

### 6.1.1.1 SECTION LIFT EFFECTIVENESS OF HIGH-LIFT AND CONTROL DEVICES

Lift effectiveness is defined and used in the literature in several ways. For linear systems, the rate of change of lift with control or flap deflection at constant angle of attack is frequently used. This parameter is defined as

$$c_{\ell_\delta} = \left( \frac{\partial c_\ell}{\partial \delta} \right)_\alpha \quad 6.1.1.1-a$$

In cases where nonlinear effects must be accounted for, it is customary to use lift increments for flap deflections at constant angle of attack. Another convention frequently used is the rate of change of zero-lift angle of attack with flap deflection.

$$\left( \frac{\partial \alpha}{\partial \delta} \right)_{c_\ell=0} = \alpha_\delta = - \frac{\left( c_{\ell_\delta} \right)_\alpha}{\left( c_{\ell_\alpha} \right)_\delta} \quad 6.1.1.1-b$$

Again, for nonlinear characteristics, increments in angle of attack at zero lift are used. Several of these definitions of lift effectiveness are used in this section, depending upon the particular device being discussed.

In the linear-lift range,  $\alpha_\delta$  can be obtained from  $c_{\ell_\delta}$ , and vice versa, by means of Equations 6.1.1.1-a and 6.1.1.1-b.

The methods presented in this section are limited to subsonic flow.

#### A. TRAILING-EDGE FLAPS

Trailing-edge flaps operating in the linear-lift range change the lift of the basic airfoil by changing the effective airfoil angle of attack. The means by which each type of flap accomplishes this end is discussed in the following paragraphs. Various types of flaps in common usage are illustrated in Section 6.1.1.3.

##### Plain Trailing-Edge Flaps

For plain, sealed trailing-edge flaps the theoretical derivative  $c_{\ell_\delta}$  is a function of flap-chord-to-wing-chord ratio and airfoil thickness ratio. Increasing airfoil thickness increases the theoretical lift increment for a given flap deflection.

The boundary layer for plain flapped airfoils is shed at the trailing edge of the flap. Lift increments are therefore sensitive to the conditions of the boundary layer — the thicker the boundary layer the lower the value of  $c_{\ell_\delta}$  derived from the flap. Since boundary layers are thicker on thick airfoils than on thin airfoils, actual  $c_{\ell_\delta}$  values tend to be lower for the thick airfoils.

In general, for a given increase in airfoil thickness ratio the reduction in  $c_{\ell_\delta}$  due to viscous effects is greater than the increase in  $c_{\ell_\delta}$  as predicted from inviscid-flow theory. In the charts of this section, viscous effects are accounted for by using the experimental lift-curve slope as a parameter, since  $c_{\ell_\alpha}$  is influenced by viscous effects in the same manner as  $c_{\ell_\delta}$ .

Because of the sensitivity of plain flaps to the boundary layer, the flow separates over the flap surface at relatively small deflection angles. The linear range of  $c_{\ell_\delta}$  for plain flaps is therefore limited to the range from 0 to  $10^\circ$  or  $15^\circ$  of flap deflection. An empirical correction factor is applied in this section to account for the nonlinear effects at high flap deflection.

### **Slotted Trailing-Edge Flaps**

For efficiently designed slotted trailing-edge flaps the airfoil boundary layer is shed at the slot lip and a new boundary layer forms over the flap surface. The lift derived from efficiently designed slotted flaps is therefore not affected by the boundary layer of the basic airfoil. Experimental data for slotted flaps support this observation.

### **Fowler Flaps**

Many flap designs have been developed in which the instantaneous center of rotation moves rearward as the flap deflects. An example of such a flap is the Fowler flap.

Aerodynamically, Fowler flaps function in the same way as single-slotted flaps. Additional lift benefits are derived from such flaps because of the increase in planform area due to flap translation.

The effect of translation can be approximated by calculating the increase in airfoil chord as a function of flap deflection.

### **Split Flaps**

The deflection of split trailing-edge flaps causes a wide wake to appear behind the airfoil. This wake prevents the realization of the full increase in circulation due to flap deflection. The rate of increase of lift with flap deflection is therefore lower than that for the corresponding plain flap. The rate also decreases continuously with increasing flap deflection, because the wake widens as the flap deflection is increased.

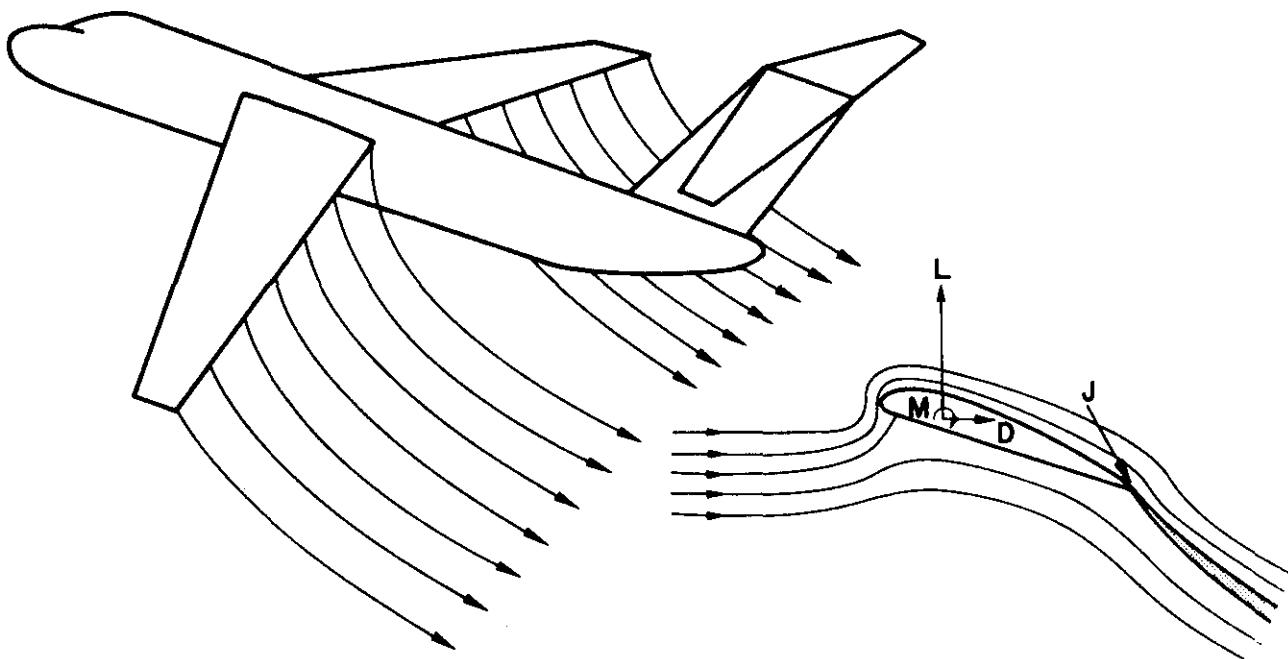
## **B. JET FLAPS**

The term jet flap has been used to describe a propulsive jet emitted from the wing trailing edge as a plane jet at an angle of inclination to the mainstream. In three dimensions, the jet is distributed in the spanwise direction on a wing. Such an integrated jet-flap system is depicted schematically in Sketch (a), along with a definition of the section jet momentum coefficient  $C_\mu$ .

In order that the Datcom user may better understand the jet-flap concept, a brief discussion covering the salient aspects of the jet-flap principle is presented. This general discussion is taken essentially from References 1 and 2.

The primary objective of a jet-flap system is to increase significantly the lift component beyond that which a conventional mechanical flap system can possibly attain. The lift of a jet flap can be attributed to three different sources as follows:

1. Direct-lift component of the jet reaction. This is directly proportional to the jet momentum emitted at the trailing edge.
2. Circulation generated around the airfoil. Since the amount of circulation greatly exceeds that of a corresponding pure airfoil, it is sometimes termed supercirculation. Physically, this additional increase in lift may be explained as follows: The air on the upper surface of the airfoil is drawn down by the deflected jet, creating a suction, while the air flow below is blocked by the jet, producing pressure. Both effects tend to increase lift on the airfoil. Scientists investigating jet lift prefer to call this circulation effect the magnification of the direct jet lift.
3. Automatic boundary-layer control. The jet tends to prevent the flow above the airfoil from separating by reducing the adverse pressure gradient which the boundary layer must negotiate. Some reduction of the adverse pressure gradient can be attributed to the jet entrainment.



$$C_{\mu} = \frac{m_j V_j}{1/2 \rho V^2 c} = \frac{J}{qc} \quad \text{and} \quad C'_{\mu} = \frac{m_j V_j}{1/2 \rho V^2 c'} = \frac{J}{qc'}$$

where

$C_{\mu}$  is the section nondimensional trailing-edge jet momentum coefficient.

$m_j$  is the mass-flow rate of the gas efflux (per section).

$V_j$  is the velocity of the gas efflux leaving the trailing edge of the airfoil.

$J$  is the jet momentum; i.e., the product of  $m_j$  and  $V_j$ .

$\rho$  is the density of the free stream.

$V$  is the velocity of the free stream.

$c$  is the airfoil chord.

$c'$  is the extended airfoil chord (see Figures 6.1.1.1-44 through -46 and Figure 6.1.1.1-48).

$q$  is the free-stream dynamic pressure.

#### SKETCH (a)

The above effect that dominates the lift contribution depends on the magnitude of the jet momentum. The boundary-layer control effect is most significant when the jet momentum is small ( $C_{\mu} < 1$ ), while the supercirculation effect predominates when the momentum is moderate or large.

With respect to the supercirculation, the downward extending jet acts generally in a manner similar to that of a mechanical flap. Although the jet sheet extends downstream to infinity, only its initial portion, before it has been curved around so as to become almost straight, could significantly affect

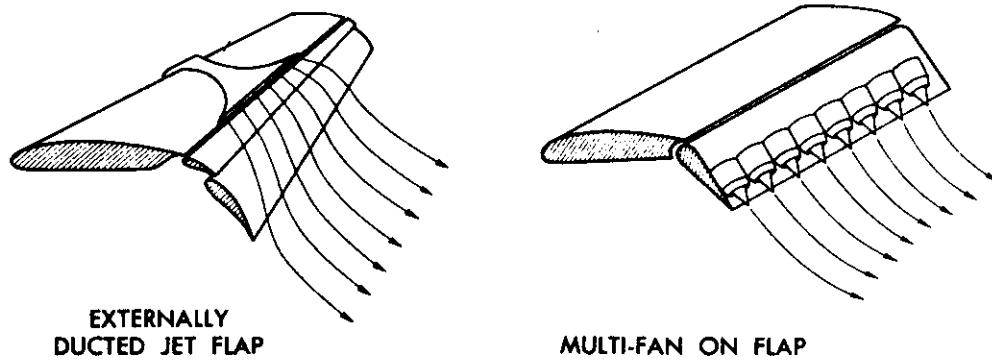
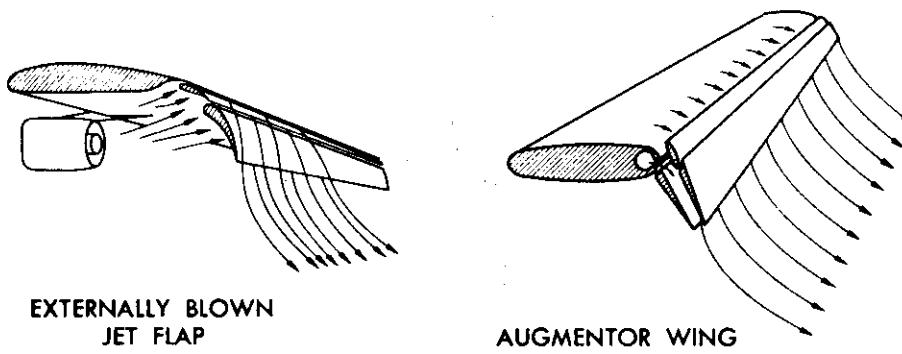
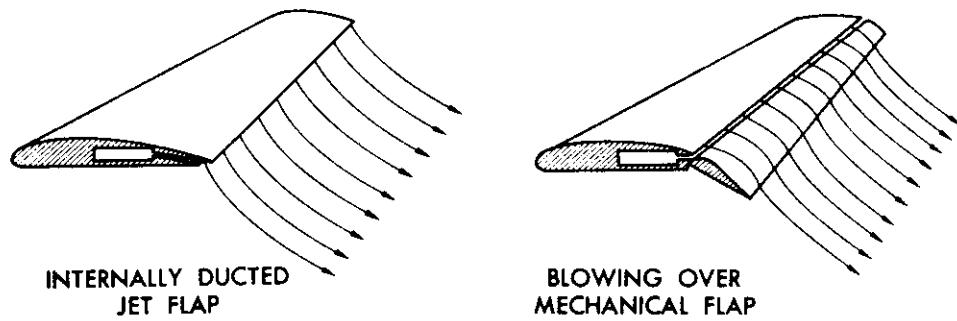
the flow. Therefore, its effect is analogous to some specific mechanical flap of finite extension. As the jet momentum is increased, the jet would penetrate farther into the mainstream, corresponding to a larger mechanical flap. The name "jet flap" was derived from such analogy.

The basic jet-flap scheme, often referred to as an internal-flow system, essentially requires the gas to be ducted through the wing either to the trailing edge or to a slot at the knee of a flap which is used for varying the jet angle. Several alternatives to the basic jet-flap scheme have been devised for directing the gas efflux to the trailing edge. Some of these concepts are shown in Sketch (b). For the external-flow system shown in Sketch (b), the gas from the engine is ducted or directed outside the wing. With an underslung podded engine, the round jet may be guided to impinge on a mechanical flap system and form a flattened jet sheet. Alternatively, with the engine mounted on the top, the exit nozzle may be elongated spanwise to generate a plane jet sheet. Another approach shown in Sketch (b) is the augmentor-wing concept. With this scheme the jet efflux can also be used to drive an ejector system that will, in turn, augment the thrust by the entrainment of the free-stream flow.

The fact that all these concepts exhibit a flat jet sheet at the trailing edge, which characteristically has the same effect of inducing supercirculation, provides the basis for a common theoretical analysis.

The analysis of jet-flap problems inherently requires that the wing and jet be treated as an integrated system. Thus far, theoretical treatments of jet-flap aerodynamic problems have been based on linearized small-disturbance concepts. In the context of linearized theory, the basic difference between the jet wing and a conventional wing is that, in addition to the wing planform, the jet sheet itself should be regarded as a discontinuity sheet in longitudinal velocity. Roughly speaking, the jet-flapped wing may be treated as if the wing planform were extended to infinity. Unfortunately, the shape of the jet sheet, unlike that of the wing, is not known. Thus a dynamic boundary condition must be introduced for the jet, in contrast to the kinematic boundary condition for the wing. Therefore, the development of an analytical solution for aerodynamic characteristics of a jet-flapped wing encounters two difficulties. One is due to the mixed boundary conditions; the other is due to the fact that the boundary conditions are prescribed over a region of semi-infinite extent. An elegant solution for the two-dimensional jet-flap problem has been obtained by Spence in References 3 and 4. His approach is based on the assumptions that the flows inside and outside the jet are irrotational and at constant, although not necessarily equal, densities. Since entrainment into the jet is neglected, it can be regarded as if bounded by streamlines. These simplifications enable a relation between the pressure differences across the jet and its curvature to be found. The limiting case of a thin, high-speed jet is considered by assuming that the jet has zero thickness but finite momentum. Airfoil thickness is neglected, the airfoil and jet are assumed near zero angle of attack, and the airfoil and jet boundary conditions are transferred to the semi-infinite line through the trailing edge and parallel to the undisturbed flow. The result of these approximations is the representation of the flow by a mixed-boundary-value problem on this semi-infinite line. Spence has obtained three basic solutions: angle of attack, flap deflection, and jet deflection. Close agreement has been obtained between Spence's theory and the experimental results of Dimmock (Reference 5) over the range of jet momentum and jet deflection angles of practical interest.

Several experimental and theoretical studies have been conducted to investigate the effects of ground proximity on jet-flapped wings. Insofar as theoretical methods are concerned, however, only a simple mathematical representation of the two-dimensional jet-flap airfoil has been formulated (Reference 6).



SKETCH (b)

### C. LEADING-EDGE FLAPS AND SLATS

#### Leading-Edge Flaps

Leading-edge flaps change the lift of an airfoil by changing the effective angle of attack in the same way that trailing-edge flaps do. Unlike trailing-edge flaps, however, a positive leading-edge-flap deflection (nose down) causes a loss in lift instead of an increase in lift. In general, the change in lift per degree of flap deflection is smaller for leading-edge flaps than for trailing-edge flaps.

Leading-edge-flap effectiveness is not affected by the airfoil boundary layer.

#### Leading-Edge Slats

The lift parameter  $c_{q\delta}$  for leading-edge slats is affected by two factors. First, the deflection or rotation of the slat causes a loss in lift similar to that of leading-edge flaps. Secondly, slat extension or translation increases the planform area.

### D. SPOILERS

Spoilers are generally used for two reasons – for roll control when deflected asymmetrically and for high drag generation when deflected symmetrically. Only the section-lift aspects of spoilers are discussed herein.

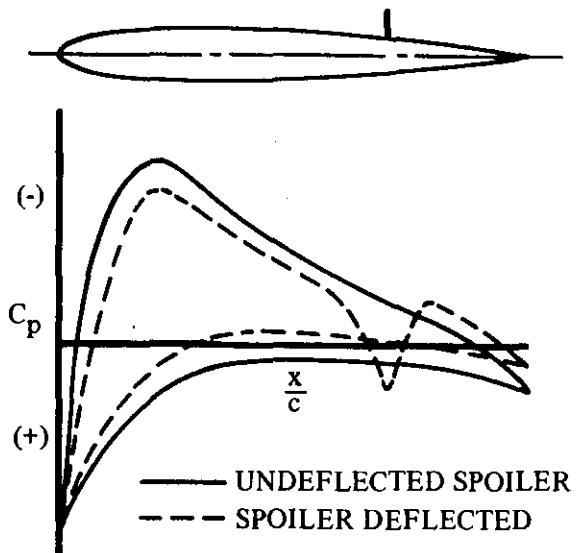
Many types of spoilers have been developed, depending upon control-power limitations, structural limitations, and aerodynamic requirements. Some of the more commonly used types are illustrated in Sketch (c).



SKETCH (c) TYPICAL SPOILER ARRANGEMENTS

Unlike flaps, spoilers operate by causing a loss in airfoil lift – rather than an increase – by separating the flow downstream. The effective angle of attack is decreased and the lift correspondingly reduced. There are two viewpoints that can be used in explaining the operation of spoilers. One is to consider the pressure field over the airfoil and the other is to consider the effect of the spoiler on the wake pattern. These viewpoints are discussed in the following paragraphs.

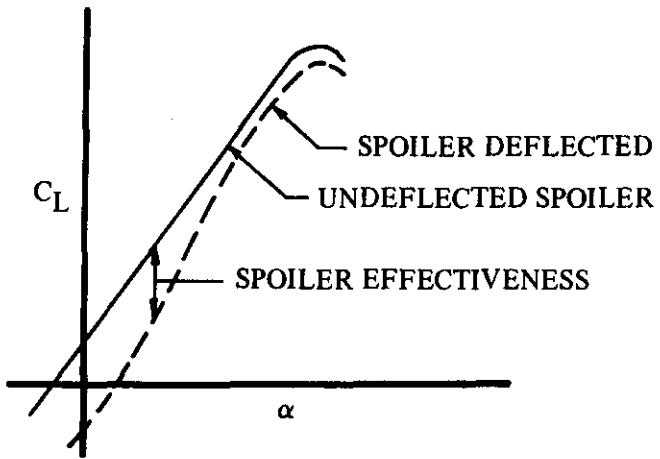
For flap- and plug-type spoilers the pressure loading forward of the spoiler (difference in upper- and lower-surface pressures) is reduced, and the local lift is reduced accordingly. Aft of the spoiler the pressure loading is increased because of high suction pressures behind the spoiler on the upper surface. The increase in lift aft of the spoiler, however, does not offset the decrease in lift forward of the spoiler, and a total loss in lift results. These phenomena are illustrated in Sketch (d).



SKETCH (d) TYPICAL AIRFOIL PRESSURE DISTRIBUTION FOR PLUG-TYPE SPOILER

For large spoiler deflections a wide wake exists behind the spoiler, the width of which depends upon spoiler height, location, and airfoil angle of attack. The lift generated from the airfoil is related to the width and direction of the wake with respect to the free stream.

At subsonic and transonic speeds the wake characteristics vary nonlinearly with angle of attack and spoiler deflection. Therefore, the corresponding lift characteristics are also nonlinear, as shown in Sketch (e). The loss in effectiveness at high angles of attack should be noted. This loss, which is particularly pronounced for thin wings, can be greatly alleviated by the use of leading-edge flaps (Reference 7) or by incorporating a slot behind the spoiler, as discussed below (Reference 8).



SKETCH (e) TYPICAL LIFT CURVES FOR PLUG-TYPE SPOILER

For small deflections of plug- and flap-type spoilers, the flow reattaches behind the spoiler and the spoiler becomes ineffective. This generally occurs for spoiler deflections less than one percent of the airfoil chord. This problem is discussed in detail in Reference 9.

One commonly used variation of the flap-type spoiler is the slotted spoiler with a deflector on the lower surface (see Sketch (c)). This system has several advantages. First, the air that is ducted from the underside of the airfoil relieves the upper-surface suction pressures behind the spoiler and increases the spoiler effectiveness. Secondly, the problem of flow reattachment does not occur for small spoiler deflections. Thirdly, the opposing aerodynamic loads on the spoiler and deflector can be used to achieve low actuation power requirements.

The information presented in this section is limited to the region near zero lift, where the spoiler lift characteristics are essentially linear with angle of attack.

## DATCOM METHODS

### A. TRAILING-EDGE FLAPS

#### Plain Flaps

The section lift increment due to the deflection of plain trailing-edge flaps with sealed gaps, based on the method of Reference 10, is given by

$$\Delta c_L = \delta_f \left[ \frac{c_{L\delta}}{(c_{L\delta})_{\text{theory}}} \right] (c_{L\delta})_{\text{theory}} K' \quad 6.1.1.1-c$$

where

$(c_{L\delta})_{\text{theory}}$  is the theoretical flap-lift effectiveness from Figure 6.1.1.1-39a for a given airfoil thickness ratio and flap-chord-to-airfoil-chord ratio.

$\frac{c_{L\delta}}{(c_{L\delta})_{\text{theory}}}$  is an empirical correction factor obtained from Figure 6.1.1.1-39b

The parameter  $c_{L\delta}/(c_{L\delta})_{\text{theory}}$  used in reading this chart is obtained from Section 4.1.1.2 (Figure 4.1.1.2-8a).

$\delta_f$  is the flap deflection.

$K'$  is an empirical correction factor from Figure 6.1.1.1-40. This factor has been derived from a large body of test data (References 11 through 28). It corrects  $\Delta c_L$  for nonlinear effects at high flap deflections.

This method does not include the effects of unsealed gaps, beveled trailing edges, or compressibility.

In general, the effectiveness of the control is reduced when the gap is unsealed. This effect is more pronounced for airfoils with beveled trailing edges than for airfoils with true-contour trailing edges.

The method may be applied to true-contour airfoils or airfoils with slightly modified trailing-edge contours. The method should not be applied to airfoils with beveled trailing edges. Not enough experimental data are available to allow a quantitative prediction of the effect of bevel. However, the data do show a decrease in control effectiveness with increasing bevel.

Compressibility will have serious effects on the lift effectiveness of plain trailing-edge controls. Experimental data (References 17, 18, and 57 through 59) show decreases in lift effectiveness up to one half the low-speed values at high subsonic speeds. Although there are not enough data to allow a quantitative prediction of compressibility effects, they do demonstrate significant effects of airfoil thickness, control size, and trailing-edge angle on the control effectiveness as the Mach number is increased. The onset of an abrupt loss in control effectiveness is delayed to higher Mach numbers by a reduction in airfoil thickness (References 58 and 59), an increase in control size (Reference 17), or a reduction in trailing-edge angle (References 56 and 57).

A comparison of low-speed test data with  $\Delta c_L$  of plain-flapped airfoils calculated by this method is presented as Table 6.1.1.1-A.

### Single-Slotted Flaps

Two methods are presented for estimating the section lift increment due to the deflection of single-slotted flaps. Both methods are applicable in the high-flap-deflection range and limited to the low-speed regime. Method 1 is preferable when test data are available for the section lift-curve slope of the unflapped airfoil. When no section lift-curve-slope test data are available, Method 2 should be used.

#### Method 1

The section lift increment due to the deflection of single-slotted flaps is given by

$$\Delta c_L = -c_{L_\alpha} \alpha_s \delta_f \quad 6.1.1.1-d$$

where

$c_{L_\alpha}$  is the section lift-curve slope of the unflapped airfoil, including the effects of compressibility, obtained from test data or Section 4.1.1.2.

$\alpha_s$  is the section lift-effectiveness parameter of single-slotted flaps obtained from the empirical correlation of Figure 6.1.1.1-41. This parameter, based on the data of References 29 through 50, is presented as a function of flap deflection for several values of the ratio of flap chord to airfoil chord  $c_f/c$ .

$\delta_f$  is the flap deflection.

A comparison of test data with  $\Delta c_L$  due to single-slotted flaps calculated by this method is presented as Table 6.1.1.1-B.

#### Method 2

This method (Reference 70) uses the theoretical lift effectiveness of a simple trailing-edge flap as obtained from thin-airfoil theory, modified by an empirical lift-effectiveness parameter. The section-lift increment due to the deflection of single-slotted flaps is given by

$$\Delta c_L = c_{L_\alpha} \delta_f \eta_1 \frac{c'}{c} \quad 6.1.1.1-e$$

where

$c_{\ell \delta}$  is the theoretical lift effectiveness from thin-airfoil theory of a simple trailing-edge flap, obtained from Figure 6.1.1.1-42 as a function of flap-chord ratio  $c_1/c$  (see Figure 6.1.1.1-44 for a geometric representation of  $c_1/c$ ).

$\delta_f$  is the flap deflection in degrees.

$\eta_1$  is the empirical lift-efficiency factor for single-slotted flaps, obtained from Figure 6.1.1.1-43a as a function of the effective turning angle  $\Phi$ ,

where

$$\Phi = \delta_f + \phi_{TE_{upper}} \quad 6.1.1.1-f$$

where

$$\phi_{TE_{upper}} = \tan^{-1} \left( \frac{Y_{90} - Y_{100}}{0.10} \right) \quad 6.1.1.1-g$$

$Y_{90}$  is the upper-surface ordinate of the flap at 90% chord in the retracted position, in fractions of the chord.

$Y_{100}$  is the upper-surface ordinate of the flap at 100% chord in the retracted position, in fractions of the chord.

$\frac{c'}{c}$  is the ratio of the extended-wing chord to the basic wing chord. (See Figure 6.1.1.1-44 for a schematic definition.)

A comparison of test data with  $\Delta c_\ell$  due to single-slotted flaps calculated by this method is presented as Table 6.1.1.1-C. These data are the same data that appear in Table 6.1.1.1-B.

It is virtually impossible to present quantitative information on the effects of the various geometric and aerodynamic variables involved because of the lack of systematic experimental data. Although a large body of test data is available, the data consist of a large number of unrelated combinations of airfoils and slotted flaps. The configurations listed in Table 6.1.1.1-B include wide variations in chordwise position of slot lip, slot-entry shape, slot-lip shape, flap-nose shape, and position of the flap with respect to the slot lip.

Because of the number of variables involved and the design parameters not considered in the Datcom methods, the comparison between theory and experiment cannot be analyzed by examining the isolated effect of any one variable.

### Fowler Flaps

Section lift increments for Fowler flaps are obtained by using the methods presented for single-slotted flaps. Fowler flaps are included in the empirical correlation of slotted-flap lift effectiveness in Figure 6.1.1.1-41 of Method 1. It should be noted, however, that this design chart

applies only when the Fowler flap is near its fully extended position and the slot is properly developed. Method 2 predicts an increase in lift increment that is directly proportional to the ratio of the extended chord to the retracted chord.

Not enough test data for airfoils are available to fully substantiate these methods. However, the accuracy of the methods when applied to Fowler flaps near their fully extended position and with a properly developed slot should be comparable to that shown for the single-slotted flap methods in Tables 6.1.1.1-B and 6.1.1.1-C.

### Double-Slotted Flaps

Two methods, taken from Reference 70, are presented for estimating the section lift increment due to the deflection of a double-slotted flap. Both methods are applicable in the high-flap-deflection range and limited to the low-speed regime. Method 1 is applicable to the conventional vane-plus-aft-flap configuration as shown in Figure 6.1.1.1-45 where  $c_1/c_2 \leq 0.60$ . Method 2 is applicable to a double-slotted configuration where the two flap-chord segments are approximately equal (see Figure 6.1.1.1-46). This configuration is referred to as a double-deflected flap in several references.

#### Method 1

The section lift increment due to the deflection of double-slotted flaps of the conventional vane-plus-aft-flap combination is given by

$$\Delta c_L = \eta_1 c_{\delta f_1} \delta_{f_1} \left( \frac{c + c_1}{c} \right) + \eta_2 c_{\delta f_2} (\delta_{f_1} + \delta_{f_2}) \left( \frac{c'}{c} \right) \quad 6.1.1.1-h$$

where

$\eta_1, \eta_2$  are the empirical lift-efficiency factors for the vane and aft-flap segments obtained from Figure 6.1.1.1-43a, based on  $c_1/c$  and  $c_2/c$ , respectively, and the effective turning angle  $\Phi$ ,

where

$$\Phi = \delta_{f_1} + \phi_{TE_{upper}} \quad (\text{vane segment})$$

$$\Phi = \delta_{f_1} + \delta_{f_2} + \phi_{TE_{upper}} \quad (\text{flap segment})$$

and  $\phi_{TE_{upper}}$  is defined in Equation 6.1.1.1-g.

$c_{\delta f_1}, c_{\delta f_2}$  are the theoretical lifting-efficiency factors for the vane and aft-flap segments obtained from Figure 6.1.1.1-42 and based on  $c_1/c$  and  $c_2/c$ , respectively.

All remaining parameters are illustrated and defined in Figure 6.1.1.1-45.

A comparison of test data with  $\Delta c_L$  due to double-slotted flaps calculated by this method is presented in Table 6.1.1.1-D.

## Method 2

The section lift increment due to the deflection of double-slotted flaps with approximately equal flap-chord segments is given by

$$\Delta c_L = \eta_1 c_{\delta f_1} \delta_{f_1} \left( \frac{c'_a}{c} \right) + \eta_2 \eta_t c_{\delta f_2} \delta_{f_2} \left( 1 + \frac{c' - c'_a}{c} \right) \quad 6.1.1.1-i$$

where

$\eta_1, \eta_2$  are the empirical lift-efficiency factors for the forward- and aft-flap segments obtained from Figure 6.1.1.1-43a, based on  $c'_1/c$  and  $c'_2/c$ , respectively, and the effective turning angle  $\Phi$ ,

where

$$\Phi = \delta_{f_1} + \phi_{TE_{upper}} \quad (\text{forward segment})$$

$$\Phi = \delta_{f_2} + \phi_{TE_{upper}} \quad (\text{aft segment})$$

and  $\phi_{TE_{upper}}$  is defined in Equation 6.1.1.1-g.

$c_{\delta f_1}, c_{\delta f_2}$  are the theoretical lifting-efficiency factors for the forward- and aft-flap segments obtained from Figure 6.1.1.1-42, based on  $c'_1/c$  and  $c'_2/c$ , respectively.

$\eta_t$  is the turning-efficiency factor of the aft flap obtained from Figure 6.1.1.1-43b, based on the forward- and aft-flap-deflection angles.

All remaining parameters are illustrated and defined in Figure 6.1.1.1-46.

No substantiation table is presented for this method because of the lack of test data for this type of configuration. However, for those cases that have been evaluated, the accuracy of the method is analogous to that of Method 1 above.

The double-slotted flap may be defined as a single-slotted flap with a turning vane in the slot. Consequently, the important design parameters for double-slotted flaps are more complicated than those for single-slotted flaps, particularly in relation to determining the efficiency of flow through the slot. As in the case for single-slotted flaps, a lack of systematic test data precludes quantitative examination of the effects of the various geometric and aerodynamic variables involved.

Because of the design parameters not considered in the Datcom method, the comparison between theory and experiment cannot be analyzed by examining the isolated effect of any one variable.

## Split Flaps

The section lift increment due to the deflection of split flaps is given by

$$\Delta c_L = -c_{L_\alpha} \alpha_\delta \delta_f \quad 6.1.1.1-j$$

where

$c_{L_\alpha}$  is the section lift-curve slope of the unflapped airfoil, including the effects of compressibility, obtained from Section 4.1.1.2.

$\alpha_\delta$  is the section lift-effectiveness parameter of split flaps obtained from the empirical curves of Figure 6.1.1.1-47. This parameter, based on the curves presented in Reference 53, is presented as a function of flap deflection for several values of the ratio of flap chord to airfoil chord  $c_f/c$ .

$\delta_f$  is the flap deflection, measured tangent to airfoil lower-surface contour at trailing edge.

A comparison of test data with  $\Delta c_L$  due to split flaps calculated by this method is presented as Table 6.1.1.1-E.

## B. JET FLAPS

Methods that are adaptable to a handbook application are not available for all jet-flap schemes. The method presented below is applicable to the pure jet-flap concept and the internally-blown-flap (IBF) and externally-blown-flap (EBF) concepts with a plain trailing-edge flap. For an IBF or EBF concept with a single-slotted or multislotted flap configuration, this method should be used only as a first approximation. No handbook method is currently available to analyze the section lift increment due to an augmentor-wing concept.

The method presented herein is a combination of methods presented in References 2 and 70 (based on Spence's theoretical results). The pertinent geometrical parameters are defined and illustrated in Figure 6.1.1.1-48. No substantiation of the method is presented herein; however, the method has been acknowledged as being substantiated in the literature (References 1 and 4).

This method is capable of estimating the lift increments in the linear-lift range (preferably at zero angle of attack) for three types of configurations:

1. Pure jet flap
2. IBF or EBF
3. Combination jet-flap and plain-flap deflection (see Figure 6.1.1.1-48)

It is of particular interest to note that the factor  $[1 + k_t(t/c')]$  in Equation 6.1.1.1-k below corrects the pressure lift contribution for thickness effects, under the constraint of no trailing-edge separation. No values for the lifting-efficiency factor are available as a function of flap setting and jet momentum coefficient. For this reason, the user must exercise caution not to apply the method to conditions where trailing-edge separation exists and/or low values of jet momentum coefficient prevail.

It should be noted that the flap-chord value  $c_f/c'$  used in Figure 6.1.1.1-49 is not the true mechanical flap length for flaps with Fowler-type motion. For Fowler-type flaps, the flap chord is the length from the flap trailing edge to the intersection of the flap-chord and wing-chord lines.

The section lift increment due to flap deflection and jet efflux of a jet-flap combination, based on the retracted airfoil chord  $c$ , is given by

$$\Delta c_q = \left\{ \left[ 1 + k_t \left( \frac{t}{c'} \right) \right] \delta_f \left( c_{q_{\delta_f}} - C'_\mu \right) + C'_\mu \delta_f \right. \\ \left. + \left[ 1 + k_t \left( \frac{t}{c'} \right) \right] \delta_j \left( c_{q_{\delta_j}} - C'_\mu \right) + C'_\mu \delta_j \right\} \frac{c'}{c} \quad 6.1.1.1-k$$

where

$k_t$  is the airfoil-theory thickness factor; i.e.,

$k_t = 1.0$  for elliptic airfoils

$= 0.637$  for parabolic airfoils

For airfoil sections other than elliptic or parabolic, a value of 0.80 for  $k_t$  is suggested (Reference 70).

$\frac{t}{c'}$  is the airfoil thickness ratio, based on the extended chord; see Figure 6.1.1.1-48.

$c_{q_{\delta_f}}$  is the rate of change of section lift coefficient with respect to flap deflection obtained from Figure 6.1.1.1-49 as a function of the trailing-edge jet momentum  $C'_\mu$  and the ratio of the flap chord to the extended wing chord  $c_f/c'$ . (The term  $c'_{q_\alpha}$  appearing in Figure 6.1.1.1-49 is the jet-flap lift-curve slope uncorrected for thickness effects.)

As noted above, the flap-chord value  $c_f$  is the length from the flap trailing edge to the intersection of the flap-chord and wing-chord lines.

$C'_\mu$  is the section nondimensional trailing-edge jet-momentum coefficient based on the extended airfoil chord (defined in Sketch (a) of this section).

$\delta_f$  is the flap deflection in radians, see Figure 6.1.1.1-48.

$c_{q_{\delta_j}}$  is the rate of change of section lift coefficient with respect to the jet deflection obtained from Figure 6.1.1.1-49 as a function of the trailing-edge jet momentum  $C'_\mu$ .

$\delta_j$  is the trailing-edge jet momentum angle in radians, with respect to the trailing-edge camber line, see Figure 6.1.1.1-48.

$\frac{c'}{c}$  is the ratio of the extended wing chord to the retracted wing chord.

### C. LEADING-EDGE FLAPS AND SLATS

The available experimental section characteristics for leading-edge devices (References 15, 69, and 76) are insufficient to allow substantiation of the methods presented. However, the methods should provide results that are suitable for first approximations for flapped airfoils with geometric parameters within the boundaries of thin-airfoil theory. Consequently, the methods are considered applicable for airfoil-flap configurations with  $t/c \leq 0.10$  and with small flap deflections, in the linear-lift range (preferably at zero angle of attack).

It should be noted that the  $c_{\ell_\delta}$  values for all leading-edge devices are of opposite sign from the values for trailing-edge flaps.

#### Leading-Edge Flaps

The method presented below is taken from Reference 70 and is based on thin-airfoil theory. The section lift increment due to leading-edge flap deflection is given by

$$\Delta c_\ell = c_{\ell_\delta} \delta_f \quad 6.1.1.1-l$$

where

$c_{\ell_\delta}$  is the leading-edge flap-effectiveness parameter obtained from Figure 6.1.1.1-50 as a function of the nose-flap-chord to wing-chord ratio  $c_f/c$ .

$\delta_f$  is the nose-flap deflection in degrees, as shown in Figure 6.1.1.1-51.

#### Krueger Flaps

The method presented below is a modification of the method presented immediately above (Reference 70), to account for the chord extension associated with Krueger leading-edge devices.

No substantiation of this method is presented because of the lack of test data. The section lift increment due to a Krueger leading-edge flap deflection is given by

$$\Delta c_\ell = c_{\ell_\delta} \delta_f \frac{c'}{c} \quad 6.1.1.1-m$$

where

$c_{\ell_\delta}$  is the leading-edge flap-effectiveness parameter obtained from Figure 6.1.1.1-50 as a function of the Krueger flap-chord to wing-chord ratio  $c_f/c'$ .

$\delta_f$  is the Krueger flap deflection, in degrees, as shown in Figure 6.1.1.1-51.

$\frac{c'}{c}$  is the ratio of the extended wing chord to airfoil chord as shown in Figure 6.1.1.1-51.

### Leading-Edge Slats

The method presented here is a modification of the method presented for leading-edge flaps (Reference 70); i.e., it is modified to account for the chord extension associated with leading-edge slats. The section lift increment due to a leading-edge slat deflection is given by

$$\Delta c_l = c_{l_s} \delta_f \frac{c'}{c} \quad 6.1.1.1-m$$

where

$c_{l_s}$  is the leading-edge flap-effectiveness parameter obtained from Figure 6.1.1.1-50 as a function of the leading-edge-slat-chord to wing-chord ratio  $c_f/c'$ .

$\delta_f$  is the slat deflection, in degrees, as shown in Figure 6.1.1.1-51.

$\frac{c'}{c}$  is the ratio of the extended wing chord to airfoil chord as shown in Figure 6.1.1.1-51.

### D. SPOILERS

The section lift increment due to either plug or flap spoilers is given by

$$\Delta c_l = -c_{l_\alpha} \Delta \alpha'_s \quad 6.1.1.1-n$$

where

$c_{l_\alpha}$  is the lift-curve slope of the basic airfoil, including compressibility effects, from Section 4.1.1.2.

$\Delta \alpha'_s$  is the spoiler lift-effectiveness parameter expressed in terms of change in zero-lift angle of attack, from Figure 6.1.1.1-52. This design chart, taken from Reference 55, was developed from data obtained by testing a series of airfoils with various plug-spoiler configurations.

In Figure 6.1.1.1-52, the parameter  $x_s$  is the distance from the nose of the airfoil to the spoiler lip, and  $h_s$  is the height of the spoiler measured from and normal to the airfoil mean line at  $x_s$ .

Experimental section characteristics (Reference 77) for airfoils with plain or plug spoilers are too meager to allow substantiation of this method. However, if a reliable value of  $c_{l_\alpha}$  is used, the method should provide results that can be used with confidence within the limitations of the design chart for determining  $\Delta \alpha'_s$ .

The lift effectiveness of a slotted spoiler with a deflector on the lower surface is greater (causes larger lift loss) than that of plug and flap spoilers. No known method is available for predicting the section lift effectiveness of slotted spoilers.

### Sample Problems

#### 1. Plain Trailing-Edge Flap

Given: The flapped airfoil of Reference 13.

$$\text{NACA 0009 airfoil} \quad c_f/c = 0.20 \quad \delta_f = 50^\circ \quad R_\infty = 2.76 \times 10^6$$

$$\tan \frac{1}{2} \phi'_{TE} = 0.099 \text{ (streamwise airfoil geometry)}$$

Compute:

$$\left( \frac{c_{q_\delta}}{c} \right)_{\text{theory}} = 3.61 \text{ per rad} = 0.063 \text{ per deg} \quad (\text{Figure 6.1.1.1-39a})$$

$$\frac{\frac{c_{q_\alpha}}{c}}{\left( \frac{c_{q_\delta}}{c} \right)_{\text{theory}}} = 0.837 \quad (\text{Figure 4.1.1.2-8a})$$

$$\frac{\frac{c_{q_\delta}}{c}}{\left( \frac{c_{q_\delta}}{c} \right)_{\text{theory}}} = 0.725 \quad (\text{Figure 6.1.1.1-39b})$$

$$K' = 0.543 \quad (\text{Figure 6.1.1.1-40})$$

Solution:

$$\Delta c_q = \delta_f \left[ \frac{\frac{c_{q_\delta}}{c}}{\left( \frac{c_{q_\delta}}{c} \right)_{\text{theory}}} \right] \left( \frac{c_{q_\delta}}{c} \right)_{\text{theory}} K' \quad (\text{Equation 6.1.1.1-c})$$

$$= (50)(0.725)(0.063)(0.543)$$

$$= 1.24$$

This compares with a test value of 1.15 from Reference 13.

#### 2. Single-Slotted Trailing-Edge Flap (Method 1)

Given: The flapped airfoil of Reference 41 with the slot lip at 0.84 c.

$$\text{NACA 65-210 airfoil} \quad c_f/c = 0.25 \quad \delta_f = 50^\circ$$

$$\text{Low Speed; } \beta = 1.0 \quad R_\infty = 6.0 \times 10^6$$

$$\tan \frac{1}{2} \phi'_{TE} = 0.084 \text{ (streamwise airfoil geometry)}$$

Compute:

$c_{q_\alpha}$  (Section 4.1.1.2)

$$\frac{c_{q_\alpha}}{(c_{q_\alpha})_{\text{theory}}} = 0.879 \quad (\text{Figure 4.1.1.2-8a})$$

$$(c_{q_\alpha})_{\text{theory}} = 6.78 \text{ per rad} \quad (\text{Figure 4.1.1.2-8b})$$

$$c_{q_\alpha} = \frac{1.05}{\beta} \left[ \frac{c_{q_\alpha}}{(c_{q_\alpha})_{\text{theory}}} \right] (c_{q_\alpha})_{\text{theory}} \quad (\text{Equation 4.1.1.2-a})$$

$$= \frac{1.05}{1.0} (0.879) (6.78)/57.3 = 0.109 \text{ per deg}$$

$$\alpha_\delta = -0.300 \quad (\text{Figure 6.1.1.1-41})$$

Solution:

$$\Delta c_q = -c_{q_\alpha} \alpha_\delta \delta_f \quad (\text{Equation 6.1.1.1-d})$$

$$= -(0.109) (-0.300) (50)$$

$$= 1.64$$

This compares with a test value of 1.73 from Reference 41.

### 3. Single-Slotted Trailing-Edge Flap (Method 2)

Given: The flapped airfoil of Reference 41 with the slot lip at 0.84 c  
(same sample problem as presented for Method 1)

$$\text{NACA 65-210 airfoil} \quad \frac{c_f}{c} = 0.25 \quad \frac{c'}{c} = 1.078 \quad \alpha = 0$$

$$Y_{90} = 0.01327 c \quad Y_{100} = 0 \quad \delta_f = 50^\circ$$

Low Speed;  $\beta = 1.0$

Compute:

$$c_{q_\delta} = 0.0668 \text{ per deg} \quad (\text{Figure 6.1.1.1-42})$$

$$\begin{aligned}\phi_{TE_{upper}} &= \tan^{-1} \left( \frac{Y_{90} - Y_{100}}{0.10} \right) \quad (\text{Equation 6.1.1.1-g}) \\ &= \tan^{-1} \left( \frac{0.01327 - 0}{0.10} \right) \\ &= 7.56^\circ\end{aligned}$$

$$\Phi = \delta_f + \phi_{TE_{upper}} \quad (\text{Equation 6.1.1.1-f})$$

$$= 50 + 7.56 = 57.56^\circ$$

$$\eta_1 = 0.455 \quad (\text{Figure 6.1.1.1-43a})$$

$$\Delta c_l = c_{q_{\delta_f}} \delta_f \eta_1 \frac{c'}{c} \quad (\text{Equation 6.1.1.1-e})$$

$$= (0.0668)(50)(0.455)(1.078)$$

$$= 1.64$$

This compares with a test value of 1.73 from Reference 41.

#### 4. Double-Slotted Trailing-Edge Flap (Method 1)

**Given:** The flapped airfoil of Reference 64.

$$\begin{array}{llll} \text{NACA 64-208 airfoil} & c_1/c = 0.056 & c_2/c = 0.25 & c'/c = 1.127 \\ M = 0.18 & \delta_{f_1} = 25^\circ & \delta_{f_2} = 25^\circ & \alpha = 0 \\ Y_{90} = 0.01067c & Y_{100} = 0 & & \end{array}$$

**Compute:**

$$c_{q_{\delta_{f_1}}} = 0.0327 \text{ per deg} \quad (\text{Figure 6.1.1.1-42})$$

$$c_{q_{\delta_{f_2}}} = 0.0668 \text{ per deg} \quad (\text{Figure 6.1.1.1-42})$$

$$\phi_{TE_{upper}} = \tan^{-1} \left( \frac{Y_{90} - Y_{100}}{0.10} \right) \quad (\text{Equation 6.1.1.1-g})$$

$$= \tan^{-1} \left( \frac{0.01067 - 0}{0.10} \right)$$

$$= 6.1^\circ$$

$$\Phi = \delta_{f_1} + \phi_{TE_{upper}} \text{ (vane segment)}$$

$$= 25 + 6.1 = 31.1^\circ$$

$$\Phi = \delta_{f_1} + \delta_{f_2} + \phi_{TE_{upper}} \text{ (flap segment)}$$

$$= 25 + 25 + 6.1 = 56.1^\circ$$

$$\left. \begin{array}{l} \eta_1 = 0.640 \\ \eta_2 = 0.470 \end{array} \right\} \quad (\text{Figure 6.1.1.1-43a})$$

$$\Delta c_q = \eta_1 c_{q_{\delta f_1}} \delta_{f_1} \left( \frac{c + c_1}{c} \right) + \eta_2 c_{q_{\delta f_2}} \left( \delta_{f_1} + \delta_{f_2} \right) \left( \frac{c'}{c} \right) \quad (\text{Equation 6.1.1.1-h})$$

$$= (0.640)(0.0327)(25)(1.056) + (0.470)(0.0668)(50)(1.127)$$

$$= 0.552 + 1.770$$

$$= 2.32$$

This compares with a test value of 2.07 from Reference 64.

## 5. Double-Slotted Trailing-Edge Flap (Method 2)

Given: The flapped airfoil of Reference 78.

$$\text{NACA 23012 airfoil} \quad c'_1/c = 0.40 \quad c_2/c = 0.2566$$

$$c'_2/c = 1.10 \quad c'/c = 1.14 \quad \delta_{f_1} = 30^\circ \quad \delta_{f_2} = 20^\circ$$

$$\text{Low Speed; } \beta = 1.0 \quad Y_{90} = 0.0168c \quad Y_{100} = 0.0013c$$

Compute:

$$c_{q_{\delta f_1}} = 0.082 \text{ per deg} \quad (\text{Figure 6.1.1.1-42})$$

$$c_{q_{\delta f_2}} = 0.0672 \text{ per deg} \quad (\text{Figure 6.1.1.1-42})$$

$$\begin{aligned}\phi_{TE_{upper}} &= \tan^{-1} \left( \frac{Y_{90} - Y_{100}}{0.10} \right) \quad (\text{Equation 6.1.1.1-g}) \\ &= \tan^{-1} \left( \frac{0.0168 - 0.0013}{0.10} \right) \\ &= 8.8^\circ\end{aligned}$$

$$\begin{aligned}\Phi &= \delta_{f_1} + \phi_{TE_{upper}} \quad (\text{forward segment}) \\ &= 30 + 8.8 = 38.8^\circ\end{aligned}$$

$$\begin{aligned}\Phi &= \delta_{f_2} + \phi_{TE_{upper}} \quad (\text{aft segment}) \\ &= 20 + 8.8 = 28.8^\circ\end{aligned}$$

$$\left. \begin{array}{l} \eta_1 = 0.69 \\ \eta_2 = 0.71 \end{array} \right\} \quad (\text{Figure 6.1.1.1-43a})$$

$\eta_t = 0.84$  (extrapolated from Figure 6.1.1.1-43b)

$$\begin{aligned}\Delta c_\alpha &= \eta_1 c_{\alpha_{\delta f_1}} \delta_{f_1} \left( \frac{c'}{c} \right) + \eta_2 \eta_t c_{\alpha_{\delta f_2}} \eta_{f_2} \left( 1 + \frac{c' - c'_a}{c} \right) \quad (\text{Equation 6.1.1.1-i}) \\ &= (0.69)(0.082)(30)(1.10) + (0.71)(0.84)(0.0672)(20)[1 + (1.14 - 1.10)] \\ &= 1.867 + 0.834 \\ &= 2.70\end{aligned}$$

This compares with a test value of 2.69 from Reference 78.

## 6. Split Trailing-Edge Flap

Given: The flapped airfoil of Reference 75

$$\delta_f = 60^\circ \quad \text{NACA 23012 airfoil} \quad c_f/c = 0.40$$

$$c_{\alpha_\alpha} = 0.107 \text{ per deg (test data)}$$

Compute:

$$\alpha_\delta = -0.30 \quad (\text{Figure 6.1.1.1-47})$$

Solution:

$$\Delta c_q = -c_{q_\alpha} \alpha_\delta \delta_f \quad (\text{Equation 6.1.1.1-j})$$

$$= -(0.107)(-0.30)(60)$$

$$= 1.92$$

This compares with a test value of 1.71 from Reference 75.

## 7. Jet Flaps

Given: The pure jet-flap configuration of Reference 5.

Elliptic airfoil

$$\frac{t}{c} = 0.125$$

$$C_\mu = 4.0$$

$$\frac{c'}{c} = 1.0$$

$$\frac{c_f}{c} = 0$$

$$\delta_f = 0$$

$$\alpha = 0$$

$$\delta_j = 31.4^\circ$$

Compute:

$$k_t = 1.0 \text{ (elliptic value)}$$

$$c_{q_{\delta_j}} = 9.60 \text{ per rad} \quad (\text{Figure 6.1.1.1-49})$$

$$\begin{aligned} \Delta c_q &= \left\{ \left[ 1 + k_t \left( \frac{t}{c'} \right) \right] \delta_f \left( c_{q_{\delta_f}} - C'_\mu \right) + C'_\mu \delta_f \right. \\ &\quad \left. + \left[ 1 + k_t \left( \frac{t}{c'} \right) \right] \delta_j \left( c_{q_{\delta_j}} - C'_\mu \right) + C'_\mu \delta_j \right\} \frac{c'}{c} \quad (\text{Equation 6.1.1.1-k}) \end{aligned}$$

Since  $\delta_f = 0$ , the first two terms drop out.

$$\Delta c_q = [1 + (1.0)(0.125)] \frac{31.4}{57.3} (9.60 - 4.0) + 4.0 \left( \frac{31.4}{57.3} \right)$$

$$= 3.452 + 2.192$$

$$= 5.64 \text{ (based on } c)$$

This compares with a test value of 5.59 from Reference 5.

## 8. Leading-Edge Flaps

Given: The flapped airfoil of Reference 15.

$$\text{NACA 0006 airfoil} \quad c_f/c = 0.15 \quad \delta_f = 20^\circ$$

$$M = 0.15$$

Compute:

$$c_{q_\delta} = -0.00286 \text{ per deg} \quad (\text{Figure 6.1.1.1-50})$$

$$\Delta c_q = c_{q_\delta} \delta_f \quad (\text{Equation 6.1.1.1-l})$$

$$= (-0.00286) (20)$$

$$= -0.057$$

This compares with a test value of -0.07 from Reference 15.

## 9. Leading-Edge Slats

Given: The flapped airfoil of Reference 69.

$$\text{NACA 65A010 airfoil} \quad c_f/c = 0.17 \quad \delta_f = 25.6^\circ$$

$$\text{Low Speed} \quad R_x = 7.0 \times 10^6 \quad c'/c = 1.12$$

Compute:

$$c_{q_\delta} = -0.00350 \text{ per deg} \quad (\text{Figure 6.1.1.1-50})$$

$$\Delta c_q = c_{q_\delta} \delta_f \frac{c'}{c} \quad (\text{Equation 6.1.1.1-m})$$

$$= (-0.00350) (25.6) (1.12)$$

$$= -0.100$$

This compares with a test value of -0.19 from Reference 69.

## REFERENCES

1. Lopez, M.L., and Shen, C.C.: Recent Developments in Jet Flap Theory and Its Application to STOL Aerodynamic Analysis. AIAA Paper 71-578, 1971. (U)
2. Lopez, M.L., Shen, C.C., and Wasson, N.F.: A Theoretical Method for Calculating the Aerodynamic Characteristics of Arbitrary Jet-Flapped Wings. Douglas Aircraft Company, MDC J5519-01, 1972. (U)
3. Spence, D.A.: Lift Coefficient of a Thin Jet-Flapped Wing. Proc. Roy. Soc., Vol. A238, 1956. (U)
4. Spence, D.A.: The Lift on a Thin Aerofoil With a Jet Augmented Flap. Aero. Quart. Vol. 9, 1958. (U)
5. Dimmock, N.A.: Some Early Jet Flap Experiments. Aero. Quart. Vol. 8, 1957. (U)
6. Lissaman, P.B.S.: A Linear Theory for the Jet Flap in Ground Effect. AIAA Jour. Vol. 6, 1968. (U)
7. Fitzpatrick, J.E., and Woods, R.L.: Low-Speed Lateral-Control Characteristics of an Unswept Wing With Hexagonal Airfoil Sections and Aspect Ratio 2.5 Equipped With Spoilers and With Sharp- and Thickened-Trailing-Edge Flap-Type Ailerons at a Reynolds Number of  $7.6 \times 10^6$ . NACA RM L52B15, 1952. (U)
8. Lowry, J.G.: Data on Spoiler-Type Ailerons. NACA RM L53I24a, 1953. (U)
9. Newman, B.G.: The Reattachment of a Turbulent Boundary Layer Behind a Spoiler. Rept. A.64, Aero. Res. Lab. (Melbourne), October 1949. (U)
10. Anon.: Royal Aeronautical Society Data Sheets - Aerodynamics, Vol. IV. (Controls 01.01.03), 1956. (U)
11. Spearman, M.L.: Wind-Tunnel Investigation of an NACA 0009 Airfoil With 0.25- and 0.50-Airfoil-Chord Plain Flaps Tested Independently and in Combination. NACA TN 1517, 1948. (U)
12. Rogallo, F.M.: Collection of Balanced Aileron Test Data. NACA WR L-419, 1944. (U)
13. Sears, R.I.: Wind-Tunnel Data on the Aerodynamic Characteristics of Airplane Control Surfaces. NACA WR L-663, 1943. (U)
14. Rose, L.M., and Altman, J.M.: Low-Speed Experimental Investigation of a Thin Fairied, Double-Wedge Airfoil Section With Nose and Trailing-Edge Flaps. NACA TN 1934, 1949. (U)
15. Gambucci, B.J.: Section Characteristics of the NACA 0006 Airfoil With Leading-Edge and Trailing-Edge Flaps. NACA TN 3797, 1956. (U)
16. Abbott, I.H., von Doenhoff, A.E., and Stivers, L.S., Jr.: Summary of Airfoil Data. NACA TR 824, 1945. (U)
17. Ilk, R.J.: Characteristics of a 15-Percent-Chord and a 35-Percent-Chord Plain Flap on the NACA 0006 Airfoil Section at High Subsonic Speeds. NACA RM A7H19, 1947. (U)
18. Luoma, A.A.: An Investigation of the Section Characteristics of Plain Unsealed Ailerons on an NACA 66, 1-115 Airfoil Section in the Langley 8-Foot High-Speed Tunnel. NACA TN 1596, 1949. (U)
19. Spearman, L.M.: Wind-Tunnel Investigation of Control-Surface Characteristics. XXIII - A 0.25-Airfoil-Chord Flap With Tab Having a Chord Twice the Flap Chord on an NACA 0009 Airfoil. NACA WR L-47, 1945. (U)
20. Street, W.G., and Ames, M.B., Jr.: Pressure-Distribution Investigation of an N.A.C.A. 0009 Airfoil With a 50-Percent-Chord Plain Flap and Three Tabs. NACA TN 734, 1939. (U)
21. Ames, M.B., Jr. and Sears, R.I.: Pressure-Distribution Investigation of an N.A.C.A. 0009 Airfoil With a 30-Percent-Chord Plain Flap and Three Tabs. NACA TN 759, 1940. (U)

22. Ames, M.B., Jr., and Sears, R.I.: Determination of Control-Surface Characteristics From NACA Plain-Flap and Tab Data. NACA TR 721, 1941. (U)
23. Breslow, A.L.: Two-Dimensional Wind-Tunnel Investigation of Sealed 0.22-Airfoil-Chord Internally Balanced Ailerons of Different Contour on an NACA 65<sub>(112)</sub>-213 Airfoil. NACA TN 1099, 1946. (U)
24. Lockwood, V.E.: Wind-Tunnel Investigation of Control-Surface Characteristics. XVII Beveled-Trailing-Edge Flaps of 0.20, 0.30, and 0.40 Airfoil Chord on an NACA 0009 Airfoil. NACA WR L-666, 1944. (U)
25. Klein, M.M.: Pressure Distributions and Force Tests of an NACA 65-210 Airfoil Section With a 50-Percent-Chord Flap. NACA TN 1167, 1947. (U)
26. Abbott, I.H., and Greenburg, H.: Tests in the Variable-Density Wind Tunnel of the NACA 23012 Airfoil With Plain and Split Flaps. NACA TR 661, 1949. (U)
27. Ames, M.B., Jr.: Wind-Tunnel Investigation of Two Airfoils With 25-Percent-Chord Gwinn and Plain Flaps. NACA TN 763, 1940. (U)
28. Cahill, J.F., et al: Aerodynamic Forces and Loadings on Symmetrical Circular-Arc Airfoils with Plain Leading-Edge and Plain Trailing-Edge Flaps. NACA TR 1146, 1953. (U)
29. Harris, T.A., and Purser, P.E.: Wind-Tunnel Investigation of an NACA 23012 Airfoil With Two Sizes of Balanced Split Flap. NACA WR L-441, 1940. (U)
30. Underwood, W.J., and Abbott, F.T., Jr.: Test of NACA 66,2-116, a = 0.6 Airfoil Section Fitted With Pressure Balance and Slotted Flaps for the Wing of the XP-63 Airplane. NACA WR L-701, 1942. (U)
31. Holtzclaw, R.W.: Wind-Tunnel Investigation of the Effects of Spoilers on the Characteristics of a Low-Drag Airfoil Equipped With a 0.25-Chord Slotted Flap. NACA WR A-92, 1945. (U)
32. Holtzclaw, R.W., and Weisman, Y.: Wind-Tunnel Investigation of the Effects of Slot Shape and Flap Location on the Characteristics of a Low-Drag Airfoil Equipped With a 0.25-Chord Slotted Flap. NACA WR A-80, 1944. (U)
33. Swanson, R.S., and Schuldenfrei, M.J.: Wind-Tunnel Investigation of an NACA 23021 Airfoil With Two Sizes of Balanced Split Flaps. NACA WR L-449, 1941. (U)
34. Bogdonoff, S.M.: Tests of Two Models Representing Intermediate Inboard and Outboard Wing Sections of the XB-36 Airplane. NACA WR L-662, 1943. (U)
35. Abbott, I.H.: Tests of Four Models Representing Intermediate Sections of the XB-33 Airplane Including Sections With Slotted Flap and Ailerons. NACA WR L-704, 1942. (U)
36. Duschik, F.: Wind-Tunnel Investigation of an N.A.C.A. 23021 Airfoil With Two Arrangements of a 40-Percent-Chord Slotted Flap. NACA TN 728, 1939. (U)
37. Recant, I.G.: Wind-Tunnel Investigation of an N.A.C.A. 23030 Airfoil With Various Arrangements of Slotted Flaps. NACA TN 755, 1940. (U)
38. Harris, T.A.: Wind-Tunnel Investigation of an N.A.C.A. 23012 Airfoil With Two Arrangements of a Wide-Chord Slotted Flap. NACA TN 715, 1939. (U)
39. Lowry, J.G.: Wind-Tunnel Investigation of an NACA 23012 Airfoil With Several Arrangements of Slotted Flaps With Extended Lips. NACA TN 808, 1941. (U)
40. Racisz, S.F.: Investigation of NACA 65<sub>(112)</sub>A111 (Approx.) Airfoil With 0.35-Chord Slotted Flap at Reynolds Numbers Up to 25 Million. NACA TN 1463, 1947. (U)
41. Cahill, J.F.: Two-Dimensional Wind-Tunnel Investigation of Four Types of High-Lift Flap on an NACA 65-210 Airfoil Section. NACA TN 1191, 1947. (U)
42. Goodwin, M.D.: Single-Slotted Trailing-Edge Flap Combined With Plain or Slotted Leading-Edge Flap. WADC TR 6356, Part 3, 1953. (U)

43. Wenzinger, C.J., and Harris, T.A.: Wind-Tunnel Investigation of an N.A.C.A. 23021 Airfoil With Various Arrangements of Slotted Flaps. NACA TR 677, 1939. (U)
44. Jones, R., and Bell, A.H.: Further Experiments on an NACA 23021 Aerofoil With a 15-Percent Handley Page Slotted Flap in the Compressed Air Tunnel. ARC R&M 2519, 1954. (U)
45. Harris, T.A., and Lowry, J.G.: Pressure Distribution Over an NACA 23021 Airfoil With a Slotted and a Split Flap. NACA TR 718, 1941. (U)
46. Wenzinger, C.J., and Harris, T.A.: Wind-Tunnel Investigation of an N.A.C.A. 23012 Airfoil With Various Arrangements of Slotted Flaps. NACA TR 664, 1939. (U)
47. Wenzinger, C.J., and Gauvain, W.E.: Wind-Tunnel Investigation of an N.A.C.A. 23012 Airfoil With A Slotted Flap and Three Types of Auxiliary Flap. NACA TR 679, 1939. (U)
48. Wenzinger, C.J., and Delano, J.B.: Pressure Distribution Over an N.A.C.A. 23012 Airfoil With a Slotted and Plain Flap. NACA TR 633, 1938. (U)
49. Abbott, I.H., and Fullmer, F.F., Jr.: Wind-Tunnel Investigation of an NACA 63, 4-420 Section With 25-Percent-Chord Slotted Flap. NACA ACR 3121, 1943. (U)
50. Wenzinger, C.J., and Anderson, W.B.: Pressure Distribution Over Airfoils With Fowler Flaps. NACA TR 620, 1938. (U)
51. Anon: Royal Aeronautical Society Data Sheets - Aerodynamics. Vol. IV (Flaps 01.01.08), 1949. (U)
52. Anon: Royal Aeronautical Society Data Sheets - Aerodynamics. Vol. IV (Flaps 01.01.09), 1959. (U)
53. James, H. A., and Hunton, L. W.: Estimation of Incremental Pitching Moments Due to Trailing-Edge Flaps on Swept and Triangular Wings. NACA TN 4040, 1957. (U)
54. Roshko, A.: Computation of the Increment of Maximum Lift Due to Flaps, Douglas Aircraft Company Rept., SM 23626, 1959. (U)
55. Franks, R.W.: The Application of a Simplified Lifting-Surface Theory to the Prediction of the Rolling Effectiveness of Plain Spoiler Ailerons at Subsonic Speeds. NACA RM A54H26a, 1954. (U)
56. Stevenson, D.B., and Adler, A.A.: High-Speed Wind-Tunnel Tests of an NACA 0009-64 Airfoil Having a 33.4-Percent-Chord Flap With an Overhang 20.1 Percent of the Flap Chord. NACA TN 1417, 1947. (U)
57. Stevenson, D.B., and Byrne, R.W.: High-Speed Wind-Tunnel Tests of an NACA 16-009 Airfoil Having a 32.9-Percent-Chord Flap With an Overhang 20.7 Percent of the Flap Chord. NACA TN 1406, 1947. (U)
58. Lindsey, W.F.: Effect of Compressibility on the Pressures and Forces Acting on a Modified NACA 65,3-019 Airfoil Having a 0.20-Chord Flap. NACA WR L-76, 1946. (U)
59. Stivers, L.S., Jr.: The Effectiveness at High Speeds of a 20-Percent-Chord Plain Trailing-Edge Flap on the NACA 65-210 Airfoil Section. NACA RM A7A17, 1947. (U)
60. Underwood, W.J., Braslow, A.L., and Cahill, J.F.: Two-Dimensional Wind-Tunnel Investigation of 0.20-Airfoil-Chord Plane Ailerons of Different Contour on an NACA 65,-210 Airfoil Section. NACA WR L-151, 1945. (U)
61. Wenzinger, C.J.: Wind-Tunnel Investigation of Ordinary and Split Flaps on Airfoils of Different Profile. NACA TR 554, 1936. (U)
62. Purser, P.E., Fischel, J., and Riebe, J.M.: Wind-Tunnel Investigation of an NACA 23012 Airfoil With a 0.30-Airfoil-Chord Double Slotted Flap. NACA WR L-469, 1943. (U)
63. Fischel, J., and Riebe, J.M.: Wind-Tunnel Investigation of an NACA 23021 Airfoil With a 0.32-Airfoil-Chord Double Slotted Flap. NACA WR L-7, 1944. (U)
64. Cahill, J.F., and Racisz, S.F.: Wind-Tunnel Investigation of Seven Thin NACA Airfoil Sections to Determine Optimum Double Slotted Flap Configurations. NACA TN 1545, 1948. (U)
65. Quinn, J.H., Jr.: Tests of the NACA 64,1A212 Airfoil Section With a Slat, a Double Slotted Flap, and Boundary-Layer Control By Suction. NACA TN 1293, 1947. (U)
66. Bogdonoff, S.M.: Wind-Tunnel Investigation of a Low-Drag Airfoil Section With a Double Slotted Flap. NACA WR L-697, 1943. (U)

67. Quinn, J.H. Jr.: Wind-Tunnel Investigation of Boundary-Layer Control By Suction on the NACA 65<sub>3</sub>-418,  $a = 1.0$  Airfoil Section With a 0.29-Airfoil-Chord Double Slotted Flap. NACA TN 1071, 1948. (U)
68. Quinn, J.H., Jr.: Wind-Tunnel Investigation of the NACA 65<sub>4</sub>-421 Airfoil Section With a Double Slotted Flap and Boundary-Layer Control by Suction. NACA TN 1395, 1947. (U)
69. Kelly, J.A., and Hayter, N-L.F.: Lift and Pitching Moment at Low Speeds of the NACA 64A010 Airfoil Section Equipped With Various Combinations of a Leading-Edge Slat, Leading-Edge Flap, Split Flap, and Double Slotted Flap. NACA TN 3007, 1953. (U)
70. Ramsey, J.C., and Laudeman, E.C.: STOL Tactical Aircraft Investigation State-of-the-Art Design Compendium. Prepared under USAF Contract F33615-71-C-1754, 1971. (U)
71. Visconti, F.: Wind-Tunnel Investigation of Air Loads Over a Double Slotted Flap on the NACA 65(216)-215,  $a = 0.8$  Airfoil Section, NACA RM L7A30, 1947. (U)
72. Cahill, J.F.: Aerodynamic Data for a Wing Section of the Republic XF-12 Airplane Equipped With a Double Slotted Flap. NACA WR L-544, 1946. (U)
73. McKee, P.B., Jr.: Double Slotted Trailing-Edge Flap Combined With a Plain or Slotted Leading-Edge Flap. WADC TR 6356, Part 2, 1952. (U)
74. Fullmer, F.F.: Wind-Tunnel Investigation of NACA 66(215)-216, 66,1-212, and 65<sub>1</sub>-212 Airfoils With 0.20-Airfoil-Chord Split Flaps. NACA WR L-140, 1944. (U)
75. Wenzinger, C.J., and Harris, T.A.: Wind-Tunnel Investigation of N.A.C.A. 23012, 23021, and 23030 Airfoils With Various Sizes of Split Flap. NACA TR 668, 1939. (U)
76. McKee, P.B., Jr.: Plain and Slotted Leading-Edge Flaps With a Conventional Split Trailing-Edge Flap. WADC TR 6356, Part 1, 1951. (U)
77. Velasco, C.E.: High-Speed Wind-Tunnel Investigation of Spoilers for Lateral Control on the NACA 65,-210 Airfoil Section. NACA MR A5K02, 1945. (U)
78. Harris, T.A., and Recant, I.G.: Wind-Tunnel Investigation of NACA 23012, 23021 and 23030 Airfoils Equipped With 40-Percent-Chord Double-Slotted Flaps. NACA TR 723, 1941. (U)

TABLE 6.1.1.1-A  
PLAIN TRAILING-EDGE FLAP EFFECTIVENESS  
DATA SUMMARY AND SUBSTANTIATION

Ref.	Airfoil Section	M	$R_f \times 10^{-8}$	$c_f/c$	$\delta_f$ (deg)	K'	$\Delta c_f$ Calc	$\Delta c_f$ Test	* Percent Error
47	23012	.105	3.5	0.10	10	1.000	0.267	0.265	0.8
					20	.900	0.478	0.430	11.2
					30	.710	0.566	0.545	3.9
					40	.640	0.680	0.685	- 0.7
					50	.595	0.790	0.795	- 0.6
					60	.560	0.893	0.895	- 0.2
61	Clark Y	.105	0.61	0.10	10	1.000	0.18	0.22	-18.2
					30	.710	0.39	0.40	- 2.5
					45	.615	0.501	0.545	- 8.1
					60	.560	0.61	0.60	1.7
13	0009	.10	2.76	0.15	10	1.000	0.37	0.39	- 5.1
					20	.890	0.65	0.57	14.0
					30	.695	0.76	0.73	4.1
					40	.616	0.90	0.84	7.1
					50	.567	1.03	0.97	6.2
					60	.531	1.16	1.09	6.4
20	0009	.09	3.4	0.15	10	1.000	0.37	0.40	- 7.5
					20	.890	0.66	0.60	10.0
					30	.695	0.77	0.73	5.5
17	0006	.3	1.0	0.15	5.5	1.000	0.21	0.24	-12.5
					10.5	1.000	0.39	0.45	-13.3
30	66,2 - 116 $\epsilon = 0.6$	-	6.0	0.167	10	.887	0.66	0.62	6.5
					30	.685	0.762	0.845	- 9.8
					40	.610	0.905	1.045	-13.4
					50	.560	1.038	1.180	-12.0
13	0009	.10	2.76	0.20	10	1.000	0.43	0.42	2.4
					20	.880	0.76	0.74	2.7
					30	.670	0.87	0.86	2.4
					40	.592	1.02	0.99	3.0
					50	.540	1.19	1.15	3.5
					60	.501	1.30	1.24	4.8

TABLE 6.1.1.1-A (CONT'D)

Ref.	Airfoil Section	M	$R_f \times 10^{-6}$	$c_t/c$	$\delta_t$ (deg)	$k'$	$\Delta c_l$ Calc	$\Delta c_l$ Test	* Percent Error
48	23012	.106	3.5	0.20	15	.978	0.595	0.660	- 9.8
↓		↓	↓	↓	30	.670	0.815	0.860	- 5.2
46	23012	.106	3.5	0.20	10	1.000	0.407	0.355	14.6
↓		↓	↓	↓	20	.880	0.714	0.655	9.0
					30	.670	0.815	0.797	2.3
					45	.565	1.031	1.025	0.6
↓			↓	↓	60	.501	1.219	1.245	- 2.1
61	23012	.105	0.61	0.20	15	.978	0.43	0.50	-14.0
↓		↓	↓	↓	30	.670	0.58	0.67	-13.4
					45	.565	0.74	0.89	-16.9
↓			↓	↓	60	.501	0.87	1.02	-14.7
28	Circular Arc 0.06c	.15	6.0	0.20	20	.880	0.82	0.87	- 5.7
↓		↓	↓	↓	40	.592	1.10	1.07	2.8
					60	.501	1.40	1.39	0.7
↓			↓	↓	20	.880	0.67	0.69	- 2.9
					40	.592	0.90	1.07	-15.9
↓			↓	↓	60	.501	1.15	1.37	-16.1
60	65 <sub>1</sub> - 210	.07	1.0	0.20	5	1.000	0.24	0.28	-14.3
↓		↓	↓	↓	10	1.000	0.49	0.60	-18.3
					5	1.000	0.28	0.25	12.0
↓			↓	↓	10	1.000	0.55	0.48	14.6
					15	.978	0.81	0.67	20.9
↓			↓	↓	20	.880	0.97	0.81	19.8
16	63, 3 - 618	.2	6.0	0.20	10	1.000	0.45	0.45	0
↓		↓	↓	↓	20	.880	0.79	0.654	20.8
					30	.670	0.90	0.80	12.5
↓			↓	↓	40	.592	1.06	0.97	9.3
					50	.540	1.21	1.09	11.0
↓			↓	↓	60	.501	1.35	1.20	12.5

TABLE 6.1.1.1-A (CONT'D)

Ref.	Airfoil Section	M	$R_f \times 10^{-6}$	$c_f/c$	$\delta_t$ (deg)	$K'$	$\Delta c_f$ Calc	$\Delta c_f$ Test	% Percent Error
12	66 (215) - 216 $a = 1.0$	.2	6.0	0.20	10	1.000	0.40	0.43	- 7.0
					20	.880	0.71	0.70	1.4
16	66 (215) - 216	.2	6.0	0.20	10	1.000	0.40	0.44	- 9.1
					40	.592	0.95	1.10	-13.6
					50	.540	1.08	1.34	-19.4
					60	.501	1.21	1.50	-19.3
23	65 (112) - 213	.15	8.0	0.22	10	1.000	0.53	0.58	- 8.6
					15	.978	0.78	0.68	14.7
					20	.870	0.93	0.86	8.1
11	0009	.09	2.58	0.25	5	1.000	0.246	0.235	4.0
					10	1.000	0.493	0.473	4.2
					15	.978	0.720	0.680	5.9
					20	.840	0.825	0.800	3.1
					25	.701	0.860	0.835	3.0
					30	.640	0.943	0.850	10.9
27	23015	.105	0.61	0.25	10	1.000	0.29	0.287	1.0
					30	.640	0.56	0.530	5.7
					45	.540	0.703	0.725	- 3.0
					60	.480	0.833	0.933	-10.7
14	Double Wedge	.17	5.8	0.25	10	1.000	0.57	0.60	- 5.0
					20	.840	0.96	1.08	-11.1
					40	.569	1.30	1.30	0
					50	.518	1.48	1.50	- 1.3
					60	.480	1.65	1.65	0
13	0008	.10	2.76	0.30	10	1.000	0.55	0.59	- 6.8
					20	.800	0.88	0.87	1.1
					30	.607	1.00	0.96	4.2
15	0006	.15	4.5	0.30	20	.800	0.95	1.10	-13.6
					35	.607	1.26	1.32	- 4.5
					50	.495	1.47	1.62	- 9.3

TABLE 6.1.1.1-A (CONT'D)

Ref.	Airfoil Section	M	$R_A \times 10^{-8}$	$c_f/c$	$\delta_f$ (deg)	K'	$\Delta c_L$ Calc	$\Delta c_L$ Test	% Percent Error
21	0009	.09	3.4	0.30	10	1.000	0.56	0.55	1.8
					20	.800	0.89	0.80	11.3
					30	.607	1.02	0.90	13.3
					40	.540	1.21	1.07	13.1
					45	.515	1.15	1.28	-10.2
13	0015	.10	2.76	0.30	20	.800	0.75	0.78	-3.8
					30	.607	0.85	0.99	-14.1
61	Clark Y	.105	0.61	0.30	10	1.000	0.391	0.475	-17.7
					30	.607	0.712	0.755	-5.7
					45	.540	0.951	0.935	1.7
					60	.460	1.080	1.040	3.8
13	66-009	.105	1.43	0.30	10	1.000	0.56	0.57	-1.8
					20	.800	0.90	0.80	12.5
					30	.607	1.03	0.90	14.4
57	16-009	.4	1.1	0.329	10.3	1.000	0.43	0.47	-8.5
56	0009-64	.4	1.1	0.334	5.9	1.000	0.288	0.332	-13.3
					7.9	1.000	0.386	0.415	-7.0
					9.9	1.000	0.483	0.495	-2.4
17	0006	.3	1.0	0.35	4.9	1.000	0.30	0.34	-11.8
					10.2	1.000	0.62	0.68	-8.8
11	0009	.09	2.58	0.50	5	1.000	0.37	0.36	2.8
					10	.998	0.74	0.71	4.2
					15	.910	1.01	0.99	2.0
					20	.685	1.01	1.02	-1.0
					25	.590	1.09	1.05	3.8
					30	.542	1.20	1.14	5.3
20	0009	.09	3.4	0.50	10	.998	0.75	0.80	-6.3
					20	.685	1.03	1.02	1.0
					30	.542	1.22	1.25	-2.4
					40	.485	1.46	1.52	-3.9
					45	.466	1.58	1.65	-4.2
25	65-210	< .15	6.0	0.50	4	1.000	0.33	0.31	6.5
					7	1.000	0.57	0.65	-12.3
					10	1.000	0.82	0.85	-3.5
Average Error = $\frac{\sum  e }{n} = 7.75\%$									

**TABLE 6.1.1.1-B.**  
**SINGLE-SLOTTED TRAILING-EDGE FLAP EFFECTIVENESS**  
**DATA SUMMARY AND SUBSTANTIATION**

Ref.	Airfoil Section	Config. (1)	M	$\beta$	$R_f \times 10^{-6}$	$c_f/c$	$\delta_f$ (deg)	$\frac{c_f}{c} \alpha$ (per deg)	$-\alpha \delta$	$\Delta c_f$ Calc	$\Delta c_f$ Test	% Percent Error
29	23012	2a*	0.105	0.995	3.5	0.15	30	0.104	.322	1.00	1.00	0
33	23021	2a*	0.105	0.995	3.5	0.15	60	0.097	.150	0.87	1.20	-27.5
44	23021	2b	LS	1.0	7.1	0.15	60	0.097	.150	0.87	0.83	4.8
34	63(420) - 222 $s = 0.1$	1b	LS	1.0	9.0	0.243	30	0.118	.445	1.58	1.41	12.1
							40		.385	1.82	1.58	15.2
							45		.345	1.83	1.46	25.3
							20		.480	1.13	1.12	1.0
							30		.445	1.58	1.40	12.9
41	65-210	2c	LS	1.0	6.0	0.25	30	0.109	.453	1.48	1.46	1.4
							40		.397	1.73	1.78	-2.8
							45		.356	1.75	1.87	-6.4
							50		.300	1.62	1.73	-6.4
							30		.453	1.48	1.54	-3.9
							36.3		.421	1.67	1.72	-2.9
							41.3		.388	1.75	1.82	-3.8
							46.5		.340	1.72	1.73	-0.6
							30		.453	1.48	1.41	5.0
							35		.428	1.63	1.54	5.8
							40		.397	1.73	1.81	-4.4
29	23012	2a*	0.105	0.995	3.5	0.25	40	0.104	.397	1.65	1.76	-6.3
31	66.2 - 216 $s = 0.6$	1c	0.19	0.982	5.1	0.25	10	0.105	.509	0.53	0.47	12.8
							20		.490	1.03	0.995	3.5
							30		.453	1.43	1.33	7.5
							40		.397	1.67	1.56	7.1
							45		.356	1.68	1.63	3.1
32	66.2 - 216 $s = 0.6$	2c	0.19	0.982	5.1	0.25	10	0.105	.509	0.53	0.48	10.4
							20		.490	1.03	1.00	3.0
							30		.453	1.43	1.335	7.1
							40		.397	1.67	1.565	6.7
							45		.356	1.68	1.63	3.1
							10		.509	0.534	0.495	7.9
							20		.490	1.03	1.01	2.0
							30		.453	1.43	1.53	-6.5
							40		.397	1.67	1.70	-1.8
							45		.366	1.68	1.61	4.3

TABLE 6.1.1.1-B. (CONT'D)

Ref.	Airfoil Section	Config. <sup>(1)</sup>	M	$\beta$	$R_L \times 10^{-6}$	$c_f/c$	$\delta_f$ (deg)	$\frac{c_L}{c} \alpha$ (per deg)	$-\alpha \delta$	$\Delta c_L$ Calc	$\Delta c_L$ Test	$\epsilon$ Percent Error
30	66, 2 - 116 $s = 0.6$	1b	LS	1.0	6.0	0.25	15	0.110	.500	0.83	0.70	18.6
↓	↓	↓	↓	↓	↓	↓	45	↓	.356	1.76	1.80	- 2.3
33	23021	2a*	0.105	0.995	3.5	0.25	40	0.097	.397	1.54	1.76	-12.5
42	Mod. Double Wedge	1b	0.25	0.97	6.9	0.263	40	0.101	.398	1.61	1.60	0.6
35	65, 2-222 $s = 0.1$	1a	LS	1.0	6.0	0.256	20	0.120	.495	1.19	1.06	12.3
↓	↓	↓	↓	↓	↓	↓	30	↓	.460	1.66	1.50	10.7
47	23012	1b	0.105	0.995	3.5	0.257	10	0.104	.515	0.54	0.48	12.5
↓	↓	↓	↓	↓	↓	↓	20	↓	.495	1.03	1.00	3.0
43	23021	2b	0.105	0.995	3.5	0.257	10	0.097	.515	0.50	0.49	2.0
↓	↓	↓	↓	↓	↓	↓	20	↓	.495	0.96	1.05	- 8.6
↓	↓	↓	↓	↓	↓	↓	30	↓	.460	1.34	1.30	3.1
↓	↓	↓	↓	↓	↓	↓	40	↓	.400	1.55	1.52	2.0
↓	↓	↓	↓	↓	↓	↓	50	↓	.305	1.48	1.60	- 7.5
↓	↓	↓	↓	↓	↓	↓	60	↓	.220	1.28	1.71	-25.1
↓	↓	↓	↓	↓	↓	↓	1b	↓	.495	0.96	0.98	- 2.0
↓	↓	↓	↓	↓	↓	↓	20	↓	.460	1.34	1.23	8.9
↓	↓	↓	↓	↓	↓	↓	30	↓	.400	1.55	1.17	32.5
↓	↓	↓	↓	↓	↓	↓	40	↓	.305	1.48	1.37	8.0
↓	↓	↓	↓	↓	↓	↓	50	↓	.220	1.28	1.46	-12.3
37	23030	1b	0.105	0.995	3.5	0.257	10	0.080	.515	0.41	0.41	0
↓	↓	↓	↓	↓	↓	↓	20	↓	.495	0.79	0.90	-12.2
↓	↓	↓	↓	↓	↓	↓	30	↓	.460	1.10	1.15	- 4.3
↓	↓	↓	↓	↓	↓	↓	40	↓	.400	1.28	1.18	8.5
↓	↓	↓	↓	↓	↓	↓	50	↓	.305	1.22	1.20	1.7
↓	↓	↓	↓	↓	↓	↓	60	↓	.220	1.06	1.40	-24.3
46	23012	2a*	0.105	0.995	3.5	0.267	30	0.104	.469	1.46	1.71	-14.6
↓	↓	2b	↓	↓	↓	↓	50	↓	.313	1.63	1.53	6.5
39	23012	1b*	0.105	0.995	3.5	0.30	40	0.104	.440	1.83	1.84	- 0.5
↓	↓	1a	↓	↓	↓	↓	10	↓	.550	0.57	0.57	0
↓	↓	↓	↓	↓	↓	↓	20	↓	.531	1.10	1.02	7.8
↓	↓	↓	↓	↓	↓	↓	30	↓	.496	1.55	1.48	4.7
↓	↓	↓	↓	↓	↓	↓	40	↓	.440	1.83	1.82	0.5
↓	↓	↓	↓	↓	↓	↓	50	↓	.338	1.76	1.96	-10.2

TABLE 6.1.1.1-B. (CONTD)

Ref.	Airfoil Section	Config. <sup>(1)</sup>	M	$\beta$	$R_f \times 10^{-6}$	$c_f/c$	$\delta_f$ (deg)	$\frac{c_f}{c} \alpha$ (per deg)	$-\alpha \delta$	$\Delta c_1$ Calc	$\Delta c_2$ Test	e Percent Error
39	23012	1b	0.105	0.995	3.5	0.30	10	0.104	.550	0.57	0.54	5.6
							20		.531	1.10	1.16	- 5.2
							30		.496	1.55	1.58	- 1.9
							40		.440	1.83	1.58	15.8
40	65(112) A111	2c	0.20	0.98	9.0	0.35	35	0.105	.499	1.83	1.95	- 6.2
							40		.466	1.96	1.85	5.9
							45		.425	2.01	2.13	- 5.6
38	23012	1b	0.105	0.995	3.5	0.40	10	0.104	.597	0.62	0.63	- 1.6
							20		.583	1.21	1.32	- 8.3
							30		.550	1.72	1.91	- 9.9
							40		.492	2.05	1.76	16.5
							50		.398	2.07	2.09	- 1.0
		1a					10		.597	0.62	0.48	29.2
							20		.583	1.21	1.24	- 2.4
							30		.560	1.72	1.78	- 3.4
							40		.492	2.05	1.73	18.5
							50		.398	2.07	2.06	0.5
36	23021	1b	0.105	0.995	3.5	0.40	10	0.100	.597	0.60	0.65	- 7.7
							20		.583	1.17	1.17	0
							30		.550	1.65	1.53	7.8
							40		.492	1.97	1.53	28.8
							50		.398	1.99	1.73	15.0
37	23030	1b	0.105	0.995	3.5	0.40	10	0.080	.597	0.48	0.52	- 7.7
							20		.583	0.93	1.07	-13.1
							30		.550	1.32	1.36	- 2.2
							40		.492	1.57	1.40	12.1
							50		.398	1.59	1.66	- 4.2

<sup>\*</sup>Fowler flap

(1) Slot-flap configuration (see sketch below)

$$\text{Average Error} = \frac{\sum |e|}{n} = 7.9\%$$

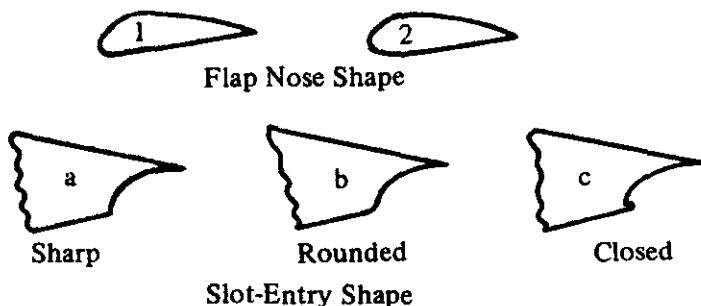


TABLE 6.1.1.1-C  
SINGLE-SLOTTED TRAILING-EDGE FLAP EFFECTIVENESS  
DATA SUMMARY AND SUBSTANTIATION  
(See TABLE 6.1.1.1-B for slot-flap configuration)

Ref.	Airfoil Section	M	$R_q \times 10^{-6}$	$c_t/c$	$\delta_f$ (deg)	$\frac{c_1}{c}$	$\Phi$ (deg)	$c_{q\delta}$ (per deg)	$\eta_1$	$\Delta c_{q\delta}^{calc}$	$\Delta c_{q\delta}^{test}$	e Percent Error
29	23012	0.105	3.5	0.15	30	1.149	38.80	0.0528	0.615	1.12	1.00	12.0
33	23021	0.105	3.5	0.15	60	1.157	74.25	0.0528	0.350	1.28	1.20	6.7
44	23021	LS	7.1	0.15	60	1.03	73.9	0.0528	0.35	1.14	0.83	37.3
34	63(420)-422 $a = 0.1$	LS	9.0	0.243	30	1.07	42.1	0.066	0.62	1.32	1.41	-6.4
					40		52.1		0.52	1.48	1.58	-6.3
					45		57.1		0.46	1.47	1.46	0.7
					20		32.1		0.697	0.99	1.12	-11.6
					30		42.1		0.62	1.32	1.40	-5.7
41	65-210	LS	6.0	0.25	29.1	1.075	37.6	0.0668	0.66	1.38	1.45	-4.8
					39.1	1.078	47.6		0.57	1.61	1.78	-9.4
					44.1	1.076	52.56		0.51	1.63	1.86	-12.4
					49.1	1.076	57.56		0.455	1.61	1.72	-6.4
					28.2	1.144	37.0		0.66	1.42	1.52	-6.6
					34.5	1.141	43.3		0.61	1.60	1.71	-6.4
					39.5	1.135	48.3		0.56	1.68	1.80	-6.7
					44.7	1.146	53.5		0.50	1.70	1.73	-1.7
					2.4		27.5		0.69	1.57	1.40	12.1
							32.5		0.65	1.76	1.53	15.0
							37.5		0.61	1.89	1.80	5.0
29	23012	0.105	3.5	0.25	40	1.25	48.8	0.0668	0.56	1.87	1.98	-5.5
31	66.2-216 $a = 0.6$	0.19	5.1	0.25	10	1.029	21	0.0668	0.73	0.50	0.47	6.4
					20	1.043	31		0.70	0.976	0.995	-1.9
					30	1.058	41		0.633	1.34	1.33	0.8
					40	1.068	51		0.53	1.51	1.56	-3.2
					45	1.073	56		0.47	1.52	1.63	-6.7
32	66.2-216 $a = 0.6$	0.19	5.1	0.25	10	1.029	21	0.0668	0.73	0.50	0.48	4.2
					20	1.043	31		0.73	0.976	1.00	-2.4
					30	1.058	41		0.633	1.34	1.335	0.4
					40	1.068	51		0.53	1.51	1.565	-3.5
					45	1.073	56		0.47	1.52	1.63	-6.7
					10	1.014	21		0.73	0.495	0.495	0
					20	1.029	31		0.70	0.96	1.01	-5.0
					30	1.043	41		0.633	1.32	1.53	-13.7
					40	1.058	51		0.53	1.50	1.70	-11.8
					45	1.066	56		0.47	1.51	1.61	-6.2
30	66.2-116 $a = 0.6$	LS	6.0	0.25	15	1.023	26.3	0.0668	0.718	0.74	0.70	5.7
					45	1.066	56.3		0.467	1.50	1.80	-16.7
33	23021	0.105	3.5	0.25	40	1.255	54.25	0.0668	0.49	1.64	1.76	-6.8
42	Mod. Double Wedge	0.25	6.9	0.253	40	1.006	46.42	0.0672	0.58	1.57	1.60	-1.9
35	66.2-222 $a = 0.1$	LS	6.0	0.256	20	1.058	31.3	0.0675	0.70	1.00	1.06	-5.7
					30		41.3		0.63	1.35	1.50	-10.0
					40		51.3		0.53	1.51	1.52	-0.7
47	23012	0.105	3.5	0.257	10	1.03	18.8	0.0676	0.73	0.51	0.48	6.3
					20	1.05	28.8		0.71	1.01	1.00	1.0
					30	1.06	38.8		0.65	1.40	1.48	-5.4
					40	1.0705	48.8		0.56	1.62	1.64	-1.2
					50	1.08	58.8		0.445	1.62	1.59	1.9

TABLE 6.1.1.1-C (CONT'D)

Ref.	Airfoil Section	M	$R_q \times 10^{-6}$	$c_f/c$	$\delta_f$ (deg)	$\frac{c_1}{c}$	$\Phi$ (deg)	$c_{\theta_f}$ (per deg)	$\eta_1$	$\Delta c_d$ calc	$\Delta c_d$ test	e Percent Error
43	23021	0.105	3.5	0.257	10	1.035	24.25	0.0676	0.72	0.50	0.49	2.0
					20	1.035	34.25		0.685	0.96	1.05	-8.6
					30	1.07	44.25		0.603	1.31	1.30	-0.8
					40	1.07	54.25		0.49	1.42	1.52	-6.6
					50	1.07	64.25		0.405	1.46	1.60	-8.8
					60	1.06	74.25		0.36	1.55	1.77	-12.4
					20	1.037	34.25		0.685	0.96	0.98	-2.0
					30	1.05	44.25		0.603	1.28	1.23	4.1
					40	1.063	54.25		0.49	1.41	1.17	20.5
					50	1.054	64.25		0.405	1.44	1.37	5.1
37	23030	0.105	3.5	0.257	60	1.065	74.25		0.36	1.55	1.46	6.2
					20	1.02	29.57	0.0676	0.706	0.49	0.41	19.5
					20	1.072	39.57		0.644	0.93	0.90	3.3
					30	1.08	49.57		0.550	1.20	1.15	4.3
					40	1.103	59.57		0.438	1.31	1.18	11.0
					50	1.122	69.57		0.403	1.53	1.20	27.5
46	23012	0.105	3.5	0.267	60	1.118	79.57		0.35	1.59	1.40	13.6
					30	1.26	38.8	0.069	0.65	1.69	1.86	-9.1
					40	1.31	48.8	0.0725	0.57	1.95	2.17	-10.1
					10	1.20	18.8		0.743	0.65	0.78	-16.7
					20		28.8		0.72	1.25	1.22	2.5
					30		38.8		0.664	1.73	1.67	3.6
					40		48.8		0.57	1.98	2.01	-1.5
					50		58.8		0.458	1.99	2.16	-7.9
					10	1.20	18.8	0.0725	0.743	0.65	0.73	-11.0
					20		28.8		0.72	1.25	1.38	-9.4
40	65(112)A111	0.20	2.4	0.35	30	1.186	43.13	0.0775	0.64	2.06	1.95	5.6
					40	1.2	48.15		0.49	1.83	1.85	-1.1
					45	1.2	53.15		0.525	2.20	2.13	3.3
					10	1.065	18.8	0.082	0.77	0.67	0.63	6.3
					20	1.088	28.8		0.75	1.34	1.32	1.5
					30	1.103	38.8		0.69	1.87	1.91	2.1
38	23012	0.105	3.5	0.40	40	1.093	48.8		0.59	2.12	1.76	20.5
					50	1.09	58.8		0.48	2.15	2.09	2.9
					10	1.082	18.8		0.77	0.68	0.57	19.3
					20	1.10	28.8		0.75	1.35	1.24	8.9
					30	1.102	38.8		0.69	1.87	1.78	5.1
					40	1.11	48.8		0.59	2.15	1.73	24.3
					50	1.09	58.8		0.48	2.15	2.06	4.4
					10	1.032	24.25	0.082	0.761	0.64	0.65	-1.5
					20	1.075	34.25		0.724	1.28	1.17	9.4
					30	1.085	44.25		0.639	1.71	1.53	11.8
36	23021	0.105	3.5	0.40	40	1.095	54.25		0.53	1.90	1.53	24.2
					50	1.09	58.8		0.435	1.95	1.73	12.7
					10	1.04	29.57	0.082	0.745	0.64	0.52	23.0
					20	1.08	39.57		0.684	1.21	1.07	13.1
					30	1.10	49.57		0.583	1.58	1.35	17.0
					40	1.15	59.57		0.475	1.79	1.40	27.9
37	23030	0.105	3.5	0.40	50	1.16	69.57		0.402	1.91	1.66	15.1

$$\text{Average Error} = \frac{\sum |e|}{n} = 8.3\%$$

TABLE 6.1.1.1-D  
DOUBLE-SLOTTED TRAILING-EDGE FLAP EFFECTIVENESS  
DATA SUMMARY AND SUBSTANTIATION

Ref.	Airfoil Section	M	$\phi_{TE\text{UPPER}}$ (deg)	$\frac{c'}{c}$	$\frac{c_1}{c}$	$\frac{c_2}{c}$	$\delta f_1$ (deg)	$\delta f_2$ (deg)	$\Delta c_L \text{ calc}$	$\Delta c_L \text{ test}$	e Percent Error
73	Wedge	0.25	7.2	1.085	0.04	0.25	20	30	2.04	1.96	4.1
64	64-208	0.18	6.1	1.127	0.056	0.25	25	25	2.33	2.17	7.4
41	65-210	—	7.6	1.139	0.075	0.25	15	25	2.14	1.99	7.5
				1.146			20		2.29	2.14	7.0
				1.143			25		2.40	2.26	6.2
				1.148			30		2.51	2.30	9.1
				1.133	↓	↓	35	↓	2.57	2.23	15.2
64	1410	0.18	8.0	1.141	0.075	0.25	25	25	2.36	2.49	-5.2
	63-210		6.4	1.133	0.075	0.25			2.44	2.51	-2.8
	65-210		7.6	1.143	0.075	0.25			2.36	2.23	5.8
	66-210		8.9	1.144	0.075	0.25		30	2.36	2.36	0
	64-208		6.1	1.148	0.075	0.25	30	15	2.62	2.364	10.8
	64-212		7.4	1.152	0.075	0.25		20	2.51	2.52	-0.4
	64-210		6.8	1.139	0.075	0.25		25	2.53	2.61	-3.1
69	64A010	0.06	5.9	1.133	0.075	0.25	30	22.7	2.54	2.34	8.6
		0.20	5.9	↓	↓	↓	↓	↓	2.54	2.26	12.4
65	64-A212	—	9.8	1.106	0.083	0.229	26	29	2.24	2.55	-12.0
71	65(216)-215 a = 0.8	0.12	8.0	1.114	0.096	0.248	10	15	1.59	1.61	-1.2
				1.118				20	1.76	1.85	-4.9
				1.121				25	1.92	1.98	-3.0
				1.125				30	2.00	2.165	-7.6
				1.133				40	2.01	2.37	-15.2
				1.137				45	2.04	2.50	-18.4
				1.151	↓	↓	↓	60	2.29	2.55	-10.2
72	R-440-318-1	—	16.5	1.137	0.092	0.238	5	35	1.52	1.74	-12.6
	R-440-413-6			1.155			20	20	1.96	1.68	16.7
				1.216			25	35	2.33	2.50	-6.8
				1.180	↓	↓	↓	40	2.32	2.63	-11.8
64	66-210	0.18	8.9	1.172	0.10	0.25	25	35	2.54	2.28	11.4
66	65 <sub>3</sub> 118	0.105	9.0	1.175	0.10	0.245	23	42	2.51	2.83	-11.3
67	65 <sub>3</sub> 418	—	13.2	1.163	0.106	0.236	21	44	2.37	2.62	-9.6
62	23012	0.105	8.8	1.221	0.1165	0.2566	25	35	2.69	2.53	6.5
68	65 <sub>4</sub> 421	—	14.1	1.166	0.109	0.235	20	31	2.17	2.23	-2.7
63	23021	0.105	14.3	1.229	0.147	0.2566	30	40	3.07	2.78	10.5
$\text{Average Error} = \frac{\sum  e }{n} = 8.2\%$											

TABLE 6.1.1.1-E  
SPLIT TRAILING-EDGE FLAP EFFECTIVENESS  
DATA SUMMARY AND SUBSTANTIATION

Ref	Airfoil Section	M	$R_g \times 10^{-6}$	$c_f/c$	$\delta_f$	$\Delta c_Q$ Calc	$\Delta c_Q$ Test	e Percent Error
75	23012	0.105	3.5	0.10	15	0.38	0.37	2.7
	23021				30	0.62	0.64	-3.1
					45	0.835	0.82	1.8
					60	0.985	0.94	4.8
					75	1.05	1.02	2.9
					15	0.35	0.32	9.4
					30	0.57	0.63	-9.5
					45	0.765	0.88	-13.1
					60	0.90	1.05	-14.3
					75	0.96	1.15	-16.5
69	64A010	0.06 0.12 0.17 0.20	2 4 6 7	0.20	66	1.31	1.35	-3.0
						1.43	1.36	5.1
						1.43	1.36	5.1
						1.43	1.36	5.1
26	23012	—	8		5	0.23	0.17	37.5
					10	0.39	0.32	21.9
					15	0.51	0.45	13.3
					20	0.615	0.58	6.0
					30	0.83	0.84	-1.2
					45	1.12	1.09	2.8
46		0.105	3.5		60	1.34	1.34	0
74	66,1-212	~0.15	6		75	1.51	1.41	7.1
					40	0.99	1.09	-9.2
					50	1.16	1.25	-7.2
					60	1.29	1.37	-5.8
					70	1.41	1.42	-0.7
					40	1.05	1.06	-0.9
					50	1.23	1.205	2.1
					60	1.37	1.36	0.7
					70	1.50	1.36	10.3
					40	1.11	1.17	-5.1
					50	1.29	1.37	-5.8
					60	1.44	1.44	0
					70	1.58	1.54	2.6
45	23021	0.085	3.56		15	0.47	0.51	-7.8
					30	0.76	0.95	-20.0
					45	1.03	1.27	-18.9
					60	1.23	1.52	-19.1
					75	1.38	1.65	-16.4
75	23012	0.105	3.5	0.30	15	0.665	0.63	5.6
	23021				30	1.05	1.06	-0.9
					45	1.41	1.37	2.9
					60	1.72	1.55	11.0
					75	1.99	1.64	21.3
					15	0.61	0.67	-9.0
					30	0.96	1.20	-20.0
					45	1.29	1.59	-18.9
					60	1.57	1.84	-14.7
					75	1.82	1.96	-7.1
					15	0.77	0.70	10.0
					30	1.21	1.22	-0.8
					45	1.59	1.55	2.6
					60	1.93	1.71	12.9
					15	0.70	0.80	-12.5
					30	1.11	1.42	-21.8
					45	1.46	1.86	-21.5
					60	1.76	2.12	-17.0
$\text{Average Error} = \frac{\sum  e }{n} = 9.3\%$								

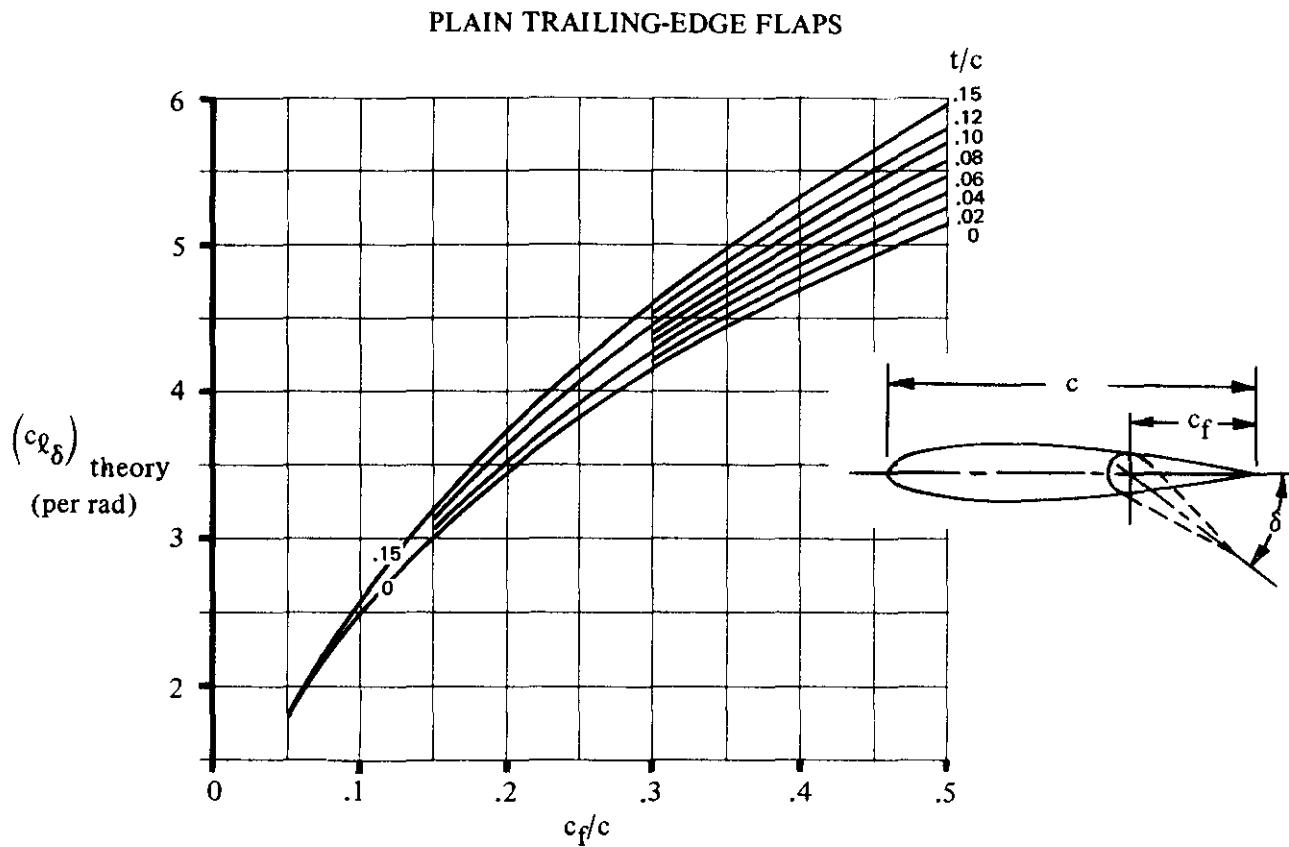


FIGURE 6.1.1.1-39a THEORETICAL LIFT EFFECTIVENESS OF PLAIN TRAILING-EDGE FLAPS

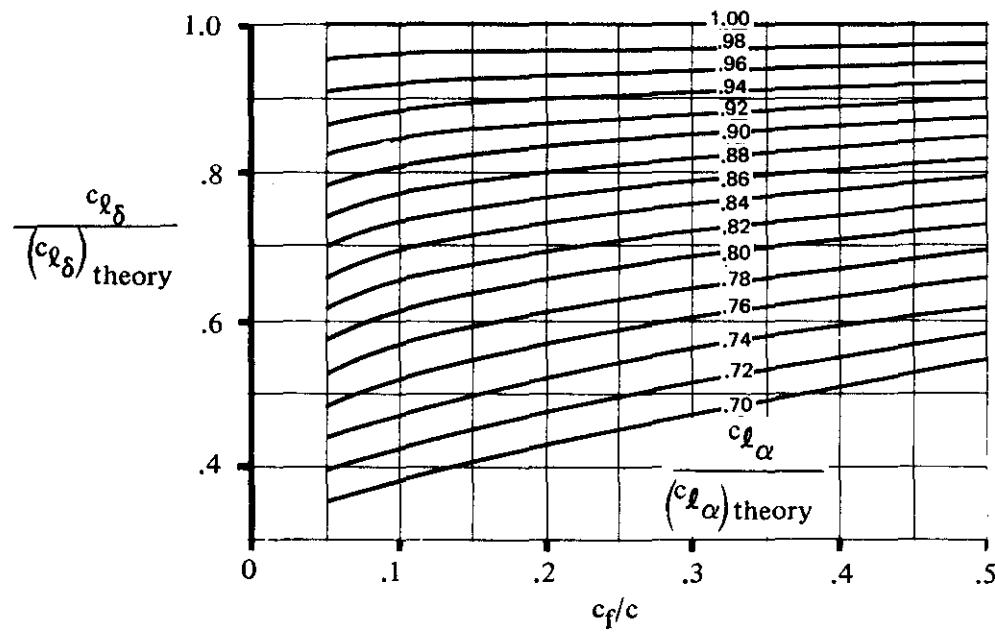


FIGURE 6.1.1.1-39b EMPIRICAL CORRECTION FOR LIFT EFFECTIVENESS OF PLAIN TRAILING-EDGE FLAPS

PLAIN TRAILING-EDGE FLAPS

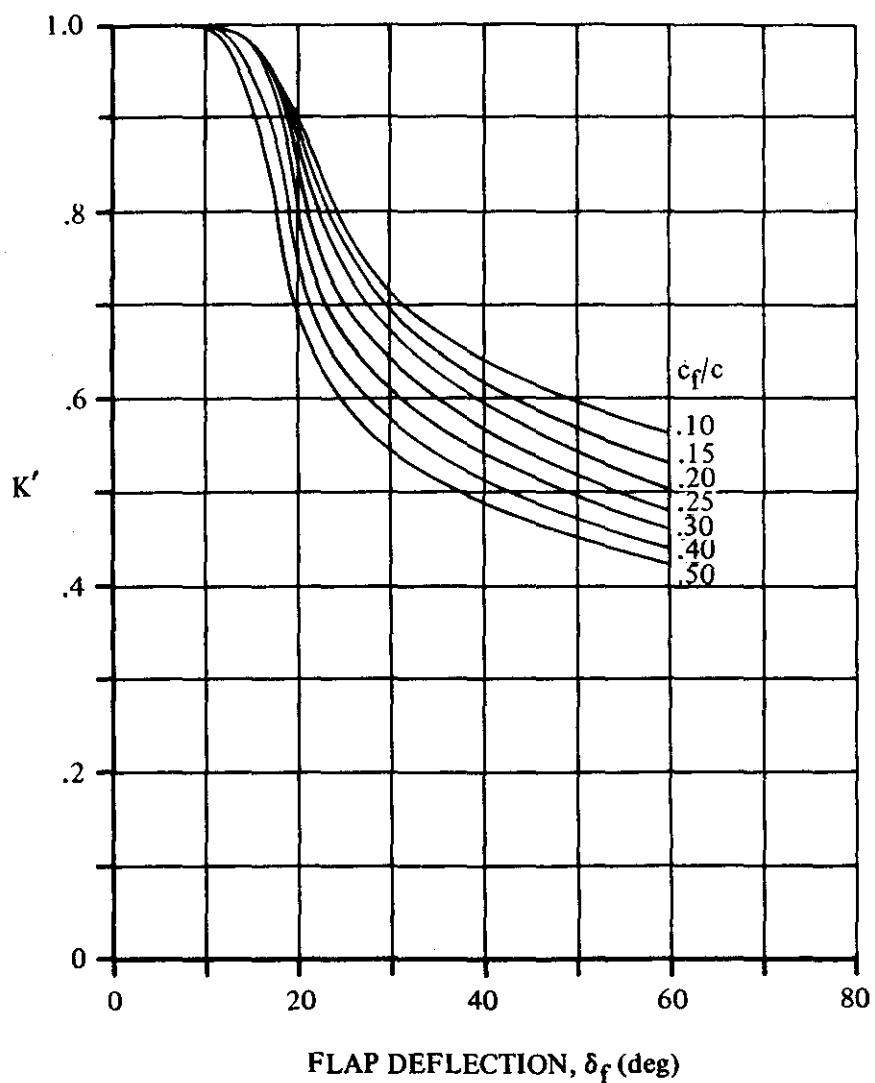


FIGURE 6.1.1.1-40 EMPIRICAL CORRECTION FOR LIFT EFFECTIVENESS OF PLAIN TRAILING-EDGE FLAPS AT HIGH FLAP DEFLECTIONS

### SINGLE-SLOTTED FLAPS

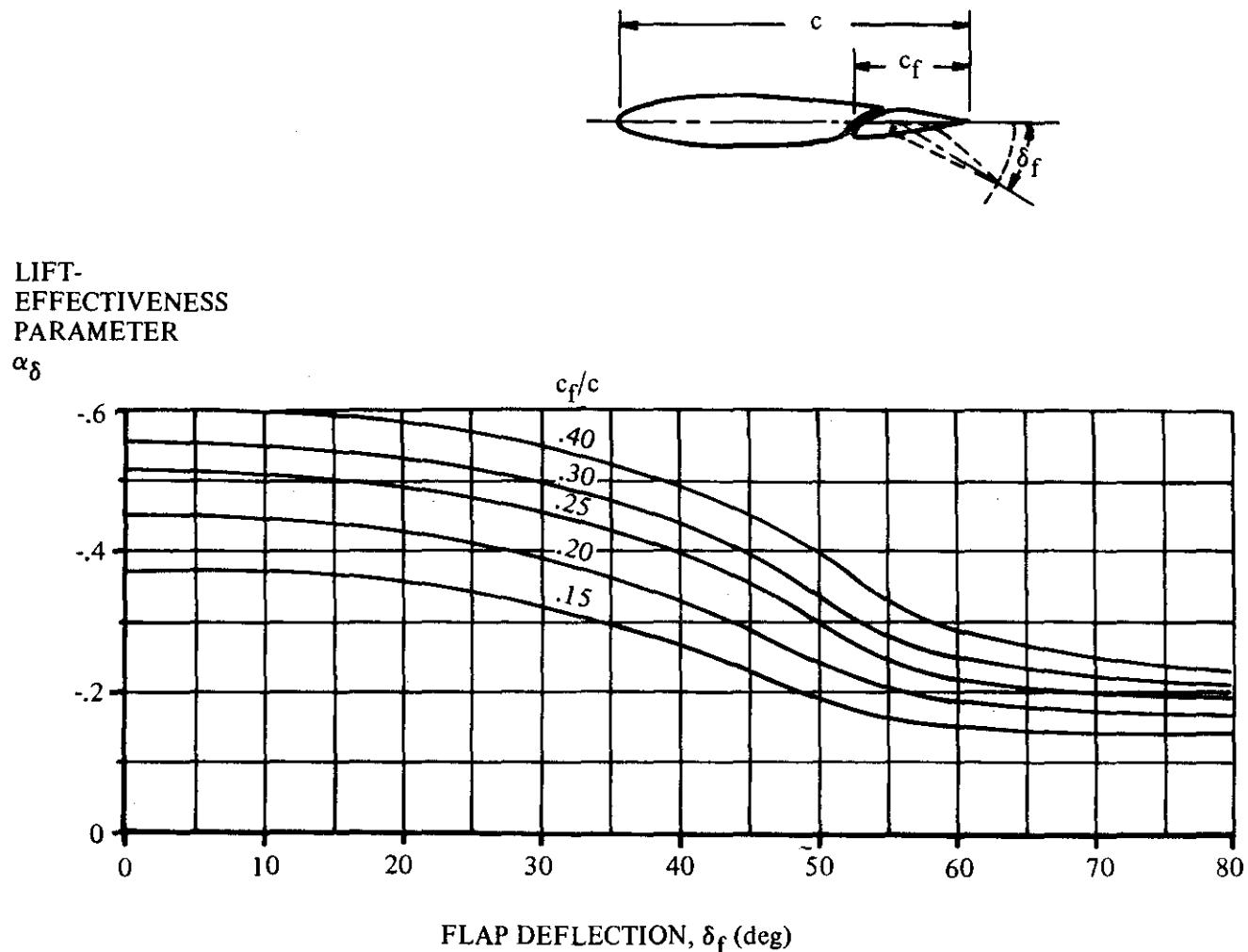
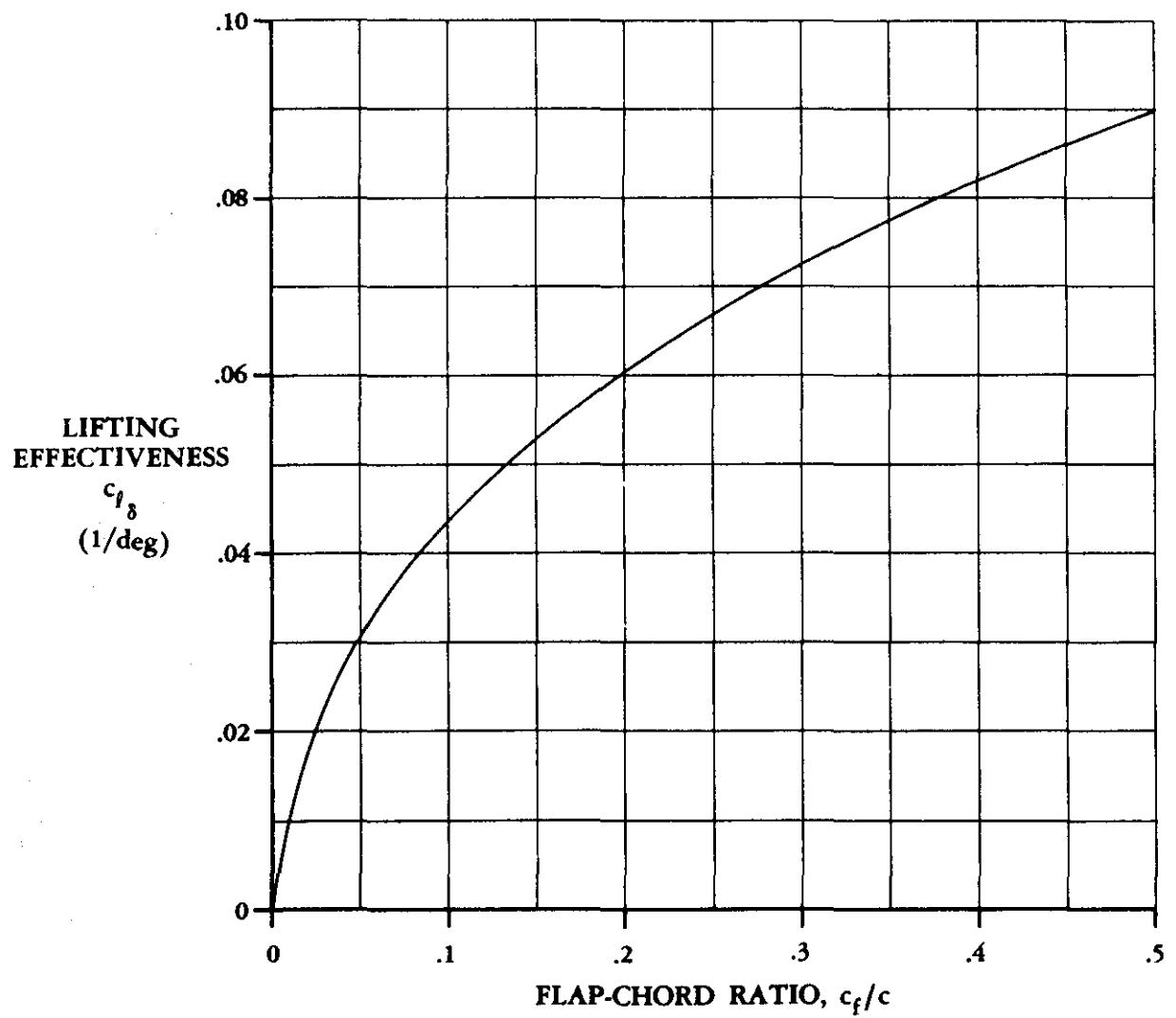


FIGURE 6.1.1.1-41 SECTION LIFT-EFFECTIVENESS PARAMETER OF SINGLE-SLOTTED FLAPS



Note: The  $c_f/c$  values needed for using this figure are defined under "Datcom Methods," based on the geometric parameters shown in Figures 6.1.1.1-44 through -46.

**FIGURE 6.1.1.1-42 THEORETICAL LIFTING EFFECTIVENESS OF TRAILING-EDGE FLAPS**

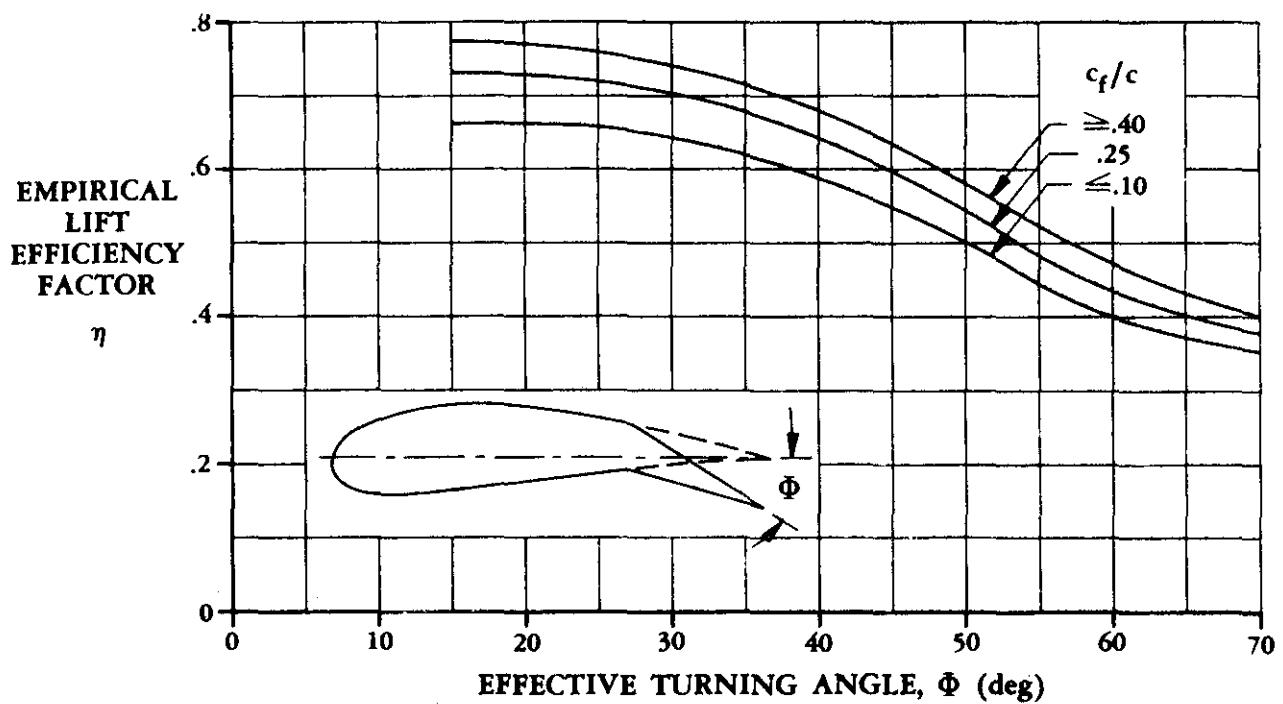


FIGURE 6.1.1.1-43a EMPIRICAL LIFTING-EFFICIENCY FACTORS FOR SLOTTED FLAPS

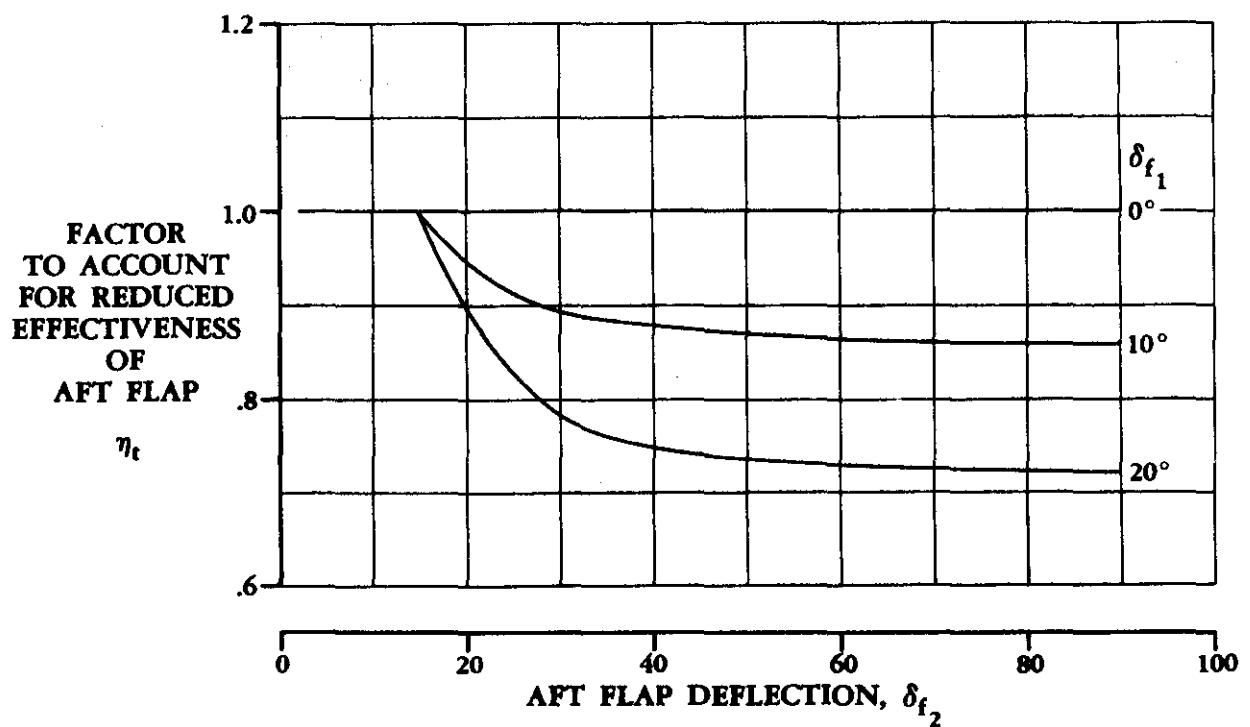
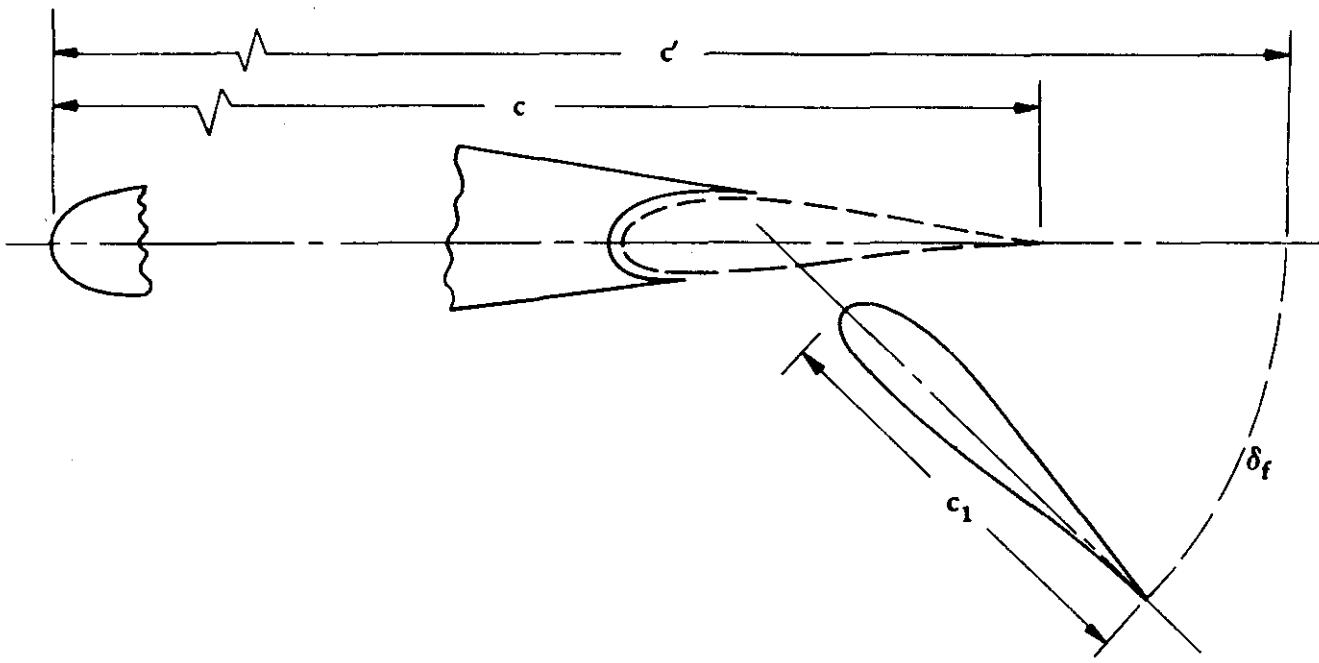


FIGURE 6.1.1.1-43b TURNING EFFICIENCY OF AFT FLAPS



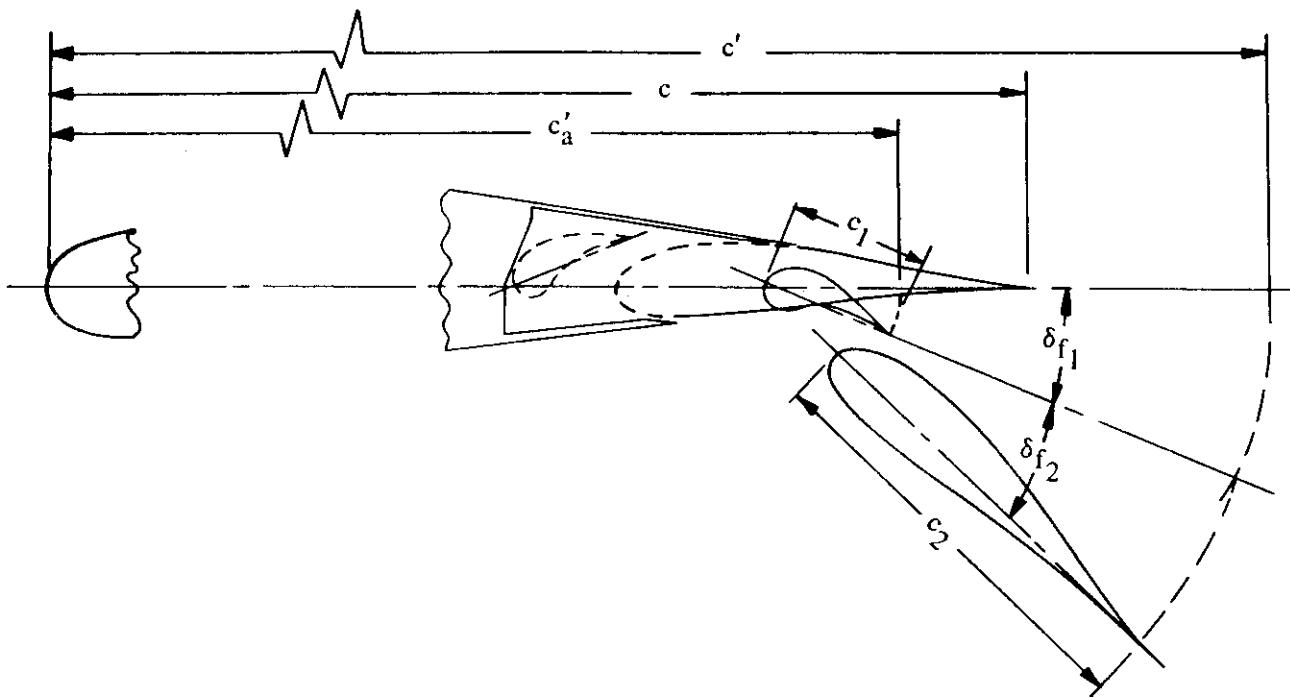
$c$  wing chord (flap in neutral position).

$c_1$  flap chord.

$c'$  extended wing chord due to flap extension. In measuring  $c'$ , the flap trailing edge is rotated from its deflected position about the intersection of the flap chord and the chord of the airfoil section, until the two chords coincide.

$\delta_f$  flap deflection.

FIGURE 6.1.1.1-44 SINGLE-SLOTTED FLAP GEOMETRIC PARAMETERS



$c$  wing chord (flap in neutral position).

$c'$  extended wing chord due to forward-flap extension. In measuring  $c_a'$ , first rotate the forward flap from its deflected position about the point of intersection of the forward-flap chord and the chord of the airfoil section, until the two chords coincide.

$c'$  extended wing chord due to the double-slotted flaps. In measuring  $c'$ , the aft flap is first rotated from its deflected position about the point of intersection of the aft-flap chord and the chord of the forward flap, until the two chords coincide. Then both flaps are rotated from the deflection of the forward flap about the point of intersection of the forward-flap chord with the wing chord, until these two coincide.

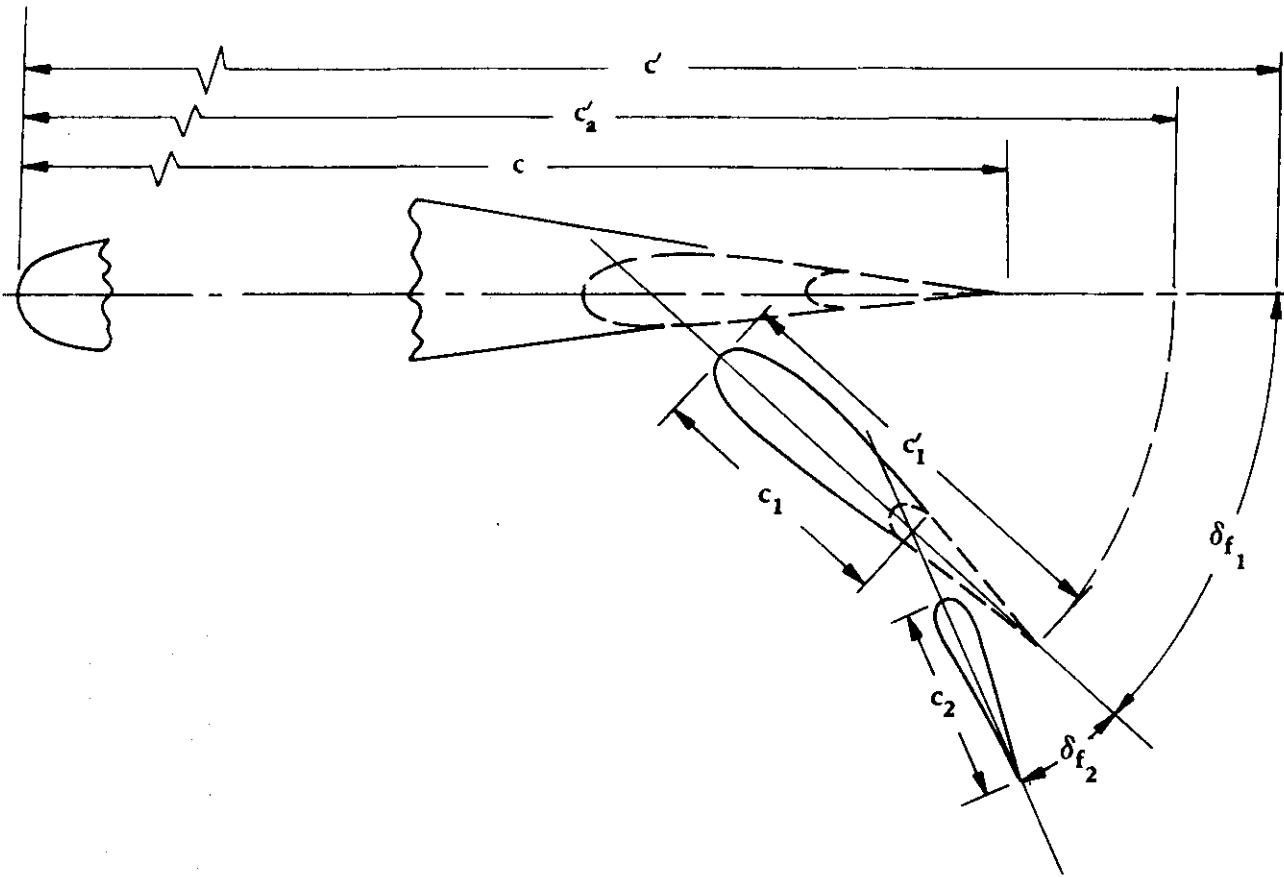
$\delta_{f1}$  flap deflection of the forward flap.

$\delta_{f2}$  flap deflection of the aft flap.

$c_1$  forward-flap chord.

$c_2$  aft-flap chord.

FIGURE 6.1.1.1-45 DOUBLE-SLOTTED FLAP GEOMETRIC PARAMETERS



$c$  wing chord (flap in neutral position).

$c'_a$  extended wing chord due to complete forward-flap extension. In measuring  $c'_a$ , first rotate the complete forward flap (usually includes aft flap) about the point of intersection of the forward-flap chord and the chord of the airfoil section, until the two chords coincide.

$c'$  extended wing chord due to the deflection of the double-slotted flaps. In measuring  $c'$ , the aft flap is first rotated from its deflected position about the point of intersection of the aft-flap chord and the chord of the forward flap, until the two chords coincide. Then both flaps are rotated from the deflection position of the forward flap about the point of intersection of the forward-flap chord with the wing chord, until these two coincide.

$c_1$  forward-flap chord (actual).

$c'_1$  forward-flap chord (complete airfoil).

$c_2$  aft-flap chord.

$\delta_{f_1}$  flap deflection of the forward flap.

$\delta_{f_2}$  flap deflection of the aft flap.

FIGURE 6.1.1-46 DOUBLE-SLOTTED FLAP GEOMETRIC PARAMETERS

## SPLIT FLAPS

LIFT-EFFECTIVENESS  
PARAMETER

$\alpha_{\delta}$

- .8

- .7

- .6

- .5

- .4

- .3

- .2

- .1

0

0

10

20

30

40

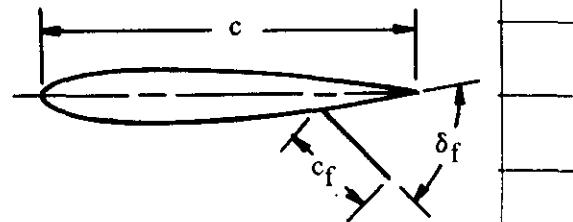
50

60

70

80

FLAP DEFLECTION,  $\delta_f$  (deg)



$c_f/c$

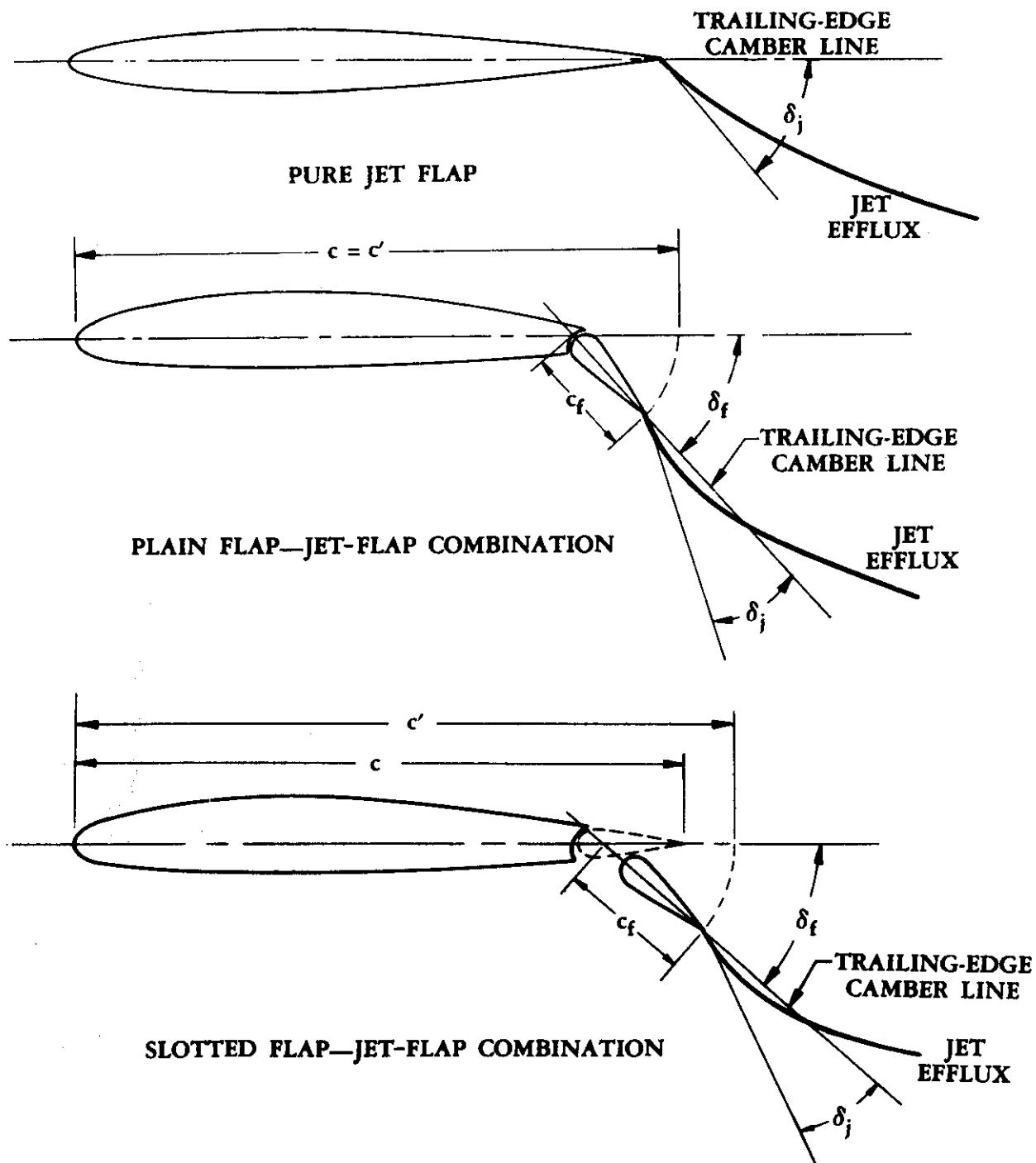
.40

.30

.20

.10

FIGURE 6.1.1.1-47 SECTION LIFT-EFFECTIVENESS PARAMETER OF SPLIT FLAPS



$\delta_j$  is the initial trailing-edge jet momentum angle in radians, measured with respect to the trailing-edge camber line of the airfoil.

$\delta_f$  is the flap deflection in radians, measured with respect to the airfoil chord.

FIGURE 6.1.1-48 JET-FLAP GEOMETRIC PARAMETERS

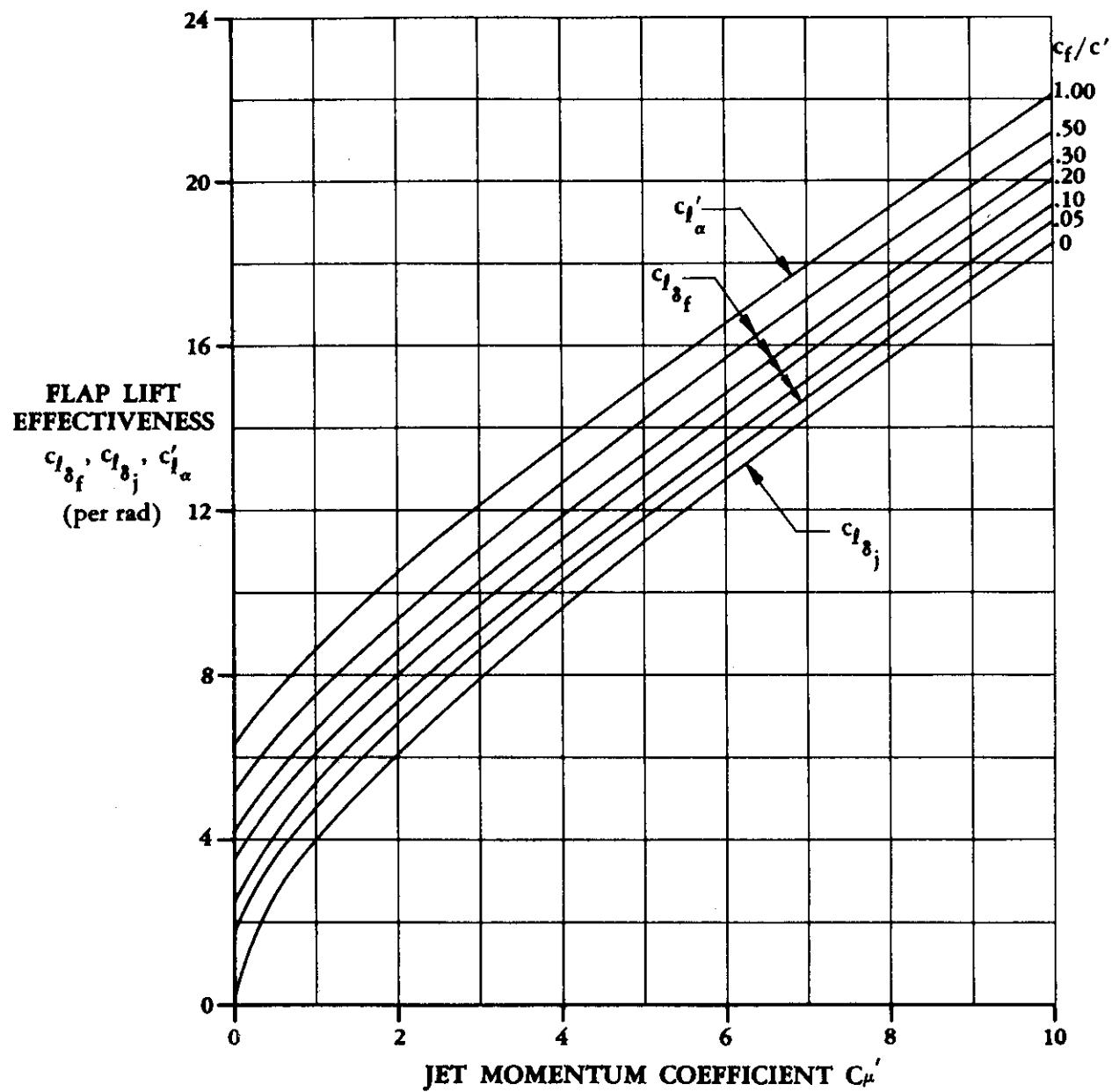
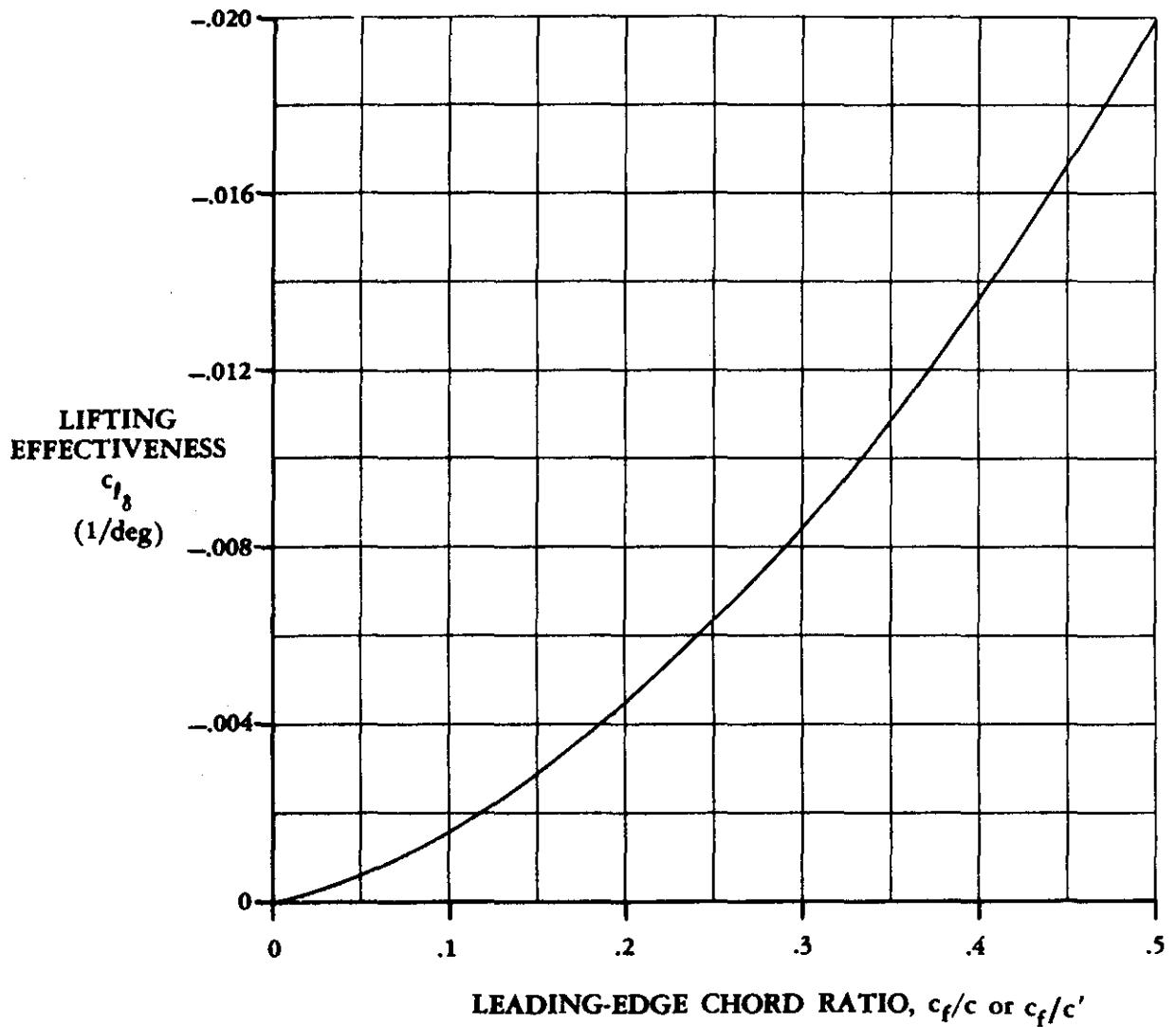
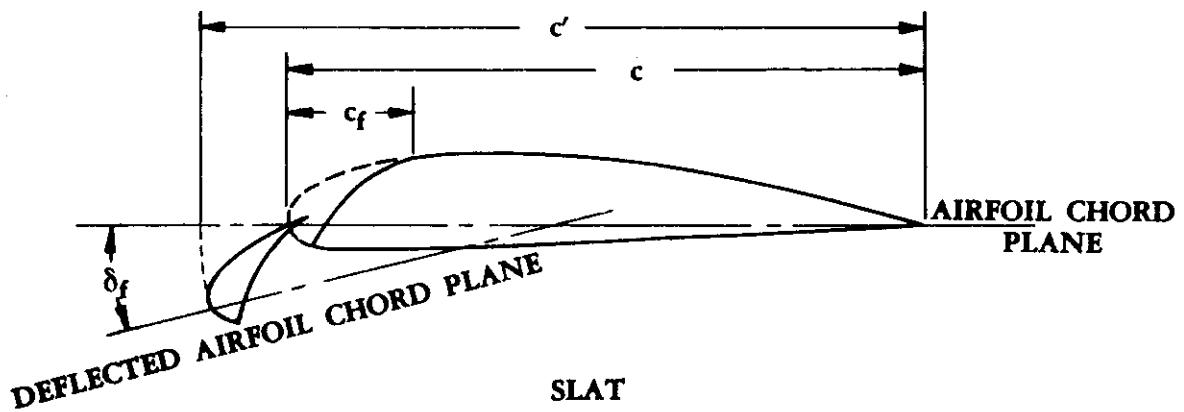
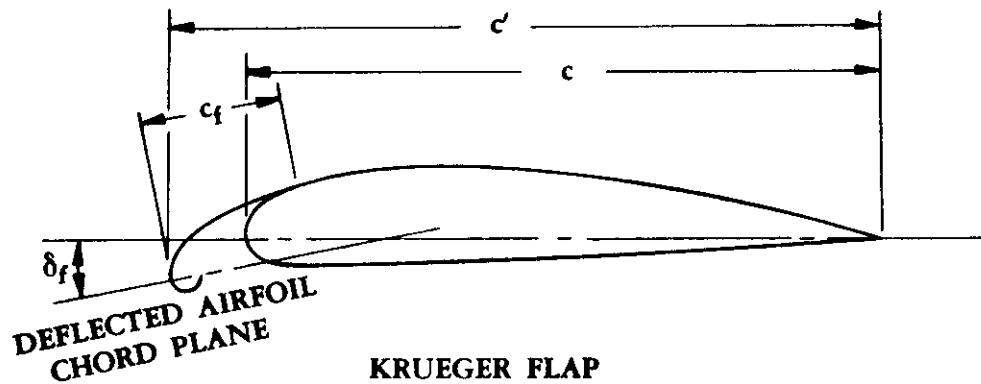
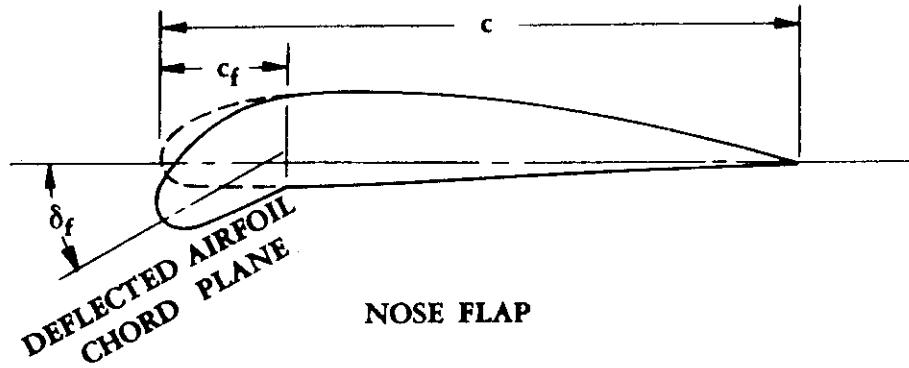


FIGURE 6.1.1.1-49 TWO DIMENSIONAL JET-FLAP THEORETICAL RESULTS



Note: The  $c_f/c$  or  $c_f/c'$  values needed for using this figure are schematically illustrated in the next figure.

**FIGURE 6.1.1.1-50 THEORETICAL LIFTING EFFECTIVENESS OF LEADING-EDGE DEVICES**



$c'$  is the extended wing chord due to the deflection of the leading-edge device. In measuring  $c'$  the leading-edge device is rotated to the wing-chord line from its deflected position, about the point of intersection of the leading-edge-flap chord and the wing chord.

**FIGURE 6.1.1.1-51 GEOMETRY OF LEADING-EDGE DEVICES**

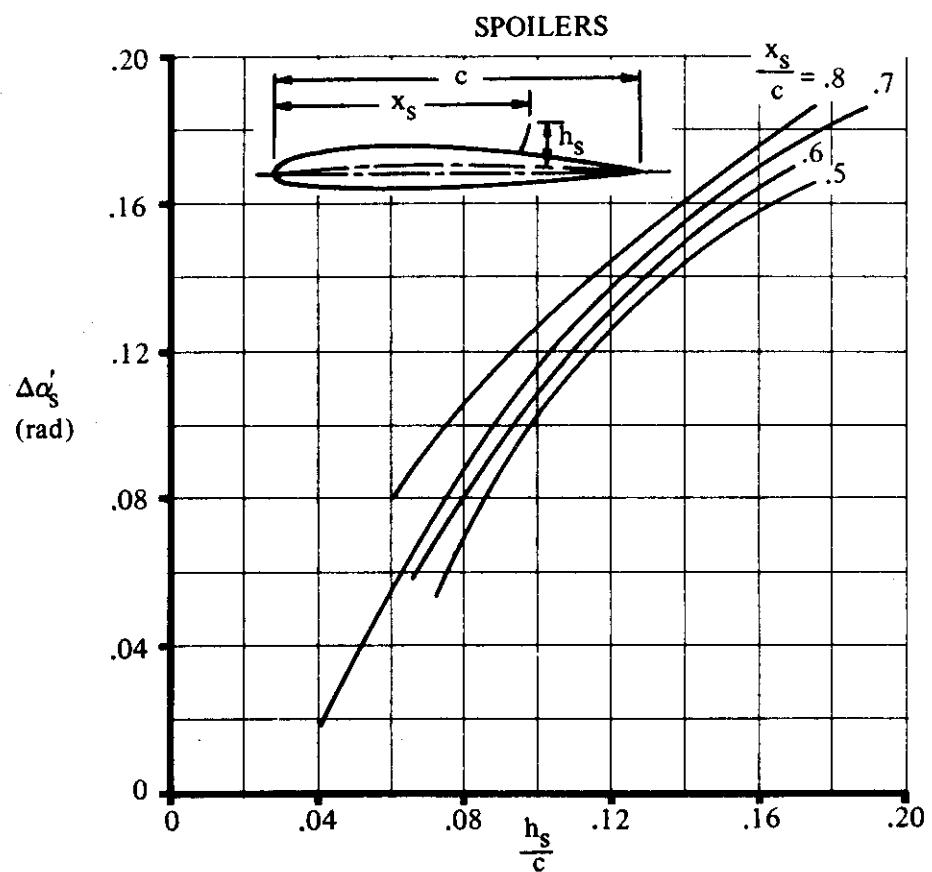


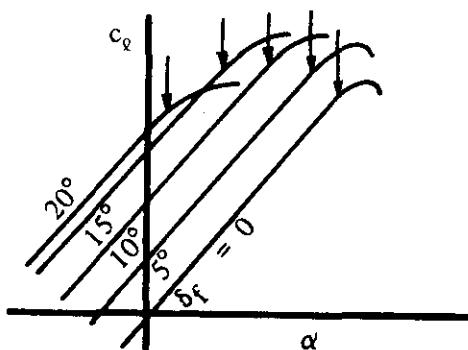
FIGURE 6.1.1.1-52 SPOILER LIFT EFFECTIVENESS – LOW SPEEDS

### 6.1.1.2 SECTION LIFT-CURVE SLOPE WITH HIGH-LIFT AND CONTROL DEVICES

#### Trailing-Edge Flaps

Thin-airfoil theory shows that the lift-curve slope of a cambered section is the same as that of the corresponding uncambered airfoil. Experimental data verify this theoretical prediction for the angle-of-attack and flap-deflection ranges for which the flow is attached over both the wing and flap surfaces.

Flow separation on the wing or flap causes the lift-curve slope to be lower than the theoretical value. Sketch (a) shows a typical set of lift curves for trailing-edge flaps at various deflections. The approximate points at which the curves become appreciably nonlinear for a given flap deflection are shown by the arrows.



SKETCH (a) TYPICAL LIFT CURVES FOR TRAILING-EDGE FLAPS

The sketch is typical of all types of trailing-edge flaps except split flaps, which have somewhat different lift characteristics. When a split flap is deflected, a reduced pressure exists in the wedge-shaped region between the flap and the wing. This reduced pressure creates a favorable pressure gradient near the wing trailing edge, which causes the boundary layer at the upper-surface trailing edge to be thinner for the flap-deflected condition than for the undeflected condition. Consequently, the lift-curve slope for small split-flap deflections is greater than that of the unflapped airfoil. This effect is particularly pronounced on thick airfoils.

For flaps that translate as they deflect, the lift-curve slope is increased because of the increased effective area of the flapped section. Fowler flaps are the most commonly used flaps of this type.

Reference 1 contains a comprehensive summary of two-dimensional trailing-edge control-surface data, including data for the nonlinear angle-of-attack and flap-deflection ranges.

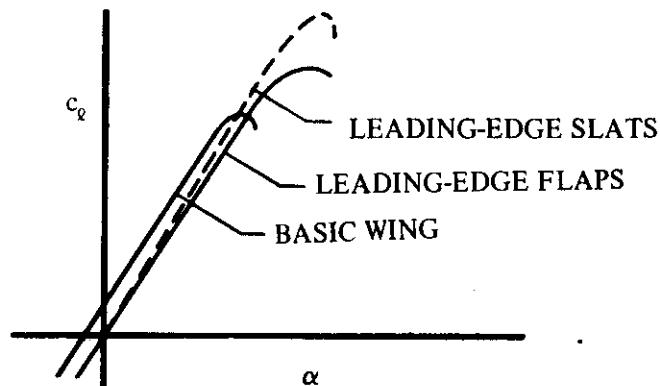
#### Jet Flaps

The lift-curve slope for a jet-flap airfoil is dependent upon the jet momentum trailing-edge coefficient  $C_\mu$ . The method presented herein is Spence's adaptation of thin-airfoil theory as presented in References 2 and 3. In summary, Spence applies thin-airfoil theory to inviscid, incompressible flow past a thin, two-dimensional wing at a small incidence, with a jet of zero thickness and finite momentum emerging at a small angle of incidence from the trailing edge. The flow inside the jet is assumed to be irrotational and is bounded by vortex sheets that prevent mixing

with the mainstream. For flaps that extend as well as rotate, a correction is applied to account for the increased planform area. For more details regarding the fundamental concepts of jet flaps, the reader is referred to the discussion presented in Section 6.1.1.1.

### Leading-Edge Flaps

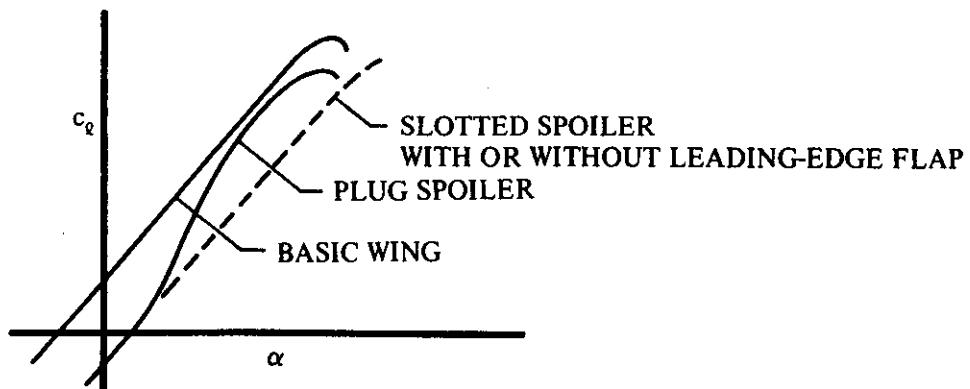
The lift-curve slope of an airfoil with a leading-edge flap is very nearly the same as that of the unflapped airfoil. For slats that extend forward as well as rotate, a correction must be made for the increased planform area. Typical lift curves are shown in Sketch (b).



**SKETCH (b) TYPICAL LIFT CURVES FOR LEADING-EDGE FLAPS AND SLATS**

### Spoilers

The lift curves of airfoils with spoilers extended are extremely nonlinear, particularly at subsonic speeds. Sketch (c) shows a typical set of lift curves for an airfoil with and without plug and slotted spoilers. Leading-edge flaps in conjunction with plug spoilers tend to linearize the lift curve at high angles of attack. This effect is similar to that achieved by adding a slot and deflector behind a plug spoiler.



**SKETCH (c) EFFECT OF SLOT AND LEADING-EDGE FLAP ON SPOILER LIFT CURVES**

The Datcom methods presented below for trailing-edge flaps, jet flaps, leading-edge flaps and slats, and spoilers are limited to subsonic flow.

## DATCOM METHODS

The approximate flap deflections at which flow separation and appreciable lift-curve-slope losses occur with increasing flap deflection are shown in Table 6.1.1.2-A for various types of flaps. Values for both good and poor designs are shown. Flap design is very critical to airfoil section and flap geometry. The effects of these variables on maximum lift are discussed in detail in Section 6.1.1.3.

### 1. Fixed-Hinge Trailing- and Leading-Edge Flaps

For these flaps the lift-curve slope is assumed to be the same as that of the unflapped section for unseparated flow conditions.

### 2. Translating Trailing-Edge Flaps and Leading-Edge Devices (Slats and Krueger Flaps)

For devices whose hinge line translates with deflection, the lift-curve slope is given by

$$\left( c_{q_\alpha} \right)_\delta = \frac{c'}{c} \left( c_{q_\alpha} \right)_{\delta=0} \quad 6.1.1.2-a$$

where

$\left( c_{q_\alpha} \right)_{\delta=0}$  is the lift-curve slope of the unflapped airfoil, including compressibility effects, from Section 4.1.1.2

$\left( c_{q_\alpha} \right)_\delta$  is the lift-curve slope at leading- or trailing-edge deflection  $\delta$ .

$c$  is the chord of the unflapped airfoil.

$c'$  is the effective chord of the flapped airfoil at any flap deflection. In measuring  $c'$  of a single-slotted trailing-edge flap or a leading-edge device, the flap or leading-edge device is rotated from its deflected position about the point of intersection of the flap or leading-edge-device chord with the wing chord, until the two coincide. In measuring  $c'$  of a double-slotted flap, the reader is referred to Figures 6.1.1.1-45 and 6.1.1.1-46.

### 3. Jet Flaps

The method presented here applies to the same configurations as indicated for the jet-flap method of Section 6.1.1.1; i.e., the pure jet flap and the internally-blown-flap (IBF) and externally-blown-flap (EBF) concepts with plain trailing-edge flaps. For an IBF or EBF concept with a single-slotted or multislotted flap configuration, this method should be used only as a first approximation.

No substantiation of the method is presented; however, the method has been acknowledged as being substantiated in the literature (References 4 and 5).

It should be noted that the term  $[1 + k_t(t/c')]$  is used as a correction for airfoil thickness effects and applies to the pressure lift contribution calculated by thin-airfoil theory. This correction can be justified only if there is no trailing-edge separation.

For jet-flap configurations the total section lift-curve slope, based on the retracted airfoil chord, is given by

$$c_{q_\alpha} = \left\{ \left[ 1 + k_t \left( \frac{t}{c'} \right) \right] \left( c'_{q_\alpha} - C'_\mu \right) + C'_\mu \right\} \frac{c'}{c} \quad 6.1.1.2-b$$

where

$k_t$  is the airfoil-theory thickness factor; i.e.,

$k_t = 1.0$  for elliptic airfoils

$= 0.637$  for parabolic airfoils

For airfoil sections other than elliptic or parabolic, a value of 0.80 for  $k_t$  is suggested (Reference 2).

$\frac{t}{c'}$  is the airfoil thickness ratio, based on the extended wing chord

$c'_{q_\alpha}$  is the jet-flap lift-curve slope uncorrected for thickness effects obtained from Figure 6.1.1.1-49, based on the extended wing chord, as a function of  $C'_\mu$ .

$C'_\mu$  is the section nondimensional trailing-edge jet momentum coefficient, based on the extended wing chord (defined in Sketch (a) of Section 6.1.1.1).

$\frac{c'}{c}$  is the ratio of the extended wing chord to airfoil chord, where  $c'$  is obtained as described in Section 6.1.1.1 for the appropriate flap geometry.

#### 4. Spoilers

For the purposes of the Datcom the lift-curve slope of an airfoil with a spoiler, for the conditions  $\alpha > 0$  and  $c_q < 0$ , is assumed to be the same as that of the basic airfoil.

### Sample Problems

#### 1. Translating Trailing-Edge Flap

Given: The flapped airfoil of Reference 7.

NACA 23012 airfoil

Single-slotted flap

$\delta_f = 30^\circ$

$c'/c = 1.154$

$M = 0.105; \beta = 0.995$

$R_x = 3.5 \times 10^6$

$\tan 1/2 \phi'_{TE} = 0.132$  (streamwise airfoil geometry)

#### 6.1.1.2-4

Compute:

$$(c_{q_\alpha})_{\delta=0} = 0.102 \text{ per deg} \quad (\text{Section 4.1.1.2})$$

Solution:

$$(c_{q_\alpha})_{\delta} = \frac{c'}{c} (c_{q_\alpha})_{\delta=0} \quad (\text{Equation 6.1.1.2-a})$$

$$= (1.154)(0.102)$$

$$= 0.118 \text{ per deg}$$

This compares with a test value of 0.120 per degree from Reference 7.

## 2. Jet Flap

Given: The pure jet-flap configuration of Reference 6.

$$\text{Elliptic airfoil} \quad \frac{t}{c} = 0.125 \quad C_\mu = 4.0$$

$$\frac{c_f}{c} = 0 \quad \delta_f = 0 \quad \delta_j = 31.4^\circ \quad \frac{c'}{c} = 1.0$$

Compute:

$$k_t = 1.0 \text{ (elliptic airfoil)}$$

$$c'_{q_\alpha} = 13.63 \text{ per rad} \quad (\text{Figure 6.1.1.1-49})$$

$$c_{q_\alpha} = \left\{ \left[ 1 + k_t \left( \frac{t}{c'} \right) \right] (c'_{q_\alpha} - C'_\mu) + C'_\mu \right\} \frac{c'}{c} \quad (\text{Equation 6.1.1.2-b})$$

$$= \{ [1 + (1.0)(0.125)] (13.63 - 4.0) + 4.0 \} 1.0$$

$$= 14.83 \text{ per rad (based on } c)$$

This compares with a test value of 16.1 from Reference 6.

## REFERENCES

1. Sears, R.L.: Wind-Tunnel Data on the Aerodynamic Characteristics of Airplane Control Surfaces. NACA WR L-663, 1943. (U)
2. Ramsey, J.C., and Laudeman, E.C.: STOL Tactical Aircraft Investigation State-of-the-Art Design Compendium. Prepared under USAF Contract F33615-71-C-1754, 1971. (U)
3. Hayashi, T.T.: The Two Dimensional Jet Flap Theory. Douglas Aircraft Company, MDC J1089, to be published. (U)
4. Lopez, M.L., and Shen, C.C.: Recent Developments in Jet Flap Theory and Its Application to STOL Aerodynamic Analysis. AIAA Paper 71-578, 1971. (U)
5. Spence, D.A.: Lift Coefficient of a Thin Jet-Flapped Wing. Proc. Roy. Soc., Vol. A238, 1956. (U)
6. Dimmock, N.A.: Some Early Jet Flap Experiments. Aero. Quart. Vol. 8, 1957. (U)
7. Harris, T.A., and Purser, P.E.: Wind-Tunnel Investigations of an NACA 23012 Airfoil with Two Sizes of Balanced Split Flap. NACA WR L-441, 1940. (U)

TABLE 6.1.1.2-A

APPROXIMATE RANGE OF FLAP DEFLECTION FOR LINEAR-LIFT CHARACTERISTICS  
AT ZERO ANGLE OF ATTACK

Flap Type	$\delta_f$ (deg)	
	Poor Design	Good Design
Plain	0 to 10	0 to 20
Single Slotted and Fowler	0 to 20	0 to 30
Double Slotted	0 to 30	0 to 60
Split	0 to 30 or 45	

### 6.1.1.3 SECTION MAXIMUM LIFT WITH HIGH-LIFT AND CONTROL DEVICES

The maximum-lift increments obtainable by the use of leading- and trailing-edge flaps are strongly influenced by the flow characteristics of unflapped sections near the stall. The lift of unflapped sections near and at the stall is discussed in detail in Sections 4.1.1.3 and 4.1.1.4.

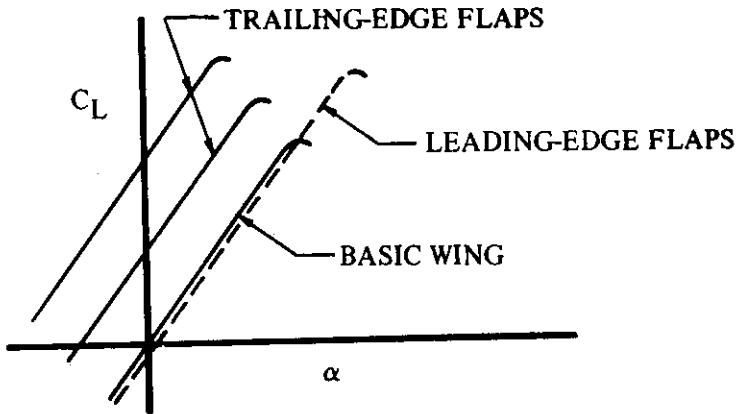
A discussion of the aerodynamic aspects of airfoil flaps is given in Reference 1, some of the more salient points of which are summarized in the following paragraphs.

Trailing-edge flaps increase the maximum lift of a section by means of the camber effect. Theoretically, the incremental load distribution due to flap deflection reaches a peak in the region of the flap hinge line, has a smaller peak at the leading edge, and falls to zero at the trailing edge. Thus the pressure gradient of the upper surface forward of the flap is relieved, although the gradient over the flap itself is greatly increased. The flow over the flap therefore separates at moderate angles, i.e.,  $10^\circ$  to  $15^\circ$  for plain flaps. However, the separation is contained behind the flap hinge line and does not progress forward over the wing until the flap deflections become large. Lift continues to increase with flap deflection after separation takes place over the flap, but the rate of increase is considerably less than that for the small flap-deflection range where the flow is completely attached. Maximum lift is obtained just before the separation progresses forward of the flap or the flow separates from the leading edge.

Leading-edge flaps increase the maximum lift of airfoils by lowering the high peak suction pressures near the nose and thereby delaying leading-edge separation. Nose-flap deflection has only a second-order effect on the flow near the trailing edge. Maximum lift for a given flap deflection is achieved when the angle of attack is increased to the point where the pressure distribution around the nose approximates the pressure distribution of the unflapped section just before the stall. Leading-edge stall ensues as in the case of the unflapped section. This problem is treated theoretically in Reference 2.

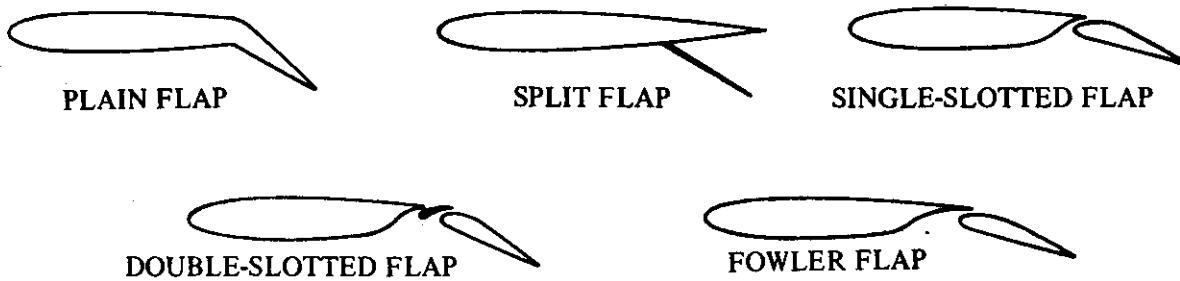
Thin airfoils stall as a result of leading-edge separation, and thick airfoils as a result of trailing-edge separation (see Section 4.1.1.3). Since trailing-edge flaps primarily affect trailing-edge separation without significantly altering the nose pressures, they are most effective on thick wings. Leading-edge flaps, on the other hand, delay leading-edge separation without significantly altering the trailing-edge flow and are therefore most effective on thin wings.

The stall angle of attack of an airfoil having a leading-edge flap is quite different from that of an airfoil having a trailing-edge flap. Leading-edge flaps produce increases in lift by enabling the airfoil to reach higher angles of attack. Therefore, the angle of attack at stall is considerably higher for an airfoil having a leading-edge flap than that for the unflapped airfoil. Trailing-edge flaps, on the other hand, produce increases in maximum lift by means of the camber effect and actually stall at an angle of attack below that of the unflapped airfoil. These trends are illustrated in the accompanying sketch. A consideration of these stalling angles is often a critical item in practice.



**SKETCH (a) TYPICAL LIFT CURVES FOR LEADING-EDGE AND TRAILING-EDGE FLAPS**

Specific comments concerning high-lift trailing-edge devices in common use are given in the following paragraphs. The accompanying sketch illustrates the various types of flaps. Not all of those shown are explicitly discussed.



**SKETCH (b) TYPICAL TRAILING-EDGE FLAPS**

### Plain Flaps

The preceding discussion of trailing-edge flaps is applicable to plain flaps and no further comments are required.

### Split Flaps

When a split flap is deflected, a region of reduced pressure exists between the upper surface of the flap and the lower surface of the airfoil. This reduced pressure creates a favorable pressure gradient over the top rear surface of the airfoil. Trailing-edge separation is thus suppressed, and final stall often occurs at the airfoil nose.

### Slotted Flaps

The crucial factor in the design of a slotted flap is the slot. The slot sheds the boundary layer at the slot lip and allows a new boundary layer to develop over the flap. The slot also directs air in a direction tangential to the surface of the flap. Flow attachment can therefore be maintained to relatively large flap deflections. For instance, efficiently designed double-slotted flaps can prevent flow separation at deflections as high as 60°.

The design of slots for slotted flaps is very critical. Several rules of thumb have been developed for efficiently designing these flaps. First, the flap (and vane) and airfoil must overlap for all deflections when viewed in planform. Secondly, the jet issuing from the slot should also be directed in a direction tangential to the flap surface. Long shroud lengths often show advantages, since they have better control over the direction of the jet.

The flaps (and vanes) of a slotted flap carry considerably more lift than the corresponding plain flap with the same chord and deflection angle. These surfaces are, in reality, in tandem with the wing and derive beneficial induced-camber effects associated with tandem configurations.

### Fowler Flaps

Aerodynamically, Fowler flaps function in the same way as single-slotted flaps. Additional lift benefits are obtained, however, from the increased chord due to translation of these flaps.

### Jet Flaps

The recent developments in high-lift technology have led to the widespread consideration of the jet-flap scheme (see Section 6.1.1.1 for a sketch of the various types and a discussion of the salient aspects). Comments regarding the maximum lift increment due to power effects of a jet-flap scheme are given in the following paragraphs.

The increment in lift due to power effects of a jet-flap configuration is strongly dependent upon the trailing-edge jet momentum coefficient  $C_\mu$ . Since the jet-flap theory as developed by Spence assumes inviscid flow, it cannot be utilized to predict the achievable maximum lift coefficient. An expression has been developed in Reference 3 for the increment in maximum lift of a two-dimensional jet-flapped airfoil with supercirculation. The analysis is limited to airfoils that exhibit a leading-edge stall. Under these circumstances it is suggested that the pressure distribution around the leading edge would be similar for the flapped- and plain-wing sections at stall.

Reference 4 summarizes an attempt to correlate test data with the method presented in Reference 3. The predicted values of  $\Delta C_{L_{max}}$  due to power underestimated the experimental data by a considerable margin. These results tend to indicate that an airfoil with blowing does not stall at the same leading-edge pressure coefficient as the airfoil without blowing, but at considerably lower pressure coefficients. The test data used for the attempted correlation indicated a wide scatter band as a function of  $C_\mu$ . This scatter prevents the application of an empirical modification to the method. Consequently, no method is presented herein. Further investigations are required and more test data needed to yield a more accurate and reliable method.

## DATCOM METHODS

The following Datcom methods for trailing-edge and leading-edge flaps are limited to subsonic flow.

### 1. Trailing-Edge Flaps

An empirical method from Reference 2 for predicting maximum lift increments for plain, split, and slotted flaps is presented in Figures 6.1.1.3-12a through 6.1.1.3-13b. The maximum lift increment is given by

$$\Delta c_{\ell_{\max}} = k_1 k_2 k_3 (\Delta c_{\ell_{\max}})_{\text{base}} \quad 6.1.1.3-a$$

where

$(\Delta c_{\ell_{\max}})_{\text{base}}$  is the section maximum lift increment for 25-percent chord flaps at the reference flap-deflection angle from Figure 6.1.1.3-12a. (Reference flap-deflection angles are denoted in Figure 6.1.1.3-13a.)

$k_1$  is a factor accounting for flap-chord-to-airfoil-chord ratios other than 0.25 from Figure 6.1.1.3-12b.

$k_2$  is a factor accounting for flap deflections other than the reference values from Figure 6.1.1.3-13a.

$k_3$  is a factor accounting for flap motion as a function of flap deflection from Figure 6.1.1.3-13b.

A comparison of experimental data with results based on these charts is shown in Table 6.1.1.3-A.

### 2. Leading-Edge Flaps

A method is developed in Reference 5 for predicting the maximum lift increment for leading-edge flaps, slats, and Krueger flaps. The method is based on an extension of thin-airfoil theory, using empirical factors that were developed using available test data.

The available Krueger-flap test data were found to be dependent largely upon the trailing-edge flap deflection. Consequently, the method for Krueger flaps from Reference 5 is not presented, since it does not account for the trailing-edge flap deflections.

The method presented herein gives reasonable results when applied to leading-edge flap deflections less than 30°, as indicated by the comparison of test data with predicted results, shown in Table 6.1.1.3-B.

For leading-edge slats it is not advisable to use the method herein for deflections greater than 20°. The method tends to overpredict the maximum lift increment for larger deflections, as shown in Table 6.1.1.3-B.

The maximum lift increment for leading-edge flaps and slats is given by

$$\Delta c_{\ell_{\max}} = c_{\ell_{\delta_{\max}}} \eta_{\max} \eta_{\delta} \delta_f \frac{c'}{c} \quad 6.1.1.3-b$$

where

$c_{\ell_{\delta_{\max}}}$  is the theoretical maximum lifting effectiveness obtained from Figure 6.1.1.3-14 as a function of the leading-edge flap-chord ratio  $c_f/c$ .

$\eta_{\max}$  is the empirical factor accounting for the maximum lifting efficiency obtained from Figure 6.1.1.3-15 as a function of the ratio of the leading-edge radius to the thickness ratio of the airfoil.

The reason for the discontinuity in the slat curve presented in Figure 6.1.1.3-15 is that older NACA test data are used to establish the left-hand portion of the curve, while more recent test data (as indicated in Reference 5) are used for the right-hand portion. An attempt was made to resolve this discontinuity; however, no modifications were made because of the lack of test data in the region of the discontinuity.

$\eta_{\delta}$  is the empirical factor accounting for changes in flap deflection from the optimum deflection obtained from Figure 6.1.1.3-16 as a function of deflection angle.

$\delta_f$  is the leading-edge deflection angle in radians (see Figure 6.1.1.1-51).

$\frac{c'}{c}$  is the ratio of the extended wing chord due to leading-edge flap extension to the retracted wing chord (see Figure 6.1.1.1-51).

### Sample Problems

#### 1. Trailing-Edge Flap

Given: The flapped airfoil of Reference 6.

NACA 65-210 airfoil      Double-slotted flap       $\delta_{f_1} = 15^\circ$        $\delta_{f_2} = 25^\circ$

$\delta_f = 40^\circ$        $c_f/c = 0.312$        $R_\ell = 6.0 \times 10^6$

Compute:

$(\Delta c_{\ell_{\max}})_{\text{base}} = 1.165$       (Figure 6.1.1.3-12a)

$k_1 = 1.250$       (Figure 6.1.1.3-12b, extrapolated)

$$k_2 = 0.950 \quad (\text{Figure 6.1.1.3-13a})$$

$$\frac{\text{Actual Flap Angle}}{\text{Reference Flap Angle}} = \frac{40}{50} = 0.80$$

$$k_3 = 0.870 \quad (\text{Figure 6.1.1.3-13b})$$

Solution:

$$\begin{aligned}\Delta c_{q_{\max}} &= k_1 k_2 k_3 (\Delta c_{q_{\max}})_{\text{base}} \quad (\text{Equation 6.1.1.3-a}) \\ &= (1.250)(0.950)(0.870)(1.165) \\ &= 1.20\end{aligned}$$

This compares with a test value of 1.33 from Reference 6.

## 2. Leading-Edge Flap

Given: The flapped airfoil of Reference 7.

NACA 64A010 airfoil • Leading-edge radius = 0.687% c

$$\frac{t}{c} = 0.10 \quad \text{Nose flap} \quad \delta_f = 30^\circ \quad \frac{c_f}{c} = 0.15 \quad \frac{c'}{c} = 1.0$$

Compute:

$$c_{q_{\delta_{\max}}} = 1.44 \text{ per rad} \quad (\text{Figure 6.1.1.3-14})$$

$$\eta_{\max} = 0.99 \quad (\text{Figure 6.1.1.3-15})$$

$$\eta_{\delta} = 0.82 \quad (\text{Figure 6.1.1.3-16})$$

Solution:

$$\begin{aligned}\Delta c_{q_{\max}} &= c_{q_{\delta_{\max}}} \eta_{\max} \eta_{\delta} \delta_f \frac{c'}{c} \quad (\text{Equation 6.1.1.3-b}) \\ &= (1.44)(0.99)(0.82) \frac{30}{57.3} (1.0) \\ &= 0.612\end{aligned}$$

This compares with a test value of 0.56 from Reference 7.

## REFERENCES

1. Nonweiler, T.: Flaps, Slots, and Other High-Lift Aids. Aircraft Engineering, September 1955. (U)
2. Anon.: Approximate Relationships for Determining Airplane Maximum Lift Coefficients. Douglas Aircraft Company Report SM 13874, 1950. (U)
3. Perry, D. H.: A Review of Some Published Data on the External-Flow Jet-Augmented Flap. ARC CP 1194, 1972. (U)
4. Levinsky, E. S., and Ramsey, J. C.: Methodology for Estimating STOL Aircraft High Lift System Characteristics. AIAA Paper 72-779, Aug. 1972. (U)
5. Ramsey, J. C., and Laudeman, E. C.: STOL Tactical Aircraft Investigation State-of-the-Art Design Compendium. Prepared Under USAF Contract F33615-71-C-1754, 1971. (U)
6. Cahill, J. F.: Two-Dimensional Wind-Tunnel Investigation of Four Types of High-Lift Flap on an NACA 65-210 Airfoil Section. NACA TN 1191, 1947. (U)
7. Kelly, J. A., and Hayter, N. L. F.: Lift and Pitching Moment at Low Speeds of the NACA 64A010 Airfoil Section Equipped with Various Combinations of a Leading-Edge Slat, Leading-Edge Flap, Split Flap, and Double Slotted Flap. NACA TN 3007, 1953. (U)
8. Roshko, A.: Computation of the Increment of Maximum Lift Due to Flaps. Douglas Aircraft Company Report SM 23626, 1959. (U)
9. Speerman, M. L.: Wind-Tunnel Investigation of an NACA 0009 Airfoil with 0.25- and 0.50-Airfoil-Chord Plain Flaps Tested Independently and in Combination. NACA TN 1517, 1948. (U)
10. Rose, L. M., and Altman, J. M.: Low-Speed Experimental Investigation of a Thin, Faired, Double-Wedge Airfoil Section with Nose and Trailing-Edge Flaps. NACA TN 1934, 1949. (U)
11. Gambucci, B. J.: Section Characteristics of the NACA 0006 Airfoil with Leading-Edge and Trailing-Edge Flaps. NACA TN 3797, 1956. (U)
12. Cahill, J. F., Underwood, W. J., Nuber, R. J., and Cheesman, G. A.: Aerodynamic Forces and Loadings on Symmetrical Circular-Arc Airfoils with Plain Leading-Edge and Plain Trailing-Edge Flaps. NACA TR 1146, 1953. (U)
13. Lockwood, V. E.: Wind-Tunnel Investigation of Control-Surface Characteristics. XVII – Beveled-Trailing-Edge Flaps of 0.20, 0.30, and 0.40 Airfoil Chord of an NACA 0009 Airfoil. NACA WR L-666, 1944. (U)
14. Jacobs, E. N., Pinkerton, R. M., and Greenberg, H.: Tests of Related Forward-Camber Airfoils in the Variable-Density Wind Tunnel. NACA TR 610, 1937. (U)
15. Cahill, J. F., and Racisz, S. F.: Wind-Tunnel Investigation of Seven Thin NACA Airfoil Sections to Determine Optimum Double-Slotted-Flap Combinations. NACA TN 1545, 1948. (U)
16. Wenzinger, C. J., and Harris, T. A.: Wind-Tunnel Investigation of an NACA 23012 Airfoil with Various Arrangements of Slotted Flaps. NACA TR 664, 1939. (U)
17. Wenzinger, C. J., and Harris, T. A.: Wind-Tunnel Investigation of NACA 23012, 23021, and 23030 Airfoils with Various Sizes of Split Flap. NACA TR 668, 1939. (U)
18. Underwood, W. J., and Abbott, F. T., Jr.: Test of NACA 66,2-116,  $a = 0.6$  Airfoil Section Fitted with Pressure Balance and Slotted Flaps for the Wing of the XP-63 Airplane. NACA WR L-701, 1942. (U)
19. Lowry, J. G.: Wind-Tunnel Investigation of an NACA 23012 Airfoil with Several Arrangements of Slotted Flaps with Extended Lips. NACA TN 808, 1941. (U)
20. Holtzclaw, R. W.: Wind-Tunnel Investigation of the Effects of Spoilers on the Characteristics of a Low-Drag Airfoil Equipped with a 0.25-Chord Slotted Flap. NACA WR A-92, 1945. (U)
21. Rogallo, F. M.: Aerodynamic Characteristics of a Slot-Lip Aileron and Slotted Flap for Dive Brakes. NACA WR L-337, 1941. (U)

22. Harris, T. A.: Wind-Tunnel Investigation of an NACA 23012 Airfoil with Two Arrangements of a Wide-Chord Slotted Flap. NACA TN 715, 1938. (U)
23. Cahill, J. F.: Aerodynamic Data for a Wing Section of the Republic XF-12 Airplane Equipped with a Double Slotted Flap. NACA WR L-544, 1946. (U)
24. Bogdonoff, S. M.: Wind-Tunnel Investigation of a Low-Drag Airfoil Section with a Double Slotted Flap. NACA WR L-697, 1943. (U)
25. Fischel, J., and Riebe, J. M.: Wind-Tunnel Investigation of an NACA 23021 Airfoil with a 0.32-Airfoil-Chord Double Slotted Flap. NACA WR L-7, 1944. (U)
26. Purser, P. E., Fischel, J., and Riebe, J. M.: Wind-Tunnel Investigation of an NACA 23012 Airfoil with a 0.30-Airfoil-Chord Double Slotted Flap. NACA WR L-469, 1943. (U)
27. Harris, T. A., and Recant, I. G.: Wind-Tunnel Investigation of NACA 23012, 23021, and 23030 Airfoils Equipped with 40-Percent-Chord Double Slotted Flaps. NACA TR 723, 1941. (U).
28. Wenzinger, C. J., and Anderson, W. B.: Pressure Distribution Over Airfoils with Fowler Flaps. NACA TR 620, 1938. (U)
29. Rose, L. M., and Altman, J. M.: Low-Speed Investigation of a Thin, Faired, Double-Wedge Airfoil Section with Nose Flaps of Various Chords. NACA TN 2018, 1950. (U)
30. Gottlieb, S. M.: Two-Dimensional Wind-Tunnel Investigation of Two NACA 6-Series Airfoils with Leading-Edge Slats. NACA L8K22, 1949. (U)
31. Hunton, L. W., and James, H. A.: Use of Two-Dimensional Data in Estimating Loads on a 45° Sweptback Wing with Slats and Partial-Span Flaps. NACA TN 3040, 1953. (U)
32. Weick, F. E., and Platt, R. C.: Wind-Tunnel Tests on Model Wing with Fowler Flap and Specially Developed Leading-Edge Slot. NACA TN 459, 1933. (U)
33. Moss, G. F.: Systematic Wind-Tunnel Tests with Slats on a 10 Percent Thick Symmetrical Wing Section (EQ 1040 Profile). ARC R&M 2705, 1952. (U)
34. Wenzinger, C. J., and Shortal, J. A.: The Aerodynamic Characteristics of a Slotted Clark Y Wing as Affected by the Auxiliary Airfoil Position. NACA TR 400, 1931. (U)
35. Koven, W., and Graham, R. R.: Wind-Tunnel Investigation of High-Lift and Stall-Control Devices on a 37° Sweptback Wing of Aspect Ratio 6 at High Reynolds Numbers. NACA RM L8D29, 1948. (U)

TABLE 6.1.1.3-A  
LOW-SPEED SECTION MAXIMUM-LIFT INCREMENTS FOR TRAILING-EDGE FLAP DEFLECTION  
DATA SUMMARY AND SUBSTANTIATION

Ref.	Airfoil	Flap Type	$R_f \times 10^{-6}$	$c_f/c$	$\delta_f$ (deg)	$c_{l\max} (\delta_f = 0)$	$\Delta c_{l\max}$ Calc	$\Delta c_{l\max}$ Test	*Percent Error
9	NACA 0009	Plain	2.58	.25	10	.885	.27	.23	17.4
10	Double Wedge t/c = 4.23%		5.8	.25	60	.84	.97	.89	9.0
11	NACA 0006		4.5	.30	50	.94	.91	.76	19.7
12	6-percent-thick circular arc		6.0	.20	60	.73	.84	.91	-7.7
12	10-percent-thick circular arc		6.0	.20	60	.67	.75	.98	-23.5
13	NACA 0009		2.76	.20	30	1.15	.56	.43	-30.2
13	NACA 0009		2.39	.30	30	.975	.64	.57	12.3
13	NACA 0009		2.39	.40	30	1.0	.66	.53	24.5
6	NACA 65-210	Split	6.0	.20	60	1.29	.75	.78	-3.8
14	NACA 0012		8.0	.20	60	1.66	.84	.69	21.7
15	NACA 1410		6.0	.20	60	1.51	.74	.82	-9.8
16	NACA 23012		3.5	.20	60	1.55	.84	.98	-14.3
17	NACA 23012		3.5	.10	60	1.55	.59	.75	-21.3
17	NACA 23021		3.5	.40	60	1.36	1.73	1.54	12.3
18	NACA 66,2-116 $a = .6$	Single Slotted	6.0	.2505	45	1.45	1.67	1.29	29.5
6	NACA 65-210		2.4	.25	30	1.22	.79	.90	-12.2
6	NACA 65-210		2.4	.25	30	1.22	.79	.84	-6.0
19	NACA 23012		3.5	.30	40	1.55	1.24	1.36	-8.8
20	NACA 66,2-216 $a = .6$		5.1	.25	45	1.46	1.67	1.42	17.6
21	NACA 23012		3.5	.2566	30	1.52	.88	1.03	-14.6
22	NACA 23012		3.5	.40	40	1.53	1.27	1.30	-2.3
6	NACA 65-210	Double Slotted	2.4	.312	40	1.22	1.20	1.30	-7.7
6	NACA 65-210		6	.312	40	1.29	1.20	1.33	-9.8
6	NACA 65-210		9	.312	50	1.4	1.47	1.20	22.5
23	Between R-4,40-318-1 and R-4,40-313-6		3.5	.238	40	1.39	1.37	1.35	1.5
23	Between R-4,40-318-1 and R-4,40-313-6		14	.238	40	1.55	1.37	1.31	4.6
24	NACA 65,3-118 $a = 1.0$		6	.309	45	1.61	1.98	1.59	24.5
25	NACA 23021		3.5	.32	50	1.35	2.30	1.86	23.7
26	NACA 23012		3.5	.30	50	1.55	1.65	1.63	1.2
27	NACA 23012		3.5	.40	40	1.55	1.82	1.91	-4.7
15	NACA 63-210		6	.25	50	1.52	1.17	1.38	-15.2
6	NACA 65-210	Fowler	2.4	.25	35	1.22	1.03	.99	4.0
6	NACA 65-210		9	.25	35	1.4	1.03	1.04	-1.0
16	NACA 23012		3.5	.2667	40	1.55	1.47	1.09	34.9
19	NACA 23012		3.5	.30	40	1.55	1.65	1.75	-5.7
28	NACA 23012		2.9	.40	30	1.16	1.71	1.70	0.6
28	Clark Y		~2	.20	30	1.35	.84	1.16	-27.6

\*based on flapped airfoil

$$\text{Average Error} = \frac{\sum |e_i|}{n} = 13.7\%$$

TABLE 6.1.1.3-B

LOW-SPEED SECTION MAXIMUM-LIFT INCREMENTS FOR LEADING-EDGE FLAP AND SLAT DEFLECTION  
DATA SUMMARY AND SUBSTANTIATION

Ref.	Airfoil	Type	t/c	c <sub>f</sub> /c	δ <sub>f</sub> (deg)	Δc <sub>l</sub> <sub>max</sub> Calc	Δc <sub>l</sub> <sub>max</sub> Test	Δ(Δc <sub>l</sub> <sub>max</sub> <sub>calc</sub> - Δc <sub>l</sub> <sub>max</sub> <sub>test</sub> )
7	64A010	Flap	0.10	0.15	15	0.373	0.39	-0.017
					30	0.612	0.56	0.052
					45	0.280	0.46	-0.180
29	Double Wedge		0.0423	0.12	5	0.068	0.145	-0.077
				0.16		0.076	0.145	-0.069
				0.20		0.085	0.155	-0.070
				0.12	10	0.136	0.14	-0.004
				0.16		0.155	0.17	-0.015
				0.20		0.170	0.20	-0.030
				0.25		0.182	0.225	-0.043
				0.12	15	0.204	0.185	0.019
				0.16		0.232	0.26	-0.028
				0.20		0.254	0.28	-0.026
				0.12	20	0.272	0.255	0.017
				0.16		0.310	0.335	-0.025
				0.20		0.339	0.345	-0.006
				0.25		0.364	0.445	-0.081
				0.12	25	0.320	0.37	-0.050
				0.16		0.364	0.445	-0.081
				0.20		0.399	0.41	-0.011
				0.25		0.428	0.515	-0.087
				0.12	30	0.335	0.41	-0.075
				0.16		0.381	0.485	-0.104
				0.20		0.417	0.465	-0.048
				0.25		0.448	0.515	-0.067
				0.12	35	0.314	0.43	-0.116
				0.16		0.368	0.195	0.163
				0.20		0.392	0.18	0.212
				0.25		0.421	0.515	-0.094
7	64A010	Slat	0.10	0.17	25.6	0.736	0.90	-0.164
30	64-212		0.12	0.14	14.3	0.70	0.60	0.100
	65A109		0.09		24.3	0.61	0.69	-0.080
31	64A010		0.10	0.17	15	0.577	0.66	-0.083
32	Clark Y		0.117	0.13	11.5	0.456	0.76	-0.304
					14	0.556	0.79	-0.234

TABLE 6.1.1.3-B (CONT'D)

Ref.	Airfoil	Type	t/c	c <sub>f</sub> /c	$\delta_f$ (deg)	$\Delta c_{\ell \max}$ Calc	$\Delta c_{\ell \max}$ Test	$\Delta(\Delta c_{\ell \max \text{calc}} - \Delta c_{\ell \max \text{test}})$
32	Clark Y	Slat	0.117	0.13	16.5	0.646	0.76	-0.114
					14	0.542	0.705	-0.163
					19	0.685	0.77	-0.085
					21.5	0.720	0.55	0.170
					19	0.691	0.683	0.008
					24	0.734	0.722	0.012
					26.5	0.729	0.715	0.014
33	EQ 1040	0.10	0.20	5.1	5.1	0.204	0.340	-0.136
					11.1	0.443	0.585	-0.142
					16.4	0.641	0.600	0.041
					20.7	0.946	0.190	0.756
					0.30	16.2	0.780	0.785
					18.2	0.843	0.852	-0.009
					20.3	0.880	0.910	-0.030
		0.30	0.20	22.3	22.3	0.907	0.642	0.265
					8.0	0.403	0.630	-0.227
					11.1	0.559	0.730	-0.171
					15.1	0.760	0.755	0.005
					13.9	0.656	0.682	-0.026
					15.9	0.742	0.685	0.057
					19.0	0.850	0.698	0.152
34	Clark Y	0.117	0.13	32.5	32.5	0.602	0.223	0.379
					25	0.723	0.344	0.379
					16.5	0.641	0.507	0.134
					7.5	0.302	0.436	-0.134
					20.5	0.680	0.213	0.467
					15	0.573	0.472	0.101
					8.5	0.332	0.521	-0.189
					9.5	0.351	0.289	0.062
					5.5	0.209	0.483	-0.274
					14	0.286	0.15	0.136
35	64 <sub>1</sub> -212	0.12	0.14	14	Average $\Delta(\Delta c_{\ell \max \text{calc}} - \Delta c_{\ell \max \text{test}}) = 0.116$			

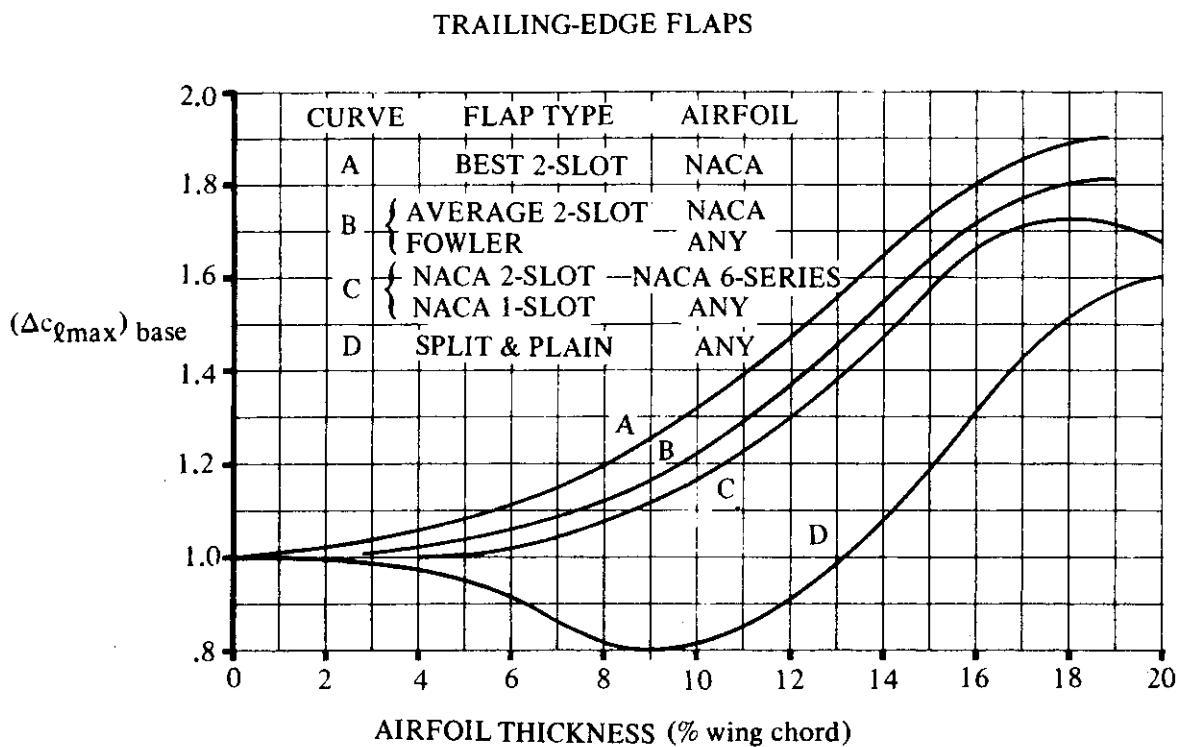


FIGURE 6.1.1.3-12a MAXIMUM-LIFT INCREMENTS FOR 25%-CHORD FLAPS AT REFERENCE FLAP ANGLE

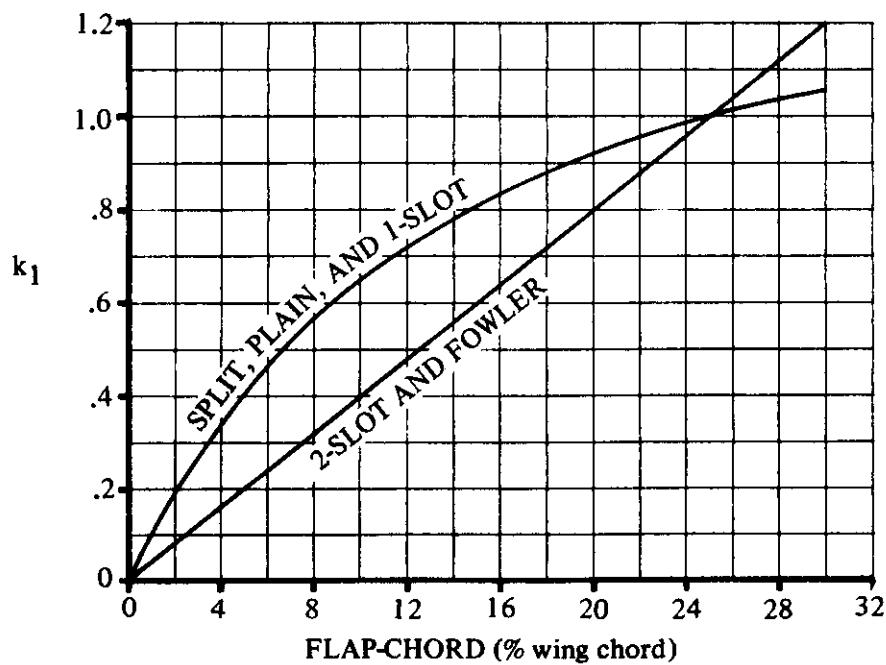
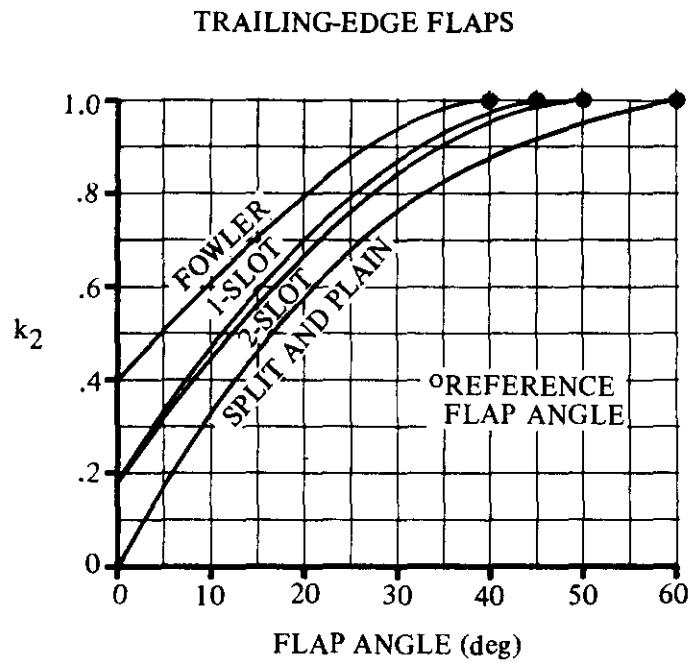
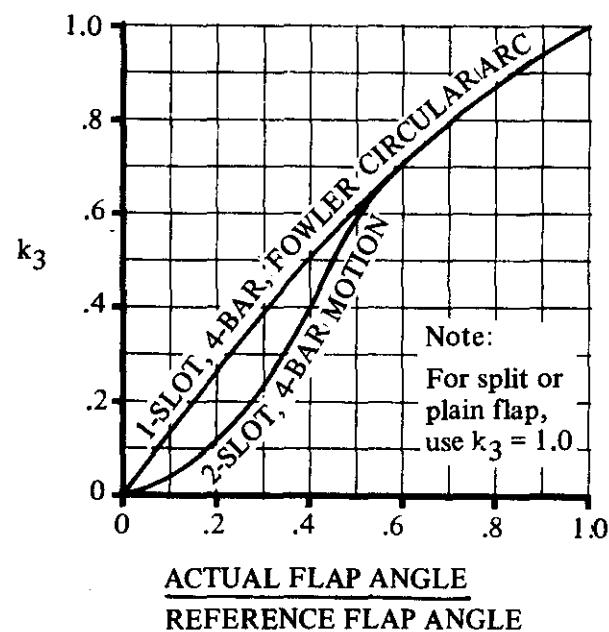


FIGURE 6.1.1.3-12b FLAP-CHORD CORRECTION FACTOR



**FIGURE 6.1.1.3-13a FLAP-ANGLE CORRECTION FACTOR**



**FIGURE 6.1.1.3-13b FLAP-MOTION CORRECTION FACTOR**

## LEADING-EDGE FLAPS AND SLATS

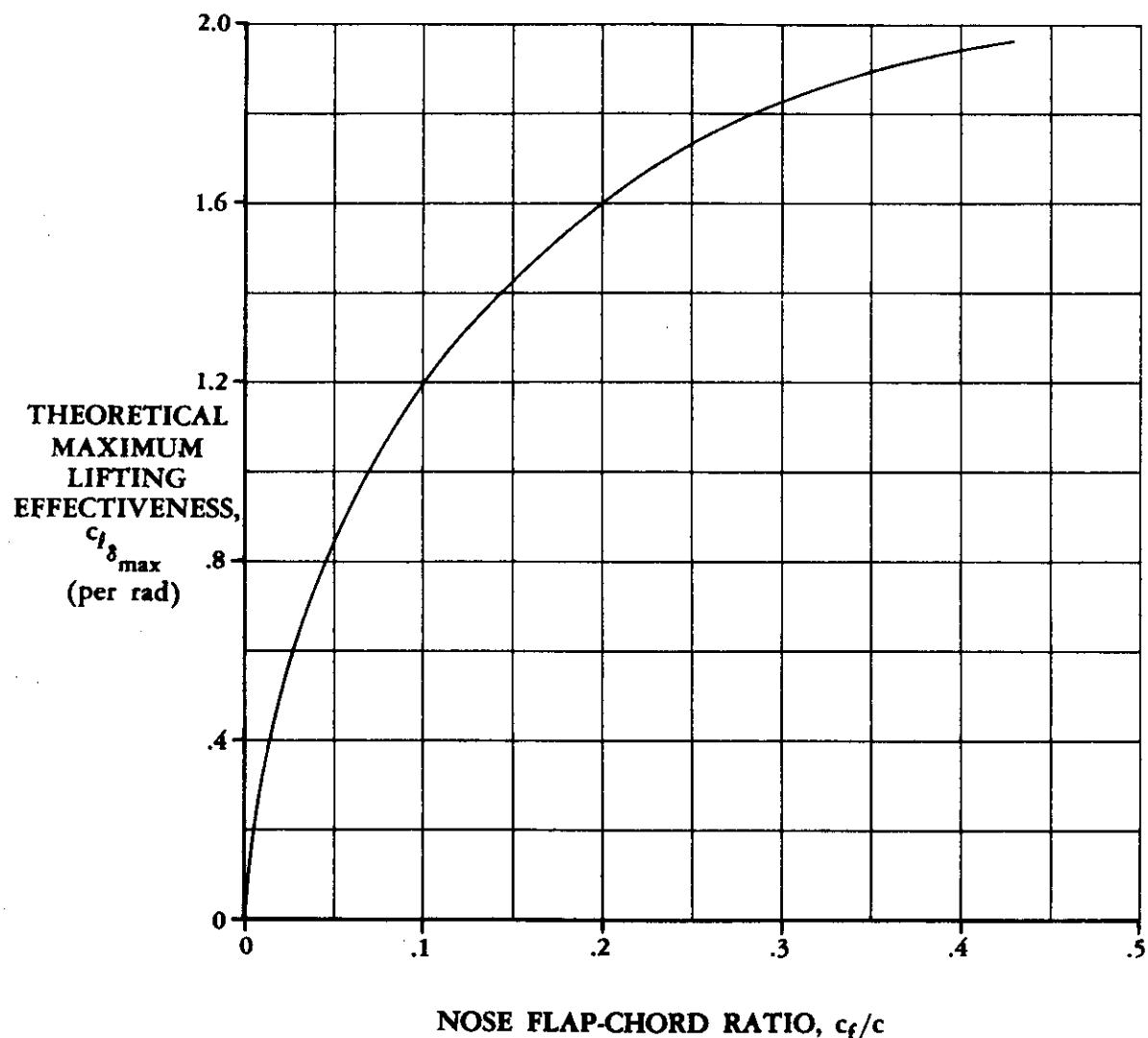


FIGURE 6.1.1.3-14 THEORETICAL MAXIMUM-LIFT EFFECTIVENESS

## LEADING-EDGE FLAPS AND SLATS

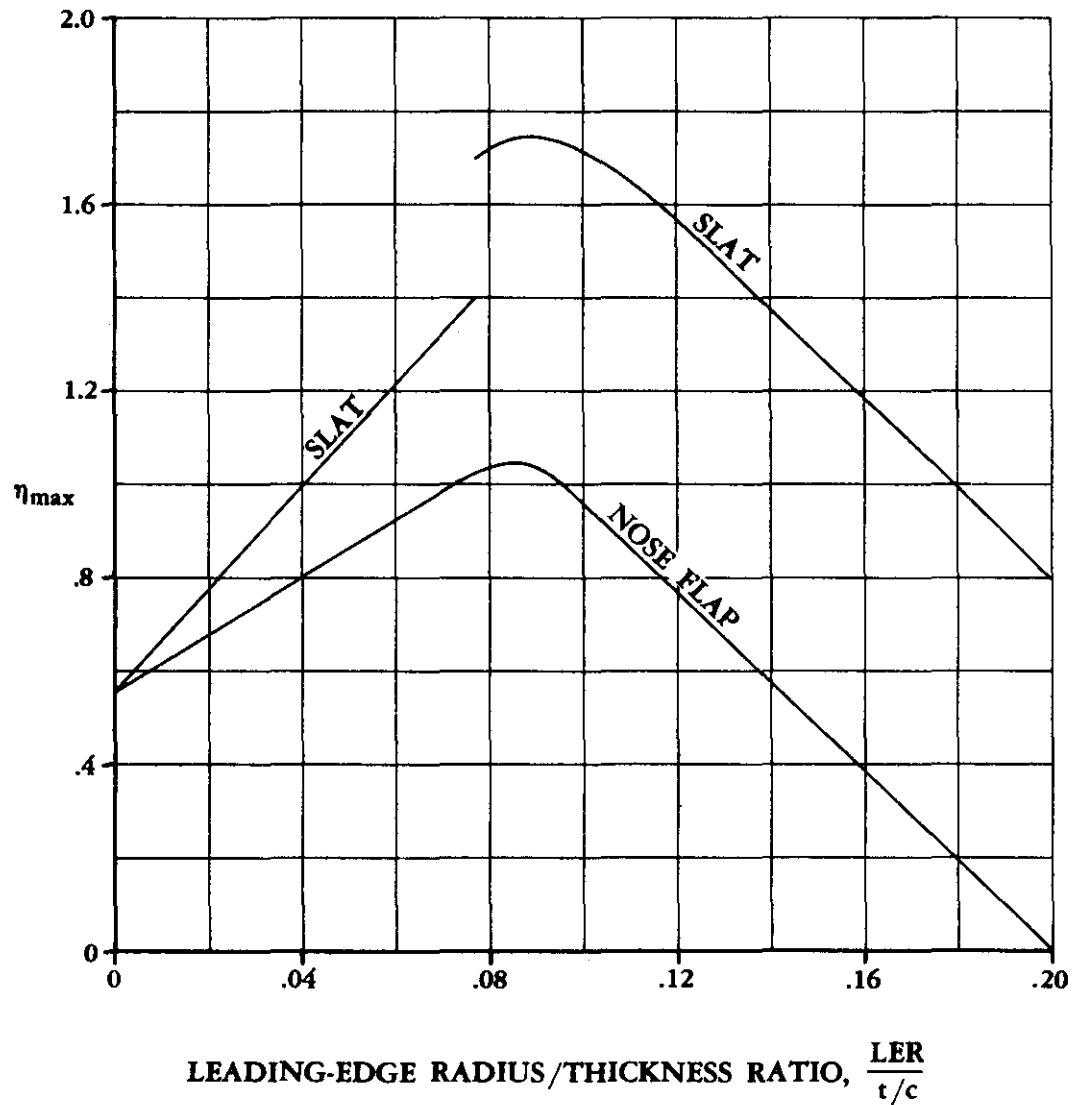


FIGURE 6.1.1.3-15 MAXIMUM-LIFT EFFICIENCY FOR LEADING-EDGE DEVICES

## LEADING-EDGE FLAPS AND SLATS

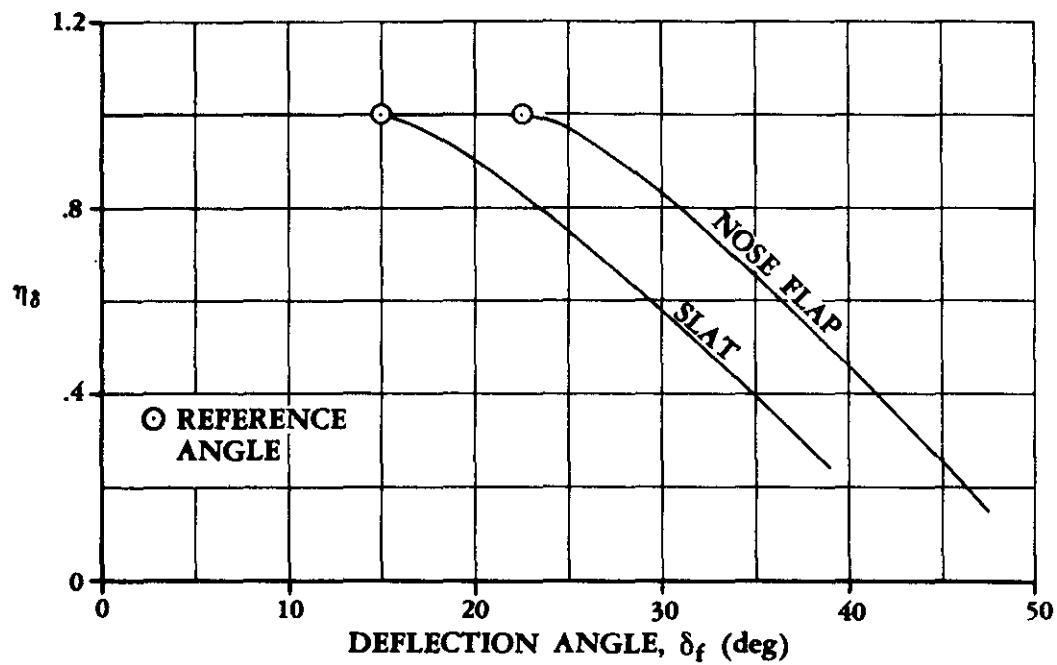


FIGURE 6.1.1.3-16 DEFLECTION-ANGLE CORRECTION FACTOR

## 6.1.2 SECTION PITCHING MOMENT WITH HIGH-LIFT AND CONTROL DEVICES

### 6.1.2.1 SECTION PITCHING-MOMENT INCREMENT $\Delta c_m$ DUE TO HIGH-LIFT AND CONTROL DEVICES

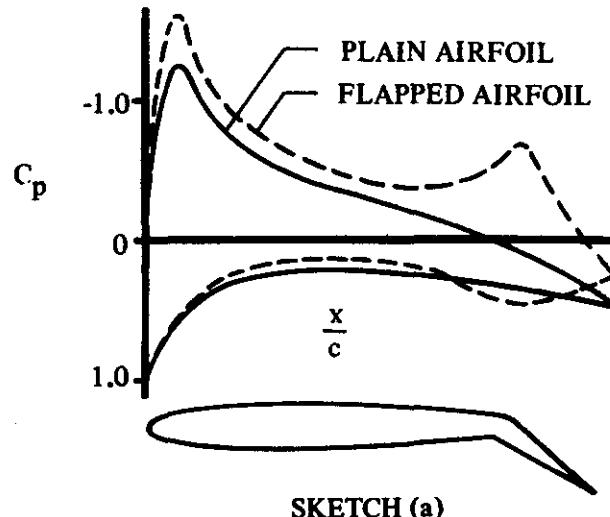
The use of high-lift and control devices alters the basic airfoil load distribution, thus affecting the section pitching moment, as well as the lift.

Methods are presented in this section for estimating the pitching-moment characteristics for most common high-lift devices in use today and for some of the blown flaps being considered for STOL aircraft. These methods are valid only in the subsonic regime in the linear-lift region (preferably near zero angle of attack). The effect of these devices on the variation of pitching moment with angle of attack is presented in Section 6.1.2.2, except for the jet flap, which is presented in this section. Considerations of clarity and simplicity of presentation dictated this deviation from standard Datcom practice.

The assumption is made that the characteristics of a trailing-edge flap are independent of any leading-edge device, and/or the characteristics of a leading-edge device are independent of any mechanical trailing-edge flap. In reality this is not quite true, but the methods of this section are not sufficiently refined to account for these interference effects. This assumption cannot be justified in the case of the more powerful jet flap.

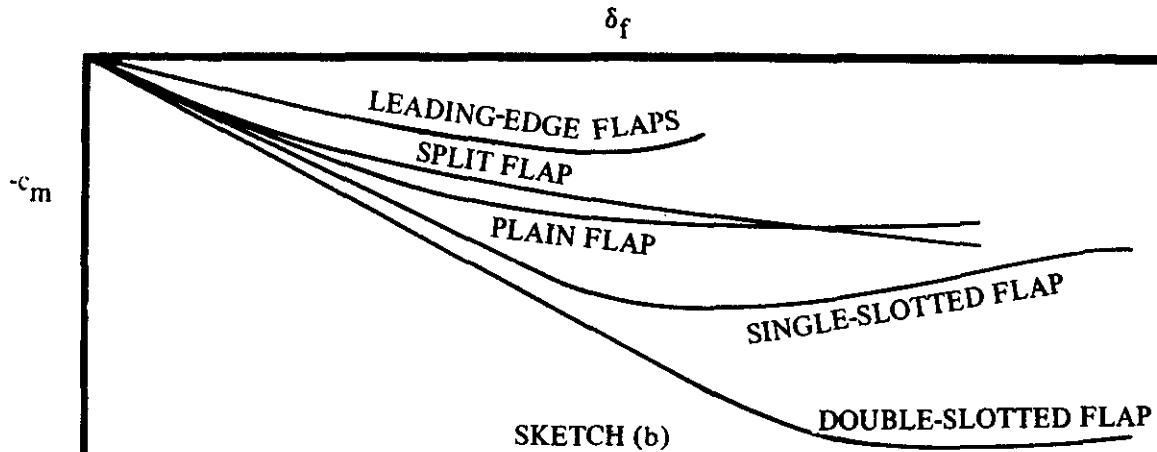
#### Trailing-Edge Mechanical Flaps

Sketch (a) shows a typical loading on an airfoil with a plain flap deflected and undeflected. The incremental load due to the flap exhibits a peak over the airfoil leading edge and a peak over the hinge line. The higher loading at the hinge predominates, giving a nose-down moment.



For conditions where the flow is attached, the center-of-pressure location of the additional load due to flaps does not shift position with flap deflection. Therefore, the pitching moment is directly proportional to the lift increment. As the flow breaks down, the center of pressure usually moves forward by a small amount, causing a mild pitch-up. The Datcom method is fairly accurate, even for high values of flap deflection.

Sketch (b) illustrates typical flap pitching-moment curves plotted as a function of flap deflection for a given ratio of flap chord to wing chord. The lift and pitching-moment variation with flap angle are usually linear as long as the flow is attached. Plain flaps maintain attached flow and exhibit linear characteristics at small angles of attack and flap deflections. Single-, double-, and triple-slotted flaps assure attached flow for increasingly higher angles of incidence and flap deflections and give linear characteristics over a much larger range. Split flaps have no significant range of linear characteristics as a result of the wide wake caused by the split trailing edge.



Theoretically, the center-of-pressure location is a function of the ratio of the flap chord to airfoil chord, showing a forward shift with increasing flap-chord ratios. Although test data for plain and split flaps do not match the theoretical center-of-pressure location, they do show the same trend as theory. Slotted flaps do not follow this trend. Data for slotted flaps were analyzed for extended airfoil chords of 10 to 40 percent. Virtually all of the data indicated a center-of-pressure location between 41 and 47 percent of the extended airfoil chord, showing no dependence upon the ratio of flap chord to airfoil chord. Therefore, an average center-of-pressure location of 44 percent has been assumed (see Figure 6.1.2.1-35a) for all slotted flaps, independent of the ratio of flap chord to airfoil chord.

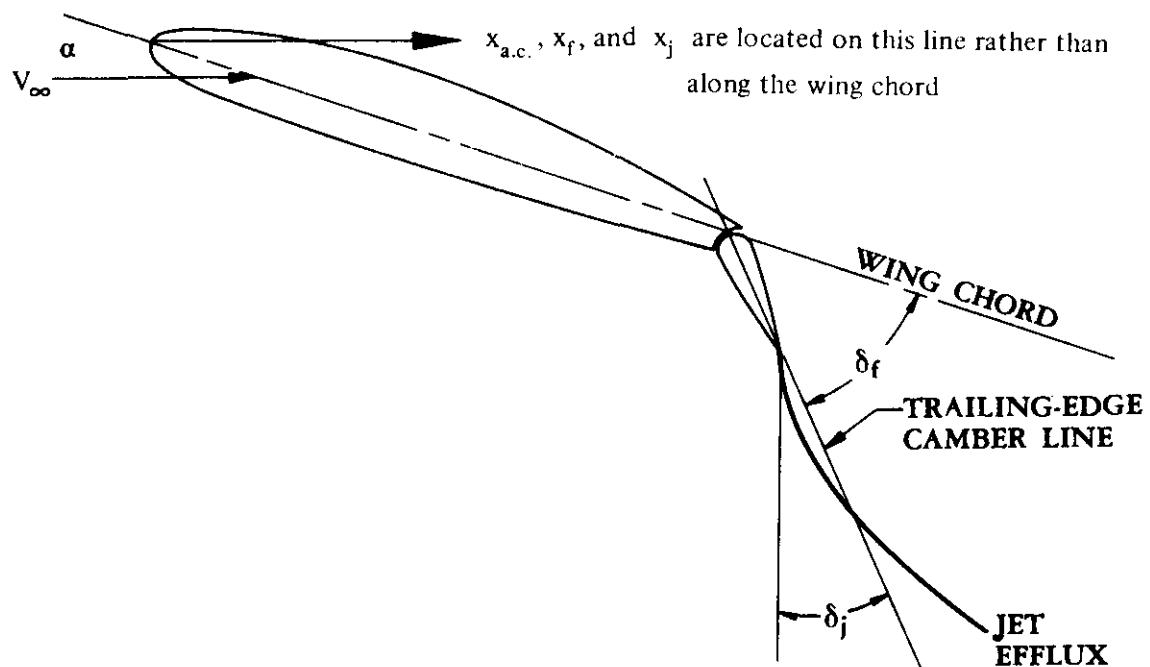
#### Leading-Edge Mechanical Devices

Leading-edge devices produce a nose-down pitching moment, similar to trailing-edge flaps, because they delay the stall by lowering the high peak loading at the leading edge. The method presented is for conventional leading-edge devices, based on thin-wing theory from Reference 1. Efforts to substantiate this method by using available test data have proved unsatisfactory. The test data exhibit nonlinear characteristics which linear theory is intrinsically unable to handle. Therefore, this method should be applied only to thin airfoils with small leading-edge devices.

#### Jet Flaps

The pitching-moment increment for a jet-flap airfoil is dependent upon the jet momentum trailing-edge coefficient  $C'_\mu$  and the ratio of flap chord to the extended wing chord. The method presented herein is Spence's adaptation of thin-airfoil theory as presented in Reference 2. In summary, Spence applies thin-airfoil theory to inviscid, incompressible flow past a thin, two-dimensional wing at small incidence, with a jet emerging at a small angle of incidence from the trailing edge. The flow inside the jet is assumed to be irrotational. In addition, the jet is bounded by vortex sheets that prevent mixing with the mainstream and maintains finite momentum as its thickness decreases to zero. For flaps that extend as well as rotate, a correction is applied to account for the increased chord length.

The definitions of aerodynamic center  $x_{a.c.}$  and center of pressure  $x_{c.p.}$  are well established for conventional aircraft. However, for jet-flap configurations the jet reaction is a new component that must be accounted for when considering the location of the aerodynamic center and center of pressure. In order to maintain consistency, the Datcom defines the aerodynamic center for jet-flap configurations as that point about which the *total* pitching moment is invariant with the *total* lift; i.e.,  $dC_m/dC_L = 0$  at a given Mach number and trailing-edge jet momentum coefficient. In essence, the aerodynamic center is a function of the trailing-edge jet momentum coefficient  $C_\mu$ . For conventional wing sections the aerodynamic center is located on the wing chord line. However, for jet-flap configurations it becomes necessary to define the measurement of  $x_{a.c.}$  off the wing-chord line, as shown in Sketch (c), to simplify the calculation of the pitching moment about any reference location.



$$\frac{x_f}{c} = -\frac{c_m \delta_f}{c_{\ell \delta_f}} \quad \frac{x_j}{c} = -\frac{c_m \delta_j}{c_{\ell \delta_j}}$$

where

$c_{m \delta_f}$  is the flap pitching-moment effectiveness measured about the leading edge.

$c_{\ell \delta_f}$  is the rate of change of section lift effectiveness due to flap deflection.

$c_{m \delta_j}$  is the rate of change of pitching-moment coefficient measured about the leading edge with respect to the jet deflection. (The parameters  $c_{m \delta_j}$  and  $c_{\ell \delta_j}$  are due to the jet efflux not being emitted at the same angle as the trailing-edge camber line, i.e., the flap deflection.)

$c_{\ell \delta_j}$  is the rate of change of section lift coefficient with respect to the jet deflection.

#### SKETCH (c) JET-FLAP AERODYNAMIC CENTER AND CENTER OF LIFT

There are two additional parameters shown and defined in Sketch (c),  $x_f$  and  $x_j$ . The center-of-lift term  $x_f$  is analogous to the conventional flap center-of-pressure location, except that it also includes the reaction component of the jet. For this reason it is not the true "center-of-pressure location"; i.e., it is the location where the total lift increment due to flap deflection is assumed to act.

The term  $x_j$  is analogous to a center-of-pressure location of the incremental load due to the jet efflux acting at an angle to the trailing-edge camber line. However, it is not a true center-of-pressure location for this incremental load, because of the inclusion of the reaction component; therefore, it is also referred to as the center of lift.

For more details regarding the fundamental concepts of jet flaps, the reader is referred to the discussion presented in Section 6.1.1.1. (Sketch (b) of Section 6.1.1.1 illustrates some of the blown-flap concepts now being investigated for STOL aircraft.)

### Spoilers

Pitching-moment changes due to spoilers are generally smaller than those for flap-type control surfaces. For this reason they are useful on thin, swept wings where wing twist due to control deflection is a problem. Many wind-tunnel programs have therefore been conducted on swept wings, but few have been conducted on airfoil sections. Reference 3, published in 1953, contains a comprehensive bibliography of spoiler studies made up to that time.

Because of the scarcity of two-dimensional spoiler data, no generalized methods are presented in this section for section pitching moment due to spoiler deflection.

## DATCOM METHODS

### 1. Trailing-Edge Mechanical Flaps

Two methods are presented for estimating the section pitching-moment increment due to the deflection of mechanical trailing-edge flaps. Method 1 is applicable to plain, split, and multislotted flaps with or without extensible flaps. Method 2 is applicable only to plain flaps.

In view of the ease of application of Method 2 and the fact that it predicts plain-flap section pitching moments as accurately as Method 1 does, Method 2 is the preferred Datcom plain-flap method.

#### Method 1 (Plain, Split, and Multislotted Flaps)

This method is empirical in nature and limited to the low-speed regime. The section pitching-moment increment due to trailing-edge flaps, based on the square of the wing chord  $c^2$ , is given by

$$\Delta c_m = \Delta c_2 \left[ \frac{x_{ref}}{c} - \left( \frac{x_{c.p.}}{c'} \right) \left( \frac{c}{c} \right) \right] \quad 6.1.2.1-a$$

where

$\Delta c_2$  is the lift increment for a given flap type and deflection, from test data or as determined by the appropriate method of Section 6.1.1.1.

$$\frac{x_{ref}}{c}$$

is the desired pitching-moment reference point expressed as a fraction of the basic airfoil chord, measured positive aft from the airfoil leading edge, parallel to the wing chord.

$$\frac{x_{c,p.}}{c}$$

is the center-of-pressure location of the incremental load due to flaps, expressed as a fraction of the extended airfoil chord, measured positive aft from the airfoil leading edge, parallel to the wing chord. This parameter is obtained from Figure 6.1.2.1-35a as a function of the ratio of flap chord to airfoil chord  $c_f/c$ .

$$\frac{c'}{c}$$

is the ratio of the extended wing chord to the airfoil chord as shown in Figures 6.1.1.1-44 through -46.

A comparison of low-speed test data with calculated values of  $\Delta c_m$  using this method is presented in Tables 6.1.2.1-A and -C through -E.

### Method 2 (Plain Flaps)

Pitching-moment increments for plain trailing-edge flaps are presented in Figure 6.1.2.1-35b. These increments are given about the quarter-chord, based on the square of the airfoil chord  $c^2$ , as a function of flap deflection and the ratio of flap chord to airfoil chord  $c_f/c$ . This figure is limited to the linear-lift range and subcritical Mach numbers.

A comparison of low-speed test data with  $\Delta c_m$  calculated by this method is presented in Table 6.1.2.1-B.

## 2. Conventional Leading-Edge Devices

The section pitching-moment increment due to mechanical leading-edge devices, based on the square of the wing chord  $c^2$ , is given by thin-airfoil theory as

$$\begin{aligned} \Delta c_{m,LE} = & c'_{m,LE} \left( \frac{c'}{c} \right)^2 \delta_{f,LE} + \left( \frac{x_{ref}}{c} + \frac{c' - c}{c} \right) \Delta c_\ell \\ & + c_m \left[ \left( \frac{c'}{c} \right)^2 - 1 \right] + 0.75 c_\ell \left( \frac{c'}{c} \right) \left( \frac{c'}{c} - 1 \right) \end{aligned} \quad 6.1.2.1-b$$

where

$$c'_{m,LE}$$

is the theoretical flap pitching-moment effectiveness (about the leading edge), obtained from Figure 6.1.2.1-36 as a function of the ratio of the leading-edge flap chord to the extended airfoil chord  $c_{f,LE}/c'$ .

$$\frac{c'}{c}$$

is the ratio of the extended wing chord to the basic airfoil chord as shown in Figure 6.1.1.1-51.

$$\delta_{f,LE}$$

is the deflection of the leading-edge device in degrees (see Figure 6.1.1.1-51).

$\frac{x_{ref}}{c}$  is the desired pitching-moment reference point expressed as a fraction of the basic airfoil chord, measured positive aft from the airfoil leading edge with the leading-edge device retracted, parallel to the wing chord.

$\Delta c_q$  is the lift increment due to a given leading-edge-device deflection, from test data or as determined by the appropriate method in Section 6.1.1.1, based on  $c$ .

$c_m$  is the section pitching-moment coefficient with the flaps retracted, based on  $c^2$ . This parameter should be obtained from the test data, if available, or from Section 4.1.2.1.

$c_q$  is the section lift coefficient with the flaps retracted, based on  $c$ . This parameter should be obtained from test data, if available, or from Sections 4.1.1.1 and 4.1.1.2.

The use of this method is demonstrated in Sample Problem 3.

### 3. Jet Flaps

Methods that are adaptable to a handbook application are not available for all jet-flap schemes. The method presented below is applicable to the pure jet-flap concept, and the internally-blown-flap (IBF) and externally-blown-flap (EBF) concepts with a plain trailing-edge flap. For an IBF or EBF concept with a single-slotted or multislotted flap configuration, this method should be used only as a first approximation. No handbook method is currently available to analyze the section pitching-moment increment due to an augmentor-wing concept.

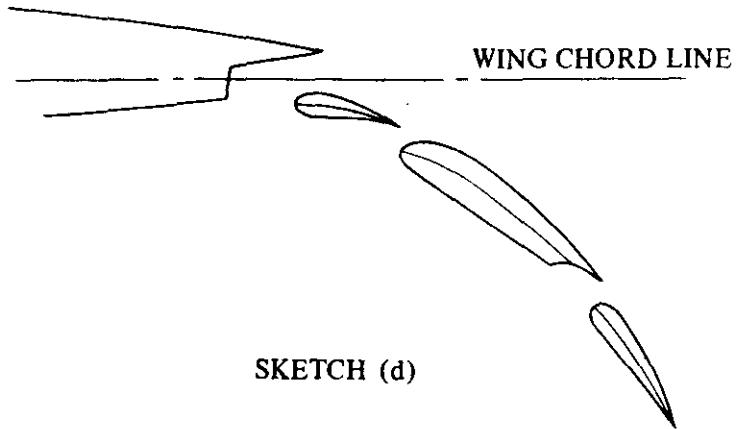
For EBF flaps the user is cautioned that if the flap does not "capture" or "intercept" all of the jet exhaust, the result of this method may be erroneous. Reference 57 considers a design where part of the jet passes below the flap. Furthermore, a technique to be used in analyzing such a design is proposed. Unfortunately, this technique is cumbersome, and no satisfactory cases to check its accuracy have been found in the available literature. Therefore, it is not included in the Datcom. It should be noted, however, that the lack of such a technique is not a serious restriction, since most configurations avoid the problem by use of jet deflectors and/or canted thrust axes to ensure that the entire engine exhaust is flattened and directed at the flap knee.

It should be noted that the airfoil thickness correction used in the method of Section 6.1.1.1 in determining the section lift increment of a jet-flap combination (see Equation 6.1.1.1-p) does not apply to the section pitching moment. Therefore, the lift coefficients calculated in this section for use in determining section pitching moment are not the same as those calculated in Sections 6.1.1.1 and 6.1.1.2 and should be considered only as intermediate values generated during the calculation of the pitching moment. The actual lift of the airfoil must be calculated by using the more exact procedures of Sections 6.1.1.1 and 6.1.1.2.

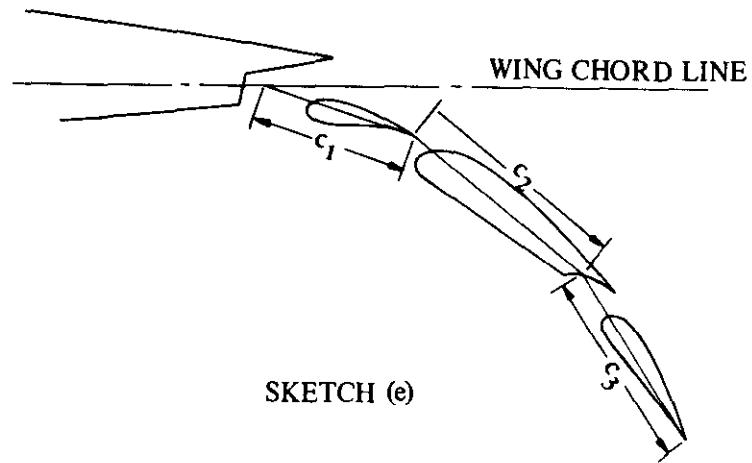
The user is reminded that the theory on which this method is based is linear and as such cannot predict any nonlinearities; e.g., those that may arise from separated flow.

The flap deflection angles and the flap-chord values to be used in this method are not defined in the conventional manner. Instead, the user must use his best judgment to approximate the particular flap system by constructing a simple-hinged multideflected flap system. The primary goal of the simple-hinged multideflected flap system is to duplicate the mean-camber-line distribution of the actual flap system. A schematic illustration is presented in the following discussion (Sketches (d) through (f)) that depicts the determination of the flap chords and flap angles for a triple-slotted-flap system. The treatment of less complex flap systems follows from this example.

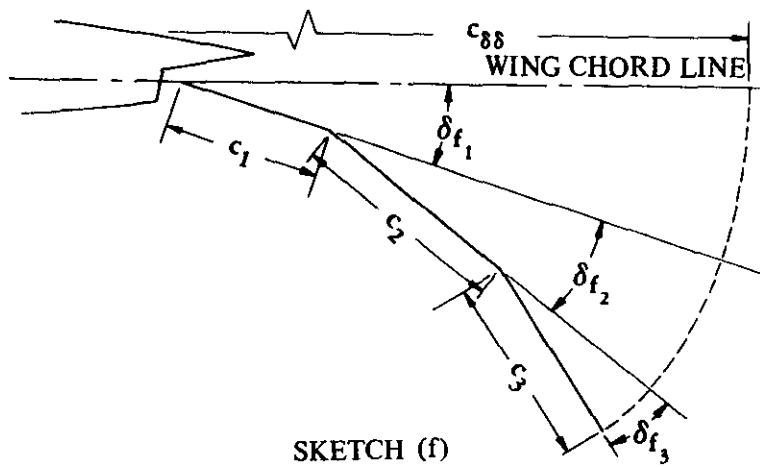
Determine the mean-camber-line distributions of the flap components as in Sketch (d).



Approximate the actual mean-camber-line distribution with straight-line segments (keeping in mind the total mean-camber-line distribution) as in Sketch (e). Extend the straight-line segments until they intersect each other, so as to define the flap-chord lengths as shown.



Determine the flap deflection angles from the straight-line segments relative to the wing chord line as shown in Sketch (f).



The determination of the extended wing-chord  $c_{\delta\delta}$  in Sketch (f) is found by the following procedure. The aft flap segment  $c_3$  is first rotated from its deflected position about the point of intersection of  $c_2$  and  $c_3$ , until the two chords coincide. Then the total chord of  $c_2$  and  $c_3$  is rotated about the intersection of  $c_1$  and  $c_2$  until these two chords coincide. Then the total chord of  $c_1$ ,  $c_2$ , and  $c_3$  is rotated about the intersection of the wing chord and  $c_1$  until it intersects the wing chord.

In the method outlined below, the computation of the pitching moment is broken down into components due to the leading-edge device, the angle of attack, the mechanical flap, and the jet flap. This division can be somewhat misleading because in each term there appears the parameter  $c_{\delta\delta}/c$ , which is the ratio of the airfoil chord with all flaps extended to the basic airfoil chord. Thus each term is actually dependent upon the total extended airfoil chord  $c_{\delta\delta}$ . For example, a change in  $c_{\delta\delta}$  due to a deflection of the leading-edge device will affect the contribution of each component, not just the component due to the leading-edge device.

No substantiation is given for the method presented below; however, the method has been acknowledged in the literature as being accurate to within 10 percent (References 12 and 16). Although an insufficient number of configurations have been analyzed to provide a meaningful substantiation table, the ones that have been analyzed indicate that this method is more accurate in estimating the pitching-moment change with flap angle than in estimating the variation of pitching moment with angle of attack. This may be accounted for by the tendency of wings developing very high lift coefficients to have significant flow separation even at low angles of attack. The variation in the amount of separated flow with angle of attack may be affecting  $c_{m\alpha}$  significantly.

The section pitching-moment increment of an airfoil due to a trailing-edge jet flap at an angle of attack, based on the square of the wing chord  $c^2$ , is given by

$$\Delta c_m = (\Delta c_m)_{\delta f_{LE}} + (\Delta c_m)_\alpha + (\Delta c_m)_{\delta f} + (\Delta c_m)_{\delta j} \quad 6.1.2.1-c$$

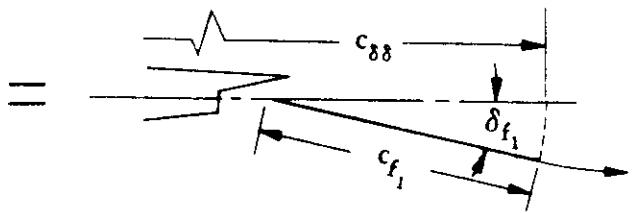
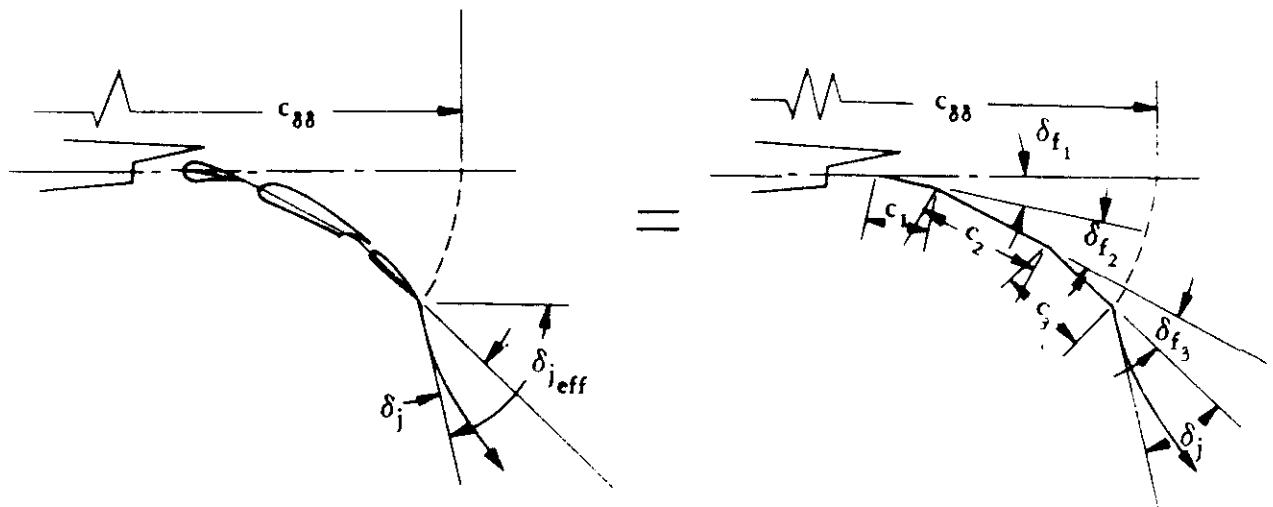
where

$(\Delta c_m)_{\delta f_{LE}}$  is the pitching-moment increment due to the deflection of a leading-edge device. (If there is no leading-edge device,  $(\Delta c_m)_{\delta f_{LE}} = 0$ .)

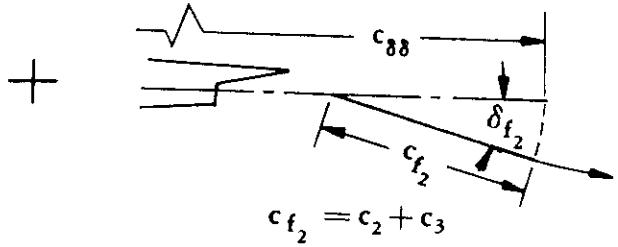
$(\Delta c_m)_\alpha$  is the pitching-moment increment due to the angle of attack of the airfoil. (If  $\alpha = 0$ ,  $(\Delta c_m)_\alpha = 0$ .)

$(\Delta c_m)_{\delta f}$  is the pitching-moment increment due to trailing-edge flaps. The flap system is treated as a series of plain flaps using the principle of superposition. The pitching moments of all of these flaps are then summed to give the total. This is illustrated schematically in Sketch (g) by using a triple-slotted flap. The treatment of less complex flap systems follows from this example. (For airfoils with no trailing-edge mechanical flaps,  $(\Delta c_m)_{\delta f} = 0$ .)

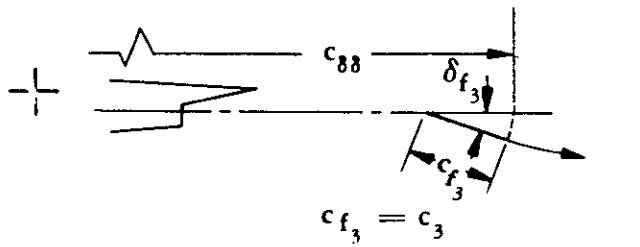
$(\Delta c_m)_{\delta j}$  is the pitching-moment increment due to the jet sheet acting at an angle  $\delta_j$  to the trailing-edge camber line. This term may be present with a pure jet flap, or in the case of EBF and IBF systems where the total turning angle of the jet exceeds the total deflection angle of the mechanical flap segments. (If  $\delta_j = 0$ ,  $(\Delta c_m)_{\delta j} = 0$ .)



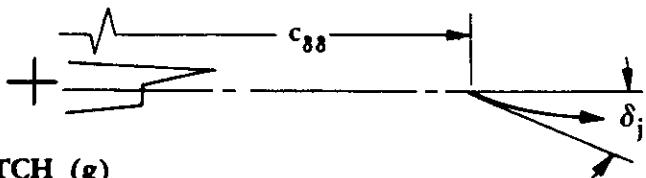
$$c_{f1} = c_1 + c_2 + c_3$$



$$c_{f2} = c_2 + c_3$$



$$c_{f3} = c_3$$



SKETCH (g)

The above terms of Equation 6.1.2.1-c are evaluated by using Steps 1 through 4, respectively, below.

Step 1. Determine  $(\Delta c_m)_{\delta f_{LE}}$  by

$$(\Delta c_m)_{\delta f_{LE}} = \Delta c_1 x_1 - \Delta c_2 x_2 + \Delta c_m_3 \quad 6.1.2.1-d$$

a. Evaluate the following expressions:

$$\Delta c_1 = \frac{\delta f_{LE}}{57.3} K c_{\delta \delta_a} \quad 6.1.2.1-e$$

$$\Delta c_2 = \frac{\delta f_{LE}}{57.3} K c_{\delta \alpha} \quad 6.1.2.1-f$$

where

$\Delta c_1, \Delta c_2$  are terms analogous to section lift coefficients. However, the thickness correction is not applied.

$\delta f_{LE}$  is the deflection of the leading-edge device in degrees, as shown in Figure 6.1.1.1-51.

K is equal to  $c_{\delta \delta}/c$ , the ratio of the extended wing chord to the retracted wing chord. (Note that the extended wing chord includes the extensions of both leading- and trailing-edge flaps. The definition of the extended chord lengths is shown in Figures 6.1.1.1-44 through -46 for trailing-edge flaps and Figure 6.1.1.1-51 for leading-edge flaps.)

$c_{\delta \delta_a}$  is the section lift effectiveness due to the deflection of a hypothetical flap of chord  $c_a$ .

$$c_a = c_{\delta \delta} - c_{f_{LE}} \quad 6.1.2.1-g$$

where  $c_{f_{LE}}$  is the chord of the leading-edge flap defined in Figure 6.1.1.1-51. This parameter is obtained from Figure 6.1.1.1-49 as a function of  $c_a/c_{\delta \delta}$ \* and the trailing-edge jet momentum  $C'_\mu$ .  $C'_\mu$  is the section nondimensional trailing-edge jet momentum coefficient based on the extended airfoil chord

$$c_{\delta \delta}, C'_\mu = C_\mu \frac{c}{c_{\delta \delta}} \text{ (see Sketch (a) Section 6.1.1.1).}$$

\*When using Figure 6.1.1.1-49 in this section, it is necessary to substitute  $c_a/c_{\delta \delta}$  or  $c_f/c_{\delta \delta}$  for  $c_f/c'$  on the figure.

$c_{\delta\alpha}$  is the jet-flap lift-curve slope obtained from Figure 6.1.1.1-49 at  $c_f/c_{\delta\delta} = 1$ ,\* as a function of the trailing-edge jet momentum coefficient  $C'_\mu$ .

b. Determine the corresponding moment arms:

$$x_1 = \frac{x_m}{c} + \left( \frac{c'_{LE}}{c} - 1 \right) - \frac{x_a}{c_{\delta\delta}} \frac{c_{\delta\delta}}{c} \quad 6.1.2.1-h$$

$$x_2 = \frac{x_m}{c} + \left( \frac{c'_{LE}}{c} - 1 \right) - \frac{x_{a.c.}}{c_{\delta\delta}} \frac{c_{\delta\delta}}{c} \quad 6.1.2.1-i$$

where

$$\frac{x_m}{c}$$

is the desired pitching-moment reference point expressed as a fraction of the basic airfoil chord, measured positive aft from the basic airfoil leading edge, parallel to the wing chord.

$$\frac{c'_{LE}}{c}$$

is the ratio of the airfoil chord with only the leading-edge device extended to the basic airfoil chord.

$$\frac{x_a}{c_{\delta\delta}}$$

is the center-of-lift location of the incremental load due to flap deflection. This parameter is obtained from Figure 6.1.2.1-37 as a function of  $c_a/c_{\delta\delta}$  and the trailing-edge jet momentum  $C'_\mu$ . It is measured positive aft from the extended-airfoil leading edge, parallel to the free stream.

$$\frac{x_{a.c.}}{c_{\delta\delta}}$$

is the aerodynamic-center location obtained from Figure 6.1.2.1-37 at  $c_f/c_{\delta\delta} = 1.0$ , as a function of  $C'_\mu$ . It is measured positive aft from the extended-airfoil leading edge, parallel to the free stream.

$$\frac{c_{\delta\delta}}{c}$$

is defined in Step 1a. (See definition of  $K$ .)

c. Determine  $\Delta c_{m3}$  from

$$\Delta c_{m3} = C_\mu \frac{c_{f,LE}}{c} \sin \delta_{f,LE} \quad 6.1.2.1-j$$

---

\*When using Figure 6.1.1.1-49 in this section, it is necessary to substitute  $c_a/c_{\delta\delta}$  or  $c_f/c_{\delta\delta}$  for  $c_f/c'$  on the figure.

where

$C_\mu$  is the section nondimensional trailing-edge jet momentum coefficient based on the basic airfoil chord (see Sketch (a) Section 6.1.1.1).

$\frac{c_{LE}}{c}$  is the ratio of the chord of the leading-edge flap, as defined in Figure 6.1.1.1-51, to the basic airfoil chord.

$\delta_{LE}$  is defined in Step 1a.

Step 2. Determine  $(\Delta c_m)_\alpha$  by

$$(\Delta c_m)_\alpha = \Delta c_4 x_2 + \Delta c_{m4} \quad 6.1.2.1-k$$

a. Evaluate  $\Delta c_4$  from

$$\Delta c_4 = \frac{\alpha}{57.3} K c_{l\alpha} \quad 6.1.2.1-l$$

where

$\Delta c_4$  is a term analogous to the section lift coefficient. However, the thickness correction is not applied.

$\alpha$  is the angle of attack of the airfoil in degrees.

$K$  and  $c_{l\alpha}$  are defined in Step 1a above.

b. Evaluate  $\Delta c_{m4}$  from

$$\Delta c_{m4} = -C_\mu \left[ \frac{x_m}{c} + \left( \frac{c'_{LE}}{c} - 1 \right) \right] \frac{\alpha}{57.3} \quad 6.1.2.1-m$$

All terms have been previously defined in the preceding steps.

Step 3. Determine  $(\Delta c_m)_{\delta_f}$  from

$$(\Delta c_m)_{\delta_f} = \sum_{i=1}^n (\Delta c_5)_i (x_5)_i \quad 6.1.2.1-n$$

The subscript  $n$  refers to the total flap segments; i.e., in triple-slotted flaps,  $n = 3$ , double-slotted flaps,  $n = 2$ , and single-slotted or plain flaps,  $n = 1$ . The subscript  $i$  refers to a particular flap segment, where the forward segment is 1 and the aft segment is  $n$ .

a. Evaluate  $(\Delta c_s)_i$  from

$$(\Delta c_s)_i = \frac{\delta_{f_i}}{57.3} K c_{\partial f_i} \quad 6.1.2.1-o$$

where

$(\Delta c_s)_i$  is a term analogous to the section lift coefficient. However, the thickness correction is not applied.

$\delta_{f_i}$  is the deflection of the  $i^{\text{th}}$  flap segment in degrees. The value of the last flap segment used in this instance depends upon the effective jet angle  $\delta_{\text{eff}}$ , determined by using Equation 6.1.4.1-d

of Section 6.1.4.1 or obtained from test data. If  $\delta_{\text{eff}} > \sum_{i=1}^n \delta_{f_i}$ ,

then the last flap deflection is that determined from constructing the straight line elements relative to the wing-chord line as

depicted in Sketches (f) and (g). If  $\delta_{\text{eff}} \leq \sum_{i=1}^n \delta_{f_i}$ , then the last

flap deflection is given by

$$\delta_{f_n} = \delta_{\text{eff}} - \sum_{i=1}^{n-1} \delta_{f_i} \quad 6.1.2.1-p$$

$c_{\partial f_i}$  is the rate of change of section lift coefficient with respect to flap deflection. The value is obtained from Figure 6.1.1.1-49 as a function of the trailing-edge jet momentum coefficient  $C'_\mu$  and the ratio of the flap chord (of the  $i^{\text{th}}$  flap segment) to the extended airfoil chord  $c_{f_i}/c_{\delta\delta}$ . For flaps with Fowler-type motion, the flap chord is defined as shown in Sketch (g).

$K$  is defined in Step 1a.

b. Determine the corresponding moment arm

$$(x_s)_i = \frac{x_m}{c} + \left( \frac{c'_{LE}}{c} - 1 \right) - \frac{x_{f_i}}{c_{\delta\delta}} \frac{c_{\delta\delta}}{c} \quad 6.1.2.1-q$$

where

$$\frac{x_{f_i}}{c_{\delta\delta}}$$

is the center-of-lift location of the incremental load due to the deflection of the  $i^{\text{th}}$  flap segment. This parameter is obtained from Figure 6.1.2.1-37 as a function of the trailing-edge jet momentum  $C'_\mu$  and the ratio of the flap chord to the extended wing-chord  $c_{f_i}/c_{\delta\delta}$ .

All other terms have been defined in Step 1b above.

Step 4. Determine  $(\Delta c_m)_{\delta_j}$  from

$$(\Delta c_m)_{\delta_j} = \Delta c_6 x_6$$

6.1.2.1-r

a. Evaluate  $\Delta c_6$  from

$$\Delta c_6 = \frac{\delta_j}{57.3} K c_{\alpha_{\delta_j}}$$

6.1.2.1-s

where

$$\Delta c_6$$

is a term analogous to the section lift coefficient. However, the thickness correction is not applied.

$$\delta_j$$

is the deflection of a pure jet flap, in degrees, relative to the trailing-edge camber line (see Sketch (g)). For IBF and EBF systems if

$$\delta_{j_{\text{eff}}} > \sum_{i=1}^n \delta_{f_i}, \text{ then}$$

$$\delta_j = \delta_{j_{\text{eff}}} - \sum_{i=1}^n \delta_{f_i}$$

6.1.2.1-t

If not, then  $\delta_j = 0$ . Terms are defined in Step 3a.

$$c_{\alpha_{\delta_j}}$$

is the rate of change of section lift coefficient with respect to jet deflection, obtained from Figure 6.1.1.1-49 at  $c_f/c_{\delta\delta} = 0$ , as a function of the trailing-edge jet momentum coefficient  $C'_\mu$ .

$$K$$

is defined in Step 1a.

b. Determine the corresponding moment arm

$$x_6 = \frac{x_m}{c} + \left( \frac{c'_{LE}}{c} - 1 \right) - \frac{x_j}{c_{\delta\delta}} \frac{c_{\delta\delta}}{c}$$

6.1.2.1-u

where

$\frac{x_j}{c_{\delta\delta}}$  is the center-of-lift location of the incremental load due to the jet deflection. This parameter is obtained from Figure 6.1.2.1-37 at  $c_f/c_{\delta\delta} = 0$ , as a function of the trailing-edge jet momentum coefficient  $C'_\mu$ .

All other terms have been defined in Step 1b above.

Theoretically, this equation, within the context of linearized theory, is exact only for an airfoil of zero thickness. Unlike the lift equation, no comparable wing-chord thickness correction exists for the pitching-moment increment.

### Sample Problems

#### 1. Plain Trailing-Edge Flap (Method 1)

Given: A flapped airfoil from Reference 11.

$$\text{Clark Y airfoil} \quad c_f/c = 0.30 \quad \delta_f = 45^\circ \quad t/c = 0.117$$

$$R_\ell = 0.61 \times 10^6 \quad \tan \frac{1}{2} \phi'_{TE} = 0.142 \quad x_{ref}/c = 0.25 \quad c'/c = 1.0$$

Compute:

$$(c_{\ell\delta})_{\text{theory}} = 4.51 \text{ per rad} \quad (\text{Figure 6.1.1.1-39a})$$

$$\frac{c_{\ell\alpha}}{(c_{\ell\alpha})_{\text{theory}}} = 0.721 \quad (\text{Figure 4.1.1.2-8a})$$

$$\frac{c_{\ell\delta}}{(c_{\ell\delta})_{\text{theory}}} = 0.516 \quad (\text{Figure 6.1.1.1-39b})$$

$$K' = 0.518 \quad (\text{Figure 6.1.1.1-40})$$

6.1.2.1-15

$$\Delta c_q = \delta_f \left[ \frac{c_{q,\delta}}{(c_{q,\delta})_{\text{theory}}} \right] (c_{q,\delta})_{\text{theory}} K' \quad (\text{Equation 6.1.1.1-c})$$

$$= \frac{45}{57.3} (0.516)(4.51)(0.518)$$

$$= 0.947$$

$$x_{c,p.}/c' = 0.425 \quad (\text{Figure 6.1.2.1-35a})$$

Solution:

$$\Delta c_m = \Delta c_q \left[ \frac{x_{ref}}{c} - \left( \frac{x_{c,p.}}{c'} \right) \left( \frac{c'}{c} \right) \right] \quad (\text{Equation 6.1.2.1-a})$$

$$= (0.947) [0.25 - (0.425)(1)]$$

$$-0.166 \text{ (based on } c^2 \text{ and measured about } c/4)$$

This compares with a test value of  $-0.195$  from Reference 11.

## 2. Plain Trailing-Edge Flap (Method 2)

Given: A flapped airfoil from Reference 40.

$$\text{NACA } 65_1-210 \text{ airfoil} \quad c_f/c = 0.20 \quad \delta_f = 15^\circ \quad x_{ref}/c = 0.25$$

Solution:

$$\Delta c_m = -0.130 \text{ (based on } c^2 \text{ and measured about } c/4) \quad (\text{Figure 6.1.2.1-35b})$$

This compares with a test value of  $-0.142$  from Reference 40.

## 3. Plain Leading-Edge Flap

Given: The flapped airfoil of Reference 9.

$$\text{NACA 0006 airfoil} \quad c_{f,LE}/c = 0.15 \quad \delta_{f,LE} = 20^\circ \quad M = 0.15$$

$$x_{ref}/c = 0.25 \quad \Delta c_q = -0.057 \text{ (Example 8, Section 6.1.1.1)}$$

$$c'/c = 1.0 \quad \alpha = 0 \quad c_q = 0 \quad c_m = 0$$

Compute:

$$c_{m\delta_{LE}} = -0.00116 \text{ per deg} \quad (\text{Figure 6.1.2.1-36})$$

$$\Delta c_{m\delta_{LE}} = c'_{m\delta_{LE}} \left( \frac{c'}{c} \right)^2 \delta_{f_{LE}} + \left[ \frac{x_{ref}}{c} + \frac{c' - c}{c} \right] \Delta c_\ell + c_m \left[ \left( \frac{c'}{c} \right)^2 - 1 \right] + 0.75 c_\ell \left( \frac{c'}{c} \right) \left( \frac{c'}{c} - 1 \right)$$

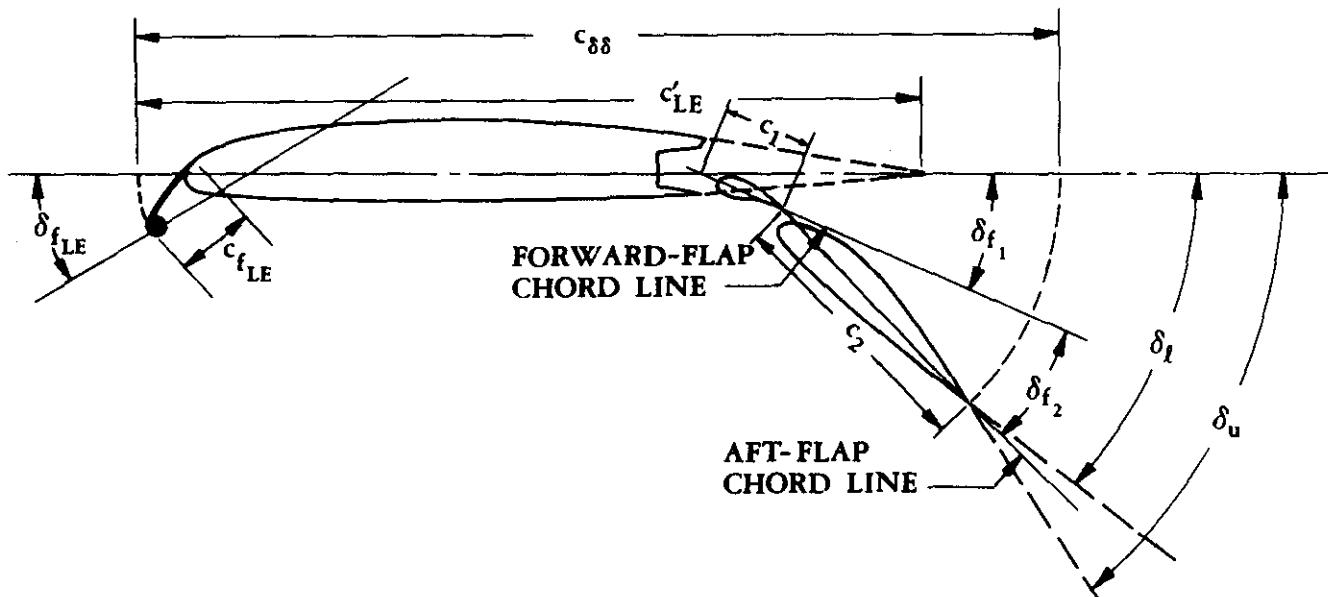
(Equation 6.1.2.1-b)

$$\begin{aligned}
 &= -0.00116 (1.0)^2 (20) + (0.25 + 0)(-0.057) + 0[(1.0)^2 - 1.0] + 0.75 (0)(1)(1 - 1) \\
 &= -0.0232 - 0.0143 \\
 &= -0.0375 \text{ (based on } c^2 \text{ and measured about } c/4)
 \end{aligned}$$

This compares with a test value of -0.026 from Reference 9.

#### 4. Jet Flaps

Given: The IBF airfoil with a double-slotted trailing-edge Fowler flap and leading-edge Krueger flap.



$$C_u = 5.0$$

$$\frac{c_{BB}}{c} = 1.174$$

$$\frac{c_{f_{LE}}}{c} = 0.105$$

$$\frac{c'_{LE}}{c} = 1.068$$

$$\frac{c_2}{c} = 0.306$$

$$\frac{c_1}{c} = 0.074$$

$$\frac{x_m}{c} = 0.25$$

$$\alpha = 3.0^\circ$$

$$\delta_{f_{LE}} = 30^\circ$$

$$\delta_{f_1} = 30^\circ$$

$$\delta_{f_2} = 15^\circ$$

$$\delta_u = 56^\circ$$

$$\delta_\ell = 38^\circ$$

Compute:

Step 1.  $(\Delta c_m)_{\delta f_{LE}}$

$$K = \frac{c_{\delta\delta}}{c} = 1.174$$

$$c_a = c_{\delta\delta} - c_{f_{LE}} \quad (\text{Equation 6.1.2.1-g})$$

$$\frac{c_a}{c_{\delta\delta}} = 1 - \frac{c_{f_{LE}}}{c} \Big/ \frac{c_{\delta\delta}}{c}$$

$$= 1 - \frac{0.105}{1.174}$$

$$= 0.9106$$

$$C'_\mu = \frac{C_\mu}{c_{\delta\delta}/c}$$

$$= \frac{5.0}{1.174}$$

$$= 4.259$$

$$\left. \begin{array}{l} c_{q_{\delta_a}} = 13.83 \text{ per rad} \\ c_{q_\alpha} = 14.00 \text{ per rad} \end{array} \right\} \quad (\text{Figure 6.1.1.1-49})$$

$$\Delta c_1 = \frac{\delta f_{LE}}{57.3} K c_{q_{\delta_a}} \quad (\text{Equation 6.1.2.1-e})$$

$$= \frac{30}{57.3} (1.174)(13.83)$$

$$= 8.501$$

$$\Delta c_2 = \frac{\delta f_{LE}}{57.3} K c_{q_\alpha} \quad (\text{Equation 6.1.2.1-f})$$

$$= \frac{30}{57.3} (1.174)(14.00)$$

$$= 8.605$$

$$\left. \begin{array}{l} \frac{x_a}{c_{\delta\delta}} = 0.235 \\ \frac{x_{a.c.}}{c_{\delta\delta}} = 0.202 \end{array} \right\} \quad (\text{Figure 6.1.2.1-37})$$

$$x_1 = \frac{x_m}{c} + \left( \frac{c'_{LE}}{c} - 1 \right) - \frac{x_a}{c_{\delta\delta}} \frac{c_{\delta\delta}}{c} \quad (\text{Equation 6.1.2.1-h})$$

$$= 0.25 + (1.068 - 1) - (0.235)(1.174)$$

$$= 0.0421$$

$$x_2 = \frac{x_m}{c} + \left( \frac{c'_{LE}}{c} - 1 \right) - \frac{x_{a.c.}}{c_{\delta\delta}} \frac{c_{\delta\delta}}{c} \quad (\text{Equation 6.1.2.1-i})$$

$$= 0.25 + (1.068 - 1) - (0.202)(1.174)$$

$$= 0.0809$$

$$\Delta c_m = C_\mu \frac{c'_{fLE}}{c} \sin \delta_{fLE} \quad (\text{Equation 6.1.2.1-j})$$

$$= (5.0)(0.105)(\sin 30^\circ)$$

$$= 0.2625$$

$$(\Delta c_m)_{\delta f_{LE}} = \Delta c_1 x_1 - \Delta c_2 x_2 + \Delta c_m \quad (\text{Equation 6.1.2.1-d})$$

$$= (8.501)(0.0421) - (8.605)(0.0809) + (0.2625)$$

$$= -0.0757$$

**Step 2.**  $(\Delta c_m)_\alpha$

$$\Delta c_4 = \frac{\alpha}{57.3} K c_{\varrho_\alpha} \quad (\text{Equation 6.1.2.1-l})$$

$$= \frac{3.0}{57.3} (1.174)(14.00)$$

$$= 0.861$$

$$\begin{aligned}\Delta c_{m4} &= -C_\mu \left[ \frac{x_m}{c} + \left( \frac{c'_{LE}}{c} - 1 \right) \right] \frac{\alpha}{57.3} \quad (\text{Equation 6.1.2.1-m}) \\ &= -(5.0)[0.25 + (1.068 - 1)] \frac{(3.0)}{57.3} \\ &= -0.0832\end{aligned}$$

$$\begin{aligned}(\Delta c_m)_\alpha &= \Delta c_4 x_2 + \Delta c_{m4} \quad (\text{Equation 6.1.2.1-k}) \\ &= (0.861)(0.0809) - 0.0832 \\ &= -0.0135\end{aligned}$$

Step 3.  $(\Delta c_m)_{\delta_f}$

$n = 2$ , since there are two flap segments

$$\begin{aligned}\delta_{\text{eff}} &= \frac{1}{2}(\delta_u + \delta_r) \quad (\text{Equation 6.1.4.1-d}) \\ &= \frac{1}{2}(56 + 38) \\ &= 47^\circ\end{aligned}$$

Therefore, since  $\delta_{\text{eff}} > \sum_{i=1}^n \delta_{f_i} = (\delta_{f_1} + \delta_{f_2}) = 45^\circ$ ,  $\delta_{f_2} = 15^\circ$  (see Step 3a)

$$\frac{c_{f_1}}{c} = \frac{c_1}{c} + \frac{c_2}{c} \quad (\text{See Sketch (g)})$$

$$= 0.074 + 0.306$$

$$= 0.380$$

$$\frac{c_{f_1}}{c_{\delta\delta}} = \frac{c_{f_1}}{c} / \frac{c_{\delta\delta}}{c}$$

$$= 0.380/1.174$$

$$= 0.3237$$

For  $i = 1$  (forward flap segment)

$$c_{\delta\delta f_1} = 12.33 \text{ per rad} \quad (\text{Figure 6.1.1-49})$$

$$(\Delta c_5)_1 = \frac{\delta_{f1}}{57.3} K_{c_{\delta f1}} \quad (\text{Equation 6.1.2.1-o})$$

$$= \frac{30}{57.3} (1.174)(12.33)$$

$$= 7.579$$

$$\frac{x_{f1}}{c_{\delta\delta}} = 0.490 \quad (\text{Figure 6.1.2.1-37})$$

$$(x_{\delta})_1 = \frac{x_m}{c} + \left( \frac{c'_{LE}}{c} - 1 \right) - \frac{x_{f1}}{c_{\delta\delta}} \frac{c_{\delta\delta}}{c} \quad (\text{Equation 6.1.2.1-q})$$

$$= 0.25 + (1.068 - 1) - (0.490)(1.174)$$

$$= -0.2573$$

For i = 2 (aft flap segment)

$$\frac{c_{f2}}{c_{\delta\delta}} = \frac{c_{f2}}{c} / \frac{c_{\delta\delta}}{c}$$

$$= 0.306/1.174 = 0.2606$$

$$c_{\delta f2} = 12.05 \text{ per rad} \quad (\text{Figure 6.1.1.1-49})$$

$$(\Delta c_5)_2 = \frac{\delta_{f2}}{57.3} K_{c_{\delta f2}} \quad (\text{Equation 6.1.2.1-o})$$

$$= \frac{15}{57.3} (1.174)(12.05)$$

$$= 3.703$$

$$\frac{x_{f2}}{c_{\delta\delta}} = 0.521 \quad (\text{Figure 6.1.2.1-37})$$

$$(x_{\delta})_2 = \frac{x_m}{c} + \left( \frac{c'_{LE}}{c} - 1 \right) - \frac{x_{f2}}{c_{\delta\delta}} \frac{c_{\delta\delta}}{c} \quad (\text{Equation 6.1.2.1-q})$$

$$= 0.25 + (1.068 - 1) - (0.521)(1.174)$$

$$= -0.2937$$

$$(\Delta c_m)_{\delta_f} = \sum_{i=1}^n (\Delta c_5)_i (x_5)_i \quad (\text{Equation 6.1.2.1-n})$$

$$\begin{aligned} &= (\Delta c_5)_1 (x_5)_1 + (\Delta c_5)_2 (x_5)_2 \\ &= (7.579)(-0.2573) + (3.703)(-0.2937) \\ &= -3.0376 \end{aligned}$$

**Step 4.**  $(\Delta c_m)_{\delta_j}$

$$c_{\theta_{\delta_j}} = 10.07 \text{ per rad} \quad (\text{Figure 6.1.1.1-49})$$

Since  $\delta_{j_{\text{eff}}} > \sum_{i=1}^n \delta_{f_i}$  (Step 3), then

$$\begin{aligned} \delta_j &= \delta_{j_{\text{eff}}} - \sum_{i=1}^n \delta_{f_i} \\ &= \delta_{j_{\text{eff}}} - (\delta_{f_1} + \delta_{f_2}) \\ &= 47 - (30 + 15) \\ &= 2^\circ \end{aligned}$$

$$\Delta c_6 = \frac{\delta_j}{57.3} K c_{\theta_{\delta_j}} \quad (\text{Equation 6.1.2.1-s})$$

$$\begin{aligned} &= \frac{2}{57.3} (1.174)(10.07) \\ &= 0.4126 \end{aligned}$$

$$\frac{x_j}{c_{\delta\delta}} = 0.658 \quad (\text{Figure 6.1.2.1-37})$$

$$\begin{aligned} x_6 &= \frac{x_m}{c} + \left( \frac{c'_{LE}}{c} - 1 \right) - \frac{x_j}{c_{\delta\delta}} \cdot \frac{c_{\delta\delta}}{c} \quad (\text{Equation 6.1.2.1-u}) \\ &= 0.25 + (1.068 - 1) - (0.658)(1.174) \\ &= -0.4545 \end{aligned}$$

$$(\Delta c_m)_{\delta_j} = \Delta c_6 \times 6 \quad (\text{Equation 6.1.2.1-r})$$

$$= (0.4164)(-0.4545)$$

$$= -0.1875$$

Solution:

$$\Delta c_m = (\Delta c_m)_{\delta_{fLE}} + (\Delta c_m)_\alpha + (\Delta c_m)_{\delta_f} + (\Delta c_m)_{\delta_j} \quad (\text{Equation 6.1.2.1-c})$$

$$= -0.0757 - 0.0135 - 3.0376 - 0.1875$$

$$= -3.314 \quad (\text{based on } c^2)$$

## REFERENCES

1. Hebert, J.: Procedure for Estimating the Aerodynamic Characteristics of Two-Dimensional Passive High Lift Devices. General Dynamics Convair Division TN-70-AVLABS-07, 1970. (U)
2. Hayashi, T. T.: The Two Dimensional Jet Flap Theory. Douglas Aircraft Company, MDC J1089, to be published. (U)
3. Lowry, J. G.: Data on Spoiler-Type Ailerons. NACA RM L53I24a, 1953. (U)
4. Dimmock, N. A.: An Experimental Introduction to the Jet Flap. ARC CP 344, 1957. (U)
5. Spence, D. A.: The Lift on a Thin Airfoil with a Blown Flap. RAE TN Aero 2450, 1956. (U)
6. Cahill, J. F.: Two-Dimensional Wind-Tunnel Investigation of Four Types of High-Lift Flap on an NACA 65-210 Airfoil Section. NACA TN 1191, 1947. (U)
7. Harris, T. A., and Recant, I. G.: Wind-Tunnel Investigation of NACA 23012, 23021, and 23030 Airfoils Equipped with 40-Percent-Chord Double Slotted Flaps. NACA TR 723, 1941. (U)
8. Wenzinger, C. J., and Harris, T. A.: Wind-Tunnel Investigation of NACA 23012, 23021, and 23030 Airfoils with Various Sizes of Split Flap. NACA TR 668, 1939. (U)
9. Gambucci, B. J.: Section Characteristics of the NACA 0006 Airfoil with Leading-Edge and Trailing-Edge Flaps. NACA TN 3797, 1956. (U)
10. Kelly, J. A., and Hayter, N. L. F.: Lift and Pitching Moment at Low Speeds of the NACA 64A010 Airfoil Section Equipped with Various Combinations of a Leading-Edge Slat, Leading-Edge Flap, Split Flap and Double Slotted Flap. NACA TN 3007, 1953. (U)
11. Wenzinger, C. J.: Wind-Tunnel Investigation of Ordinary and Split Flaps on Airfoils of Different Profile. NACA TR 554, 1936. (U)
12. Ramsey, J. C., and Laudeman, E. C.: STOL Tactical Aircraft Investigation State-of-the-Art Design Compendium. Prepared under USAF Contract F33615-71-C-1754, 1971. (U)
13. May, F. W.: State-of-the-Art Design Compendium – STOL Aerodynamic Technology (Internally Blown Flaps). Boeing D180-14299-1, 1972. (U)
14. Kriechbaum, G., et al.: State-of-the-Art Design Compendium – STOL Aerodynamic Technology (Vectorized Thrust and Mechanical Flaps). Boeing D180-14239-1, 1972. (U)

15. Jacobs, W. F., and Paterson, J. H.: The Jet-Flapped Wing in Two- and Three-Dimensional Flow. IAS Preprint 791, 1968. (U)
16. Korbacher, G. K., and Sridhar, K.: A Review of the Jet Flap. UTIA Review No. 14, 1960. (U)
17. Rogallo, F. M.: Collection of Balanced Aileron Test Data. NACA WR L-419, 1944. (U)
18. Rose, L. M., and Altman, J. M.: Low-Speed Experimental Investigation of a Thin Faired, Double-Wedge Airfoil Section with Nose and Trailing-Edge Flaps. NACA TN 1934, 1949. (U)
19. Street, W. G., and Ames, M. B., Jr.: Pressure Distribution Investigation of an NACA 0009 Airfoil with a 50-Percent Chord Plain Flap and Three Tabs. NACA TN 734, 1939. (U)
20. Ames, M. B., Jr. and Sears, R. I.: Pressure-Distribution Investigation of an NACA 0009 Airfoil with a 30-Percent Chord Plain Flap and Three Tabs. NACA TN 759, 1940. (U)
21. Abbott, I. H., and Greenburg, H.: Tests in the Variable-Density Wind Tunnel of the NACA 23012 Airfoil with Plain and Split Flaps. NACA TR 661, 1949. (U)
22. Cahill, J. F., et al.: Aerodynamic Forces and Loadings on Symmetrical Circular-Arc Airfoils with Plain Leading-Edge and Plain Trailing-Edge Flaps. NACA TR 1146, 1953. (U)
23. Harris, T. A., and Purser, P. E.: Wind-Tunnel Investigation of an NACA 23012 Airfoil with Two Sizes of Balanced Split Flap. NACA WR L-441, 1940. (U)
24. Holtzclaw, R. W.: Wind-Tunnel Investigation of the Effects of Spoilers on the Characteristics of a Low-Drag Airfoil Equipped with a 0.25-Chord Slotted Flap. NACA WR A-92, 1945. (U)
25. Holtzclaw, R. W., and Weisman, Y.: Wind-Tunnel Investigation of the Effects of Slot Shape and Flap Location on the Characteristics of a Low-Drag Airfoil Equipped with a 0.25-Chord Slotted Flap. NACA WR A-80, 1944. (U)
26. Swanson, R. S., and Schuldenfrei, M. J.: Wind-Tunnel Investigation of an NACA 23021 Airfoil with Two Sizes of Balanced Split Flaps. NACA WR L-449, 1941. (U)
27. Bogdonoff, S. M.: Tests of Two Models Representing Intermediate Inboard and Outboard Wing Sections of the XB-36 Airplane. NACA WR L-662, 1943. (U)
28. Duschik, F.: Wind-Tunnel Investigation of an NACA 23021 Airfoil with Two Arrangements of a 40-Percent-Chord Slotted Flap. NACA TN 728, 1939. (U)
29. Recant, I. G.: Wind-Tunnel Investigation of an NACA 23030 Airfoil with Various Arrangements of Slotted Flaps. NACA TN 755, 1940. (U)
30. Harris, T. A.: Wind-Tunnel Investigation of an NACA 23012 Airfoil with Two Arrangements of a Wide-Chord Slotted Flap. NACA TN 715, 1939. (U)
31. Lowry, J. G.: Wind-Tunnel Investigation of an NACA 23012 Airfoil with Several Arrangements of Slotted Flaps with Extended Lips. NACA TN 808, 1941. (U)
32. Wenzinger, C. J., and Harris, T. A.: Wind-Tunnel Investigation of an NACA 23021 Airfoil with Various Arrangements of Slotted Flaps. NACA TR 677, 1939. (U)
33. Jones, R., and Bell, A. H.: Further Experiments on an NACA 23021 Aerofoil with a 15-Percent Handley Page Slotted Flap in the Compressed Air Tunnel. ARC R&M 2519, 1954. (U)
34. Harris, T. A., and Lowry, J. G.: Pressure Distribution Over an NACA 23021 Airfoil with a Slotted and a Split Flap. NACA TR 718, 1941. (U)
35. Wenzinger, C. J., and Harris, T. A.: Wind-Tunnel Investigation of an NACA 23012 Airfoil with Various Arrangements of Slotted Flaps. NACA TR 664, 1939. (U)
36. Wenzinger, C. J., and Gauvain, W. E.: Wind-Tunnel Investigation of an NACA 23012 Airfoil with a Slotted Flap and Three Types of Auxiliary Flap. NACA TR 679, 1939. (U)
37. Wenzinger, C. J., and Delano, J. B.: Pressure Distribution Over an NACA 23012 Airfoil with a Slotted and Plain Flap. NACA TR 633, 1938. (U)

38. Stevenson, D. B., and Adler, A. A.: High-Speed Wind-Tunnel Tests of an NACA 0009-64 Airfoil Having a 33.4-Percent Chord Flap with an Overhang 20.1 Percent of the Flap Chord. NACA TN 1417, 1947. (U)
39. Stevenson, D. B., and Byrne, R. W.: High-Speed Wind-Tunnel Tests of an NACA 16-009 Airfoil Having a 32.9-Percent Chord Flap with an Overhang 20.7 Percent of the Flap Chord. NACA TN 1406, 1947. (U)
40. Underwood, W. J., Braslow, A. L., and Cahill, J. F.: Two-Dimensional Wind-Tunnel Investigation of 0.20-Airfoil-Chord Plain Ailerons of Different Contour on an NACA 65<sub>1</sub>-210 Airfoil Section. NACA WR L-151, 1945. (U)
41. Purser, P. E., Fischel, J., and Riebe, J. M.: Wind-Tunnel Investigation of an NACA 23012 Airfoil with a 0.30-Airfoil-Chord Double Slotted Flap. NACA WR L-469, 1943. (U)
42. Fischel, J., and Riebe, J. M.: Wind-Tunnel Investigation of an NACA 23021 Airfoil with a 0.32-Airfoil-Chord Double Slotted Flap. NACA WR L-7, 1944. (U)
43. Cahill, J. F., and Racisz, S. F.: Wind-Tunnel Investigation of Seven Thin NACA Airfoil Sections to Determine Optimum Double-Slotted-Flap Configurations. NACA TN 1545, 1948. (U)
44. Bogdonoff, S. M.: Wind-Tunnel Investigation of a Low-Drag Airfoil Section with a Double Slotted Flap. NACA WR L-697, 1943. (U)
45. Quinn, J. H., Jr.: Wind-Tunnel Investigation of Boundary-Layer Control by Suction on the NACA 66<sub>3</sub>-418,  $a = 1.0$  Airfoil Section with a 0.29-Airfoil-Chord Double Slotted Flap. NACA TN 1071, 1945. (U)
46. Fullmer, F. F.: Wind-Tunnel Investigation of NACA 66(215)-216, 66,1-212 and 65<sub>1</sub>-212 Airfoils with 0.20-Airfoil-Chord Split Flaps. NACA WR L-140, 1944. (U)
47. Gauvain, W. E.: Wind-Tunnel Tests of a Clark Y Wing with "Maxwell" Leading Edge Slots. NACA TN 598, 1937. (U)
48. McKee, P. B., Jr.: Plain and Slotted Leading-Edge Flaps with a Conventional Split Trailing-Edge Flap. WADC TR 6356, Part 1, 1951. (U)
49. Spence, D. A.: Lift Coefficient of a Thin Jet-Flapped Wing. Proc. Roy. Soc., Vol. A238, 1956. (U)
50. Cahill, J. F.: Summary of Section Data on Trailing-Edge High-Lift Devices. NACA TR 938, 1949. (U)
51. James, H. A., and Hunton, L. W.: Estimation of Incremental Pitching Moments Due to Trailing-Edge Flaps on Swept and Triangular Wings. NACA TN 4040, 1957. (U)
52. Sears, R. I.: Wind-Tunnel Data on the Aerodynamic Characteristics of Airplane Control Surfaces. NACA WR L-663, 1943. (U)
53. Cahill, J. F.: Aerodynamic Data for a Wing Section of the Republic XF-12 Airplane Equipped with a Double-Slotted Flap. NACA WR L-544, 1946. (U)
54. Rose, L. M., and Altman, J. M.: Low-Speed Investigation of a Thin, Faired, Double-Wedge Airfoil Section with Nose Flaps of Various Chord. NACA TN 2018, 1950. (U)
55. Kelly, J. A.: Effects of Modifications to the Leading-Edge Region on the Stalling Characteristics of the NACA 63<sub>1</sub>-012 Airfoil Section. NACA TN 2228, 1950. (U)
56. Nuber, R. J., and Gottlieb, S. M.: Two-Dimensional Wind-Tunnel Investigation at High Reynolds Numbers of an NACA 65A006 Airfoil with High-Lift Devices. NACA RM L7K06, 1948. (U)
57. Renselaer, D. J. and Kelly, R.: Aerodynamic Design Compendium for Externally Blown Flaps. North American Rockwell NA-71-1105, 1971. (U)

**TABLE 6.1.2.1-A**  
**PLAIN TRAILING-EDGE FLAP PITCHING-MOMENT EFFECTIVENESS**  
**(METHOD 1)**  
**DATA SUMMARY AND SUBSTANTIATION**

Ref.	Airfoil Section	$c_f/c$	$x_{ref}/c$	$\delta_f$ (deg)	$\Delta c_m$ Calc.	$\Delta c_m$ Test	$\epsilon$ Percent Error
36	23012	0.10	0.238	10 20 30 40 50 60	-0.063 -0.113 -0.134 -0.161 -0.187 -0.212	-0.070 -0.105 -0.130 -0.160 -0.180 -0.195	-10.0 7.6 3.1 0.6 3.9 8.7
11	Clark Y	0.10	0.250	10 30 45 60	-0.041 -0.088 -0.113 -0.137	-0.070 -0.125 -0.159 -0.165	-41.4 -29.6 -28.9 -17.0
35	23012	0.20	0.238	10 20 30 45 60	-0.086 -0.151 -0.173 -0.219 -0.258	-0.090 -0.150 -0.180 -0.215 -0.240	-4.4 0.7 -3.9 1.9 7.5
37	23012	0.20	0.250	15 30	-0.119 -0.163	-0.122 -0.170	-2.5 -4.1
11	23012	0.20	0.250	15 30 45 60	-0.086 -0.116 -0.148 -0.174	-0.130 -0.178 -0.220 -0.235	-33.8 -34.8 -32.7 -26.0
22	Circular Arc 0.06c	0.20	0.250	20 40 60	-0.164 -0.220 -0.280	-0.133 -0.174 -0.220	23.3 26.4 27.3
	Circular Arc 0.10c	0.20	0.250	20 40 60	-0.134 -0.180 -0.230	-0.130 -0.188 -0.220	3.1 -4.3 4.5
40	65 <sub>1</sub> -210	0.20	0.250	5 10 5 10 15 20	-0.048 -0.098 -0.056 -0.110 -0.162 -0.194	-0.062 -0.110 -0.051 -0.101 -0.142 -0.166	-22.6 -10.9 9.8 8.9 14.1 16.9

TABLE 6.1.2.1-A (CONT'D)

Ref.	Airfoil Section	$c_t/c$	$x_{ref}/c$	$\delta_t$ (deg)	$\Delta c_m$ Calc.	$\Delta c_m$ Test	e Percent Error
18	Double Wedge	0.25	0.250	10	-0.107	-0.100	7.0
				20	-0.180	-0.163	10.4
				40	-0.244	-0.194	25.8
				50	-0.278	-0.220	26.4
				60	-0.309	-0.225	37.3
9	0006	0.30	0.250	20	-0.166	-0.180	-7.8
				35	-0.221	-0.205	7.8
				50	-0.257	-0.250	2.8
20	0009	0.30	0.250	10	-0.098	-0.100	-2.0
				20	-0.156	-0.160	-2.5
				30	-0.179	-0.170	5.3
				40	-0.212	-0.200	6.0
				45	-0.201	-0.220	-8.6
11	Clark Y	0.30	0.250	10	-0.068	-0.100	-32.0
				30	-0.125	-0.170	-26.5
				45	-0.166	-0.195	-14.9
				60	-0.189	-0.185	2.2
39	16-009	0.329	0.250	10.3	-0.072	-0.075	-4.0
38	0009-64	0.334	0.250	5.9	-0.048	-0.059	-18.7
				7.9	-0.064	-0.072	-11.7
				9.9	-0.080	-0.089	-10.1
19	0009	0.50	0.250	10	-0.094	-0.086	9.3
				20	-0.129	-0.150	-14.0
				30	-0.153	-0.196	-21.9
				40	-0.183	-0.239	-23.4
				45	-0.198	-0.258	-23.3
$\text{Average Error} = \frac{\sum  e }{n} = 14.2\%$							

**TABLE 6.1.2.1-8**  
**PLAIN TRAILING-EDGE FLAP PITCHING-MOMENT EFFECTIVENESS**  
**(METHOD 2)**  
**DATA SUMMARY AND SUBSTANTIATION**

Ref.	Airfoil Section	$c_f/c$	$\delta_f$ (deg)	$\Delta c_m c/4$ Calc.	$\Delta c_m c/4$ Test	$e$ Percent Error
36	23012	0.10	10	-0.053	-0.073	-27.4
			20	-0.103	-0.110	-6.4
			30	-0.140	-0.137	2.2
			40	-0.162	-0.168	-3.6
			50	-0.173	-0.190	-8.9
			60	-0.178	-0.206	-13.6
11	Clark Y	0.10	10	-0.053	-0.070	-24.3
			30	-0.140	-0.125	12.0
			45	-0.168	-0.159	5.7
			60	-0.178	-0.165	7.9
35	23012	0.20	10	-0.090	-0.094	-4.3
			20	-0.162	-0.158	2.5
			30	-0.200	-0.190	5.3
			45	-0.223	-0.227	-1.8
			60	-0.236	-0.255	-7.5
			15	-0.130	-0.122	6.6
37	23012	0.20	30	-0.200	-0.170	17.6
			15	-0.130	-0.130	0
			30	-0.200	-0.178	12.4
			45	-0.223	-0.220	1.4
11	23012	0.20	60	-0.236	-0.235	0.4
			20	-0.162	-0.133	21.8
			40	-0.217	-0.174	24.7
			60	-0.236	-0.220	7.3
			20	-0.162	-0.130	24.6
			40	-0.217	-0.188	15.4
22	Circular Arc 0.06c	0.20	60	-0.236	-0.220	7.3
			20	-0.162	-0.133	21.8
			40	-0.217	-0.174	24.7
	Circular Arc 0.10c	0.20	60	-0.236	-0.220	7.3
			20	-0.162	-0.130	24.6
			40	-0.217	-0.188	15.4

TABLE 6.1.2.1-B (CONTD)

Ref.	Airfoil Section	c <sub>t</sub> /c	$\delta_t$ (deg)	$\Delta c_{m,c/4}$ Calc.	$\Delta c_{m,c/4}$ Test	e Percent Error
40	65 <sub>1</sub> -210	0.20	5	-0.048	-0.062	-22.6
			10	-0.090	-0.110	-18.2
			5	-0.048	-0.051	-5.9
			10	-0.090	-0.101	-10.9
			15	-0.130	-0.142	-8.5
			20	-0.162	-0.166	-2.4
18	Double Wedge	0.25	10	-0.110	-0.100	10.0
			20	-0.195	-0.163	19.6
			40	-0.268	-0.194	38.1
			50	-0.283	-0.220	28.6
			60	-0.292	-0.225	29.8
9	0006	0.30	20	-0.167	-0.180	-7.2
			35	-0.237	-0.205	15.6
			50	-0.258	-0.250	3.2
20	0009	0.30	10	-0.090	-0.100	-10.0
			20	-0.167	-0.160	4.4
			30	-0.218	-0.170	28.2
			40	-0.243	-0.200	21.5
			45	-0.252	-0.220	14.5
11	Clark Y	0.30	10	-0.090	-0.100	-10.0
			30	-0.218	-0.170	28.2
			45	-0.252	-0.195	29.2
			60	-0.265	-0.185	43.2
39	16-009	0.329	10.3	-0.093	-0.075	24.0
38	0009-64	0.334	5.9	-0.051	-0.059	-13.6
			7.9	-0.070	-0.072	-3.4
			9.9	-0.090	-0.089	1.1
19	0009	0.50	10	-0.077	-0.086	-10.5
			20	-0.144	-0.150	-4.0
			30	-0.195	-0.196	-0.5
			40	-0.235	-0.239	-1.7
			45	-0.250	-0.258	-3.1
$\text{Average Error} = \frac{\sum  e }{n} = 12.6\%$						

**TABLE 6.1.2.1-C**  
**SINGLE-SLOTTED TRAILING-EDGE FLAP PITCHING-MOMENT EFFECTIVENESS**  
**(METHOD 1)**  
**DATA SUMMARY AND SUBSTANTIATION**

Ref.	Airfoil Section	$c_f/c$	$c'/c$	$x_{ref}/c$	$\delta_f$ (deg)	$\Delta c_m$ Calc.	$\Delta c_m$ Test	e Percent Error
23	23012	0.15	1.150	0.238	30	-0.300	-0.300	0
26	23021	0.15	1.150	0.223	60	-0.366	-0.380	-3.7
27	63(420)-222, $a = 0.1$	0.243	1.070	0.260	40	-0.327	-0.300	9.0
23	23012	0.25	1.250	0.238	40	-0.583	-0.620	-6.0
26	23021	0.25	1.250	0.223	40	-0.540	-0.520	3.8
24	66,2-216, $a = 0.6$	0.25	1.029	0.250	10	-0.101	-0.105	-3.8
			1.043		20	-0.204	-0.240	-15.0
			1.058		30	-0.289	-0.327	-11.6
			1.068		40	-0.332	-0.384	-13.5
			1.073		50	-0.338	-0.405	-16.5
25	66,2-216, $a = 0.6$	0.25	1.014	0.260	10	-0.097	-0.112	-13.4
			1.029		20	-0.194	-0.234	-17.1
			1.043		30	-0.276	-0.360	-23.3
			1.058		40	-0.323	-0.410	-21.2
			1.066		50	-0.331	-0.400	-17.3
6	65-210	0.25	1.144	0.250	28.2	-0.359	-0.425	-15.5
			1.141		34.5	-0.404	-0.445	-9.2
			1.135		39.5	-0.420	-0.500	-16.0
			1.146		44.7	-0.428	-0.462	-7.4
					29.1	-0.308	-0.360	-14.4
					39.1	-0.361	-0.420	-14.1
					44.1	-0.363	-0.445	-18.4
					49.1	-0.359	-0.396	-9.1
36	23012	0.257	1.030	0.238	10	-0.110	-0.110	0
			1.050		20	-0.226	-0.240	-5.8
			1.060		30	-0.320	-0.355	-9.9
			1.070		40	-0.377	-0.395	-4.6
			1.080		50	-0.384	-0.355	8.2
21	23021	0.257	1.035	0.223	10	-0.116	-0.130	-10.8
			1.035		20	-0.223	-0.270	-17.4
			1.070		30	-0.324	-0.350	-7.4
			1.070		40	-0.352	-0.400	-12.0
			1.070		50	-0.362	-0.405	-10.6
			1.060		60	-0.377	-0.405	-6.9

TABLE 6.1.2.1-C (CONTD)

Ref.	Airfoil Section	$c_f/c$	$c'/c$	$x_{ref}/c$	$\delta_f$ (deg)	$\Delta c_m$ Calc.	$\Delta c_m$ Test	e Percent Error
21	23021	0.257	1.037	0.223	20	-0.224	-0.255	-12.2
			1.050		30	-0.306	-0.330	-7.3
			1.063		40	-0.345	-0.320	7.8
			1.054		50	-0.347	-0.340	2.1
			1.065		60	-0.381	-0.360	5.8
35	23012	0.267	1.260	0.238	30	-0.533	-0.600	-11.2
31	23012	0.30	1.200	0.238	10	-0.189	-0.205	-7.8
					20	-0.363	-0.325	11.7
					30	-0.502	-0.435	15.4
					40	-0.574	-0.540	6.3
					50	-0.577	-0.560	3.0
			1.310		10	-0.189	-0.220	-14.1
					20	-0.363	-0.395	-8.1
					30	-0.502	-0.500	0.4
					40	-0.574	-0.515	11.5
28	23021	0.40	1.032	0.223	10	-0.148	-0.155	-4.5
					20	-0.320	-0.310	3.2
					30	-0.435	-0.400	8.8
					40	-0.458	-0.390	17.5
					50	-0.505	-0.425	18.8
29	23030	0.40	1.040	0.140	10	-0.203	-0.195	4.1
					20	-0.406	-0.410	-1.0
					30	-0.544	-0.545	-0.2
					40	-0.655	-0.570	14.9
					50	-0.707	-0.650	8.8
30	23012	0.40	1.065	0.238	10	-0.155	-0.145	6.9
					20	-0.323	-0.300	7.7
					30	-0.462	-0.440	5.0
					40	-0.515	-0.355	45.1
					50	-0.519	-0.420	23.6
$\text{Average Error} = \frac{\sum  e }{n} \approx 11.2\%$								

**TABLE 6.1.2.1-D**  
**DOUBLE-SLOTTED TRAILING-EDGE FLAP PITCHING-MOMENT EFFECTIVENESS**  
**(METHOD 1)**  
**DATA SUMMARY AND SUBSTANTIATION**

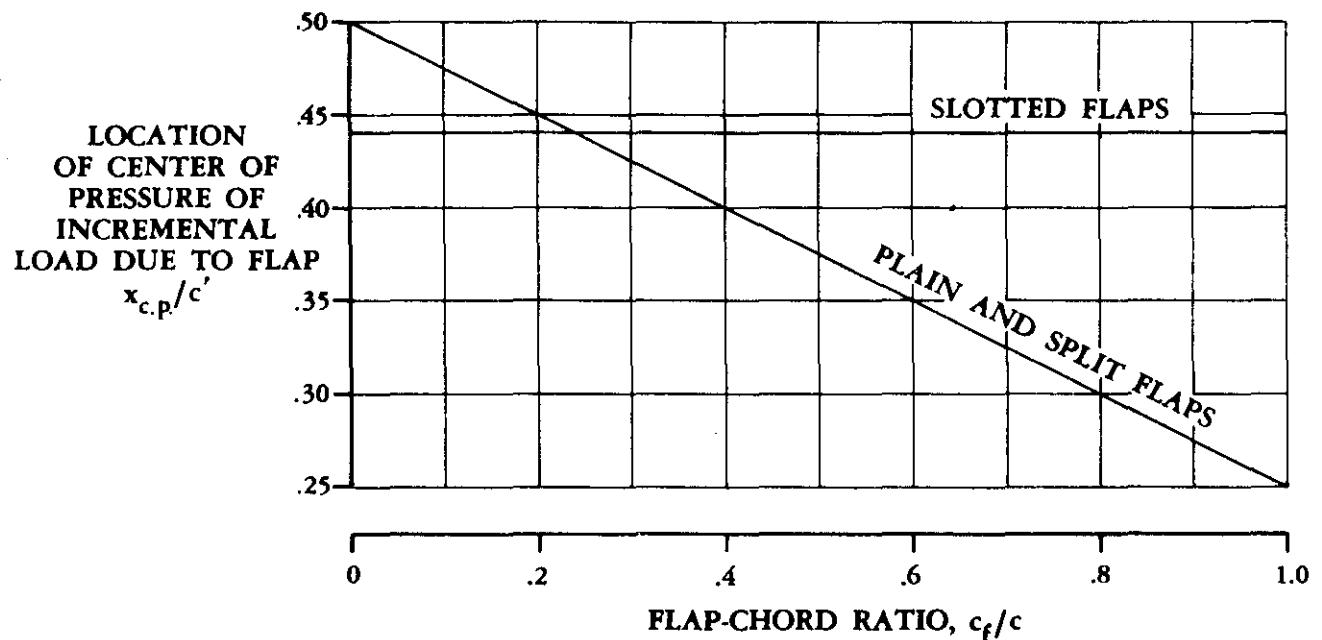
Ref.	Airfoil Section	$c_1/c$	$c_2/c$	$c'/c$	$x_{ref}/c$	$\delta_{r_1}$ (deg)	$\delta_{r_2}$ (deg)	$\Delta c_m$ Calc.	$\Delta c_m$ Test	$\frac{\epsilon}{c} \times 10^3$ Percent Error
41	23012	0.170	0.257	1.221	0.238	25	35	-0.804	-0.713	12.8
42	23021	0.147	0.257	1.229	0.223	30	40	-0.976	-0.773	26.3
43	64-208	0.056	0.250	1.127	0.250	25	25	-0.573	-0.541	5.9
	1410	0.075	0.250	1.141		25	25	-0.595	-0.606	-1.8
	63-210			1.138		25	25	-0.612	-0.578	5.9
	65-210			1.143		25	25	-0.597	-0.584	2.2
	66-210			1.144		25	30	-0.598	-0.583	2.6
	64-208			1.148		30	15	-0.668	-0.568	17.6
	64-212			1.152		30	20	-0.645	-0.606	6.4
	64-210			1.139		30	25	-0.635	-0.633	0.3
	66-210	0.100	0.250	1.172		25	35	-0.675	-0.563	19.9
6	65-210	0.075	0.250	1.139	0.250	15	25	-0.537	-0.550	-2.3
				1.146		20	25	-0.582	-0.583	-0.2
				1.143		25	25	-0.607	-0.590	2.9
				1.148		30	25	-0.640	-0.590	8.5
				1.133		35	25	-0.639	-0.557	14.7
10	64A010	0.075	0.250	1.133	0.250	30	22.7	-0.631	-0.550	14.7
				1.133		30	22.7	-0.631	-0.520	21.4
44	65-118	0.100	0.245	1.175	0.250	23	42	-0.670	-0.714	-6.2
7	23012	0.143	0.257	1.145	0.238	30	20	-0.737	-0.654	12.7
				1.160		30	30	-0.808	-0.703	14.9
				1.110		10	40	-0.509	-0.527	-3.4
				1.110		20	10	-0.459	-0.472	-2.8
				1.115		40	0	-0.545	-0.410	32.9
				1.101		0	30	-0.358	-0.342	4.7
$\text{Average Error} = \frac{\sum  e }{n} = 9.8\%$										

TABLE 6.1.2.1-E  
 SPLIT TRAILING-EDGE FLAP PITCHING-MOMENT EFFECTIVENESS  
 (METHOD 1)  
 DATA SUMMARY AND SUBSTANTIATION

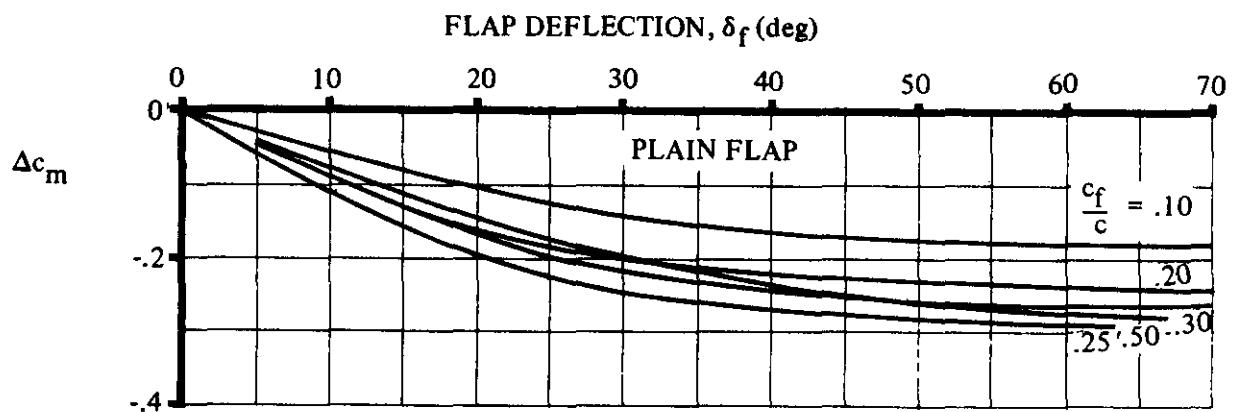
Ref.	Airfoil Section	$c_f/c$	$x_{ref}/c$	$\delta_f$ (deg)	$\Delta c_m$ Calc.	$\Delta c_m$ Test	$\epsilon$ Percent Error
8	23012	0.10	0.238	15	-0.085	-0.085	0
				30	-0.147	-0.145	1.4
				45	-0.185	-0.185	0
				60	-0.211	-0.195	8.2
				75	-0.225	-0.185	21.6
8	23021	0.10	0.223	15	-0.123	-0.080	53.8
				30	-0.207	-0.150	38.0
				45	-0.267	-0.210	27.2
				60	-0.305	-0.250	22.0
				75	-0.328	-0.250	31.2
46	66,1-212	0.20	0.250	40	-0.204	-0.205	-0.5
				50	-0.228	-0.219	4.1
				60	-0.246	-0.235	4.7
				70	-0.258	-0.234	10.3
46	65 <sub>1</sub> -212	0.20	0.250	40	-0.204	-0.191	6.8
				50	-0.228	-0.212	7.5
				60	-0.246	-0.221	11.3
				70	-0.258	-0.211	22.3
46	66(215)-216	0.20	0.250	40	-0.236	-0.232	1.7
				50	-0.264	-0.257	2.7
				60	-0.286	-0.262	9.2
				70	-0.304	-0.264	15.2
21	23012	0.20	0.238	5	-0.036	-0.026	38.5
				10	-0.070	-0.060	16.7
				15	-0.106	-0.090	17.8
				20	-0.134	-0.116	15.5
				30	-0.179	-0.170	5.3
				45	-0.228	-0.214	6.5

TABLE 6.1.2.1-E (CONTD)

Ref.	Airfoil Section	$c_t/c$	$x_{ref}/c$	$\delta_t$ (deg)	$\Delta c_m$ Calc	$\Delta c_m$ Test	$\epsilon$ Percent Error
34	23021	0.20	0.250	15 30 45 60 75	-0.134 -0.224 -0.292 -0.332 -0.358	-0.103 -0.200 -0.252 -0.280 -0.271	30.1 12.0 15.9 18.6 32.1
8	23012	0.30	0.238	15 30 45 60	-0.110 -0.185 -0.236 -0.267	-0.115 -0.185 -0.230 -0.242	-4.3 0 2.6 10.3
8	23021	0.30	0.223	15 30 45 60 75	-0.160 -0.267 -0.345 -0.394 -0.422	-0.140 -0.245 -0.325 -0.360 -0.365	14.3 9.0 6.2 9.4 15.6
8	23012	0.40	0.238	15 30 45 60	-0.110 -0.188 -0.238 -0.269	-0.102 -0.185 -0.230 -0.245	7.8 1.6 3.5 9.8
8	23021	0.40	0.223	15 30 45 60	-0.163 -0.271 -0.350 -0.402	-0.153 -0.272 -0.360 -0.407	6.5 -0.4 -2.8 -1.2
$\text{Average Error} = \frac{\sum  \epsilon }{n} = 12.5\%$							



**FIGURE 6.1.2.1-35a** EMPIRICAL LOCATION OF CENTER OF PRESSURE OF INCREMENTAL LOAD DUE TO TRAILING-EDGE, MECHANICAL FLAPS



**FIGURE 6.1.2.1-35b** EFFECT OF TRAILING-EDGE FLAP DEFLECTION AND FLAP-CHORD-TO-WING-CHORD RATIO ON SECTION INCREMENTAL PITCHING MOMENT DUE TO PLAIN FLAPS

## LEADING-EDGE DEVICES

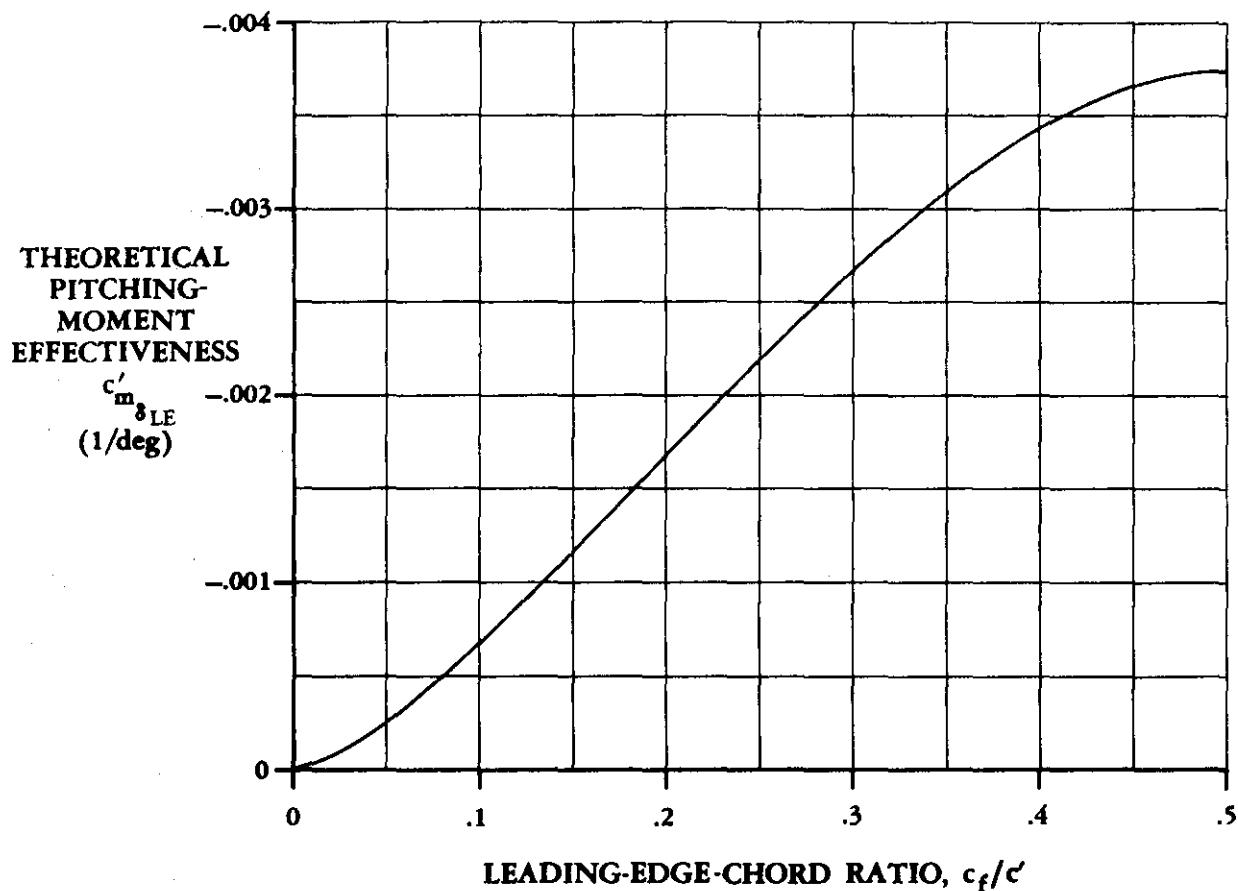


FIGURE 6.1.2.1-36 THEORETICAL PITCHING-MOMENT EFFECTIVENESS OF LEADING-EDGE DEVICES

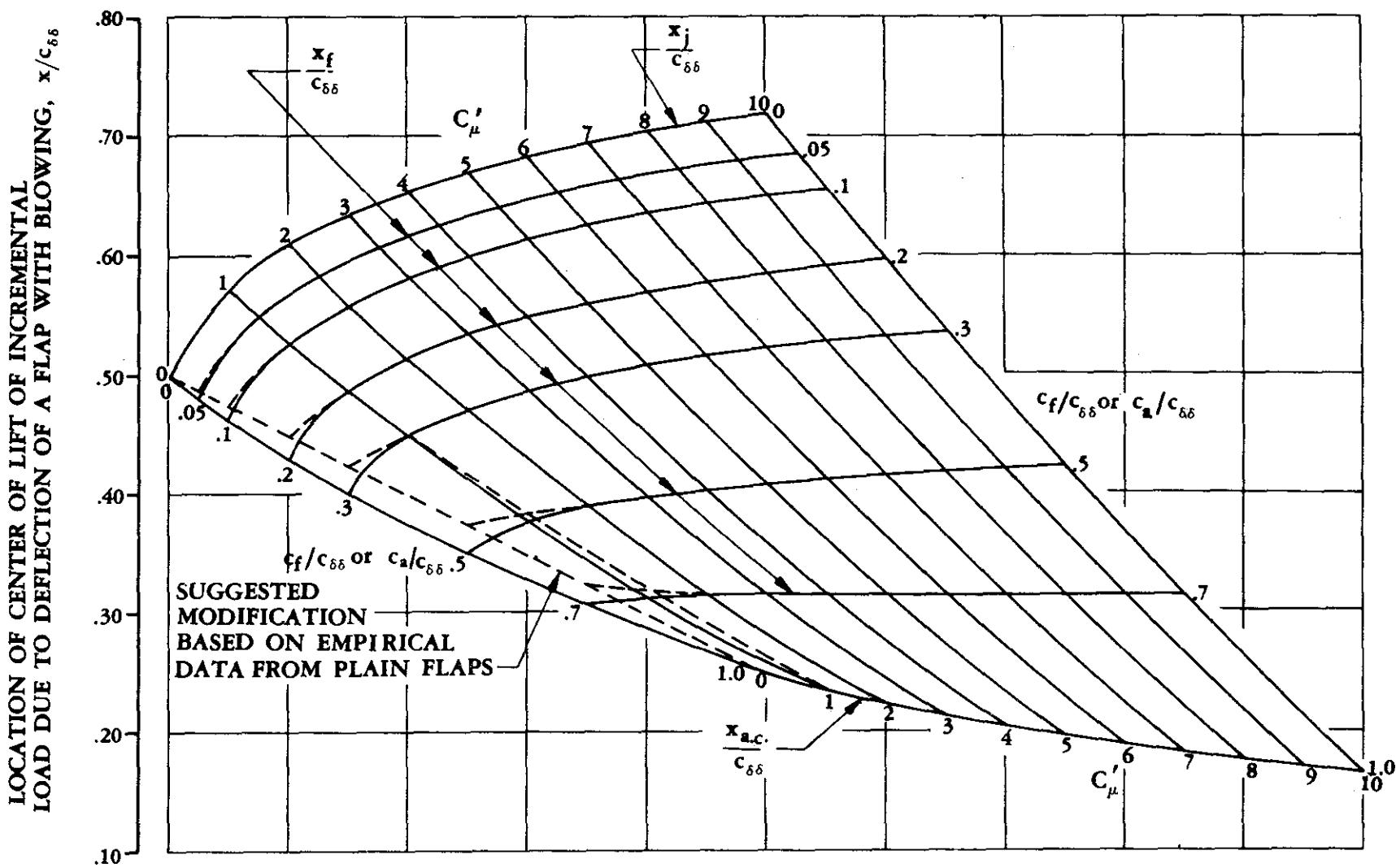


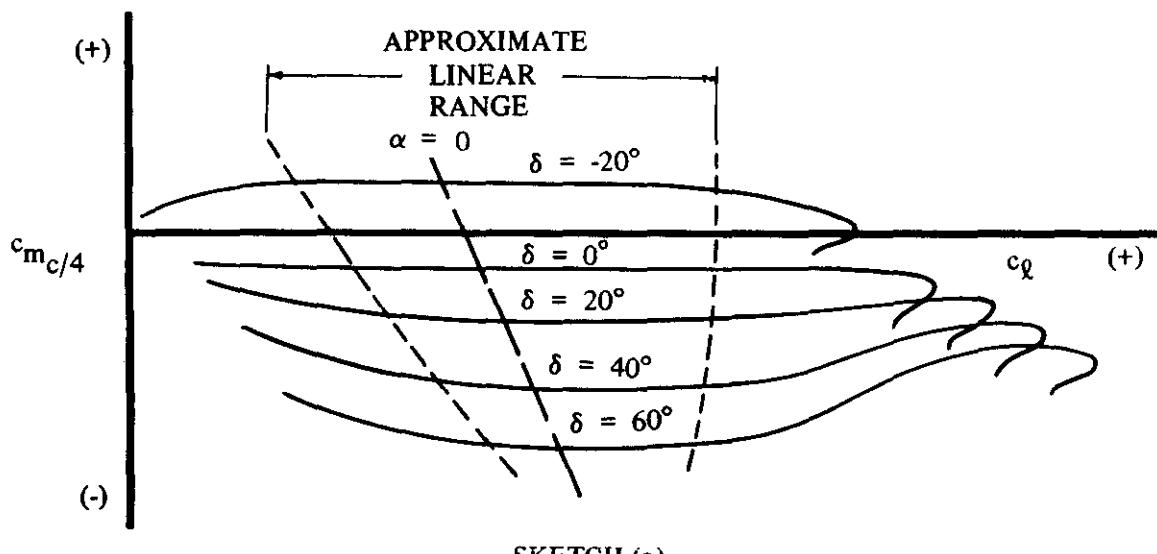
FIGURE 6.1.2.1-37 THEORETICAL LOCATION OF CENTER OF PRESSURE OF INCREMENTAL LOAD DUE TO DEFLECTION OF A FLAP WITH A JET EMERGING FROM THE TRAILING EDGE

### 6.1.2.2 SECTION DERIVATIVE $c_{m\alpha}$ WITH HIGH-LIFT AND CONTROL DEVICES

#### Mechanical Flaps

According to thin-airfoil theory, camber, such as that due to flaps, does not affect the moment-curve slope of an airfoil section. Experimental data verify this for the angle-of-attack and flap-deflection ranges for which the flow is attached over the airfoil and flap surfaces. This aspect of the subject is discussed with respect to lift for various types of flaps in Section 6.1.1.2.

A typical set of data is shown in Sketch (a) for plain trailing-edge flaps.



The approximate linear range is noted in the sketch. At angles of attack above the linear range the flow separates over the flap surface, and the additional loading due to the flap is lost. A pitch-up tendency results. At angles of attack below the linear range the flow separates on the underside of the airfoil, causing a forward shift in center of pressure and a nose-up moment change.

Theoretically, the pitching-moment-curve slope is affected both by leading- and trailing-edge devices that extend beyond the chord of the basic airfoil. These changes, predicted by thin-airfoil theory, along with a recommended empirical factor for trailing-edge devices, are presented in Reference 1. Attempts to substantiate these equations by using available test data of References 2 through 8 have proved unsatisfactory. The test data from these references do not indicate a consistent dependence of pitching-moment-curve slope upon airfoil-chord extension as predicted by thin-airfoil theory.

#### Jet Flaps

The aerodynamic-center location for a jet-flap airfoil is dependent upon the trailing-edge jet momentum coefficient  $C_j$  and upon the extent to which leading- and trailing-edge flaps extend beyond the basic airfoil.

Considerations of clarity and simplicity of presentation dictated a deviation from normal Datcom practice in that the effect of jet flaps on  $c_{m\alpha}$  was included in Section 6.1.2.1, which deals with the pitching-moment increment  $\Delta c_m$ .

## DATCOM METHODS

### 1. Leading- and Trailing-Edge Mechanical Flaps

The parameter  $dc_m/dc_\alpha$  for various flap deflections is the same as that for zero flap deflection for angles of attack near zero. However, the linear range for this parameter becomes very small at the higher flap deflections.

### 2. Jet Flaps

The variation of pitching moment with angle of attack for airfoil sections equipped with jet flaps is covered in the jet-flap method of Section 6.1.2.1. The range of applicability and the limitations of the method are discussed there and in Section 6.1.1.1.

## REFERENCES

1. Hebert, J., Jr., et al.: STOL Tactical Aircraft Investigation. Volume II Design Compendium. AFFDL-TR-73-21-Volume II, 1973. (U)
2. Recant, I. G.: Wind-Tunnel Investigation of an N.A.C.A. 23030 Airfoil with Various Arrangements of Slotted Flaps. NACA TN 755, 1940. (U)
3. Wenzinger, C. J., and Harris, T. A.: Wind-Tunnel Investigation of an N.A.C.A. 23021 Airfoil with Various Arrangements of Slotted Flaps. NACA TR 677, 1939. (U)
4. Harris, T. A., and Purser, P. E.: Wind-Tunnel Investigation of an N.A.C.A. 23012 Airfoil with Two Sizes of Balanced Split Flap. NACA WR L-441, 1940. (U)
5. Swanson, R. S., and Schuldenfrei, M. J.: Wind-Tunnel Investigation of an N.A.C.A. 23021 Airfoil with Two Sizes of Balanced Split Flaps. NACA WR L-449, 1941. (U)
6. Holtzclaw, R. W., and Weisman, Y.: Wind-Tunnel Investigation of the Effects of Slot Shape and Flap Location on the Characteristics of a Low-Drag Airfoil Equipped with a 0.25-Chord Slotted Flap. NACA WR A-80, 1944. (U)
7. Holtzclaw, R. W.: Wind-Tunnel Investigation of the Effects of Spoilers on the Characteristics of a Low-Drag Airfoil Equipped with a 0.25-Chord Slotted Flap. NACA WR A-92, 1945. (U)
8. Harris, T. A., and Recant, I. G.: Wind-Tunnel Investigation of N.A.C.A. 23012, 23021, and 23030 Airfoils Equipped with 40-Percent-Chord Double Slotted Flaps. NACA TR 723, 1941. (U)
9. Sears, R. I.: Wind-Tunnel Data on the Aerodynamic Characteristics of Airplane Control Surfaces. NACA WR L-663, 1943. (U)
10. Lowry, T. G.: Wind-Tunnel Investigation of an N.A.C.A. 23012 Airfoil with Several Arrangements of Slotted Flaps with Extended Lips. NACA TN 808, 1941. (U)
11. Wenzinger, C. J., and Harris, T. A.: Wind-Tunnel Investigation of an N.A.C.A. 23012 Airfoil with Various Arrangements of Slotted Flaps. NACA TR 664, 1939. (U)

### 6.1.2.3 SECTION PITCHING MOMENT NEAR MAXIMUM LIFT WITH HIGH-LIFT AND CONTROL DEVICES

It is shown in reference 1 that near maximum-lift conditions the pitching-moment increment due to flap deflection is a function of the corresponding lift increment and is nearly independent of flap and airfoil geometry. The summary chart from this reference is presented in this section for estimating pitching-moment increments due to flap deflection at high angles of attack. The flap types covered include plain, slotted, and Fowler trailing-edge flaps and leading-edge flaps and slats. The chart is applicable only to that part of the  $c_m$  versus  $c_l$  curve just below the moment break.

#### DATCOM METHOD

Section pitching-moment increments due to high-lift and control devices are obtained from figure 6.1.2.3-3. The section-lift increment  $\Delta c_l$  used in reading this chart is obtained from the appropriate method of Section 6.1.1.1. The section-lift increment for airfoils with both leading-edge and trailing-edge devices is obtained by adding the individual increments calculated by the methods of Section 6.1.1.1.

The design chart is based on the test data of references 2 through 28. The accuracy of the method, within the boundaries of the test points on the chart, is dependent upon the accuracy of the value of  $\Delta c_l$  used in reading the design chart. The limitations of the method are the same as those of the methods of Section 6.1.1.1 for determining the section-lift increments.

#### REFERENCES

1. Bidwell, J.M., and Cahill, J.F.: Survey of Two-Dimensional Data on Pitching-Moment Changes Near Maximum Lift Caused by Deflection of High-Lift Devices. NACA RM L9J03, 1949. (U)
2. Cahill, J.F.: Summary of Section Data on Trailing-Edge High-Lift Devices. NACA RM L8D09, 1948. (U)
3. Wenzinger, C.J., and Harris, T.A.: Wind-Tunnel Investigation of an NACA 23012 Airfoil With Various Arrangements of Slotted Flaps. NACA TR 664, 1939. (U)
4. Abbott, I.H., and Greenberg, H.: Tests in the Variable-Density Wind Tunnel of the NACA 23012 Airfoil with Plain and Split Flaps. NACA TR 661, 1939. (U)
5. Klein, M.M.: Pressure Distributions and Force Tests of an NACA 65-210 Airfoil Section with a 50-Percent-Chord Flap. NACA TN 1167, 1947. (U)
6. Wenzinger, C.J., and Harris, T.A.: Wind-Tunnel Investigation of NACA 23012, 23021, and 23030 Airfoils with Various Sizes of Split Flap. NACA TR 668, 1939. (U)
7. Schuldenfrei, M.J.: Wind-Tunnel Investigation of an NACA 23012 Airfoil with a Handley Page Slat and Two Flap Arrangements. NACA WR L-261, 1942. (U)
8. Harris, T.A., and Purser, P.E.: Wind-Tunnel Investigation of an NACA 23012 Airfoil with Two Sizes of Balanced Split Flap. NACA WR L-441, 1940. (U)
9. Lowry, J.G.: Wind-Tunnel Investigation of an NACA 23012 Airfoil with Several Arrangements of Slotted Flaps with Extended Lips. NACA TN 808, 1941. (U)
10. Harris, T.A.: Wind-Tunnel Investigation of an NACA 23012 Airfoil with Two Arrangements of a Wide-Chord Slotted Flap. NACA TN 715, 1939. (U)
11. Purser, P.E., Fischel, J., and Riebe, J.M.: Wind-Tunnel Investigation of an NACA 23012 Airfoil with a 0.30-Airfoil-Chord Double Slotted Flap. NACA WR L-469, 1943. (U)

12. Wenzinger, C.J., and Harris, T.A.: Wind-Tunnel Investigation of an NACA 23021 Airfoil with Various Arrangements of Slotted Flaps. NACA TR 677, 1939. (U)
13. Duschik, F.: Wind-Tunnel Investigation of an NACA 23021 Airfoil with Two Arrangements of a 40-Percent-Chord Slotted Flap. NACA TN 728, 1939. (U)
14. Fischel, J., and Riebe, J.M.: Wind-Tunnel Investigation of an NACA 23021 Airfoil with a 0.32-Airfoil-Chord Double Slotted Flap. NACA WR L-7, 1944. (U)
15. Holtzclaw, R.W., and Weisman, Y.: Wind-Tunnel Investigation of the Effects of Slot Shape and Flap Location on the Characteristics of Low-Drag Airfoil Equipped with a 0.25-Chord Slotted Flap. NACA WR A-92, 1944. (U)
16. Abbott, I.H., and Fullmer, F.F., Jr.: Wind-Tunnel Investigation of NACA 63, 4-420 Airfoil with 25-Percent-Chord Slotted Flap. NACA ACR 3121, 1943. (U)
17. Gillis, C.L., and McKee, J.W.: Wind-Tunnel Investigation of an NACA 23012 Airfoil with an 18.05-Percent-Chord Maxwell Slat and with Trailing-Edge Flaps. NACA WR L-574, 1941. (U)
18. Lowry, J.G., and McKee, J.W.: Wind-Tunnel Investigation of an NACA 23012 Airfoil with a 30-Percent-Chord Maxwell Slat and With Trailing-Edge Flaps. NACA WR L-693, 1941. (U)
19. Weick, F.E., and Platt, R.C.: Wind-Tunnel Tests on Model Wing With Fowler Flap and Specially Developed Leading-Edge Slot. NACA TN 459, 1933. (U)
20. Lemme, H.G.: Force and Pressure-Distribution Measurements on a Rectangular Wing with a Slotted Droop Nose and with Either Plain and Split Flaps in Combination or a Slotted Flap. NACA TM 1108, 1947. (U)
21. Lemme, H.A.: Force and Pressure-Distribution Measurements on a Rectangular Wing with Double-Hinged Nose. NACA TM 1117, 1947. (U)
22. Gauvain, W.E.: Wind-Tunnel Tests of a Clark Y Wing with "Maxwell" Leading-Edge Slots. NACA TN 598, 1937. (U)
23. Fullmer, F.F., Jr.: Two-Dimensional Wind-Tunnel Investigation of the NACA 641-012 Airfoil Equipped with Two Types of Leading-Edge Flap. NACA TN 1277, 1947. (U)
24. Fullmer, F.F., Jr.: Two-Dimensional Wind-Tunnel Investigation of an NACA 64-009 Airfoil Equipped with Two Types of Leading-Edge Flap. NACA TN 1624, 1948. (U)
25. Underwood, W.J., and Nuber, R.J.: Two-Dimensional Wind-Tunnel Investigation at High Reynolds Numbers of Two Symmetrical Circular-Arc Airfoil Sections with High-Lift Devices. NACA RM L6K22, 1947. (U)
26. Nuber, R.J., and Cheesman, G.A.: Two-Dimensional Wind-Tunnel Investigation of a 6-Percent-Thick Symmetrical Circular-Arc Airfoil Section with Leading-Edge and Trailing-Edge High-Lift Devices Deflected in Combination. NACA RM L9G20, 1949. (U)
27. Nuber, R.J., and Gottlieb, S.M.: Two-Dimensional Wind-Tunnel Investigation at High Reynolds Numbers of an NACA 65A006 Airfoil with High-Lift Devices. NACA RM L7K06, 1948. (U)
28. Thompson, M.J.: A Simple Method for Determining the Aerodynamic Center of an Airfoil. Jour. Aero. Sci., February 1938. (U)

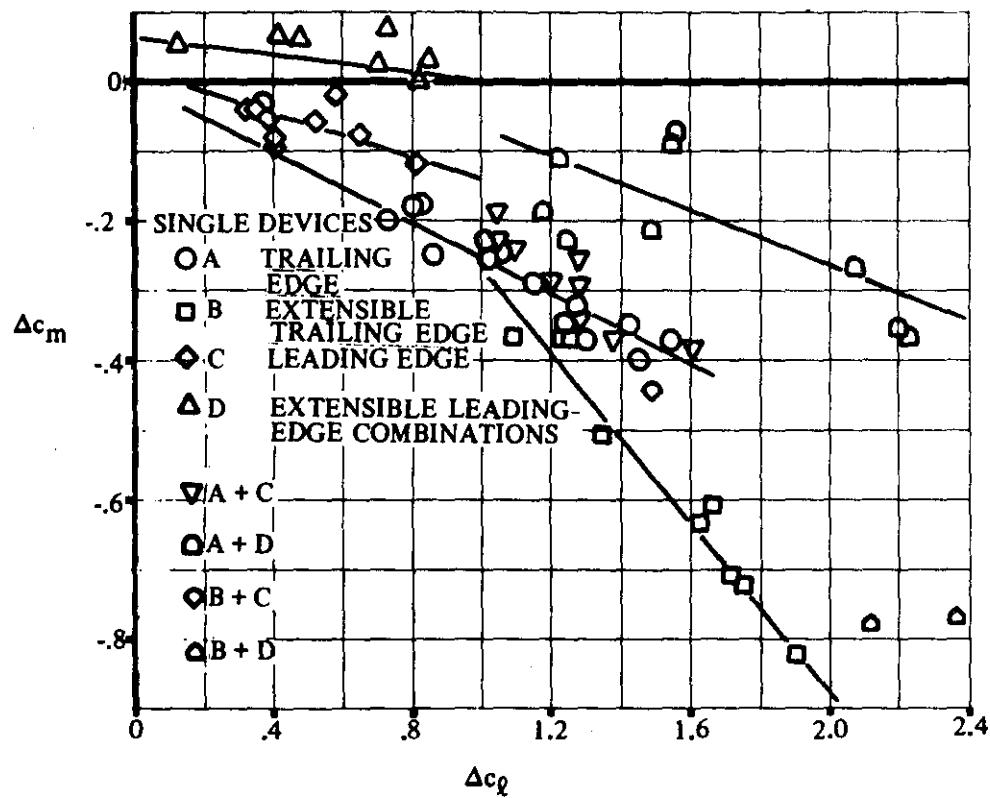


**FIGURE 6.1.2.3-3 SECTION PITCHING-MOMENT INCREMENTS OF VARIOUS TYPES OF HIGH-LIFT DEVICES**

### 6.1.3 SECTION HINGE MOMENT OF HIGH-LIFT AND CONTROL DEVICES

Hinge moments are affected by many factors, such as balance ratio, balance shape, basic airfoil characteristics, trailing-edge angle, trailing-edge bluntness, gap size and geometry, tab controls and trimmers, etc. Hinge moments are also nonlinear with angle of attack and flap deflection, particularly at moderate to large angles. The hinge moments of trailing-edge controls are sensitive to boundary-layer conditions and hence to Reynolds-number effects. All of the above items cause the prediction of hinge moments to be very difficult. Test data on the particular configuration under consideration or one closely resembling it should always be preferred to characteristics obtained from generalized methods. (Summaries of early hinge-moment test data used in determining the effects of various factors on hinge moments can be found in References 1 and 2.)

The methods presented in subsequent sections are limited to the range of flap deflections and angles of attack for which the hinge moments are linear, i.e., those conditions for which the flow is attached over the control surface. The angles of attack and flap deflections at which the flow separates over a plain, sealed control are interrelated and depend upon the flap-chord-to-wing-chord ratio. Approximate boundaries for linear control effectiveness are presented in Figure 6.1.3-2. This chart, taken from Reference 3, is based on test data on an NACA 0009 airfoil.

The sign convention for hinge moments is that a positive hinge moment tends to rotate the control-surface trailing edge down, i.e., a positive control deflection.

### REFERENCES

1. Sears, R. I.: Wind-Tunnel Data on the Aerodynamic Characteristics of Airplane Control Surfaces. NACA WR L-663, 1943. (U)
2. Axelson, J. A.: A Summary and Analysis of Wind Tunnel Data on the Lift and Hinge-Moment Characteristics of Control Surfaces up to a Mach Number of 0.90. NACA RM A7L02, 1948. (U)
3. Ames, M. B., Jr., and Sears, R. I.: Determination of Control-Surface Characteristics from NACA Plain-Flap and Tab Data. NACA TR 721, 1941. (U)

### SUBSONIC SPEEDS

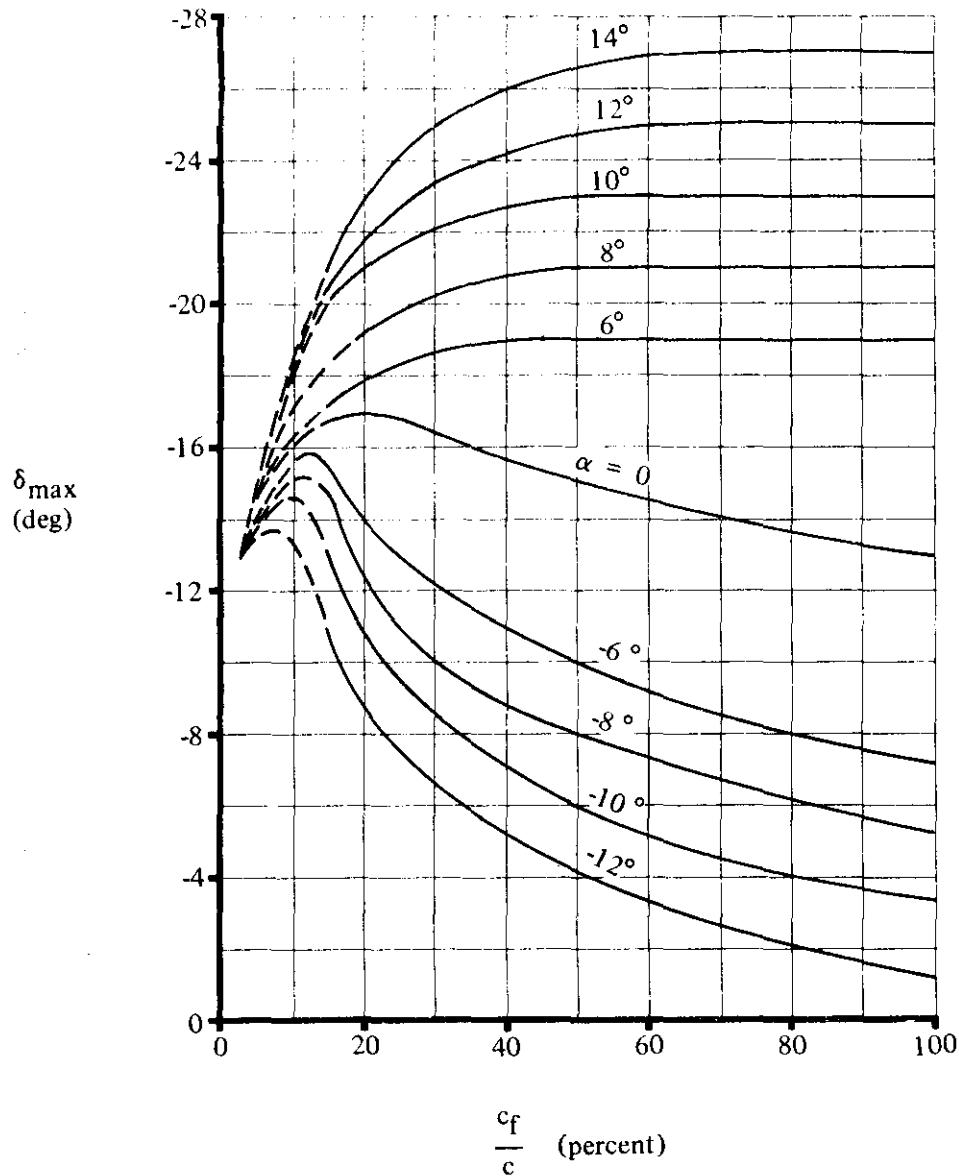


FIGURE 6.1.3-2 APPROXIMATE MAXIMUM CONTROL-SURFACE DEFLECTIONS FOR LINEAR CONTROL CHARACTERISTICS OF A PLAIN, SEALED FLAP (NACA 0009 AIRFOIL)

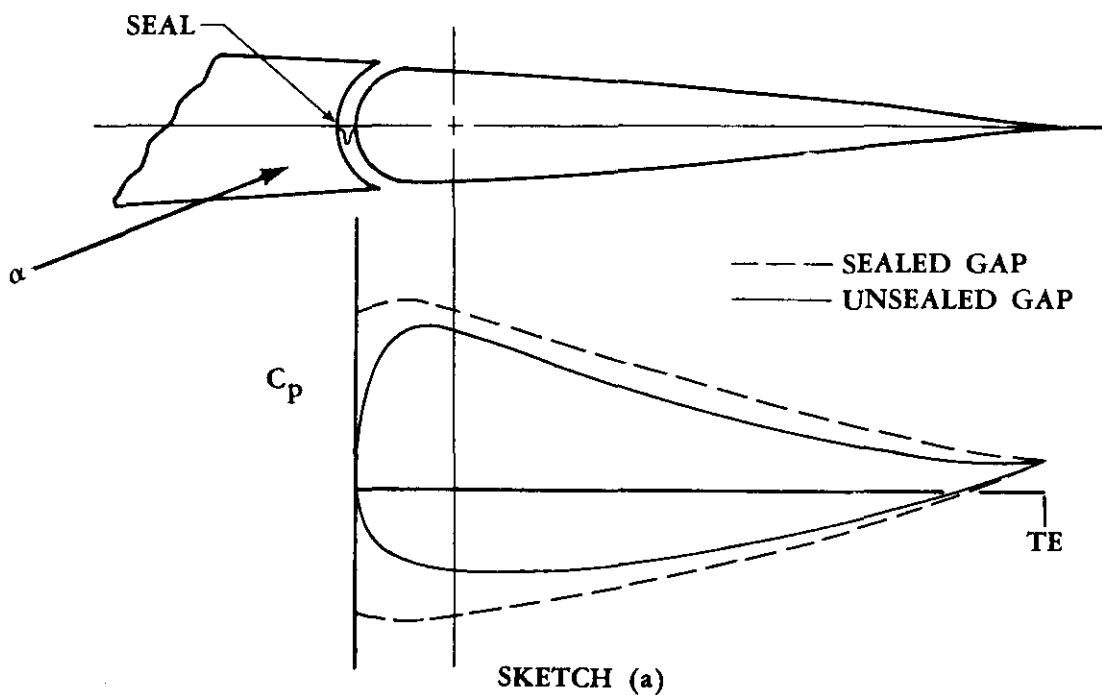
### 6.1.3.1 SECTION HINGE-MOMENT DERIVATIVE $c_{h\alpha}$ OF HIGH-LIFT AND CONTROL DEVICES

For the angle-of-attack range where the flow is attached over the control surface, the variation of hinge moment with angle of attack is linear. At some angle of attack, depending upon the control deflection and airfoil and control geometry, the flow separates from the flap surface. The rate of change of hinge moment with flap deflection increases beyond this point at an increased rate. This increase can be attributed to the increased loading at the trailing edge on the leeward side that accompanies separation, i.e., the aft movement of the center-of-pressure location. The approximate angle of attack at which the flow separates from the surface of a plain, sealed flap on an NACA 0009 airfoil is shown as a function of flap deflection angle and flap-chord-to-control-chord ratio in Figure 6.1.3-2.

Those additional parameters that restrict the linear range are large trailing-edge angles, large nose-balance ratios, blunt (control) nose shapes, and relatively large airfoil thickness ratios. The linear hinge-moment range is generally smaller than the corresponding linear lift-increment range due to control deflection.

#### Seal and Gap Effects

Unsealing the gap between the nose of the control surface and the basic airfoil affects the hinge-moment derivative of both plain and balanced controls. For most cases, the hinge-moment derivative  $c_{h\alpha}$  becomes more positive when the gap is unsealed. Experimental data indicate that this effect tends to be larger for balanced controls. The method presented herein does not quantitatively account for the effect of unsealing the gap. In effect, seals or gaps produce a change in the pressure distribution along the control surface. Therefore, many factors must be considered when analyzing the effects of gaps or seals, i.e., type and/or location of seal, nose shape, balancing, and the particular pressure distribution of the airfoil. Sketch (a) illustrates the pressure distributions for a



sealed and unsealed gap on a particular control. (This pressure distribution should not be construed as being true for all configurations.) In viewing the change in the pressure distribution, the effect of the hinge-line location (balanced control) becomes evident when determining the effect of the seal or gap on the hinge-moment derivative.

In view of the difficulty of predicting the effects of seals and gaps, experimental data should be used whenever possible. Figures 6.1.3.1-9 and -10 (from Reference 1) show the effects of fixing transition and sealing the tab gap on a modified NACA 65<sub>1</sub>-012 airfoil. For these data, the flap-chord-to-wing-chord ratio is 0.25, the tab-chord-to-flap-chord ratio is 0.25, and the flap gap is sealed.

## DATCOM METHOD

### A. SUBSONIC

The method presented for estimating the hinge moment of trailing-edge controls due to angle of attack at low speeds is taken from Reference 2. It is based on the theories and data of References 3, 4, and 5, and applies to sealed controls (at the nose) in the linear hinge-moment range only. It is not valid for horn-balanced controls. The hinge-moment derivative  $c_{h\alpha}$  is based on the control chord squared  $c_f^2$  (where the control chord  $c_f$  is measured from the hinge line aft to the trailing edge).

The method is broken down into a logical sequence of calculations that account for various factors in the following order:

1. Radius-nose, sealed, plain trailing-edge control for which the thickness condition

$$\tan \frac{\phi'_{TE}}{2} = \tan \frac{\phi''_{TE}}{2} = \tan \frac{\phi_{TE}}{2} = \frac{t}{c}$$

is satisfied.

2. Thickness distribution when

$$\tan \frac{\phi'_{TE}}{2} = \tan \frac{\phi''_{TE}}{2} = \tan \frac{\phi_{TE}}{2} = \frac{t}{c}$$

is not satisfied.

3. Various control nose shapes and the effect of nose balance.

4. Effects of Mach number.

The semiempirical method for determining the section hinge-moment derivative  $c_{h\alpha}$  is as follows:

**Step 1.** Calculate the hinge-moment derivative  $c'_{h\alpha}$  for a radius-nose, sealed, trailing-edge flap for the following thickness condition:

$$\tan \frac{\phi'_{TE}}{2} = \tan \frac{\phi''_{TE}}{2} = \tan \frac{\phi_{TE}}{2} = \frac{t}{c}$$

by

$$c'_{h\alpha} = \left[ \frac{c'_{h\alpha}}{(c'_{h\alpha})_{theory}} \right] (c'_{h\alpha})_{theory} \quad (\text{per radian}) \quad 6.1.3.1-a$$

where

$\phi'_{TE}$  is the trailing-edge angle defined as the angle between straight lines passing through points at 90 and 99 percent of the chord on the upper and lower airfoil surfaces.

$\phi''_{TE}$  is the trailing-edge angle defined as the angle between straight lines passing through points at 95 and 99 percent of the chord on the upper and lower airfoil surfaces.

$\phi_{TE}$  is the trailing-edge angle defined as the angle between tangents to the upper and lower airfoil surfaces at the trailing edge.

$\frac{c'_{h\alpha}}{(c'_{h\alpha})_{theory}}$  is the ratio of the actual to the theoretical hinge-moment derivative for a radius-nose, sealed-gap, plain trailing-edge flap, obtained from Figure 6.1.3.1-11a.

$(c'_{h\alpha})_{theory}$  is the theoretical hinge-moment derivative for airfoils having  
 $\tan \frac{\phi'_{TE}}{2} = \tan \frac{\phi''_{TE}}{2} = \tan \frac{\phi_{TE}}{2} = \frac{t}{c}$ .  
 This parameter is obtained from Figure 6.1.3.1-11b.

The parameter  $c_{q\alpha}/(c_{q\alpha})_{theory}$  used in reading this chart is obtained from Figure 4.1.1.2-8a.

**Step 2.** If the thickness condition in Step 1 is satisfied, Step 2 may be omitted. However, if the thickness condition in Step 1 is not satisfied, correct the hinge-moment derivative  $c'_{h\alpha}$  of Step 1 to account for the particular thickness distribution by

$$c''_{h\alpha} = c'_{h\alpha} + 2(c_{q\alpha})_{theory} \left[ 1 - \frac{c_{q\alpha}}{(c_{q\alpha})_{theory}} \right] \left( \tan \frac{\phi''_{TE}}{2} - \frac{t}{c} \right) \quad (\text{per radian}) \quad 6.1.3.1-b$$

where

$c'_{h\alpha}$  is obtained from Equation 6.1.3.1-a in Step 1.

$(c_{l\alpha})_{\text{theory}}$  is the theoretical section lift-curve slope obtained from Figure 4.1.1.2-8b as a function of airfoil thickness ratio.

The parameters  $c_{l\alpha}/(c_{l\alpha})_{\text{theory}}$  and  $\frac{\phi''_{TE}}{2}$  are obtained as noted above in Step 1.

For a beveled trailing edge,  $\phi''_{TE}$  should be taken as equal to the angle of the bevel.

It is stated in Reference 2 that under the restriction that there is no separated flow,  $c_{h\alpha}$  for a radius-nose control can be determined by using the above equations with an accuracy of  $\pm 0.05$  per radian.

- Step 3. Correct the hinge-moment derivative to account for nose-shape and nose-balance effects by using the following equation (taken from Reference 5):

$$(c_{h\alpha})_{\text{balance}} = c''_{h\alpha} \left[ \frac{(c_{h\alpha})_{\text{balance}}}{c''_{h\alpha}} \right] \quad (\text{per radian}) \quad 6.1.3.1-c$$

where

$c''_{h\alpha}$  is obtained from Step 2, or is equal to  $c'_{h\alpha}$  from Step 1 if the thickness correction is not required.

$\frac{(c_{h\alpha})_{\text{balance}}}{c''_{h\alpha}}$  is obtained from Figure 6.1.3.1-12a for noses of various shapes. The nose shapes corresponding to the curves in Figure 6.1.3.1-12a are shown in Figure 6.1.3.1-12b. The balance ratio used in Figure 6.1.3.1-12a is defined by

$$\text{Balance ratio} = \sqrt{\left(\frac{c_b}{c_f}\right)^2 - \left(\frac{t_c}{2c_f}\right)^2} \quad 6.1.3.1-d$$

where

$c_b$  is the chord of the balance.

$c_f$  is the chord of the control aft of the hinge line.

$t_c$  is the thickness of the control at the hinge line.

Figure 6.1.3.1-12a is taken from Reference 6 and is based on a limited amount of experimental data on sealed controls. Small changes in nose shape, trailing-edge contour, and air flow may have significant effects on the hinge-moment derivative of balanced control surfaces.

- Step 4. Mach-number effects should be approximated by the use of test data whenever possible. However, when no test data are available, the Mach-number effects may be roughly approximated by using the Prandtl-Glauert correction; i.e.,

$$(c_{h\alpha})_M = \frac{(c_{h\alpha})_{\text{low speed}}}{\sqrt{1 - M^2}}$$

### Sample Problem

Given: The flapped airfoil of Reference 7.

NACA 0015 airfoil	Plain trailing-edge flap	$c_f/c = 0.30$
Round-nose control	$c_b/c_f = 0.35$	$t_c/(2c_f) = 0.1527$
Sealed gap	$\tan \frac{\phi'_{TE}}{2} = 0.164$	$\tan \frac{\phi''_{TE}}{2} = 0.169$
Low speed	$R_\infty = 2.76 \times 10^6$	$\tan \frac{\phi_{TE}}{2} = 0.169$

Compute:

Determine the hinge-moment derivative for a radius-nose, sealed, trailing-edge flap

$$(c_{h\alpha})_{\text{theory}} = -0.507 \text{ per rad} \quad (\text{Figure 6.1.3.1-11b})$$

$$\frac{c_{q\alpha}}{(c_{q\alpha})_{\text{theory}}} = 0.760 \quad (\text{Figure 4.1.1.2-8a})$$

$$\frac{c'_{h\alpha}}{(c_{h\alpha})_{\text{theory}}} = 0.320 \quad (\text{Figure 6.1.3.1-11a})$$

$$c'_{h\alpha} = \left[ \frac{c'_{h\alpha}}{(c_{h\alpha})_{\text{theory}}} \right] (c_{h\alpha})_{\text{theory}} \quad (\text{Equation 6.1.3.1-a})$$

$$= (0.320)(-0.507)$$

$$= -0.162 \text{ per rad}$$

Determine if the thickness condition is satisfied; i.e.,

$$\tan \frac{\phi'_{TE}}{2} = \tan \frac{\phi''_{TE}}{2} = \tan \frac{\phi_{TE}}{2} = \frac{t}{c}$$

$$0.164 \neq 0.169 = 0.169 \neq 0.15$$

Determine the hinge-moment derivative accounting for the thickness distribution

$$(c_{q_\alpha})_{\text{theory}} = 7.04 \text{ per rad} \quad (\text{Figure 4.1.1.2-8b})$$

$$c''_{h_\alpha} = c'_{h_\alpha} + 2(c_{q_\alpha})_{\text{theory}} \left[ 1 - \frac{c_{q_\alpha}}{(c_{q_\alpha})_{\text{theory}}} \right] \left( \tan \frac{\phi''_{TE}}{2} - \frac{t}{c} \right) \quad (\text{Equation 6.1.3.1-b})$$

$$= -0.162 + 2(7.04)[1 - 0.760](0.169 - 0.150)$$

$$= -0.0978 \text{ per rad}$$

Determine the effect of nose shape and nose balance

$$\text{Balance ratio} = \sqrt{\left(\frac{c_b}{c_f}\right)^2 - \left(\frac{t_c}{2c_f}\right)^2} \quad (\text{Equation 6.1.3.1-d})$$

$$= \sqrt{(0.35)^2 - (0.1527)^2}$$

$$= 0.315$$

$$\frac{(c_{h_\alpha})_{\text{balance}}}{c''_{h_\alpha}} = 0.50 \quad (\text{Figure 6.1.3.1-12a})$$

$$(c_{h_\alpha})_{\text{balance}} = c''_{h_\alpha} \left[ \frac{(c_{h_\alpha})_{\text{balance}}}{c''_{h_\alpha}} \right] \quad (\text{Equation 6.1.3.1-c})$$

$$= (-0.0978)(0.50)$$

$$= -0.0489 \text{ per rad}$$

$$= -0.000853 \text{ per deg}$$

This compares with a test value of  $-0.00145$  per degree from Reference 7.

## B. TRANSONIC

No method is available for predicting the section hinge-moment derivative  $c_{h_\alpha}$  at transonic speeds.

## C. SUPERSONIC

The method for determining  $c_{h_\alpha}$  at supersonic speeds is based on the theory of Reference 8. The theory applies to airfoils with sharp leading and trailing edges, where the angles of attack and flap-deflection angles are small. In addition, the flow field is assumed to be everywhere supersonic and inviscid.

### DATCOM METHOD

The hinge-moment derivative  $c_{h_\alpha}$  at supersonic speeds for a symmetric, straight-sided flap with  $c_f/c < 1/2$ , regardless of the airfoil section ahead of the flap, is given by

$$c_{h_\alpha} = -C_1 + C_2 \phi_{TE} \quad 6.1.3.1-e$$

where  $C_1$  and  $C_2$  are thickness correction factors to the supersonic flat-plate derivative.

$$C_1 = \frac{2}{\sqrt{M^2 - 1}} \text{ per radian}$$

$$C_2 = \frac{(\gamma + 1)M^4 - 4(M^2 - 1)}{2(M^2 - 1)^2} \text{ per radian}$$

$\phi_{TE}$  is the trailing-edge angle in radians.

$\gamma$  is the ratio of specific heats,  $\gamma = 1.4$ .

For a symmetric, circular-arc airfoil with  $c_f/c < 1/2$ ,  $c_{h_\alpha}$  is given by

$$c_{h_\alpha} = -C_1 + \left( \frac{\Delta c_{h_\alpha}}{t/c} \right) \frac{t}{c} \quad 6.1.3.1-f$$

where  $C_1$  is defined above, and

$\frac{\Delta c_{h_\alpha}}{t/c}$  is a thickness correction factor for symmetric, circular-arc airfoils obtained from Figure 6.1.3.1-13.

The method becomes somewhat complicated for more general airfoil shapes. Other airfoil shapes are treated in Reference 8.

### Sample Problem

Given: Symmetric, circular-arc airfoil.

$$t/c = 0.06$$

$$c_f/c = 0.30$$

$$M = 2.0$$

Compute:

$$C_1 = \frac{2}{\sqrt{M^2 - 1}} \cdot \frac{1}{57.3} = 0.020 \text{ per deg}$$

$$\frac{\Delta c_{h_\alpha}}{t/c} = 0.0008 \text{ per deg} \quad (\text{Figure 6.1.3.1-13})$$

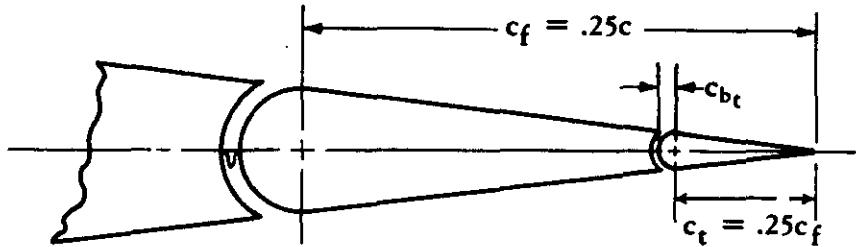
Solution:

$$\begin{aligned} c_{h_\alpha} &= -C_1 + \left( \frac{\Delta c_{h_\alpha}}{t/c} \right) \frac{t}{c} \quad (\text{Equation 6.1.3.1-f}) \\ &= -0.020 + (0.0008)(0.06) \\ &= -0.01995 \text{ per deg} \end{aligned}$$

### REFERENCES

1. Brewer, J. D., and Queijo, M. J.: Wind-Tunnel Investigation of the Effect of Tab Balance on Tab and Control-Surface Characteristics. NACA TN 1403, 1947. (U)
2. Anon.: Royal Aeronautical Society Data Sheets – Aerodynamics, Vol. IV, (Controls 04.01.01), 1956. (U)
3. Anon.: Royal Aeronautical Society Data Sheets – Aerodynamics, Vol. IV, (Controls 04.01.00), 1950. (U)
4. Garner, H. C.: Charts for Low-Speed Characteristics of Two-Dimensional Trailing Edge Flaps. ARC 18,528, 1956. (U)
5. Woods, L. C.: The Theory of Aerofoils with Hinged Flaps in Two-Dimensional Compressible Flow. ARC CP 138, 1952. (U)
6. Anon.: Royal Aeronautical Society Data Sheets – Aerodynamics, Vol. IV, (Controls 04.01.03), 1949. (U)
7. Sears, R. I., and Hoggard, H. P., Jr.: Wind-Tunnel Investigation of Control-Surface Characteristics. VII – A Medium Aerodynamic Balance of Two Nose Shapes Used with a 30-Percent-Chord Flap on an NACA 0015 Airfoil. NACA WR L-448, 1942. (U)
8. Lock, C. N. H.: Examples of the Application of Busemann's Formula to Evaluate the Aerodynamic Force Coefficients on Supersonic Aerofoils. ARC R&M 2101, 1944. (U)

SUBSONIC SPEEDS



TAB GAP	TRANSITION STRIPS
— .004c	AT .01c
— SEALED	AT .01c
— .004c	OFF
— SEALED	OFF

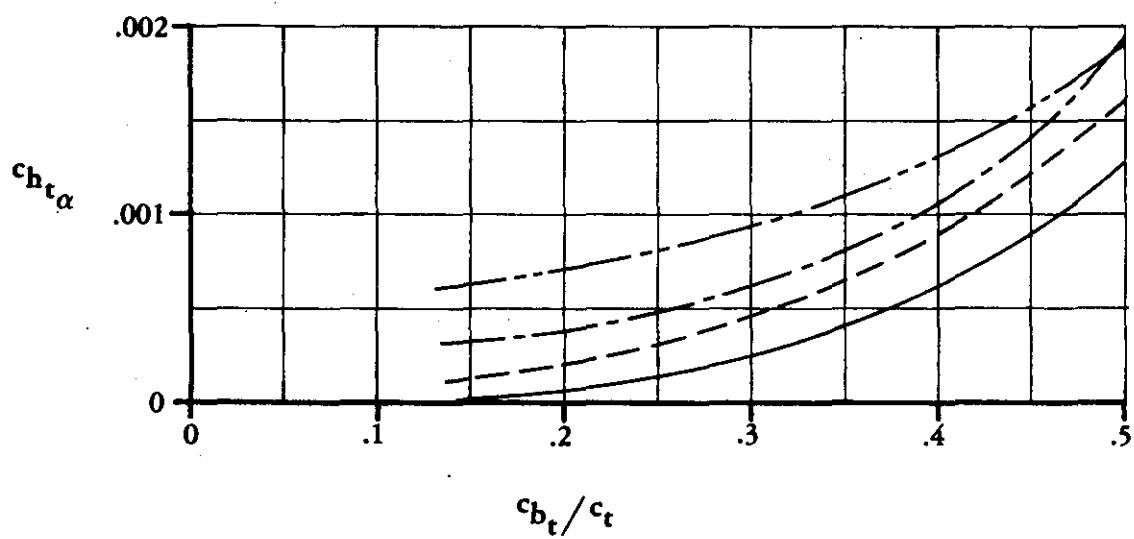
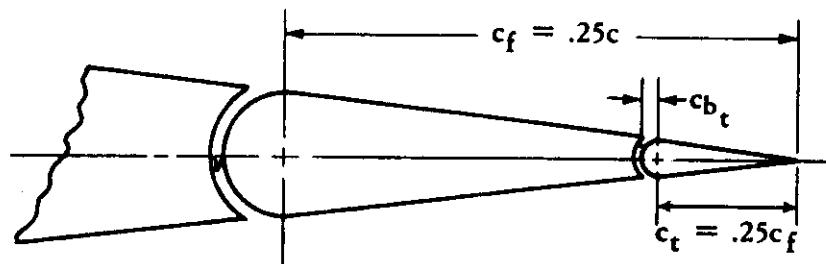


FIGURE 6.1.3.1-9 EFFECT OF SEALED AND UNSEALED TAB GAPS AND TRANSITION STRIPS ON TAB SECTION HINGE MOMENTS

SUBSONIC SPEEDS



TAB GAP	TRANSITION STRIPS
— .004c	AT .01c
- - - SEALED	AT .01c
— .004c	OFF
- - - SEALED	OFF

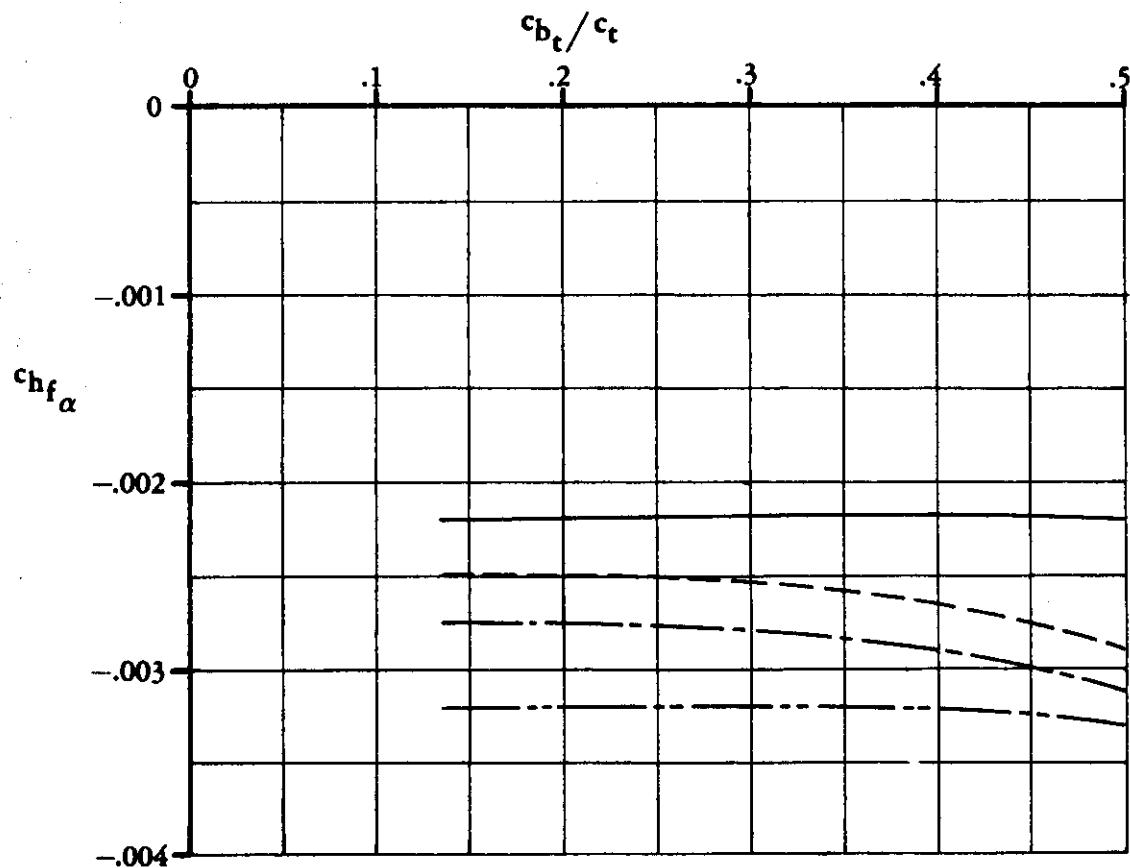


FIGURE 6.1.3.1-10 EFFECT OF SEALED AND UNSEALED TAB GAPS AND TRANSITION STRIPS ON FLAP SECTION HINGE MOMENTS

SUBSONIC SPEEDS

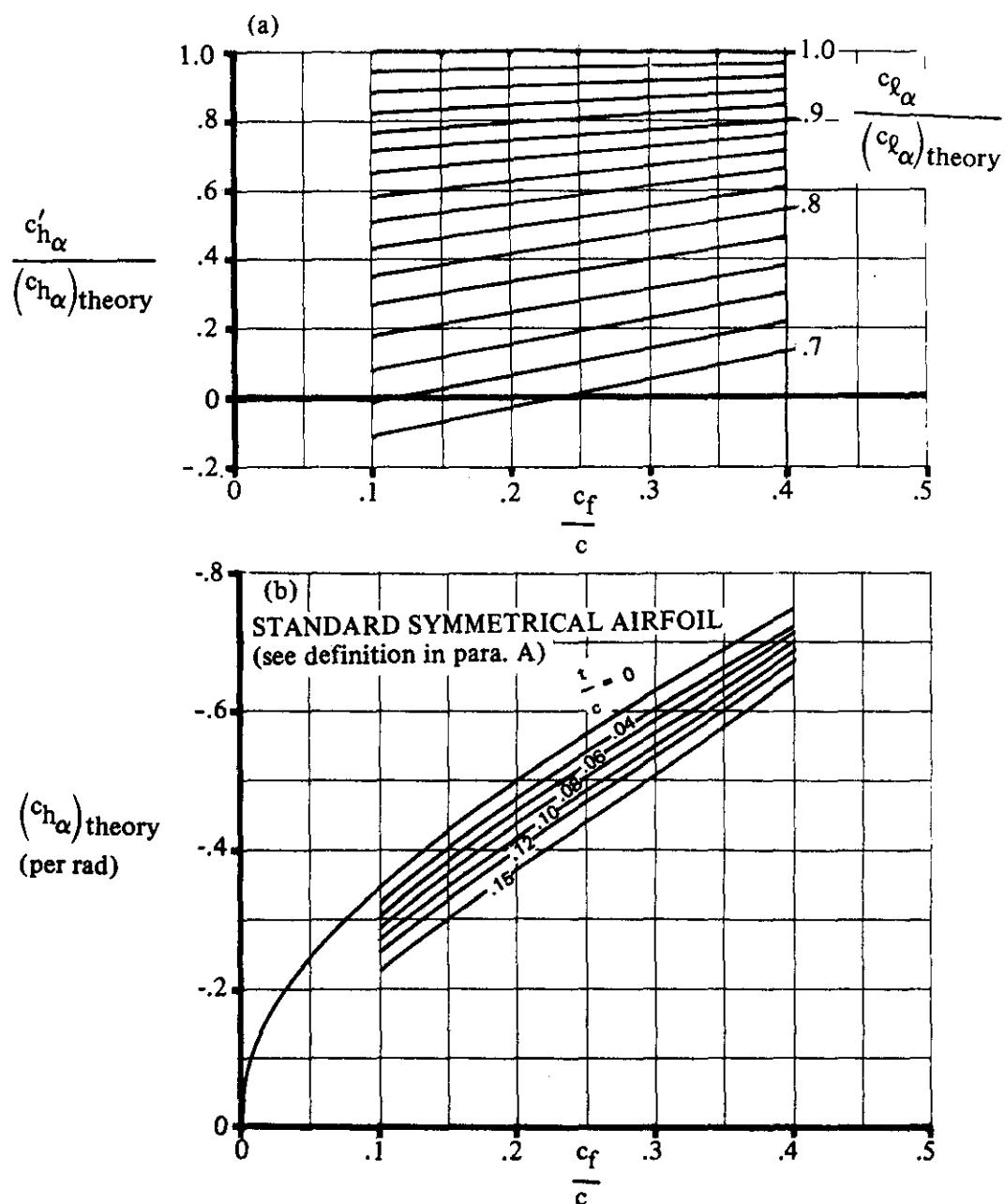
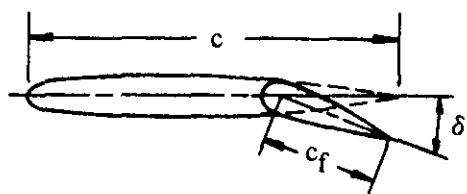


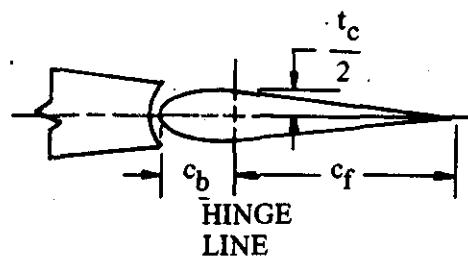
FIGURE 6.1.3.1-11 RATE OF CHANGE OF SECTION HINGE-MOMENT COEFFICIENT WITH ANGLE OF ATTACK FOR A PLAIN FLAP

- NACA 0009
- NACA 0015
- NACA 66009
- NACA 0009
- NACA 0015
- △ NACA 0009

ROUND NOSE

ELLIPTIC NOSE

SHARP NOSE



SUBSONIC SPEEDS

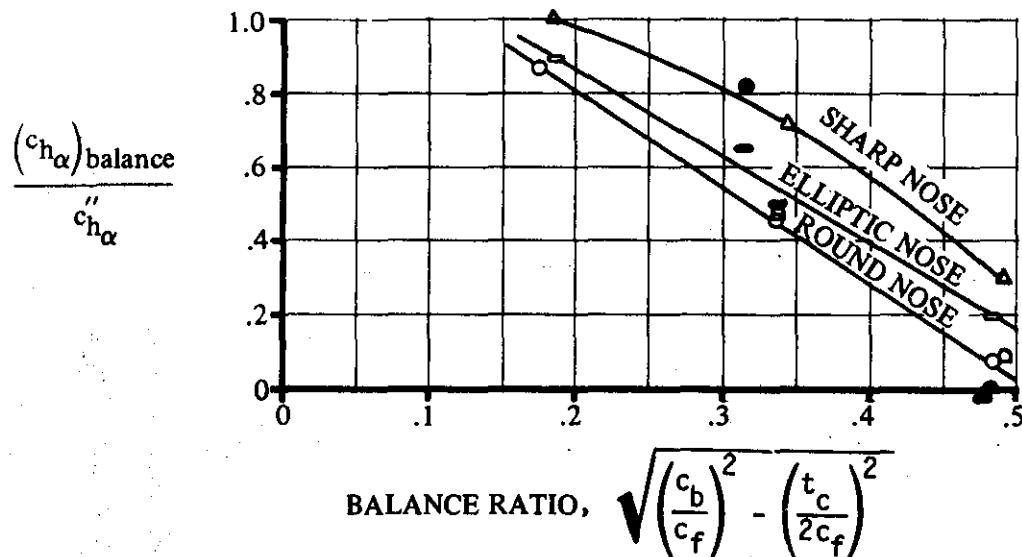


FIGURE 6.1.3.1-12a

EFFECT OF NOSE BALANCE ON SECTION CONTROL HINGE-MOMENT COEFFICIENT

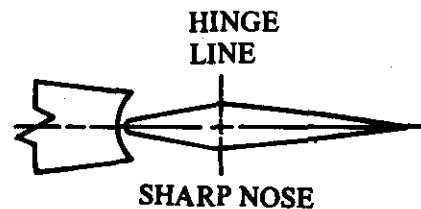
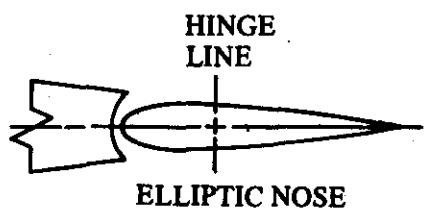
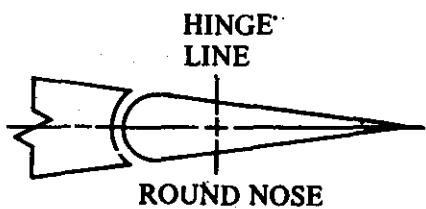
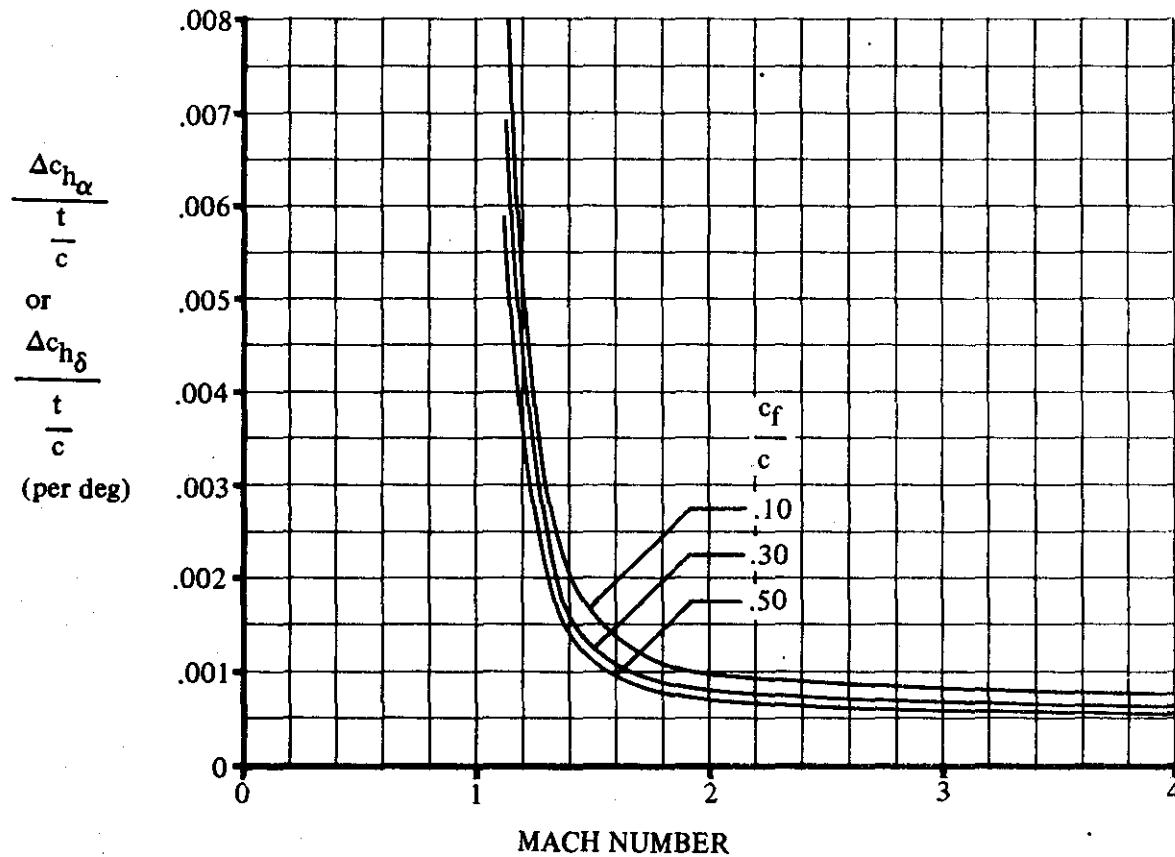


FIGURE 6.1.3.1-12b

CONTROL-SURFACE SECTION NOSE SHAPES SHOWN FOR A 35% BALANCE

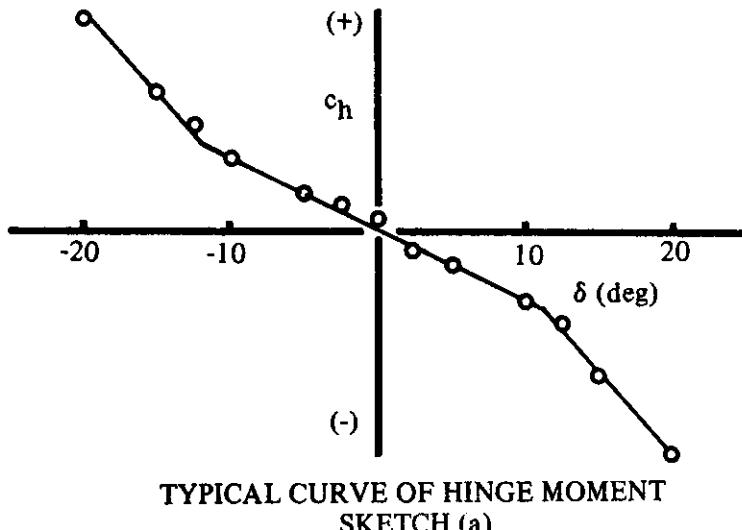
## SUPersonic SPEEDS



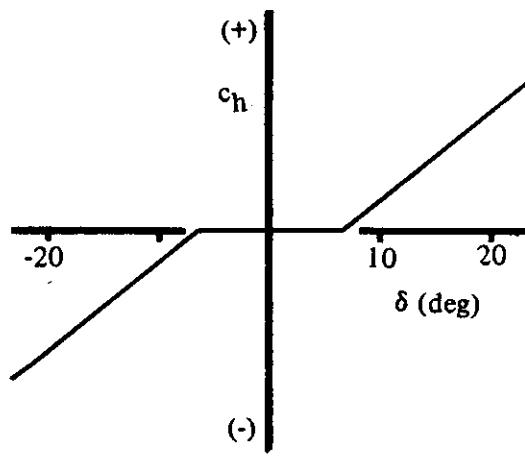
**FIGURE 6.1.3.1-13 THICKNESS CORRECTION FACTOR FOR HINGE-MOMENT DERIVATIVES FOR SYMMETRIC, CIRCULAR-ARC AIRFOILS**

### 6.1.3.2 SECTION HINGE-MOMENT DERIVATIVE $c_{h\delta}$ OF HIGH-LIFT AND CONTROL DEVICES

For small control deflections, where the flow is attached over the control surface, the variation of hinge moment with control deflection is linear. At some deflection angle, depending upon the angle of attack and airfoil and control geometry, the flow separates from the flap surface. The rate of change of hinge moment with flap deflection increases beyond this point at an increased rate, as shown in Sketch (a). This increase can be attributed to the increased loading at the trailing edge on the leeward side that accompanies separation; i.e., the aft movement of the center-of-pressure location. The approximate deflection angle at which the flow separates from the surface of a plain, sealed flap on an NACA 0009 airfoil is shown as a function of angle of attack and flap-chord-to-control-chord ratio in Figure 6.1.3-2.

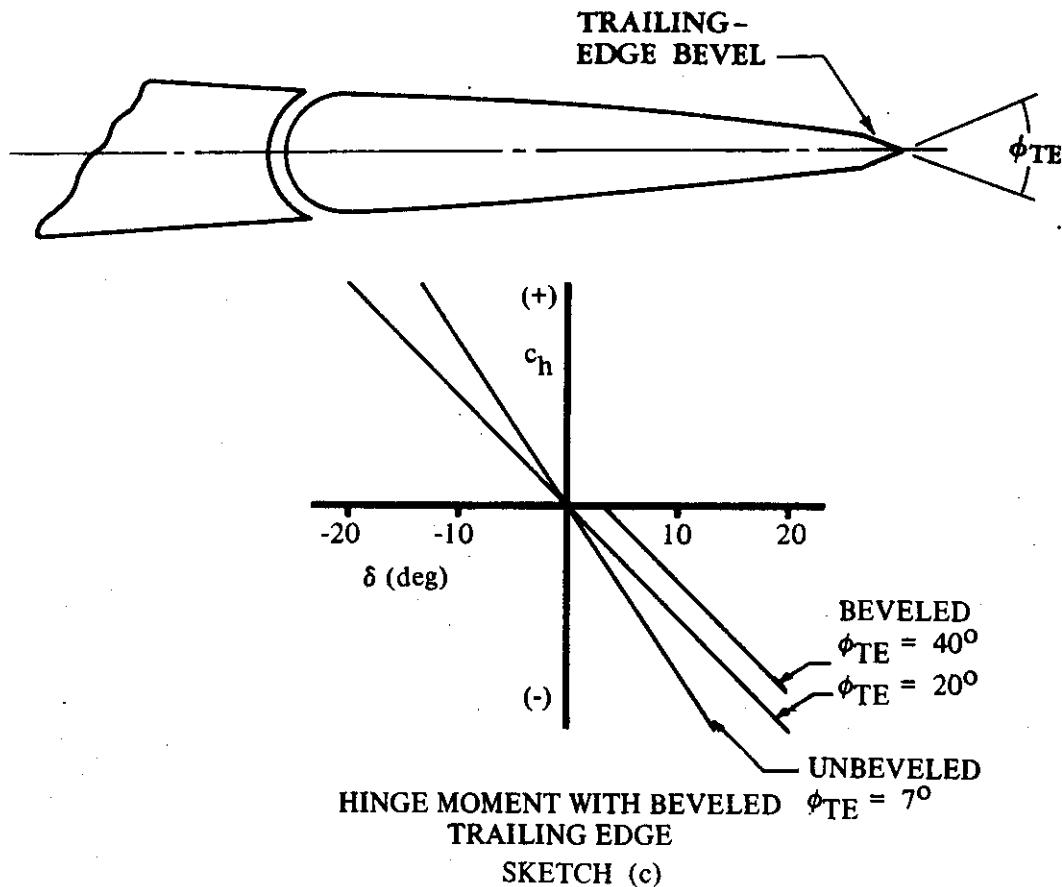


The additional parameters that restrict the linear range are large trailing-edge angles, large nose-balance ratios, blunt (control) nose shapes, and relatively large airfoil thickness ratios. The effect of large nose-balance ratios is shown in Sketch (b) (from Reference 1).



HINGE MOMENT WITH VERY  
LARGE NOSE BALANCE  
SKETCH (b)

The effect of beveled trailing edges is shown in Sketch (c) (from Reference 1). The linear hinge-moment range is generally smaller than the corresponding linear lift-increment range due to control deflection.



Unsealing the gap between the nose of the control surface and the basic airfoil affects the hinge-moment derivative of both plain and balanced controls. The method presented herein does not quantitatively account for the effect of unsealing the gap (see Section 6.1.3.1 for a discussion of the salient aspects). Figures 6.1.3.2-10 and -11 (from Reference 2) illustrate the effect of fixing transition and sealing the tab gap on a modified NACA 65<sub>1</sub>-012 airfoil. For these data, the flap-chord-to-wing-chord ratio is 0.25, the tab-chord-to-flap-chord ratio is 0.25, and the flap gap is sealed.

## DATCOM METHOD

## A. SUBSONIC

The method presented for estimating the hinge moment due to trailing-edge control deflection at low speeds is taken from Reference 3 and closely parallels the method presented in Section 6.1.3.1 for predicting the hinge-moment derivative  $c_{h\alpha}$ . This method is based on the theories and data of References 4, 5, and 6. The method applies to sealed controls (at the nose) in the linear hinge-moment range only. It is not valid for horn-balanced controls. The hinge-moment derivative  $c_{h\delta}$  is based on the control chord squared  $c_f^2$  (where the control chord  $c_f$  is measured from the hinge line aft to the trailing edge).

The method is broken down into a logical sequence of calculations that account for various factors in the following order:

1. Radius-nose, sealed, plain trailing-edge control for which the condition

$$\tan \frac{\phi'_{TE}}{2} = \tan \frac{\phi''_{TE}}{2} = \tan \frac{\phi_{TE}}{2} = \frac{t}{c}$$

is satisfied.

2. Thickness distribution when

$$\tan \frac{\phi'_{TE}}{2} = \tan \frac{\phi''_{TE}}{2} = \tan \frac{\phi_{TE}}{2} = \frac{t}{c}$$

is not satisfied.

3. Various control nose shapes and the effect of nose balance.

4. Effects of Mach number.

The semiempirical method for determining the section hinge-moment derivative  $c'_{h\delta}$  is as follows:

- Step 1. Calculate the hinge-moment derivative  $c'_{h\delta}$  for a radius-nose, sealed, trailing-edge flap for the following thickness condition

$$\tan \frac{\phi'_{TE}}{2} = \tan \frac{\phi''_{TE}}{2} = \tan \frac{\phi_{TE}}{2} = \frac{t}{c}$$

by

$$c'_{h\delta} = \left[ \frac{c'_{h\delta}}{(c'_{h\delta})_{theory}} \right] (c'_{h\delta})_{theory} \quad (\text{per radian}) \quad 6.1.3.2-a$$

where

$\phi'_{TE}$  is the trailing-edge angle defined as the angle between straight lines passing through points at 90 and 99 percent of the chord on the upper and lower airfoil surfaces.

$\phi''_{TE}$  is the trailing-edge angle defined as the angle between straight lines passing through points at 95 and 99 percent of the chord on the upper and lower airfoil surfaces.

$\phi_{TE}$

is the trailing-edge angle defined as the angle between tangents to the upper and lower airfoil surfaces at the trailing edge.

$$\frac{c'_{h\delta}}{(c_{h\delta})_{theory}}$$

is the ratio of the actual to the theoretical hinge-moment derivative for a radius-nose, sealed-gap, plain trailing-edge flap, obtained from Figure 6.1.3.2-12a.

The parameter  $c_{l\alpha}/(c_{l\alpha})_{theory}$  used in reading this chart is obtained from Figure 4.1.1.2-8a.

$$(c_{h\delta})_{theory}$$

is the theoretical hinge-moment derivative for airfoils having

$$\tan \frac{\phi'_{TE}}{2} = \tan \frac{\phi''_{TE}}{2} = \tan \frac{\phi_{TE}}{2} = \frac{t}{c}$$

This parameter is obtained from Figure 6.1.3.2-12b.

- Step 2. If the thickness condition in Step 1 is satisfied, Step 2 may be omitted. However, if the thickness condition in Step 1 is not satisfied, correct the hinge-moment derivative  $c'_{h\delta}$  of Step 1 to account for the particular thickness distribution by

$$c''_{h\delta} = c'_{h\delta} + 2(c_{l\delta})_{theory} \left[ 1 - \frac{c_{l\delta}}{(c_{l\delta})_{theory}} \right] \left( \tan \frac{\phi''_{TE}}{2} - \frac{t}{c} \right) \quad (\text{per radian})$$

6.1.3.2-b

where

$$c'_{h\delta}$$

is obtained from Equation 6.1.3.2-a in Step 1.

$$(c_{l\delta})_{theory}$$

is the theoretical lift due to flap deflection, obtained from Figure 6.1.1.1-39a.

$$\frac{c_{l\delta}}{(c_{l\delta})_{theory}}$$

is the ratio of the actual to the theoretical lift due to flap deflection, obtained from Figure 6.1.1.1-39b as a function of  $c_{l\alpha}/(c_{l\alpha})_{theory}$  and  $c_f/c$ .

The parameters  $c_{l\alpha}/(c_{l\alpha})_{theory}$  and  $\tan \frac{\phi''_{TE}}{2}$  are obtained as noted in Step 1.

For a beveled trailing edge,  $\phi''_{TE}$  should be taken as equal to the angle of bevel.

It is stated in Reference 3 that under the restriction that there is no separated flow,  $c_{h\delta}$  for a radius-nose control can be determined from the above equations with an accuracy of  $\pm 0.05$  per radian.

- Step 3. Correct the hinge-moment derivative to account for nose-shape and nose-balance effects (taken from Reference 5) by

$$(c_{h\delta})_{balance} = c''_{h\delta} \left[ \frac{(c_{h\delta})_{balance}}{c''_{h\delta}} \right] \text{ (per radian)} \quad 6.1.3.2-c$$

where

$c''_{h\delta}$  is obtained from Equation 6.1.3.2-b, or is equal to  $c'_{h\delta}$  in Step 1, if the thickness correction is not required.

$\frac{(c_{h\delta})_{balance}}{c''_{h\delta}}$  is obtained from Figure 6.1.3.2-13 for noses of various shapes. The nose shapes corresponding to the curves in Figure 6.1.3.2-13 are shown in Figure 6.1.3.1-12b of Section 6.1.3.1. The balance ratio as used in Figure 6.1.3.2-13 is defined by Equation 6.1.3.1-d of Section 6.1.3.1.

Figure 6.1.3.2-13 is taken from Reference 6 and is based on a limited amount of experimental data on sealed controls. Small changes in nose shape, trailing-edge contour, and air flow may have significant effects on the hinge-moment derivative of balanced control surfaces.

- Step 4. Mach-number effects should be approximated by the use of test data whenever possible. However, when no test data are available, the Mach-number effects may be roughly approximated by using the Prandtl-Glauert correction; i.e.,

$$(c_{h\delta})_M = \frac{(c_{h\delta})_{low speed}}{\sqrt{1 - M^2}} \quad 6.1.3.2-e$$

#### Sample Problem

Given: The flapped airfoil of Reference 8. This is the same configuration as that of the sample problem of Paragraph A, Section 6.1.3.1.

NACA 0015 airfoil	Plain trailing-edge flap	$c_f/c = 0.30$
Round-nose control	$c_b/c_f = 0.35$	$t_c/(2c_f) = 0.1527$
Sealed gap	$\tan \frac{\phi'_{TE}}{2} = 0.164$	$\tan \frac{\phi''_{TE}}{2} = 0.169$
Low speed	$R_g = 2.76 \times 10^6$	$\tan \frac{\phi_{TE}}{2} = 0.169$

Compute:

Determine the hinge-moment derivative for a radius-nose, sealed, trailing-edge flap

$$(c_{h\delta})_{\text{theory}} = -0.825 \text{ per rad} \quad (\text{Figure 6.1.3.2-12b})$$

$$\frac{c_{q\alpha}}{(c_{q\alpha})_{\text{theory}}} = 0.760 \quad (\text{Figure 4.1.1.2-8a})$$

$$\frac{c'_{h\delta}}{(c_{h\delta})_{\text{theory}}} = 0.780 \quad (\text{Figure 6.1.3.2-12a})$$

$$c'_{h\delta} = \left[ \frac{c'_{h\delta}}{(c_{h\delta})_{\text{theory}}} \right] (c_{h\delta})_{\text{theory}} \quad (\text{Equation 6.1.3.2-a})$$

$$= (0.780)(-0.825)$$

$$= -0.644 \text{ per rad}$$

Determine if the thickness condition is satisfied; i.e.,

$$\tan \frac{\phi'_{TE}}{2} = \tan \frac{\phi''_{TE}}{2} = \tan \frac{\phi_{TE}}{2} = \frac{t}{c}$$

$$0.164 \neq 0.169 = 0.169 \neq 0.15$$

Determine the hinge-moment derivative accounting for the thickness distribution

$$(c_{q\delta})_{\text{theory}} = 4.60 \text{ per rad} \quad (\text{Figure 6.1.1.1-39a})$$

$$\frac{c_{q\delta}}{(c_{q\delta})_{\text{theory}}} = 0.605 \quad (\text{Figure 6.1.1.1-39b})$$

$$c''_{h\delta} = c'_{h\delta} + 2(c_{q\delta})_{\text{theory}} \left[ 1 - \frac{c_{q\delta}}{(c_{q\delta})_{\text{theory}}} \right] \left( \tan \frac{\phi''_{TE}}{2} - \frac{t}{c} \right) \quad (\text{Equation 6.1.3.2-b})$$

$$= -0.644 + 2(4.60)[1 - 0.605](0.169 - 0.150)$$

$$= -0.575 \text{ per rad}$$

Determine the effect of nose shape and nose balance

$$\text{Balance ratio} = \sqrt{\left(\frac{c_b}{c_f}\right)^2 - \left(\frac{t_c}{2c_f}\right)^2} \quad (\text{Equation 6.1.3.1-d})$$

$$= \sqrt{(0.35)^2 - (0.1527)^2}$$

$$= 0.315$$

$$\frac{(c_{h\delta})_{\text{balance}}}{c''_{h\delta}} = 0.42 \quad (\text{Figure 6.1.3.2-13})$$

$$(c_{h\delta})_{\text{balance}} = c''_{h\delta} \left[ \frac{(c_{h\delta})_{\text{balance}}}{c''_{h\delta}} \right] \quad (\text{Equation 6.1.3.2-c})$$

$$= (-0.575)(0.42)$$

$$= -0.2415 \text{ per rad}$$

$$= -0.00421 \text{ per deg}$$

This compares with a test value of  $-0.0030$  per degree from Reference 8.

## B. TRANSONIC

No method is available for predicting the section hinge-moment derivative  $c_{h\delta}$  at transonic speeds.

## C. SUPERSONIC

The method for determining  $c_{h\delta}$  at supersonic speeds is based on the theory of Reference 7. The theory applies to airfoils with sharp leading and trailing edges, where the angles of attack and flap deflection angles are small. In addition, the flow field is assumed to be everywhere supersonic and inviscid.

### DATCOM METHOD

The hinge-moment derivative  $c_{h\delta}$  at supersonic speeds for a symmetric, straight-sided flap with  $c_f/c < 1/2$ , regardless of the airfoil section ahead of the flap, is given by

$$c_{h\delta} = -C_1 + C_2 \phi_{TE} \quad 6.1.3.2-d$$

where  $C_1$  and  $C_2$  are thickness correction factors to the supersonic flat-plate derivative.

$$C_1 = \frac{2}{\sqrt{M^2 - 1}} \text{ per radian}$$

$$C_2 = \frac{(\gamma + 1)M^4 - 4(M^2 - 1)}{2(M^2 - 1)^2} \text{ per radian}$$

$\phi_{TE}$  is the trailing-edge angle in radians.

$\gamma$  is the ratio of specific heats,  $\gamma = 1.4$ .

For a symmetric, circular-arc airfoil with  $c_f/c < 1/2$ ,  $c_{h_\delta}$  is given by

$$c_{h_\delta} = -C_1 + \left( \frac{\Delta c_{h_\delta}}{t/c} \right) \frac{t}{c} \quad 6.1.3.2-e$$

where  $C_1$  is defined above, and

$\frac{\Delta c_{h_\delta}}{t/c}$  is a thickness correction factor for symmetric, circular-arc airfoils, obtained from Figure 6.1.3.1-13.

The method becomes somewhat complicated for more general airfoil shapes. Other airfoil shapes are treated in Reference 7.

### Sample Problem

Given: Symmetric, circular-arc airfoil.

$$t/c = 0.06 \quad c_f/c = 0.30 \quad M = 2.0$$

Compute:

$$C_1 = \frac{2}{\sqrt{M^2 - 1}} \frac{1}{57.3} = 0.020 \text{ per deg}$$

$$\frac{\Delta c_{h_\delta}}{t/c} = 0.0008 \text{ per deg} \quad (\text{Figure 6.1.3.1-13})$$

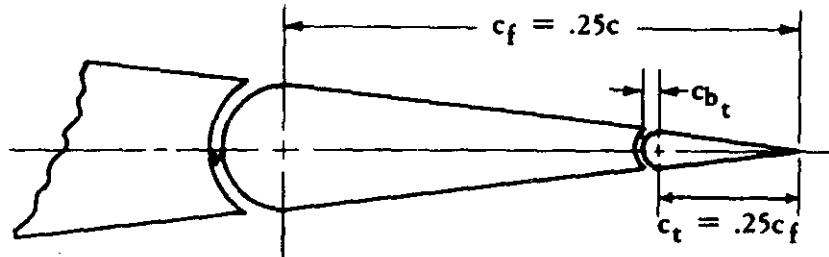
Solution:

$$\begin{aligned} c_{h\delta} &= -C_1 + \left( \frac{\Delta c_{h\delta}}{t/c} \right) \frac{t}{c} \quad (\text{Equation 6.1.3.2-e}) \\ &= -0.020 + (0.0008)(0.06) \\ &= -0.01995 \text{ per deg} \end{aligned}$$

## REFERENCES

1. Anon.: Royal Aeronautical Society Data Sheets — Aerodynamics, Vol. IV, (Controls 04.01.00), 1950. (U)
2. Brewer, J. D., and Queijo, M. J.: Wind-Tunnel Investigation of the Effect of Tab Balance on Tab and Control-Surface Characteristics. NACA TN 1403, 1947. (U)
3. Anon.: Royal Aeronautical Society Data Sheets — Aerodynamics, Vol. IV, (Controls 04.01.02), 1956. (U)
4. Garner, H. C.: Charts for Low-Speed Characteristics of Two-Dimensional Trailing Edge Flaps. ARC 18,528, 1956. (U)
5. Woods, L. C.: The Theory of Aerofoils with Hinged Flaps in Two-Dimensional Compressible Flow. ARC CP 138, 1952. (U)
6. Anon.: Royal Aeronautical Society Data Sheets — Aerodynamics, Vol. IV, (Controls 04.01.03), 1949. (U)
7. Lock, C. N. H.: Examples of the Application of Busemann's Formula to Evaluate the Aerodynamic Force Coefficients on Supersonic Aerofoils. ARC R&M 2101, 1944. (U)
8. Sears, R. I., and Hoggard, H. P., Jr.: Wind-Tunnel Investigation of Control-Surface Characteristics. VII — A Medium Aerodynamic Balance of Two Nose Shapes Used with a 30-Percent-Chord Flap on an NACA 0015 Airfoil. NACA WR L-448, 1942. (U)

SUBSONIC SPEEDS



TAB GAP	TRANSITION STRIPS
— .004c	AT .01c
— — — SEALED	AT .01c
— - .004c	OFF
— - — SEALED	OFF

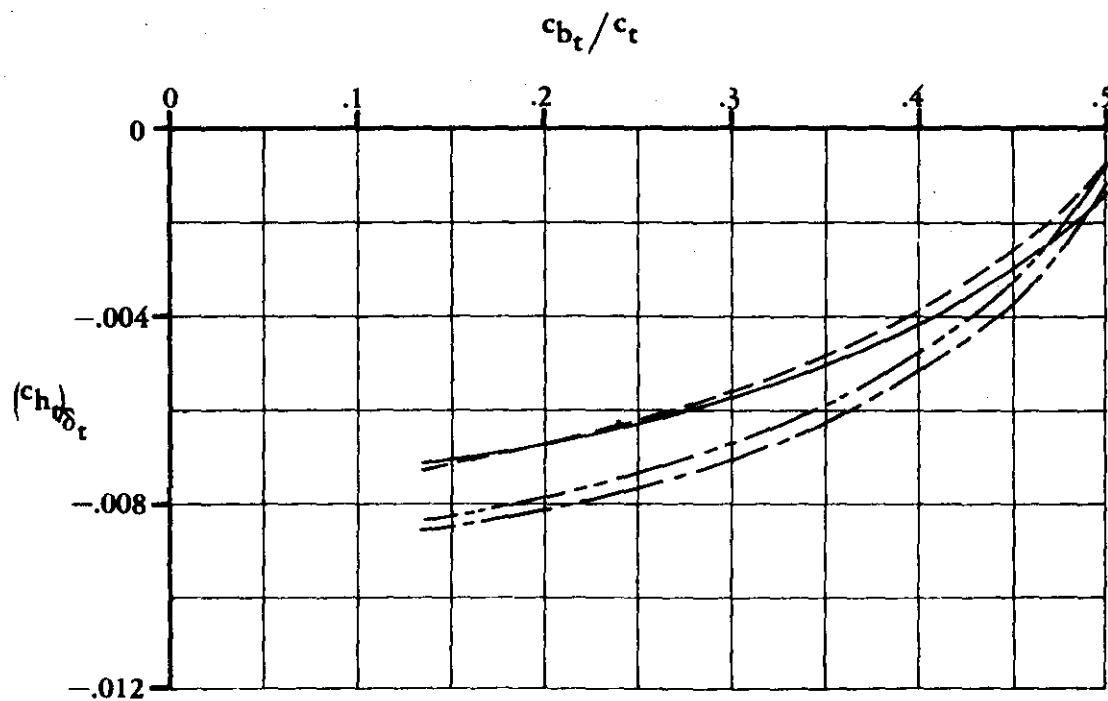
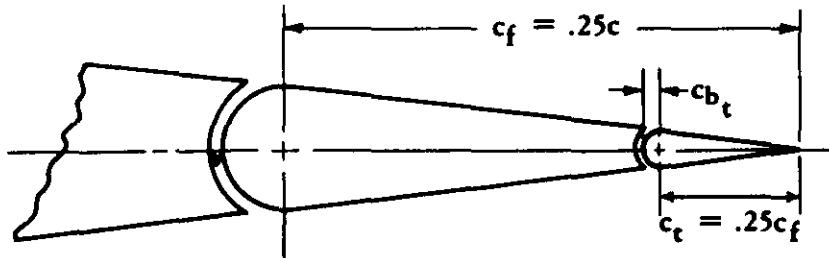


FIGURE 6.1.3.2-10 EFFECT OF SEALED AND UNSEALED TAB GAPS AND TRANSITION STRIPS ON TAB SECTION HINGE MOMENTS

SUBSONIC SPEEDS



TAB GAP	TRANSITION STRIPS
— .004c	AT .01c
— — — SEALED	AT .01c
— - .004c	OFF
— - — SEALED	OFF

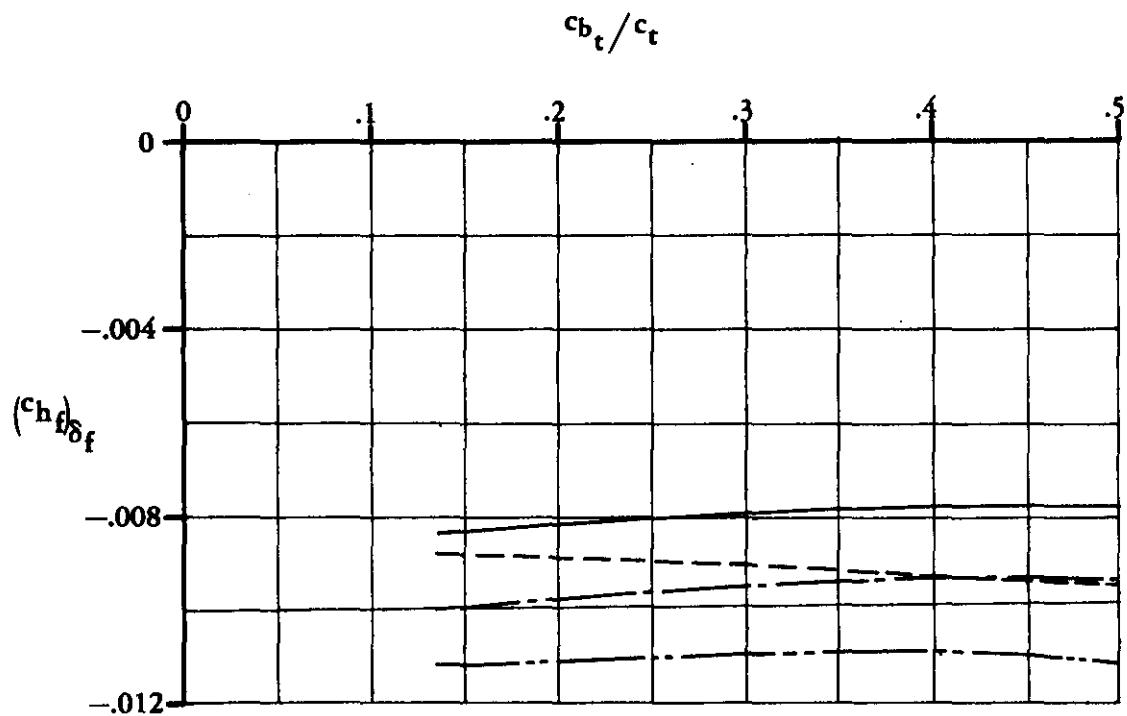
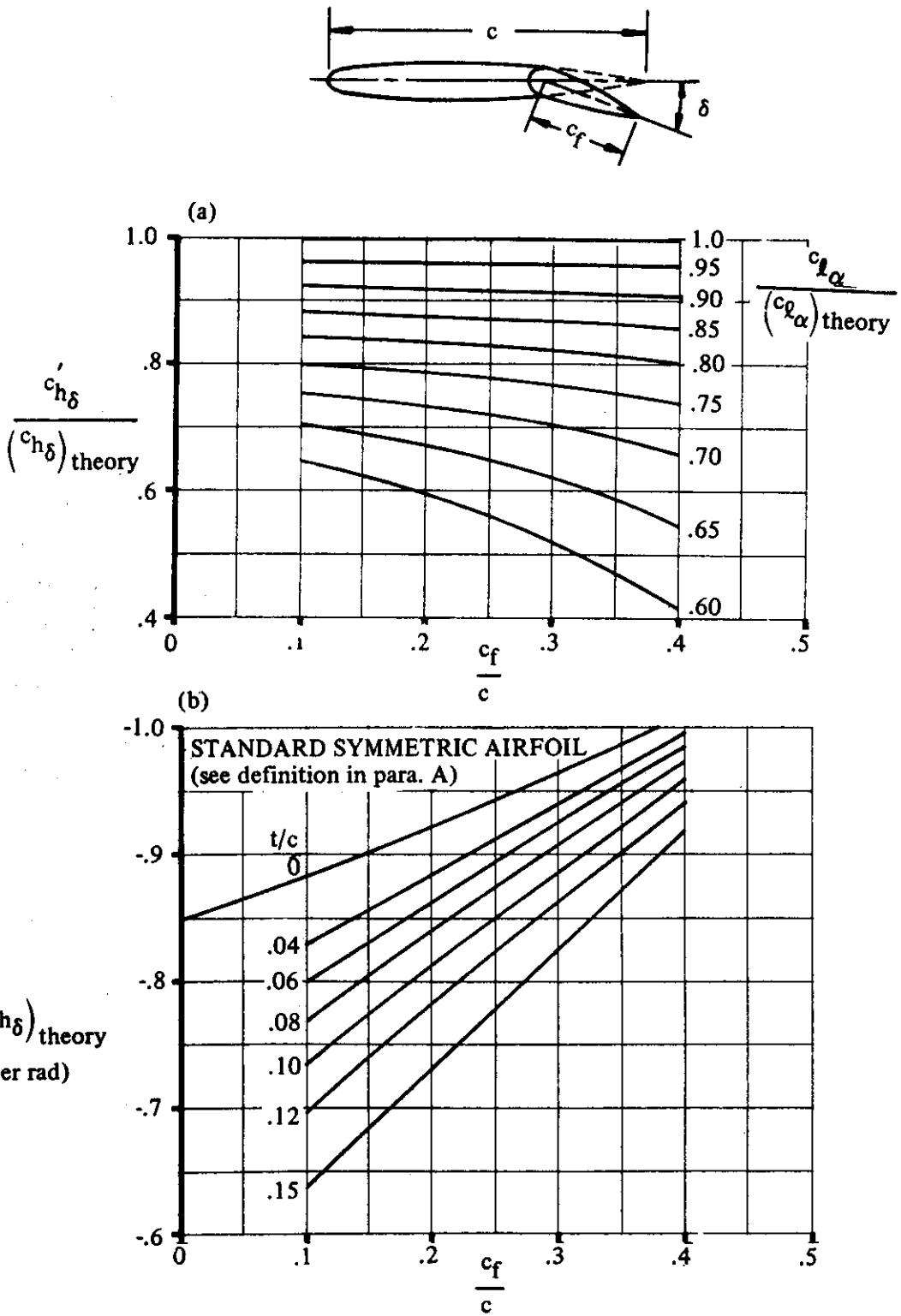


FIGURE 6.1.3.2-11 EFFECT OF SEALED AND UNSEALED TAB GAPS AND TRANSITION STRIPS ON FLAP SECTION HINGE MOMENTS



**FIGURE 6.1.3.2-12 RATE OF CHANGE OF HINGE-MOMENT COEFFICIENT WITH CONTROL DEFLECTION FOR A PLAIN FLAP**

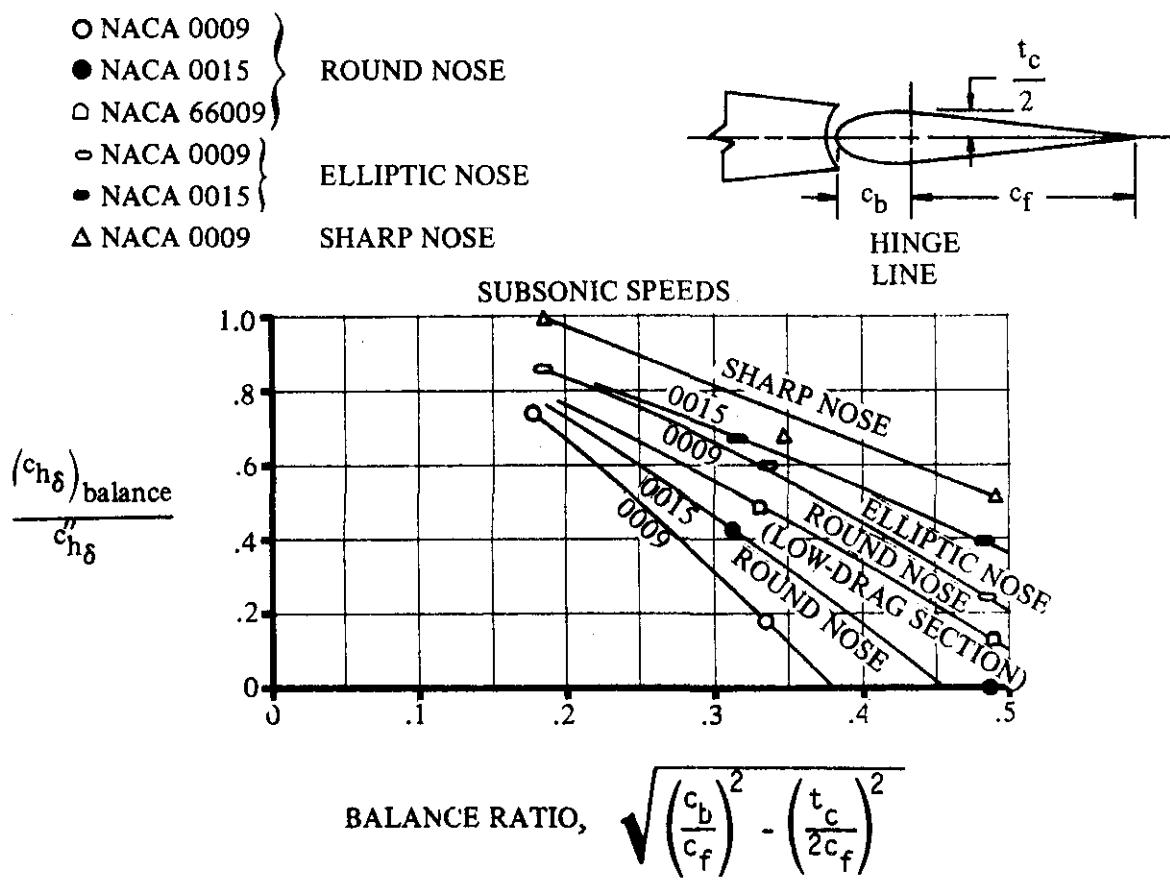


FIGURE 6.1.3.2-13 EFFECT OF NOSE BALANCE ON SECTION CONTROL HINGE-MOMENT COEFFICIENT

### 6.1.3.3 SECTION HINGE-MOMENT DERIVATIVE ( $c_{hf} \delta_t$ ) OF CONTROL SURFACE DUE TO CONTROL TABS

A deflected tab on a control surface causes pressure changes on the surfaces of the tab and control. Because of the large moment arms associated with these incremental pressures, large changes in control-surface hinge moments result. In addition, these incremental changes in the pressure distribution can be influenced by a sealed or unsealed surface where the tab meets the control.

#### DATCOM METHOD

The following method is taken from Reference 1 and is based on the two-dimensional NACA 0009 airfoil test data for round-nose, unbalanced controls with sealed flap and tab gaps. This method is limited to the low-speed linear hinge-moment range and should be restricted to tab deflections of approximately  $\pm 18^\circ$  and the combinations of control deflection and angle of attack as indicated in Figure 6.1.3-2.

The change in the low-speed section hinge-moment coefficient of a control due to tab deflection, measured at constant values of angle of attack and flap deflection, can be expressed as

$$\left( \frac{\partial c_{hf}}{\partial \delta_t} \right)_{\alpha, \delta_f} = \left( \frac{\partial c_{hf}}{\partial \delta_t} \right)_{c_\ell, \delta_f} - \left( \frac{\partial c_{hf}}{\partial c_\ell} \right)_{\delta_t, \delta_f} \left( \frac{\partial c_\ell}{\partial \alpha} \right)_{\delta_t, \delta_f} \left( \frac{\partial \alpha}{\partial \delta_t} \right)_{c_\ell, \delta_f} \quad 6.1.3.3-a$$

where

$\left( \frac{\partial c_{hf}}{\partial \delta_t} \right)_{c_\ell, \delta_f}$  is the change in control section hinge-moment coefficient due to tab deflection, measured at constant values of lift and flap deflection. This value is obtained from Figure 6.1.3.3-4a.

$\left( \frac{\partial c_{hf}}{\partial c_\ell} \right)_{\delta_t, \delta_f}$  is the change in control section hinge-moment coefficient due to lift variation, measured at constant values of tab and flap deflection. This value is obtained from Figure 6.1.3.3-4b (modified from Reference 1 to reflect the characteristics of a flat-sided flap contour – like a conventional elevator).

$\left( \frac{\partial c_\ell}{\partial \alpha} \right)_{\delta_t, \delta_f}$  is the section lift-curve slope of the primary panel (wing, horizontal tail, etc.) at constant values of tab and flap deflection. This value can be obtained from Section 4.1.1.2.

$\left( \frac{\partial \alpha}{\partial \delta_t} \right)_{c_\ell, \delta_f}$  is the rate of change of angle of attack due to a change in tab deflection in the linear range at constant values of lift and flap deflection. This value can be obtained from Figure 6.1.3.3-5.

The above method does not quantitatively account for the effect of unsealing the tab gap. In view of the difficulty of predicting the effects of seals and gaps, experimental data should be used whenever possible. Figure 6.1.3.3-6a (from Reference 2) shows the effects of fixing transition and sealing the tab gap on a modified NACA 65<sub>1</sub>-012 airfoil. For these data, the flap-chord-to-wing-chord ratio is 0.25, the tab-chord-to-flap-chord ratio is 0.25, and the flap gap is sealed.

The effects of tab nose shape are also not accounted for in the above method, and experimental data should be used whenever possible. However, the effect of tab nose shape as a function of nose balance is presented in Figure 6.1.3.3-6b (from Reference 2) for a NACA 65<sub>1</sub>-012 airfoil with a tab gap of 0.004c and transition strips at 0.01c.

Other parameters not accounted for in this method include the effects of airfoil thickness and trailing-edge angle. Unfortunately, not enough data are available to evaluate the effects of either of these variables on the section hinge-moment derivative. Additional test data, including the effects of these variables on a limited number of flapped configurations, are presented in References 3 through 9.

### Sample Problem

Given: The flap and tab configuration of Reference 2.

NACA 65<sub>1</sub>-012 airfoil

Plain trailing-edge flap (sealed)

$c_f/c = 0.25$

Round-nose flap

Plain trailing-edge tab (sealed)

$c_t/c_f = 0.25$

Round-nose tab

Low speed

$R_q = 4.59 \times 10^6$

Compute:

$$\left( \frac{\partial c_{hf}}{\partial \delta_t} \right)_{c_q, \delta_f} = -0.0124 \text{ per deg} \quad (\text{Figure 6.1.3.3-4a})$$

$$\left( \frac{\partial c_{hf}}{\partial c_q} \right)_{\delta_t, \delta_f} = -0.046 \quad (\text{Figure 6.1.3.3-4b})$$

$$\left( \frac{\partial \alpha}{\partial \delta_t} \right)_{c_q, \delta_f} = -0.255 \quad (\text{Figure 6.1.3.3-5})$$

$$c_{q_\alpha} = 0.11 \text{ per deg} \quad (\text{Table 4.1.1-B})$$

Solution:

$$\left( \frac{\partial c_{h_f}}{\partial \delta_t} \right)_{\alpha, \delta_f} = \left( \frac{\partial c_{h_f}}{\partial \delta_t} \right)_{c_\alpha, \delta_f} - \left( \frac{\partial c_{h_f}}{\partial c_\alpha} \right)_{\delta_t, \delta_f} \left( \frac{\partial c_\alpha}{\partial \alpha} \right)_{\delta_t, \delta_f} \left( \frac{\partial \alpha}{\partial \delta_t} \right)_{c_\alpha, \delta_f}$$

(Equation 6.1.3.3-a)

$$= -0.0124 - (-0.046)(0.11)(-0.255)$$

$$= -0.0124 - 0.0013$$

$$= -0.0137 \text{ per deg}$$

This compares with test values of  $-0.0115$  per degree with transition strips and  $-0.0138$  per degree without transition strips, from Reference 2.

## REFERENCES

1. Ames, M. B., Jr., and Sears, R. I.: Determination of Control-Surface Characteristics from NACA Plain Flap and Tab Data. NACA TR 721, 1941. (U)
2. Brewer, J. D., and Queijo, M. J.: Wind-Tunnel Investigation of the Effect of Tab Balance on Tab and Control-Surface Characteristics. NACA TN 1403, 1947. (U)
3. Batson, A. S., and Skelton, W. C.: Lift and Hinge Moment on Two-Dimensional Tabbed Controls at Low Speeds. ARC 17285, 1955. (U)
4. Sears, R. I., and Liddell, R. B.: Wind-Tunnel Investigation of Control-Surface Characteristics. VI — A 30-Percent-Chord Plain Flap on the 0015 Airfoil. NACA L-454, 1942. (U)
5. Sears, R. I., and Hoggard, H. P., Jr.: Wind-Tunnel Investigation of Control-Surface Characteristics. VII — A Medium Aerodynamic Balance of Two Nose Shapes Used with a 30-Percent-Chord Flap on an NACA 0015 Airfoil. NACA L-448, 1942. (U)
6. Sears, R. I., and Clarence, G. L.: Wind-Tunnel Investigation of Control-Surface Characteristics. VIII — A Large Aerodynamic Balance of Two Nose Shapes Used with a 30-Percent-Chord Flap on an NACA 0015 Airfoil. NACA L-378, 1942. (U)
7. Clarence, G. L., and Lockwood, V. E.: Wind-Tunnel Investigation of Control-Surface Characteristics. XIII — Various Flap Overhangs Used with a 30-Percent-Chord Flap on an NACA 66-009 Airfoil. NACA L-314, 1943. (U)
8. Wright, K. C.: Measurements of Two-Dimensional Derivatives on a Wing-Aileron-Tab System with a 1541 Section Aerofoil. Part II — Direct Tab and Cross Aileron-Tab Derivatives. ARC R&M 3029, 1958. (U)
9. Ames, M. B., Jr.: Wind-Tunnel Investigation of Control-Surface Characteristics. III — A Small Aerodynamic Balance of Various Nose Shapes Used with a 30-Percent-Chord Flap on an NACA 0009 Airfoil. NACA L-301, 1941. (U)

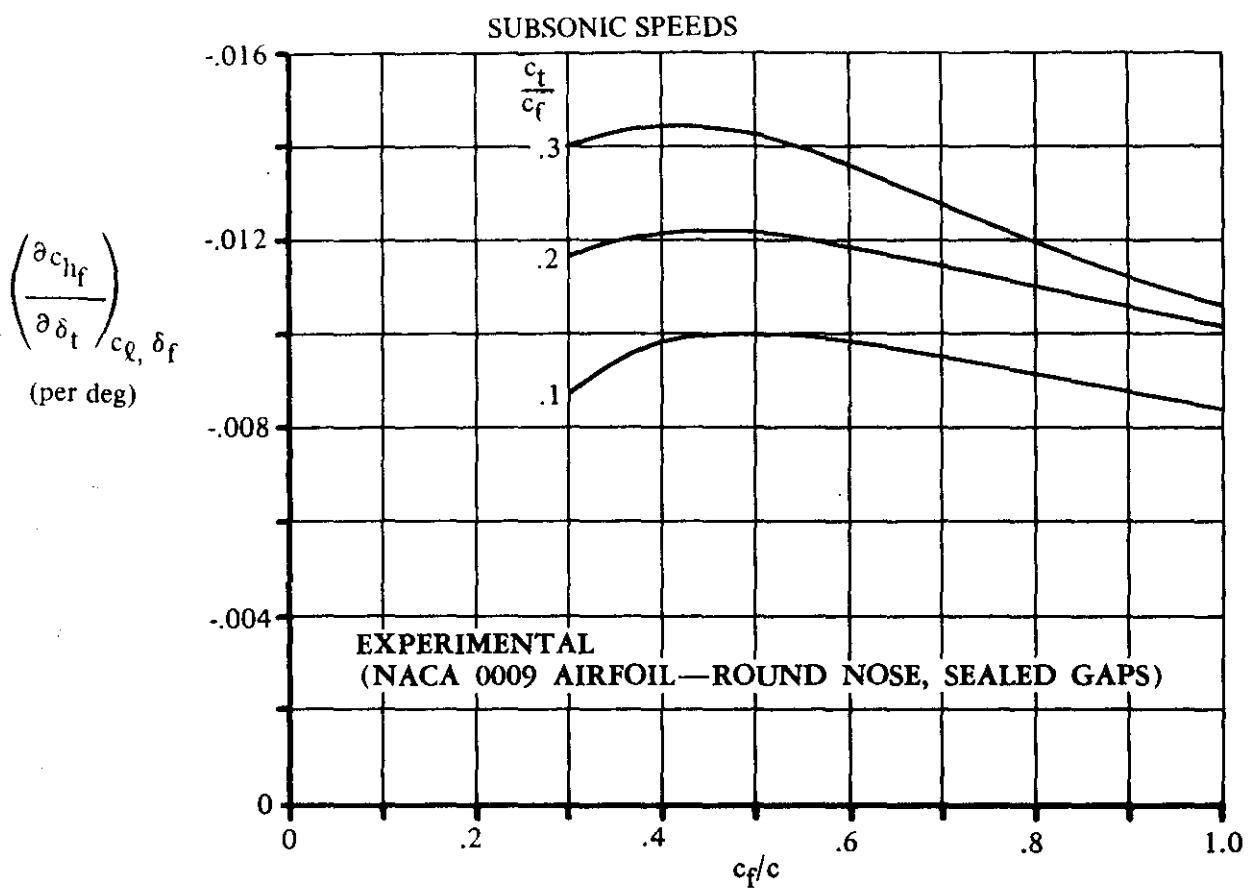


FIGURE 6.1.3.3-4a EFFECT OF TAB DEFLECTION ON CONTROL-SURFACE SECTION HINGE MOMENTS

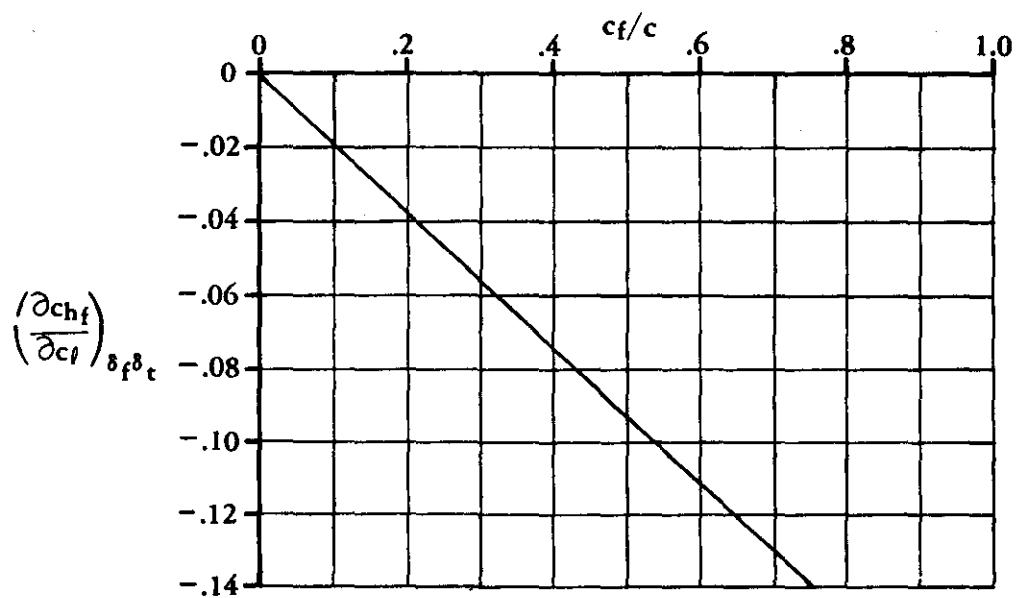
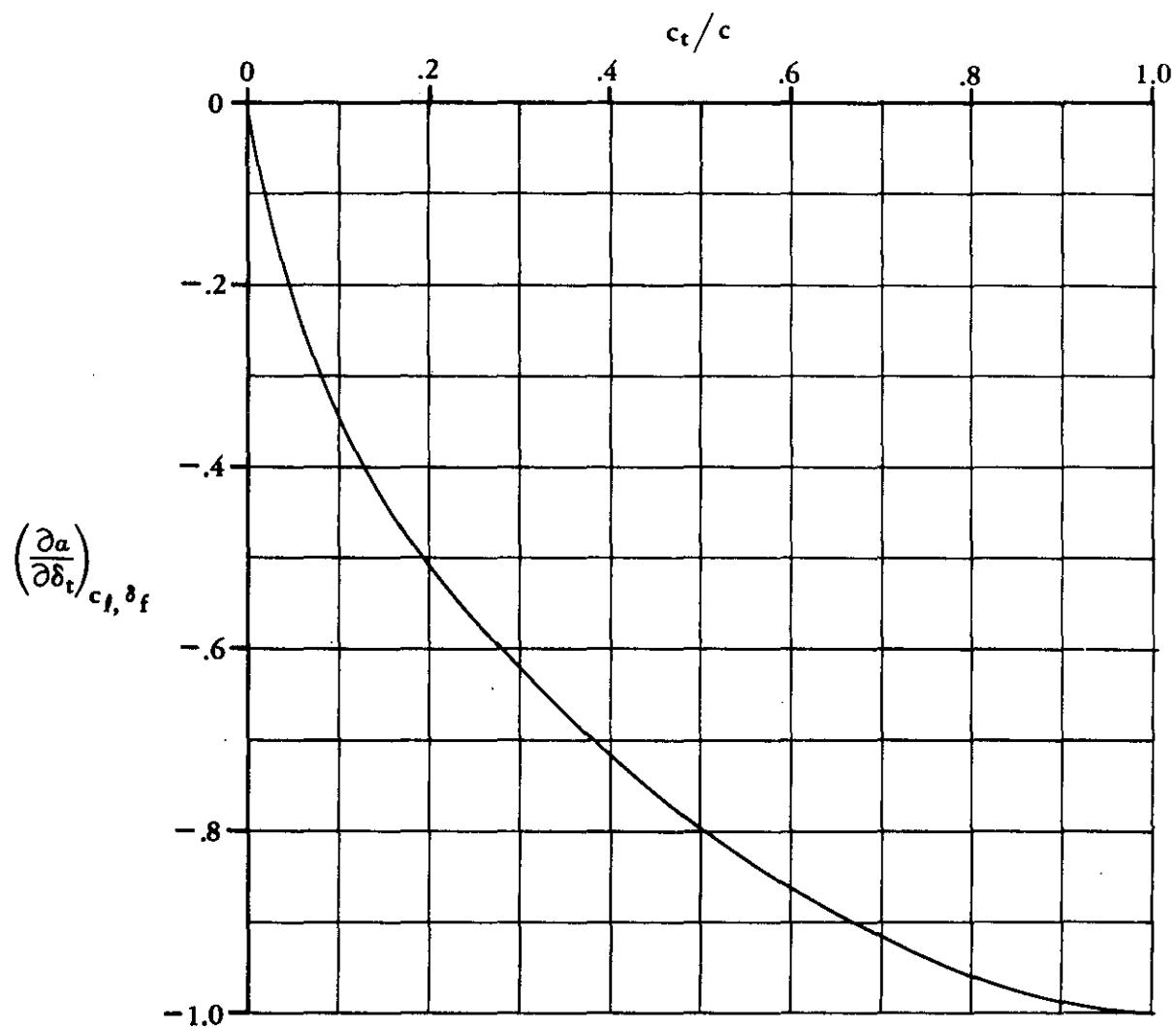


FIGURE 6.1.3.3-4b EFFECT OF SECTION LIFT COEFFICIENT ON FLAP SECTION HINGE MOMENTS

SUBSONIC SPEEDS



**FIGURE 6.1.3.3-5 RATE OF CHANGE OF ANGLE OF ATTACK DUE TO A CHANGE IN TAB DEFLECTION**

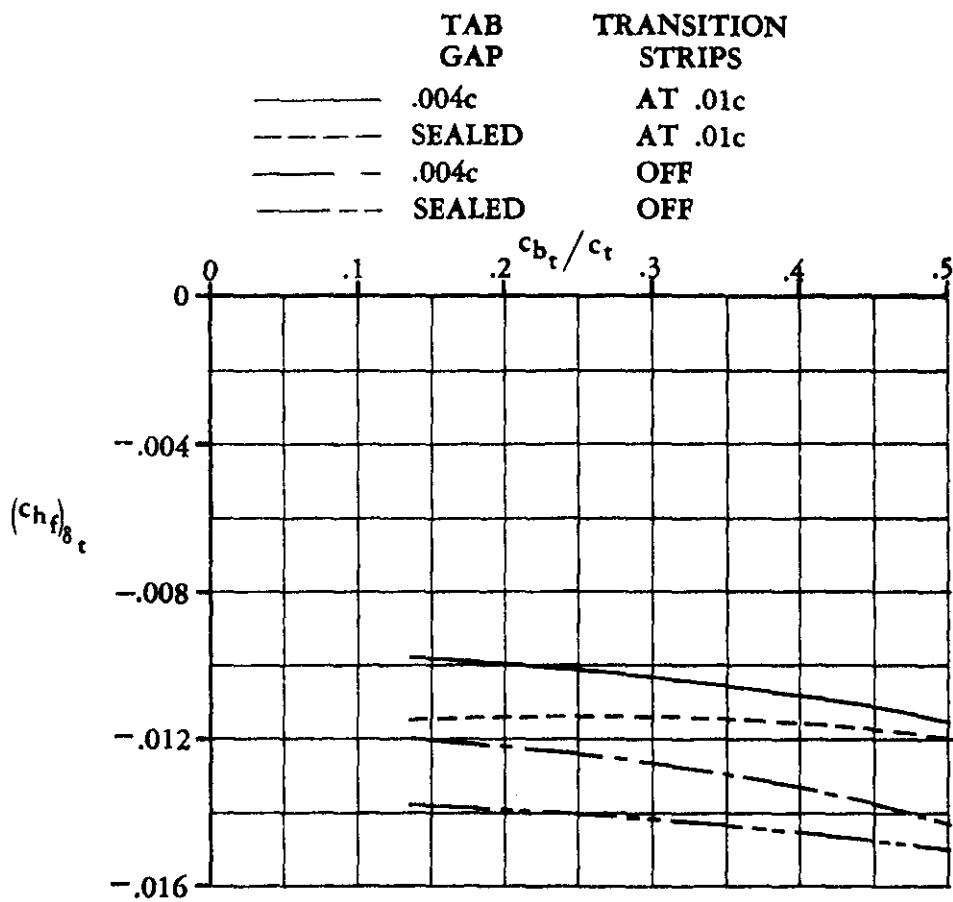


FIGURE 6.1.3.3-6a EFFECT OF SEALED AND UNSEALED TAB GAPS AND TRANSITION STRIPS ON FLAP SECTION HINGE MOMENTS

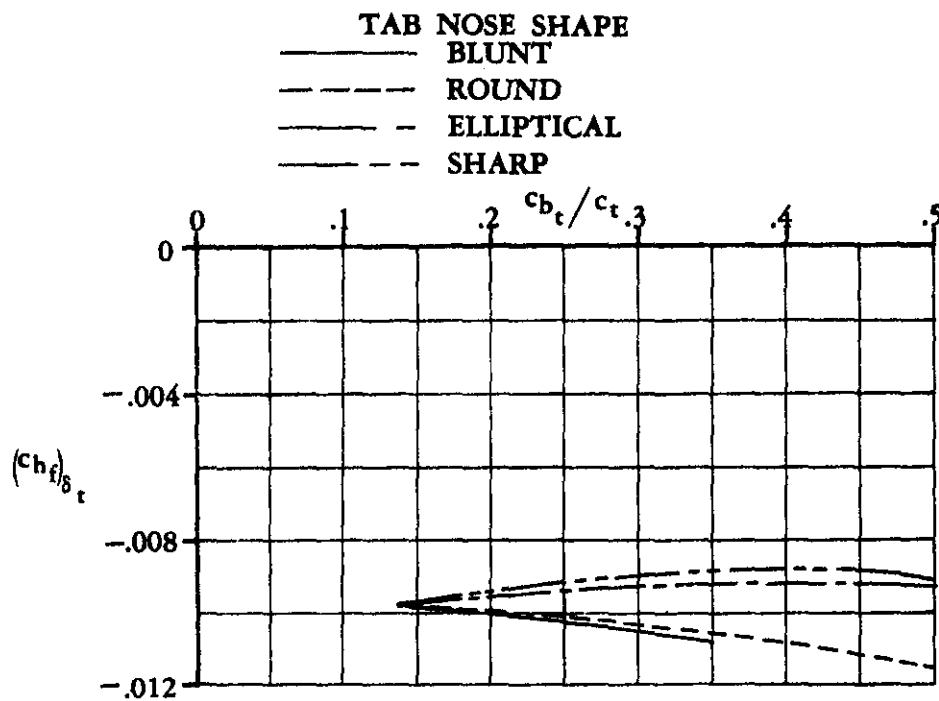


FIGURE 6.1.3.3-6b EFFECT OF TAB NOSE SHAPE AND AERODYNAMIC BALANCE ON FLAP SECTION HINGE MOMENTS

#### 6.1.3.4 SECTION HINGE-MOMENT DERIVATIVE ( $c_{h_t}$ ) <sub>$\delta_f$</sub> OF CONTROL TAB DUE TO CONTROL SURFACE

A deflected flap or control surface causes pressure changes on the surfaces of the tab and control. These pressure changes on the tab generally result in a change in the tab hinge moment.

#### DATCOM METHOD

The following method is taken from Reference 1 and is based on the two-dimensional NACA 0009 airfoil test data for round-nose, unbalanced controls, with sealed flap and tab gaps. This method is limited to the low-speed linear hinge-moment range and should be restricted to flap deflections of approximately  $\pm 18^\circ$  and the combinations of control deflection and angle of attack as indicated in Figure 6.1.3-2.

The change in the low-speed tab section hinge-moment coefficient due to flap deflection, measured at constant values of angle of attack and tab deflection, can be expressed as

$$\left( \frac{\partial c_{h_t}}{\partial \delta_f} \right)_{\alpha, \delta_t} = \left( \frac{\partial c_{h_t}}{\partial \delta_f} \right)_{c_2, \delta_t} - \left( \frac{\partial c_{h_t}}{\partial c_2} \right)_{\delta_f, \delta_t} \left( \frac{\partial c_2}{\partial \alpha} \right)_{\delta_f, \delta_t} \left( \frac{\partial \alpha}{\partial \delta_f} \right)_{c_2, \delta_t} \quad 6.1.3.4-a$$

where

$\left( \frac{\partial c_{h_t}}{\partial \delta_f} \right)_{c_2, \delta_t}$  is the change in tab section hinge-moment coefficient due to control deflection, measured at constant values of lift and tab deflection. This value is obtained from Figure 6.1.3.4-4a.

$\left( \frac{\partial c_{h_t}}{\partial c_2} \right)_{\delta_f, \delta_t}$  is the change in tab section hinge-moment coefficient with respect to lift coefficient, measured at constant values of flap and tab deflections. This value is obtained from Figure 6.1.3.4-4b.

$\left( \frac{\partial c_2}{\partial \alpha} \right)_{\delta_f, \delta_t}$  is the section lift-curve slope of the primary panel (wing, horizontal tail, etc.) at constant values of tab and flap deflection. This value can be obtained from Section 4.1.1.2.

$\left( \frac{\partial \alpha}{\partial \delta_f} \right)_{c_2, \delta_t}$  is the rate of change of angle of attack due to a change in flap deflection in the linear range at constant values of lift and tab deflection. This value can be obtained from Figure 6.1.3.4-5.

The above method does not quantitatively account for the effect of unsealing the tab gap. In view of the difficulty of predicting the effects of seals and gaps, experimental data should be used whenever possible. Figure 6.1.3.4-6a (from Reference 2) shows the effects of fixing transition and sealing the tab gap on a modified NACA 65<sub>1</sub>-012 airfoil. For these data, the flap-chord-to-wing-chord ratio is 0.25, the tab-chord-to-flap-chord ratio is 0.25, and flap gap is sealed.

The effects of tab nose shape are not accounted for in the above method and experimental data should be used whenever possible. However, the effect of tab nose shape as a function of nose balance is presented in Figure 6.1.3.4-6b (from Reference 2) for a NACA 65<sub>1</sub>-012 airfoil with a tab gap of 0.004c and transition strips at 0.01c.

Other parameters not accounted for in the above method include the effects of airfoil thickness and trailing-edge angle. Unfortunately, not enough test data are available to evaluate the effects of either of these variables on the section hinge-moment derivative. Additional test data, including the effects of these variables on a limited number of flapped configurations, are presented in References 3 through 9 of Section 6.1.3.3.

### Sample Problem

Given: The flap and tab configuration of Reference 2.

NACA 65<sub>1</sub>-012 airfoil

Plain trailing-edge flap (sealed)

$c_f/c = 0.25$

Round-nose flap

Plain trailing-edge tab (sealed)

$c_t/c_f = 0.25$

Round-nose tab

Low speed

$R_e = 4.59 \times 10^6$

Compute:

$$\left( \frac{\partial c_{ht}}{\partial \delta_f} \right)_{c_f, \delta_t} = -0.00188 \text{ per deg} \quad (\text{Figure 6.1.3.4-4a})$$

$$\left( \frac{\partial c_{ht}}{\partial c_f} \right)_{\delta_f, \delta_t} = -0.011 \quad (\text{Figure 6.1.3.4-4b})$$

$$\left( \frac{\partial \alpha}{\partial \delta_f} \right)_{c_f, \delta_t} = -0.569 \quad (\text{Figure 6.1.3.4-5})$$

$$c_{\alpha} = 0.11 \text{ per deg} \quad (\text{Table 4.1.1-B})$$

Solution:

$$\left( \frac{\partial c_{h_t}}{\partial \delta_f} \right)_{\alpha, \delta_t} = \left( \frac{\partial c_{h_t}}{\partial \delta_f} \right)_{c_\ell, \delta_t} - \left( \frac{\partial c_{h_t}}{\partial c_\ell} \right)_{\delta_f, \delta_t} \left( \frac{\partial c_\ell}{\partial \alpha} \right)_{\delta_f, \delta_t} \left( \frac{\partial \alpha}{\partial \delta_f} \right)_{c_\ell, \delta_t}$$

(Equation 6.1.3.4-a)

$$= -0.00188 - (-0.011)(0.11)(-0.569)$$
$$= -0.00188 - 0.00069$$
$$= -0.00257 \text{ per deg}$$

This compares with test values of -0.0012 per degree with transition strips and -0.0026 per degree without transition strips, from Reference 2.

## REFERENCES

1. Ames, M. B., Jr., and Sears, R. I.: Determination of Control-Surface Characteristics from NACA Plain Flap and Tab Data. NACA TR 721, 1941. (U)
2. Brewer, J. D., and Queijo, M. J.: Wind-Tunnel Investigation of the Effect of Tab Balance on Tab and Control-Surface Characteristics. NACA TN 1403, 1947. (U)

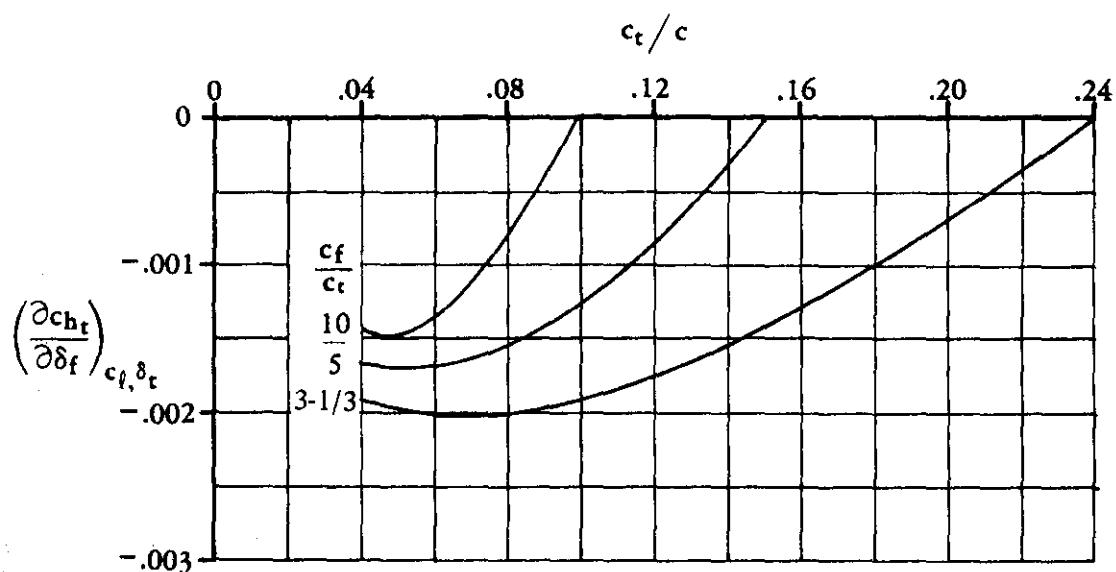


FIGURE 6.1.3.4-4a EFFECT OF FLAP DEFLECTION ON TAB SECTION HINGE MOMENTS

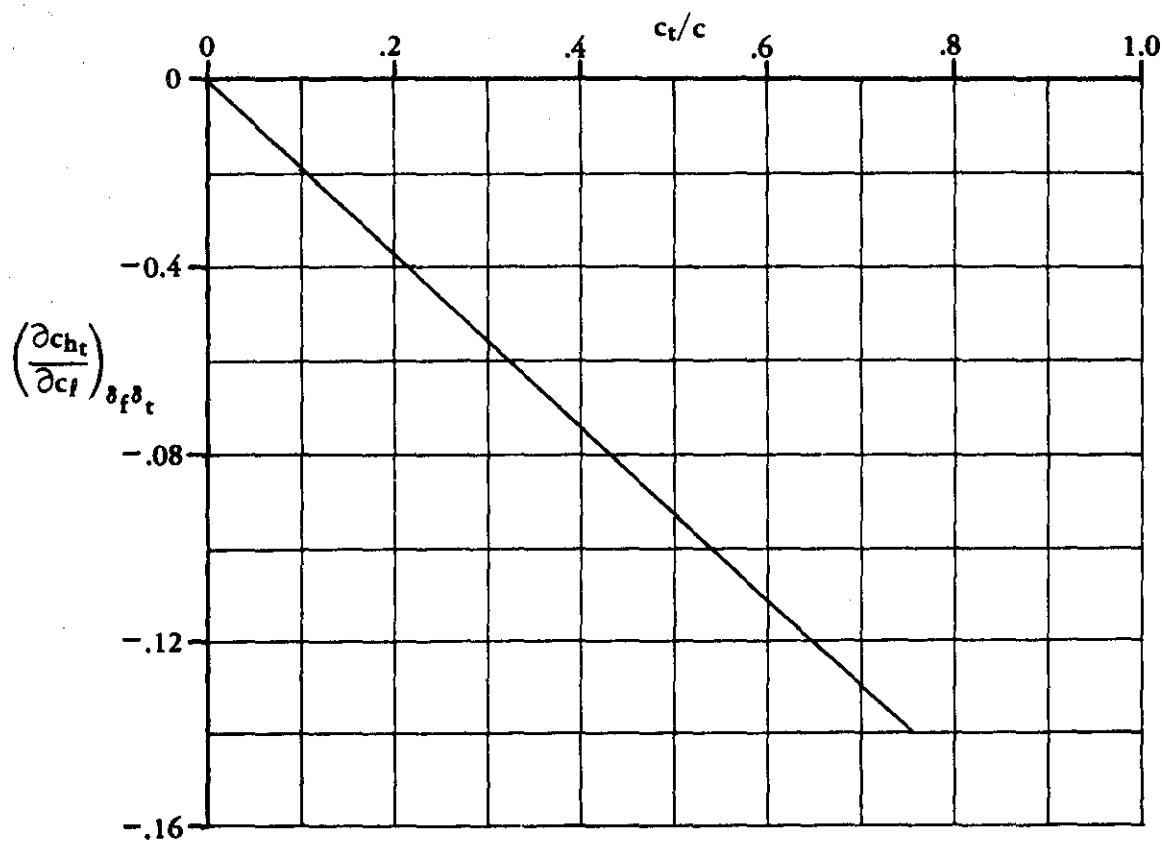
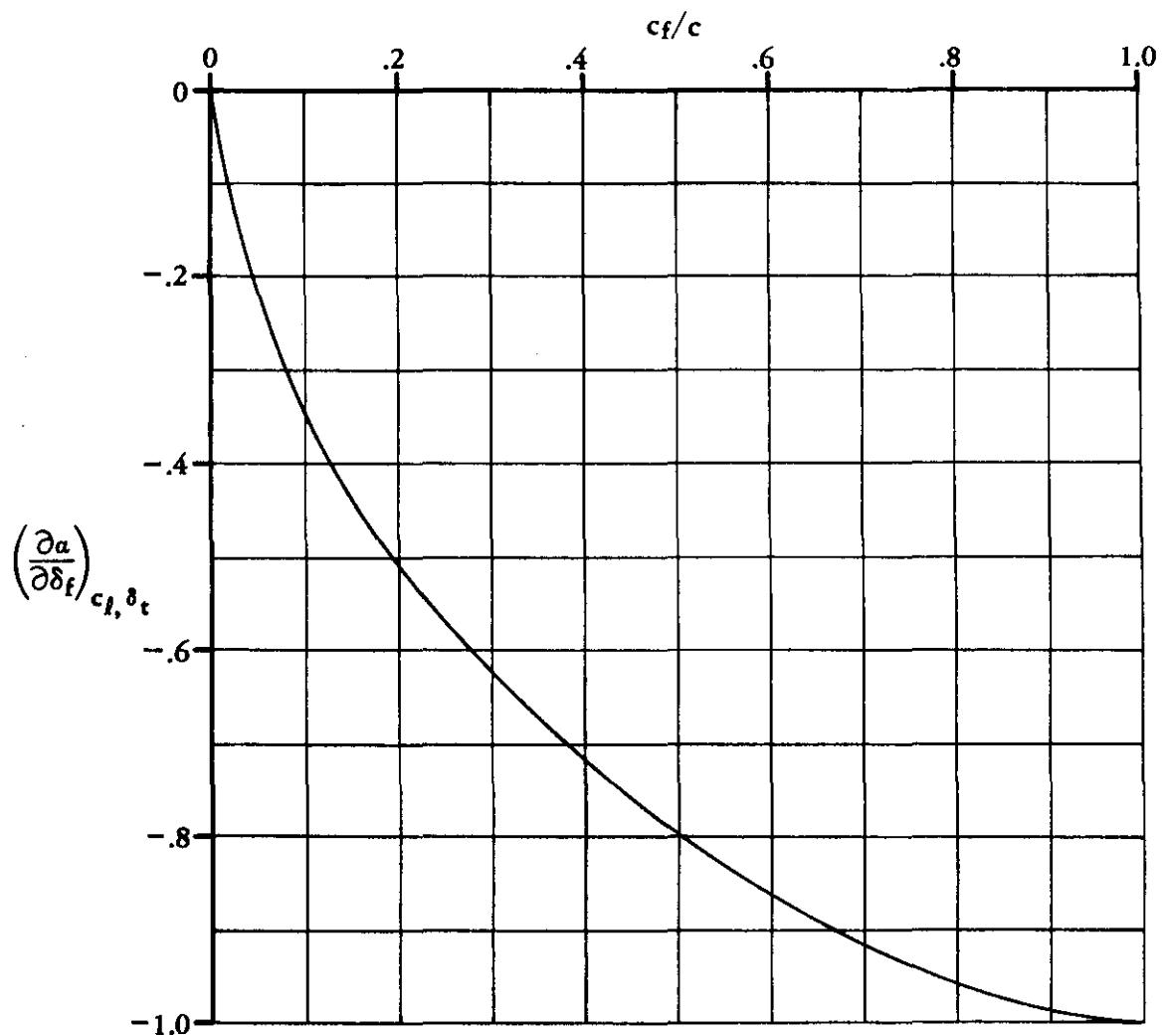
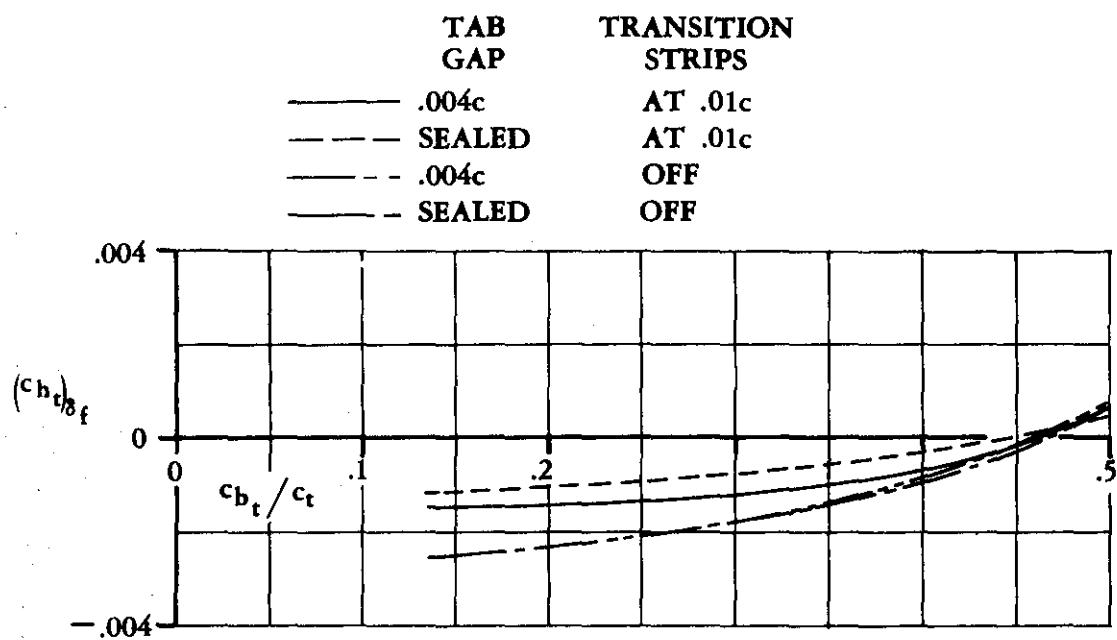


FIGURE 6.1.3.4-4b EFFECT OF SECTION LIFT COEFFICIENT ON TAB SECTION HINGE MOMENTS

SUBSONIC SPEEDS



**FIGURE 6.1.3.4-5 RATE OF CHANGE OF ANGLE OF ATTACK DUE TO A CHANGE IN FLAP DEFLECTION**



**FIGURE 6.1.3.4-6 a EFFECT OF SEALED AND UNSEALED TAB GAPS AND TRANSITION STRIPS ON TAB SECTION HINGE MOMENTS**

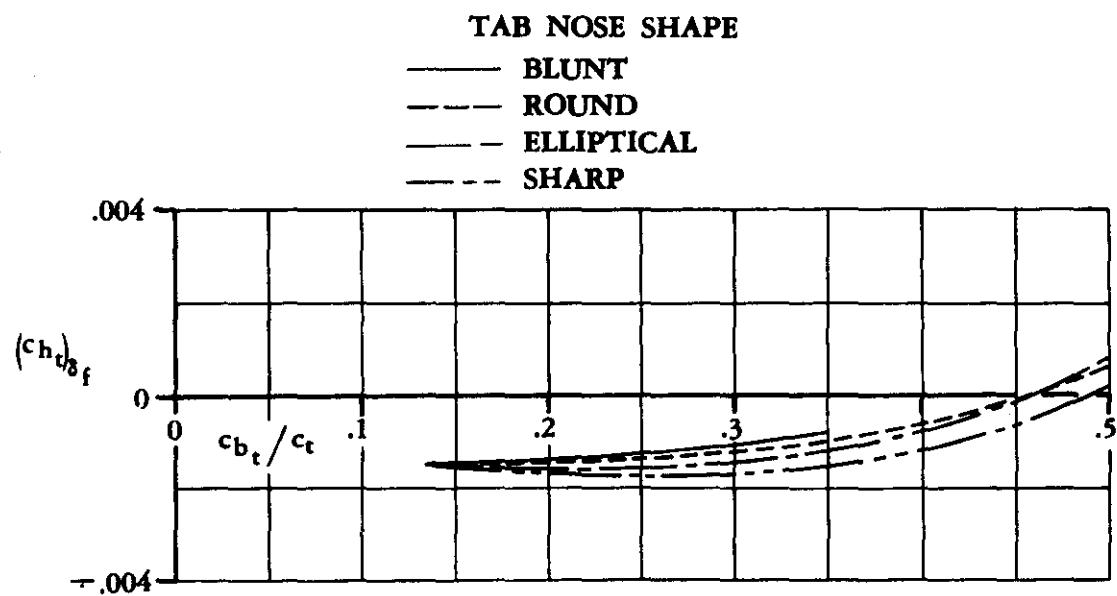


**FIGURE 6.1.3.4-6 b EFFECT OF TAB NOSE SHAPE AND AERODYNAMIC BALANCE ON TAB SECTION HINGE MOMENTS**

### 6.1.4 WING LIFT WITH HIGH-LIFT AND CONTROL DEVICES

#### 6.1.4.1 CONTROL DERIVATIVE $C_{L\delta}$ OF HIGH-LIFT AND CONTROL DEVICES

##### A. SUBSONIC

###### Mechanical Flaps

The method used to estimate lift due to flap deflection at subsonic speeds is designed to make maximum use of experimental airfoil section data when such data are available. This approach is taken from Reference 1, wherein various existing methods have been combined to obtain a simple procedure with general application.

###### Jet Flaps

Two methods are presented for estimating the jet-flap lift increment at small angles of attack (see Section 6.1.1.1 for a sketch of the various jet-flap types and a discussion of the salient aspects). More accurate and sophisticated lift methods than those presented here have been developed for analyzing jet-flap configurations (such as the method presented in Reference 2). However, the more sophisticated methods are not amenable to a handbook solution; i.e., they require the use of a computer. Other modifications and approaches to the jet-flap problem are presented and discussed in detail in Reference 3.

The first method (taken from Reference 4) evaluates the lift increment due to both flap deflection and power effects for an internally-blown-flap (IBF) configuration. This method is based on the theoretical two-dimensional jet-flap lift increment modified by Maskell's theoretical correction factor for finite-aspect-ratio effects and a crude part-span factor to account for partial-span flaps. This method has not been substantiated because of the lack of published three-dimensional IBF data. However, the method has yielded results within ten percent of test data for those cases that have been evaluated (References 4 and 5).

The second method (taken from Reference 6) is used to evaluate the lift increment due only to power effects for an externally-blown-flap (EBF) configuration. This method is based on Spence's two-dimensional jet-flap lift increment, modified by Hartunian's theoretical correction factor for finite-aspect-ratio effects and the ratio of flapped wing area to reference wing area to account for partial-span effects. Substantiation of this method has not been presented here; however, a substantiation of the method does appear in Reference 6 with an indicated average error of about 10 percent.

The nondimensional trailing-edge jet momentum coefficient for three-dimensional jet-flap configurations is denoted by  $C_J$ . The relationship to the two-dimensional jet momentum coefficient  $C_\mu$  (see Section 6.1.1.1 for definition) can be expressed as

$$C_J = \frac{1}{qS} \int_{-b/2}^{b/2} J dy$$

$$= \frac{1}{S} \int_{-b/2}^{b/2} c C_\mu dy$$

where

$J$  is the jet momentum at the trailing edge.

$dy$  is the spanwise wing increment.

$q$  is the free-stream dynamic pressure.

$S$  is the reference wing area.

$b$  is the wing span.

$c$  is the wing chord.

## DATCOM METHODS

### 1. Mechanical Leading- and Trailing-Edge Devices

The lift increment developed by deflection of a control surface is given by

$$\Delta C_L = \Delta c_\delta \left( \frac{C_{L\alpha}}{c_{L\alpha}} \right) \left[ \frac{(\alpha_\delta)_{C_L}}{(\alpha_\delta)_{c_\delta}} \right] K_b \quad 6.1.4.1-a$$

where

$\Delta c_\delta$  is the section lift increment due to control deflection. Test data on the particular flapped airfoil are preferred, but the increment can be estimated by the applicable method of Section 6.1.1.1.

$C_{L\alpha}$  is the lift-curve slope of the wing with the flap retracted, based on the wing reference area, obtained from the appropriate wing method of Paragraph A of Section 4.1.3.2.

$c_{L\alpha}$  is the section lift-curve slope of the basic airfoil, including the effects of compressibility, obtained from Section 4.1.1.2.

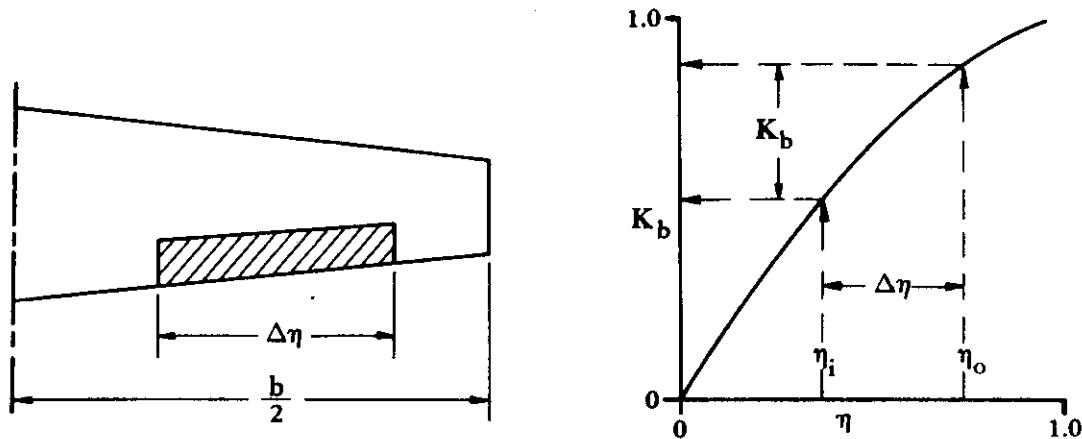
$\frac{(\alpha_\delta)_{C_L}}{(\alpha_\delta)_{c_\delta}}$  is the ratio of the three-dimensional flap-effectiveness parameter to the two-dimensional flap-effectiveness parameter, obtained from Figure 6.1.4.1-14 as a function of wing aspect ratio and the theoretical value of  $(\alpha_\delta)_{c_\delta}$ . The theoretical value of  $(\alpha_\delta)_{c_\delta}$  is obtained from the inset chart of Figure 6.1.4.1-14.

When experimental values of the section lift increment  $\Delta c_\delta$  are used in Equation 6.1.4.1-a, the value of  $(\alpha_\delta)_{c_\delta}$  used to obtain  $(\alpha_\delta)_{C_L}/(\alpha_\delta)_{c_\delta}$  from Figure 6.1.4.1-14 should be calculated using

$$(\alpha_\delta)_{c_\delta} = - \frac{(\Delta c_\delta)_{\text{experiment}}}{(c_{L\alpha}) \delta_f}$$

with one exception; i.e., for area-suction- and blowing-type flaps, use the inset chart of Figure 6.1.4.1-14.

$K_b$  is the flap-span factor obtained from Figure 6.1.4.1-15 as illustrated in Sketch (a).  
 (Note:  $\eta$  is the span station,  $\eta = \frac{\text{control span ordinate}}{b/2}$ .)



SKETCH (a)

It should be noted that the control deflection angles and all dimensions are measured in planes parallel or perpendicular to the plane of symmetry.

This method is restricted to the limitations of the methods used to evaluate the section lift increments from Section 6.1.1.1.

Equation 6.1.4.1-a is applicable to leading-edge flaps and slats, and plain, split, and slotted trailing-edge flaps. The lift increment due to combinations of leading-edge and trailing-edge devices may be estimated by applying Equation 6.1.4.1-a to each device separately and adding the individual increments.

For the case of arbitrary spanwise distribution of control chord (constant-chord controls on tapered wings or tapered controls on untapered wings), the control can be divided into spanwise steps and the lift increment found by the summation of  $\Delta C_L$  values due to each spanwise step based on the average values of  $\Delta c_\delta$  and  $(\alpha_\delta)_{c_\delta}$  over that spanwise step.

Low-speed values of  $\Delta C_L$  at  $\alpha = 0$ , calculated using the Datcom method, are compared with test values in Figures 6.1.4.1-16a, -16b, and -16c for wing-control combinations employing plain, split, and slotted trailing-edge controls, respectively. All parameters used in the calculations were estimated by using methods from the appropriate sections of the Datcom. The values of  $(\alpha_\delta)_{c_\delta}$  used in the calculations were obtained from the inset of Figure 6.1.4.1-14. The ranges of Reynolds numbers and geometric parameters of the test configurations are noted on the correlation charts.

## 2. Jet-Flap IBF Configuration

The lift increment due to flap deflection and power effects for an IBF configuration is given by

$$\Delta C_L = \Delta c_\alpha \left[ \frac{A_t + \frac{2C'_J}{\pi}}{A_t + 2 + 0.604(C'_J)^{1/2} + 0.876 C'_J} \right] \frac{S_{Wf}}{S_W} \quad 6.1.4.1-b$$

where

$\Delta c_\alpha$  is the section lift increment due to flap deflection and power effects. Test data on the particular flapped airfoil are preferred, but the increment can be estimated by the jet-flap method of Section 6.1.1.1. (When using Section 6.1.1.1 the value of  $C'_J$  is substituted for the value of  $C'_\mu$ .)

$A_t$  is the aspect ratio of the wing based on the total wing area  $S_t$ , including any increase in wing area due to flap extension.

$C'_J$  is the three-dimensional trailing-edge jet momentum coefficient, based on the blown-flap affected wing area  $S_{Wf}$ , i.e.,

$$C'_J = C_J \frac{S_W}{S_{Wf}}$$

$\frac{S_{Wf}}{S_W}$  is the ratio of the blown-flap affected wing area (schematically illustrated in Section 2.2.2) to the wing reference area. The blown-flap affected area includes any increase in wing area due to flap extension.

As indicated above, this method has not been thoroughly substantiated and therefore should be applied with caution.

It should be noted that the total lift coefficient for an IBF configuration can be found by adding the lift increment from Equation 6.1.4.1-b to the flaps-retracted power-off lift coefficient, obtained from test data or the appropriate methods of Section 4.

## 3. Jet-Flap EBF Configuration

The effective jet deflection angle  $\delta_{j,eff}$  and the trailing-edge momentum coefficient  $C_J$  are not specifically defined for EBF configurations. This is due to the jet sheet being somewhat diffuse rather than infinitesimally thin as assumed in jet-flap theory. For this reason it becomes necessary to obtain the effective jet angle from static force tests, or to relate the jet angle to the trailing-edge flap geometry. From correlation of test data (indicated in Reference 6), the best results are obtained when the engine exhaust jet momentum is used directly to define the trailing-edge momentum coefficient. Any losses in thrust must therefore be considered in the determination of drag.

The lift increment due to power effects for an EBF configuration is given by

$$\Delta C_L = 4\pi d_o \left[ \frac{\pi A_t + 2C'_J}{\pi A_t + c_{\ell_\alpha} + 2.01 C'_J} \right] \frac{\delta_{j_{\text{eff}}}}{57.3} \frac{S_{W_f}}{S_W} \quad 6.1.4.1-c$$

where

$4\pi d_o$  is the theoretical effect of blowing on the lift derivative. This parameter is obtained from Figure 6.1.4.1-18 as a function of the flap chord ratio  $c_f/c'$  and trailing-edge jet momentum coefficient  $C'_J$ . (See Figure 6.1.4.1-19a for a schematic definition of  $c_f/c'$ .)

$A_t$  is the aspect ratio of the wing based on the total wing area  $S_t$ , including any increase in wing area due to flap extension.

$C'_J$  is the three-dimensional trailing-edge jet momentum coefficient, based on the blown-flap-affected wing area  $S_{W_f}$ , i.e.,  $C'_J = C_J S_W / S_{W_f}$ .

$c_{\ell_\alpha}$  is the two-dimensional jet-flap lift-curve slope uncorrected for thickness effects. This term is obtained from Figure 6.1.1.1-49, using the trailing-edge jet momentum coefficient  $C'_J$  in place of  $C'_\mu$ .

$\delta_{j_{\text{eff}}}$  is the effective jet deflection angle with respect to the airfoil chord, in degrees. If possible, this value should be obtained from static force tests. When test data are not available, the effective flap deflection angle may be approximated by using

$$\delta_{j_{\text{eff}}} = \frac{1}{2} (\delta_u + \delta_\ell) \quad 6.1.4.1-d$$

where the values for  $\delta_u$  and  $\delta_\ell$  are shown schematically in Figure 6.1.4.1-19b.

$\frac{S_{W_f}}{S_W}$  is the ratio of the flap-affected wing area (schematically illustrated in Section 2.2.2) to the wing reference area. The flap-affected area includes any increase in wing area due to flap extension.

It should be noted that the total lift coefficient for an EBF configuration can be found by adding the lift increment from Equation 6.1.4.1-c, the power-off mechanical-flap lift increment from Equation 6.1.4.1-a, and the flap-retracted power-off lift coefficient, obtained from test data or the appropriate methods of Section 4.

### Sample Problems

#### 1. Mechanical Flaps

Given: The sweptback wing of Reference 7.

$$A = 3.78$$

$$\lambda = 0.586$$

$$\Lambda_{c/2} = 45.46^\circ$$

NACA 65A006 airfoil	Plain trailing-edge flap	$c_f/c = 0.224$
$b_f/b = 0.469$	$\eta_i = 0.141$	$\eta_o = 0.610$
Low speed; $\beta = 1.0$		$R_\infty = 6.1 \times 10^6$
$\tan(\phi'_{TE}/2) = 0.0717$ (streamwise airfoil section geometry)		

Compute:

$c_{q_\alpha}$  and  $\Delta c_{q_\alpha}$  (Sections 4.1.1.2 and 6.1.1.1)

$$\frac{c_{q_\alpha}}{(c_{q_\alpha})_{\text{theory}}} = 0.887 \quad (\text{Figure 4.1.1.2-8a})$$

$$(c_{q_\alpha})_{\text{theory}} = 6.58 \text{ per rad} \quad (\text{Figure 4.1.1.2-8b})$$

$$c_{q_\alpha} = \frac{1.05}{\beta} \left[ \frac{c_{q_\alpha}}{(c_{q_\alpha})_{\text{theory}}} \right] (c_{q_\alpha})_{\text{theory}} \quad (\text{Equation 4.1.1.2-a})$$

$$= (1.05)(0.887)(6.58) = 6.13 \text{ per rad}$$

$$(c_{q_\delta})_{\text{theory}} = 3.77 \text{ per rad} \quad (\text{Figure 6.1.1.1-39a})$$

$$\frac{c_{q_\delta}}{(c_{q_\delta})_{\text{theory}}} = 0.817 \quad (\text{Figure 6.1.1.1-39b})$$

$$K' = 0.780 \quad (\text{Figure 6.1.1.1-40})$$

$$\Delta c_q = \delta_f \left[ \frac{c_{q_\delta}}{(c_{q_\delta})_{\text{theory}}} \right] (c_{q_\delta})_{\text{theory}} K' \quad (\text{Equation 6.1.1.1-c})$$

$$= \left( \frac{22.1}{57.3} \right) (0.817)(3.77)(0.780)$$

$$= 0.927$$

Wing lift-curve slope (Section 4.1.3.2)

$$\kappa = \frac{c_{q_\alpha}}{2\pi} = \frac{6.13}{2\pi} = 0.976$$

$$\frac{A}{\kappa} \left( \beta^2 + \tan^2 \Lambda_{c/2} \right)^{1/2} = \frac{3.78}{0.976} [1.0 + (1.0162)^2]^{1/2} = 5.52$$

$$\frac{C_{L_\alpha}}{A} = 0.798 \text{ per rad} \quad (\text{Figure 4.1.3.2-49})$$

$$C_{L_\alpha} = 3.016 \text{ per rad}$$

$$(\alpha_\delta)_{c_2} = -0.576 \quad (\text{Inset, Figure 6.1.4.1-14})$$

$$\frac{(\alpha_\delta)_{CL}}{(\alpha_\delta)_{c_2}} = 1.083 \quad (\text{Figure 6.1.4.1-14})$$

$$\left. \begin{array}{l} (K_b)_{n_i} = 0.190 \\ (K_b)_{n_o} = 0.740 \end{array} \right\} \quad (\text{Figure 6.1.4.1-15})$$

$$K_b = (K_b)_{n_o} - (K_b)_{n_i} = 0.550$$

Solution:

$$\begin{aligned} \Delta C_L &= \Delta c_2 \left( \frac{C_{L_\alpha}}{c_{L_\alpha}} \right) \left[ \frac{(\alpha_\delta)_{CL}}{(\alpha_\delta)_{c_2}} \right] K_b \quad (\text{Equation 6.1.4.1-a}) \\ &= (0.927) \frac{3.016}{6.13} (1.083)(0.550) \\ &= 0.272 \end{aligned}$$

This compares with a test value of 0.255 from Reference 7.

## 2. Jet-Flap IBF Configuration

Given: The IBF configuration of Reference 5.

$$\text{NACA 4424 airfoil} \quad \delta_f = 30^\circ \quad \delta_j = 22^\circ$$

$$\frac{c_f}{c} = 0.11 \quad \frac{c'}{c} = 1.0 \quad A = 6.0 \quad A_t = 6.0$$

$$C_J = 2.80 \quad \frac{t}{c} = 0.24 \quad \frac{S_{W_f}}{S_W} = 0.783 \quad \frac{S_t}{S_W} = 1.0$$

Compute:

$$C'_J = C_J \frac{S_w}{S_{w_f}}$$

$$= (2.80) \frac{1}{0.783}$$

$$= 3.576$$

$$k_t = 0.80 \text{ (average airfoil)}$$

$$\left. \begin{array}{l} c_{\ell \delta f} = 10.0 \text{ per rad} \\ c_{\ell \delta j} = 8.9 \text{ per rad} \end{array} \right\}$$

Figure 6.1.1.1-49

$$\Delta c_\ell = \left\{ \left[ 1 + k_t \left( \frac{t}{c'} \right) \right] \delta_f (c_{\ell \delta f} - C'_\mu) + C'_\mu \delta_f \right. \\ \left. + \left[ 1 + k_t \left( \frac{t}{c'} \right) \right] \delta_j (c_{\ell \delta j} - C'_\mu) + C'_\mu \delta_j \right\} \frac{c'}{c} \quad (\text{Equation 6.1.1.1-k})$$

$$= [1 + (0.80)(0.24)] \frac{30}{57.3} (10.0 - 3.576) + 3.576 \frac{30}{57.3}$$

$$+ [1 + (0.80)(0.24)] \frac{22}{57.3} (8.9 - 3.576) + 3.576 \frac{22}{57.3}$$

$$= 4.01 + 1.87 + 2.44 + 1.37$$

$$= 9.69$$

Solution:

$$\Delta C_L = \Delta c_\ell \left[ \frac{A_t + \frac{2C'_J}{\pi}}{A_t + 2 + 0.604 (C'_J)^{1/2} + 0.876 C'_J} \right] \frac{S_{w_f}}{S_w} \quad (\text{Equation 6.1.4.1-b})$$

$$= 9.69 \left[ \frac{6.0 + \frac{2(3.576)}{\pi}}{6.0 + 2.0 + 0.604 (3.576)^{1/2} + 0.876 (3.576)} \right] 0.783$$

$$= 5.12 \text{ (lift increment due to flap deflection and power effects)}$$

This compares with a test value of 5.03 from Reference 5.

### 3. Jet-Flap EBF Configuration

Given: The EBF configuration of Reference 8.

$$\frac{c_f}{c} = 0.556 \quad \frac{c'}{c} = 1.336 \text{ (without leading-edge extension)} \quad \frac{t}{c} \approx 0.12$$

$$S_w = 8.43 \text{ ft}^2 \quad S_{w_f} = 9.58 \text{ ft}^2 \quad S_t = 10.84 \text{ ft}^2$$

$$A_t = 7.23 \quad A_t = 5.62 \quad C_J = 1.74$$

$$\delta_u = 61^\circ \quad \delta_g = 50^\circ$$

Compute:

$$C'_J = C_J \left( \frac{S_w}{S_{w_f}} \right)$$

$$= 1.74 \left( \frac{8.43}{9.58} \right) = 1.53$$

$$\delta_{j_{\text{eff}}} = \frac{1}{2} (\delta_u + \delta_g) \quad (\text{Equation 6.1.4.1-d})$$

$$= \frac{1}{2} (61 + 50)$$

$$= 55.5^\circ$$

$$\frac{c_f}{c'} = \left( \frac{c_f}{c} \right) \left( \frac{c}{c'} \right)$$

$$= \frac{0.556}{1.336} = 0.416$$

$$c'_{g_\alpha} = 9.66 \text{ per rad} \quad (\text{Figure 6.1.1.1-49})$$

$$4\pi d_o = 3.48 \quad (\text{Figure 6.1.4.1-18})$$

Solution:

$$\Delta C_L = 4\pi d_o \left[ \frac{\pi A_t + 2C'_J}{\pi A_t + c'_{g_\alpha} + 2.01 C'_J} \right] \left( \frac{\delta_{j_{\text{eff}}}}{57.3} \right) \left( \frac{S_{w_f}}{S_w} \right) \quad (\text{Equation 6.1.4.1-c})$$

$$= 3.48 \left[ \frac{\pi(5.62) + (2)(1.53)}{\pi(5.62) + 9.66 + (2.01)(1.53)} \right] \left( \frac{55.5}{57.3} \right) \left( \frac{9.58}{8.43} \right)$$

$$= 2.61 \text{ (lift increment due to power effects only)}$$

This compares with a test value of 2.45 from Reference 8.

## B. TRANSONIC

No accurate method is available for predicting the control derivative  $C_{L\delta}$  at transonic speeds. Mixed flow conditions and interrelated shockwave and boundary-layer-separation effects cause extreme nonlinearities in this parameter in the transonic regime. The method presented herein is based on the observation that experimental data indicate that  $C_{L\delta}$  follows the same trend as the lift-curve slope through the transonic regime.

### DATCOM METHOD

A first-order approximation to the control derivative  $C_{L\delta}$  at transonic speeds for mechanical trailing-edge flaps is given by

$$C_{L\delta} = C_{L\delta M=0.6} \left( \frac{C_{I\delta}}{C_{I\delta M=0.6}} \right) \quad 6.1.4.1-e$$

where

$C_{L\delta M=0.6}$  is the lift effectiveness, calculated by the method of Paragraph A of this section, at  $M = 0.6$ , i.e.,

$$C_{L\delta} = \frac{\Delta C_L}{\delta_f}$$

$\frac{C_{I\delta}}{C_{I\delta M=0.6}}$  is the ratio of the rolling-effectiveness parameter at the Mach number in question to that at  $M = 0.6$ , obtained by the method of Paragraph B of Section 6.2.1.1.

## C. SUPERSONIC

At supersonic speeds, the lift effectiveness of plain trailing-edge controls is predicted by the theoretical method presented in Reference 9. The restrictions used in the derivation of the method are as follows:

1. Leading and trailing edges of the control surface are swept ahead of the Mach lines from the deflected controls.
2. Control root and tip chords are parallel to the plane of symmetry.
3. Controls are located either at the wing tip or far enough inboard so that the outermost Mach lines from the deflected controls do not cross the wing tip.
4. Innermost Mach lines from the deflected controls do not cross the wing root chord.
5. Wing planform has leading edges swept ahead of the Mach lines and has streamwise tips.

6. Controls are not influenced by the tip conical flow from the opposite wing panel or by the interaction of the wing-root Mach cone with the wing tip.

### DATCOM METHOD

The trailing-edge flap effectiveness  $C_{L\delta}$  at supersonic speeds for a symmetric, straight-sided flap is given by

$$C_{L\delta} = \left(1 - \frac{C_2}{C_1}\phi_{TE}\right) C'_{L\delta} \frac{S_f}{S_w} \quad 6.1.4.1-f$$

where  $\left(1 - \frac{C_2}{C_1}\phi_{TE}\right)$  is a thickness correction factor to the supersonic flat-plate derivative.

$$C_1 = \frac{2}{\sqrt{M^2 - 1}} \text{ (per radian)}$$

$$C_2 = \frac{(\gamma + 1)M^4 - 4(M^2 - 1)}{2(M^2 - 1)^2} \text{ (per radian)}$$

$\phi_{TE}$  is the trailing-edge angle in radians, measured normal to the control hinge line.

$\gamma$  is the ratio of specific heats,  $\gamma = 1.4$ .

$C'_{L\delta}$  is the lift effectiveness of one symmetric, straight-sided flap, based on the area of the flap. This parameter is obtained from Figures 6.1.4.1-20a through 6.1.4.1-20j for flaps located at the wing tip and from Figure 6.1.4.1-25 for flaps located inboard from the wing tip.

$\frac{S_f}{S_w}$  is the ratio of the total flap area (both sides of wing) to the total wing area.

It should be noted that control deflection angles are measured streamwise.

Not enough supersonic test data are available to allow substantiation of this method.

#### Sample Problem

Given: A wing-flap configuration with the following characteristics:

$$S_w = 46.5 \text{ sq ft}$$

$$\bar{c}_w = 4.0 \text{ ft}$$

$$b_w = 12.0 \text{ ft}$$

$$\lambda_w = 0.55$$

$$\Lambda_{LE} = 42^\circ$$

$$\Lambda_{TE} = 27.7^\circ$$

Symmetric, straight-sided inboard flap

$$\Lambda_{HL} = 30.8^\circ \quad S_f = 4.71 \text{ sq ft} \quad b_f = 6.5 \text{ ft} \quad \lambda_f = 0.715 \quad \phi_{TE} = 3^\circ$$

Additional Characteristics:

$$M = 1.90; \beta = 1.62$$

Compute:

$$C_1 = \frac{2}{\sqrt{M^2 - 1}} = 1.235 \text{ per rad}$$

$$C_2 = \frac{(\gamma + 1)M^4 - 4(M^2 - 1)}{2(M^2 - 1)^2} \text{ per rad}$$

$$= \frac{(2.4)(1.90)^4 - 4[(1.90)^2 - 1]}{2[(1.90)^2 - 1]^2} = \frac{20.84}{13.62} = 1.53 \text{ per rad}$$

$$\frac{\tan \Lambda_{TE}}{\beta} = \frac{0.5250}{1.62} = 0.324$$

$$\beta C'_{L\delta} = 0.074 \text{ per deg} \quad (\text{Figure 6.1.4.1-25})$$

$$C'_{L\delta} = 0.0457 \text{ per deg}$$

Solution:

$$C_{L\delta} = \left(1 - \frac{C_2}{C_1} \phi_{TE}\right) C'_{L\delta} \frac{S_f}{S_w} \quad (\text{Equation 6.1.4.1-f})$$

$$= \left[1 - \left(\frac{1.53}{1.235}\right) \left(\frac{3.0}{57.3}\right)\right] (0.0457) \frac{4.71}{46.5}$$

$$= 0.00433 \text{ per deg}$$

## REFERENCES

1. Lowry, J. G., and Polhamus, E. C.: A Method for Predicting Lift Increment Due to Flap Deflection at Low Angles of Attack in Incompressible Flow. NACA TN 3911, 1957. (U)
2. Lopez, M. L., and Shen, C. C.: Recent Developments in Jet Flap Theory and Its Application to STOL Aerodynamic Analysis. AIAA Paper 71-578, 1971. (U)
3. Korbacher, G. K., and Sridher, K.: A Review of the Jet Flap. Univ. of Toronto, UTIA Review 14, 1960. (U)

4. Alexander, A. J., and Williams, J.: Wind-Tunnel Experiments on a Rectangular-Wing Jet-Flap Model of Aspect Ratio 6. ARC R&M 3329, 1964. (U)
5. Butler, S. F. J., Guyett, M. B., and Moy, B. A.: Six-Component Low-Speed Tunnel Tests of Jet-Flap Complete Models with Variation of Aspect Ratio, Dihedral and Sweepback, Including the Influence of Ground Proximity. ARC R&M 3441, 1961. (U)
6. May, F., and Widdison, C. A.: STOL High-Lift Design Study. Vol. I – State-of-the-Art Review of STOL Aerodynamic Technology. AFFDL-TR-71-26 Vol. I, 1971. (U)
7. Barnett, U. R., Jr., and Lipson, S.: Effects of Several High-Lift and Stall-Control Devices on the Aerodynamic Characteristics of a Semispan  $49^{\circ}$  Sweptback Wing. NACA RM L52D17a, 1952. (U)
8. Grafton, S. B., Parlett, L. P., and Smith, C. C.: Dynamic Stability Derivatives of a Jet Transport Configuration with High Thrust-Weight Ratio and An Externally Blown Jet Flap. NASA TN D-6440, 1971. (U)
9. Goin, K. L.: Equations and Charts for the Rapid Estimation of Hinge-Moment and Effectiveness Parameters for Trailing-Edge Controls Having Leading and Trailing Edges Swept Ahead of the Mach Lines. NACA TR 1041, 1951. (U)
10. Abbott, I. H., and Greenberg, H.: Tests in the Variable-Density Wind Tunnel of the NACA 23012 Airfoil with Plain and Split Flaps. NACA TR 661, 1939. (U)
11. Smith, D. W., and Reed, V. D.: Subsonic Static Longitudinal Stability and Control Characteristics of a Wing-Body Combination Having a Pointed Wing of Aspect Ratio 2 With Constant-Percent-Chord Trailing Edge Elevons. NACA RM A53C20, 1953. (U)
12. Wenzinger, C. J.: Wind-Tunnel Investigation of Ordinary and Split Flaps on Airfoils of Different Profile. NACA TR 554, 1936. (U)
13. Lipson, S., and Barnett, U. R., Jr.: Comparison of Semispan and Full-Span Tests of a  $47.5^{\circ}$  Sweptback Wing with Symmetrical Circular-Arc Sections and Having Drooped-Nose Flaps, Trailing-Edge Flaps, and Ailerons. NACA RM L51H15, 1951. (U)
14. Schwier, W.: Lift Increase by Blowing Out Air, Tests on Airfoil of 12 Percent Thickness, Using Various Types of Flap. NACA TM 1148, 1947. (U)
15. Guryansky, E. R., and Lipson, S.: Effect of High-Lift Devices on the Longitudinal and Lateral Characteristics of a  $45^{\circ}$  Sweptback Wing With Symmetrical Circular-Arc Sections. NACA RM L8D06, 1948. (U)
16. Pearson, H. A., and Anderson, R. F.: Calculation of the Aerodynamic Characteristics of Tapered Wings With Partial-Span Flaps. NACA TR 665, 1939. (U)
17. Pratt, G. L., and Shields, E. R.: Low-Speed Longitudinal Characteristics of a  $45^{\circ}$  Sweptback Wing of Aspect Ratio 8 With High-Lift and Stall-Control Devices at Reynolds Numbers from 1,500,000 to 4,800,000. NACA RM L51J04, 1952. (U)
18. Sivells, J. C., and Spooner, S. H.: Investigation in the Langley 19-Foot Pressure Tunnel of Two Wings of NACA 65-210 Airfoil Sections with Various Type Flaps. NACA TR 942, 1949. (U)
19. Graham, R. R., and Conner, D. W.: Investigation of High-Lift and Stall-Control Devices on an NACA 64-Series  $42^{\circ}$  Sweptback Wing With and Without Fuselage. NACA RM L7G09, 1947. (U)
20. Woods, R. L., and Spooner, S. H.: Effects of High-Lift and Stall-Control Devices, Fuselage, and Horizontal Tail on a Wing Sweptback  $42^{\circ}$  at the Leading Edge and Having Symmetrical Circular-Arc Airfoil Sections at Reynolds Number of  $6.9 \times 10^6$ . NACA RM L9B11, 1949. (U)
21. Foster, G. V., and Fitzpatrick, J. E.: Longitudinal-Stability Investigation of High-Lift and Stall-Control Devices on a  $52^{\circ}$  Sweptback Wing With and Without Fuselage and Horizontal Tail at a Reynolds Number of  $6.8 \times 10^6$ . NACA RM LR108, 1948. (U)
22. Graham, D., and Koenig, D. G.: Tests in the Ames 40- by 80-Foot Wind Tunnel of an Airplane Configuration With an Aspect Ratio 2 Triangular Wing and an All-Moveable Horizontal Tail – Longitudinal Characteristics. NACA RM A51B21, 1951. (U)
23. Spooner, S. H., and Mollenberg, E. F.: Positioning Investigation of Single Slotted Flaps on a  $47.7^{\circ}$  Sweptback Wing at Reynolds Numbers of  $4.0 \times 10^6$  and  $6.0 \times 10^6$ . NACA RM L50H29, 1950. (U)
24. Mollenberg, E. F., and Spooner, S. H.: Low-Speed Investigation of the Effects of Single Slotted and Doubled Slotted Flaps on a  $47.7^{\circ}$  Sweptback Wing – Fuselage Combination at a Reynolds Number of  $6.0 \times 10^6$ . NACA RM L51E24, 1951. (U)

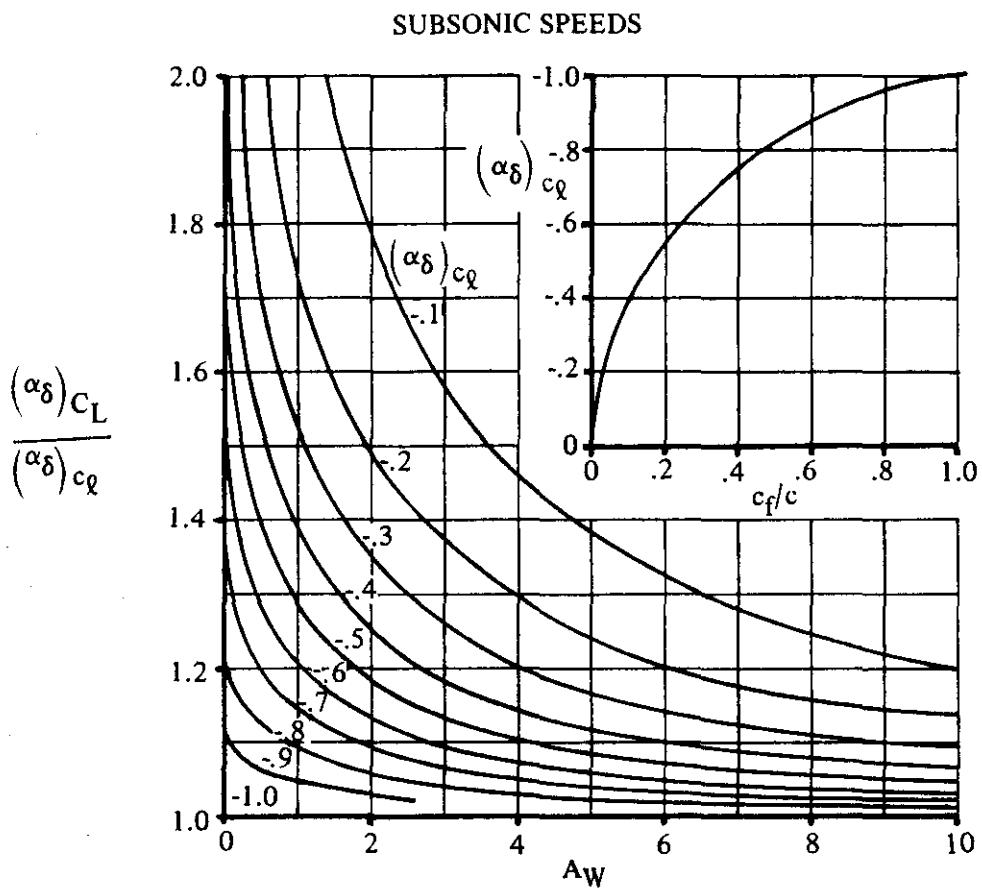


FIGURE 6.1.4.1-14 FLAP-CHORD FACTOR

SUBSONIC SPEEDS

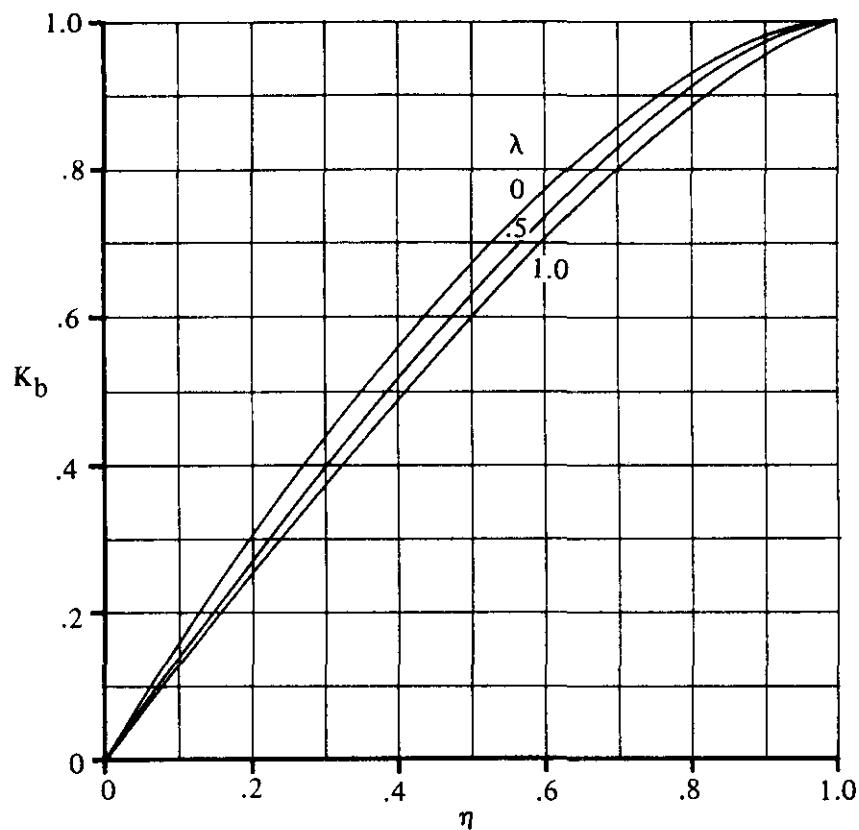


FIGURE 6.1.4.1-15 SPAN FACTOR FOR INBOARD FLAPS

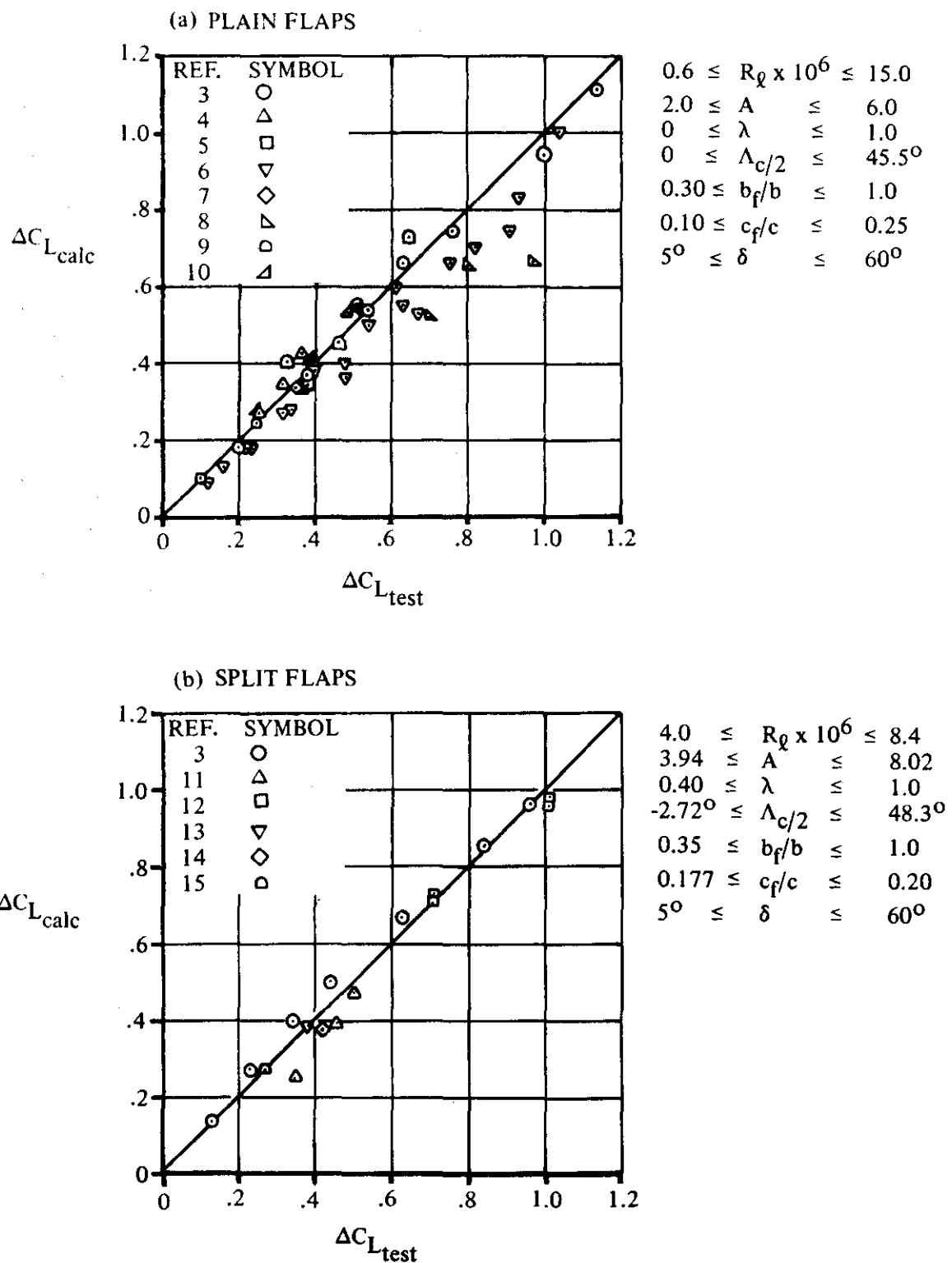


FIGURE 6.1.4.1-16 CORRELATION OF CALCULATED AND EXPERIMENTAL DATA FOR THE INCREMENTAL LIFT DEVELOPED BY DEFLECTION OF CONTROLS AT SUBSONIC SPEEDS

(c) SLOTTED FLAPS

SINGLE SLOTTED

$$\begin{aligned} 4.0 &\leq R_\ell \times 10^6 \leq 14.6 \\ 2.0 &\leq A \leq 9.02 \\ 0 &\leq \lambda \leq 0.40 \\ -2.72^\circ &\leq \Lambda_{c/2} \leq 56.3^\circ \\ 0.306 &\leq b_f/b \leq 0.975 \\ 0.20 &\leq c_f/c \leq 0.22 \\ 9.4^\circ &\leq \delta \leq 45^\circ \end{aligned}$$

DOUBLE SLOTTED

$$\begin{aligned} R_\ell &= 4.4 \times 10^6 \\ A &= 9.02 \\ \lambda &= 0.40 \\ \Lambda_{c/2} &= -2.72^\circ \\ b_f/b &= 0.60 \\ c'/c &= 1.144 \\ \delta &= 50^\circ \end{aligned}$$

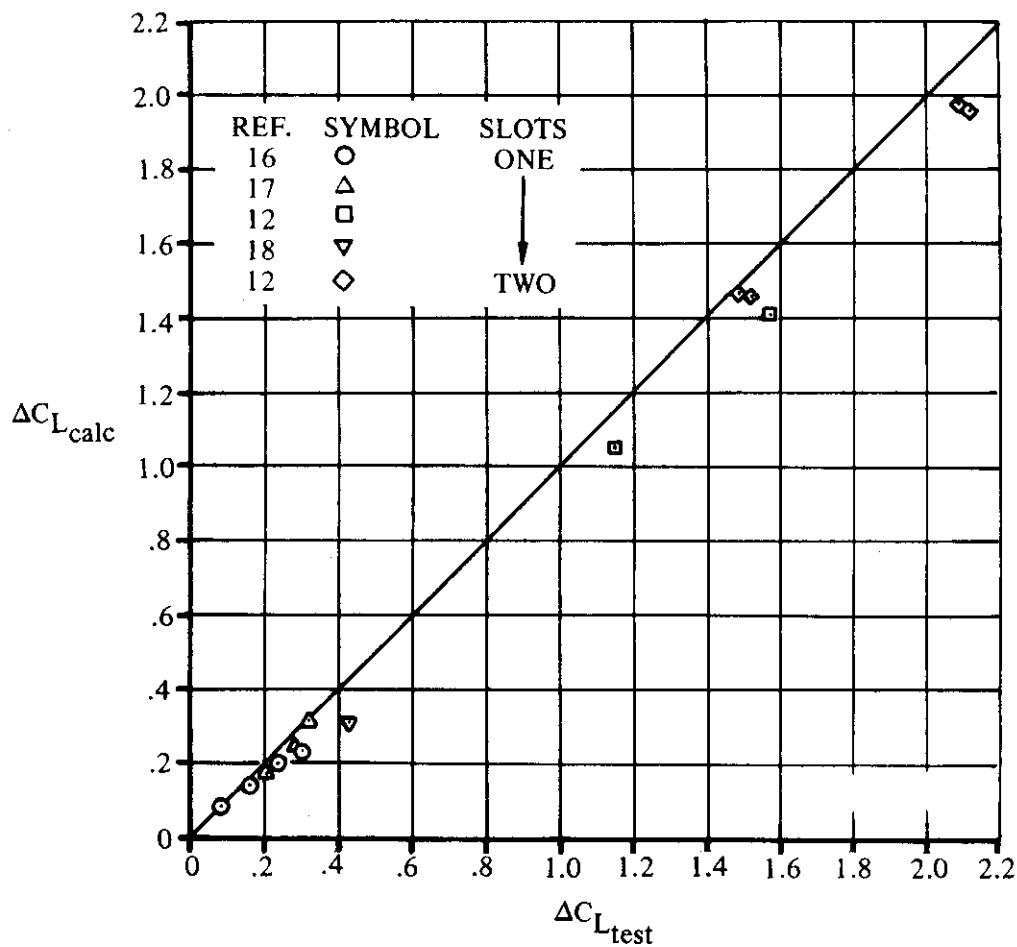


FIGURE 6.1.4.1-16 (CONTD)

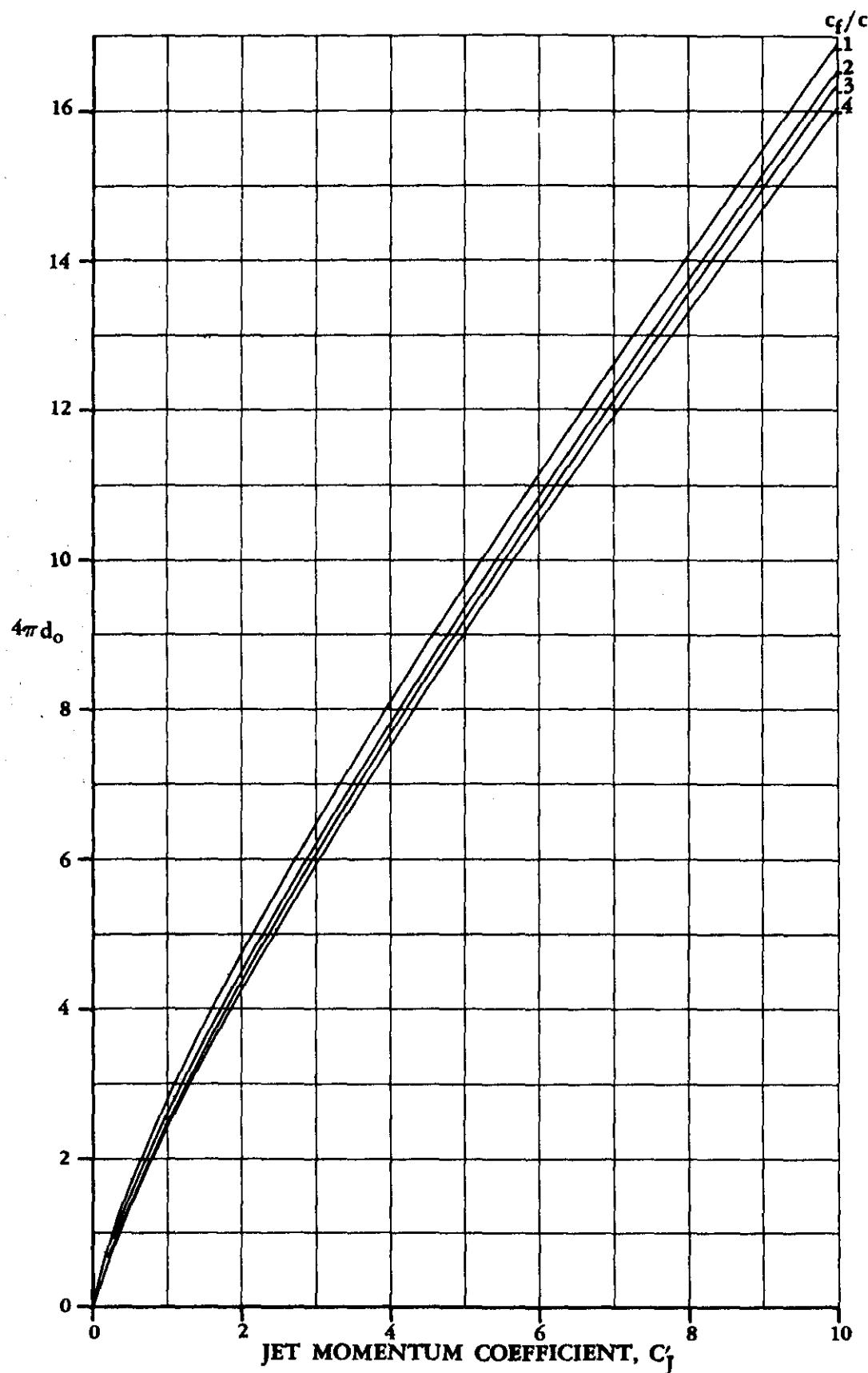


FIGURE 6.1.4.1-18 THEORETICAL CHANGE IN LIFT DERIVATIVE DUE TO BLOWING

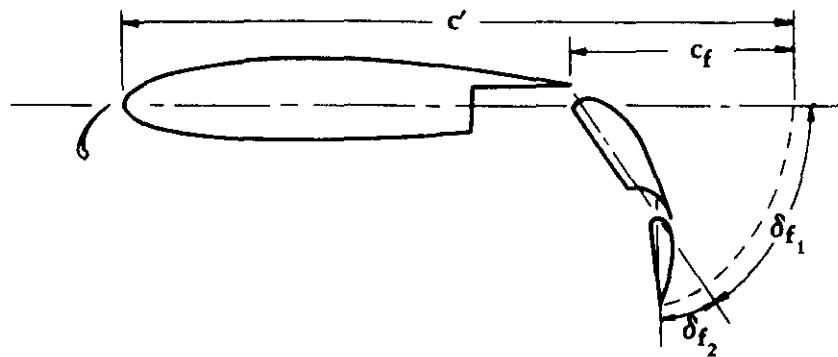


FIGURE 6.1.4.1-19a. FLAP CHORD FOR AN EBF CONFIGURATION

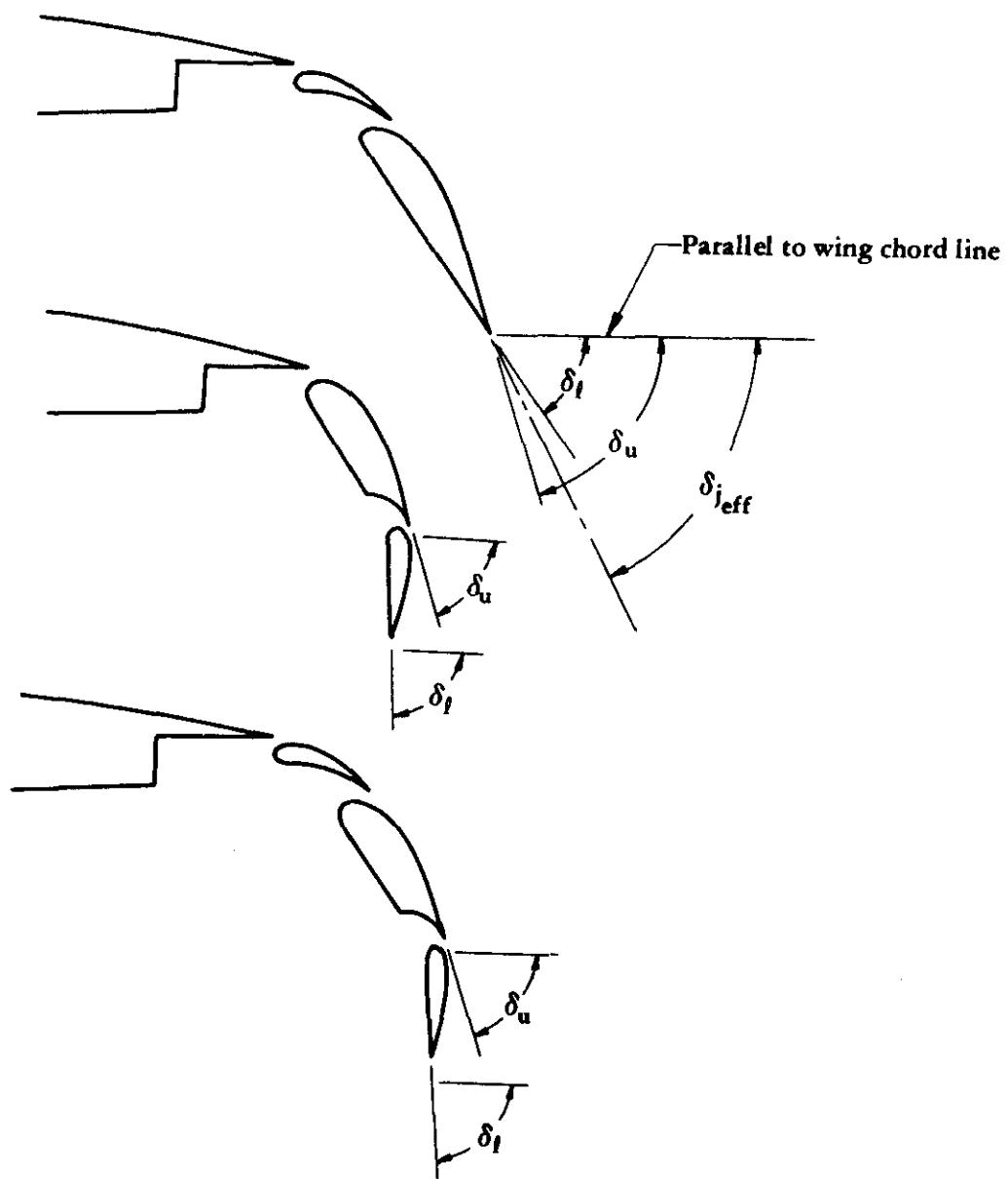


FIGURE 6.1.4.1-19b. EFFECTIVE JET DEFLECTION ANGLE FOR AN EBF CONFIGURATION

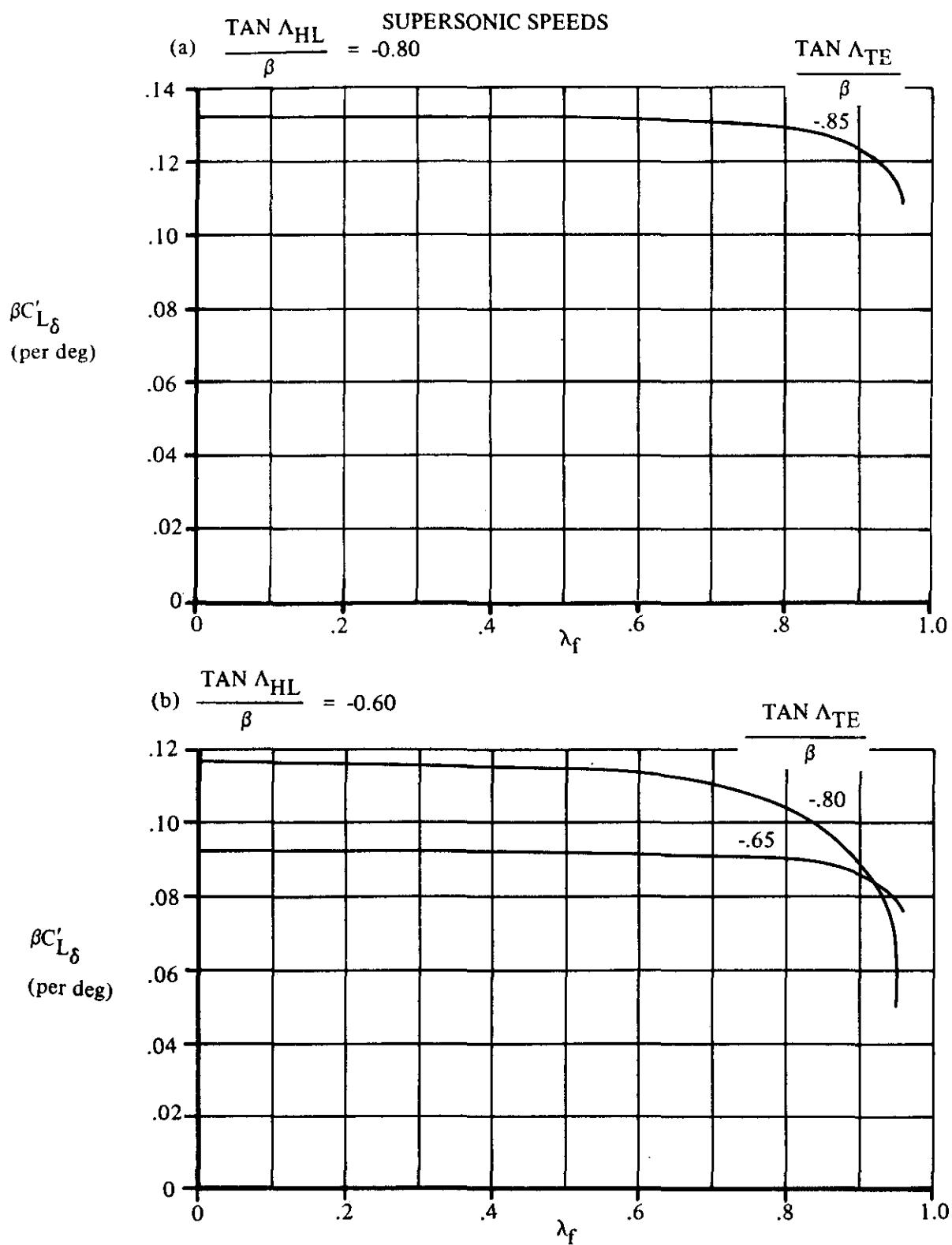
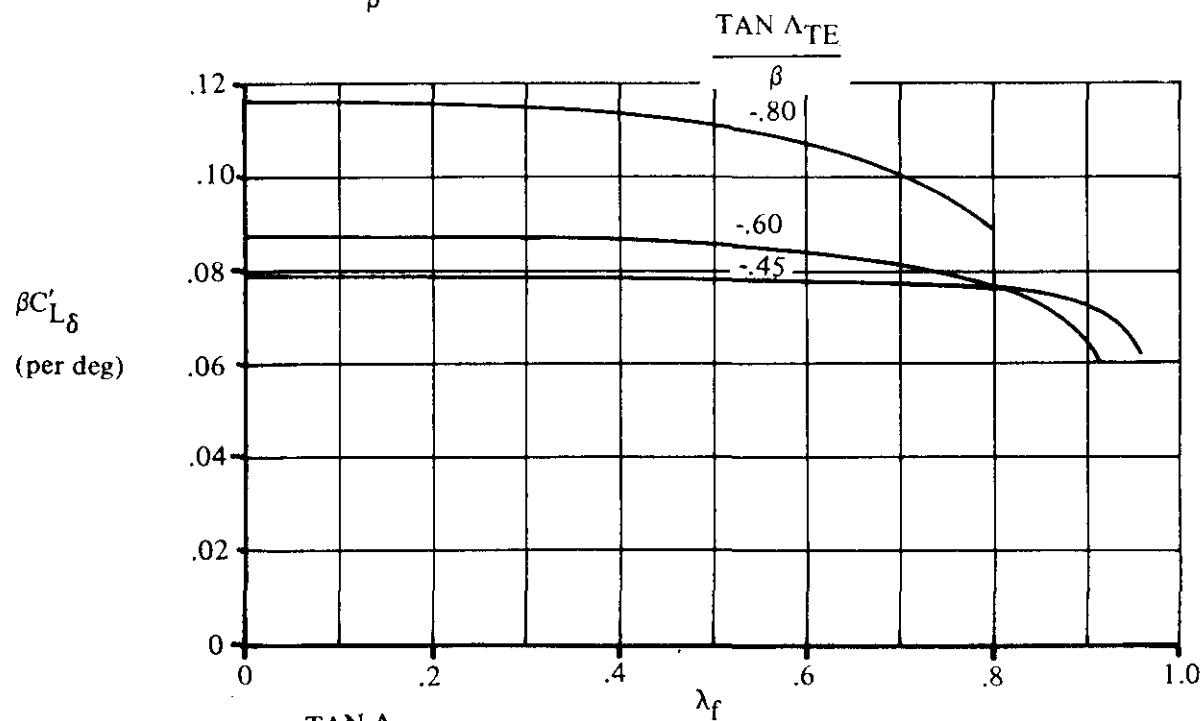


FIGURE 6.1.4.1-20 LIFT PARAMETER FOR DEFLECTED TRAILING-EDGE FLAPS LOCATED AT THE WING TIP

SUPersonic SPEEDS

$$(c) \frac{\tan \Lambda_{HL}}{\beta} = -0.40$$



$$(d) \frac{\tan \Lambda_{HL}}{\beta} = -0.20$$

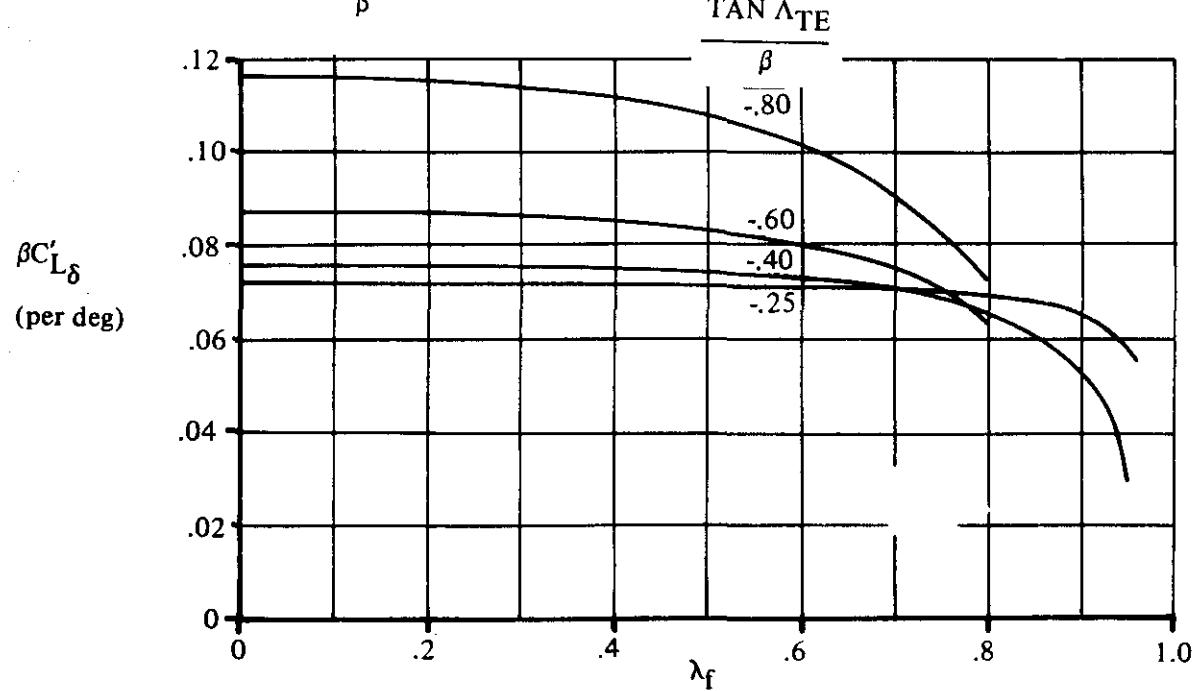
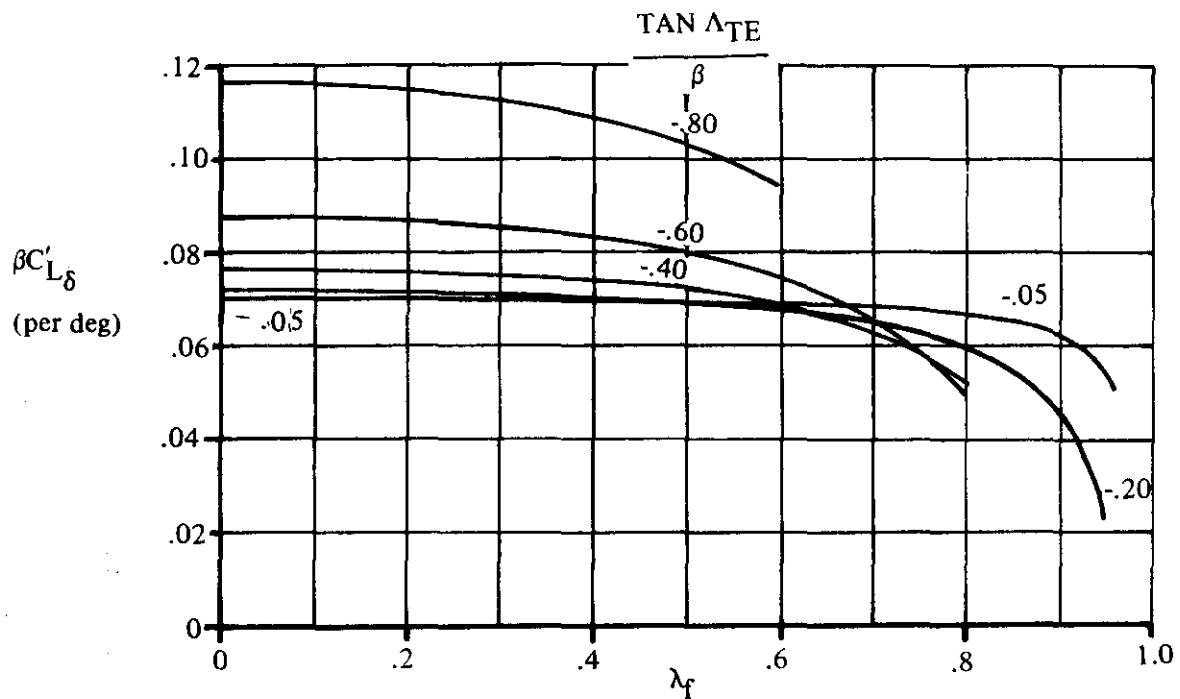


FIGURE 6.1.4.1-20 (CONT'D)

SUPersonic SPEEDS

$$(e) \frac{\tan \Lambda_{HL}}{\beta} = 0$$



$$(f) \frac{\tan \Lambda_{HL}}{\beta} = 0.20$$

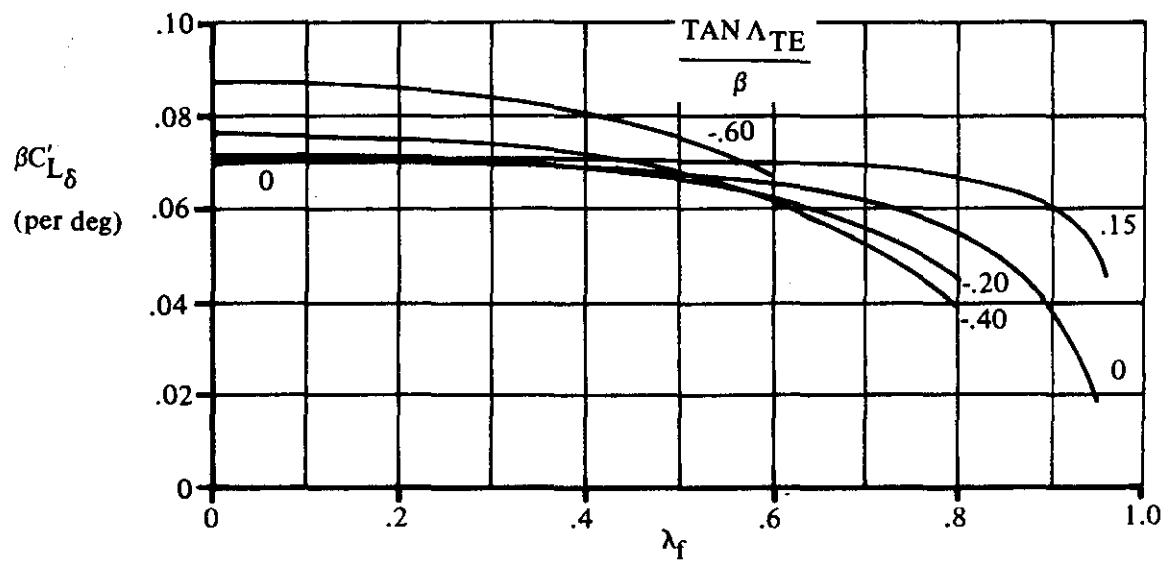


FIGURE 6.1.4.1-20(CONTD)

SUPersonic SPEEDS

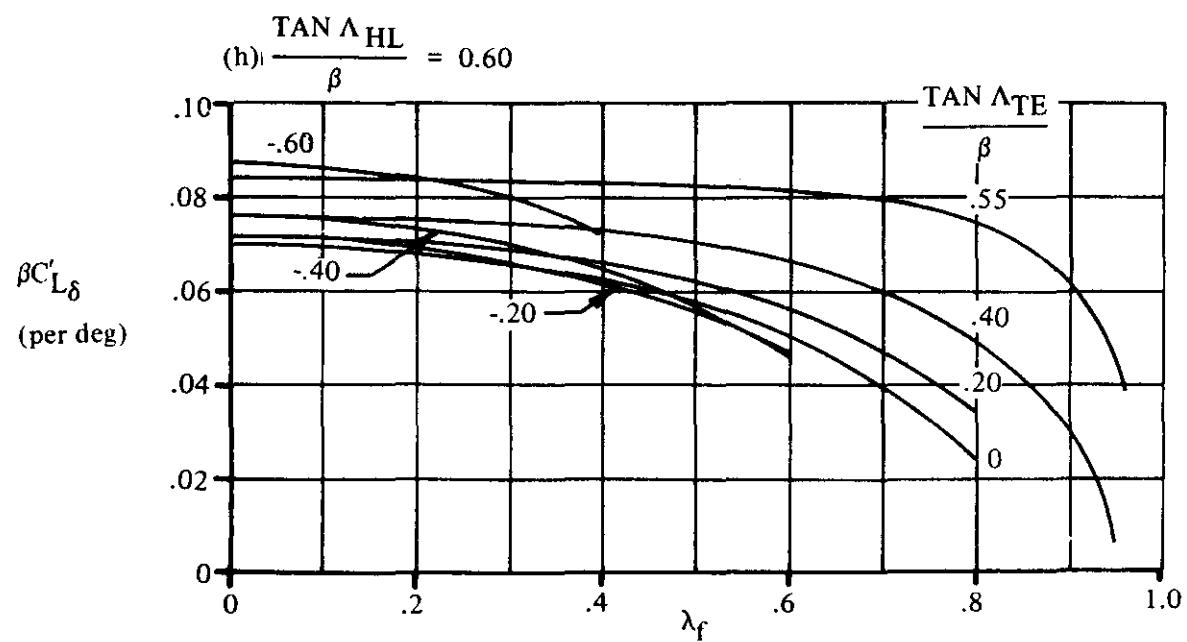
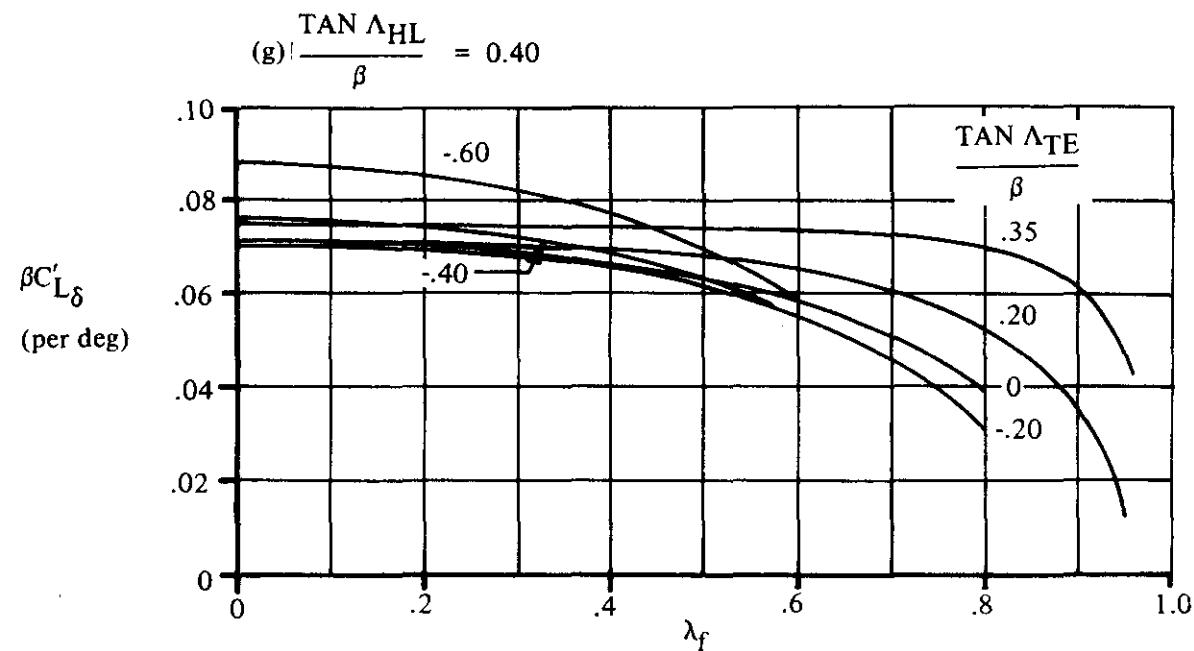


FIGURE 6.1.4.1-20 (CONT'D)

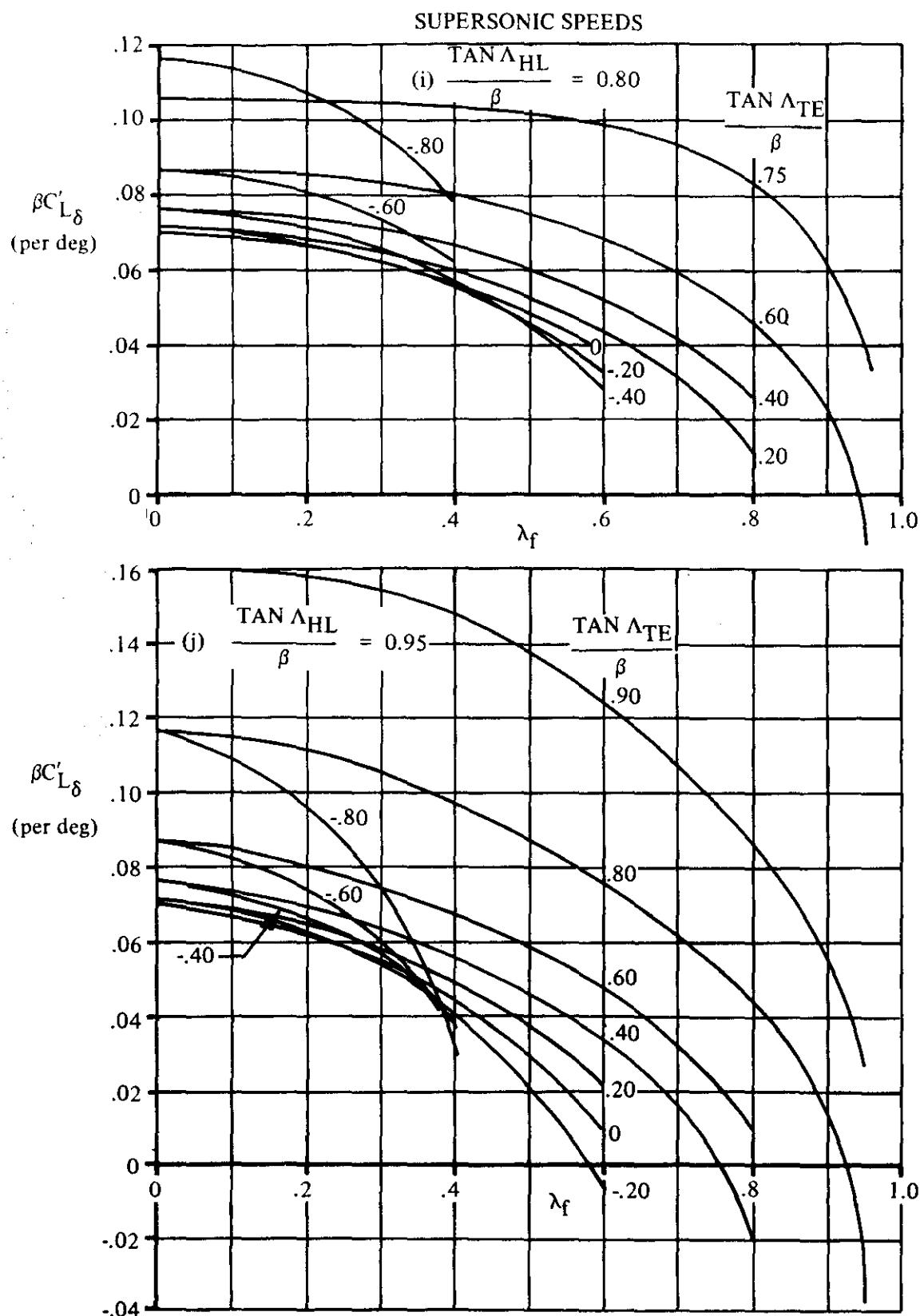


FIGURE 6.1.4.1-20 (CONTD)

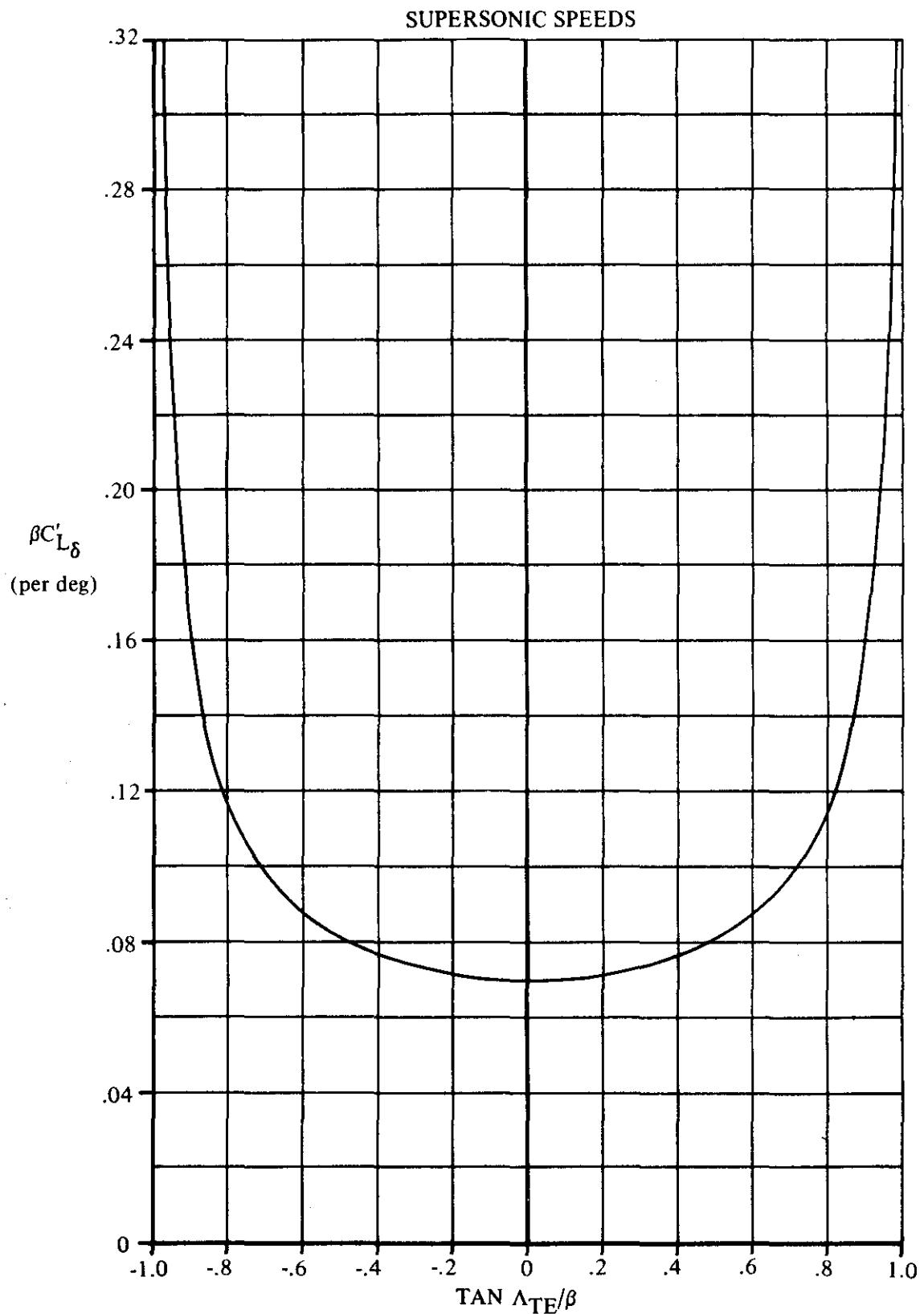


FIGURE 6.1.4.1-25 LIFT PARAMETERS FOR DEFLECTED TRAILING-EDGE FLAPS LOCATED INBOARD FROM WING TIP

#### 6.1.4.2 WING LIFT-CURVE SLOPE WITH HIGH-LIFT AND CONTROL DEVICES

According to linear wing theory, camber, such as that due to flaps, does not affect the lift-curve slope. Linear theory also predicts that, for translating types of leading- or trailing-edge flaps, the lift-curve slope will increase as a result of the additional wing area. Recently, linear theory has also been applied to wings with blown flaps and shows an increase in lift-curve slope with increasing trailing-edge jet momentum. Within the limitation that the flow does not separate from the surface of the wing or flap, experimental data verify these predictions.

The effects of these devices on the two-dimensional airfoil section lift-curve slope are discussed in Section 6.1.1.2. The discussion and methods of that section are directly applicable to the three-dimensional wing.

#### DATCOM METHODS

##### 1. Leading- and Trailing-Edge Mechanical Flaps

For wings with nontranslating leading- and trailing-edge flaps, the lift-curve slope of the flap-deflected wing is assumed to be the same as that of the flap-retracted wing, as given in Section 4.1.3.2. This assumption is valid for the linear-lift range of angles of attack and flap deflection.

For wings with translating leading- and trailing-edge flaps, a correction is made to the flaps-up lift-curve slope by means of the equation

$$(C_{L_\alpha})_\delta = \left[ \left( \frac{c'}{c} - 1 \right) \frac{S_{W_f}}{S_W} \right] (C_{L_\alpha})_{\delta=0} + (C_{L_\alpha})_{\delta=0} \quad 6.1.4.2-a$$

where

$(C_{L_\alpha})_\delta$  is the lift-curve slope of the flap-deflected wing, based on the area of the flap-retracted wing.

$(C_{L_\alpha})_{\delta=0}$  is the lift-curve slope of the flap-retracted wing from test data or Section 4.1.3.2.

$\frac{S_{W_f}}{S_W}$  is the ratio of the flap-affected wing area to the wing reference area. The area  $S_{W_f}$  is schematically illustrated in Section 2.2.2, and does not include any increase in wing due to flap extensions.

$\frac{c'}{c}$  is the ratio of the extended wing chord to the chord of the flap-retracted wing. In measuring  $c'$  of a single-slotted trailing-edge flap or a leading-edge slat, the flap or slat is rotated from its deflected position about the point of intersection of the flap or slat chord with the wing chord until the two coincide. In measuring  $c'$  of a double-slotted flap, the aft flap is first rotated from its deflected position about the point of intersection of the aft-flap chord and the chord of the forward flap until the two chords coincide; then both flaps are rotated from the deflection of the

forward flap about the point of intersection of the forward-flap chord with the wing chord until these two coincide. (See Figures 6.1.1.1-44 through -46, and -51.)

For the case of arbitrary spanwise distribution of flap chord (constant-chord flaps on tapered wings or tapered flaps on untapered wings), the flap can be divided into spanwise steps and the correction factor to be applied to the flaps-up lift-curve slope found by the summation of the correction factors due to each spanwise step based on the average value of  $c'/c$  and  $S_{w_f}/S_w$  over that spanwise step.

## 2. Jet Flaps

The method presented herein for estimating the lift-curve slope of a wing with a blown flap is a modification of the method presented in Reference 1. Similar methods appear in References 2 and 3. The assumptions made in the development of the method are as follows: inviscid flow, elliptical loading, high-aspect-ratio configuration, full-span trailing-edge flaps, and constant spanwise sectional momentum coefficient. Despite these limitations, the theory has been successfully adapted to handle configurations outside the range of these assumptions. Specifically, this method is strictly valid only for the pure jet-flap and the internally-blown-flap (IBF) systems; however, it has been applied with good success to wings with externally-blown flaps (EBF).

This method uses an aspect-ratio correction factor based on Hartunian's work (Reference 4). Mathematically, the aspect-ratio correction factor allows the method to be applied to wings of any aspect ratio. However, the validity of the method for aspect ratios less than five is unknown. The fact that the data presented in Figure 6.1.4.2-9 allow the method to be applied to low-aspect-ratio configurations must not be construed to mean that the Datcom recommends such use.

The corrections of the method for part-span blowing and large trailing-edge flap deflections are not inherent in Hartunian's aspect-ratio correction factor.

An implicit assumption of this method is that the flow on the unblown wing is attached. Unfortunately, the blown-flap systems now being tested do not always exhibit attached flow for an unblown condition. However, such designs are acceptable, since blowing provides a type of automatic boundary-layer control that causes the flow to reattach. But it does prohibit the use of experimental data to determine the lift-curve slope of the unblown flap-deflected wing where separation is a possibility.

The lift-curve slope (near zero angle of attack) of a wing with a trailing-edge jet flap, based on the flap-retracted wing area, is given by

$$C_{L_\alpha} = (C_{L_\alpha})_s \left\{ [K(A_t, C_J') - 1] K_b + 1 \right\} + \frac{C_J (\cos \delta_{j_{eff}} - 1)}{57.3} \quad 6.1.4.2-b$$

where

$(C_{L_\alpha})_s$  is the lift-curve slope of the unblown flap-deflected wing, with attached flow. This parameter can be obtained from experimental data if no separation exists, or from the mechanical-flap method of this section.

$K(A_t, C_J')$  is the jet momentum aspect-ratio correction factor obtained from Figure 6.1.4.2-9 as a function of  $A_t$  and  $C_J'$ , where

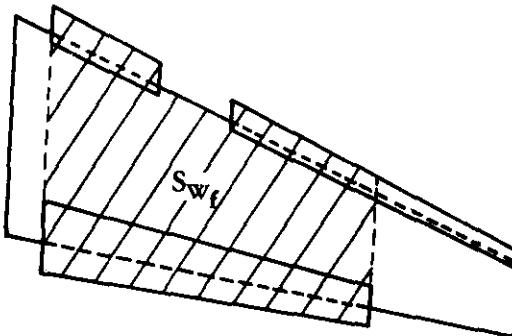
$A_t$  is the aspect ratio of the wing based on the total wing area  $S_t$ , including any increase in wing area due to flap extension.

$C'_J$  is the three-dimensional trailing-edge jet momentum coefficient based on the blown-flap affected area  $S_{W_f}$ ; i.e.,

$$C'_J = C_J \frac{S_W}{S_{W_f}}$$

where

$S_{W_f}/S_W$  is the ratio of the blown-flap affected area (schematically illustrated in Sketch(a)) to the wing reference area. The blown-flap affected area includes any increase in wing area due to flap extensions.



SKETCH (a)

$K_b$  is the flap-span factor from Figure 6.1.4.1-15, using the  $\lambda = 1$  curve, as illustrated in Sketch (a) of Section 6.1.4.1.

$C_J$  is the trailing-edge jet momentum coefficient based on the flap-retracted wing area.

$\delta_{j_{\text{eff}}}$  is the effective jet deflection angle with respect to the airfoil chord, in degrees. If possible, this value should be obtained from static force tests. When test data are not available for an externally-blown-flap (EBF) configuration, the effective flap deflection angle may be approximated by using Equation 6.1.4.1-d, i.e.,

$$\delta_{j_{\text{eff}}} = \frac{1}{2} (\delta_u + \delta_e)$$

where the values for  $\delta_u$  and  $\delta_e$  are shown schematically in Figure 6.1.4.1-19b.

A data summary and substantiation of this method are presented in Table 6.1.4.2-A.

### Sample Problems

#### 1. Leading-edge slat

Given: The wing of Reference 5 with a 50-percent-span leading-edge slat.

$$A = 6.0 \quad \Lambda_{c/2} = 32.8^\circ \quad \lambda = 0.50 \quad c'/c = 1.10 \quad S_{Wf}/S_W = 0.429$$

$$\text{Low speed; } \beta = 1.0 \quad \kappa = 1.0 \text{ (assumed)}$$

Compute:

$$\frac{A}{\kappa} [\beta^2 + \tan^2 \Lambda_{c/2}]^{1/2} = (6.0)[1.0 + (0.6445)^2]^{1/2} = 7.14$$

$$\frac{(C_{L\alpha})_{\delta=0}}{A} = 0.67 \text{ per rad} \quad (\text{Figure 4.1.3.2-49})$$

$$(C_{L\alpha})_{\delta=0} = 4.02 \text{ per rad} = 0.0702 \text{ per deg}$$

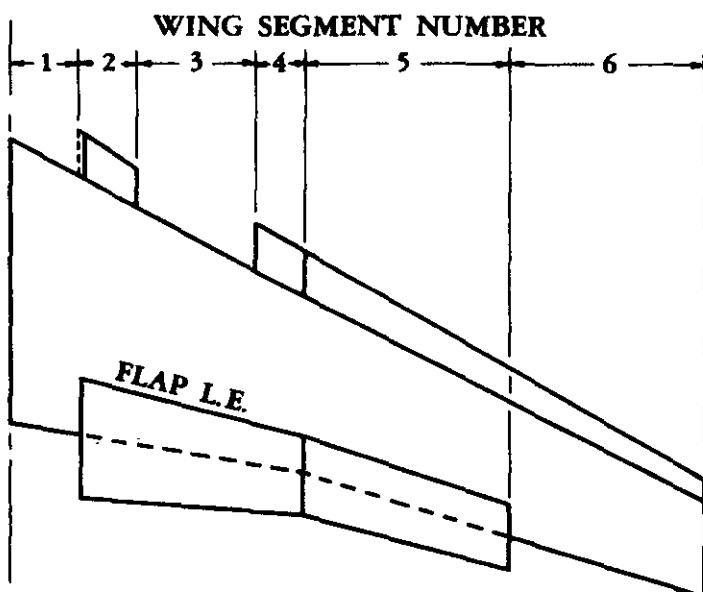
Solution:

$$\begin{aligned} (C_{L\alpha})_{\delta} &= \left[ \left( \frac{c'}{c} - 1 \right) \frac{S_{Wf}}{S_W} \right] (C_{L\alpha})_{\delta=0} + (C_{L\alpha})_{\delta=0} \quad (\text{Equation 6.1.4.2-a}) \\ &= [(1.10 - 1.0)(0.420)] 0.0702 + 0.0702 \\ &= 0.0732 \text{ per deg (based on } S_W) \end{aligned}$$

This compares with a test value of 0.0720 per degree from Reference 5.

#### 2. Jet Flap

Given: The sweptback wing-body configuration of Reference 6 with a trailing-edge double-slotted EBF system.



Note: All leading-edge and trailing-edge devices are shown rotated into the wing plane.

**Wing Characteristics:**

$$A = 7.75$$

$$S_w = 7.87 \text{ ft}^2$$

$$b = 95.08 \text{ in.}$$

$$\lambda = 0.336$$

$$c_r = 19.49 \text{ in.}$$

$$c_t = 6.54 \text{ in.}$$

$$\bar{c} = 13.22 \text{ in.}$$

$$y_{\bar{c}} = 19.33 \text{ in.}$$

To facilitate calculations, the wing has been divided into segments as shown in the preceding sketch. The divisions are made at the sweep discontinuity and at the discontinuities in leading- and trailing-edge flaps.

Sections	$S(\text{ft}^2)$ (flaps retracted)	$c'/c$	$S_t(\text{ft}^2)$ (flaps extended)
1	1.253	1.000	1.253
2	0.909	1.421	1.311
3	1.650	1.253	2.069
4	0.617	1.521	0.933
5	2.076	1.521	3.178
6	1.365	1.268	1.847
Value for the entire wing	7.870		10.59 $\text{ft}^2$

**Flap Characteristics:**

**Double-slotted trailing-edge flap:**

$$\text{Forward segment: } c_f/c = 0.22 \quad \delta_{f1} = 30^\circ$$

$$\text{Aft segment: } c_f/c = 0.24 \quad \delta_{f2} = 30^\circ$$

$$\eta_i = 0.102 \quad \eta_o = 0.720 \quad \delta_{\text{eff}} = 60^\circ$$

**Krueger leading-edge flap:**

$$\text{Inboard segment: } c_f/c = 0.168$$

$$\text{Outboard segment: } c_f/c = 0.268$$

Additional Characteristics:

$$R_e = 0.35 \times 10^6 \quad V = 50 \text{ ft/sec} \quad C_J = 3.18$$

$$\text{Low speed; } \beta = 1.0 \quad \kappa = 1.0 \text{ (assumed)} \quad \Lambda_{c/2} = 21.1^\circ \text{ (average value)}$$

Compute:

Determine the unblown lift-curve slope for both leading- and trailing-edge flap extension.

$$\frac{A}{\kappa} [\beta^2 + \tan^2 \Lambda_{c/2}]^{1/2} = \frac{7.75}{1.0} [1.0 + (0.3859)^2]^{1/2} = 8.307$$

$$\frac{(C_{L\alpha})_{\delta=0}}{A} = 0.602 \text{ per rad} \quad (\text{Figure 4.1.3.2-49})$$

$$(C_{L\alpha})_{\delta=0} = 4.666 \text{ per rad} = 0.0814 \text{ per deg}$$

Since the wing has been divided into 6 segments, Equation 6.1.4.2-a should be written as

$$\begin{aligned} (C_{L\alpha})_{\delta} &= \sum_{n=1}^6 \left[ \left( \frac{c'}{c} - 1 \right) \frac{S_{Wf}}{S_w} \right] (C_{L\alpha})_{\delta=0} + (C_{L\alpha})_{\delta=0} \quad (\text{Equation 6.1.4.2-a}) \\ &= \left[ (1.0 - 1.0) \frac{0}{7.87} + (1.421 - 1.0) \frac{0.909}{7.87} + (1.253 - 1.0) \frac{1.650}{7.87} + (1.521 - 1.0) \frac{0.617}{7.87} \right. \\ &\quad \left. + (1.521 - 1.0) \frac{2.076}{7.87} + (1.278 - 1.0) \frac{1.365}{7.87} \right] 0.0814 + 0.0814 \\ &= (0.3264)(0.0814) + 0.0814 \\ &= 0.108 \end{aligned}$$

Determine the blown lift-curve slope for both leading- and trailing-edge flap extension.

$$A_t = \frac{(95.08)^2}{(144)(10.59)} = 5.928$$

The value of  $S_{Wf}$  is found by adding the flap-extended wing area for segments 2 through 5; i.e.,  $S_{Wf} = 7.491 \text{ ft}^2$ .

$$C'_J = C_J \frac{S_w}{S_{Wf}}$$

$$= 3.18 \frac{7.87}{7.491}$$

$$= 3.34$$

$$K(A_t, C'_J) = 1.795 \quad (\text{Figure 6.1.4.2-9})$$

$$\left. \begin{array}{l} (K_b)_{\eta_i} = 0.13 \\ (K_b)_{\eta_o} = 0.82 \end{array} \right\} \quad (\text{Figure 6.1.4.1-15})$$

$$K_b = 0.82 - 0.13 = 0.69$$

Solution:

$$\begin{aligned} C_{L_\alpha} &= (C_{L_\alpha})_0 \{ [K(A_t, C'_J) - 1] K_b + 1 \} + \frac{C_J(\cos \delta_{\text{eff}} - 1)}{57.3} \quad (\text{Equation 6.1.4.2-b}) \\ &= (0.108) \{ [1.795 - 1](0.69) + 1 \} + \frac{3.18(0.50 - 1)}{57.3} \\ &= 0.167 - 0.0277 \\ &= 0.139 \text{ per deg} \end{aligned}$$

This compares with a test value of 0.130 per degree from Reference 6.

## REFERENCES

1. May, F.W.: State-of-the-Art Design Compendium — STOL Aerodynamic Technology (Internally Blown Jet Flaps). Boeing D180-14299-1, 1971. (U)
2. Ramsey, J.C., and Laudeman, E.C.: STOL Tactical Aircraft Investigation State-of-the-Art Design Compendium. Prepared under USAF Contract F33615-71-C-1754, 1971. (U)
3. May, F.W., and Widdison, C.A.: STOL High-Lift Design Study. Vol. 1. State-of-the-Art Review of STOL Aerodynamic Technology. AFFDL-TR-71-26, Vol. 1, 1971. (U)
4. Hartunian, R.A.: The Finite Aspect Ratio Jet Flap. CAL A1-1190-A-3, 1959. (U)
5. Koven, W., and Graham, R.R.: Wind-Tunnel Investigation of High-Lift and Stall Control Devices on a 37° Sweptback Wing of Aspect Ratio 6 at High Reynolds Numbers. NACA RM L8D29, 1948. (U)
6. Freeman, D.C., Jr., Parlett, L.P., and Henderson, R.L.: Wind-Tunnel Investigation of a Jet Transport Airplane Configuration with an External-Flow Jet Flap and Inboard Pod-Mounted Engines. NASA TN D-7004, 1970. (U)
7. Smith, C.C., Jr.: Effect of Engine Position and High-Lift Devices on Aerodynamic Characteristics of an External-Flow Jet-Flap STOL Model. NASA TN D-6222, 1971. (U)
8. Alexander, A.J., and Williams, J.: Wind-Tunnel Experiments on a Rectangular-Wing Jet-Flap Model of Aspect Ratio 6. ARC R&M 3329, 1964. (U)
9. Aoyagi, K., and Hall, L.P.: Wind-Tunnel Investigation of a Large 35° Swept-Wing Jet Transport Model with an External-Flow Jet-Augmented Double-Slotted Flap. NASA TN D-6482, 1971. (U)
10. Vogler, R.D.: Wind-Tunnel Investigation of a Four-Engine Externally Blown Jet-Flap STOL Airplane Model. NASA TN D-7034, 1970. (U)

11. Turner, T.R.: Low-Speed Investigation of a Full-Span Internal-Flow Jet-Augmented Flap on a High-Wing Model with a 35° Swept Wing of Aspect Ratio 7.0. NASA TN D-434, 1960. (U)
12. Campbell, J.P., and Johnson, J.L., Jr.: Wind-Tunnel Investigation of an External-Flow Jet-Augmented Slotted Flap Suitable for Application to Airplanes with Pod-Mounted Jet Engines. NACA TN 3898, 1956. (U)
13. Aerodynamic Subdivision, Douglas Aircraft Company: Summary of Low Speed Wind Tunnel Data on Several Externally Blown Flap STOL Transport Configurations. MDC J5431, 1972. (U)

**TABLE 6.1.4.2-A**  
**EFFECT OF JET MOMENTUM ON LIFT-CURVE SLOPE**  
**DATA SUMMARY AND SUBSTANTIATION**  
**SUBSONIC**

Ref	A	$\Delta c/2$ (deg)	$\delta_{j,eff}$ (deg)	Flap Type	$C_J$	$C_{L\alpha}$ Calc	$C_{L\alpha}$ Test	$e$ Percent Error
6	7.75	21.1	60	Double-slotted EBF with L. E. Krueger	1.06 2.12 3.18 4.24	0.122 0.133 0.141 0.146	0.110 0.130 0.130 0.139	10.9 2.3 8.5 5.0
7*	7.0	0	35	Double-slotted EBF with L. E. slat	2.76 4.13 5.50 4.13 5.50	0.153 0.168 0.181 0.167 0.179	0.178 0.200 0.220 0.160 0.192	-14.0 -16.0 -17.7 4.4 -6.8
8	6.0	0	30	Plain IBF	0.95 2.07	0.097 0.115	0.100 0.116	-3.0 -0.9
9	7.82	32.4	20	Double-slotted EBF with L. E. slat	2.0 2.0	0.128 0.118	0.145 0.114	-11.7 3.5
10	7.0	21.3	60	Double-slotted EBF with L. E. slat	2.0 3.0	0.120 0.127	0.120 0.127	0 0
13	7.0	21.8	23	Double-slotted EBF with L. E. slat & flap	2.0 3.0	0.125 0.124	0.147 0.144	-15.0 -13.9
	7.0	3.1	60	L. E. slat	2.9	0.158	0.133	18.8
11	7.0	31.9	18.8	Plain IBF	3.09	0.125	0.149	-16.1
12	6.62	26.9	60	Single-slotted EBF	2.95	0.103	0.112	-8.0
$\text{Average Error} = \frac{\sum  e }{n} = 8.8\%$								

\*The data indicate that the flow is probably unattached, which may account for the large errors in this case.

6.1.4.2-9

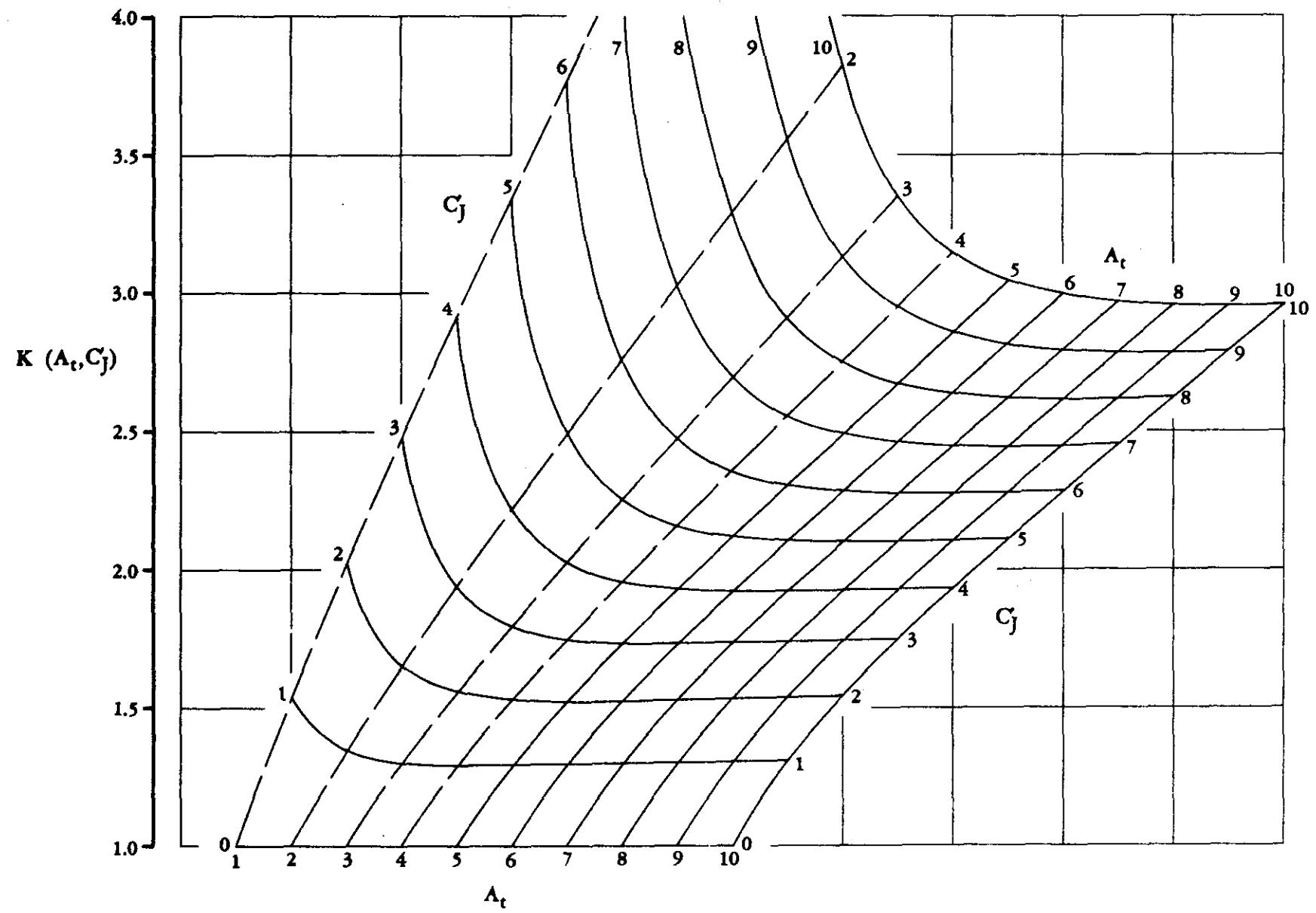


FIGURE 6.1.4.2-9 JET MOMENTUM FACTOR FOR BLOWN FLAPS

### 6.1.4.3 WING MAXIMUM LIFT WITH HIGH-LIFT AND CONTROL DEVICES

The estimation of wing maximum-lift coefficient is at best approximate. The stalling characteristics of various kinds of wings often take on an entirely different character from the stalling characteristics of airfoil sections. Stall may begin at the wing tips or may occur initially at the inboard flapped sections, depending upon the amount of sweep, taper ratio, and the difference in stall angle between the flapped and unflapped sections. Leading-edge devices can markedly alter the character of the stall. Large crossflow components on the wing at the stall make estimates based on section data inaccurate.

Tabulated data from 142 reports are presented in Reference 1. Results are shown for many planforms with and without various configurations of leading- and trailing-edge flaps, fences, and slats. Values of  $C_{L_{max}}$  and  $\alpha_{C_{L_{max}}}$  are given in tabular form. Summary data from Reference 1 are shown in Figures 6.1.4.3-7 through 6.1.4.3-9.

Figure 6.1.4.3-7 illustrates the effect of sweep on the maximum lift effectiveness of trailing-edge flaps. It can be seen that at high angles of sweep, flap deflection can actually decrease maximum lift. This results partially from the additional induced effects when flaps are deflected, causing the tips to stall. Figure 6.1.4.3-8 shows representative effects on  $C_{L_{max}}$  of two sweptback wings with varying flap-span ratios.

Because of their boundary-layer-control properties, double-slotted flaps are capable of producing larger  $C_{L_{max}}$  increments.

Maximum lift increments of leading-edge and trailing-edge flaps cannot, in general, be added when these devices are used in combination. A brief summary of maximum lift coefficients for swept wings is presented in Figure 6.1.4.3-9.

Separate methods are presented herein for estimating the wing maximum lift due to each of the following: mechanical trailing-edge flaps, slats, and jet flaps (externally-blown flaps only).

#### Mechanical Trailing-Edge Flaps

The Datcom method for trailing-edge flaps is semiempirical and converts two-dimensional data into three-dimensional characteristics as affected by wing planform, airfoil section characteristics across the span, flap type and geometry, and flap span. The method is intended to be used as a first-order approximation of wing maximum-lift coefficients when experimental data are not available.

#### Slats

The Datcom method for slats is an empirical method that assumes a section maximum-lift value of 1.28. This method estimates the maximum obtainable lift increment for a particular slat span, slat-chord-to-wing-chord ratio, and wing quarter-chord sweep. If a test value for the slat section maximum lift is available, it can be substituted for the assumed value of 1.28. Attempts to use the predicted section maximum-lift value from Section 6.1.1.3 have been unsatisfactory, as the resulting estimates underpredicted the test values. The method has not been substantiated beyond the test data that were used to formulate the method (which indicated a variation in agreement). Therefore, the method is intended to be used only as a first approximation of the slat maximum-lift increment when experimental data are not available.

#### Jet Flaps

The jet-flap method presented is for predicting the maximum-lift coefficient for an externally-blown-flap (EBF) configuration; no method is currently presented for an internally-blown-flap (IBF) configuration. The Datcom method for EBF configurations is an empirical approximation

taken from Reference 2. The maximum-lift coefficient therein is reasoned to be a function of the total camber of the wing, and blowing is considered to act as an effective camber increase. The measurement of the increase in camber is taken to be the component of thrust normal to the airfoil. This method is intended to be a first-order approximation of the maximum-lift increment due to power effects. Substantiation of this method is not presented here; however, a substantiation of the method does appear in References 2 and 3.

A semiempirical method for an EBF configuration, based on the assumption of a leading-edge stall and the use of basic jet-flap theory, is given in Reference 3. The method provides good correlation with measured values when an empirical factor is added. However, the use of this method depends upon the availability of test data for the effective jet deflection angle, the measured turning efficiency, and the power-off stall angle of attack. If these test data are available, this method is preferable to the Datcom method presented herein.

## DATCOM METHODS

### 1. Mechanical Trailing-Edge Flaps

The increment in maximum-lift coefficient due to trailing-edge flap deflection is given by the equation

$$\Delta C_{L_{\max}} = \Delta c_{L_{\max}} \frac{S_{W_f}}{S_W} K_A \quad 6.1.4.3-a$$

where

$\Delta c_{L_{\max}}$  is the increment in airfoil section maximum-lift coefficient due to trailing-edge flaps, obtained from Section 6.1.1.3.

$\frac{S_{W_f}}{S_W}$  is the ratio of the flap-affected wing area to the total wing area. The flap-affected wing area does not include any increase in wing area due to flap extension.

$K_A$  is an empirically derived correction factor that accounts for the effects of wing planform. This parameter is obtained from Figure 6.1.4.3-10 as a function of the sweepback of the wing quarter-chord line.

It should be noted that the flap deflection angles and all dimensions are measured in planes parallel or perpendicular to the plane of symmetry.

### 2. Slats

The increment in maximum-lift coefficient due to leading-edge slat deflection, based on the wing reference area, is given by

$$\Delta C_{L_{\max}} = 1.28 \left( \frac{c_f/c}{0.18} \right) \left( \frac{b_{slat}}{b_e} \right)^2 \cos^2 \Lambda_{c/4} \quad 6.1.4.3-b$$

where

$\frac{c_f}{c}$  is the ratio of the leading-edge-slat chord to the wing chord (see Figure 6.1.1.1-51).

6.1.4.3-2

$$\frac{b_{\text{slat}}}{b_e}$$

is the ratio of the total slat span to the exposed wing span. For a segmented leading-edge slat,  $b_{\text{slat}}$  is the total span of the segments. (See Section 4.3.1.2 for the definition of the exposed wing span.)

$$\Lambda_{c/4}$$
 is the sweep of the quarter chord.

### 3. Jet Flaps

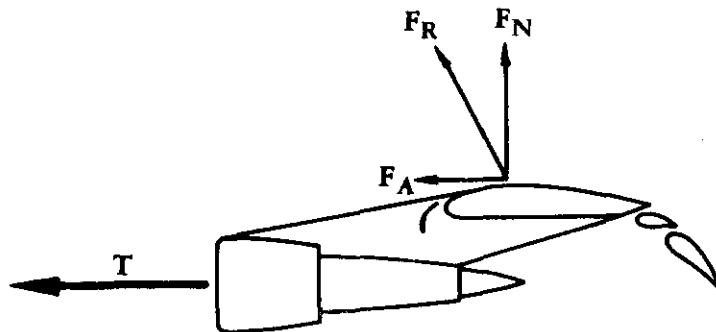
The increment in maximum-lift coefficient due to power effects for an EBF configuration is approximated from Figure 6.1.4.3-12, as a function of the thrust normal to the airfoil, defined as

$$\eta_t C_J \sin \delta_{j_{\text{eff}}}$$

where

$$\eta_t$$

is the static turning efficiency defined as the resultant force divided by the gross thrust. This value should be obtained from test data if available, or it may be approximated for double- or triple-slotted flaps from Figure 6.1.4.3-11, as a function of the effective jet deflection angle. (See Sketch (a).)



$$\delta_{j_{\text{eff}}} = \tan^{-1} (F_N / F_A)$$

$$\eta_t = F_R / T$$

**SKETCH (a)**

$$C_J$$

is the nondimensional trailing-edge jet momentum coefficient based on the gross engine thrust and the wing reference area. (See Section 6.1.4.1 for a definition.)

$$\delta_{j_{\text{eff}}}$$

is the effective jet deflection angle with respect to the airfoil chord. If possible, this value should be obtained from static force tests. When test data are not available, the effective flap deflection angle may be approximated by using Equation 6.1.4.1-d; i.e.,

$$\delta_{j_{\text{eff}}} = \frac{1}{2} (\delta_u + \delta_\ell)$$

where  $\delta_u$  and  $\delta_\ell$  are defined in Section 6.1.4.1.

### Sample Problems

#### 1. Mechanical Trailing-Edge Flaps

Given: The wing-flap configuration of Reference 2.

$$A = 5.1$$

$$\lambda = 0.383$$

$$\Lambda_{c/4} = 46^\circ$$

NACA 64-210 airfoil (L286c)

$$(t/c)_{\text{streamwise}} = 0.072$$

Single-slotted flap

$$c_f/c = 0.258$$

$$\delta_f = 15.6^\circ$$

$$\frac{S_{w_f}}{S_w} = 0.378$$

$$R_g = 6.0 \times 10^6$$

Compute:

$\Delta c_{\ell_{\max}}$  (Section 6.1.1.3)

$$\left( \Delta c_{\ell_{\max}} \right)_{\text{base}} = 1.045 \quad (\text{Figure 6.1.1.3-12a})$$

$$k_1 = 1.010 \quad (\text{Figure 6.1.1.3-12b})$$

$$k_2 = 0.605 \quad (\text{Figure 6.1.1.3-13a})$$

$$\frac{\text{Actual flap angle}}{\text{Reference flap angle}} = \frac{15.6}{45} = 0.347$$

$$k_3 = 0.445 \quad (\text{Figure 6.1.1.3-13b})$$

$$\Delta c_{\ell_{\max}} = k_1 k_2 k_3 \left( \Delta c_{\ell_{\max}} \right)_{\text{base}} \quad (\text{Equation 6.1.1.3-a})$$

$$= (1.010) (0.605) (0.445) (1.045)$$

$$= 0.284$$

$$K_A = 0.730 \quad (\text{Figure 6.1.4.3-10})$$

Solution:

$$\Delta C_{L_{\max}} = \Delta c_{\ell_{\max}} \frac{S_{w_f}}{S_w} K_A \quad (\text{Equation 6.1.4.3-a})$$

$$= (0.284) (0.378) (0.730)$$

$$= 0.0784 \quad (\text{based on } S_w)$$

This compares with a test value of 0.075 from Reference 2.

## 2. Slats

Given: The wing-body configuration of an A4D-1 Flight Trainer

$$\frac{c_f}{c} = 0.177 \quad \Lambda_{c/4} = 33.2^\circ \quad \frac{b_{slat}}{b_e} = 0.535$$

Compute:

$$\begin{aligned} \Delta C_{L_{max}} &= 1.28 \left( \frac{c_f/c}{0.18} \right) \left( \frac{b_{slat}}{b_e} \right)^2 \cos^2 \Lambda_{c/4} && \text{(Equation 6.1.4.3-b)} \\ &= (1.28) \left( \frac{0.177}{0.18} \right) (0.535)^2 (0.700) \\ &= 0.252 \text{ (based on } S_w) \end{aligned}$$

This compares with a test value of 0.295.

## 3. Jet-Flap EBF Configuration

Given: The wing-body configuration of Reference 5.

$$C_j = 3.18 \quad \delta_f = 60^\circ \quad \delta_u \approx 73^\circ \quad \delta_\ell \approx 52^\circ$$

Double-Slotted Flaps

Compute:

$$\begin{aligned} \delta_{j_{eff}} &= \frac{1}{2} (\delta_u + \delta_\ell) && \text{(Equation 6.1.4.1-d)} \\ &= \frac{1}{2} (73 + 52) \\ &= 62.5^\circ \end{aligned}$$

$$\eta_t = 0.583 \quad \text{(Figure 6.1.4.3-11)}$$

$$\eta_t C_j \sin \delta_{j_{eff}} = (0.583) (3.18) (0.887) = 1.644$$

$$\Delta C_{L_{max}} = 4.65 \quad \text{(Figure 6.1.4.3-12, lift increment due only to power effects, based on } S_w)$$

This compares with a test value of 5.35 from Reference 5.

## REFERENCES

1. Furlong, G. C., and McHugh, J. G.: A Summary and Analysis of the Low-Speed Longitudinal Characteristics of Swept Wings at High Reynolds Number. NACA TR 1339, 1957. (U)
2. May, F., and Widdison, C. A.: STOL High-Lift Design Study. Vol. I — State-of-the-Art Review of STOL Aerodynamic Technology. AFDL-TR-71-26, Vol. I, 1971. (U)
3. Moorhouse, D. J.: A Practical Look at the Stall and High-Lift Operation of Externally Blown Flap STOL Transport Configurations. AGARD Preprint No. 102, 1972. (U)
4. Spooner, S. H., and Mollenberg, E. F.: Positioning Investigation of Single-Slotted Flaps on a 47.7° Sweptback Wing at Reynolds Numbers of  $4.0 \times 10^6$  and  $6.0 \times 10^6$ . NACA RM L50H29, 1950. (U)
5. Freeman, D. C., Jr., Parlett, L. P., and Henderson, R. L.: Wind-Tunnel Investigation of a Jet Transport Airplane Configuration with an External-Flow-Jet Flap and Inboard Pod-Mounted Engines. NASA TN D-7004, 1970. (U)

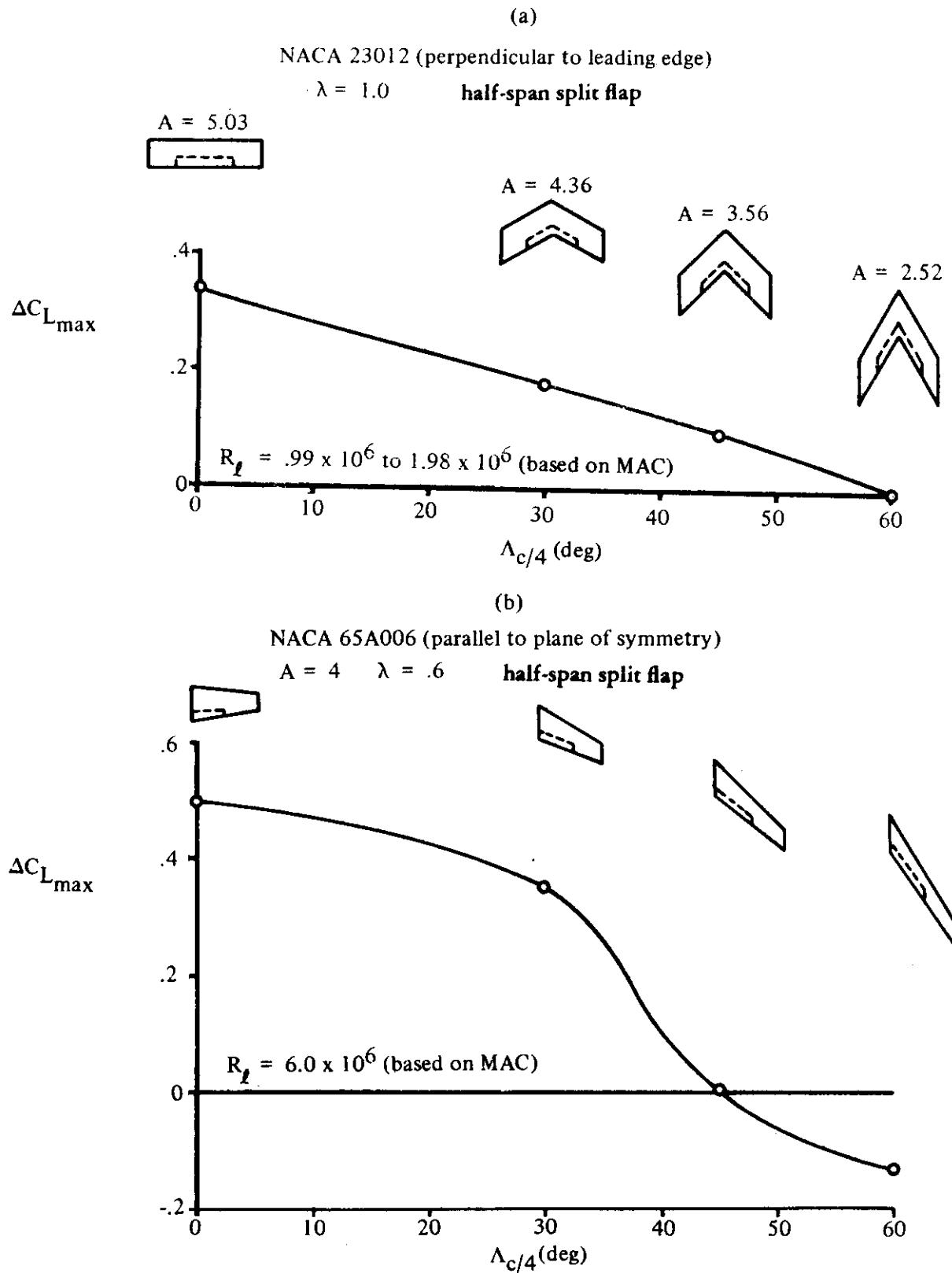


FIGURE 6.1.4.3-7 TYPICAL EFFECTS OF WING SWEEP ON MAXIMUM-LIFT INCREMENTS DUE TO SPLIT TRAILING-EDGE FLAPS

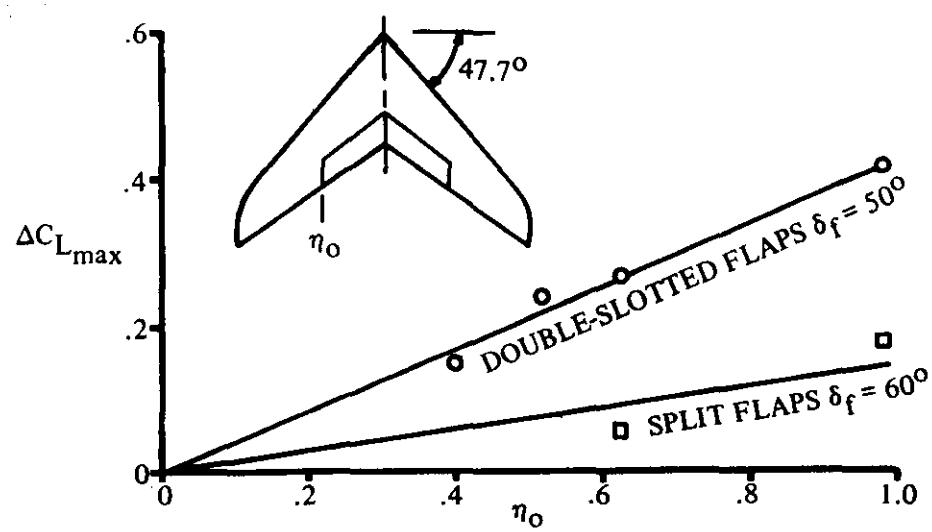
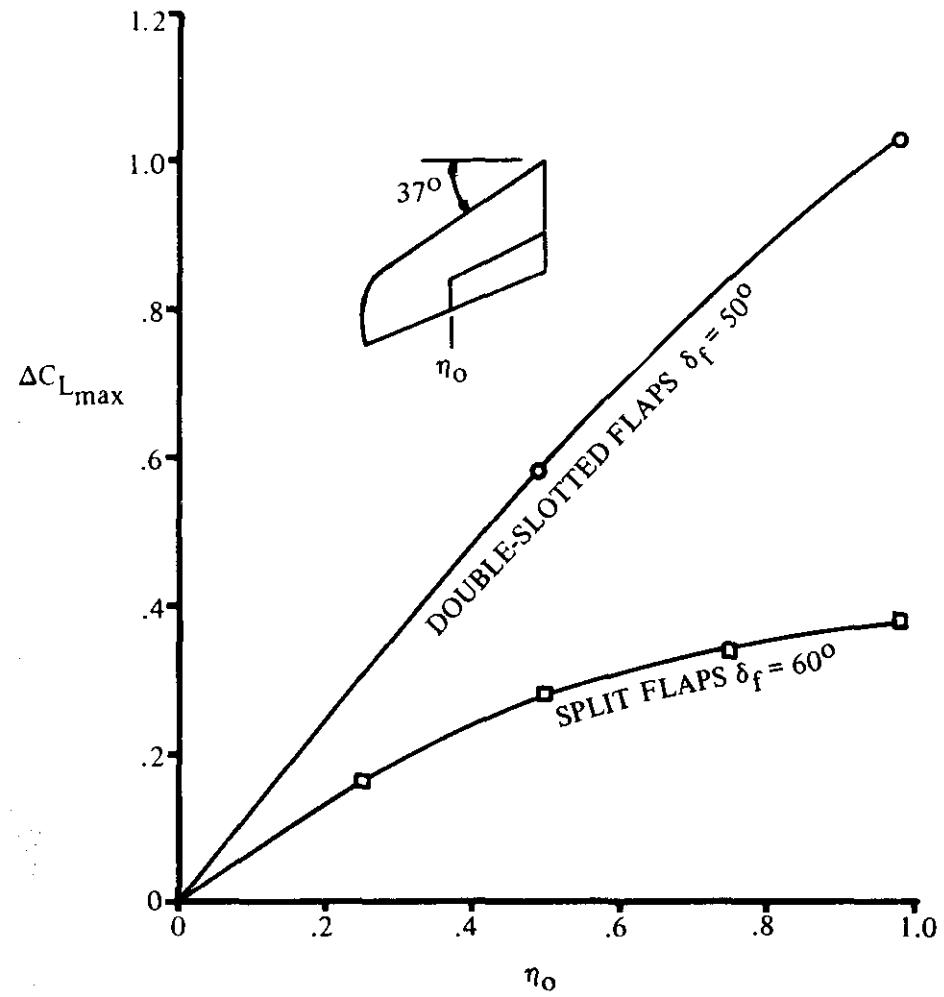


FIGURE 6.1.4.3-8 EFFECT OF SPANWISE FLAP EXTENT ON WING MAXIMUM LIFT INCREMENT

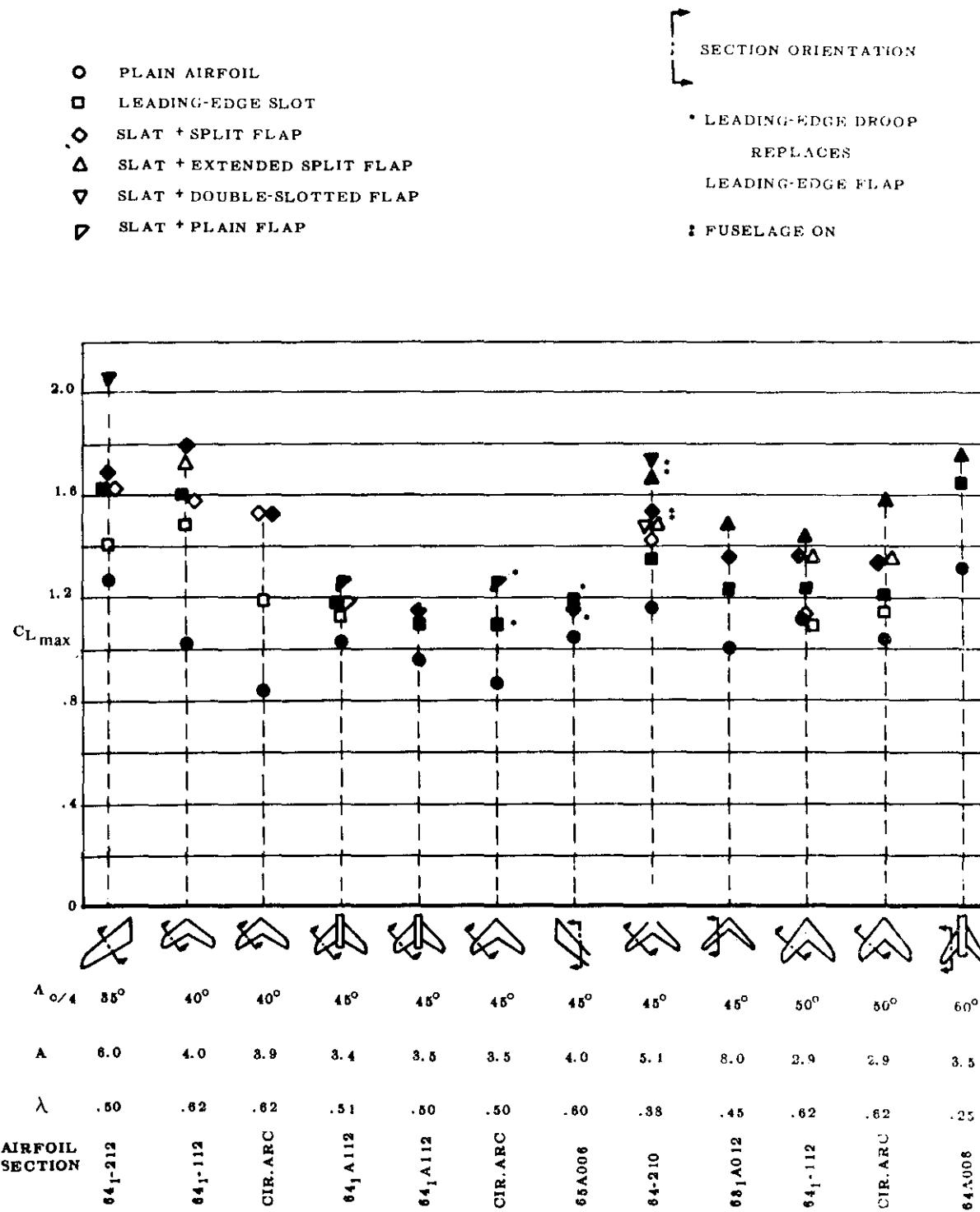


FIGURE 6.1.4.3-9 SUMMARY CHART OF MAXIMUM LIFT COEFFICIENTS OBTAINED WITH VARIOUS TYPES OF TRAILING-EDGE FLAPS

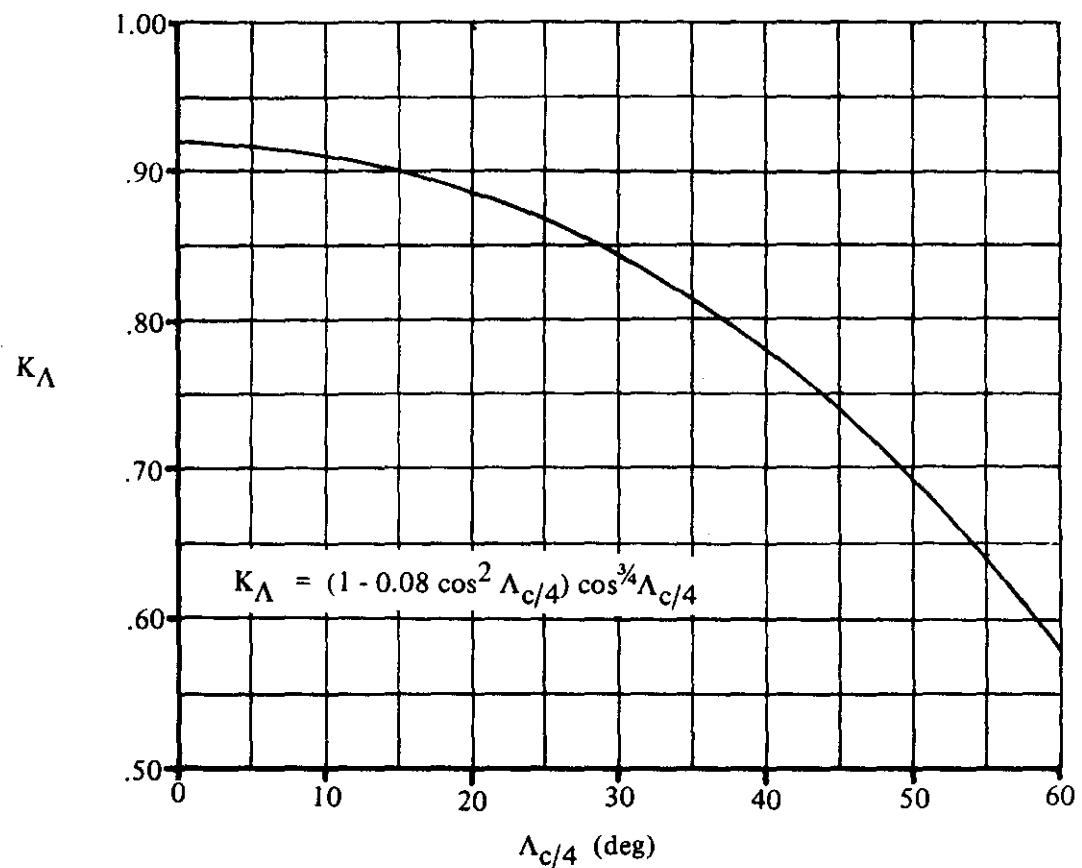


FIGURE 6.1.4.3-10 PLANFORM CORRECTION FACTOR — TRAILING-EDGE FLAPS

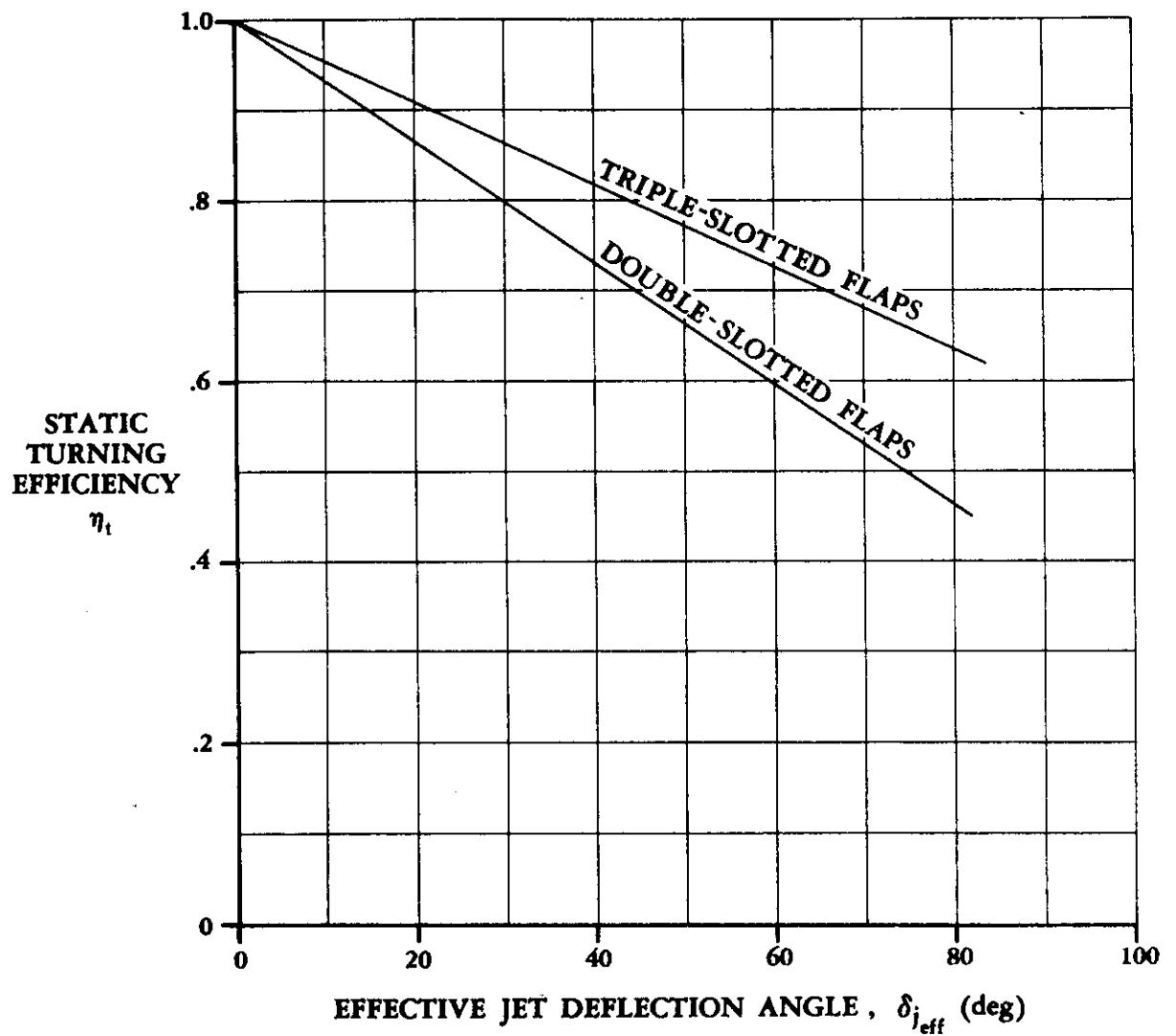
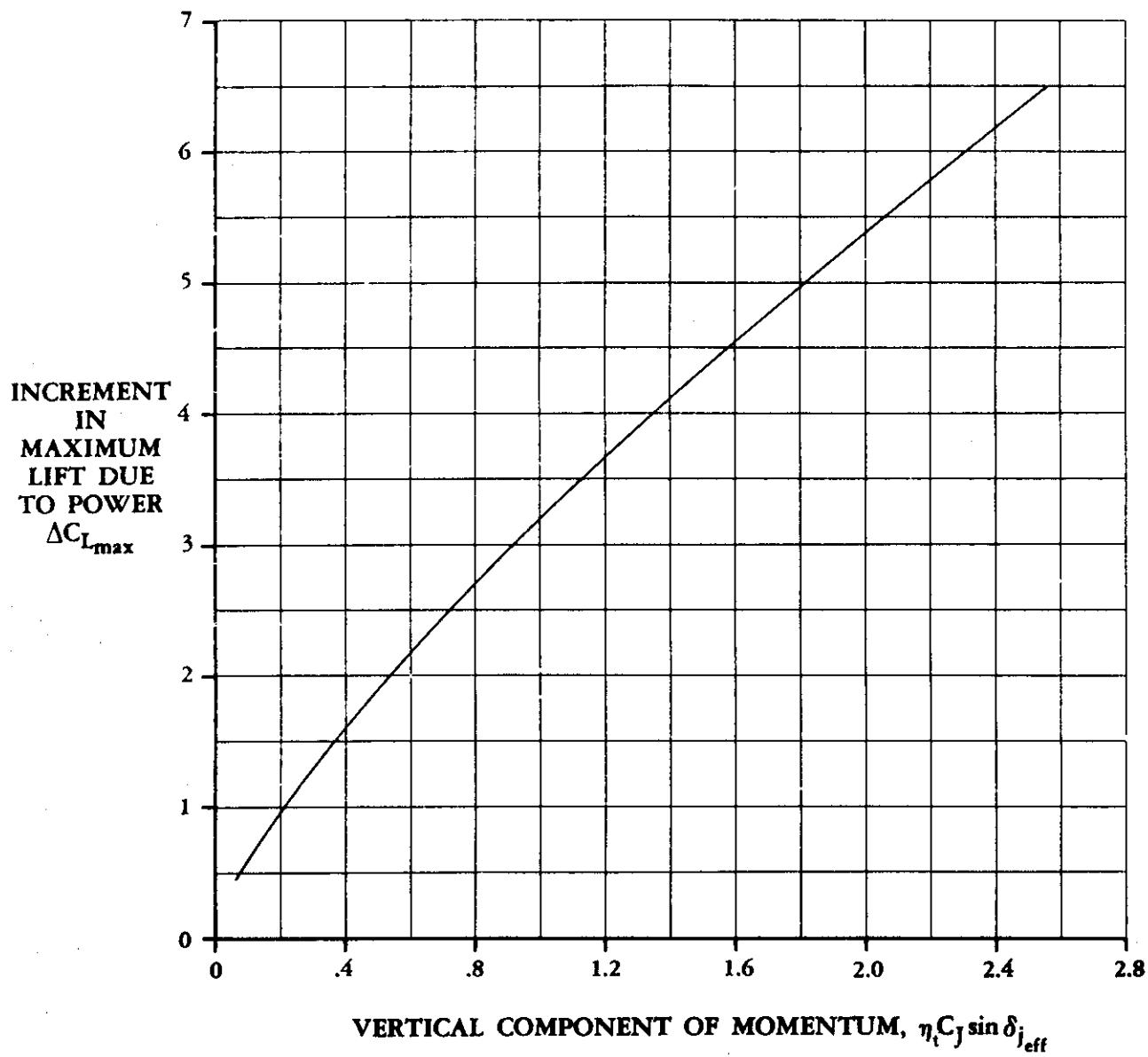


FIGURE 6.1.4.3-11 FLAP TURNING EFFICIENCY



**FIGURE 6.1.4.3-12 CORRELATION OF MAXIMUM LIFT DUE TO POWER**

### **6.1.5 WING PITCHING MOMENT WITH HIGH-LIFT AND CONTROL DEVICES**

The following sections give the effect of flap deflection on wing pitching-moment coefficient at subsonic, transonic, and supersonic speeds. Section data from other portions of the Datcom are used. Although the methods are developed for trailing-edge flaps, they can be applied to leading-edge flaps, slats, and spoilers, provided the proper section data are available or can be estimated. However, the methods presented are applicable to the angle-of-attack and flap-deflection ranges for which linear aerodynamic control characteristics exist. A chart showing the linear-lift range for a particular airfoil is shown in Section 6.1.3. In general, the linear-lift range for wings is considerably shorter than that shown in this chart, particularly for swept and low-aspect-ratio wings. For swept wings, the effects of spanwise boundary-layer flow, induced camber, and leading-edge vortices are pronounced and tend to nonlinearize the control or flap characteristics. For low-aspect-ratio wings, section characteristics are not important and, generally, the linear range is shorter than those of their section counterparts.

Leading- and trailing-edge flaps frequently have a pronounced effect upon the longitudinal stability characteristics of wings. Reference 1 gives a summary of these effects. Figures 6.1.5-2a and 6.1.5-2b are reproduced from this reference. Figure 6.1.5-2a shows the increase in stability that can be obtained from leading-edge flaps, slats, and fences. The basic curve is also shown in Section 4.1.4.3. Figure 6.1.5-2b shows the effect of spanwise extent of leading- and trailing-edge flaps on longitudinal stability for a particular wing.

### **REFERENCE**

1. Furlong, G.C., and McHugh, J.G.: *A Summary and Analysis of the Low-Speed Longitudinal Characteristics of Swept Wings at High Reynolds Number*, NACA TR 1339, 1957. (U)

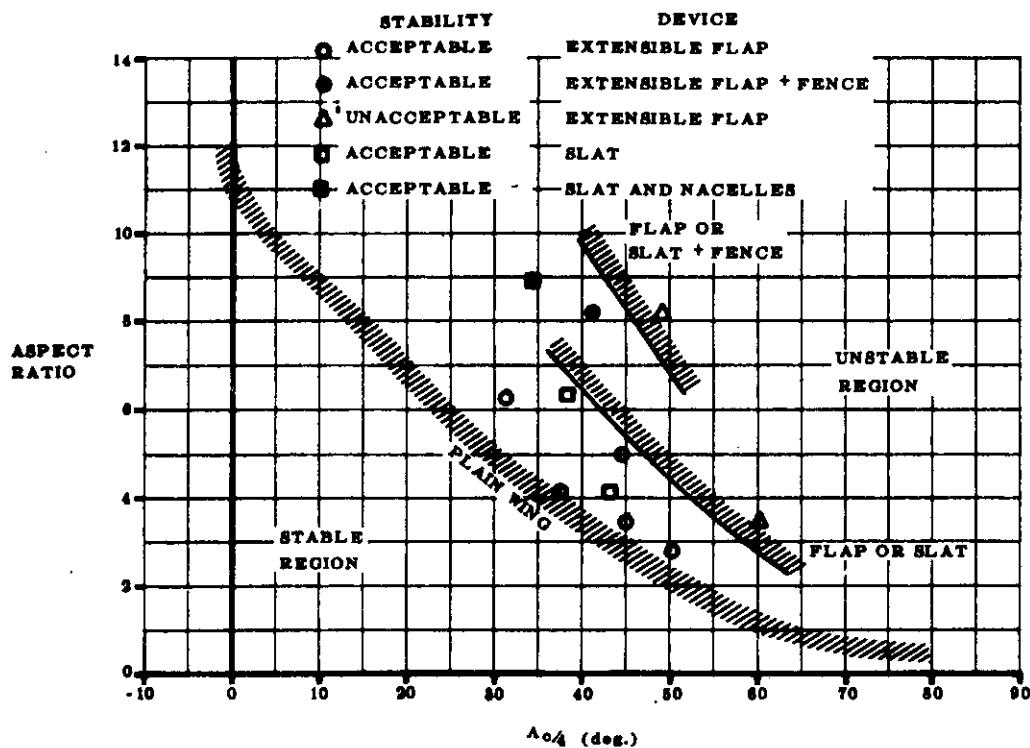


FIGURE 6.1.5-2a INFLUENCE OF SEVERAL TYPES OF STALL-CONTROL DEVICES ON LONGITUDINAL STABILITY BOUNDARY FOR WINGS WITH  $\lambda > .4$

■■■■■ UNSTABLE AT MAXIMUM LIFT  
 ■■■■■ STABLE AT  $C_{L_{max}}$  WITH UNSTABLE SHIFT OF a.o. GREATER THAN  $0.15^\circ$  PRIOR TO  $C_{L_{max}}$   
 ■■■■■ STABLE AT  $C_{L_{max}}$  WITH UNSTABLE SHIFT OF a.o. LESS THAN  $0.15^\circ$  PRIOR TO  $C_{L_{max}}$   
 ■■■■■ STABLE AT  $C_{L_{max}}$  WITH UNSTABLE SHIFT OF a.o. LESS THAN  $0.05^\circ$  PRIOR TO  $C_{L_{max}}$

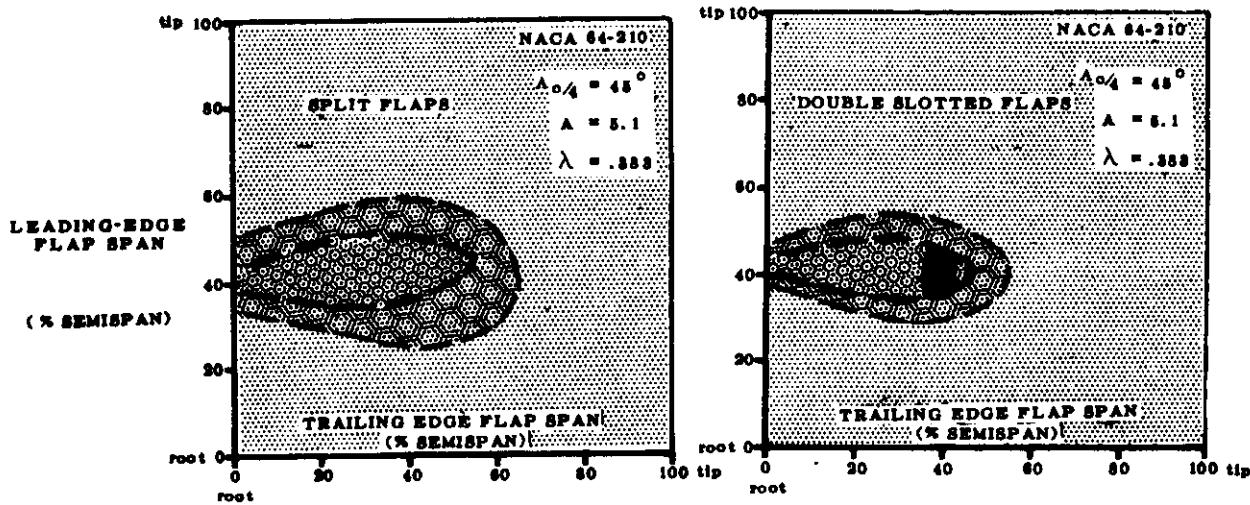


FIGURE 6.1.5-2b EFFECTS OF LEADING-EDGE AND TRAILING-EDGE FLAPS ON LONGITUDINAL STABILITY CHARACTERISTICS OF A SWEPTBACK WING

### 6.1.5.1 PITCHING-MOMENT INCREMENT $\Delta C_m$ DUE TO HIGH-LIFT AND CONTROL DEVICES

#### A. SUBSONIC

Methods are presented in this section for estimating the pitching-moment characteristics for most common high-lift devices in use today and for some of the blown flaps being considered for STOL aircraft. These methods are valid only in the linear-lift region (preferably near zero angle of attack). The effect of these devices on the variation of pitching moment with angle of attack is presented in Section 6.1.5.2, except for the jet flap, which is presented in this section. Considerations of clarity and simplicity of presentation dictated this deviation from standard Datcom practice. The reader is referred to Sections 6.1.1.1 and 6.1.2.1 for a discussion of the salient aspects regarding the various types of high-lift devices.

The assumption is made that the characteristics of a trailing-edge flap are independent of any leading-edge device, and/or the characteristics of a leading-edge device are independent of any mechanical trailing-edge flap. In reality this is not quite true, but the methods of this section are not sufficiently refined to account for these interference effects. This assumption cannot be justified in the case of the more powerful jet flap.

#### Trailing-Edge Mechanical Flaps

Two methods are presented for estimating the pitching-moment increment due to trailing-edge mechanical flaps at small angles of attack and low speeds. Both methods are applicable to all types of flaps and to high-flap-deflection ranges, provided proper section data are used.

Method 1 (Reference 1) is substantially easier to apply than Method 2 (Reference 2). A data summary and substantiation of Method 1 are presented in Table 6.1.5.1-A. The resulting mean error of the pitching-moment increment due to flap deflection is  $\pm 0.053$ . For configurations with quarter-chord sweep angles greater than  $45^\circ$ , caution should be exercised, since the accuracy of the method is questionable in this range.

Method 2 uses linear theory for subsonic compressible flow, together with two-dimensional airfoil data adjusted for the effects of sweep. The additional feature of this method is that it requires the determination of the spanwise loading of the wing due to flap deflection. It is this feature that makes this method cumbersome to use. This method is not substantiated here; however, a substantiation of the method does appear in Reference 2 with a reported mean error of pitching-moment increment due to flap deflection of  $\pm 0.02$ .

#### Leading-Edge Mechanical Devices

Although the second method described above should be equally applicable to leading-edge devices, no substantiation of such use has been found. The use of a method as complex as this one cannot be justified when the small pitching moments and nonlinear characteristics of leading-edge devices are considered. Therefore, a simpler method is presented for estimating the effect of conventional leading-edge devices on the pitching moment. This method is based on the thin-airfoil, two-dimensional method, uncorrected for three-dimensional effects. Although the accuracy of the method is not as good as desired, no trends in three-dimensional parameters, such as aspect ratio, taper ratio, or sweep, have been observed that would improve the accuracy.

The lack of accuracy is to be expected, since the linear theory is intrinsically unable to handle the large deflections typical of leading-edge devices or to predict the nonlinear characteristics evident in the test data.

### Jet Flaps

The method presented herein (taken in part from Reference 3) adapts the jet-flap method for airfoils, presented in Section 6.1.2.1, for use on finite-aspect-ratio wings. As such, it applies to the same concepts and is subject to the same limitations that are listed in that section. The user is referred to the discussions in Sections 6.1.1.1 and 6.1.2.1 for a complete understanding of this method.

The jet-flap method assumes that the entire flap is immersed in a uniform-jet-flow field. For externally-blown-flap (EBF) systems on swept wings, where this assumption is obviously not valid, the method contains a procedure for making an approximate estimate of the spanwise distribution of the jet. However, this cannot be expected to yield better than a rough estimate of the true pitching moment. This is due to the fact that the pitching moment cannot be accurately estimated without a detailed knowledge of the spanwise extent of the wing influenced by the jet.

Unfortunately, the jet spreading problem is very difficult to treat, and to date little in the way of analytical or empirical methods has been developed. Solution of the problem, which is simply to determine the spanwise distribution of trailing-edge jet momentum, requires that the flow details of the impingement, spreading, and turning process be known. Such a flow solution, which involves the viscid/inviscid interaction of the jet impinging on the wing-flap system, is clearly beyond the scope of the Datcom.

The wing pitching moment is calculated by applying correction factors for finite aspect ratio to Spence's adaptation of thin-airfoil theory to the two-dimensional jet-flap problem. The correction factors adjust the center-of-lift location and the magnitude of the lift increment. The first is from Reference 4 and is based on conventional flap data; the second is from Reference 38 and is based on Maskell's theoretical correction for three-dimensional effects. This method does not account for sweep or taper effects, except insofar as they affect the geometric relationship between the center of gravity and the wing. This should not be a serious restriction, since the jet-flap system is usually applied to high-aspect-ratio wings with low to moderate sweepback. The maximum sweep angle and taper ratio for which this method is valid have not been determined.

## DATCOM METHODS

### 1. Trailing-Edge Mechanical Flaps

#### Method 1

This method assumes a constant flap-chord-to-wing-chord ratio. In the case of arbitrary spanwise distribution of flap chord (constant-chord flaps on tapered wings or tapered flaps on untapered wings), the flaps should be divided into spanwise steps. The pitching-moment contributions from each spanwise step are then calculated and added together to obtain the total increment for the flap.

At low angles of attack, the change in pitching-moment increment due to flap deflection based on  $S_w \bar{c}_w$  taken about  $\bar{c}_w/4$  is given by

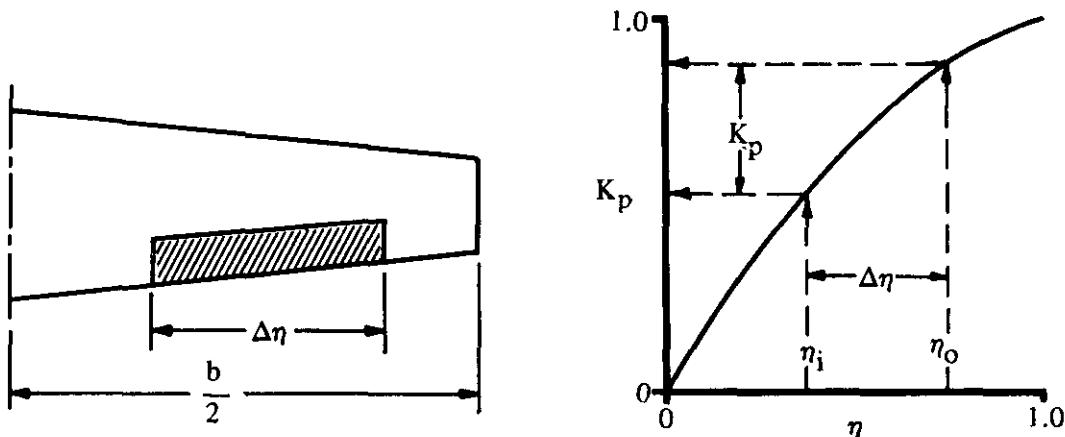
$$\Delta C_{m_f} = \Delta C_m + K_A \left( \frac{A}{1.5} \right) \Delta C_L \tan \Lambda_{c/4} \quad 6.1.5.1-a$$

where

$$\Delta C_m = K_p \left\{ \left( \frac{\Delta C'_m}{\Delta C_L} \right) \Delta C_L \left( \frac{c'}{c} \right)^2 - 0.25 C_L \left( \frac{c'}{c} \right) \left( \frac{c'}{c} - 1 \right) + C_m \left[ \left( \frac{c'}{c} \right)^2 - 1 \right] \right\} \quad 6.1.5.1-b$$

where

$K_p$  is the flap-span factor as a function of taper ratio and flap location, obtained from Figure 6.1.5.1-61 as illustrated in Sketch (a). Note:  $\eta$  is the span station,  $\eta = \frac{\text{control span ordinate}}{b/2}$



SKETCH (a)

$\frac{\Delta C'_m}{\Delta C_L}$  is the ratio of the pitching-moment increment to lift increment for a full-span flap on a rectangular wing, obtained from Figure 6.1.5.1-60 as a function of wing thickness and flap-chord-to-extended-wing-chord ratio.

$\Delta C_L$  is the lift increment due to flap deflection, obtained from the appropriate equation (determined by the particular flap type) of Section 6.1.4.1 using the following assumptions:

1. full-span flap
2. wing aspect ratio of 6
3. no sweep,  $\Lambda_{c/2} = 0$

(Note: the above assumptions are to be used for all calculations involved in calculating  $\Delta C_L$ .)

- $\frac{c'}{c}$  is the ratio of the extended wing chord to the retracted wing chord (see Figures 6.1.1.1-44 through -46 for a graphical illustration).
- $C_L$  is the wing-body lift coefficient with the flap retracted. This value should be obtained from test data if available, or from Sections 4.1.3.1\* and 4.3.1.2.
- $C_m$  is the wing-body pitching-moment coefficient with the flap retracted. This value should be obtained from test data if available, or from Section 4.3.2.2 supplemented with a test-data value for  $(C_{m0})_{WB}$ .
- $K_A$  is the conversion factor for a partial-span flap on a sweptback wing obtained from Figure 6.1.5.1-57 in a similar manner as  $K_p$ ; i.e., see the illustration in Sketch (a).
- $A$  is the wing aspect ratio.
- $\Lambda_{c/4}$  is the sweep of the wing quarter-chord.

## Method 2

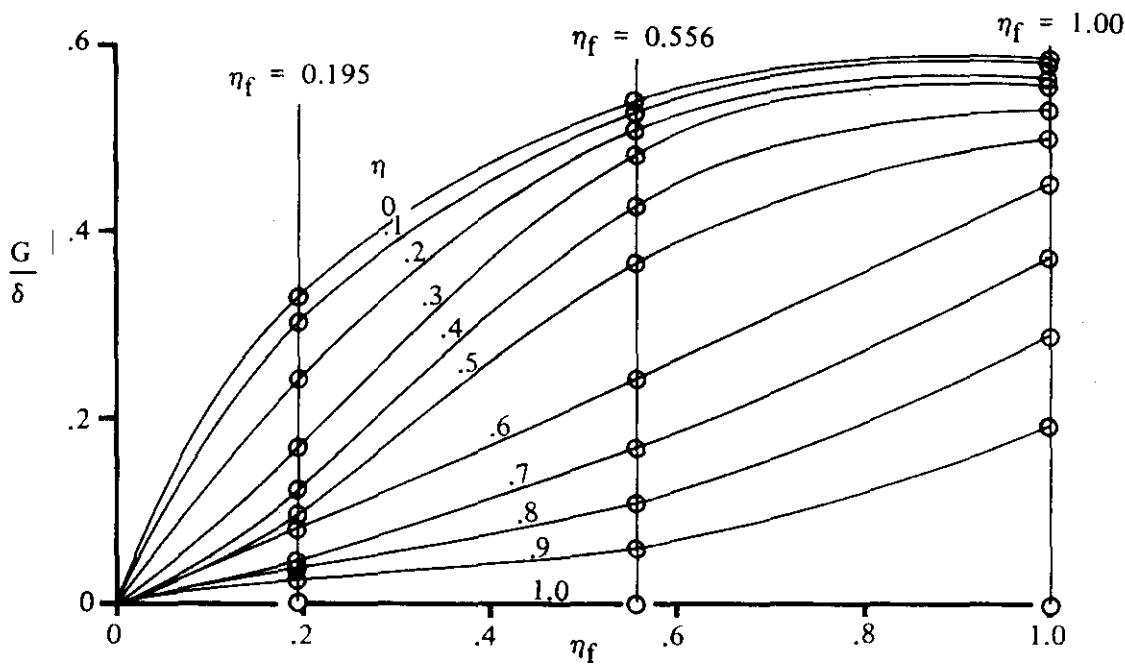
This method requires the determination of the span loading due to flap deflection (Reference 5) and the chordwise center-of-pressure location for stations across the span. Once these quantities are determined, the incremental pitching moment can be calculated by an integration process. The pitching-moment increment  $\Delta C_{mf}$  is obtained by using the procedure outlined in the following steps:

- Step 1. Determine the spanwise loading coefficient  $G/\delta$  of full wing-chord flaps. The spanwise loading coefficient  $G/\delta$  of full wing-chord flaps is obtained as a function of span station,  $\eta = \frac{\text{span ordinate}}{b/2}$ , from Figures 6.1.5.1-62a through 6.1.5.1-62d for appropriate values of  $\beta A/\kappa$ ,  $\Lambda_\beta$ , and  $\lambda$ , where  $\kappa = c_{\ell\alpha M}/(2\pi/\beta)$  and  $\Lambda_\beta = \tan^{-1}(\tan \Lambda_{c/4}/\beta)$ .

It should be noted that Figures 6.1.5.1-62a through 6.1.5.1-62d present the spanwise loading coefficients for full wing-chord flaps that extend from the plane of symmetry out to span stations of  $\eta_0 = 0.195$ ,  $\eta_0 = 0.556$ , and  $\eta_0 = 1.0$  (Figure 6.1.5.1-62a also includes  $\eta_0 = 0.831$ ). The results for other flap spans are obtained by interpolating the results of the particular flap spans presented in Figures 6.1.5.1-62a through 6.1.5.1-62d. The final step in the interpolation procedure is to cross-plot the results of the variation of the loading parameter at given stations as a function of flap span  $\eta_f$  for desired values of the parameters  $\beta A/\kappa$ ,  $\Lambda_\beta$ , and  $\lambda$  (see Sketch (b)).

---

\*The wing-body zero-lift angle of attack is obtained from the wing-alone data of Section 4.1.3.1. Test data from a similar configuration should be used if available. Wing surface velocity is increased by the presence of the fuselage; therefore, when the fuselage is below the wing, the lift is reduced, and with the fuselage above the wing, the lift will be increased. This effect is generally small, unless wing-mounted bodies, such as stores or nacelles, are close to the fuselage or to each other.

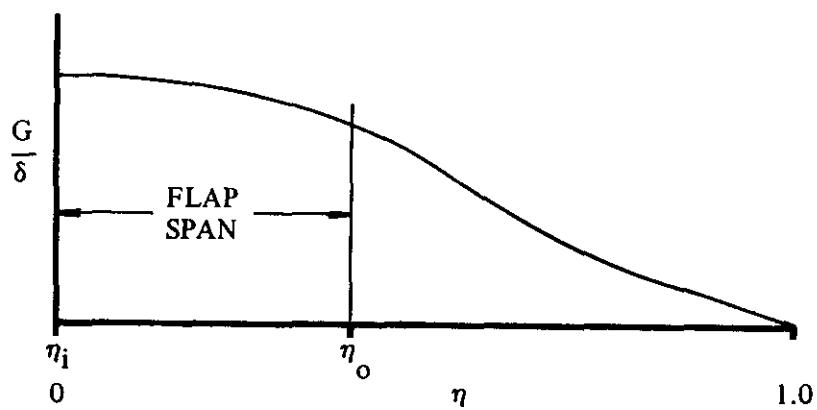


SKETCH (b)

The spanwise loading is then read from this cross plot at the desired values of  $\eta_f$  ( $\eta_i$  and  $\eta_o$ ). Note that for cases where Figure 6.1.5.1-62a applies, i.e., where  $\beta A/\kappa = 0$ , the cross plot represented by Sketch (b) is obtained directly, since no intermediate steps are required to interpolate for  $\lambda$  or  $\Lambda_\beta$ .

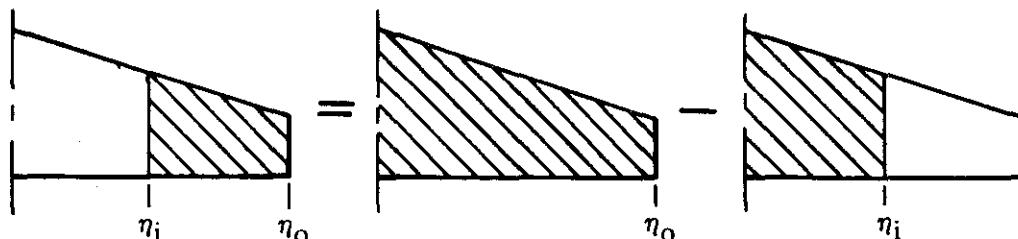
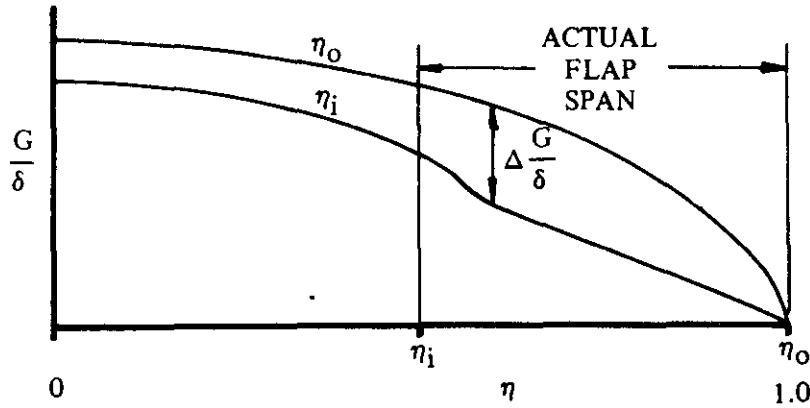
The following procedure is used to determine the spanwise loading of the actual flap:

- For flaps that extend from the plane of symmetry outboard, tabulate the loading for an inboard flap extending from the plane of symmetry to the outboard station of the actual flap, as shown in Sketch (c).



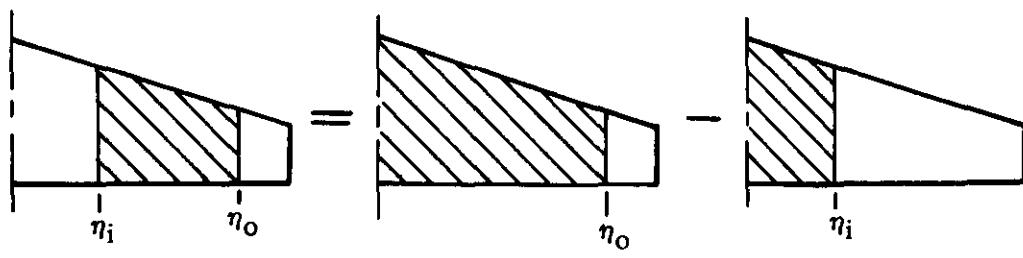
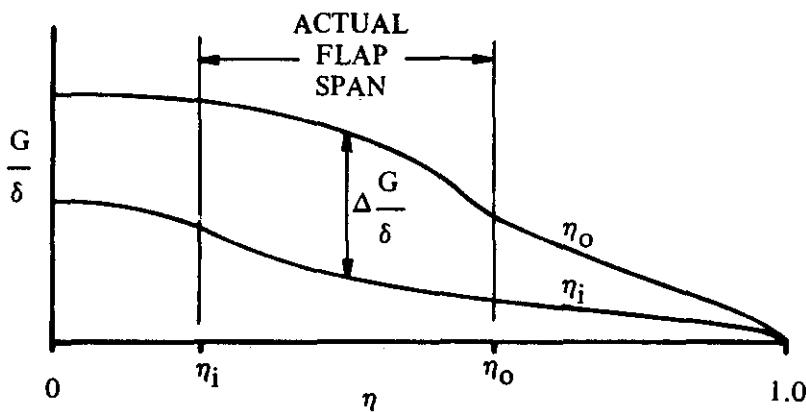
SKETCH (c)

- For partial-span flaps that extend from the wing tip inboard, the charts are used as follows: Tabulate the loading  $G/\delta$  for a full-span flap. Tabulate the loading  $G/\delta$  for an inboard flap extending from the plane of symmetry to the inboard station of the actual flap. Subtract the loadings of the above tabulations at each span station to obtain the loading of the actual flap (see Sketch (d)).



SKETCH (d)

- c. For partial-span flaps that have outboard ends inboard of the wing tip and inboard ends outboard of the plane of symmetry, the charts are used as follows: Tabulate the loading function  $G/\delta$  for flaps extending from the plane of symmetry to the outboard station of the actual flap. Tabulate the loading function  $G/\delta$  for a flap extending from the plane of symmetry to the inboard end of the actual flap. Subtract the loadings of the above tabulations at each span station to obtain the loading of the actual flap (see Sketch(e)).



SKETCH (e)

**Step 2.** Determine the incremental section lift coefficient as a function of span station  $\eta$  by\*

$$c_{q_A} = -\frac{2b}{c} \frac{G}{\delta} \alpha_\delta \delta \quad 6.1.5.1-c$$

where

$c_{q_A}$  is the incremental section lift coefficient due to flap deflection.

$b$  is the total wing span.

$c$  is the local chord at the span station in question.

$\frac{G}{\delta}$  is the loading coefficient of a full wing-chord flap at the span station in question, obtained from Step 1.

$\alpha_\delta$  is the two-dimensional lift-effectiveness parameter expressed as

$$\alpha_\delta = -\frac{(c_{q_\delta})_\alpha}{(c_{q_\alpha})_\delta} \quad (\text{Equation 6.1.1.1-b})$$

where

$c_{q_\delta}$  is the lift effectiveness of the flapped airfoil from the appropriate method of Section 6.1.1.1.

$c_{q_\alpha}$  is the airfoil section lift-curve slope (including the effects of compressibility) from Section 4.1.1.2.

For area-suction and blowing-type flaps the theoretical value of  $\alpha_\delta$  is presented as a function of  $c_f/c$  in the inset of Figure 6.1.4.1-14.

When experimental values of the section lift increment  $\Delta c_q$  are available for plain, split, or slotted flaps, the lift-effectiveness parameter should be calculated using

$$\alpha_\delta = -\frac{(\Delta c_q)_{\text{experiment}}}{(c_{q_\alpha})_\delta \delta}$$

$\delta$  is the streamwise flap deflection in radians. This value may be obtained from

$$\delta = \tan^{-1} (\cos \Lambda_{HL} \tan \delta_{HL}) \quad 6.1.5.1-d$$

---

\*In the theory, sections of a yawed infinite wing are dealt with. See Reference 2 for details of the theoretical treatment of sweep and taper.

where

$\Lambda_{HL}$  is the sweep angle of the flap hinge line.

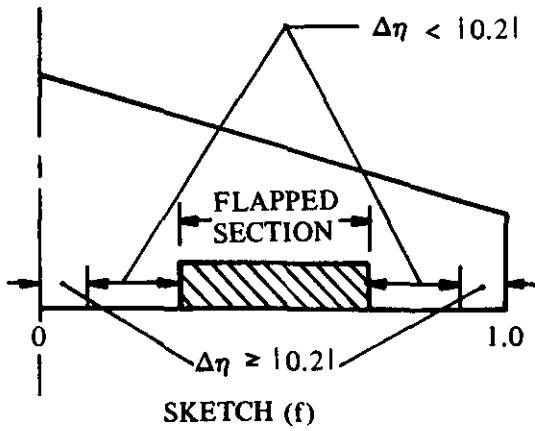
$\delta_{1HL}$  is the flap deflection measured normal to the flap hinge line.

The product  $(G/\delta)\alpha_\delta$  in Equation 6.1.5.1-c converts the spanwise loading distribution of full wing-chord flaps,  $c_f/c = 1.0$ , to the spanwise loading distribution of partial wing-chord flaps. For the case of arbitrary spanwise distribution of flap chord (constant-chord flaps on tapered wings or tapered flaps on untapered wings), the flap can be divided into spanwise steps and a new value for  $\alpha_\delta$  for each segment determined. The load distribution due to each spanwise step is then determined by the product of  $G/\delta$  and the average value of  $\alpha_\delta$  over that spanwise step.

**Step 3.** Determine the chordwise center-of-pressure location  $x_{c,p.}$  for stations across the span.

For this calculation the wing span is divided into not more than three types of regions. These regions are illustrated schematically in Sketch (f), and consist of:

- Span stations included in the flapped section.
- Span stations adjacent to the flap ends where the distance from the ends of the flap  $\Delta\eta$  is less than  $|0.20|$ .
- Span stations not influenced by the flap span,  $\Delta\eta \geq |0.20|$ .



The chordwise center-of-pressure location in each region is obtained as follows:

- For the span stations included in the flapped section

$$x_{c,p.} = 0.25 - \frac{\Delta c_m}{c_{\ell_A} = 0} \quad 6.1.5.1-e$$

where

$$\Delta c_m$$

is the section incremental pitching moment obtained from Section 6.1.2.1 by the appropriate trailing-edge mechanical-flap method using  $c_f/c$  and  $\delta'$ , where  $\delta'$  is the flap deflection in the plane normal to the constant-percent chord line through  $x_{c,p,b}$ , given by

$$\delta' = \tan^{-1} \frac{\tan \delta}{\cos \Lambda_b} \quad 6.1.5.1-t$$

where  $\Lambda_b$  is the sweepback of the constant-percent chord line through the center-of-pressure of the basic loading, given by

$$\tan \Lambda_b = \tan \Lambda_{c/4} - \frac{4}{A} (x_{c,p,b} + 0.25) \frac{1 - \lambda}{1 + \lambda}$$

6.1.5.1-g

where  $x_{c,p,b}$  is the chordwise center-of-pressure position (basic loading) for a plain flap from Figure 6.1.5.1-67b.

$$c_{q_A} = 0$$

is the incremental section lift coefficient as a function of span station, referred to the basic load line, by

$$c_{q_A} = 0 = \frac{c_{q_A}}{\cos^2 \Lambda_b} \quad 6.1.5.1-h$$

where  $c_{q_A}$  is obtained from Step 2.

- b. For the span stations adjacent to the flap ends where the distance from the ends of the flap  $\Delta\eta$  is less than |0.20|,

$$x_{c,p.} = 0.25 - K \left( \frac{\Delta c_m}{c_{q_A} = 0} \right)_{\substack{\text{edge of} \\ \text{flap}}} \quad 6.1.5.1-i$$

where

$$K$$

is obtained from Figure 6.1.5.1-67a as a function of distance from the end of the flap.

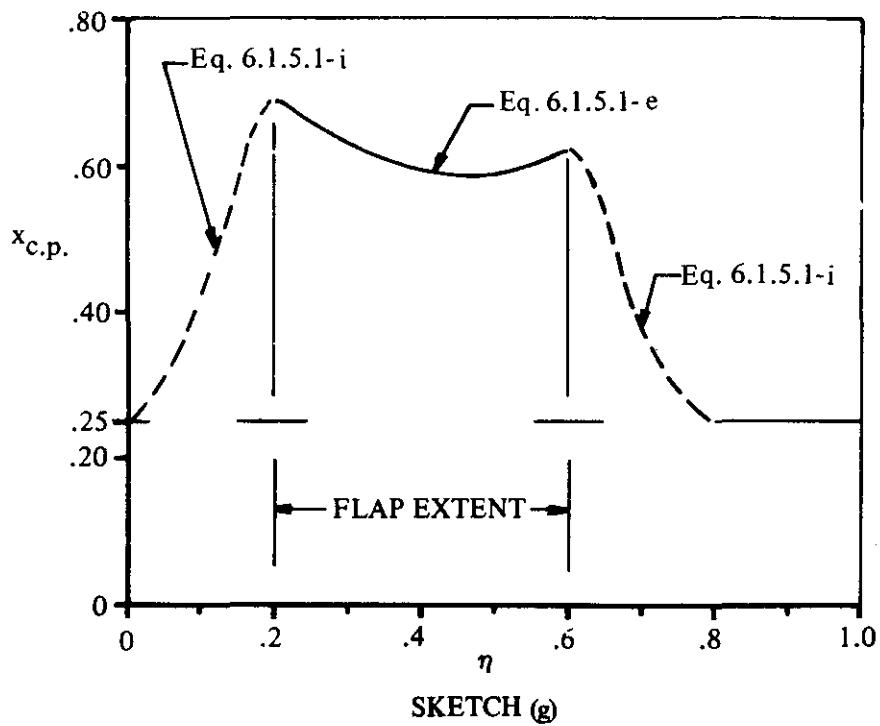
6.1.5.1-9

$$\left( \frac{\Delta c_m}{c_{\ell \Lambda} = 0} \right)_{\text{edge of flap}}$$

is the value determined in Step 3a at the span station corresponding to the edge of the flap.

- c. For span stations not influenced by the flap span, i.e.,  $\Delta\eta \geq |0.20|$ , the theoretical chordwise center-of-pressure position is assumed to be the quarter-chord point.

A typical variation of chordwise center-of-pressure location for stations across the span is illustrated in Sketch (g).



Step 4. For wings with swept quarter-chord, the chordwise center-of-pressure position at each span station must be referred to the quarter-chord of the MAC by

$$\frac{x}{c} = (\eta - \bar{\eta}) \frac{b/2}{\bar{c}} \tan \Lambda_{c/4} + \frac{c (x_{c.p.} - 0.25)}{\bar{c}} \quad 6.1.5.1-j$$

where

$\bar{\eta}$  is the lateral distance of the wing MAC from the body center line in semispans.

$x$  is the distance of the local center of pressure aft of the quarter-chord of the MAC.

- Step 5. With the local centers of pressure and the span loading known, determine the change in pitching moment due to flap deflection, based on  $S_w \bar{c}_w$  taken about the quarter-chord of the wing MAC, by integrating across the span as follows:

$$\Delta C_{m_f} = \int_0^{1.0} \left[ c_{q_A} \frac{c}{c_{av}} \left( \frac{x}{\bar{c}} \right) \right] d\eta \quad 6.1.5.1-k$$

where  $c_{q_A}$  is from Step 2,  $(x/\bar{c})$  is from Steps 3 and 4, and  $c/c_{av}$  is the ratio of the local chord at a given span station to the average chord ( $c_{av} = S_w/b_w$ ).

## 2. Leading-Edge Devices

This method assumes a constant flap-chord-to-wing-chord ratio. In the case of an arbitrary spanwise distribution of leading-edge flap chord, the flaps should be divided into spanwise steps. The pitching-moment contributions from each spanwise step are then calculated and added to obtain the total increment for the leading-edge device.

The pitching-moment increment due to mechanical leading-edge devices, based on  $S_w \bar{c}_w$ , is given by

$$\Delta C_m = \left[ c'_{m\delta_{LE}} \left( \frac{\bar{c}'}{\bar{c}} \right) + \left( \frac{x_m}{\bar{c}} - \frac{x_{LE}}{\bar{c}} \right) c'_{q\delta} \right] \frac{S_w f}{S_w} \delta_f + \left\{ C_m \left[ \left( \frac{\bar{c}'}{c} \right)^2 - 1 \right] + 0.75 C_L \left( \frac{\bar{c}'}{c} \right) \left( \frac{\bar{c}' - c}{c} \right) \right\} \Delta \eta \quad 6.1.5.1-\ell$$

where

$c'_{m\delta_{LE}}$  is the theoretical two-dimensional, flap pitching-moment effectiveness about the leading edge, obtained from Figure 6.1.2.1-36 as a function of the ratio of flap chord to the extended airfoil chord  $c_f/c'$ . (See Figures 6.1.1.1-51 for the definition of flap chord  $c_f$ .)

$\bar{c}'$  is the mean aerodynamic chord of the wing segment affected by the leading-edge device (see Sketch (h)). The wing chord is the extended-wing chord due to an extension of the leading-edge device. The trailing-edge flaps, if any, are considered retracted.

$\bar{c}$  is the wing mean aerodynamic chord (MAC).

$c$  is the retracted or basic-airfoil chord at the spanwise station of the MAC of the wing segment affected by the leading-edge device (see Sketch (h)).

$\frac{x_m}{\bar{c}}$  is the moment-reference-center location in fractions of the wing MAC, measured positive aft from the aircraft reference-axis origin (usually the aircraft nose or wing apex) parallel to the longitudinal axis.

$$\frac{x_{LE}}{\bar{c}}$$

is the location of the leading edge of the mean aerodynamic chord of the wing segment affected by the leading-edge device, in fractions of the wing MAC. This parameter is measured positive aft from the aircraft reference-axis origin (see Sketch (h)).

$$c'_{\delta}$$

is the two-dimensional leading-edge flap effectiveness parameter obtained from Figure 6.1.1.1-50 as a function of the flap-chord ratio  $c_f/\bar{c}'$ , instead of  $c_f/c$ .

$$S_{Wf}$$

is the area of the wing segment affected by the leading-edge device (see Sketch (h)).

$$S_W$$

is the wing reference area.

$$\delta_f$$

is the leading-edge-device deflection, measured parallel to the free stream in degrees (see Figure 6.1.1.1-51).

$$C_m$$

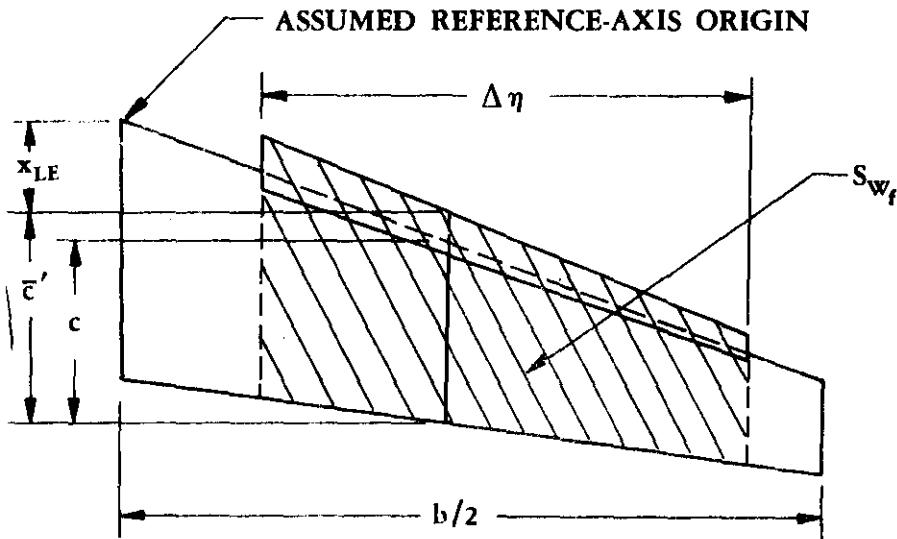
is the wing-body pitching-moment coefficient at a given angle of attack, with the leading- and trailing-edge flaps retracted. This parameter should be obtained from test data, if available, or by using Section 4.3.2.2 supplemented with a test-data value for  $(C_{m0})_{WB}$ .

$$C_L$$

is the wing-body lift coefficient at a given angle of attack, with the leading-edge and trailing-edge flaps retracted. This parameter should be obtained from test data, if available, or from Sections 4.1.3.1\*, 4.1.3.2, and 4.3.1.2.

$$\Delta\eta$$

is the flap span in fractions of the wing semispan (see Sketch (h)).



SKETCH (h)

\*The wing-body zero-lift angle of attack is obtained from the wing-alone data of Section 4.1.3.1. Test data from a similar configuration should be used if available.

### 3. Jet Flaps

The method presented herein pertains to the same concepts as noted in Section 6.1.1.1; i.e., the pure jet-flap concept and the IBF and EBF concepts with a plain trailing-edge flap. For an IBF or EBF concept with a single-slotted or multislotted flap configuration, this method should be used only as a first approximation.

Because of the complexity of calculating the pitching moment due to a trailing-edge jet flap, the method is presented in a stepwise procedure. This procedure assumes that the wing employs a leading-edge device; however, it will also handle configurations without leading-edge devices. In using the method, all flap-chord lengths and flap deflections are measured in a streamwise direction.

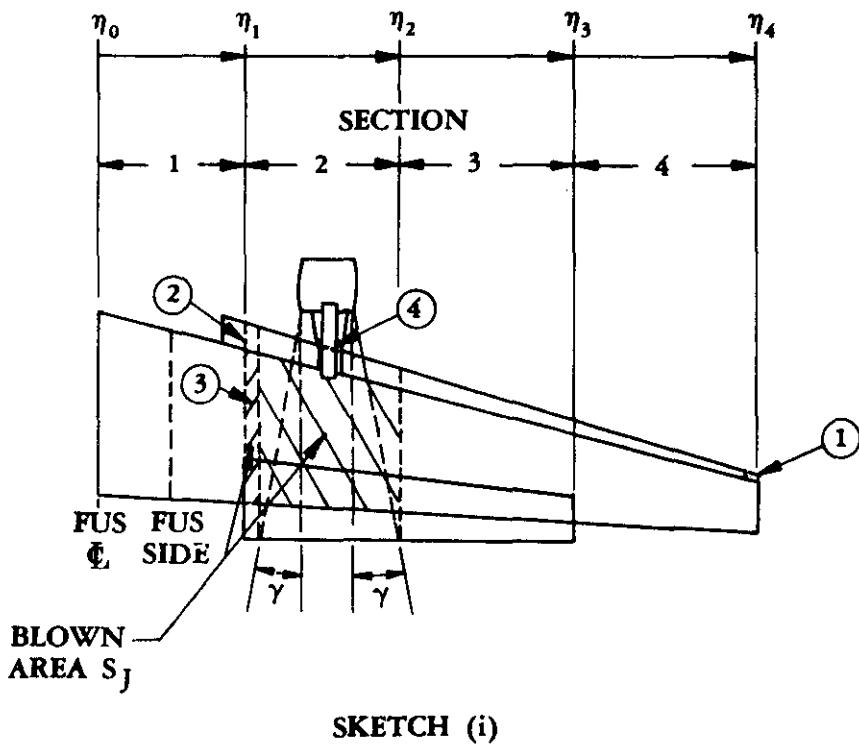
The computation of the pitching moment is broken down into components due to the leading-edge device, the angle of attack, the mechanical flap, and the jet flap. This division can be somewhat misleading because in each term there appears the parameter  $c_{\delta\delta}/c$ , which is the ratio of the airfoil chord with all flaps extended to the basic airfoil chord. Thus each term is actually dependent upon the total extended airfoil chord  $c_{\delta\delta}$ . For example, a change in  $c_{\delta\delta}$  due to a deflection of the leading-edge device will affect the contribution of each component, not just the component due to the leading-edge device.

No substantiation of the method is presented herein because of the scarcity of data for which enough information is available to make a meaningful comparison. The available data indicate an average error of approximately  $\pm 20$  percent. For those configurations that have been analyzed by using this method, the results indicate that this method is more accurate in estimating the pitching-moment increment due to flap deflection than in estimating the variation of pitching moment with angle of attack. This may be accounted for by the tendency of wings developing very high lift coefficients to have significant flow separation even at low angles of attack. The variation in the amount of separated flow with angle of attack may be affecting  $C_{m\alpha}$  significantly.

The wing pitching-moment increment (omitting the zero-lift pitching moment at  $C_\mu = 0$ ) due to a trailing-edge jet flap with or without a leading-edge device is obtained from the following procedure. All of the area terms are assumed to be total values, not semispan values, i.e., to include both the left- and right-wing contributions.

Step 1. Divide the wing into spanwise sections that exhibit the same geometric and flow characteristics, i.e., no geometric discontinuities.

- a. The blown wing area will determine one or more spanwise sections. The blown wing area is defined as the basic wing area that is affected by the jet flap, excluding any increase in wing area due to Fowler motion of the leading-and/or trailing-edge devices. For a pure jet-flap configuration with the efflux at the trailing edge,  $S_j$  is defined as the streamwise basic wing area ahead of the jet flap. For EBF configurations, the jet spreading angle  $\gamma$  must be considered before  $S_j$  can be determined. Therefore, it is suggested that the user determine the spreading angle for his particular configuration from test data on a similar configuration. However, if no such test data are available, the Datcom recommends that a value of  $12^\circ$  be used for the spreading angle  $\gamma$ . An example for determining  $S_j$  for an EBF configuration is presented in Sketch (i). In this example the value of  $S_j$  has been increased slightly so as to include that portion of the wing ahead of the inboard tip of the flap. The reason for this adjustment is explained in part (b).



- b. The basic criterion for dividing the wing is the avoidance of discontinuities. The sections are determined such that the ratio of the extended wing chord (including both leading- and trailing-edge devices) to the basic wing chord is constant or approximately constant, and the ratio of the flap chord to the basic wing chord is constant or approximately constant; i.e.,  $c_{\delta\delta}/c$  is constant and  $c_f/c$  is constant. A schematic illustration for determining these spanwise sections for an EBF configuration is presented in Sketch (i). In order to minimize the number of spanwise sections, it is suggested that small changes are assumed to be made to the actual configuration. In Sketch (i) some of the assumptions made were: 1) the outboard wing slat station was assumed to be at the wing tip, 2) the inboard tip of the slat was neglected, 3) the jet spreading was assumed to extend to the inboard station of the flap, and 4) no discontinuity was assumed in the slat due to the engine pylon.

- Step 2. The pitching-moment increment of each spanwise section is now calculated by treating each wing section as a two-dimensional airfoil. The calculation of the pitching-moment increments is performed by strictly applying the jet-flap method of Section 6.1.2.1 (not the mechanical leading- or trailing-edge methods) to evaluate each section individually. To prevent a duplication of effort, the material of Section 6.1.2.1 is not repeated here. It is therefore advised that the reader become familiar with the jet-flap method of Section 6.1.2.1 before proceeding further. However, before the jet-flap method of Section 6.1.2.1 can be applied to the three-dimensional wing sections, the following terms  $x_m/c$ ,  $C_\mu$ ,  $K$ ,  $x_f/c_{\delta\delta}$ ,  $x_j/c_{\delta\delta}$ , and  $\alpha_L$  (for  $\alpha$ ) must be redefined as follows:

$\frac{x_m}{c}$  redefined as the ratio of the distance from the wing leading edge to the unique unswept reference line (which may lie on or aft of a conventional wing configuration) to the local chord, such that  $x_m/c$  has a constant value for straight-tapered wings. (This reference location eliminates the need for calculating the spanwise center-of-pressure location for each wing section.) For non-straight-tapered wings there can be more than one value. Sketch (j) presents an example of a non-straight-tapered wing where two values of  $x_m/c$  are required. The determination of  $x_m/c$  is defined by

$$\frac{x_m}{c} = \frac{1 + \lambda}{1 - \lambda} \left( \frac{A_s}{4} \right) \tan \Lambda_{LE}$$

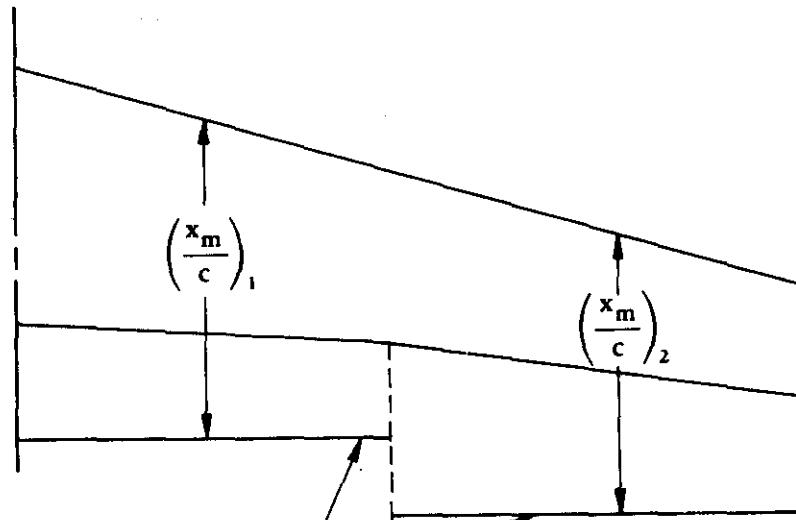
6.1.5.1-m

where

$\lambda$  is the taper ratio of the particular spanwise wing section.

$A_s$  is the aspect ratio of the particular spanwise wing section.

$\Lambda_{LE}$  is the sweep of the leading-edge angle of the particular spanwise wing section.



Reference lines defined  
by Equation 6.1.5.1-m

SKETCH (j)

However, a problem arises in the case of untapered wings ( $\lambda = 1$ ), since  $x_m/c$  in Equation 6.1.5.1-m becomes indeterminate. Therefore, for an untapered wing or wing section, Equation 6.1.5.1-m is modified to the following:

$$\frac{x_m}{c} = \frac{\Delta x_r}{c}$$

6.1.5.1-n

6.1.5.1-15

where

$\Delta x_t$  is the distance between the wing apex and the desired moment reference center, measured positive aft.

c is the basic wing chord.

$C_\mu$  is the section nondimensional trailing-edge jet momentum coefficient. For those sections that are outside of the blown area,  $C_\mu = 0$ . For those sections within the blown area, the following approximation is used to determine the relationship between  $C_\mu$  and  $C_J$ :

$$C_\mu = C_J \eta_t \frac{S_w}{S_J} \quad 6.1.5.1-o$$

where

$C_J$  is the nondimensional trailing-edge jet momentum coefficient based on the gross engine thrust and the wing reference area. (See Section 6.1.4.1 for an exact definition.)

$\eta_t$  is the static turning efficiency defined as the resultant force divided by the gross thrust (see Section 6.1.4.3, Sketch (a)). This value should be obtained from test data if possible, or from Figure 6.1.4.3-11 for slotted flaps. Although Figure 6.1.4.3-11 represents a reasonable average of the available data, the data scatter is large. Since this method cannot be expected to yield good results if the error in  $\eta_t$  is large, it is imperative that test data be used if available.

$\frac{S_w}{S_J}$  is the ratio of the wing reference area to the blown wing area.

K redefined here to apply to each wing section individually, based on the following expression

$$K = \left[ \frac{A_t + 2 C'_\mu / \pi}{A_t + 2 + 0.604 (C'_\mu)^{1/2} + 0.876 C'_\mu} \right] \frac{c_{ss}}{c} \quad 6.1.5.1-p$$

where

$\frac{c_{ss}}{c}$  is the ratio of the extended wing chord, including the extensions of both the leading- and trailing-edge devices, to the basic wing chord of the particular spanwise wing section.

$A_t$  is the aspect ratio of the total wing based on the extended wing chord, i.e.,  $A_t = A(c/c_{\delta\delta})$ , using the particular section value for  $c/c_{\delta\delta}$ .

$C'_\mu$  is the section nondimensional trailing-edge jet momentum coefficient based on the extended wing chord  $c_{\delta\delta}$ , i.e.,  $C'_\mu = C_\mu (c/c_{\delta\delta})$ .

$$\frac{x_{f_i}}{c_{\delta\delta}}, \frac{x_j}{c_{\delta\delta}}$$

are the center-of-lift location of the incremental load due to the deflection of the  $i^{\text{th}}$  flap segment and the center-of-lift location of the incremental load due to the jet deflection, respectively. In this section these terms are applied to each spanwise wing section and are corrected for three-dimensional effects by

$$\frac{x_{f_i}}{c_{\delta\delta}} = \left( \frac{x_{f_i}}{c_{\delta\delta}} \right)_{2D} \left[ \frac{(x_{c,p.})_{3D}}{(x_{c,p.})_{2D}} \right]_i \quad 6.1.5.1-q$$

$$\frac{x_j}{c_{\delta\delta}} = \left( \frac{x_j}{c_{\delta\delta}} \right)_{2D} \left[ \frac{(x_{c,p.})_{3D}}{(x_{c,p.})_{2D}} \right]_j \quad 6.1.5.1-r$$

where

$$\left( \frac{x_{f_i}}{c_{\delta\delta}} \right)_{2D}$$

is the two-dimensional center-of-lift location of the incremental load due to deflection of the  $i^{\text{th}}$  trailing-edge flap segment. This parameter is obtained, as defined in Section 6.1.2.1, from Figure 6.1.2.1-37 as a function of the ratio of the flap chord to the extended airfoil chord  $c_{f_i}/c_{\delta\delta}$  and  $C'_\mu$ .

$$\left[ \frac{(x_{c,p.})_{3D}}{(x_{c,p.})_{2D}} \right]_i$$

is the ratio of the center-of-lift location for a finite-aspect-ratio wing to the center-of-lift location for an infinite-aspect-ratio wing for the incremental load due to deflection of the  $i^{\text{th}}$  trailing-edge flap segment. This parameter is obtained from Figure 6.1.5.1-68 as a function of  $c_{f_i}/c_{\delta\delta}$  and  $1/A_t$ .

$$\left( \frac{x_j}{c_{\delta\delta}} \right)_{2D}$$

is the two-dimensional center-of-lift location of the incremental load due to the jet momentum acting at some angle to the trailing-edge camber line. This parameter is obtained from Figure 6.1.2.1-37 at  $c_f/c_{\delta\delta} = 0$ , as a function of the trailing-edge jet momentum  $C'_\mu$ .

$$\left[ \frac{(x_{c.p.})_{3D}}{(x_{c.p.})_{2D}} \right]_j$$

is the ratio of the center-of-lift location for a finite-aspect-ratio wing to the center-of-lift location for an infinite-aspect-ratio wing for the incremental load due to the jet momentum acting at some angle to the trailing-edge camber line. This parameter is obtained from Figure 6.1.5.1-68 at  $c_f/c_{\delta\delta} = 0$ , as a function of  $1/A_t$ .

$$\alpha_L$$

is the local angle of attack for the particular spanwise wing section under consideration. For wings with twist, this value will change from section to section. It is suggested that the change be approximated by using the average twist incidence for each section.

- Step 3. Compute the sum of the wing section pitching-moment increments from Step 2 according to the following:

$$C_{m_m} = \sum_{k=1}^p \Delta c_m (K_{b_k} - K_{b_{k-1}}) \quad 6.1.5.1-s$$

where

$$k$$

is the number of the wing section (numbered from the fuselage center line outboard).

$$p$$

is the total number of wing sections.

$$\Delta c_m$$

is the section pitching-moment increment for the particular spanwise section, obtained from the jet-flap procedure of Section 6.1.2.1.

$$K_{b_k}, K_{b_{k-1}}$$

are the values of the span factor for the outboard and inboard ends, respectively, of the  $k^{th}$  wing section. This parameter is obtained from Figure 6.1.4.1-15 as a function of basic-wing taper ratio  $\lambda$  and the span stations  $\eta_k$  and  $\eta_{k-1}$  of the streamwise cuts defining the  $k^{th}$  wing section nondimensionalized by the wing semispan (see Sketch (i)).

- Step 4. Calculate the lift contribution to the pitching-moment increment for each wing section according to

$$C_{\lambda_k} = \left[ \Delta c_1 - \Delta c_2 + \Delta c_4 + \sum_{i=1}^n (\Delta c_5)_i + \Delta c_6 \right] (K_{b_k} - K_{b_{k-1}}) \quad 6.1.5.1-t$$

where

$\Delta c_1, \Delta c_2, \Delta c_4, (\Delta c_5)_i$ , and  $\Delta c_6$  are the terms analogous to lift generated during the execution of the jet-flap procedure of Section 6.1.2.1.

$K_{b_k}, K_{b_{k-1}}$  are defined in Step 3 above.

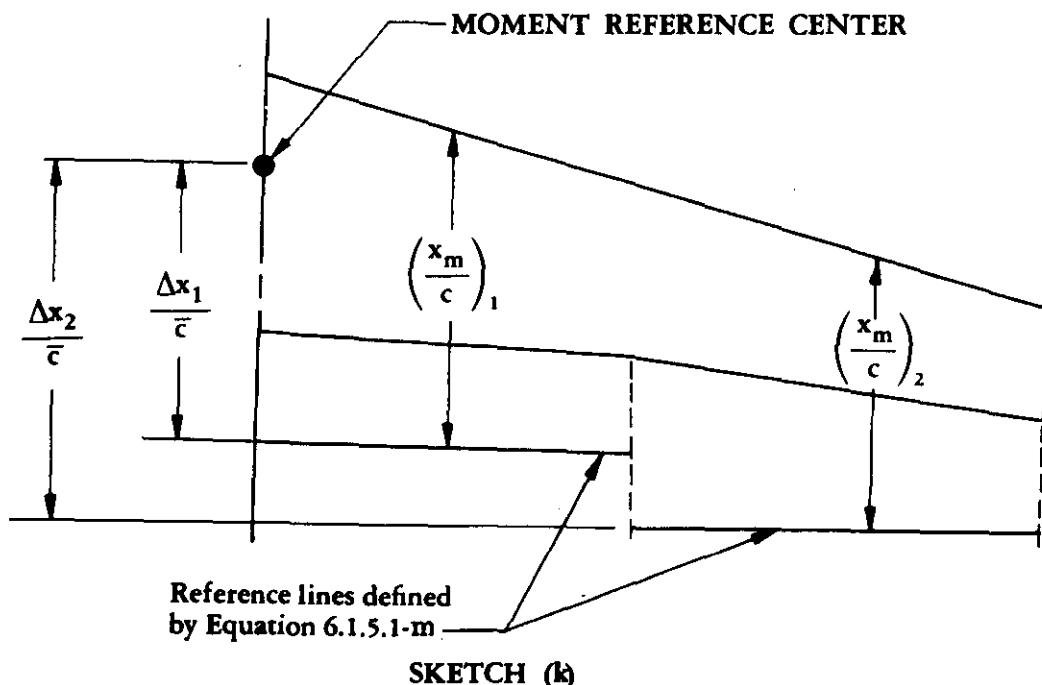
- Step 5. The total wing pitching-moment increment due to a jet flap at some angle of attack is calculated by using one of two equations presented below. For a tapered wing, Equation 6.1.5.1-u is used; while for an untapered wing, Equation 6.1.5.1-v should be used. Both equations convert the pitching moments for each wing panel about  $x_m/c_{\delta\delta}$  to the desired moment-reference-center location, based on  $S_w \bar{c}_w$ .

$$\Delta C_m = C_{m_m} + \eta_t C_J \frac{\Delta z}{\bar{c}} + \sum_{k=1}^P \left\{ \left[ C_\mu \frac{\alpha_L}{57.3} \frac{S_k}{S_w} - C_{\lambda_k} \right] \frac{\Delta x_k}{\bar{c}} \right\} \quad 6.1.5.1-u$$

where

$\frac{\Delta z}{\bar{c}}$  is the vertical distance between the desired moment-reference-center location and the quarter-chord of the MAC, positive for the wing below the desired location. (This is an approximation because an exact solution would require accounting for the vertical distance for each blown wing section.)

$\frac{\Delta x_k}{\bar{c}}$  is the longitudinal distance between the moment-reference-center location and the location of the chord station for zero sweep. This parameter is measured positive aft from the moment reference center as illustrated in Sketch (k).



For an untapered wing this distance can be found by using

$$\frac{\Delta x_k}{c} = \frac{\eta_k - \eta_{k-1}}{2} \frac{b}{2} \frac{\tan \Lambda}{c}$$

6.1.5.1-v

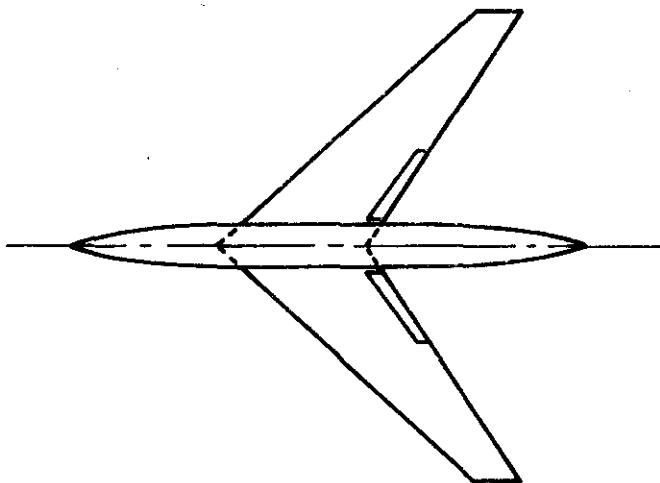
$S_k$  is the area of the  $k^{\text{th}}$  wing section with all flaps retracted.

All remaining terms have been defined in the previous steps.

### Sample Problems

#### 1. Single-Slotted Trailing-Edge Flap (Method 1)

Given: The sweptback wing-body configuration of Reference 32 with a single-slotted flap.



Wing Characteristics:

$$A = 5.1 \quad b/2 = 74.75 \text{ in.} \quad \lambda = 0.383 \quad \Lambda_{c/4} = 44.6^\circ$$

$$c_t = 42.36 \text{ in.} \quad c_t = 16.24 \text{ in.} \quad S_w = 30.35 \text{ ft}^2 \quad \bar{c} = 31.22 \text{ in.}$$

$$\text{NACA } 64-210 \perp 0.286 c \quad \frac{t}{c} = 0.075 \text{ (streamwise)} \quad \frac{Y_{90}}{2} = 0.671 \% c$$

$$\frac{Y_{99}}{2} = 0.04 \% c \quad a = 0 \quad C_m = -0.034 \text{ (test data)}$$

$$C_L = 0.025 \text{ (test data)}$$

**Flap Characteristics:**

$$\text{Single-slotted flap} \quad \frac{c_f}{c} = 0.286 \text{ (streamwise)} \quad \frac{c'}{c} = 1.05$$

$$\eta_i = 0.144 \quad \eta_o = 0.45 \quad \delta_f = 30.68^\circ \text{ (streamwise)}$$

**Additional Characteristics:**

$$M = 0.14; \beta = 0.99 \quad R_q = 6 \times 10^6$$

**Compute:**

$$\begin{aligned} \tan \frac{1}{2} \phi'_{TE} &= \frac{\frac{Y_{90}}{2} - \frac{Y_{99}}{2}}{9} \\ &= \frac{0.671 - 0.04}{9} = 0.07 \end{aligned}$$

$$\left( \frac{c_{q_\alpha}}{(c_{q_\alpha})_{\text{theory}}} \right) = 0.873 \quad (\text{Figure 4.1.1.2-8a})$$

$$(c_{q_\alpha})_{\text{theory}} = 6.66 \text{ per rad} \quad (\text{Figure 4.1.1.2-8b})$$

$$c_{q_\alpha} = \frac{1.05}{\beta} \left[ \frac{c_{q_\alpha}}{(c_{q_\alpha})_{\text{theory}}} \right] (c_{q_\alpha})_{\text{theory}} \quad (\text{Equation 4.1.1.2-a})$$

$$= \frac{1.05}{0.99} (0.873) (6.66)$$

$$= 6.167 \text{ per rad}$$

$$\alpha_6 = -0.483 \quad (\text{Figure 6.1.1.1-41})$$

$$\Delta c_q = -c_{q_\alpha} \alpha_6 \delta_f \quad (\text{Equation 6.1.1.1-d})$$

$$= -(6.167) (-0.483) \frac{30.68}{57.3}$$

$$= 1.595$$

$$\left. \begin{array}{l} A = 6.0 \\ \Lambda_{c/2} = 0 \end{array} \right\} \text{Method 1 assumptions for calculating } \Delta C_L$$

$$\kappa = \frac{c_{q_\alpha}}{\beta} / \frac{2\pi}{\beta} = \frac{6.167}{2\pi} = 0.9815$$

$$\frac{A}{\kappa} \left[ \beta^2 + \tan^2 \Lambda_{c/2} \right]^{1/2} = \frac{6}{0.9815} (0.99) = 6.05$$

$$\frac{C_{L_\alpha}}{A} = 0.747 \text{ per rad} \quad (\text{Figure 4.1.3.2-49})$$

$$C_{L_\alpha} = 6(0.747) = 4.48 \text{ per rad}$$

$$(\alpha_\delta)_{c_q} = -0.655 \quad (\text{Figure 6.1.4.1-14 insert})$$

$$\frac{(\alpha_\delta)_{C_L}}{(\alpha_\delta)_{c_q}} = 1.04 \quad (\text{Figure 6.1.4.1-14})$$

$$K_b = 1.0 \quad (\text{assume full-span flaps for calculating } \Delta C_L)$$

$$\begin{aligned} \Delta C_L &= \Delta c_q \left( \frac{C_{L_\alpha}}{c_{q_\alpha}} \right) \left[ \frac{(\alpha_\delta)_{C_L}}{(\alpha_\delta)_{c_q}} \right] K_b \quad (\text{Equation 6.1.4.1-a}) \\ &= (1.595) \left( \frac{4.48}{6.167} \right) (1.04) (1.0) \\ &= 1.205 \end{aligned}$$

$$\frac{c_f}{c'} = \frac{c_f}{c} \frac{c}{c'}$$

$$= \frac{0.286}{1.05} = 0.272$$

$$\frac{\Delta C'_m}{\Delta C_L} = -0.271 \quad (\text{Figure 6.1.5.1-60})$$

$$(K_p)_{\eta=0.144} = 0.27 \quad (\text{Figure 6.1.5.1-61})$$

$$(K_p)_{\eta=0.45} = 0.72 \quad (\text{Figure 6.1.5.1-61})$$

$$K_p = (K_p)_{\eta_0} - (K_p)_{\eta_i}$$

$$= 0.72 - 0.27 = 0.45$$

$$\Delta C_m = K_p \left\{ \left( \frac{\Delta C'_m}{\Delta C_L} \right) \Delta C_L \left( \frac{c'}{c} \right)^2 - 0.25 C_L \left( \frac{c'}{c} \right) \left( \frac{c'}{c} - 1 \right) + C_m \left[ \left( \frac{c'}{c} \right)^2 - 1 \right] \right\}$$

(Equation 6.1.5.1-b)

$$= 0.45 \left\{ (-0.271)(1.205)(1.05)^2 - 0.25(0.025)(1.05)(0.05) - 0.034 \left[ (1.05)^2 - 1 \right] \right\}$$

$$= 0.45 \{ -0.36 - 0.0003 - 0.0035 \}$$

$$= -0.164$$

$$(K_\Lambda)_{\eta=0.144} = 0.0365 \quad (\text{Figure 6.1.5.1-57a through -57d, interpolated})$$

$$(K_\Lambda)_{\eta=0.45} = 0.0615 \quad (\text{Figure 6.1.5.1-57a through -57d, interpolated})$$

$$K_\Lambda = (K_\Lambda)_{\eta_0} - (K_\Lambda)_{\eta_i}$$

$$= 0.0615 - 0.0365 = 0.025$$

Solution:

$$\Delta C_{mf} = \Delta C_m + K_\Lambda \left( \frac{A}{1.5} \right) \Delta C_L \tan \Lambda_{c/4} \quad (\text{Equation 6.1.5.1-a})$$

$$= -0.164 + (0.025) \left( \frac{5.1}{1.5} \right) (1.205) (0.9874)$$

$$= -0.164 + 0.101$$

= -0.063 (based on the product of wing area and wing mean aerodynamic chord and referred to a moment center at  $\bar{c}/4$ )

This compares with a test value of  $\Delta C_{mf} = -0.074$  from Reference 32.

## 2. Plain Trailing-Edge Flap (Method 2)

Given: The sweptback wing of Reference 13 with a partial-span plain trailing-edge flap. This is the same configuration as Sample Problem 1 of Paragraph A of Section 6.1.4.1.

Wing Characteristics:

$$\begin{array}{llll} A = 3.78 & b/2 = 16.97 \text{ ft} & \lambda = 0.586 & \Lambda_{c/4} = 47.35^\circ \\ c_r = 11.315 \text{ ft} & \bar{\eta} = 0.456 & \bar{c} = 9.09 \text{ ft} & c_{av} = 8.98 \text{ ft} \end{array}$$

NACA 65A006 airfoil (streamwise)

Flap Characteristics:

$$\begin{array}{llll} \text{Plain trailing-edge flap} & \Lambda_{HL} = 43^\circ & c_f/c = 0.224 \text{ (streamwise)} \\ \eta_i = 0.10 & \eta_o = 0.58 & \delta_{HL} = 30^\circ & \delta = 22.1^\circ \text{ (streamwise)} \end{array}$$

Additional Characteristics:

$$\text{Low speed; } \beta = 1.0 \quad R_\alpha = 6.1 \times 10^6$$

Compute:

Step 1. Determine the spanwise loading coefficient  $G/\delta$  (see Step 1c of Datcom Method 2)

$$c_{q_\alpha} = 6.13 \text{ per rad (Sample Problem 1, Paragraph A, Section 6.1.4.1)}$$

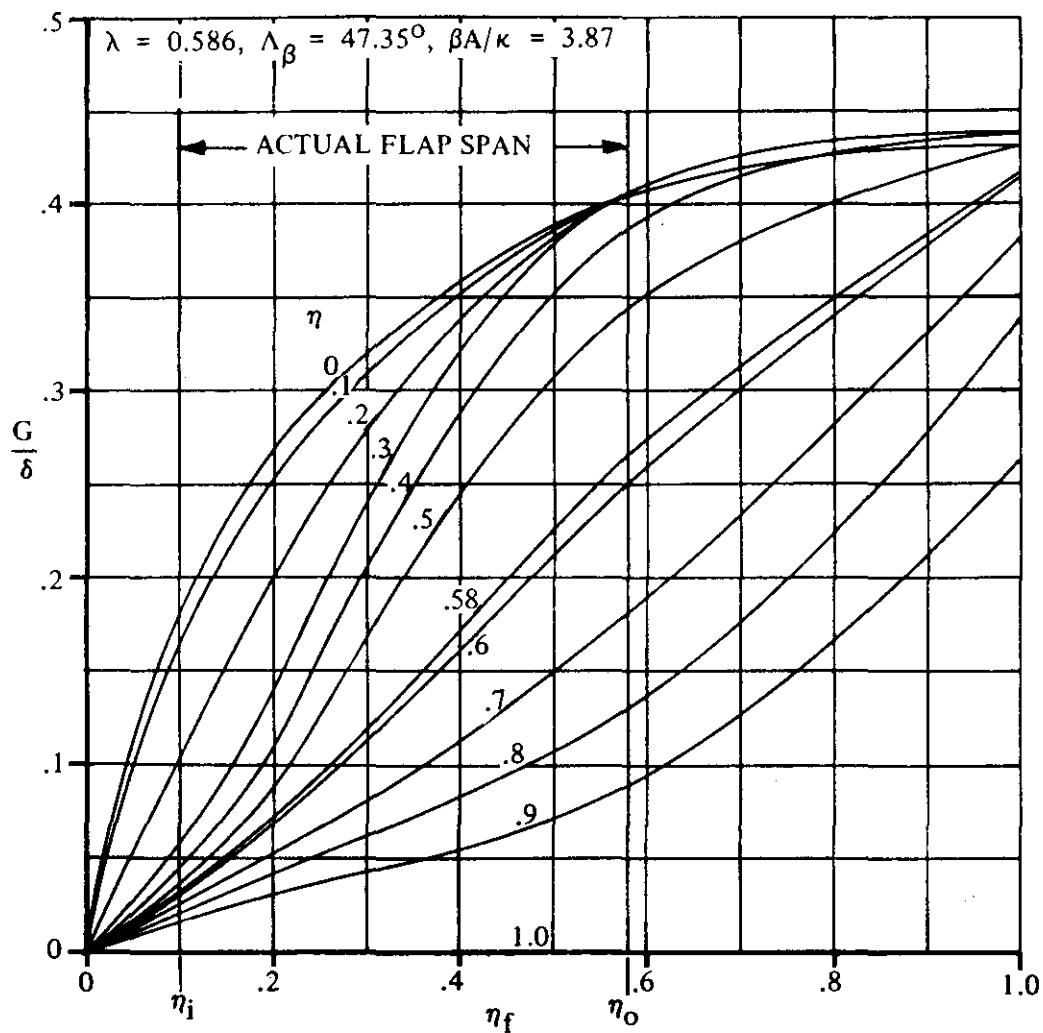
$$\kappa = \frac{c_{q_\alpha}}{2\pi} = \frac{6.13}{2\pi} = 0.976$$

$$\frac{\beta A}{\kappa} = \frac{(1.0)(3.78)}{0.976} = 3.87$$

$$\Lambda_\beta = \tan^{-1} \left( \frac{\tan \Lambda_{c/4}}{\beta} \right) = \tan^{-1} \left( \frac{\tan 47.35^\circ}{1.0} \right) = 47.35^\circ$$

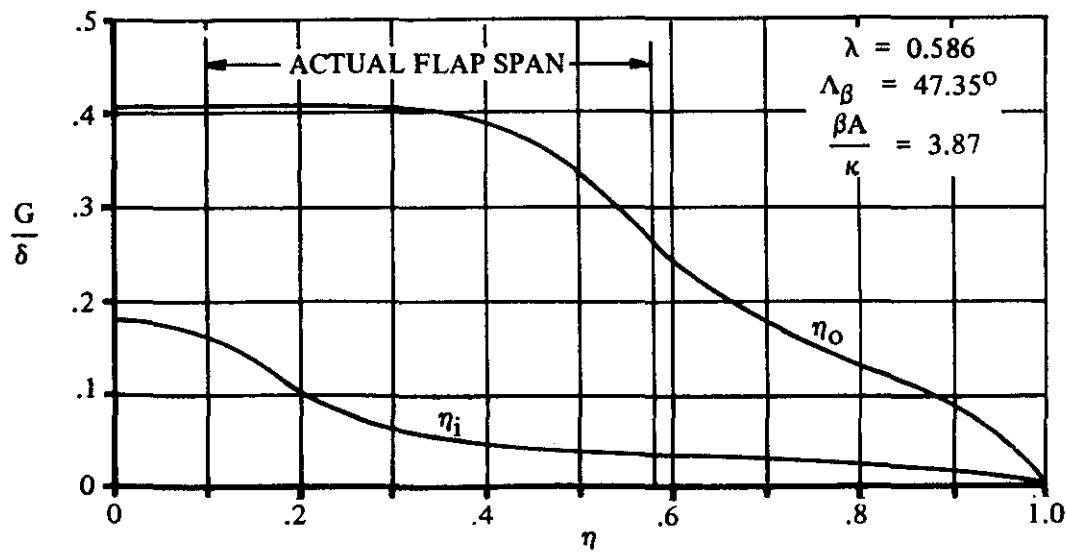
Obtain the spanwise loading coefficient  $G/\delta$  for a full wing-chord flap extending from the plane of symmetry to the inboard station of the actual flap ( $\eta_i = 0.10$ ), and for a full wing-chord flap extending from the plane of symmetry to the outboard end of the actual flap ( $\eta_o = 0.58$ ). Since the span loadings for these particular flap spans are not presented in Figures 6.1.5.1-62a through 6.1.5.1-62d, the interpolation procedure described in Step 1 of Datcom Method 2 must be applied. The cross-plotted results of the variation of the loading parameter at given span stations as a function of flap span for the desired values of  $\beta A/\kappa$ ,  $\Lambda_\beta$ , and  $\lambda$  are presented in Sketch(h).

The spanwise loading coefficients for a full wing-chord flap that extends from the plane of symmetry to the inboard station  $\eta_i = 0.100$  and for a full wing-chord flap that extends from the plane of symmetry to the outboard station  $\eta_o = 0.58$  are read from Sketch(h) at  $\eta_i$  and  $\eta_o$ . These spanwise loading coefficients are presented in Sketch(i).



VARIATION OF LOADING COEFFICIENT WITH FLAP SPAN

SKETCH (h)



VARIATION OF SPANWISE LOADING COEFFICIENT

SKETCH (i)

Step 2. Determine the incremental section lift coefficient as a function of span station  $\eta$ .

$$c_{\ell \Delta} = - \frac{2b}{c} \frac{G}{\delta} \alpha_{\delta} \delta \quad (\text{Equation 6.1.5.1-c})$$

$$\Delta c_{\ell} = 0.927 \quad (\text{Sample Problem 1, Paragraph A, Section 6.1.4.1})$$

$$\alpha_{\delta} = - \frac{(c_{\ell \delta})_{\alpha}}{(c_{\ell \alpha})_{\delta}} \quad (\text{Equation 6.1.1.1-b})$$

$$= - \frac{\Delta c_{\ell}}{(c_{\ell \alpha})_{\delta}} = - \frac{0.927}{(6.13) \frac{22.1}{57.3}} = -0.392$$

#### INCREMENTAL SECTION LIFT COEFFICIENT

(1)	(2)	(3)	(4)	(5)	(6)	(7)
$\eta$	$\left(\frac{G}{\delta}\right)_{\eta_0} = 0.58$	$\left(\frac{G}{\delta}\right)_{\eta_i} = 0.10$	$\frac{G}{\delta}$ - (2) - (3)	$\alpha_{\delta} \delta$ (rad)	Local Chord (ft)	$-2b \frac{c_{\ell \Delta}}{(4)(5)} / (6)$ Eq. 6.1.5.1-c
0	0.404	0.180	0.224	-0.151	11.315	0.203
$\eta_i$	0.404	0.163	0.241		10.847	0.228
.2	0.404	0.103	0.301		10.379	0.297
.3	0.405	0.057	0.348		9.911	0.360
.4	0.386	0.045	0.341		9.443	0.370
.5	0.344	0.036	0.308		8.975	0.352
$\eta_0$	0.265	0.031	0.234		8.600	0.279
.6	0.250	0.030	0.220		8.507	0.265
.7	0.180	0.025	0.155		8.039	0.198
.8	0.129	0.021	0.108		7.571	0.146
.9	0.088	0.016	0.072		7.103	0.104
1.0	0	0	0		6.635	0

Step 3. Determine the chordwise center-of-pressure location  $x_{c.p.}$  for stations across the span.

$$x_{c.p.b} = 0.665 \quad (\text{Figure 6.1.5.1-67b})$$

$$\tan \Lambda_b = \tan \Lambda_c / 4 \cdot \frac{4}{A} \left( x_{c.p.b} - 0.25 \right) \left( \frac{1-\lambda}{1+\lambda} \right) \quad (\text{Equation 6.1.5.1-g})$$

$$= 1.0856 - \frac{4}{3.78} (0.665 - 0.25) \left( \frac{0.414}{1.586} \right) = 0.9710$$

$$\Lambda_b = \tan^{-1}(0.9710) = 44.15^\circ$$

$$\cos \Lambda_b = 0.7175$$

$$\cos^2 \Lambda_b = 0.5148$$

$$\delta' = \tan^{-1} \left( \frac{\tan \delta}{\cos \Lambda_b} \right) \quad (\text{Equation 6.1.5.1-f})$$

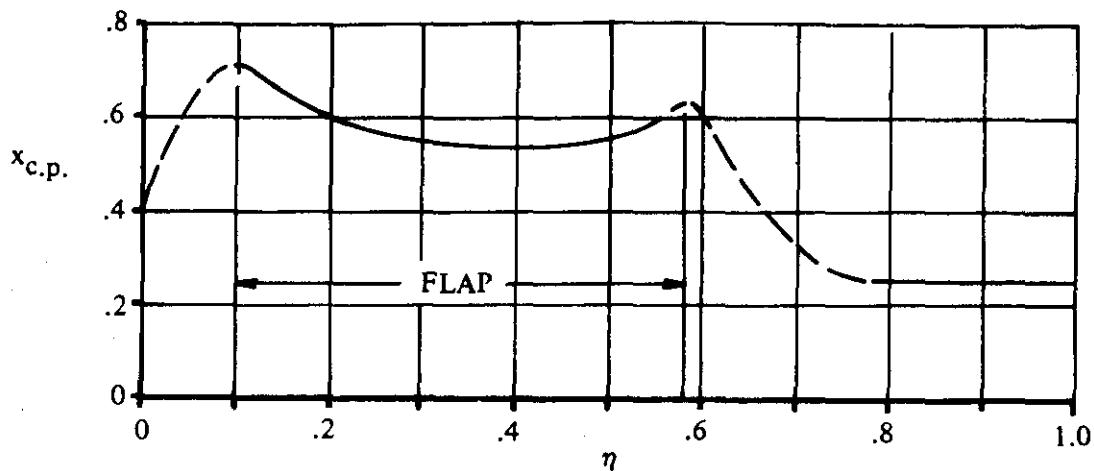
$$= \tan^{-1} \left( \frac{\tan 22.1^\circ}{\cos 44.15^\circ} \right) = \tan^{-1} (0.5660) = 29.5^\circ$$

$$\Delta c_{m_f} = -0.205 \quad (\text{Figure 6.1.2.1-35b at } \delta' \text{ and } c_f/c)$$

CHORDWISE CENTER-OF-PRESSURE LOCATION

$\eta$	FLAPPED SECTION			ADJACENT TO FLAP ENDS, $\Delta\eta <  0.20 $			$x_{c.p.}$ Summary
	(8)	(9)	(10)	(11)	(12)	(13)	
	$c_l \Lambda = 0$ $\text{Eq. 6.1.5.1-h}$	$\frac{\Delta c_{m_f}}{c_l \Lambda = 0}$ $-0.205$ (8)	$x_{c.p.}$ Flapped Section 0.25- (9)		$\left( \frac{\Delta c_{m_f}}{c_l \Lambda = 0} \right)$ edge of flap	$x_{c.p.}$ $\text{@ } \Delta\eta <  0.20 $ $0.25 - (11)(12)$ $\text{Eq. 6.1.5.1-i}$	
0	—	—	—	0.33	-0.463	0.403	0.403
$\eta_i$	0.443	-0.463	0.713	—	—	—	0.713
.2	0.577	-0.355	0.605	—	—	—	0.605
.3	0.699	-0.293	0.543	—	—	—	0.543
.4	0.719	-0.285	0.535	—	—	—	0.535
.5	0.684	-0.300	0.550	—	—	—	0.550
$\eta_o$	0.542	-0.378	0.628	—	—	—	0.628
.6	—	—	—	0.955	-0.378	0.611	0.611
.7	—	—	—	0.210	-0.378	0.329	0.329
.8	—	—	—	—	—	—	0.250
.9	—	—	—	—	—	—	0.250
1.0	—	—	—	—	—	—	0.250

The calculated variation of chordwise center-of-pressure location for stations across the span is plotted in Sketch (j)



VARIATION OF CHORDWISE CENTER-OF-PRESSURE LOCATION  
SKETCH (j)

Solution:

$$\Delta C_{m_f} = \int_0^{1.0} - \left[ c_{\ell} \Lambda \left( \frac{c}{c_{av}} \right) \left( \frac{x}{c} \right) \right] d\eta \quad (\text{Equation 6.1.5.1-k})$$

$$\frac{x}{c} = (\eta - \bar{\eta}) \frac{b/2}{c} \tan \Lambda_c/4 + \frac{c(x_{c.p.} - 0.25)}{c} \quad (\text{Equation 6.1.5.1-j})$$

(15)

(16)

(17)

(18)

(19)

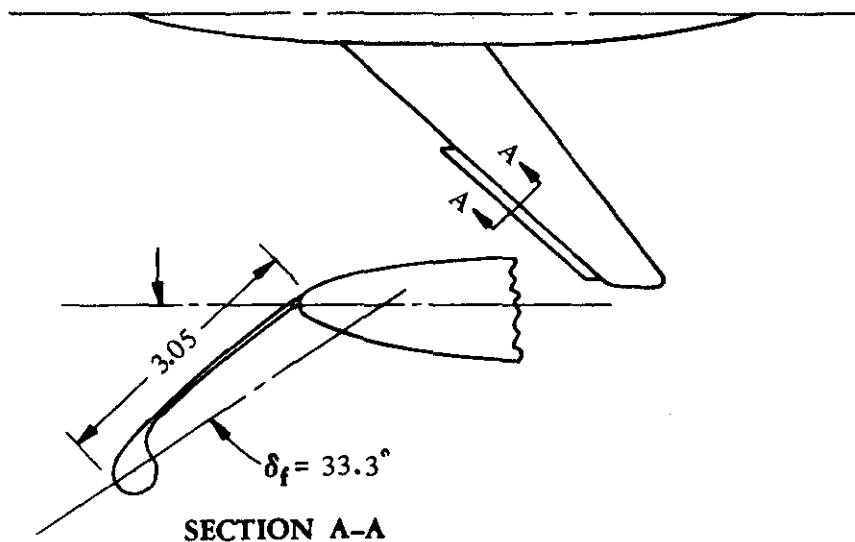
(20)

$\eta$	$\frac{c}{c_{av}}$ (6) 8.98	$\frac{c}{c}$ (6) 9.09	$(\eta - \bar{\eta}) \frac{b/2}{c} \tan \Lambda_c/4$	$(x_{c.p.} - .25) \frac{c}{c}$ [(14) - .25] (16)	$\frac{x}{c}$ (17) + (18)	$\Delta C_{m_f}$ Eq. 6.1.5.1-k $\Delta \eta$
0	1.260	1.245	-0.924	0.190	-0.734	0.00939
$\eta_i$	1.208	1.193	-0.721	0.552	-0.169	0.00465
.2	1.156	1.142	-0.519	0.405	-0.114	0.00391
.3	1.104	1.090	-0.316	0.319	0.003	-0.00012
.4	1.051	1.039	-0.113	0.296	0.183	-0.00712
.5	0.999	0.987	0.089	0.296	0.385	-0.01354
$\eta_o$	0.958	0.946	0.251	0.358	0.609	-
.6	0.947	0.936	0.292	0.338	0.630	-0.01581
.7	0.895	0.884	0.494	0.070	0.564	-0.00999
.8	0.843	0.833	0.697	0	0.697	-0.00858
.9	0.791	0.781	0.899	0	0.899	-0.00740
1.0	0.739	0.730	1.102	0	1.102	0
$\Delta C_{m_f} = \Sigma =$						-0.0473

This compares with a test value of  $\Delta C_{m_f} = -0.040$  from Reference 13.

### 3. Krueger Leading-Edge Flap

Given: The sweptback wing-body configuration of Reference 35 with a leading-edge Krueger flap.



#### Wing Characteristics:

$$\begin{array}{lllll} A = 5.1 & b/2 = 74.75 \text{ in.} & \lambda = 0.383 & \Lambda_{c/4} = 45.35^\circ & \Lambda_{LE} = 47.72^\circ \\ c_t = 42.36 \text{ in.} & c_t = 16.24 \text{ in.} & S_w = 30.35 \text{ ft}^2 & & \bar{c} = 31.22 \text{ in.} \\ y_{\bar{c}} = 31.81 \text{ in.} & \alpha = 2^\circ & & & \end{array}$$

#### Flap Characteristics:

$$\begin{array}{lll} \text{Krueger leading-edge flap} & c_{f_{LE}} = 3.05 \text{ in.} & \delta_{f_{LE}}^* = 33.3^\circ \\ \text{Constant flap chord} & \eta_i = 0.50 & \eta_o = 0.975 \end{array}$$

#### Additional Characteristics:

$$\begin{array}{lll} M = 0.14; \beta = 0.99 & R_2 = 6 \times 10^6 & C_L = 0.17 \\ x_m = 42.79 \text{ in. (aft of wing apex)} & C_m = -0.040 \text{ (flaps retracted)} & \end{array}$$

\* $\delta_f$  is defined according to Figure 6.1.1-51, not as defined in Reference 35.

Compute:

Determine  $\bar{c}'$

$$c_{f_{LE}} = \frac{c_{f_{LE}}}{\cos \Lambda_{LE}} = \frac{3.05}{0.6727} = 4.53 \text{ in.}$$

$$c = c_r - \eta (c_r - c_t) \quad (\text{see Section 2.2.2})$$

$$\text{At } \eta_i, c = 42.36 - (0.50)(42.36 - 16.24) = 29.30 \text{ in.}$$

$$c' = c + c_f = 29.30 + 4.53 = 33.83 \text{ in.}$$

$$\text{At } \eta_o, c = 42.36 - (0.975)(42.36 - 16.24) = 16.89 \text{ in.}$$

$$c' = 16.89 + 4.53 = 21.42 \text{ in.}$$

$$\lambda_f = \frac{(c')_{\eta_o}}{(c')_{\eta_i}} = \frac{21.42}{33.83} = 0.633$$

$$\bar{c}' = \frac{2}{3} (c')_{\eta_i} \left( \frac{1 + \lambda_f + \lambda_f^2}{1 + \lambda_f} \right) \quad (\text{Section 2.2.2})$$

$$= \frac{2}{3} (33.83) \left( \frac{1 + 0.633 + 0.633^2}{1 + 0.633} \right)$$

$$= 28.09 \text{ in.}$$

Determine  $c_{m_{\delta LE}}'$  and  $c_{q_{\delta}}'$  (assuming constant flap-to-chord ratio)

$$\frac{c_{f_{LE}}}{\bar{c}'} = \frac{4.53}{28.09} = 0.161$$

$$c_{m_{\delta LE}}' = -0.00127 \text{ per deg} \quad (\text{Figure 6.1.2.1-36})$$

$$c_{q_{\delta}}' = -0.00320 \text{ per deg} \quad (\text{Figure 6.1.1.1-50})$$

Determine  $x_{LE}$

$$y_{\bar{c}'} = \frac{1}{3} (\Delta\eta)(b/2) \left( \frac{1 + 2\lambda_f}{1 + \lambda_f} \right) + (\eta_i)(b/2) \quad (\text{Section 2.2.2})$$

$$= \frac{1}{3} (0.975 - 0.50)(74.75) \left( \frac{1 + 2(0.633)}{1 + 0.633} \right) + 0.5(74.75)$$

$$= 16.42 + 37.375 = 53.80 \text{ in.}$$

$$\begin{aligned}
x_{LE} &= y_{\bar{c}'} \tan \Lambda_{LE} - c_f \\
&= 53.80 (1.0998) - 4.53 \\
&= 54.64 \text{ in.}
\end{aligned}$$

Determine  $S_{W_f}$

$$\begin{aligned}
S_{W_f} &= [(c')_{\eta_i} + (c')_{\eta_o}] (\Delta\eta)(b/2) \\
&= (33.83 + 21.42)(0.975 - 0.50)(74.75) \\
&= 1961.72 \text{ in.}^2 = 13.62 \text{ ft}^2
\end{aligned}$$

Determine  $\delta_f$  (streamwise)

$$\begin{aligned}
\delta_f &= \tan^{-1} (\tan \delta_{f_{LE}} \cos \Lambda_{LE}) \quad (\text{Equation 6.1.5.1-d}) \\
&= \tan^{-1} [(0.6569)(0.6727)] \\
&= 23.84^\circ \text{ (streamwise)}
\end{aligned}$$

Determine  $c$

$$\text{At } \eta_{\bar{c}'} \text{, } c = c_r - \frac{y_{\bar{c}'}}{b/2} (c_r - c_t) \quad (\text{Section 2.2.2})$$

$$= 42.36 - \frac{53.80}{74.75} (42.36 - 16.24) = 23.56 \text{ in.}$$

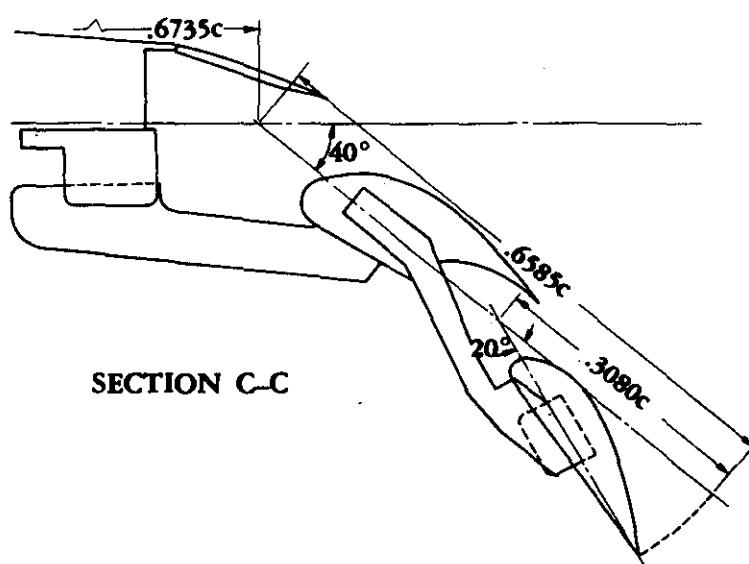
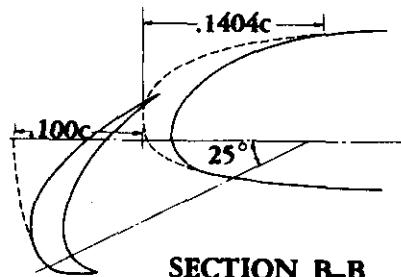
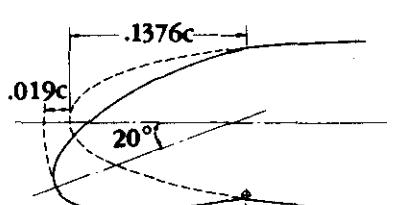
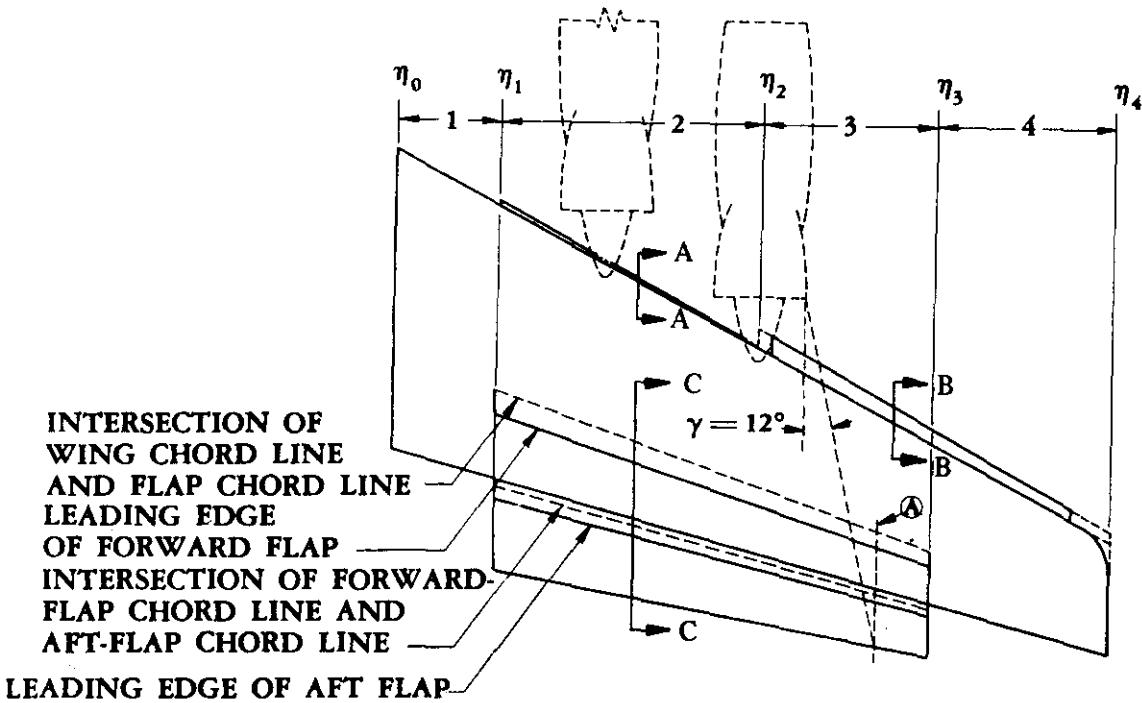
Solution:

$$\begin{aligned}
\Delta C_m &= \left[ c_{m_{\delta_{LE}}} \left( \frac{\bar{c}'}{\bar{c}} \right) + \left( \frac{x_m}{\bar{c}} - \frac{x_{LE}}{\bar{c}} \right) c_{\delta_b} \right] \frac{S_{W_f}}{S_w} \delta_f \\
&\quad + \left\{ C_m \left[ \left( \frac{\bar{c}'}{c} \right)^2 - 1 \right] + 0.75 C_L \left( \frac{\bar{c}'}{c} \right) \left( \frac{\bar{c}'}{c} - 1 \right) \right\} \Delta\eta \quad (\text{Equation 6.1.5.1-q}) \\
&= \left[ (-0.00127) \left( \frac{28.09}{31.22} \right) + \left( \frac{42.79}{31.22} - \frac{54.64}{31.22} \right) (-0.00320) \right] \frac{13.62}{30.35} (23.84) \\
&\quad + \left\{ (-0.040) \left[ \left( \frac{28.09}{23.56} \right)^2 - 1 \right] + 0.75 (0.17) \left( \frac{28.09}{23.56} \right) \left( \frac{28.09}{23.56} - 1 \right) \right\} (0.975 - 0.50) \\
&= (-0.00114 + 0.00121)(10.70) + (-0.0169 + 0.0293)(0.475) \\
&= 0.00075 + 0.00589 \\
&= 0.00664
\end{aligned}$$

This compares with a test value of  $\Delta C_m = 0.003$  from Reference 35.

#### 4. Trailing-Edge Jet Flap

Given: The wing with the EBF system shown below.



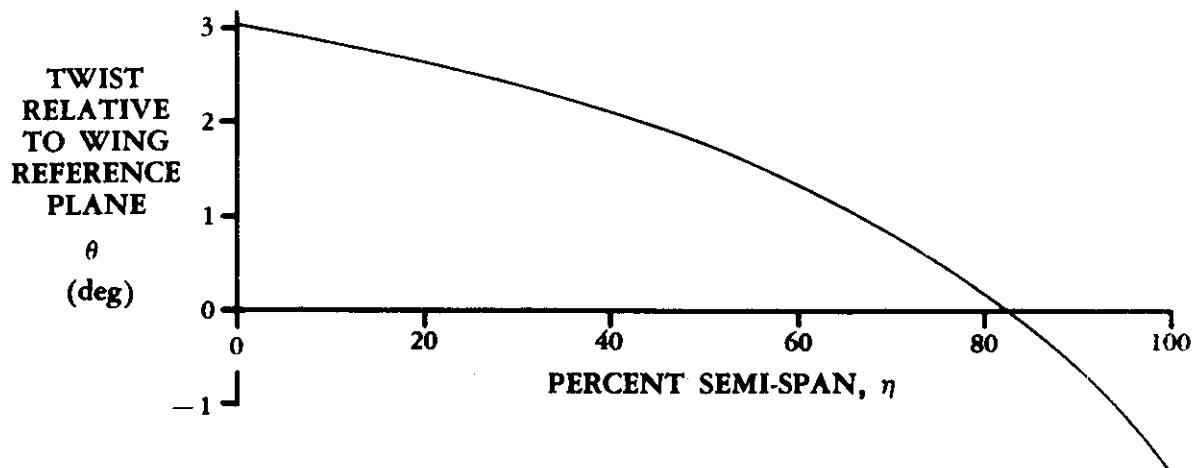
$$A = 7.0 \quad \lambda = 0.3714 \quad b = 5.9360 \text{ ft} \quad \Lambda_{c/4} = 25^\circ$$

$$c_r = 14.84 \text{ in.} \quad \bar{c} = 10.8886 \text{ in.} \quad S_w = 5.0337 \text{ ft}^2$$

$$x_{c.g.} = 10.72 \text{ in. aft of wing apex} \quad \Delta z_{c.g.} = -1.922 \text{ in. (below MAC quarter-chord)}$$

$$\alpha_w = 0 \quad C_J = 3.0 \quad \eta_t = 0.81 \quad \left. \begin{array}{l} \\ \\ \delta_{\text{leff}} = 57.5^\circ \end{array} \right\} \text{(from static force-test data)}$$

$$\delta_{f_1} = 40^\circ \quad \delta_{f_2} = 20^\circ$$



Wing section, $k$	1	2	3	4
Span station of outboard streamwise cut, $\eta_k$	0.1443	0.5076	0.7515	1.0
Span station of inboard streamwise cut, $\eta_{k-1}$	0	0.1443	0.5076	0.7515
Leading-edge device	None	Drooped leading edge	Slat	Slat
$\delta_{f,LE}$	0	$20^\circ$	$25^\circ$	$25^\circ$
Trailing-edge device	None	Double-slot Fowler flap	Double-slot Fowler flap	None
$c_{f,LE}/c$	0	0.1376	0.1404	0.1404
$c'_{LE}/c$	1.0	1.019	1.100	1.100
$c_1/c$	0	0.3505	0.3505	0
$c_2/c$	0	0.3080	0.3080	0
$c_{\delta\delta}/c$	1.0	1.351	1.432	1.100

Compute:

- Step 1. Divide the wing into four sections as indicated in the drawing. The wing-tip is squared off and the slats extended to avoid definition of additional small wing sections. It was assumed that blowing affects the entire trailing-edge flap.\*

Find  $S_J = S_2 + S_3$  (the area ahead of the flap)

$$c_t = \lambda c_r = (0.3714)(14.84) = 5.512 \text{ in.}$$

$$c = c_r - \eta_k(c_r - c_t)$$

$$\text{At } \eta_1, c = 14.84 - 0.1443(14.84 - 5.51) = 13.49 \text{ in.}$$

$$\text{At } \eta_2, c = 14.84 - 0.5076(14.84 - 5.51) = 10.10 \text{ in.}$$

$$\text{At } \eta_3, c = 14.84 - 0.7515(14.84 - 5.51) = 7.83 \text{ in.}$$

$$S_2 = \frac{1}{2} \frac{(13.49 + 10.10)}{12} (0.5076 - 0.1443)(5.9360) = 2.120 \text{ ft}^2$$

$$S_3 = \frac{1}{2} \frac{(10.10 + 7.83)}{12} (0.7515 - 0.5076)(5.9360) = 1.082 \text{ ft}^2$$

$$S_J = 2.120 + 1.082 = 3.202 \text{ ft}^2$$

Because of the lengthiness of the calculations for various parameters in Steps 2 through 5, the calculations for only wing section 2 will be presented in detail. However, the calculated components for each wing section are listed in summary tables with the detailed calculations for wing section 2.

\*For purposes of illustration only, an additional division, (A) in the sketch, is shown. It is made at the intersection of the jet and the extended flap trailing edge, by assuming that the jet spreading is 12 degrees. If the wing had been equipped with a full-span trailing-edge flap, division A would have been used as  $\eta_3$  instead of  $\eta_3 = 0.7515$ .

Step 2.  $\Delta c_m$  (Section 6.1.2.1. Note, however, that several terms have been redefined in Section 6.1.5.1; e.g.,  $C_\mu$ ,  $K$ ,  $\frac{x_m}{c}$ ,  $\alpha_L$ ,  $\frac{x_{f_i}}{c_{\delta\delta}}$ , and  $\frac{x_j}{c_{\delta\delta}}$ )

Find  $(\Delta c_m)_{\delta f_{LE}}$  (Wing Section 2)

$$\left. \begin{array}{l} \delta_{f_{LE}} = 20^\circ \\ \frac{c_{f_{LE}}}{c} = 0.1376 \end{array} \right\} \text{(given)}$$

$$c_a = c_{\delta\delta} - c_{f_{LE}} \quad (\text{Equation 6.1.2.1-g})$$

$$\frac{c_a}{c_{\delta\delta}} = 1 - \frac{c_{f_{LE}}}{c} / \frac{c_{\delta\delta}}{c}$$

$$= 1 - \frac{0.1376}{1.351}$$

$$= 0.8981$$

$$C_\mu = C_J \eta_t \frac{S_w}{S_J} \quad (\text{Equation 6.1.5.1-o})$$

$$= (3.0)(0.81) \frac{5.0337}{3.202}$$

$$= 3.820$$

$$C_\mu' = C_\mu \frac{c}{c_{\delta\delta}} \quad (\text{defined in Section 6.1.2.1 Step 1a})$$

$$= 3.820/1.351$$

$$= 2.828$$

$$c_{\theta_{\delta a}} = 11.6 \text{ per rad} \quad (\text{Figure 6.1.1.1-49})$$

$$c_{\theta_a} = 11.8 \text{ per rad} \quad (\text{Figure 6.1.1.1-49})$$

$$A_t = A \frac{c}{c_{\delta\delta}} = \frac{7.0}{1.351} = 5.181$$

$$K = \left[ \frac{A_t + 2 C'_\mu / \pi}{A_t + 2 + 0.604(C'_\mu)^{1/2} + 0.876 C'_\mu} \right] \frac{c_{\delta\delta}}{c} \quad (\text{Equation 6.1.5.1-p})$$

$$= \left[ \frac{5.181 + 2(2.828)/\pi}{5.181 + 2 + 0.604(2.828)^{1/2} + 0.876(2.828)} \right] \quad (1.351)$$

$$= \frac{6.981(1.351)}{10.674}$$

$$= 0.8836$$

$$\Delta c_1 = \frac{\delta_{fLE}}{57.3} K c_{q_{\delta_a}} \quad (\text{Equation 6.1.2.1-e})$$

$$= \frac{20}{57.3} (0.8836)(11.6)$$

$$= 3.5776$$

$$\Delta c_2 = \frac{\delta_{fLE}}{57.3} K c_{q_\alpha} \quad (\text{Equation 6.1.2.1-f})$$

$$= \frac{20}{57.3} (0.8836)(11.8)$$

$$= 3.6393$$

$$\tan \Lambda_{LE} = \tan \Lambda_{c/4} - \frac{4}{A} \left( -\frac{1}{4} \right) \frac{1-\lambda}{1+\lambda} \quad (\text{Section 2.2.2})$$

$$= 0.4663 - \frac{4}{7} \left( -\frac{1}{4} \right) \frac{1-0.3714}{1.3714}$$

$$= 0.5318$$

$$\frac{x_m}{c} = \left( \frac{1+\lambda}{1-\lambda} \right) \frac{A_s}{4} \tan \Lambda_{LE} \quad (\text{Equation 6.1.5.1-m})$$

$$= \left( \frac{1.3714}{1 - 0.3714} \right) \frac{7}{4} (0.5318)$$

$$= 2.0304$$

$$\frac{x_a}{c_{\delta\delta}} = 0.245 \quad (\text{Figure 6.1.2.1-37})$$

$$\frac{x_{a.c.}}{c_{\delta\delta}} = 0.215 \quad (\text{Figure 6.1.2.1-37})$$

$$x_1 = \frac{x_m}{c} + \left( \frac{c'_{LE}}{c} - 1 \right) - \frac{x_a}{c_{\delta\delta}} \frac{c_{\delta\delta}}{c} \quad (\text{Equation 6.1.2.1-h})$$

$$= 2.0304 + (1.019 - 1) - 0.245 (1.351)$$

$$= 1.718$$

$$x_2 = \frac{x_m}{c} + \left( \frac{c'_{LE}}{c} - 1 \right) - \frac{x_{a.c.}}{c_{\delta\delta}} \frac{c_{\delta\delta}}{c} \quad (\text{Equation 6.1.2.1-i})$$

$$= 2.0304 + (1.019 - 1) - 0.215 (1.351)$$

$$= 1.759$$

$$\Delta c_{m3} = C_\mu \frac{c_{fLE}}{c} \sin \delta_{fLE} \quad (\text{Equation 6.1.2.1-j})$$

$$= 3.820 (0.1376)(0.3420)$$

$$= 0.1798$$

$$(\Delta c_m)_{\delta f_{LE}} = \Delta c_1 x_1 - \Delta c_2 x_2 + \Delta c_{m3} \quad (\text{Equation 6.1.2.1-d})$$

$$= (3.5776)(1.718) - (3.6393)(1.759) + 0.1798$$

$$= -0.0754 \quad (\text{for Wing Section 2})$$

$(\Delta c_m)_{\delta f_{LE}}$  Summary

Wing Section	1	2	3	4
$\delta f_{LE}$ (given)	0	20°	25°	25°
$\frac{c_f LE}{c}$ (given)	0	0.1376	0.1404	0.1404
$\frac{c_a}{c_{\delta \delta}}$ (From Eq. 6.1.2.1-g)		0.8981	0.9020	0.8724
$C_\mu$ (Eq. 6.1.5.1-o)	0	3.820	3.820	0
$C'_\mu$	0	2.828	2.668	0
$c_Q \delta_a$ (per rad) (Fig. 6.1.1.1-49)		11.6	11.4	6.1
$c_Q \alpha$ (per rad) (Fig. 6.1.1.1-49)		11.8	11.6	6.3
$A_t$	7.0	5.181	4.888	6.364
$K$ (Eq. 6.1.5.1-p)	0.7778	0.8836	0.9237	0.8370
$\Delta c_1$ (Eq. 6.1.2.1-e)		3.5776	4.594	2.228
$\Delta c_2$ (Eq. 6.1.2.1-f)		3.6393	4.675	2.301
$\frac{x_m}{c}$ (Eq. 6.1.5.1-m)		2.0304	2.0304	2.0304
$\frac{x_a}{c_{\delta \delta}}$ (Fig. 6.1.2.1-37)		0.245	0.246	0.274
$\frac{x_{a.c.}}{c_{\delta \delta}}$ (Fig. 6.1.2.1-37)		0.215	0.216	0.249
$x_1$ (Eq. 6.1.2.1-h)		1.718	1.778	1.829
$x_2$ (Eq. 6.1.2.1-i)		1.759	1.821	1.8665
$\Delta c_{m3}$ (Eq. 6.1.2.1-j)		0.1798	0.2267	0
$(\Delta c_m)_{\delta f_{LE}}$ (Eq. 6.1.2.1-d)	0 (no LE device)	-0.0754	-0.1183	-0.1968

Find  $(\Delta c_m)_x$

$$\alpha_L = \alpha_w + \theta$$

$$= 0 + \theta$$

Wing Section	1	2	3	4
$\alpha_L = \theta$ (from given plot)	2.91	2.30	1.19	-0.42
*K	0.7778	0.8836	0.9237	0.8370
* $c_{L\alpha}$ (per rad)	6.3	11.8	11.6	6.3
$\Delta c_4 = \frac{\alpha_L}{57.3} K c_{L\alpha}$ (Eq. 6.1.2.1-l)	0.2489	0.4185	0.2225	-0.03866
* $C_\mu$	0	3.820	3.820	0
* $\frac{x_m}{c}$		2.0304	2.0304	2.0304
$\frac{c'_{LE}}{c}$ (given)	1.0	1.019	1.100	1.100
$\Delta c_{m4} = -C_\mu \left[ \frac{x_m}{c} + \left( \frac{c'_{LE}}{c} - 1 \right) \right] \frac{\alpha_L}{57.3}$ (Eq. 6.1.2.1-m)	0	-0.3142	-0.1690	0
* $x_2$	1.781	1.759	1.821	1.8565
$(\Delta c_m)_x = \Delta c_4 x_2 + \Delta c_{m4}$ (Eq. 6.1.2.1-k)	0.4433	0.4219	0.2362	-0.0717

\*From preceding  $(\Delta c_m)_{\delta f_{LE}}$  calculations.

Find  $(\Delta c_m)_{\delta_f}$  (Wing Section 2)

$$n = 2$$

Forward flap

$$\delta_{f_1} = 40^\circ$$

$$c_{f_1} = c_1 + c_2 \quad (\text{Sketch (g) Section 6.1.2.1})$$

$$\begin{aligned} \frac{c_{f_1}}{c_{\delta\delta}} &= \frac{c_1 + c_2}{c} \Big/ \frac{c_{\delta\delta}}{c} \\ &= (0.3505 + 0.3080)/1.351 \\ &= 0.4874 \end{aligned}$$

$$C'_\mu = 2.828 \quad (\text{previous } (\Delta c_m)_{\delta f_{LE}} \text{ calculations})$$

$$c_{q_{\delta f_1}} = 10.6 \text{ per rad} \quad (\text{Figure 6.1.1.1-49})$$

$$K = 0.8836 \quad (\text{see previous table for } (\Delta c_m)_\alpha)$$

$$\begin{aligned} (\Delta c_S)_1 &= \frac{\delta_{f_1}}{57.3} K c_{q_{\delta f_1}} \quad (\text{Equation 6.1.2.1-o}) \\ &= \frac{40}{57.3} (0.8836)(10.6) \\ &= 6.538 \end{aligned}$$

$$\left( \frac{x_{f_1}}{c_{\delta\delta}} \right)_{2D} = 0.402 \quad (\text{Figure 6.1.2.1-37})$$

$$A_t = 5.181 \quad (\text{previous } (\Delta c_m)_{\delta f_{LE}} \text{ calculations})$$

$$\frac{1}{A_t} = \frac{1}{5.181} = 0.1930$$

$$\left[ \frac{(x_{c,p.})_{3D}}{(x_{c,p.})_{2D}} \right]_1 = 1.085 \quad (\text{Figure 6.1.5.1-68})$$

$$\begin{aligned} \frac{x_{f1}}{c_{\delta\delta}} &= \left( \frac{x_{f1}}{c_{\delta\delta}} \right)_{2D} \left[ \frac{(x_{c,p.})_{3D}}{(x_{c,p.})_{2D}} \right]_1 \quad (\text{Equation 6.1.5.1-q}) \\ &= (0.402)(1.085) \\ &= 0.436 \end{aligned}$$

$$\begin{aligned} (x_5)_1 &= \frac{x_m}{c} + \left( \frac{c'_{LE}}{c} - 1 \right) - \frac{x_{f1}}{c_{\delta\delta}} \frac{c_{\delta\delta}}{c} \quad (\text{Equation 6.1.2.1-q}) \\ &= 2.0304 + (1.019 - 1) - 0.436(1.351) \\ &= 1.460 \end{aligned}$$

### Aft flap

$$\delta_{f2} = \delta_{leff} - \sum_{i=1}^{n-1} \delta_{fi} \quad (\text{Equation 6.1.2.1-p})$$

$$= 57.5 - 40$$

$$= 17.5^\circ$$

$$c_{f2} = c_2 \quad (\text{Sketch (g) Section 6.1.2.1})$$

$$\frac{c_{f2}}{c_{\delta\delta}} = \frac{c_2}{c} / \frac{c_{\delta\delta}}{c}$$

$$= 0.3080/1.351$$

$$= 0.2280$$

$$C'_\mu = 2.828 \quad (\text{previous } (\Delta c_m)_{\delta f_{LE}} \text{ calculations})$$

$$c_{\alpha_{\delta f_2}} = 9.5 \text{ per rad} \quad (\text{Figure 6.1.1.1-49})$$

$$K = 0.8836 \quad (\text{see previous table for } (\Delta c_m)_\alpha)$$

$$(\Delta c_5)_2 = \frac{\delta_{f2}}{57.3} K_{c_{\delta\delta} f_2} \quad (\text{Equation 6.1.2.1-o})$$

$$= \frac{17.5}{57.3} (0.8836)(9.5)$$

$$= 2.564$$

$$\left( \frac{x_{f2}}{c_{\delta\delta}} \right)_{2D} = 0.518 \quad (\text{Figure 6.1.2.1-37})$$

$$A_t = 5.181 \quad (\text{previous } (\Delta c_m)_{\delta f_{LE}} \text{ calculations})$$

$$\frac{1}{A_t} = \frac{1}{5.181} = 0.1930$$

$$\left[ \frac{(x_{c,p.})_{3D}}{(x_{c,p.})_{2D}} \right]_2 = 1.140 \quad (\text{Figure 6.1.5.1-68})$$

$$\frac{x_{f2}}{c_{\delta\delta}} = \left( \frac{x_{f2}}{c_{\delta\delta}} \right)_{2D} \left[ \frac{(x_{c,p.})_{3D}}{(x_{c,p.})_{2D}} \right]_2 \quad (\text{Equation 6.1.5.1-q})$$

$$= (0.518)(1.140)$$

$$= 0.5905$$

$$(x_5)_2 = \frac{x_m}{c} + \left( \frac{c'_{LE}}{c} - 1 \right) - \frac{x_{f2}}{c_{\delta\delta}} \frac{c_{\delta\delta}}{c} \quad (\text{Equation 6.1.2.1-q})$$

$$= 2.0304 + (1.019 - 1) - 0.5905(1.351)$$

$$= 1.252$$

$$(\Delta c_m)_{\delta f} = \sum_{i=1}^n (\Delta c_5)_i (x_5)_i \quad (\text{Equation 6.1.2.1-n})$$

$$= (6.538)(1.460) + (2.564)(1.252)$$

$$= 12.7556 \quad (\text{for Wing Section 2})$$

$(\Delta c_m)_{\delta_f}$  Summary

Wing Section	1	2	3	4
* $C'_\mu$		2.828	2.668	
*K		0.8836	0.9237	
* $1/A_t$		0.1930	0.2046	
<b>Forward Flap</b>				
$c_{\delta \delta} \delta f_1$ (per rad) (Fig. 6.1.1.1-49)		10.6	10.4	
$(\Delta c_5)_1$ (Eq. 6.1.2.1-o)		6.538	6.706	
$\left( \frac{x_{f_1}}{c_{\delta \delta}} \right)_{2D}$ (Fig. 6.1.2.1-37)		0.402	0.400	
$\left[ \frac{(x_{c,p.})_{3D}}{(x_{c,p.})_{2D}} \right]_1$ (Fig. 6.1.5.1-68)		1.085	1.090	
$\frac{x_{f_1}}{c_{\delta \delta}}$ (Eq. 6.1.5.1-q)		0.436	0.436	
$(x_5)_1$ (Eq. 6.1.2.1-q)		1.460	1.5060	
<b>Aft Flap</b>				
$c_{\delta \delta} \delta f_2$ (per rad) (Fig. 6.1.1.1-49)		9.5	9.25	
$(\Delta c_5)_2$ (Eq. 6.1.2.1-o)		2.564	2.609	
$\left( \frac{x_{f_2}}{c_{\delta \delta}} \right)_{2D}$ (Fig. 6.1.2.1-37)		0.518	0.515	
$\left[ \frac{(x_{c,p.})_{3D}}{(x_{c,p.})_{2D}} \right]_2$ (Fig. 6.1.5.1-68)		1.140	1.147	

\*From preceding  $(\Delta c_m)_{\delta f_{LE}}$  calculations

Wing Section	1	2	3	4
$\frac{x_{f_2}}{c_{\delta\delta}}$ (Eq. 6.1.5.1-q)		0.5905	0.5907	
$(x_5)_2$ (Eq. 6.1.2.1-q)		1.252	1.2845	
$(\Delta c_m)_{\delta_f} = \sum_{i=1}^n (\Delta c_5)_i (x_5)_i$ (Equation 6.1.2.1-n)	0 (no TE flaps)	12.7556	13.4505	0 (no TE flaps)

Find  $(\Delta c_m)_{\delta_j}$

$$\delta_{j_{\text{eff}}} < \sum_{i=1}^n \delta_{f_i}$$

For  $57.5 < 40 + 20$ , then  $\delta_j = 0$

$$\Delta c_6 = \frac{\delta_j}{57.3} K c_{\delta\delta_j} \quad (\text{Equation 6.1.2.1-s})$$

= 0 (all wing sections)

$$(\Delta c_m)_{\delta_j} = \Delta c_6 x_6 \quad (\text{Equation 6.1.2.1-r})$$

= 0

$$\Delta c_m = (\Delta c_m)_{\delta_{f_{LE}}} + (\Delta c_m)_\alpha + (\Delta c_m)_{\delta_f} + (\Delta c_m)_{\delta_j} \quad (\text{Equation 6.1.2.1-c})$$

Wing Section	1	2	3	4
$(\Delta c_m)_{\delta_{f_{LE}}}$ (Eq. 6.1.2.1-d)	0	-0.0754	-0.1183	-0.1968
$(\Delta c_m)_\alpha$ (Eq. 6.1.2.1-k)	0.4433	0.4219	0.2363	-0.0717
$(\Delta c_m)_{\delta_f}$ (Eq. 6.1.2.1-n)	0	12.7556	13.4505	0
$(\Delta c_m)_{\delta_j}$ (Eq. 6.1.2.1-r)	0	0	0	0
$\Delta c_m$ (Eq. 6.1.2.1-c)	0.4433	13.10	13.57	-0.2685

**Step 3.  $C_{m_m}$**

Wing Section, k	1	2	3	4
$\eta_k$	0.1443	0.5076	0.7515	1.0
$\eta_{k-1}$	0	0.1443	0.5076	0.7515
$K_{b_k}$ (Fig. 6.1.4.1-15)	0.205	0.650	0.880	1.0
$K_{b_{k-1}}$ (Fig. 6.1.4.1-15)	0	0.205	0.650	0.880
$K_{b_k} - K_{b_{k-1}}$	0.205	0.445	0.230	0.120
$\Delta c_m$ (from preceding Step 2)	0.4433	13.10	13.57	-0.2673

$$\begin{aligned}
 C_{m_m} &= \sum_{k=1}^p \Delta c_m (K_{b_k} - K_{b_{k-1}}) \quad (\text{Equation 6.1.5.1-s}) \\
 &= (0.4433)(0.205) + (13.10)(0.445) + (13.57)(0.230) + (-0.2673)(0.120) \\
 &= 9.009
 \end{aligned}$$

**Step 4.  $C_{\lambda_k} = [\Delta c_1 - \Delta c_2 + \Delta c_4 + \sum_{i=1}^n (\Delta c_5)_i + \Delta c_6] (K_{b_k} - K_{b_{k-1}})$  (Equation 6.1.5.1-t)**

Wing Section, k	1	2	3	4
* $\Delta c_1$	0	3.5776	4.594	2.228
* $\Delta c_2$	0	3.6393	4.675	2.301
* $\Delta c_4$	0.2489	0.4185	0.2225	-0.03865
* $\sum_{i=1}^n (\Delta c_5)_i$	0	6.538+ 2.564	6.706+ 2.609	0
* $\Delta c_6$	0	0	0	0
** $(K_{b_k} - K_{b_{k-1}})$	0.205	0.445	0.230	0.120
$C_{\lambda_k}$ (Eq. 6.1.5.1-t)	0.0510	4.212	2.175	-0.01340

\*From preceding Step 2

\*\*From preceding Step 3

Step 5.  $\Delta C_m$

$$\frac{\Delta z}{\bar{c}} = \frac{-1.922}{10.8886} = -0.1765$$

$$\begin{aligned}\frac{\Delta x_k}{\bar{c}} &= \frac{x_m}{c} \left( \frac{c}{\bar{c}} \right) - \frac{x_{c.g.}}{\bar{c}} \\ &= 2.0304 \left( \frac{14.84}{10.8886} \right) - \frac{10.72}{10.8886} \\ &= 1.783\end{aligned}$$

Wing Section, k	1	2	3	4
$C_{\lambda_k}$ (preceding Step 4)	0.0510	4.212	2.175	-0.0134
$C_\mu$ (preceding Step 2)	0	3.820	3.820	0
$\frac{\alpha_L}{57.3}$ (preceding Step 2)		0.04014	0.02977	
$\frac{S_k}{S_w}$ (preceding Step 1)		0.4212	0.2150	
$C_\mu \frac{\alpha_L}{57.3} \frac{S_k}{S_w}$	0	0.0646	0.0171	0

$$\Delta C_m = C_{m_m} + \eta_t C_J \frac{\Delta z}{\bar{c}} + \sum_{k=1}^p \left\{ \left[ C_\mu \frac{\alpha_L}{57.3} \frac{S_k}{S_w} - C_{\lambda_k} \right] \frac{\Delta x_k}{\bar{c}} \right\} \quad (\text{Equation 6.1.5.1-u})$$

$$= 9.009 + (0.81)(3.0)(-0.1765)$$

$$+ \{(0 - 0.0510) + (0.0646 - 4.212) + (0.0171 - 2.175) + [0 - (-0.0134)]\} \quad (1.783)$$

$$= 9.009 - 0.4289 - 11.310$$

$$= -2.729 \quad (\text{based on } S_w \bar{c}_w)$$

## B. TRANSONIC

The following method for the estimation of  $C_{m\delta}$  at transonic speeds is based on a procedure similar to that of Reference 6 and is developed empirically from test data of References 7 through 10. The only readily available test data for pitching-moment effectiveness at transonic speeds are those of References 7 through 10. Therefore, the method has not been substantiated independently of these test data.

### DATCOM METHOD

A first-order approximation to the pitching-moment effectiveness at transonic speeds is given by

$$C_{m\delta} = -C_{L\delta} \frac{x}{c} \quad 6.1.5.1-w$$

where

$C_{L\delta}$  is the lift effectiveness of the control surfaces from the method of Paragraph B of Section 6.1.4.1.

$\frac{x}{c}$  is the distance, in percent of MAC, of the chordwise center-of-pressure location aft of the wing moment reference point.

$$\frac{x}{c} = -\frac{b}{c} \tan \Lambda_{LE} \left[ \frac{1+2\lambda}{6(1+\lambda)} + 2 \frac{(C_{l\delta})_{M=0.6}}{(C_{L\delta})_{M=0.6}} \right] + \left( \frac{x_{c.p.}}{c_{c.p.}} \right) \frac{c_{c.p.}}{c} - \frac{x_{MRP}}{c} \quad 6.1.5.1-x$$

where

$(C_{l\delta})_{M=0.6}$  is the roll effectiveness of the control surface at  $M = 0.6$ , based on the total wing span with one control deflected. This parameter is one-half the value of  $C_{l\delta}$  obtained by the method of Paragraph A of Section 6.2.1.1.

$(C_{L\delta})_{M=0.6}$  is the lift effectiveness of the control surfaces at  $M = 0.6$  from Paragraph A of Section 6.1.4.1.

$\frac{x_{MRP}}{c}$  is the distance, in percent of MAC, from the leading edge of the MAC to the moment reference point, positive for the moment reference point aft of the leading edge of the MAC.

$\frac{x_{c.p.}}{c_{c.p.}}$  is the empirically derived chordwise center-of-pressure location of the incremental load due to surface deflection, determined by

$$\frac{x_{c.p.}}{c_{c.p.}} = \left( \frac{x_{c.p.}}{c_{c.p.}} \right)_1 + K \left( \frac{c_f}{c} - 0.2 \right) \quad 6.1.5.1-y$$

where  $(x_{c.p.}/c_{c.p.})_1$  and  $K$  are empirically derived factors presented as functions of Mach number and  $\Lambda_{c/4}$  in Figures 6.1.5.1-69a and 6.1.5.1-69b, respectively. The flap-chord ratio  $c_f/c$  is measured in the streamwise direction.

$$\frac{c_{c.p.}}{\bar{c}}$$

is the wing chord at the spanwise center-of-pressure location, in percent of MAC given by

$$\frac{c_{c.p.}}{\bar{c}} = \frac{c_r}{\bar{c}} \left[ 1 - 4(1 - \lambda) \frac{(C_l \delta)_{M=0.6}}{(C_L \delta)_{M=0.6}} \right] \quad 6.1.5.1-z$$

where  $(C_l \delta)_{M=0.6}$  and  $(C_L \delta)_{M=0.6}$  are defined above.

The planform parameters of the empirical data used to derive Figures 6.1.5.1-69a and 6.1.5.1-69b are:  $A = 4.0$ ,  $\lambda = 0.6$ ,  $t/c = 0.06$ ,  $0 \leq \Lambda_{c/4} \leq 60^\circ$ , and a 0.30c plain sealed flap.

### Sample Problem

Given: The configuration of Reference 8 with a partial-span plain trailing-edge flap.

Wing Characteristics:

$$A = 4.0 \quad b/2 = 4.243 \text{ in.} \quad \lambda = 0.60 \quad \Lambda_{c/4} = 35^\circ \quad \Lambda_{LE} = 37.33^\circ$$

NACA 65A006 airfoil (streamwise)  $x_{MRP} = \frac{\bar{c}}{4}$   $c_r/\bar{c} = 1.183$   $\frac{b}{\bar{c}} = 3.918$

Flap Characteristics:

$$\begin{array}{lll} \text{Plain trailing-edge flap} & c_f/c = 0.30 & \Lambda_{HL} = 30.44^\circ \\ \eta_i = 0.57 & \eta_o = 1.0 & \delta = 16^\circ \text{ (streamwise)} \end{array}$$

Additional Characteristics:

$$M = 0.90 \quad (C_l \delta)_{M=0.6} = 0.0014 \text{ per deg (test value for semispan model, based on } S_W \text{ and } b_W)$$

$$(C_l \delta)_{M=0.9} = 0.00135 \text{ per deg (test value for semispan model, based on } S_W \text{ and } b_W)$$

$$(C_L \delta)_{M=0.6} = 0.0105 \text{ per deg (test value for full-span model, based on } S_W)$$

Compute:

Chordwise center-of-pressure location

$$\frac{c_{c.p.}}{\bar{c}} = \frac{c_r}{\bar{c}} \left[ 1 - 4(1 - \lambda) \frac{\left( C_{l\delta} \right)_{M=0.6}}{\left( C_{L\delta} \right)_{M=0.6}} \right] \quad (\text{Equation 6.1.5.1-z})$$

$$= 1.183 \left[ 1 - 4(0.4) \frac{0.0014}{0.0105} \right]$$

$$= 0.931$$

$$\left( \frac{x_{c.p.}}{c_{c.p.}} \right)_1 = 0.880 \quad (\text{Figure 6.1.5.1-69 a})$$

$$K = -0.690 \quad (\text{Figure 6.1.5.1-69b})$$

$$\frac{x_{c.p.}}{c_{c.p.}} = \left( \frac{x_{c.p.}}{c_{c.p.}} \right)_1 + K \left( \frac{c_f}{c} - 0.2 \right) \quad (\text{Equation 6.1.5.1-y})$$

$$= (0.880) + (-0.690) (0.30 - 0.20)$$

$$= 0.811$$

$$\frac{x}{\bar{c}} = -\frac{b}{\bar{c}} \tan \Lambda_{LE} \left[ \frac{1+2\lambda}{6(1+\lambda)} - 2 \frac{\left( C_{l\delta} \right)_{M=0.6}}{\left( C_{L\delta} \right)_{M=0.6}} \right] + \left( \frac{x_{c.p.}}{c_{c.p.}} \right) \frac{c_{c.p.}}{\bar{c}} - \frac{x_{MRP}}{\bar{c}} \quad (\text{Equation 6.1.5.1-x})$$

$$= (-3.918) (0.7626) \left[ \frac{2.20}{9.60} - 2 \left( \frac{0.0014}{0.0105} \right) \right] + (0.811) (0.931) - 0.25$$

$$= 0.112 + 0.755 - 0.25$$

$$= 0.617$$

Lift effectiveness at  $M = 0.9$  (Section 6.1.4.1)

$$C_{L\delta} = \left( C_{L\delta} \right)_{M=0.6} \left( \frac{C_{l\delta}}{\left( C_{l\delta} \right)_{M=0.6}} \right) \quad (\text{Equation 6.1.4.1-e})$$

$$= 0.0105 \left( \frac{0.00135}{0.0014} \right)$$

$$= 0.0101 \text{ per deg}$$

Solution:

$$\begin{aligned} C_{m\delta} &= -C_{L\delta} \frac{x}{\bar{c}} \text{ (Equation 6.1.5.1-w)} \\ &= - (0.0101) (0.617) \\ &= -0.00623 \text{ per deg} \end{aligned}$$

The test value at  $M = 0.90$  from Reference 8 is  $-0.0065$  per degree.

### C. SUPERSONIC

The procedure for estimating trailing-edge control effectiveness at supersonic speeds is based on the method presented in Reference 11. The restrictions used in the derivation of the method are listed below.

1. Leading and trailing edges of the control surface are swept ahead of the Mach lines from the deflected controls.
2. Control root and tip chords are parallel to the plane of symmetry.
3. Controls are located either at the wing tip or far enough inboard so that the outermost Mach lines from the deflected controls do not cross the wing tip.
4. Innermost Mach lines from the deflected controls do not cross the wing root chord.
5. Wing planform has leading edges swept ahead of the Mach lines and has streamwise tips.
6. Controls are not influenced by the tip conical flow from the opposite wing panel or by the interaction of the wing-root Mach cone with the wing tip.

### DATCOM METHOD

The pitching-moment effectiveness  $C_{m\delta}$  at supersonic speeds for symmetric, straight-sided controls, based on total wing area and  $\bar{c}$ , is given by

$$C_{m\delta} = K_1 \frac{1}{3} \frac{b_f}{\bar{c}} \frac{c_{rf}}{S_W} C'_{m\delta} - K_2 \frac{1}{2} \frac{b_f}{\bar{c}} \frac{S_f}{S_W} C'_{l\delta} - K_3 \frac{x_f}{\bar{c}} \frac{S_f}{S_W} C'_{L\delta} \quad 6.1.5.1-aa$$

where

$$K_1 = \left( 1 - \frac{C_2}{C_1} \phi_{TE} \right) (1 + \lambda_f + \lambda_f^2)$$

$$K_2 = \left( 1 - \frac{C_2}{C_1} \phi_{TE} \right) \tan \Lambda_{HL}$$

$$K_3 = \left( 1 - \frac{C_2}{C_1} \phi_{TE} \right)$$

where  $\left(1 - \frac{C_2}{C_1} \phi_{TE}\right)$  is a thickness correction factor to the supersonic flat-plate derivative.

$$C_1 = \frac{2}{\sqrt{M^2 - 1}} \text{ per radian}$$

$$C_2 = \frac{(\gamma + 1) M^4 - 4(M^2 - 1)}{2(M^2 - 1)^2} \text{ per radian}$$

$\phi_{TE}$  is the trailing-edge angle in radians, measured normal to the control hinge line.

$\gamma$  is the ratio of specific heats,  $\gamma = 1.4$ .

$b_f$  is the control span (both sides of wing).

$S_f$  is the control area (both sides of wing).

$\lambda_f$  is the taper ratio of the control.

$\Lambda_{HL}$  is the sweep of the control hinge line.

$c_{rf}$  is the root chord of the control.

$x_f$  is the distance of the leading edge of the control root chord behind the wing axis of pitch.

$C'_{m\delta}$  is the pitching-moment effectiveness of one symmetric, straight-sided control, based on twice its moment area about the hinge line, from Figures 6.1.5.1-70 through 6.1.5.1-73b, according to the control planform as follows:

- (a) Tapered controls with outboard edge coincident with wing tip, use Figure 6.1.5.1-70.
- (b) Tapered controls with outboard edge not coincident with wing tip, use Figure 6.1.5.1-73a.
- (c) Untapered controls with outboard edge coincident with wing tip, use Figure 6.1.5.1-73b.
- (d) Untapered controls with outboard edge not coincident with wing tip, use Figure 6.1.5.1-73a.

$C'_{L\delta}$  is the lift effectiveness of one symmetric, straight-sided control, based on the area of the control, obtained from Paragraph C of Section 6.1.4.1.

$C'_{I\delta}$  is the rolling-moment effectiveness of one symmetric, straight-sided control about its root chord line, based on the area and span of one control, obtained from Paragraph C of Section 6.2.1.1.

It should be noted that control deflection angles are measured streamwise.

For swept-forward wings and controls with inverse taper, see Reference 11 for the proper values of  $C_{m_\delta}$ ,  $C_{L_\delta}$  and  $C'_{l_\delta}$ .

Thickness correction factors for other than symmetrical, straight-sided controls can be determined from Reference 11.

The computation of pitching-moment effectiveness for leading-edge controls and trailing-edge controls with subsonic leading edges can be accomplished with the aid of Reference 12.

Not enough test data are available to allow substantiation of the method.

### Sample Problem

Given: A wing-control configuration with the following characteristics:

Wing Characteristics:

$$S_W = 46.5 \text{ sq ft} \quad \bar{c} = 4.0 \text{ ft} \quad b = 12.0 \text{ ft} \quad \Lambda_{LE} = 42^\circ$$

$$\Lambda_{TE} = 27.7^\circ$$

Control Characteristics:

Symmetric, straight-sided inboard flap

$$S_f = 4.71 \text{ sq ft (both sides of wing)} \quad b_f = 6.5 \text{ ft (both sides of wing)}$$

$$\lambda_f = 0.715 \quad c_{rf} = 0.85 \text{ ft} \quad x_f = 1.768 \text{ ft} \quad \phi_{TE} = 3^\circ$$

$$\Lambda_{HL} = 30.8^\circ$$

Additional Characteristics:

$$M = 1.90; \beta = 1.62$$

Compute:

$$C_1 = \frac{2}{\sqrt{M^2 - 1}} = 1.235$$

$$C_2 = \frac{(\gamma + 1) M^4 - 4(M^2 - 1)}{2(M^2 - 1)^2} = \frac{(2.4)(1.90)^4 - 4[(1.90)^2 - 1]}{2[(1.90)^2 - 1]^2} = \frac{20.84}{13.62} = 1.53$$

$$K_1 = \left( 1 + \frac{C_2}{C_1} \phi_{TE} \right) \left( 1 + \lambda_f + \lambda_f^2 \right)$$

$$K_2 = \left[ 1 - \left( \frac{1.53}{1.235} \right) \left( \frac{3.0}{57.3} \right) \right] \left[ 1 + 0.715 + (0.715)^2 \right] = (0.935)(2.226) = 2.08$$

$$K_2 = \left( 1 - \frac{C_2}{C_1} \phi_{TE} \right) (\tan \Lambda_{HL}) = (0.935)(0.5961) = 0.557$$

$$K_3 = \left( 1 - \frac{C_2}{C_1} \phi_{TE} \right) = 0.935$$

$$\frac{\tan \Lambda_{TE}}{\beta} = \frac{0.5250}{1.62} = 0.324$$

$$\frac{\tan \Lambda_{HL}}{\beta} = \frac{0.5961}{1.62} = 0.368$$

$$\beta C'_{m\delta} = -0.0360 \text{ per deg (Figure 6.1.5.1-73a)}$$

$$C'_{m\delta} = -0.0222 \text{ per deg}$$

$$\beta C'_{L\delta} = 0.0750 \text{ per deg (Figure 6.1.4.1-25)}$$

$$C'_{L\delta} = 0.0463 \text{ per deg}$$

$$\beta C'_{l\delta} = 0.0340 \text{ per deg (Figure 6.2.1.1-28, interpolated)}$$

$$C'_{l\delta} = 0.0210 \text{ per deg}$$

Solution:

$$C_{m\delta} = K_1 \frac{1}{3} \frac{b_f}{c} \frac{c_{rf}}{S_W} C'_{m\delta} - K_2 \frac{1}{2} \frac{b_f}{c} \frac{S_f}{S_W} C'_{l\delta} - K_3 \frac{x_f}{c} \frac{S_f}{S_W} C'_{L\delta} \quad (\text{Equation 6.1.5.1-a a})$$

$$= (2.08) \frac{1}{3} \left( \frac{6.5}{4.0} \right) \left( \frac{0.85}{46.5} \right) (-0.0222) - (0.557) \frac{1}{2} \left( \frac{6.5}{4.0} \right) \left( \frac{4.71}{46.5} \right) (0.0210)$$

$$- (0.935) \left( \frac{1.768}{4.0} \right) \left( \frac{4.71}{46.5} \right) (0.0463)$$

$$= (-0.000457) - (0.000963) - (0.00194)$$

$$= -0.00336 \text{ per deg}$$

## REFERENCES

1. Anon: Royal Aeronautical Society Data Sheets – Aerodynamics, Vol. IV. (Flaps 08.01.01 and 08.01.02), 1956. (U)
2. James, H. A., and Hunton, L. W.: Estimation of Incremental Pitching Moments Due to Trailing-Edge Flaps on Swept and Triangular Wings. NACA TN 4040, 1957. (U)
3. May, F., and Widdison, C. A.: STOL High-Lift Design Study. Vol. 1. State-of-the-Art Review of STOL Aerodynamic Technology. AFFDL-TR-71-26 Vol. 1, 1971. (U)
4. Campbell, L. J., Blanks, C. F., and Leaver, D. A.: Aerodynamic Characteristics of Rectangular Wings of Small Aspect Ratio. ARC R&M 3142, 1960. (U)
5. DeYoung, J.: Theoretical Symmetric Span Loading Due to Flap Deflection for Wings of Arbitrary Plan Form at Subsonic Speeds. NACA TR 1071, 1952. (U)
6. Decker, J., et al.: USAF Stability and Control Handbook. M-03671, 1956. (C) Title Unclassified
7. Smith, W. G.: Wind-Tunnel Investigation at Subsonic and Supersonic Speeds of a Model of a Tailless Fighter Airplane Employing a Low-Aspect-Ratio Sweptback Wing – Stability and Control. NACA RM A52J30, 1953. (U)
8. Thompson, R. F.: Lateral-Control Investigation of Flap-Type Controls on a Wing with Quarter-Chord Line Swept Back 35°, Aspect Ratio 4, Taper Ratio 0.6, and NACA 65A006 Airfoil Section. NACA RM L9L12a, 1950. (U)
9. Vogler, R. D.: Lateral-Control Investigation of Flap-Type Controls on a Wing with Quarter-Chord Line Swept Back 45°, Aspect Ratio 4, Taper Ratio 0.6, and NACA 65A006 Airfoil Section. Transonic-Bump Method. NACA RM L9F29a, 1949. (U)
10. Hammond, A. D.: Lateral-Control Investigation of Flap-Type Controls on a Wing with Unswept Quarter-Chord Line, Aspect Ratio 4, Taper Ratio 0.6, and NACA 65A006 Airfoil Section. NACA RM L50A03, 1950. (U)
11. Goin, K. L.: Equations and Charts for the Rapid Estimation of Hinge-Moment and Effectiveness Parameters for Trailing-Edge Controls Having Leading and Trailing Edges Swept Ahead of the Mach Lines. NACA TR 1041, 1951. (U)
12. Heaslet, M. A., and Spreiter, J. R.: Reciprocity Relations in Aerodynamics. NACA TN 2700, 1952. (U)
13. Barnett, U. R., Jr., and Lipson, S.: Effects of Several High-Lift and Stall-Control Devices on the Aerodynamic Characteristics of a Semispan 49° Sweptback Wing. NACA RM L52D17a, 1952. (U)
14. Maki, R. L., and Embry, U. R.: Effects of High-Lift Devices and Horizontal-Tail Location on the Low-Speed Characteristics of a Large-Scale 45° Swept-Wing Airplane Configuration. NACA RM A54E10, 1954. (U)
15. Kelly, M. W., and Tolhurst, W. H., Jr.: The Use of Area Suction to Increase the Effectiveness of a Trailing-Edge Flap on a Triangular Wing of Aspect Ratio 2. NACA RM A54A25, 1954. (U)
16. Fink, M. P., and Cocke, B. W.: A Low-Speed Investigation of the Aerodynamic Control, and Hinge-Moment Characteristics of Two Types of Controls and Balancing Tabs on a Large-Scale Thin Delta-Wing – Fuselage Model. NACA RM L54B03, 1954. (U)
17. Lock, R. C., Ross, J. G., and Meiklem, P.: Wind-Tunnel Tests on a 90°-Apex Delta Wing of Variable Aspect Ratio (Sweepback 36.8°). Part II – Measurements of Downwash and Effect of High Lift Devices. ARC CP 83, 1948. (U)
18. Trouncer, J., and Moss, G. F.: Low-Speed Wind-Tunnel Tests on Two 45 Degree Sweptback Wings of Aspect Ratios 4.5 and 3.0 (Models A and B) ARC R&M 2710, 1953. (U)
19. Franks, R. W.: Tests in the Ames 40- by 80-foot Wind Tunnel of Two Airplane Models Having Aspect Ratio 2 Trapezoidal Wings of Taper Ratios 0.33 and 0.20. NACA RM A52L16, 1953. (U)
20. Riebe, J. M., and MacLeod, R. G.: Low-Speed Wind-Tunnel Investigation of a Thin 60° Delta Wing with Double Slotted, Single Slotted, Plain, and Split Flaps. NACA RM L52J29, 1953. (U)
21. Riebe, J. M., and Graven, J. C., Jr.: Low-Speed Investigation of the Effects of Location of a Delta and a Straight Tail on the Longitudinal Stability and Control of a Thin Delta Wing with Extended Double Slotted Flaps. NACA RM L53J26, 1954. (U)
22. Guryansky, E. R., and Lipson, S.: Effect of High-Lift Devices on the Longitudinal and Lateral Characteristics of a 45° Sweptback Wing with Symmetrical Circular-Arc Sections. NACA RM 1RD06, 1948. (U)
23. Foster, G. V., Mollenberg, E. F., and Woods, R. L.: Low-Speed Longitudinal Characteristics of an Unswept Hexagonal Wing with and without a Fuselage and a Horizontal Tail Located at Various Positions at Reynolds Numbers from  $2.8 \times 10^6$  to  $7.6 \times 10^6$ . NACA RM L52L11b, 1953. (U)

24. Pratt, G. L., and Shields, E. R.: Low-Speed Longitudinal Characteristics of a  $45^0$  Sweptback Wing of Aspect Ratio 8 with High-Lift and Stall-Control Devices at Reynolds Numbers from 1,500,000 to 4,800,000. NACA L51J04, 1952. (U)
25. Franks, R. W.: Tests in the Ames 40- by 80-Foot Wind Tunnel of an Airplane Model with an Aspect Ratio 4 Triangular Wing and an All-Movable Horizontal Tail — High Lift Devices and Lateral Controls. NACA A52K13, 1953. (U)
26. Weiberg, J. A., and Page, V. R.: Large-Scale Wind-Tunnel Tests of an Airplane Model with an Unswept, Aspect Ratio-10 Wing, Four Propellers, and Blowing Flaps. NASA TN D-25, 1959. (U)
27. Goodson, K. W., and Few, A. G., Jr.: Low-Speed Static Longitudinal and Lateral Stability Characteristics of a Model with Leading-Edge Chord-Extensions Incorporated on a  $40^0$  Sweptback Circular-Arc Wing of Aspect Ratio 4 and Taper Ratio 0.50. NACA RM L52I18, 1952. (U)
28. Griner, R. F., and Foster, G. V.: Low-Speed Longitudinal and Wake Air-Flow Characteristics at a Reynolds Number of  $6.0 \times 10^6$  of a  $52^0$  Sweptback Wing Equipped with Various Spans of Leading-Edge and Trailing-Edge Flaps, a Fuselage, and a Horizontal Tail at Various Vertical Positions. NACA RM L50K29, 1951. (U)
29. Salmi, R. J.: Horizontal-Tail Effectiveness and Downwash Surveys for Two  $47.7^0$  Sweptback Wing-Fuselage Combinations with Aspect Ratios of 5.1 and 6.0 at a Reynolds Number of  $6.0 \times 10^6$ . NACA RM L50K06, 1951. (U)
30. Foster, G. V., and Griner, R. F.: Low-Speed Longitudinal and Wake Air-Flow Characteristics at a Reynolds Number of  $5.5 \times 10^6$  of a Circular-Arc  $52^0$  Sweptback Wing with a Fuselage and a Horizontal Tail at Various Vertical Positions. NACA RM L51C30, 1951. (U)
31. Tinling, B. E., and Lopez, A. E.: The Effects of Nacelles and of Extended Split Flaps on the Longitudinal Characteristics of a Wing-Fuselage-Tail Combination Having a Wing with  $40^0$  of Sweepback and an Aspect Ratio of 10. NACA RM A53D06, 1953. (U)
32. Spooner, S. H., and Mollenberg, E. F.: Positioning Investigation of Single Slotted Flaps on a  $47.4^0$  Sweptback Wing at Reynolds Numbers of  $4.0 \times 10^6$  and  $6.0 \times 10^6$ . NACA RM L50H29, 1950. (U)
33. Riebe, J. M., and Graven, J. C., Jr.: Low-Speed Investigation of the Effects of Location of a Delta Horizontal Tail on the Longitudinal Stability and Control of a Fuselage and Thin Delta Wing with Double Slotted Flaps Including the Effects of a Ground Board. NACA RM L53H19a, 1953. (U)
34. Anderson, A. E.: An Investigation at Low Speed of a Large-Scale Triangular Wing of Aspect Ratio Two — II. The Effect of Airfoil Section Modifications and the Determination of the Wake Downwash. NACA RM A7H28, 1947. (U)
35. Mollenberg, E. F. and Spooner, S. H.: Low-Speed Investigation of the Effects of Single Slotted and Double Slotted Flaps on a  $47.7^0$  Sweptback-Wing-Fuselage Combination at a Reynolds Number of  $6.0 \times 10^6$ . NACA RM L51E24, 1951. (U)
36. Freeman, D. C., Jr., Parlett, L. P., and Henderson, R. L.: Wind-Tunnel Investigation of a Jet Transport Airplane Configuration with an External-Flow Jet Flap and Inboard Pod-Mounted Engines. NASA TN D-7004, 1970. (U)
37. Smith, C. C., Jr.: Effect of Engine Position and High-Lift Devices on Aerodynamic Characteristics of an External-Flow Jet-Flap STOL Model. NASA TN D-6222, 1971. (U)
38. Alexander, A. J. and Williams, J.: Wind-Tunnel Experiments on a Rectangular-Wing Jet-Flap Model of Aspect-Ratio 6. ARC R&M 3329, 1964. (U)
39. Koenig, D. G., and Corsiglia, V. R.: Aerodynamic Characteristics of a Large-Scale Model with an Unswept Wing and Augmented Jet Flap. NASA TN D-4610, 1968. (U)
40. Campbell, J. P., and Johnson, J. L.: Wind-Tunnel Investigation of an External-Flow Jet-Augmented Slotted Flap Suitable for Application to Airplanes with Pod-Mounted Jet Engines. NACA TN 3898, 1956. (U)
41. Renselaer, D. J., and Kelly, R.: Aerodynamic Design Compendium for Externally Blown Flaps. NA-71-1105, 1971. (U)
42. Krichbaum, G., Letsinger, G., May, F. W., Morell, E. J., and Vincent, J. H.: State of the Art Design Compendium — STOL Aerodynamic Technology (Vectorized Thrust and Mechanical Flaps), Boeing D180-14239-1, 1971. (U)
43. May, F. W.: State of the Art Design Compendium — STOL Aerodynamic Technology (Internally Blown Jet Flaps). Boeing, D180-14299-1, 1971. (U)
44. Hebert, J., Jr., et al.: STOL Tactical Aircraft Investigation. Vol II Design Compendium. AFFDL-TR-73-21-Vol II, 1973. (U)

**TABLE 6.1.5.1-A**  
**EFFECT OF FLAP DEFLECTION ON PITCHING MOMENT**  
**DATA SUMMARY AND SUBSTANTIATION**  
**METHOD 1 SUBSONIC**

Ref.	A	$\lambda$	$\Delta c/4$ (deg)	t/c	Flap Type	$\delta_f$ (deg)	$(\Delta C_m)_{\delta_f}$ calc.	$(\Delta C_m)_{\delta_f}$ test	$\Delta(\Delta C_m)_{\delta_f}$ calc.-test
13	3.78	0.586	47.35	0.06	Plain	30	-0.065	-0.04	-0.025
↓	↓	↓	↓	↓		45	-0.087	-0.05	-0.037
14	3.5	0.3	45	0.10	Double Slotted	50	-0.370	-0.280	-0.090
Unpub. data	6.8	0.3	35	0.115	Double Slotted	45	-0.351	-0.418	0.067
15	2.0	0	56.3	0.05	Plain	59	-0.258	-0.185	-0.073
16	2.31	0	52.4	0.03	Plain	30	-0.146	-0.196	0.050
17	3.0	0.143	36.9	0.10	Split	60	-0.228	-0.184	-0.044
18	4.5	0.25	45	0.14	Split	60	-0.091	-0.103	0.012
↓	3.0	↓	↓	↓		↓	-0.150	-0.123	-0.027
19	2.0	0.33	36.87	0.05	Single Slotted	40	-0.329	-0.263	-0.066
↓	↓	0.20	45	↓		↓	-0.330	-0.260	-0.070
20	2.31	0	52.4	0.03	Plain	54	-0.254	-0.165	-0.089
↓	↓	↓	↓	↓		↓	-0.154	-0.164	0.010
21	2.31	0	52.4	0.03	Single Slotted	59.75	-0.252	-0.172	-0.080
↓	↓	↓	↓	↓	Double Slotted	64	-0.547	-0.413	-0.134
21	2.31	0	52.4	0.03	Single Slotted	40.3	-0.249	-0.336	0.087
22	3.5	0.5	44.9	0.074	Double Slotted	61.3	-0.440	-0.622	0.182
↓	↓	↓	↓	↓	Plain	52.2	-0.092	-0.072	-0.020
23	2.5	0.625	5.27	0.06	Plain	50	-0.031	-0.089	0.058
↓	↓	↓	↓	↓		↓	-0.221	-0.151	-0.070
24	8.0	0.45	45	0.12	Split	50	-0.068	-0.008	-0.060
25	4.0	0	36.9	0.05	Single Slotted	40	-0.244	-0.153	-0.091
26	9.86	0.5	0	0.17	Plain	40	-0.080	-0.170	0.090
27	4.0	0.5	40	0.08	Plain	41.7	-0.063	-0.060	-0.003
28	2.88	0.625	50.24	0.08	Split	48.1	-0.033	-0.021	-0.012
↓	↓	↓	↓	↓		↓	-0.072	-0.082	0.010
29	5.1	0.383	45.35	0.075	Split	50.8	-0.028	-0.080	-0.041
↓	6.0	0.313	↓	↓		↓	-0.039	-0.020	-0.008
↓	5.1	0.383	↓	↓	Double Slotted	36.5	-0.114	-0.050	-0.064
↓	6.0	0.313	↓	↓		↓	-0.078	-0.087	0.009
30	2.84	0.616	49.9	0.053	Split	49.3	-0.103	-0.135	0.032
↓	↓	↓	↓	↓		↓	-0.029	-0.033	0.004
31	10.0	0.4	40	0.10	Split	23.86	-0.023	+0.010	-0.033
↓	↓	↓	↓	↓		↓	+0.027	+0.039	-0.012
32	5.1	0.383	44.6	0.075	Single Slotted	30.7	-0.063	-0.074	0.011
33	2.31	0	52.4	0.03	Double Slotted	40.3	-0.303	-0.328	0.025
34	2.0	0	56.3	0.05	Split	44.5	-0.229	-0.174	-0.055

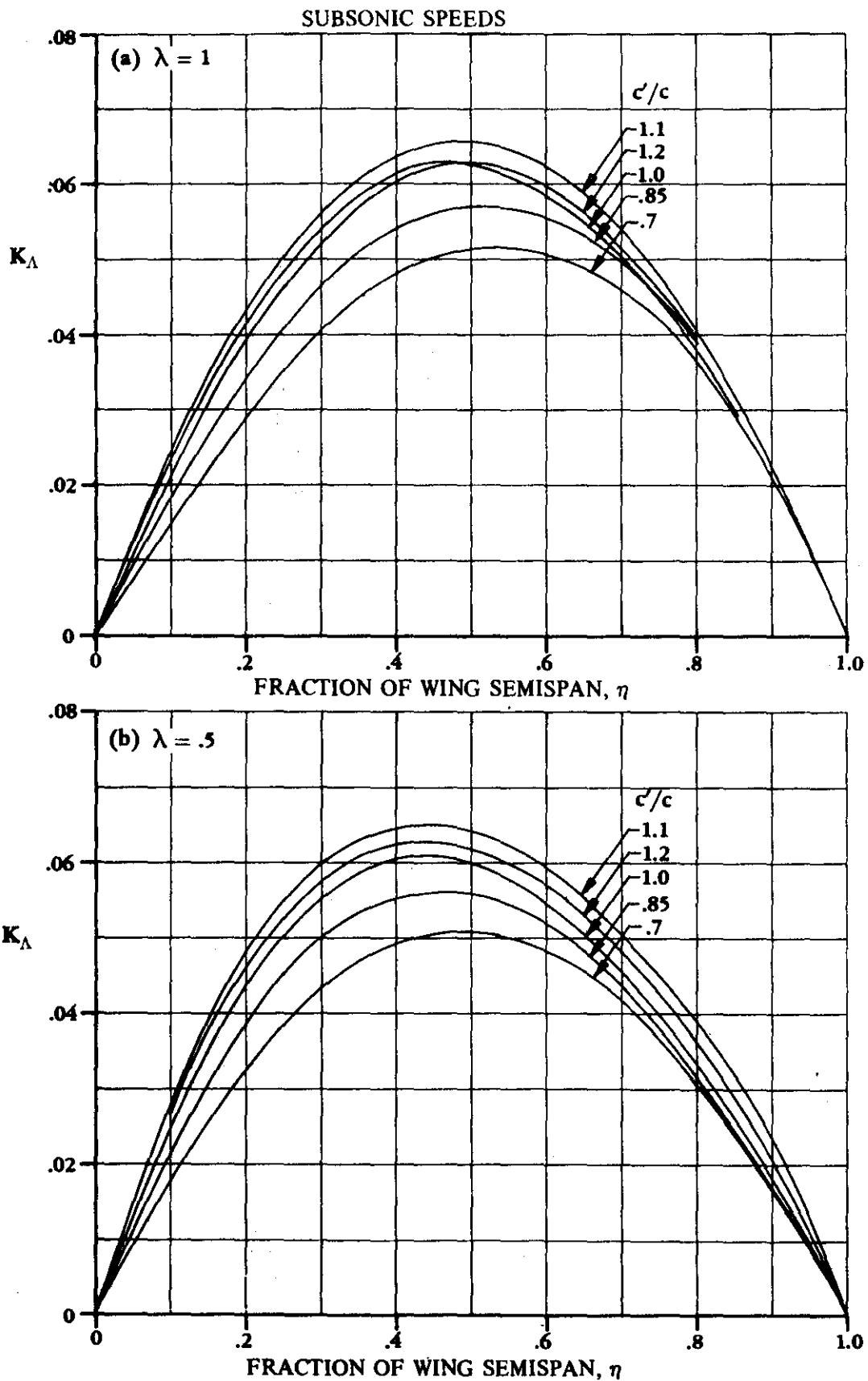


FIGURE 6.1.5.1-57 SPAN FACTOR FOR SWEPT WINGS

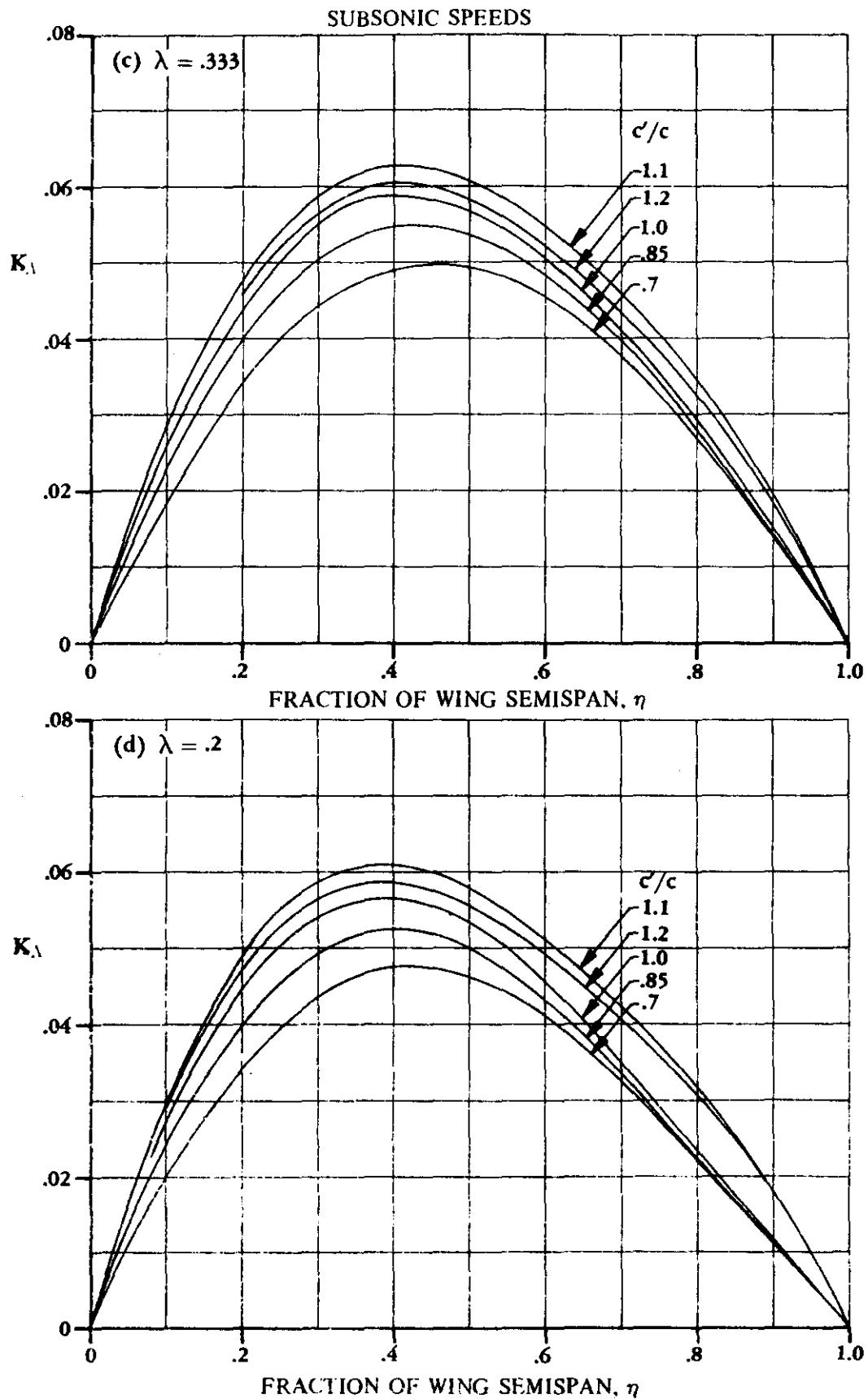
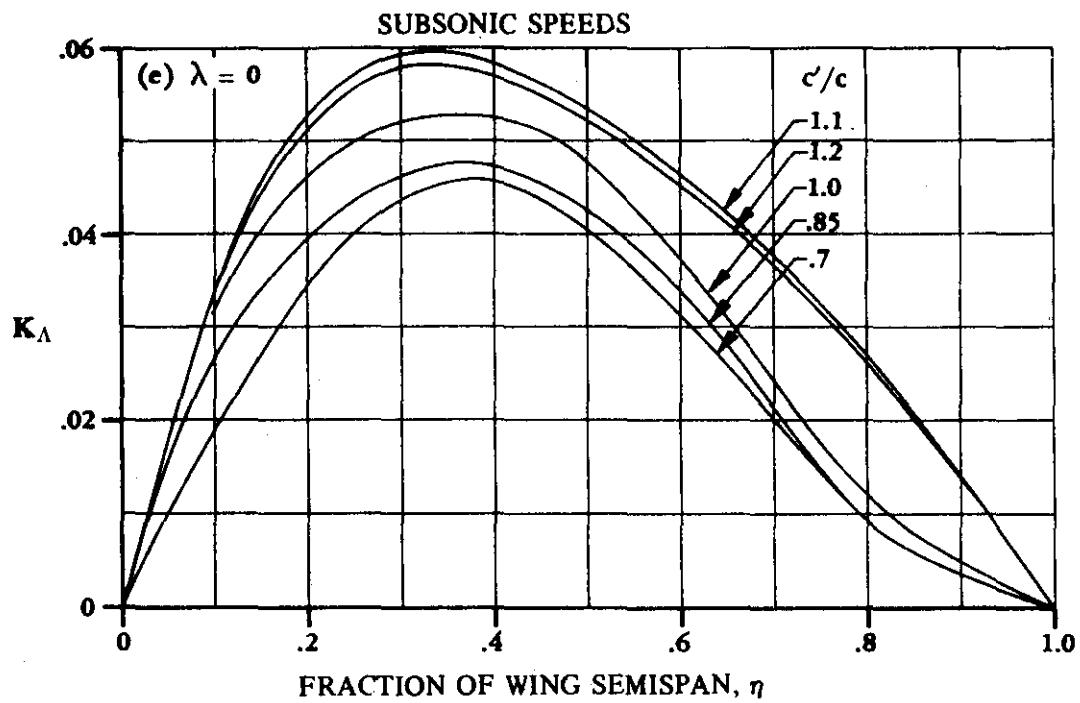


FIGURE 6.1.5.1-57 (CONT'D)



**FIGURE 6.1.5.1-57 (CONTD)**

SUBSONIC SPEEDS

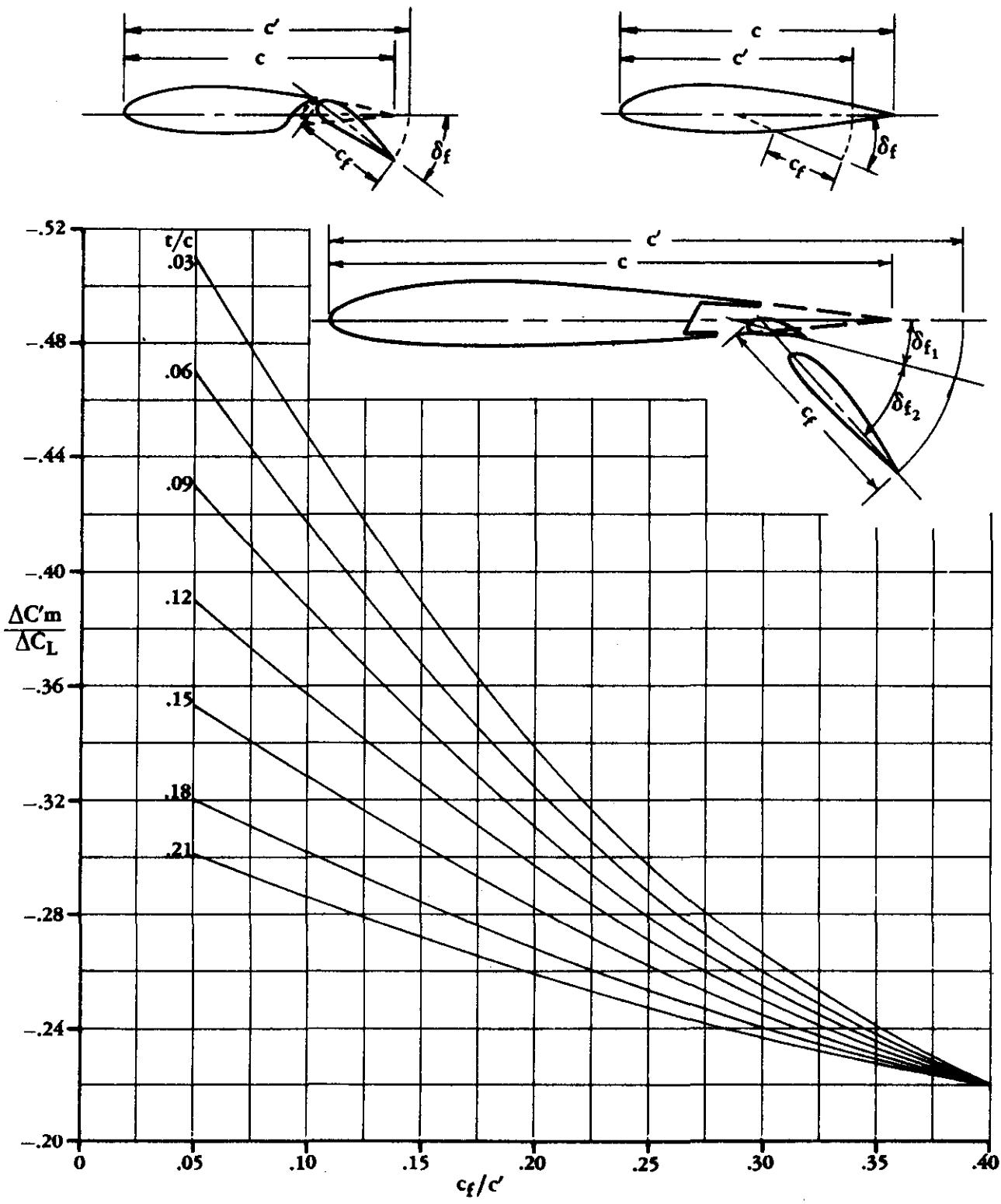
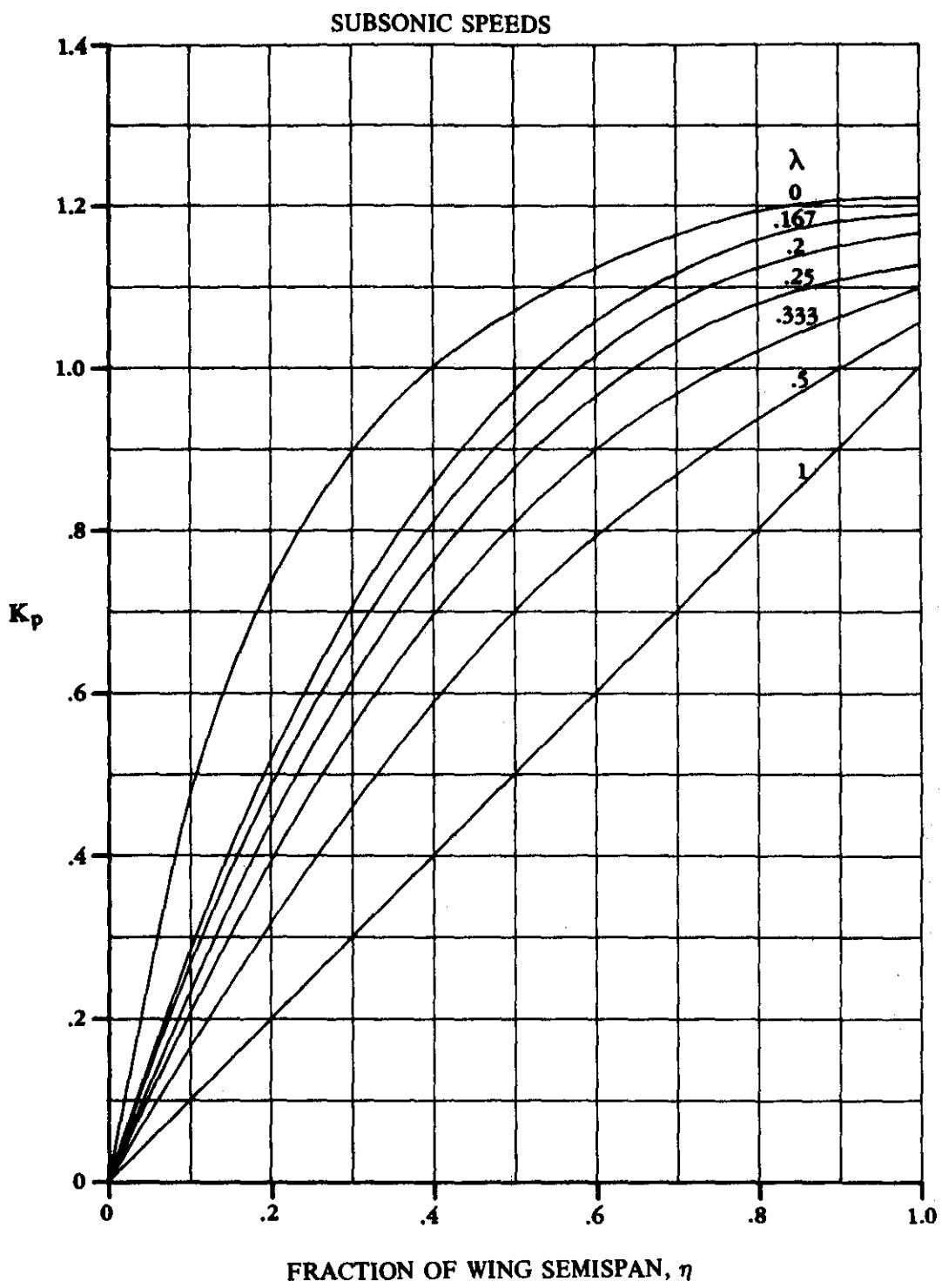


FIGURE 6.1.5.1-60 RATIO OF PITCHING-MOMENT-COEFFICIENT INCREMENT TO LIFT-COEFFICIENT INCREMENT DUE TO FLAPS FOR UNSWEPT WINGS



**FIGURE 6.1.5.1-61 CONVERSION FACTOR FOR PARTIAL-SPAN FLAPS**

SUBSONIC SPEEDS

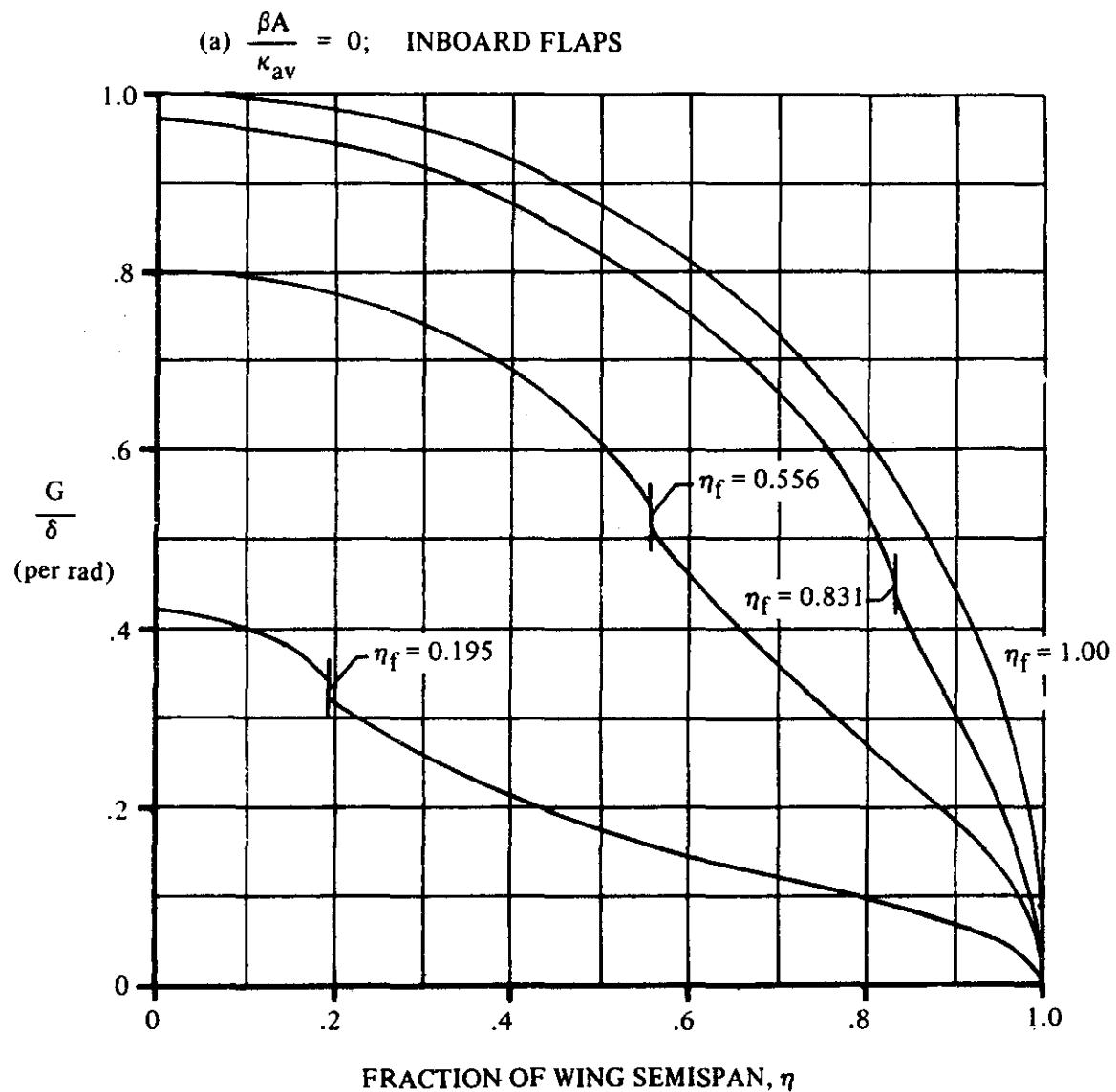


FIGURE 6.1.5.1-62 SPANWISE LOAD DISTRIBUTION DUE TO SYMMETRIC FLAP DEFLECTION FOR STRAIGHT-TAPERED WING.  $c_f/c = 1$ .

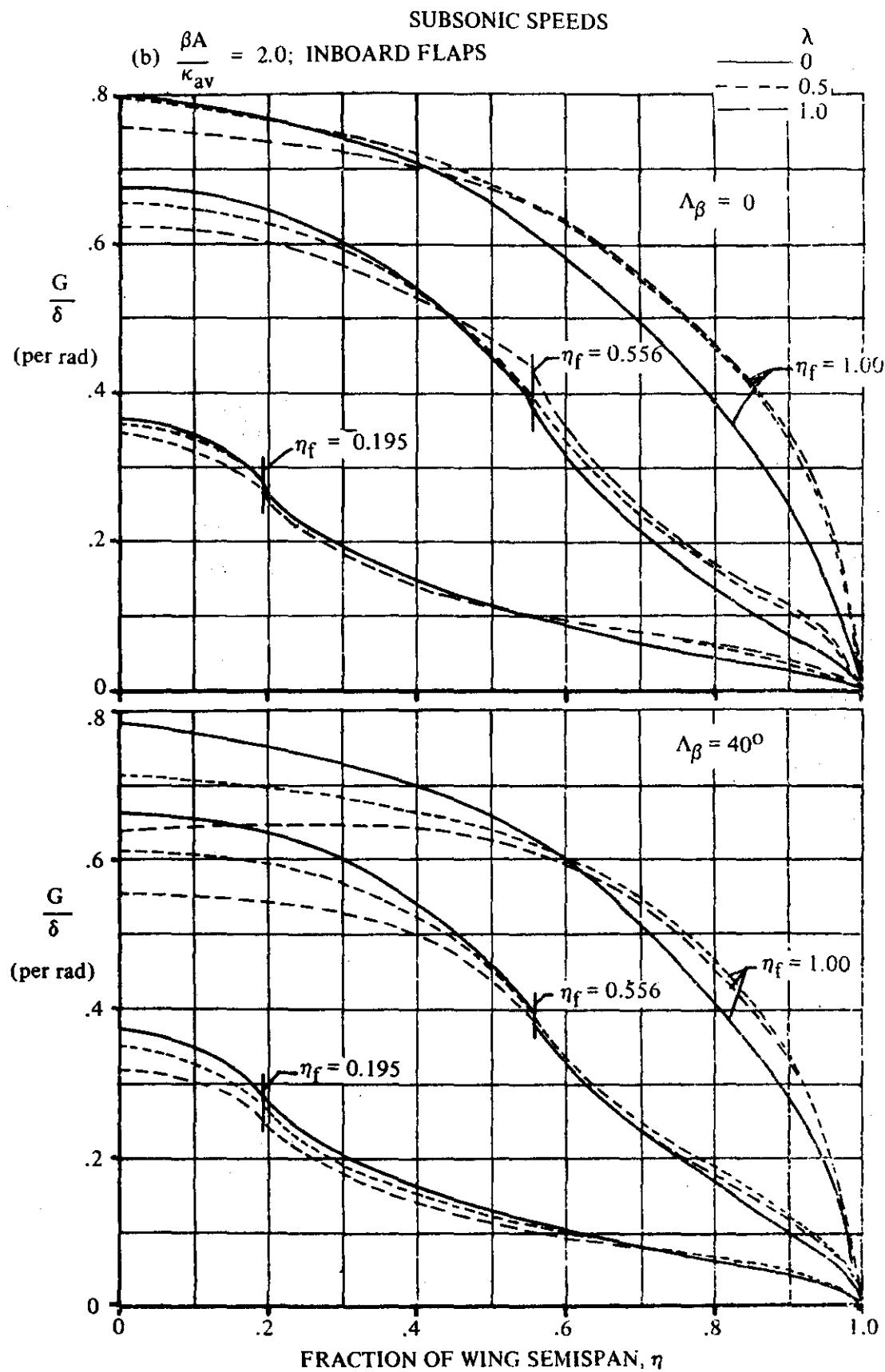


FIGURE 6.1.5.1-62 (CONTD)

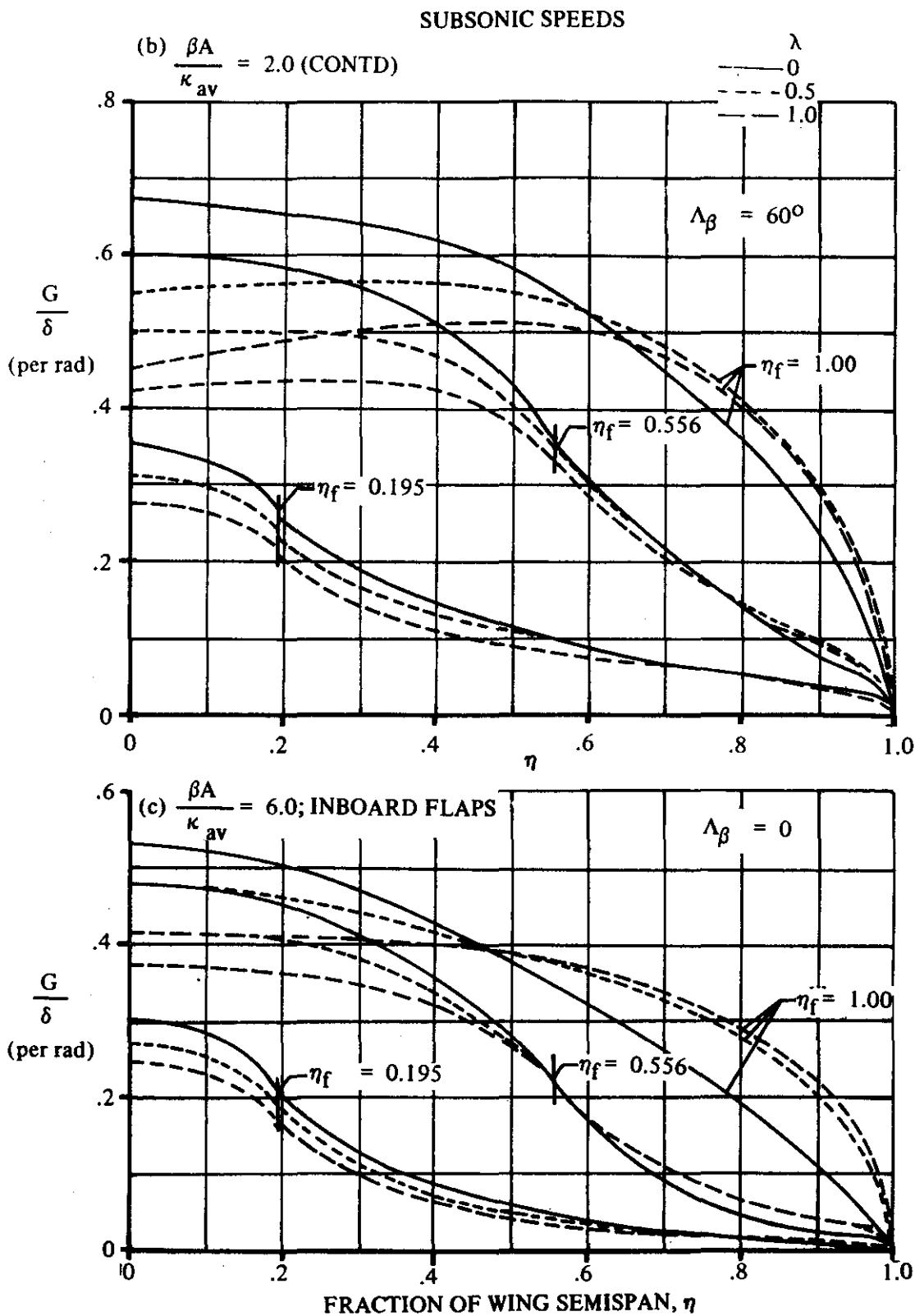


FIGURE 6.1.5.1-62 (CONTD)

SUBSONIC SPEEDS

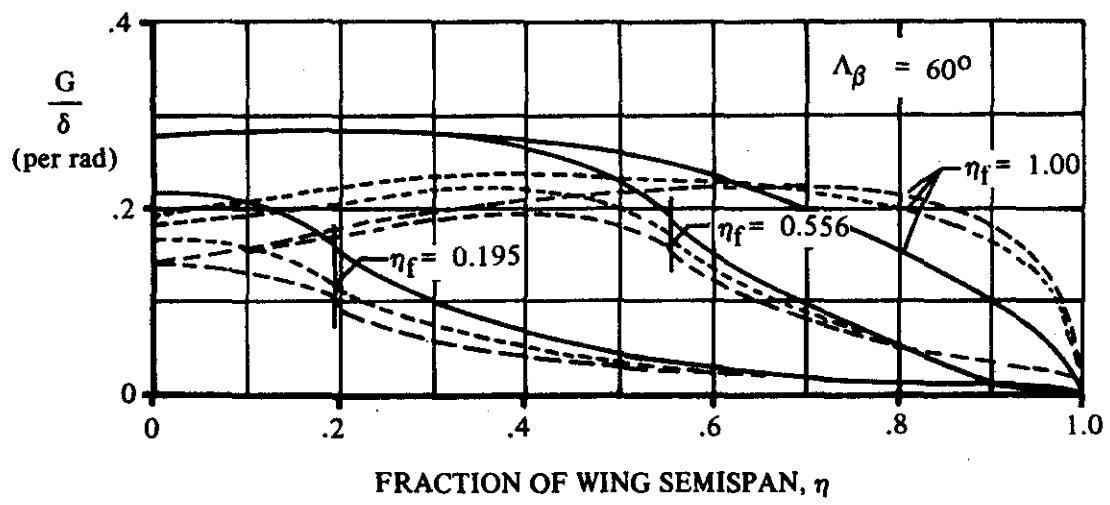
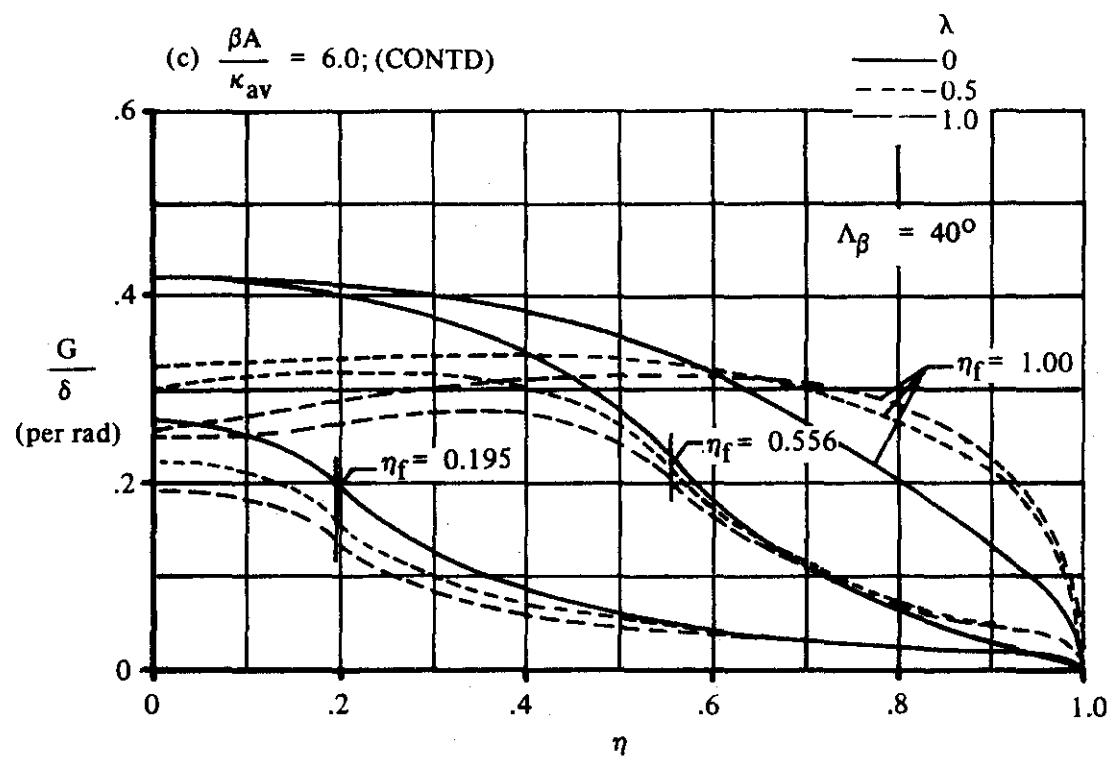


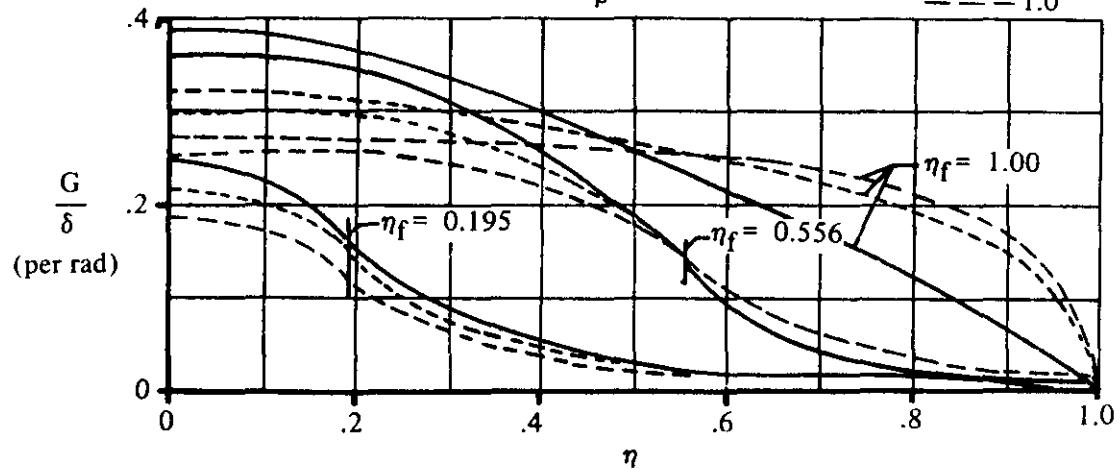
FIGURE 6.1.5.1-62 (CONTD)

SUBSONIC SPEEDS

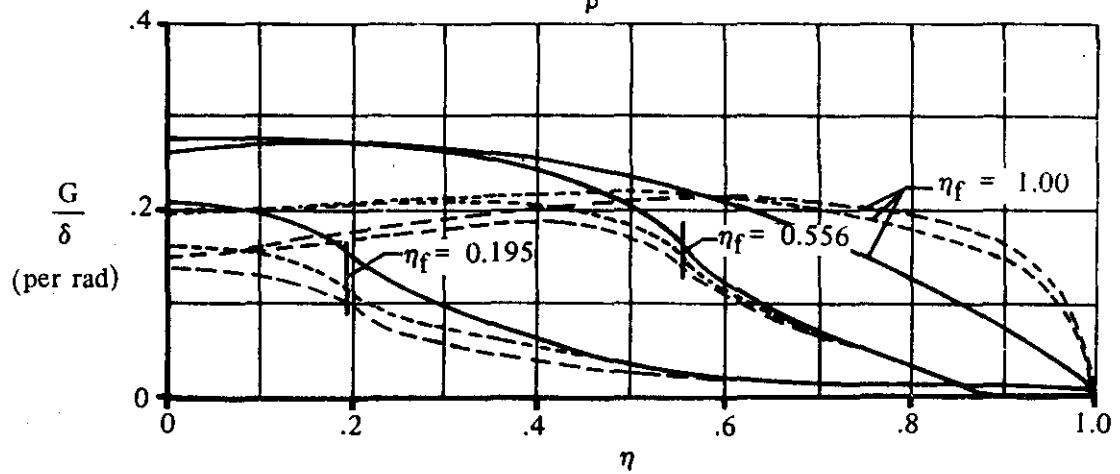
(d)  $\frac{\beta A}{\kappa_{av}} = 10.0$ ; INBOARD FLAPS

$\Lambda_\beta = 0$

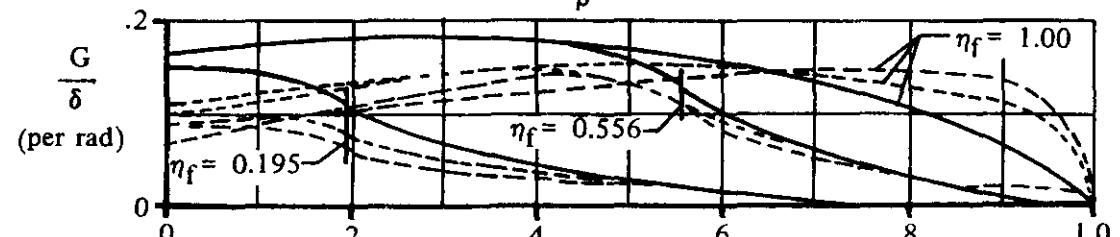
$\lambda$   
— 0  
- - - 0.5  
- - - 1.0



$\Lambda_\beta = 40^\circ$



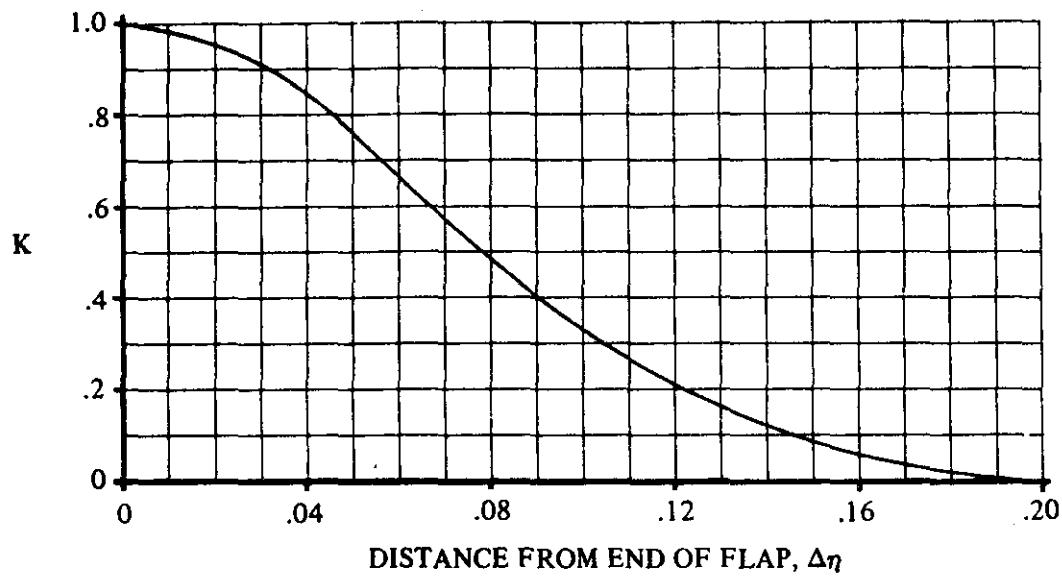
$\Lambda_\beta = 60^\circ$



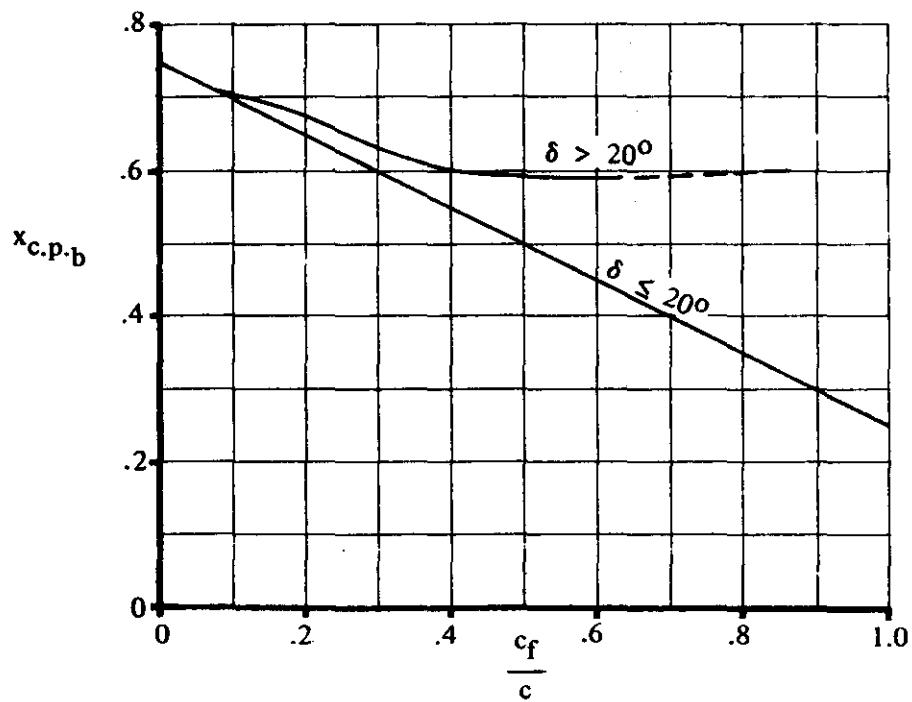
FRACTION OF WING SEMISPAN,  $\eta$

FIGURE 6.1.5.1-62 (CONTD)

SUBSONIC SPEEDS



**FIGURE 6.1.5.1-67a** ESTIMATION OF SECTION CENTER-OF-PRESSURE LOCATION FOR UNFLAPPED SECTIONS NEAR END OF FLAPS



**FIGURE 6.1.5.1-67b** VARIATION OF SECTION-BASIC-LOADING CENTER OF PRESSURE WITH FLAP-CHORD RATIO

6.1.5.1-68

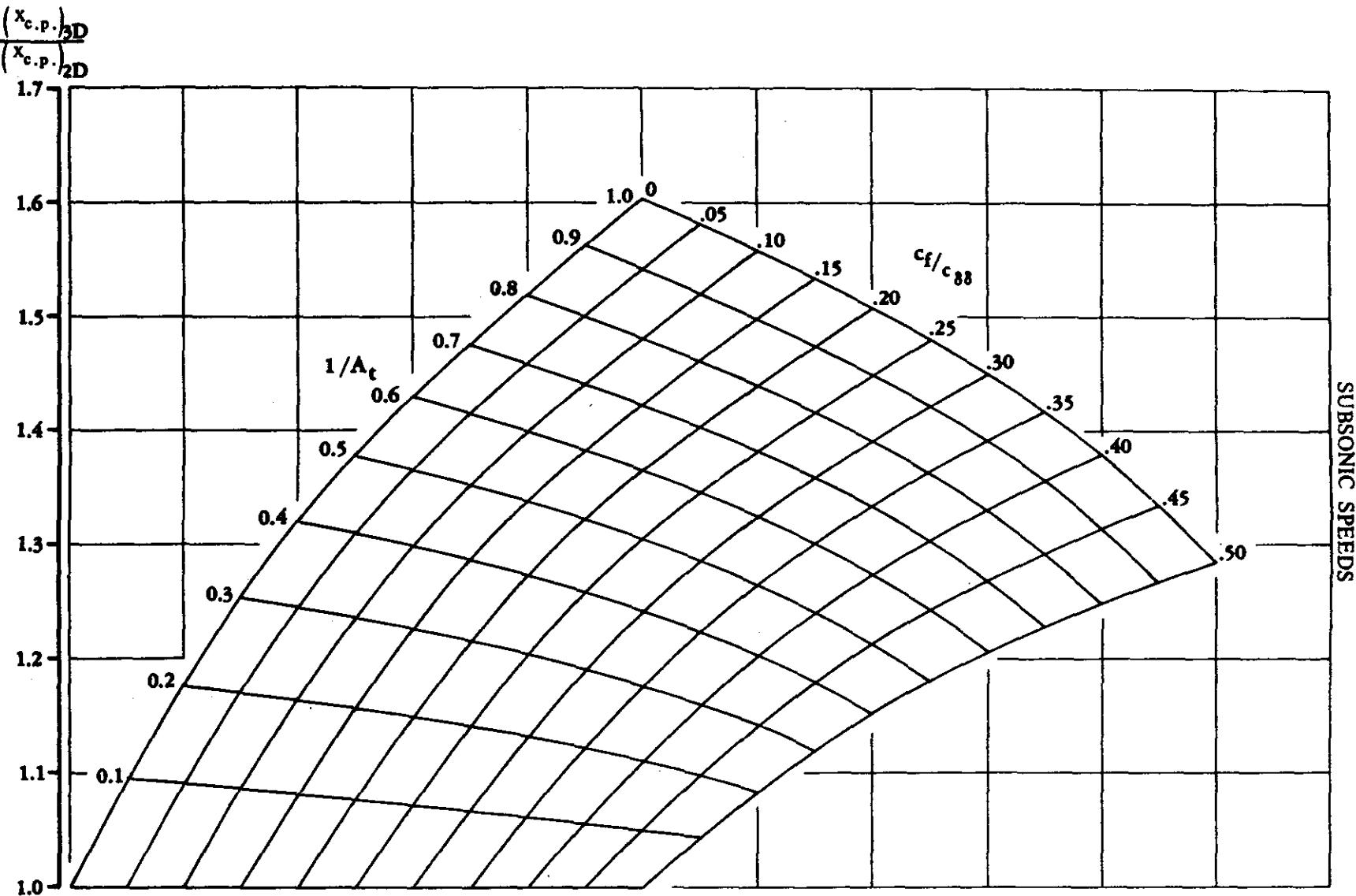
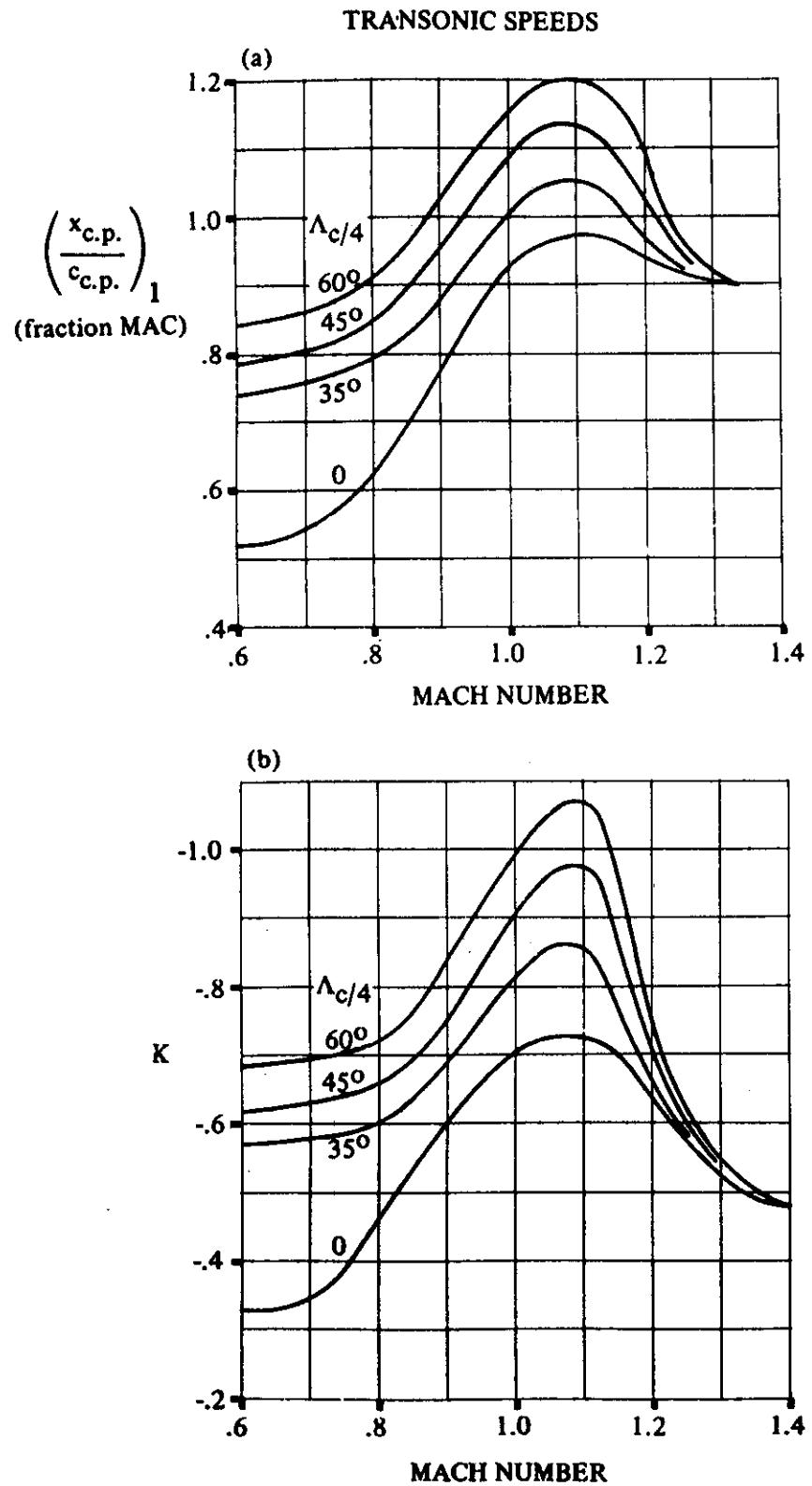
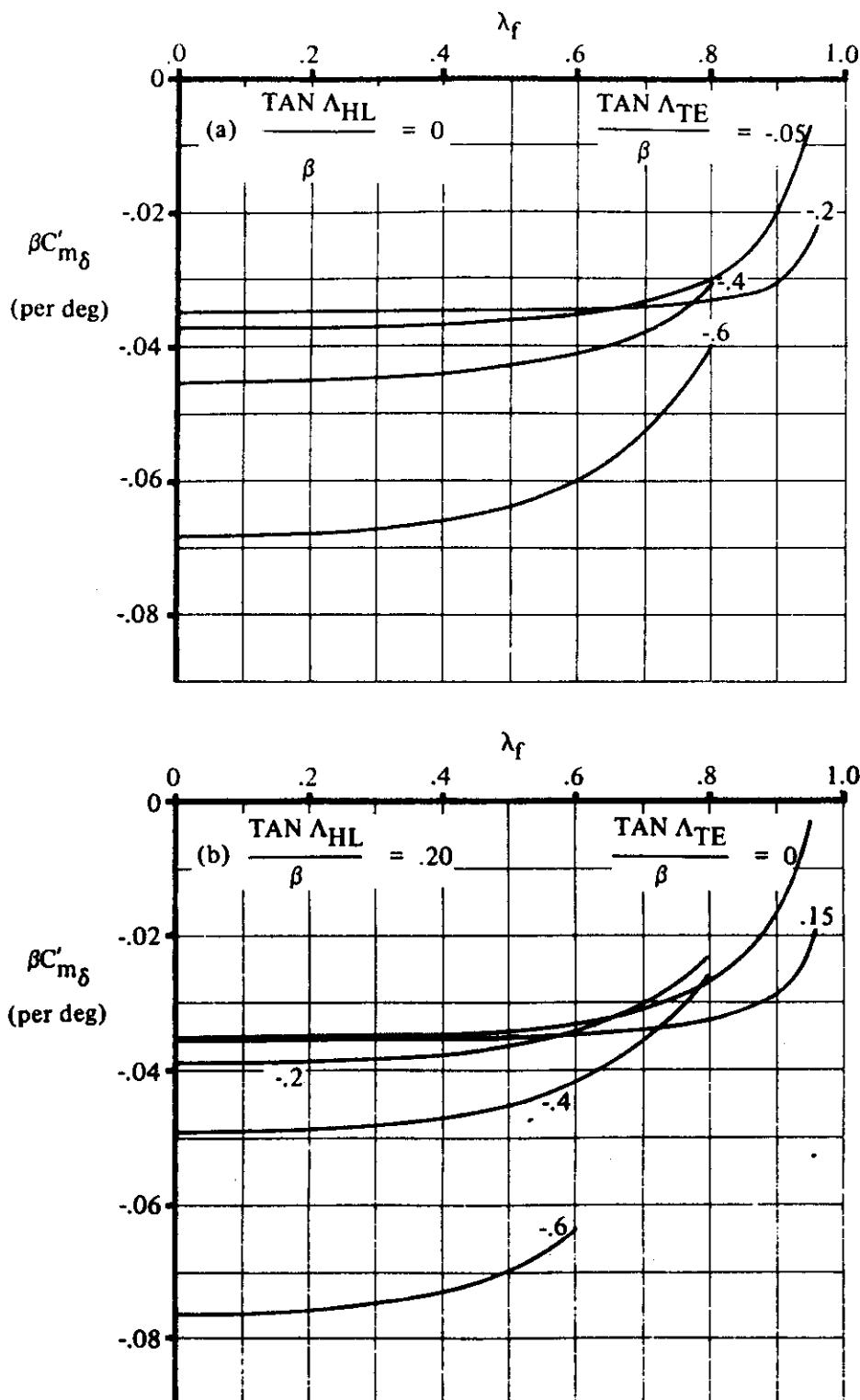


FIGURE 6.1.5.1-68 RATIO OF CENTER OF PRESSURE LOCATION FOR A WING  
TO CENTER OF PRESSURE LOCATION FOR AN AIRFOIL



**FIGURE 6.1.5.1-69 TRANSONIC CONTROL-SURFACE PITCH-EFFECTIVENESS PARAMETERS**

SUPersonic SPEEDS



**FIGURE 6.1.5.1-70 PITCHING-MOMENT DERIVATIVE FOR TAPERED CONTROL SURFACES HAVING OUTBOARD EDGE COINCIDENT WITH WING TIP**

SUPersonic SPEEDS

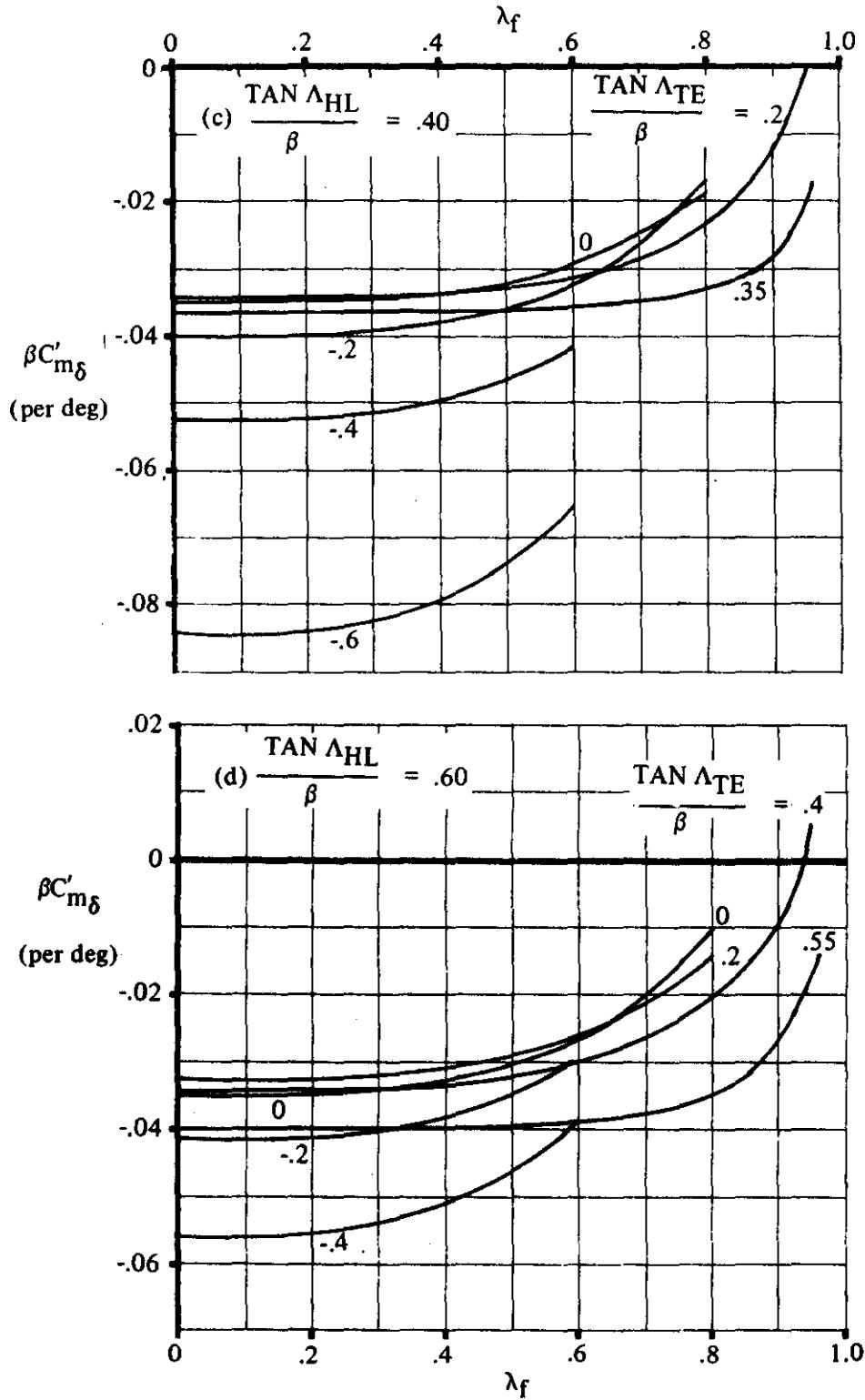
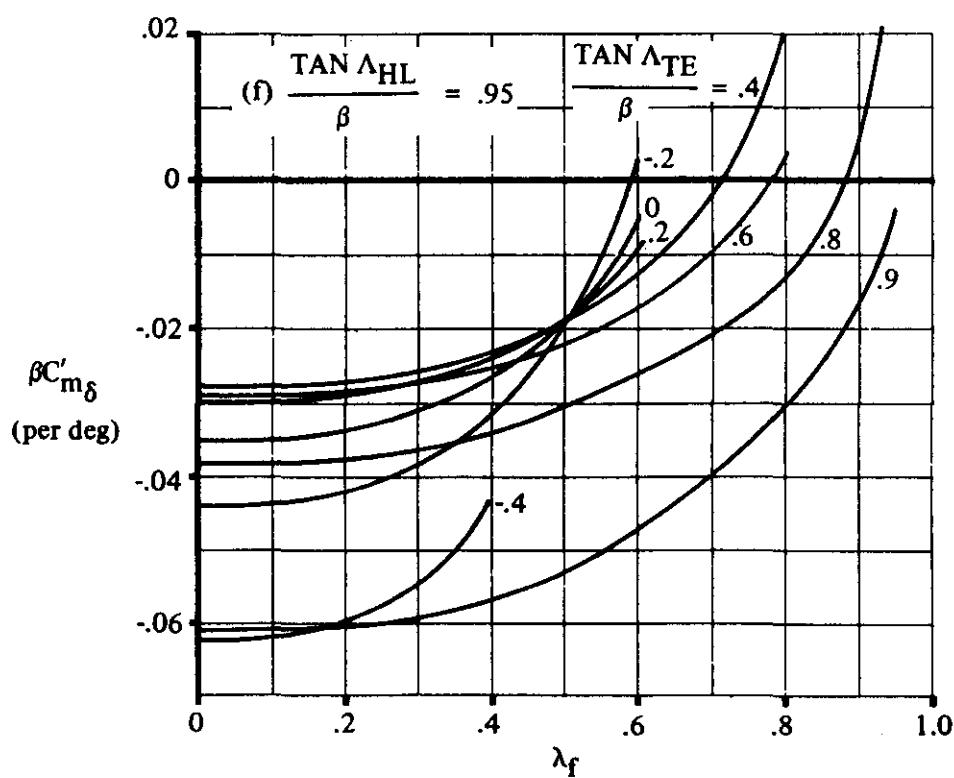
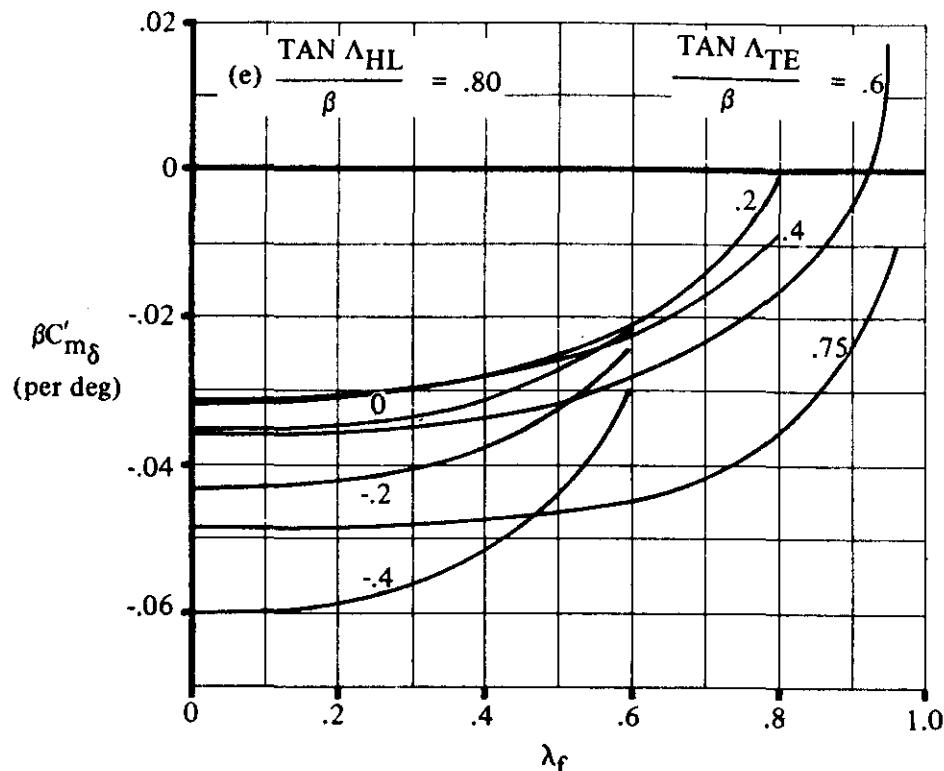


FIGURE 6.1.5.1-70 (CONTD)

**SUPersonic SPEEDS**



**FIGURE 6.1.5.1-70 (CONT'D)**

SUPersonic SPEEDS

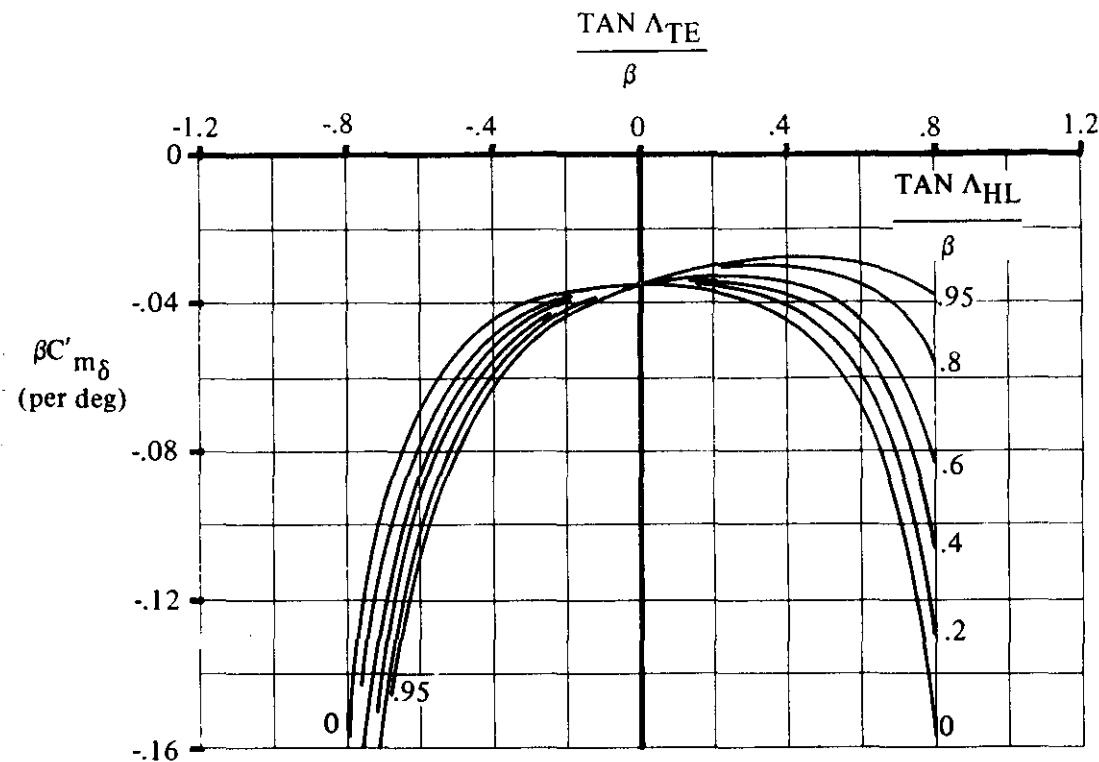


FIGURE 6.1.5.1-73a PITCHING-MOMENT DERIVATIVE FOR TAPERED AND UNTAPERED TRAILING-EDGE FLAPS HAVING OUTBOARD EDGE NOT COINCIDENT WITH WING TIP

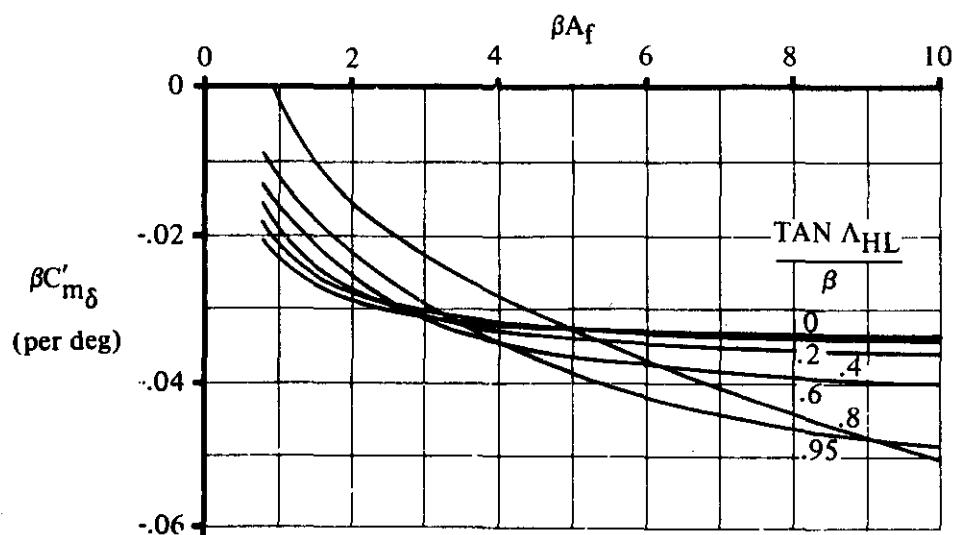


FIGURE 6.1.5.1-73b PITCHING-MOMENT DERIVATIVE FOR UNTAPERED TRAILING-EDGE CONTROL SURFACES LOCATED AT THE WING TIP

### 6.1.5.2 WING DERIVATIVE $C_{m_\alpha}$ WITH HIGH-LIFT AND CONTROL DEVICES

#### Mechanical Flaps

According to lifting-line or lifting-surface theory, camber, such as that due to flaps, does not affect the variation of pitching moment with angle of attack over the region where there is no flow separation. The theory is substantiated by experiment over the linear angle-of-attack and flap-deflection ranges (References 1 and 2).

Theoretically, the pitching-moment-curve slope of both wings and airfoils is affected by leading- and/or trailing-edge flaps that extend beyond the basic airfoil chord. However, the changes in  $C_{m_\alpha}$  for airfoils (as predicted by linear theory) cannot be substantiated with test data (see Section 6.1.2.2). In addition, the effect of extended flaps on  $C_{m_\alpha}$  for a wing of finite aspect ratio is not treated in detail in any of the literature surveyed for Datcom. Therefore, no method is presented to account for the effects of extended flaps on  $C_{m_\alpha}$ .

#### Jet Flaps

The aerodynamic-center location for a wing with a jet flap is dependent upon the trailing-edge jet momentum coefficient  $C_m$  and upon the extent to which leading- and trailing-edge flaps extend beyond the basic wing.

Considerations of clarity and simplicity of presentation dictated a deviation from normal Datcom practice in that the effect of jet flaps on  $C_{m_\alpha}$  was included in Section 6.1.5.1, which deals with the pitching-moment increment  $\Delta C_m$ .

### DATCOM METHOD

#### 1. Mechanical Flaps

The variation of wing pitching moment with angle of attack for various flap deflections is assumed to be the same as that for zero flap deflection over the linear-lift range (see Section 6.1.3, particularly Figure 6.1.3-2).

#### 2. Jet Flaps

The variation of pitching moment with angle of attack for wings equipped with jet flaps is covered in the jet-flap method of Section 6.1.5.1. The range of applicability and the limitations of the method are discussed there and in Sections 6.1.1.1 and 6.1.2.1.

### REFERENCES

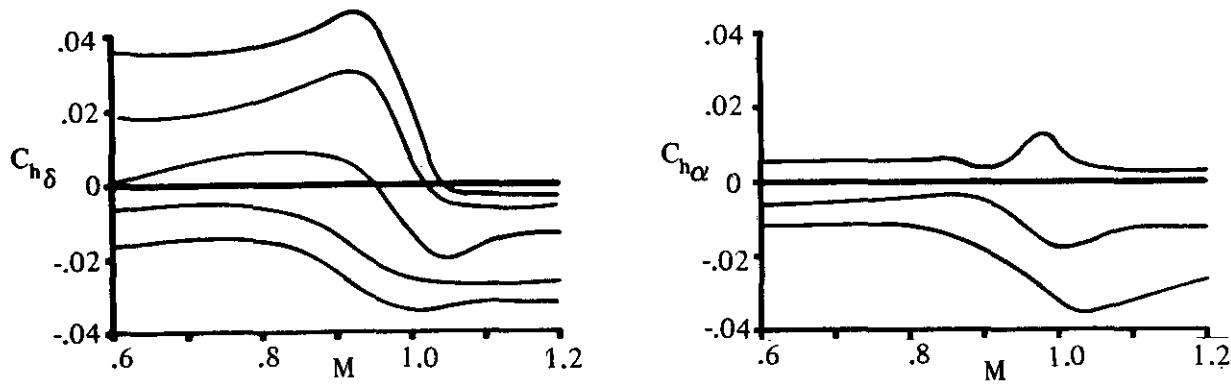
1. Boyd, J. W., and Pfyl, F. A.: Experimental Investigation of Aerodynamically Balanced Trailing-Edge Control Surfaces on an Aspect Ratio 2 Triangular Wing at Subsonic and Supersonic Speeds. NACA RM A52L04, 1953. (U)
2. Furlong, G. C., and McHugh, J. G.: A Summary and Analysis of the Low-Speed Longitudinal Characteristics of Swept Wings at High Reynolds Number. NACA TR 1339, 1957. (U)

### 6.1.6 HINGE MOMENTS OF HIGH-LIFT AND CONTROL DEVICES

This section presents approximate methods for determining hinge-moment derivatives at subsonic and supersonic speeds. At subsonic speeds the method, based on lifting-line theory, is believed to be of sufficient accuracy to be used for preliminary-design work. This method is best suited for higher-aspect-ratio wings.

The methods presented for supersonic speeds have one stringent restriction: the leading edges of the wing planform must be swept ahead of the Mach lines. The methods are based on conical-flow solutions. Since hinge-moment variation with Mach number at transonic speeds becomes somewhat erratic, no method is presented for calculating transonic hinge moments. However, some trends in the transonic range can be noted from References 1 through 4. As the critical Mach number is passed, a shock forms on the upper surface of the airfoil and moves rearward with increasing Mach number. The airfoil pressure distribution changes from one that is approximately triangular, with a peak negative pressure forward, to one more nearly rectangular, with lower pressures at the trailing edge. In general, this causes hinge moments to become more negative. Sketch (a) presents some typical hinge-moment-derivative variations with Mach number.

It should be noted that in the more normal or stable case, where  $C_{h\alpha}$  and  $C_{h\delta}$  are negative at subsonic speeds, hinge-moment derivatives decrease in a somewhat regular fashion through the transonic range and then increase slightly to their supersonic value. Most of the very erratic variations of  $C_{h\alpha}$  and  $C_{h\delta}$  occur when these values are near zero or positive at subsonic speeds. It can also be seen that in the transonic region some hinge-moment derivatives can change sign.



SKETCH (a)

### REFERENCES

- Thompson, R. F.: Investigation of a 42.7° Sweptback Wing Model to Determine the Effects of Trailing - Edge Thickness on the Aileron Hinge-Moment and Flutter Characteristics at Transonic Speeds. NACA RM L50J06, 1950. (U)
- Lord, D. R., and Czarnecki, K. R.: Recent Information on Flap and Tip Controls. NACA RM L53I17a, 1953. (U)
- Thompson, R.F.: Hinge-Moment, Lift, and Pitching-Moment Characteristics of a Flap-Type Control Surface Having Various Hinge-Line Locations on a 4-Percent-Thick 60° Delta Wing – Transonic Bump Method. NACA RM L54B08, 1954. (U)
- Hieser, G.: Transonic Investigation of the Effectiveness and Loading Characteristics of a Flap-Type Aileron With and Without Paddle Balances on an Unswept-Wing–Fuselage Model. NACA RM L56B02, 1956. (U)
- Runkel, J. F., and Hieser, G.: Normal-Force and Hinge-Moment Characteristics at Transonic Speeds of Flap-Type Ailerons at Three Spanwise Locations on a 4-Percent-thick Sweptback-Wing—Body Model and Pressure-Distribution Measurements on an Inboard Aileron. NACA RM L57I23, 1957. (U)

### 6.1.6.1 HINGE-MOMENT DERIVATIVE $C_{h_\alpha}$ OF HIGH-LIFT AND CONTROL DEVICES

#### A. SUBSONIC

The hinge-moment derivative due to angle of attack can be approximated from the method of Reference 1. The method is based on lifting-line theory, with additional lifting-surface corrections to account for sweep.

The method is based on equations in terms of section parameters; therefore, the accuracy of the method is dependent upon the accuracy with which the section characteristics can be estimated. Test data on the particular airfoil-flap combination under consideration or one closely resembling it should always be preferred to characteristics obtained from generalized methods. Calculated values and test data for several different configurations are presented in Table 6.1.6.1-A to illustrate the accuracy of the method and summarize available test data.

The method is directly applicable to control surfaces having constant chord ratios and constant airfoil contours across the span. For configurations with variable chord ratios or variable airfoil contours across the span, it is suggested that average values of the section characteristics be used. Furthermore, the accuracy of the method in predicting the effects of finite-wing parameters decreases as the wing aspect ratio decreases. Application of the method to wings with aspect ratios of three or less should be avoided.

Experimental data have shown that for sweptback wings the shape of the ends of the control surface can have a critical effect on the hinge-moment parameters. The Datcom method is applicable to controls with the control-surface ends cut parallel to the plane of symmetry. For configurations with wing cutouts, or with control surfaces that do not have ends parallel to the plane of symmetry, it is suggested that empirical procedures be used to estimate  $C_{h_\alpha}$ .

The effect of subcritical Mach-number corrections on hinge moments appears to be small for control surfaces having trailing-edge angles less than approximately 12°. Therefore the Datcom method, which neglects subcritical Mach-number effects, may be applied over a large portion of the subcritical Mach-number range.

#### DATCOM METHOD

The hinge-moment derivative due to angle of attack of a sealed, plain trailing-edge control at subsonic speeds, based on the product of the control-surface area and the control-surface chord  $S_c c_c$  (area and chord aft of the hinge line), is approximated by

$$C_{h_\alpha} = \frac{A \cos \Lambda_{c/4}}{A + 2 \cos \Lambda_{c/4}} \left( C_{h_\alpha} \right)_{\text{balance}} + \Delta C_{h_\alpha} \quad 6.1.6.1-a$$

where

$\left( C_{h_\alpha} \right)_{\text{balance}}$  is the section hinge-moment derivative due to angle of attack. Test data on the particular flapped airfoil are preferred, but the derivative can be approximated by the method of Paragraph A of Section 6.1.3.1. (This term could be  $c'_{h_\alpha}$  or  $c''_{h_\alpha}$  from Section 6.1.3.1.)

6.1.6.1-1

$\Delta C_{h_\alpha}$  is an approximate lifting-surface correction which accounts for induced-camber effects.

It is obtained by multiplying the quantity  $\frac{\Delta C_{h_\alpha}}{c_{\ell_\alpha} B_2 K_\alpha \cos \Lambda_{c/4}}$ , from Figure 6.1.6.1-19a, by its denominator

where

$c_{\ell_\alpha}$  is the airfoil section lift-curve slope obtained by using the method of Section 4.1.1.2.

$B_2$  accounts for the effect of control-surface and balance chord ratios. This parameter is obtained from Figure 6.1.6.1-19c. The primed values of the control-surface and balance chord ratios, used in reading Figure 6.1.6.1-19c, refer to measurements normal to the wing quarter-chord line.

$K_\alpha$  accounts for the effect of control-surface span. This parameter is defined by

$$K_\alpha = \frac{(K_\alpha)_{\eta_i} (1 - \eta_i) + (K_\alpha)_{\eta_o} (1 - \eta_o)}{\eta_o - \eta_i} \quad 6.1.6.1-b$$

where

$\eta_i$  is the inboard span station of the control,  
 $\eta_i = \frac{\text{inboard span ordinate}}{b/2}$

$(K_\alpha)_{\eta_i}$  is obtained from Figure 6.1.6.1-19b as a function of the inboard spanwise location ( $\eta_i$ ) of the control panel.

$\eta_o$  is the outboard span station of the control,  
 $\eta_o = \frac{\text{outboard span ordinate}}{b/2}$

$(K_\alpha)_{\eta_o}$  is obtained from Figure 6.1.6.1-19b as a function of the outboard spanwise location ( $\eta_o$ ) of the control panel.

### Sample Problem

Given: The flapped wing configuration of Reference 8

Wing Characteristics:

$$A = 3.43 \quad \lambda = 0.44 \quad \Lambda_{c/4} = 48.7^\circ$$

$$t/c = 0.086 \text{ (streamwise)}$$

$$\tan \frac{\phi'_{TE}}{2} = 0.0697 \text{ (streamwise)}$$

$$\tan \frac{\phi''_{TE}}{2} = 0.0523 \text{ (streamwise)}$$

NACA 65-012 airfoil (normal to .50c of unswept wing)

Flap Characteristics:

Plain trailing-edge flap	Sealed gap	$\Lambda_{HL} = 41^\circ$
$c_f/c = 0.167$ (streamwise)	$c'_f/c' = 0.20$ (normal to .25c)	
$c_b/c_f = 0.090$ (streamwise)	$c'_b/c'_f = 0.115$ (normal to .25c)	
$t_c/(2c_f) = 0.090$ (streamwise)	Round-nosed control	
$\eta_i = 0.586$	$\eta_o = 0.99$	

Additional Characteristics:

$$\text{Low speed } R_\ell = 2.2 \times 10^6$$

Compute:

Section hinge-moment derivative  $c_{h\alpha}$  (Section 6.1.3.1)

$$(c_{h\alpha})_{\text{theory}} = -0.384 \text{ per rad} \quad (\text{Figure 6.1.3.1-11b})$$

$$\frac{c_{h\alpha}}{(c_{h\alpha})_{\text{theory}}} = 0.855 \quad (\text{Figure 4.1.1.2-8a})$$

$$\frac{c'_{h\alpha}}{(c_{h\alpha})_{\text{theory}}} = 0.600 \quad (\text{Figure 6.1.3.1-11a})$$

$$c'_{h\alpha} = \left[ \frac{c'_{h\alpha}}{(c_{h\alpha})_{\text{theory}}} \right] (c_{h\alpha})_{\text{theory}} \quad (\text{Equation 6.1.3.1-a})$$

$$= (0.600)(-0.384) = -0.230 \text{ per rad}$$

$$(c_{h\alpha})_{\text{theory}} = 6.715 \text{ per rad} \quad (\text{Figure 4.1.1.2-8b})$$

$$\text{Balance ratio} = \sqrt{\left(\frac{c_b}{c_f}\right)^2 - \left(\frac{t_c}{2c_f}\right)^2} = 0 \quad (\text{Equation 6.1.3.1-d})$$

$$(c_{h\alpha})_{\text{balance}} / c''_{h\alpha} = 1.0 \quad (\text{Figure 6.1.3.1-12a})$$

$$c''_{h\alpha} = c'_{h\alpha} + 2 \left( c_{l\alpha} \right)_{\text{theory}} \left[ 1 - \frac{c_{l\alpha}}{\left( c_{l\alpha} \right)_{\text{theory}}} \right] \left( \tan \frac{\phi''_{TE}}{2} \cdot \frac{t}{c} \right) \quad (\text{Equation 6.1.3.1-b})$$

$$= -0.230 + 2 (6.715) [1 - 0.855] (0.0523 - 0.086)$$

$$= -0.296 \text{ per rad} = -0.00516 \text{ per deg}$$

$$\left( c_{h\alpha} \right)_{\text{balance}} = c''_{h\alpha} \left[ \left( c_{h\alpha} \right)_{\text{balance}} / c''_{h\alpha} \right] \quad (\text{Equation 6.1.3.1-c})$$

$$= -0.00516 \text{ per deg}$$

Induced camber effect  $\Delta C_{h\alpha}$

$$c_{l\alpha} = \frac{1.05}{\beta} \left[ \frac{c_{l\alpha}}{\left( c_{l\alpha} \right)_{\text{theory}}} \right] \left( c_{l\alpha} \right)_{\text{theory}} \quad (\text{Equation 4.1.1.2-a})$$

$$= \left( \frac{1.05}{1.0} \right) (0.855) (6.715)$$

$$= 6.03 \text{ per rad}$$

$$= 0.105 \text{ per deg}$$

$$B_2 = 0.885 \quad (\text{Figure 6.1.6.1-19c})$$

$$\left. \begin{array}{l} (K_\alpha)_{\eta_i} = 2.18 \\ (K_\alpha)_{\eta_o} = 4.20 \end{array} \right\} \quad (\text{Figure 6.1.6.1-19b})$$

$$K_\alpha = \frac{(K_\alpha)_{\eta_i} (1 - \eta_i) - (K_\alpha)_{\eta_o} (1 - \eta_o)}{\eta_o - \eta_i} \quad (\text{Equation 6.1.6.1-b})$$

$$= \frac{(2.18)(1 - 0.586) - (4.20)(1 - 0.99)}{0.99 - 0.586}$$

$$= 2.13$$

$$c_{l\alpha} B_2 K_\alpha \cos \Lambda_{c/4} = (0.105)(0.885)(2.13)(0.66) = 0.1306 \text{ per deg}$$

$$\frac{\Delta C_{h\alpha}}{c_{l\alpha} B_2 K_\alpha \cos \Lambda_{c/4}} = 0.0125 \quad (\text{Figure 6.1.6.1-19a})$$

$$\Delta C_{h\alpha} = (0.0125)(0.1306) = 0.00163 \text{ per deg}$$

Solution:

$$\begin{aligned} C_{h\alpha} &= \frac{A \cos \Lambda_{c/4}}{A + 2 \cos \Lambda_{c/4}} (C_{h\alpha})_{\text{balance}} + \Delta C_{h\alpha} \quad (\text{Equation 6.1.6.1-a}) \\ &= \frac{(3.43)(0.6600)}{(3.43) + (2)(0.6600)} (-0.00516) + 0.00163 \\ &= -0.00083 \text{ per deg} \end{aligned}$$

This compares with a test value of  $-0.0014$  per degree from Reference 8.

## B. TRANSONIC

No method is available for the prediction of the hinge-moment derivative  $C_{h\alpha}$  at transonic speeds. Because of the mixed-flow conditions and interrelated shock-wave and boundary-layer-separation effects encountered at transonic speeds, the prediction of  $C_{h\alpha}$  by theoretical means is extremely difficult. Experimental results for  $C_{h\alpha}$  at transonic speeds are presented in References 2 through 5.

## C. SUPERSONIC

The supersonic three-dimensional hinge moment due to angle of attack can be computed for trailing-edge control surfaces by the method presented in Reference 6. The method is based on linearized theory and applies to tapered and untapered trailing-edge control surfaces, with the following restrictions:

1. Control root and tip chords are parallel to the plane of symmetry.
2. Wing planform has leading edges swept ahead of the Mach lines and has streamwise tips.
3. Controls are not influenced by the tip conical flow from the opposite wing panel or by the interaction of the wing-root Mach cone with the wing tip.

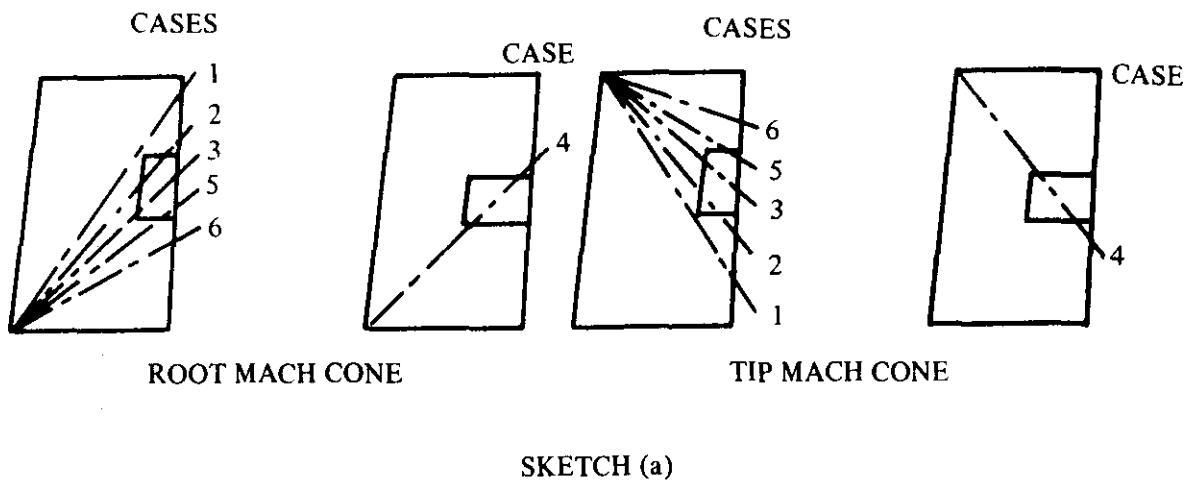
Calculated values and test data for several different configurations are presented in Table 6.1.6.1-B to illustrate the accuracy of the method and summarize available test data.

For leading-edge control surfaces or for trailing-edge control surfaces with subsonic leading edges, reverse-flow techniques (see Reference 7) can be used.

## DATCOM METHOD

The method consists of determining the pressure-area-moment for an infinitely thin flat-plate control by assuming two-dimensional loading and then subtracting the losses in loading resulting from the interference of the wing-root and wing-tip conical flows.

Combinations of wing-root and wing-tip conical-flow cases for a typical wing-planform-control configuration are illustrated by the relative positions of the Mach lines in Sketch (a).



For a given Mach number and wing-control combination (which determines the wing-root and wing-tip conical-flow case), the conical-flow losses are obtained by dividing the conical regions into a series of triangular segments, each having its origin at the apex of the Mach cone, and summing the loss in pressure-area-moment  $P'S_L x$  for those segments. The procedure to be followed in summing  $P'S_L x$  for the triangular segments is illustrated for the most general wing-root and wing-tip conical-flow case (Case 1) in Figure 6.1.6.1-21. Table 6.1.6.1-C is a general computing form for summing a pressure-area-moment parameter representing a loss in loading from the two-dimensional loading of the triangular segments of the conical-flow region defined by Case 1.

Figure 6.1.6.1-21 and Table 6.1.6.1-C can be adapted to compute the pressure-area-moment parameter for wing-root and wing-tip conical-flow Cases 2 through 5 by determining the proper regions that will be affected by the Mach cones. For wing-root and wing-tip conical-flow Case 6, there is no loss in loading from the two-dimensional loading value.

The hinge-moment derivative  $C_{h_\alpha}$  at supersonic speeds for a symmetric, straight-sided control, based on the product of the control-surface area and the control-surface chord  $S_c c_c$  (area and chord aft of hinge line), is given by

$$\left( C_{h_\alpha} \right)_{t/c} = \left( 1 - \frac{C_2}{C_1} \phi_{TE} \right) \left( C_{h_\alpha} \right)_{t/c = 0} \quad 6.1.6.1-c$$

where

$\left( 1 - \frac{C_2}{C_1} \phi_{TE} \right)$  is a thickness correction factor to the supersonic flat-plate derivative.

$$C_1 = \frac{2}{\sqrt{M^2 - 1}} \quad \text{per radian}$$

$$C_2 = \frac{(\gamma + 1) M^4 - 4(M^2 - 1)}{2(M^2 - 1)^2} \quad \text{per radian}$$

$\phi_{TE}$  is the trailing-edge angle in radians, measured normal to the control hinge line.

$\gamma$  is the ratio of specific heats,  $\gamma = 1.4$ .

For a symmetrical biconvex airfoil the thickness correction factor in Equation 6.1.6.1-c is

$$1 - \frac{2 C_2 \left( \frac{t}{c} \right)' }{3 C_1 (1 + k) \cos(\Lambda_{LE} - \Lambda_{HL})} \left\{ 2 \left[ 1 + 2 \left( \frac{x_h}{c} \right)' \right] - k \left[ 1 - \left( \frac{x_h}{c} \right)' \right]^2 \right\}$$

where

$\left( \frac{t}{c} \right)'$  is the maximum airfoil-thickness ratio, measured in a plane normal to the control hinge axis.

$\left( \frac{x_h}{c} \right)'$  is the chordwise location of the control hinge axis, measured in a plane normal to the control hinge axis.

$$k = \tan(\Lambda_{LE} - \Lambda_{HL}) \tan(\Lambda_{LE} - \Lambda_{TE})$$

Thickness correction factors for other airfoil sections can be determined from Reference 6.

$(C_h \alpha)_{t/c = 0}$  is the supersonic flat-plate hinge-moment derivative.

The procedure for calculating  $(C_h \alpha)_{t/c = 0}$  is outlined in the following steps:

**Step 1.** Construct the wing-root and wing-tip Mach lines on a layout of the wing-control configuration, and determine the wing-root and wing-tip conical-flow case by referring to Sketch (a).

If the wing-root and wing-tip conical-flow case is Case 6, there is no loss of loading from the two-dimensional value. For this case calculate  $\beta$  and  $g$  as presented in Step 2, then

$$(C_h \alpha)_{t/c = 0} = \frac{-2}{57.3 \beta \sqrt{1 - g^2}} \quad (\text{per degree}) \quad 6.1.6.1-d$$

**Step 2.** Compute the following geometric and Mach-number parameters (see Sketch (b)):

$$\beta = \sqrt{M^2 - 1}$$

$$g = \frac{\tan \Lambda_{LE}}{\beta}$$

$$a = \frac{\tan \Lambda_{HL}}{\beta}$$

$$d = \frac{\tan \Lambda_{TE}}{\beta}$$

$$K_1 = \beta y_o$$

$$K_2 = \beta y_i$$

$$K_3 = \beta \left( \frac{b}{2} - y_i \right)$$

$$K_4 = \beta \left( \frac{b}{2} - y_o \right)$$

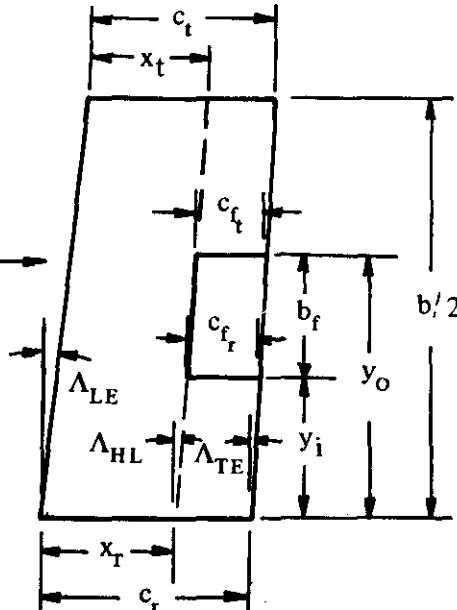
$$K_5 = \beta (y_o)^2$$

$$K_6 = \frac{1}{\beta (1 - d)}$$

$$K_7 = \frac{1}{\beta (1 - a)}$$

$$K_8 = \beta (y_i)^2$$

$$K_9 = \beta \left( \frac{b}{2} - y_i \right)^2$$



SKETCH (b)

$$K_{10} = \frac{1}{\beta (1 + d)}$$

$$K_{11} = \frac{1}{\beta (1 + a)}$$

$$K_{12} = \beta \left( \frac{b}{2} - y_o \right)^2$$

Step 3. Determine the regions (triangular segments numbered ① through ⑧ on Figure 6.1.6.1-21) that are affected by the wing-root and wing-tip conical-flow case determined in Step 1.

The regions affected for each case are:

Conical-Flow Case (Sketch (a))	Wing-Root and Wing-Tip Conical Flow Regions Affected
1	1, 2, 3, 4, 5, 6, 7, 8
2	1, 3, 4, 5, 7, 8
3	3, 5, 7, 8
4	1, 3, 4, 7
5	3, 7
6	None

Step 4. Calculate the pressure-area-moment parameter representing a loss in loading from the two-dimensional loading value for each of the wing-root and wing-tip conical-flow regions affected by using the computing procedure presented in Table 6.1.6.1-C.

Step 5. Sum the values of the pressure-area-moment parameter calculated in Step 4 for the affected regions and obtain  $(C_h \alpha)_{t/c = 0}$  by

$$(C_h \alpha)_{t/c = 0} = \frac{-2}{57.3 \beta \sqrt{1 - g^2}} \left\{ 1 - \frac{\sum P' (3x \sqrt{1 + \beta^2 a^2}) 2S_L}{2M_a [3\sqrt{1 + \beta^2 a^2}]} \right\} \text{(per deg)} \quad 6.1.6.1-e$$

where

$$2M_a [3 \sqrt{1 + \beta^2 a^2}] = b_f \frac{(c_{f_r})^3 - (c_{f_t})^3}{c_{f_r} - c_{f_t}} \quad 6.1.6.1-f$$

for tapered controls, and

$$2M_a [3 \sqrt{1 + \beta^2 a^2}] = 3 b_f (c_{f_r})^2 \quad 6.1.6.1-g$$

for untapered controls.

#### SYMBOLS AND DEFINITIONS USED IN COMPUTATION OF $(C_h \alpha)_{t/c = 0}$

$n, r'$  nondimensional coordinates used in integration of wing-root and wing-tip conical pressures. Equations are given in column 1 of Table 6.1.6.1-C for calculating  $n$  and  $r'$ . Values of  $n$  are required to enter the design charts for  $P'$  and  $t_{c,p}$  for conical-flow Regions 3, 4, 5, and 6. Values of  $r'$  are required to enter the design charts for  $P'$  and  $t_{c,p}$  for conical-flow Regions 1, 2, 7, and 8.

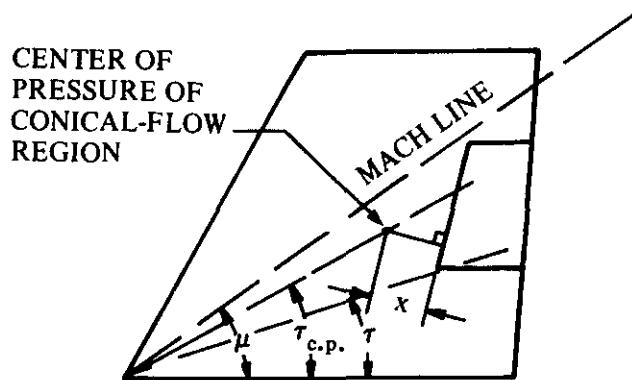
$P'$  the loss of loading of the average value of the local pressure ratio  $(C_p/C_{p_0})$  over the conical-flow region. This parameter is obtained from Figure 6.1.6.1-22 for conical-flow regions intersecting the wing-root Mach cone and from Figure 6.1.6.1-34 for conical-flow regions intersecting the wing-tip Mach cone.

$C_p$  is the pressure coefficient ( $\Delta p/q$ ) for a three-dimensional wing.

$C_{p_0}$  is the two-dimensional pressure coefficient.

$t_{c,p}$  nondimensional parameter used in calculating the moment-arm parameter  $3x \sqrt{1 + \beta^2 a^2}$ .  $t_{c,p}$  is obtained from Figure 6.1.6.1-22 for conical-flow regions intersecting the wing-root Mach cone and from Figure 6.1.6.1-34 for conical-flow regions intersecting the wing-tip Mach cone.

- x distance of the center of loading of a conical-flow region from the control hinge axis measured normal to the hinge axis (see Sketch (c)). Equations are given in Column ④ of Table 6.1.6.1-C for calculating the moment-arm parameter  $3x\sqrt{1 + \beta^2 a^2}$  for the appropriate conical-flow region; hence, explicit values of  $x$  are not required.



SKETCH (c)

$\tau_{c.p.}$  angle of a ray in the conical-flow field which passes through the center of pressure.

$\tau$  angle denoting an arbitrary position of the ray in the conical-flow field.

$S_L$  area of a loaded region. Equations are given in Column ⑤ of Table 6.1.6.1-C for determining  $2S_L$ .

$M_a$  area moment of a control surface about its hinge axis.

$$M_a = \frac{(c_f r)^2 b_f}{6} \cos \Lambda_{HL} (\lambda_f^2 + \lambda_f + 1)$$

where  $\lambda_f$  is the control-surface taper ratio.

$\eta$  angle of sweep of the line intersecting conical-flow regions of the wing at angle of attack. In reading values of  $P'$  and  $\tau_{c.p.}$  from Figures 6.1.6.1-22a through 6.1.6.1-22j, and from Figures 6.1.6.1-34a through 6.1.6.1-34d,  $\eta = \Lambda_{HL}$  for conical-flow Regions 5 and 6, and  $\eta = \Lambda_{TE}$  for conical-flow Regions 3 and 4.

The sample problem below illustrates use of the method for obtaining  $(C_{h\alpha})_{t/c = 0}$

### Sample Problem

Given: A wing-control configuration with the following characteristics:

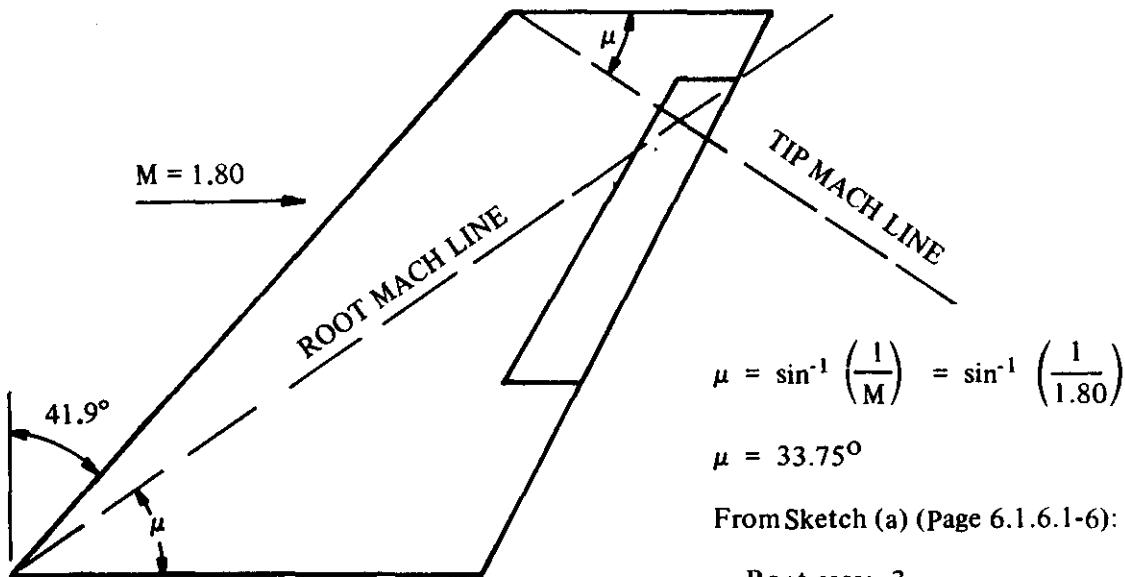
$$\begin{aligned}
 A &= 6.19 & \lambda &= 0.55 & b/2 &= 6.0 \text{ ft} & \Lambda_{LE} &= 41.9^\circ \\
 \Lambda_{TE} &= 27.57^\circ & \Lambda_{HL} &= 30.85^\circ & c_t &= 2.75 \text{ ft} & c_r &= 5.0 \text{ ft} \\
 x_t &= 2.20 \text{ ft} & x_r &= 4.0 \text{ ft} & c_{f_t} &= 0.606 \text{ ft} & c_{f_r} &= 0.850 \text{ ft} \\
 b_f &= 3.25 \text{ ft} & y_i &= 2.0 \text{ ft} & y_o &= 5.25 \text{ ft}
 \end{aligned}$$

Additional Characteristics:

$$M = 1.80; \beta = 1.4967$$

Compute:

Step 1. Determine the wing-root and wing-tip conical-flow case.



Root case: 3

Tip case: 3

Step 2. Compute the required geometric and Mach-number parameters.

$$g = \frac{\tan \Lambda_{LE}}{\beta} = \frac{0.8972}{1.4967} = 0.5995$$

$$a = \frac{\tan \Lambda_{HL}}{\beta} = \frac{0.5973}{1.4967} = 0.3991$$

$$d = \frac{\tan \Lambda_{TE}}{\beta} = \frac{0.5221}{1.4967} = 0.3488$$

$$K_1 = \beta y_o = (1.4967)(5.25) = 7.8577 \text{ ft}$$

$$K_2 = \beta y_i = (1.4967)(2.0) = 2.9934 \text{ ft}$$

$$K_3 = \beta \left( \frac{b}{2} - y_i \right) = (1.4967)(6.0 - 2.0) = 5.9868 \text{ ft}$$

$$K_4 = \beta \left( \frac{b}{2} - y_o \right) = (1.4967)(6.0 - 5.25) = 1.1225 \text{ ft}$$

$$K_5 = \beta (y_o)^2 = (1.4967)(5.25)^2 = 41.2528 \text{ sq ft}$$

$$K_6 = \frac{1}{\beta(1-d)} = \frac{1}{(1.4967)(1-0.3488)} = 1.0260$$

$$K_7 = \frac{1}{\beta(1-a)} = \frac{1}{(1.4967)(1-0.3991)} = 1.1119$$

$$K_8 = \beta (y_i)^2 = (1.4967)(2.0)^2 = 5.9868 \text{ sq ft}$$

$$K_9 = \beta \left( \frac{b}{2} - y_i \right)^2 = (1.4967)(6.0 - 2.0)^2 = 23.9472 \text{ sq ft}$$

$$K_{10} = \frac{1}{\beta(1+d)} = \frac{1}{(1.4967)(1+0.3488)} = 0.4954$$

$$K_{11} = \frac{1}{\beta(1+a)} = \frac{1}{(1.4967)(1+0.3991)} = 0.4775$$

$$K_{12} = \beta \left( \frac{b}{2} - y_o \right)^2 = (1.4967)(6.0 - 5.25)^2 = 0.8419 \text{ sq ft}$$

**Step 3.** Determine the wing-root and wing-tip conical-flow regions affected.

From the chart of Step 3 of the Datcom method the affected wing-root and wing-tip conical-flow regions are: 3, 5, 7, and 8.

**Step 4.** Using the computing form, presented as Table 6.1.6.1-C, calculate the pressure-area-moment parameter representing a loss in loading from the two-dimensional loading value of the affected conical-flow regions.

	(1)	(2)	(3)	(4)	(5)	(6)
Conical-Flow Region	n or r' See Column 1 Table 6.1.6.1-C	p' See Table 6.1.6.1-C	t <sub>c.p.</sub> See Table 6.1.6.1-C	3x $\sqrt{1 + \beta^2 a^2}$ See Column 4 Table 6.1.6.1-C	2S <sub>L</sub> See Column 5 Table 6.1.6.1-C	$p' (3x \sqrt{1 + \beta^2 a^2}) 2S_L$ (cu ft)
ROOT MACH CONE	3	0.6101	0.258	0.736	-2.4978	15.649
	5	0.5503	0.245	-	4.00	9.7901
	7	1.0191	0.300	0.645	5.1073	6.1011
	8	0.7354	0.277	0.695	-5.7755	4.4027
TIP MACH CONE	3	0.4495	0.280	0.662	-0.9512	1.6840
	5	0.2862	0.224	-	2.20	0.6614
	7	1.1011	0.314	0.609	2.0177	0.9270
	8	0.5608	0.236	0.751	-2.7147	0.4721
$\sum p' (3x \sqrt{1 + \beta^2 a^2}) 2S_L = \sum (6) =$						1.9760

Solution:

$$2M_a \left[ 3 \sqrt{1 + \beta^2 a^2} \right] = b_f \frac{(c_{f_r})^3 - (c_{f_t})^3}{c_{f_r} - c_{f_t}} \quad (\text{Equation 6.1.6.1-f})$$

$$= 3.25 \frac{(0.850)^3 - (0.606)^3}{(0.850) - (0.606)} = 5.22 \text{ cu ft}$$

$$\begin{aligned} (C_{h\alpha})_{t/c=0} &= \frac{-2}{57.3 \beta \sqrt{1 - g^2}} \left\{ 1 - \frac{\sum p' (3x \sqrt{1 + \beta^2 a^2}) 2S_L}{2M_a [3 \sqrt{1 + \beta^2 a^2}]} \right\} \\ &= \frac{-2}{(57.3)(1.4967) \left( \sqrt{1 - (0.5995)^2} \right)} \left\{ 1 - \frac{1.9760}{5.22} \right\} \\ &= -0.0181 \text{ per deg} \end{aligned} \quad (\text{Equation 6.1.6.1-e})$$

## REFERENCES

- Toll, T. A., and Schneiter, L. E.: Approximate Relations for Hinge-Moment Parameters of Control Surfaces on Swept wings at Low Mach Numbers. NACA TN 1711, 1948. (U)
- Thompson, R. F.: Hinge-Moment, Lift, and Pitching-Moment Characteristics of a Flap-Type Control Surface Having Various Hinge-Line Locations on a 4-Percent-Thick 60° Delta Wing — Transonic-Bump Method. NACA RM L54B08, 1954. (U)
- Thompson, R. F.: Investigation of a 42.7° Sweepback Wing Model to Determine the Effects of Trailing-Edge Thickness on the Aileron Hinge-Moment and Flutter Characteristics at Transonic Speeds. NACA RM L50J06, 1950. (U)

4. Hieser, G.: Transonic Investigation of the Effectiveness and Loading Characteristics of a Flap-Type Aileron With and Without Paddle Balances on an Unswept-Wing-Fuselage Model. NACA RM L56B02, 1956. (U)
5. Runkel, J. F., and Hieser, G.: Normal-Force and Hinge-Moment Characteristics at Transonic Speeds of Flap-Type Ailerons at Three Spanwise Locations on a 4-Percent-Thick Sweptback-Wing-Body Model and Pressure Distribution Measurements on an Inboard Aileron. NASA TN D-842, 1961. (U)
6. Goin, K. L.: Equations and Charts for the Rapid Estimation of Hinge-Moment and Effectiveness Parameters for Trailing-Edge Controls Having Leading and Trailing Edges Swept Ahead of the Mach Lines. NACA TR 1041, 1951. (U)
7. Heaslet, M. A., and Spreiter, J. R.: Reciprocity Relations in Aerodynamics, NACA TN 2700, 1952. (U)
8. Fischel, J., and Schneiter, L. E.: An Investigation at Low Speed of a  $51.3^{\circ}$  Sweptback Semispan Wing Equipped With 16.7-Percent-Chord Plain Flaps and Ailerons Having Various Spans and Three Trailing-Edge Angles. NACA RM L&H20, 1948. (U)
9. Dods, J. B., Jr.: Wind-Tunnel Investigation of Horizontal Tails. III – Unswept and  $35^{\circ}$  Swept-back Plan Forms of Aspect Ratio 6. NACA RM A8H30, 1948. (U)
10. Tinling, B. E., and Dickson, J. K.: Tests of a Model Horizontal Tail of Aspect Ratio 4.5 in the Ames 12-Foot Pressure Wind Tunnel. I – Quarter-Chord Line Swept Back  $35^{\circ}$ . NACA RM A9G13, 1949 (U)
11. Kolbe, C. D., and Bandettini, A.: Investigation in the Ames 12-Foot Pressure Wind Tunnel of a Model Horizontal Tail of Aspect Ratio 3 and Taper Ratio 0.5 Having the Quarter-Chord Line Swept Back  $45^{\circ}$ . NACA RM A51D02, 1951. (U)
12. Johnson, H. I.: Measurements of Aerodynamic Characteristics of a  $35^{\circ}$  Sweptback NACA 65-009 Airfoil Model with 1/4-Chord Plain Flap by the NACA Wing-Flow Method. NACA RM L7F13, 1947. (U)
13. Morrill, C. P., Jr., and Boddy, L. E.: High-Speed Stability and Control Characteristics of a Fighter Airplane Model with a Swept-Back Wing and Tail. NACA RM A7K28, 1948. (U)
14. Cleary, J. W., and Boddy, L. E.: Wind-Tunnel Investigation of a  $45^{\circ}$  Swept-Back Wing Having a Symmetrical Root and a Highly Cambered Tip, Including the Effects of Fences and Lateral Controls. NACA RM A53I21, 1953. (U)
15. Pfyl, F. A.: Aerodynamic Study of a Wing-Fuselage Combination Employing a Wing Swept Back  $63^{\circ}$  – Effectiveness of an Inboard Elevon as a Longitudinal and Lateral-Control Device at Subsonic and Supersonic Speeds. NACA RM A51I18, 1951. (U)
16. Hammond, A. D.: The Effect of Various Aerodynamic Balances on the Low-Speed Lateral-Control and Hinge-Moment Characteristics of a 0.20-Chord Partial-Span Outboard Aileron on a Wing with Leading Edge Swept Back  $51.3^{\circ}$ . NACA RM L52G03, 1952. (U)
17. Schneiter, L. E., and Hagerman, J. R.: Wind-Tunnel Investigation at High Subsonic Speeds of the Lateral-Control Characteristics of an Aileron and a Stepped Spoiler on a Wing with Leading Edge Swept Back  $51.3^{\circ}$ . NACA RM L9D06, 1949. (U)
18. Fischel, J., and Schneiter, L. E.: An Investigation at Low Speeds of a  $51.3^{\circ}$  Sweptback Semispan Wing with a Raked Tip and with 16.7-Percent-Chord Ailerons Having Three Spans and Three Trailing-Edge Angles. NACA RM L8F29, 1948. (U)
19. Dods, J. B., Jr.: Wind-Tunnel Investigation of Horizontal Tails. II – Unswept and  $35^{\circ}$  Swept-Back Plan Forms of Aspect Ratio 4.5. NACA RM A8B11, 1948. (U)
20. Harper, J. J.: Wind-Tunnel Investigation of Effects of Various Aerodynamic Balance Shapes and Sweepback on Control Surface Characteristics of Semispan Tail Surfaces with NACA 0009, 0015, 66-009, 66(215)-014, and Circular-Arc Airfoil Sections. NACA TN 2495, 1951. (U)
21. Lord, D. R., and Driver, C.: Investigation of the Effect of Balancing Tabs on the Hinge-Moment Characteristics of a Trailing-Edge Flap-Type Control on a Trapezoidal Wing at a Mach Number of 1.61. NACA RM L54F22, 1954. (U)
22. Sivells, J. C., and Goin, K. L.: Experimental and Calculated Hinge Moments of Two Ailerons on a  $42.7^{\circ}$  Sweptback Wing at a Mach Number of 1.9. NACA RM L8K24a, 1949. (U)
23. Conner, D. W., and Mitchell, M. H., Jr.: Control Effectiveness and Hinge- Moment Measurements at a Mach Number of 1.9 of a Nose Flap and Trailing-Edge Flap on a Highly Tapered Low-Aspect-Ratio Wing. NACA RM L8K17a, 1949. (U)
24. Lord, D. R., and Czarnecki, K. R.: Aerodynamic Characteristics of Several Flap-Type Trailing-Edge Controls on a Trapezoidal Wing at Mach Numbers of 1.61 and 2.01. NACA RM L54D19, 1954. (U)
25. Spearman, M. L., and Webster, R. A.: An Investigation at Mach Numbers of 1.40 and 1.59 of the Effects of Aileron Profile on the Aerodynamic Characteristics of a Complete Model of a Supersonic Aircraft Configuration. NACA RM L50J31, 1951. (U)
26. Boatright, W. B., and Rainey, R. W.: Hinge-Moment Measurement of a Wing with Leading-Edge and Trailing-Edge Flaps at a Mach Number of 1.93. NACA RM L8K12a, 1949. (U)

27. Dunning, R. W., and Ulman, E. F.: Aerodynamic Characteristics at Mach Number 4.04 of a Rectangular Wing of Aspect Ratio 1.33 having a 6-Percent-Thick Circular-Arc Profile and a 30-Percent-Chord Full-Span Trailing-Edge Flap. NACA RM L53D03, 1953. (U)
28. Robinson, R. L.: An Investigation of a Supersonic Aircraft Configuration having a Tapered Wing with Circular-Arc Sections and 40° Sweepback — Static Lateral Control Characteristics at Mach Numbers of 1.40 and 1.59. NACA RM L50I11, 1950. (U)

**TABLE 6.1.6.1-A**  
**SUBSONIC HINGE-MOMENT DERIVATIVE DUE TO ANGLE OF ATTACK**  
**DATA SUMMARY AND SUBSTANTIATION**

Ref.	M	A	$\Lambda_{c/4}$ (deg)	$\lambda$	Type of Control Surface	$C_{h\alpha}$ Calc	$C_{h\alpha}$ Test	$\Delta C_{h\alpha}$ Calc-Test
9	0.23	6.0	5.7	0.5	Elevator	-0.00268	-0.0030	0.0003
10	0.21	4.5	35.3	0.5	Elevator	-0.00273	-0.0034	0.0007
	0.6					-0.00209	-0.0028	0.0007
	0.8					-0.00310	-0.0022	-0.0009
	0.85					-0.00365	-0.0016	-0.0021
	0.9					-0.00460	-0.0015	-0.0031
11	0.25	3.0	45.6	0.5	Elevator	-0.00167	-0.0030	0.0013
	0.6					-0.00145	-0.0030	0.0015
	0.8					-0.00231	-0.0027	0.0004
	0.9					-0.00360	-0.0025	-0.0011
12	0.55	3.04	35.0	1.0	Flap	-0.00211	-0.0057	0.0036
	0.8					-0.00368	-0.0045	0.0008
	0.9					-0.00558	-0.0044	-0.0012
13	0.3	4.785	35.22	0.513	Aileron	0.00296	-0.0024	0.0054
	0.6					0.00234	-0.0022	0.0045
	0.8					0.00233	0	0.00233
	0.85					0.00238	-0.002	0.00438
	0.875					0.00241	0	0.00241
	0.9					0.00249	-0.004	0.00649
	0.3	4.65	35.59	0.450	Elevator	0.00154	0	0.00154
	0.6					0.00101	-0.0015	0.0025
	0.8					0.000889	-0.0028	0.0037
	0.85					0.000866	-0.0026	0.0035
	0.875					0.000851	-0.0042	0.0051
	0.9					0.000847	-0.0047	0.0055
4	0.7	4.0	4.8	0.5	Aileron	-0.00418	-0.0013	-0.0029
	0.8					-0.00546	-0.0030	-0.0025
	0.9					-0.00842	0.0013	-0.0097
14	0.25	5.515	45.0	0.532	Aileron	-0.000982	-0.00244	0.00146
	0.8					-0.00280	-0.00195	-0.00085
	0.9					-0.00392	-0.00280	-0.00112
	0.25					-0.000986	-0.00244	0.00145
	0.8					-0.00280	-0.00195	-0.00085
	0.9					-0.00393	-0.0028	-0.0011
15	0.6	3.50	60.8	0.25	Elevon	-0.000858	-0.0039	0.0030
	0.9					-0.00166	-0.0059	0.0042
16	0.328	3.06	38.7	0.49	Aileron	-0.000753	-0.0002	-0.0006
	0.328				Aileron	0.000920	0.0011	-0.0002

TABLE 6.1.6.1-A (CONTD)

Ref.	M	A	$\Delta c/4$ (deg)	$\lambda$	Type of Control Surface	$C_{h\alpha}$ Calc	$C_{h\alpha}$ Test	$\Delta C_{h\alpha}$ Calc-Test
17	0.302	3.06	38.7	0.49	Aileron	-0.000713	-0.001	0.0003
						-0.00113	-0.001	-0.0001
						-0.00184	-0.001	-0.0008
						-0.00255	-0.001	-0.0016
8	0.12	3.43	48.6	0.44	Aileron	0.000427	-0.0024	0.0028
						0.000661	-0.0015	0.0022
						0.00124	-0.0011	0.0023
						-0.000303	-0.0025	0.0022
						0.000143	-0.0011	0.0012
						0.00472	0.0015	0.0032
						-0.000214	-0.0015	0.0013
18	0.12	3.58	48.7	0.44	Aileron	-0.00141	-0.0035	0.0021
						0.0000304	-0.0016	0.0016
						0.00351	0.0022	0.0013
						-0.00123	-0.0026	0.0014
						0.000207	-0.0011	0.0013
						0.00369	0.0026	0.0011
						-0.000754	-0.0019	0.0011
						0.000683	-0.0008	0.0015
						0.00417	0.0027	0.0015
						-0.00240	-0.0020	-0.0004
19	0.17	4.5	7.6	0.5	Elevator	-0.00158	-0.0021	0.0005
						-0.000532	0	-0.0005
20	0.12	3.36	13.5	0.4	Flap	-0.00118	-0.0003	-0.0009
						-0.00581	-0.0028	-0.0030
						-0.000417	-0.0012	0.0008
						0.00109	0.0040	-0.0029
						0.000920	0.0039	-0.0030
						-0.00262	-0.0036	0.0010
						-0.000860	-0.0037	0.0028
						-0.00169	-0.0038	0.0021
						-0.00104	0	-0.00104
						0.0000177	-0.0002	0.00022
						-0.000520	-0.0003	-0.0002
						0.000369	0	0.00037
						0.000800	0.0006	0.0002
						0.000511	0.0004	0.0001
3.36	3.36	13.5	0.4	Flap		0.000181	-0.0022	0.0024
						0.000626	-0.0034	0.0040
						0.000325	-0.0044	0.0047
						0.00374	0.001	0.0027
						0.00283	0.0013	0.0015
						0.00317	0.0008	0.0024
Average $\Delta \left  C_{h\alpha}^{\text{calc}} - C_{h\alpha}^{\text{test}} \right  = 0.0020$								

**TABLE 6.1.6.1-B**  
**SUPERSONIC HINGE-MOMENT DERIVATIVE DUE TO ANGLE OF ATTACK**  
**DATA SUMMARY AND SUBSTANTIATION**

Ref.	M	A	$\Lambda_{LE}$ (deg)	$\lambda$	$C_{h\alpha}$ Calc	$C_{h\alpha}$ Test	$\Delta (C_{h\alpha})$ Calc-Test
21	1.61	3.1	23	0.4	-0.0193	-0.0183	-0.001
22	1.9	4.0	42.7	0.5	-0.0177	-0.010	-0.0077
					-0.0177	-0.014	-0.0037
23	1.9	1.06	45	0.31	-0.0056	-0.003	-0.0026
24	1.61	3.1	23	0.4	-0.0278	-0.0133	-0.0145
					-0.0203	-0.020	-0.0003
					-0.0222	-0.019	-0.0032
					-0.0193	-0.0175	-0.0018
					-0.0215	-0.023	0.0015
					-0.0236	-0.0217	-0.0019
		2.01			-0.0168	-0.0163	-0.0005
					-0.0172	-0.015	-0.0022
					-0.0154	-0.0146	-0.0008
25	1.59	4.0	42.7	0.5	-0.0108	-0.012	0.0012
					-0.0108	-0.012	0.0012
					-0.0108	-0.013	0.0022
					-0.0108	-0.017	0.0062
26	1.93	3.14	9.33	0.59	-0.0127	-0.009	-0.0037
27	4.04	1.33	0	1.0	-0.00479	-0.006	0.00121
28	1.59	1.0	42.7	0.5	-0.0107	-0.0163	0.0056
	1.59	1.17	40.6	0.337	-0.0041	-0.0043	0.0002
Average $\Delta  C_{h\alpha_{calc}} - C_{h\alpha_{test}}  = 0.00301$							

**TABLE 6.1.6.1-C**  
**COMPUTING FORM FOR SUMMING PRESSURE-AREA-MOMENT PARAMETER OF TRIANGULAR  
 SEGMENTS OF WING-ROOT AND WING-TIP CONICAL-FLOW REGIONS**

Figures for Determining Columns (2) & (3)	Conical-Flow Region	Enter Figure at Following Value of n or r	P'	t <sub>c.p.</sub>	Value of $3x \sqrt{1 + \beta^2 s^2}$	Value of $2S_L$	$P' (3x \sqrt{1 + \beta^2 s^2}) 2S_L$
ROOT MACH CONE	6.1.6.1-22k through 6.1.6.1-22l	1 $r' = \frac{c_r}{K_1} \cdot (1-d)$			$\frac{2K_1(1-at_{c.p.})}{t_{c.p.}} - 3x_r$	$(1) K_5$	
	2 $r' = \frac{x_r}{K_1} \cdot (1-a)$				$3x_r \cdot \frac{2K_1(1-at_{c.p.})}{t_{c.p.}}$	$(1) K_5$	
	3 $n = 1 - \frac{K_2}{c_r} \cdot (1-d)$				$\frac{2c_r(1-at_{c.p.})}{(1-dt_{c.p.})} - 3x_r$	$(1)(c_r)^2 K_6$	
	4 $n = 1 - \frac{K_1}{c_r} \cdot (1-d)$				$3x_r \cdot \frac{2c_r(1-at_{c.p.})}{(1-dt_{c.p.})}$	$(1)(c_r)^2 K_6$	
	5 $n = 1 - \frac{K_2}{x_r} \cdot (1-a)$			-	$x_r$	$(1)(x_r)^2 K_7$	
	6 $n = 1 - \frac{K_1}{x_r} \cdot (1-a)$			-	$-x_r$	$(1)(x_r)^2 K_7$	
	7 $r' = \frac{c_t}{K_2} \cdot (1-d)$				$3x_t \cdot \frac{2K_2(1-at_{c.p.})}{t_{c.p.}}$	$(1) K_8$	
	8 $r' = \frac{x_t}{K_2} \cdot (1-a)$				$3x_t \cdot \frac{2K_2(1-at_{c.p.})}{t_{c.p.}} - 3x_t$	$(1) K_8$	
TIP MACH CONE	6.1.6.1-34e through 6.1.6.1-34f	1 $r' = \frac{c_t}{K_3} \cdot (1+d)$			$\frac{2K_3(1+at_{c.p.})}{t_{c.p.}} - 3x_t$	$(1) K_9$	
	2 $r' = \frac{x_t}{K_3} \cdot (1+a)$				$3x_t \cdot \frac{2K_3(1+at_{c.p.})}{t_{c.p.}}$	$(1) K_9$	
	3 $n = 1 - \frac{K_4(1+d)}{c_t}$				$\frac{2c_t(1+at_{c.p.})}{(1+dt_{c.p.})} - 3x_t$	$(1)(c_t)^2 K_{10}$	
	4 $n = 1 - \frac{K_3(1+d)}{c_t}$				$3x_t \cdot \frac{2c_t(1+at_{c.p.})}{(1+dt_{c.p.})}$	$(1)(c_t)^2 K_{10}$	
	5 $n = 1 - \frac{K_4(1+a)}{x_t}$			-	$x_t$	$(1)(x_t)^2 K_{11}$	
	6 $n = 1 - \frac{K_3(1+a)}{x_t}$			-	$-x_t$	$(1)(x_t)^2 K_{11}$	
	7 $r' = \frac{c_t}{K_4} \cdot (1+d)$				$3x_t \cdot \frac{2K_4(1+at_{c.p.})}{t_{c.p.}}$	$(1) K_{12}$	
	8 $r' = \frac{x_t}{K_4} \cdot (1+a)$				$3x_t \cdot \frac{2K_4(1+at_{c.p.})}{t_{c.p.}} - 3x_t$	$(1) K_{12}$	

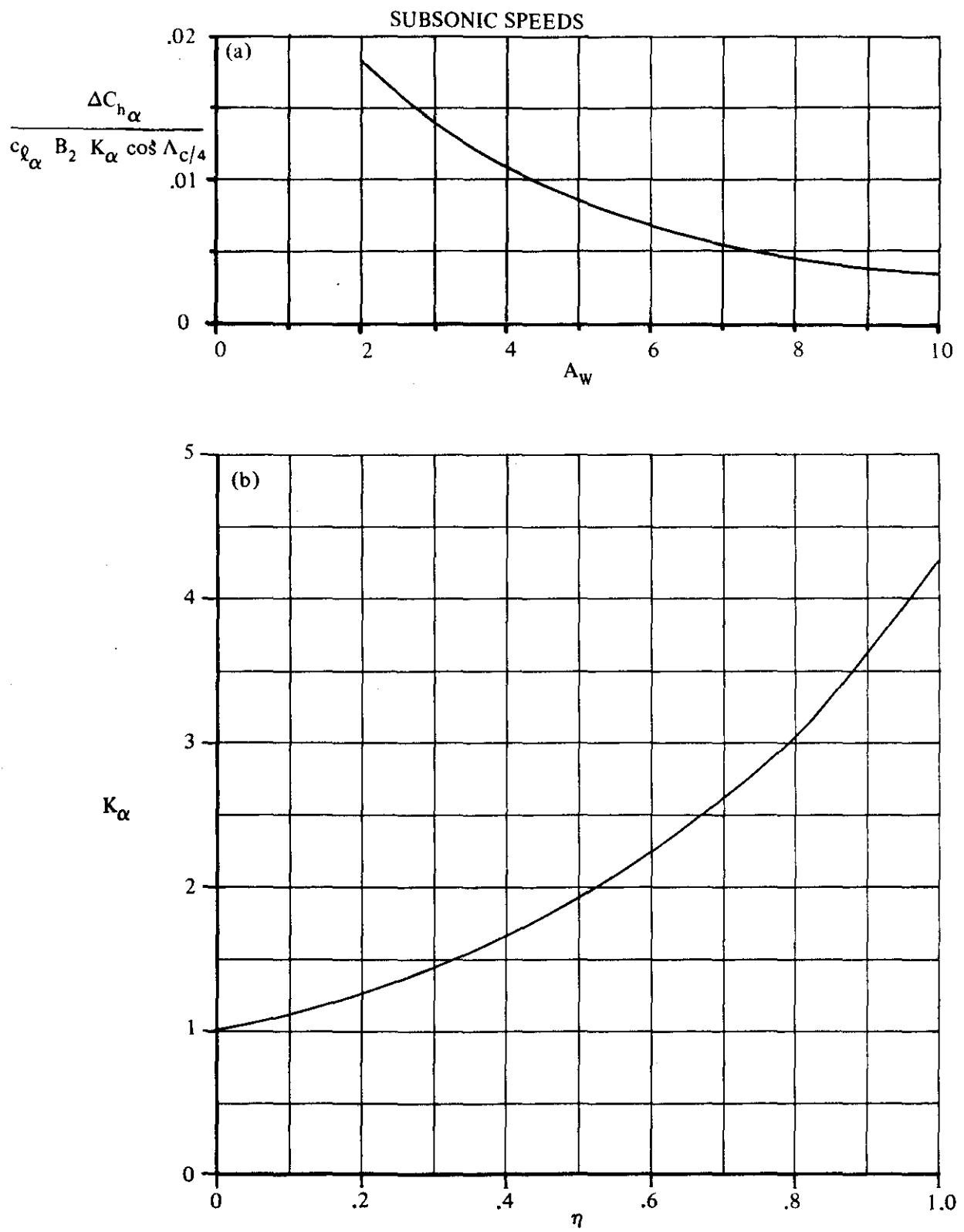


FIGURE 6.1.6.1-19 CHARTS FOR INDUCED-CAMBER CORRECTIONS TO HINGE-MOMENT PARAMETERS OF FINITE-SPAN WINGS

SUBSONIC SPEEDS

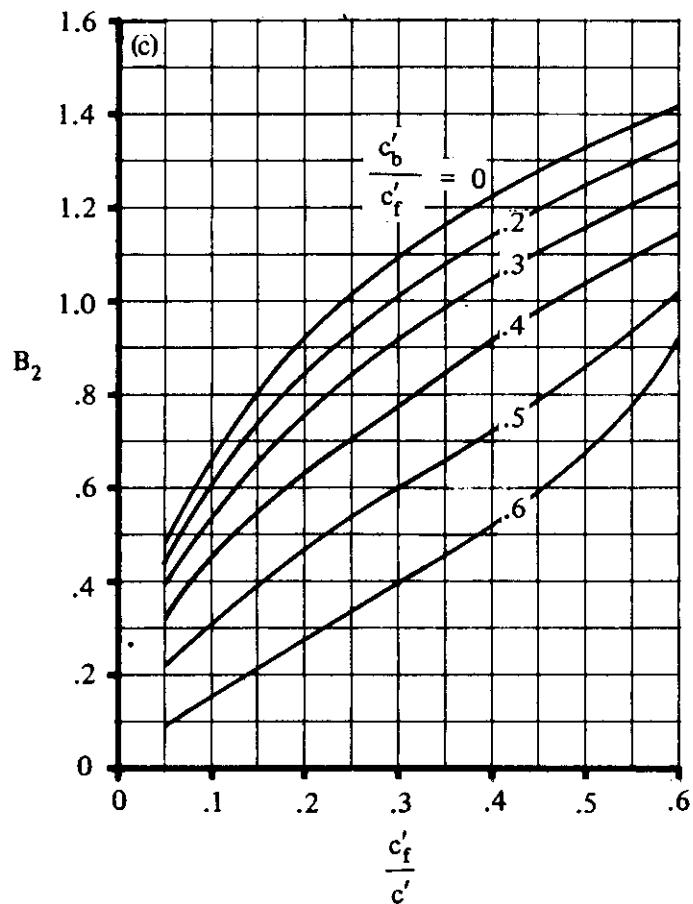
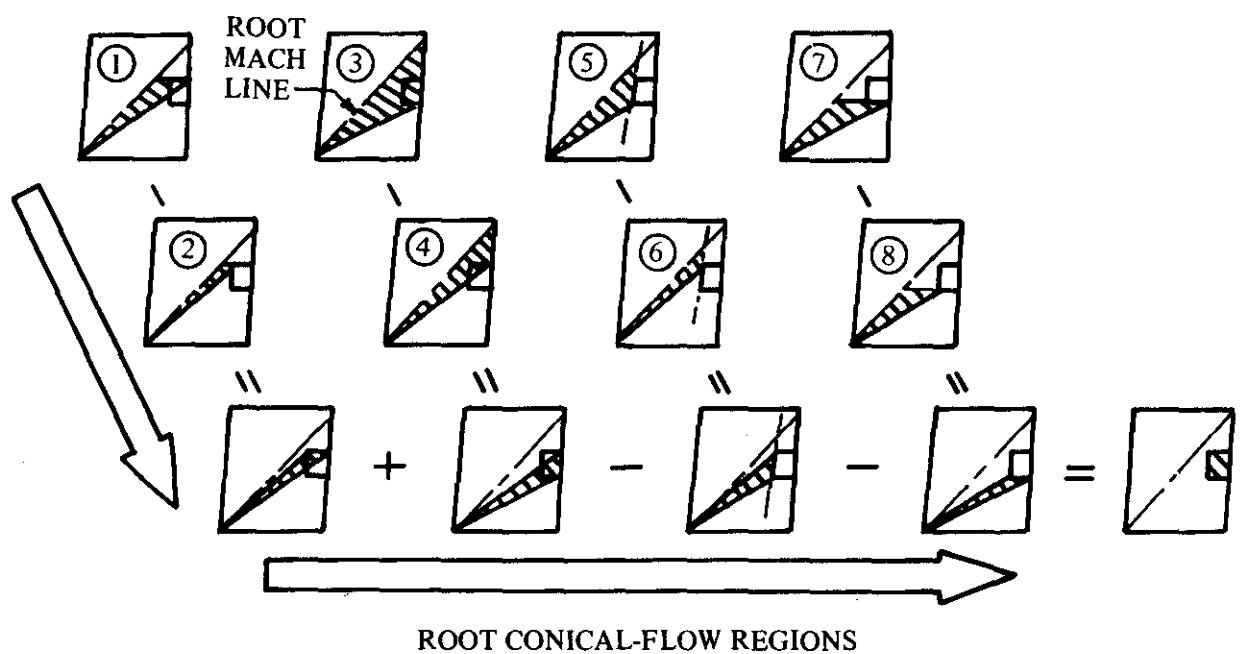
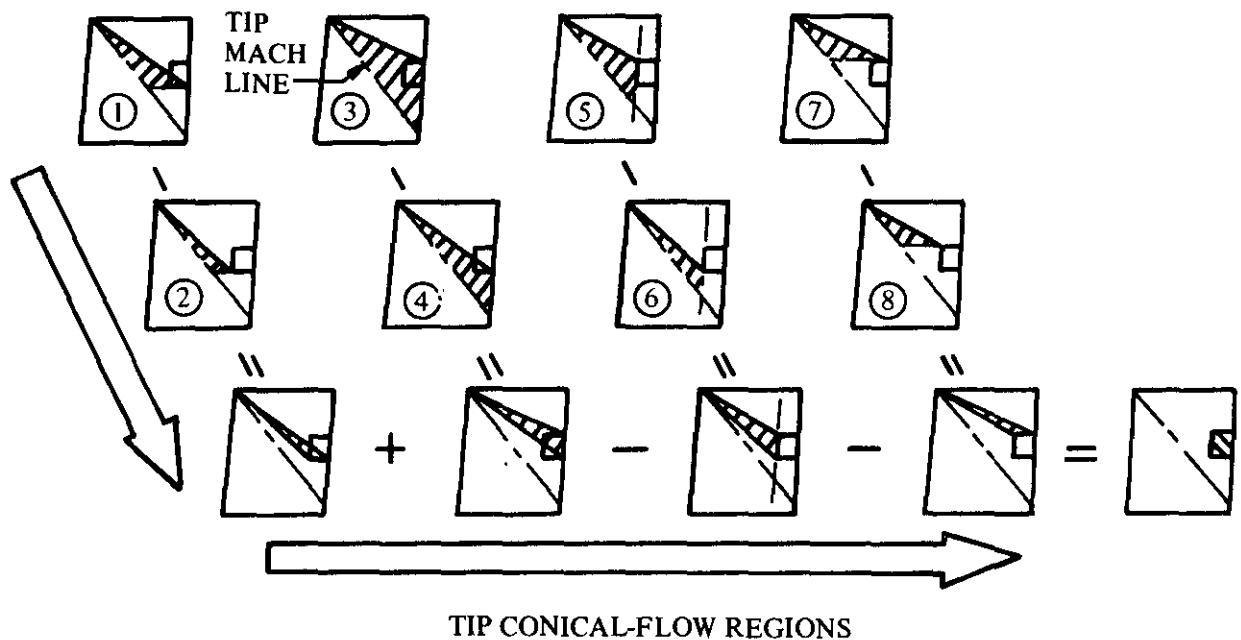


FIGURE 6.1.6.1-19 (CONTD)



Arrows show procedure for summing pressure-area-moment parameter. (Encircled numbers correspond to regions as designated in computing form for pressure-area-moment parameter.)  
Table 6.1.6.1-A

FIGURE 6.1.6.1-21 DEFINITION OF CONICAL-FLOW REGIONS

SUPERSONIC SPEEDS

$$(a) \frac{\tan \Lambda_{LE}}{\beta} = 0.10$$

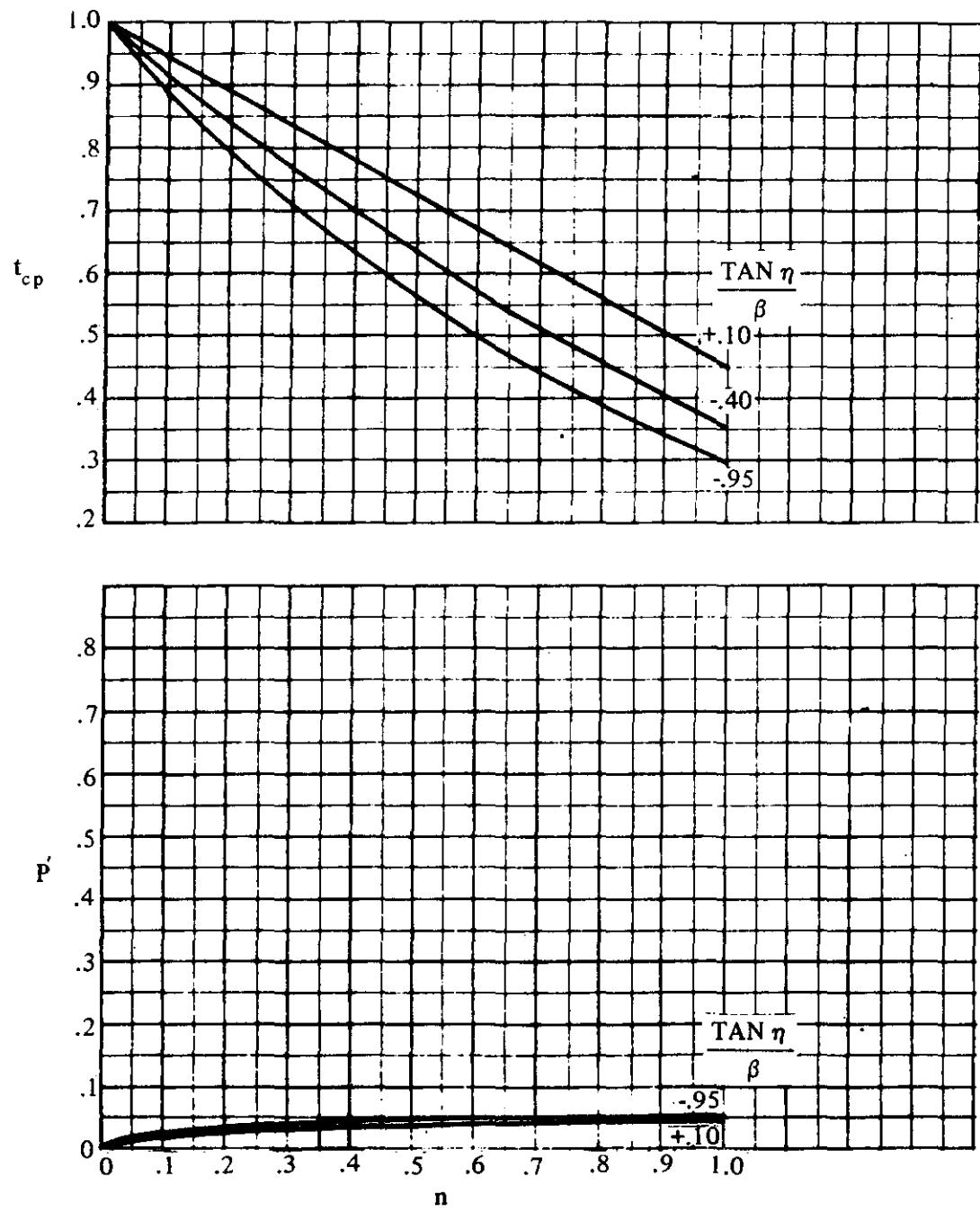


FIGURE 6.1.6.1-22 LOADING DISTRIBUTIONS IN THE CONICAL-FLOW REGIONS  
INTERSECTING THE WING-ROOT MACH CONE

SUPersonic SPEEDS

$$(b) \quad \frac{\tan \Lambda_{LE}}{\beta} = 0.20$$

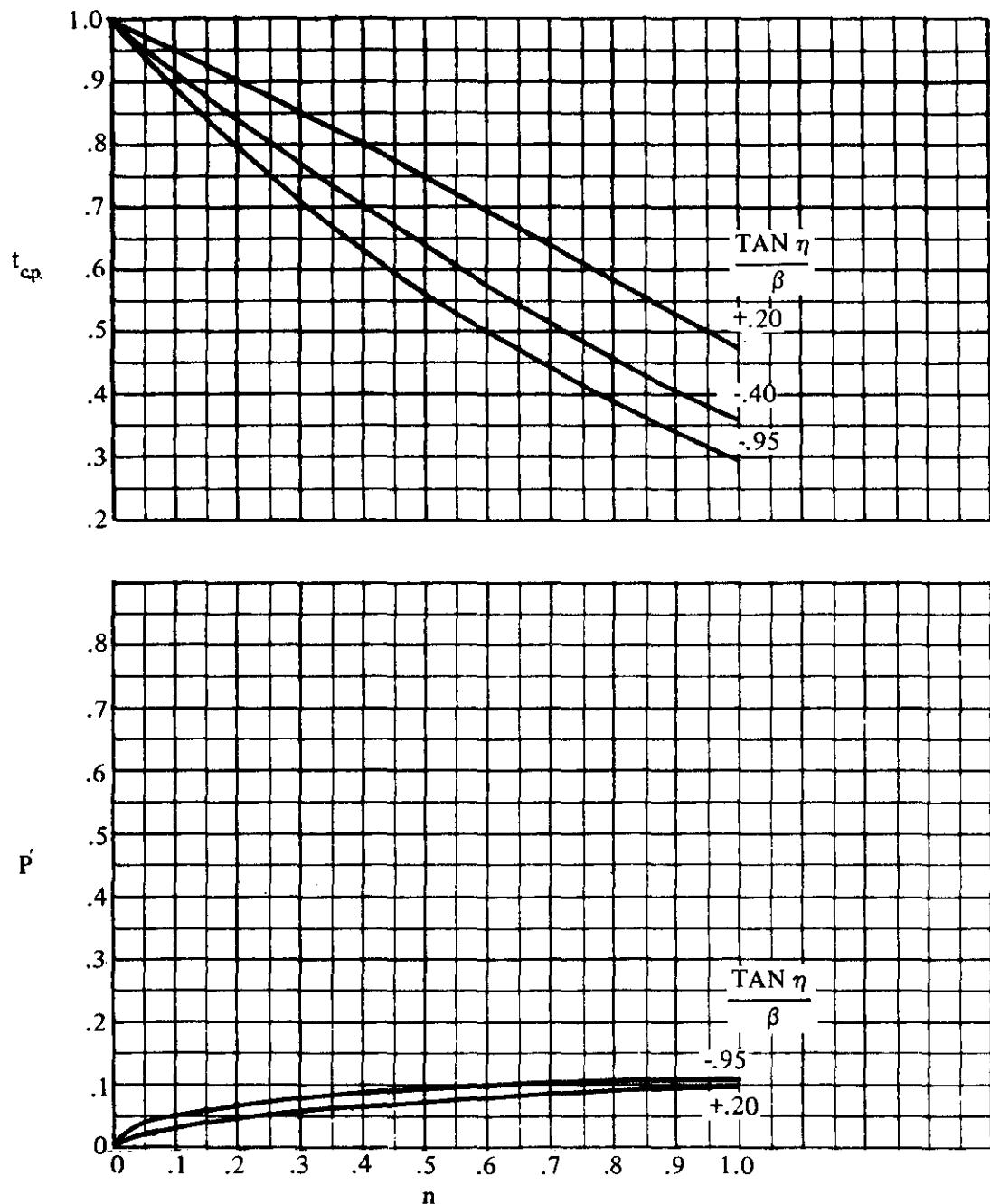
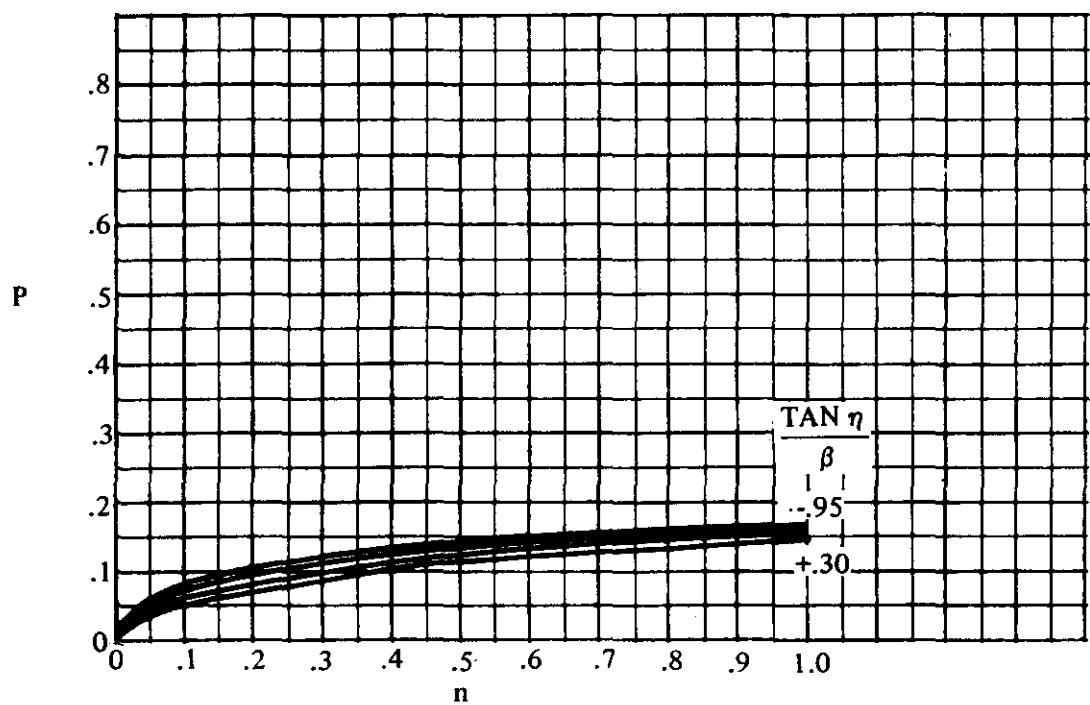
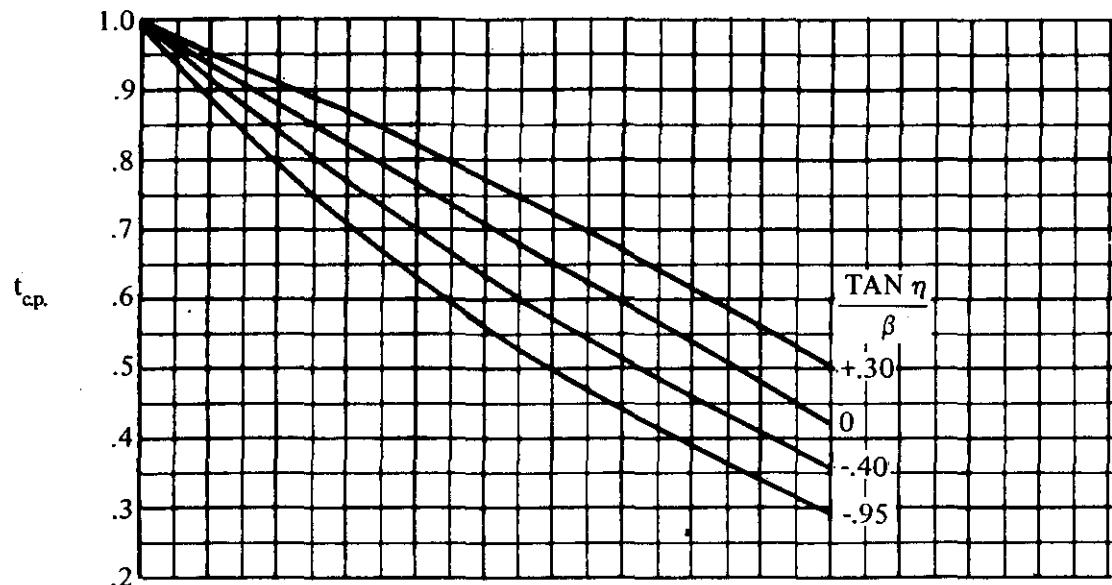


FIGURE 6.1.6.1-22 (CONTD)

## SUPersonic SPEEDS

$$(c) \quad \frac{\tan \Lambda_{LE}}{\beta} = 0.30$$



**FIGURE 6.1.6.1-22 (CONTD)**

SUPersonic SPEEDS

$$(d) \quad \frac{\tan \Lambda_{LE}}{\beta} = 0.40$$

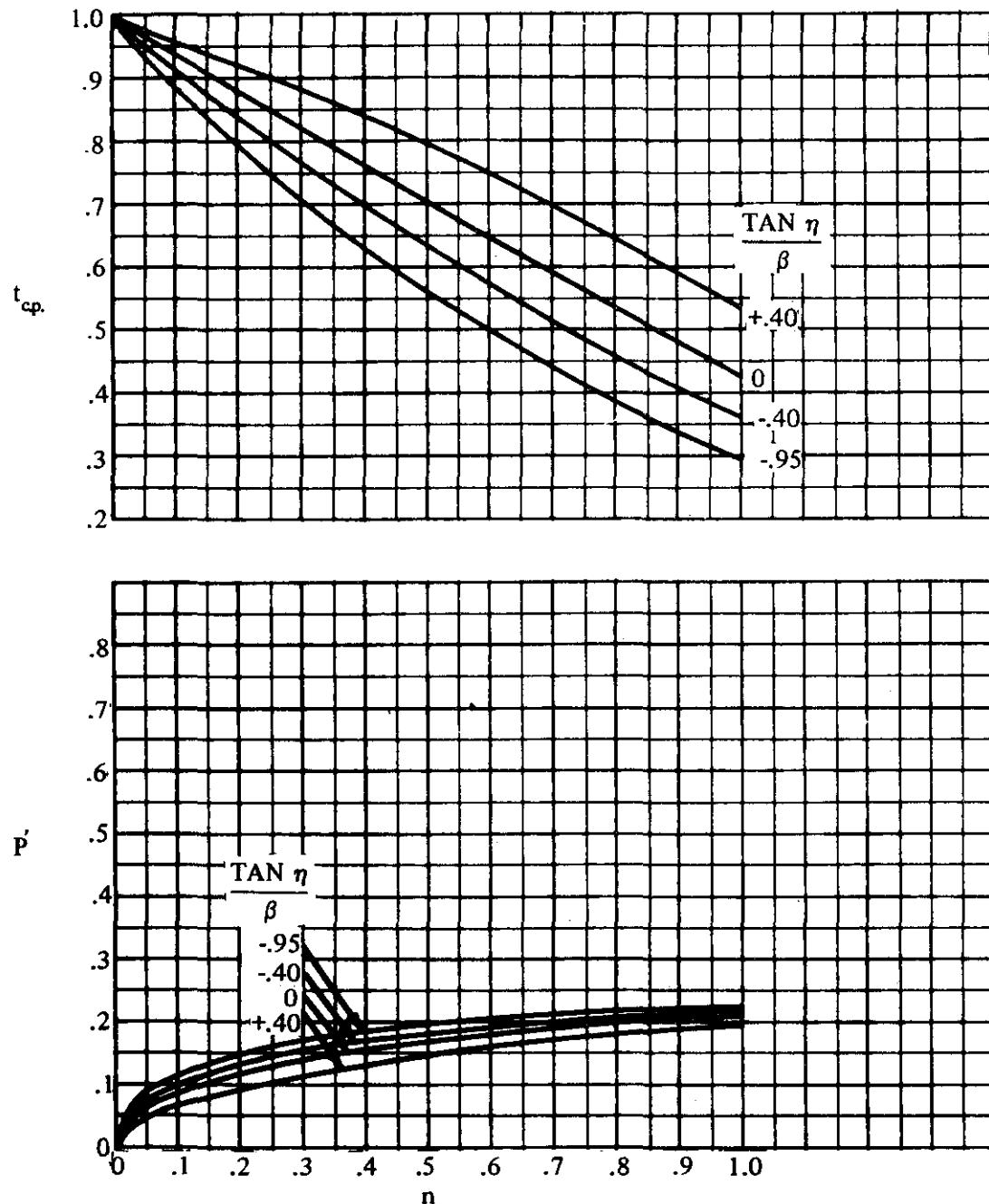


FIGURE 6.1.6.1-22 (CONT'D)

SUPersonic SPEEDS

$$(e) \frac{\tan \Lambda_{LE}}{\beta} = 0.50$$

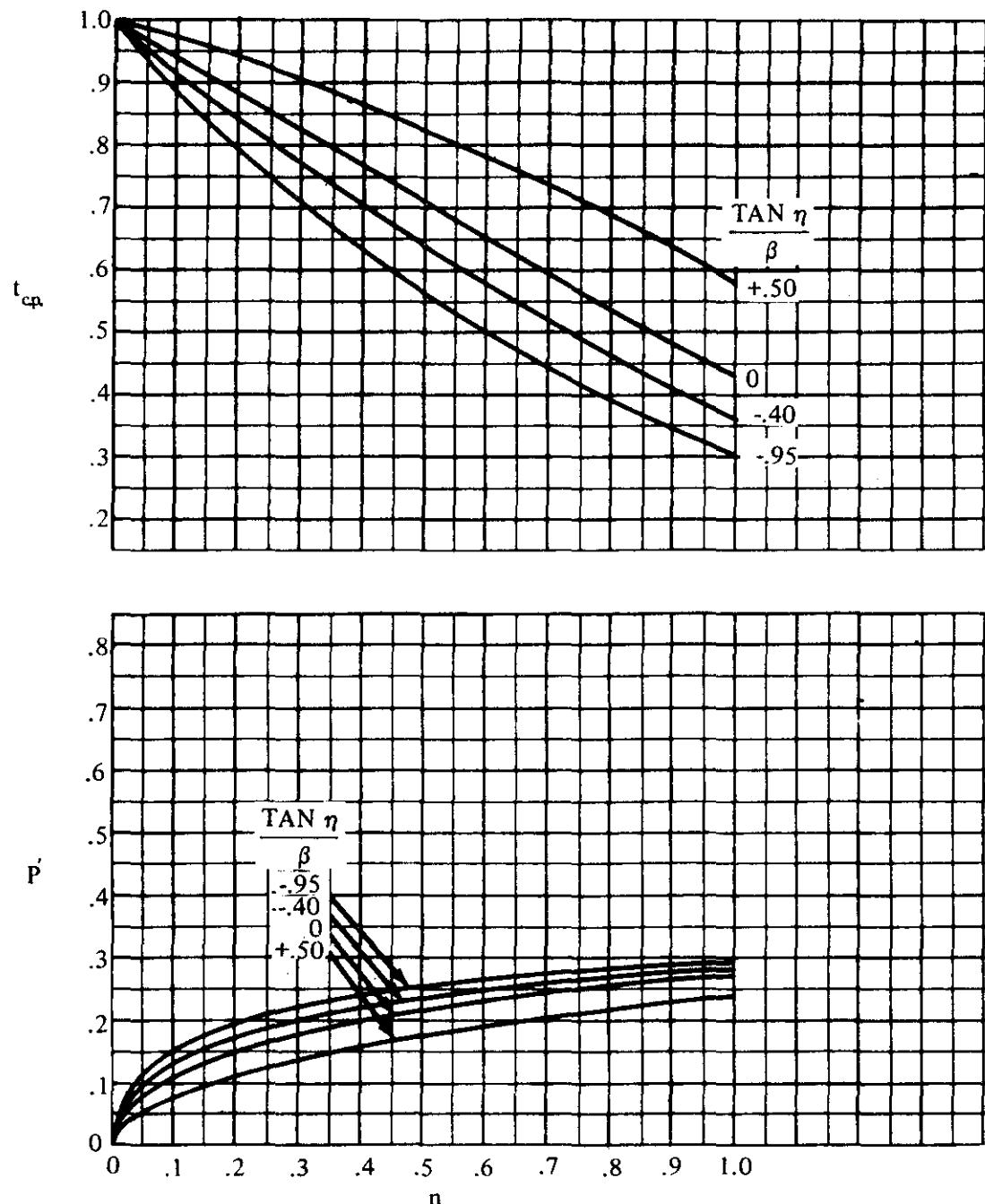


FIGURE 6.1.6.1-22 (CONTD)

SUPersonic SPEEDS

$$(f) \frac{\tan \Lambda_{LE}}{\beta} = 0.60$$

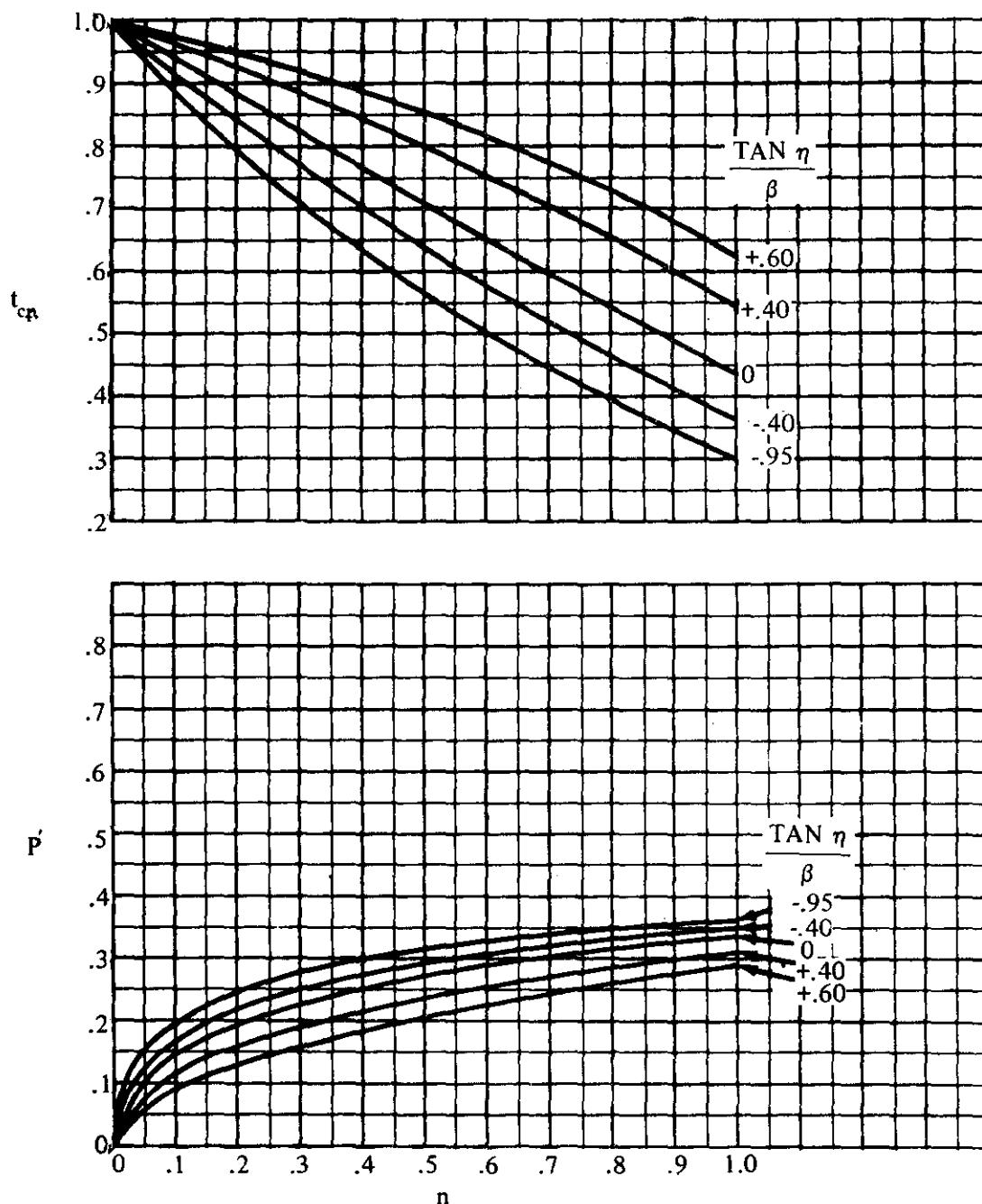


FIGURE 6.1.6.1-22 (CONTD)

SUPersonic SPEEDS

$$(g) \quad \frac{\tan \Lambda_{LE}}{\beta} = 0.70$$

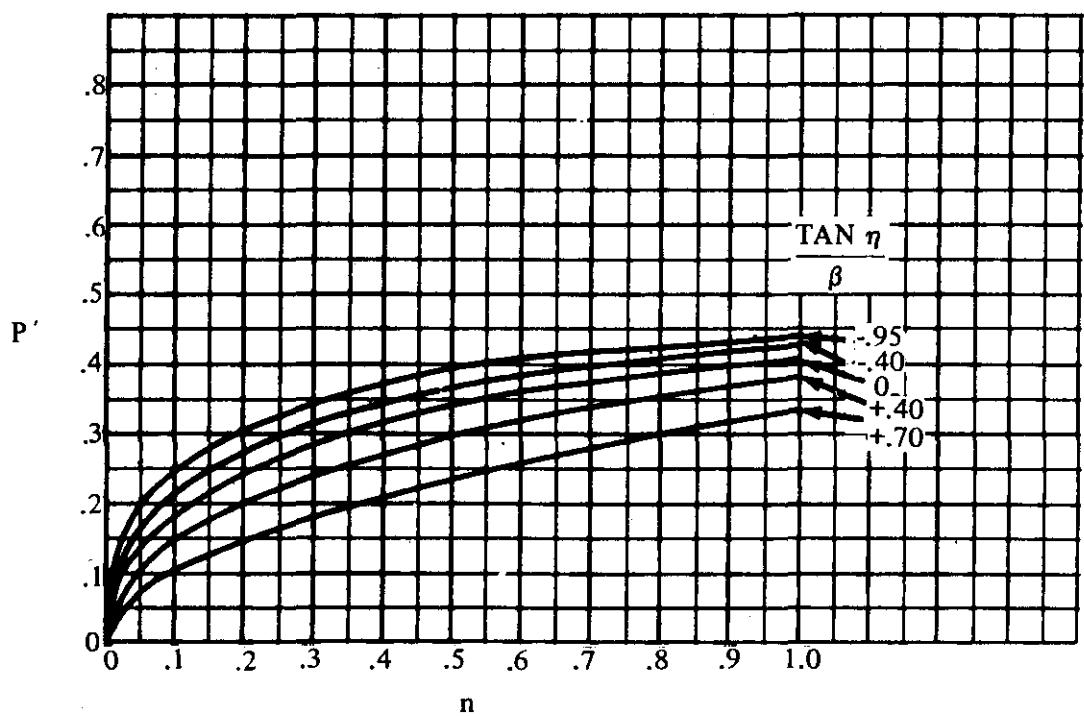
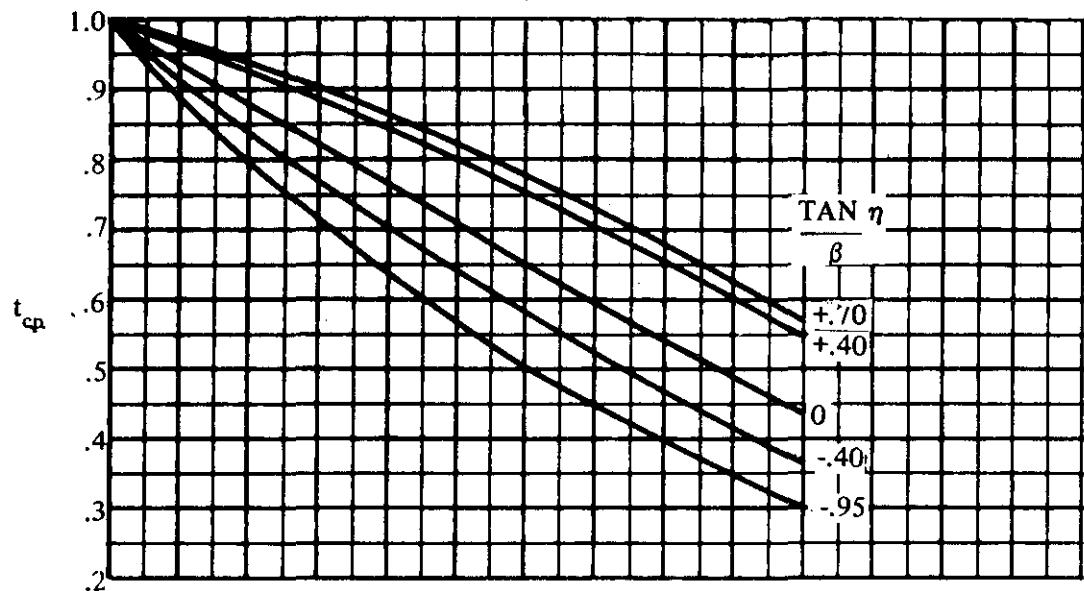


FIGURE 6.1.6.1-22 (CONTD)

SUPersonic SPEEDS

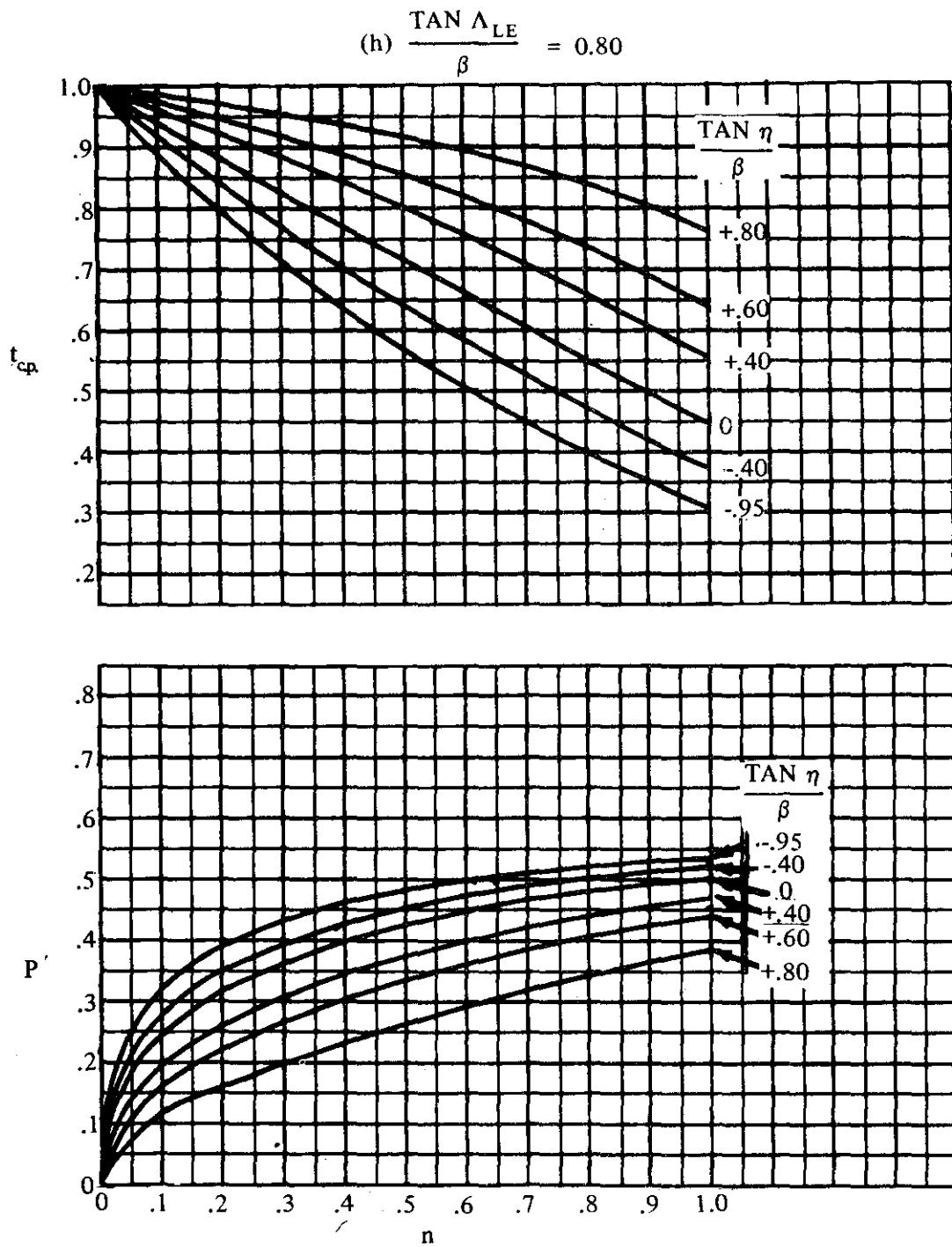


FIGURE 6.1.6.1-22 (CONTD)

SUPersonic SPEEDS

$$(i) \frac{\tan \Lambda_{LE}}{\beta} = 0.90$$

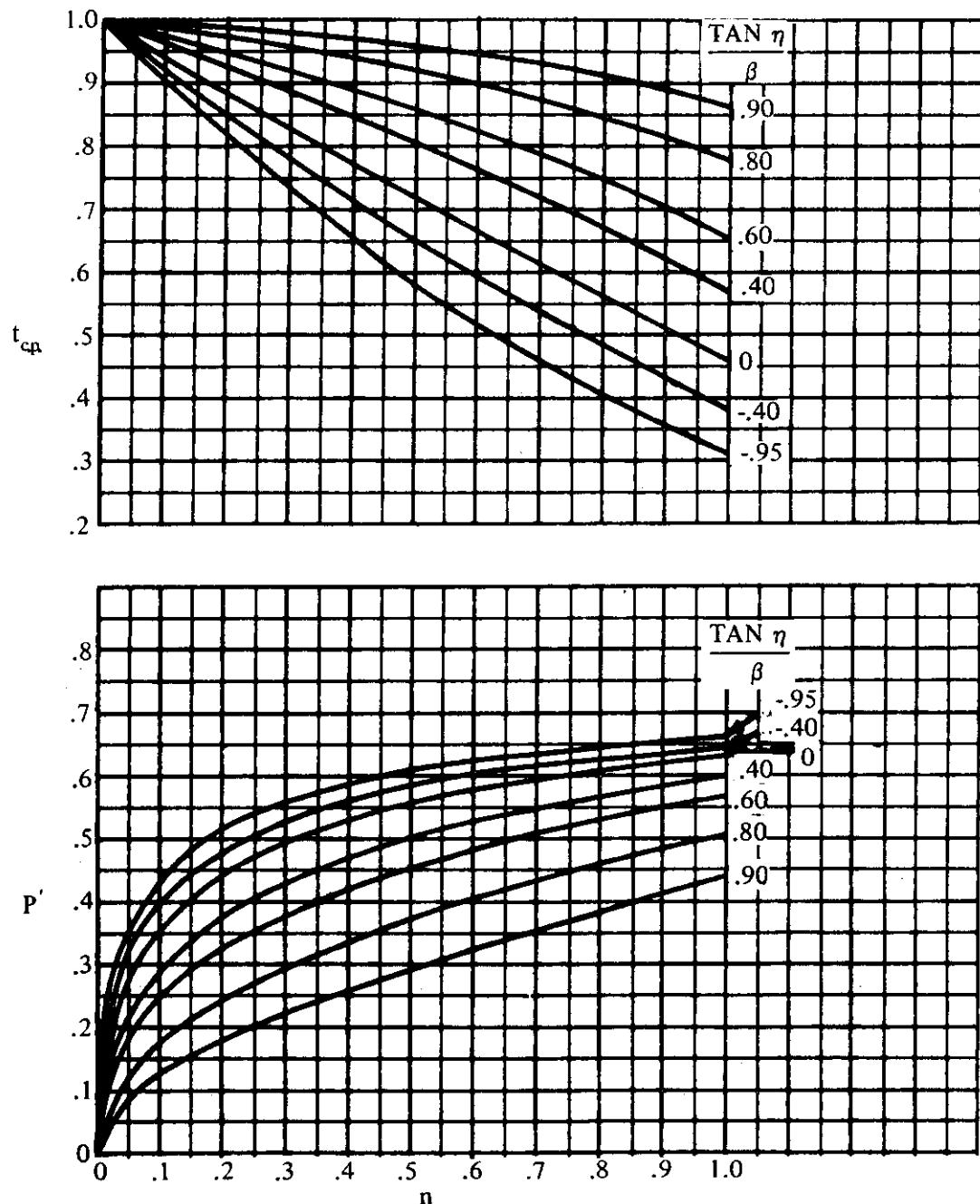


FIGURE 6.1.6.1-22 (CONTD)

SUPersonic SPEEDS

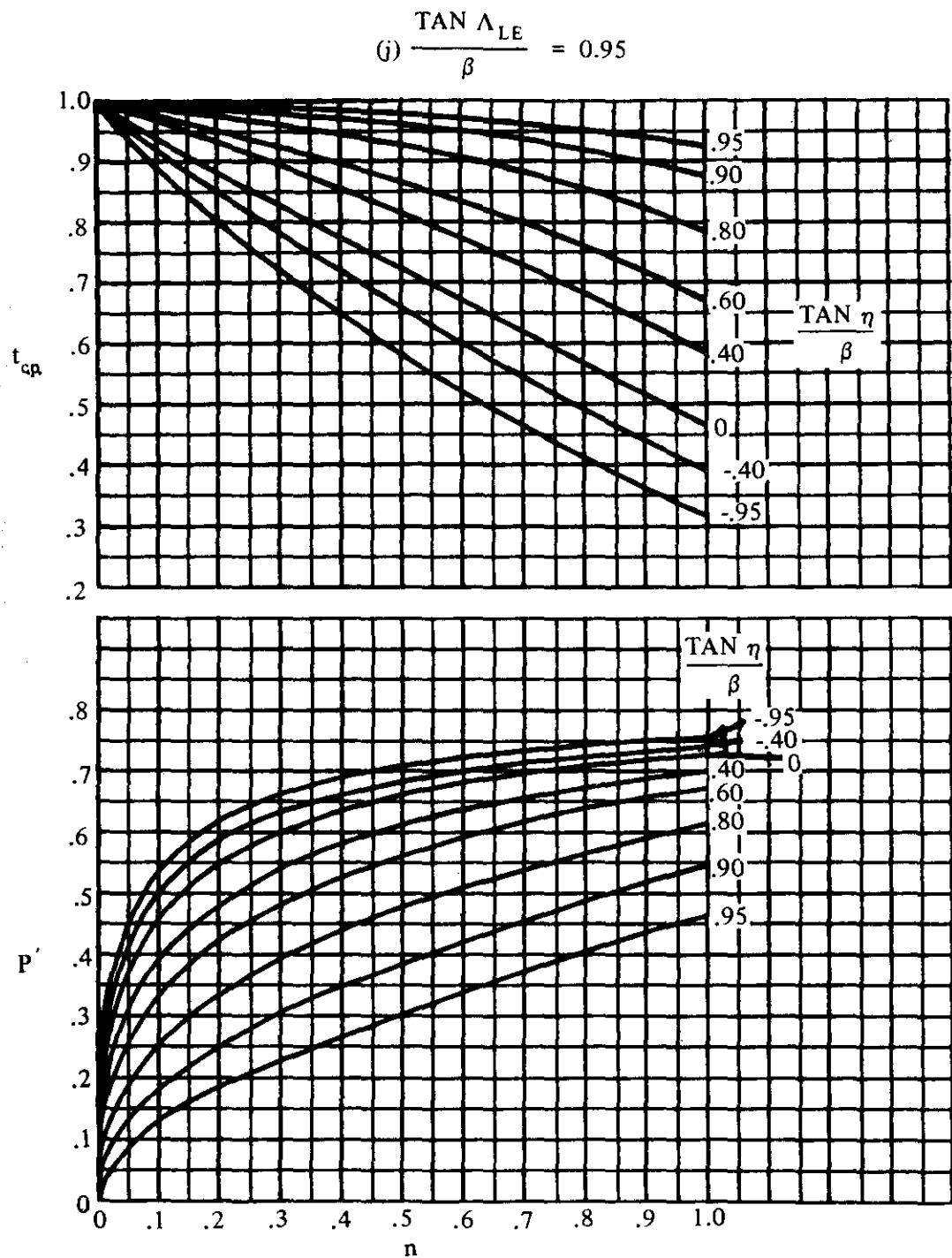


FIGURE 6.1.6.1-22 (CONTD)

SUPersonic SPEEDS

(k)  $r' = 0$  TO 1.0

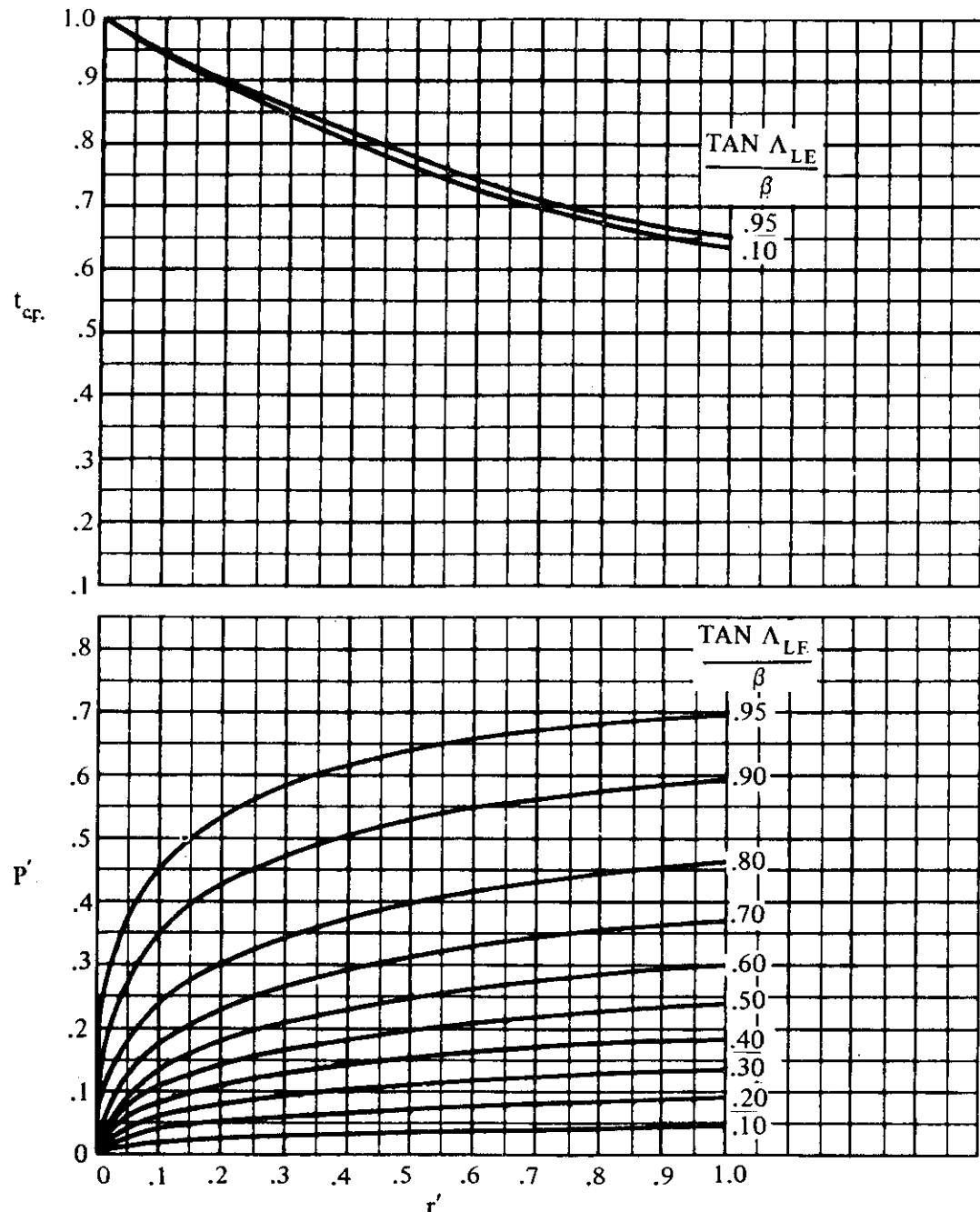


FIGURE 6.1.6.1-22 (CONTD)

SUPersonic SPEEDS

( $t$ )  $r' = 1.0$  TO 10.0

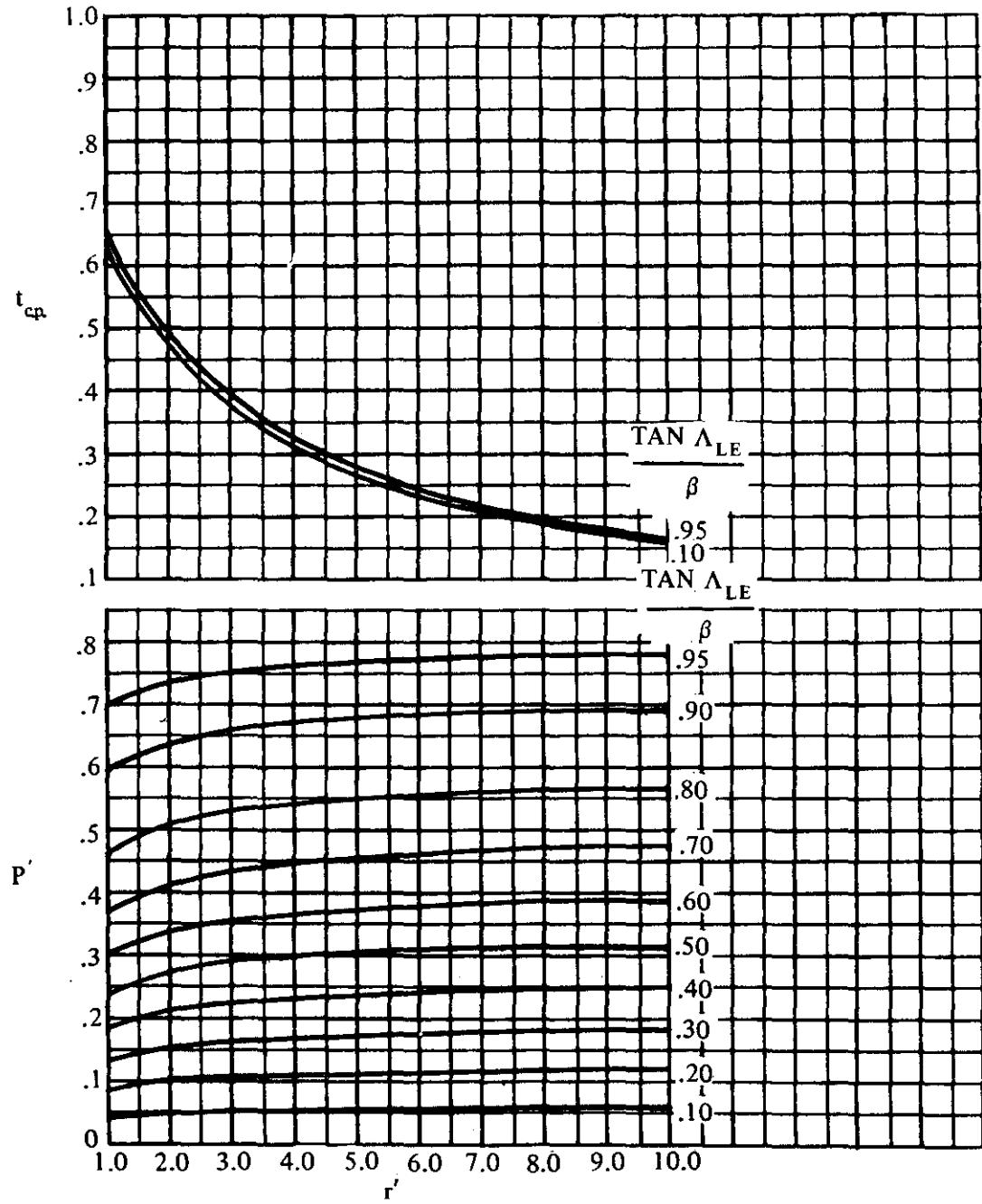


FIGURE 6.1.6.1-22 (CONTD)

SUPersonic SPEEDS

$$(a) \frac{\tan \Lambda_{LE}}{\beta} = 0$$

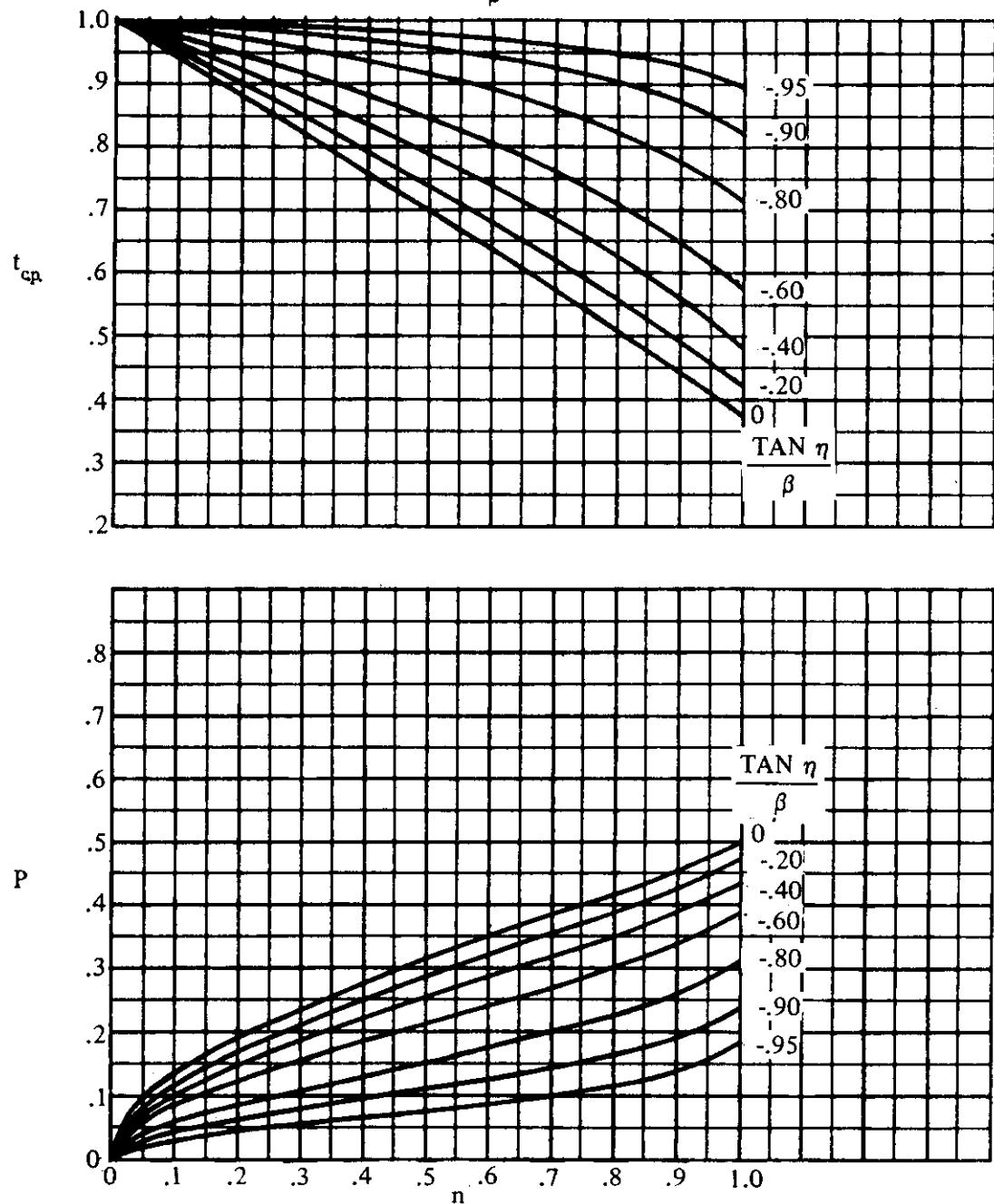


FIGURE 6.1.6.1-34 LOADING DISTRIBUTION IN THE CONICAL-FLOW REGIONS  
INTERSECTING THE WING-TIP MACH CONE

SUPersonic SPEEDS

$$(b) \frac{\tan \Lambda_{LE}}{\beta} = 0.20$$

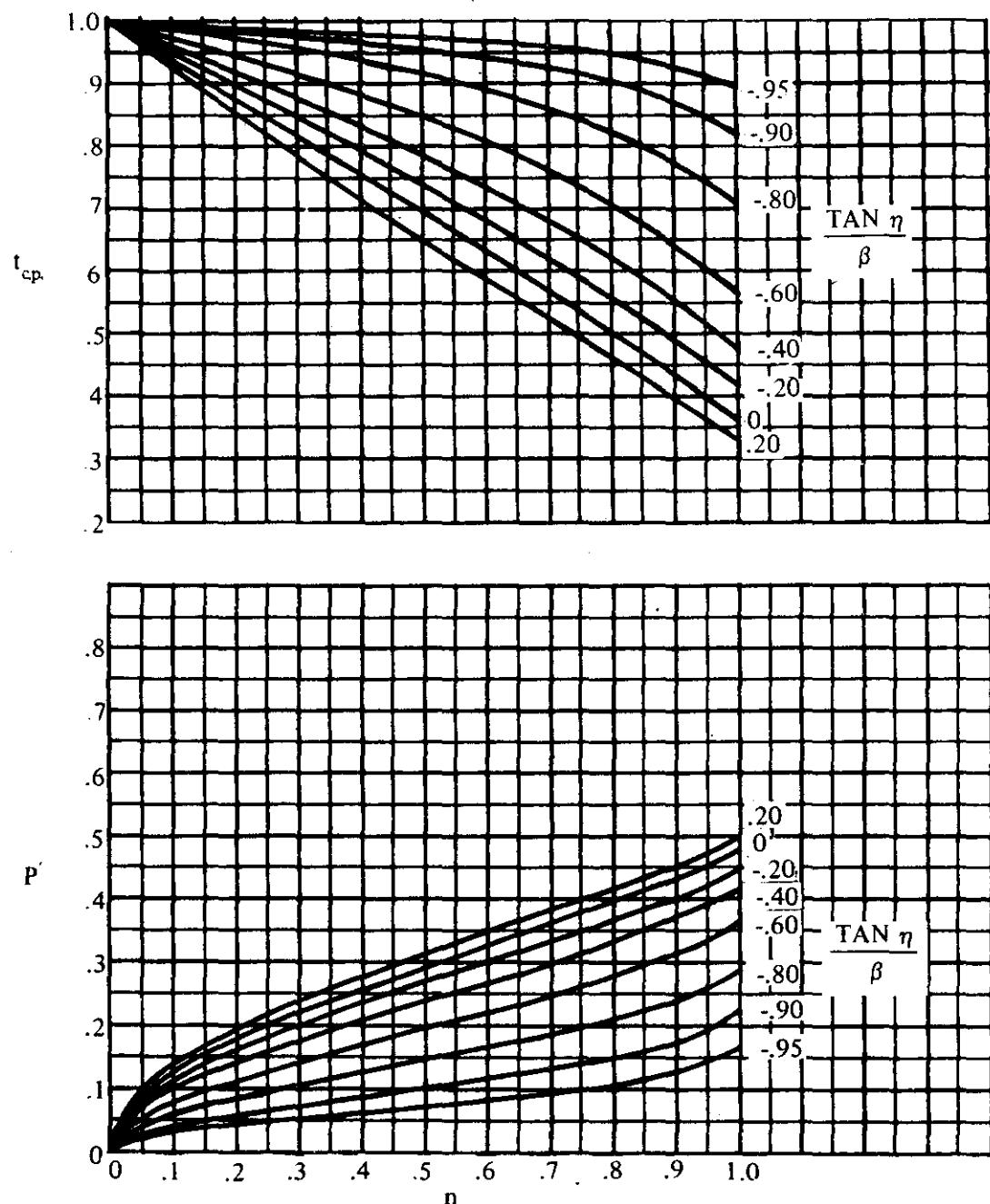


FIGURE 6.1.6.1-34 (CONTD)

SUPersonic SPEEDS

$$(c) \frac{\tan \Lambda_{LE}}{\beta} = 0.50$$

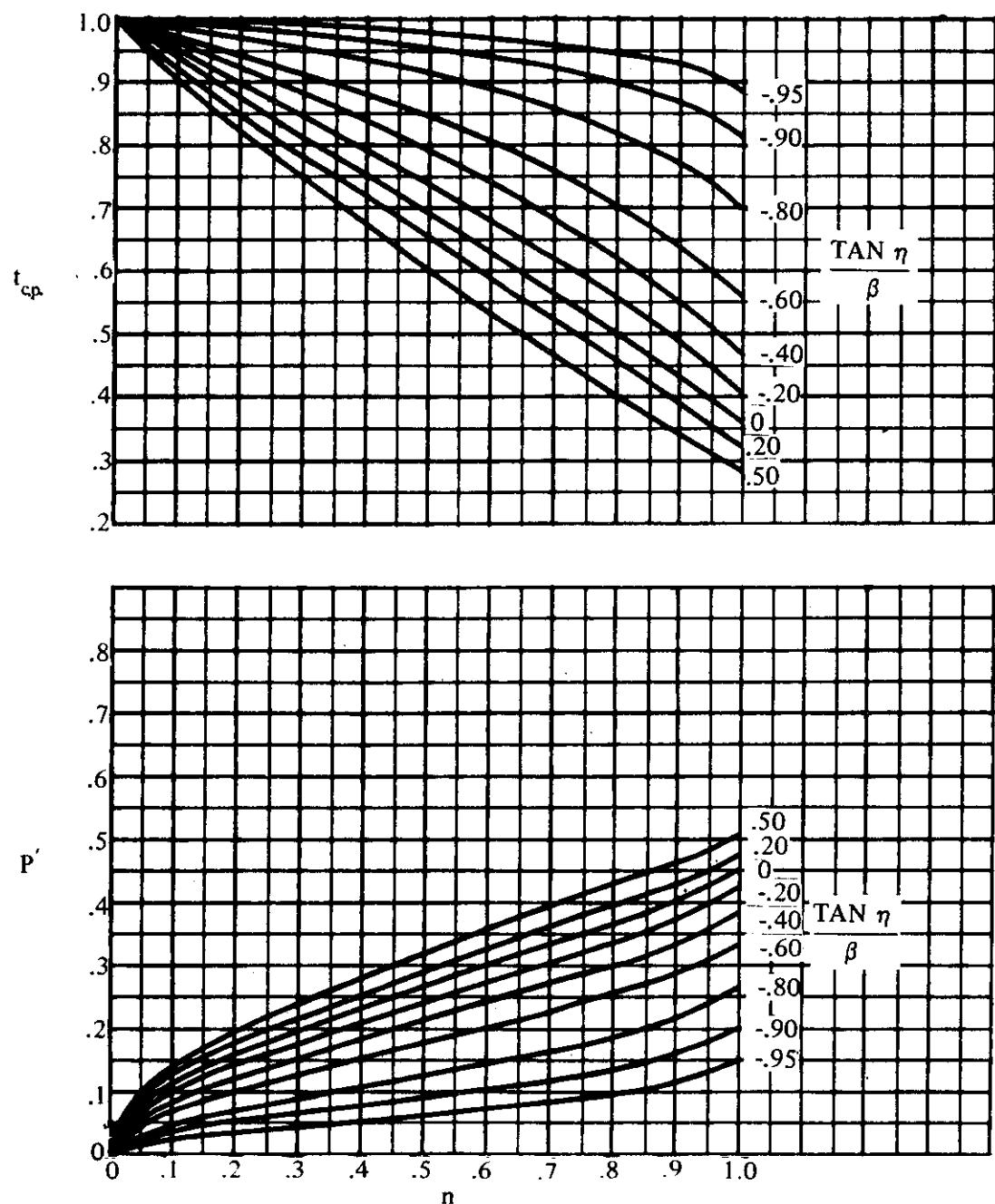


FIGURE 6.1.6.1-34 (CONTD)

SUPersonic SPEEDS

$$(d) \frac{\tan \Lambda_{LE}}{\beta} = 0.95$$

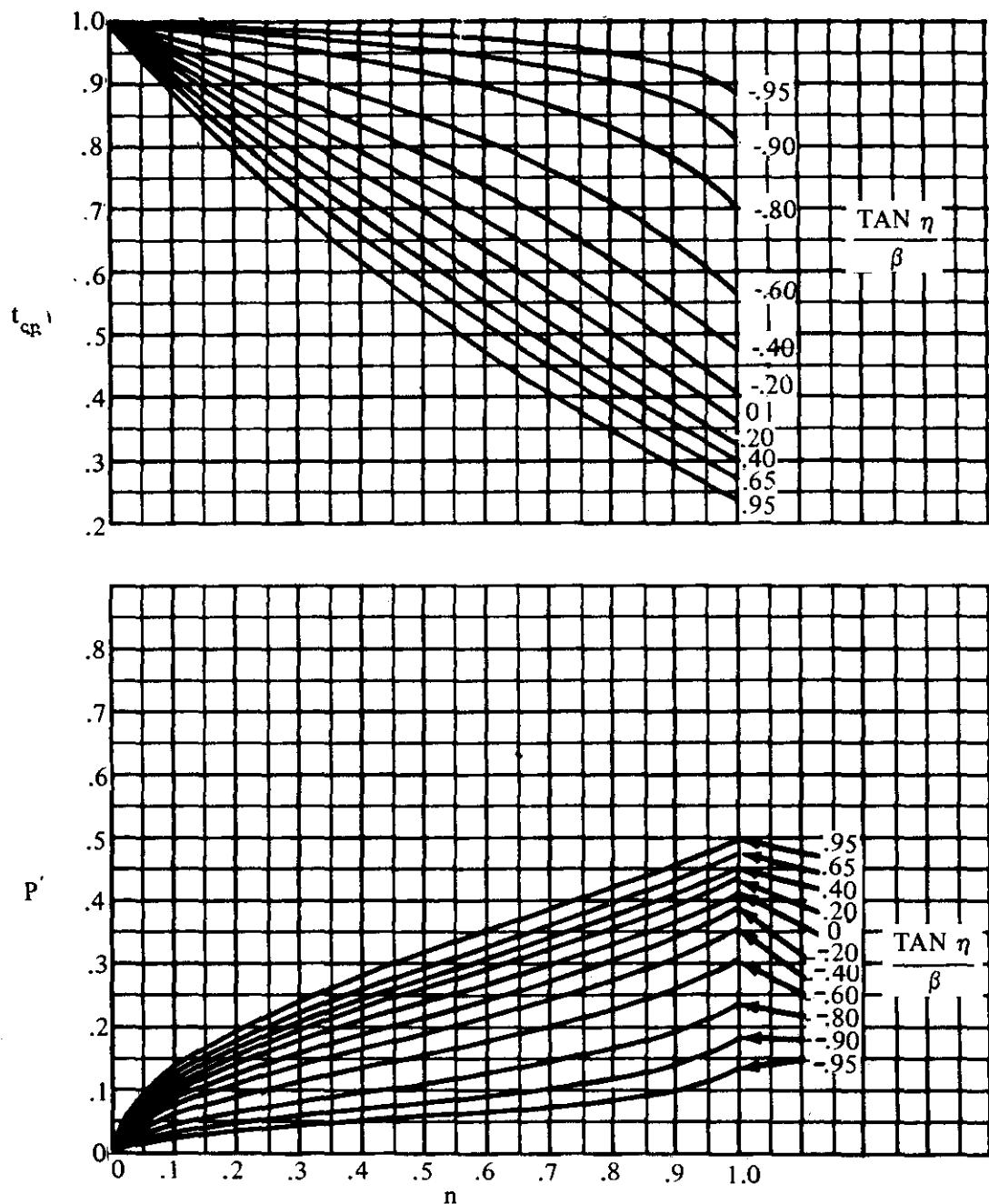


FIGURE 6.1.6.1-34 (CONT'D)

SUPersonic SPEEDS

(e)  $r' = 0$  TO 1.0

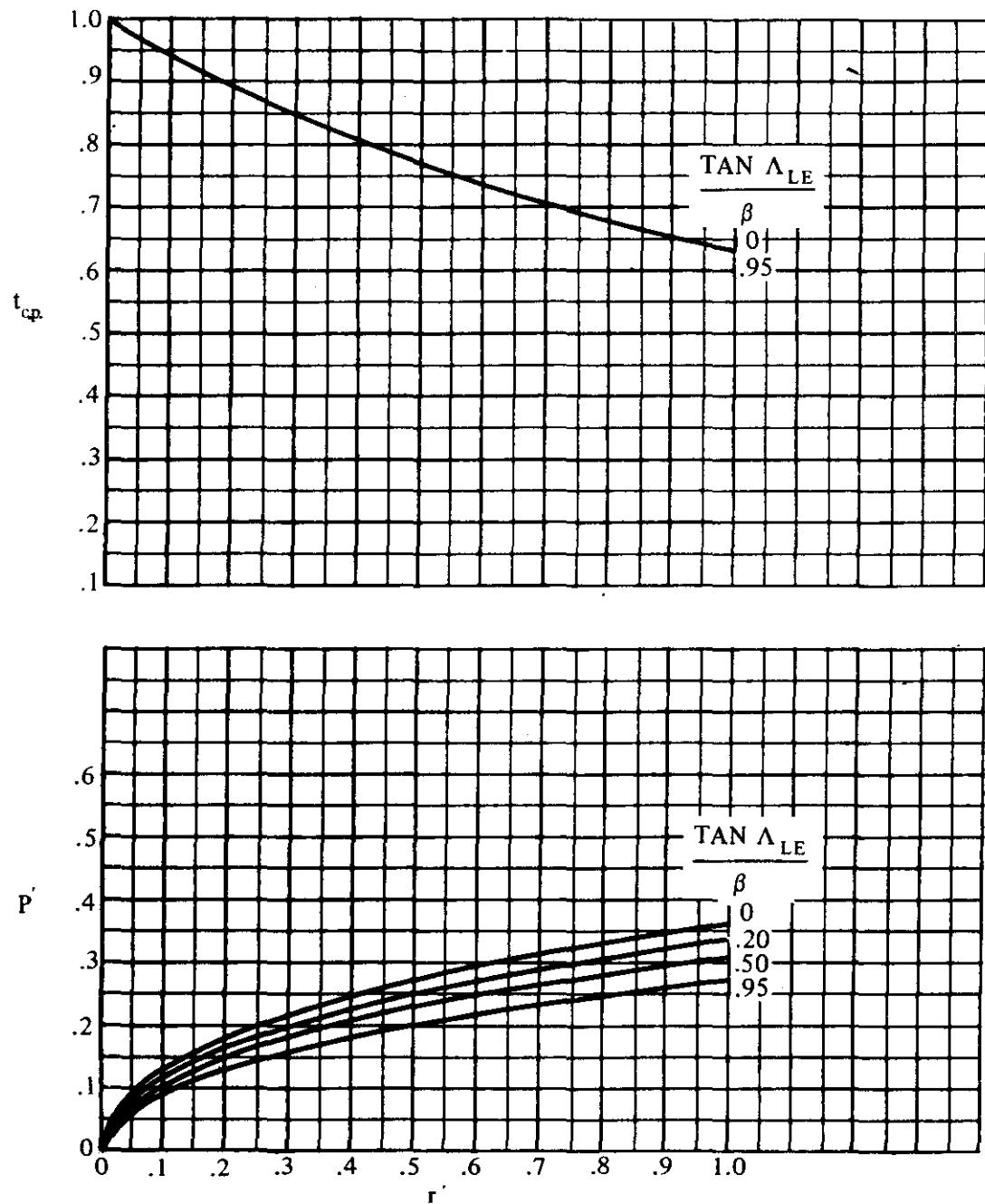


FIGURE 6.1.6.1-34 (CONTD)

SUPersonic SPEEDS

(f)  $r' = 1.0$  TO 10.0

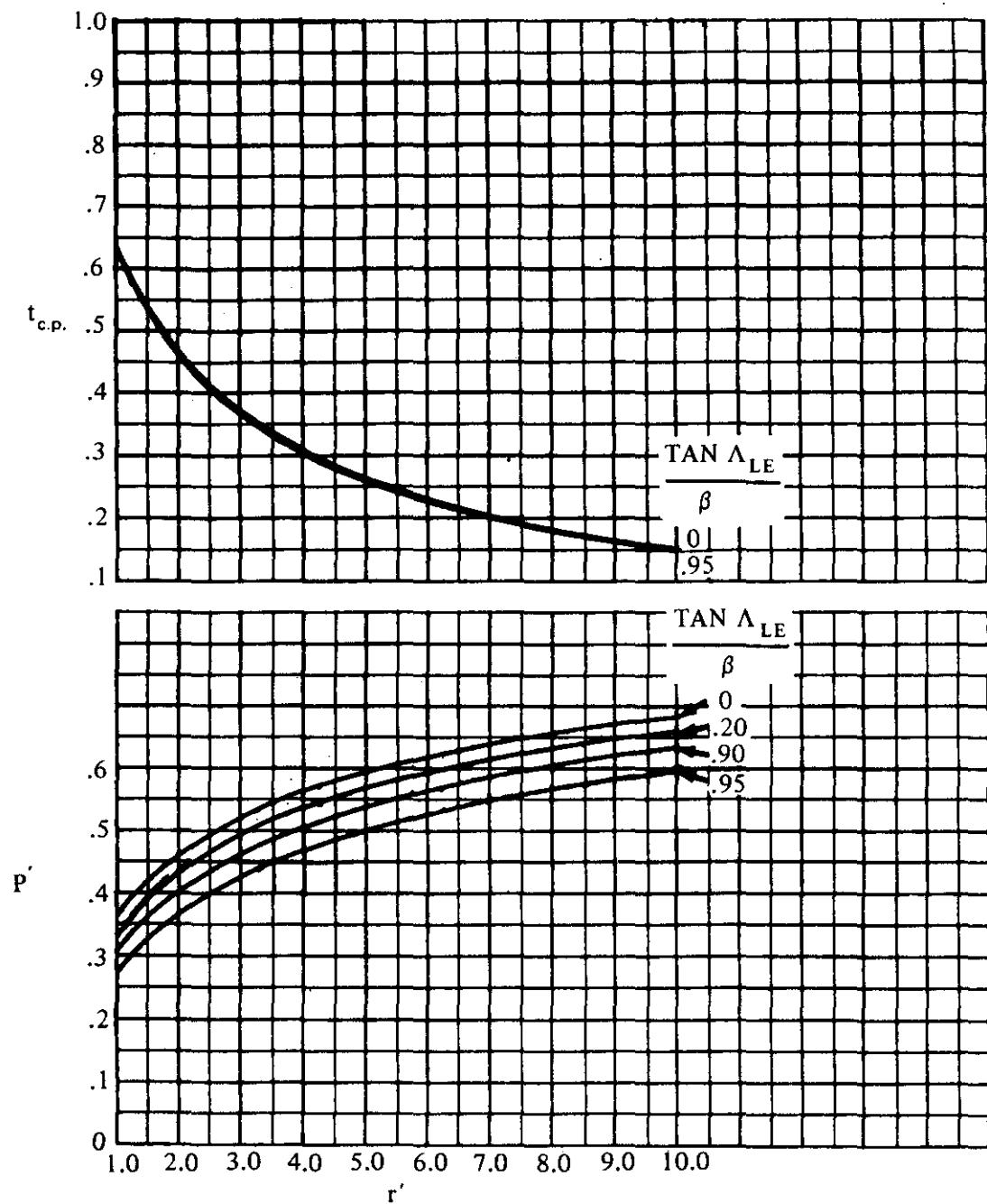


FIGURE 6.1.6.1-34 (CONTD)

### 6.1.6.2 HINGE-MOMENT DERIVATIVE $C_{h_\delta}$ OF HIGH-LIFT AND CONTROL DEVICES

#### A. SUBSONIC

The hinge-moment derivative due to control deflection can be approximated from the method of Reference 1. The method is based on lifting-line theory, with additional lifting-surface corrections to account for sweep.

The method is based on equations in terms of section parameters; therefore, the accuracy of the method is dependent upon the accuracy with which the section characteristics can be estimated. Test data on the particular airfoil-flap combination under consideration or one closely resembling it should always be preferred to characteristics obtained from generalized methods. Calculated values and test data for several different configurations are presented in Table 6.1.6.2-A to illustrate the accuracy of the method and summarize available test data.

The method is directly applicable to control surfaces having constant chord ratios and constant airfoil contours across the span. For configurations with variable chord ratios or variable airfoil contours across the span, it is suggested that average values of the section characteristics be used. Furthermore, the accuracy of the method in predicting the effects of finite-wing parameters decreases as the wing aspect ratio decreases. Application of the method to wings with aspect ratios of three or less should be avoided.

Experimental data have shown that for sweptback wings the shape of the ends of the control surface can have a critical effect on the hinge-moment parameters. The Datcom method is applicable to controls with the control-surface ends cut parallel to the plane of symmetry. For configurations with wing cutouts, or with control surfaces that do not have ends parallel to the plane of symmetry, it is suggested that empirical procedures be used to estimate  $C_{h_\delta}$ .

The effect of subcritical Mach-number corrections on hinge moments appears to be small for control surfaces having trailing-edge angles less than approximately  $12^\circ$ . Therefore, the Datcom method, which neglects subcritical Mach-number effects, may be applied over a large portion of the subcritical Mach-number range.

#### DATCOM METHOD

The hinge-moment derivative due to the deflection of a sealed, plain trailing-edge control at subsonic speeds, based on the product of the control-surface area and the control-surface chord  $S_c c_c$  (area and chord aft of the hinge line), is approximated by

$$C_{h_\delta} = \cos \Lambda_{c/4} \cos \Lambda_{HL} \left[ \left( C_{h_\delta} \right)_{balance} + \alpha_\delta \left( C_{h_\alpha} \right)_{balance} \frac{2 \cos \Lambda_{c/4}}{A + 2 \cos \Lambda_{c/4}} \right] + \Delta C_{h_\delta} \quad 6.1.6.2-a$$

where

$(c_{h_\alpha})_{\text{balance}}$  is the section hinge-moment derivative due to angle of attack. Test data on the particular flapped airfoil are preferred, but the derivative can be approximated by the method of Paragraph A of Section 6.1.3.1. (This term could be  $c'_{h_\alpha}$  or  $c''_{h_\alpha}$  from Section 6.1.3.1.)

$(c_{h_\delta})_{\text{balance}}$  is the section hinge-moment derivative due to control deflection. Test data on the particular flapped airfoil are preferred, but the derivative can be approximated by the method of Paragraph A of Section 6.1.3.2. (This term could be  $c'_{h_\delta}$  or  $c''_{h_\delta}$  from Section 6.1.3.2.)

$\alpha_\delta$  is the two-dimensional lift-effectiveness parameter expressed as

$$\alpha_\delta = - \frac{(c_{q_\delta})_\alpha}{(c_{q_\alpha})_\delta} \quad (\text{Equation 6.1.1.1-b})$$

where

$c_{q_\delta}$  is the lift effectiveness of the sealed, plain trailing-edge control obtained by using the method of Section 6.1.1.1.

$c_{q_\alpha}$  is the airfoil section lift-curve slope (including the effects of compressibility) from Section 4.1.1.2.

When experimental values of the section lift increment  $\Delta c_q$  are available, the lift effectiveness parameter should be calculated using

$$(\alpha_\delta)_{c_q} = - \frac{(\Delta c_q)_{\text{experiment}}}{(c_{q_\alpha})_\delta}$$

$\Delta C_{h_\delta}$  is an approximate lifting-surface correction which accounts for induced-camber effects. It is obtained by multiplying the quantity  $\frac{\Delta C_{h_\delta}}{c_{q_\delta} B_2 K_\delta \cos \Lambda_{c/4} \cos \Lambda_{HL}}$  from Figure 6.1.6.2-15a, by its denominator. The primed values of the control-surface and wing chord ratios, used in reading Figure 6.1.6.2-15a, refer to measurements normal to the wing quarter-chord line.

The terms in the denominator are defined below, except for  $c_{q_\delta}$ , which is defined above.

$B_2$  accounts for the effect of the control surface and balance chord ratios. This parameter is obtained from Figure 6.1.6.1-19c, where the primed values of the control-surface and balance-chord ratios refer to measurements normal to the quarter-chord line.

$K_\delta$  accounts for the effect of control-surface span. This parameter is defined by

$$K_\delta = \frac{(K_\delta)_{\eta_i} (1 - \eta_i) - (K_\delta)_{\eta_o} (1 - \eta_o)}{\eta_o - \eta_i} \quad 6.1.6.2-b$$

where

$\eta_i$  is the inboard span station of the control,

$$\eta_i = \frac{\text{inboard span ordinate}}{b/2}$$

$(K_\delta)_{\eta_i}$  is obtained from Figure 6.1.6.2-15b as a function of the inboard spanwise location ( $\eta_i$ ) of the control panel.

$\eta_o$  is the outboard span station of the control,

$$\eta_o = \frac{\text{outboard span ordinate}}{b/2}$$

$(K_\delta)_{\eta_o}$  is obtained from Figure 6.1.6.2-15b as a function of the outboard spanwise location ( $\eta_o$ ) of the control panel.

### Sample Problem

Given: The flapped wing configuration of Reference 8. This is the configuration of the sample problem of Paragraph A, Section 6.1.6.1. The characteristics are repeated.

#### Wing Characteristics:

$$A = 3.43 \quad \lambda = 0.44 \quad \Lambda_{c/4} = 48.7^\circ \quad \text{NACA 65-012 airfoil (normal to .50c of unswept wing)}$$

$$t/c = 0.086 \text{ (streamwise)}$$

$$\tan \frac{\phi'_{TE}}{2} = 0.0697 \text{ (streamwise)}$$

$$\tan \frac{\phi''_{TE}}{2} = 0.0523 \text{ (streamwise)}$$

Flap Characteristics:

$$\text{Plain trailing-edge flap} \quad \text{Sealed gap} \quad \Lambda_{HL} = 41^\circ$$

$$c_f/c = 0.167 \text{ (streamwise)} \quad c'_f/c' = 0.20 \text{ (normal to .25c)}$$

$$c_b/c_f = 0.090 \text{ (streamwise)} \quad c'_b/c'_f = 0.115 \text{ (normal to .25c)}$$

$$t_c/(2c_f) = 0.090 \text{ (streamwise)} \quad \text{Round-nosed control}$$

$$\eta_i = 0.586 \quad \eta_o = 0.99 \quad \delta = 0$$

Additional Characteristics:

$$\text{Low speed} \quad R_\ell = 2.2 \times 10^6$$

$$(c_{h\alpha})_{\text{balance}} = -0.00516 \text{ per deg}$$

$$c_{\ell\alpha} = 0.105 \text{ per deg}$$

$$\frac{c_{\ell\alpha}}{(c_{\ell\alpha})_{\text{theory}}} = 0.855$$

} (Sample Problem, Paragraph A, Section 6.1.6.1)

Compute:

Lift effectiveness (Section 6.1.1.1)

$$(c_{\ell\delta})_{\text{theory}} = 3.29 \text{ per rad} \quad (\text{Figure 6.1.1.1-39a})$$

$$\frac{c_{\ell\delta}}{(c_{\ell\delta})_{\text{theory}}} = 0.745 \quad (\text{Figure 6.1.1.1-39b})$$

$$K' = 1.0 \quad (\text{Figure 6.1.1.1-40})$$

$$c_{\ell\delta} = \frac{\Delta c_{\ell\delta}}{\delta_f} = \left[ \frac{c_{\ell\delta}}{(c_{\ell\delta})_{\text{theory}}} \right] (c_{\ell\delta})_{\text{theory}} K' \quad (\text{Equation 6.1.1.1-c})$$

$$= (0.745)(3.29)(1.0) = 2.45 \text{ per rad}$$

$$\alpha_\delta = - \frac{(c_{\ell\delta})_\alpha}{(c_{\ell\alpha/\delta})} \quad (\text{Equation 6.1.1.1-b})$$

$$= - \frac{2.45}{(0.105)} \frac{1}{57.3} = -0.407$$

Section hinge-moment derivative  $c_{h\delta}$  (Section 6.1.3.2)

$$(c_{h\delta})_{\text{theory}} = -0.810 \text{ per rad} \quad (\text{Figure 6.1.3.2-12b})$$

$$\frac{c'_{h\delta}}{(c_{h\delta})_{\text{theory}}} = 0.883 \quad (\text{Figure 6.1.3.2-12a})$$

$$c'_{h\delta} = \left[ \frac{c'_{h\delta}}{(c_{h\delta})_{\text{theory}}} \right] (c_{h\delta})_{\text{theory}} \quad (\text{Equation 6.1.3.2-a})$$

$$= (0.883)(-0.810) = -0.715 \text{ per rad}$$

$$\text{Balance ratio} = \sqrt{\left(\frac{c_b}{c_f}\right)^2 \cdot \left(\frac{t_c}{2c_f}\right)^2} = 0 \quad (\text{Equation 6.1.3.1-d})$$

$$\frac{(c_{h\delta})_{\text{balance}}}{c''_{h\delta}} = 1.0 \quad (\text{Figure 6.1.3.2-13})$$

$$c''_{h\delta} = c'_{h\delta} + 2(c_{\ell\delta})_{\text{theory}} \left[ 1 - \frac{(c_{\ell\delta})}{(c_{\ell\alpha/\delta})_{\text{theory}}} \right] \left( \tan \frac{\phi''_{TE}}{2} - \frac{t}{c} \right) \quad (\text{Equation 6.1.3.2-b})$$

$$= (-0.715) + 2(3.29) [1 - 0.745] (0.0523 - 0.086)$$

$$= -0.7715 \text{ per rad} = -0.0135 \text{ per deg}$$

$$(c_{h\delta})_{\text{balance}} = c''_{h\delta} \left[ \frac{(c_{h\delta})_{\text{balance}}}{c''_{h\delta}} \right] \quad (\text{Equation 6.1.3.2-c})$$

$$= -0.0135 \text{ per deg}$$

Induced camber effect  $\Delta C_{h_\delta}$

$$B_2 = 0.885 \quad (\text{Figure 6.1.6.1-19c})$$

$$\left. \begin{array}{l} (K_\delta)_{\eta_i} = 2.0 \\ (K_\delta)_{\eta_o} = 4.25 \end{array} \right\} \quad (\text{Figure 6.1.6.2-15b})$$

$$K_\delta = \frac{(K_\delta)_{\eta_i} (1 - \eta_i) - (K_\delta)_{\eta_o} (1 - \eta_o)}{\eta_o - \eta_i} \quad (\text{Equation 6.1.6.2-b})$$

$$= \frac{(2.0)(1 - 0.586) - (4.25)(1 - 0.99)}{0.99 - 0.586}$$

$$= 1.944$$

$$c_{q_\delta} B_2 K_\delta \cos \Lambda_{c/4} \cos \Lambda_{HL} = \frac{2.45}{57.3} (0.885)(1.944)(0.660)(0.7547)$$

$$= 0.03665 \text{ per deg}$$

$$\frac{\Delta C_{h_\delta}}{c_{q_\delta} B_2 K_\delta \cos \Lambda_{c/4} \cos \Lambda_{HL}} = 0.0218 \quad (\text{Figure 6.1.6.2-15a})$$

$$\Delta C_{h_\delta} = (0.0218)(0.03665) = 0.000799 \text{ per deg}$$

Solution:

$$C_{h_\delta} = \cos \Lambda_{c/4} \cos \Lambda_{HL} \left[ \left( c_{h_\delta} \right)_{\text{balance}} + \alpha_\delta \left( c_{h_\alpha} \right)_{\text{balance}} \frac{2 \cos \Lambda_{c/4}}{A + 2 \cos \Lambda_{c/4}} \right] + \Delta C_{h_\delta} \quad (\text{Equation 6.1.6.2-a})$$

$$= (0.6600)(0.7547) \left[ (-0.0135) + (-0.407)(-0.00516) \frac{2(0.6600)}{3.43 + 2(0.6600)} \right] + 0.000799$$

$$= -0.00563 \text{ per deg}$$

The test value from Reference 8 is  $-0.0031$  per degree.

## B. TRANSONIC

No method is available for the prediction of the hinge-moment derivative  $C_{h\delta}$  at transonic speeds. Because of the mixed-flow conditions and interrelated shock-wave and boundary-layer-separation effects encountered at transonic speeds, the prediction of  $C_{h\delta}$  by theoretical means is extremely difficult. Experimental results for  $C_{h\delta}$  at transonic speeds are presented in References 2 through 5.

## C. SUPERSONIC

The supersonic three-dimensional hinge moment due to control deflection can be computed for trailing-edge surfaces by the method of Reference 6. The method is based on linearized theory and applies to tapered and untapered control surfaces with the following restrictions:

1. Leading and trailing edges of the control surface are swept ahead of the Mach lines from the deflected controls.
2. Control root and tip chords are parallel to the plane of symmetry.
3. Controls are located either at the wing tip or far enough inboard so that the outermost Mach lines from the deflected controls do not cross the wing tip.
4. Innermost Mach lines from the deflected controls do not cross the wing root chord.
5. The wing planform has leading edges swept ahead of the Mach lines and has streamwise tips.
6. Controls are not influenced by the tip conical flow from the opposite wing panel or by the interaction of the wing-root Mach cone with the wing tip.

Calculated values and test data for several different configurations are presented in Table 6.1.6.2-B to illustrate the accuracy of the method and summarize available test data.

For leading-edge control surfaces and for trailing-edge control surfaces with subsonic leading edges, reverse-flow techniques (see Reference 7) can be used.

### DATCOM METHOD

The hinge-moment derivative  $C_{h\delta}$  at supersonic speeds for a symmetric, straight-sided control, based on the product of the control-surface area and the control-surface chord  $S_c c_c$  (area and chord aft of the hinge line), is approximated by

$$C_{h\delta} = \frac{1}{\beta} \left( 1 - \frac{C_2}{C_1} \phi_{TE} \right) \beta C'_{h\delta} \quad 6.1.6.2-c$$

where

$\left(1 - \frac{C_2}{C_1} \phi_{TE}\right)$  is a thickness correction factor to the supersonic flat-plate derivative.

$$C_1 = \frac{2}{\sqrt{M^2 - 1}} \text{ per radian}$$

$$C_2 = \frac{(\gamma + 1) M^4 + 4(M^2 - 1)}{2(M^2 - 1)^2} \text{ per radian}$$

$\phi_{TE}$  is the trailing-edge angle in radians, measured normal to the control hinge line.

$\gamma$  is the ratio of specific heats,  $\gamma = 1.4$ .

For a symmetrical biconvex airfoil the airfoil thickness correction factor in Equation 6.1.6.2-c is

$$1 - \frac{4}{3} \frac{C_2}{C_1} \left(\frac{t}{c}\right)' \left[1 + 2 \left(\frac{x_h}{c}\right)'\right]$$

where

$\left(\frac{t}{c}\right)'$  is the maximum airfoil-thickness ratio, measured in a plane normal to the control hinge axis.

$\left(\frac{x_h}{c}\right)'$  is the chordwise location of the control hinge axis, measured in a plane normal to the control hinge axis.

Thickness correction factors for other airfoil sections can be determined from Reference 6.

$\beta C'_{h\delta}$  is the supersonic flat-plate hinge-moment parameter obtained from Figure 6.1.6.2-17. For tapered controls this parameter is a function of  $\tan \Lambda_{HL}/\beta$ ,  $\tan \Lambda_{TE}/\beta$ , and the control taper ratio  $\lambda_f$ . For untapered controls it is a function of  $\tan \Lambda_{HL}/\beta$ ,  $\tan \Lambda_{TE}/\beta$ , and the control aspect-ratio parameter  $\beta A_f$ .

### Sample Problem

Given: Wing with a tapered, trailing-edge control.

$$\Lambda_{HL} = 31^\circ \quad \Lambda_{TE} = 27.6^\circ \quad \lambda_f = 0.713 \quad \phi_{TE} = 3^\circ$$

$$\text{Symmetric, flat-sided section} \quad M = 1.80; \quad \beta = 1.50$$

Compute:

$$C_1 = \frac{2}{\sqrt{M^2 - 1}} = \frac{2}{1.5} = 1.33 \text{ per rad}$$

$$C_2 = \frac{(\gamma+1) M^4 - 4(M^2 - 1)}{2(M^2 - 1)^2} = \frac{(2.4)(1.8)^4 - 4(2.24)}{2(2.24)^2} = 1.62 \text{ per rad}$$

$$\left(1 - \frac{C_2}{C_1} \phi_{TE}\right) = \left[1 - \left(\frac{1.62}{1.33}\right) \frac{3.0}{57.3}\right] = 0.936$$

$$\frac{\tan \Lambda_{HL}}{\beta} = \frac{0.6009}{1.5} = 0.401$$

$$\frac{\tan \Lambda_{TE}}{\beta} = \frac{0.5228}{1.5} = 0.349$$

$$\beta C'_h \delta = -0.0335 \text{ per deg} \quad (\text{Figure 6.1.6.2-1 7c})$$

Solution:

$$C_h \delta = \frac{1}{\beta} \left(1 - \frac{C_2}{C_1} \phi_{TE}\right) \beta C'_h \delta \quad (\text{Equation 6.1.3.2-c})$$

$$= \frac{0.936}{1.5} (-0.0335) = -0.0209 \text{ per deg}$$

## REFERENCES

1. Toll, T. A., and Schneiter, L. E.: Approximate Relations for Hinge-Moment Parameters of Control Surfaces on Swept wings at Low Mach Numbers. NACA TN 1711, 1948. (U)
2. Thompson, R. F.: Hinge-Moment, Lift, and Pitching-Moment Characteristics of a Flap-Type Control Surface Having Various Hinge-Line Locations on a 4-Percent-Thick 60° Delta Wing — Transonic-Bump Method. NACA RM L54B08, 1954. (U)
3. Thompson, R. F.: Investigation of a 42.7° Sweptback Wing Model to Determine the Effects of Trailing-Edge Thickness on the Aileron Hinge-Moment and Flutter Characteristics at Transonic Speeds. NACA RM L50J06, 1950. (U)
4. Hieser, G.: Transonic Investigation of the Effectiveness and Loading Characteristics of a Flap-Type Aileron With and Without Paddle Balances on an Unswept-Wing-Fuselage Model. NACA RM L56B02, 1956. (U)
5. Runckel, J. F., and Hieser, G.: Normal-Force and Hinge-Moment Characteristics at Transonic Speeds of Flap-Type Ailerons at Three Spanwise Locations on a 4-Percent-Thick Sweptback-Wing-Body Model and Pressure Distribution Measurements on an Inboard Aileron. NASA TN D-842, 1961. (U)
6. Goin, K. L.: Equations and Charts for the Rapid Estimation of Hinge-Moment and Effectiveness Parameters for Trailing-Edge Controls Having Leading and Trailing Edges Swept Ahead of the Mach Lines. NACA TR 1041, 1951. (U)
7. Heaslet, M. A., and Spreiter, J. R.: Reciprocity Relations in Aerodynamics, NACA TN 2700, 1952. (U)
8. Fischel, J., and Schneiter, L. E.: An Investigation at Low Speed of a 51.3° Sweptback Semispan Wing Equipped With 16.7-Percent-Chord Plain Flaps and Ailerons Having Various Spans and Three Trailing-Edge Angles. NACA RM L&H20, 1948. (U)

9. Dods, J. B., Jr.: Wind-Tunnel Investigation of Horizontal Tails. III – Unswept and 35° Swept-back Plan Forms of Aspect Ratio 6. NACA RM A8H30, 1948. (U)
10. Tinting, B. E., and Dickson, J. K.: Tests of a Model Horizontal Tail of Aspect Ratio 4.5 in the Ames 12-Foot Pressure Wind Tunnel. I – Quarter-Chord Line Swept Back 35°. NACA RM A9G13, 1949. (U)
11. Kolbe, C. D., and Bandettini, A.: Investigation in the Ames 12-Foot Pressure Wind Tunnel of a Model Horizontal Tail of Aspect Ratio 3 and Taper Ratio 0.5 Having the Quarter-Chord Line Swept Back 45°. NACA RM A51D02, 1951. (U)
12. Johnson, H. I.: Measurements of Aerodynamic Characteristics of a 35° Sweptback NACA 65-009 Airfoil Model with 1/4-Chord Plain Flap by the NACA Wing-Flow Method. NACA RM L7F13, 1947. (U)
13. Morrill, C. P., Jr., and Boddy, L. E.: High-Speed Stability and Control Characteristics of a Fighter Airplane Model with a Swept-Back Wing and Tail. NACA RM A7K28, 1948. (U)
14. Cleary, J. W., and Boddy, L. E.: Wind-Tunnel Investigation of a 45° Swept-Back Wing Having a Symmetrical Root and a Highly Cambered Tip, Including the Effects of Fences and Lateral Controls. NACA RM A53I21, 1953. (U)
15. Pfyl, F. A.: Aerodynamic Study of a Wing-Fuselage Combination Employing a Wing Swept Back 63° – Effectiveness of an Inboard Elevon as a Longitudinal and Lateral-Control Device at Subsonic and Supersonic Speeds. NACA RM A51I18, 1951. (U)
16. Hammond, A. D.: The Effect of Various Aerodynamic Balances on the Low-Speed Lateral-Control and Hinge-Moment Characteristics of a 0.20-Chord Partial-Span Outboard Aileron on a Wing with Leading Edge Swept Back 51.3°. NACA RM L52G03, 1952. (U)
17. Schneiter, L. E., and Hagerman, J. R.: Wind-Tunnel Investigation at High Subsonic Speeds of the Lateral-Control Characteristics of an Aileron and a Stepped Spoiler on a Wing with Leading Edge Swept Back 51.3°. NACA RM L9D06, 1949. (U)
18. Moseley, W. C., Jr., and Gainer, T. G.: Some Effects of Control Profile and Control Trailing-Edge Angle on the Oscillating Hinge-Moment and Flutter Characteristics of Flap-Type Controls at Transonic Speeds. NASA TM X-170, 1960. (U)
19. Fischel, J., and Schneiter, L. E.: An Investigation at Low Speeds of a 51.3° Sweptback Semispan Wing with a Raked Tip and with 16.7-Percent-Chord Ailerons Having Three Spans and Three Trailing-Edge Angles. NACA RM L8F29, 1948. (U)
20. Dods, J. B., Jr.: Wind-Tunnel Investigation of Horizontal Tails. II – Unswept and 35° Swept-Back Plan Forms of Aspect Ratio 4.5. NACA RM A8B11, 1948. (U)
21. Harper, J. J.: Wind-Tunnel Investigation of Effects of Various Aerodynamic Balance Shapes and Sweepback on Control-Surface Characteristics of Semispan Tail Surfaces with NACA 0009, 0015, 66-009, 66(215)-014, and Circular-Arc Airfoil Sections. NACA TN 2495, 1951. (U)
22. Lord, D. R., and Driver, C.: Investigation of the Effect of Balancing Tabs on the Hinge-Moment Characteristics of a Trailing-Edge Flap-Type Control on a Trapezoidal Wing at a Mach Number of 1.61. NACA RM L54F22, 1954. (U)
23. Sivells, J. C., and Goin, K. L.: Experimental and Calculated Hinge Moments of Two Ailerons on a 42.7° Sweptback Wing at a Mach Number of 1.9. NACA RM L8K24a, 1949. (U)
24. Conner, D. W., and Mitchell, M. H., Jr.: Control Effectiveness and Hinge-Moment Measurements at a Mach Number of 1.9 of a Nose Flap and Trailing-Edge Flap on a Highly Tapered Low-Aspect-Ratio Wing. NACA RM L8K17a, 1949. (U)
25. Lord, D. R., and Czarnecki, K. R.: Aerodynamic Characteristics of Several Flap-Type Trailing-Edge Controls on a Trapezoidal Wing at Mach Numbers of 1.61 and 2.01. NACA RM L54D19, 1954. (U)
26. Spearman, M. L., and Webster, R. A.: An Investigation at Mach Numbers of 1.40 and 1.59 of the Effects of Aileron Profile on the Aerodynamic Characteristics of a Complete Model of Supersonic Aircraft Configuration. NACA RM L50J31, 1951. (U)
27. Boatright, W. B., and Rainey, R. W.: Hinge-Moment Measurement of a Wing with Leading-Edge and Trailing-Edge Flaps at a Mach Number of 1.93. NACA RM L8K12a, 1949. (U)
28. Dunning, R. W., and Ulman, E. F.: Aerodynamic Characteristics at Mach Number 4.04 of a Rectangular Wing of Aspect Ratio 1.33 having a 6-Percent-Thick Circular-Arc Profile and a 30-Percent-Chord Full-Span Trailing-Edge Flap. NACA RM L53D03, 1953. (U)
29. Robinson, R. L.: An Investigation of a Supersonic Aircraft Configuration having a Tapered Wing with Circular-Arc Sections and 40° Sweepback – Static Lateral Control Characteristics at Mach Numbers of 1.40 and 1.59. NACA RM L50I11, 1950. (U)

TABLE 6.1.6.2-A  
SUBSONIC HINGE-MOMENT DERIVATIVE DUE TO CONTROL DEFLECTION  
DATA SUMMARY AND SUBSTANTIATION

Ref.	M	A	$\Delta c/4$ (deg)	$\lambda$	Type of Control Surface	$C_{h_h}$ Calc	$C_{h_h}$ Test	$\Delta C_{h_h}$ Calc-Test
9	0.23	6	5.7	0.5	Elevator	-0.0118	-0.0104	-0.0014
10	0.21	4.5	35.3	0.5	Elevator	-0.00830	-0.0081	-0.0002
	0.6					-0.00976	-0.0094	-0.0004
	0.8					-0.0132	-0.0118	-0.0014
	0.85					-0.0151	-0.0128	-0.0023
	0.9					-0.0184	-0.0147	-0.0037
11	0.25	3	45.6	0.5	Elevator	-0.00608	-0.0067	0.0006
	0.6					-0.00725	-0.0079	0.0006
	0.8					-0.00991	-0.0083	-0.0016
	0.9					-0.0139	-0.0087	-0.0052
12	0.55	3.04	35.0	1.0	Flap	-0.00956	-0.0085	-0.0011
	0.8					-0.0136	-0.010	-0.0036
	0.9					-0.0190	-0.010	-0.0090
13	0.3	4.785	35.22	0.513	Aileron	-0.00431	-0.0057	0.0014
	0.6					-0.00586	-0.0046	-0.0013
	0.8					-0.00829	-0.0043	-0.0040
	0.85					-0.00962	-0.0040	-0.0056
	0.875					-0.0106	-0.0040	-0.0066
	0.9					-0.0119	-0.0055	-0.0064
	0.3	4.65	35.59	0.450	Elevator	-0.00593	-0.0063	0.0004
	0.6					-0.00755	-0.0040	-0.0036
	0.8					-0.0103	-0.0024	-0.0079
	0.85					-0.0119	-0.0020	-0.0099
	0.875					-0.0130	-0.0006	-0.0124
	0.9					-0.0144	0	-0.0144
4	0.7	4.0	4.8	0.5	Aileron	-0.0164	-0.0110	-0.0054
	0.8					-0.0199	-0.0130	-0.0069
	0.9					-0.0281	-0.0185	-0.0096
14	0.25	5.515	45.0	0.532	Aileron	-0.00554	-0.005	-0.0005
	0.8					-0.00945	-0.006	-0.0035
	0.9					-0.0131	-0.006	-0.0071
	0.25					-0.00552	-0.005	-0.0005
	0.8					-0.00941	-0.006	-0.0034
	0.9					-0.0130	-0.006	-0.0070
15	0.6	3.50	60.8	0.25	Elevon	-0.00337	-0.0029	-0.0005
	0.9					-0.00626	-0.0035	-0.0028
16	0.328	3.06	38.7	0.49	Aileron	-0.00571	-0.0031	-0.0026
	0.328					0.00363	-0.0013	0.0049

TABLE 6.1.6.2-A (CONT'D)

Ref.	M	A	$\Lambda_{c/4}$ (deg)	$\lambda$	Type of Control Surface	$C_{h\delta}$ Calc	$C_{h\delta}$ Test	$\Delta C_{h\delta}$ Calc-Test
17	0.302	3.06	38.7	0.49	Aileron	-0.00566	-0.0043	-0.0014
	0.499					-0.00633	-0.0043	-0.0020
	0.7					-0.00787	-0.0047	-0.0032
	0.8					-0.00955	-0.0048	-0.0048
18	0.6	3.0	0	1.0	Flap	-0.00225	-0.005	0.0027
	0.7					-0.00262	-0.004	0.0014
	0.8					-0.00327	-0.0026	-0.0007
	0.85					-0.00383	-0.0095	0.0057
	0.9					-0.00478	-0.005	0.0002
	0.6					-0.00301	-0.005	0.0020
	0.7					-0.00347	-0.004	0.0005
	0.8					-0.00429	-0.005	0.0007
	0.85					-0.00499	-0.0055	0.0005
	0.9					-0.00619	-0.002	-0.0042
	0.6					-0.00390	-0.0053	0.0014
	0.7					-0.00447	-0.0043	-0.0002
	0.8					-0.00547	-0.001	-0.0045
	0.85					-0.00634	-0.004	-0.0023
	0.9					-0.00782	-0.0043	-0.0035
	0.6					-0.00564	-0.012	0.0064
	0.7					-0.00641	-0.011	0.0046
	0.8					-0.00779	-0.011	0.0032
	0.85					-0.00901	-0.012	0.0030
	0.9					-0.0111	-0.0145	0.0034
8	0.12	3.43	48.6	0.44	Aileron	-0.00477	-0.0064	0.0016
						-0.00469	-0.0060	0.0013
						-0.00447	-0.0057	0.0012
						-0.00504	-0.0067	0.0017
						-0.00489	-0.0064	0.0015
						-0.00178	-0.0035	0.0017
						-0.00543	-0.0069	0.0015
19	0.12	3.58	48.7	0.44	Aileron	-0.00592	-0.0071	0.0012
						-0.00494	-0.0056	0.0007
						-0.00219	-0.0025	0.0003
						-0.00586	-0.0073	0.0014
						-0.00488	-0.0058	0.0009
						-0.00214	-0.0028	0.0007
						-0.00568	-0.0070	0.0013

TABLE 6.1.6.2-A (CONTD)

Ref.	M	A	$\Delta c/4$ (deg)	$\lambda$	Type of Control Surface	$C_{h\delta}$ Calc	$C_{h\delta}$ Test	$\Delta C_{h\delta}$ Calc-Test
19	0.12	3.68	48.7	0.44	Aileron	-0.00471	-0.0057	0.0010
↓	↓	↓	↓	↓		-0.00199	-0.0023	0.0003
20	0.17	4.5	7.6	0.5	Elevator	-0.0109	-0.0095	-0.0014
↓	↓	↓	35.3	↓		-0.00775	-0.0069	-0.0009
21	0.12	3.36	13.5	0.4	Flap	-0.0102	-0.0068	-0.0034
↓	↓	↓	↓	↓		-0.00558	-0.0032	-0.0024
		3.30	40.0	0.4	Flap	-0.00768	-0.0041	-0.0036
		↓	↓	↓		-0.00698	-0.0078	0.0008
		3.36	13.5	0.4	Flap	-0.00376	-0.0049	0.0011
		↓	↓	↓		-0.00455	-0.0012	-0.0034
		3.36	13.5	0.4	Flap	-0.00251	0.0005	-0.0030
		↓	↓	↓		-0.00735	-0.0100	0.0026
		3.36	13.5	0.4	Flap	-0.00392	-0.0082	0.0043
		↓	↓	↓		-0.00550	-0.0086	0.0031
		3.36	13.5	0.4	Flap	-0.00608	-0.0059	-0.0002
		↓	↓	↓		-0.00318	-0.0054	0.0022
		3.36	13.5	0.4	Flap	-0.00452	-0.0054	0.0009
		↓	↓	↓		-0.00536	-0.0048	-0.0006
		3.36	13.5	0.4	Flap	-0.00335	-0.0036	0.0002
		↓	↓	↓		-0.00412	-0.0040	-0.0001
		3.36	13.5	0.4	Flap	-0.00539	-0.0110	0.0056
		↓	↓	↓		-0.00279	-0.0094	0.0066
		3.36	13.5	0.4	Flap	-0.00426	-0.0112	0.0069
		↓	↓	↓		-0.00197	-0.0019	-0.0001
		3.36	13.5	0.4	Flap	-0.000815	-0.0022	0.0014
		↓	↓	↓		-0.00149	-0.0027	0.0012
Average $\Delta  C_{h\delta}^{\text{calc}} - C_{h\delta}^{\text{test}}  = 0.0029$								

**TABLE 6.1.6.2-B**  
**SUPersonic HINGE-MOMENT DERIVATIVE DUE TO CONTROL DEFLECTION**  
**DATA SUMMARY AND SUBSTANTIATION**

Ref.	M	A	$\Delta_{LE}$ (deg)	$\lambda$	$C_{h\delta}$ Calc	$C_{h\delta}$ Test	$\Delta(C_{h\delta})$ Calc-Test
22	1.61	3.1	23	0.4	-0.0209	-0.0210	0.0001
23	1.9	4.0	42.7	0.5	-0.0122	-0.010	-0.0022
↓	↓	↓	↓	↓	-0.0122	-0.014	0.0018
24	1.9	1.06	45	0.31	-0.0151	-0.010	-0.0051
25	1.61	3.1	23	0.4	-0.0192	-0.021	0.0018
↓	↓	↓	↓	↓	-0.0196	-0.019	-0.0006
26	1.59	4.0	42.7	0.5	-0.0169	-0.012	-0.0049
↓	↓	↓	↓	↓	-0.0169	-0.012	-0.0049
27	1.93	3.14	9.33	0.59	-0.0124	-0.011	-0.0014
28	4.04	1.33	0	1.0	-0.00464	-0.0056	0.001
29	1.59	4.0	42.7	0.5	-0.0166	-0.0157	-0.0009
↓	1.59	1.17	40.6	0.337	-0.0149	-0.0031	-0.0118
Average $\Delta  C_{h\delta}^{calc} - C_{h\delta}^{test}  = 0.0020$							

SUBSONIC SPEEDS

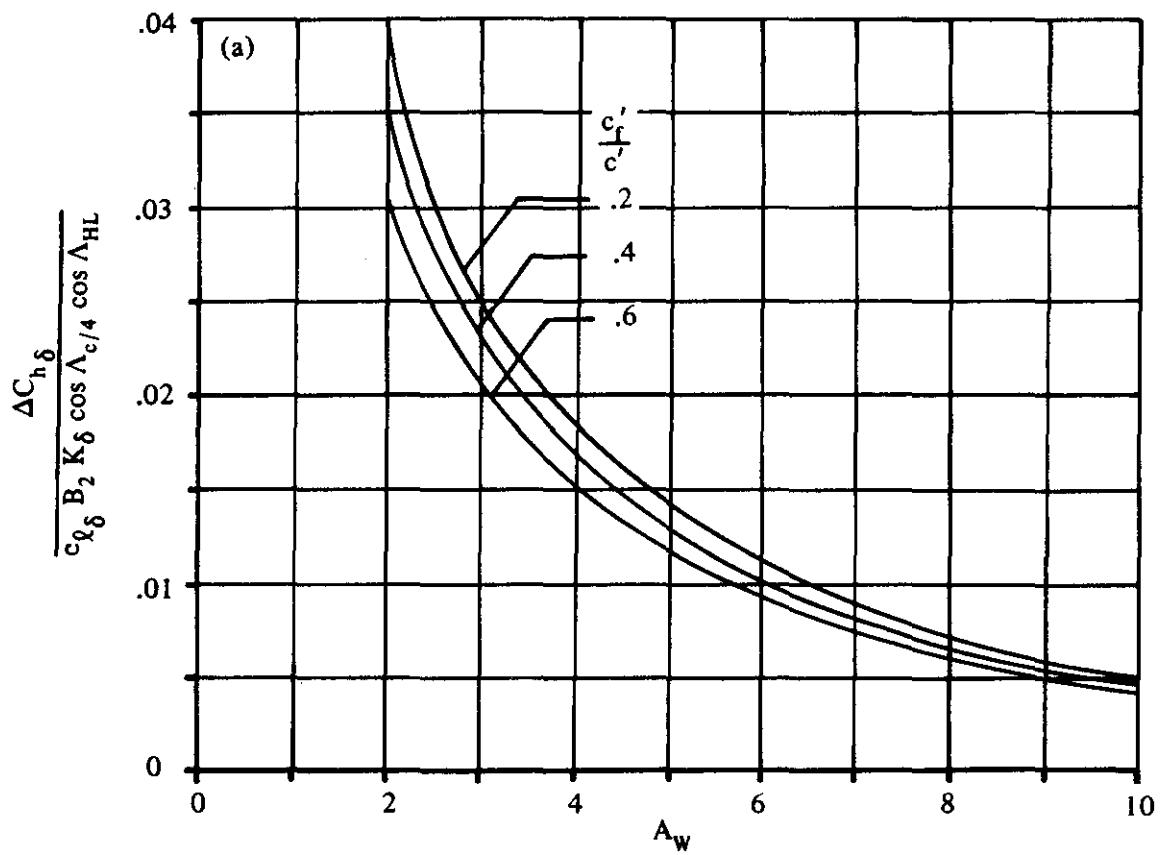


FIGURE 6.1.6.2-15 CHARTS FOR INDUCED-CAMBER CORRECTIONS TO HINGE-MOMENT PARAMETERS OF FINITE-SPAN WINGS

SUBSONIC SPEEDS

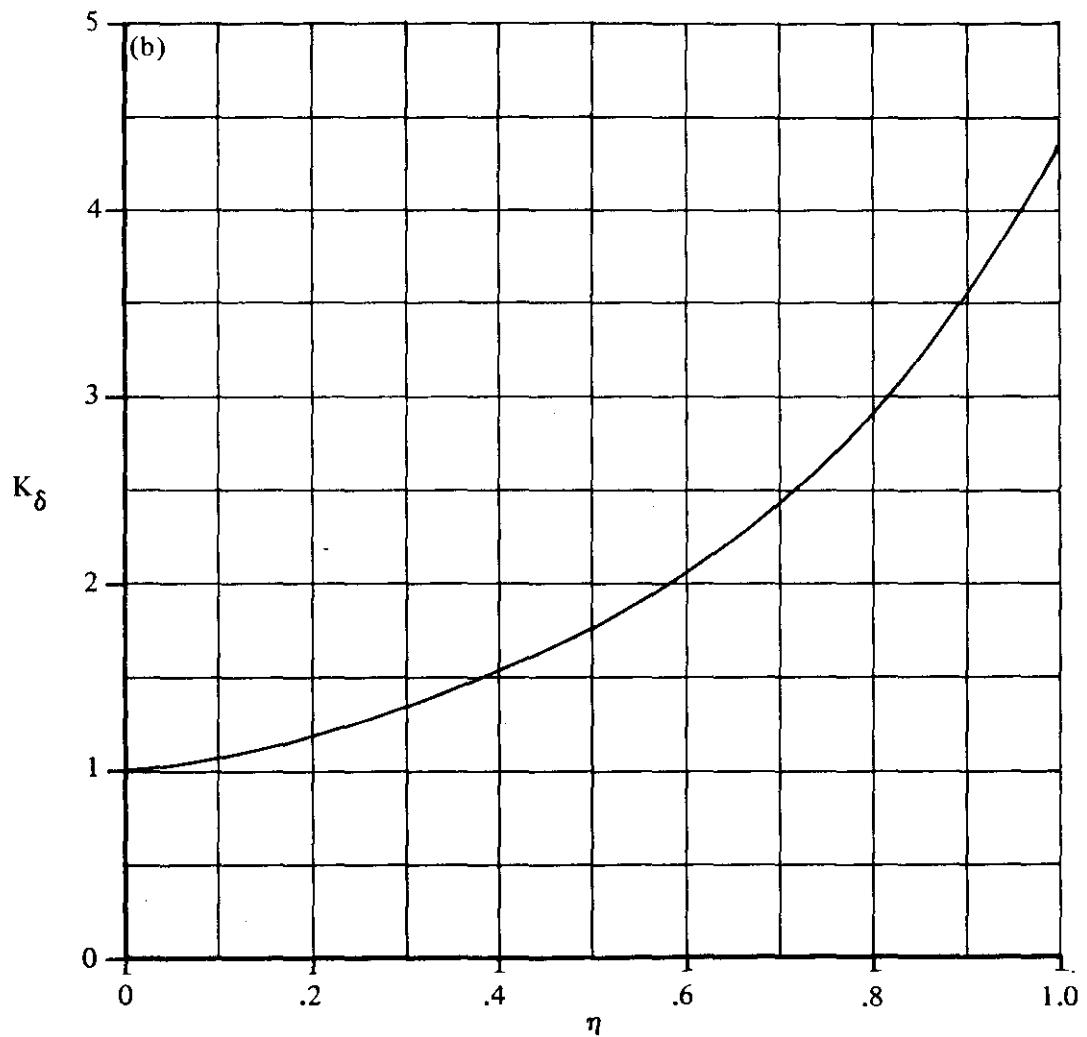


FIGURE 6.1.6.2-15 (CONTD)

### SUPersonic SPEEDS

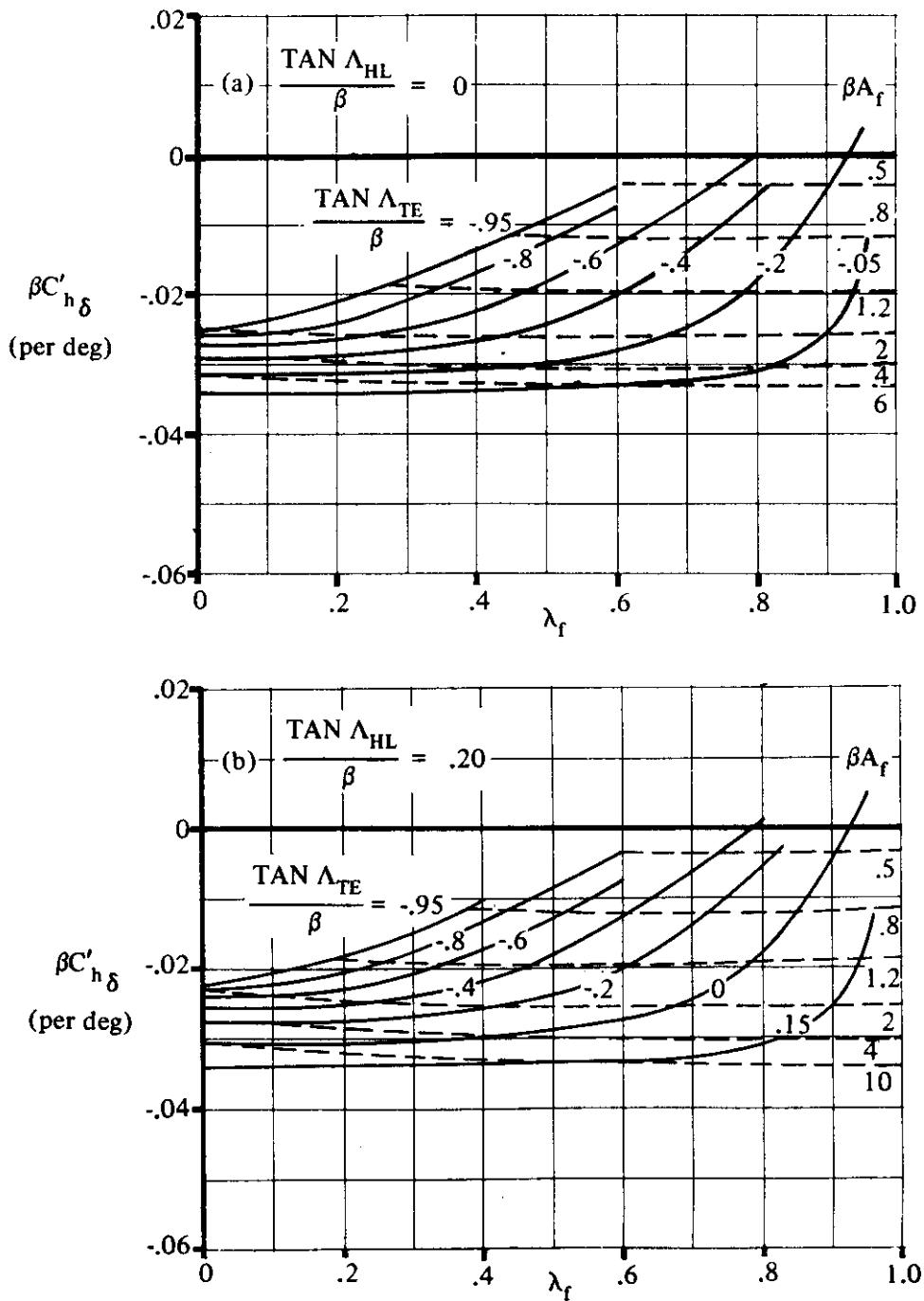


FIGURE 6.1.6.2-17 SUPersonic THEORETICAL HINGE-MOMENT DERIVATIVE  $C_{h\delta}$

6.1.6.2-17

### SUPersonic SPEEDS

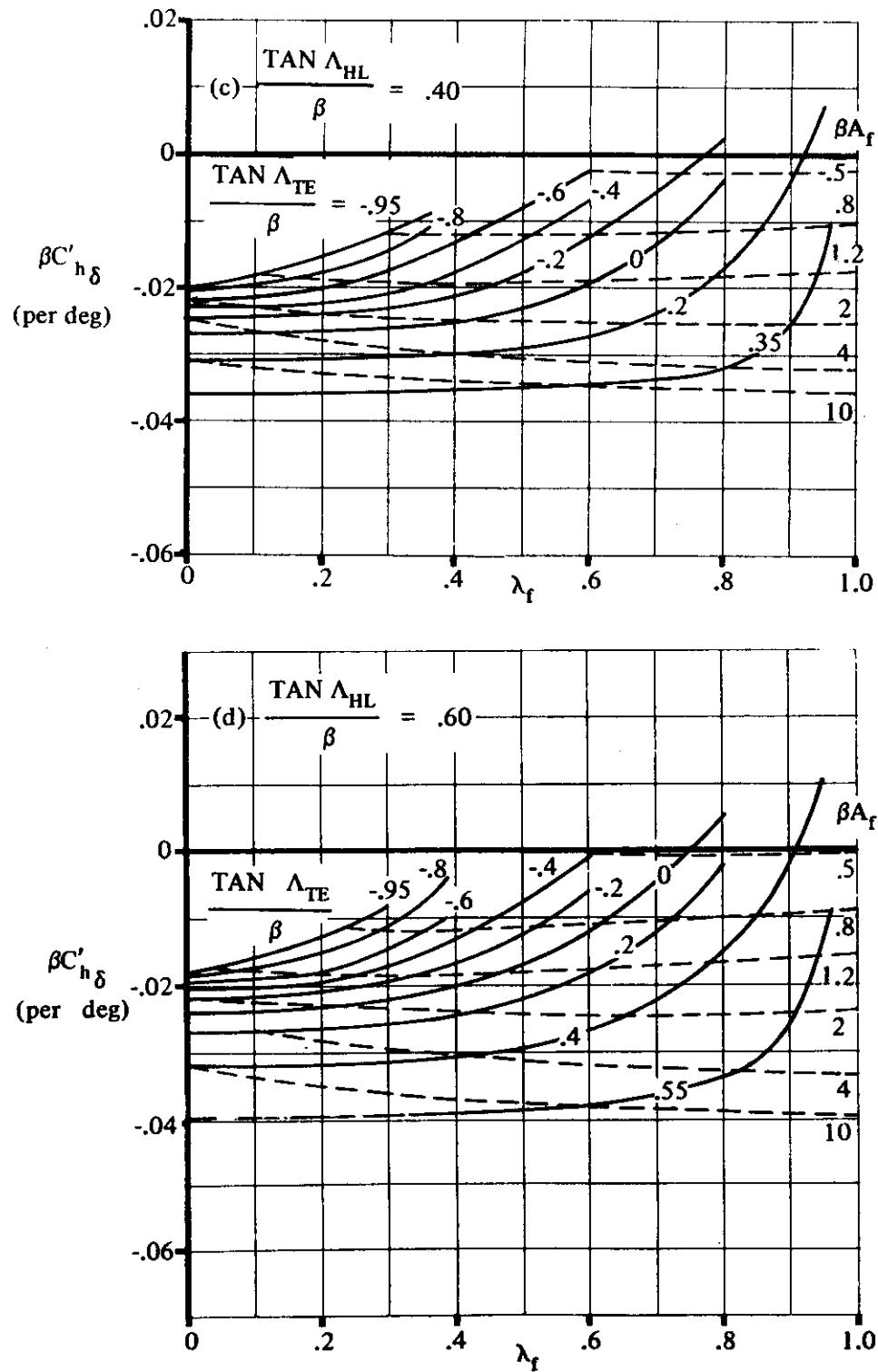


FIGURE 6.1.6.2-17 (CONT'D)

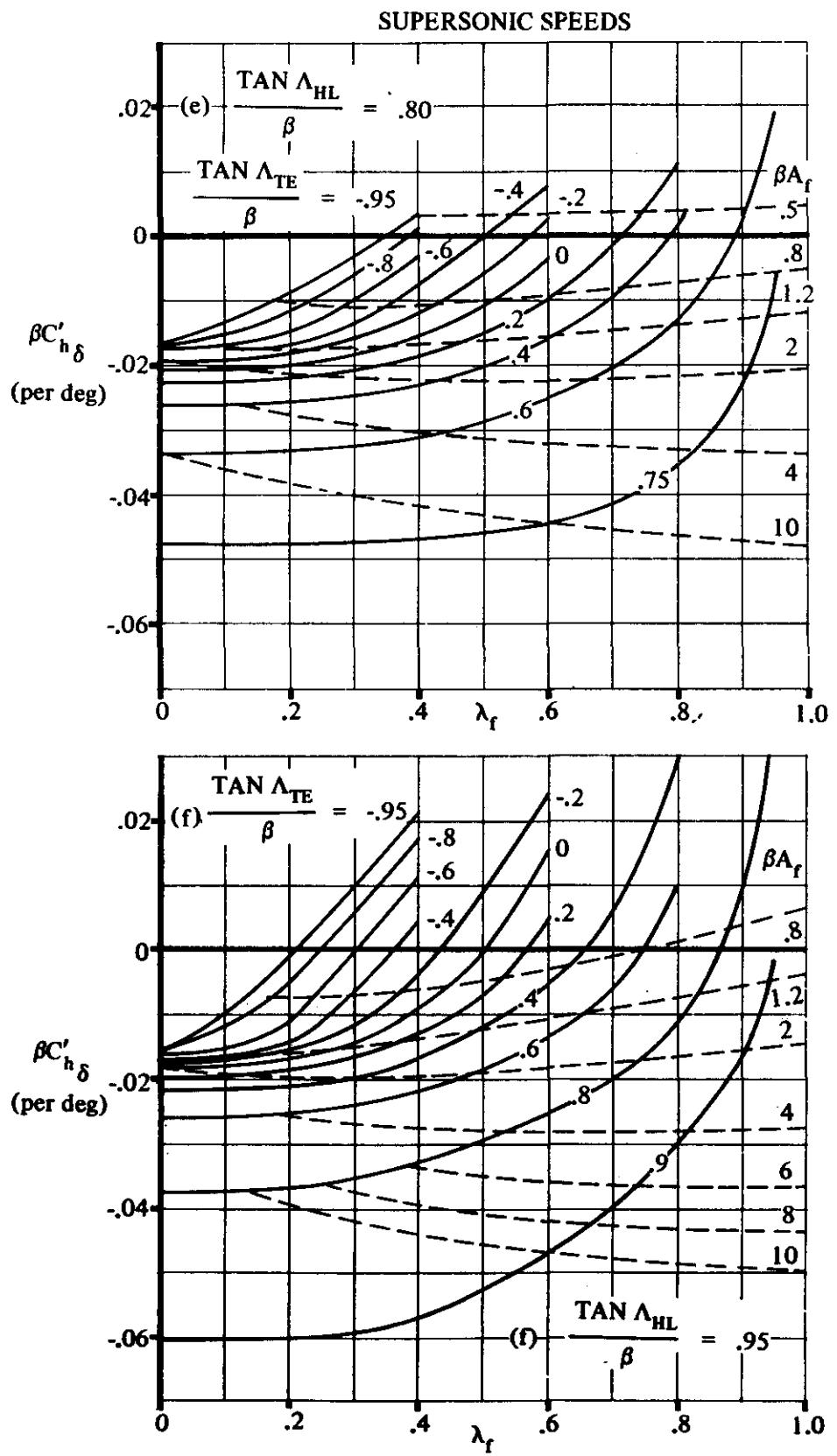


FIGURE 6.1.6.2-17 (CONTD)

### 6.1.7 DRAG OF HIGH-LIFT AND CONTROL DEVICES

There are two types of movable control surfaces. Control surfaces or flaps may exist as movable portions of primary lifting surfaces, such as ailerons on a wing or elevators attached to stabilizers. A control surface may also exist as an independent lifting surface, such as an "all-flying" horizontal tail. The drag due to deflection of the latter type of control is treated simply as the drag of the surface at a different angle of attack. This section of the Datcom is therefore concerned only with the drag due to deflection of flaps or control surfaces that are movable parts of primary lifting surfaces.

The deflection of flaps or control surfaces causes two increments of drag. First, the profile drag of the primary-surface-movable-surface combination is changed. Second, if the two surfaces are producing a force normal to the local flow direction, the deflection of the control surface will produce a different span-loading distribution and may therefore change the induced drag of the surfaces. Both profile-drag and induced-drag effects are considered in the Datcom.

#### A. SUBSONIC

The changes of both induced drag and profile drag due to control or flap deflection are considered. The change of induced drag is caused by a change in span-loading distribution. The induced drag is calculated first without flap or control surfaces deflected and then with these surfaces deflected. The increment of drag thus obtained is the change of induced drag due to flap or control-surface deflection.

The method of calculating induced drag used in this Section is limited to the flap deflections and angles of attack for which the flow is attached over the control surface. The approximate maximum control deflections for linear control characteristics are given in figure 6.1.3-2. This chart, based on test data for an NACA 0009 airfoil, is intended only to serve as a guide.

#### DATCOM METHOD

To calculate the induced drag for a spanwise symmetrically loaded wing, the span-loading distribution is determined by the method of Section 6.1.5.1. A finite number  $m$  of spanwise stations on the full-span wing is chosen. Each station is indicated by the integers  $v$  and  $n$ , which are related to span location by the equation

$$\eta = \cos \frac{v\pi}{m+1} = \cos \frac{n\pi}{m+1} \quad 6.1.7-a$$

The number of span stations  $m$  must be an odd integer. If the span loading is a smooth curve,  $m$  may be relatively small, for example, 7, 9, or 11. If the span loading is not smooth,  $m$  should be larger, for example, 13, 15, or 17.

For a given flap deflection  $\delta$ , the span loading is given by

$$G_v = -\left(\frac{G}{\delta}\right)_v (\alpha_\delta) \delta \quad 6.1.7-b$$

where  $\alpha_\delta$  is obtained from Section 6.1.1.1,  $\delta$  is the streamwise control deflection, and  $(G/\delta)_v$  is determined as outlined in step 1 of Method 2 in paragraph A of Section 6.1.5.1.

The induced drag can be expressed, by the method of reference 1, as

$$C_{D_i} = \frac{\pi A}{m+1} \left[ G_k \left\{ b_{kk} G_k - \sum_{n=1}^k (1 - \delta_{kn}) B_{kn} G_n \right\} + 2 \sum_{v=1}^{k-1} G_v \left\{ b_{vv} G_v - \sum_{n=1}^k (1 - \delta_{vn}) B_{vn} G_n \right\} \sin \phi_v \right] \quad 6.1.7-c$$

where

$$k = \frac{m+1}{2} \quad 6.1.7-d$$

$$b_{vv} = \frac{m+1}{4 \sin \phi_v} \quad \text{for } n = v \quad 6.1.7-e$$

$$= b_{kk} \quad \text{for } v = n = k$$

$$b_{vn} = \frac{\sin \phi_n}{(\cos \phi_n - \cos \phi_v)^2} \left( \frac{1 - (-1)^{n-v}}{2(m+1)} \right) \quad \text{for } n \neq v \quad 6.1.7-f$$

$$\delta_{vn} = 1 \quad \text{for } v = n \quad 6.1.7-g$$

$$\delta_{vn} = 0 \quad \text{for } v \neq n \quad 6.1.7-h$$

$$B_{vn} = b_{vn} \quad \text{for } n = \frac{m+1}{2} = k \quad 6.1.7-i$$

$$B_{vn} = b_{vn} + b_{v,m+1-n} \quad \text{for } n \neq \frac{m+1}{2} = k \quad 6.1.7-j$$

$$\phi = \cos^{-1} \eta \quad 6.1.7-k$$

$$\phi_v = \frac{v\pi}{m+1} \quad 6.1.7-l$$

$$\phi_n = \frac{n\pi}{m+1} \quad 6.1.7-m$$

$$G_v = -\left(\frac{C}{\delta}\right)_v (\alpha_\delta) \delta \quad (\text{equation 6.1.7-b})$$

$$= G_n \quad \text{for } n = v$$

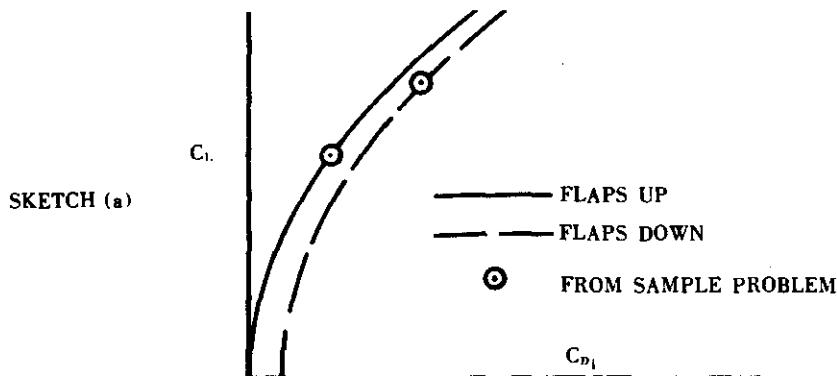
$$= G_k \quad \text{for } n = k$$

The sample problem at the end of this section demonstrates the use of equation 6.1.7-c. Step 1 of the sample problem is an evaluation of the terms of equation 6.1.7-c that are functions only of  $m$ , and hence of  $n$  and  $v$ . Once calculated for a given number of span locations  $m$ , Step 1 need not be repeated. Therefore, when using  $m = 11$  or  $m = 21$ , one may utilize the results of Step 1 in the sample problem, and begin the calculations at Step 2.

Equation 6.1.7-c gives the induced drag coefficient at a given angle of attack and a given flap deflection. The corresponding lift coefficient is

$$C_L = \frac{\pi A}{m+1} \left[ G_k + 2 \sum_{n=1}^{k-1} G_n \sin \phi_n \right] \quad 6.1.7-n$$

where the terms of equation 6.1.7-n are defined as in equation 6.1.7-c.



Equations 6.1.7-c and 6.1.7-n are evaluated at several angles of attack, both with flaps up and with flaps down. The induced drag coefficient  $C_{D_i}$  is then plotted versus  $C_L$  for flaps up and flaps down, as shown in sketch (a). The increment of  $C_{D_i}$  between these curves, at constant  $C_L$ , is the induced drag due to flap deflection at a given lift coefficient.

The increment of profile drag due to control or flap deflection can be expressed as a change of the minimum drag coefficient for the polar of the primary surface with undeflected control or flap. The minimum drag coefficient is then

$$(C_D)_{\min} = (C_{D\min})_{\text{flaps up}} + \Delta C_{D\min} \quad 6.1.7-o$$

where

$$\Delta C_{D\min} = \Delta c_{d_f} K_b + K' \frac{(\Delta C_{L_f})^2}{\pi A} \quad 6.1.7-p$$

$\Delta c_{d_f}$  is the airfoil section drag coefficient with deflected flap given in figures 6.1.7-22 and 6.1.7-23 as a function of deflection and of  $\frac{c_f}{c}$  for plain and for single-slotted flaps.

$K_b$  is given in figure 6.1.4.1-15 as a function of taper ratio and flap span ratio.

$K'$  is the flap span factor given in figures 6.1.7-24(a), (b), and (c), taken from reference 2.

$\Delta C_{L_f}$  is determined by the mechanical flap method of Section 6.1.4.1

The shift of the polar without flap or control deflection can now be drawn (figure 6.1.7-27). The increment of induced drag due to flap or control deflection is added to the basic polar. The resulting curve is then translated parallel to the  $C_D$ -axis until the minimum  $C_D$  agrees with the value given by equation 6.1.7-o.

### Sample Problem

Given: The flapped-wing configuration with the following characteristics.

Wing Characteristics:

$$A = 6.35 \quad \lambda = 0.50 \quad \Lambda_{c/4} = 40^\circ \quad S_W = 567 \text{ sq ft}$$

$$c_r = 12.6 \text{ ft} \quad \bar{c} = 9.8 \text{ ft} \quad b_w/2 = 30.0 \text{ ft}$$

$$\text{NACA } 63_1012 \text{ airfoil (streamwise)} \quad \tan \frac{\phi'_{TE}}{2} = 0.073$$

Flap Characteristics:

Plain trailing-edge flap Sealed gap

$$\eta_l = 0.195 \quad \eta_o = 0.556 \quad \delta = 11.3^\circ \text{ (streamwise)}$$

$$c_f/c = 0.20 \text{ (streamwise)}$$

Additional characteristics:

$$\text{Low speed; } \beta = 1.0 \quad \left( C_{D_{\min}} \right)_{\delta=0} = 0.0203 \quad \alpha = 10^{\circ}$$

$$R_f = 9.0 \times 10^6$$

Compute:

Step 1. Parameters that are functions of  $m$  are evaluated. These parameters remain constant for any particular value of  $m$ . Tables are presented in this section for  $m = 11$  and  $21$ , (tables 6.1.7-A through 6.1.7-F). In case it is desired to use some other value of  $m$ , the procedure for calculating these parameters is outlined below. Equations 6.1.7-a through 6.1.7-m are used.

$$\text{Let } m = 11$$

$$m + 1 = 12$$

$$k = \frac{m+1}{2} = 6$$

$$v = 1 \text{ to } k (1 \text{ to } 6)$$

$$n = 1 \text{ to } k (1 \text{ to } 6)$$

(1)

$v$	$\phi_v$	$\sin \phi_v$	$\cos \phi_v$ $= \eta$
1			
2			
3			
4			
5			
6			

Equation 6.1.7-1

(2)

		$(\cos \phi_n - \cos \phi_v)^2$					
		v					
n		1	2	3	4	5	6
1							
2							
3							
4							
5							
6							

(3)

$$\frac{1 - (-1)^{n-v}}{2(m+1)}$$

n	v					
	1	2	3	4	5	6
1						
2						
3						
4						
5						
6						

(4)

n	b <sub>vn</sub>						
	v	1	2	3	4	5	6
1							
2							
3							
4							
5							
6							

Equations 6.1.7-e and 6.1.7-f

(5)

$$(\cos \phi_{m+1-n} - \cos \phi_v)^2$$

n	v					
	1	2	3	4	5	6
1						
2						
3						
4						
5						
6						

(6)

$$\frac{1 - (-1)^{(m+1-n)-v}}{2(m+1)}$$

n	v					
	1	2	3	4	5	6
1						
2						
3						
4						
5						
6						

(7)

$b_{v, m+1-n}$						
n	v					
	1	2	3	4	5	6
1						
2						
3						
4						
5						
6						

Equations 6.1.7-e and 6.1.7-f, with  
 $(m + 1 - n)$  substituted for n

(8)

$1 - \delta_{vn}$						
n	v					
	1	2	3	4	5	6
1						
2						
3						
4						
5						
6						

Equations 6.1.7-g and 6.1.7-h

(9)

$B_{vn}$						
n	v					
	1	2	3	4	5	6
1						
2						
3						
4						
5						
6						

Equations 6.1.7-i and 6.1.7-j

(10)

$(1 - \delta_{vn}) B_{vn}$						
n	v					
	1	2	3	4	5	6
1						
2						
3						
4						
5						
6						

Step 2. Spanwise loading coefficient  $G_v$ .

The following spanwise loading coefficients must be obtained:

1. Basic loading without flaps
  2. Incremental loading due to flap deflection
  3. Basic loading with flaps
1. Basic loading without flaps:

The variation of  $G/\delta$  with  $\eta_v$  is determined as outlined in step 1 of Method 2 in paragraph A of Section 6.1.5.1.

$$c_{l\alpha} = 0.116 \text{ per deg} = 6.65 \text{ per rad (table 4.1.1-B)}$$

$$\kappa = \frac{c_{l\alpha}}{2\pi} = \frac{6.65}{2\pi} = 1.06$$

$$\frac{\beta A}{\kappa} = \frac{(1.0)(6.35)}{1.06} = 6.0$$

$$\Lambda_\beta = \tan^{-1} \left( \frac{\tan \Lambda_{c/4}}{\beta} \right) = \tan^{-1} \left( \frac{\tan 40^\circ}{1.0} \right) = 40^\circ$$

The variation of  $G/\delta$  with  $\eta_v$  is then the spanwise loading from figure 6.1.5.1-62c with  $\eta_o = 1.0$  (wing treated as a full-span flap). The desired loading coefficient  $G_v$  is calculated as follows:

$$G_v = - \left( \frac{G}{\delta} \right) \alpha_\delta \delta \quad (\text{equation 6.1.7-b})$$

$$\alpha_\delta = -1.0 \text{ (wing treated as a full wing-chord flap)}$$

$$\delta = \sigma \text{ (radians)} = 0.175 \text{ rad}$$

Then

$$G_v = \left( \frac{G}{\delta} \right)_v \alpha$$

The calculation is shown below.

$\eta$	$\left(\frac{G}{\delta}\right)_v$ per rad	$\alpha$ rad	$G_v$
0	.32	.175	.0560
.1	.33	.175	.0578
.2	.34	.175	.0595
.3	.34	.175	.0595
.4	.34	.175	.0595
.5	.33	.175	.0578
.6	.32	.175	.0560
.7	.30	.175	.0525
.8	.26	.175	.0455
.9	.21	.175	.0368
1.0	0	.175	0

2. Incremental loading due to flap deflection:

The variation of  $G/\delta$  with  $\eta_v$  may be read directly from figure 6.1.5.1-62c at  $\eta_i = 0.195$  and  $\eta_o = 0.556$ . Then, the difference in the spanwise loading of those tabulations at each span station is the spanwise loading of the actual full-chord flap. (See sketch (b), Section 6.1.5.1.)

Flap effectiveness  $\alpha_\delta$

$$\frac{c_{l\alpha}}{\left(c_{l\alpha}\right)_{\text{theory}}} = 0.899 \quad (\text{figure 4.1.1.2-8a})$$

$$\frac{c_{l\delta}}{\left(c_{l\delta}\right)_{\text{theory}}} = 0.836 \quad (\text{figure 6.1.1.1-39b})$$

$$\left(c_{l\delta}\right)_{\text{theory}} = 3.68 \text{ per rad} \quad (\text{figure 6.1.1.1-39a})$$

$$K' = 0.999 \quad (\text{figure 6.1.1.1-40})$$

$$\Delta c_l = \delta \left[ \frac{c_{l\delta}}{\left(c_{l\delta}\right)_{\text{theory}}} \right] \left(c_{l\delta}\right)_{\text{theory}} K' \quad (\text{equation 6.1.1.1-c})$$

$$= \frac{11.3}{57.3} (0.836) (3.68) (0.999) = 0.606$$

$$\alpha_{\delta} = - \frac{\Delta c_l}{(c_l \alpha)_{\delta}} \quad (\text{equation 6.1.1.1-b})$$

$$= - \frac{0.606}{(0.116)(11.3)} = -0.462$$

$$G_v = - \left( \frac{G}{\delta} \right)_v \alpha_{\delta} \delta \quad (\text{equation 6.1.7-b})$$

$$= - \left( \frac{G}{\delta} \right)_v (-0.462)(11.3/57.3) = 0.0911 \left( \frac{G}{\delta} \right)_v$$

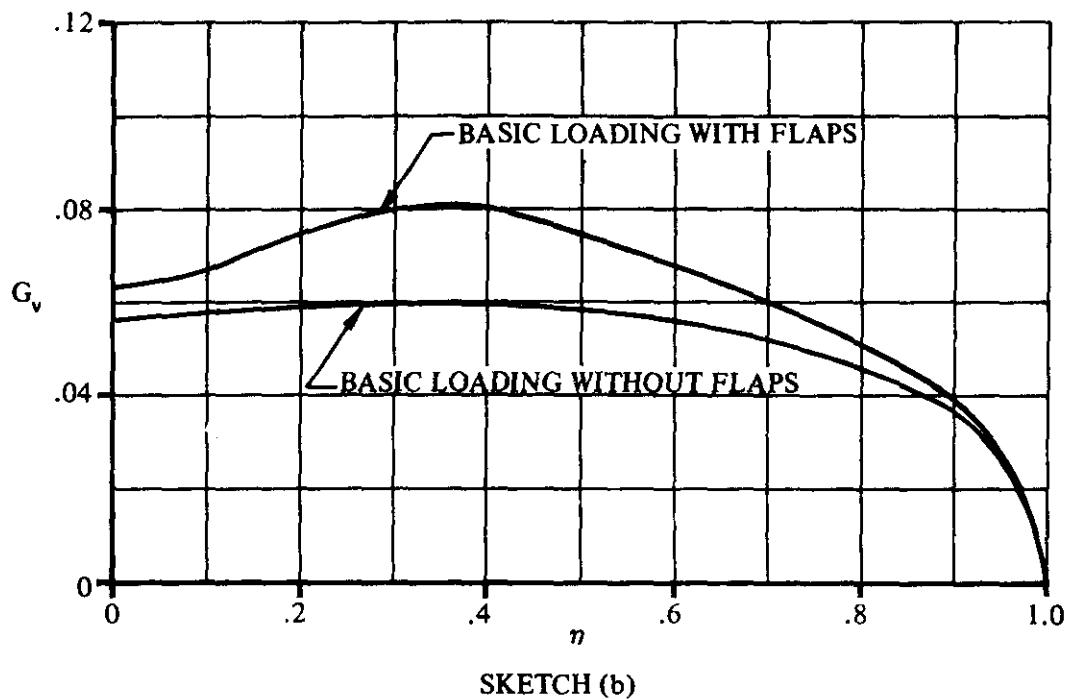
$\eta$	$\left( \frac{G}{\delta} \right)_{\eta_o} = 0.556$ (fig. 6.1.5.1-62c)	$\left( \frac{G}{\delta} \right)_{\eta_i} = 0.195$ (fig. 6.1.5.1-62c)	$\left( \frac{G}{\delta} \right)_v (\eta_o - \eta_i)$	$G_v$
0	0.30	0.22	0.08	0.0073
.1	0.31	0.21	0.10	0.0091
.2	0.32	0.15	0.17	0.0155
.3	0.32	0.10	0.22	0.0200
.4	0.30	0.07	0.23	0.0210
.5	0.23	0.05	0.18	0.0164
.6	0.17	0.04	0.13	0.0118
.7	0.11	0.03	0.08	0.0073
.8	0.07	0.02	0.05	0.0046
.9	0.05	0.02	0.03	0.0027
1.0	0	0	0	0

### 3. Basic loading with flaps:

The incremental loading due to flap deflection is added to the basic loading without flaps to obtain the basic loading with flaps.

$\eta$	$G_v$ basic loading without flaps	$G_v$ incremental loading due to flaps	$G_v$ basic loading with flaps
0	0.0560	0.0073	0.0633
.1	0.0578	0.0091	0.0669
.2	0.0595	0.0155	0.0750
.3	0.0595	0.0200	0.0795
.4	0.0595	0.0210	0.0805
.5	0.0578	0.0164	0.0742
.6	0.0560	0.0118	0.0678
.7	0.0525	0.0073	0.0598
.8	0.0455	0.0046	0.0501
.9	0.0368	0.0027	0.0395
1.0	0	0	0

The above loadings are plotted in sketch (b), in order that values of  $G_v$  may be read for any desired  $\eta_v$ .



Step 3  $C_{D_i}$  due to flaps

$$\text{Let } C_{D_i} = \frac{\pi A}{m+1} [N_1 + N_2] \quad (\text{equation 6.1.7-c})$$

where

$$N_1 = G_k \left\{ b_{kk} G_k - \sum_{n=1}^k \left[ (1 - \delta_{vn}) B_{kn} G_n \right] \right\}$$

$$N_2 = 2 \sum_{v=1}^{k-1} \left( G_v \left\{ b_{vv} G_v - \sum_{n=1}^k \left[ (1 - \delta_{vn}) B_{vn} G_n \right] \right\} \sin \phi_v \right)$$

$$m+1 = 12 \quad k = 6 \quad \frac{\pi A}{m+1} = \frac{\pi (6.35)}{12} = 1.662$$

$C_{D_i}$  must be calculated for the following loadings:

Case 1. Basic loading without flaps

Case 2. Basic loading with flaps

Case 1. (Calculations for basic loading without flaps)

Tabulate  $G_v$  for  $v = 1$  to  $k$

$v$	$\eta$ (table 6.1.7-A)	$G_v$ [from sketch (b)]
1	.9659	.0205
2	.8660	.0400
3	.7071	.0520
4	.5000	.0578
5	.2588	.0595
6	0	.0560

Calculate  $N_1$

for  $v = k = 6, n = k = 6$

①	②	③
$G_k$	$b_{nk}$ table 6.1.7-B	$b_{nk} G_k$ = ① ③
.0560	3.000	.1680

for  $v = k = 6$

①	②	③	④
$n$	$(1 - \delta_{vn}) B_{vn}$ table 6.1.7-C	$G_n$	① ③
1	.04622	.0205	.0009
2	0	.0400	0
3	.2356	.0520	.0123
4	0	.0578	0
5	2.404	.0595	.1430
6	0	.0560	0

$$\sum_{n=1}^k \textcircled{4} = 0.1562$$

$$N_1 = 0.560 \{0.1680 - 0.1562\} = 0.000661$$

Calculate  $N_2$

for  $v = 1$

(1)	(2)	(3)	(4)	(5)
v	n	$(1 - \delta_{vn}) B_{vn}$ table 6.1.7-C	$G_n$	$\sum (4)$
1	1	0	.0205	0
	2	4.187	.0400	.1675
	3	0	.0520	0
	4	.3660	.0578	.0212
	5	0	.0595	0
	6	.08931	.0560	.0050

$$\sum_{n=1}^k (5) = 0.1937$$

Repeat the above calculation for  $v = 2$  through 5. The summations are listed below.

$$(6) = \sum_{n=1}^k (1 - \delta_{vn}) B_{vn} G_n \text{ for } v = 1 \text{ to } k-1$$

v	1	2	3	4	5
(6)	.1937	.1838	.1762	.1664	.1544

(1)	(2)	(3)	(4)	(5)	(6)	(7)	(8)
v	$\sin \phi_v$ table 6.1.7-A	$b_{vv}$ table 6.1.7-B	$G_v$	$b_{vv} G_v$ = (3)(4)	(6)	$(7) - (6)$	$(1)(2)(3)$
1	.2588	11.59	.0205	.2376	.1937	.0439	.000233
2	.5000	6.000	.0400	.2400	.1838	.0562	.001124
3	.7071	4.243	.0520	.2206	.1762	.0444	.001633
4	.8660	3.464	.0578	.2002	.1664	.0358	.001692
5	.9659	3.106	.0595	.1848	.1544	.0304	.001747

$$2 \sum_{v=1}^{k-1} (6) = 0.01286$$

Solution for Case 1

$$C_{D_i} = \frac{\pi A}{m+1} [N_1 + N_2] = 1.662 [0.000661 + 0.01286] \\ = 0.0225 \text{ (basic loading without flaps)}$$

Case 2. (Calculations for basic loading with flaps at  $\alpha = 10^\circ$ )

Tabulate  $G_v$  for  $v = 1$  to  $k$

$v$	$n$	$G_v$ sketch (b)
1	.9659	.0220
2	.8660	.0432
3	.7071	.0590
4	.5000	.0747
5	.2588	.0784
6	0	.0635

Calculate  $N_1$

for  $v = k = 6, n = k = 6$

(1) $G_k$	(2) $b_{kk}$ table 6.1.7-B	(3) $b_{kk} G_k$ (1)(2)
.0635	3.00	.1905

for  $v = k = 6$

(1) $n$	(2) $(1 - \delta_{vn}) B_{kn}$ table 6.1.7-C	(3) $G_n$	(4) $(1 - \delta_{kn}) B_{kn} G_n$ (2)(3)
1	.04622	.0220	.00102
2	0	.0432	0
3	.2356	.0590	.01390
4	0	.0747	0
5	2.404	.0784	.1885
6	0	.0635	0

$$\sum_{n=1}^k (4) = 0.2034$$

$$N_1 = 0.0635 \{0.1905 - 0.2034\} = -0.000819$$

Calculate  $N_2$

for  $v = 1$

(1)	(2)	(3)	(4)	(5)
v	n	$(1 - \delta_{vn}) B_{vn}$ (table 6.1.7-C)	$G_n$	$(1 - \delta_{vn}) B_{vn} G_n$ (3) (4)
1	1	0	.0220	0
	2	4.187	.0432	.1809
	3	0	.0590	0
	4	.3660	.0747	.0273
	5	0	.0784	0
	6	.08931	.0635	.0057

$$\sum_{n=1}^k (5) = 0.2139$$

Repeat the above calculation for  $v = 2$  through 5. The summations are listed below.

$$(6) = \sum_{n=1}^k (1 - \delta_{vn}) B_{vn} G_n \text{ for } v = 1 \text{ to } k-1$$

v	1	2	3	4	5
(6)	.2139	.2089	.2121	.2052	.1873

(1)	(2)	(3)	(4)	(5)	(6)	(7)	(8)
v	$\sin \phi_v$ table 6.1.7-A	$b_{vv}$ table 6.1.7-B	$G_v$	$b_{vv} G_v$ (3) (4)	(6)	(5) - (6)	(7) (4) (2)
1	.2588	11.59	.0220	.2550	.2139	.0411	.000234
2	.5000	6.00	.0432	.2592	.2089	.0503	.001086
3	.7071	4.243	.0590	.2503	.2121	.0382	.001595
4	.8660	3.464	.0747	.2588	.2052	.0536	.003465
5	.9659	3.106	.0784	.2435	.1873	.0562	.002456

$$N_2 = 2 \sum_{v=1}^{k-1} (8) = 0.02127$$

$$C_{D_i} = \frac{\pi A}{m+1} [N_1 + N_2] = 1.662 [-0.000819 + 0.02127]$$

$$= 0.0340 \text{ (basic loading with flaps deflected } 11.3^\circ \text{ at } \alpha = 10^\circ)$$

Step 4. Determine the lift coefficient  $C_L$  for Cases 1 and 2.

Case 1. (Basic Loading without flaps)

Case 2. (Basic Loading with flaps)

$$G_k = 0.0635 \text{ for } v = k = 6$$

(1) n	(2) $G_n$	(3) $\sin \phi_n$ table 6.1.7-A	(4) $G_n \sin \phi_n$ (2) (3)
1	.0220	.2588	.00569
2	.0432	.5000	.02160
3	.0590	.7071	.04172
4	.0747	.8660	.06469
5	.0784	.9659	.07573

$$2 \sum_{n=1}^{k-1} (4) = 0.4189$$

$$C_L = \frac{\pi A}{m + 1} \left[ G_k + 2 \sum_{n=1}^{k-1} G_n \sin \phi_n \right] \quad (\text{equation 6.1.7-n})$$

$$= 1.662 [0.0635 + 0.4189]$$

$$= 0.8017 \text{ (basic loading with flaps deflected } 11.3^\circ \text{ at } \alpha = 10^\circ)$$

Step 5. Determine the profile drag increment due to flaps  $\Delta C_{D_{\min}}$

$$\Delta c_{d_f} = 0.0050 \text{ (figure 6.1.7-22)}$$

$$\left. \begin{array}{l} K_b(\eta_0 = 0.568) = 0.688 \\ K_b(\eta_1 = 0.195) = 0.265 \end{array} \right\} \quad (\text{figure 6.1.4.1-15})$$

$$K_b = K_b(\eta_0) - K_b(\eta_1) = 0.424$$

$$K' \approx 1.31 \text{ (figures 6.1.7-24a through -24c, interpolated)}$$

$$\Delta C_{L_f} \text{ (Section 6.1.4.1)}$$

$$\left. \begin{array}{l} \Delta c_L = 0.606 \\ \alpha_\delta = -0.462 \\ c_{L\alpha} = 6.65 \text{ per rad} \end{array} \right\} \quad (\text{Step 2, above})$$

$$\frac{(\alpha_\delta)_{c_L}}{(\alpha_\delta)_{c_L}} = 1.056 \quad (\text{figure 6.1.4.1-14}) \quad (\text{at } (\alpha_\delta)_{c_L} = 0.55 \text{ from inset of figure 6.1.4.1-14})$$

$$\frac{A}{\kappa} \left[ \beta^2 + \tan^2 \Lambda_{c/2} \right]^{1/2} = \frac{6.35}{1.06} [1 + (0.7866)^2]^{1/2} = 7.62$$

$$C_{L\alpha}/A = 0.640 \text{ per rad} \quad (\text{figure 4.1.3.2-49})$$

$$C_{L\alpha} = (0.640)(6.35) = 4.06 \text{ per rad}$$

$$\Delta C_{L_f} = \Delta c_L \left( \frac{C_{L\alpha}}{c_{L\alpha}} \right) \left[ \frac{(\alpha_\delta)_{c_L}}{(\alpha_\delta)_{c_L}} \right] K_b \quad (\text{equation 6.1.4.1-a})$$

$$= (0.606) \left( \frac{4.06}{6.65} \right) [1.056] (0.424)$$

$$= 0.166$$

$$\Delta C_{D_{min}} = \Delta c_d K_b + K' \frac{(\Delta C_{L_f})^2}{\pi A} \quad (\text{equation 6.1.7-p})$$

$$= (0.0050)(0.424) + (1.31) \frac{(0.166)^2}{\pi(6.35)}$$

$$= 0.00212 + 0.00181$$

$$= 0.00393$$

**Step 6. Determine the minimum drag coefficient with flaps deflected**

$$C_D_{min} = \left( C_{D_{min}} \right)_{\delta=0} + \Delta C_{D_{min}} \quad (\text{equation 6.1.7-o})$$

$$= 0.0203 + 0.0039$$

$$= 0.0242$$

At this point, the lift coefficients and induced-drag coefficients are known at  $\alpha = 10^\circ$  for flaps deflected  $11.3^\circ$ . The minimum drag coefficient with flaps deflected is also known. Steps 2 through 4 must now be repeated at several angles of attack to determine the variation of  $C_{D_1}$  with  $C_L$ , as shown in sketch (a)

on page 6.1.7-2 for flaps undeflected and flaps deflected  $11.3^\circ$ . These values are plotted in the form of figure 6.1.7-27 to give a flap-deflected drag polar.

## B. TRANSONIC

At transonic Mach numbers, the drag increment due to control deflection is extremely difficult to estimate. The transonic flow about an airfoil, which has locally subsonic and supersonic regions, is very sensitive to changes in airfoil section. The supersonic flow regions frequently terminate with a nearly normal shock wave, causing an abrupt increase in pressure at that point. The location of this shock wave can be greatly influenced by control deflection, which results in changes to the pressure distribution, and hence causes an unpredictable drag increment. The complexity of the mixed flows prevents the use of either simple theory or empirical analysis for general treatment of the problem.

## DATCOM METHOD

Because of the extreme sensitivity of the mixed flows at transonic Mach numbers, no Datcom Method is given to estimate the drag increment due to control deflection.

## C. SUPERSONIC

At supersonic speeds, the drag due to control-surface deflection can be considered in two parts - a change of wave or pressure drag, and a change of skin-friction drag.

## DATCOM METHOD

The increment of wave drag of the primary surface with control surface deflected is

$$\Delta(C_{D_{wave}}) = \left[ \frac{(C_{D_{wave}})}{(C_{D_{wave}})_{\delta=0}} - 1 \right] (C_{D_{wave}})_{\delta=0} \quad 6.1.7-q$$

where  $(C_{D_{wave}})_{\delta=0}$  is determined by the method of Section 4.1.5.1.

The ratio  $\frac{(C_{D_{wave}})}{(C_{D_{wave}})_{\delta=0}}$  can be estimated by linear theory and is approximated by

$$\frac{(C_{D_{wave}})}{(C_{D_{wave}})_{\delta=0}} = \left[ 1 - \frac{\bar{c}_t}{c} \right] + \left[ \frac{\bar{c}_t}{c} \right] \left[ \frac{\alpha + \delta}{\alpha} \right]^2 \left[ \frac{S_{a1} + \frac{1}{2} S_1}{S} + 1 - \frac{S_{a1} + S_1}{S} \right] \quad 6.1.7-r$$

where

$\frac{\bar{c}_t}{c}$  is the ratio of mean flap chord to primary-surface chord

$\alpha$  is the angle of attack of the primary surface with  $\delta=0$

$\delta$  is the deflection of the control surface relative to the primary surface, positive for trailing edge down

$S_{a1}$  is the part of the primary-surface planform area forward of and including the flap area that is not influenced by the primary-surface tip [see figure 6.1.7-28 (b)]

$S_1$  is the part of the primary-surface planform area forward of and including the flap area that is influenced by the primary-surface tip [see figure 6.1.7-28 (b)]

The effect of control surface or flap deflection on drag is

$$(C_D)_\delta = (C_D)_{\delta=0} + \Delta(C_{D_{wave}}) + \Delta(C_{f_f}) \quad 6.1.7-s$$

Although procedures can be devised for estimating the change of skin-friction drag due to control surface or flap deflection, the estimated changes are so small as to be of the order of the reading accuracy of the charts of reference 3 that are used in the calculations. Therefore the change of skin-friction drag due to control deflection will be assumed to be zero.

### Sample Problem

Given:

Configuration of sample problem 1, Method 1, paragraph C, Section 4.1.5.1.

$$\Lambda_{r/s} = 35^\circ$$

$$A = 4.0$$

$$t/c = 0.06$$

Smooth surface

Stabilized flight

$$R_f = 10'$$

Round-nose airfoil

$$M = 2.0$$

$$(C_D)_s = 0.00521$$

$$(C_{D_{\text{wave}}})_{\delta=0} = (\Delta C_D)_{\delta=0} = 0.0171$$

Additional characteristics:

$$\frac{S_w}{2} = 200 \text{ sq ft}$$

$$\frac{b_w}{2} = 20 \text{ ft}$$

$$\lambda = 0.3$$

$$c_t = 15.40 \text{ ft}$$

full-span flap

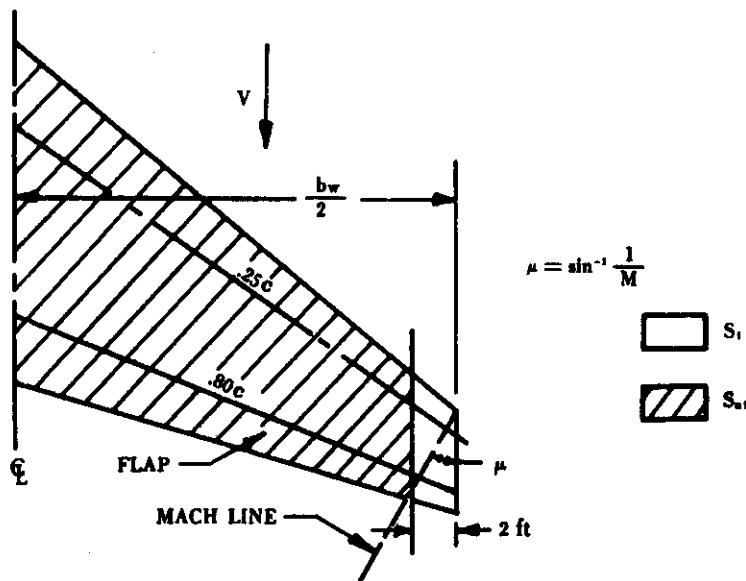
$$\frac{\bar{c}_t}{c} = 0.20$$

$$\alpha = 5^\circ$$

$$\delta = -8^\circ$$

$$(C_D)_{\delta=0} = 0.0395 \text{ (at } \alpha = 5^\circ)$$

The pertinent Mach line is shown below.



$$S_t = 10 \text{ sq ft}$$

$$S_{st} = 190 \text{ sq ft}$$

Compute:

$\Delta C_{D_{\text{wave}}}$  calculation:

$$\left[ 1 - \frac{\bar{c}_t}{c} \right] = 0.8$$

$$\left[ \frac{\alpha + \delta}{\alpha} \right]^2 = 0.36$$

$$\left[ \frac{S_{a1} + \frac{1}{2} S_1}{S} \right] = \frac{195}{200} = 0.975$$

$$\left[ \frac{S_{a1} + S_1}{S} \right] = 1.0$$

$$\begin{aligned} \frac{C_{D_{wave}}}{(C_{D_{wave}})_{\delta=0}} &= \left[ 1 - \frac{\bar{c}_t}{c} \right] + \left[ \frac{\bar{c}_t}{c} \right] \left[ \frac{\alpha + \delta}{\alpha} \right]^2 \left[ \frac{S_{a1} + \frac{1}{2} S_1}{S} + 1 - \frac{S_{a1} + S_1}{S} \right] \quad (\text{equation 6.1.7-r}) \\ &= 0.8 + 0.2 (0.36) (0.975) \\ &= 0.8702 \end{aligned}$$

$$\begin{aligned} \Delta C_{D_{wave}} &= \left[ \frac{C_{D_{wave}}}{(C_{D_{wave}})_{\delta=0}} - 1 \right] (C_{D_{wave}})_{\delta=0} \quad (\text{equation 6.1.7-q}) \\ &= [0.8702 - 1] (0.0171) \\ &= -0.00222 \end{aligned}$$

Solution for drag with flap deflection:

For  $\alpha = 5^\circ$

$$\begin{aligned} (C_D)_{\delta=-5^\circ} &= (C_D)_{\delta=0} + \Delta C_{D_{wave}} + \Delta C_{D_f} \quad (\text{equation 6.1.7-s}) \\ &= 0.0395 + (-0.00222) + 0 \\ &= 0.03728 \end{aligned}$$

TABLE 6.1.7-A

$v$	$\phi_v$ deg	$\sin \phi_v$	$\cos \phi_v$ $= \eta$
1	15.0	.2588	.9659
2	30.0	.5000	.8660
3	45.0	.7071	.7071
4	60.0	.8660	.5000
5	75.0	.9659	.2588
6	90.0	1.0	0

TABLE 6.1.7-B

n	$b_{vn}$					
	1	2	3	4	5	6
1	11.59	2.161	0	.09934	0	.02311
2	4.175	6.000	1.650	0	.1130	0
3	0	2.334	4.243	1.374	0	.1178
4	.3324	0	1.683	3.464	1.240	0
5	0	.2183	0	1.383	3.106	1.202
6	.08931	0	.1667	0	1.244	3.000

TABLE 6.1.7-C

n	(1 - $\delta_{vn}$ ) B <sub>vn</sub>					
	v					
1	2	3	4	5	6	
1	0	2.167	0	.1094	0	.04622
2	4.187	0	1.667	0	.1459	0
3	0	2.358	0	1.414	0	.2356
4	.3660	0	1.733	0	1.365	0
5	0	.2819	0	1.523	0	2.404
6	.08931	0	.1667	0	1.244	0

Note: m = 11 for tables 6.1.7-A, -B, and -C

m = 21 for tables 6.1.7-D, -E, and -F

TABLE 6.1.7-D

v	$\phi_v$ deg	$\sin \phi_v$	$\cos \phi_v$ $= \eta$
1	8.18	.1423	.9898
2	16.36	.2817	.9595
3	24.54	.4153	.9097
4	32.73	.5407	.8412
5	40.91	.6549	.7557
6	49.09	.7557	.6549
7	57.27	.8412	.5407
8	65.46	.9097	.4153
9	73.64	.9595	.2817
10	81.82	.9898	.1423
11	90.00	1.0	0

TABLE 6.1.7-E

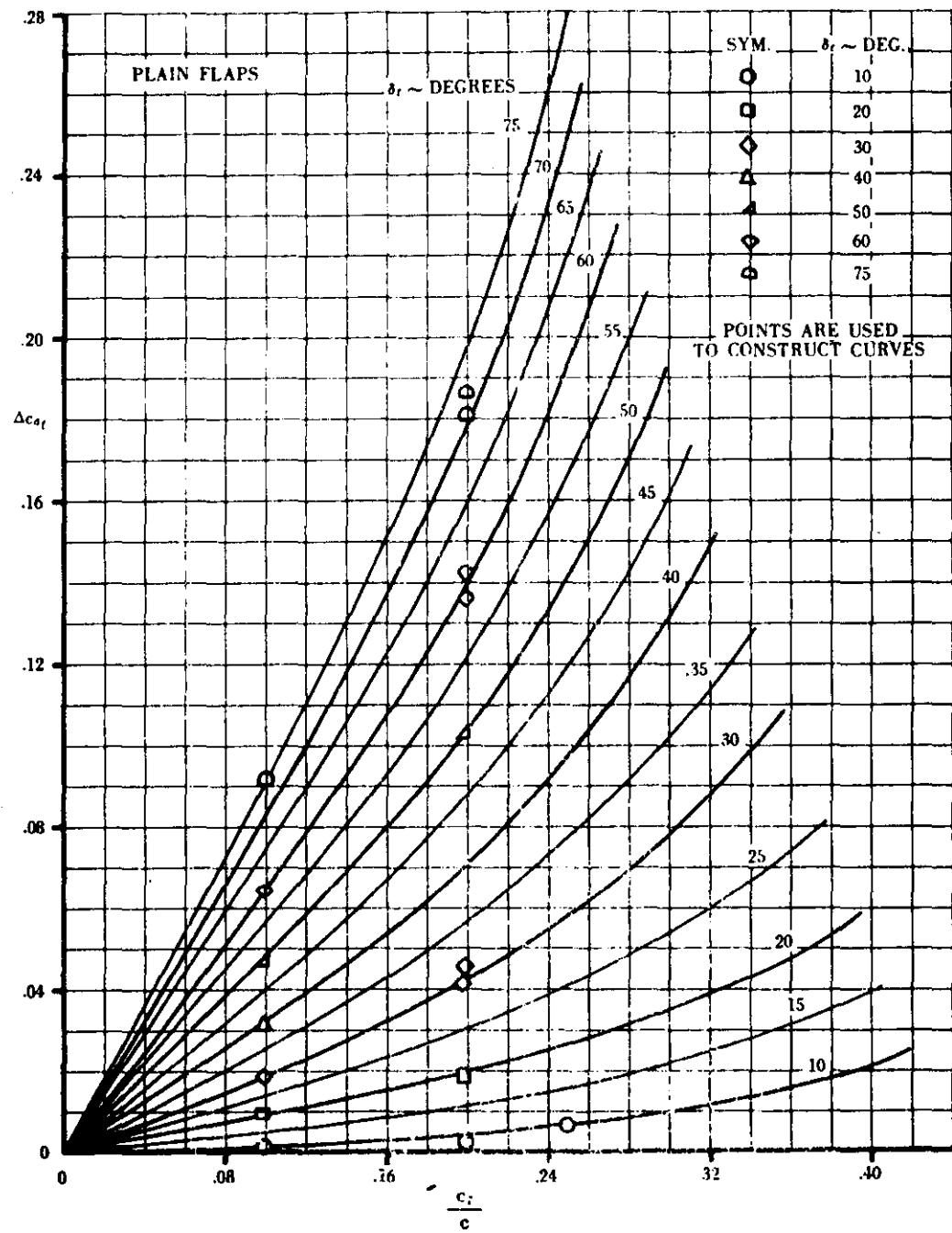
n	$b_{vn}$										
	v										
1	2	3	4	5	6	7	8	9	10	11	
1	38.65	7.044	0	.2929	0	.05764	0	.01959	0	.009004	0
2	13.95	19.52	5.163	0	.3083	0	.07300	0	.02787	0	.01391
3	0	7.611	13.24	4.023	0	.2907	0	.07723	0	.03205	0
4	1.113	0	5.238	10.17	3.362	0	.2721	0	.07851	0	.03473
5	0	.7167	0	4.072	8.398	2.930	0	.2568	0	.07910	0
6	.3061	0	.5291	0	3.381	7.278	2.634	0	.2466	0	.08008
7	0	.2180	0	.4234	0	2.932	6.538	2.431	0	.2409	0
8	.1253	0	.1692	0	.3567	0	2.628	6.046	2.316	0	.2397
9	0	.09493	0	.1393	0	.3131	0	2.443	5.732	2.244	0
10	.06263	0	.07639	0	.1195	0	.2835	0	2.315	5.557	2.222
11	0	.04937	0	.06423	0	.1060	0	.2635	0	2.244	5.500

TABLE 6.1.7-F

n	$(1 - \delta_{vn}) B_{vn}$										
	v										
1	2	3	4	5	6	7	8	9	10	11	
1	0	7.046	0	.2948	0	.06003	0	.02287	0	.01405	0
2	13.95	0	5.167	0	.3127	0	.07869	0	.03618	0	.02782
3	0	7.616	0	4.029	0	.2984	0	.08798	0	.04910	0
4	1.120	0	5.246	0	3.372	0	.2850	0	.09800	0	.06946
5	0	.7268	0	4.084	0	2.945	0	.2785	0	.1160	0
6	.3188	0	.5431	0	3.398	0	2.658	0	.2858	0	.1602
7	0	.2310	0	.4384	0	2.951	0	2.459	0	.2883	0
8	.1463	0	.1928	0	.3869	0	2.673	0	2.401	0	.4794
9	0	.1232	0	.1739	0	.3628	0	2.533	0	2.487	0
10	.09772	0	.1170	0	.1753	0	.3799	0	2.565	0	4.444
11	0	.04937	0	.06423	0	.1060	0	.2635	0	2.244	0

## REFERENCES

1. DeYoung, J.: Theoretical Symmetric Span Loading Due to Flap Deflection for Wings of Arbitrary Plan Form at Subsonic Speeds. NACA Report 1071, 1952. (U)
2. Young, A. D.: The Aerodynamic Characteristics of Flaps. British Report No. Aero 2185, February 1947. (U)
3. Ames Research Staff: Equations, Tables, and Charts for Compressible Flow. NASA Report 1135, 1953. (U)



**FIGURE 6.1.7-22 TWO-DIMENSIONAL DRAG INCREMENT DUE TO FLAPS**

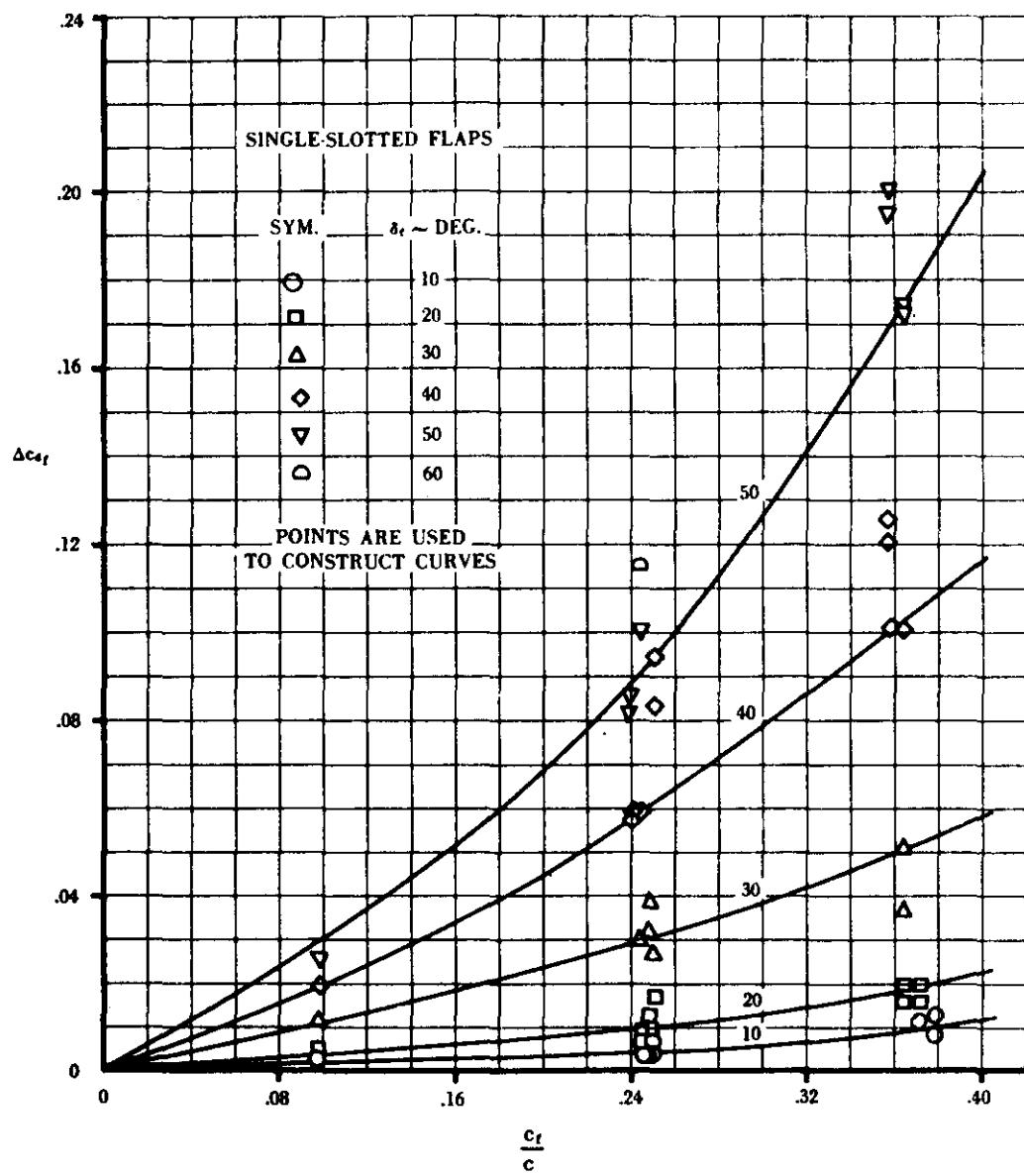


**FIGURE 6.1.7-23 TWO-DIMENSIONAL DRAG INCREMENT DUE TO FLAPS**

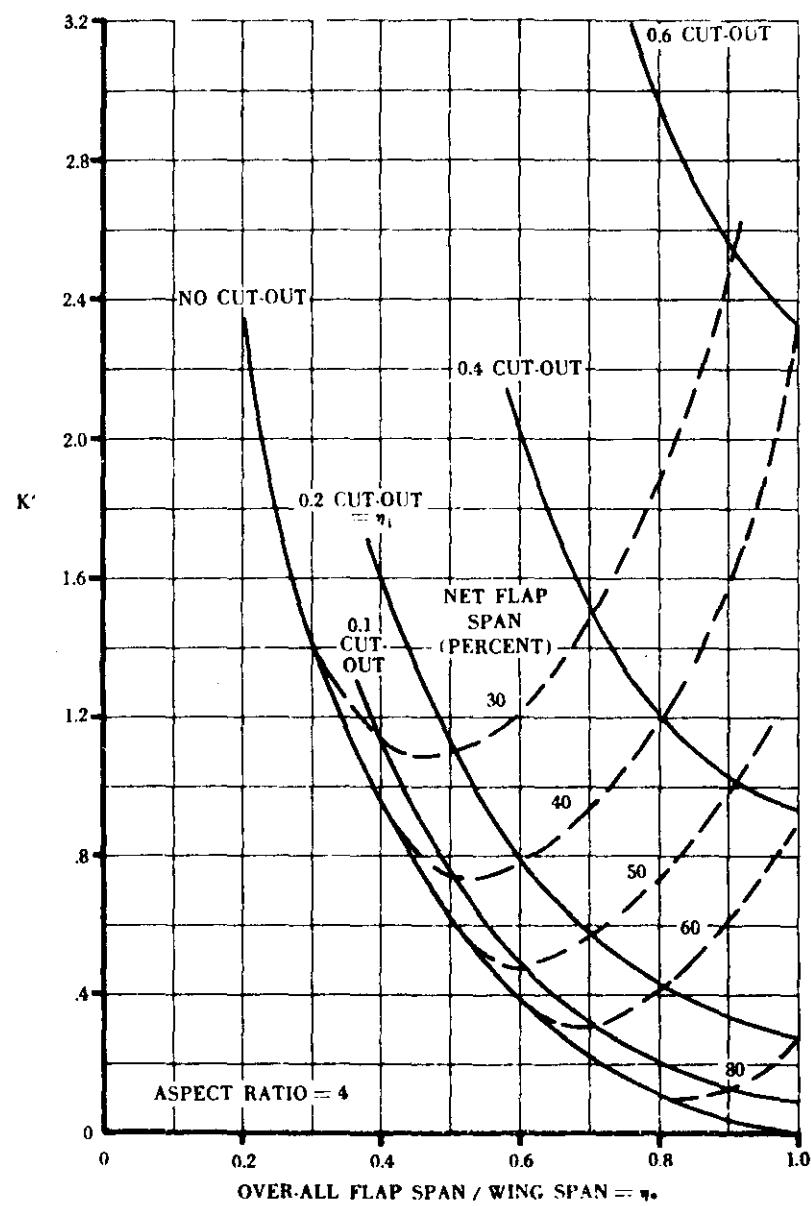


FIGURE 6.1.7-24 (a) FACTOR  $K'$  FOR CALCULATING INDUCED DRAG OF AN ELLIPTIC WING WITH PART-SPAN FLAPS AND CUT-OUT

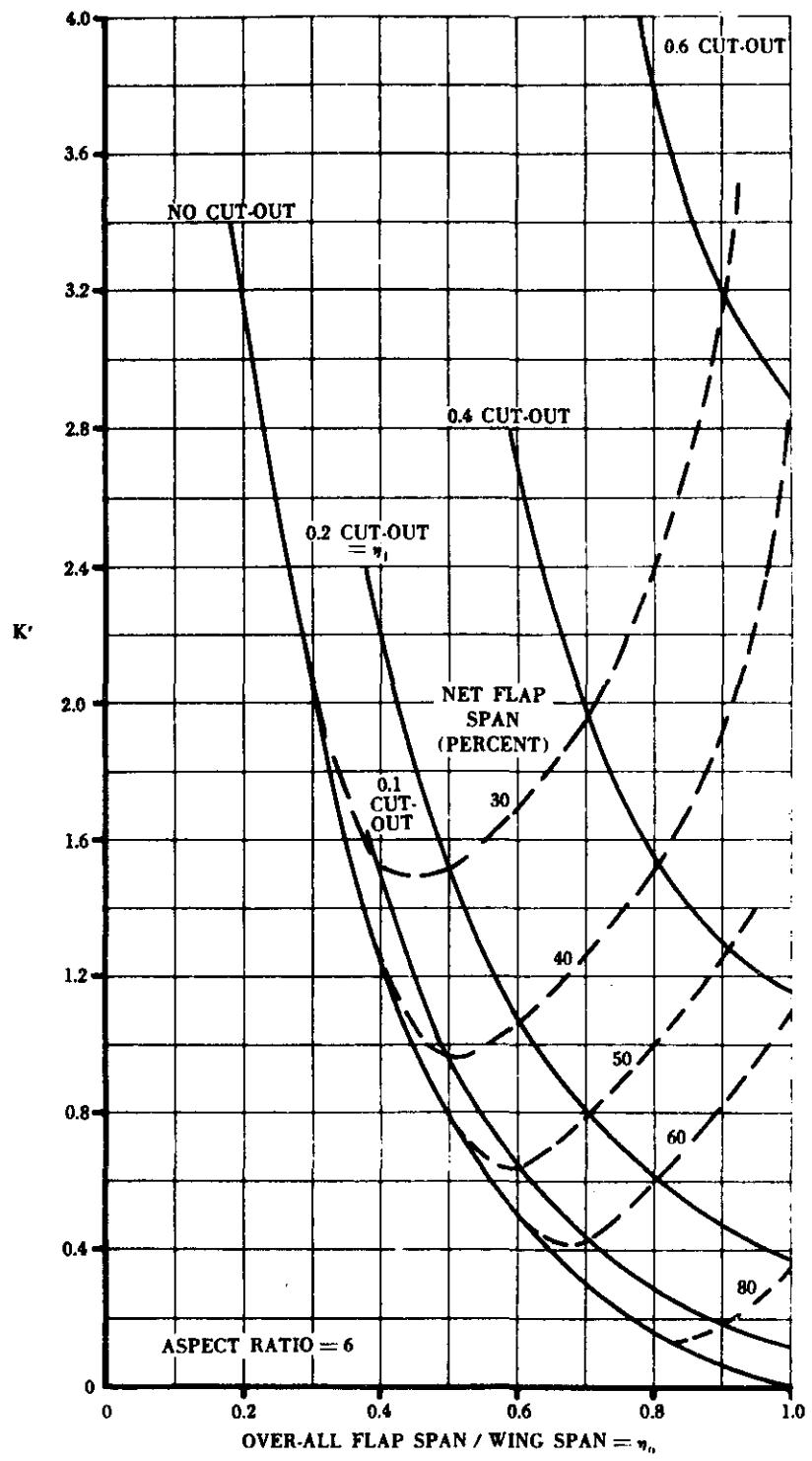


FIGURE 6.1.7-24 (b) FACTOR  $K'$  FOR CALCULATING INDUCED DRAG OF AN ELLIPTIC WING WITH PART-SPAN FLAPS AND CUT-OUT

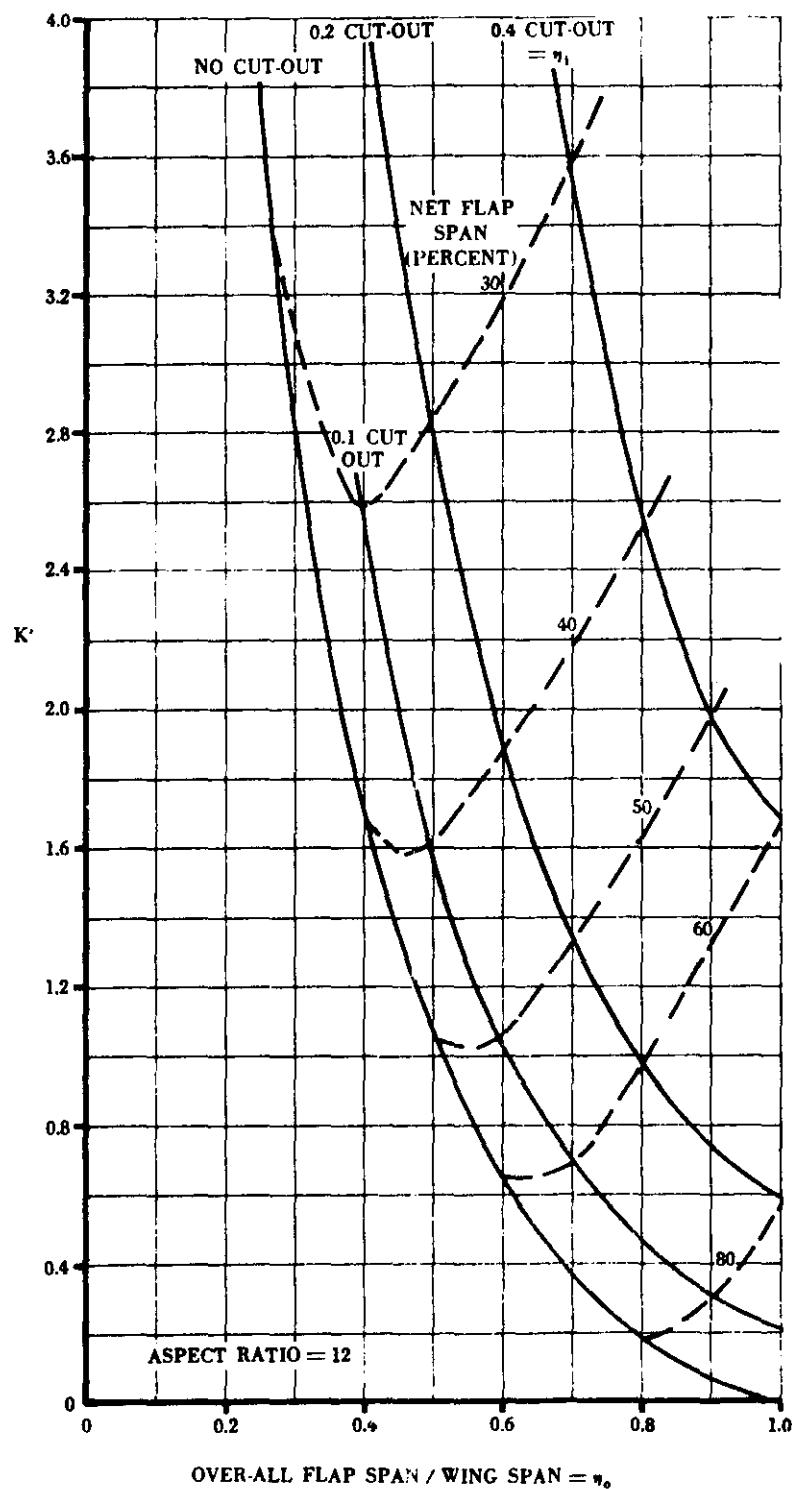


FIGURE 6.1.7-24 (c) FACTOR  $K'$  FOR CALCULATING INDUCED DRAG OF AN ELLIPTIC WING WITH PART-SPAN FLAPS AND CUT-OUT

- BASIC POLAR WITH NO CONTROL OR FLAP DEFLECTION
- — BASIC POLAR WITH INDUCED-DRAG INCREMENT DUE TO FLAPS
- - — BASIC POLAR WITH INDUCED-DRAG INCREMENT DUE TO FLAPS SHIFTED TO THE PROPER  $C_{D\text{MIN}}$

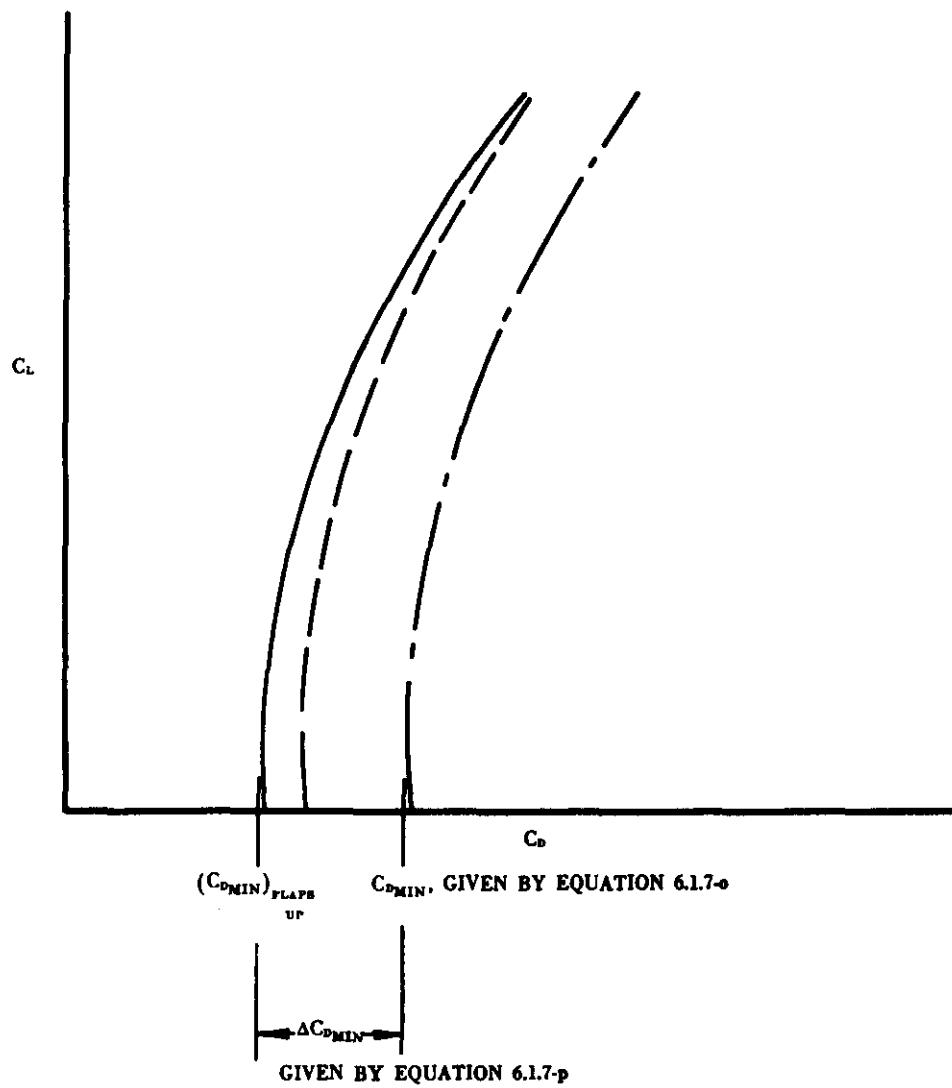


FIGURE 6.1.7-27 CONSTRUCTION OF FLAPS-DEFLECTED DRAG POLAR

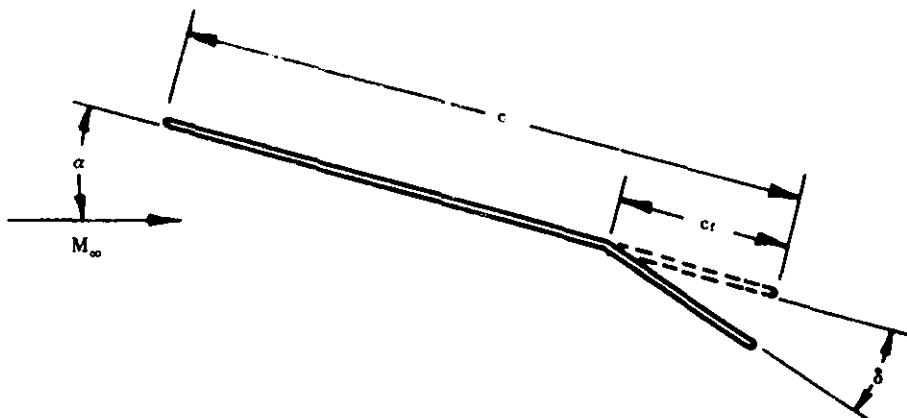


FIGURE 6.1.7-28 (a) CROSS SECTION OF AERODYNAMIC SURFACE

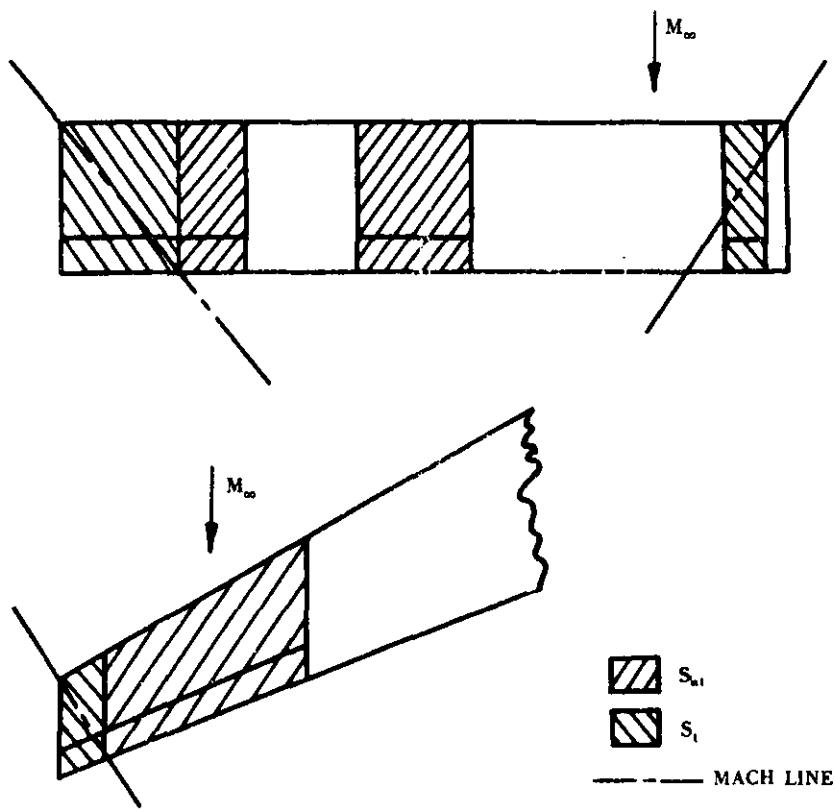


FIGURE 6.1.7-28 (b) EXAMPLES OF  $S_{el}$  AND  $S_t$

## 6.2 ASYMMETRICALLY DEFLECTED CONTROLS ON WING-BODY AND TAIL-BODY CONTROL COMBINATIONS

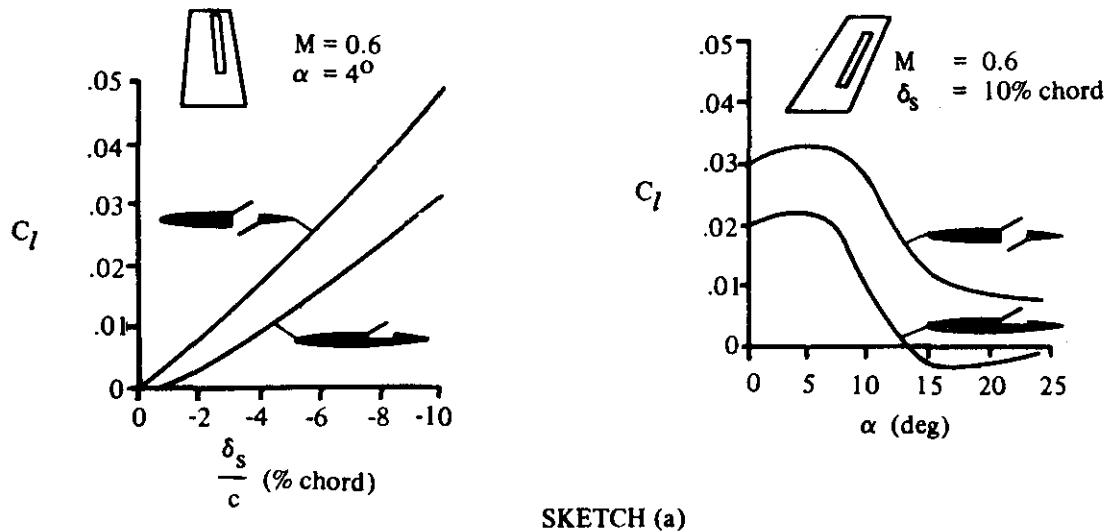
### 6.2.1 ROLLING MOMENT DUE TO ASYMMETRIC DEFLECTION OF CONTROL DEVICES

#### 6.2.1.1 ROLLING MOMENT DUE TO CONTROL DEFLECTION

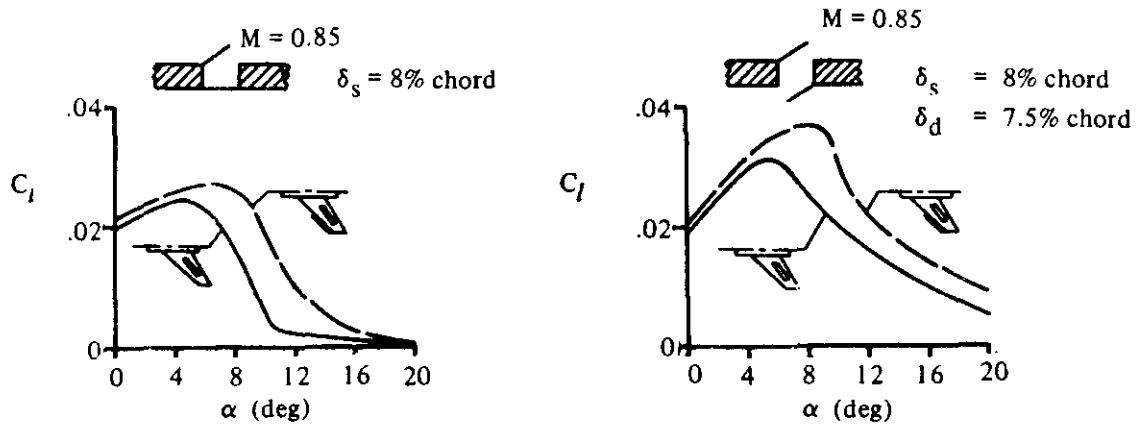
Methods are presented in this section for estimating the rolling moment due to control deflection at subsonic, transonic, and supersonic speeds. Plain trailing-edge flap-type controls and spoilers are included. The fundamental means by which each of these devices changes the lift of a wing, and hence the rolling moment, is discussed in Section 6.1.1.1.

A discussion of the aerodynamic aspects of spoilers on three-dimensional wings is given in reference 1. This reference also contains an extensive bibliography of spoiler tests. The following discussion summarizes the conclusions of this reference.

At subsonic and transonic speeds, spoilers do not, in general, provide linear variation of effectiveness with spoiler projection, particularly at small deflections (see sketch (a)). This deficiency can be corrected by the use of a slot or slot-deflector behind the spoiler.



For thin wings at high angles of attack plain spoilers are ineffective. This ineffectiveness can be partially overcome by the use of a slot behind the spoiler and by the use of leading-edge devices. Sketch (b) shows the effect of a drooped leading-edge extension on the rolling effectiveness of a plain and of a slotted spoiler.

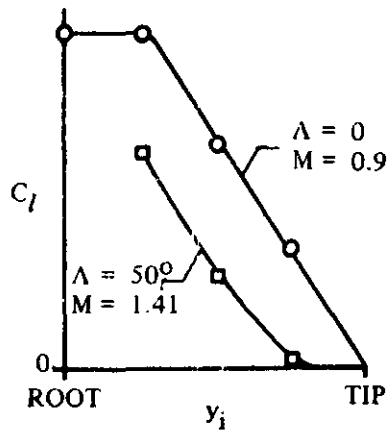


EFFECT OF DROOPED WING LEADING-EDGE EXTENSION ON SPOILER EFFECTIVENESS  
SKETCH (b)

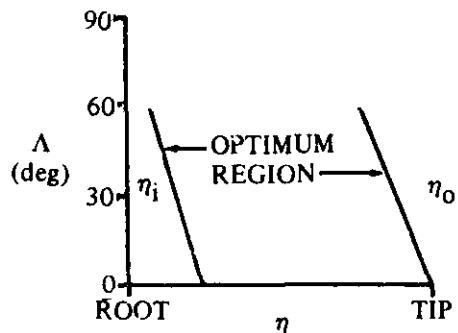
In order to achieve maximum effectiveness, spoilers should be located toward the rear portion of the wing for the following reasons:

1. The ineffectiveness of spoilers at small deflections increases with distance from the trailing edge.
2. The lag time at low speeds becomes excessively long for forward-mounted spoilers.

The optimum spanwise extent and position of spoilers are determined primarily by wing sweep. The higher the sweep angle, the farther inboard the spoilers should be placed. Sketch (c) shows the spoiler rolling moment for a spoiler extending from the wing tip to any inboard station  $y_i$ . The ineffectiveness of tip-located spoilers on swept wings is apparent.



SKETCH (c)



SKETCH (d)

The optimum spanwise location of spoilers as a function of wing sweep is shown in sketch (d).

## A. SUBSONIC

### Plain Trailing-Edge Flaps

A simplified lifting-surface theory is used in reference 2 to obtain the rolling-moment effectiveness  $C_{l\delta}$  for plain trailing-edge controls at subcritical Mach numbers. The theory is applicable to wings for which  $\beta A \geq 2$  and  $\Lambda_\beta < 60^\circ$ , where  $\Lambda_\beta = \tan^{-1}(\tan \Lambda_{c/4}/\beta)$ . The Prandtl-Glauert compressibility correction is used to account for subcritical compressibility effects. In this section the theory of reference 2 is used up to  $M = 0.6$ . Since the theory is based on potential flow, the results are valid for attached-flow conditions only, i.e., wing angle of attack and surface deflection where no flow separation exists.

Two-dimensional lift-curve slopes for specific wing sections are used to adjust the wing lift distribution. It should be noted that the design charts from reference 2 give results for two full-chord controls anti-symmetrically deflected. Then, absolute values of the section-lift effectiveness  $|\alpha_\delta|$  for a specific configuration are used to adjust the theory to realistic values. This results in positive values of  $C_{l\delta}$  for anti-

symmetric control deflections. The proper sign of the rolling-moment coefficient will result from the

$$\text{expression } C_l = C_{l\delta} \frac{(\delta_L - \delta_R)}{2} *$$

### Spoilers

The method for predicting the effectiveness of plug and flap type spoilers is taken from reference 3. The method is based on the simplified lifting-surface theory developed for flap-type controls in reference 2, used with section spoiler data and an empirical correction for the effective spanwise location on swept wings. The results are valid for attached flow conditions only.

A design chart based on the empirical results of reference 4 is presented for the prediction of the subsonic rolling effectiveness of spoiler-slot-deflector controls.

## DATCOM METHODS

### Plain Trailing-Edge Flaps

The wing trailing-edge control derivative  $C_{l\delta}$  at subcritical Mach numbers, based on the total wing area and wing span, is obtained from the procedure outlined in the following steps:

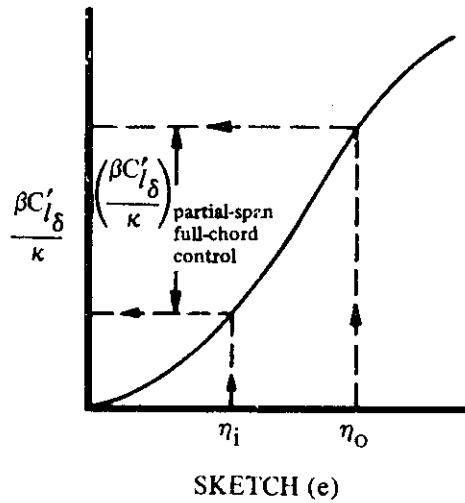
Step 1. Obtain the rolling-moment effectiveness parameter  $\beta C'_{l\delta}/\kappa$  of two full-chord controls ( $c_f/c = 1.0$ ) antisymmetrically deflected, as a function of  $\beta A/\kappa$  and  $\Lambda_\beta$ , from figure 6.2.1.1-23.

The parameter  $\kappa$  is the ratio of the two-dimensional lift-curve slope at the appropriate Mach number to  $2\pi/\beta$ , i.e.,  $(c_{L\alpha})_M/(2\pi/\beta)$ . The two-dimensional lift-curve slope is obtained from Section 4.1.1.2. For wings with airfoil sections varying in a reasonably linear manner with span, the lift-curve slope of the section at the MAC of the flapped portion of the wing is adequate.

The parameter  $\Lambda_\beta$  is the compressible sweep parameter, given as  $\Lambda_\beta = \tan^{-1}(\tan \Lambda_{c/4}/\beta)$ .

\*The usual convention is implied. Positive rolling moment is right wing down. Positive control deflection is trailing edge down.

Figure 6.2.1.1-23 gives directly the effectiveness parameter for control spans measured from the plane of symmetry outboard. For partial-span controls having the inboard edge of the control at spanwise station  $\eta_i$  and the outboard edge at  $\eta_o$ , the effectiveness parameter is obtained as illustrated in sketch (e).



SKETCH (e)

Step 2. Determine the rolling effectiveness of two full-chord controls antisymmetrically deflected by

$$C'_{l\delta} = \frac{\kappa}{\beta} \left( \frac{\beta C'_l \delta}{\kappa} \right) \quad 6.2.1.1-a$$

Step 3. Determine the rolling effectiveness of the partial-chord controls ( $c_f/c \approx 1.0$ ) of constant-percent-chord ( $c_f/c = \text{constant}$ ) antisymmetrically deflected by

$$\tilde{C}'_{l\delta} = |\alpha_\delta| C'_{l\delta} \quad 6.2.1.1-b$$

where  $C'_{l\delta}$  is obtained from equation 6.2.1.1-a and  $|\alpha_\delta|$  is the absolute value of the section lift effectiveness.  $\alpha_\delta$  is obtained from Section 6.1.1.1 for the particular control under consideration. For antisymmetric control deflections the value of  $\alpha_\delta$  is based on the deflection of one surface.

The effect of a differential control deflection is taken into account by considering  $C'_{l\delta}$  of each control as one-half the antisymmetric value (equation 6.2.1.1-b) where  $|\alpha_\delta|$  is considered separately for each control and based on its respective deflection. Then, the total rolling-moment coefficient for differential-control deflection is obtained by

$$C_l = \left( \frac{C'_{l\delta}}{2} \right)_L \delta_L - \left( \frac{C'_{l\delta}}{2} \right)_R \delta_R$$

For arbitrary spanwise distribution of control chord (constant-chord controls on tapered wings or tapered controls on untapered wings), the control is divided into spanwise steps, and the total  $C_{l\delta}$  value is found by summing the  $C_{l\delta}$  values due to each spanwise step, based on the average  $|\alpha_\delta|$  values over that spanwise step.

It should be noted that in applying this method the control deflection angles and all dimensions are measured in planes parallel and perpendicular to the plane of symmetry.

The relationship between streamwise control deflection  $\delta$ , control deflection measured normal to the control hinge line  $\delta_{\perp_{HL}}$ , and sweep of the flap hinge line  $\Lambda_{HL}$  is

$$\tan \delta = \cos \Lambda_{HL} \tan \delta_{\perp_{HL}}$$

The relationship between a  $C_{l\delta}$  value defined for a streamwise deflection and the corresponding value defined normal to the hinge line is

$$C_{l\delta} = C_{l\delta_{\perp_{HL}}} \cos \Lambda_{HL}$$

Sample problem 1 on page 6.2.1.1-7 illustrates the use of this method.

There are not enough experimental data available to substantiate this method. However, for configurations within the limitations of the method it is expected that the accuracy of the calculated results will be within  $\pm 10$  percent.

### Spoilers

#### Plug or Flap-Type Spoilers

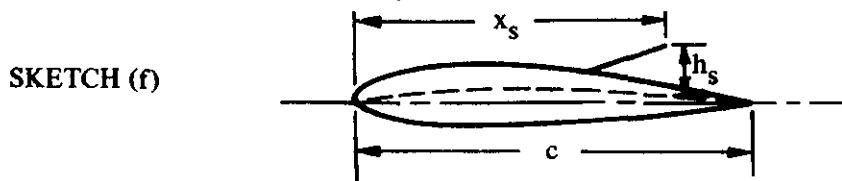
The rolling-moment coefficient of a plug or a flap-type spoiler deflected on one wing panel only, based on the total wing area and wing span, is given by

$$C_l = \frac{C'_{l\delta}}{2} \Delta\alpha'_s \quad 6.2.1.1-c$$

where

$C'_{l\delta}$  is the rolling-moment effectiveness of two full-chord controls antisymmetrically deflected, obtained as outlined in the above method for plain-trailing-edge controls, but with effective locations of the inboard and outboard ends of the control used in place of their geometric locations in reading figure 6.2.1.1-23.

$\Delta\alpha'_s$  is the spoiler lift effectiveness expressed in terms of the change in zero-lift angle of attack. This parameter is presented as a function of effective spoiler height for four spoiler chordwise locations in figure 6.1.1.1-52. In using this figure,  $x_s$  is the distance from the nose of the airfoil to the spoiler lip, and  $h_s$  is the height of the spoiler measured from and normal to the airfoil mean line at  $x_s$  (see sketch (f)).



The effective locations of the inboard and outboard ends of the spoiler, used in reading figure 6.2.1.1-23, are given by

$$\left. \begin{aligned} \eta_{i\text{eff}} &= \eta_i + \Delta\eta_i \\ \eta_{o\text{eff}} &= \eta_o + \Delta\eta_o \end{aligned} \right\} \quad 6.2.1.1.-d$$

where  $\eta_i$  and  $\eta_o$  are the spanwise locations of the inboard and outboard ends of the spoiler, respectively, and  $\Delta\eta_i$  and  $\Delta\eta_o$  are effective increments in the spoiler spanwise locations due to the spanwise flow of the spoiler wake for partial-span spoilers. These increments in spoiler spanwise locations are given by

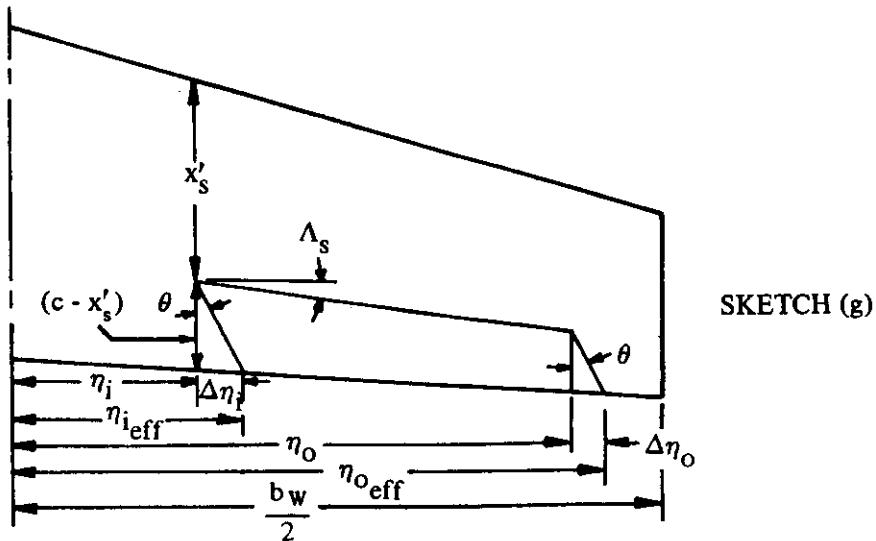
$$\left. \begin{aligned} \Delta\eta_i &= \frac{4}{A(1+\lambda)} \left[ 1 - (1-\lambda)\eta_i \right] \frac{\cos \Lambda_{TE} \sin \theta}{\cos(\Lambda_{TE} + \theta)} \\ \Delta\eta_o &= \frac{4}{A(1+\lambda)} \left[ 1 - (1-\lambda)\eta_o \right] \frac{\cos \Lambda_{TE} \sin \theta}{\cos(\Lambda_{TE} + \theta)} \end{aligned} \right\} \quad 6.2.1.1.-e$$

where  $\theta$  is an empirically determined angle obtained from figure 6.2.1.1-26a as a function of the spoiler sweepback. The spoiler sweepback is determined from the expression

$$\tan \Lambda_s = \tan \Lambda_{c/4} - \frac{4 \left[ 0.75 - \left( 1 - \frac{x'_s}{c} \right) \right]}{A} \left( \frac{1-\lambda}{1+\lambda} \right)$$

In using this method, if  $\eta_{o\text{eff}}$  exceeds 1.0, which would be the case for the spoiler extending almost to the wing tip on a highly swept wing, the value of  $C'_{l\delta}$  at  $\eta_o = 1.0$  is used.

The effective spanwise extent of an arbitrarily located spoiler as used in this method is illustrated in sketch (g).



Sample problem 2 on page 6.2.1.1-9 illustrates the use of this method.

Comparisons of test data with results calculated by using this method are presented as table 6.2.1.1-A. Additional comparisons between test and calculated values are given in reference 3.

Only spoilers of constant-percent-chord height ( $h_s/c = \text{constant}$ ) were included in the analysis of reference 3; however, it is implied therein that the method should give acceptable results for arbitrary spanwise distribution of spoiler control chord.

#### Spoiler-Slot-Deflector

The rolling-moment coefficient of a spoiler-slot-deflector on one wing panel, based on the total wing area and wing span, is given by

$$(C_l)_{\text{spoiler-slot-deflector}} = K(C_l)_{\text{plain spoiler}} \quad 6.2.1.1-f$$

where

$(C_l)_{\text{plain spoiler}}$  is the rolling-moment coefficient of a plain flap-type spoiler deflected on one wing panel, based on the total wing area and wing span, determined by using equation 6.2.1.1-c.

K is the ratio of the rolling-moment coefficient of a spoiler-slot-deflector to that of a plain spoiler, obtained from figure 6.2.1.1-26b, as a function of the ratio of spoiler deflection to deflector deflection  $\delta_s/\delta_d$ . The spoiler and deflector deflections are illustrated in figure 6.2.1.1-26b. Note the difference between the spoiler-height measurement  $h_s$  used in determining  $C_l$  of the plain spoiler and the  $\delta_s$  and  $\delta_d$  measurements for the spoiler-slot-deflector control.

Figure 6.2.1.1-26b is based on the empirical results of reference 4. The wing planform of the test configuration is a straight-tapered wing with  $A = 4.0$ ,  $\lambda = 0.6$ ,  $\Lambda_{c/4} = 32.6^\circ$ , and with an NACA 65006 airfoil section in the streamwise direction. The method has not been verified by comparison with other test results. Nevertheless, the method is expected to give acceptable results over the linear-lift range for configurations with  $\beta A \geq 2$  and  $\Lambda_\beta < 60^\circ$ , and at Mach numbers up to 0.6.

The use of this method is illustrated in sample problem 3 on page 6.2.1.1-12.

#### Sample Problems

##### 1. Plain Trailing-Edge-Flap Ailerons

Given: The following wing-aileron configuration:

Wing Characteristics:

$$A_w = 3.78 \quad \lambda_w = 0.586 \quad \Lambda_{c/4} = 47.35^\circ$$

NACA 65009 airfoil (streamwise)  $\tan \phi'_{TE}/2 = 0.0776$  (streamwise airfoil section geometry)

Aileron Characteristics:

$$\text{Plain trailing-edge flap} \quad c_f/c = 0.30 \quad \eta_i = 0.75 \quad \eta_o = 0.95$$

$$\delta_L = 15^\circ \quad \delta_R = -15^\circ$$

Additional Characteristics:

$$M = 0.40; \quad \beta = 0.917 \quad R_\ell = 9 \times 10^6$$

Compute:

$$C'_{l\delta}$$

$$\frac{c_{l\alpha}}{(c_{l\alpha})_{\text{theory}}} = 0.893 \quad (\text{figure 4.1.1.2-8a})$$

$$(c_{l\alpha})_{\text{theory}} = 6.58 \text{ per rad} \quad (\text{figure 4.1.1.2-8b})$$

$$(c_{l\alpha})_M = \frac{1.05}{\beta} \left[ \frac{c_{l\alpha}}{(c_{l\alpha})_{\text{theory}}} \right] (c_{l\alpha})_{\text{theory}} \quad (\text{equation 4.1.1.2-a})$$

$$= \frac{1.05}{0.917} (0.893) (6.58) = 6.73 \text{ per rad}$$

$$\kappa = \frac{(c_{l\alpha})_M}{2\pi/\beta} = \frac{6.73}{2\pi/\beta} = 0.981$$

$$\frac{\beta A}{\kappa} = \frac{(0.917)(3.78)}{0.981} = 3.53$$

$$\Lambda_\beta = \tan^{-1} \frac{\tan \Lambda_c/4}{\beta} = \tan^{-1} \left( \frac{1.0856}{0.917} \right) = 49.8^\circ$$

$$\left. \begin{aligned} \left( \frac{\beta C'_{l\delta}}{\kappa} \right)_{\eta_i=0.75} &= 0.320 \text{ per rad} \\ \left( \frac{\beta C'_{l\delta}}{\kappa} \right)_{\eta_o=0.95} &= 0.420 \text{ per rad} \end{aligned} \right\} \quad (\text{figures 6.2.1.1-23a through -23c, interpolated})$$

$$C'_{l\delta} = \frac{\kappa}{\beta} \left[ \left( \frac{\beta C'_{l\delta}}{\kappa} \right)_{\eta_o} - \left( \frac{\beta C'_{l\delta}}{\kappa} \right)_{\eta_i} \right] \quad (\text{equation 6.2.1.1-a})$$

$$= \frac{0.981}{0.917} [0.420 - 0.320] = 0.107 \text{ per rad}$$

Section lift effectiveness  $\alpha_\delta$  (Section 6.1.1.1)

$$\left(\frac{c_{\ell_\delta}}{c_{\ell_\delta}}\right)_{\text{theory}} = 4.35 \text{ per rad (figure 6.1.1.1-39a)}$$

$$\frac{\left(\frac{c_{\ell_\delta}}{c_{\ell_\delta}}\right)}{\left(\frac{c_{\ell_\delta}}{c_{\ell_\delta}}\right)_{\text{theory}}} = 0.840 \text{ (figure 6.1.1.1-39b)}$$

$$K' = 0.98 \text{ (figure 6.1.1.1-40)}$$

$$\Delta c_{\ell} = \delta \left[ \frac{c_{\ell_\delta}}{\left(\frac{c_{\ell_\delta}}{c_{\ell_\delta}}\right)_{\text{theory}}} \right] \left(\frac{c_{\ell_\delta}}{c_{\ell_\delta}}\right)_{\text{theory}} K' \text{ (equation 6.1.1.1-c)}$$

$$= \frac{15.0}{57.3} (0.840) (4.35) (0.98) = 0.937$$

$$\alpha_\delta = -\frac{\left(\frac{c_{\ell_\delta}}{c_{\ell_\alpha}}\right)_\alpha}{\left(\frac{c_{\ell_\delta}}{c_{\ell_\alpha}}\right)_\delta} \text{ (equation 6.1.1.1-b)}$$

$$= -\frac{\Delta c_{\ell}}{\left(\frac{c_{\ell_\alpha}}{c_{\ell_\alpha}}\right)_\delta} \delta = -\frac{(0.937)}{(6.73) \frac{15.0}{57.3}} = -0.532$$

**Solution:**

$$C_{l_\delta} = C_{l_\delta} |\alpha_\delta| \text{ (equation 6.2.1.1-b)}$$

$$= (0.107)(0.532) = 0.0569 \text{ per rad}$$

The rolling-moment coefficient is given by

$$\begin{aligned} C_l &= \left( \frac{C_{l_\delta}}{2} \right)_L \delta_L - \left( \frac{C_{l_\delta}}{2} \right)_R \delta_R \\ &= \frac{0.0569}{2(57.3)} [15 - (-15)] = 0.0149 \text{ (based on } S_W b_W) \end{aligned}$$

## 2. Spoiler

Given: The wing-body configuration of reference 4 with a partial-span constant-chord spoiler hinged at the 55-percent-chord line.

**Wing Characteristics:**

$$A_W = 4.0 \quad \lambda_W = 0.60 \quad S_W = 324.0 \text{ sq in.} \quad b_W = 36.0 \text{ in.}$$

$$\Lambda_{c/4} = 32.6^\circ \quad \Lambda_{TE} = 24.3^\circ \quad \text{NACA 65006 airfoil (streamwise)}$$

**Spoiler Characteristics:**

$$\eta_i = \frac{y_i}{b/2} = 0.139$$

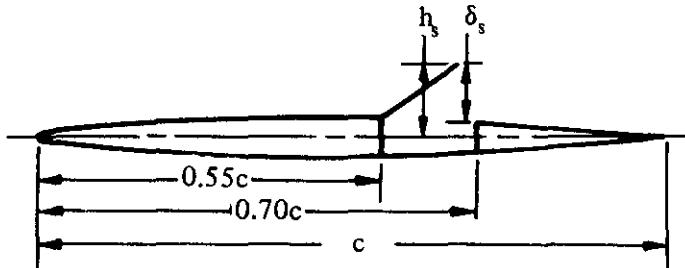
$$\eta_o = \frac{y_o}{b/2} = 0.639$$

$$\frac{c_s}{c} = 0.150$$

Spoiler projection  $\delta_s$  measured from the airfoil surface at  $0.70c$ , and corresponding spoiler chordwise location

$$\frac{\delta_s}{c} = 0.100$$

$$\frac{x_s}{c} = 0.662$$



**Additional Characteristics:**

$$M = 0.40; \beta = 0.917$$

Compute:

Determine  $C'_{l\delta}$

$$c_{\ell\alpha} = 0.105 \text{ per deg} = 6.02 \text{ per rad (table 4.1.1-B)}$$

$$(c_{\ell\alpha})_M = \frac{c_{\ell\alpha}}{\beta} = \frac{6.02}{0.917} = 6.56 \text{ per rad}$$

$$\kappa = \frac{(c_{\ell\alpha})_M}{2\pi/\beta} = \frac{6.56}{2\pi/\beta} = 0.958$$

$$\Lambda_\beta = \tan^{-1} \frac{\tan \Lambda_{c/4}}{\beta} = \tan^{-1} \frac{0.6395}{0.917} = 34.9^\circ$$

$$\frac{\beta A}{\kappa} = \frac{0.917 (4.0)}{0.958} = 3.85$$

Determine  $\eta_{i_{\text{eff}}}$  and  $\eta_{o_{\text{eff}}}$

$$\tan \Lambda_s = \tan \Lambda_{c/4} - \frac{4 \left[ 0.75 - \left( 1 - \frac{x_s}{c} \right) \right]}{A} \left( \frac{1 - \lambda}{1 + \lambda} \right)$$

$$= 0.6395 - \frac{4}{4.0} [0.75 - (1 - 0.662)] \frac{0.40}{1.60}$$

$$= 0.6395 - (0.412)(0.25) = 0.5365$$

$$\Lambda_s = \tan^{-1} 0.5365 = 28.2^\circ$$

$$\theta = 28.3^\circ \text{ (figure 6.2.1.1-26a)}$$

$$\frac{\cos \Lambda_{TE} \sin \theta}{\cos (\Lambda_{TE} + \theta)} = \frac{0.9114 (0.4741)}{0.6074} = 0.7114$$

$$\frac{4 \left(1 - \frac{x'_s}{c}\right)}{A(1 + \lambda)} = \frac{4(1 - 0.662)}{4.0(1.60)} = 0.211$$

$$[1 - (1 - \lambda) \eta_i] = [1 - (1 - 0.6)(0.139)] = 0.944$$

$$[1 - (1 - \lambda) \eta_o] = [1 - (1 - 0.6)(0.639)] = 0.744$$

$$\left. \begin{aligned} \Delta \eta_i &= \frac{4 \left(1 - \frac{x'_s}{c}\right)}{A(1 + \lambda)} [1 - (1 - \lambda) \eta_i] \frac{\cos \Lambda_{TE} \sin \theta}{\cos (\Lambda_{TE} + \theta)} \\ &= (0.211)(0.944)(0.7114) = 0.142 \end{aligned} \right\} \quad \text{(equation 6.2.1.1-e)}$$

$$\left. \begin{aligned} \Delta \eta_o &= \frac{4 \left(1 - \frac{x'_s}{c}\right)}{A(1 + \lambda)} [1 - (1 - \lambda) \eta_o] \frac{\cos \Lambda_{TE} \sin \theta}{\cos (\Lambda_{TE} + \theta)} \\ &= (0.211)(0.744)(0.7114) = 0.112 \end{aligned} \right\}$$

$$\left. \begin{aligned} \eta_{i_{\text{eff}}} &= \eta_i + \Delta \eta_i = 0.139 + 0.142 = 0.281 \\ \eta_{o_{\text{eff}}} &= \eta_o + \Delta \eta_o = 0.639 + 0.112 = 0.751 \end{aligned} \right\} \quad \text{(equation 6.2.1.1-d)}$$

$$\left. \begin{aligned} \left( \frac{\beta C_l \delta}{\kappa} \right)_{\eta_{i_{\text{eff}}}} &= 0.061 \text{ per rad} \\ \left( \frac{\beta C_l \delta}{\kappa} \right)_{\eta_{o_{\text{eff}}}} &= 0.350 \text{ per rad} \end{aligned} \right\} \quad \text{(figures 6.2.1.1-23a through -23c, interpolated)}$$

$$C'_{l\delta} = \frac{\kappa}{\beta} \left[ \left( \frac{\beta C'_l \delta}{\kappa} \right) \eta_{o_{\text{eff}}} - \left( \frac{\beta C'_l \delta}{\kappa} \right) \eta_{i_{\text{eff}}} \right] \quad (\text{equation 6.2.1.1-a})$$

$$= \frac{0.958}{0.917} [0.350 - 0.061] = 0.302 \text{ per rad}$$

Determine  $\Delta\alpha'_s$

The upper-surface ordinate of the NACA 65006 airfoil section at 0.70c is 0.0194c. (see reference 5)

$$\frac{h_s}{c} = \frac{\delta_s}{c} + 0.0194 = 0.100 + 0.0194 = 0.1194$$

$$\Delta\alpha'_s = 0.134 \quad (\text{figure 6.1.1.1-52 at } x_s/c, h_s/c)$$

Solution:

$$C_l = \frac{C'_{l\delta}}{2} \Delta\alpha'_s \quad (\text{equation 6.2.1.1-c})$$

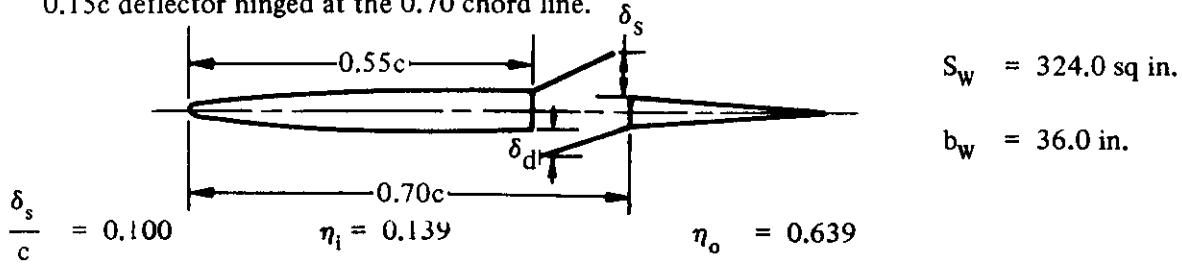
$$= \left( \frac{0.302}{2} \right) (0.134)$$

$$= 0.0202 \text{ (based on } S_w b_w \text{ ) (Spoiler deflected on one wing panel)}$$

This result compares with a test value of 0.0215 from reference 4.

### 3. Spoiler-Slot-Deflector

Given: The wing-body configuration of reference 4 with a partial-span constant-chord spoiler-slot-deflector on one wing panel. This is the configuration of sample problem 2 with the addition of a slot opening between the 55- and 70-percent-chord lines extending from  $\eta_i = 0.139$  to  $\eta_o = 0.639$ , and a 0.15c deflector hinged at the 0.70 chord line.



$$(C_l)_{\text{plain spoiler}} = 0.0202 \quad (\text{sample problem 2})$$

$$\frac{\delta_d}{c} = 0.025, 0.050, 0.075, 0.100$$

Solution:

$$(C_l)_{\text{spoiler-slot-deflector}} = K(C_l)_{\text{plain spoiler}} \quad (\text{equation 6.2.1.1-f})$$

$$= (0.0202) K \quad (\text{based on } S_w b_w)$$

(1)	(2)	(3)	(4)	(5)	(6)
$\frac{\delta_s}{c}$	$\frac{\delta_d}{c}$	$\delta_s/\delta_d$ ① / ②	K figure 6.2.1.1-26b	$(C_l)_{\text{spoiler-slot-deflector}}$ (0.0202) ④	$(C_l)_{\text{spoiler-slot-deflector}}$ (Test)
0.100	0.025	4.00	1.35	0.0273	0.0290
0.100	0.050	2.00	1.70	0.0343	0.0350
0.100	0.075	1.33	1.57	0.0317	0.0350
0.100	0.100	1.00	1.34	0.0271	0.0300

## B. TRANSONIC

No accurate method is available for predicting  $C_{l\delta}$  at transonic speeds. Mixed flow conditions and inter-related shock-wave and boundary-layer-separation effects cause extreme nonlinearities in this parameter. The discussion of paragraph B of Section 4.1.3.2 gives some insight into these effects for plain wings.

The method presented here is intended to give a first-order approximation only and to provide a guide to aid in fairing between subcritical and supersonic speeds.

Published experimental data in the transonic speed range are available for only a specific flap-type control tested on a wing-planform series in which only the wing sweep was varied (references 6 through 9).

## DATCOM METHOD

No specific charts are presented for determining the transonic rolling effectiveness of lateral-control devices. The best source of information of this type is experimental data on similar configurations. If such information is not available, the following approach may be used as a guide in fairing between subcritical and supersonic speeds.

A first-order approximation of the transonic rolling effectiveness of lateral-control devices is given by

$$C_l = (C_l)_{M=0.6} \frac{(C_{L\alpha})}{(C_{L\alpha})_{M=0.6}} \quad 6.2.1.1-g$$

where

$(C_l)_{M=0.6}$  is the rolling effectiveness of the control at  $M = 0.6$ , obtained by using the appropriate method of paragraph A of this section.

$(C_L \alpha)$ 

is the transonic wing-lift-curve slope, obtained from paragraph B of Section 4.1.3.2.

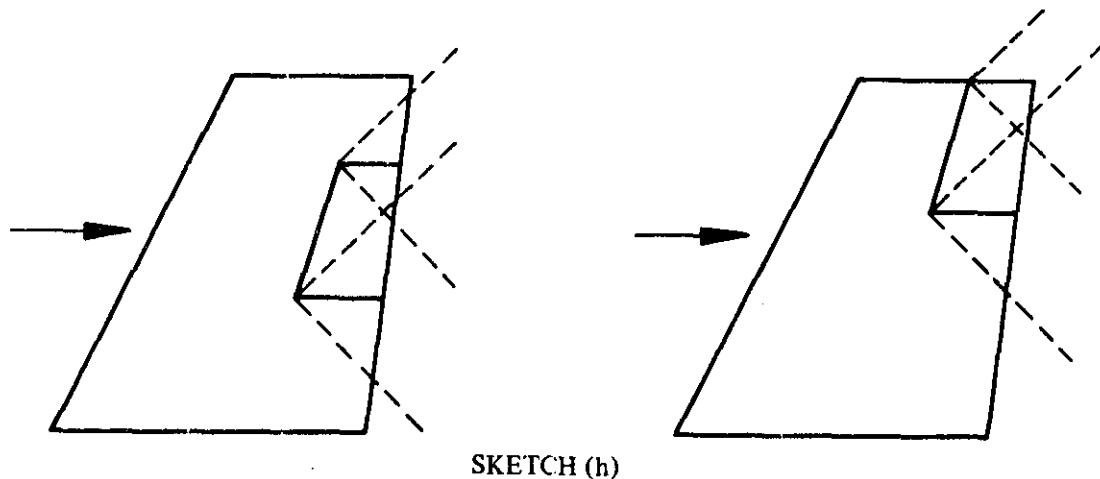
 $(C_L \alpha)_{M=0.6}$ 

is the wing-lift-curve slope at  $M = 0.6$ , obtained by using the straight-tapered wing method of paragraph A of Section 4.1.3.2 (figure 4.1.3.2-41).

### C. SUPERSONIC

#### Plain Trailing-Edge Flaps

Supersonic linear theory is used in reference 10 to derive conical-flow solutions for the rolling effectiveness of wing trailing-edge flap-type control surfaces. The theory is based on the following assumptions (see sketch (h)):



1. The leading (hinge line) and trailing edges of the control surface are supersonic (swept ahead of the Mach lines).
2. The control surfaces are located at the wing tip or are far enough inboard to prevent the outermost Mach lines from the control surface from crossing the wing tip.
3. The innermost Mach lines from the deflected control surface do not cross the root chord.
4. The root and tip chords of the control surfaces are streamwise.
5. Controls are not influenced by the tip conical flow from the opposite wing panel or by the interaction of the wing-root Mach cone with the wing tip.

An approximate correction is given in reference 10 to account for the effect of airfoil thickness in the case of slab-sided controls.

#### Spoilers

The method presented for determining the supersonic rolling moment due to spoilers is taken from reference 11. The derivation is based on an analysis, presented in reference 12, of the pressure distributions adjacent to the spoiler. Although data on spoiler rolling characteristics at supersonic speeds are limited, the method appears satisfactory for both plug and flap-type spoilers within the Mach number range of the available data ( $M = 1.6$  to  $3.0$ ).

No method is presented for determining the supersonic rolling moment due to spoiler-slot-deflectors. Published test data on spoiler-slot-deflector characteristics at supersonic speeds are extremely limited. References 13 and 14 present test data on spoiler-slot-deflector controls at supersonic speeds.

## DATCOM METHODS

### Plain Trailing-Edge Flaps

The supersonic rolling effectiveness of plain trailing-edge flap-type controls is given by

$$C_{l\delta} = \left( 1 - \frac{C_2}{C_1} \phi_{TE} \right) C'_{L\delta} \frac{S_f}{S_w} - \frac{1}{2} \left[ \frac{y_i}{b_w} + \left( \frac{b_f}{2 b_w} \right) \frac{C'_{L\delta}}{C_{L\delta}} \right] \quad 6.2.1.1-h$$

where

$C_{l\delta}$  is the control-surface rolling effectiveness of one control surface deflected on one wing panel, based on the total wing area and span.

$C'_{l\delta}$  is the theoretical rolling-moment derivative based on total control area  $S_f$  for thin wings for the following cases:

- (a) Tapered control surfaces with outboard edge coincident with wing tip (use figure 6.2.1.1-27).
- (b) Tapered control surfaces with outboard edge not coincident with wing tip (use figure 6.2.1.1-28).
- (c) Untapered control surfaces with outboard edge coincident with wing tip (use figure 6.2.1.1-29a).
- (d) Untapered control surface with outboard edge not coincident with wing tip (use figure 6.2.1.1-29b).

$\frac{S_f}{S_w}$  is the ratio of the total control area (both sides of wing) to the total wing area.

$\frac{b_f}{b_w}$  is the ratio of the total control span (both sides of wing) to the total wing span.

$\frac{y_i}{b_w}$  is the distance from the wing root chord to the control root chord in wing spans.

$\left( 1 - \frac{C_2}{C_1} \phi_{TE} \right)$  is a thickness correction factor to the supersonic flat-plate derivative.

$$C_1 = \frac{2}{\sqrt{M^2 - 1}} \text{ (per radian)}$$

$$C_2 = \frac{(\gamma + 1) M^4 - 4(M^2 - 1)}{2(M^2 - 1)^2} \text{ (per radian)}$$

$\theta_{TE}$  is the trailing-edge angle in radians, measured normal to the control hinge line.

$\gamma$  is the ratio of specific heats,  $\gamma = 1.4$ .

$C'_{L\delta}$  is the lift-effectiveness of one symmetric, straight-sided control, based on the area of the control. This parameter is obtained from figures 6.1.4.1-20a through 6.1.4.1-20j for controls located at the wing tip, and from figure 6.1.4.1-25 for controls located inboard from the wing tip.

It should be noted that in applying this method the control deflection angle and all dimensions (with the exception of  $\phi_{TE}$ ) are measured in planes parallel and perpendicular to the plane of symmetry.

The limitations of this method are noted in the introduction to paragraph C. A comparison of test values with results calculated by this method is presented as table 6.2.1.1-B.

Sample problem 1 at the conclusion of this paragraph illustrates the use of the method.

#### Spoilers

##### Plug and Flap-Type Spoilers

The supersonic rolling-moment coefficient of a plug or a flap-type spoiler deflected on one panel, based on the total wing area and span, is obtained from figure 6.2.1.1-30 as a function of Mach number and configuration geometry.

A comparison of test values with results calculated by using this method is presented as table 6.2.1.1-C.

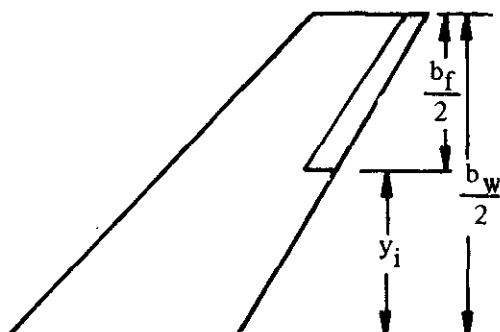
Sample problem 2 at the conclusion of this paragraph illustrates the use of the method.

#### Sample Problems

##### 1. Plain Trailing-Edge-Flap Ailerons

Given: The wing-body-tail configuration of reference 18, with plain trailing-edge ailerons.

##### Wing Characteristics:



$$S_W = 166.8 \text{ sq in.} \quad b_W = 25.86 \text{ in.}$$

$$\lambda_W = 0.50 \quad A_W = 4.0$$

$$\Lambda_{c/4} = 40^\circ \quad \Lambda_{TE} = 30.5^\circ$$

$$\Lambda_{LE} = 42.7^\circ$$

**Control Characteristics:**

$$\begin{aligned} \text{Symmetric, straight-sided outboard control} \quad \Lambda_{HL} &= 33.26^\circ \quad \lambda_f = 0.666 \\ b_f &= 12.93 \text{ in. (both sides of wing)} \quad S_f = 13.89 \text{ sq in. (both sides of wing)} \\ \frac{y_i}{b_w} &= 0.25 \quad \phi_{TE} = 6^\circ \quad c_f/c = 0.20 \end{aligned}$$

**Additional Characteristics:**

$$M = 1.61; \beta = 1.262; M^2 - 1 = 1.592$$

**Compute:**

$$C_1 = \frac{1}{\sqrt{M^2 - 1}} = \frac{1}{1.262} = 0.792 \text{ per rad}$$

$$C_2 = \frac{(\gamma + 1) M^4 - 4(M^2 - 1)}{2(M^2 - 1)^2} = \frac{(2.40)(1.61)^4 - 4(1.592)}{2(1.592)^2} = 1.925 \text{ per rad}$$

$$\frac{\tan \Lambda_{HL}}{\beta} = \frac{0.6558}{1.262} = 0.520; \quad \frac{\tan \Lambda_{TE}}{\beta} = \frac{0.5891}{1.262} = 0.467$$

$$\beta C'_{L\delta} = 0.0745 \text{ per deg (figures 6.1.4.1-20g through -20i, interpolated)}$$

$$C'_{L\delta} = 0.0590 \text{ per deg}$$

$$\beta C'_{l\delta} = 0.0370 \text{ per deg (figure 6.2.1.1-27)}$$

$$C'_{l\delta} = 0.0293 \text{ per deg}$$

**Solution:**

$$\begin{aligned} C_{l\delta} &= \left(1 - \frac{C_2}{C_1} \phi_{TE}\right) C'_{L\delta} \frac{S_f}{S_w} \frac{1}{2} \left[ \frac{y_i}{b_w} + \left( \frac{b_f}{2b_w} \right) \frac{C'_{l\delta}}{C'_{L\delta}} \right] \text{ (equation 6.2.1.1-h)} \\ &= \left[ 1 - \frac{1.925}{0.792} \left( \frac{6}{57.3} \right) \right] (0.0590) \frac{13.89}{166.8} \left( \frac{1}{2} \right) \left[ 0.25 + \frac{6.465}{25.86} \left( \frac{0.0293}{0.0590} \right) \right] \\ &= 0.000686 \text{ per deg (based on } S_w b_w \text{) (one control surface deflected on one wing panel)} \end{aligned}$$

This compares with a test value of 0.00056 per degree from reference 18.

## 2. Plug and Flap-Type Spoilers

Given: The wing-body-tail configuration of reference 18, equipped with plug and flap-type spoilers.

Wing Characteristics:

$$A_w = 4.0 \quad \lambda_w = 0.500 \quad \Lambda_{c/4} = 40^\circ$$

Spoiler Characteristics:

Case	Type	$\frac{y_i}{b_w/2}$	$\frac{y_o}{b_w/2}$	Chordwise Location %c	$\frac{\delta_s}{c}$
1	Plug	0.15	0.95	0.55	0.05
2	Flap	0.15	0.95	0.55	0.05
3	Plug	0.15	0.95	0.65	0.02
4	Plug	0.15	0.55	0.65	0.05
5	Plug	0.15	0.55	0.65	0.02

Additional Characteristics:

$$M = 1.61$$

Compute:

Case	$\frac{y_i + y_o}{b_w/2}$	$\frac{b_s}{b_w/2}$	$(C_l)_{\text{calc}}$ figure 6.2.1.1-30	$(C_l)_{\text{test}}$ $@ \alpha = 0^\circ$
1	1.10	0.80	0.0070	0.0085
2	1.10	0.80	0.0070	0.0080
3	1.10	0.80	0.0030	0.0017
4	0.70	0.40	0.0030	0.0045
5	0.70	0.40	0.0016	0.0006

## REFERENCES

1. Lowry, J.G.: Data on Spoiler-Type Ailerons. NACA RM L53I24a, 1953. (U)
2. DeYoung, J.: Theoretical Antisymmetric Span Loading for Wings of Arbitrary Planform at Subsonic Speeds. NACA TR 1056, 1951. (U)
3. Franks, R.: The Application of a Simplified Lifting-Surface Theory to the Prediction of the Rolling Effectiveness of Plain Spoiler Ailerons at Subsonic Speeds. NACA RM A54H26a, 1954. (U)
4. Vogler, R.D.: Wind-Tunnel Investigation at High Subsonic Speeds of a Spoiler-Slot-Deflector Combination on an NASA 65A006 Wing with Quarter-Chord Line Swept Back 32.6°. NACA RM L53D17, 1953. (U)
5. Abbott, I.H., von Doenhoff, A.E., and Stivers, L.S., Jr.: Summary of Airfoil Data. NACA TR 824, 1945. (U)

6. Hammond, A.D.: Lateral-Control Investigation of Flap-Type Controls on a Wing with Unswept Quarter-Chord Line, Aspect Ratio 4, Taper Ratio 0.6 and NACA 65A006 Airfoil Section—Transonic Bump Method. NACA RM L50A03, 1950. (U)
7. Thompson, R.F.: Lateral-Control Investigation of Flap-Type Controls on a Wing With Quarter-Chord Line Swept Back  $35^{\circ}$ , Aspect Ratio 4, Taper Ratio 0.6, and NACA 65A006 Airfoil Section. NACA RM L9L12a, 1950. (U)
8. Vogler, R.D.: Lateral-Control Investigation of Flap-Type Controls on a Wing With Quarter-Chord Line Swept Back  $45^{\circ}$ , Aspect Ratio 4, Taper Ratio 0.6, and NACA 65A006 Airfoil Section—Transonic-Bump Method. NACA RM L9F29a, 1949. (U)
9. Vogler, R.D.: Lateral-Control Investigation of Flap-Type Controls on a Wing With Quarter-Chord Line Swept Back  $60^{\circ}$ , Aspect Ratio 4, Taper Ratio 0.6, and NACA 65A006 Airfoil Section—Transonic-Bump Method. NACA RM L50A17, 1950. (U)
10. Goin, K.L.: Equations and Charts for the Rapid Estimation of Hinge-Moment and Effectiveness Parameters for Trailing-Edge Controls Having Leading and Trailing Edges Swept Ahead of the Mach Lines. NACA TR 1041, 1951. (U)
11. Decker, J.L., et al: USAF Stability and Control Handbook. M-03671, 1956. (C) Title Unclassified
12. Lord, D.R., and Czarnecki, K.R.: Loads Associated with Spoilers at Supersonic Speeds. NACA RM L55E12a, 1955. (U)
13. Foster, G.V.: Effects of Spoiler-Slot Deflector Control on the Aerodynamic Characteristics at a Mach Number of 2.01 of a Variable-Wing-Sweep Configuration With the Outer Wing Panels Swept Back  $75^{\circ}$ . NASA TM X-273, 1960. (U)
14. Lord, D.R., and Moring, R.: Aerodynamic Characteristics of a Spoiler-Slot-Deflector Control on a  $45^{\circ}$  Sweptback Wing at Mach Numbers of 1.61 and 2.01. NACA RM L57E16a, 1957. (U)
15. Franks, R.W.: Tests in the Ames 40- by 80-Foot Wind Tunnel of the Aerodynamic Characteristics of Four Airplane Models with Plain Spoiler Ailerons. NACA RM A54H26, 1954. (U)
16. Vogler, R.D.: Wind-Tunnel Investigation at High Subsonic Speeds of Spoilers of Large Projection on an NACA 65A006 Wing With Quarter-Chord Line Swept Back  $32.5^{\circ}$ . NACA RM L51L10, 1952. (U)
17. Fischel, J., and Hegerman, J.R.: Effect of Aspect Ratio and Sweepback on the Low-Speed Lateral Control Characteristics of Untapered Low-Aspect-Ratio Wings Equipped With Retractable Ailerons. NACA TN 2347, 1951. (U)
18. Hamilton, C.V., and Driver, C.: An Investigation of a Supersonic Aircraft Configuration Having a Tapered Wing with Circular-Arc Sections and  $40^{\circ}$  Sweepback. — Stability and Control Characteristics at a Mach Number of 1.61 of the Complete Configuration Equipped With Spoilers. NACA RM L54F15, 1954. (U)
19. Conner, D.W., and Mitchell, M.H., Jr.: Effect of Spoiler on Airfoil Pressure Distribution and Effects of Size and Location of Spoilers on the Aerodynamic Characteristics of a Tapered Unswept Wing of Aspect Ratio 2.5 at a Mach Number of 1.90. NACA RM L50L20, 1951. (U)
20. Wong, N.D.: An Investigation of the Control Effectiveness of Tip Ailerons and Spoilers on a Low-Aspect-Ratio Trapezoidal-Wing Airplane Model at Mach Numbers From 1.55 to 2.35. NACA RM A57I26a, 1957. (U)
21. Kindell, W.H.: Effects of Span and Spanwise and Chordwise Location on the Control Effectiveness of Spoilers on a  $60^{\circ}$  Sweptback Wing at Mach Numbers of 1.41 and 1.96. NACA RM L53B09, 1953. (U)
22. Guy, L.D.: Effects of Overhang Balance on the Hinge-Moment and Effectiveness Characteristics of an Unswept Trailing-Edge Control on a  $60^{\circ}$  Delta Wing at Transonic and Supersonic Speeds. NACA RM L54G12a, 1954. (U)
23. Spearman, M.L., and Driver, C.: Longitudinal and Lateral Stability and Control Characteristics at Mach Number 2.01 of a  $60^{\circ}$  Delta-Wing Airplane Configuration Equipped with a Canard Control and With Wing Trailing-Edge Flap Controls. NACA RM L58A20, 1958. (U)
24. Guy, L.D.: Hinge-Moment and Effectiveness Characteristics of an Aspect-Ratio-8.2 Flap-Type Control on a  $60^{\circ}$  Delta Wing at Mach Numbers From 0.72 to 1.96. NACA RM L56J17, 1957. (U)
25. Guy, L.D., and Brown, H.V.: Effects of an Inset Tab on the Hinge-Moment and Effectiveness Characteristics of an Unswept Trailing-Edge Control on a  $60^{\circ}$  Delta Wing at Mach Numbers From 0.75 to 1.96. NACA RM L54K16a, 1955. (U)

**TABLE 6.2.1.1-A**  
**SUBSONIC ROLLING-MOMENT EFFECTIVENESS OF PLUG**  
**AND FLAP-TYPE SPOILERS**

DATA SUMMARY

Ref.	Airfoil Section	A	$\lambda$	$\Lambda_{c/4}$ (deg)	$\frac{\delta}{c}$	$\frac{h}{c}$	$\frac{x_s}{c}$	$\frac{\eta_1}{b/2}$	$\frac{\eta_3}{b/2}$	$\frac{b_s}{b/2}$	M	$C_I$ / Calc	$C_I$ / Test	$\Delta C_I$ / Calc-Test
15	NACA65A006	3.00	0.40	40.6	0.10 0.15 0.10 0.10 0.10	0.1174 0.1674 0.1174 0.1174 0.1366	0.70 0.15 0.60 0.80 0.70	0.15 0.15 0.15 0.60 0.10	0.60 0.80 0.60 0.80 0.60	0.45 0.65 0.45 0.65 0.50	0.13 0.13 0.13 0.13 0.13	0.0148 0.0208 0.0225 0.0289 0.0287	0.0166 0.0215 0.0261 0.0300 0.0300	-0.0007 -0.0007 -0.0036 -0.0031 -0.0013
	NACA0012-64	4.78	0.51	36.0	0.10 0.10 0.10 0.10 0.10	0.1174 0.1174 0.1174 0.1174 0.1366	0.60 0.80 0.80 0.80 0.70	0.15 0.15 0.15 0.60 0.10	0.60 0.80 0.60 0.80 0.60	0.45 0.45 0.45 0.40 0.50	0.13 0.13 0.13 0.13 0.13	0.0139 0.0152 0.0291 0.0344 0.0287	0.0112 0.0190 0.0344 0.0027 0.0300	0.0027 -0.0038 -0.0063 -0.0027 -0.0013
16	NACA65A006	4.0	0.60	32.6	0.15	0.1694	0.70	0.139	0.639	0.50	0.40	0.0281	0.0322	-0.0041
	NACA65A006	4.0	0.60	32.6	0.05 0.075 0.10	0.0694 0.0944 0.1194	0.692 0.681 0.662	0.139 0.639 0.639	0.60 0.40 0.50	0.60 0.60 0.40	0.0290 0.0298 0.0220	0.0360 0.0341 0.0215	-0.0060 -0.0043 0.0006	
4	NACA65A006	4.0	0.60	32.6	0.05 0.075 0.10	0.0694 0.0944 0.1194	0.692 0.681 0.662	0.139 0.639 0.639	0.60 0.40 0.50	0.40 0.40 0.40	0.0112 0.0169 0.0220	0.0100 0.0160 0.0215	0.0012 0.0009 0.0006	
17	NACA64A010	4.13	1.00	0	0.02 0.06	0.0483 0.0883	0.07 0.07	0.376 0.976	0.60 0.26	0.26 0.26	0.0077 0.0233	0.0085 0.0270	-0.0008 -0.0037	

$$\text{Average Error} = \frac{\sum |\Delta C_I|}{n} = 0.0027$$

**TABLE 6.2.1.1-B**  
**SUPersonic ROLLING EFFECTIVENESS OF PLAIN TRAILING-EDGE-FLAP AILERONS**

**DATA SUMMARY**

Ref.	$\lambda_T$	$\Delta_{HL}$ (deg)	$\Delta_{TE}$ (deg)	$\phi_{TE}$ (deg)	$\frac{b_f}{b_W}$	$\frac{s_f}{s_W}$	$\frac{v_i}{b_W}$	M	$C_l \delta$ (per deg) Calc	$C_l \delta$ (per deg) Test	$\Delta C_l \delta$ (per deg) Calc-Test
18	0.886	33.26	30.5	6.0	0.50	0.0834	0.25	1.61	0.000686	0.000680	0.000126
22	1.00	0	0	7.62	0.536	0.0746	0.086	1.96	0.000242	0.000223	0.000019
23	1.00	0	0	9.2	0.338	0.0615	0.0776	2.01	0.000151	0.000180	-0.000029
24	1.00	0	0	7.62	0.536	0.0401	0.086	1.96	0.000130	0.000098	0.000032
25	1.00	0	0	7.84	0.402	0.075	0.180	1.96	0.000312	0.000270	0.000042
								1.41	0.000615	0.000418	0.000100
$\Sigma  \Delta C_l \delta $											Average Error = $\frac{\Sigma  \Delta C_l \delta }{n} = 0.000050$

**TABLE 6.2.1.1-C**  
**SUPersonic ROLLING MOMENT DUE TO SPOILER DEFLECTION**

**DATA SUMMARY**

Ref.	Spoiler	A	$\lambda$	$\Delta_{c/4}$ (deg)	$\frac{v_i}{b_W/2}$	$\frac{v_o}{b_W/2}$	Spoiler Chordwise Location (% c)	$\frac{\delta_s}{c}$	M	$C_l$ Calc	$C_l$ Test	$\Delta C_l$ Calc-Test
18	Plug	4.0	0.50	40.0	0.15	0.96	0.65	0.06	1.61	0.0070	0.0085	-0.0015
	Flap						0.65	0.02		0.0070	0.0080	-0.0010
	Plug					0.55	0.06	0.02		0.0030	0.0017	0.0013
14	Flap	3.80	0.30	46.0	0.13	0.78	0.75	0.04	1.61	0.0049	0.0056	-0.0006
							0.06	0.0066		0.0100	-0.0034	
							0.075	0.0087		0.0115	-0.0028	
							0.04	0.0040	2.01	0.0030	0.0010	
							0.06	0.0055		0.0052	0.0003	
							0.075	0.0080		0.0085	-0.0006	

TABLE 6.2.1.1-C (CONTD)

Ref.	Spoiler	A	$\lambda$	$\Lambda_{c/4}$ (deg)	$\frac{V_l}{b_w/2}$	$\frac{V_o}{b_w/2}$	Spoiler Chordwise Location (%)	$\frac{\delta_s}{c}$	M	$C_l$ Calc	$C_l$ Test	$\Delta C_l$ Calc-Test
19	Plug	2.50	0.626	5.3	0.20	0.96	0.75	0.06	1.90	0.0067	0.0075	-0.0008
					↓			0.02		0.0019	0.0030	-0.0011
					0.45			0.06		0.0062	0.0060	-0.0008
					↓			0.02		0.0019	0.0017	0.0002
					0.70			0.06		0.0024	0.0033	-0.0009
					↓			0.02		0.0020	0.0018	0.0002
					0.45	0.70		0.06		0.0024	0.0032	-0.0008
					↓			0.02	↓	0.0012	0.0013	-0.0001
20	Flap	3.20	0.40	19.2	0.28	0.76	0.77	0.037	1.55	0.0031	0.0035	-0.0004
					↓			0.095	↓	0.0084	0.0078	0.0006
					0.037			0.037	1.90	0.0028	0.0026	0.0003
					↓			0.095	↓	0.0069	0.0053	0.0016
					0.037			0.037	2.35	0.0027	0.0011	0.0016
					↓			0.095	↓	0.0065	0.0037	0.0028
21	Plug	2.50	0.626	47.16	0.20	0.95	0.65	0.04	1.41	0.0075	0.0084	-0.0009
					↓			0.06	↓	0.0130	0.0110	0.0020
					0.04			0.04	1.96	0.0046	0.0045	0.0001
					↓			0.06	↓	0.0082	0.0075	0.0007
					0.70			0.04	1.41	0.0052	0.0075	-0.0023
					↓			0.06	↓	0.0062	0.0092	-0.0030
					0.45			0.04	1.96	0.0029	0.0035	-0.0006
					↓			0.06	↓	0.0043	0.0050	-0.0007
					0.45			0.04	1.41	0.0020	0.0034	-0.0014
					↓			0.06	↓	0.0030	0.0060	-0.0030
					0.45			0.04	1.96	0.0011	0.0020	-0.0009
					↓			0.06	↓	0.0020	0.0040	-0.0020
$\text{Average Error} = \frac{\sum  \Delta C_l }{n} = 0.0012$												

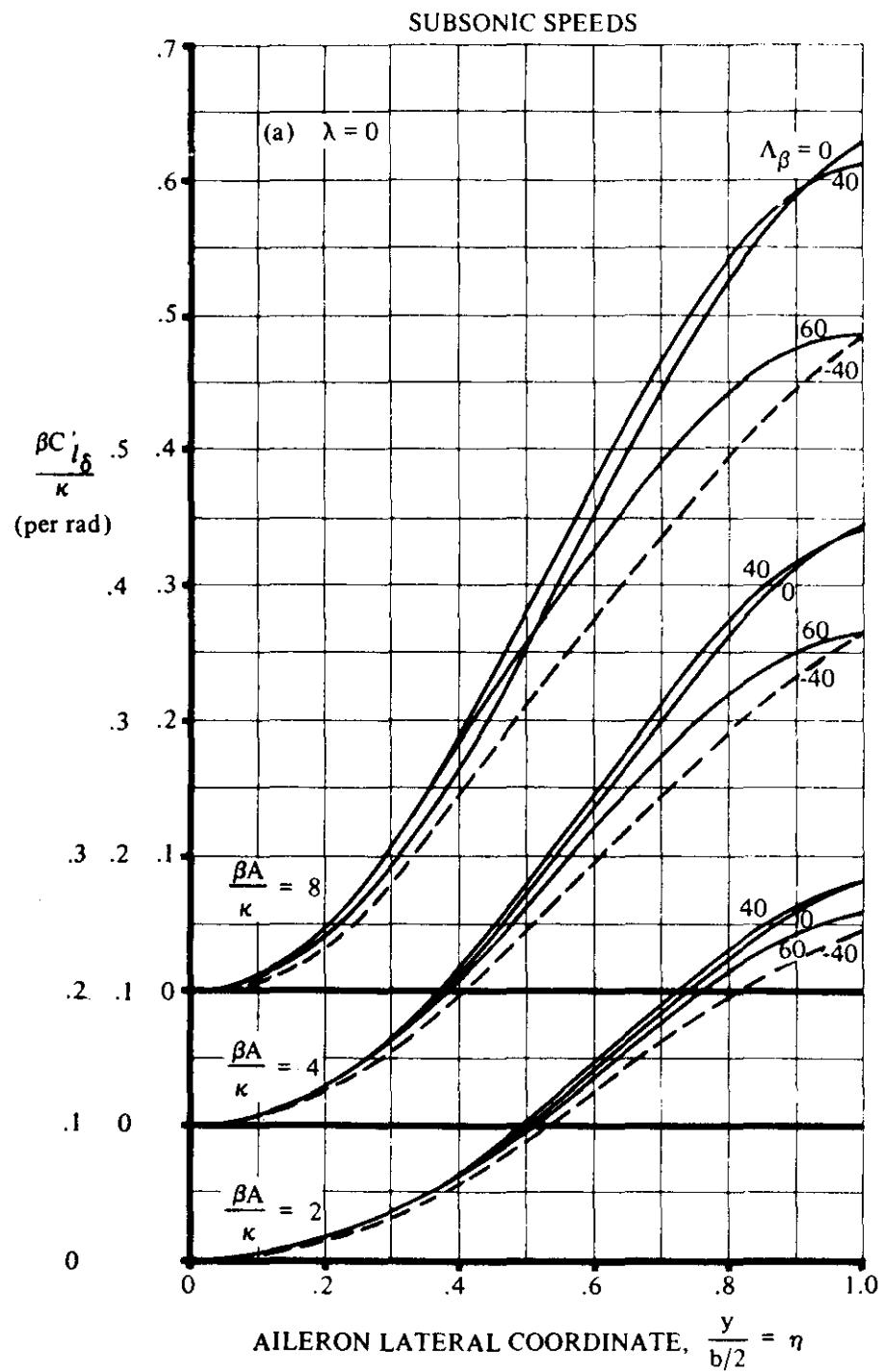


FIGURE 6.2.1.1-23 SUBSONIC AILERON ROLLING-MOMENT PARAMETER

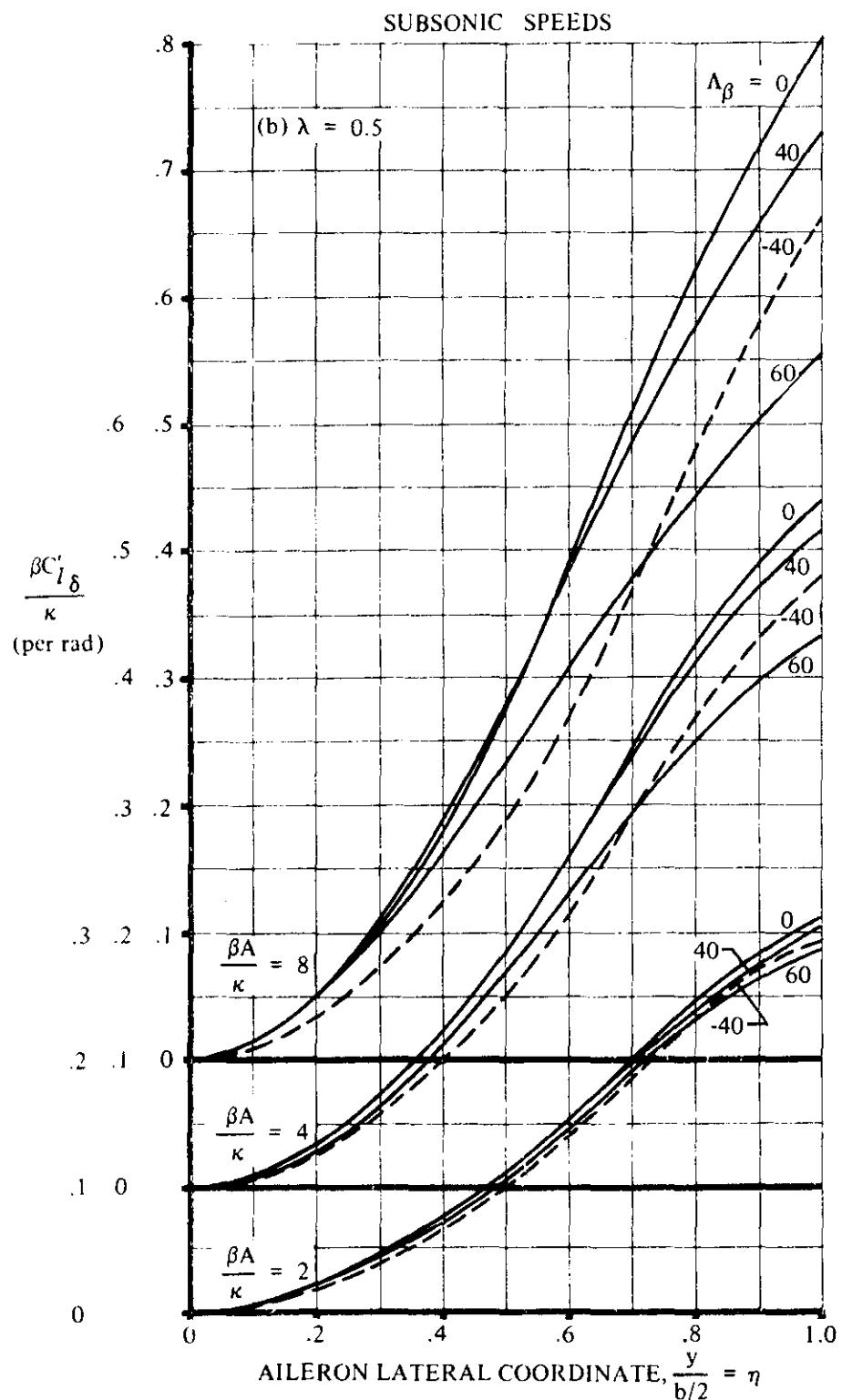


FIGURE 6.2.1.1-23 (CONTD)

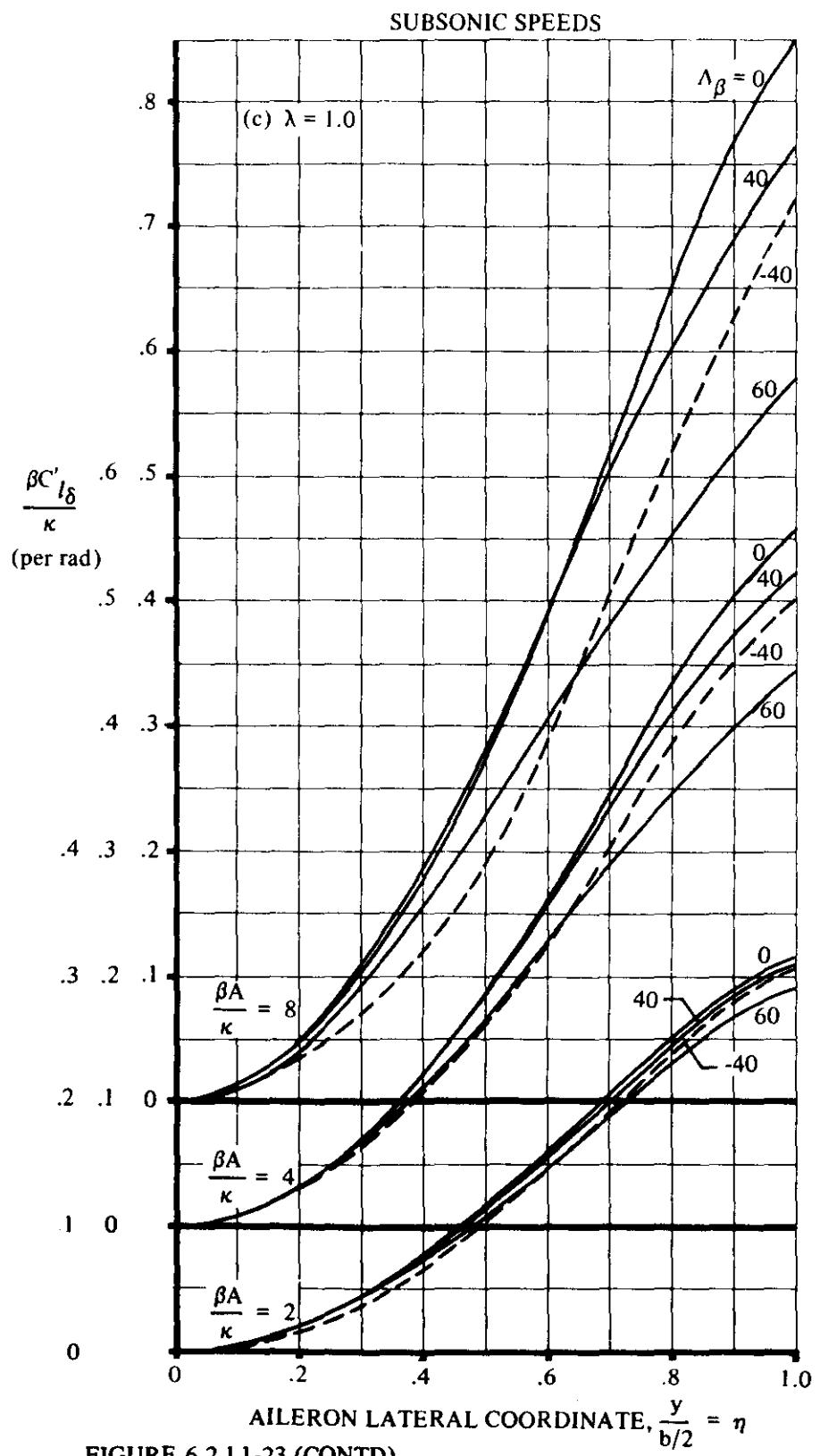


FIGURE 6.2.1.1-23 (CONTD)

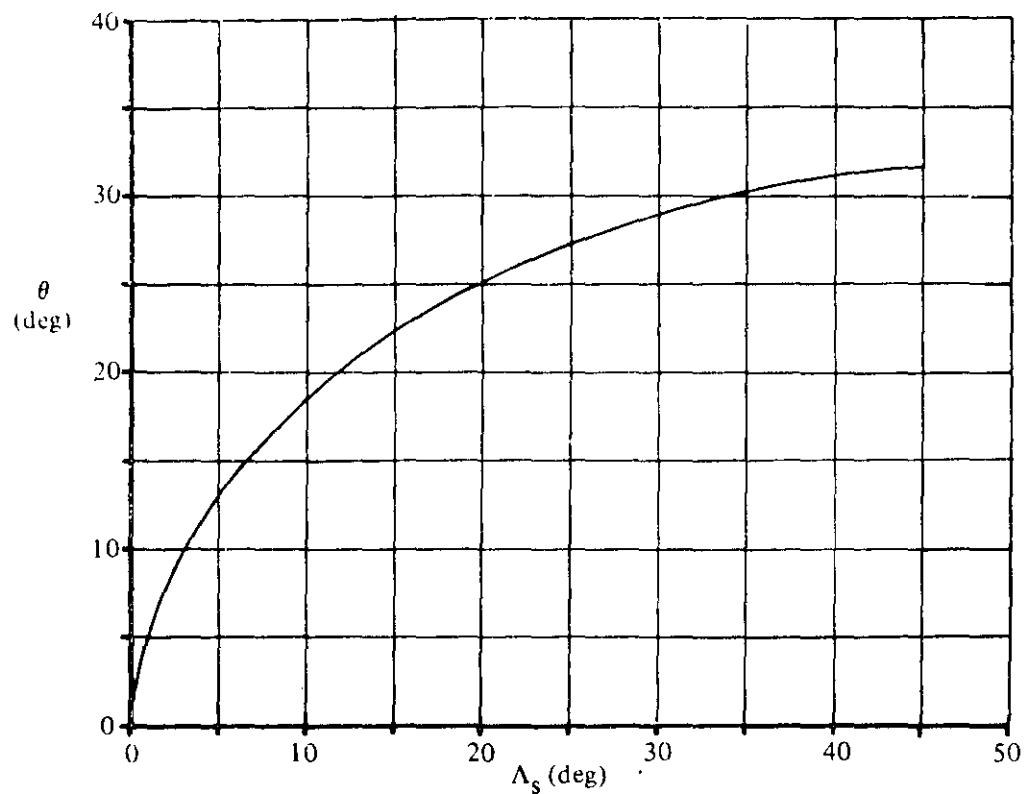


FIGURE 6.2.1.1-26a VARIATION OF  $\theta$  WITH ANGLE OF SWEEPBACK OF SPOILER

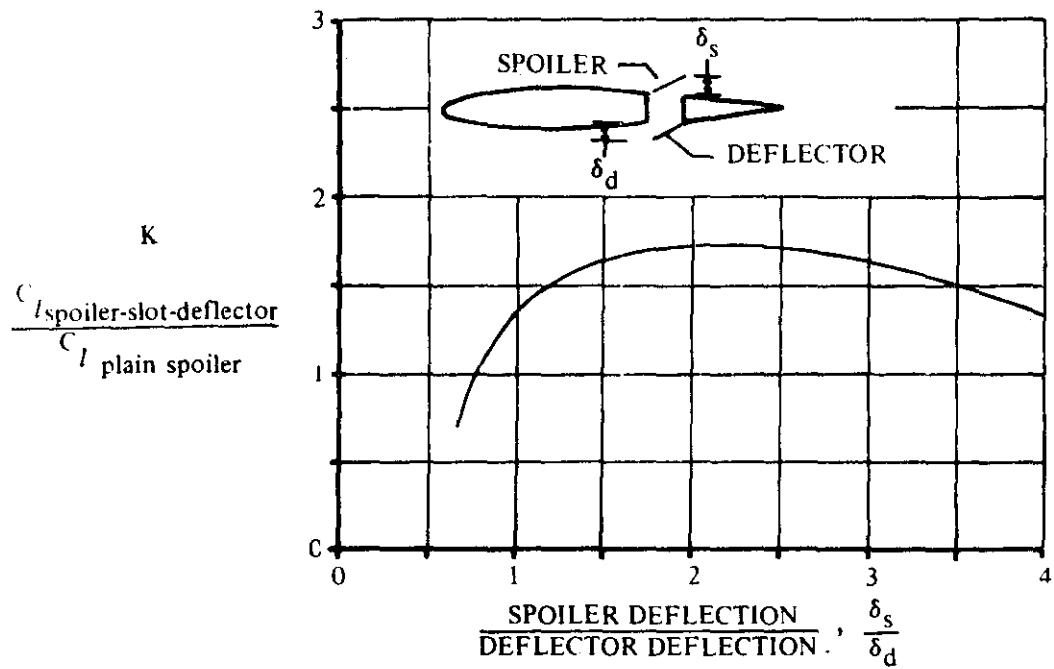


FIGURE 6.2.1.1-26b EFFECT OF SPOILER SLOT AND DEFLECTOR ON SPOILER ROLLING EFFECTIVENESS

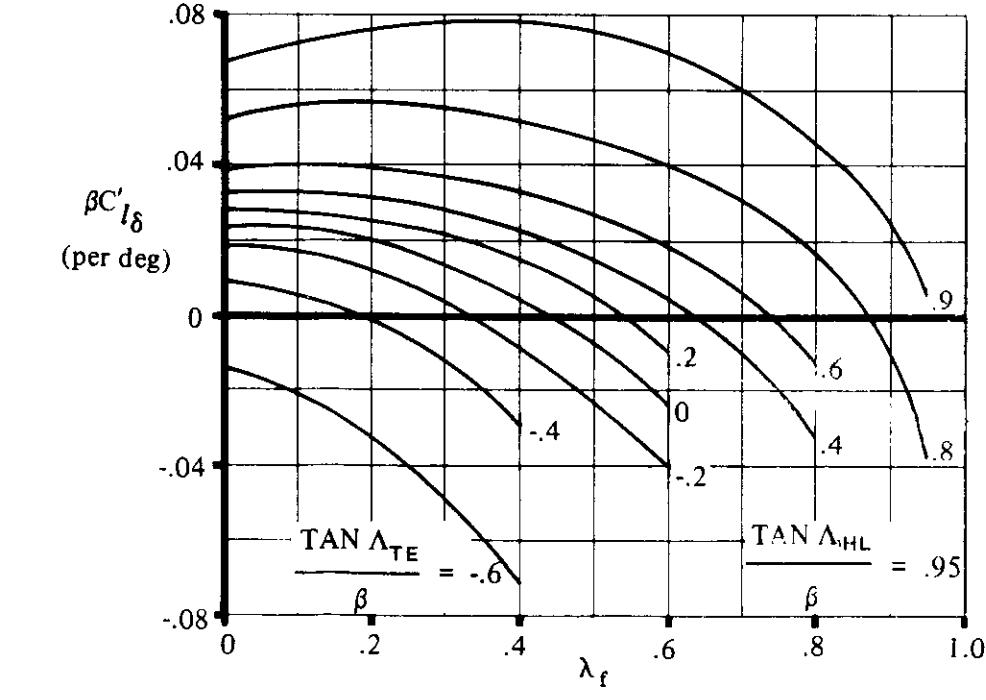
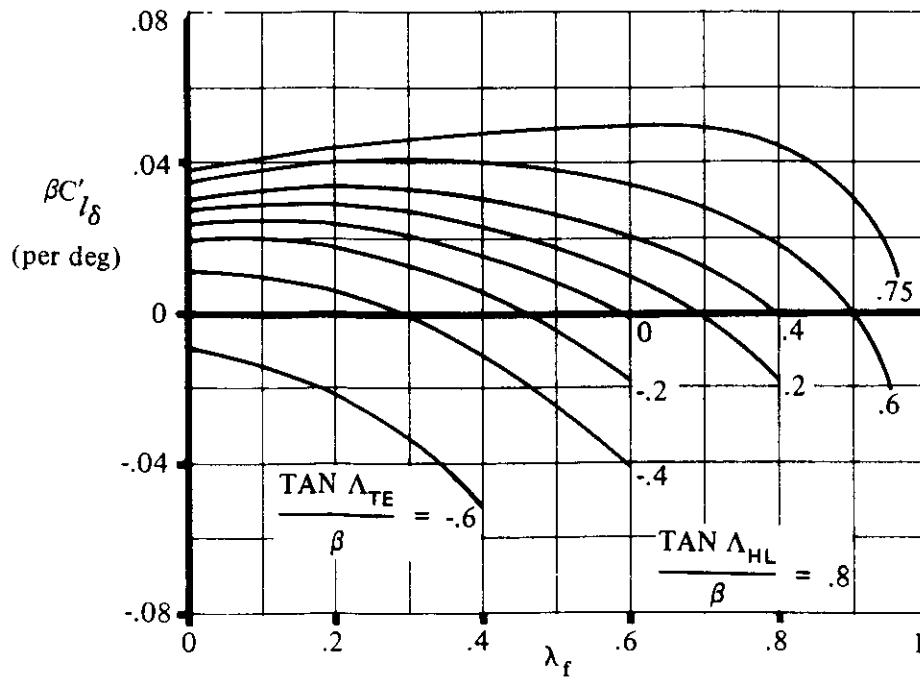
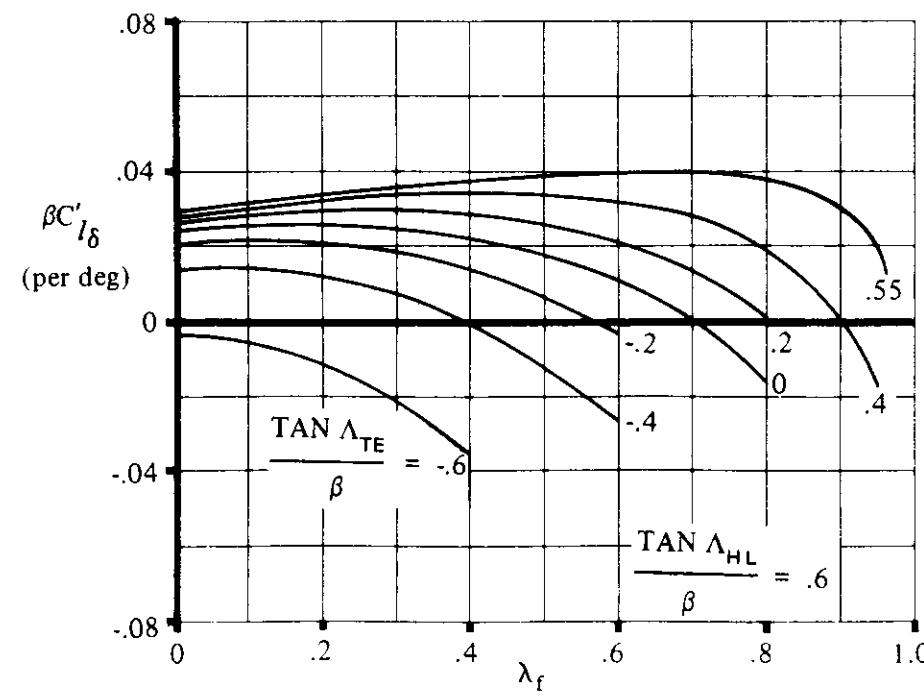
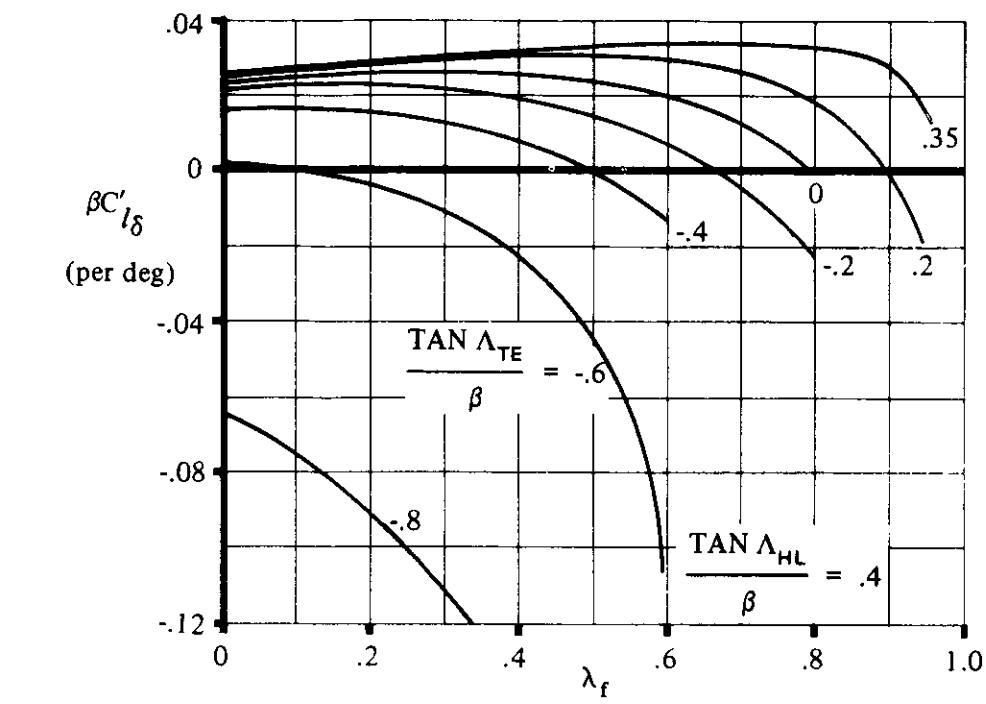
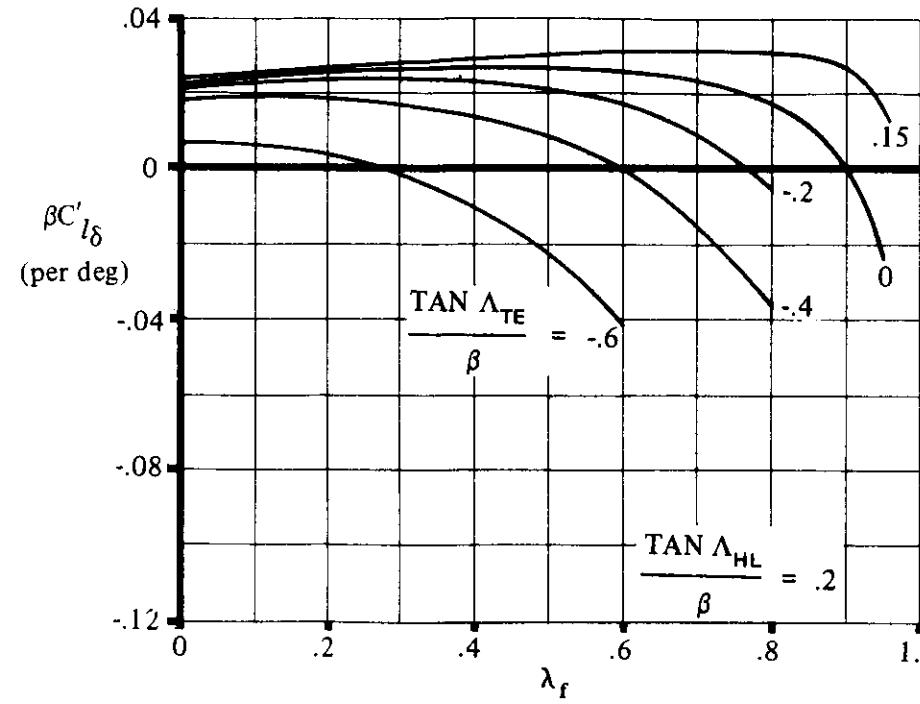
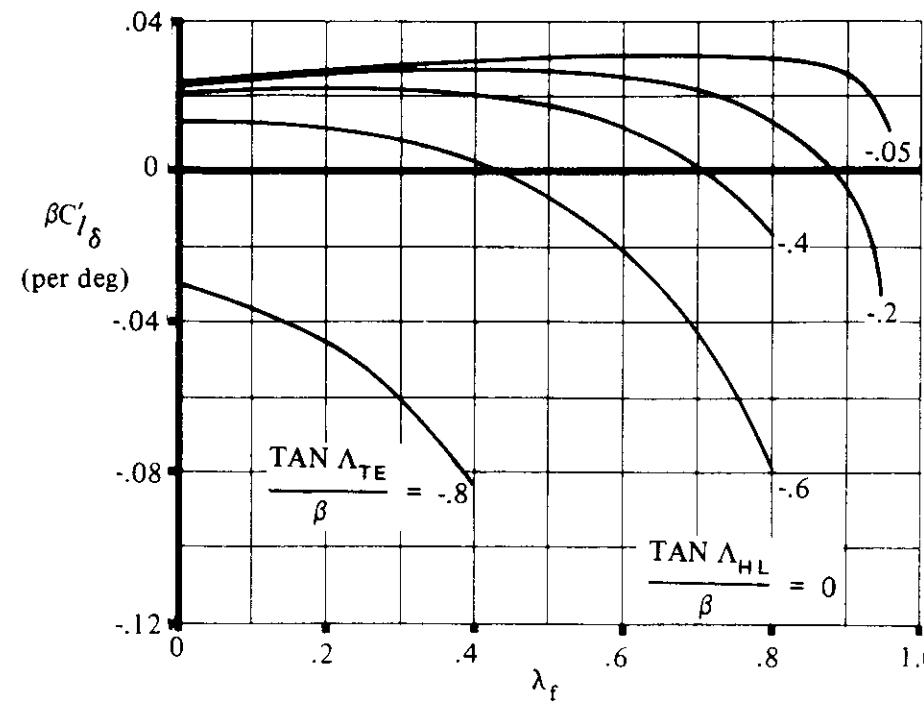


FIGURE 6.2.1.1-27 ROLLING-MOMENT DERIVATIVE FOR TAPERED CONTROL SURFACES HAVING OUTBOARD EDGE COINCIDENT WITH WING TIP

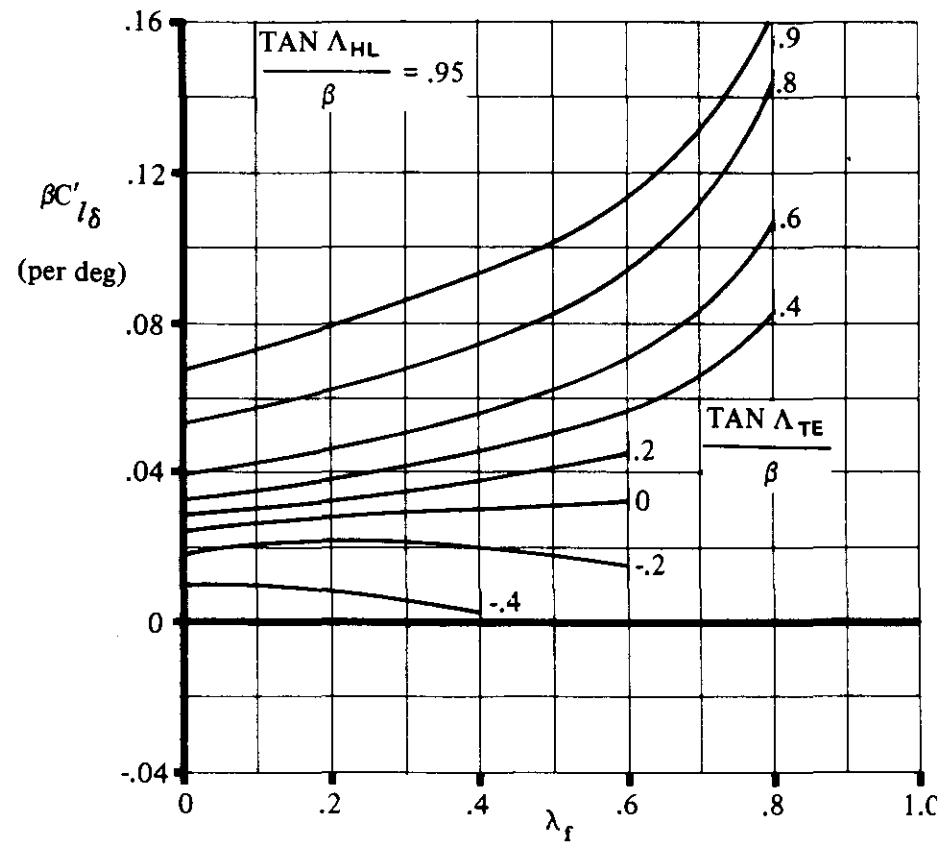
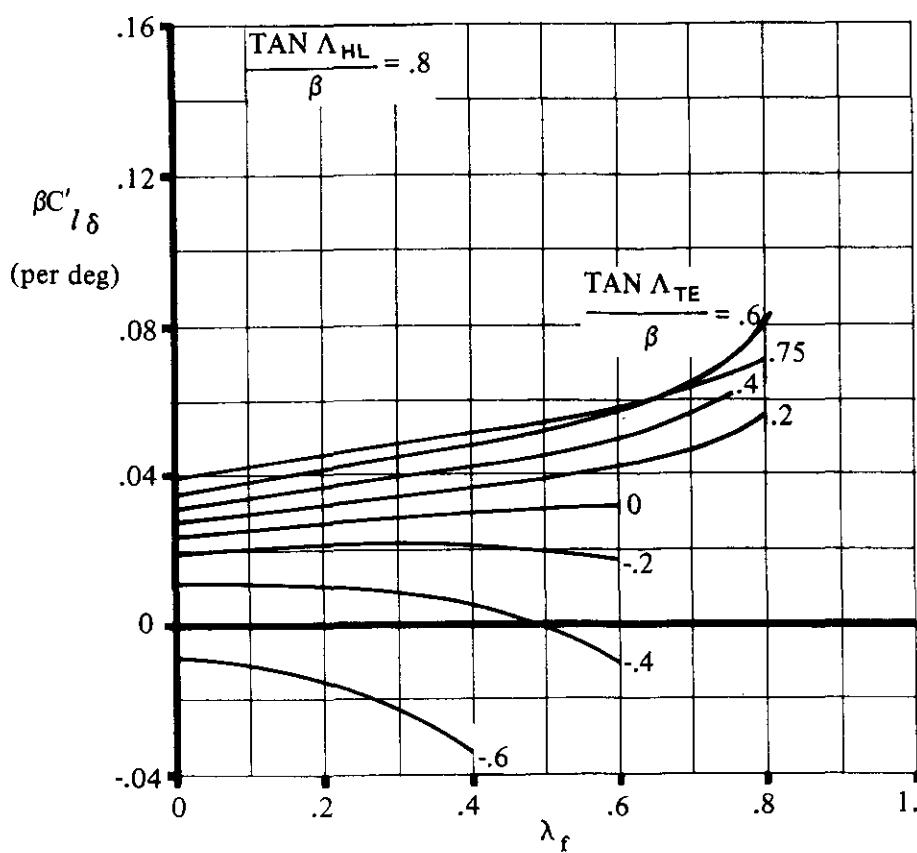
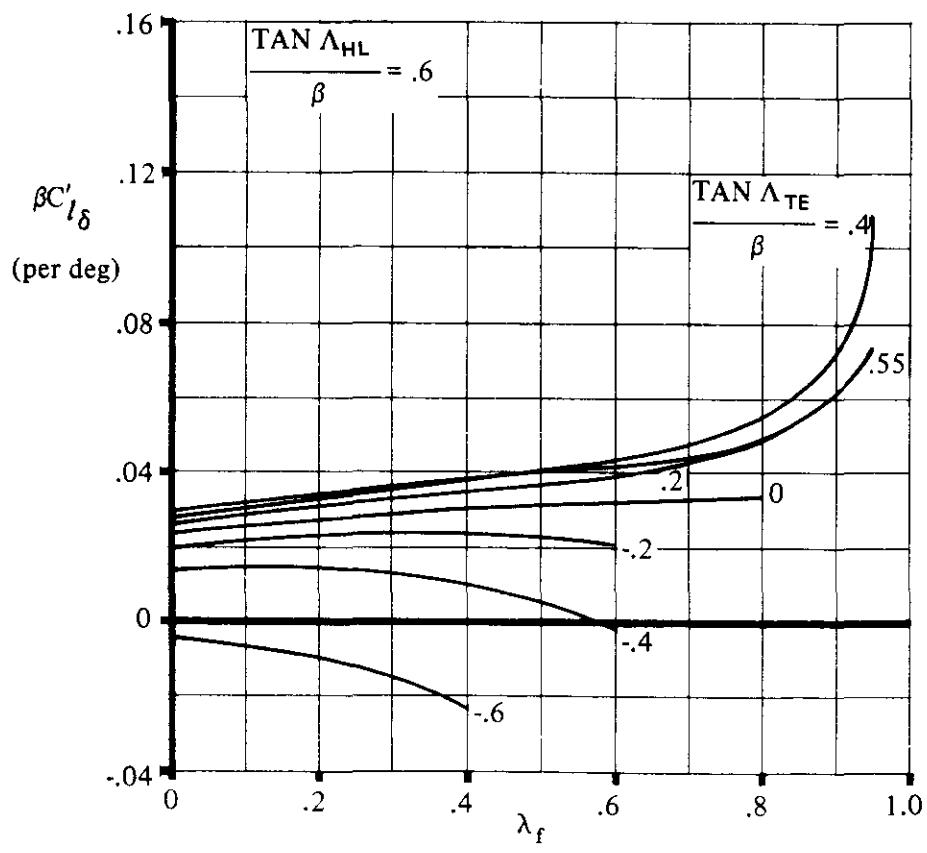
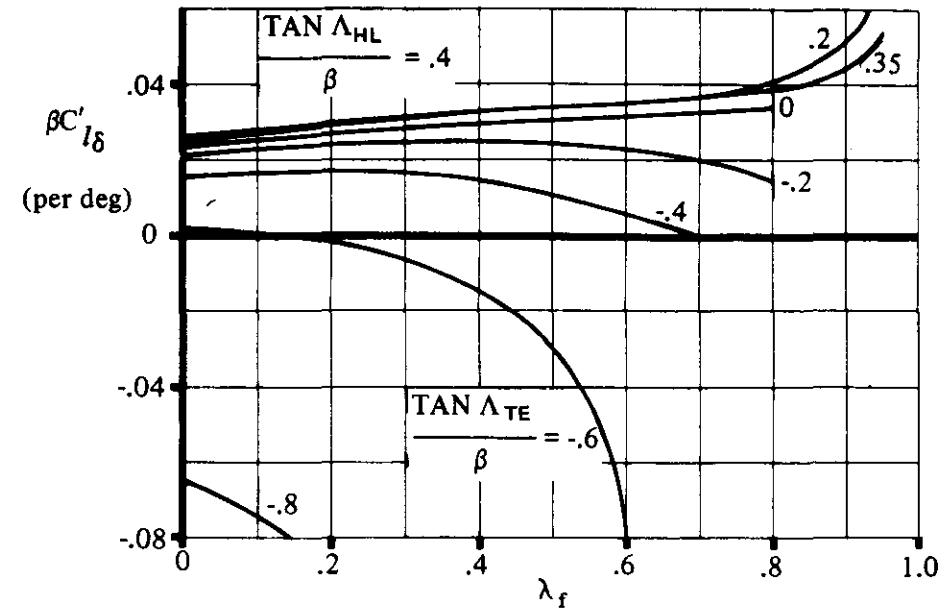
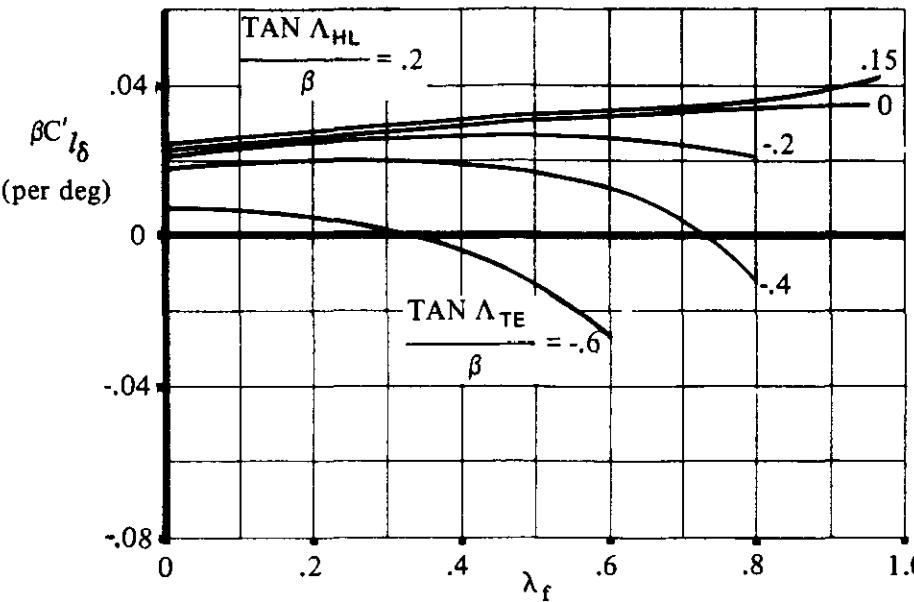
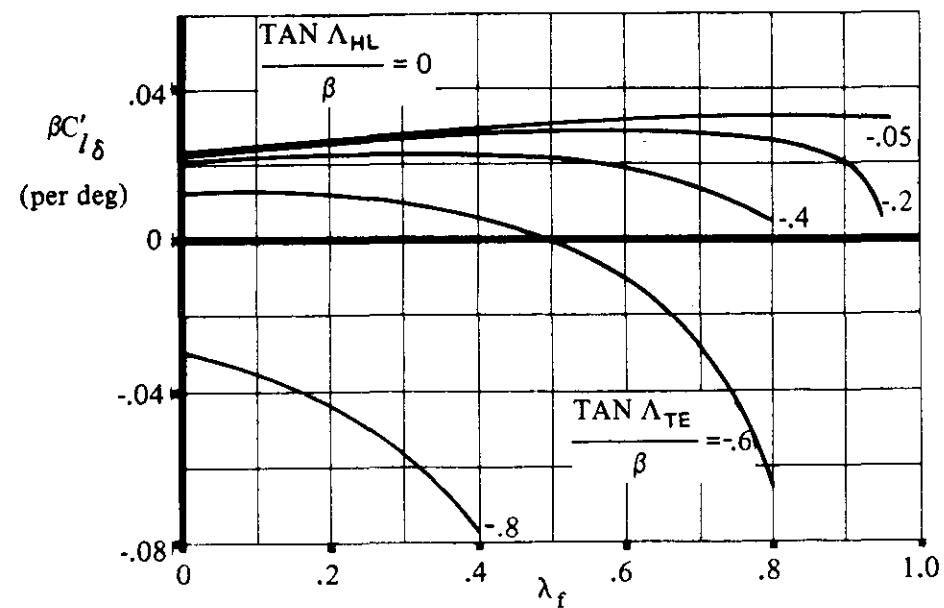


FIGURE 6.2.1.1-28 ROLLING-MOMENT DERIVATIVE FOR TAPERED CONTROL SURFACES HAVING OUTBOARD EDGE NOT COINCIDENT WITH WING TIP

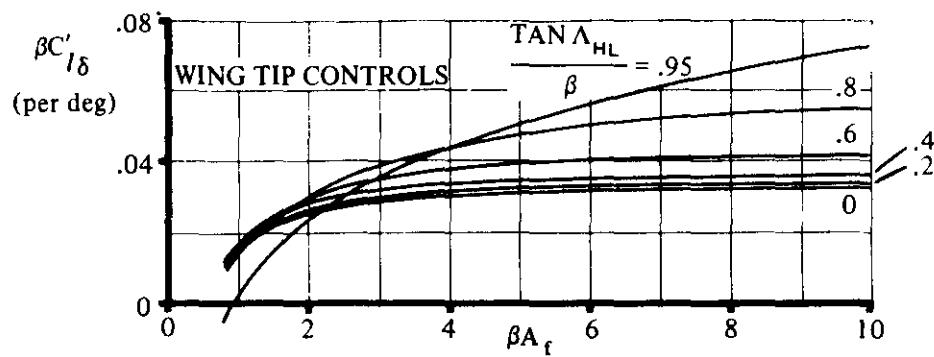


FIGURE 6.2.1.1-29a ROLLING-MOMENT DERIVATIVE FOR UNTAPERED CONTROL SURFACES HAVING OUTBOARD EDGE COINCIDENT WITH WING TIP

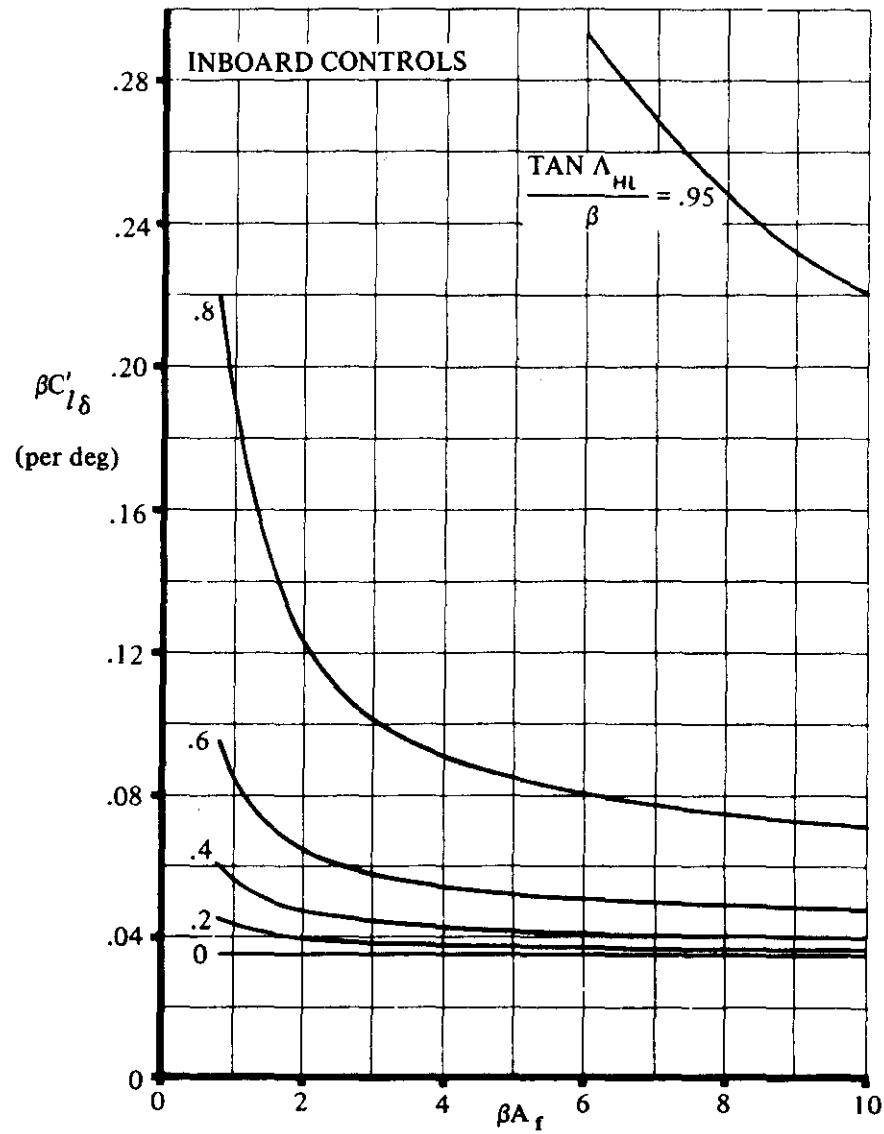


FIGURE 6.2.1.1-29b ROLLING-MOMENT DERIVATIVE FOR UNTAPERED CONTROL SURFACES HAVING OUTBOARD EDGE NOT COINCIDENT WITH WING TIP

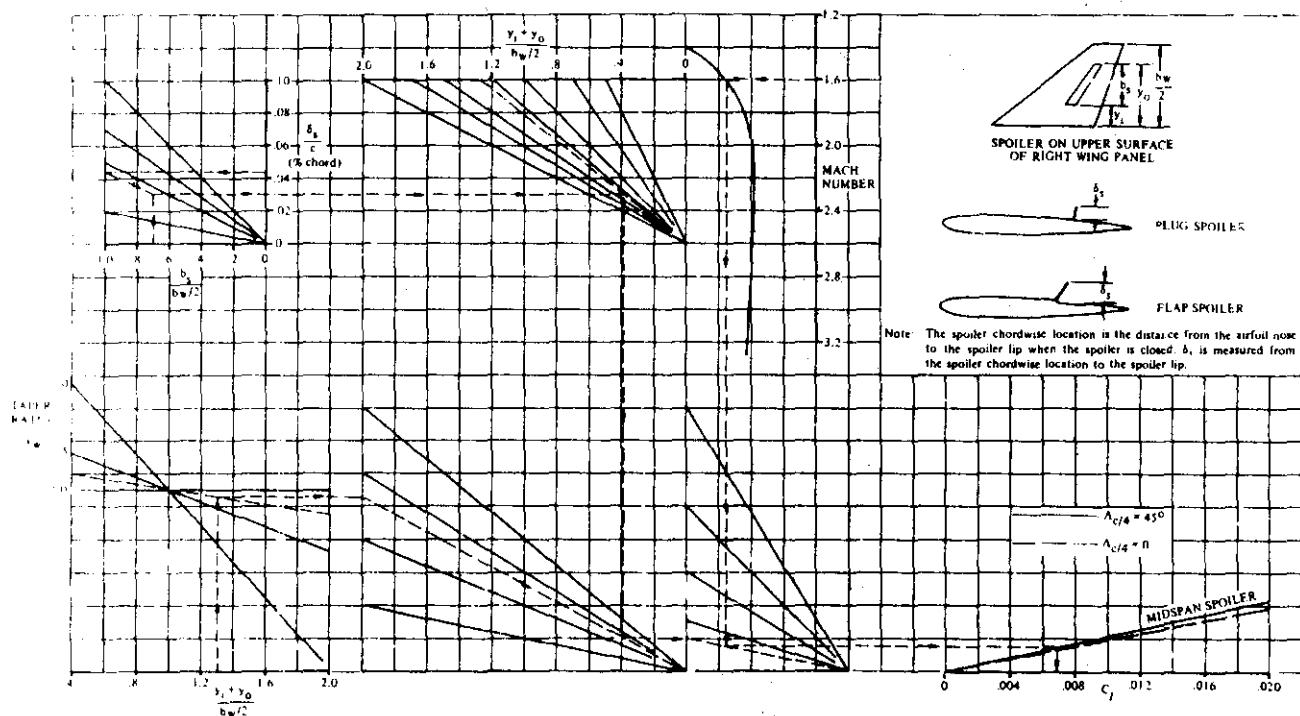


FIGURE 6.2.1.1-10 SPOILER ROLLING MOMENTS AT SUPERSONIC SPEEDS BASED ON TOTAL WING AREA

### 6.2.1.2 ROLLING MOMENT DUE TO A DIFFERENTIALLY DEFLECTED HORIZONTAL STABILIZER

A large amount of theoretical and experimental work has been directed toward the development of efficient roll-control devices. The initial studies and tests concentrated on ailerons, optimizing their size and location to maximize the available roll-control power. However, the more recent studies have investigated auxiliary surfaces or techniques that supplement aileron control to improve aircraft maneuverability. Among these auxiliary devices considered is the differentially deflected horizontal stabilizer.

Methods are presented in this section for estimating the rolling moments generated by a differentially deflected horizontal tail, at subsonic, transonic, and supersonic speeds. These methods are valid only for body-mounted horizontal tails (due to the empirical tail-effectiveness parameter) and are applicable throughout the angle-of-attack range until separation is encountered on the horizontal tail. No provisions are made to estimate the effects of flap deflections, horizontal-tail dihedral, or the rolling-moment contribution of the vertical tail; i.e., they are assumed to be negligible. Comparisons of the estimated and experimental values indicate relatively good correlation to moderate angles of attack (see Tables 6.2.1.2-A and -B).

Body vortices can have a strong influence on the horizontal-tail loading at high angles of attack. For body vortices, the flow separates just above or behind the area of minimum pressure along the side of the body near the nose and wraps up into a pair of symmetrical vortices that proceed downstream. The point at which separation first takes place depends upon the angle of attack (the higher the angle of attack, the nearer the nose separation occurs), the nose-profile shape (the blunter the nose, the nearer the nose separation occurs), and body cross-sectional shape (sharply curving lateral contours promote early separation). The vortices increase in size and strength with increasing downstream distance. These body vortices are accounted for in the methods herein by using the vortex interference charts found in Section 4.3.1.3. However, the effect of the wing shock-expansion field on the body vortices is neglected in the supersonic method.

Wing vortices are of equal interest in determining the horizontal-tail loading at high angles of attack. For closely-coupled configurations having wings and tails of nearly equal span, the wing-vortex effects can be of particular significance. The wing-vortex effects are accounted for in the downwash gradient parameter  $\partial\bar{e}/\partial\alpha$  calculated in Section 4.4.1. (Care should be used to select the method best suited for the configuration.)

To familiarize the reader with the more salient aspects associated with horizontal-tail roll control, a basic discussion is presented. The discussion is supplemented by graphical comparisons of tail-roll-control and aileron-roll-control characteristics to illustrate similarities and differences. (Both the discussion and the illustrations are taken from Reference 1, except where noted.)

The interest in evaluating roll control for a differentially deflected horizontal tail is, in general, due to the inadequate roll-control power provided by conventional roll-control systems; i.e., ailerons and/or spoilers in the transonic and supersonic speed regimes. This inadequacy is due primarily to wing twist and shock-induced separation of the boundary layer ahead of the control surface. For a thin flexible wing of a high-speed airplane, the deflection of conventional outboard ailerons can produce a substantial amount of wing twist that can result in a significant reduction in roll-control

effectiveness. The boundary-layer separation results in a loss of roll-control effectiveness, as well as an increase in buffet and drag and a decrease in lift.

The most recent results of tail-roll-control investigations (Reference 2) indicate that tail roll control is best suited as an auxiliary roll-control device, where only moderate differential deflections are required.

In general, three basic considerations should be kept in mind when designing a tail-roll-control system:

- (1) The tail must provide adequate effectiveness without excessive deflections (large tail and good effectiveness).
- (2) The longitudinal trim requirements of the tail should be minimized to avoid interaction of roll and pitch controls.
- (3) The horizontal tail should be positioned vertically to avoid excessive favorable or adverse yawing moments.

The first item requires no discussion, as the advantages are apparent. The second item can be a critical factor and is worthy of careful consideration. For a specific configuration, a wind-tunnel test is required to determine the interaction effects, since no methods presently exist for estimating this effect. Both the effects of roll control on pitching moments and the variation of roll control with angle of attack for different stabilizer settings must be considered. It is necessary to avoid stabilizer trim settings where the roll control might be limited or significantly reduced because of separation on the horizontal tail as a result of high angles of attack. For example, the landing configuration for some aircraft may produce control interaction problems. The effects of Item 3 above are discussed in detail in Section 6.2.2.2.

#### **Mach Number Effects**

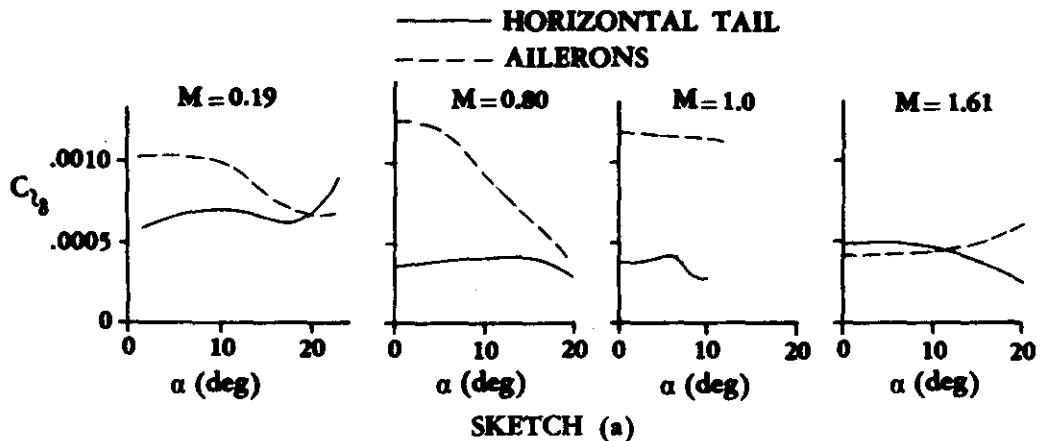
From the limited available test data (References 1 through 8), it can be concluded that the variation of tail-roll-control effectiveness  $C_{l\delta}$  with Mach number is small. Within the subsonic regime, the effectiveness is relatively constant. In the supersonic regime, a slight increase in  $C_{l\delta}$  is noted at a Mach number of approximately 1.2, and then a progressive decrease in effectiveness is noted with increasing Mach number because of the decreasing lift-curve slope of the horizontal tail.

In the subsonic regime, values for  $C_{l\delta}$  due to tail roll control are approximately one-half to one-third of those produced by conventional ailerons at comparable speeds. In the supersonic speed regime, values for  $C_{l\delta}$  due to tail roll control are comparable to those obtained by using ailerons. However, since there will usually be more control deflection available for the ailerons, they will provide more roll control, assuming no aileron reversal is encountered due to wing twist.

#### **Angle-of-Attack Effects**

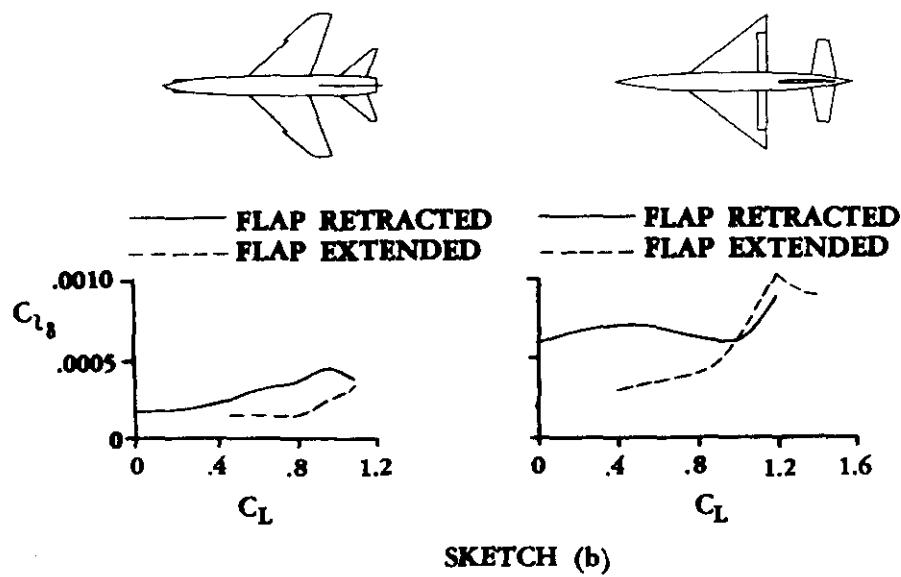
For subsonic Mach numbers, the variation of  $C_{l\delta}$  with angle of attack is not large for most configurations. However, for some configurations  $C_{l\delta}$  can decrease to one-half its original value at

$\alpha = 16^\circ$  to  $20^\circ$  (Reference 8). For aileron control at subsonic speeds, the effectiveness generally drops off rapidly with increasing angle of attack, so that at high angles of attack the values of  $C_{l\delta}$  can begin to approximate those for tail roll control (Reference 3). Sketch (a) presents representative trends for both aileron and horizontal-tail deflections at four different Mach numbers as a function of angle of attack. (These results were obtained on wind-tunnel models with essentially rigid wings.) In contrast to the subsonic speed regime, at  $M = 1.61$  the aileron effectiveness increases with angle of attack while the tail roll control decreases with angle of attack.



#### Flap Effects

The effects of flaps on the tail roll control are shown in Sketch (b) for two different configurations. Both configurations show a detrimental effect of flaps at low lift coefficients. However, as the lift coefficient is increased, the tail roll control increases to equal or exceed the flap-retracted value of  $C_{l\delta}$ . Insufficient data exist to determine if this trend is consistent for all configurations.

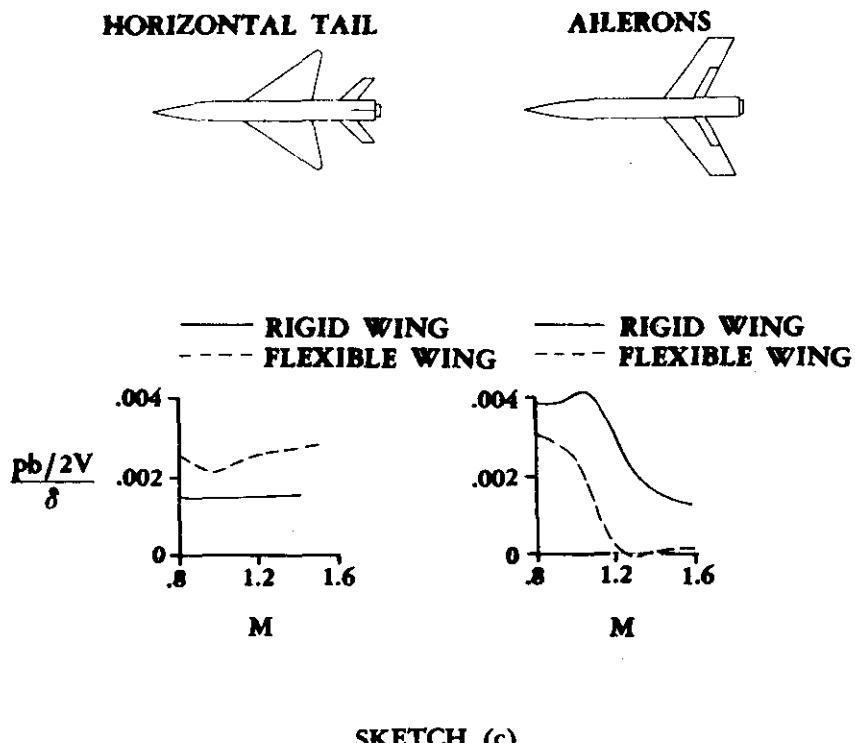


### Dihedral Effects

Reference 6 presents the results of a systematic variation of dihedral angle from 0 to  $-30^\circ$  on the lateral-control effectiveness and the stabilizer characteristics for tail roll control at subsonic speeds. The results of the investigation show a small variation in the roll effectiveness  $C_{l\delta}$  with negative tail-dihedral angle. These small variations did not form a set pattern, but rather were dependent upon the initial stabilizer angle prior to differential deflection.

### Aeroelastic Effects

The effects of wing flexibility are analyzed in the literature (References 1 and 4) through an overall rolling effectiveness parameter  $(pb/2V)/\delta$ , which can be expressed as  $C_{l\delta}/C_{l_p}$ . Thus, for a flexible-wing airplane in comparison to a rigid-wing airplane, greater rolling effectiveness will be realized for the flexible-wing aircraft because of the reduction in the wing contribution to roll damping  $C_{l_p}$ . Sketch (c) presents a comparison of data for a stiff and a flexible wing for both tail roll control and aileron roll control as a function of Mach number. These data illustrate the wing-twist problem encountered for thin flexible wings employing ailerons at supersonic speeds. In contrast, the horizontal-tail roll control shows no adverse effects, but rather an increase for the flexible wing. Thus one can conclude that for certain cases, i.e., a thin flexible-wing configuration at supersonic speeds, the tail-roll-control contribution may be superior to that of conventional ailerons.



## A SUBSONIC

### DATCOM METHOD

The following method is a modification of the method found in Reference 1, with the additional terms accounting for the effects of downwash, body vortices, and tail effectiveness. At angles of attack less than six degrees the body vortex interference factor  $i_{vB(H)}$  can be neglected. The roll-control effectiveness of a body-mounted differentially deflected horizontal stabilizer, based on  $S_w b_w$ , is given by

$$C_{I_\delta} = \frac{1}{2} \left[ \left( 1 - \frac{\pi A_w}{57.3} \frac{\partial \bar{\epsilon}}{\partial \alpha} \right) + i_{vB(H)} \left( \frac{\Gamma}{2\pi \alpha V_r} \right) \left( \frac{r}{b_{H_e}/2} \right) \right] \eta \left( \frac{q_H}{q} \right) \frac{\bar{y}_H S_{H_e}}{b_w S_w} (C_{L_{\alpha H}})_e \quad 6.2.1.2-a$$

The proper sign of the rolling-moment coefficient will result from the expression  $C_I = C_{I_\delta}^* (\delta_L - \delta_R)$ . The subscript e refers to the exposed surface (see Section 4.3.1.2 for a definition of exposed surfaces), and

$A_w$  is the aspect ratio of the total wing.

$\frac{\partial \bar{\epsilon}}{\partial \alpha}$  is the average rate of change of downwash with respect to angle of attack at the horizontal tail, obtained from Section 4.4.1. Care should be exercised to select the method of Section 4.4.1 best suited for the aircraft configuration.

$i_{vB(H)}$  is the vortex interference factor for a lifting surface mounted on the body center line. This parameter is given in Figures 4.3.1.3-7a through-7d for various exposed-tail taper ratios, relative exposed-tail sizes, and vortex center-line positions.

The vertical and lateral vortex positions required to obtain  $i_{vB(H)}$  are  $\frac{z_0}{r}$  and  $\frac{y_0}{r}$ , respectively. At any given station x, they may be obtained from Figures 4.3.1.3-13b and 4.3.1.3-14, respectively, as functions of the parameter  $\frac{\alpha(x - x_s)}{r}$  where

$\alpha$  is the angle of attack in radians.

x is the distance from the body nose to the quarter-chord point of the MAC of the exposed horizontal tail for subsonic flow. (However, for supersonic flow x is measured to the midchord point of the MAC of the exposed horizontal tail.)

r is the average body radius in the region of the horizontal tail. For noncircular bodies use the average body depth in the region of the horizontal tail.

\*It should be noted that the definition of  $C_{I_\delta}$  based on the total differential deflection (consistent with the literature) does not agree with  $C_{I_\delta}$  in other sections.

$\frac{x_s}{r}$  is the nondimensional position of vortex separation, from Figure 4.3.1.3-13a.

It should be noted that Figures 4.3.1.3-7a through -7l give the vortex interference factors for a lifting surface mounted on the body center line. If the lifting surface is not mounted on the body center line, the vertical distance of the body vortices from the body center line, obtained from Figure 4.3.1.3-13b, must be corrected to their distance from the tail before obtaining  $i_{vB(H)}$ . This is illustrated in the sample problem following the subsonic method.

In using Figures 4.3.1.3-7a through -7l a possible problem can develop when interpolation must be made with respect to  $\lambda$  and  $\frac{r}{b_w/2}$ . For positions of

the vortex near the body, the interpolation in  $\frac{r}{b_w/2}$  can carry the vortex inside the body. Under these circumstances, it is recommended that the interpolation be made using  $\frac{y_o - r}{b_w/2 - r}$  for the vortex lateral position in place of  $\frac{y_o}{b_w/2}$ , to avoid vortex positions inside the body.

For noncylindrical bodies, caution must be exercised in using the curves in Section 4.3.1.3 as they are based entirely on cylindrical body shapes.

$$\frac{\Gamma}{2\pi\alpha V r}$$

$\frac{r}{b_{H_e}/2}$  is the ratio of the average radius of the body (or average fuselage depth for noncircular bodies) in the region of the tail to the semispan of the exposed tail.

$$\eta \left( \frac{q_H}{q} \right)$$

is the tail-effectiveness factor for configurations with body-mounted horizontal tails, obtained from Figure 6.2.1.2-22 (from Reference 9).

$$b_w$$

is the total wing span.

$$\frac{S_{H_e}}{S_w}$$

is the ratio of the area of the exposed horizontal tail to the total wing area.

$$\bar{y}_H$$

is the lateral c.p. coordinate of the horizontal tail, measured from and normal to the longitudinal axis. This parameter is given by

$$\bar{y}_H = \eta_{c.p.} \left( \frac{b_{H_e}}{2} \right) + r \quad 6.2.1.2-b$$

where

$\eta_{c.p.}$  is the spanwise location of the c.p. of the exposed horizontal tail (based on the exposed aspect ratio, sweep, and exposed taper ratio), obtained from Figure 6.2.1.2-23 (from Reference 10).

$\frac{b_{H_e}}{2}$  is the semispan of the exposed horizontal tail.

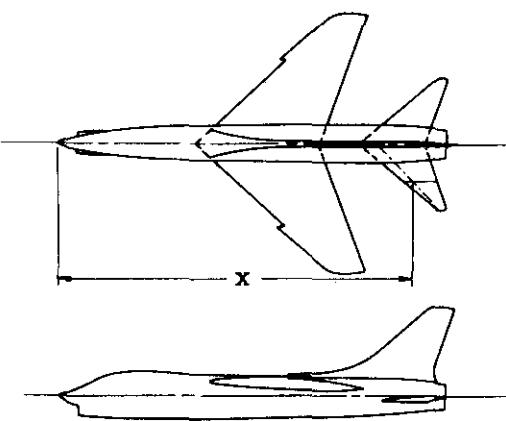
$r$  is the body radius in the region of the horizontal tail. For noncircular bodies use the average body depth in the region of the horizontal tail.

$(C_{L_{\alpha H}})_e$  is the lift-curve slope of the exposed horizontal stabilizer, obtained from Section 4.1.3.2. Care should be exercised to use the appropriate method in determining this parameter because of its significant influence.

The total angular deflection of the control surfaces  $\delta$  is measured in a plane parallel to the plane of symmetry, and is positive for the left control surface deflected trailing edge down and the right control surface deflected trailing edge up.

### Sample Problem

Given: The configuration of Reference 3



#### Wing Characteristics:

$$S_w = 666.7 \text{ sq in.} \quad b_w = 47.56 \text{ in.} \quad A_w = 3.39$$

$$\lambda_w = 0.247 \quad \Lambda_{c/4} = 42^\circ \quad \text{Root Section NACA 65-006}$$

Tip Section NACA 65-005

Horizontal-Tail Characteristics:

$$S_{H_e} = 102.4 \text{ sq in.} \quad b_{H_e} = 18.24 \text{ in.} \quad b_H = 24.11 \text{ in.}$$

$$A_{H_e} = 3.25 \quad A_H = 3.50 \quad \lambda_{H_e} = 0.187$$

$$\lambda_H = 0.148 \quad \Lambda_{c/4} = 45^\circ \quad \Lambda_{c/2} = 38.2^\circ$$

$$h_H = -3.0 \text{ in.} \quad \ell_H = 18.25 \text{ in.}$$

Additional Characteristics:

$$\text{Low speed: } \beta \approx 1.0 \quad d_H = 5.87 \text{ in.} \quad x = 66.0 \text{ in.}$$

$$r = 2.935 \text{ in.} \quad z' = 0.49 \text{ in.}$$

Compute:

Calculate  $(C_{L_{\alpha_H}})_e$  from Section 4.1.3.2

$$c_{q_\alpha} = 0.105 \text{ per deg} \quad (\text{Table 4.1.1-B, for 65-006})$$

$$\kappa = \frac{(c_{q_\alpha})_M}{2\pi/\beta} = \frac{c_{q_\alpha}/\beta}{2\pi/\beta} = \frac{57.3(0.105)}{2\pi} = 0.9576$$

$$\frac{A_{H_e}}{\kappa} \left[ \beta^2 + \tan^2 \Lambda_{c/2} \right]^{1/2} = \frac{3.25}{0.9576} \left[ 1.0 + (0.788)^2 \right]^{1/2} = 4.32$$

$$\frac{(C_{L_{\alpha_H}})_e}{A_{H_e}} = 0.935 \text{ per rad} \quad (\text{Figure 4.1.3.2-49})$$

$$(C_{L_{\alpha_H}})_e = 3.039 \text{ per rad}$$

$$= 0.0530 \text{ per deg}$$

Calculate  $\eta \left( \frac{q_H}{q} \right)$

$$\frac{d_H}{b_H} = \frac{5.87}{24.11} = 0.243$$

$$\eta \left( \frac{q_H}{q} \right) = 0.789 \quad (\text{Figure 6.2.1.2-22})$$

Calculate  $\bar{y}_H$

$$(\Delta_\beta)_H = \tan^{-1} \left( \frac{\tan \Delta_{c/4}}{\beta} \right) = \tan^{-1} \left( \frac{1}{1} \right) = 45^\circ$$

$$\frac{\beta A_{He}}{\kappa} = \frac{(1)(3.25)}{0.9576} = 3.394$$

$$\eta_{c.p.} = 0.429 \quad (\text{Figure 6.2.1.2-23})$$

$$\bar{y}_H = \eta_{c.p.} \left( \frac{b_{He}}{2} \right) + r \quad (\text{Equation 6.2.1.2-b})$$

$$= (0.429) \left( \frac{18.24}{2} \right) + 2.935 = 6.85$$

$$\frac{\bar{y}_H S_{He}}{b_w S_w} = \frac{6.85}{47.56} \frac{102.4}{666.7} = 0.0221$$

Calculate  $\frac{\partial \bar{\epsilon}}{\partial \alpha}$  from Section 4.4.1. (Method 2 is used because this configuration is similar to other configurations used in the substantiation of the method presented in Table 4.4.1-B.)

$$\frac{\partial \bar{\epsilon}}{\partial \alpha} = 4.44 \left[ K_A K_\lambda K_H (\cos \Delta_{c/4})^{1/2} \right]^{1.19} \quad (\text{Equation 4.4.1-h})$$

$$K_A = 0.183 \quad (\text{Figure 4.4.1-69a})$$

$$K_\lambda = 1.324 \quad (\text{Figure 4.4.1-69b})$$

$$\frac{2\ell_H}{b} = \frac{2(18.25)}{47.56} = 0.767$$

$$\frac{2h_H}{b} = \frac{2(-3.0)}{47.56} = -0.126$$

$$K_H = 1.16 \quad (\text{Figure 4.4.1-70, extrapolated})$$

$$\frac{\partial \bar{\epsilon}}{\partial \alpha} = 4.44 [(0.183)(1.324)(1.16)(0.862)]^{1.19}$$

$$= 4.44 [0.2423]^{1.19} = 4.44 [0.1851]$$

$$= 0.822$$

Calculate the body vortex interference factors from Section 4.3.1.3

$$\frac{r}{(b_{H_e}/2)} = \frac{2.935}{9.12} = 0.322$$

$$\alpha \left( \frac{x - x_s}{r} \right) = \frac{\alpha}{57.3} \left( \frac{66.0}{2.935} - \frac{x_s}{r} \right) = \frac{\alpha}{57.3} \left( 22.5 - \frac{x_s}{r} \right)$$

(1)                          (2)                          (3)                          (4)                          (5)                          (6)                          (7)                          (8)

$\alpha$ (deg)	$x_s/r$ (Fig. 4.3.1.3-13a)	$\frac{\alpha}{57.3} \left( \frac{x - x_s}{r} \right)$ (Fig. 4.3.1.3-14)	$y_o/r$ (Fig. 4.3.1.3-14)	$z_o/r$ (Fig. 4.3.1.3-13b)	$z_o/r$ (corrected)*	$\frac{\Gamma}{2\pi\alpha Vr}$ (Fig. 4.3.1.3-15)	$\frac{y_o}{b_{H_e}/2}$ (4) (0.322)
0	—	—	—	—	—	—	—
4	—	—	—	—	—	—	—
8	16.9	0.782	0.600	1.13	1.297	0.55	0.193
12	11.25	2.356	0.705	1.62	1.787	0.895	0.227
16	8.55	3.895	0.747	1.90	2.067	1.215	0.241
20	7.0	5.410	0.762	2.075	2.242	1.58	0.245

(1)                          (9)                          (10)                          (11)

$\alpha$ (deg)	$\frac{z_o}{b_{H_e}/2}$ (6) (0.322)	$i_{vB(H)}$ (Fig. 4.3.1.3-7a-q)	$i_{vB(H)} \left( \frac{\Gamma}{2\pi\alpha Vr} \right) \left( \frac{r}{b_{H_e}/2} \right)$ (10) (7) (0.322)
0	—	—	—
4	—	—	—
8	0.418	-0.190	-0.03365
12	0.575	-0.300	-0.08646
16	0.666	-0.296	-0.1158
20	0.722	-0.297	-0.1511

\*The vertical location of the body vortex must be adjusted to account for the true location of the horizontal tail (Figures 4.3.1.3-7a through -7l assume the horizontal tail is mounted on the body center line). Since the horizontal tail is located below the body center line, the vertical distance of the vortex is increased; i.e.,  $\left( \frac{z_o}{r} \right)_{\text{corrected}} = \frac{z_o}{r} + \frac{z'}{r}$  where  $z'$  is the distance of the horizontal tail below the center line.

Solution:

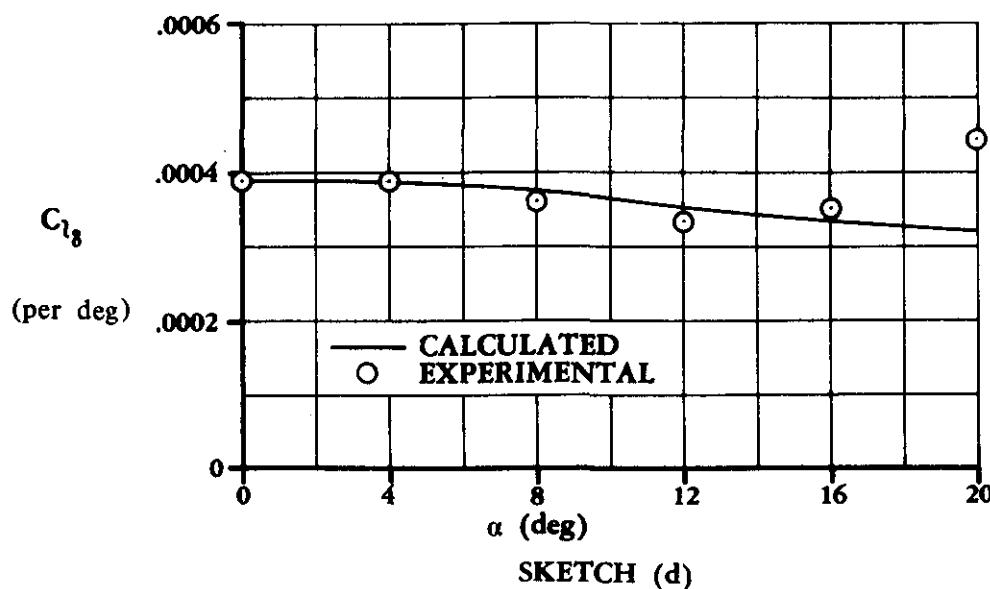
$$C_{l\delta} = \frac{1}{2} \left[ \left( 1 - \frac{\pi A_w}{57.3} \frac{\partial \bar{\epsilon}}{\partial a} \right) + i_{v_{B(H)}} \left( \frac{\Gamma}{2\pi\alpha V_r} \right) \left( \frac{r}{b_{H_e}/2} \right) \right] \eta \left( \frac{q_H}{q} \right) \frac{\bar{y}_H S_{H_e}}{b_w S_w} \left( C_{L\alpha H} \right)_e$$

(Equation 6.2.1.2-a)

$$\begin{aligned} &= \frac{1}{2} \left[ \left\{ 1 - \frac{\pi(3.39)}{57.3} (0.822) \right\} + i_{v_{B(H)}} \left( \frac{\Gamma}{2\pi\alpha V_r} \right) \left( \frac{r}{b_{H_e}/2} \right) \right] (0.789) (0.0221) (0.0530) \\ &= 0.000391 + 0.000462 \left[ i_{v_{B(H)}} \left( \frac{\Gamma}{2\pi\alpha V_r} \right) \left( \frac{r}{b_{H_e}/2} \right) \right] \end{aligned}$$

$\alpha$ (deg)	$i_{v_{B(H)}} \left( \frac{\Gamma}{2\pi\alpha V_r} \right) \left( \frac{r}{b_{H_e}/2} \right)$	$C_{l\delta}$ (per deg)
0	—	0.000391
4	—	0.000391
8	-0.03365	0.000375
12	-0.08646	0.000351
16	-0.1158	0.000338
20	-0.1511	0.000321

The calculated results are compared with test values from Reference 3 in Sketch (d).



## B. TRANSONIC

### DATCOM METHOD

Because Mach number effects on roll-control effectiveness are very small, no separate solution is presented in the transonic regime. The existing methods are considered to be applicable in the transonic regime; i.e., the subsonic method for  $M < 1.0$ , and the supersonic method for  $M > 1.0$ . However, it should be emphasized that the transonic methods must be used to calculate the various components of the roll-control-effectiveness equations; i.e., the values of  $\partial\bar{e}/\partial\alpha$ ,  $(C_{L\alpha H})_e$ , and  $(C_{N\alpha H})_e$ , in the transonic speed regime.

## C. SUPERSONIC

### DATCOM METHOD

The following method is a modification of the method found in Reference 1, with the additional terms accounting for the effects of body vortices and tail effectiveness. In contrast to the subsonic method, this method accounts for the tail effectiveness and the downwash due to wing vortices in the empirical factor of 0.35. At angles of attack less than six degrees the body vortex interference factor  $i_{vB(H)}$  can be neglected. The roll-control effectiveness of a body-mounted differentially deflected horizontal stabilizer, based on  $S_w b_w$ , is given by

$$C_{I\delta} = 0.35 \left[ i_{vB(H)} \left( \frac{\Gamma}{2\pi\alpha Vr} \right) \left( \frac{r}{b_{H_e}/2} \right) + (k_{H(B)} + k_{B(H)}) \right] \left( C_{N\alpha H} \right)_e \frac{\bar{y}_H S_{H_e}}{b_w S_w} \quad 6.2.1.2-c$$

The proper sign of the rolling-moment coefficient will result from the expression  $C_I = C_{I\delta} (\delta_L - \delta_R)$ . The subscript e refers to the exposed surface (see Section 4.3.1.2 for a definition of exposed surfaces), and

$k_{H(B)}$  and  $k_{B(H)}$  are tail-body interference factors obtained from Figures 4.3.1.2-12b and -12a, respectively, of Section 4.3.1.2. Care should be taken to use the appropriate empennage geometry with these figures; i.e., the average body diameter in the region of the horizontal tail and the horizontal-tail span.

$(C_{N\alpha H})_e$  is the normal-force variation with angle of attack of the exposed horizontal tail obtained from Paragraph C of Section 4.1.3.2. Care should be exercised to use the correct method for the specific geometry and to apply the appropriate correction factors where applicable, e.g., those on Figure 4.1.3.2-60.

$\bar{y}_H$  is the lateral center-of-pressure coordinate of the horizontal tail measured from and normal to the longitudinal axis. For the supersonic case, it is assumed that the lateral center-of-pressure coordinate is located at the 40-percent position of the semispan of the exposed tail; i.e.,

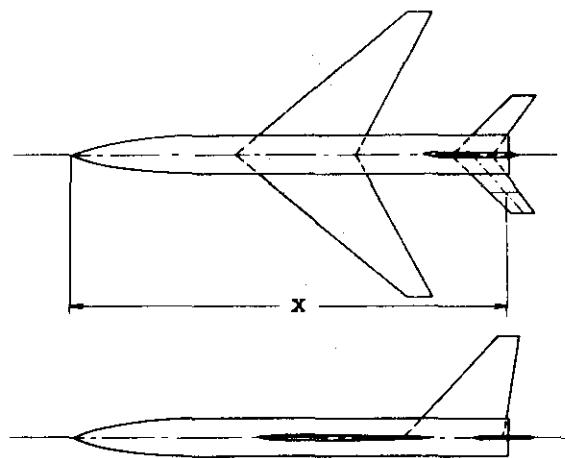
$$\bar{y}_H = 0.4 \left( \frac{b_{H_e}}{2} \right) + r \quad 6.2.1.2-d$$

All remaining terms have been previously defined in the subsonic method of this section. (It should be noted that the c.p. of the horizontal tail at supersonic speeds is assumed to be located at the midchord point of the exposed tail MAC in defining the parameter  $x$ .)

The total angular deflection of the control surfaces  $\delta$  is measured in a plane parallel to the plane of symmetry, and is positive for the left control surface deflected trailing edge down and the right control surface deflected trailing edge up.

### Sample Problem

Given: Model 2 of Reference 8



#### Wing Characteristics:

$$S_w = 144.0 \text{ sq in.} \quad b_w = 24.0 \text{ in.} \quad \Lambda_{c/4} = 45^\circ$$

#### Horizontal-Tail Characteristics:

$$S_{H_e} = 18.24 \text{ sq in.} \quad b_H = 10.73 \text{ in.} \quad b_{H_e} = 7.4 \text{ in.}$$

$$A_H = 4.0 \quad A_{H_e} = 3.0 \quad \lambda_H = 0.6 \quad \lambda_{H_e} = 0.685$$

$$\Lambda_{c/4} = 45^\circ \quad \Lambda_{LE} = 46.7^\circ \quad \text{Airfoil: Double Wedge; t/c = 0.04}$$

#### Additional Characteristics:

$$M = 2.01; \beta = 1.744 \quad r = 1.665 \text{ in.} \quad x = 36.59 \text{ in.}$$

Compute:

Calculate  $(C_{N\alpha H})_e$  from Section 4.1.3.2

$$\frac{\tan \Lambda_{LE}}{\beta} = \frac{1.0625}{1.744} = 0.609$$

$$A_{H_e} \tan \Lambda_{LE} = (3.0)(1.0625) = 3.1875$$

$$\beta(C_{N\alpha}) = 4.02 \text{ per rad} \quad (\text{Figure 4.1.3.2-56 (d), (e), (f), interpolated})$$

$$C_{N\alpha} = 2.305 \text{ per rad}$$

$$\beta \cot \Lambda_{LE} = (1.744)(0.9424) = 1.64 \text{ (supersonic leading edge)}$$

The supersonic wing lift-curve-slope correction factor will be applied because of the supersonic leading edge.

t/c = 0.04 and double-wedge airfoil

$\Delta y = 0.25$  (Figure 2.2.1-8)

$$\Delta y_\perp = \frac{\Delta y}{\cos \Lambda_{LE}} = \frac{0.25}{0.6858} = 0.365$$

$$\frac{C_{N\alpha}}{(C_{N\alpha})_{\text{theor},}} = 0.995 \quad (\text{Figure 4.1.3.2-60})$$

$$(C_{N\alpha H})_e = (0.995)(2.305) = 2.293 \text{ per rad} = 0.040 \text{ per degree}$$

Calculate the tail-body interference factors from Section 4.3.1.2

$$\frac{d_H}{b_H} = \frac{2(1.665)}{10.73} = 0.3103$$

$$k_{B(H)} = 0.324 \quad (\text{Figure 4.3.1.2-12a})$$

$$\beta A_{H_e} = (1.744)(3.0) = 5.232$$

$$k_{H(B)} = 0.983 \quad (\text{Figure 4.3.1.2-12b})$$

$$k_{B(H)} + k_{H(B)} = 0.324 + 0.983 = 1.307$$

Calculate the lateral center-of-pressure coordinate

$$\bar{y}_H = 0.4 \left( \frac{b_{He}}{2} \right) + r \quad (\text{Equation 6.2.1.2-d})$$

$$= (0.4)(3.7) + 1.665 = 3.145 \text{ in.}$$

$$\frac{\bar{y}_H S_{He}}{b_w S_w} = \frac{(3.145)(18.24)}{(24.0)(144.0)} = 0.0166$$

Calculate the body vortex interference factors from Section 4.3.1.3

$$\frac{r}{b_{He}/2} = \frac{1.665}{3.7} = 0.45$$

$$\alpha \left( \frac{x - x_s}{r} \right) = \frac{\alpha}{57.3} \left( \frac{36.59}{1.665} - \frac{x_s}{r} \right) = \frac{\alpha}{57.3} \left( 21.98 - \frac{x_s}{r} \right)$$

(1) (2) (3) (4) (5) (6) (7) (8)

$\alpha$ (deg)	$x_s/r$ (Fig. 4.3.1.3-13a)	$\frac{\alpha}{57.3} \left( \frac{x - x_s}{r} \right)$	$y_o/r$ (Fig. 4.3.1.3-14)	$z_o/r$ (Fig. 4.3.1.3-13b)	$z_o/r$ (corrected)*	$\frac{\Gamma}{2\pi\alpha Vr}$ (Fig. 4.3.1.3-15)	$\frac{y_o}{b_{He}/2}$ (4) (0.45)
0	—	—	—	—	—	—	—
4	—	—	—	—	—	—	—
8	17.0	0.695	0.590	1.110	1.110	0.54	0.265
12	11.15	2.268	0.700	1.600	1.600	0.87	0.315
16	8.52	3.758	0.742	1.880	1.880	1.18	0.334

(1) (9) (10) (11)

$\alpha$ (deg)	$\frac{z_o}{b_{He}/2}$ (6) (0.45)	$i_{vB(H)}$ (Fig. 4.3.1.3-7a-f)	$i_{vB(H)} \left( \frac{\Gamma}{2\pi\alpha Vr} \right) \left( \frac{r}{b_{He}/2} \right)$ (10) (7) (0.45)
0	—	—	—
4	—	—	—
8	0.499	-0.125	-0.0304
12	0.720	-0.226	-0.0885
16	0.846	-0.242	-0.1285

$$\left( \frac{z_o}{r} \right)_{\text{corrected}} = \frac{z_o}{r} - 0 = \frac{z_o}{r} \quad (\text{tail located on body center line}).$$

Solution:

$$C_{l\delta} = 0.35 \left[ i_{vB(H)} \left( \frac{\Gamma}{2\pi\alpha Vr} \right) \left( \frac{r}{b_{H_e}/2} \right) + \left( k_{H(B)} + k_{B(H)} \right) \right] \left( C_{N_{\alpha H}} \right)_e \frac{\bar{y}_H S_{H_e}}{b_w S_w}$$

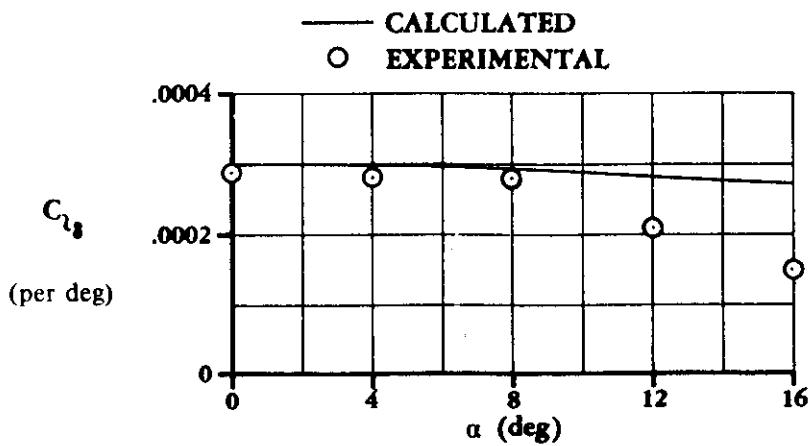
(Equation 6.2.1.2-c)

$$= 0.35 \left[ i_{vB(H)} \left( \frac{\Gamma}{2\pi\alpha Vr} \right) \left( \frac{r}{b_{H_e}/2} \right) + 1.307 \right] (0.040) (0.0166)$$

$$= 0.000232 \left[ i_{vB(H)} \left( \frac{\Gamma}{2\pi\alpha Vr} \right) \left( \frac{r}{b_{H_e}/2} \right) \right] + 0.000303$$

$\alpha$ (deg)	$i_{vB(H)} \left( \frac{\Gamma}{2\pi\alpha Vr} \right) \left( \frac{r}{b_{H_e}/2} \right)$	$C_{l\delta}$ (per deg)
0	-	0.000303
4	-	0.000303
8	-0.0304	0.000296
12	-0.0885	0.000282
16	-0.1285	0.000273

The calculated results are compared with test values from Reference 8 in Sketch (e).



SKETCH (e)

## REFERENCES

1. Campbell, J. P.: The Use of the Horizontal Tail for Roll Control. NACA RM L55L16a, 1956. (U)
2. McAllister, J. D., et al.: Wing Roll Control Devices for Transonic High Lift Conditions. Part I -- Fixed Wing Configuration. AFFDL-TR-69-124, 1970. (U)
3. Boisseau, P. C.: Low-Speed Roll Effectiveness of a Differentially Deflected Horizontal-Tail Surface on a 42° Swept-Wing Model. NACA RM L56E03, 1956. (U)
4. English, R. D.: Free-Flight Investigation, Including Some Effects of Wing Aeroelasticity, of the Rolling Effectiveness of an All-Movable Horizontal Tail With Differential Incidence at Mach Numbers from 0.6 to 1.5. NACA RM L54K30, 1955. (U)
5. Mitchell, J. L., and Vitale, A. J.: Free-Flight Investigation of the Control Effectiveness of a Differentially Deflected Horizontal Tail at Mach Numbers from 0.8 to 1.6. NACA RM L56B20, 1956. (U)
6. Fournier, P. G.: Effect of Tail Dihedral on Lateral Control Effectiveness at High Subsonic Speeds of Differentially Deflected Horizontal-Tail Surfaces on a Configuration Having a Thin Highly Tapered Wing. NASA Memo 12-1-58L, 1959. (U)
7. Critzos, C. C.: Lateral-Control Investigation at Transonic Speeds of Differentially Deflected Horizontal-Tail Surfaces for a Configuration Having a 6-Percent-Thick 45° Sweptback Wing. NACA RM L55I26, 1955. (U)
8. Spearman, M. L.: Limited Investigation of Effects of Differential Horizontal-Tail Deflection on Lateral Control Characteristics of Two Swept-Wing Airplane Models at Mach Numbers from 1.4 to 2.0. NACA RM L56I20, 1956. (U)
9. Neely, R. H., and Griner, R. F.: Summary and Analysis of Horizontal-Tail Contribution to Longitudinal Stability of Swept-Wing Airplanes at Low Speeds. NASA TR R-49, 1959. (U)
10. DeYoung, J., and Harper, C. W.: Theoretical Symmetric Span Loading at Subsonic Speeds for Wings Having Arbitrary Plan Form. NACA TR 921, 1948. (U)
11. Koenig, D. G.: Tests in the Ames 40- by 80-Foot Wind Tunnel of an Airplane Configuration with an Aspect Ratio 3 Triangular Wing and an All-Movable Horizontal Tail -- Longitudinal and Lateral Characteristics. NACA RM A52L15, 1953. (U)
12. Spearman, M. L. and Foster, G. V.: Stability and Control Characteristics at a Mach Number of 2.01 of a Variable-Sweep-Wing Configuration with Outboard Wing Panels Swept Back 75°. NASA TM X-32, 1959. (U)
13. Shaw, D. S.: Supersonic Investigation of the Static Stability, Performance, and Control of a Variable-Sweep Tactical Fighter Model. Phase 1, NASA TM X-1045, 1965. (C) Title Unclassified
14. Graham, D., and Koenig, D. G.: Tests in the Ames 40- by 80-Foot Wind Tunnel of an Airplane Configuration with an Aspect Ratio 2 Triangular Wing and an All-Movable Horizontal Tail -- Lateral Characteristics. NACA RM A51L03, 1952. (U)

**TABLE 6.2.1.2-A**  
**SUBSONIC TAIL-ROLL-CONTROL EFFECTIVENESS**  
**DATA SUMMARY AND SUBSTANTIATION**

Ref.	M	A <sub>W</sub>	$\lambda_W$	b <sub>W</sub> (in.)	$\Lambda_{LE_W}$	A <sub>H<sub>0</sub></sub>	$\lambda_{H_0}$	b <sub>H</sub> (in.)	$\Lambda_{LE_H}$	$\alpha$	C <sub>I<sub>δ</sub></sub> Calc.	C <sub>I<sub>δ</sub></sub> Test	$\Delta C_{I\delta}$
2	0.7	4.07	0.3	22.52	31.5°	2.146	0	13.06	57.5°	0	0.000872	0.00114	-0.000268
										4	0.000872	0.00116	-0.000288
										8	0.000836	0.00132	-0.000484
										12	0.000784	0.00112	-0.000336
3	0.05	3.39	0.247	47.56	47.2°	3.25	0.187	24.11	50.5°	0	0.000391	0.00039	0
										4	0.000391	0.00039	0
										8	0.000375	0.000361	0.000014
										12	0.000351	0.000336	0.000015
6	0.6	3.0	0.14	27.39	38.7°	3.084	0.588	16.12	18.8°	0	0.000575	0.00069	-0.000115
										5	0.000575	0.00069	-0.000115
										10	0.000544	0.00074	-0.000196
										15	0.000506	0.00077	-0.000264
11	0.13	2.99	0	367.7	53.2°	3.977	0.50	221.4	10°	0	0.000787	0.00055	0.000237
										4	0.000787	0.00065	0.000137
										8	0.000740	0.00081	-0.00007
										12	0.000720	0.00084	-0.00012
										16	0.000696	0.00078	-0.000084
										20	0.000674	0.00072	-0.000046

TABLE 6.2.1.2-A (CONT'D)

Ref.	M	$A_w$	$\lambda_w$	$b_w$ (in.)	$\Delta_{LE_w}$	$A_{H_s}$	$\lambda_{H_s}$	$b_h$ (in.)	$\Delta_{LE_h}$	$\alpha$	$C_l \delta$ Calc.	$C_l \delta$ Test	$\Delta C_l \delta$
7	0.96 ↓ 0.90 ↓ 0.80 ↓ 0.8 ↓	4.0 ↓ ↓ ↓ ↓ ↓ ↓	0.6 ↓ ↓ ↓ ↓ ↓ ↓	72.0 ↓ ↓ ↓ ↓ ↓ ↓	46.7° ↓ ↓ ↓ ↓ ↓ ↓	3.275 ↓ ↓ ↓ ↓ ↓ ↓	0.668 ↓ ↓ ↓ ↓ ↓ ↓	30.7 ↓ ↓ ↓ ↓ ↓ ↓	46.6° ↓ ↓ ↓ ↓ ↓ ↓	0 4 0 4 8 12 16 0 4 8 12 16 20 0 4 8 12 16 0 4 8 12 16	0.000358 0.000358 0.000367 0.000367 0.000345 0.000327 0.000311 0.000352 0.000352 0.000332 0.000315 0.000299 0.000284 0.000954 0.000954 0.000914 0.000856 0.000813 0.000913 0.000913 0.000875 0.000820 0.000774	0.000315 0.00040 0.000325 0.000373 0.00045 0.000385 0.000325 0.00035 0.00040 0.00035 0.000415 0.000368 0.000265 0.00119 0.00119 0.00130 0.00112 0.00088 0.00124 0.00122 0.00126 0.00122 0.00096	0.000043 -0.000042 0.000042 -0.000006 -0.000105 -0.000058 -0.000014 0.000002 -0.000048 -0.000018 -0.0001 -0.000069 0.000019 -0.000236 -0.000236 -0.000386 -0.000264 -0.000067 -0.000327 -0.000307 -0.000375 -0.0004 -0.000186
2	0.9 ↓ 0.8 ↓	4.07 ↓ ↓ ↓	0.3 ↓ ↓ ↓	22.52 ↓ ↓ ↓	31.5° ↓ ↓ ↓	2.146 ↓ ↓ ↓	0 ↓ ↓ ↓	13.06 ↓ ↓ ↓	57.5° ↓ ↓ ↓	0 4 8 12 16 0 4 8 12 16	0.000954 0.000954 0.000914 0.000856 0.000813 0.000913 0.000913 0.000875 0.000820 0.000774	0.00119 0.00119 0.00130 0.00112 0.00088 0.00124 0.00122 0.00126 0.00122 0.00096	-0.000236 -0.000236 -0.000386 -0.000264 -0.000067 -0.000327 -0.000307 -0.000375 -0.0004 -0.000186

**TABLE 6.2.1.2-B**  
**SUPersonic TAIL-ROLL-CONTROL EFFECTIVENESS**  
**DATA SUMMARY AND SUBSTANTIATION**

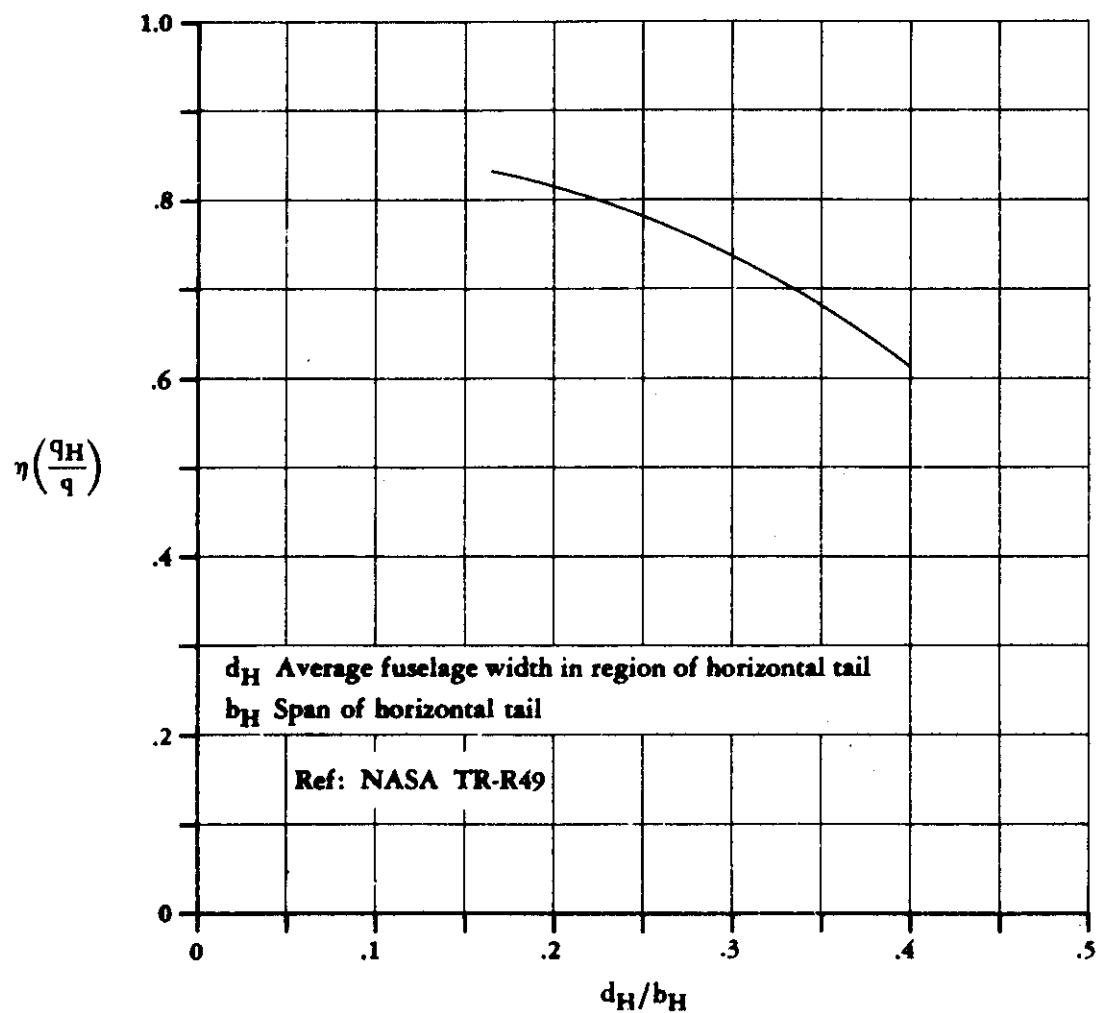
Ref.	M	A <sub>W</sub>	$\lambda_W$	b <sub>W</sub> (in.)	$\Delta LE_W$	A <sub>H<sub>e</sub></sub>	' $\lambda_{H_e}$	b <sub>H</sub> (in.)	$\Delta LE_H$	$\alpha$	C <sub>I<sub>δ</sub></sub> Calc.	C <sub>I<sub>δ</sub></sub> Test	$\Delta C_{I\delta}$
8 Model 1	1.61	4	0.5	25.31	$38.1^{\circ}$	3.0	0.468	12.12	$39.5^{\circ}$	0	0.000455	0.00049	-0.000035
										4	0.000455	0.00049	-0.000035
										8	0.000454	0.00046	-0.000006
										12	0.000435	0.000425	0.000010
										16	0.000423	0.00036	0.000063
										0	0.000371	0.00040	-0.000029
										4	0.000371	0.00040	-0.000029
										8	0.000370	0.00039	-0.000020
										12	0.000354	0.00034	0.000014
										16	0.000345	0.00025	0.000095
8 Model 2	1.41	4	0.2	24.0	$49.4^{\circ}$	3.0	0.685	10.73	$46.7^{\circ}$	0	0.000402	0.00042	-0.000018
										4	0.000402	0.00039	0.000012
										8	0.000393	0.00035	0.000043
										12	0.000374	0.00034	0.000034
										16	0.000362	0.00028	0.000082
										0	0.000303	0.00029	0.000013
										4	0.000303	0.00028	0.000023
										8	0.000296	0.00028	0.000016
										12	0.000282	0.00021	0.000072
										16	0.000273	0.00015	0.000123
12	2.01	1.86	0.13	22.68	$60^{\circ}$	2.23	0.197	15.4	$60^{\circ}$	0	0.000644	0.00050	0.000144
										4	0.000644	0.00055	0.000094
										8	0.000605	0.00050	0.000105
										12	0.000580	0.00043	0.00015
										16	0.000551	0.00038	0.000171

TABLE 6.2.1.2-B (CONT'D)

Ref.	M	$A_w$	$\lambda_w$	$b_w$ (in.)	$\Delta_{LEw}$	$A_{He}$	$\lambda_{He}$	$b_h$ (in.)	$\Delta_{LEh}$	$\alpha$	$C_{l\delta}$ Calc.	$C_{l\delta}$ Test	$\Delta C_{l\delta}$
7	1.00	4.0	0.6	72.0	46.7°	3.275	0.668	30.7	46.7°	0	0.000387	0.000350	0.000037
	1.05									4	0.000387	0.000365	0.000022
										8	0.000370	0.000300	0.000070
										0	0.00036	0.00035	0.00001
										4	0.00036	0.00040	-0.00004
2	1.20	4.07	0.3	22.52	31.5°	2.146	0	13.06	57.5°	0	0.00148	0.00135	0.00013
										4	0.00148	0.00137	0.00011
										8	0.00143	0.00140	0.00003
										12	0.00138	0.00131	0.00007
										16	0.00121	0.00112	0.00009
13	1.60	7.564	—	31.50	72.5°	2.111	0.186	14.834	57.5°	0	0.000872		
										5	0.000872		
										10	0.000840		
										15	0.000810		
										20	0.000769		
										0	0.000703		
										5	0.000703		(a)
										10	0.000678		
										15	0.000655		
										0	0.000610		
										5	0.000610		
										10	0.000588		
										15	0.000568		

(a) This information is classified CONFIDENTIAL.

**SUBSONIC SPEEDS**



**FIGURE 6.2.1.2-22 TAIL EFFECTIVENESS FOR BODY-MOUNTED HORIZONTAL TAILS**

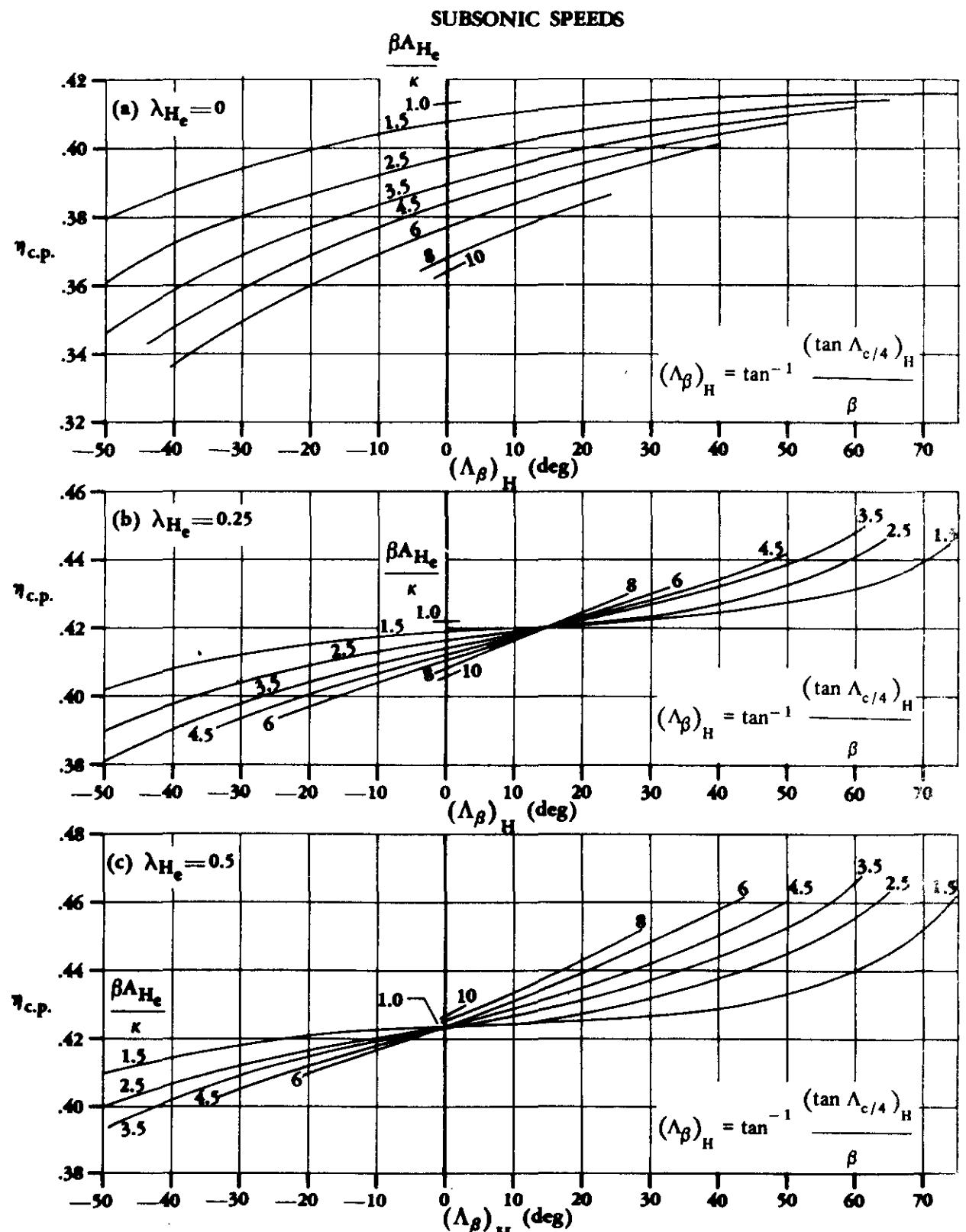


FIGURE 6.2.1.2-23 VARIATION OF SPANWISE LOCATION OF CENTER OF PRESSURE WITH COMPRESSIBLE SWEEP, ASPECT RATIO, AND TAPER RATIO

### SUBSONIC SPEEDS

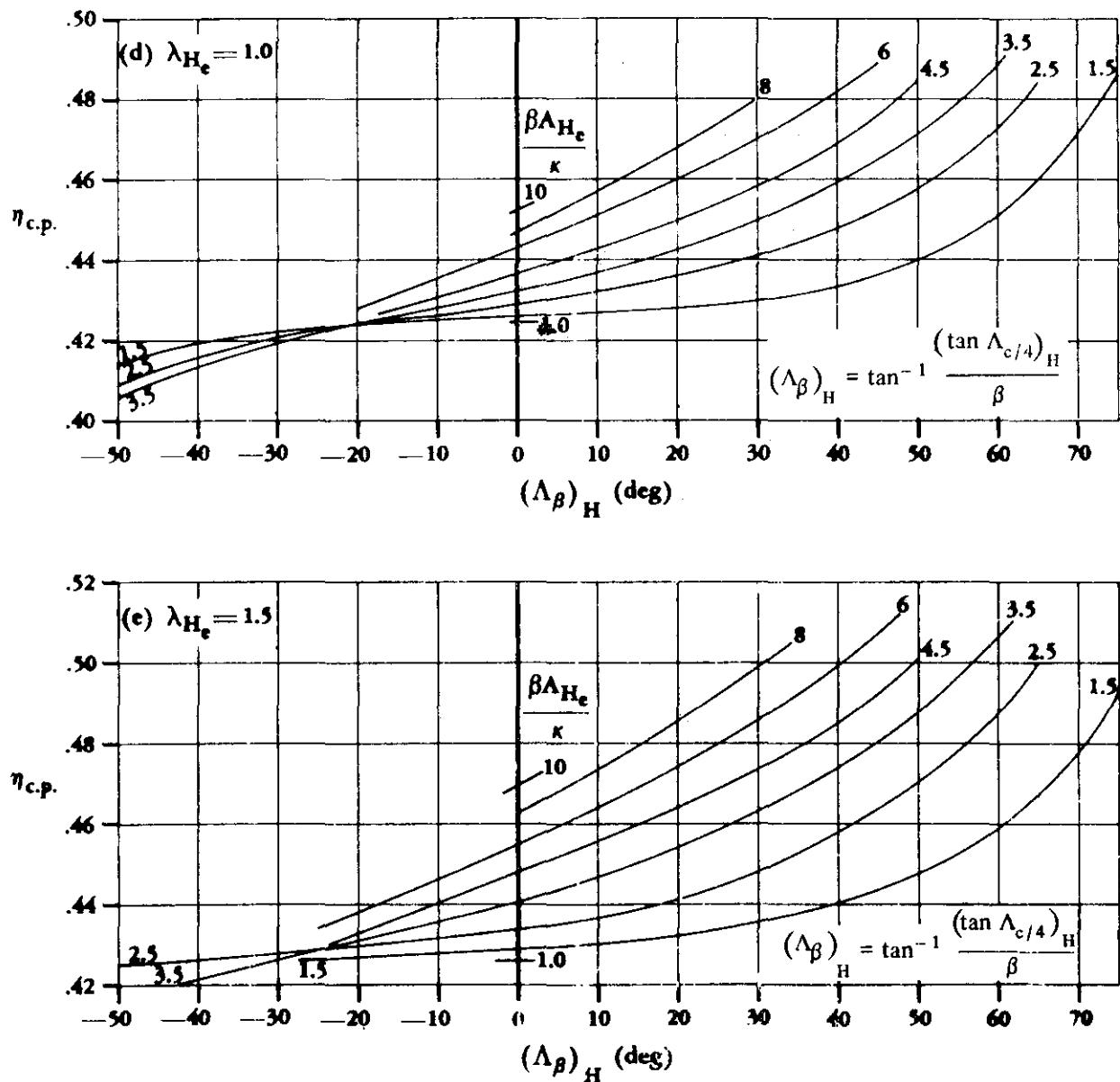


FIGURE 6.2.1.2-23 (CONT'D)

## 6.2.2 YAWING MOMENT DUE TO ASYMMETRIC DEFLECTION OF CONTROL DEVICES

### 6.2.2.1 YAWING MOMENT DUE TO CONTROL DEFLECTION

Yawing moments due to aileron deflection arise from two sources. The first is the asymmetric change in the induced drag of the wings; the induced drag of the wing with the down-going aileron increases and that of the wing with the up-going aileron decreases. The second is the increase in profile drag due to flap deflection. The profile drag increases almost equally for positive and for negative flap deflections. The yawing moments due to the profile-drag increments of antisymmetrically deflected ailerons therefore tend to cancel. The methods of this section for estimating the yawing moment due to aileron deflection are derived from induced-drag changes and neglect contributions due to profile drag.

For spoilers that deflect on one wing panel at a time, the profile drag cannot be neglected. The methods presented for estimating the yawing moment due to spoiler deflection therefore include the contributions due to induced-drag and profile-drag changes.

Additional discussion on the aerodynamic aspects of aileron and spoiler controls is found in Sections 6.1.1.1, 6.1.1.2, 6.1.1.3, and 6.2.1.1.

#### A. SUBSONIC

##### DATCOM METHODS

###### Aileron-Type Controls

The method for determining the yawing moment of plain trailing-edge-flap controls is taken from Reference 1. The method is empirical in nature and is based on a limited amount of test data.

For aileron-type controls that extend to the wing tip, the yawing moment due to aileron deflection resulting from the unsymmetrical change in induced drag may be approximated by

$$C_n = KC_L C_{l\delta} \frac{(\delta_L - \delta_R)}{2} \quad 6.2.2.1-a$$

where

$K$  is an empirical factor, depending upon planform geometry, obtained from Figure 6.2.2.1-9. This design chart is taken from Reference 1 and is based on the data of References 2 through 7.

$C_{l\delta}$  is the rolling effectiveness of the aileron (per radian), obtained by using the method of Paragraph A of Section 6.2.1.1 for the appropriate subcritical Mach number.

$C_L$  is the lift coefficient for zero aileron deflection.

$\delta_R$  is the right-hand control deflection in radians (positive trailing edge down).

$\delta_L$  is the left-hand control deflection in radians (positive trailing edge down).

For aileron-type controls not extending to the wing tip, Equation 6.2.2.1-a is used to compute the difference in the yawing moments of two hypothetical ailerons—one extending from the inboard location of the actual aileron to the wing tip and the other extending from the outboard location of the actual aileron to the wing tip. The difference in the yawing moments of these two hypothetical ailerons gives the yawing moment of the actual aileron.

The method is valid for attached-flow conditions only; i.e., wing angle of attack and control deflection where no flow separation exists.

A sample problem illustrating the use of this method is presented on Page 6.2.2.1-3.

Not enough test data are available to permit either an independent verification or an extension of this method. Therefore, caution should be used in applying the method to configurations whose geometric parameters fall outside the ranges of those of the configurations of References 2 through 7 (see Figure 6.2.2.1-9).

## Spoilers

### Plug and Flap-Type Spoilers

The subsonic yawing moment due to spoiler deflection is obtained from Figures 6.2.2.1-10 and 6.2.2.1-11 for straight wings and swept wings, respectively. The charts are from Reference 1 and are based on the data of References 6 through 11. They are applicable to plug and to flap-type spoilers at zero angle of attack and for spoiler heights above the wing surface between 2 and 10 percent of the local wing chord. However, the applicability of the charts to inboard spoilers on swept wings is questionable.

Not enough experimental data are available to permit either an independent verification or an extension of this method. Therefore, the method is limited to the ranges of parameters presented on the design charts. It should be noted that the swept-wing design chart is based on test data from configurations with a constant spoiler chordwise location of 0.70c.

The design chart values of  $C_n$  are for a spoiler deflected on one panel based on the total wing area and wing span.

Sample Problem 2 on Page 6.2.2.1-4 illustrates the use of this method.

### Spoiler-Slot-Deflector

The use of spoiler-slot-deflector combinations increases the effectiveness and hence the yawing moment due to spoiler deflection. The yawing moment due to a spoiler-slot-deflector combination at zero angle of attack, where the spoiler deflection is equal to the deflector deflection ( $\delta_s/\delta_d = 1.0$ ) is given by

$$(C_n)_{\text{spoiler-slot-deflector}} = K (C_n)_{\text{plain spoiler}} \quad 6.2.2.1-b$$

where

$K$  is the ratio of the yawing-moment coefficient of a spoiler-slot-deflector to that of a plain spoiler, obtained from Figure 6.2.2.1-12 as a function of the compressible sweep parameter  $M \cos \Lambda_c/4$ . This chart is based on data from References 12 through 14.

$(C_n)_{\text{plain spoiler}}$  is the yawing-moment coefficient of a plain flap-type spoiler deflected on one wing panel, based on the total wing area and span, obtained from either Figure 6.2.2.1-10 or 6.2.2.1-11.

For higher angles of attack, a decrease in  $C_n$  due to plug and to flap spoilers is experienced. As the stall is approached, the yawing moment for these spoilers becomes zero. The use of a slot and deflector in combination with a plug or a flap spoiler improves its effectiveness at high angles of attack (see Section 6.2.1.1) and hence gives a significant yawing-moment increment for these angles.

Not enough test data are available to extend this method to configurations employing differential spoiler-deflector deflections.

Application of this method is illustrated by Sample Problem 3 on Page 6.2.2.1-4.

### Sample Problems

#### 1. Aileron-Type Control

Given: The wing-control configuration of Reference 4.

Wing-Control Characteristics:

$$A_w = 3.94 \quad \lambda_w = 0.625 \quad \Lambda_{LE} = 42^\circ \quad b_w = 11.38 \text{ ft}$$

$$S_w = 32.8 \text{ sq ft} \quad \frac{y_i}{b_w/2} = 0.50 \quad \delta_L = 15^\circ \quad \delta_R = -15^\circ$$

Additional Characteristics:

Low speed

$\alpha$ (deg)	$C_L$	$C_{I\delta}$ (per rad)	Test results
2	0.110	0.1180	
4	0.230	0.1158	
6	0.350	0.1126	

Compute:

$$K = -0.261 \text{ (Figure 6.2.2.1-9)}$$

$$\frac{\delta_L - \delta_R}{2} = 15^\circ = 0.262 \text{ rad}$$

Solution:

$$\begin{aligned} C_n &= KC_L C_{I\delta} \frac{(\delta_L - \delta_R)}{2} \text{ (Equation 6.2.2.1-a)} \\ &= (-0.261)(0.262) C_L C_{I\delta} \\ &= -0.0684 C_L C_{I\delta} \end{aligned}$$

(1)	(2)	(3)	(4)	(5)	(6)
$\alpha$ (deg)	$C_L$	$C_{I\delta}$ (per rad)	(2)(3)	$(C_n)^{calc}$ -0.0684 (4)	$(C_n)^{test}$
2	0.110	0.1180	0.01298	-0.00089	-0.0010
4	0.230	0.1158	0.02663	-0.00182	-0.0018
6	0.360	0.1126	0.03941	-0.00270	-0.0026

These test data have been used in the derivation of Figure 6.2.2.1-9; therefore, the sample problem is not an independent verification of the method.

## 2. Spoiler

Given: The wing-control configuration of Reference 15.

Wing-Control Characteristics:

$$S_w = 324 \text{ sq in.} \quad \lambda_w = 0.60 \quad A_w = 4.0 \quad b_w = 36.0 \text{ in.} \quad \Lambda_{LE} = 35.1^\circ$$

Flap-type spoiler  $\frac{x_s}{c} = 0.70 \quad \frac{b_s}{b_w/2} = 0.50$

$$\frac{y_o}{b_w/2} = 0.639 \quad \frac{\delta_s}{c} = 0.025, 0.05, 0.075, 0.100$$

Solution:

$\frac{\delta_s}{c}$	$\frac{C_n}{\delta_s/c}$ Fig. 6.2.2.1-11	$C_n$ Calc	$C_n$ Test
.025	0.04	0.0010	0.00085
.050	0.04	0.0020	0.0020
.075	0.04	0.0030	0.0031
.100	0.04	0.0040	0.0034

## 3. Spoiler-Slot-Deflector

Given: The wing-control configuration of Reference 15. This is the configuration of Sample Problem 2 with the addition of a slot opening and a hinged deflector.

Wing-Control Characteristics:

$$S_w = 324.0 \text{ sq in.} \quad b_w = 36.0 \text{ in.} \quad \Lambda_{c/4} = 32.6^\circ \quad \frac{\delta_s}{c} = \frac{\delta_d}{c}$$

The following test values of  $(C_n)_{\text{plain spoiler}}$ :

$\frac{\delta_s}{c}$	$(C_n)_{\text{plain spoiler}}$ (test results from Ref. 15)
.025	0.00085
.050	0.0020
.075	0.0031
.100	0.0034

Additional Characteristics:

$$M = 0.40$$

Compute:

$$M \cos \Lambda_{c/4} = 0.40 (0.8425) = 0.3370$$

$$K = 2.33 \text{ (Figure 6.2.2.1-12)}$$

Solution:

$$(C_n)_{\text{spoiler-slot-deflector}} = K (C_n)_{\text{plain spoiler}} \quad (\text{Equation 6.2.2.1-b})$$

$\frac{\delta_s}{c}$	$(C_n)_{\text{plain spoiler}}$	$(C_n)_{\text{spoiler-slot-deflector}}$ Calc	$(C_n)_{\text{spoiler-slot-deflector}}$ Test
.025	0.00085	0.0020	0.0025
.050	0.0020	0.0047	0.0042
.075	0.0031	0.0072	0.0080
.100	0.0034	0.0079	0.0090

## B. TRANSONIC

Force and moment characteristics at transonic speeds are difficult to generalize because of the nonlinear nature of the flow equations and interacting shock-wave-boundary-layer separation effects (see Section 4.1.3.2). The method presented here is intended to give a first-order approximation only and to provide a guide to aid in fairing between subcritical and supersonic speeds.

### DATCOM METHOD

No specific charts are presented for determining the transonic yawing moment of lateral-control devices. The best source of information of this type is experimental data on similar configurations. If such information is not available, the following approach may be used as a guide in fairing between subcritical and supersonic speeds.

A first-order approximation of the transonic yawing moment of lateral-control devices is given by

$$C_n = (C_n)_{M=0.6} \frac{C_{L\alpha}}{(C_{L\alpha})_{M=0.6}} \quad 6.2.2.1-c$$

where

$(C_n)_{M=0.6}$  is the yawing moment of the control at  $M = 0.6$ , obtained by using the appropriate method of Paragraph A of this section.

$(C_{L\alpha})$  is the transonic wing-lift-curve slope, obtained from Paragraph B of Section 4.1.3.2.

$(C_{L\alpha})_{M=0.6}$  is the wing-lift-curve slope at  $M = 0.6$ ; obtained by using the straight-tapered-wing method of Paragraph A of Section 4.1.3.2 (Figure 4.1.3.2-49).

It should be noted that this approximation applied to spoilers neglects the effect of transonic wave drag, which can be very significant. Therefore, when applied to spoilers, the method should be considered only for the purpose of establishing the trend through the transonic region, and not as an approximation of the magnitude of the yawing moment.

### C. SUPERSONIC

Methods are presented at supersonic speeds for approximating the yawing moment due to aileron-type controls and to plug or to flap-type spoilers. No method is presented for estimating the supersonic yawing moment due to spoiler-slot-deflectors. Published test data on spoiler-slot-deflector characteristics at supersonic speeds are extremely limited. References 16 and 17 present test data on spoiler-slot-deflector controls at supersonic speeds.

#### DATCOM METHOD

##### Aileron-Type Controls

Supersonic values of yawing moment due to flap deflection are obtained from Figure 6.2.2.1-13. This chart is taken from Reference 1 and is based on the method of computing drag due to lift in Reference 18 and on a limited amount of test data from References 19 and 20.

Not enough test data are available to permit either an independent verification or an extension of this method. Therefore, caution should be used in applying the method to configurations whose geometric parameters fall outside those of the configurations of References 19 and 20 (see Figure 6.2.2.1-13).

##### Spoilers

##### Plug and Flap-Type Spoilers

The supersonic yawing-moment coefficient due to spoiler deflection of a plug or a flap-type spoiler, deflected on one panel, based on the total wing area and span, is obtained from Figure 6.2.2.1-14 as a function of Mach number and configuration geometry. The design chart is based on the data from References 10 and 21 through 23.

A comparison of test values with results calculated by using this method is presented as Table 6.2.2.1-A.

#### REFERENCES

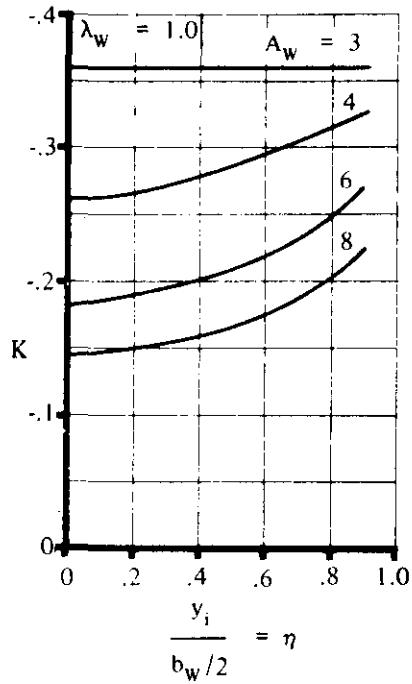
1. Decker, J., et al: USAF Stability and Control Handbook. M-03671, 1956. (C) Title Unclassified
2. Fitzpatrick, J.E., and Woods, R.L.: Low-Speed Lateral-Control Characteristics of an Unswept Wing With Hexagonal Airfoil Sections and Aspect Ratio 2.5 Equipped with Spoilers and With Sharp- and Thickened-Trailing-Edge Flap-Type Ailerons at a Reynolds Number of  $7.6 \times 10^6$ . NACA RM L52B15, 1952. (U)
3. Graham, R.R., and Koven, W.: Lateral-Control Investigation on a  $37^\circ$  Sweptback Wing of Aspect Ratio 6 at a Reynolds Number of 6,800,000. NACA RM L8K12, 1949. (U)
4. Spooner, S.H., and Woods, R.L.: Low-Speed Investigation of Aileron and Spoiler Characteristics of a Wing Having  $42^\circ$  Sweepback of the Leading Edge and Circular-Arc Airfoil Sections at Reynolds Numbers of Approximately  $6.0 \times 10^6$ . NACA RM L9A07, 1949. (U)

5. Bollech, T.V., and Pratt, G.L.: Investigation of Low-Speed Aileron Control Characteristics at a Reynolds Number of 6,800,000 of a Wing With Leading Edge Swept Back  $42^{\circ}$  With and Without High-Lift Devices. NACA RM L9E24, 1949. (U)
6. Pesamanick, J., and Sellers, T.B.: Low-Speed Investigation of the Effect of Several Flap and Spoiler Ailerons on the Lateral Characteristics of a  $47.5^{\circ}$  Sweepback-Wing-Fuselage Combination at a Reynolds Number of  $4.4 \times 10^6$ . NACA RM L50J20, 1950. (U)
7. Fischel, J., Naeseth, R.L., Hagerman, J.R., and O'Hare, W.M.: Effect of Aspect Ratio on the Low-Speed Lateral Control Characteristics of Untapered Low-Aspect-Ratio Wings Equipped With Flap and With Retractable Ailerons. NACA TR 1091, 1952. (U)
8. Franks, R.W.: Tests in the Ames 40- by 80-Foot Wind Tunnel of the Aerodynamic Characteristics of Airplane Models with Plain Spoiler Ailerons. NACA RM A54H26, 1954. (U)
9. Fischel, J., and Hammond, A.D.: Investigation of Effect of Span and Spanwise Location of Plain and Stepped Spoiler Ailerons on Lateral Control Characteristics of a Wing With Leading Edge Swept Back  $51.3^{\circ}$ . NACA RM L9K02, 1950. (U)
10. Johnson, H.S.: Wind-Tunnel Investigation at High Subsonic Speeds of the Effect of Spoiler Profile on the Lateral Control Characteristics of a Wing-Fuselage Combination With Quarter-Chord Line Swept Back  $32.6^{\circ}$  and NACA 65A006 Airfoil Section. NACA RM L53J05a, 1953. (U)
11. Fischel, J., and Tamburello, V.: Investigation of the Effect of Span, Spanwise Location, and Chordwise Location of Spoilers on Lateral Control Characteristics on a Tapered Wing. NACA TN 1294, 1947. (U)
12. Vogler, R.D.: Wind-Tunnel Investigation at Transonic Speeds of a Spoiler-Slot-Deflector Combination on an Unswept NACA 65A006 Wing. NACA RM L53J21, 1953. (U)
13. Hammond, A.D., and Brown, A.E.: Results of an Investigation at High Subsonic Speeds to Determine Lateral-Control and Hinge-Moment Characteristics of a Spoiler-Slot-Deflector Configuration on a  $35^{\circ}$  Sweepback Wing. NACA RM L57C20, 1957. (U)
14. Hammond, A.D.: Wind-Tunnel Investigation of the Effect of Aspect Ratio and Chordwise Location on Effectiveness of Plain Spoilers on Thin Untapered Wings at Transonic Speeds. NACA RM L56F20, 1956. (U)
15. Vogler, R.D.: Wind-Tunnel Investigation at High Subsonic Speeds of a Spoiler-Slot-Deflector Combination on an NACA 65A006 Wing With Quarter-Chord Line Swept Back  $32.6^{\circ}$ . NACA RM L53D17, 1953. (U)
16. Foster, G.V.: Effects of Spoiler-Slot-Deflector Control on the Aerodynamic Characteristics at a Mach Number of 2.01 of a Variable-Wing-Sweep Configuration with the Outer Wing Panels Swept Back  $75^{\circ}$ . NASA TM X-273, 1960. (U)
17. Lord, D.R., and Moring, R.: Aerodynamic Characteristics of a Spoiler-Slot-Deflector Control on a  $45^{\circ}$  Sweepback Wing at Mach Numbers of 1.61 and 2.01. NACA RM L57E16a, 1957. (U)
18. Polhamus, E.C.: Drag Due to Lift at Mach Numbers up to Two. NACA RM L53I22b, 1953. (U)
19. Mitchell, M.H., Jr.: Effects of Varying the Size and Location of Trailing-Edge Flap-Type Controls on the Aerodynamic Characteristics of an Unswept Wing at a Mach Number of 1.9. NACA RM L50F08, 1950. (U)
20. Jacobsen, C.R.: Effects on Control Effectiveness of Systematically Varying the Size and Location of Trailing-Edge Flaps on a  $45^{\circ}$  Sweepback Wing at a Mach Number of 1.9. NACA RM L51I26, 1951. (U)
21. Kindell, W.H.: Effects of Span and Spanwise and Chrodwise Location on the Control Effectiveness of Spoilers on a  $50^{\circ}$  Sweepback Wing at Mach Numbers of 1.41 and 1.96. NACA RM L53B09, 1953. (U)
22. Conner, D.W., and Mitchell, M.H., Jr.: Effects of Spoiler on Airfoil Pressure Distribution and Effects of Size and Location of Spoilers on the Aerodynamic Characteristics of a Tapered Unswept Wing of Aspect Ratio 2.5 at a Mach Number of 1.90. NACA RM L50L20, 1951. (U)
23. Wong, N.D.: An Investigation of the Control Effectiveness of Tip Ailerons and Spoilers on a Low-Aspect-Ratio Trapezoidal-Wing Airplane Model at Mach Numbers from 1.55 to 2.35. NACA RM A57I26a, 1957. (U)
24. Hamilton, C.V., and Driver, C.: An Investigation of a Supersonic Aircraft Configuration Having a Tapered Wing with Circular-Arc Sections and  $40^{\circ}$  Sweepback—Stability and Control Characteristics at a Mach Number of 1.61 of the Complete Configuration Equipped With Spoilers. NACA RM L54F15, 1954. (U)

**TABLE 6.2.2.1-A**  
**SUPersonic YAWING MOMENT DUE TO SPOILER DEFLECTION**

**DATA SUMMARY**

Ref.	Spoiler	A	$\lambda$	$\Lambda_{c/4}$ (deg)	$\frac{V_i}{b_W/2}$	$\frac{V_o}{b_W/2}$	Spoiler Chordwise Location (%c)	$\frac{\delta_s}{c}$	M	$C_n$ Calc	$C_n$ Test	$\Delta C_n$ Calc - Test
24	Plug	4.0	0.50	40.0	0.15	0.95	0.55	0.05	1.61	0.0052	0.0053	-0.0001
	Flap						0.65			0.0052	0.0062	-0.0010
	Plug					0.55		0.02		0.0052	0.0070	-0.0015
										0.0021	0.0020	0.0001
22	Plug	2.50	0.625	5.3	0.20	0.95	0.75	0.05	1.90	0.0040	0.0056	-0.0016
						0.45		0.02		0.0018	0.0021	-0.0003
						0.70		0.05		0.0030	0.0049	-0.0019
								0.02		0.0015	0.0012	0.0003
						0.45		0.05		0.0015	0.0026	-0.0011
								0.02		0.0008	0.0008	0
								0.05		0.0030	0.0020	0.0010
								0.02		0.0015	0.0004	0.0011
23	Flap	3.20	0.40	19.2	0.28	0.75	0.77	0.037	1.55	0.0025	-0.0008	0.0033
								0.095		0.0060	-0.0008	0.0068
								0.037	1.90	0.0016	0	0.0016
								0.095		0.0040	0	0.0040
21	Plug	2.50	0.625	47.16	0.20	0.95	0.65	0.037	2.35	0.0011	0.0025	-0.0014
								0.095		0.0030	0.0025	0.0005
						0.70				0.0012	0.0011	0.0001
								0.04		0.0045	0.0043	0.0002
						0.45				0.0018	0.0014	0.0004
								0.06		0.0025	0.0019	0.0006
$ \Delta C_n $												Average Error = $\frac{ \Delta C_n }{n} = 0.0012$



$1.13 \leq A_w \leq 6.13$   
 $0.5 \leq \lambda_w \leq 1.0$   
 $0 \leq \frac{y_i}{b_w/2} \leq 0.775$

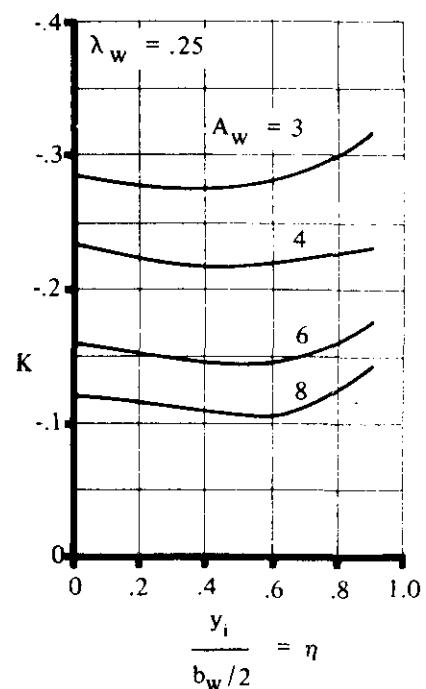
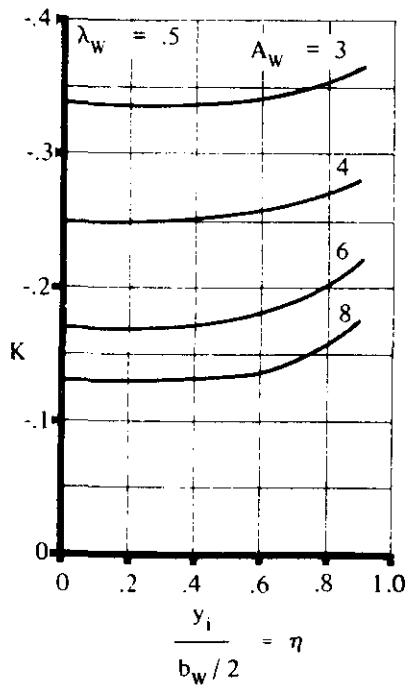
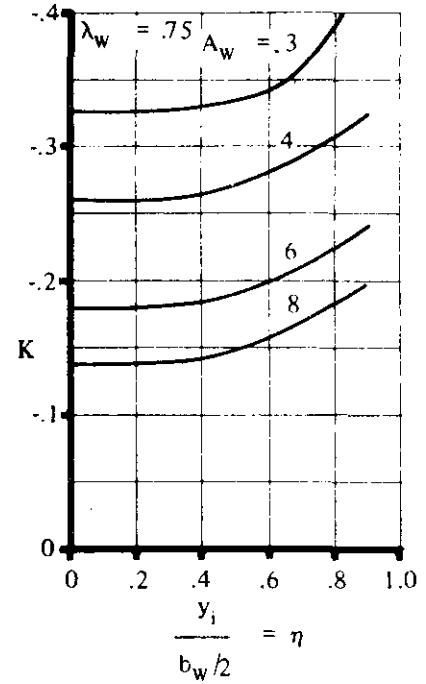


FIGURE 6.2.2.1-9 CORRELATION CONSTANT FOR DETERMINING YAWING MOMENT DUE TO AILERON DEFLECTION

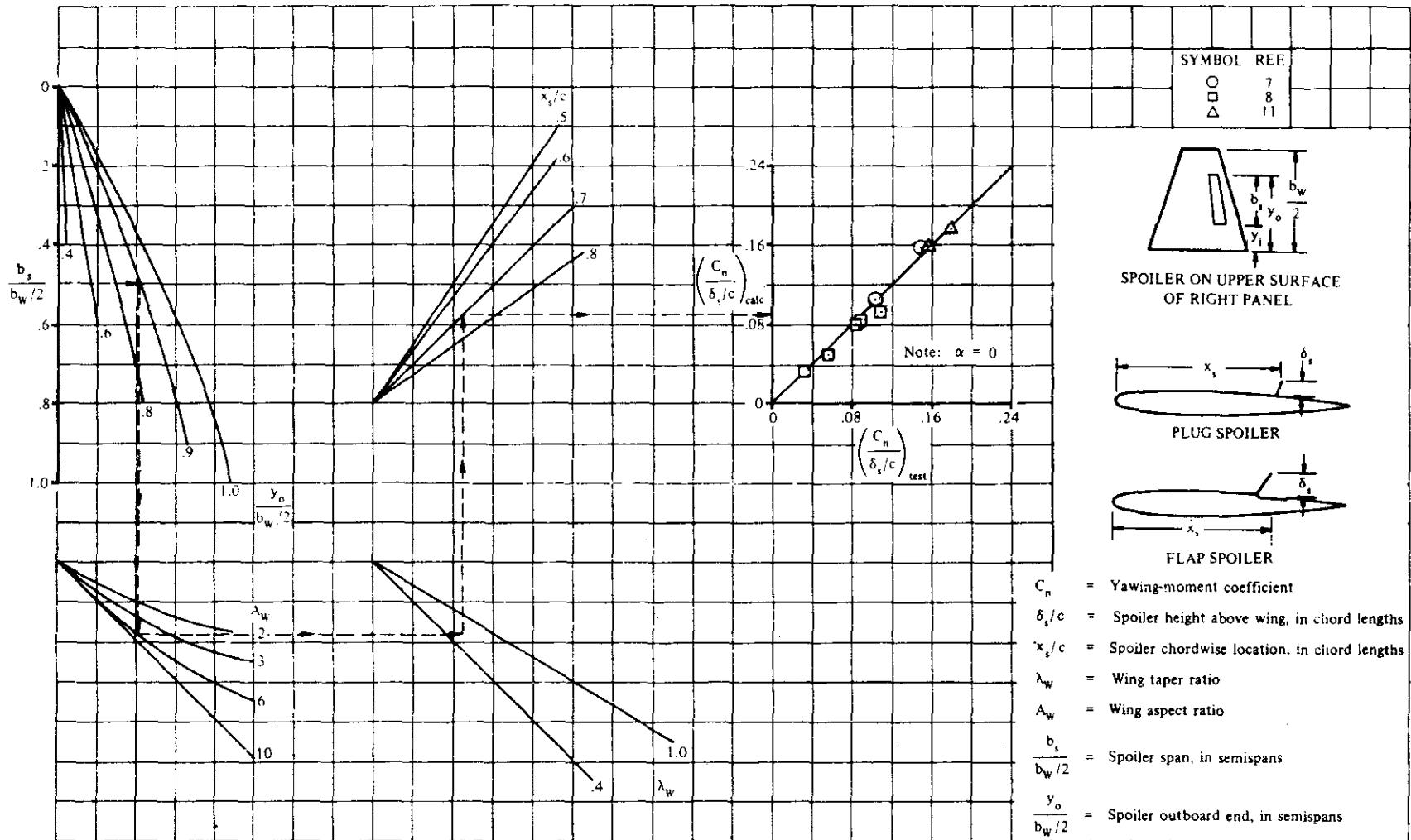


FIGURE 6.2.2.1-10 YAWING MOMENT DUE TO SPOILER CONTROL SURFACES FOR STRAIGHT WINGS AT SUBSONIC SPEEDS AT LOW ANGLES OF ATTACK

6.2.2.1-10

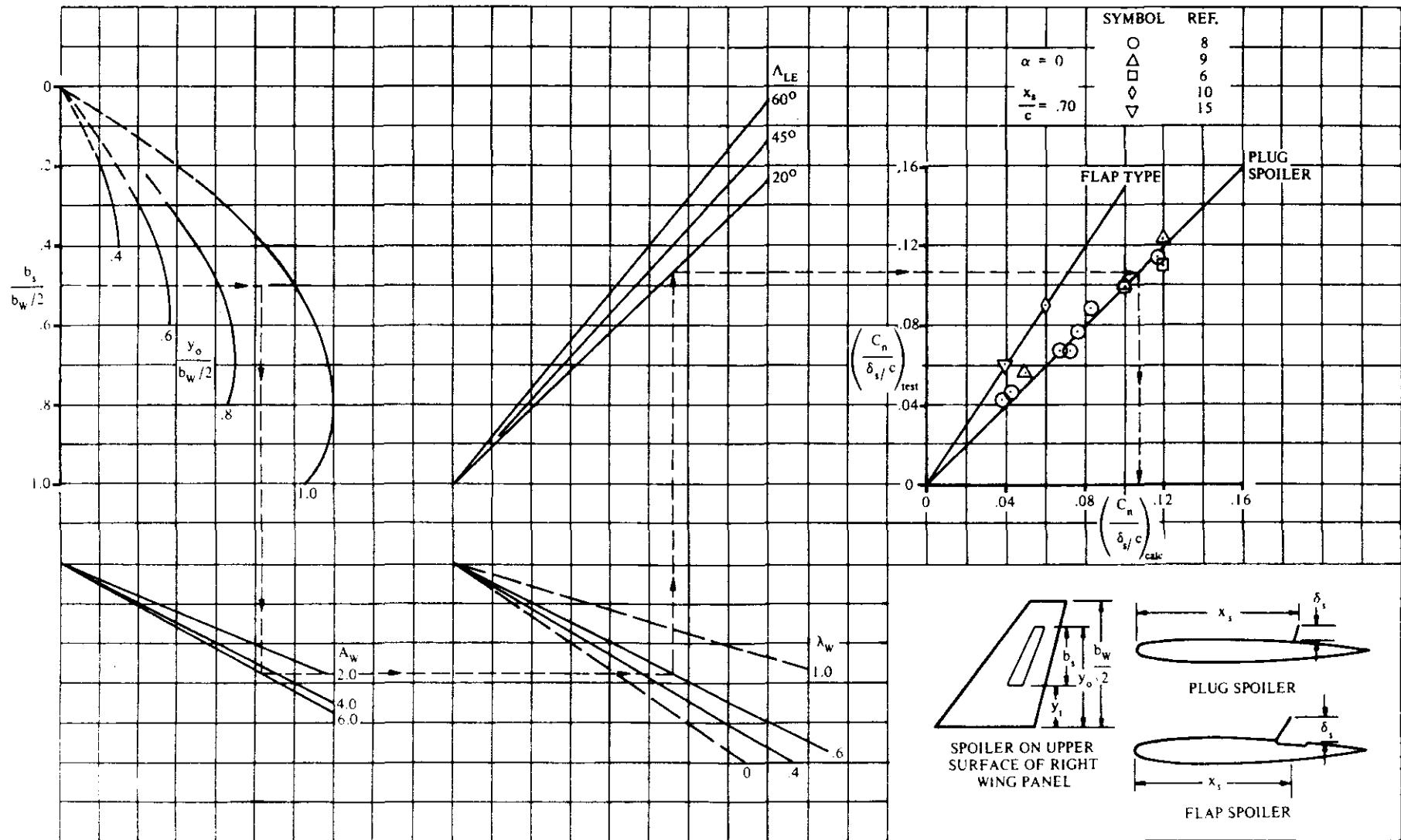


FIGURE 6.2.2.1-11 YAWING MOMENT DUE TO SPOILER CONTROL SURFACES FOR SWEPTBACK WINGS AT SUBSONIC SPEEDS AND LOW ANGLES OF ATTACK

SUBSONIC SPEEDS

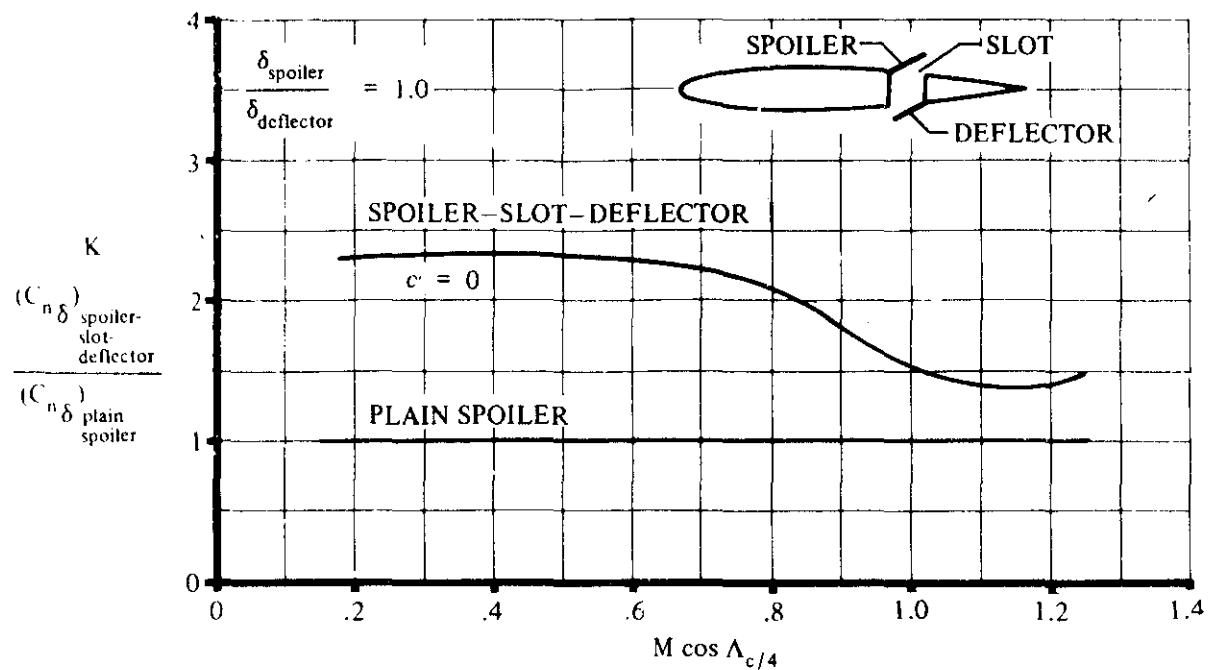


FIGURE 6.2.2.1-12 EFFECT OF SLOT AND DEFLECTOR ON SPOILER YAWING MOMENT

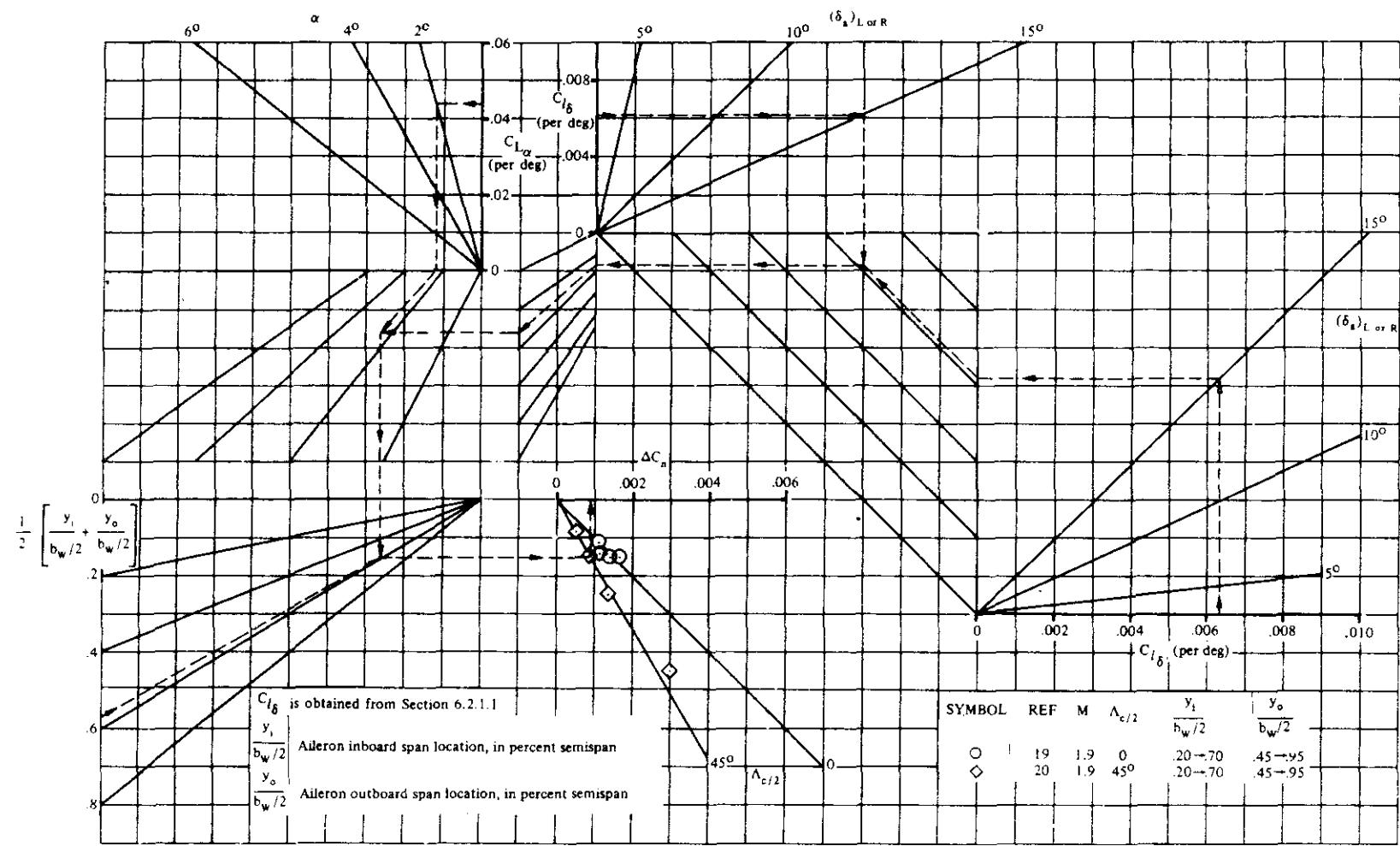


FIGURE 6.2.2.1-13 YAWING MOMENT DUE TO AILERON DEFLECTION AT SUPersonic SPEEDS

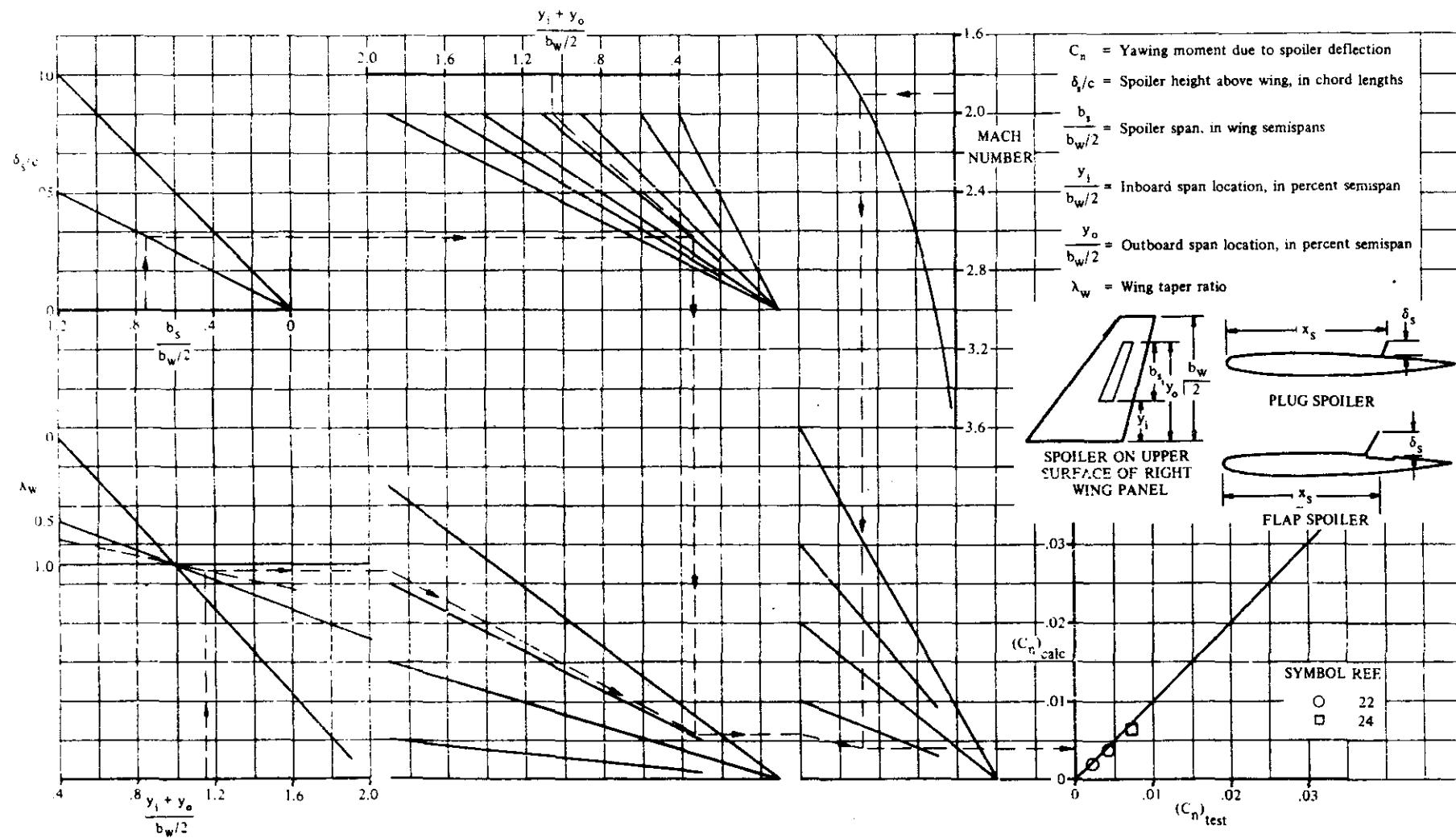


FIGURE 6.2.2.1-14 SPOILER YAWING MOMENT AT SUPERSONIC SPEEDS

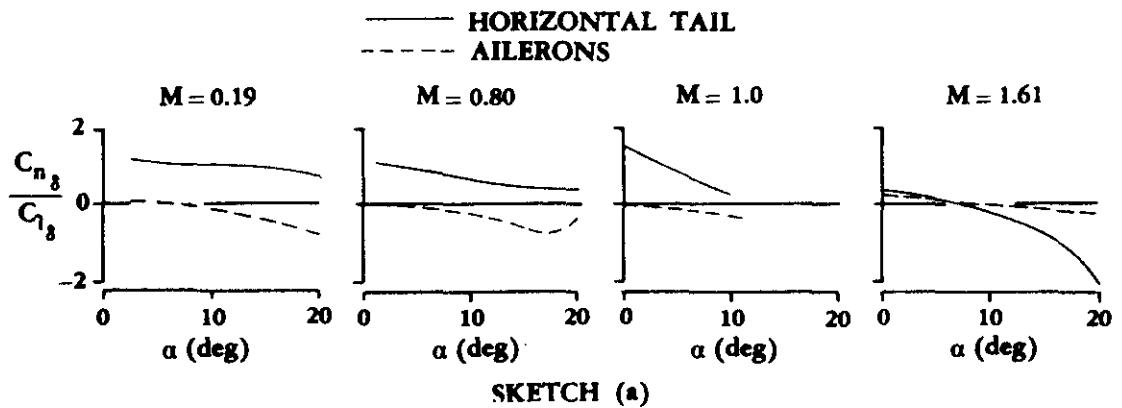
### 6.2.2.2 YAWING MOMENT DUE TO A DIFFERENTIALLY DEFLECTED HORIZONTAL STABILIZER

No methods are available for estimating the yawing moments due to a differentially deflected horizontal stabilizer, and the data available for correlation are limited. However, a brief discussion, taken essentially from Reference 1, is given pertaining to the qualitative and quantitative aspects of yawing moments associated with tail roll control.

Associated with tail roll control are yawing moments, varying in magnitude and direction as a function of Mach number, angle of attack, and vehicle geometry. These yawing moments can be attributed to (1) the pressure differential induced on the vertical tail as a result of the differentially deflected horizontal tail, (2) the drag component associated with each horizontal-tail panel, and (3) the dihedral of the horizontal tail. For most configurations and test conditions, the differential pressure on the vertical tail is the dominating factor.

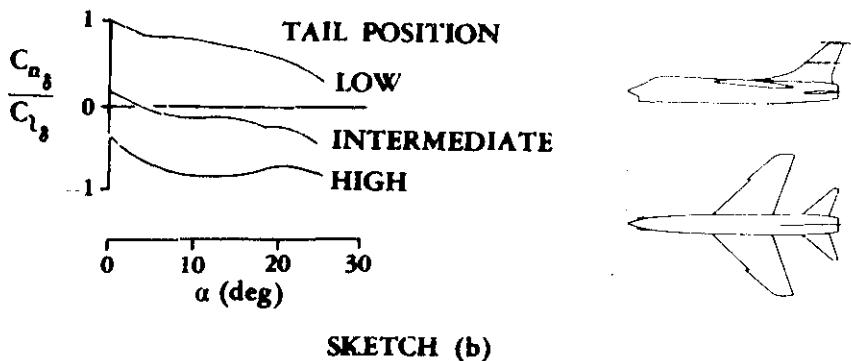
Yawing-moment data are generally presented in the form of the parameter  $C_{n\delta}/C_{l\delta}$  (ratio of yawing moment to rolling moment produced by roll control). For low-horizontal-tail configurations, tail roll control up to  $M \approx 1.0$  produces very large favorable yawing moments, which decrease with increasing angle of attack but tend to remain positive over the angle-of-attack range ( $\alpha \approx 0$  to  $22^\circ$ ) for which test data are available. These large yawing moments are due primarily to the induced pressure differential on the vertical panel. This pressure differential on the vertical tail also tends to reduce the rolling moment for a low-tail configuration.

At supersonic speeds, the load carry-over from the horizontal tail to the vertical tail decreases with increasing Mach number. The attendant result is that at supersonic speeds the tail roll control will produce smaller favorable yawing moments at low angles of attack and possibly adverse yawing moments at high angles of attack. For a specific configuration, if the Mach number is high enough, adverse yaw due to tail roll control is a possibility throughout the angle-of-attack range. Sketch (a) presents representative yawing-moment data produced by roll control for a low-tail configuration as a function of Mach number and angle of attack.



The vertical position of the horizontal tail is the most important parameter in determining the relative magnitude and direction of the yawing moment due to roll control (References 1 and 2). The variations in yawing moment due to roll control shown in Sketch (b) are representative of the

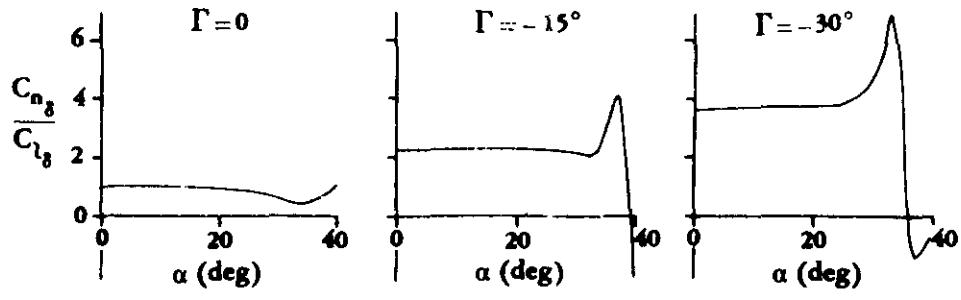
effect of the horizontal-tail location. These variations would enable the designer to position the horizontal tail to avoid large undesirable yawing moments, longitudinal stability permitting. In this connection, it may also be pointed out that if a ventral fin is used on the airplane for high-speed stability, the yawing moments for a low tail position would be smaller. If the yawing moments cannot be adjusted to a satisfactory value by positioning the tail, it might be necessary to adjust them by linking the rudder in with the tail roll control.



## Dihedral Effects

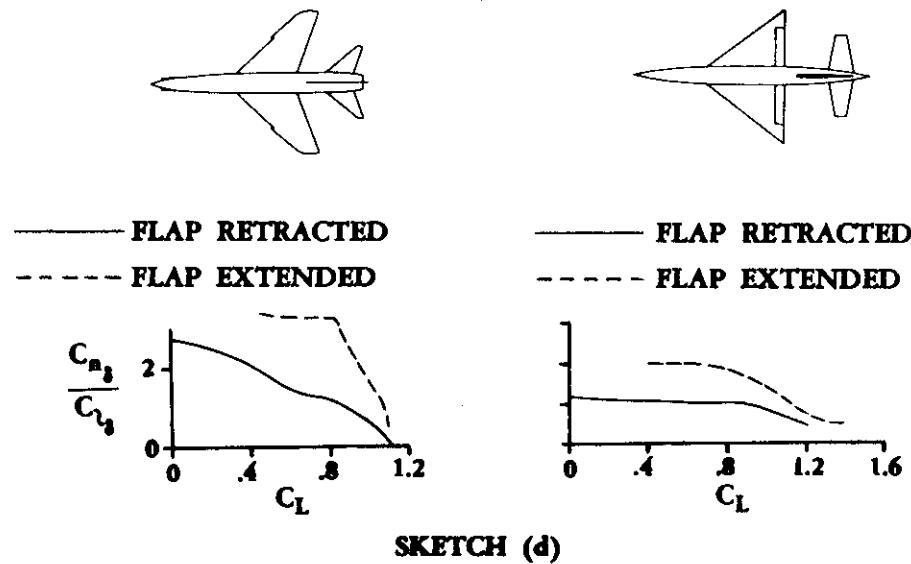
The results of dihedral variation on yawing moment due to roll  $C_{n\delta}/C_{l\delta}$  are of significant importance. The lateral component of the horizontal-tail loads increases with negative dihedral, and the load induced on the vertical tail by differential horizontal-tail deflection is reduced by increases in negative dihedral. The combined effect of these two phenomena is a substantial increase in the yawing-moment parameter  $C_{n\delta}/C_{l\delta}$  with increasing negative dihedral angle over a large angle-of-attack range. The variation of the yawing moment due to tail roll control is shown in Sketch (c) (Reference 3). Consequently, if negative tail dihedral is employed on a low-tail configuration to improve the linearity of the pitching-moment curves, for example, and differential tail deflection is utilized to augment low-speed roll control; then the favorable yawing moment associated with tail roll control will be aggravated further. Of course, if a ventral fin is employed on the configuration, the loads induced on the ventral would be increased, tending to offset the additional yawing moment due to negative dihedral; however, this effect would not be strong enough to cancel the effect created by negative dihedral. On the other hand, for low-tail configurations at supersonic speeds where the yawing moment due to tail roll control is adverse, negative tail dihedral would be favorable.

## SUBSONIC SPEEDS



### Flap Effects

The effects of flaps on yawing moment due to roll control are shown for two different configurations in Sketch (d). Both configurations show a substantial increase of  $C_{n\delta}/C_{l\delta}$  with flap deflection at low lift coefficients. This increase is primarily the result of a decrease in roll effectiveness  $C_{l\delta}$ .



### REFERENCES

1. Campbell, J. P.: The Use of the Horizontal Tail for Roll Control. NACA RM L55L16a, 1956. (U)
2. Boisseau, P. C.: Low-Speed Roll Effectiveness of a Differentially Deflected Horizontal-Tail Surface on a 42° Swept-Wing Model. NACA RM L56E03, 1956. (U)
3. Fournier, P. G.: Effect of Tail Dihedral on Lateral Control Effectiveness at High Subsonic Speeds of Differentially Deflected Horizontal-Tail Surfaces on a Configuration Having a Thin Highly Tapered Wing. NASA Memo 12-1-58L, 1959. (U)

### 6.2.3 SIDE FORCE DUE TO ASYMMETRIC DEFLECTION OF CONTROL DEVICES

The side-force increment due to the asymmetric deflection of control devices on a plain wing is usually small enough to be neglected. At supersonic speeds, however, strong shock waves can be generated from deflected controls. These shock waves frequently impinge on vehicle components and cause considerable forces and moments by means of their direct pressure effect and by boundary-layer-separation effects.

For the purpose of the Datcom, it is assumed that the side force due to asymmetric control deflection is sufficiently small to be neglected. Some data on the side force due to asymmetric control deflection on wing-body combinations at supersonic speeds may be found in reference 1.

### REFERENCE

1. Smith, W. G., and Intriuri, P. F.: Some Aspects of Aileron Deflection on the Static Lateral and Directional Aerodynamic Characteristics of Four Contemporary Airplane Models. NACA RM A57E22, 1957. (U)

## 6.3 SPECIAL CONTROL METHODS

### 6.3.1 AERODYNAMIC CONTROL EFFECTIVENESS AT HYPERSONIC SPEEDS

The interest in aircraft and re-entry vehicles operating at hypersonic speeds has created the need for establishing preliminary-design methods for predicting the effectiveness of aerodynamic controls of such vehicles at hypersonic speeds.

This section presents a procedure, taken from reference 1, for applying the correlation results presented in reference 1 to the prediction of hypersonic control effectiveness.

The development of efficient hypersonic vehicles involves solutions of complex problems associated with the severe environment of hypersonic flight. Control characteristics, particularly at hypersonic speeds, are greatly affected by flow separation phenomena. Flow separation can occur ahead of deflected flaps, on the leeward side of a surface inclined at large angles of attack, near the impingement of a shock wave upon the boundary layer of a body, and on a curved surface. Control effectiveness may be increased, limited, or completely nullified because of boundary-layer separation. Pressure distributions over the control and the basic configuration can be greatly altered because of separation effects. Heat-transfer rates are changed on the control surfaces and the basic configuration both upstream and downstream of the control. The interaction region is characterized by a reduction of local heating rates in the separated region and a substantial heating rate increase at the reattachment point. It is therefore essential to understand the flow-separation phenomena and to describe the flow conditions in the separated region.

In reference 1, semiempirical correlations are developed for the characteristic parameters of a separated flow at hypersonic speeds. These correlations describe the pressure and heat-transfer distributions in terms of local flow properties by defining characteristic magnitudes and distance parameters. Knowing these quantities, relations for incremental aerodynamic force and moment coefficients are developed.

In order that the Datcom user may better understand the control effectiveness methods presented in this section, general discussions of hypersonic flow separation and the effects of the influence of separation on controls are presented. These general discussions are essentially quoted from reference 2 and present only the salient aspects of hypersonic-flow separation and its influence on aerodynamic controls. The reader can obtain a more thorough review of hypersonic-flow separation phenomena from references 1 and 3.

#### HYPersonic-FLOW SEPARATION

Separated flows are characterized by the prevailing type of boundary layer: laminar, turbulent, or transitional. The pressure rise and the extent of the separated region depend upon the characteristics of the boundary layer.

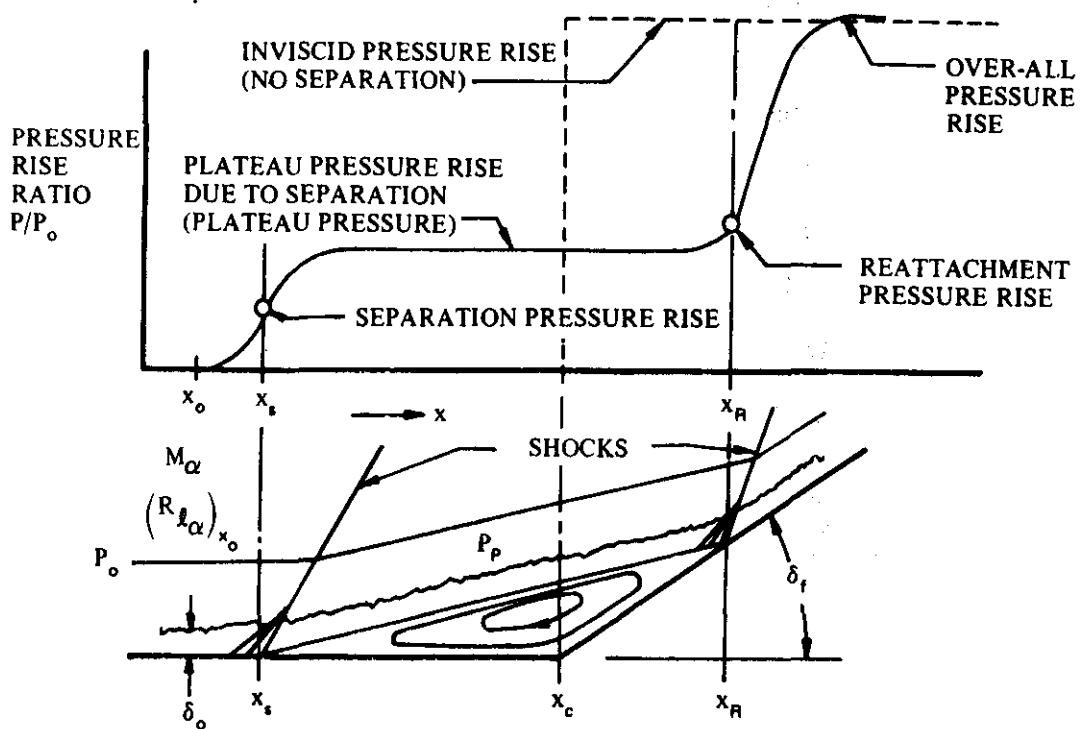
In general, boundary-layer separation occurs whenever the streamwise pressure increase along a surface is sufficient to overcome the forces acting to accelerate a fluid particle, or when the streamline curvature necessary to follow the surface contour cannot be sustained by the pressure gradient normal to the surface. In steady-flow aerodynamic problems the only forces acting to accelerate the low-momentum fluid near the wall against a pressure gradient are the shear forces between layers of fluid. Because the momentum of the fluid near the wall is quite low, a relatively small amount of deceleration by the pressure gradient is sufficient to bring about separation. Turbulent flow helps to delay the occurrence of separation, because the turbulent fluctuations increase the effective shear forces and thereby increase the adverse pressure force necessary to reverse the flow of the fluid near the wall.

The greatly increased effective viscosity due to turbulent fluctuations enables the equilibrium between pressure and shear forces near the wall to occur at much greater adverse pressure rises in turbulent boundary layers. Because of the connection between pressure rise and flow turning angle, this higher pressure corresponds to a much shorter, thicker separated zone for the same initial boundary-layer thickness. Cases presented by Schlichting (reference 4) and Howarth (reference 5) show turbulent pressure rises twice the lami-

nar ones, while the laminar separation zone extends 10 times farther than the turbulent one. A similar thickening (and simultaneous pressure rise) occurs in a transitional separation when the mixing zone becomes turbulent, and the downstream flow soon approaches a condition very similar to the equivalent turbulent separation. Upstream of the transition point, the flow has the character of the corresponding laminar separation zone. The location of the transition point therefore plays a distinct role in determining the pressure distribution (see references 6 and 7).

Present indications are that shock-induced laminar separation pressure distributions, and to a limited extent turbulent ones, are independent of the type of geometry producing separation (see reference 6). However, the turbulent peak pressure rise often depends significantly on geometry (references 6 and 8 through 11). This difference in dependence can probably be attributed to the greatly increased effective viscosity in turbulent flow enabling the wall contour within the separated zone to transmit its effect more strongly to the outer flow.

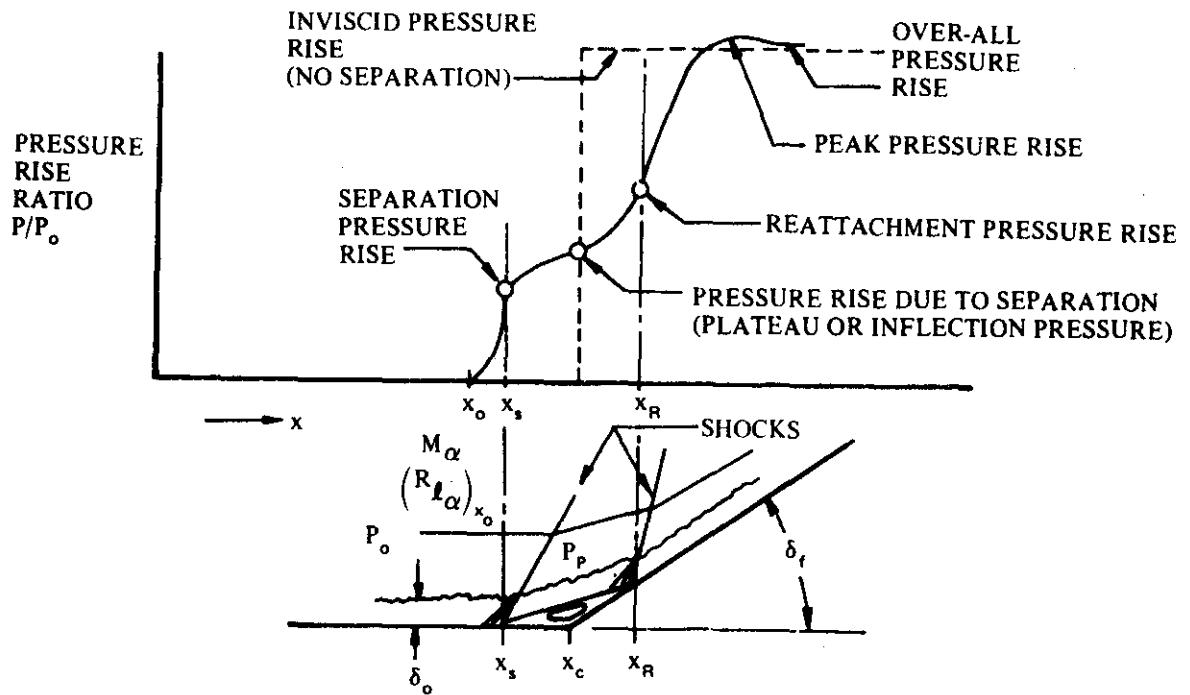
Typical surface pressure distributions for laminar and turbulent boundary layers are presented in sketches (a) and (b), respectively.



WALL PRESSURE DISTRIBUTION IN THE VICINITY OF LAMINAR SEPARATION

SKETCH (a)

The laminar boundary layer has a characteristic plateau where the pressure remains almost constant over most of the separated flow region. The separation pressure coefficient is based on the pressure rise from the undisturbed stream to the separation point. As explicitly mentioned by Love (reference 12), this is not to be confused with the pressure rise needed to cause separation.



WALL PRESSURE DISTRIBUTION IN THE VICINITY OF TURBULENT SEPARATION

SKETCH (b)

The separated turbulent boundary-layer pressure distribution has no plateau region but rises to an inflection value. The final pressure after reattachment is usually that given by inviscid theory. Occasionally, a situation arises wherein there is a pressure rise above the inviscid value followed by an expansion to the inviscid value. This is caused by a lower local entropy level due to the multiple-shock compression of the inviscid flow near the separation and reattachment points. The multiple-shock compression is a more efficient process than the single-shock compression, resulting in a higher local total pressure. It has been observed occasionally in three-dimensional hypersonic separation, and there is good reason to expect it in other situations at high Mach numbers where multiple oblique-shock compression can exist.

The critical pressure-rise coefficient, referred to herein as the incipient pressure-rise coefficient  $C_{p_{inc}}$ , corresponds to the minimum over-all pressure for which separation will occur (see references 4, 7, 9, 10, 12, and 13). The current indications are that it is independent of the particular geometry causing the pressure rise (see references 11 and 14), although this may not prove to be a general rule.  $C_{p_{inc}}$  is much greater and is a much weaker function of Reynolds number for turbulent boundary layers ( $C_{p_{inc}} \sim (R_{\ell})^{1/10}$ ) than for laminar boundary layers ( $C_{p_{inc}} \sim (R_{\ell})^{1/4}$ ). Recent correlations presented in reference 1 substantiate this 1/4-power Reynolds-number dependence for laminar boundary layers; however, the range of Reynolds numbers of the available test data is too small to validate the 1/10-power relation for turbulent boundary layers. Nevertheless, this dependence does correlate the available turbulent data over the ranges of the test conditions.

The pressure rise due to separation (plateau pressure) is of the same order of magnitude as the critical pressure rise, and exhibits the same type of dependence on Mach and Reynolds numbers. Detailed correlation formulas for predicting the pressure-distribution parameters in various situations are developed in reference 1, and are presented in the Datcom method in the form of design charts.

Two further points should be made concerning the general characteristics of laminar and turbulent separations. First, the high altitudes and large stream-to-wall temperature ratios characteristic of hypersonic flight greatly increase the probability of finding laminar flow. And second, the large viscous interaction associated with high Mach number and low Reynolds number will often make it very difficult to determine experimentally or theoretically whether separation has even occurred, let alone the separation location. For those conditions where separation is difficult to detect, the effect of separation on loads is quite small, but the understanding of the flow and the prediction of heat transfer and flow stability become uncertain.

The stability and steadiness of separated flows cannot be predicted with certainty using present information. In general, cavities appear to be the most unstable type of separated geometry. Unsteadiness can result from a hysteresis between laminar and turbulent separated-zone conditions if the flow conditions and geometry are of certain types, e.g., a sharply deflected ramp near the transition point of a flat plate. Whether all separated-zone instabilities are associated with transition or whether other mechanisms participate must be determined by future investigations. The resonant frequency of a cavity would be one important parameter in such an investigation. Violent macroscopic flow fluctuations affect heat-transfer rates and wall shear forces near the separation and reattachment points because of the Reynolds stress effect.

The relationships between heat transfer and separation in laminar and turbulent flow are poorly understood. Chapman (reference 15) theoretically estimates a ratio of heat transfer in a laminar separated zone to that in the attached layer, of 0.56. The experiments of Larson (reference 16) substantiate this estimate. Chapman mentions that turbulent separation regions can have heat-transfer rates as high as six times the equivalent rates for the attached layer at low Mach numbers, but this ratio decreases greatly with increasing Mach number. The turbulent-flow measurements of Larson do not show this high ratio at low Mach numbers, but the theory appears to approach the measurements at high Mach numbers. Larson states that the discrepancy is probably due to the failure of the theory to include the proper temperature - heat-transfer relationships for the experiments. It appears doubtful whether very large increases in heat transfer will ever be found in steady, separated regions. In short, turbulent and transitional separations may lead to heat-transfer rates higher than the equivalent attached boundary layer, but at high Mach numbers the ratio appears to be about 0.50 to 0.70, which is not indicated satisfactorily by present theory. Local increases in heat-transfer rate near reattachment are mentioned in reference 16, but these were not always found by the other investigators mentioned in reference 16.

The converse effect, i.e., the effect of heat-transfer on separation characteristics, is also not understood (see references 16 through 25). Sogin states in his survey report (reference 24) that there is much disagreement between theory and experiment regarding the effects of heat transfer on either laminar or turbulent separated flows. Thus, theoretical results for laminar boundary layers (references 17 through 23 and 32 and 33) indicate separation should be delayed by cooling; experimental results in references 32 and 33 tend to substantiate this theory, while those in references 16 and 26 through 28 do not. Gadd further states that if the turbulent boundary layer could be treated analytically it should also show separation delayed by cooling (references 26 and 27), but poor experimental agreement is obtained. The resolution of this uncertainty is very important, as it bears directly on the application of wind-tunnel data (equilibrium wall) to flight problems (usually cold wall).

#### INFLUENCE OF SEPARATION ON CONTROLS

Control characteristics, particularly at hypersonic speeds, are often greatly affected by separation. As previously noted, control effectiveness may be increased, limited, or completely nullified because of boundary-layer separation. Pressure distributions over controls and on the basic configuration may be greatly altered due to separation effects, changing drastically the moment coefficients predicted by inviscid theory. Heat-transfer rates are changed on the control surfaces and on the basic configuration both upstream and downstream of the control. Separation effects must therefore be considered in both the design and loca-

tion of controls. In general, separation tends to smooth out the sharp changes in pressure distributions predicted by inviscid theory, and can cause local "hot spots" which have heat-transfer rates many times higher than those that would exist for attached boundary layers. Separated flow phenomena are frequently unsteady and three-dimensional in nature, and undergo large changes with transition from laminar to turbulent flow, further complicating the analytical treatment of a design. Thus, for example, hysteresis effects are noticeable in the  $C_m$  versus  $\alpha$  curves for some control configurations.

Aerodynamic forces and moments on a vehicle may be changed as much by changing the pressure distribution on the basic configuration as they would be by changes in the normal forces acting on controls. Leading-edge controls, for example, usually are not directly influenced by separation but, by causing separation, they can affect the pressures and heat-transfer rates over the entire configuration. Some effects of separation associated with controls on windward and leeward surfaces and some important three-dimensional and unsteady flow effects of separation on control characteristics are presented below.

#### Leading-Edge Controls

Leading-edge controls contemplated for hypersonic vehicles include flaps, spoilers, fins, spikes, and all-movable noses. The importance of separation for such controls is in the influence on the entire flow field downstream of the control. Separation behind a deflected leading-edge flap makes any control or stabilizing surface downstream of the flap ineffectual. Heat-transfer rates on the surface are reduced in the separated-flow region, but if the boundary layer reattaches on the surface the heat-transfer rate at reattachment can be several times larger than that for an attached boundary layer. The control forces and hinge moments of leading-edge fins and flaps would not be directly influenced by separation. Fins, which may be canards, create strong vortices which can cause boundary-layer transition and contribute to the possibility of unsteady flow over the downstream surfaces of the configuration. Comparable effects would be expected for large amounts of all-movable nose deflection which, nevertheless, is anticipated to be a very effective trimming device at high angles of attack. The importance of leading-edge controls in influencing the entire afterbody is epitomized by the use of spikes. Flow-separation spikes in front of blunt bodies may reduce the total drag of the body by effectively streamlining it. Average heat-transfer rates in the separated-flow region created by the spike are significantly reduced in laminar flow, although the local heat-transfer rate at reattachment may be quite high. Deflectable spikes might be used as control devices because they alter the pressure distribution in the forward region of a body. The separated-flow region caused by spikes, however, is frequently unsteady, which is a most unsatisfactory control characteristic. If these problems can be worked out, spike controls could become a very effective system for blunt vehicles.

#### Downstream Controls

Frequently control surfaces located downstream of the leading edge are also used as stabilizing devices. Their effectiveness, however, may be greatly affected by upstream separation of the boundary layer. The inviscid estimate of the pressure rise due to deflecting a control into the local stream is a discontinuous jump in the pressure distribution on the surface at the leading edge of the control. A similar sudden increase in the inviscid pressure distribution occurs at the trailing-edge shock required to recompress the flow over an expansion surface. In the actual flow, the sudden pressure rise may be transmitted upstream through the subsonic portion of the boundary layer, and separation may occur far upstream as a result. This is particularly likely for hypersonic flow, where shocks are highly swept, and for laminar boundary layers, which have thicker subsonic portions than turbulent boundary layers. Depending upon flow conditions, the boundary layer may be separated over the major portion of the surface, thereby greatly influencing the effectiveness of controls located downstream on either compression or expansion surfaces.

Laminar boundary-layer separation ahead of a deflected flap on the windward surface of a vehicle spreads the flow-deflection pressure rise over a much larger region than does turbulent separation. The effectiveness of the flap in creating a moment is lessened both by the decrease in the pressure distribution on the flap and by any pressure increase occurring on the surface upstream of the moment reference center. These effects tend to restrict the desired rearward movement of the center of pressure and reduce the effectiveness of the control. In extreme cases the center-of-pressure location with laminar separation may be well forward of that for a turbulent boundary layer.

The extent of the separated-flow region and the pressures imposed on the surface depend on the flap deflection, flow conditions, and nature of the boundary layer ahead of the flap. Reattachment of the separated flow on the flap is usually accompanied by a local heat-transfer rate several times larger than that corresponding to an attached boundary layer; the average heat transfer to the separated-flow region, however, is reduced. Similarly, separation affects the pressure distribution on vehicles having flared-skirt-type stabilizing surfaces. Laminar boundary-layer flow ahead of small protuberances yields pressure distributions closer to the inviscid predictions than does turbulent flow. A small step on a surface is effectively streamlined by laminar separation far ahead of it, whereas for turbulent separation, a strong shock exists ahead of the step and there is a large increase in the local pressure.

Separation on the leeward side of a vehicle may make shielded controls (i.e., controls which do not "see" the free stream) useless. Several factors combine in making leading-edge separation from the leeward surface of hypersonic vehicles particularly probable. Large angles of attack may be desirable for many hypersonic flight paths. Because high Mach number flows have small limiting expansion angles, much of the upper surface feels only the leakage flow from the boundary layer where the Mach number is lower. The pressure rise due to the strong trailing-edge shock may be propagated far forward through the thick hypersonic boundary layer, thus increasing the possibility of leading-edge separation. Another factor enhancing the probability of separation is the likelihood of the boundary layer being laminar with consequently thicker subsonic regions and at the same time less able to overcome an adverse pressure gradient than the corresponding turbulent boundary layer. The effectiveness of controls located entirely within the separated-flow region, such as trailing-edge flaps or fins, would be nullified. On the other hand, flow separation over notches (cavities) may advantageously be used to control the drag of a hypersonic vehicle; for essentially the same average rate of heat transfer to a hypersonic vehicle, the drag may be increased by an order of magnitude by the employment of notches in the surface of the vehicle. Separation influences both the type and the location of control devices. Spoilers, for example, would be ineffectual on leeward surfaces of hypersonic vehicles even if they were near the leading edge. Positive controls that always "see" the free stream are required.

#### Three-Dimensional and Unsteady Flow Effects

Separated-flow regions rarely are purely two-dimensional and usually are unsteady. Although much insight into separation phenomena may be gained by using two-dimensional flow analyses, there are important effects that must be considered three-dimensionally. One such effect is the large venting of the separated region in front of a ramp of finite span. The fluid in the separated region, having low velocity and relatively high pressure, expands readily into the low-pressure stream at the tip, and the mass balance of the two-dimensional separation is upset. Another case is that associated with the streamwise flow in the corner at the juncture of a fin and the surface of the configuration. A strong vortex may be set up in such a corner with extreme rates of heat transfer associated with the vortical motion. Another important three-dimensional effect is the coupling effect of a control on another surface. The shock wave ahead of a blunt control or ahead of a separated-flow region may impinge on a transverse surface. Thus, the deflection of a vertical fin or rudder may cause nonsymmetrical separation on the horizontal surface and create an undesired rolling or pitching moment. Particularly for separation occurring near the point of transition of a laminar to turbulent boundary layer, the point of separation and the associated shock wave may

oscillate about some mean position. Large buffeting loads may be experienced on the surface and on adjoining surfaces of the configuration. Unsteady flow in cavities in the surface of a missile may also cause structural failure. Laminar boundary-layer separation with large center-of-pressure shift may be experienced at a small control deflection, while if the deflection is increased and then decreased to its initial value, the separation may be turbulent with a far different value of pitching moment because of the different center-of-pressure location. This hysteresis is extremely difficult to predict, and can be quite dangerous.

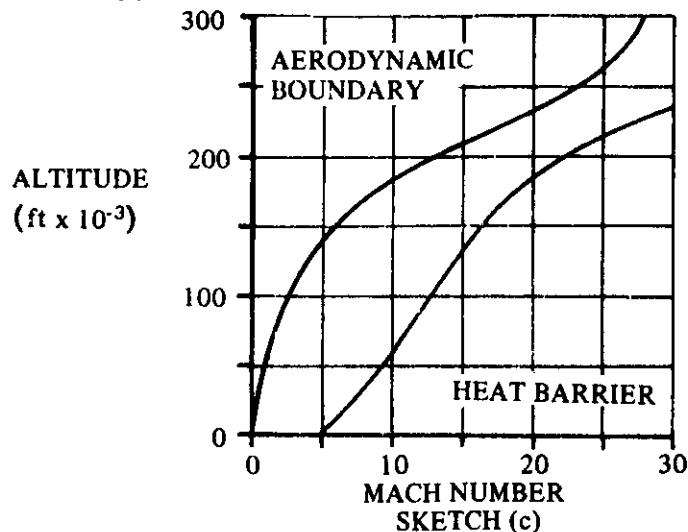
In high Mach number flows, the pressure loads produced by compression surfaces are much greater than those produced by expansion surfaces. Consequently, the most effective aerodynamic controls usually employ deflections which involve compression of the local flow. Therefore, shock-induced separation, either ahead of a compression surface or due to an incident shock, is the type most prevalent with hypersonic controls and has been treated most extensively in the literature.

When separation occurs in high-speed flight, the changes in the pressure distribution and heat-transfer rate can have catastrophic effects. Trim and stability are radically affected by sudden center-of-pressure shifts and changes in pressure magnitude. Local hot spots at separation and reattachment points can cause failure of thermal protection. Heat-transfer rates can also be greatly increased by streamwise vortices originating from three-dimensional separations.

#### HYPersonic CONTROL EFFECTIVENESS

The method presented in this section to determine the aerodynamic control effectiveness at hypersonic speeds is taken from reference 1. The method is intended for use over a broad range of flight conditions encountered by a typical hypersonic cruise/glide vehicle. However, it should be noted that the semiempirical correlation charts used in the method are based on presently available data covering a limited range of test conditions and that the validity of extrapolations for conditions outside the experimental range has not been established. The range of variables covered by experimental data is indicated on the correlation charts.

The flight conditions encountered by a typical hypersonic vehicle are illustrated by the altitude-velocity envelop presented as sketch (c).



For a given velocity the maximum attainable altitude is determined by the minimum dynamic pressure which will sustain flight, and the minimum altitude is a function of the vehicle's capability to withstand aerodynamic heating. The Datcom method is restricted to free-stream flight conditions in the flight envelop for Mach numbers greater than 5.0.

The angle of attack of the vehicle is limited by vehicle performance and structural heating conditions. The angle of attack below which the L/D ratio is favorable and structural heating is not excessive is approximately 20°. Therefore, the angle-of-attack range of the Datcom method is  $0 \leq \alpha \leq 20^\circ$ . Since the study conducted in connection with reference 1 was concerned primarily with flat-plate surfaces, the angle of attack also represents the flow-deflection angle in the method that follows.

The prediction method has been derived on the basis of compression-corner flow separation. It is limited to the analysis of controls on windward surfaces, and is applicable only to regions where the assumption of two-dimensional flow is valid.

In applying the method to complex three-dimensional configurations, the degree of deviation from two-dimensional flow should be established so that the proper method of determining the local-flow properties can be selected. Then the correlations presented herein can be applied to the separated-flow region. For such approximations exact streamline direction is not as important as static pressure and Mach number. However, there can be substantial reductions in control effectiveness due to finite span. Section V of reference 1 presents some insight into methods that can be employed to determine the degree of deviation from two-dimensional flow when the actual flow is three-dimensional. The use of flow-visualization studies, and lengthwise and spanwise pressure distributions on similar models are suggested. Reference 1 presents brief summaries of separated three-dimensional flow on fin-plate configurations, flat surfaces with compression flaps and end plates, and delta wings with variations (blunt leading edges, pyramidal configurations with and without flat-bottom surfaces, etc.)

Since leeward surfaces in hypersonic flow are generally ineffective, the restriction of the method to the analysis of controls on the windward surface is not a serious limitation.

For many practical cases the control surfaces are located near the trailing edge of essentially planar surfaces and are sufficiently far from the leading edge for bluntness effects to be negligible. For such cases, the local-flow properties upstream of the control surface are approximately the same as flow conditions behind an oblique shock, and oblique-shock properties can be used to define the local-flow properties. The Datcom method is restricted to cases of this sort.

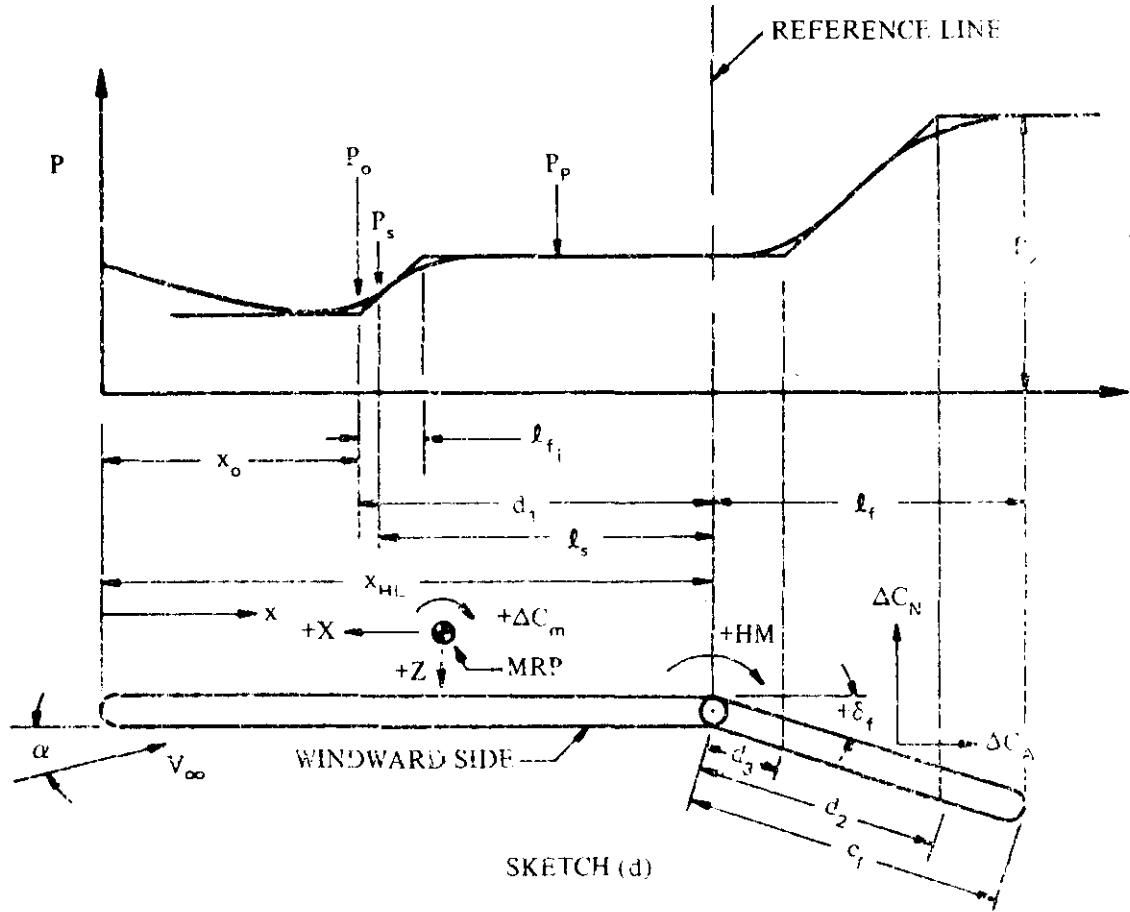
The Datcom method consists of first determining the local-flow properties upstream of the control surface. Then by using the local-flow properties, a complete pressure distribution is defined for compression-corner flow separation in terms of interaction parameters and pressure levels for either laminar or turbulent separated-flow conditions. Finally, the pressure distribution is integrated to obtain the two-dimensional force and moment increments produced by separated compression-corner flow. Force and moment equations have been developed in terms of the distances and pressure levels which define the pressure distribution. These equations are presented in the Datcom method.

The local-flow conditions have been determined by using oblique-shock properties for a number of conditions in the flight envelop. The design charts presented in this section include local-flow properties based on both perfect-gas and equilibrium-real-gas assumptions. For the flight regimes where flow properties deviate from those given by oblique-shock theory for a perfect gas, equilibrium-real-gas effects have been determined by means of similarity parameters from approximate theory and the effective ratio of specific heats presented in reference 29 (see Sections III and VI of reference 1). In using the local-flow charts (figure 6.3.1-31 through -49) the equilibrium-real-gas curves are used for velocity-altitude conditions and flow-deflection angles where the equilibrium-real-gas value differs from the perfect-gas value.

The equations used for the prediction of the separated-flow pressure distributions are developed in reference 1. Where applicable, the final equations are presented on the design charts of this section; however, the developments of the semiempirical correlations for laminar and turbulent separated flows are not discussed herein.

In reference 1 the transition phenomenon is investigated and a criterion for establishing the location of transition based on the results of Deem and Murphy (reference 30) is established. The minimum pressure rise required to cause flow separation, and incipient-separation criteria for both laminar and turbulent flow, are based on test data.

The characteristics of the separated-flow region of a typical pressure profile are illustrated in sketch (d). The distance parameters are based on a common reference line which is defined for various model configurations as a geometrical shock impingement point, hinge line (for corner flow), or the forward face of a step.



#### NOTATION

Symbol	Definition
$x_o$	beginning of pressure interaction (point where pressure just begins to rise)
$d_1$	upstream pressure interaction length (distance from the beginning of interaction to the reference line)
$l_{f_i}$	free interaction length (distance from the beginning of interaction to the point where the pressure distribution reaches the straight section of the pressure plateau)
$d_2$	downstream interaction length (distance from the reference line to the point of intersection of two lines tangent to the pressure curve in the downstream region, measured along the ship (see sketch (d))
$d_3$	distance from the reference line to the point of intersection of two lines tangent to the pressure curve as illustrated in sketch (d)
$l_s$	separation length (distance from the separation point to the reference line)

Symbol	Definition
$l_t$	length of the control (undeflected)
$c_f$	control chord
$d_{LE}$	diameter of leading edge
$x_{HL}$	distance of the control hinge line measured from the nose of the configuration
$\delta_t$	control deflection, positive trailing edge down
$b$	span of surface
$C_A$	axial-force coefficient
$C_p$	pressure coefficient
$C_m$	pitching-moment coefficient
$C_N$	normal-force coefficient
$HM$	hinge moment
$L$	reference length
$P$	pressure
$q$	dynamic pressure
$R_\ell$	Reynolds number
$S$	reference area
$T$	temperature
$V$	velocity
$x$	longitudinal coordinate, measured from leading edge to point of interest
$\alpha$	angle of attack or flow-deflection angle
$\gamma$	ratio of specific heats
$\delta$	boundary-layer thickness
$\theta$	shock-wave angle measured from upstream flow direction
$\phi$	angle associated with geometry of separation
$\Lambda_{LE}$	leading-edge-sweep angle

Symbol	Definition
<b>SUBSCRIPTS</b>	
HL	hinge line
inc	incipient
MRP	moment reference point
P	plateau
$\alpha$	local condition upstream of interaction
o	point where interaction begins
$\infty$	free stream
2	peak value, downstream portion of pressure distribution
t	transition point
c.p.	center of pressure
w	wall
s	separation
<b>SUPERSCRIPT</b>	
*	reference condition

### DATCOM METHOD

The control effectiveness at hypersonic speeds of a deflected control located on the windward surface is obtained from the procedure outlined in the following steps:\*\*

**Step 1. Determine the local-flow conditions:**

The ratios of pressure, temperature, Mach number, and Reynolds number behind an oblique shock to their respective values in the free stream are obtained from figures 6.3.1-31, -37, -43, and -49, respectively.

---

\*\*The subscript  $\alpha$  used throughout the Datcom method has two different meanings as follows: (1) The value of the parameter being considered is its local value upstream of interaction, examples being  $(C_p)_\alpha$ ,  $p_\alpha$ ,  $M_\alpha$ ,  $Rf_\alpha$ ; (2) The value of the parameter being considered is its value at some specific location downstream of interaction, referred to local conditions upstream of interaction, examples being  $(C_p)_2$ ,  $(Rf)_\alpha$ ,  $(C_p)_P$ .

The pressure coefficient upstream of the control surface, referred to free-stream conditions, is given by

$$(C_{p_\infty})_\alpha = \frac{(P_\infty/P_\infty) - 1}{\frac{\gamma}{2} M_\infty^2} \quad 6.3.1-a$$

**Step 2.** Determine if the flow is laminar or turbulent:

It is assumed that the state of the boundary layer is laminar if  $x_t > x_{HL}$ , and turbulent if  $x_t < x_{HL}$ . Based on the results of Dhem and Murphy (reference 29) and recent experimental data, the following expression for transition distance is given, in reference 1:

$$x_t (\text{feet}) = \frac{5.38 \times 10^2 + 1.94 \times 10^2 |M_\alpha - 3|^{3/2} (\cos \Lambda)^{1/2}}{(R_{\ell_\alpha}/\text{in.})^{0.6}} \quad 6.3.1-b$$

For configurations with no sweepback ( $\Lambda = 0$ ), the state of the boundary layer at the hinge line is obtained from figure 6.3.1-55 as a function of  $(R_{\ell_\alpha})_{HL}$  and  $M_\alpha$ , where

$$(R_{\ell_\alpha})_{HL} = x_{HL} (R_{\ell_\alpha})$$

Of course, if the transition Reynolds number is known, then the transition distance is given by  $x_t = (R_{\ell_\alpha})_{x_t} / R_{\ell_\alpha}$ , where  $R_{\ell_\alpha}$  is the Reynolds number per foot.

**Step 3.** Determine if flow separation exists:

Obtain the pressure coefficient for incipient separation  $(C_{p_\alpha})_{inc}$  from figure 6.3.1-56 for laminar flow or figure 6.3.1-57 for turbulent flow.

Obtain the final pressure-rise coefficient by

$$(C_{p_{\alpha/2}}) = \frac{(P_2/P_\infty) - 1}{\frac{\gamma}{2} M_\alpha^2} \quad 6.3.1-c$$

where  $P_2/P_\infty$  is obtained from figure 6.3.1-58 as a function of  $M_\alpha$ . For laminar flow the average of the isentropic and single-shock values should be used for  $M_\alpha < 6$ , and the single-shock value should be used for  $M_\alpha > 6$ . For turbulent flow use the single-shock value. If  $(C_{p_\alpha})_2 \geq (C_{p_\alpha})_{inc}$ , the flow is separated.

**Step 4.** Determine the separation location if separated flow exists:

If flow separation exists, an iterative procedure is required to determine the separation location. For a given local Mach number  $M_\alpha$ , the upstream interaction distance  $d_1$  is a function of the plateau-pressure level  $P_p$ , which is a function of the Reynolds number at the interaction point  $(R_{\ell_\alpha})_{x_0}$ .

Therefore, for any interaction point  $x_o$ , a corresponding plateau-pressure level and upstream interaction distance must be defined. In solving for the interaction location, the upstream interaction distances corresponding to a number of assumed interaction locations are calculated until the point is found for which the sum of the downstream distance to the interaction point and the upstream interaction distance is equal to the distance to the hinge line; i.e.,  $x_o + d_1 = x_{HL}$ . The procedure is as follows:

- a. Assume an interaction location  $x_o$  (For vehicles of practical dimensions the difference between  $x_o$  and  $x_{HL}$  will be small).
- b. Calculate the Reynolds number for the assumed  $x_o$  by  $(R_{\ell_\alpha})_{x_o} = x_o (R_{\ell_\alpha})$ , and obtain the plateau-pressure level  $(C_{p_\alpha})_P$  as a function of  $(R_{\ell_\alpha})_{x_o}$  and  $M_\alpha$  from figure 6.3.1-59 or figure 6.3.1-60 for laminar or turbulent flow, respectively.
- c. Obtain the upstream interaction distance, nondimensionalized by boundary-layer thickness  $d_1/\delta_o$ , as a function of  $(C_{p_\alpha})_P$  and  $M_\alpha$  from figure 6.3.1-61 or figure 6.3.1-62 for laminar or turbulent flow, respectively.
- d. For a given wall temperature, obtain the reference temperature Reynolds-number ratio  $(R_{\ell_\alpha^*}/R_{\ell_\alpha})$  as a function of  $T_w/T_\alpha$  and  $M_\alpha$  from figure 6.3.1-63 or figure 6.3.1-64 for laminar or turbulent flow, respectively.
- e. Calculate the reference temperature Reynolds number by  $R_{\ell_\alpha^*} = (R_{\ell_\alpha^*}/R_{\ell_\alpha}) R_{\ell_\alpha}$ , and obtain the corresponding boundary-layer thickness  $\delta_o$  from figure 6.3.1-65 or figure 6.3.1-66 for laminar or turbulent flow, respectively, by  $\delta_o = (\delta_o/\sqrt{x_o}) \sqrt{x_o}$ .
- f. Calculate the upstream interaction distance by  $d_1 = (d_1/\delta_o) \delta_o$ .
- g. Sum  $d_1$  and  $x_o$ . If  $d_1 + x_o \neq x_{HL}$ , repeat the procedure until  $d_1 + x_o = x_{HL}$ .

**Step 5.** Having determined the separation point  $x_o$ , define the windward pressure distribution (see sketch (d)) as follows:

- a. Calculate the Reynolds number for  $x_o$  by  $(R_{\ell_\alpha})_{x_o} = x_o (R_{\ell_\alpha})$ .
- b. Obtain the plateau-pressure level  $(C_{p_\alpha})_P$  as a function of  $(R_{\ell_\alpha})_{x_o}$  and  $M_\alpha$  from figure 6.3.1-59 or figure 6.3.1-60 for laminar or turbulent flow, respectively.
- c. Calculate the plateau pressure, referred to free-stream conditions, by

$$(C_{p_\infty})_P = (C_{p_\alpha})_P \left( \frac{M_\alpha}{M_\infty} \right)^2 \frac{P_\alpha}{P_\infty} + (C_{p_\infty})_\alpha \quad 6.3.1-d$$

where  $M_\alpha/M_\infty$ ,  $P_\alpha/P_\infty$ , and  $(C_{p_\infty})_\alpha$  are obtained from step 1.

- d. Obtain the free interaction length nondimensionalized by boundary-layer thickness  $\ell_{f_i}/\delta_o$  as a function of  $(C_{p\alpha})_P$  and  $M_\alpha$  from figure 6.3.1-67 or figure 6.3.1-68 for laminar or turbulent flow, respectively.
- e. Calculate the free interaction length by  $\ell_{f_i} = (\ell_{f_i}/\delta_o) \delta_o$  where  $\delta_o$  is the boundary-layer thickness determined as outlined in step 4e.
- f. Obtain the upstream interaction distance nondimensionalized by boundary-layer thickness  $d_1/\delta_o$  as a function of  $(C_{p\alpha})_P$  and  $M_\alpha$  from figure 6.3.1-61 or figure 6.3.1-62 for laminar or turbulent flow, respectively.
- g. Calculate the upstream interaction distance by  $d_1 = (d_1/\delta_o) \delta_o$ .
- h. Obtain the downstream interaction length  $d_2$  from figure 6.3.1-69 or figure 6.3.1-70 for laminar or turbulent flow, respectively.
- i. Determine the downstream interaction length to the pressure rise  $d_3$ . For turbulent flow  $d_3 = 0$ . For laminar flow the ratio  $d_3/d_1$  is obtained from figure 6.3.1-71 as a function of flap deflection  $\delta_f$  and the equivalent flow-deflection angle  $\phi$  for  $(C_{p\alpha})_P$ .

The equivalent flow-deflection angle for  $(C_{p\alpha})_P$  may be obtained as a function of the shock-wave angle  $\theta$  and  $M_\alpha$ . The shock-wave angle is given by

$$\theta = \sin^{-1} \sqrt{\frac{6(P_P/P_\alpha) + 1}{7(M_\alpha)^2}} \quad 6.3.1-e$$

where

$$\frac{P_P}{P_\alpha} = (C_{p\alpha})_P \frac{\gamma}{2} (M_\alpha)^2 + 1 \quad 6.3.1-f$$

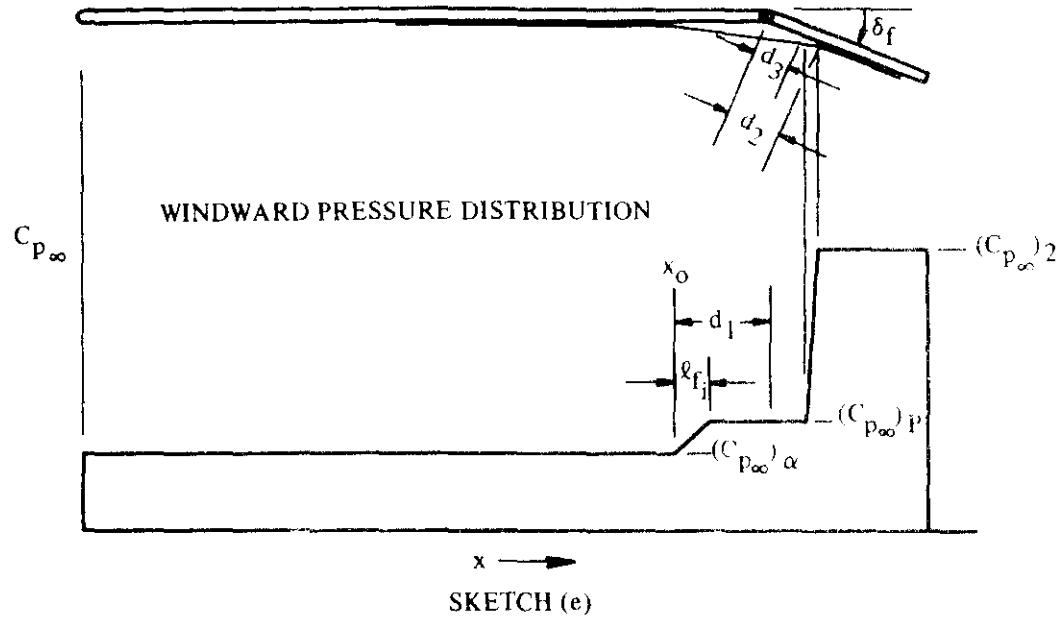
Enter figure 4.4.1-81 with  $\theta$  and  $M_\alpha$  and read  $\phi = |\delta'|$ .

- j. Calculate the peak flap pressure, referred to free-stream conditions, by

$$(C_{p\alpha})_2 = (C_{p\alpha})_2 \left( \frac{M_\alpha}{M_\infty} \right)^2 \frac{P_\alpha}{P_\infty} + (C_{p\alpha})_\alpha \quad 6.3.1-g$$

where  $M_\alpha/M_\infty$ ,  $P_\alpha/P_\infty$ , and  $(C_{p\alpha})_\alpha$  are obtained from step 1, and  $(C_{p\alpha})_2$  is obtained from step 2 (equation 6.3.1-c).

Step 6. The windward pressure distribution may now be constructed as illustrated in sketch (e).



Step 7. The two-dimensional force and moment increments produced on the windward surface of a deflected control are given by

Normal-force increment:

$$\frac{\Delta C_N S}{b} = \left[ (C_{p_\infty})_P - (C_{p_\infty})_\alpha \right] \left[ d_1 - \frac{d_1}{2} + \cos \delta_f c_f \right] + \left[ (C_{p_\infty})_2 - (C_{p_\infty})_P \right] (\cos \delta_f) \left[ c_f - \frac{d_2}{2} - \frac{d_3}{2} \right] \text{ (ft)} \quad 6.3.1-h$$

Increment of pitching moment about HL due to normal force increment:

$$\begin{aligned} \left[ \frac{(\Delta C_m)_{HL} SL}{b} \right]_{\Delta C_N} &= \left[ (C_{p_\infty})_P - (C_{p_\infty})_\alpha \right] \left[ \frac{(l_{f_i})^2}{6} - \frac{(l_{f_i})(d_1)}{2} + \frac{(d_1)^2}{2} - \frac{\cos^2 \delta_f (c_f)^2}{2} \right] \\ &\quad - \left[ (C_{p_\infty})_2 - (C_{p_\infty})_P \right] (\cos^2 \delta_f) \left[ \frac{(c_f)^2}{2} - \frac{(d_2)^2}{6} - \frac{d_2 d_3}{6} - \frac{(d_3)^2}{6} \right] \text{ (ft)}^2 \quad 6.3.1-i \end{aligned}$$

Center of pressure of normal-force increment, measured from the MRP, negative aft:

$$(x_{c.p.})_{\Delta C_N} = -(x_{HL} - x_{MRP}) + \frac{\left[ (\Delta C_m)_{HL} L \right]_{\Delta C_N}}{\Delta C_N} \text{ (ft)} \quad 6.3.1-j$$

Axial-force increment:

$$\frac{\Delta C_A S}{b} = (\sin \delta_f) \left\{ \left[ (C_{p_\infty})_P - (C_{p_\infty})_\alpha \right] c_f + \left[ (C_{p_\infty})_2 - (C_{p_\infty})_P \right] \left[ c_f - \frac{d_2}{2} - \frac{d_3}{2} \right] \right\} \text{ (ft)} \quad 6.3.1-k$$

Increment of pitching moment about HL due to axial-force increment:

$$\left[ \frac{(\Delta C_m)_{HL} S L}{b} \right]_{\Delta C_A} = - (\sin^2 \delta_f) \left\{ \left[ (C_{p_\infty})_P \cdot (C_{p_\infty})_\alpha \right] \frac{(c_f)^2}{2} + \left[ (C_{p_\infty})_2 \cdot (C_{p_\infty})_P \right] \left[ \frac{(c_f)^2}{2} - \frac{(d_2)^2}{6} - \frac{d_2 d_3}{6} - \frac{(d_3)^2}{6} \right] \right\} (ft)^2 \quad 6.3.1-l$$

Center of pressure of axial-force increment, measured from the MRP, positive down:

$$(z_{c.p.})_{\Delta C_A} = z_{HL} \cdot \frac{\left[ (\Delta C_m)_{HL} S L \right]_{\Delta C_A}}{\Delta C_A} (ft) \quad 6.3.1-m$$

Increment of pitching moment about vehicle MRP:

$$\left[ \frac{(\Delta C_m)_{MRP} S}{b} L \right] = \left[ \frac{(\Delta C_N) S}{b} (x_{c.p.}) \right]_{\Delta C_N} - \left[ \frac{(\Delta C_A) S}{b} (z_{c.p.}) \right]_{\Delta C_A} (ft)^2 \quad 6.3.1-n$$

Windward component of control hinge moment (based on absolute pressure):

$$\frac{HM}{bq} = - \left\{ (C_{p_\infty})_2 \frac{(c_f)^2}{2} \cdot \frac{1}{6} \left[ (C_{p_\infty})_2 \cdot (C_{p_\infty})_P \right] \left[ (d_2)^2 + d_2 d_3 + (d_3)^2 \right] \right\} (ft)^2 \quad 6.3.1-o$$

An approximate correction for the effect of finite control span on the two-dimensional pressure distribution in the separated region over the control is presented as figure 6.3.1-72. This empirical correlation, taken from reference 1, is based on a limited amount of test data. Unfortunately, not enough test data are available for partial-span control effect to identify the effects of Mach number, Reynolds number, or control position.

Two sample problems are presented at the conclusion of this section. The first sample problem is straightforward in that the Datcom method is directly applicable. The second sample problem illustrates an application of the method to a flight condition where the separated region extends forward to the leading edge of the configuration.

It should be recalled that the use of oblique-shock relations implies small leading-edge-bluntness effects and negligible viscous effects. On bodies with a blunted leading edge, pressure near the leading edge will be higher than that predicted by the oblique-shock theory. When leading-edge bluntness is not zero, the actual value for  $M_\alpha$  will be between that given by oblique-shock and shock-loss theories. Values of  $M_\alpha$  on surfaces with leading edges of various bluntness dimensions were obtained from test data during the analysis conducted in connection with reference 1. It is suggested therein that oblique-shock properties result in acceptable values of local Mach number  $M_\alpha$  for

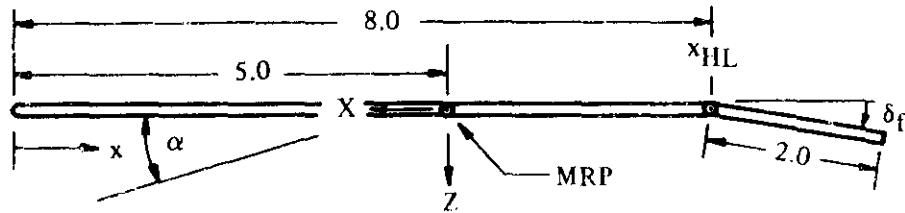
$$\frac{0.1375 \frac{x_{HL}}{d_{LE}} + 2.0}{M_\infty} > 1.0$$

If the leading-edge bluntness is comparatively large, the local-flow properties should be calculated by other available methods, such as tangent-wedge, blast-wave, or the Moeckel shock-loss theory (reference 31). Blunt leading edges or large viscous-induced pressure gradients also reduce the boundary-layer thickness. The effects of leading-edge bluntness and viscous interaction on the flow properties along a body surface are discussed in Section III of reference 1.

### Sample Problems

1.

Given: A two-dimensional flat plate with negligible thickness.



$$L = 10.0 \text{ ft} \quad x_{MRP} = 5.0 \text{ ft} \quad x_{HL} = 8.0 \text{ ft} \quad z_{HL} = 0 \quad c_f = 2.0 \text{ ft}$$

$$\delta_t = 10^0 \quad R_{\rho_\alpha} = 1.06 \times 10^5 \text{ per ft}$$

$$\text{Altitude: } 150,000 \text{ ft} \quad P_\infty = 2.84 \text{ lb}/(\text{ft})^2 \quad T_\infty = 480^\circ \text{ R}$$

$$T_w = 1500^\circ \text{ R} \quad \alpha = 15^\circ \quad \text{Negligible viscous interaction (assumed)}$$

$$M_\infty = 10.0$$

Compute:

Determine the local flow conditions:

$$\frac{P_\alpha}{P_\infty} = 13.5 \quad (\text{figure 6.3.1-31c})$$

$$\frac{T_\alpha}{T_\infty} = 3.0 \quad (\text{figure 6.3.1-37c}) \quad (\text{equilibrium real gas})$$

$$M_\alpha = 5.5 \quad (\text{figure 6.3.1-43c}) \quad (\text{equilibrium real gas})$$

$$\frac{R_{\rho_\alpha}}{R_{\rho_\infty}} = 1.94 \quad (\text{figure 6.3.1-49c}) \quad (\text{equilibrium real gas})$$

$$T_\alpha = T_\infty \frac{T_\alpha}{T_\infty} = 1440^\circ \text{ R}$$

$$R_{\rho_\alpha} = R_{\rho_\infty} \frac{R_{\rho_\alpha}}{R_{\rho_\infty}} = 2.06 \times 10^5 \text{ per ft}$$

$$\left(C_{p\infty}\right)_\alpha = \frac{(P_\alpha/P_\infty) - 1}{\frac{\lambda}{2} M_\infty^2} = \frac{\frac{13.5 - 1}{1.4}}{\frac{2}{2} (10)^2} = 0.179 \text{ (equation 6.3.1-a)}$$

Determine if the flow is laminar or turbulent:

$$(R_{\ell\alpha})_{HL} = x_{HL} (R_{\ell\alpha}) = (8.0) (2.06 \times 10^5) = 1.648 \times 10^6$$

At  $(R_{\ell\alpha})_{HL}$  and  $M_\alpha$ , figure 6.3.1-55 indicates a laminar boundary layer at the hinge line.

Determine if separation exists:

$$(C_{p\alpha})_{inc} = 0.020 \text{ (figure 6.3.1-56)}$$

$$\frac{P_2}{P_\alpha} = 3.12 \text{ (figure 6.3.1-58) (average of isentropic and single-shock values)}$$

$$\left(C_{p\alpha}\right)_2 = \frac{(P_2/P_\alpha) - 1}{\frac{\gamma}{2} M_\alpha^2} = \frac{3.12 - 1}{\frac{1.4}{2} (5.5)^2} = 0.100 \text{ (equation 6.3.1-c)}$$

Since  $\left(C_{p\alpha}\right)_2 > (C_{p\alpha})_{inc}$ , the flow is separated.

Determine the separation location (see step 4 of Datcom method for iteration procedure):

First iteration (assume  $x_o = 7.0$  ft)

$$(R_{\ell\alpha})_{x_o} = x_o (R_{\ell\alpha}) = (7.0) (2.06 \times 10^5) = 1.442 \times 10^6$$

$$(C_{p\alpha})_p = 0.0185 \text{ (figure 6.3.1-59)}$$

$$\frac{d_1}{\delta_o} = 20.0 \text{ (figure 6.3.1-61)}$$

$$\frac{T_w}{T_\alpha} = \frac{1500}{1440} = 1.042$$

$$\frac{R_{\ell\alpha}^*}{R_{\ell\alpha}} = 0.28 \text{ (figure 6.3.1-63)}$$

$$R_{\ell\alpha}^* = R_{\ell\alpha} \left( \frac{R_{\ell\alpha}^*}{R_{\ell\alpha}} \right) = (2.06 \times 10^5) (0.28) = 5.768 \times 10^4 \text{ per ft}$$

$$\frac{\delta_o}{\sqrt{x_o}} = 0.0215 \text{ (figure 6.3.1-65)}$$

$$\delta_o = \sqrt{x_o} \frac{\delta_o}{\sqrt{x_o}} = (\sqrt{7.0})(0.0215) = 0.057 \text{ ft}$$

$$d_1 = \delta_o \left( \frac{d_1}{\delta_o} \right) = (0.057)(20.0) = 1.14 \text{ ft}$$

$$d_1 + x_o = 1.14 + 7.0 = 8.14 \text{ ft} > x_{HL} \text{. Try a second iteration.}$$

Second iteration (assume  $x_o = 6.5 \text{ ft}$ )

$$(R_{\rho\alpha})_{x_o} = x_o (R_{\rho\alpha}) = (6.5)(2.06 \times 10^5) = 1.339 \times 10^6$$

$$(C_{p\alpha})_p = 0.019 \text{ (figure 6.3.1-59)}$$

$$\frac{d_1}{\delta_o} = 21.5 \text{ (figure 6.3.1-61)}$$

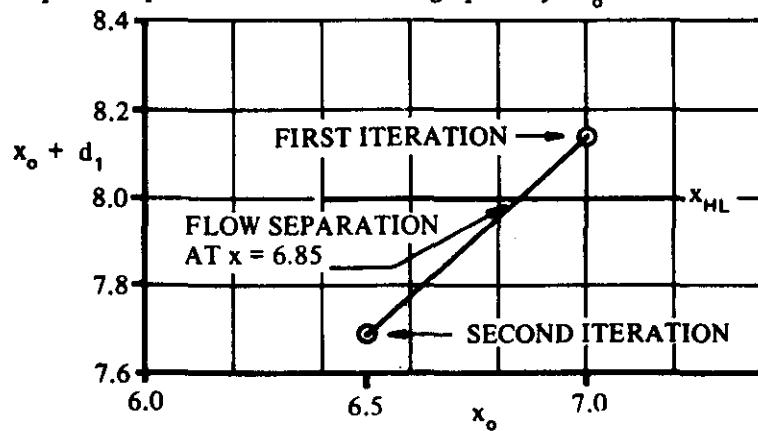
$$\frac{\delta_o}{\sqrt{x_o}} = 0.0215 \text{ (calculation to determine } \delta_o/\sqrt{x_o} \text{ is same as first iteration)}$$

$$\delta_o = \sqrt{x_o} \frac{\delta_o}{\sqrt{x_o}} = \sqrt{6.5} (0.0215) = 0.055 \text{ ft}$$

$$d_1 = \delta_o \left( \frac{d_1}{\delta_o} \right) = (0.055)(21.5) = 1.183 \text{ ft}$$

$$d_1 + x_o = 1.183 + 6.50 = 7.683 \text{ ft} < x_{HL}$$

The flow separation point is now determined graphically.  $x_o = 6.85 \text{ ft}$



Define the windward pressure distribution:

$$(R_{\rho_\alpha})_{x_0} = x_0 (R_{\rho_\alpha}) = (6.85)(2.06 \times 10^5) = 1.41 \times 10^6$$

$$(C_{p,\alpha/P})_P = 0.019 \text{ (figure 6.3.1-59)}$$

$$\begin{aligned}(C_{p,\infty})_P &= (C_{p,\alpha})_P \left( \frac{M_\alpha}{M_\infty} \right)^2 \frac{P_\alpha}{P_\infty} + (C_{p,\infty})_\alpha \text{ (equation 6.3.1-d)} \\ &= (0.019) \left( \frac{5.5}{10.0} \right)^2 (13.5) + 0.179 = 0.257\end{aligned}$$

$$\frac{\ell_{f_i}}{\delta_0} = 8.0 \text{ (figure 6.3.1-67)}$$

$$\delta_0 = \sqrt{x_0} \cdot \frac{\delta_0}{\sqrt{x_0}} = \sqrt{6.85} (0.0215) = 0.056 \text{ ft}$$

$$\ell_{f_i} = \delta_0 \left( \frac{\ell_{f_i}}{\delta_0} \right) = (0.056) (8.0) = 0.448 \text{ ft}$$

$$\frac{d_1}{\delta_0} = 21.4 \text{ (figure 6.3.1-61)}$$

$$d_1 = \delta_0 \left( \frac{d_1}{\delta_0} \right) = (0.056) (21.4) = 1.20 \text{ ft}$$

$$\frac{c_f}{d_1} = \frac{2.0}{1.20} > 1; \text{ therefore, } \frac{d_2}{\sqrt{(c_f)(d_1)}} = \frac{d_2}{d_1} = 0.506 \text{ (figure 6.3.1-69)}$$

$$d_2 = d_1 \left( \frac{d_2}{d_1} \right) = (1.20)(0.506) = 0.607 \text{ ft}$$

Equivalent flow deflection angle for  $(C_{p,\alpha/P})_P$

$$\frac{P_P}{P_\alpha} = (C_{p,\alpha/P})_P \frac{\gamma}{2} (M_\alpha)^2 + 1 \text{ (equation 6.3.1-f)}$$

$$= (0.019) \left( \frac{1.4}{2} \right) (5.5)^2 + 1 = 1.402$$

$$\theta = \sin^{-1} \sqrt{\frac{6(P_p/P_\infty) + 1}{7(M_\infty)^2}} \quad (\text{equation 6.3.1-e})$$

$$= \sin^{-1} \sqrt{\frac{6(1.402) + 1}{7(5.5)^2}} = 12.2^\circ$$

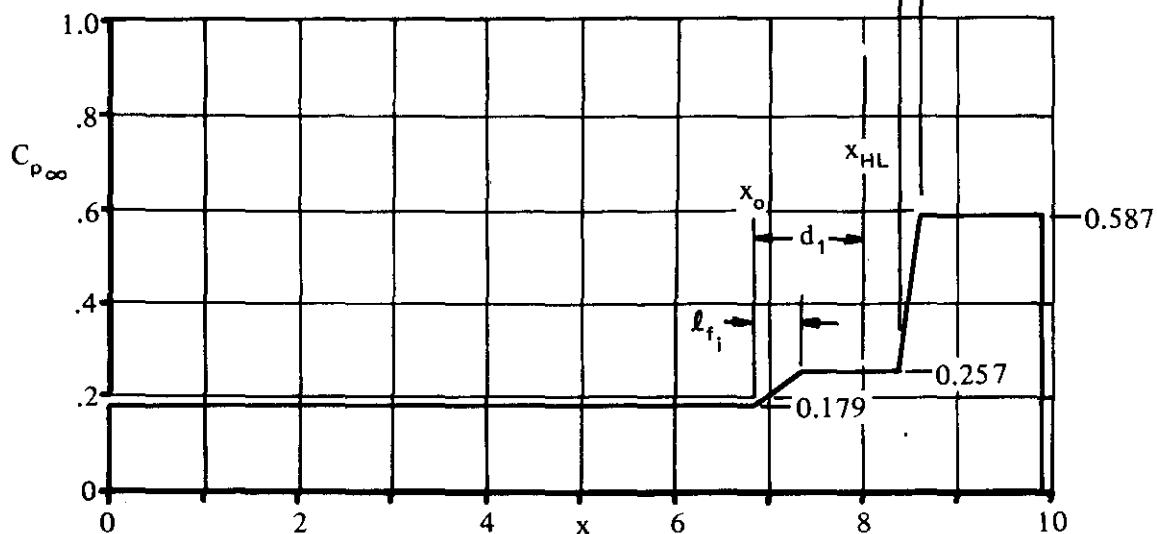
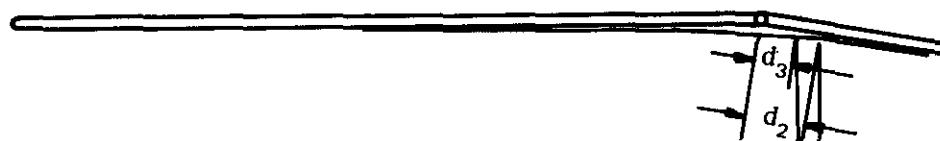
$$\phi = 2.6^\circ (\phi = |\delta'| \text{ at } M_\infty \text{ and } \theta \text{ from figure 4.4.1-81})$$

$$\frac{d_3}{d_1} = 0.35 \quad (\text{figure 6.3.1-71})$$

$$d_3 = d_1 \left( \frac{d_3}{d_1} \right) = (1.20)(0.35) = 0.42 \text{ ft}$$

$$(C_{P_\infty})_2 = (C_{P_\infty})_2 \left( \frac{M_\infty}{M_\alpha} \right)^2 \frac{P_\alpha}{P_\infty} + (C_{P_\infty})_\alpha \quad (\text{equation 6.3.1-g})$$

$$= (0.100) \left( \frac{5.5}{10.0} \right)^2 (13.5) + (0.179) = 0.587$$



Solution:

Normal-force increment:

$$\frac{\Delta C_N S}{b} = \left[ (C_{p_\infty})_P - (C_{p_\infty})_\alpha \right] \left[ d_1 - \frac{q_{f_i}}{2} + \cos \delta_f c_f \right] + \left[ (C_{p_\infty})_2 - (C_{p_\infty})_P \right] (\cos \delta_f) \left[ c_f - \frac{d_2}{2} - \frac{d_3}{2} \right]$$

(equation 6.3.1-h)

$$= [(0.257) - (0.179)] \left[ 1.20 - \frac{0.448}{2} + (0.985)(2.0) \right]$$

$$+ [(0.587) - (0.257)] (0.985) \left\{ 2.0 - \frac{0.607}{2} - \frac{0.42}{2} \right\}$$

$$= 0.713 \text{ ft}$$

Increment of pitching moment about HL due to normal force increment:

$$\left[ \frac{(\Delta C_m)_{HL} SL}{b} \right]_{\Delta C_N} = \left[ (C_{p_\infty})_P - (C_{p_\infty})_\alpha \right] \left[ \frac{(q_{f_i})^2}{6} - \frac{(q_{f_i})(d_1)^2}{2} + \frac{(d_1)^2}{2} - \frac{\cos^2 \delta_f (c_f)^2}{2} \right]$$

$$- \left[ (C_{p_\infty})_2 - (C_{p_\infty})_P \right] (\cos^2 \delta_f) \left[ \frac{(c_f)^2}{2} - \frac{(d_2)^2}{6} - \frac{(d_2 d_3)}{6} - \frac{(d_3)^2}{6} \right]$$

(equation 6.3.1-i)

$$= [(0.257) - (0.179)] \left[ \frac{(0.448)^2}{6} - \frac{(0.448)(1.20)}{2} + \frac{(1.20)^2}{2} \right.$$

$$- \left. \frac{(0.985)^2 (2.0)^2}{2} \right] - [(0.587) - (0.257)] (0.985)^2 \left[ \frac{(2.0)^2}{2} - \frac{(0.607)^2}{6} \right.$$

$$- \left. \frac{(0.607)(0.42)}{6} - \frac{(0.42)^2}{6} \right]$$

$$= -0.713 (\text{ft})^2$$

Center of pressure for normal-force increment referred to MRP:

$$(x_{c.p.})_{\Delta C_N} = -(x_{HL} - x_{MRP}) + \frac{[(\Delta C_m)_{HL} L] \Delta C_N}{\Delta C_N}$$

(equation 6.3.1-j)

$$= -(8.0 - 5.0) + \frac{-0.713}{0.713}$$

$$= -4.00 \text{ ft } (4.00 \text{ feet aft of MRP})$$

Axial-force increment:

$$\begin{aligned}\frac{\Delta C_A S}{b} &= (\sin \delta_f) \left\{ \left[ (C_{p_\infty})_P - (C_{p_\infty})_\alpha \right] c_f + \left[ (C_{p_\infty})_2 - (C_{p_\infty})_P \right] \left[ c_f - \frac{d_2}{2} - \frac{d_3}{2} \right] \right\} \text{ (equation 6.3.1-k)} \\ &= (0.174) \left\{ [(0.257) - (0.179)] (2.0) + [(0.587) - (0.257)] \left[ 2.0 - \frac{0.607}{2} - \frac{0.42}{2} \right] \right\} \\ &= 0.1125 \text{ ft}\end{aligned}$$

Increment of pitching moment about HL due to axial force:

$$\begin{aligned}\left[ \frac{(\Delta C_m)_{HL} SL}{b} \right]_{\Delta C_A} &= -(\sin^2 \delta_f) \left\{ \left[ (C_{p_\infty})_P - (C_{p_\infty})_\alpha \right] \frac{(c_f)^2}{2} + \left[ (C_{p_\infty})_2 - (C_{p_\infty})_P \right] \left[ \frac{(c_f)^2}{2} - \frac{(d_2)^2}{6} \right. \right. \\ &\quad \left. \left. - \frac{d_2 d_3}{6} - \frac{(d_3)^2}{6} \right] \right\} \text{ (equation 6.3.1-l)} \\ &= -(0.174)^2 \left\{ [(0.257) - (0.179)] \frac{(2.0)^2}{2} + [(0.587) - (0.257)] \right. \\ &\quad \left. \left[ (2.0)^2 - \frac{(0.607)^2}{6} - \frac{(0.607)(0.42)}{6} - \frac{(0.42)^2}{6} \right] \right\} \\ &= -0.0234 \text{ (ft)}^2\end{aligned}$$

Center of pressure of axial-force increment:

$$\begin{aligned}(z_{c.p.})_{\Delta C_A} &= Z_{HL} - \frac{[(\Delta C_m)_{HL} L]_{\Delta C_A}}{\Delta C_A} \text{ (equation 6.3.1-m)} \\ &= 0 - \left( \frac{-0.0234}{0.1125} \right) \\ &= 0.208 \text{ (ft)}\end{aligned}$$

Increment of pitching moment about vehicle MRP:

$$\begin{aligned}\left[ \frac{(\Delta C_m)_{MRP} S}{b} - L \right] &= \left[ \frac{(\Delta C_N) S}{b} - (x_{c.p.}) \right]_{\Delta C_N} - \left[ \frac{(\Delta C_A) S}{b} (z_{c.p.}) \right]_{\Delta C_A} \text{ (equation 6.3.1-n)} \\ &= (0.713) (-4.00) - (0.1125) (0.208) = -2.875 \text{ (ft)}^2\end{aligned}$$

Windward component of control hinge moment (based on absolute pressure):

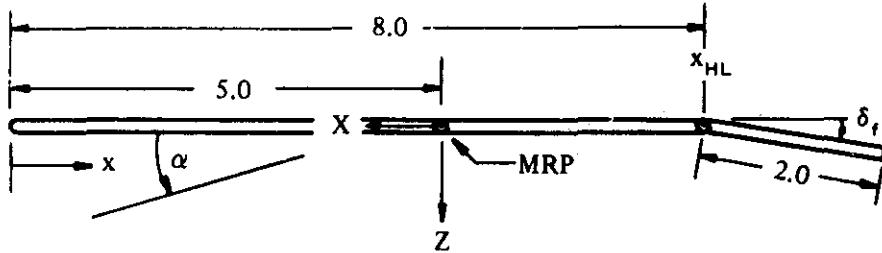
$$\frac{HM}{bq} = - \left\{ (C_{p_\infty})_2 \frac{(c_f)^2}{2} - \frac{1}{6} \left[ (C_{p_\infty})_2 - (C_{p_\infty})_P \right] [(d_2)^2 + d_2 d_3 + (d_3)^2] \right\} \text{ (equation 6.3.1-o)}$$

$$= - \left\{ (0.587) \frac{(2.0)^2}{2} + \frac{1}{6} [(0.587) - (0.257)] [(0.607)^2 + (0.607)(0.42) + (0.42)^2] \right\}$$

$$= -1.130 \text{ (ft)}^2$$

2.

Given: A two-dimensional flat plate with negligible thickness.



$$L = 10.0 \text{ ft} \quad x_{MRP} = 5.0 \text{ ft} \quad x_{HL} = 8.0 \text{ ft} \quad z_{HL} = 0$$

$$c_f = 2.0 \text{ ft} \quad \delta_f = 10^\circ \quad R_{\rho_\infty} = 3.27 \times 10^4 \text{ per ft}$$

$$\text{Altitude: } 200,000 \text{ ft} \quad P_\infty = 0.413 \text{ lb/(ft)}^2 \quad T_\infty = 458^\circ \text{ R}$$

$$T_w = 2000^\circ \text{ R} \quad \alpha = 10^\circ \quad \text{Negligible viscous interaction (assumed)}$$

$$M_\infty = 20$$

Compute:

Determine the local-flow conditions:

$$\frac{P_\alpha}{P_\infty} = 21 \quad (\text{figure 6.3.1-31d}) \quad (\text{equilibrium real gas})$$

$$\frac{T_\alpha}{T_\infty} = 4.30 \quad (\text{figure 6.3.1-37d}) \quad (\text{equilibrium real gas})$$

$$M_\alpha = 9.80 \quad (\text{figure 6.3.1-43d}) \quad (\text{equilibrium real gas})$$

$$\frac{R_{\rho_\alpha}}{R_{\rho_\infty}} = 1.87 \quad (\text{figure 6.3.1-49d}) \quad (\text{equilibrium real gas})$$

$$T_\alpha = T_\infty \frac{T_\alpha}{T_\infty} = 1970^\circ \text{ R}$$

$$R_{\rho_\alpha} = R_{\rho_\infty} \frac{R_{\rho_\alpha}}{R_{\rho_\infty}} = 6.11 \times 10^4 \text{ per ft}$$

$$\left(C_{p_\infty}\right)_\alpha = \frac{(P_\alpha/P_\infty) - 1}{\frac{\gamma}{2} M_\infty^2} = \frac{21.0 - 1}{\frac{1.4}{2} (20)^2} = 0.071 \text{ (equation 6.3.1-a)}$$

Determine if the flow is laminar or turbulent:

$$(R_{\rho_\alpha})_{HL} = x_{HL} (R_{\rho_\alpha}) = (8.0) (6.11 \times 10^4) = 4.9 \times 10^5$$

At  $(R_{\rho_\alpha})_{HL}$  and  $M_\alpha$ , figure 6.3.1-55 indicates a laminar boundary layer.

Determine if separation exists:

$$(C_{p_\alpha})_{inc} = 0.019 \text{ (figure 6.3.1-56)}$$

$$\frac{P_2}{P_\alpha} = 6.80 \text{ (figure 6.3.1-58) (single-shock value)}$$

$$(C_{p_\alpha})_2 = \frac{(P_2/P_\alpha) - 1}{\frac{\gamma}{2} M_\alpha^2} = \frac{6.80 - 1}{\frac{1.4}{2} (9.8)^2} = 0.0863 \text{ (equation 6.3.1-c)}$$

Since  $(C_{p_\alpha})_2 > (C_{p_\alpha})_{inc}$ , the flow is separated.

Determine the separation location (see step 4 of Datcom method for iteration procedure):

First iteration (assume  $x_o = 7.0 \text{ ft}$ )

$$(R_{\rho_\alpha})_{x_o} = x_o (R_{\rho_\alpha}) = (7.0) (6.11 \times 10^4) = 4.277 \times 10^5$$

$$(C_{p_\alpha})_P = 0.0185 \text{ (figure 6.3.1-59)}$$

$$\frac{d_1}{\delta_o} = 110 \text{ (figure 6.3.1-61)}$$

$$\frac{T_w}{T_\alpha} = \frac{2000}{1970} = 1.015$$

$$\frac{R_{\rho_\alpha}^*}{R_{\rho_\alpha}} = 0.079 \text{ (figure 6.3.1-63)}$$

$$R_{\ell\alpha}^* = R_{\ell\alpha} \left( \frac{R_{\ell\alpha}^*}{R_{\ell\alpha}} \right) = (6.11 \times 10^4)(0.079) = 4.83 \times 10^3$$

$$\frac{\delta_o}{\sqrt{x_o}} = 0.075 \text{ (figure 6.3.1-65)}$$

$$\delta_o = \sqrt{x_o} \frac{\delta_o}{\sqrt{x_o}} = \sqrt{7.0} (0.075) = 0.199 \text{ ft}$$

$$d_1 = \delta_o \left( \frac{d_1}{\delta_o} \right) = (0.199)(110) = 21.89 \text{ ft}$$

$$d_1 + x_o = 21.89 + 7.0 = 28.89 \text{ ft} > x_{HL} \text{. Try a second iteration.}$$

Second iteration (assume  $x_o = 4.0 \text{ ft}$ )

$$(R_{\ell\alpha})_{x_o} = x_o (R_{\ell\alpha}) = (4.0)(6.11 \times 10^4) = 2.444 \times 10^5$$

$$(C_{p\alpha/p})_P = 0.023 \text{ (figure 6.3.1-59)}$$

$$\frac{d_1}{\delta_o} = 230 \text{ (figure 6.3.1-61)}$$

$$\frac{\delta_o}{\sqrt{x_o}} = 0.075 \text{ (calculation to determine } \delta_o / \sqrt{x_o} \text{ is same as first iteration)}$$

$$\delta_o = \sqrt{x_o} \frac{\delta_o}{\sqrt{x_o}} = \sqrt{4.0} (0.075) = 0.150 \text{ ft}$$

$$d_1 = \delta_o \left( \frac{d_1}{\delta_o} \right) = (0.150)(230) = 34.50 \text{ ft}$$

$$d_1 + x_o = 34.50 + 4.0 = 38.50 \text{ ft} > x_{HL} \text{. Try a third iteration.}$$

Third iteration (assume  $x_o = 2.0 \text{ ft}$ )

$$(R_{\ell\alpha})_{x_o} = x_o (R_{\ell\alpha}) = (2.0)(6.11 \times 10^4) = 1.222 \times 10^5$$

$$(C_{p\alpha/p})_P = 0.0255 \text{ (figure 6.3.1-59)}$$

$$\frac{d_1}{\delta_o} = 350 \text{ (figure 6.3.1-61)}$$

$$\frac{\delta_o}{\sqrt{x_o}} = 0.075 \text{ (calculation to determine } \delta_o/\sqrt{x_o} \text{ is same as first and second iteration)}$$

$$\delta_o = \sqrt{x_o} \frac{\delta_o}{\sqrt{x_o}} = \sqrt{2.0} (0.075) = 0.106 \text{ ft}$$

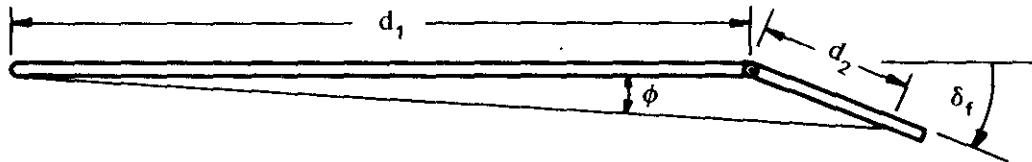
$$d_1 = \delta_o \left( \frac{d_1}{\delta_o} \right) = (0.106) (350) = 37.10 \text{ ft}$$

$$d_1 + x_o = 37.10 + 2.0 = 39.10 \text{ ft} > x_{HL}$$

The magnitudes of  $d_1$  from the iterations indicate that the region of separation extends forward to the leading edge of the plate. For this case it is assumed that the plateau-pressure region extends forward to the leading edge. Then,  $d_1 = x_{HL}$  and  $\ell_{f_i} = 0$  (see sketch (d)).

Define the windward pressure distribution:

Assume the plateau pressure corresponds to the wedge pressure for a local flow deflection angle of  $\phi$  degrees as illustrated below.



Then, by using  $d_1$ ,  $d_2$ , and  $\delta_f$  the angle  $\phi$  can be defined. Knowing  $\phi$  the plateau-pressure level is obtained by using oblique-shock relations.

Assume  $d_1 = x_{HL} = 8.0 \text{ ft}$

$$\frac{c_f}{d_1} = \frac{2.0}{8.0} = 0.25 \leq 0.25; \text{ therefore, } \frac{d_2}{\sqrt{(c_f)(d_1)}} = 2 \frac{d_2}{d_1} = 0.475 \text{ (figure 6.3.1-69)}$$

$$d_2 = \frac{0.475 d_1}{2} = 1.90 \text{ ft}$$

$$\phi = \tan^{-1} \frac{d_2 \sin \delta_f}{d_1 + d_2 \cos \delta_f} = \tan^{-1} \frac{(1.90)(0.174)}{8.0 + (1.90)(0.985)}$$

$$= \tan^{-1} 0.0335 = 1.9^\circ$$

$$\theta = 7.25^\circ (\theta \text{ is obtained from figure 4.4.1-81 at } M_\alpha = 9.8 \text{ and } \phi = |\delta'|)$$

$$\frac{P_p}{P_\alpha} = \frac{7M_\alpha^2 \sin^2 \theta - 1}{6} \quad (\text{equation 6.3.1-e})$$

$$= \frac{7(9.8)^2 (\sin 7.25^\circ)^2 - 1}{6} = 1.62$$

$$(C_{p\alpha})_p = \frac{(P_p/P_\alpha) - 1}{\frac{\gamma}{2} M_\alpha^2} \quad (\text{equation 6.3.1-f})$$

$$= \frac{(1.62) - 1}{\frac{1.4}{2} (9.8)^2}$$

$$= 0.00922$$

$$(C_{p\infty})_p = (C_{p\alpha})_p \left( \frac{M_\alpha}{M_\infty} \right)^2 \frac{P_\alpha}{P_\infty} + (C_{p\infty})_\alpha \quad (\text{equation 6.3.1-d})$$

$$= (0.00922) \left( \frac{9.8}{20.0} \right)^2 (21) + 0.071 = 0.117$$

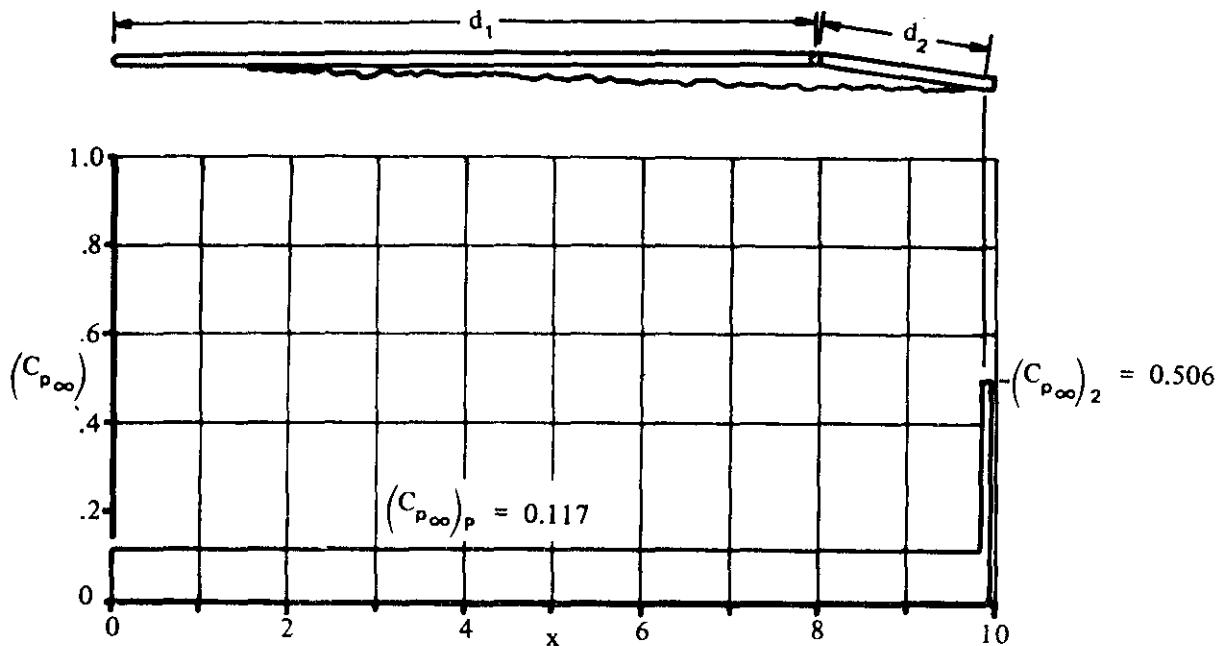
$$\left( \frac{d_3}{d_1} \right) = 0.250 \quad (\text{figure 6.3.1-71})$$

$$d_3 = d_1 \left( \frac{d_3}{d_1} \right) = (8.0)(0.25) = 2.0 \text{ ft. However, } d_3 \text{ must be less than or equal to } d_2 \\ (\text{see sketch (d)}). \text{ Therefore, let } d_3 = d_2 = 1.90 \text{ ft}$$

$$(C_{p\infty})_2 = (C_{p\alpha})_2 \left( \frac{M_\alpha}{M_\infty} \right)^2 \frac{P_\alpha}{P_\infty} + (C_{p\infty})_\alpha \quad (\text{equation 6.3.1-g})$$

$$= (0.0863) \left( \frac{9.8}{20.0} \right)^2 (21) + 0.071 = 0.506$$

The windward pressure distribution is illustrated in the following sketch. The solutions for the force and moment increments are not shown, since the use of equations 6.3.1-h through 6.3.1-o is illustrated in sample problem 1.



## REFERENCES

1. Popinski, Z., and Ehrlich, C.F.: Development of Design Methods for Predicting Hypersonic Aerodynamic Control Characteristics. AFFDL-TR-66-85, 1966. (U)
2. Kaufman, L.G., II, Oman, R.A., Hartofilis, S.A., et al: A Review of Hypersonic Flow Separation and Control Characteristics. ASD-TDR-62-168, 1962. (U)
3. Wuerer, J.E., et al: Flow Separation In High-Speed Flight, A Review of the State-of-the-Art. Douglas Aircraft Co., Report SM-46429, 1965. (U)
4. Schlichting, H.: Boundary-Layer Theory. McGraw-Hill Book Co., New York, 1955. (U)
5. Modern Developments in Fluid Dynamics – High-Speed Flow. Edited by L. Howarth, Vol. I, Oxford University Press, 1953. (U)
6. Chapman, D.R., Kuehn, D., and Larson, H.K.: Investigation of Separated Flows in Supersonic and Transonic Streams with Emphasis on the Effects of Transition. NACA TR 1356, 1958. (U)
7. Sterrett, J.R., and Emery, J. C.: Extension of Boundary-Layer-Separation Criteria to a Mach Number of 6.5 by Utilizing Flat Plates With Forward-Facing Steps. NASA TN D-618, 1960. (U)
8. Hammitt, A.G.: The Interaction of Shock Waves and Turbulent Boundary Layers. JAS, Vol. 25, No. 6, 1958. (U)
9. Lange, R.H.: Present Status of Information Relative to the Prediction of Shock-Induced Boundary-Layer Separation. NACA TN 3065, 1954. (U)
10. Reshotko, E., and Tucker, M.: Effect of a Discontinuity on Turbulent Boundary-Layer-Thickness Parameters with Application to Shock-Induced Separation. NACA TN 3454, 1955. (U)
11. Drougge, G.: An Experimental Investigation of the Influence of Strong Adverse Pressure Gradients on Turbulent Boundary Layers at Supersonic Speeds. Aero. Res. Inst. of Sweden, Report No. 46, 1953. (U)
12. Love, E.S.: Pressure Rise Associated with Shock-Induced Boundary Layer Separation. NACA TN 3601, 1955. (U)
13. Shapiro, A.H.: The Dynamics and Thermodynamics of Compressible Fluid Flow. Vol. II, The Ronald Press Co., New York, 1954. (U)

14. Schuh, H.: On Determining Turbulent Boundary-Layer Separation in Incompressible and Compressible Flow. JAS, Vol. 22, No. 5, 1955. (U)
15. Chapman, D.R.: A Theoretical Analysis of Heat Transfer in Regions of Separated Flows. NACA TN 3792, 1956. (U)
16. Larson, H.K.: Heat Transfer in Separated Flows. JAS, Vol. 26, No. 11, 1959. (U)
17. Cohen, C.B., and Reshotko, E.: Similar Solutions for the Compressible Laminar Boundary Layer With Heat Transfer and Pressure Gradient. NACA TR 1293, 1956. (U)
18. Cohen, C.B., and Reshotko, E.: The Compressible Laminar Boundary Layer With Heat Transfer and Arbitrary Pressure Gradient. NACA TR 1294, 1956. (U)
19. Gadd, G.E.: The Numerical Integration of the Laminar Compressible Boundary-Layer Equations, With Special Reference to the Position of Separation When the Wall is Cooled. ARC 15101, FM1771, 1952. (U)
20. Gadd, G.E.: A Theoretical Investigation of the Effects of Mach Number, Reynolds Number, Wall Temperature and Surface Curvature on Laminar Separation in Supersonic Flow. ARC 18449, 1956. (U)
21. Gadd, G.E.: A Review of Theoretical Work Relevant to the Problem of Heat-Transfer Effects on Laminar Separation. ARC 18495, 1956. (U)
22. Illingworth, C.R.: The Effect of Heat Transfer on the Separation of a Compressible Laminar Boundary Layer. Quart. Fluid Mech. & Appl. Math. 7, 8, 1954. (U)
23. Morduchow, M., and Grage, R.G.: Separation Stability and Other Properties of Compressible Laminar Boundary Layer With Pressure Gradient and Heat Transfer. NACA TN 3296, 1955. (U)
24. Sogin, H.H., Burkhard, K., and Richardson, P.D.: Heat Transfer in Separated Flows – Part I: Preliminary Experiments on Heat Transfer From an Infinite Bluff Plate to an Air Stream. Part II: Survey on Separated Flows With Special Reference to Heat Transfer. Aeronautical Research Lab., Melbourne, ARL-4, 1961. (U)
25. Kuo, Y.H.: Dissociation Effects in Hypersonic Viscous Flows. JAS, Vol. 24, No. 5, 1957. (U)
26. Gadd, G.E.: An Experimental Investigation of Heat Transfer Effects on Boundary Layer Separation in Supersonic Flow. Jour. Fluid Mech., Vol. 2, Part 2, 1957. (U)
27. Gadd, G.E., and Holder, D.W.: The Behavior of Supersonic Boundary Layers in the Presence of Shock Waves. IAS Paper 59-138, 1959. (U)
28. Gadd, G.E.: Boundary Layer Separation in the Presence of Heat Transfer. AGARD Rpt. 280, 1960. (U)
29. Bertram, M.H., and Cook, B.S.: The Correlation of Oblique Shock Parameters for Ratios of Specific Heats From 1 to 5/3 With Application to Real Gas Flows. NASA TR R-171, 1963. (U)
30. Deem, R.E., and Murphy, J.S.: Flat-Plate Boundary-Layer Transition at Hypersonic Speeds. AIAA Paper No. 65-128, 1965. (U)
31. Moeckel, W.E.: Some Effects of Bluntness on Boundary-Layer Transition and Heat Transfer at Supersonic Speeds. NACA TR 1312, 1957. (U)
32. Abbott, D. E., Holt, M., and Neilsen, J. N.: Investigation of Hypersonic Flow Separation and Its Effects on Aerodynamic Control Characteristics. ASD-TDR-62-963, 1962. (U)
33. Nielsen, J. N., Lynes, L. L., and Goodwin, F. K.: Calculation of Laminar Separation with Free Interaction by the Method of Integral Relations, Part II – Two-Dimensional Supersonic Nonadiabatic Flow and Axisymmetric Supersonic Adiabatic and Nonadiabatic Flows. AFFDL-TR-65-107, 1966. (U)

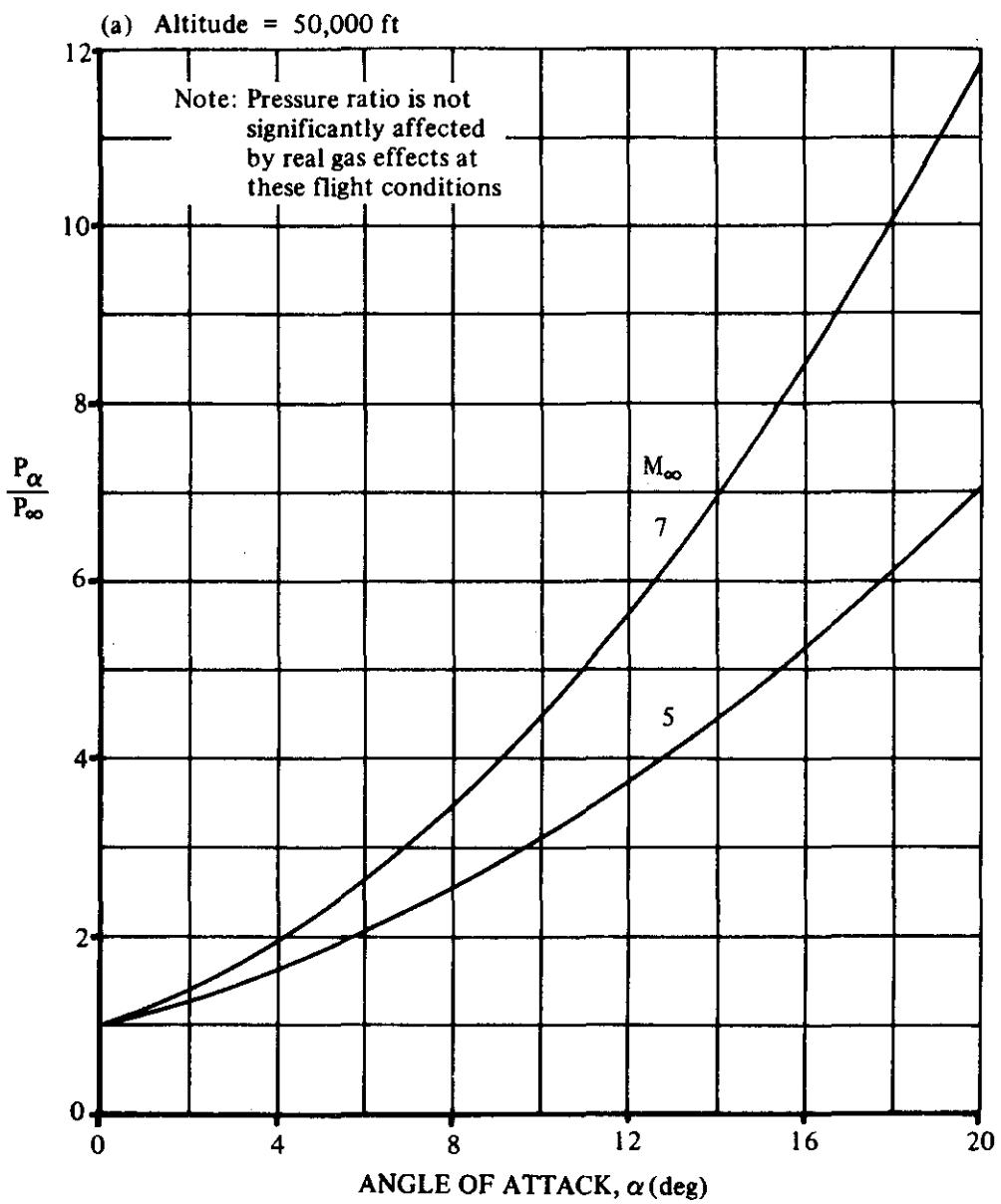


FIGURE 6.3.1-31 OBLIQUE SHOCK PRESSURE RATIO INCLUDING REAL GAS EFFECTS

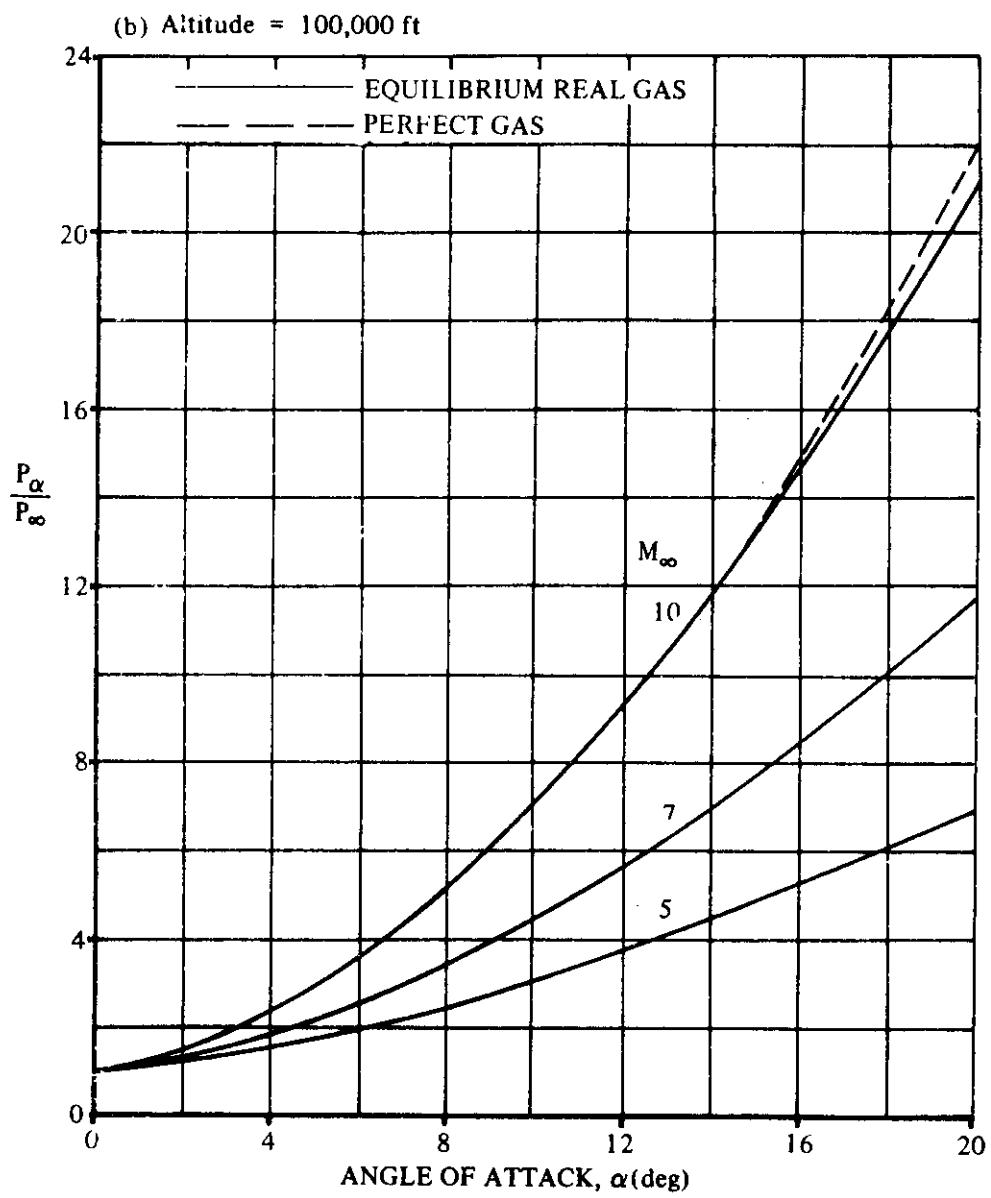


FIGURE 6.3.1-31 (CONTD)

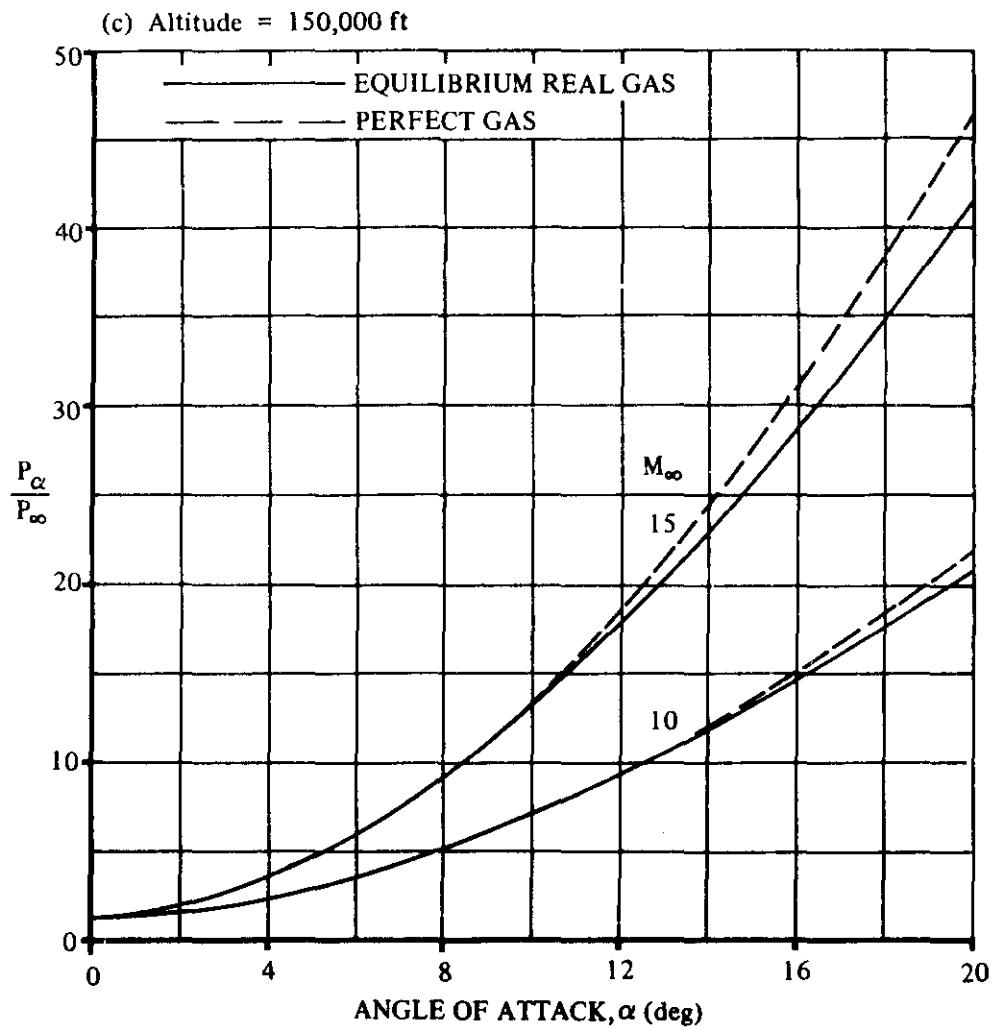


FIGURE 6.3.1-31 (CONTD)

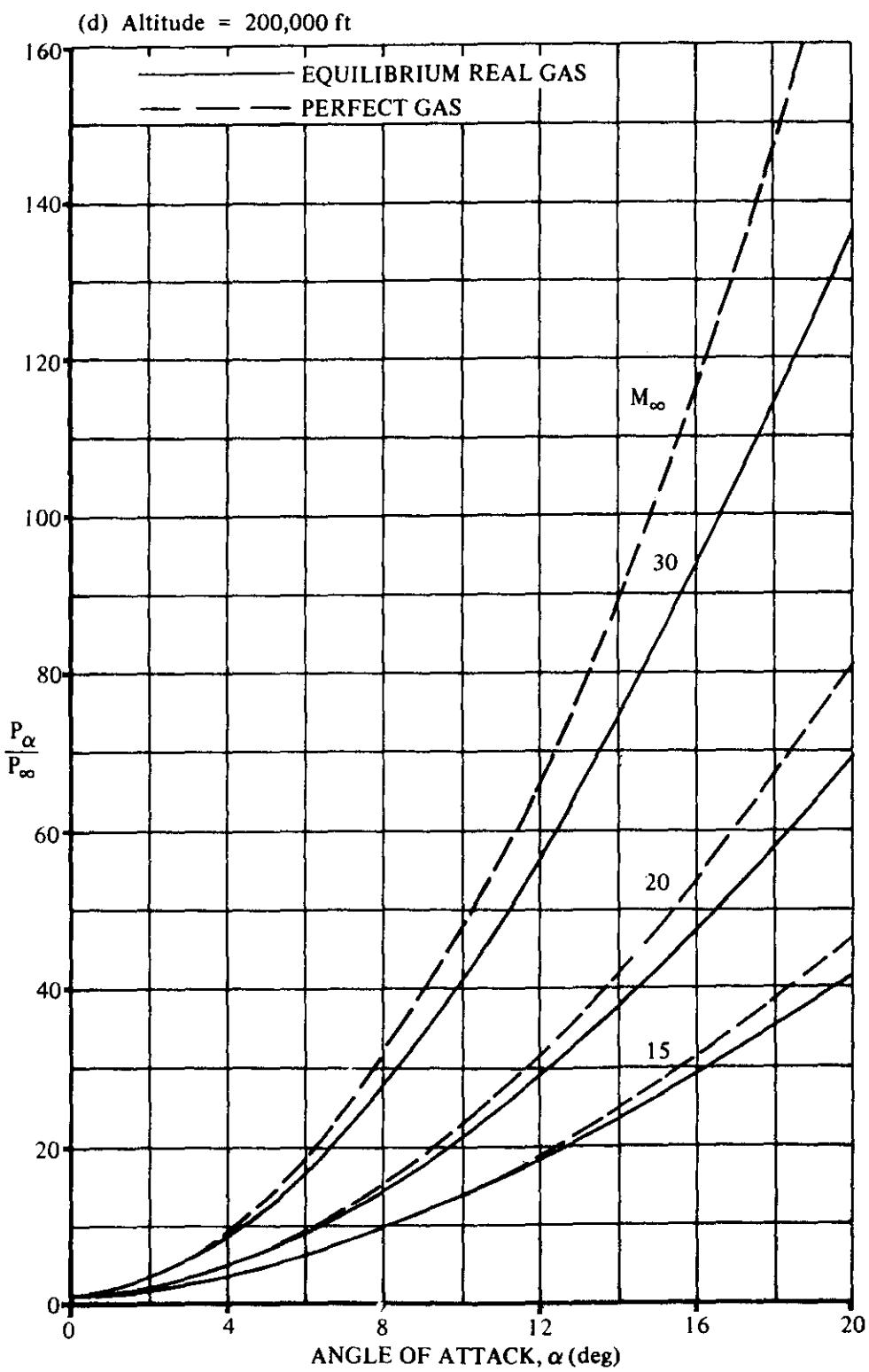


FIGURE 6.3.1-31 (CONTD)

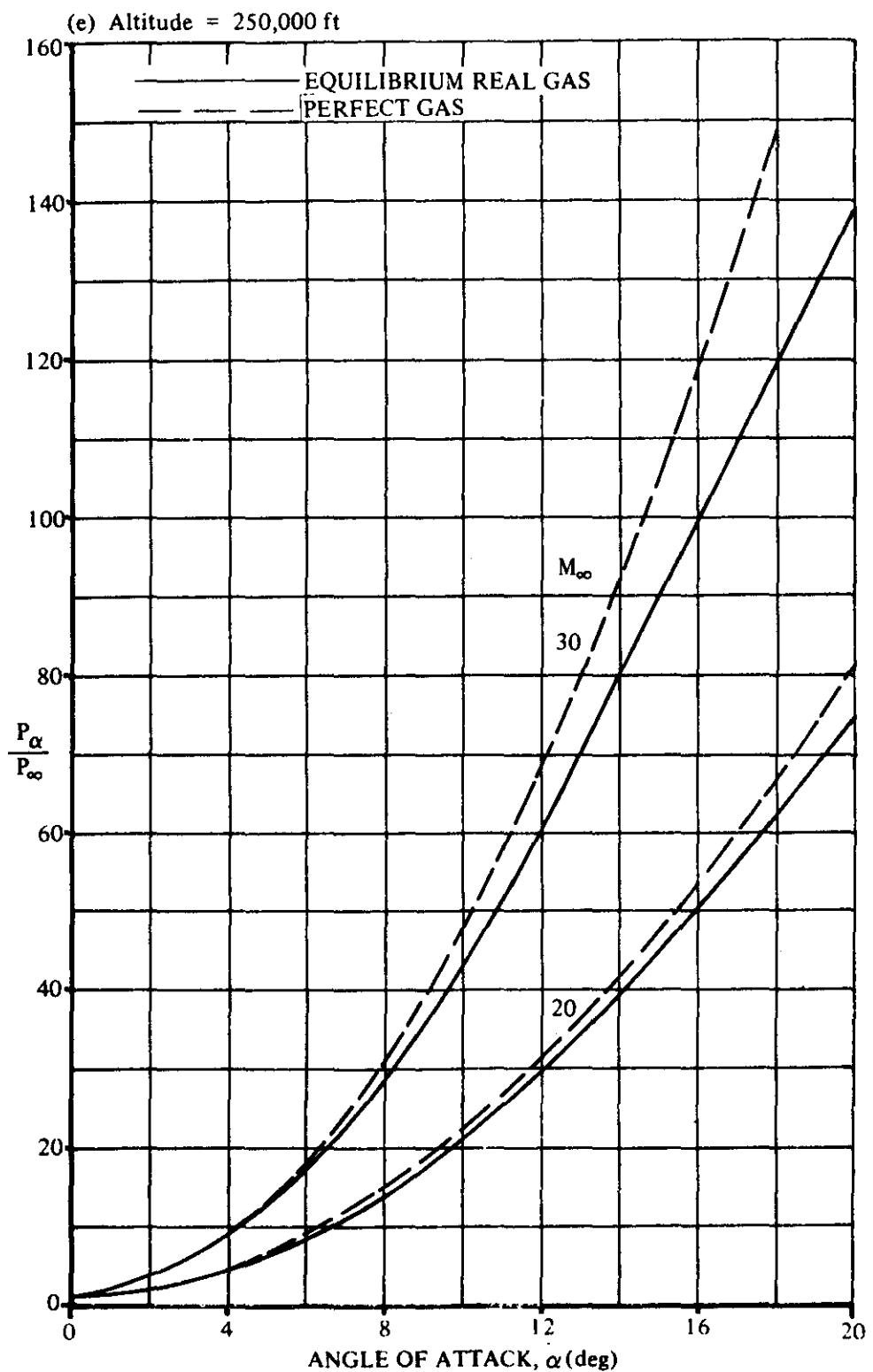


FIGURE 6.3.1-31 (CONTD)

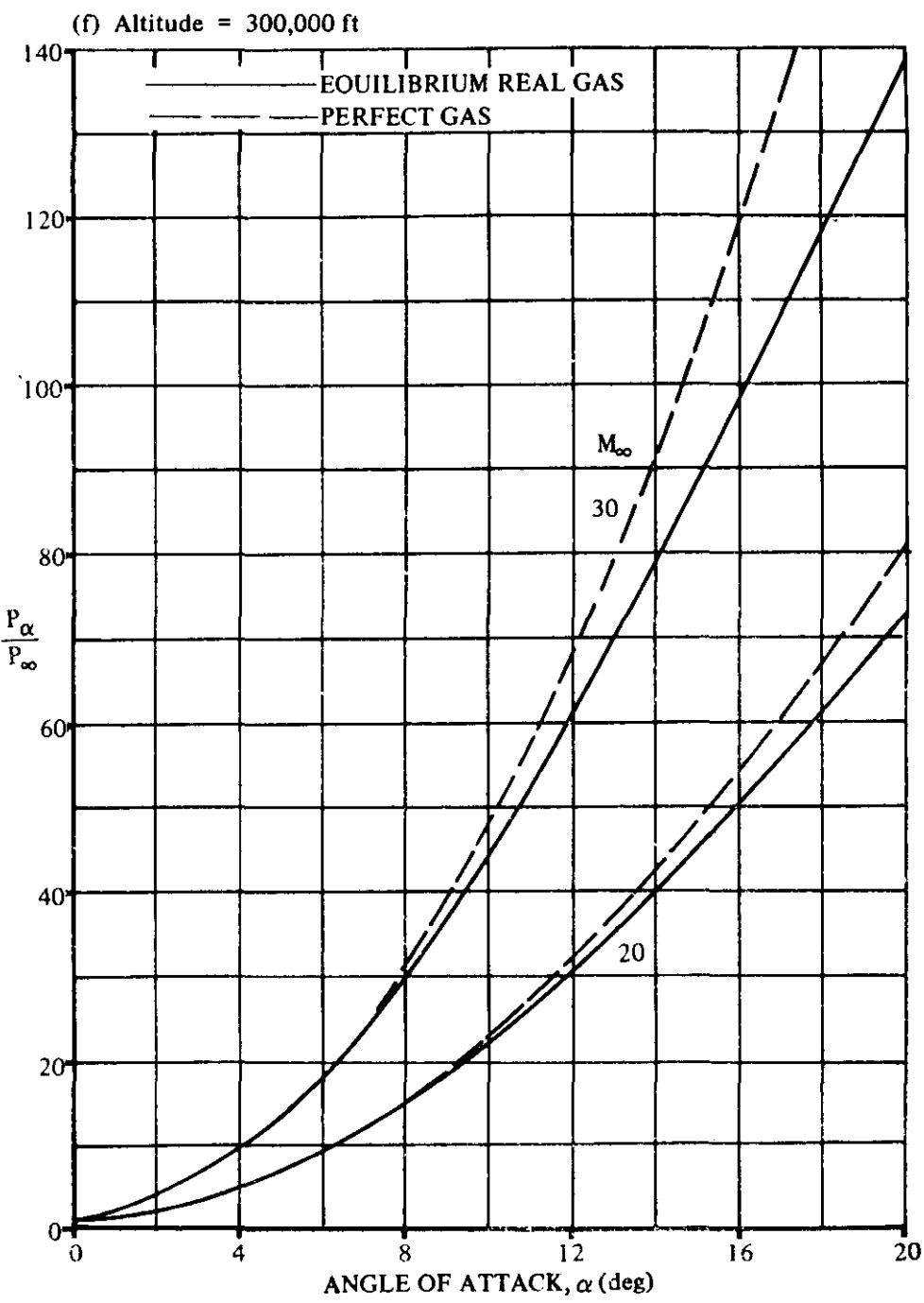


FIGURE 6.3.1-31 (CONTD)

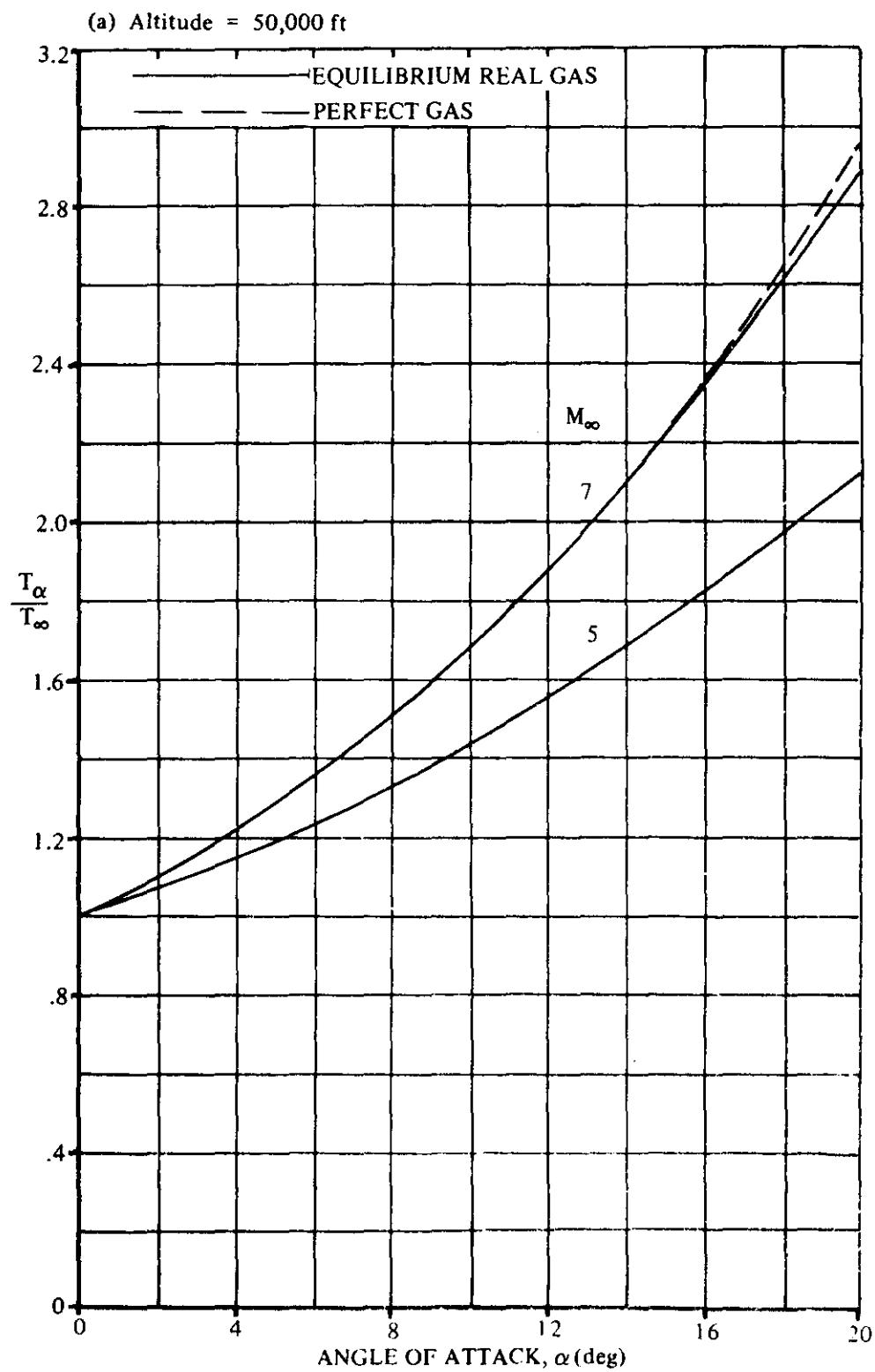


FIGURE 6.3.1-37 OBLIQUE SHOCK TEMPERATURE RATIO INCLUDING REAL GAS EFFECTS

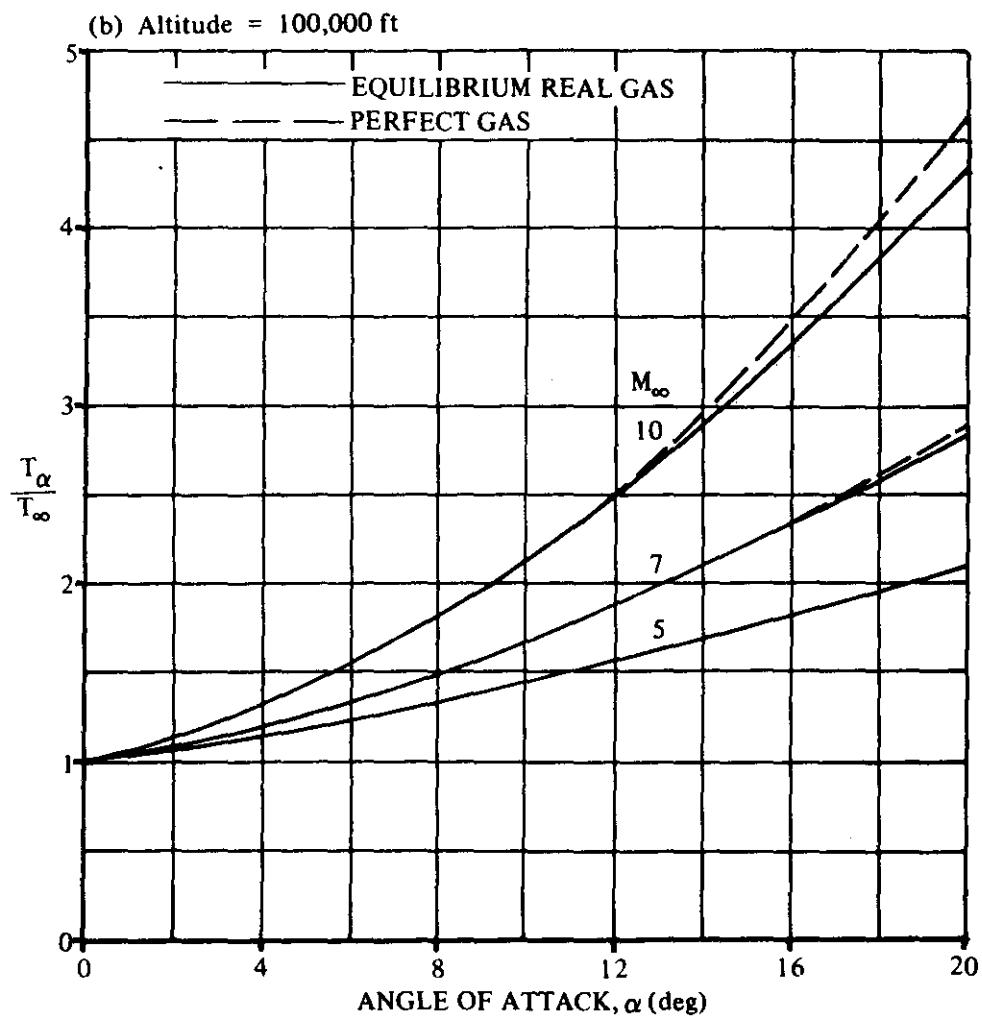


FIGURE 6.3.1-37 (CONTD)

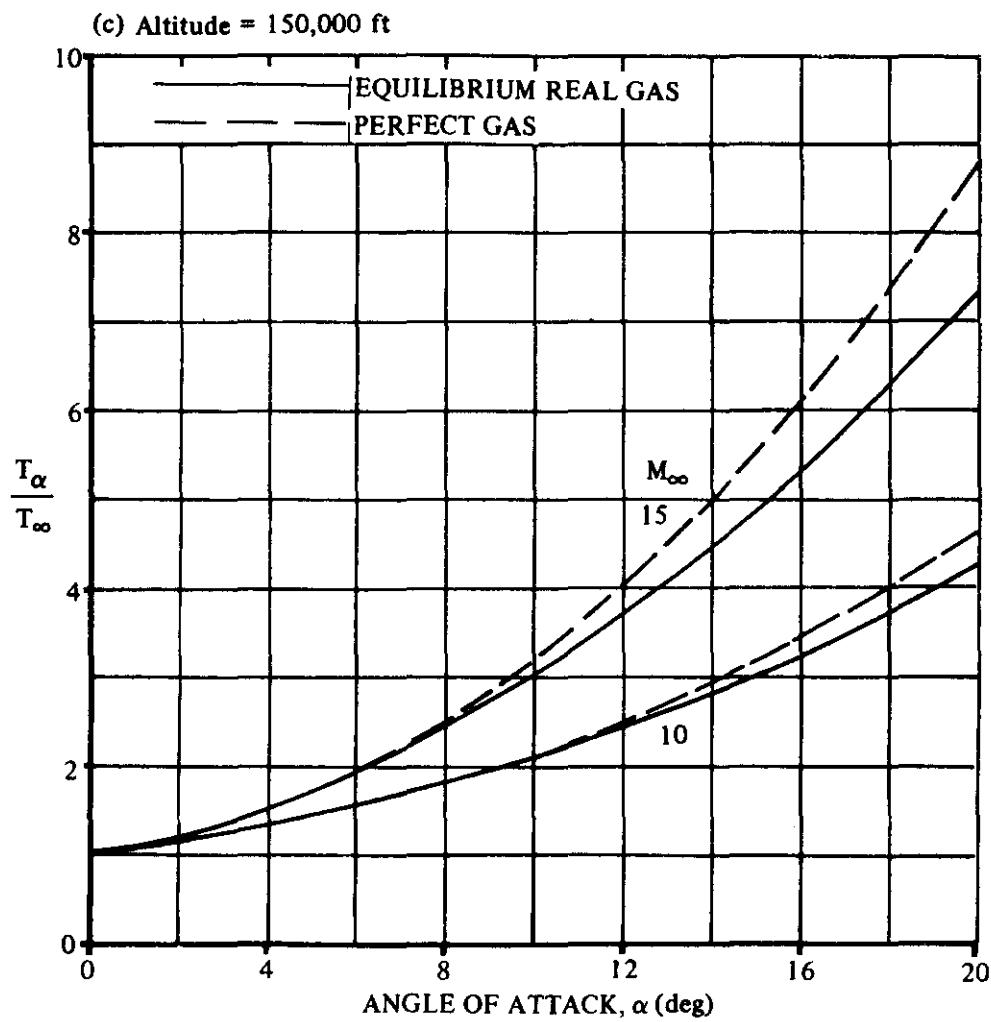


FIGURE 6.3.1-37 (CONTD)

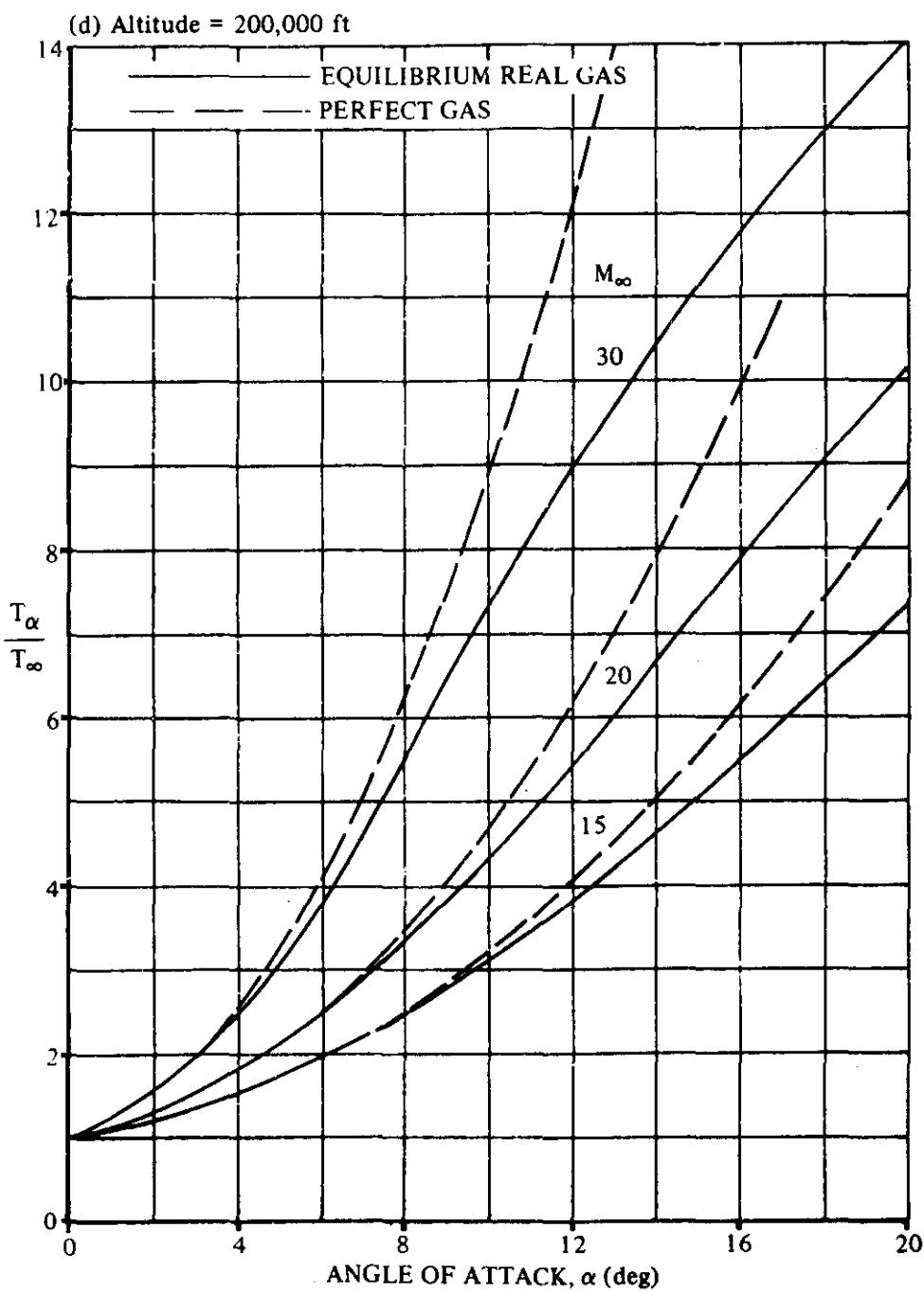


FIGURE 6.3.1-37 (CONTD)

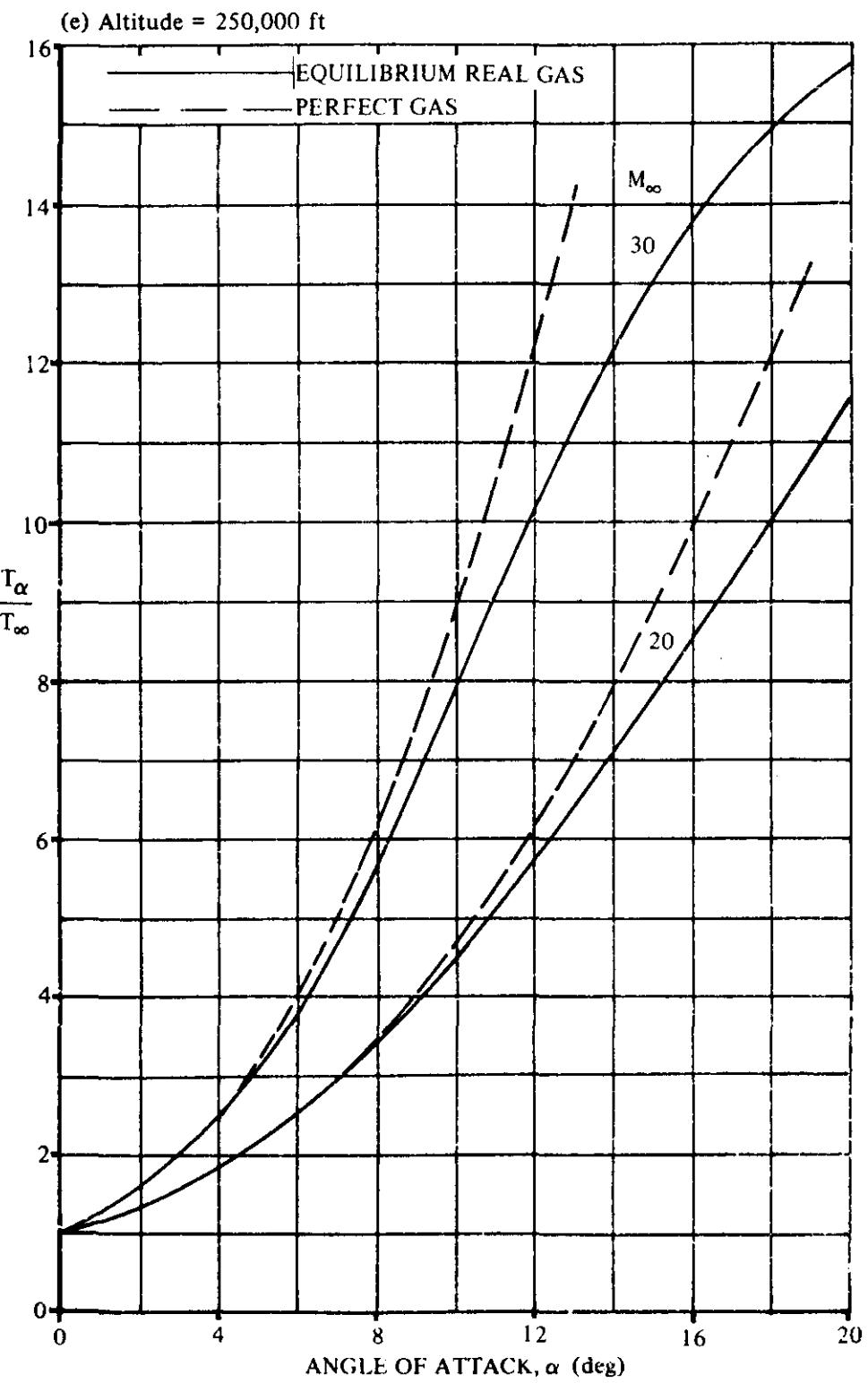


FIGURE 6.3.1-37 (CONTD)

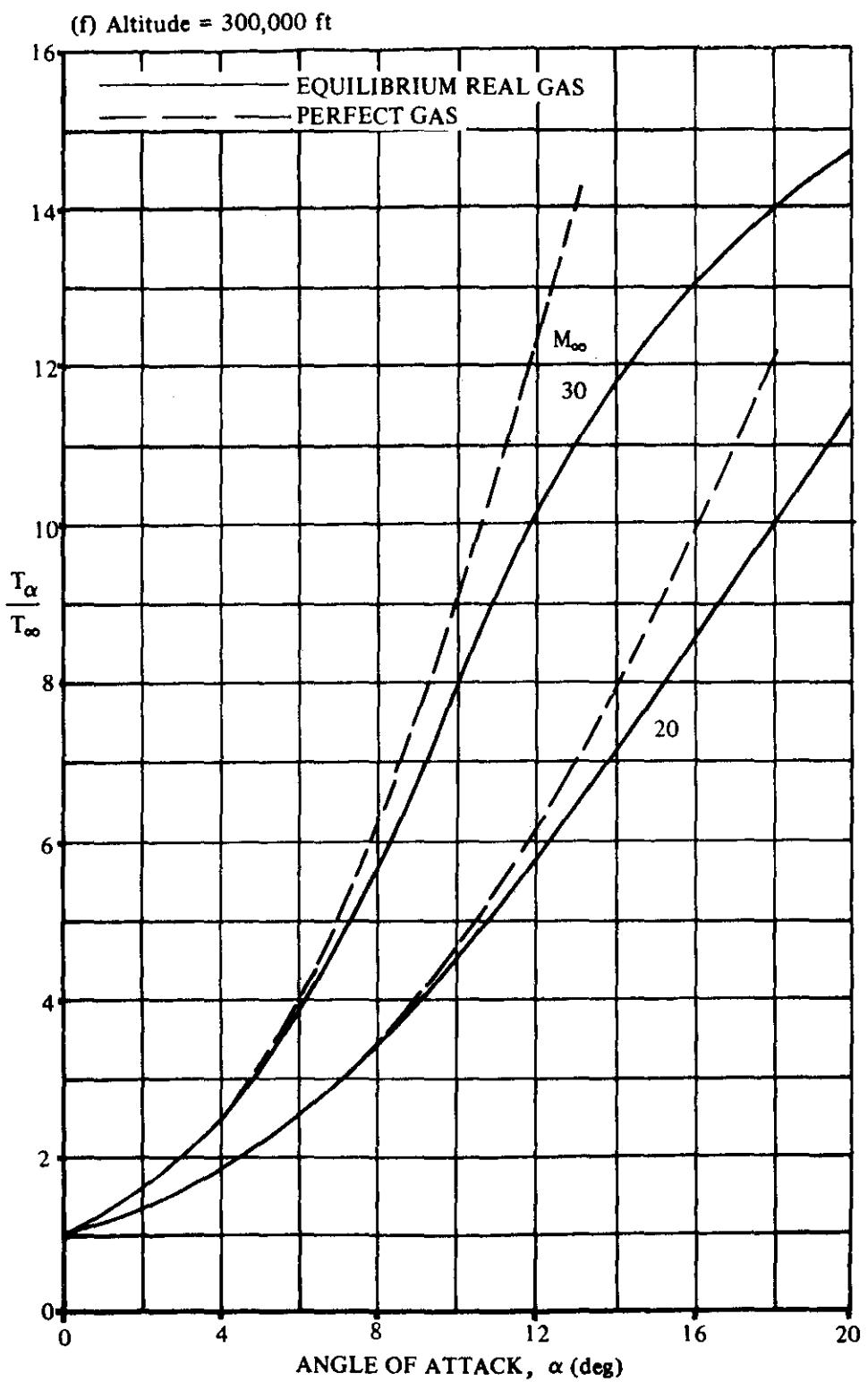


FIGURE 6.3.1-37 (CONTD)

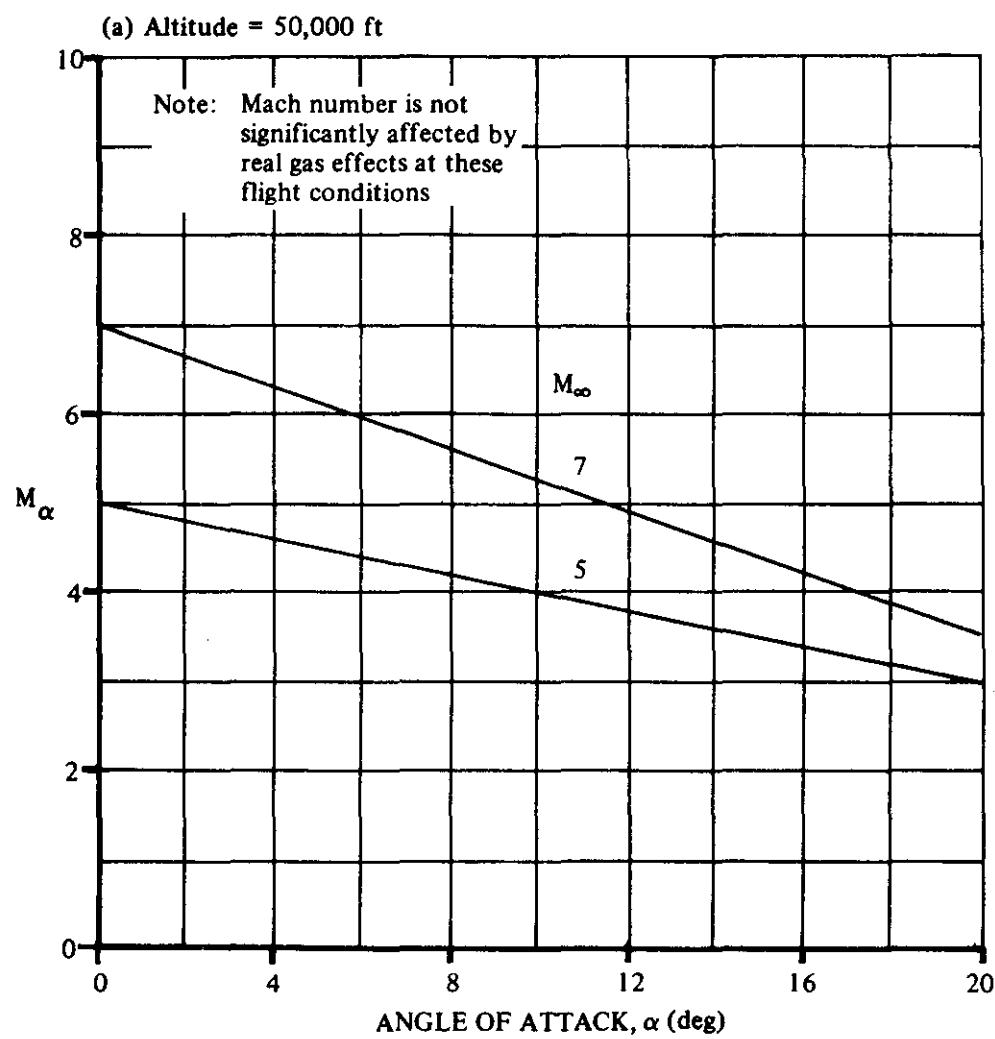


FIGURE 6.3.1-43 MACH NUMBER BEHIND AN OBLIQUE SHOCK INCLUDING REAL GAS EFFECTS

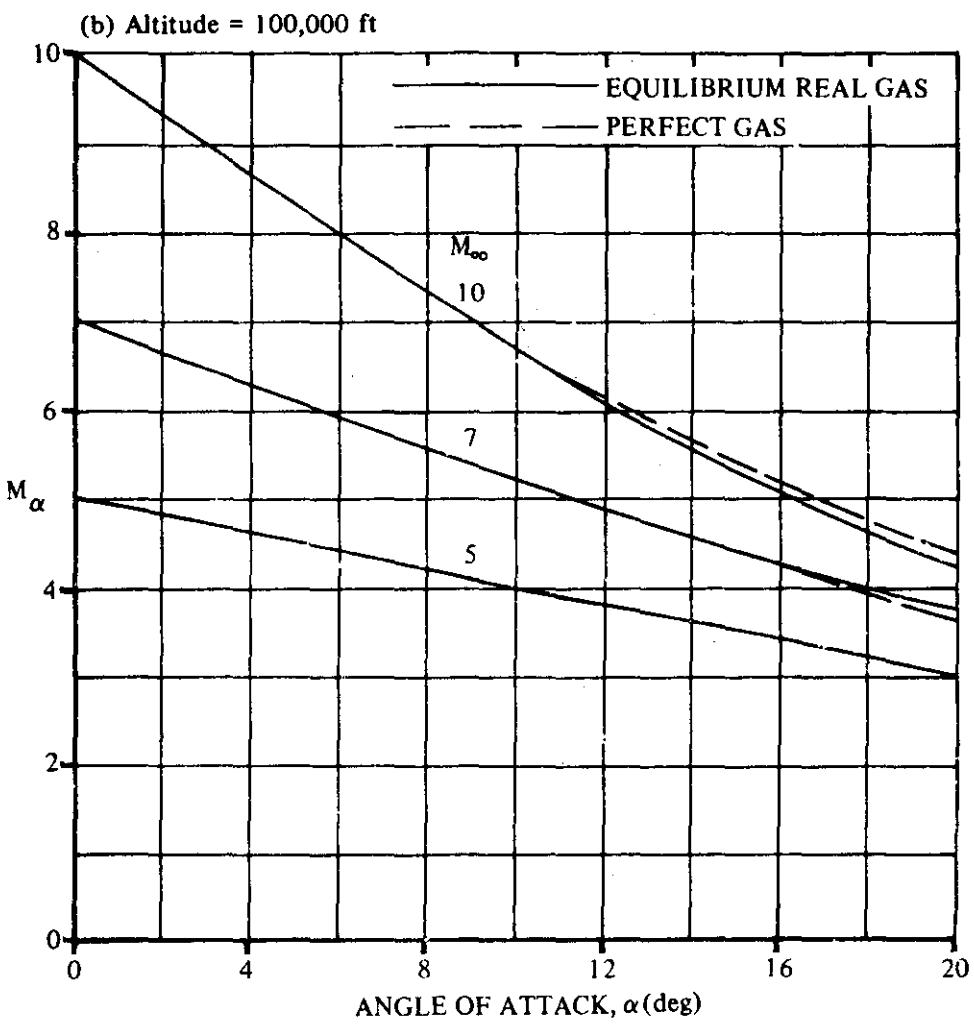


FIGURE 6.3.1-43 (CONTD)

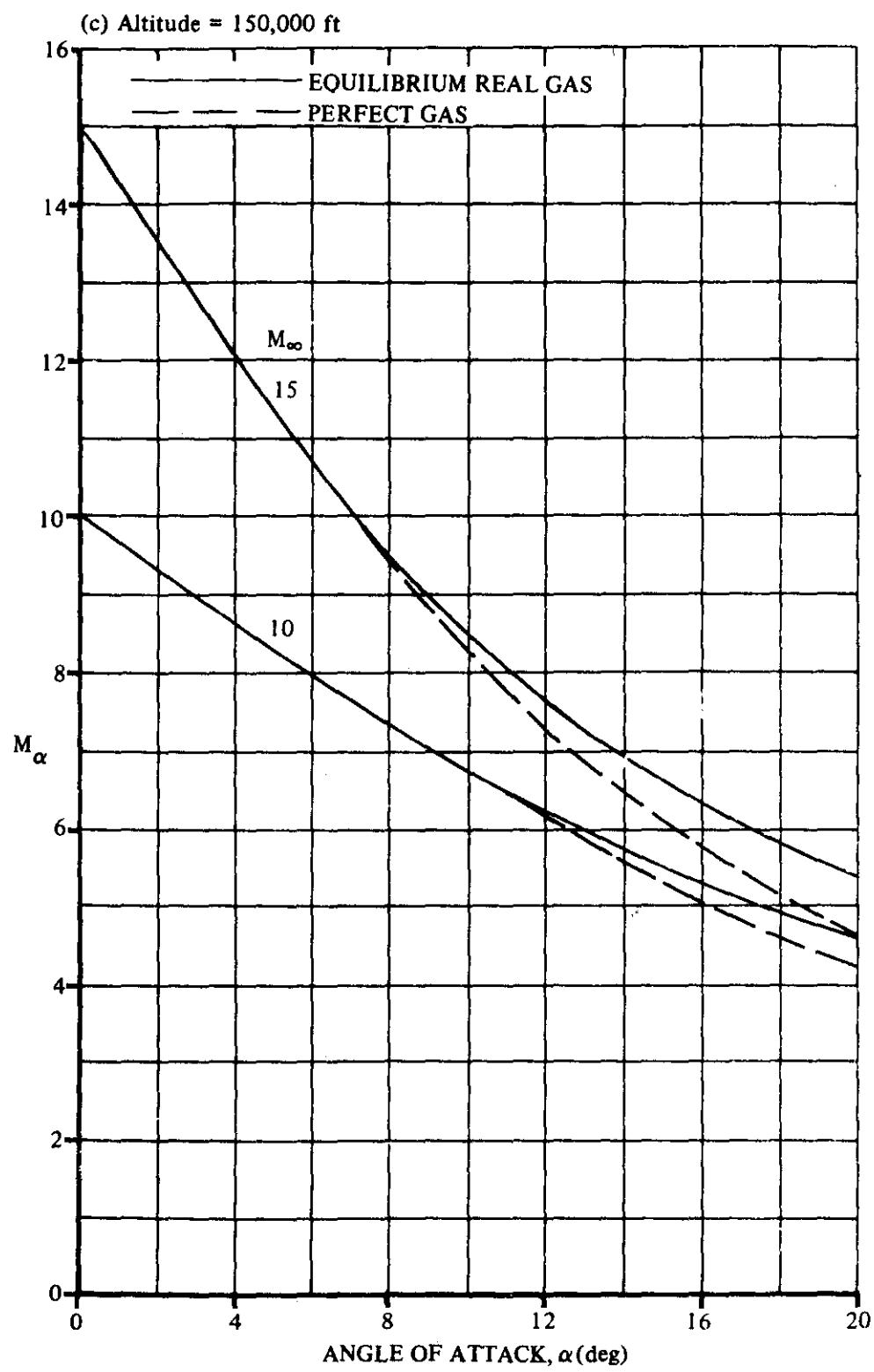


FIGURE 6.3.1-43 (CONTD)

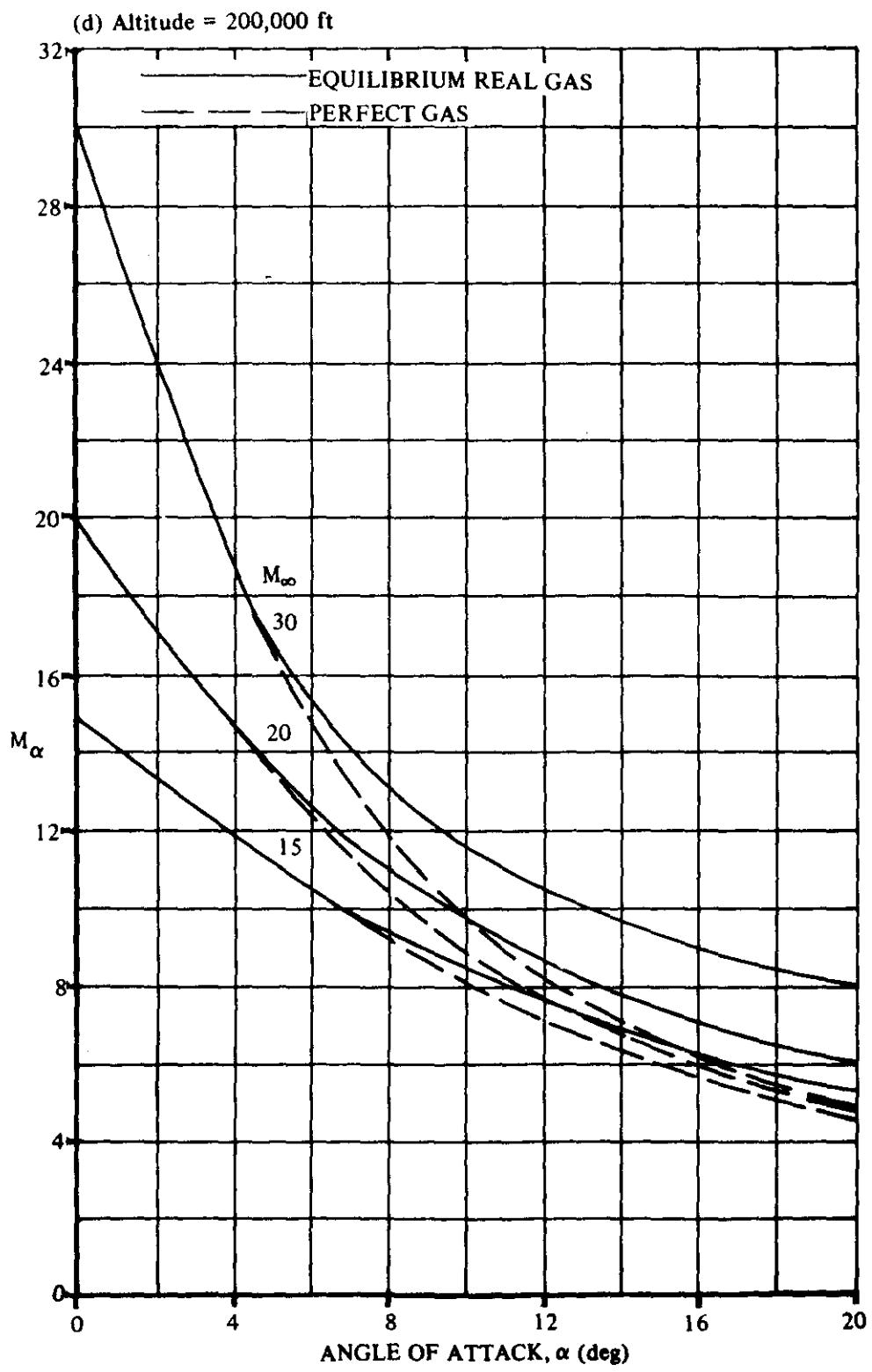


FIGURE 6.3.1-43 (CONTD)

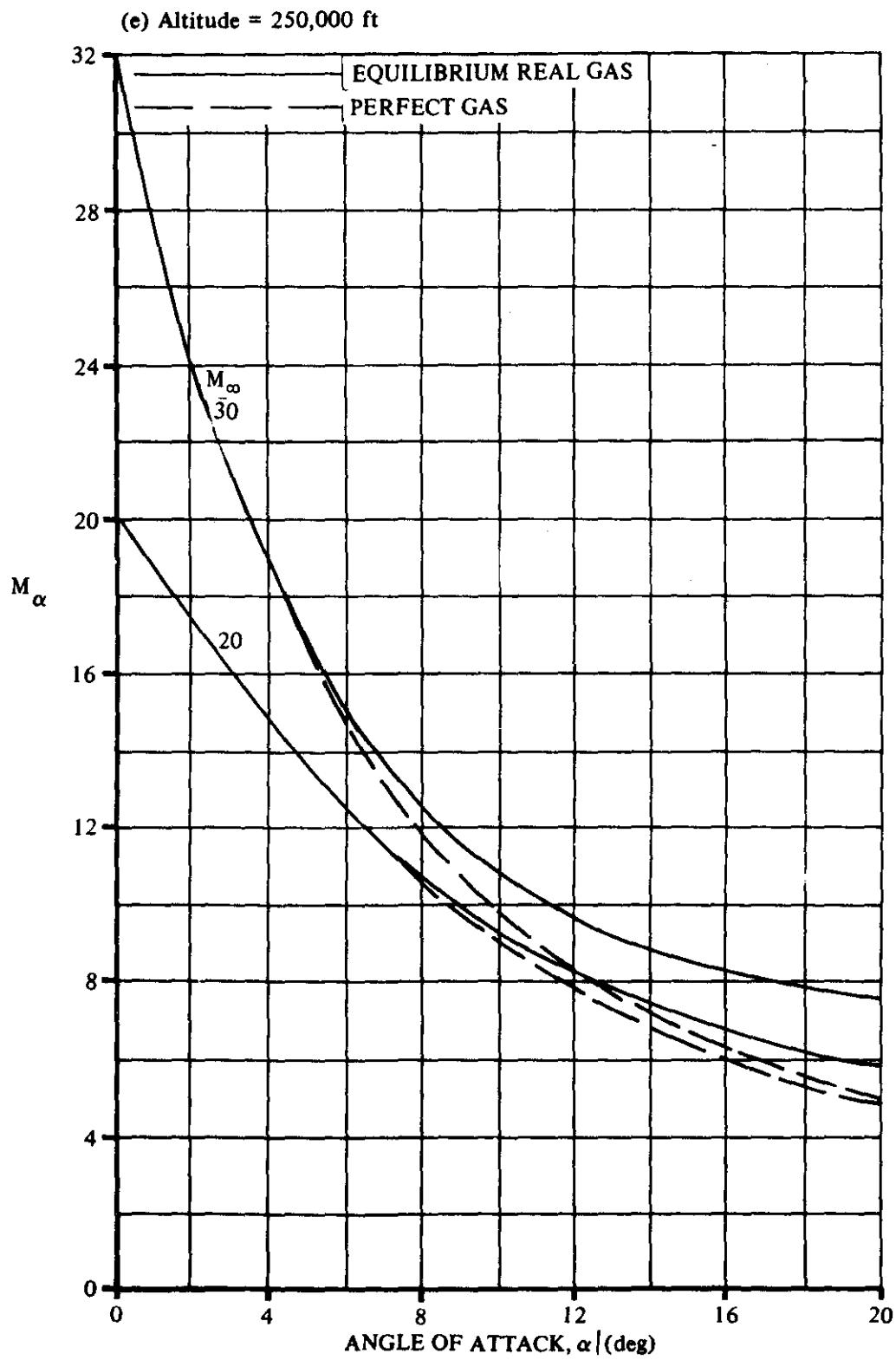


FIGURE 6.3.1-43 (CONTD)

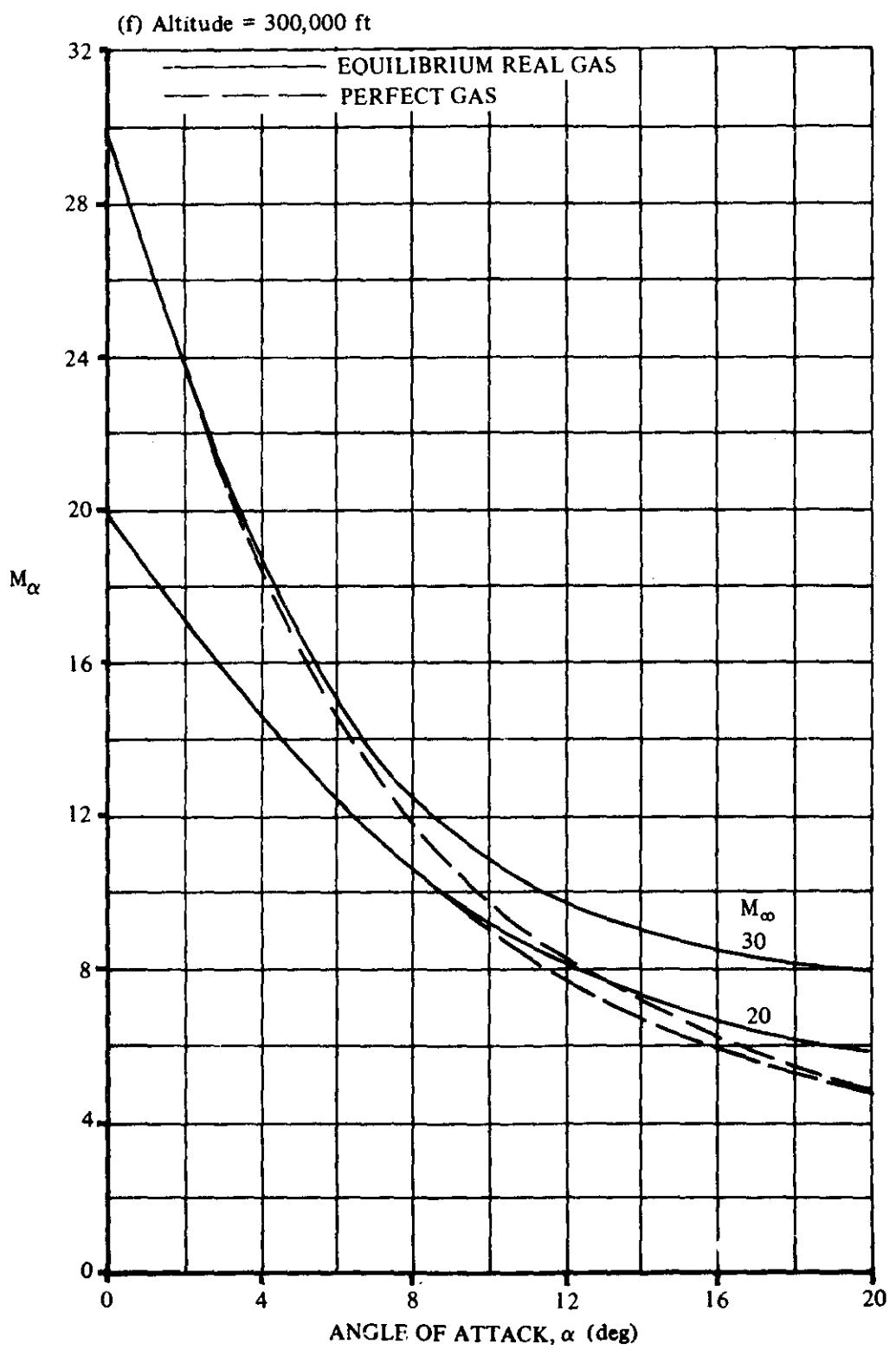


FIGURE 6.3.1-43 (CONTD)

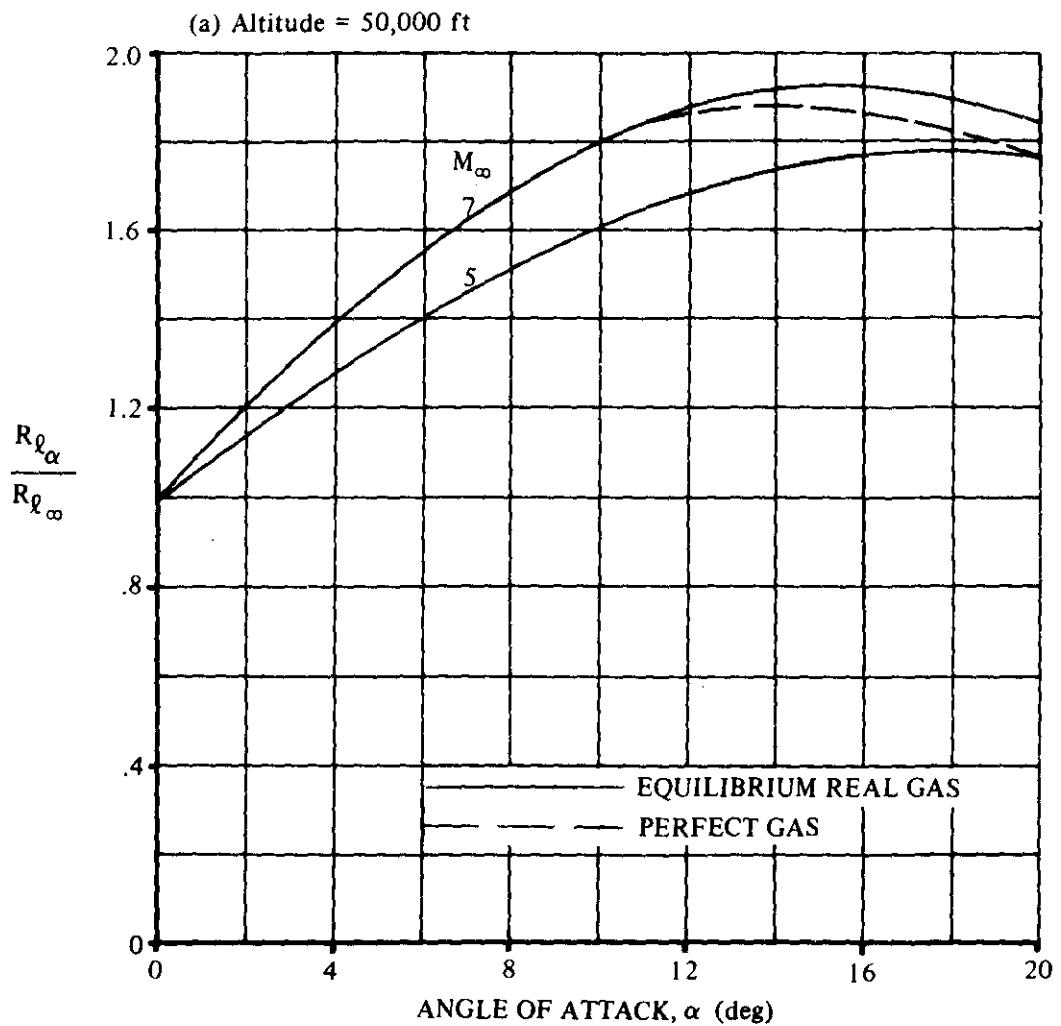


FIGURE 6.3.1-49 OBLIQUE SHOCK REYNOLDS-NUMBER RATIO INCLUDING REAL GAS EFFECTS

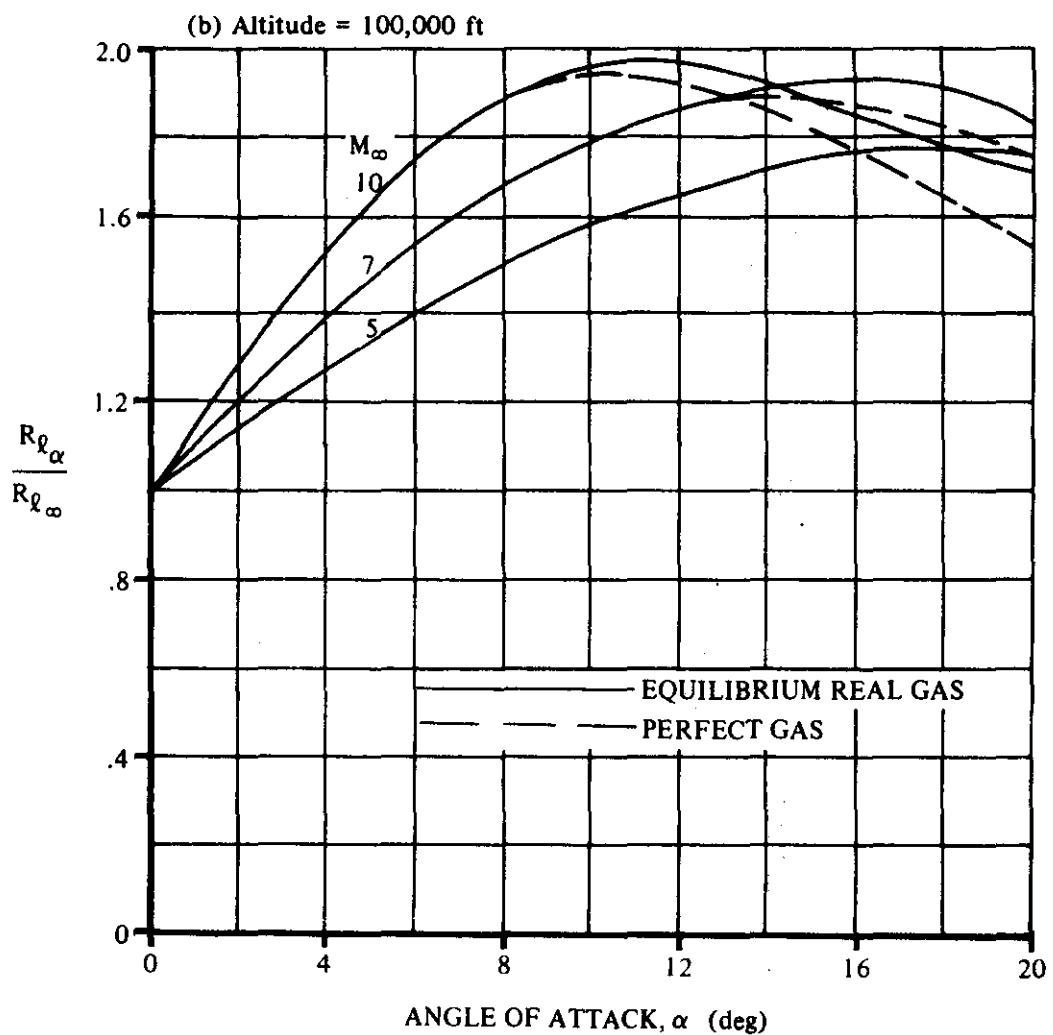


FIGURE 6.3.1-49 (CONTD)

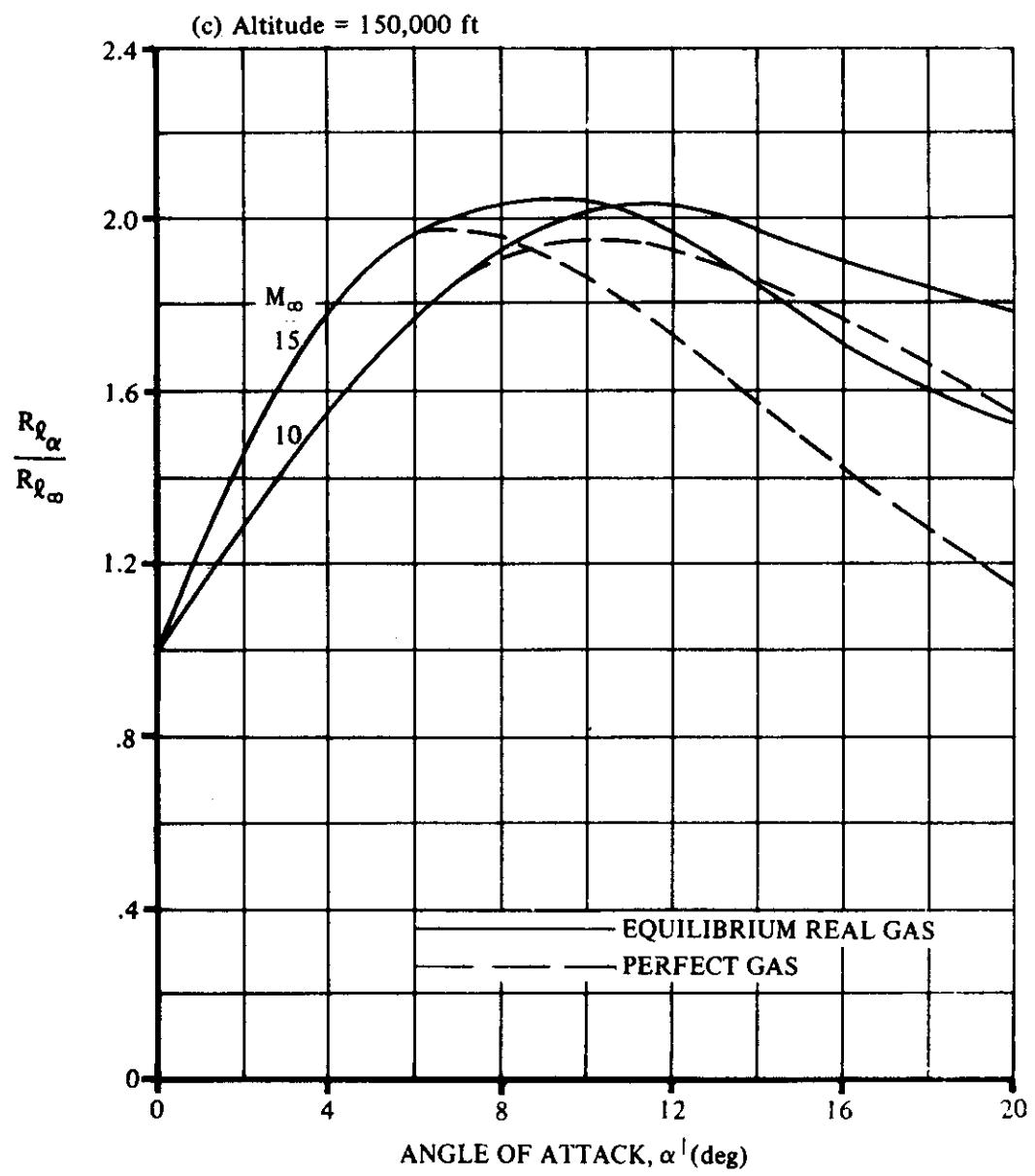


FIGURE 6.3.1-49 (CONTD)

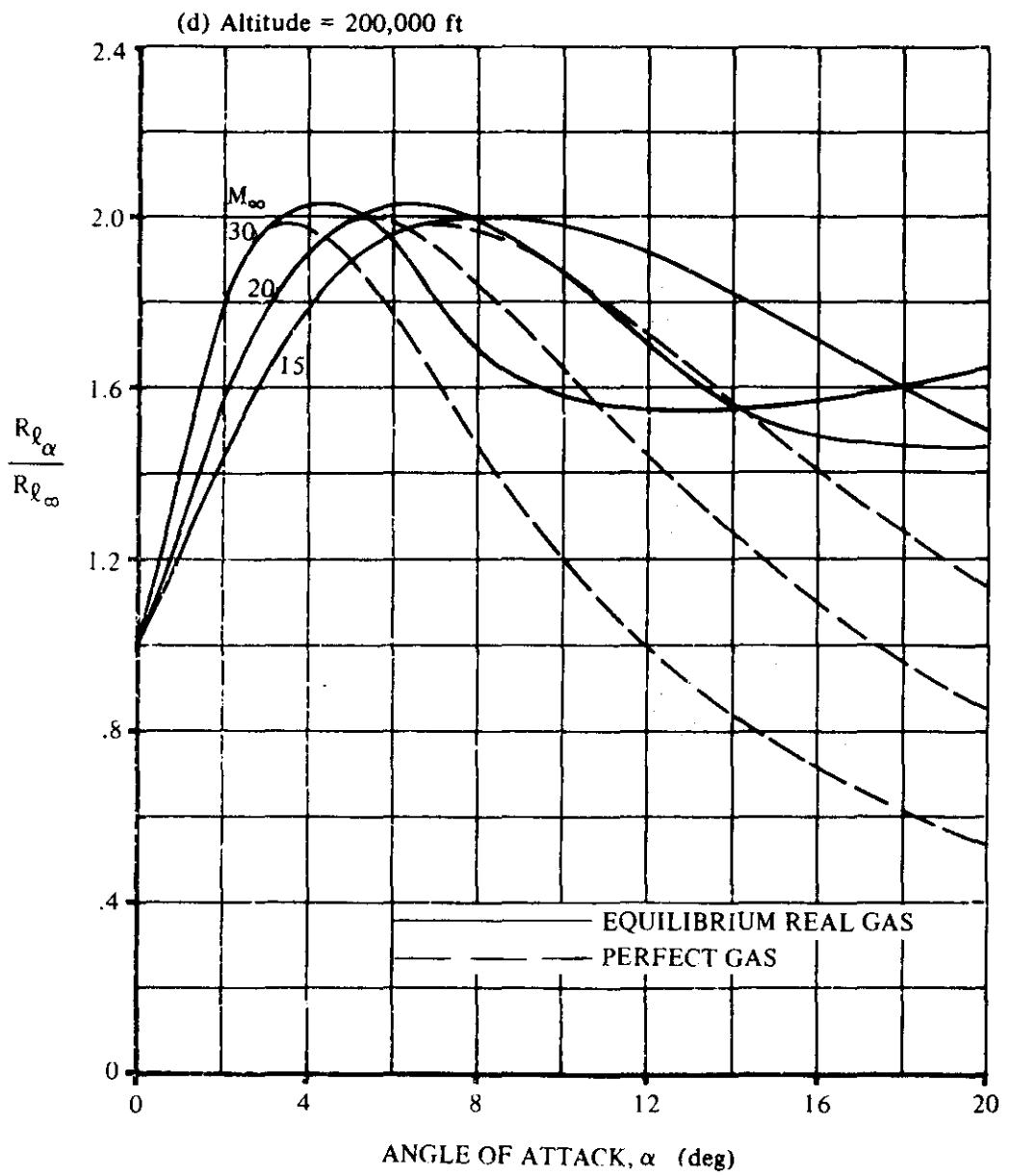


FIGURE 6.3.1-49 (CONT'D)

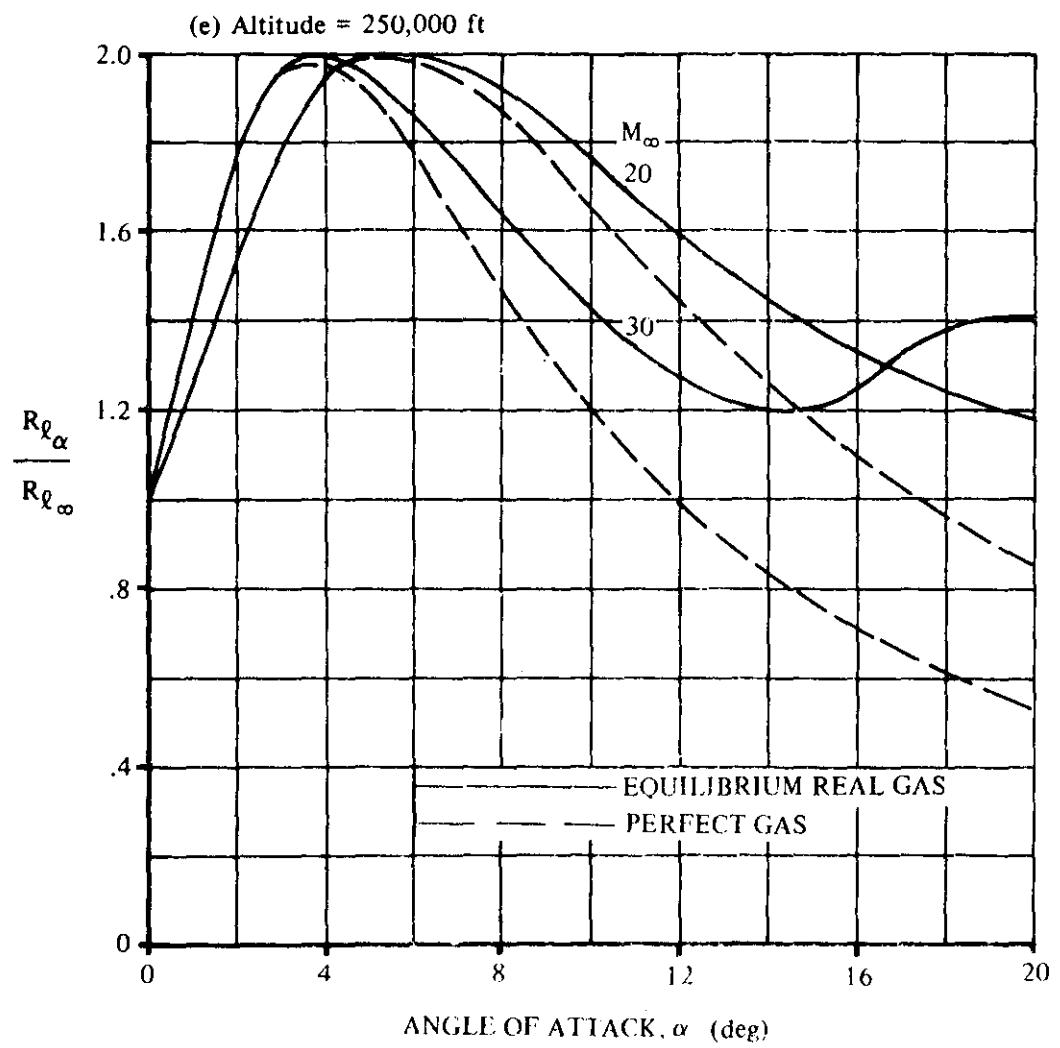


FIGURE 6.3.1-49 (CONT'D)

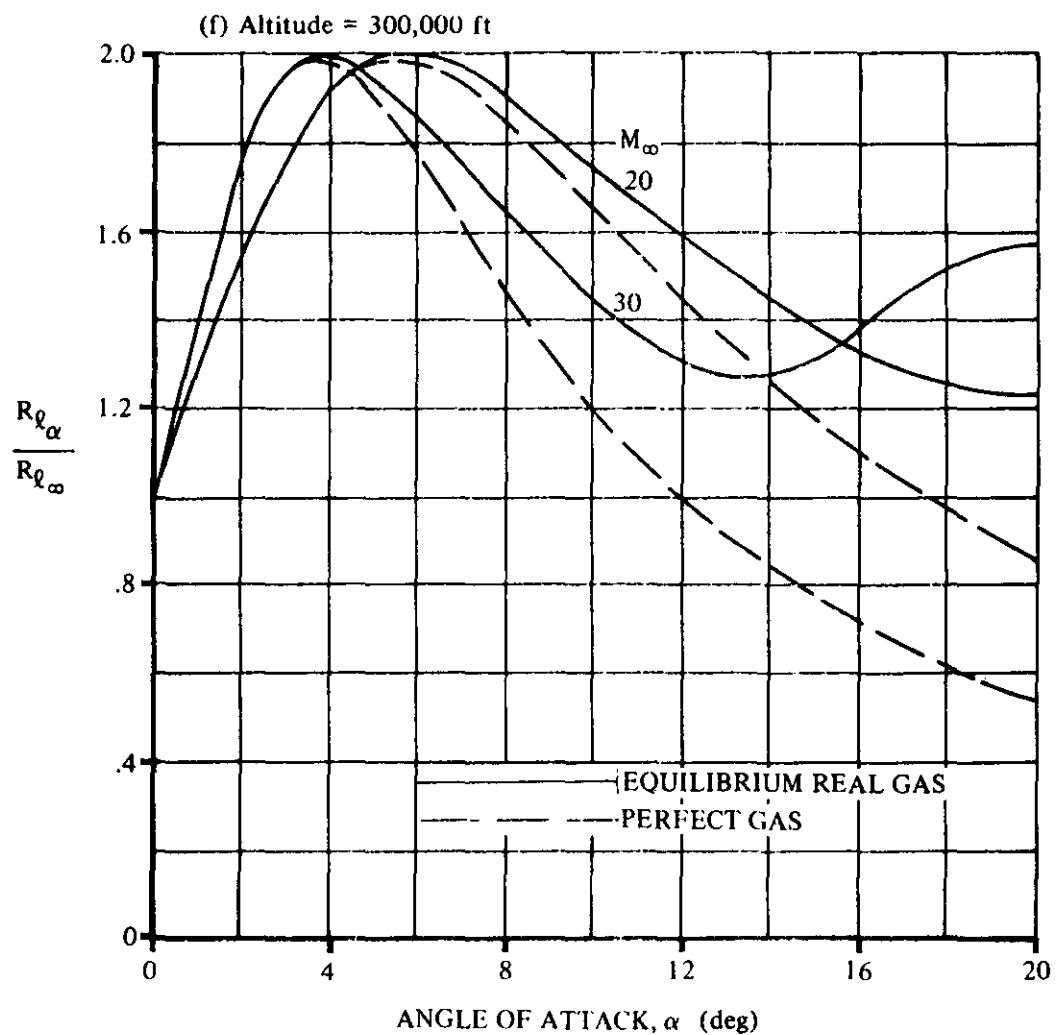
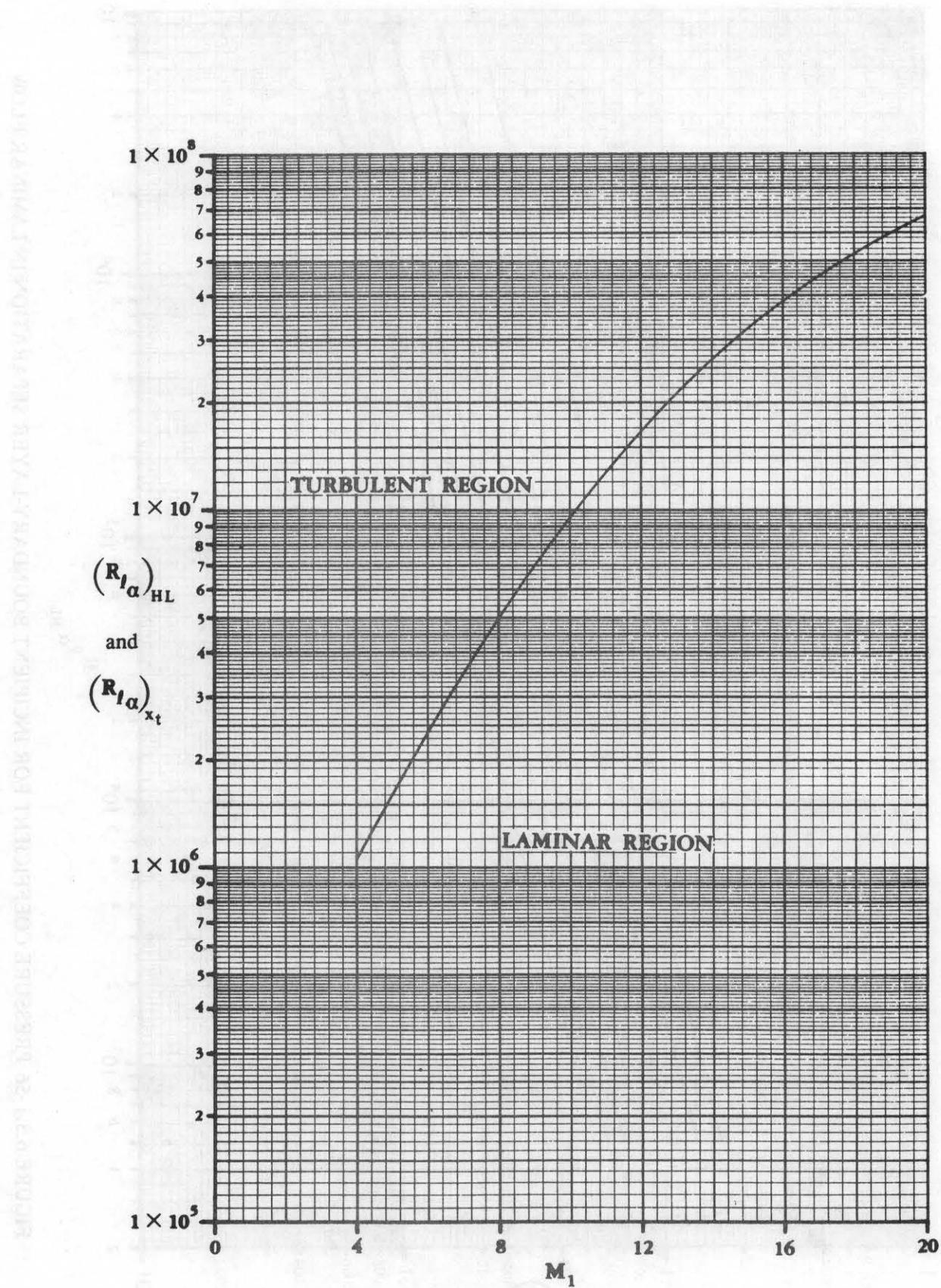


FIGURE 6.3.1-49 (CONTD)



**FIGURE 6.3.1-55 REGIONS FOR EXISTENCE OF THE LAMINAR AND TURBULENT BOUNDARY LAYERS**

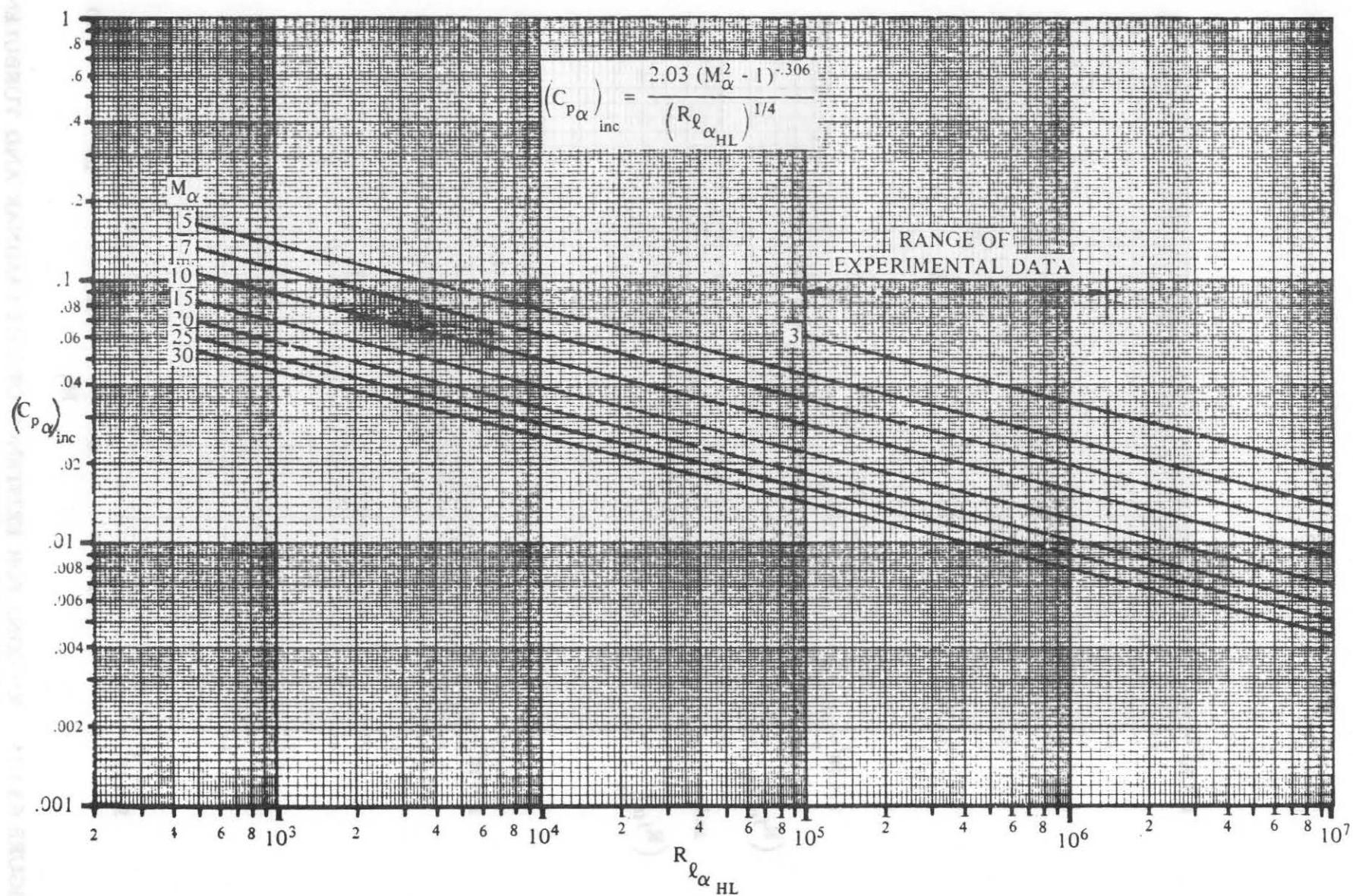


FIGURE 6.3.1-56 PRESSURE COEFFICIENT FOR INCIPIENT BOUNDARY-LAYER SEPARATION IN LAMINAR FLOW

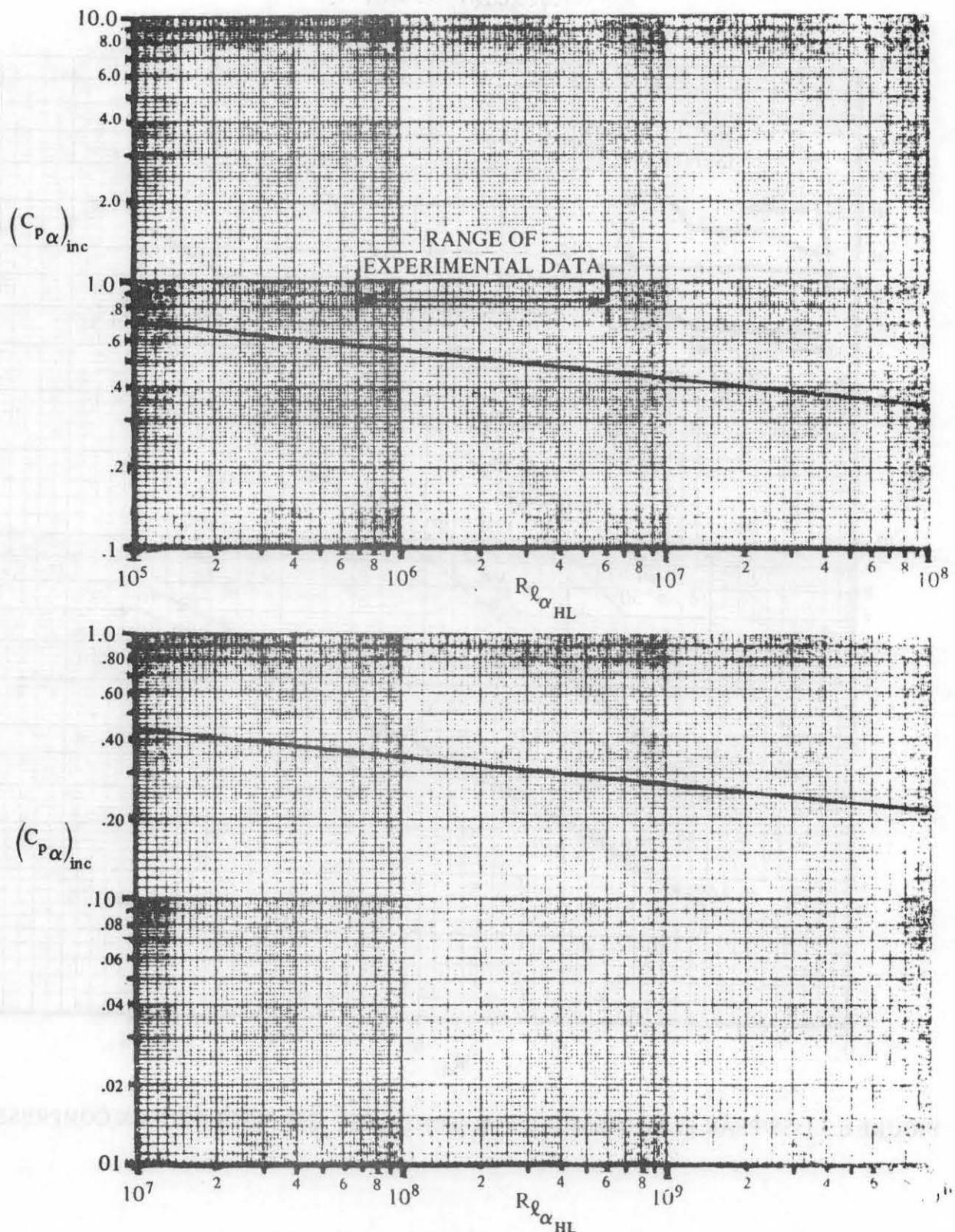


FIGURE 6.3.1-57 PRESSURE COEFFICIENT FOR INCIPIENT BOUNDARY-LAYER SEPARATION IN TURBULENT FLOW

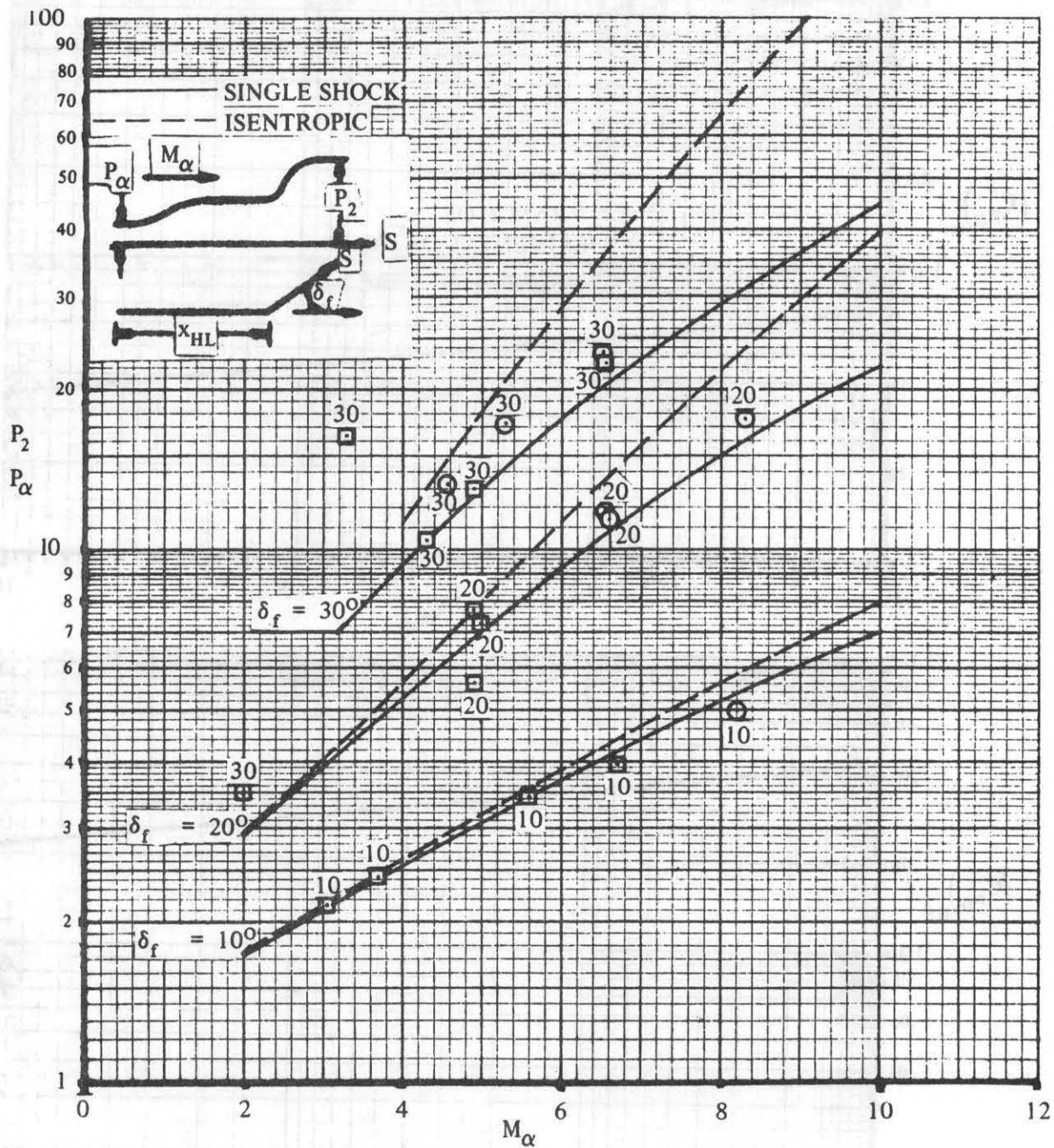


FIGURE 6.3.1-58 PEAK FLAP PRESSURE FOR ISENTROPIC AND SINGLE-SHOCK COMPRESSION

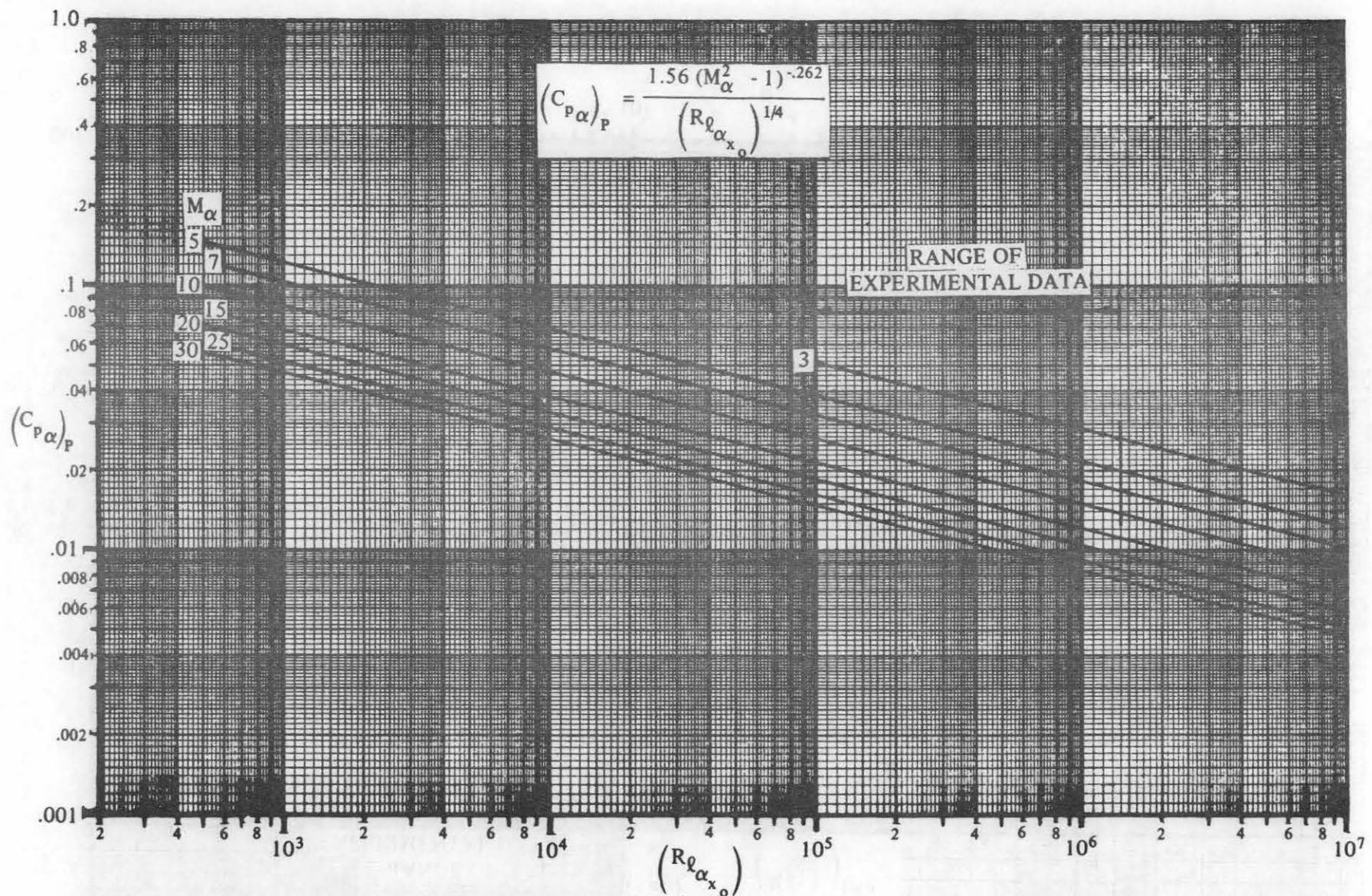


FIGURE 6.3.1-59 LAMINAR PLATEAU-PRESSURE COEFFICIENT

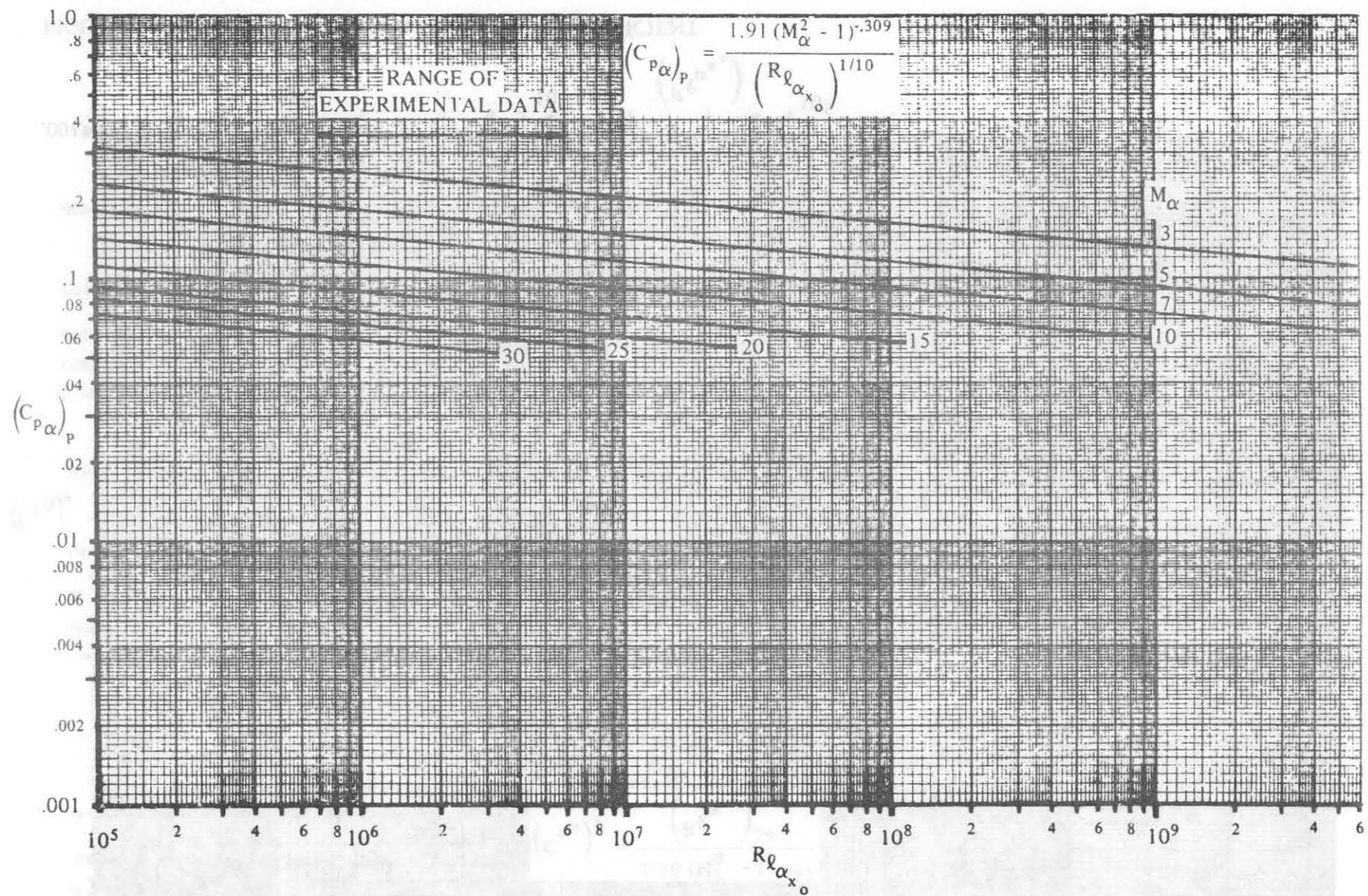


FIGURE 6.3.1-60 TURBULENT PLATEAU-PRESSURE COEFFICIENT

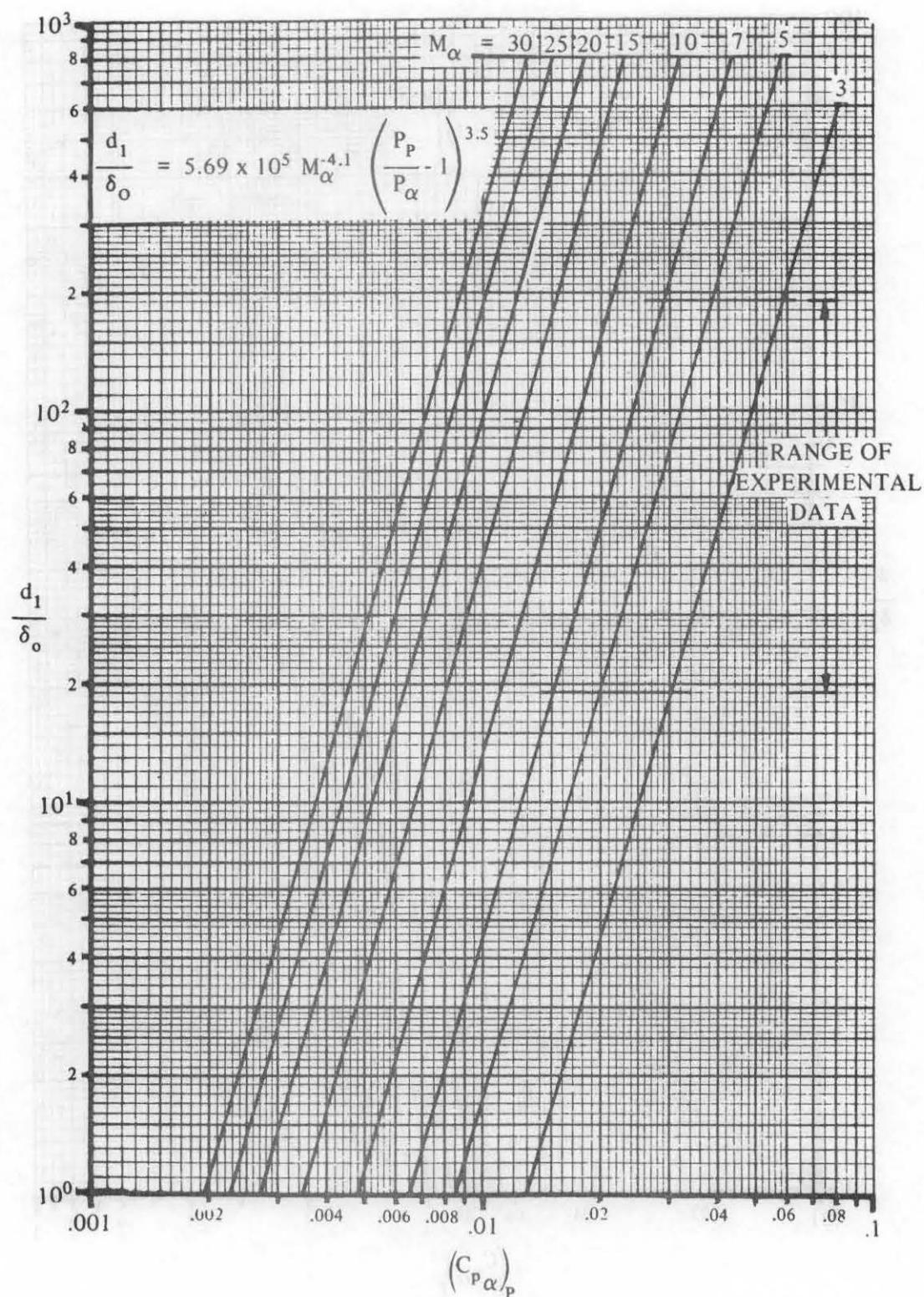


FIGURE 6.3.1-61 UPSTREAM INTERACTION DISTANCE FOR LAMINAR FLOW

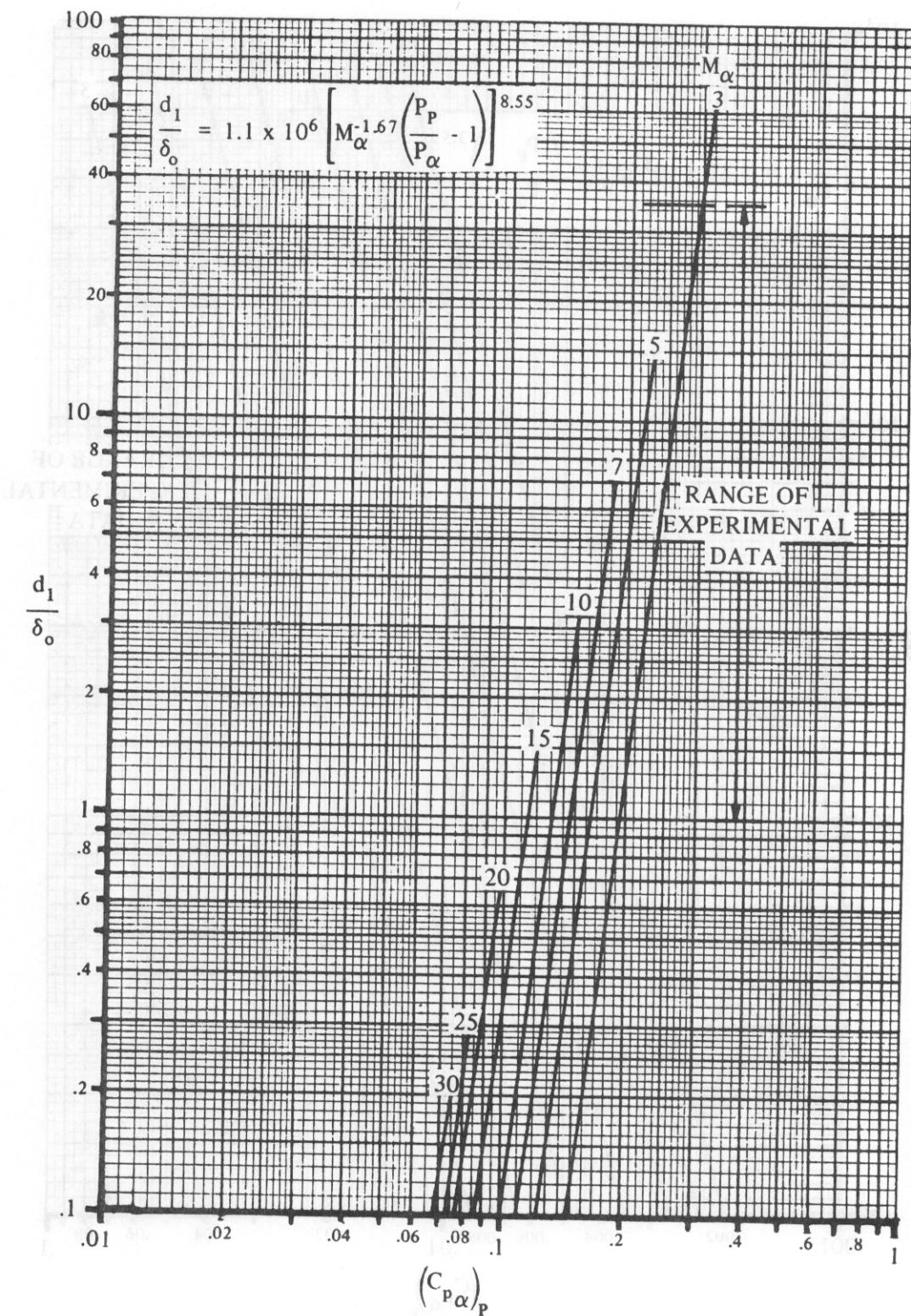


FIGURE 6.3.1 -62 UPSTREAM INTERACTION DISTANCE FOR TURBULENT FLOW

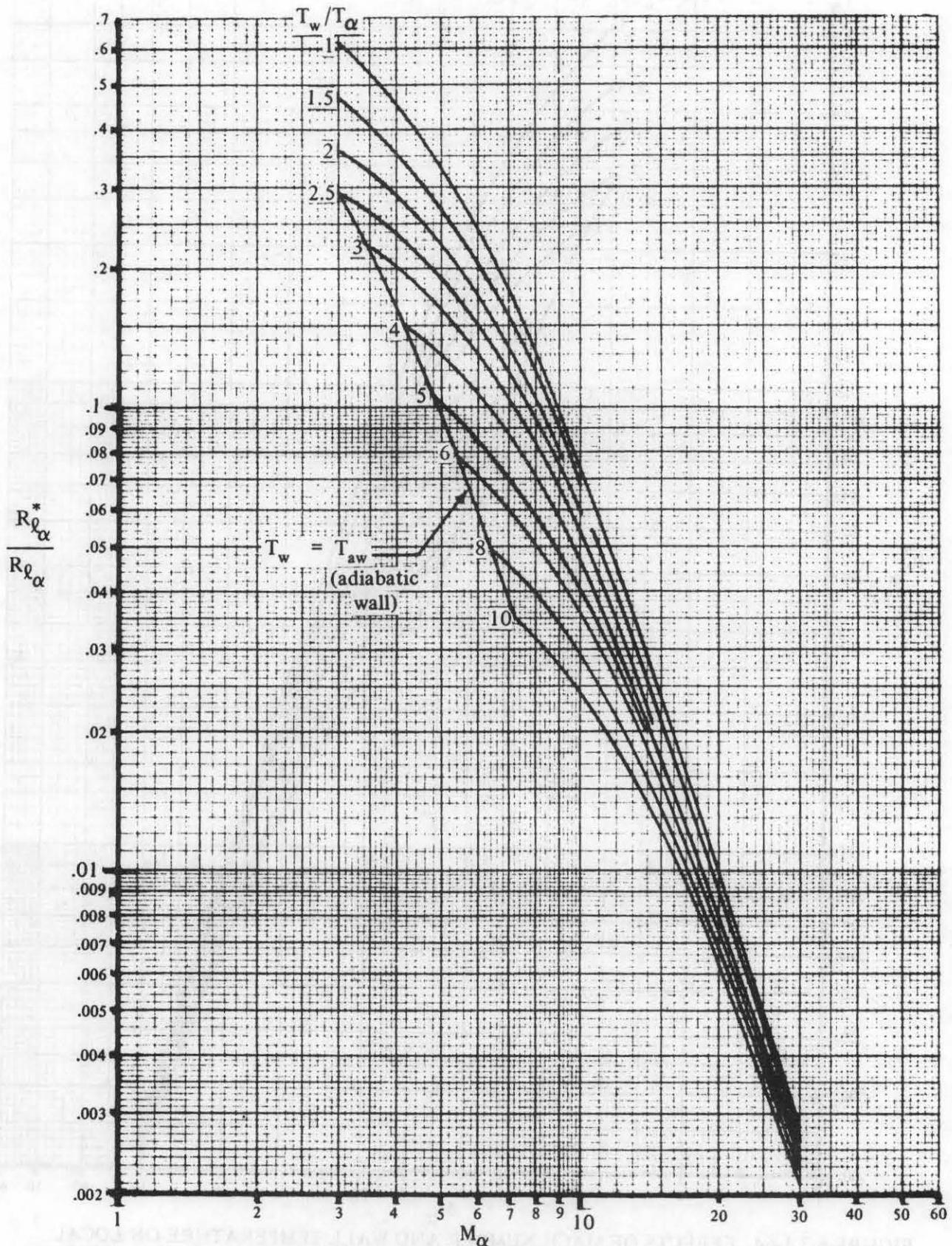


FIGURE 6.3.1-63 EFFECTS OF MACH NUMBER AND WALL TEMPERATURE ON LOCAL REFERENCE TEMPERATURE REYNOLDS-NUMBER RATIO (LAMINAR)

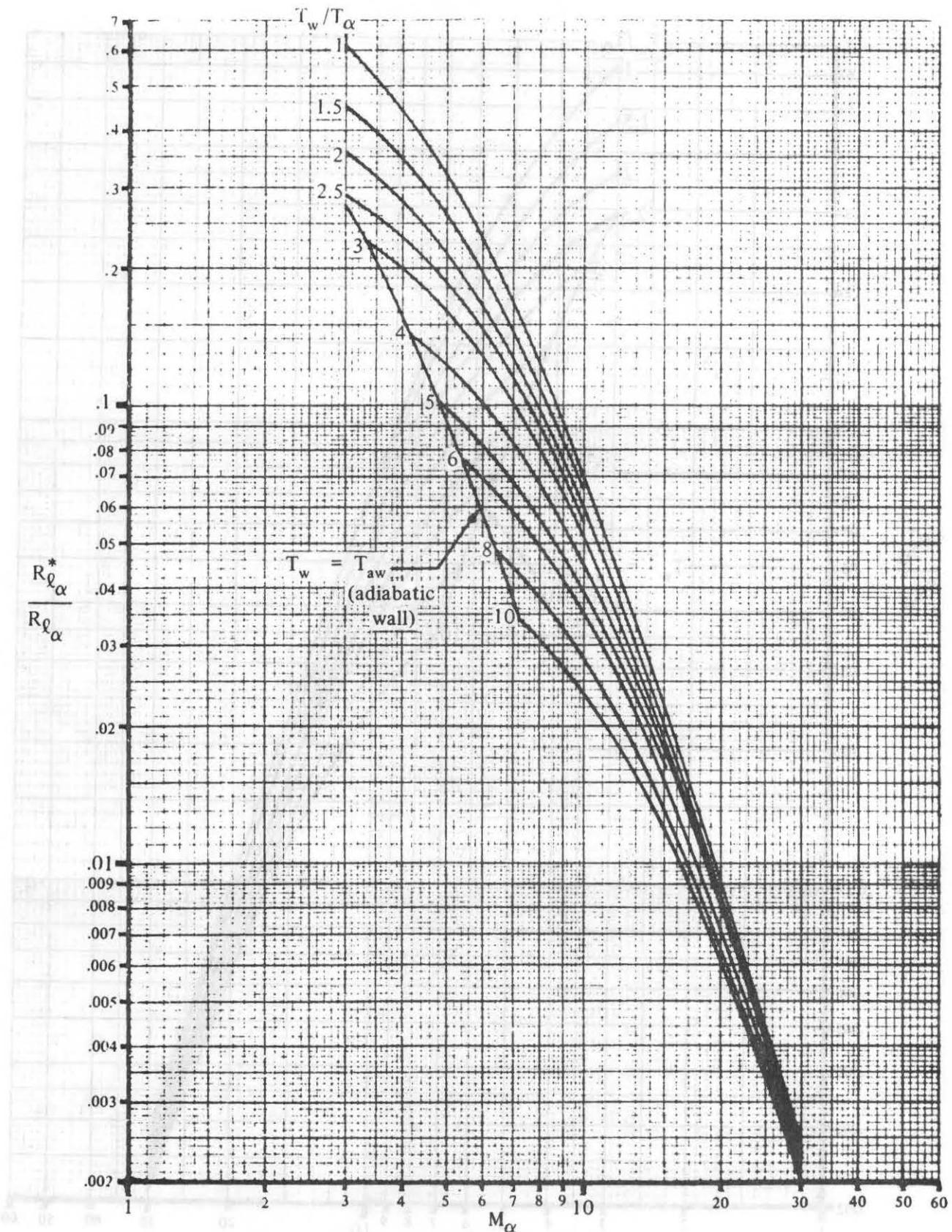


FIGURE 6.3.1-64. EFFECTS OF MACH NUMBER AND WALL TEMPERATURE ON LOCAL REFERENCE TEMPERATURE REYNOLDS- NUMBER RATIO (TURBULENT)

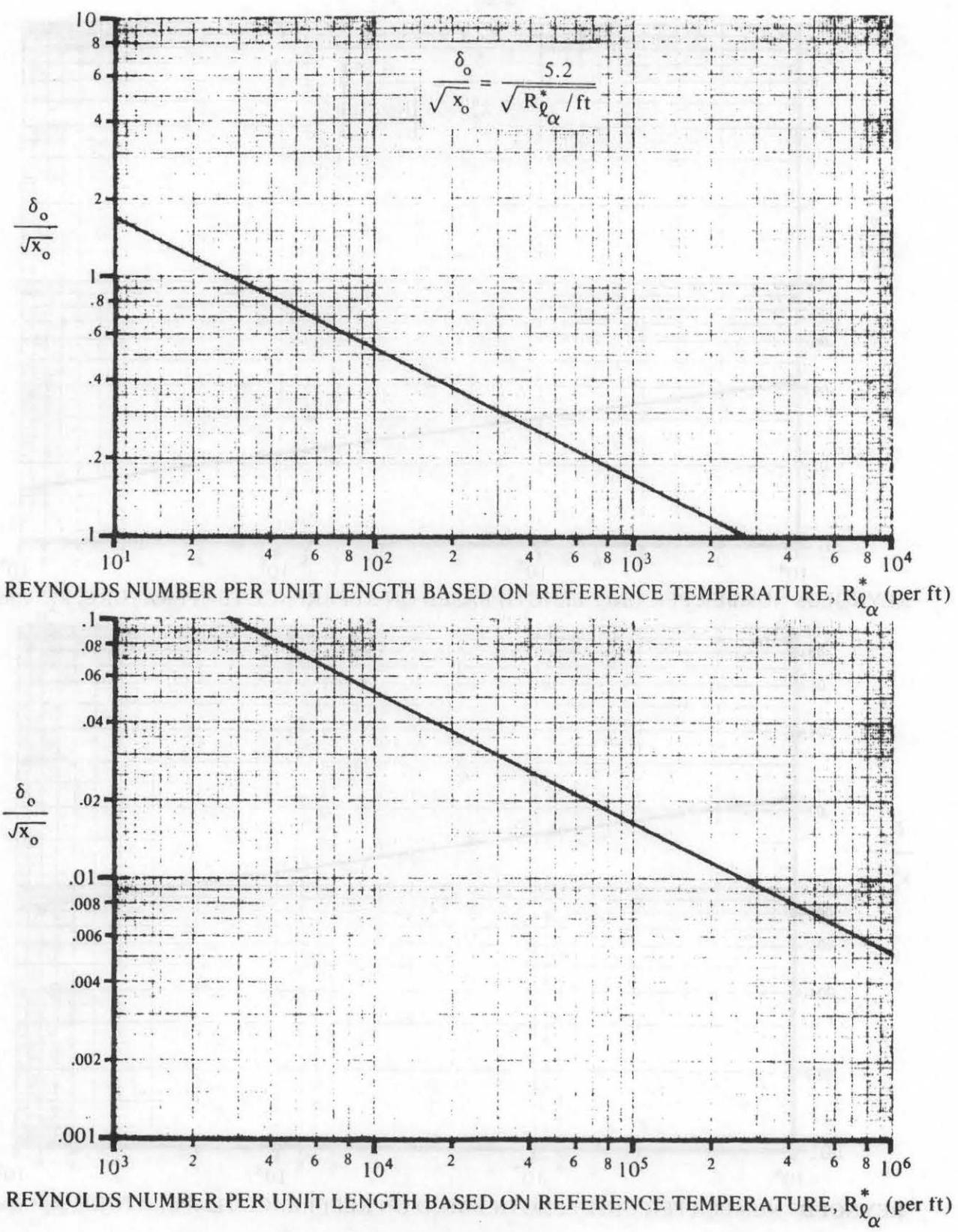
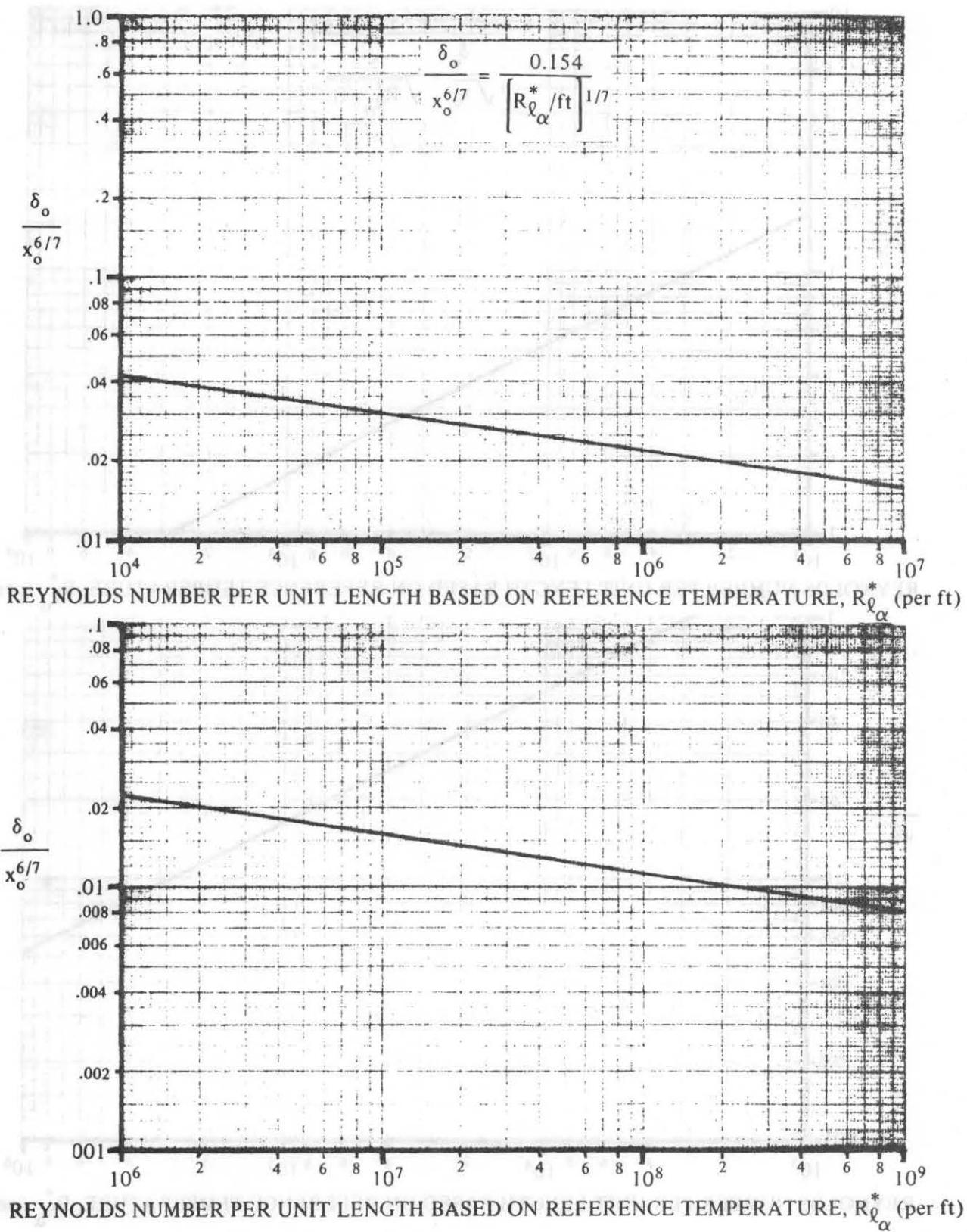


FIGURE 6.3.1-65 LAMINAR BOUNDARY-LAYER THICKNESS



**FIGURE 6.3.1-66. TURBULENT BOUNDARY LAYER THICKNESS**

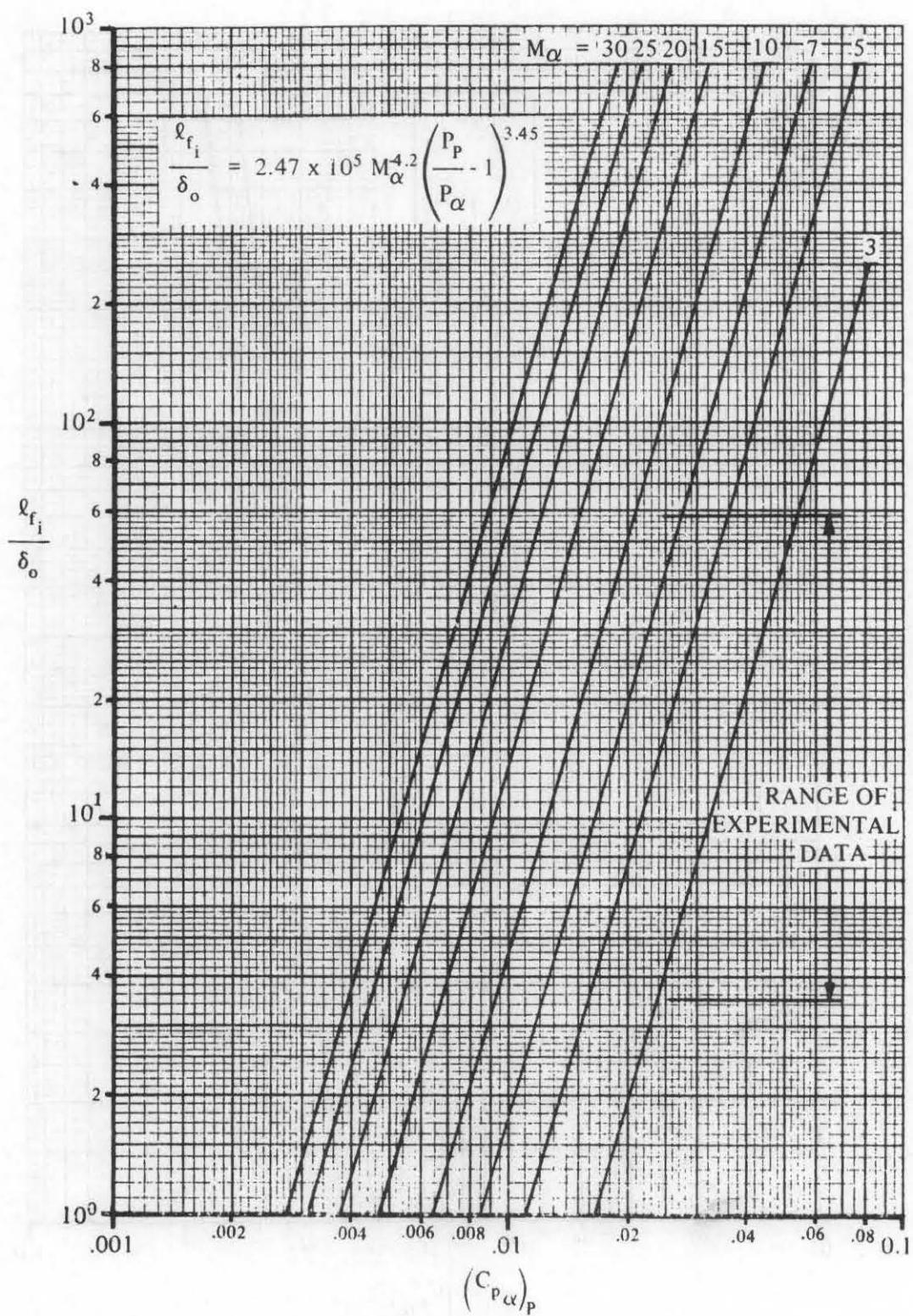


FIGURE 6.3.1-67 FREE INTERACTION LENGTH FOR LAMINAR FLOW

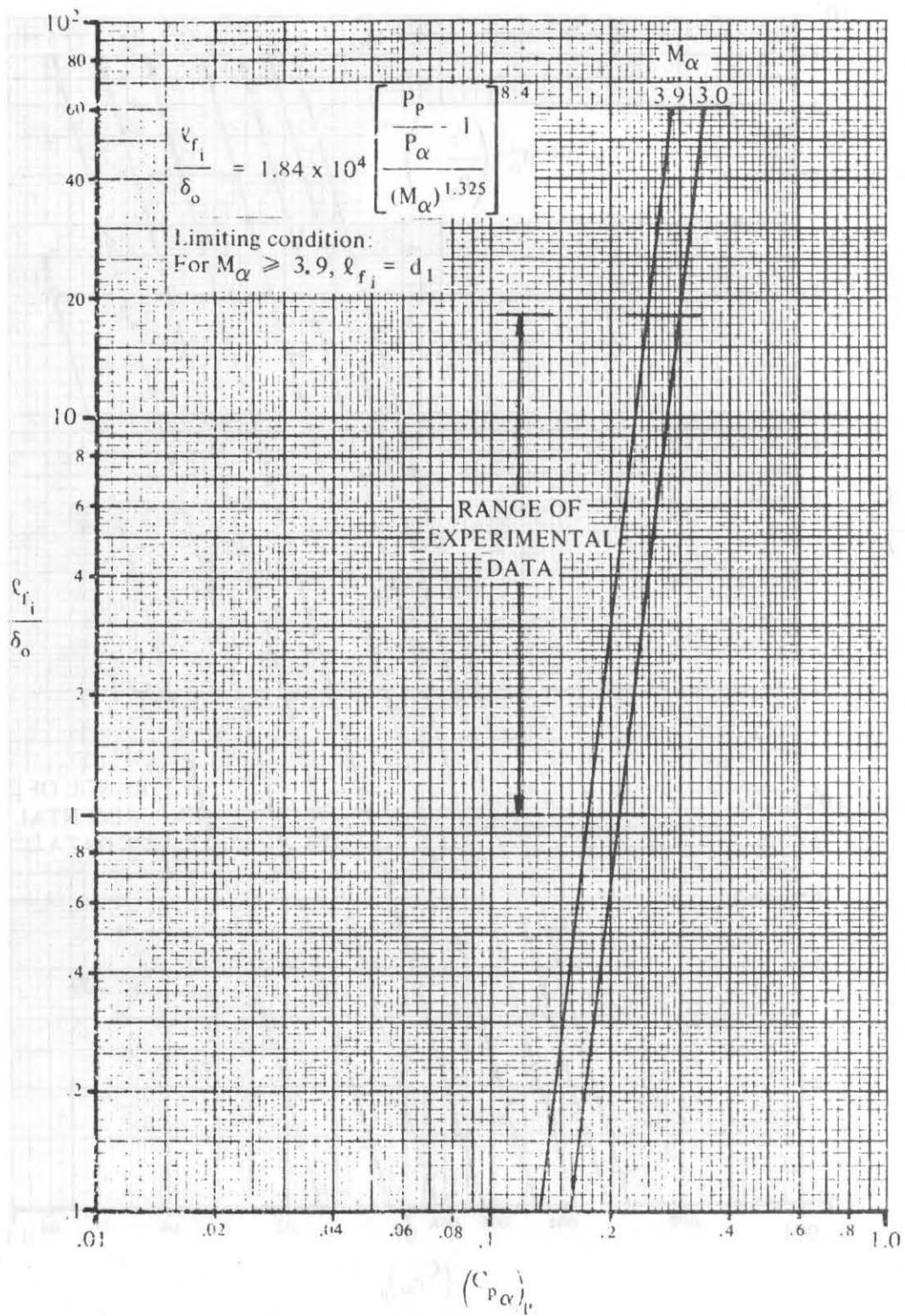
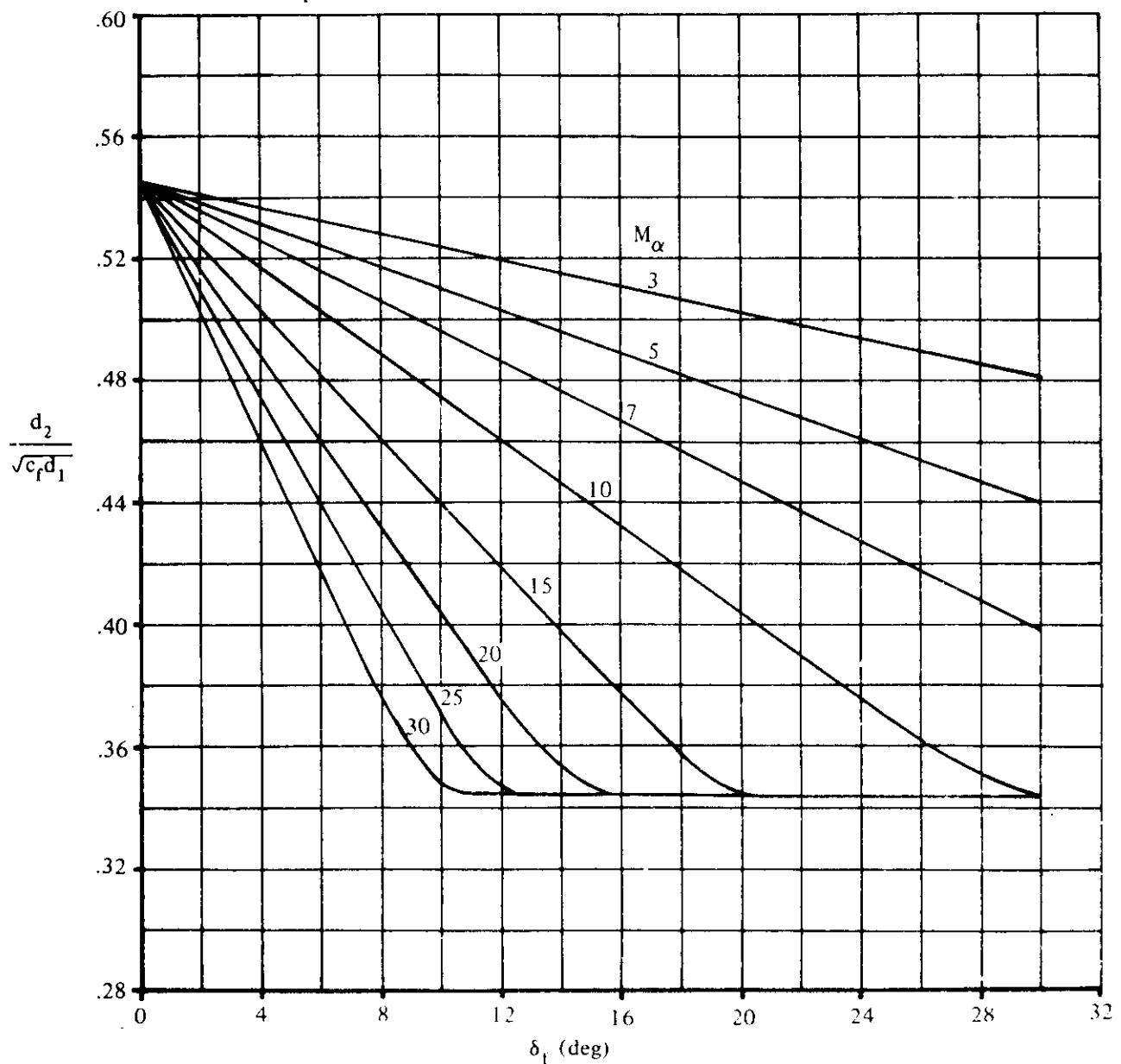


FIGURE 6.3.1-68 FREE INTERACTION LENGTH FOR TURBULENT FLOW

**Limiting conditions:**

1. If  $\frac{c_f}{d_1} \geq 1$ , then  $\frac{d_2}{\sqrt{c_f d_1}} = \frac{d_2}{d_1}$
2. If  $\frac{c_f}{d_1} \leq 0.25$ , then  $\frac{d_2}{\sqrt{c_f d_1}} = 2 \frac{d_2}{d_1}$

( $c_f$  = flap chord)



**FIGURE 6.3.1-69 DOWNSTREAM INTERACTION DISTANCE TO PEAK PRESSURE ON FLAP FOR LAMINAR FLOW**

Limiting conditions

1. If  $\frac{c_1}{d_1} \geq 1$ , then  $\frac{d_2}{\sqrt{c_1 d_1}} = \frac{d_2}{d_1}$

2. If  $\frac{c_f}{d_1} \leq 0.25$ , then  $\frac{d_2}{\sqrt{c_f d_1}} = 2 \frac{d_2}{d_1}$

( $c_f$  = flap chord)

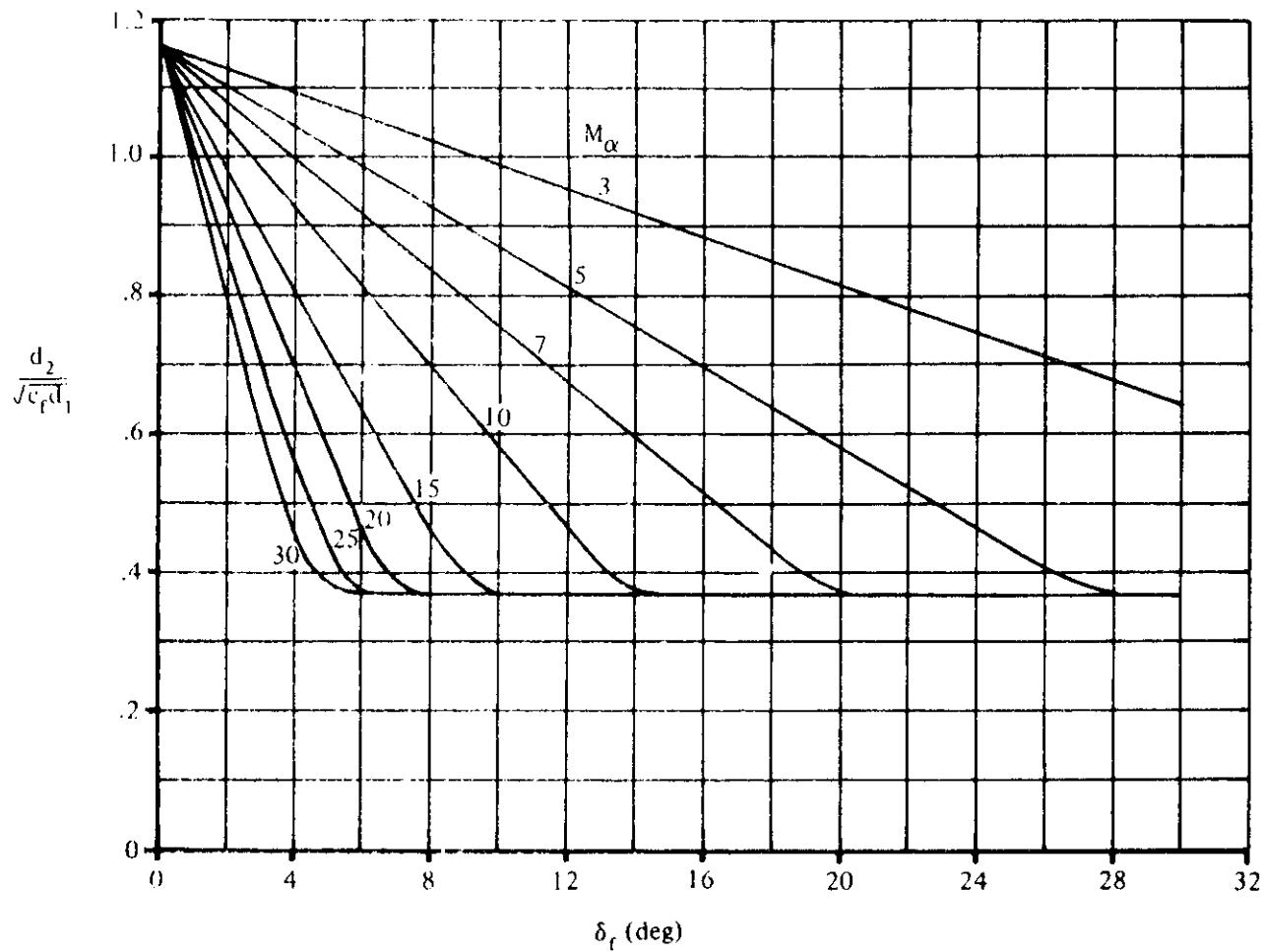


FIGURE 6.3.1-70 DOWNSTREAM INTERACTION DISTANCE TO PEAK PRESSURE ON FLAP FOR TURBULENT FLOW

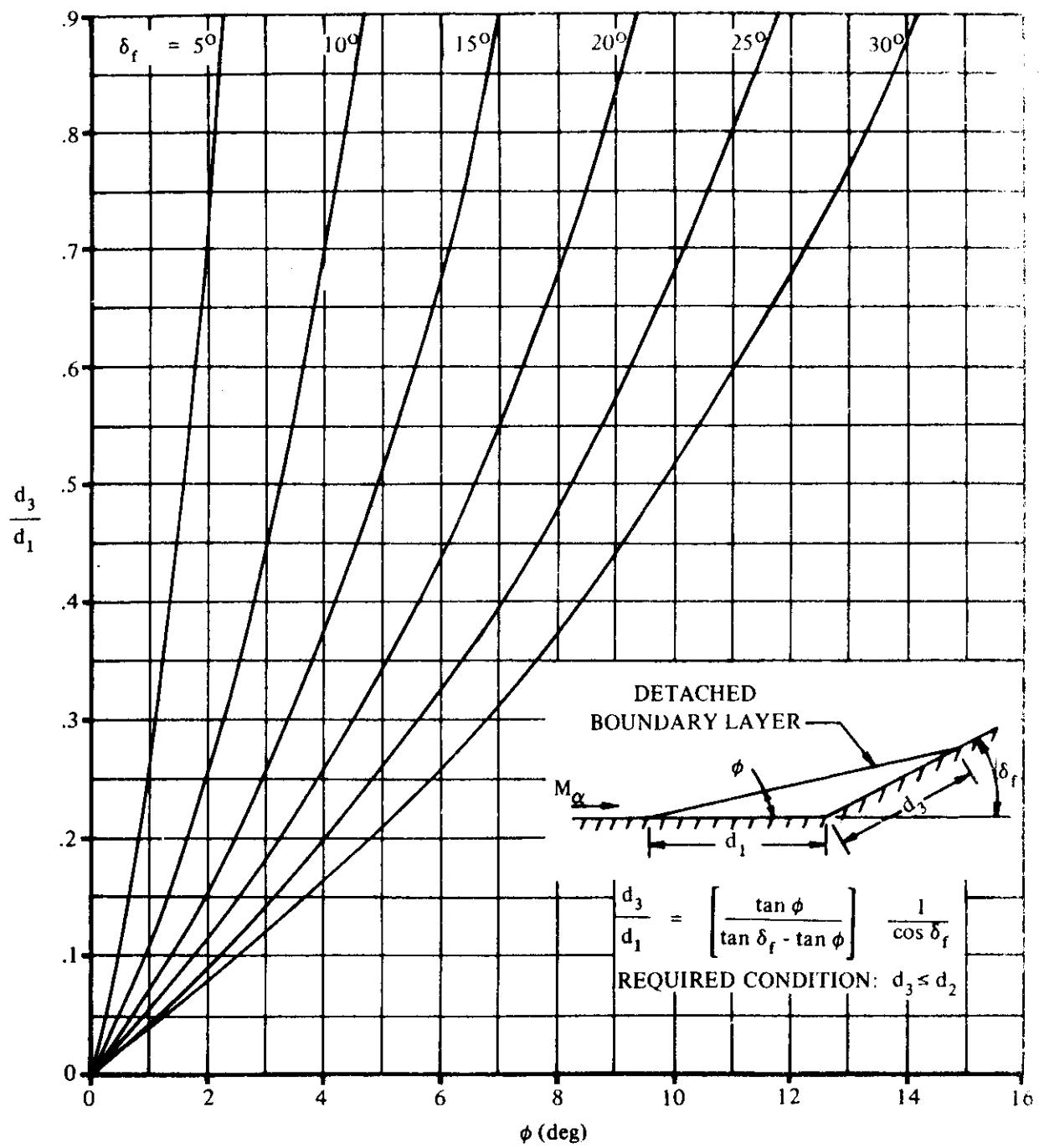


FIGURE 6.3.1-71 DOWNSTREAM INTERACTION DISTANCE TO PRESSURE RISE ON FLAP FOR LAMINAR FLOW

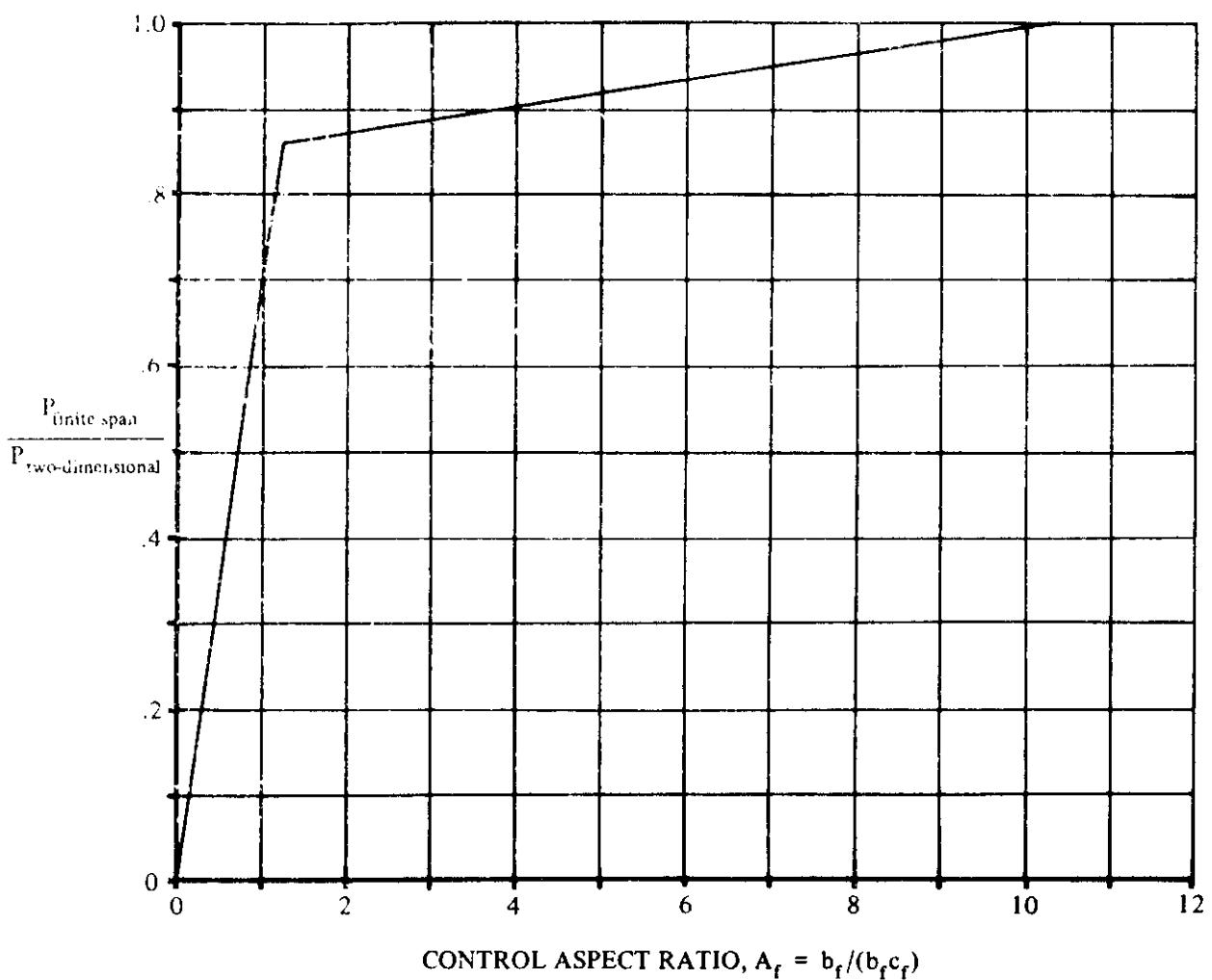


FIGURE 6.3.1-72 EFFECT OF FINITE CONTROL SPAN ON THE TWO-DIMENSIONAL PRESSURE DISTRIBUTION IN THE SEPARATED-FLOW REGION

### 6.3.2 TRANSVERSE-JET CONTROL EFFECTIVENESS

The interest in evaluating the feasibility of using transverse-jet control systems on high-speed flight vehicles within the atmosphere has created the need for establishing preliminary design methods for predicting transverse-jet control effectiveness.

This section presents a procedure, taken from reference 1, for sizing a two-dimensional transverse-jet control system in hypersonic flow.

A transverse-jet control system is a control system that uses one or more jets as spoilers. Flow separation generally limits the use of conventional flap-type systems; however, it serves as the basic phenomenon in achieving an effective transverse-jet control system. The jet spoiler creates flow separation in the region surrounding the jet by forcing the primary flow to turn around the obstruction created by the jet exhaust. Transverse-jet control systems are often referred to as jet-interaction control systems to emphasize the important contribution provided by the jet-interaction phenomenon.

Transverse-jet control systems consist of a variety of different types and sizes of thrust units mounted on aerodynamic surfaces. The thrust can be provided by solid or liquid propellant rocket engines or bleed-thrust control units. These thrust units may be large single units or a group of small units strategically located.

In analyzing the performance of transverse jets, several theories have been developed that provide estimates of the principal parameters upstream and downstream of the nozzle. However, the complexity of the interaction has prevented obtaining a detailed physical description of the flow field. This has restricted investigators to limiting the scope of their analyses until fundamentals of the flow have been firmly established. Thus, the Datcom method presented herein is subject to limitations. The primary restriction limits analyses to two-dimensional nozzles. Considerable effort (references 2, 3, 4, and 5) has been directed towards analyzing the three-dimensional problem; however, no acceptable design methods are currently available. The other limiting condition pertains to the pressure forces downstream of the nozzle exit. Because of the conflicting theories regarding the merits of the downstream forces, all nozzles are assumed to be located at the aft end of their respective surfaces. Thus, no consideration is given to possible aft-end forces in the Datcom method; however, they are considered in the discussion of interaction forces.

The advantages (reference 6) of transverse jets in high-speed flow in comparison with conventional aerodynamic control systems have provided the impetus for investigating the possible implementation of transverse-jet control systems. The primary advantage is the possibility of achieving control forces greater than the impulse provided by the jet reaction. This increased force or amplification is due to the favorable interaction of the transverse jet with the local stream flow. The jet interaction substantially alters the surface pressure distribution and results in large additional surface loads, which augment the simple reaction force of the jet. Experimental tests have indicated that properly designed systems can achieve interaction forces that exceed the reaction jet force by factors of four or five.

A second advantage is the possible reduced control response time for transverse jets in comparison to conventional systems. This reduced response time enables the vehicle to be designed with less static stability. A potential increase in reliability provides a third advantage, since redundancy is more readily achieved with a less severe weight penalty than for conventional systems and because rocket technology is felt to be more advanced than the technology involved in building high-speed actuators and the integral components required to operate in an extreme temperature environment. Another benefit is the wide range of flight conditions in which transverse jets can provide control forces, as compared with the limited envelope for conventional systems. Improvements are also derived from the elimination of structural problems associated with control surfaces and related heat-transfer problems prevalent in hypersonic flow.

Inherent with transverse jets are many problems and disadvantages which must be solved or accounted for before successful implementation can be achieved. The most crucial problem is the lack of a thorough knowledge involving the jet-interaction process. This prevents formulating a completely reliable prediction technique. Distinct disadvantages are the weight penalties imposed by the propulsion system and the limited quantity of propellant available for a given mission. Associated problems are also encountered in the growth potential when mission requirements change.

An evaluation and design comparison of transverse-jet controls and conventional aerodynamic control systems are presented in reference 6. The conclusions of the report are: (1) high L/D re-entry vehicles with the vehicle trimmed to maximum L/D are favorable to transverse-jet control systems, if trajectory control by roll control is used; (2) if a winged re-entry vehicle is to be maneuvered in pitch to angles appreciably different from the angle of attack required for maximum L/D, conventional flap-type aerodynamic controls are preferable. Additional comparisons regarding transverse jets, solid spoilers, and flap deflections can be found in references 6 and 7.

In order that the Datcom user may better understand the control-effectiveness methods presented in this section, a general discussion of hypersonic-flow separation and the effect of the jet-interaction phenomena upon augmenting the control force is presented. This general discussion is essentially quoted from Section 6.3.1 of the Datcom and from reference 1. A more detailed description of hypersonic-flow separation and jet-interaction phenomena can be found in references 1, 2, 3, 4, and 8. A summary of the literature pertaining to transverse jets can be found in reference 9. A summation of the contents of each document is given, along with a qualitative discussion of the data and/or theory presented.

### Hypersonic-Flow Separation

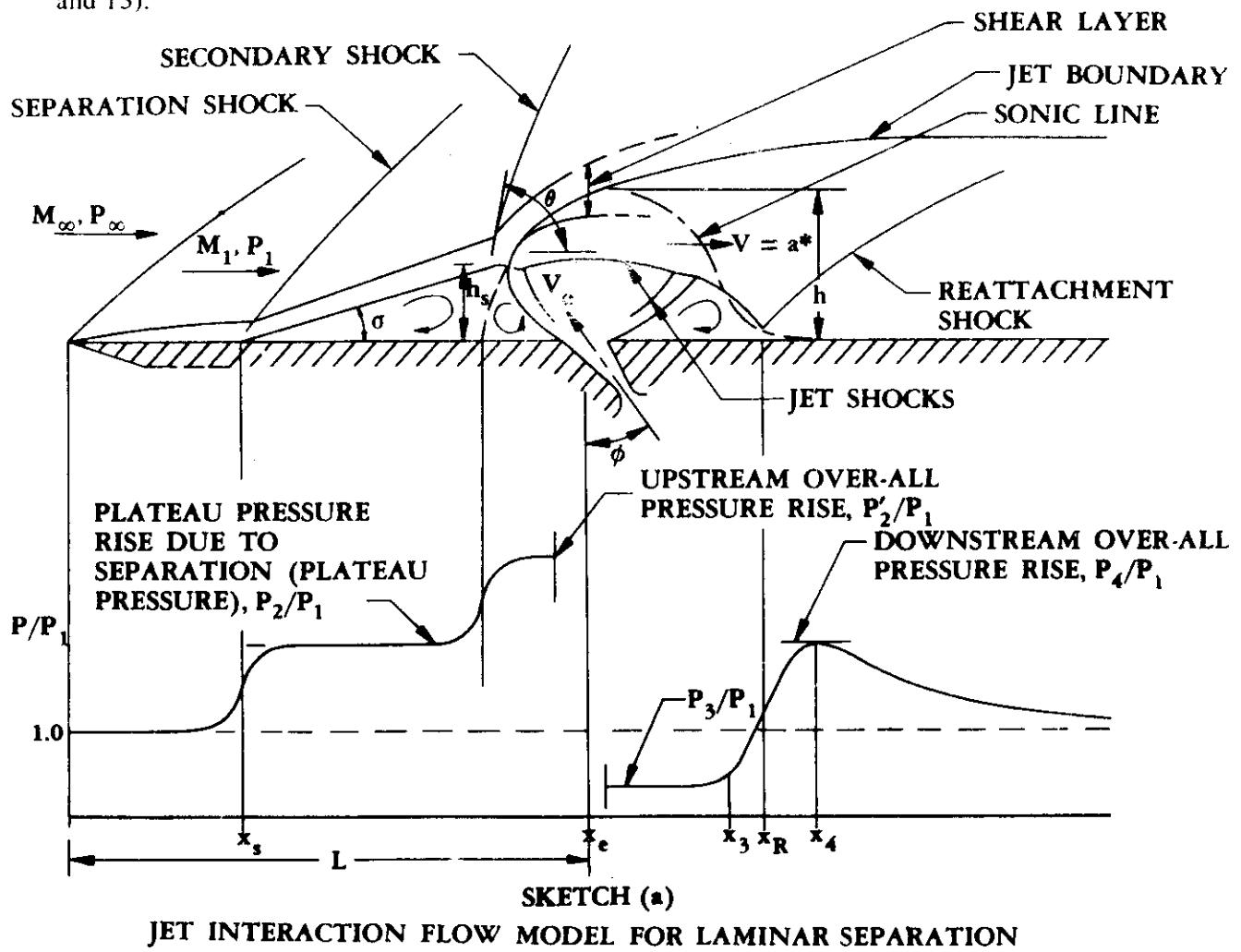
Separated flows are characterized by the prevailing type of boundary layer: laminar, turbulent, or transitional. The pressure rise and the extent of the separated region depend upon the characteristics of the boundary layer.

In general, boundary-layer separation occurs whenever the streamwise pressure increase along a surface is sufficient to overcome the forces acting to accelerate a fluid particle, or when the streamline curvature necessary to follow the surface contour cannot be sustained by the pressure gradient normal to the surface. In steady-flow aerodynamics the only forces acting to accelerate the low-momentum fluid near the wall against a pressure gradient are the shear forces between

layers of fluid. Because the momentum of the fluid near the wall is quite low, a relatively small amount of deceleration by the pressure gradient is sufficient to bring about separation. Turbulent flow helps to delay the occurrence of separation, because the turbulent fluctuations increase the effective shear forces and thereby increase the adverse pressure force necessary to reverse the flow of the fluid near the wall.

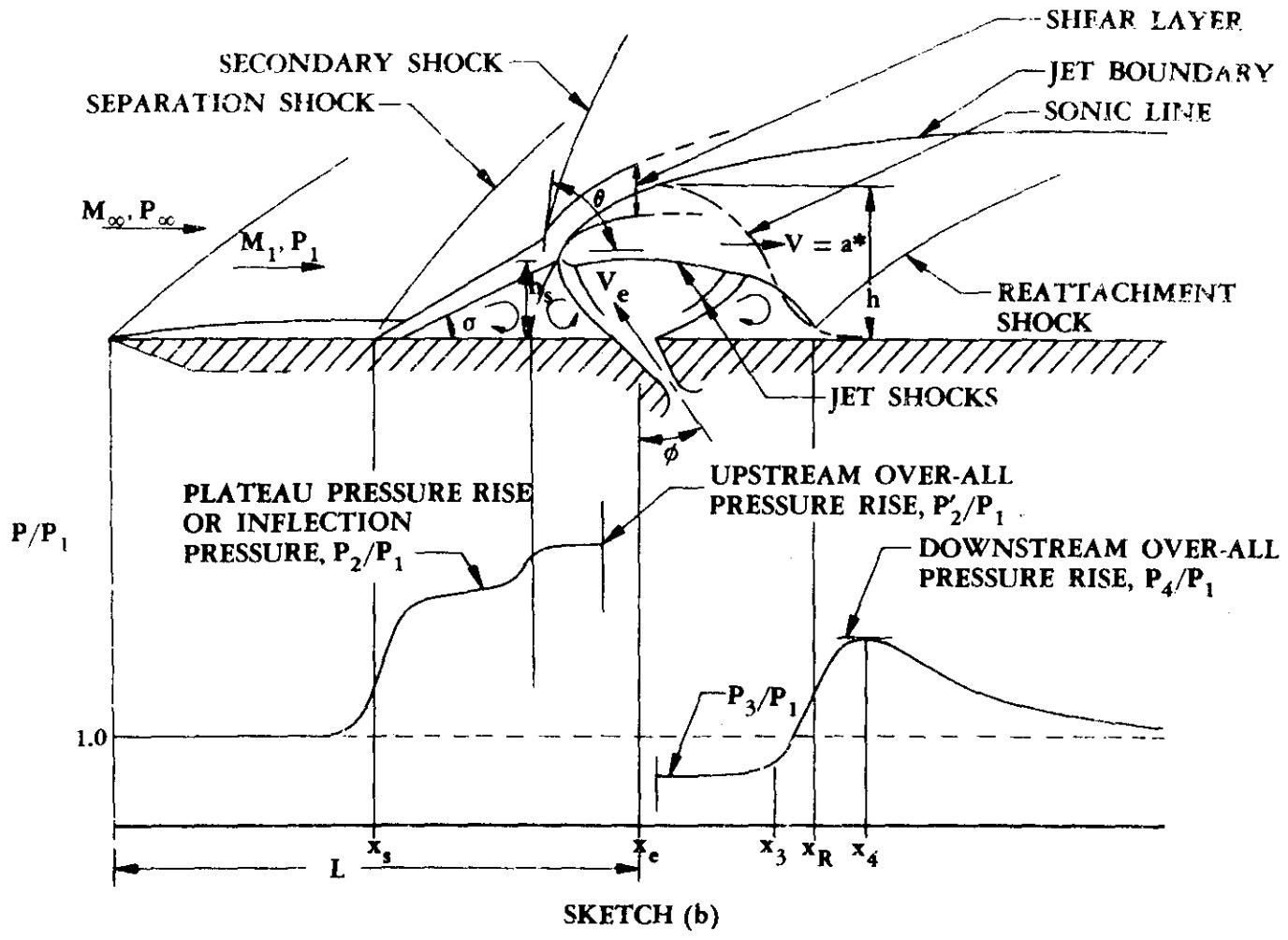
The greatly increased effective viscosity due to turbulent fluctuations enables the equilibrium between pressure and shear forces near the wall to occur at much greater adverse pressure rises in a turbulent boundary layer. Because of the connection between pressure rise and flow turning angle, this higher pressure corresponds to a much shorter, thicker separated zone for the same initial boundary-layer thickness. Cases presented by Schlichting (reference 10) and Howarth (reference 11) show turbulent pressure rises twice the laminar ones; whereas the laminar separation zone extends much farther than the turbulent one.

A similar thickening (and simultaneous pressure rise) occurs in a transitional separation when the mixing zone becomes turbulent and the downstream flow soon approaches a condition very similar to the equivalent turbulent separation. Upstream of the transition point, the flow has the character of the corresponding laminar separation zone. The location of the transition point therefore plays a significant role in determining the pressure distribution (see references 12 and 13).



Present indications are that shock-induced laminar-separation pressure distributions, and to a limited extent turbulent ones, are independent of the type of disturbing force that produces separation (see reference 12). However, the turbulent peak pressure rise often depends significantly on the disturbing force (references 12 and 14 through 17). This difference in dependence can probably be attributed to the greatly increased effective viscosity in turbulent flow, enabling the wall contour within the separated zone to transmit its effect more strongly to the outer flow.

Typical jet-interaction flow fields for laminar and turbulent boundary layers are presented in sketches (a) and (b), respectively (reference 1).



**JET INTERACTION FLOW MODEL FOR TURBULENT SEPARATION**

For the upstream region, laminar boundary-layer separation has a characteristic plateau where the pressure remains almost constant over most of the separated flow region. The plateau pressure level depends only on local flow conditions at the location of the separation point (see reference 12). The upstream turbulent boundary-layer-separation pressure distribution is not characterized by a long pressure plateau region as in the case of laminar separation. Instead, the turbulent separation produces an increasing pressure gradient that exhibits an inflection point or a very

short plateau pressure, which appears to be dependent only upon the Mach number. Although some discrepancies exist in the literature (references 1, 4, and 18) regarding upstream pressure trends with boundary-layer condition, the majority of the later references indicate that larger upstream forces are exhibited for laminar separated boundary layers. These larger forces can be attributed to the integrated loads for the longer, lower pressure regions of laminar flow, being larger than those for the shorter, higher pressure regions of turbulent flow.

The problem of locating the boundary-layer transition point is one that has received wide-spread attention from theoreticians and experimentalists. However, no universally applicable prediction technique has been obtained. The best approach for predicting the transition point is to examine wind-tunnel data that most nearly approximate the actual flow conditions. Techniques for correlating the transition data from various sources are available. Reference 19 presents one such technique for correlating data for cone-shaped configurations. In the absence of similar wind-tunnel data, the method presented in the Datcom can serve as an approximate estimation for determining the state of the boundary layer or transition point.

#### Jet-Interaction Phenomena

The most prominent feature of jet-interaction phenomena is the formation of a strong jet shock that is nearly normal to the jet flow direction, resulting in a recompression and subsonic flow on the downstream side of the nozzle. Reference 8 indicates that because the injected stream must be turned by the primary flow, it acts as an obstruction, and as such, produces a strong shock in the primary flow. This shock interacts with the boundary layer on the wall and causes it to separate. Both the initial shock and the resulting boundary-layer separation produce a region of high pressure near the point of injection. This is the source of the interaction force that augments the simple reaction force of the jet.

Kaufman, in reference 20, describes the interaction pressure downstream of the nozzle as characteristically having a low-pressure region followed by a pressure rise to the reattachment value. At reattachment, the pressure can be either larger or smaller than the undisturbed free-stream pressure. Downstream of reattachment, the pressure approaches its undisturbed value asymptotically.

The low-pressure region downstream of the nozzle can have an adverse effect on the interaction force if the nozzle is not located at the aft end. However, the increasing pressure at reattachment can in some cases predominate, yielding a favorable force if the aft end of the surface is of sufficient length to capture the major portion of the positive pressure region.

The reattachment of the boundary layer downstream of the jet is not well understood. Experiments have indicated a pressure rise similar to that at separation, with the gradient at reattachment usually being in excess of that at separation.

The downstream pressure distributions have frequently been compared to pressure distributions behind rearward-facing steps. These pressure distributions have been estimated by using various base-flow analyses. As indicated by Kaufman (reference 20), determining the proper start conditions for the base-flow models has been difficult. This is due to the existence of large gradients in the flow and no detailed flow-field measurements in this region to guide the

selection of the proper jet-flow conditions to be utilized as the initial conditions in the base-flow analyses.

As stated earlier, the Datcom method does not account for aft-end forces, because all nozzles are assumed to be located at the aft end of their respective surfaces.

### Three-Dimensional Effects

Three-dimensional flow fields result from low-aspect-ratio jets located on both flat plates and more complicated bodies. Reference 2 presents a description of the flow field and the relative differences between two- and three-dimensional flow. The more salient aspects are presented here for the reader's benefit.

Three-dimensional effects in the jet-interaction flow field are not well understood quantitatively. This is partly due to the fact that less effort has been devoted to the three-dimensional problem, but more significantly because of the general complexity of three-dimensional flow. The boundary-layer-separation problem alone is not very well understood for three-dimensional flow. Unfortunately, the more significant differences between two- and three-dimensional flow fields are observed to be the extent of the boundary-layer separation and the geometry of the shocks. In contrast to two-dimensional flow, the three-dimensional boundary-layer separation is greatly reduced as a result of the lateral flow component, allowing the boundary layer to bleed off around the sides of the plume. This minimizes the viscous effects and creates a largely inviscid phenomenon.

The most obvious concern with three-dimensional flow is the possible loss in effectiveness due to end effects. However, reference 5 points out that integration of the pressure distribution over a 7-degree cone shows that the normal-force coefficient obtained is the same as the normal-force coefficient per unit span of a two-dimensional jet with the same jet mass flux. This behavior is attributed to a favorable interaction between the cross flow and the main stream, which increases the effective span of the jet. However, this conclusion was based on limited test data and has not been corroborated for various flow conditions.

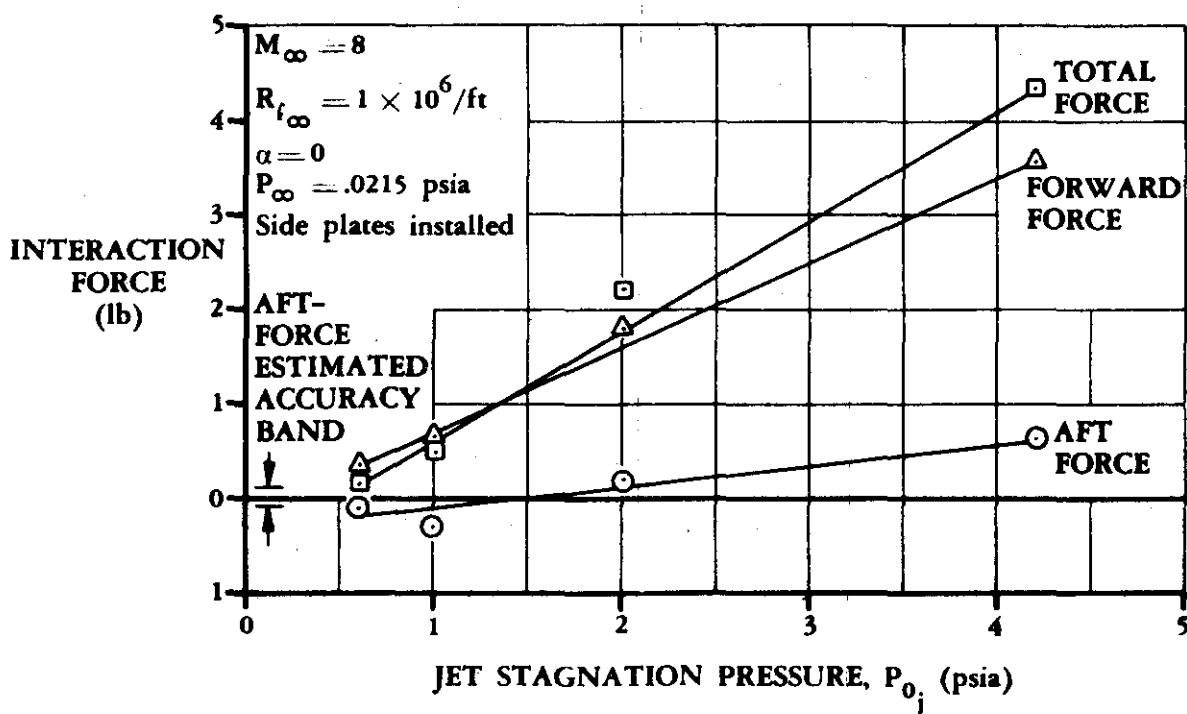
Unlike a jet on a flat plate, an adverse interaction has been observed to occur frequently on three-dimensional bodies. This is attributed to the effect of "wraparound," i.e., the propagation of the disturbance to the sides or the underside of the body. Much of the interaction force created by three-dimensional nozzles results from the high-pressure region immediately behind the bow shock, which forms a hyperbolic high-pressure ridge on the surface of the body extending out from the region of the nozzle. In addition, the low-pressure region directly downstream of the nozzle, which has an adverse effect on the interaction force, is virtually as effective on a cylindrical body as on a flat plate; therefore, negative interaction forces commonly occur on such vehicles.

Although the existing method of analysis in reference 2 provides fair agreement with experimental data, additional sophistication in the shock-body interaction analysis is contemplated, and improved correlation is expected. References 4, 5, 18, and 21 offer additional information regarding the pressure distributions and jet-interaction phenomena for three-dimensional flow.

### Jet-Interaction Control Effectiveness

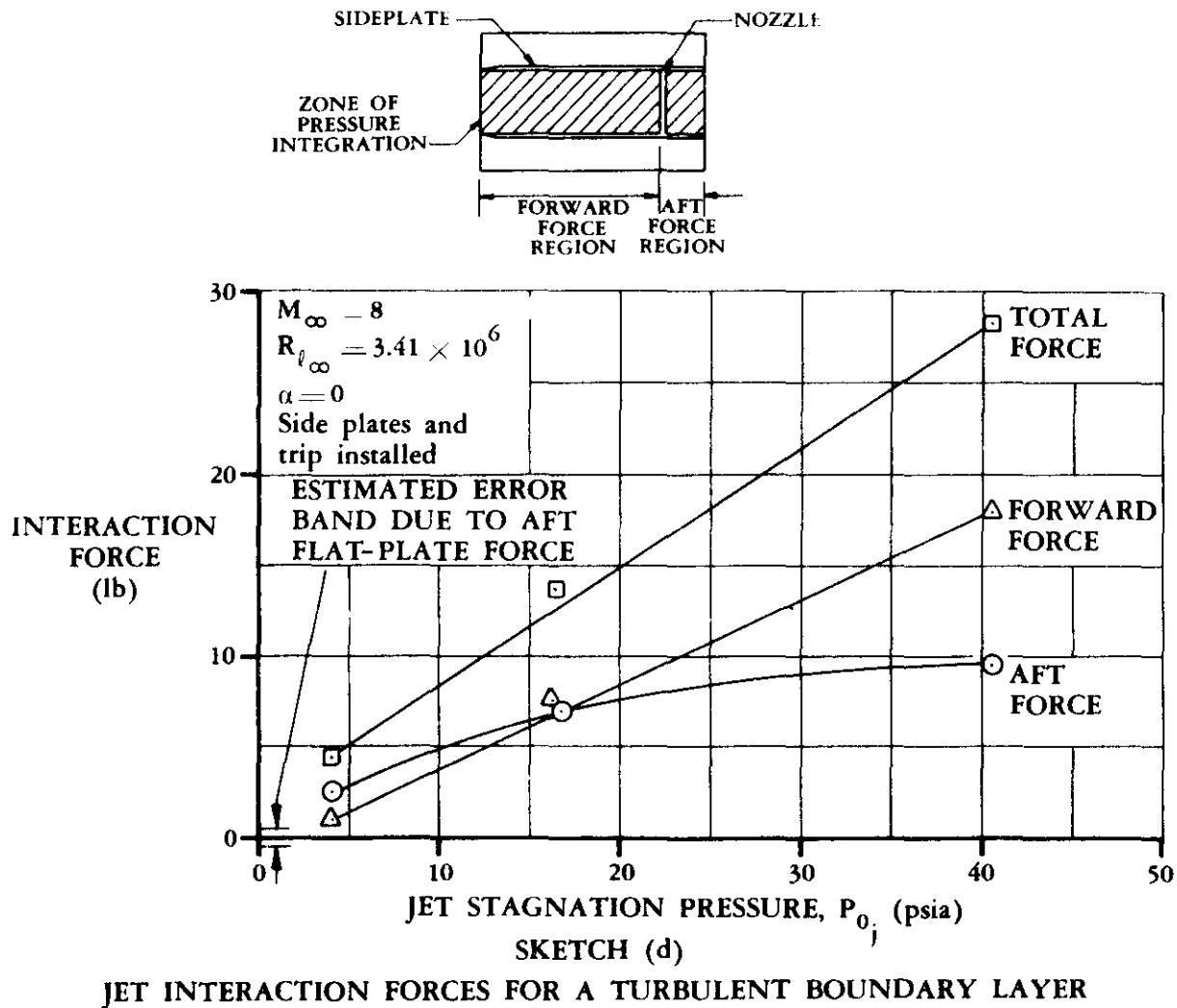
For obvious reasons it is desirable to obtain the highest possible jet-interaction forces. This leads to the consideration of various nozzle inclination angles. Figure 6.3.2-41 (reference 1) presents the amplification factor versus injection angle for various values of nozzle exit velocities and normal sonic amplification factors. From this figure it can be seen that substantial gains in performance may be achieved by inclining the nozzle upstream, provided that large amplification factors (control force normal to wall normalized with respect to vacuum thrust of sonic nozzle) are realized from a normal sonic nozzle. The reason for this is apparent when it is realized that inclining the nozzle upstream tends to increase the interaction force and to decrease the normal component of thrust. Hence, if only a moderate interaction force is realized for a normal sonic nozzle, then little may be gained by upstream injection because of the loss in the normal component of thrust. However, if injection normal to the wall produces a large interaction force relative to the thrust, then substantial improvement may be realized by inclining the nozzle. Maurer in reference 22 states that the optimum injection angles against the main stream were in the range of  $15^\circ < \phi < 45^\circ$

Inherent with obtaining the maximum control-force effectiveness is locating the nozzle to achieve the most desirable pressure distribution. Unfortunately, many discrepancies and questions are found in the literature regarding the contribution of aft-end forces. Pressure distributions downstream of the nozzle can be found in references 1, 8, 20, 23, and 24, to list a few. Barnes (reference 1) found that the aft interaction forces due to a laminar boundary layer are considerably smaller than the forward forces (see sketch (c)). In contrast, he found that for



JET INTERACTION FORCES FOR A LAMINAR BOUNDARY LAYER

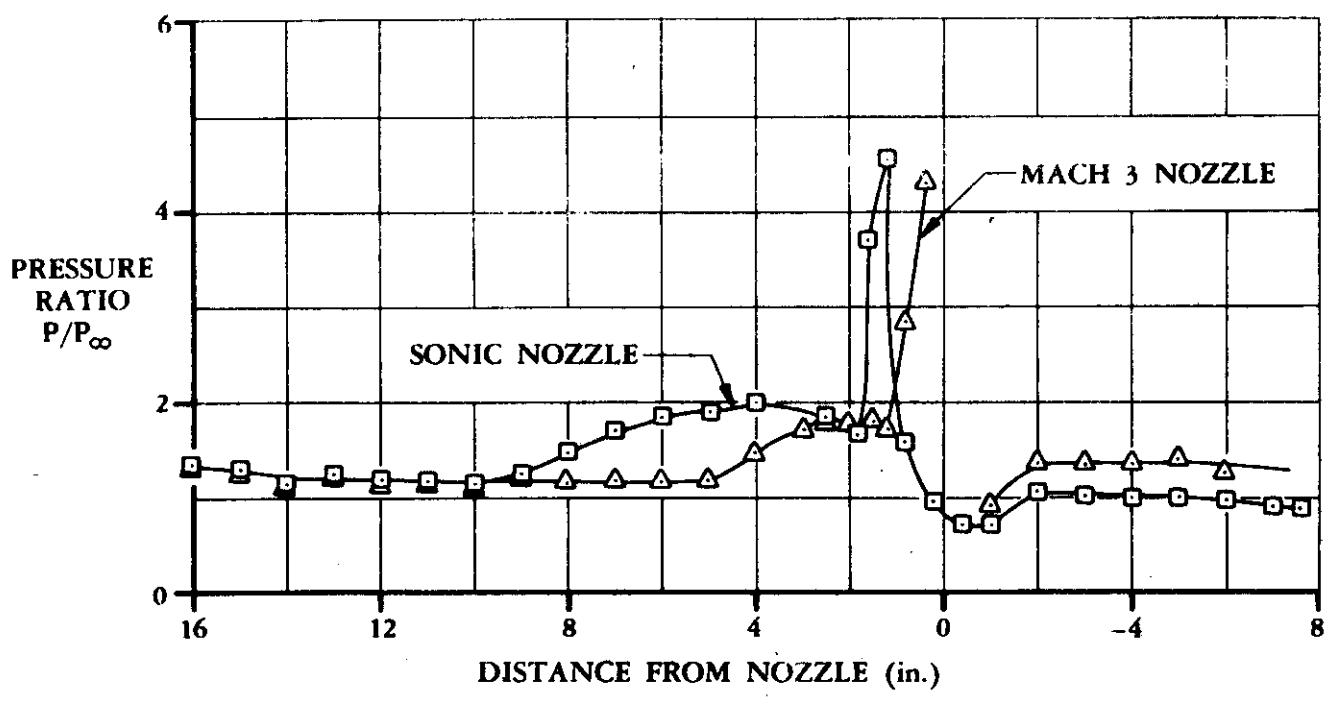
turbulent flows the aft-end forces added significantly to the total force, as is evident in sketch (d). However, the contribution of downstream forces in turbulent flow was found to decrease rapidly as the mass-flow rate increased. Although these sketches do not hold true for all nozzle configurations and flow conditions, they do indicate the relative contribution available from aft-end forces. Kaufman (reference 20), in addition to corroborating the findings of Barnes, found that the reattachment pressure increased strongly with increasing Mach number. Spaid and Zukoski, in reference 8, indicate a dependence of downstream pressure on Mach number, mass-flow rate, and injectant fluid properties. With helium as an injectant, higher downstream static pressure levels were obtained in comparison with those for nitrogen.



An iterative method, utilizing experimental data classified according to nozzle aspect ratios (span/width), is presented in reference 20, which predicts upstream and downstream pressure distributions. The results of the method agree qualitatively with experimental data, although more theoretical analyses must be developed before it becomes a reliable predicting technique.

In general, because of the complexity involved in the interaction phenomena, no consistent nozzle angle or location yields the optimum design for the large range of possible applications and environments; each case must be considered separately.

Although the supersonic jet experiences an increase in reaction force over the sonic jet, it also experiences a decrease in the interaction force; it is not obvious which occurrence dominates. The decreased interaction force is a result of a lower pressure at the exit for a supersonic jet. This prevents the jet from expanding into a full plume upon leaving the nozzle, consequently the interaction force decreases. An example of the relative effect of nozzle exit velocity on surface pressure is shown in sketch (e), from reference 1. The Datcom method predicts improved performance by obtaining supersonic velocities at the nozzle exit. Although experimental data indicate that supersonic nozzles exhausting normal to a wall produce virtually no change in control force, the Datcom method predicts a moderate gain. Experiments show that a beneficial effect occurs principally at positive upstream injection angles.



**SKETCH (e)**  
**COMPARISON OF NORMAL SONIC AND NORMAL MACH 3 CIRCULAR NOZZLE CENTER-LINE PRESSURE DISTRIBUTIONS**

Experimental data show that jet-flow parameters are dominating factors in the jet-interaction phenomena. The more prominent features of the flow are determined by the strength of the jet. For very weak jets (jets with very low pressure ratios ( $P_0/P_1$ )), the jet behavior has been described by Kaufman in reference 20 as similar to film cooling of the surface. There are no separated flow regions, and boundary-layer analysis can describe the resulting flow. In reference 25, Kaufman considers weak jets and focuses his work on the downstream pressure distributions.

Because the Datcom method applies only to strong jets (jets sufficient to induce separation of the boundary layer), it is pertinent to ascertain if separation exists. Available data are not conclusive, but it appears that the minimum nozzle exit pressure  $P_e$  to achieve separation must be of the order of twice the plateau pressure  $P_2$  in the separated boundary layer. Turbulent

flow yields a higher plateau pressure, hence it is the determining condition for establishing a minimum jet-strength requirement. The minimum jet-pressure ratio ( $P_0/P_1$ ) required to induce separation is presented in figure 6.3.2-43 (reference 1). At pressure ratios substantially below those in figure 6.3.2-43, the Datcom method is probably not valid.

When pressure ratios are above the minimum required, some discrepancy exists in the literature regarding the effect on the amplification factor. Werle in reference 26 concludes that a slight loss in effectiveness is displayed as  $P_0/P_1$  approaches infinity, while Barnes in reference 1 indicates virtually no change in amplification factor. Reference 20 contains a summary of available jet-interaction data wherein pertinent flow parameters along with the various slot geometries are tabulated.

The Datcom method does not explicitly account for variations in angle of attack. These changes in angle of attack must be accounted for in evaluating local flow conditions and the state of the boundary layer. At high angles of attack, with the jet on the leeward side, caution must be used. The flow will begin to separate, and the jet will essentially be exhausting into a dead-air region that results in the interaction force decreasing to zero. Pressure distributions for small variations in angle of attack can be found in references 1 and 20 for flat plates, and in reference 3 for an ogive-cylinder.

Several methods for modulating the control force have been suggested. The more pragmatic methods are: pulsing the jet with a constant jet pressure with a pulse duration proportional to the impulse required, using multiple nozzles which are individually actuated, varying the jet plenum pressure, and combinations of these.

The Datcom equations describing the upstream jet interaction have been obtained from a momentum balance method. Several other techniques have been used by investigators in their attempts to establish the most complete and reliable prediction scheme. Blast-wave analogy has been used in references 2 and 27. Other investigators (references 5 and 28) employ finite difference techniques in conjunction with various methods in an attempt to describe the flow field.

#### NOTATION

SYMBOL	DEFINITION
a	speed of sound
b	span of slot nozzle (normal to flow direction)
c	nozzle discharge coefficient
$C_{f_0}$	vacuum-thrust coefficient
$C_{F_c}$	control-force coefficient
$C_p$	pressure coefficient, $C_p = (P - P_1)/q_1$

SYMBOL	DEFINITION
$C_x$	drag coefficient
$d_e$	width of nozzle exit in the flow direction
$d_{LE}$	diameter of surface leading edge
$d_t$	width of nozzle throat
$F_c$	control force
$F_{j_0}$	vacuum thrust
$h$	maximum height of sonic line above surface (effective jet height)
$h_s$	maximum height of separated boundary layer above the surface
$I_{sp}$	jet vacuum specific impulse
$K$	upstream amplification factor (control force normal to the surface normalized with respect to vacuum thrust of sonic nozzle)
$K_o$	upstream amplification factor of normal sonic nozzle
$L$	distance of nozzle from plate leading edge
$M$	Mach number
$\dot{m}$	nozzle mass-flow rate
$P$	pressure
$P_{0j}$	jet plenum pressure
$q$	dynamic pressure, $q = \rho V^2/2$
$R_{\ell_L}$	Reynold number based on length $L$ (dimensionless)
$R_{\ell_s}$	Reynolds number based on the distance to the separation point (dimensionless)
$R_{\ell_\infty}$	unit Reynolds number based on free-stream conditions
SF	safety factor

SYMBOL	DEFINITION
$v$	velocity
$x_{cp}$	center-of-pressure location measured relative to leading edge
$\alpha$	angle of attack (positive with jet on lee side of model)
$\gamma$	specific-heat ratio of jet gases
$\theta$	angle of secondary shock
$\lambda$	mean free path (average distance traveled between molecular collisions)
$\xi$	pressure ratio across secondary shock
$\rho$	density
$\sigma$	boundary-layer separation angle
$\phi$	inclination of nozzle center line relative to an axis normal to surface
<b>SUBSCRIPTS</b>	
cr	corrected
e	nozzle-exit conditions
max	maximum value
min	minimum value
R	reattachment conditions
s	separation conditions
t	throat conditions
trim	trim condition
1	ambient conditions on plate in the absence of a jet
2	conditions in the region of the separated boundary layer
2'	conditions at the second peak pressure in the separated boundary layer
3	conditions in the separated region just before the reattachment shock
4	conditions in the region corresponding to the peak downstream pressure after the reattachment shock

SYMBOL	DEFINITION
--------	------------

$\infty$	undisturbed free-stream conditions
----------	------------------------------------

SUPERSCRIPT
-------------

*	sonic conditions
---	------------------

### DATCOM METHOD

A method for sizing a two-dimensional transverse-jet control system, modulated by varying the jet plenum pressure, is presented in the following procedure. This method is based on a continuum concept and is valid in the Mach number range of 2 to 20. When the mean free path of the surrounding flow  $\lambda$  approaches 0.1 of the jet width  $d_t$ , the method begins to break down. The method is completely invalid when the mean free path equals the jet width. The method is invalid because of angle-of-attack effects when (1) the angle of attack is such that the leading-edge shock interacts with the jet-interaction region; or (2) the boundary layer is separated at the jet location prior to jet discharge.

For a transverse-jet control system that is modulated by pulsing the jet with a constant jet plenum pressure, the sizing procedure is similar to the Datcom method. The primary objective is to determine the maximum jet plenum pressure required to satisfy the trim and separation requirements. This enables the nozzle throat width to be calculated.

The Datcom method consists of first obtaining a time history of the local-flow parameters at the nozzle exit prior to jet discharge. These parameters are then used in conjunction with the time history of the control force required to trim the vehicle, to obtain a control-force coefficient. This control-force coefficient is then corrected, and the sonic amplification factor is obtained as a function of the state of the boundary layer and the Reynolds number. The true value for the amplification factor is then obtained from design charts that account for the nozzle inclination angle and nozzle exit Mach number. From the local Mach number and the nozzle exit conditions, values for the minimum jet plenum pressure required to induce flow separation are obtained. This minimum jet plenum pressure and the vacuum thrust, calculated using the true amplification factor, allow calculation of the nozzle throat diameter. This in turn permits the calculation of the jet plenum pressure and propellant weight requirements to trim the vehicle.

Step 1. Determine if the boundary layer is separated at the jet location prior to jet discharge.

Because of the complex nature of boundary-layer separation at hypersonic speeds, no single criterion is available to accurately determine the location of separation. Exact locations can only be determined through wind-tunnel testing. However, for preliminary-design conditions, the simple Newtonian-shadowing criterion may be used. For a nozzle located on the leeward side, this criterion assumes the location of the separation point to be just downstream of the leading edge when the leeward surface is not directly visible to the free stream. Thus, using the Newtonian-shadowing criterion restricts the Datcom method to transverse-jet control systems located on the windward surface.

If the boundary layer is separated prior to jet discharge, the jet-interaction force is probably nil. For this case, the only force is that due to the reaction of the jet, nullifying the Datcom method.

- Step 2. Determine the time-history values required for the control force  $F_c$  to trim or maneuver the vehicle, the associated free-stream Mach Number  $M_\infty$ , and the associated angle of attack  $\alpha_\infty$ .

These parameters must be obtained from an outside source because of the numerous possibilities for vehicle design and mission trajectories. The jet-interaction center of pressure can be assumed to be located at the nozzle for determining the time history of the control force.

- Step 3. Determine the time-history values of the local-flow parameters:  $P_1$ ,  $q_1$ ,  $M_1$ , and  $R\varrho_L$  in the absence of jet exhaust. The ratios of pressure, dynamic pressure, Mach number, and Reynolds number behind an oblique shock to their respective values in the free stream can be obtained from figures 6.3.2-30, -31, -32, and -33, respectively. These oblique shock ratios are valid so long as the following relationship holds:

$$\frac{0.1375 \frac{L}{d_{LE}} + 2.0}{M_\infty} > 1.0$$

For a thick leading edge and for high Mach numbers, the above relationship becomes invalid, disallowing the calculation of the local-flow parameters by oblique-shock theory. This requires calculating the local-flow properties by other available methods, such as tangent-wedge, blast-wave, Newtonian-impact (reference 29), or the Moeckel shock-loss theory (reference 30).

- Step 4. Determine the time history of the state of the boundary layer from wind-tunnel data that approximate the actual flow conditions, or as a function of  $M_1$  and  $R\varrho_L$  from figure 6.3.2-34.

- Step 5. Make the following initial choices regarding nozzle geometry, if not already established.

- a. Assume a nozzle span  $b$  that is as large as the vehicle geometry permits.
- b. Choose a nozzle injection angle  $\phi$ , where  $0 < \phi < 45^\circ$ .

- Step 6. Determine the nozzle exit Mach number  $M_e$  and the jet vacuum specific impulse  $I_{sp}$ .

The calculation of these parameters requires knowledge of the propellant as well as of the plenum temperature and nozzle shape. It is therefore advisable that these parameters be determined by the propulsion engineer and designer.

Step 7. Determine the time-history values of the control-force coefficient  $C_{F_c}$  by

$$C_{F_c} = \frac{F_c}{q_1 bL} \quad 6.3.2-a$$

Step 8. Calculate the value of the vacuum-thrust coefficient using the value of specific-heat ratio associated with the propellant by

$$C_{f_0} = \left( \frac{2}{\gamma + 1} \right)^{\frac{\gamma}{\gamma - 1}} (\gamma + 1) \quad 6.3.2-b$$

Step 9. Calculate the time-history values of the corrected control-force coefficient by

$$(C_{F_c})_{cr} = \left( \frac{F_c}{q_1 bL} \right) \left( \frac{1.268}{C_{f_0}} \right) \quad 6.3.2-c$$

Step 10. From the Reynolds number and the state of the boundary layer at each time interval, select the appropriate figure from the sizing charts (figures 6.3.2-35 a through -35 e and -40) and determine the time-history values of the amplification factor  $K_o$  for a normal sonic nozzle. For a laminar boundary layer interpolate between figures 6.3.2-35 a through -35 e. For a turbulent boundary layer, which is independent of Reynolds number, use figure 6.3.2-40.

Step 11. Determine the time-history values of the true amplification factor  $K$  from figure 6.3.2-41 or 6.3.2-42, or by

$$K = (K_o - 1) \left[ 1 + \frac{\gamma}{\gamma + 1} \frac{V_e}{a_t} \sin \phi \right] + \left[ \frac{V_e}{a_t} + \frac{a_t}{V_e} \right] \frac{\cos \phi}{2} \quad 6.3.2-d$$

where

$$\frac{V_e}{a_t} = \left[ \frac{(\gamma + 1)M_e^2}{2 + (\gamma - 1)M_e^2} \right]^{1/2} \quad 6.3.2-e$$

Step 12. Calculate the time-history values of the vacuum thrust by

$$F_{j_0} = \frac{F_c}{K} \quad 6.3.2-f$$

Step 13. Determine a time-history value of the minimum jet plenum pressure required to induce separation  $(P_{0j})_{min}$  as follows:

- a. Obtain the time history of the minimum jet plenum pressure ratio  $(P_{0j}/P_1)_{\min}$  as a function of  $V_e/a_t$  and  $M_1$  from figure 6.3.2-43.
- b. Multiply these pressure ratios by the corresponding value of local pressure  $P_1$  to obtain  $(P_{0j})_{\min}$ ; i.e.,

$$(P_{0j})_{\min} = (P_{0j}/P_1)_{\min} P_1 \quad 6.3.2-g$$

Step 14. From the time-history values in steps 12 and 13, determine the maximum value of the vacuum thrust  $(F_{j0})_{\max}$  and the maximum value of plenum pressure  $(P_{0j})_{\max}$

Step 15. Calculate, using experimental data if available, a value for the nozzle discharge coefficient  $c$  (defined as the ratio of the actual nozzle flow to the flow calculated by isentropic laws). In reference 31, relations are given relating the nozzle discharge coefficient to the velocity coefficient, polytropic efficiency, and other nozzle parameters. However, all these relationships require some experimental knowledge of the nozzle.

If no experimental data are available for the nozzle, a value of 0.90 can be assumed with concurrence of the nozzle designer. This value was the lower bound for nozzle discharge coefficients experienced by the investigators in reference 1. However, caution must be used because values as low as 0.71 for nozzle discharge coefficients have also been reported (reference 3).

Step 16. Calculate the nozzle throat width required to provide a vacuum thrust at least as large as the peak value predicted to trim the vehicle. The use of a safety factor to allow for dynamics and contingencies may be desirable (see sample problem). Compute the nozzle throat width as follows:

$$d_t = \frac{(F_{j0})_{\max} SF}{c C_{f0} b (P_{0j})_{\max}} \quad 6.3.2-h$$

Step 17. Calculate the time-history values of the jet plenum pressure required to trim the vehicle by

$$(P_{0j})_{\text{trim}} = \frac{F_{j0}}{c C_{f0} b d_t} \quad 6.3.2-i$$

The jet plenum pressure required to trim the vehicle should always exceed the minimum jet plenum pressure required to induce separation  $(P_{0j})_{\min}$  in step 13. When the jet plenum pressure required to trim the vehicle is less than the minimum jet plenum pressure required to induce separation, two choices are available: (a) the throat width can be reduced with a corresponding increase in jet plenum pressure; (b) no

change can be made, with a loss in effectiveness (amplification factor) for a short period of time. The second choice is preferable because economically and structurally it is advantageous to keep the jet plenum pressure as low as possible.

**Step 18.** Calculate the time-history values of the mass-flow rate by

$$\dot{m} = \frac{F_{j_0}}{I_{sp}} \quad 6.3.2-j$$

**Step 19.** Calculate the required propellant weight by integrating the time history of the mass-flow rate.

**Step 20.** Revise the preliminary estimates made in step 5 and reiterate to obtain an optimum configuration based on trade-offs between system weight, jet-plenum-pressure requirements, and the available control force.

The approach described above is based on the assumption that the jet-interaction center of pressure is located at the nozzle (step 2). In many practical applications this assumption introduces only a small error, particularly for turbulent boundary layers and for relatively low-aspect-ratio nozzles. Present knowledge of jet interaction does not allow an accurate determination of the center of pressure, particularly for laminar boundary layers. However, an approximate method from reference 1 is presented.

The most extreme forward location of the center of pressure results from a two-dimensional nozzle located at the end of a plate. This location can be evaluated and used as a guide in estimating the true center-of-pressure location.

For three-dimensional nozzles the longitudinal extent of the separated boundary layer is much closer to the nozzle than for the two-dimensional case. Experimental data indicate that for most three-dimensional configurations one-half of the calculated value will be conservative and should suffice for preliminary-design purposes.

**Step 21.** Determine the time-history values of the center-of-pressure location for each time increment as follows:

a. For laminar flow

- (1) Assume a value for the separation Reynolds number  $R_{\ell_s}$  of approximately one-fifth the Reynolds number based on the nozzle location  $R_{\ell_L}$ . (It should be noted that although  $R_{\ell_s}$  is based on the separation location, it does not give an accurate value for the separation location.)
- (2) Calculate the plateau-pressure coefficient  $C_{p_2}$  by

$$C_{p_2} = \frac{1.60}{[R_{\ell_s}(M_1^2 - 1)]^{1/4}} \quad 6.3.2-k$$

where

$$C_{p_2} = \frac{P_2 - P_1}{q_1}$$

- (3) Calculate the total drag coefficient of the interaction phenomena by

$$C_x = 4.75 C_{p_2} \quad 6.3.2-\ell$$

- (4) Calculate the normalized effective jet height by

$$\frac{h}{L} = \left( \frac{P_{0j} d_t}{P_1 L} \right) \left( \frac{2 C_{f0}}{\gamma C_x M_1^2 + 2} \right) \quad 6.3.2-m$$

- (5) Calculate the plateau pressure by

$$P_2 = C_{p_2} q_1 + P_1 \quad 6.3.2-n$$

- (6) Calculate the tangent of the boundary-layer separation angle by

$$\tan \sigma = \left[ \frac{5(\xi - 1)}{7 M_1^2 - 5(\xi - 1)} \right] \left[ \frac{7 M_1^2 - (6\xi + 1)}{6\xi + 1} \right]^{1/2} \quad 6.3.2-o$$

where

$$\xi = \frac{P_2}{P_1} \quad 6.3.2-p$$

- (7) Calculate a new value for the normalized effective jet height by

$$\left( \frac{h}{L} \right)_{\text{new}} = \left( 1 - \frac{R_{\ell_s}}{R_{\ell_L}} \right) \tan \sigma \quad 6.3.2-q$$

- (8) If  $\left( \frac{h}{L} \right)_{\text{new}}$  given by equation 6.3.2-q is not equal to  $\left( \frac{h}{L} \right)$  given by equation 6.3.2-m, i.e.,  $\left( \frac{h}{L} \right)_{\text{new}} \neq \left( \frac{h}{L} \right)$ , choose a new value for  $R_{\ell_s}$  in step 21.a.(1) and iterate until  $\left( \frac{h}{L} \right)_{\text{new}} = \left( \frac{h}{L} \right)$ .

- (9) Calculate the normalized center-of-pressure location with respect to the nozzle location by

$$\frac{x_{cp}}{L} = (1 - G) + G \left[ 1 - \frac{G}{2} \left( \frac{C_{F_c}}{C_{p_2}} \right) \right] \quad 6.3.2-r$$

where

$$G \cong 1 - \frac{1}{K} \quad 6.3.2-s$$

and  $C_{p_2}$  is based on the correct value of  $R_{\ell_s}$ . (step 21.a.(2))

b. For turbulent flow

- (1) Calculate the plateau-pressure coefficient  $C_{p_2}$

For  $M_1 < 5$

$$C_{p_2} = 0.41 + 0.481 M_1 - 0.0509 M_1^2 + 0.0061 M_1^3 \quad 6.3.2-t$$

For  $M_1 > 5$

$$C_{p_2} = 0.2257 - 0.0232 M_1 + 0.0014 M_1^2 - 0.00003 M_1^3 \quad 6.3.2-u$$

- (2) Calculate the normalized center-of-pressure location with respect to the nozzle location by

$$\frac{x_{cp}}{L} = (1 - G) + G \left[ 1 - \frac{G}{2} \left( \frac{C_{F_c}}{C_{p_2}} \right) \right] \quad (\text{equation 6.3.2-r})$$

where

$$G \cong 1 - \frac{1}{K} \quad (\text{equation 6.3.2-s})$$

If the calculated value for the center of pressure appears to introduce a significant error into the determination of the required control force in step 2, a new control force should be calculated and the procedure repeated for sizing the nozzle.

### Sample Problem

Given: A transverse jet located at the trailing edge of a flat plate

$$L = 10.0 \text{ ft}$$

$$b = 2.0 \text{ ft}$$

$$\phi = 30^\circ$$

$$V_e/a_t = 2.0$$

$$M_e = 2.39$$

$$\gamma = 1.2$$

$$I_{sp} = 225.0 \text{ sec}$$

$$c = 0.90$$

The sample problem presents a hypothetical case which serves to illustrate the Datcom method. The time-history values of the control force  $F_c$  must be calculated or established prior to the application of the Datcom method. For a real problem, the time-history values of the free-stream Mach number  $M_\infty$  and the angle of attack  $\alpha_\infty$  must also be determined prior to the application of the Datcom method, in order to obtain the time-history values of the local-flow parameters.

**TABLE 6.3.2-A**  
**SAMPLE TRANSVERSE-JET SIZING CALCULATIONS**

1. Time (sec)	1	2	3	4	5
2. Control Force, $F_c$ (lb)	1000	2000	1000	500	200
3. Local Mach No., $M_1$	10.0	9.0	8.0	7.0	6.0
4. Reynolds No., $R\ell_L$	$1 \times 10^8$	$5 \times 10^7$	$1 \times 10^7$	$5 \times 10^6$	$1 \times 10^6$
5. Local Pressure, $P_1$ (lb/in. <sup>2</sup> )	1.70	0.65	0.25	0.10	0.04
6. Dynamic Pressure, $q_1$ (lb/in. <sup>2</sup> )	119	36.8	11.2	3.43	1.01
7. Boundary Layer	turb	turb	turb	turb	lam
8. Control-Force Coeff., $C_{F_c} = F_c/(q_1 b L)$	0.00292	0.0189	0.0310	0.0506	0.0688
9. Corrected Force Coeff., $(C_{F_c})_{cr}$	0.00296	0.0192	0.0314	0.0513	0.0698
10. Sonic Amplification Factor, $K_0$	2.53	2.15	2.10	2.05	2.80
11. Amplification Factor, $K$	3.44	2.86	2.78	2.70	3.86
12. Vacuum Thrust, $F_{ij_0}$ (lb)	291	700	360	185	51.8
13. Min. Pressure Ratio, $(P_{0j}/P_1)_{min}$	560	510	465	420	375
14. Min. Jet Pressure, $(P_{0j})_{min}$ (lb/in. <sup>2</sup> )	950	332	116	42	15
15. Jet Pressure, $(P_{0j})_{trim}$ (lb/in. <sup>2</sup> )	316	760	391	201	56.3
16. Mass-Flow Rate, $\dot{m}$ (lb/sec)	1.29	3.12	1.60	0.82	0.23

With the time-history values of the local-flow parameters completed in items 3 through 7 of table 6.3.2-A, the calculation for the sample problem continues for  $t = 1$  second with step 4.

Determine the state of the boundary layer from wind-tunnel test data or as a function of  $M_1$  and  $R_{\ell L}$  from figure 6.3.2-34.

Determine the control-force coefficient

$$C_{F_c} = \frac{F_c}{q_1 b L} \quad (\text{equation 6.3.2-a})$$

$$= \frac{1000}{(119)(2)(10)(144)} \\ = 0.00292$$

Determine the vacuum-thrust coefficient

$$C_{f_0} = \left( \frac{2}{\gamma + 1} \right)^{\frac{\gamma}{\gamma-1}} (\gamma + 1) \quad (\text{equation 6.3.2-b})$$

$$= \left( \frac{2}{1.2 + 1} \right)^{\frac{1.2}{1.2-1}} (1.2 + 1) \\ = 1.25$$

Determine the corrected control-force coefficient

$$\left( C_{F_c} \right)_{cr} = \left( \frac{F_c}{q_1 b L} \right) \left( \frac{1.268}{C_{f_0}} \right) \quad (\text{equation 6.3.2-c}) \\ = (0.00292) \left( \frac{1.268}{1.250} \right) \\ = 0.00296$$

Determine the sonic amplification factor

$$K_o = 2.53 \quad (\text{figure 6.3.2-40})$$

Determine the true amplification factor

$$K = 3.44 \quad (\text{figure 6.3.2-41})$$

Determine the vacuum thrust

$$F_{j_0} = \frac{F_c}{K} \quad (\text{equation 6.3.2-f})$$

$$= \frac{1.000}{3.44}$$

$$= 291 \text{ lb}$$

Determine the minimum jet plenum pressure required to induce separation

$$\left( \frac{P_{0j}}{P_1} \right)_{\min} = 560 \quad (\text{figure 6.3.2-43})$$

$$\left( P_{0j} \right)_{\min} = \left( \frac{P_{0j}}{P_1} \right)_{\min} P_1 \quad (\text{equation 6.3.2-g})$$

$$= (560) (1.70)$$

$$= 950 \text{ lb/in.}^2$$

The remaining steps cannot be based on one time segment; i.e., the total time history of the various parameters must be considered.

Determine the throat width

$$d_t = \frac{\left( F_{j_0} \right)_{\max} SF}{c C_{f_0} b \left( P_{0j} \right)_{\max}} \quad (\text{equation 6.3.2-h})$$

$$= \frac{(700) (1.25)}{(0.9) (1.25) (24) (950)}$$

$$= 0.0341 \text{ in.}$$

The safety factor is determined from the maximum thrust and the maximum jet plenum pressure. The maximum thrust required is 700 lb; however, a value of 900 lb should allow for contingencies. If the design value for the maximum jet pressure required to induce separation is chosen to be 1000 lb/in.<sup>2</sup> rather than the value of 950 lb/in.<sup>2</sup> in table 6.3.2-A, the safety factor can be expressed as

$$SF = \left| \frac{\left( F_{j_0} \right)_{\max}}{\left( P_{0j} \right)_{\max}} \right|_{\text{design}} \left| \frac{\left( P_{0j} \right)_{\max}}{\left( F_{j_0} \right)_{\max}} \right|$$

$$= \left( \frac{900}{1000} \right) \left( \frac{950}{700} \right)$$

$$= 1.21, \text{ use } 1.25$$

The jet plenum pressures required to trim the vehicle are calculated based on the throat width by using equation 6.3.2-i. These calculated plenum pressures must always exceed the plenum pressure required to induce separation (950 lb/in.<sup>2</sup> at the initial time period of one second). The jet plenum pressures required for trim (item 15 in the table) were computed as follows:

$$\left( P_{0j} \right)_{\text{trim}} = \frac{F_{j_0}}{c C_{f_0} b d_t} \quad (\text{equation 6.3.2-i})$$

$$\begin{aligned} &= \frac{F_{j_0}}{(0.9)(1.25)(24)(0.0341)} \\ &= 1.086 F_{j_0} \end{aligned}$$

It is seen that the jet plenum pressures required for trim (item 15) are less than the specified minimum value at the initial time of one second. Two choices are available: either the throat width can be reduced with a corresponding increase in jet pressure or, if this proves to be detrimental to the system weight, then some loss in effectiveness can probably be accepted for a short time period in order to avoid increasing the jet pressure. The proper choice depends upon the sensitivity of the control-system weight to an increase in jet plenum pressure.

The propellant weight required to trim the vehicle is obtained from the integral of the mass-flow rate in item 16. For the sample problem, the required propellant weight to trim the vehicle is 7.06 lb.

In order to arrive at an optimum nozzle design in any particular application, several iterations of the above procedure should be made with systematic variations in the initial assumptions. If extensive sizing studies are required and if suitable computing facilities are available, a computer program, described in reference 1, should be used.

Determine the center-of-pressure location.

Two cases are presented to illustrate the procedure: one where the boundary layer is turbulent and one where the boundary layer is laminar.

Case I             $t = 4$  seconds (turbulent flow)

$$\left. \begin{array}{l} M_1 = 7.0 \\ C_{F_c} = 0.0506 \\ K = 2.70 \end{array} \right\} \text{(table 6.3.2-A)}$$

$$C_{p_2} = 0.2257 - 0.0232 M_1 + 0.0014 M_1^2 - 0.00003 M_1^3 \quad \text{(equation 6.3.2-u)}$$

$$\begin{aligned} &= 0.2257 - 0.0232 (7) + 0.0014 (49) - 0.00003 (343) \\ &= 0.1216 \end{aligned}$$

$$G \cong 1 - \frac{1}{K} \quad \text{(equation 6.3.2-s)}$$

$$= 1 - \frac{1}{2.70} = 0.63$$

$$\frac{x_{cp}}{L} = (1 - G) + G \left[ 1 - \frac{G}{2} \left( \frac{C_{F_c}}{C_{p_2}} \right) \right] \quad \text{(equation 6.3.2-r)}$$

$$= (1 - 0.63) + 0.63 \left[ 1 - \frac{0.63}{2} \left( \frac{0.0506}{0.1216} \right) \right]$$

$$= 0.917$$

$$x_{cp} = (0.917) L$$

$$= (0.917) (10)$$

$$= 9.17 \text{ ft from leading edge}$$

Case II             $t = 5$  seconds (laminar flow)

$$\left. \begin{array}{l} M_1 = 6.0 \\ C_{F_c} = 0.0688 \\ K = 3.86 \end{array} \right\} \text{(table 6.3.2-A)}$$

$$\left. \begin{array}{l} P_{0j} = 56.3 \text{ lb/in.}^2 \\ P_1 = 0.04 \text{ lb/in.}^2 \\ q_1 = 1.01 \text{ lb/in.}^2 \end{array} \right\} \quad (\text{table 6.3.2-A})$$

First iteration (assume  $R_{\ell_s} = 1 \times 10^5$ )

$$\begin{aligned} C_{p_2} &= \frac{1.60}{[R_{\ell_s} (M_1^2 - 1)]^{1/4}} && (\text{equation 6.3.2-k}) \\ &= \frac{1.60}{[10^5 (36 - 1)]^{1/4}} \\ &= 0.037 \end{aligned}$$

$$\begin{aligned} C_x &= 4.75 C_{p_2} && (\text{equation 6.3.2-l}) \\ &= (4.75) (0.037) \\ &= 0.1758 \end{aligned}$$

$$\begin{aligned} \frac{h}{L} &= \left[ \frac{P_{0j} d_t}{P_1 L} \right] \left[ \frac{2 C_{f0}}{\gamma C_x M_1^2 + 2} \right] && (\text{equation 6.3.2-m}) \\ &= \left[ \frac{(56.3) (0.0341)}{(0.04) (10) (12)} \right] \left[ \frac{(2) (1.25)}{(1.2) (0.1758) (36) + 2} \right] \\ &= (0.400) (0.2605) \\ &= 0.104 \end{aligned}$$

$$\begin{aligned} P_2 &= C_{p_2} q_1 + P_1 && (\text{equation 6.3.2-n}) \\ &= (0.037) (1.01) + 0.04 \\ &= 0.0774 \text{ lb/in.}^2 \end{aligned}$$

$$\xi = \frac{P_2}{P_1} = \frac{0.0774}{0.04} = 1.93 \quad (\text{equation 6.3.2-p})$$

$$\tan \sigma = \left[ \frac{5(\xi - 1)}{7M_1^2 - 5(\xi - 1)} \right] \left[ \frac{7M_1^2 - (6\xi + 1)}{6\xi + 1} \right]^{1/2} \quad (\text{equation 6.3.2-o})$$

$$= \left[ \frac{5(0.93)}{7(36) - 5(0.93)} \right] \left[ \frac{7(36) - [6(1.93) + 1]}{6(1.93) + 1} \right]^{1/2}$$

$$= (0.0188)(4.36)$$

$$= 0.082$$

$$\left( \frac{h}{L} \right)_{\text{new}} = \left( 1 - \frac{R_{q_s}}{R_{q_L}} \right) \tan \sigma \quad (\text{equation 6.3.2-q})$$

$$= \left( 1 - \frac{10^5}{10^6} \right) (0.0819)$$

$$= 0.0738$$

Since  $0.0738 \neq 0.104$ , try a second iteration.

Second iteration (assume  $R_{q_s} = 5 \times 10^4$ )

$$C_{p_2} = \frac{1.60}{[(5 \times 10^4)(36 - 1)]^{1/4}} = 0.044 \quad (\text{equation 6.3.2-k})$$

$$C_x = (4.75)(0.044) = 0.209 \quad (\text{equation 6.3.2-l})$$

$$\frac{h}{L} = \left[ \frac{(56.3)(0.0341)}{(0.04)(10)(12)} \right] \left[ \frac{2(1.25)}{(1.2)(0.209)(36) + 2} \right] \quad (\text{equation 6.3.2-m})$$

$$= (0.400)(0.227)$$

$$= 0.0908$$

$$P_2 = (0.044)(1.01) + 0.04 = 0.0844 \text{ lb/in.}^2 \quad (\text{equation 6.3.2-n})$$

$$\xi = \frac{P_2}{P_1} = \frac{0.0844}{0.04} = 2.11 \quad (\text{equation 6.3.2-p})$$

$$\begin{aligned}\tan \sigma &= \left[ \frac{5(1.11)}{252 - 5(1.11)} \right] \left[ \frac{252 - [6(2.11) + 1]}{6(2.11) + 1} \right]^{1/2} \quad (\text{equation 6.3.2-o}) \\ &= (0.0225)(4.18) \\ &= 0.094\end{aligned}$$

$$\left(\frac{h}{L}\right)_{\text{new}} = \left(1 - \frac{5 \times 10^4}{10^6}\right) (0.094) = 0.0893 \quad (\text{equation 6.3.2-q})$$

Since  $0.0893 \neq 0.0908$ , try a third iteration.

Third iteration (assume  $R_{\ell_s} = 4.85 \times 10^4$ )

$$C_{p_2} = \frac{1.60}{[(4.85 \times 10^4)(36 - 1)]^{1/4}} = 0.0443 \quad (\text{equation 6.3.2-k})$$

$$C_x = (4.75)(0.0443) = 0.210 \quad (\text{equation 6.3.2-l})$$

$$\begin{aligned}\frac{h}{L} &= \left[ \frac{(56.3)(0.0341)}{(0.04)(10)(12)} \right] \left[ \frac{(2)(1.25)}{(1.2)(0.210)(36) + 2} \right] \quad (\text{equation 6.3.2-m}) \\ &= (0.400)(0.226) \\ &= 0.0904\end{aligned}$$

$$P_2 = (0.0443)(1.01) + 0.04 = 0.0847 \text{ lb/in.}^2 \quad (\text{equation 6.3.2-n})$$

$$\xi = \frac{P_2}{P_1} = \frac{0.0847}{0.04} = 2.118 \quad (\text{equation 6.3.2-p})$$

$$\begin{aligned}\tan \sigma &= \left[ \frac{5(1.118)}{252 - 5(1.118)} \right] \left[ \frac{252 - [6(2.118) + 1]}{6(2.118) + 1} \right]^{1/2} \quad (\text{equation 6.3.2-o}) \\ &= (0.0227)(4.17) \\ &= 0.0947\end{aligned}$$

$$\left(\frac{h}{L}\right)_{\text{new}} = \left(1 - \frac{4.95 \times 10^4}{10^6}\right)(0.0947) = 0.0901 \quad (\text{equation 6.3.2-q})$$

$$0.0901 \cong 0.0904; \text{ therefore } R_{\ell_s} = 4.85 \times 10^4$$

$$C_{p_2} = 0.0443$$

$$G \cong 1 - \frac{1}{K} = 1 - \frac{1}{3.86} = 0.741 \quad (\text{equation 6.3.2-s})$$

$$\begin{aligned} \frac{x_{cp}}{L} &= (1 - G) + G \left[ 1 - \frac{G}{2} \left( \frac{C_F c}{C_{p_2}} \right) \right] \quad (\text{equation 6.3.2-r}) \\ &= (1 - 0.741) + 0.741 \left[ 1 - \frac{0.741}{2} \left( \frac{0.0688}{0.0443} \right) \right] \\ &= 0.574 \end{aligned}$$

Since the value of  $x_{cp}/L = 0.574$  is a conservative estimate of the most extreme forward position for a two-dimensional nozzle, the actual value is probably close to 0.75 or 0.80 (see discussion prior to step 21). Since the center of pressure for  $t = 5$  seconds is not close to the nozzle location, it would be advisable to calculate a new control force based on the approximate value of  $x_{cp} = 7.5$  ft and repeat the sizing calculation for  $t = 5$  seconds.

## REFERENCES

1. Barnes, J. W., Davis, J. G., and Tang, H. H.: Control Effectiveness of Transverse Jets Interacting With a High-Speed Free Stream. Vol. I. Design Charts, Theoretical and Experimental Results. AFFDL TR-67-90, Vol. I, 1967. (U)
2. Cassel, L. A., Davis, J. G., and Engh, D. P.: Lateral Jet Control Effectiveness Prediction for Axisymmetric Missile Configurations. Army Missile Command, RD-TR-68-6, 1968. (U)
3. Phinney, R. E., Werle, M. J., and Knott, J.: Slot Jet Interaction Studies of an Ogive Cylinder at  $M_\infty = 4$  and 5. Naval Ordnance Lab., NOL TR-68-143, 1968. (U)
4. Strike, W. T., Schueler, C. J., and Deitering, J. S.: Interactions Produced by Sonic Lateral Jets Located on Surfaces in a Supersonic Stream. AEDC-TDR-63-22, 1963. (U)
5. Zakkay, V., Erdos, J., and Calarese, W.: An Investigation of the Interaction Between a Transverse Sonic Jet and a Hypersonic Stream. N.Y. Univ., NYU-AA-68-27, 1968. (U)
6. Swanson, R. S.: Parametric and Preliminary Design Comparison of Transverse Jet Controls and Flap-Type Aerodynamic Controls for Re-entry Vehicles and High-Speed Cruise Aircraft. AFFDL TR-68-98, 1968. (U)
7. Heyser, A., and Maurer, F.: Experimental Investigations on Solid Spoilers and Jet Spoilers at Mach Numbers of 0.6 to 2.8. Cal. Inst. of Tech., JPL, Trans. No. 32, 1964. (U)
8. Spaid, F. W., and Zukoski, E. E.: A Study of the Interaction of Gaseous Jets From Transverse Slots With Supersonic External Flows. Douglas Aircraft Company DP 4480, 1967. (U)
9. Spring, D. J., Street, T. A., and Amick, J. L.: Transverse Jet Experiments and Theories — A Survey of the Literature. US Army Missile Command RD-TR-67-4, 1967. (U)

10. Schlichting, H.: *Boundary-Layer Theory*. McGraw-Hill Co., New York, 1955. (U)
11. Howarth, L. (edit): *Modern Developments in Fluid Dynamics – High-Speed Flow*. Vol. I. Oxford Univ. Press, 1953. (U)
12. Chapman, D. R., Kuehn, D., and Larson, H. K.: *Investigation of Separated Flows in Supersonic and Transonic Streams With Emphasis on the Effects of Transition*. NACA TR 1356, 1958. (U)
13. Sterrett, J. R., and Emery, J. C.: *Extension of Boundary-Layer-Separation Criteria to a Mach Number of 6.5 by Utilizing Flat Plates With Forward-Facing Steps*. NASA TN D-618, 1960. (U)
14. Hammitt, A. G.: *The Interaction of Shock Waves and Turbulent Boundary Layers*. JAS, Vol. 25, No. 6, 1958. (U)
15. Lange, R. H.: *Present Status of Information Relative to the Prediction of Shock-Induced Boundary-Layer Separation*. NACA TN 3065, 1954. (U)
16. Reshotko, E., and Tucker, M.: *Effect of a Discontinuity on Turbulent Boundary-Layer-Thickness Parameters With Application to Shock-Induced Separation*. NACA TN 3454, 1955. (U)
17. Drougge, G.: *An Experimental Investigation of the Influence of Strong Adverse Pressure Gradients of Turbulent Boundary Layers at Supersonic Speeds*. Aero. Res. Inst. of Sweden, Rept. No. 46, 1953. (U)
18. Amick, J. L., and Hays, P. B.: *Interaction Effects of Side Jets Issuing From Flat Plates and Cylinders Alined With a Supersonic Stream*. WADD TR-60-329, 1960. (U)
19. Shaw, W. J.: *Static Stability Characteristics of Cones, Including Effects of Nose Bluntness, Ablation Interactions, and Selected Protuberance Configurations*. McDonnell Douglas Corp. DAC-63190, 1969. (U)
20. Kaufman, L. G., II, and Koch, F.: *High Speed Flows Past Transverse Jets*. Grumman Aircraft Eng. Corp. RE-348, 1968. (U)
21. Maurer, F.: *Three-Dimensional Effects in Shock-Separated Flow Regions Ahead of Lateral Control Jets Issuing From Slot Nozzles of Finite Length*. Published in the proceedings of a Specialists' Meeting, sponsored by the AGARD Fluid Dynamics Panel held in Rhode-Saint Genese, Belgium, 1966. (U)
22. Maurer, F.: *Interference Effects Produced by Gaseous Side-Jets Issuing Into a Supersonic Stream*. Deutsche Luft-und Raumfahrt Forschungsbericht 65-04, 1965. (U)
23. Volz, W. C., and Werle, M. J.: *Jet Interaction Studies*. Naval Ordnance Lab., White Oak, 1966. (U)
24. Orth, R. C., and Funk, J. A.: *An Experimental and Comparative Study in Jet Penetration in Supersonic Flow*. AIAA Paper 67-225, 1967. (U)
25. Kaufman, L. G., II: *Classification of Interactions Due to High-Speed Flows Past Transverse Jets*. Grumman Aircraft Eng. Corp., Research Rept. RE-154, 1962. (U)
26. Werle, M. J.: *A Critical Review of Analytical Methods for Estimating Control Forces Produced by Secondary Injection*. Naval Ordnance Lab., NOL TR-68-5, 1968 (U)
27. Evers, J. L.: *A Study of the Bow Shock Induced by Secondary Injection Into Supersonic and Hypersonic Flows*. Von Karman Inst. for Fluid Dynamics, TN 29, 1965. (U)
28. Cox, E. F.: *Interaction of a Two Dimensional Jet With a Deflecting Stream*. So. Carolina Univ. Ph.D. Thesis, 1967. (U)
29. Truitt, R. W.: *Hypersonic Aerodynamics*. The Ronald Press Company, New York, 1959. (U)
30. Moeckel, W. E.: *Some Effects of Bluntness on Boundary-Layer Transition and Heat Transfer at Supersonic Speeds*. NACA TR 1312, 1957. (U)
31. Emmons, H. W. (edit): *Fundamentals of Gas Dynamics*. Princeton University Press, Princeton, N.J., 1958. (U)
32. Nunn, R. H., and Ulrich, R. D.: *Jet Reaction Control for Atmospheric Flight: A Review and Summary of the Literature*. Naval Weapons Center NWC-TP-4559, 1969. (C) Title Unclassified

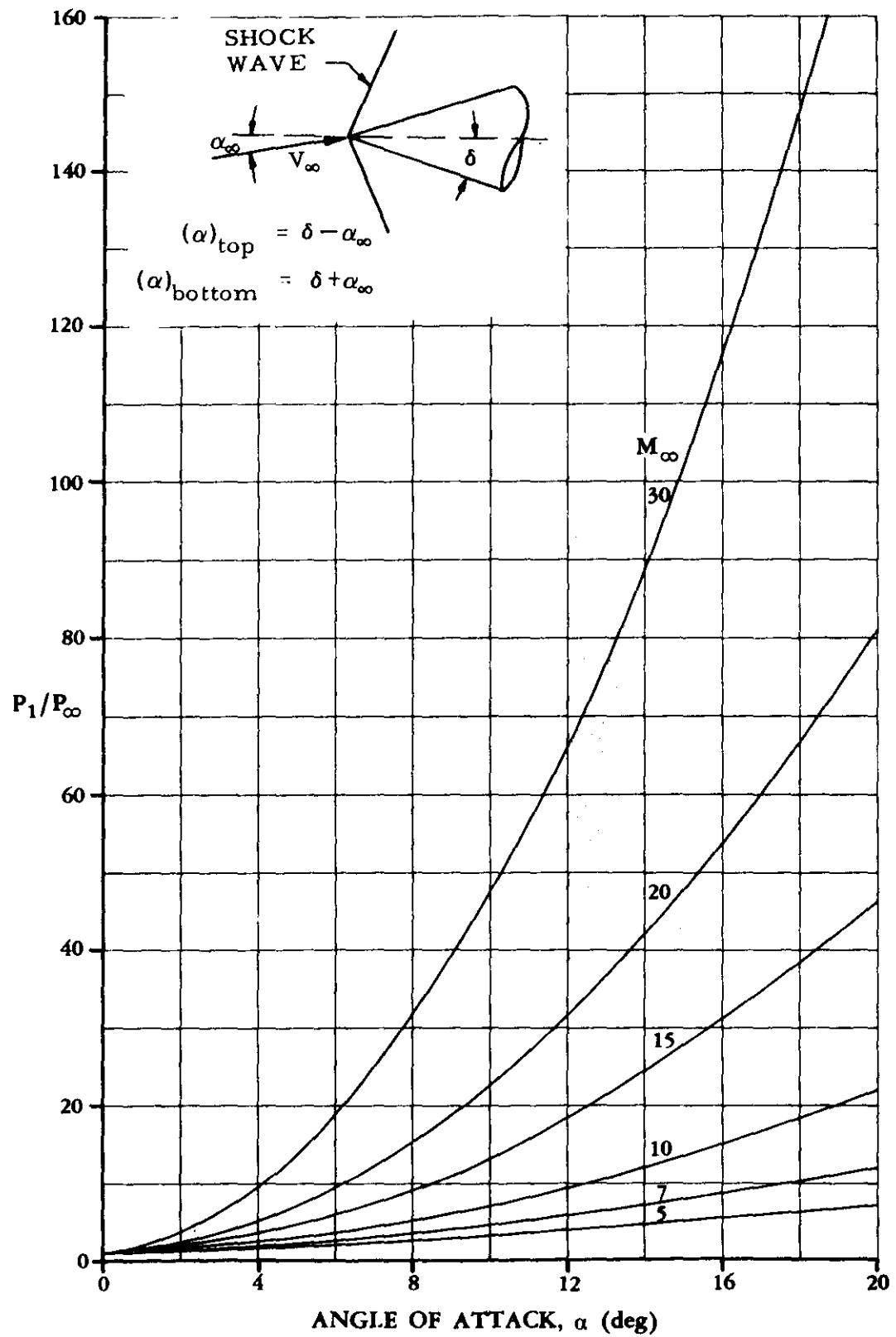


**FIGURE 6.3.2-30 OBlique SHOCK PRESSURE RATIO FOR PERFECT GAS**

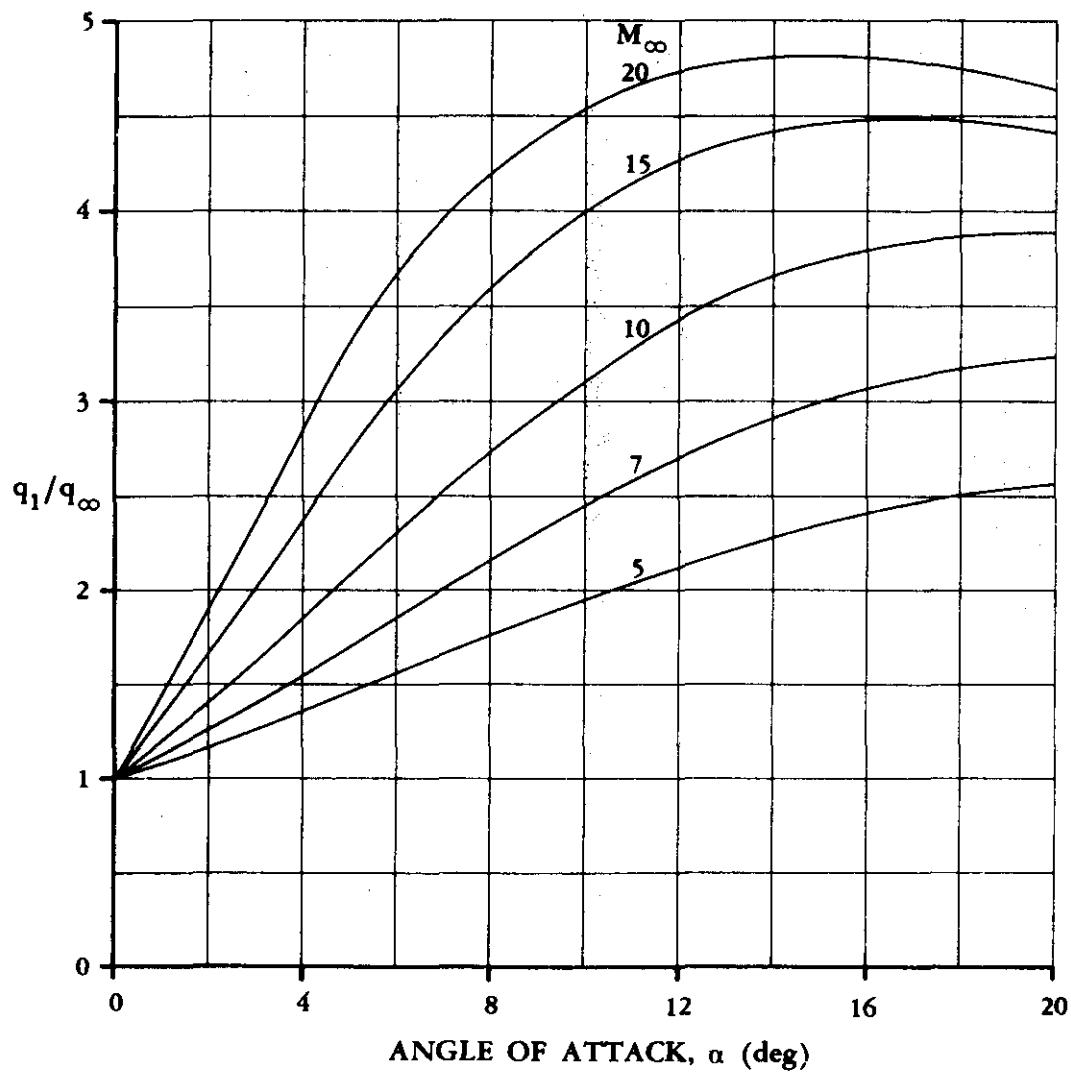
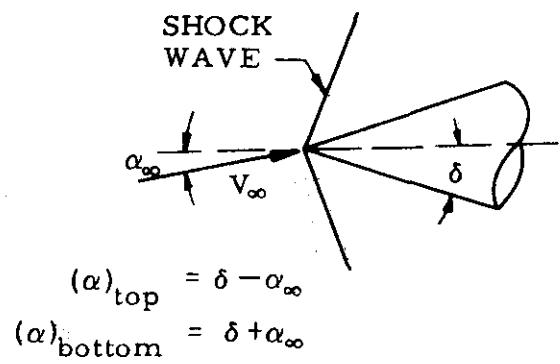
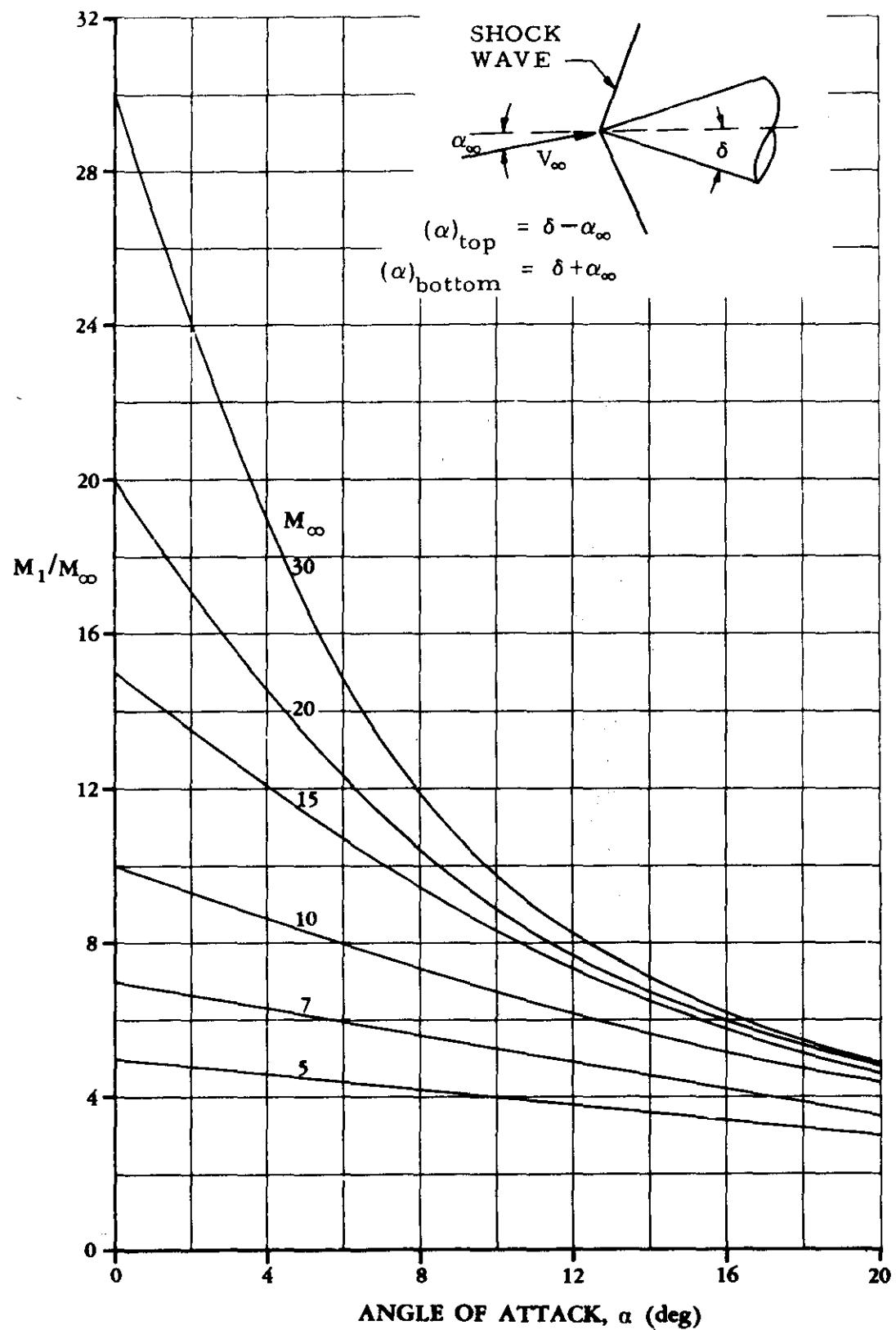


FIGURE 6.3.2-31 OBLIQUE SHOCK DYNAMIC-PRESSURE RATIO FOR PERFECT GAS



**FIGURE 6.3.2-32 OBlique SHOCK MACH NUMBER RATIO FOR PERFECT GAS**

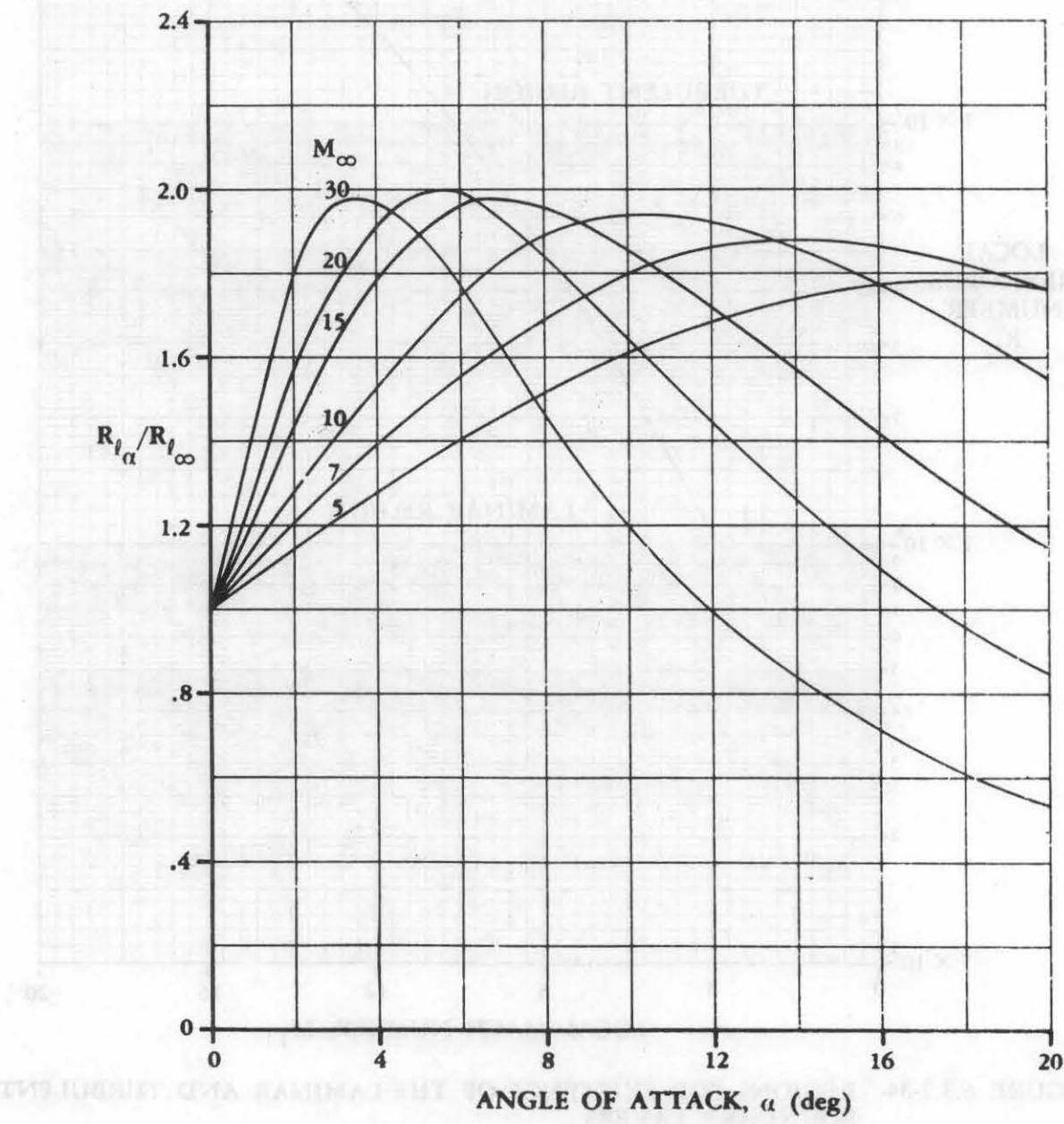
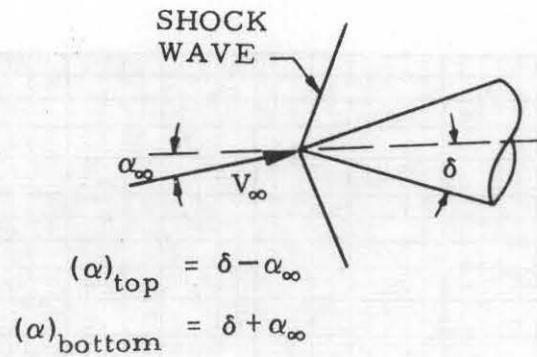
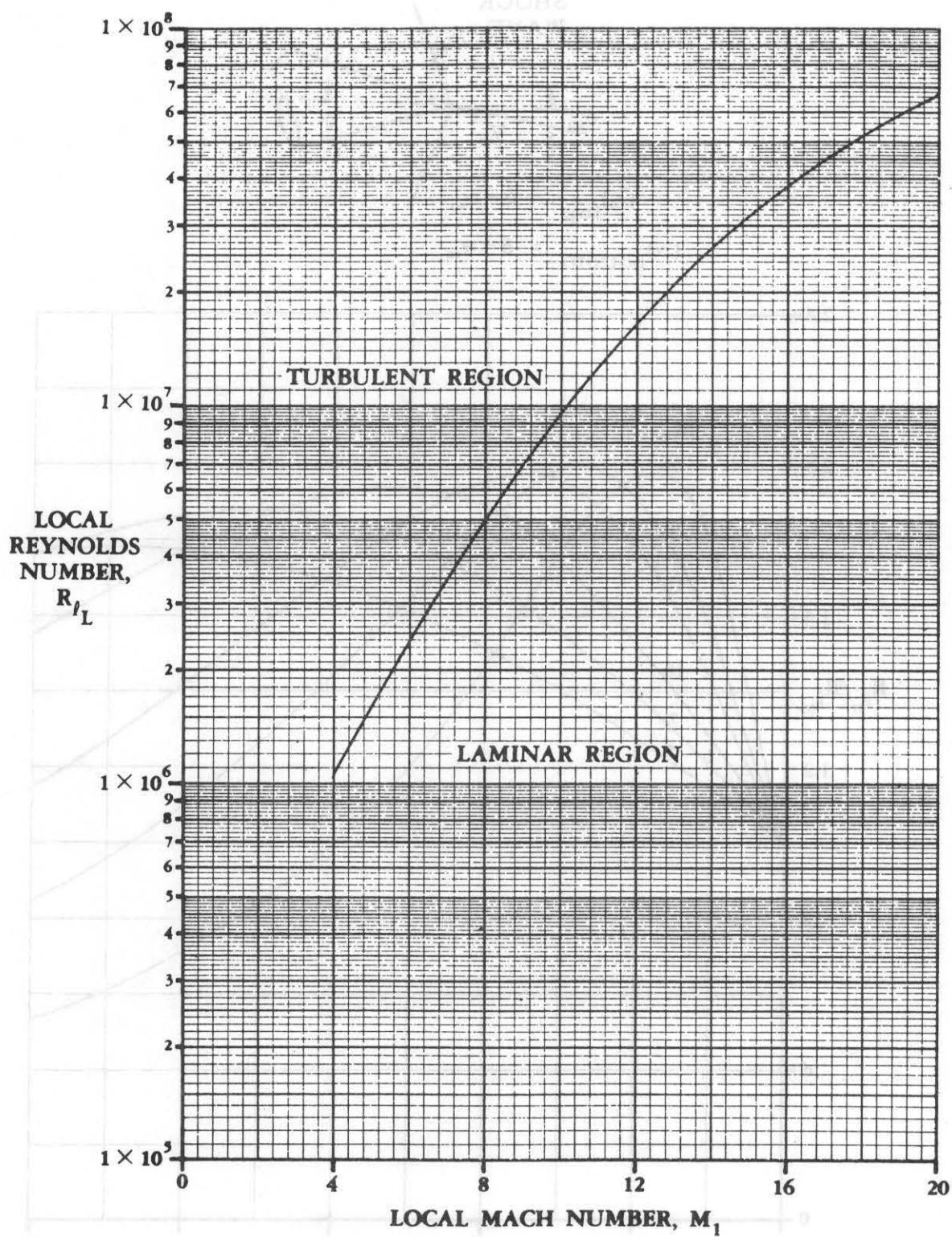


FIGURE 6.3.2-33 OBLIQUE SHOCK REYNOLDS-NUMBER RATIO FOR PERFECT GAS



**FIGURE 6.3.2-34 REGIONS FOR EXISTENCE OF THE LAMINAR AND TURBULENT BOUNDARY LAYERS**

(a)  $R_{fL} = 1 \times 10^5$

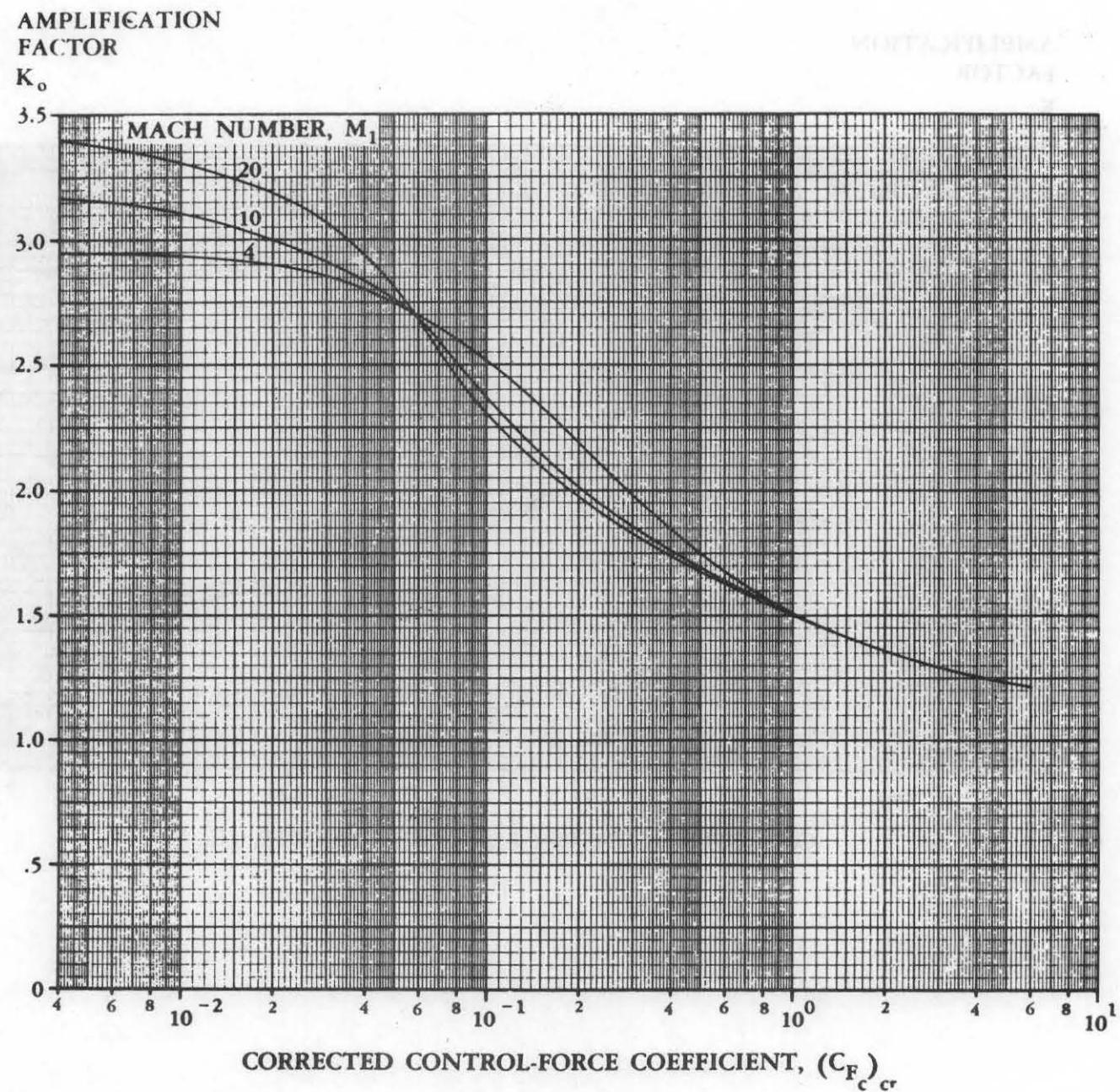


FIGURE 6.3.2-35 AMPLIFICATION FACTOR VERSUS CONTROL-FORCE COEFFICIENT FOR LAMINAR BOUNDARY LAYER

(b)  $R_{i_L} = 1 \times 10^6$

AMPLIFICATION  
FACTOR

$K_o$

MACH NUMBER,  $M_1$

20

10

6

4

2

3

2

1

0

0

4

6

8

$10^{-2}$

CORRECTED CONTROL-FORCE COEFFICIENT,  $(C_{F_c})_{cr}$

2 4 6 8 10<sup>-1</sup> 2 4 6 8 10<sup>0</sup> 2 4 6 8 10<sup>1</sup>

FIGURE 6.3.2-35 (CONTD)

FIGURE 6.3.2-35 (CONTD)  
CORRECTED CONTROL-FORCE COEFFICIENT  
 $(C_{F_c})_{cr}$  VS MACH NUMBER FOR VARIOUS  
VALUES OF INDIVIDUAL AMPLIFICATION  
FACTORS  $K_o$  AND LIFT COEFFICIENT  
 $R_{i_L}$  FOR A PLANE WITH A  
REAR-LOCATED CONTROL SURFACE

(c)  $R_{fL} = 1 \times 10^7$

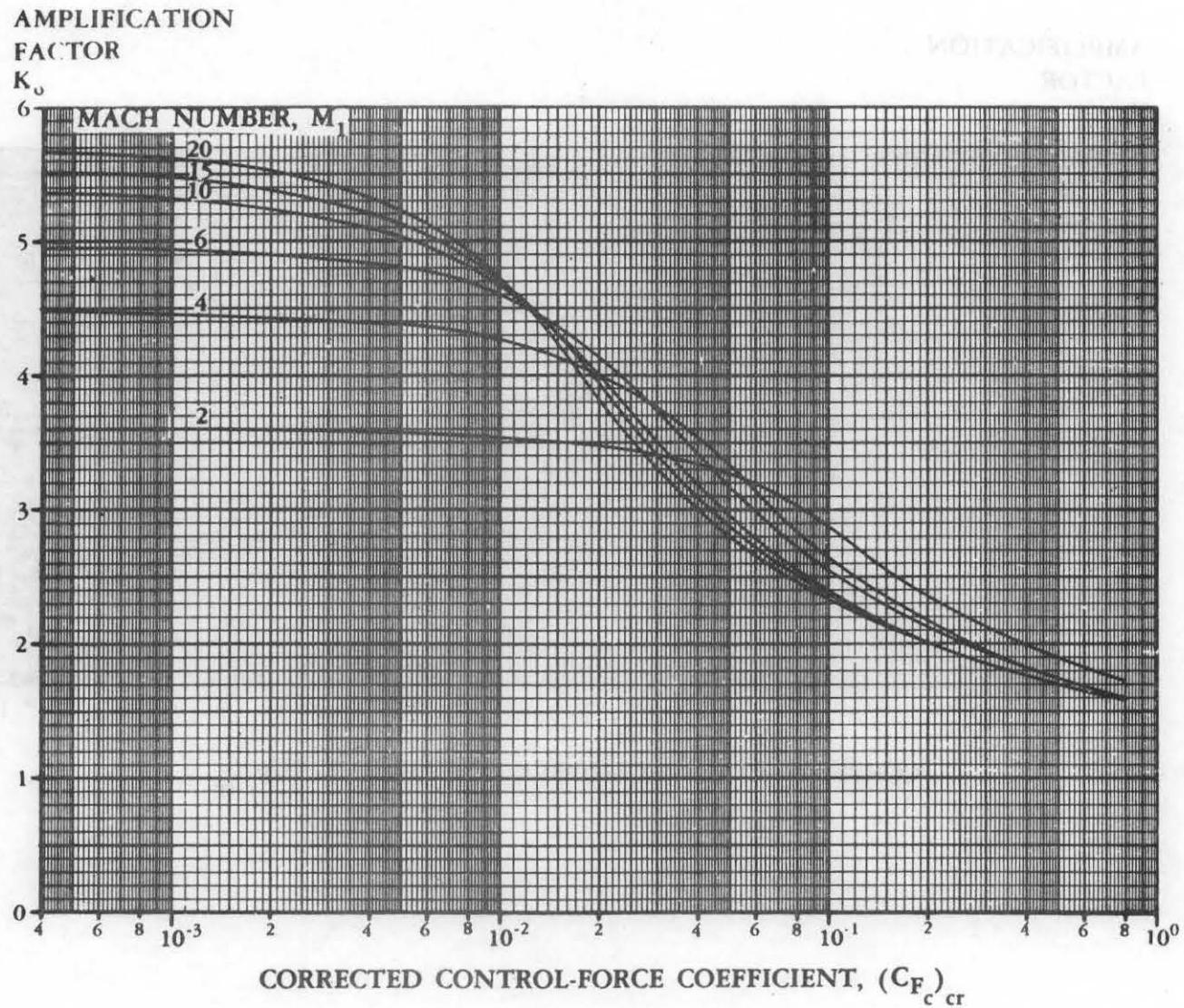


FIGURE 6.3.2-35 (CONTD)

(d)  $R_{f_L} = 1 \times 10^8$

AMPLIFICATION  
FACTOR

$K_o$

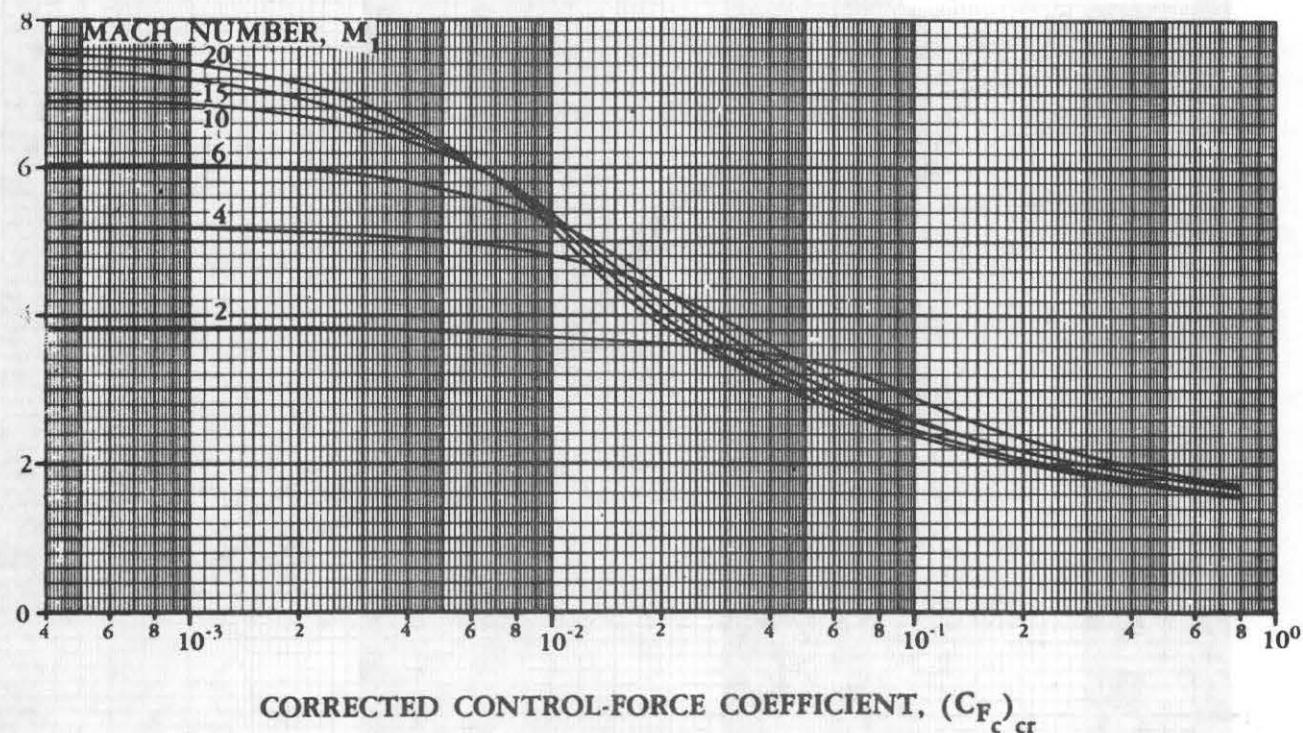


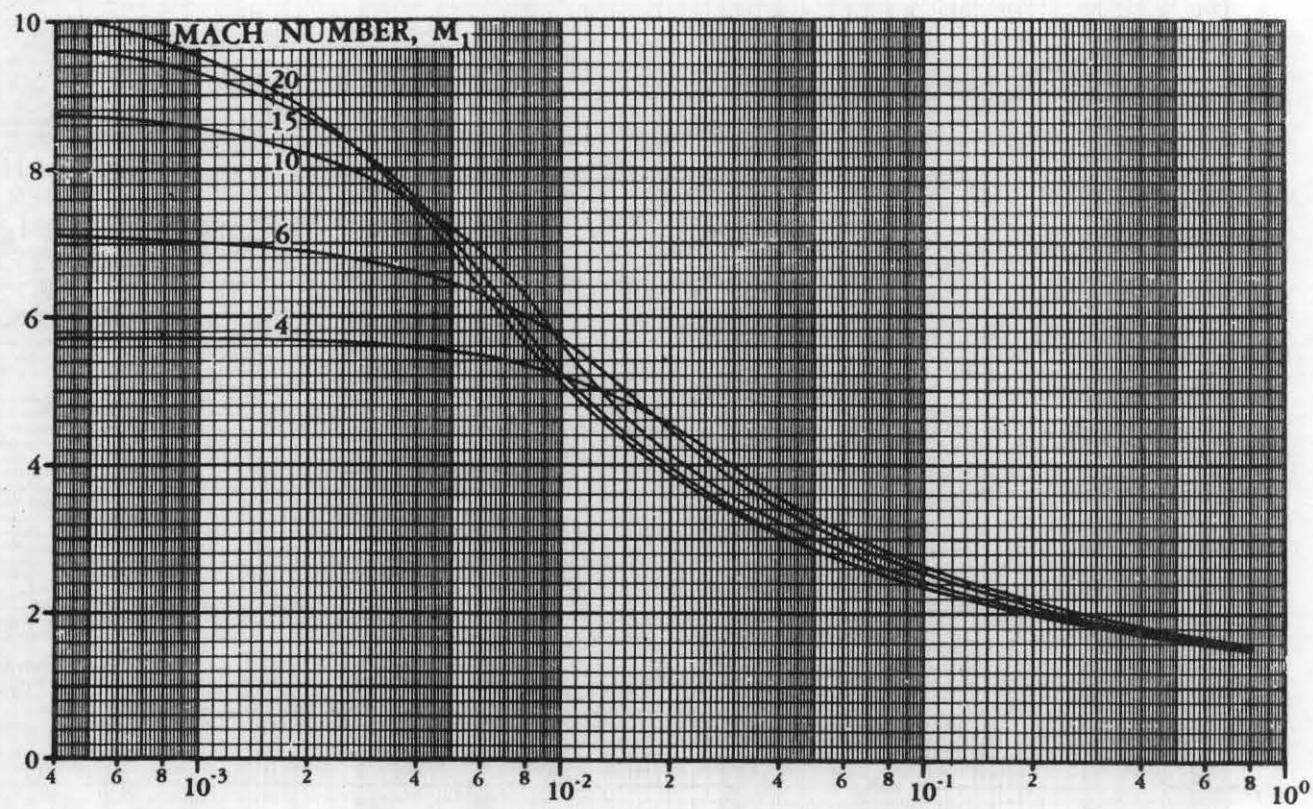
FIGURE 6.3.2-35 (CONTD)

$$(e) R_L = 1 \times 10^9$$

AMPLIFICATION

FACTOR

$K_o$



CORRECTED CONTROL-FORCE COEFFICIENT,  $(C_{Fc})_{cr}$

FIGURE 6.3.2-35 (CONTD)

## AMPLIFICATION

### FACTOR

$K_o$

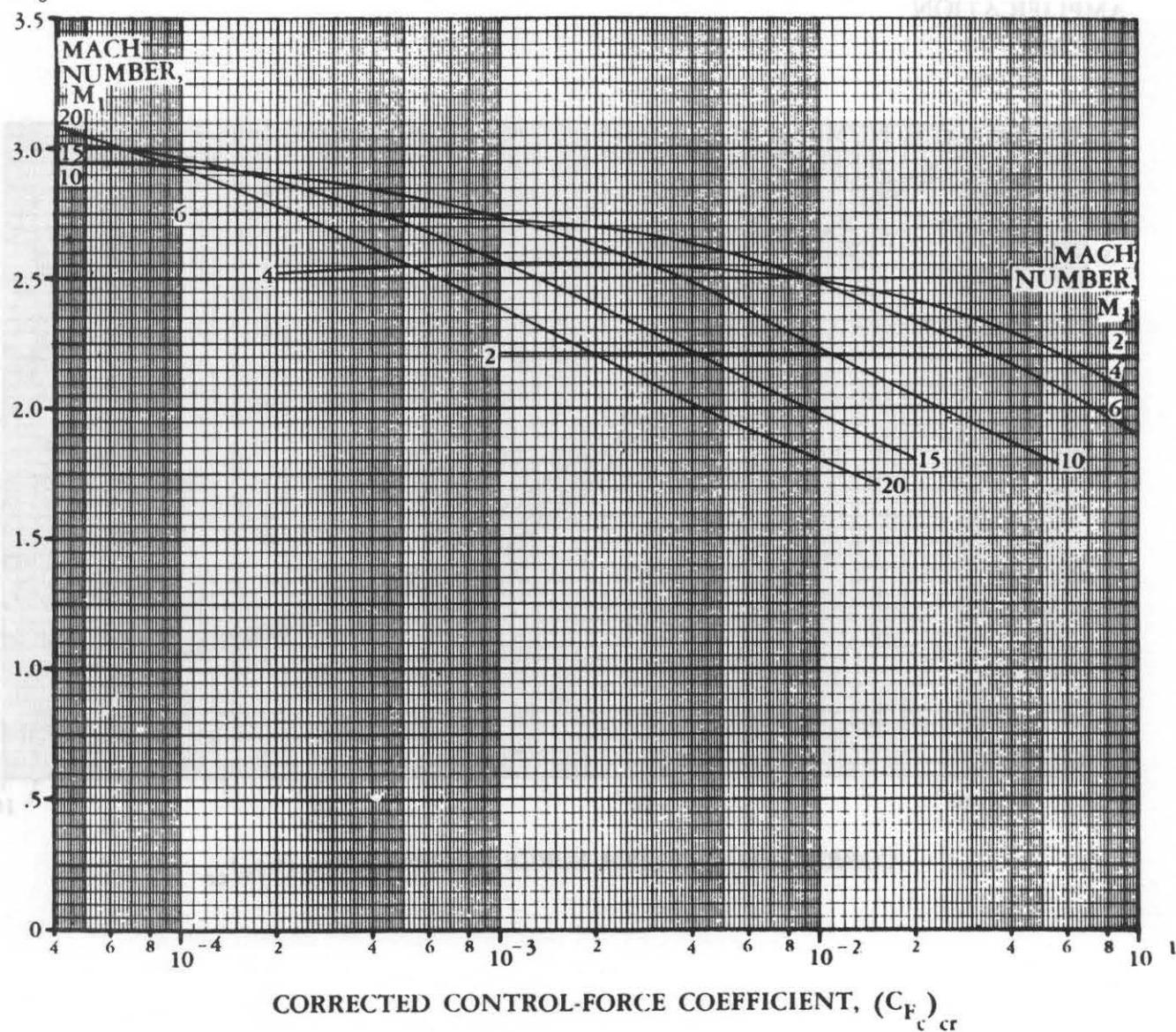


FIGURE 6.3.2-40 AMPLIFICATION FACTOR VERSUS CONTROL-FORCE COEFFICIENT FOR TURBULENT BOUNDARY LAYER

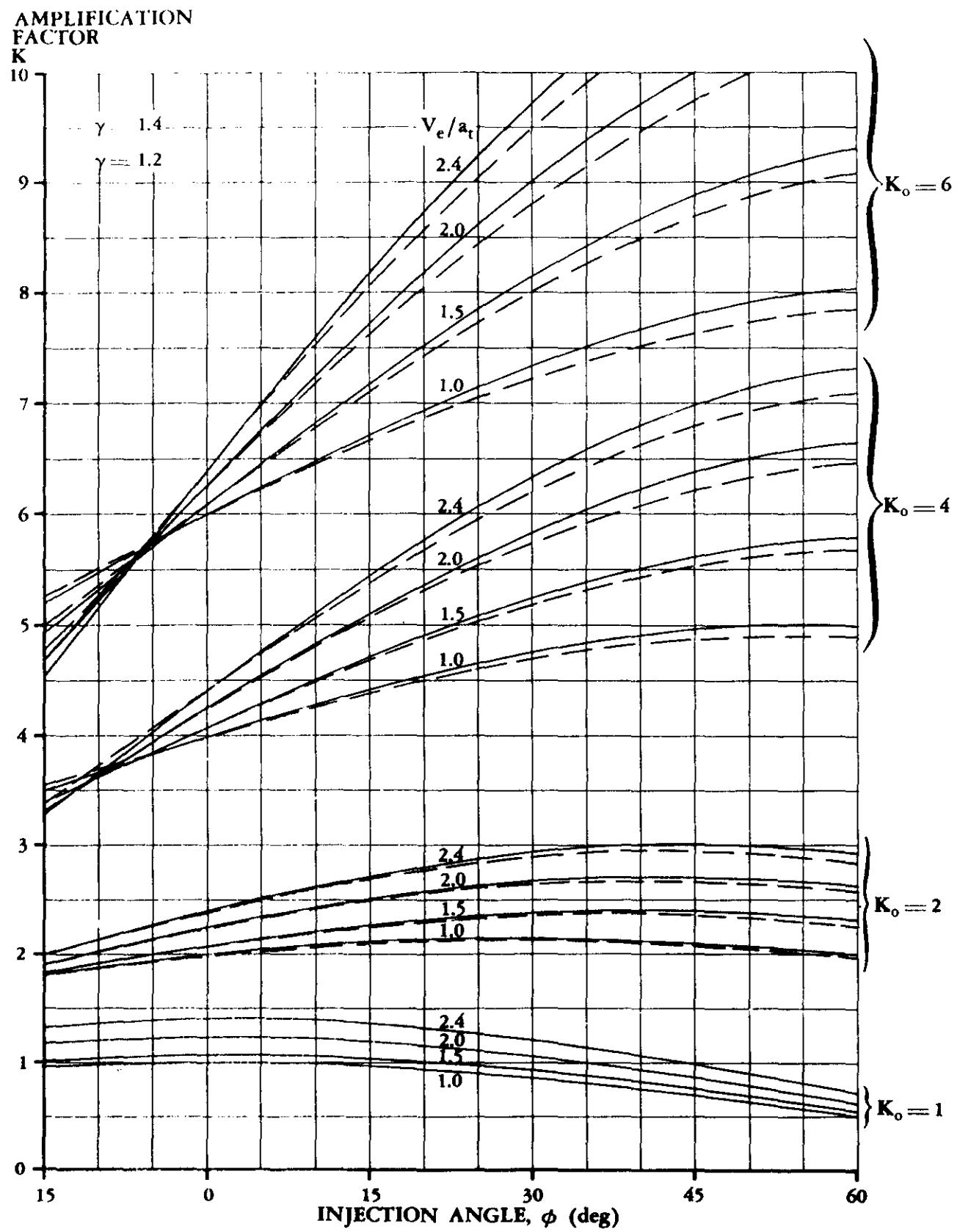
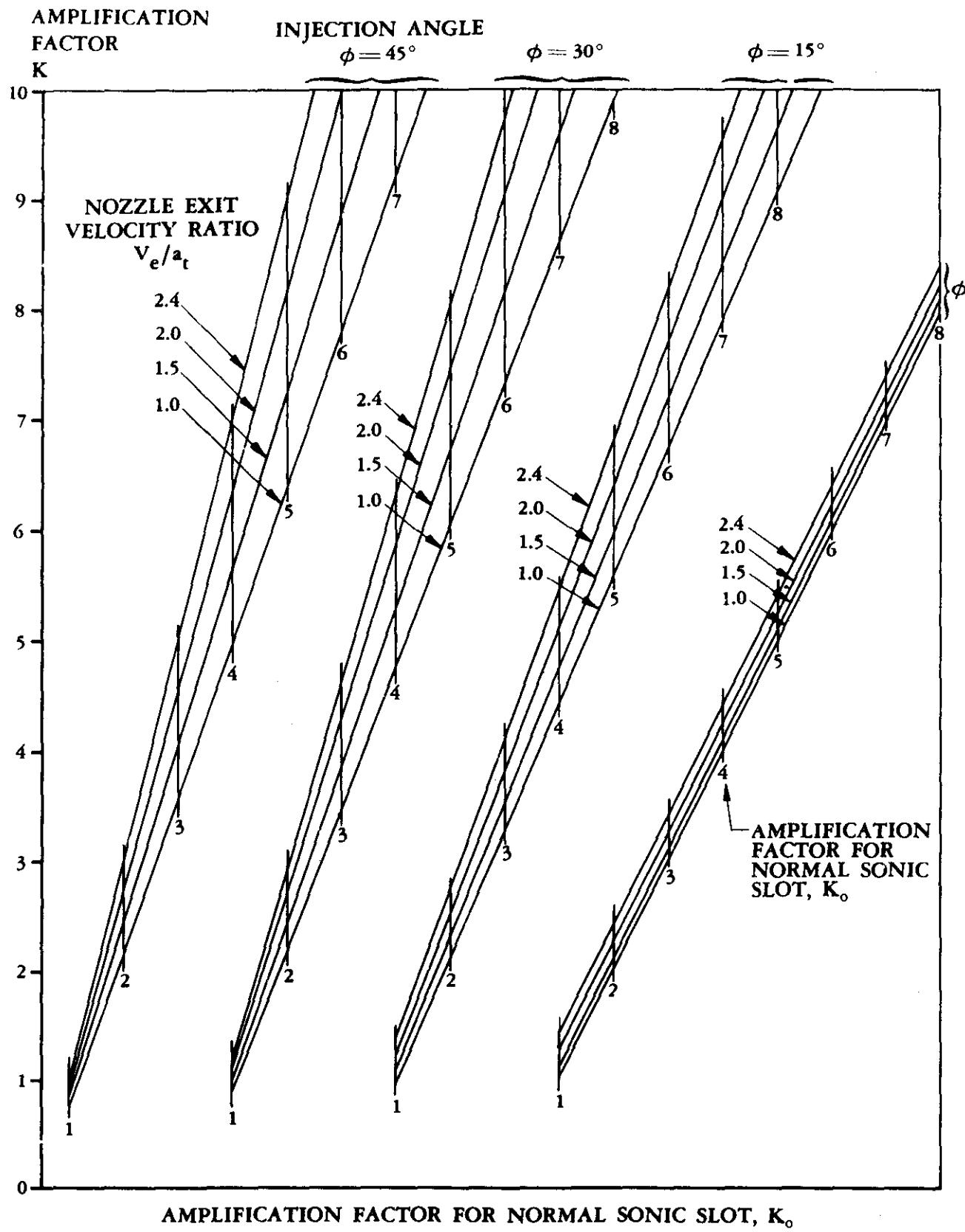
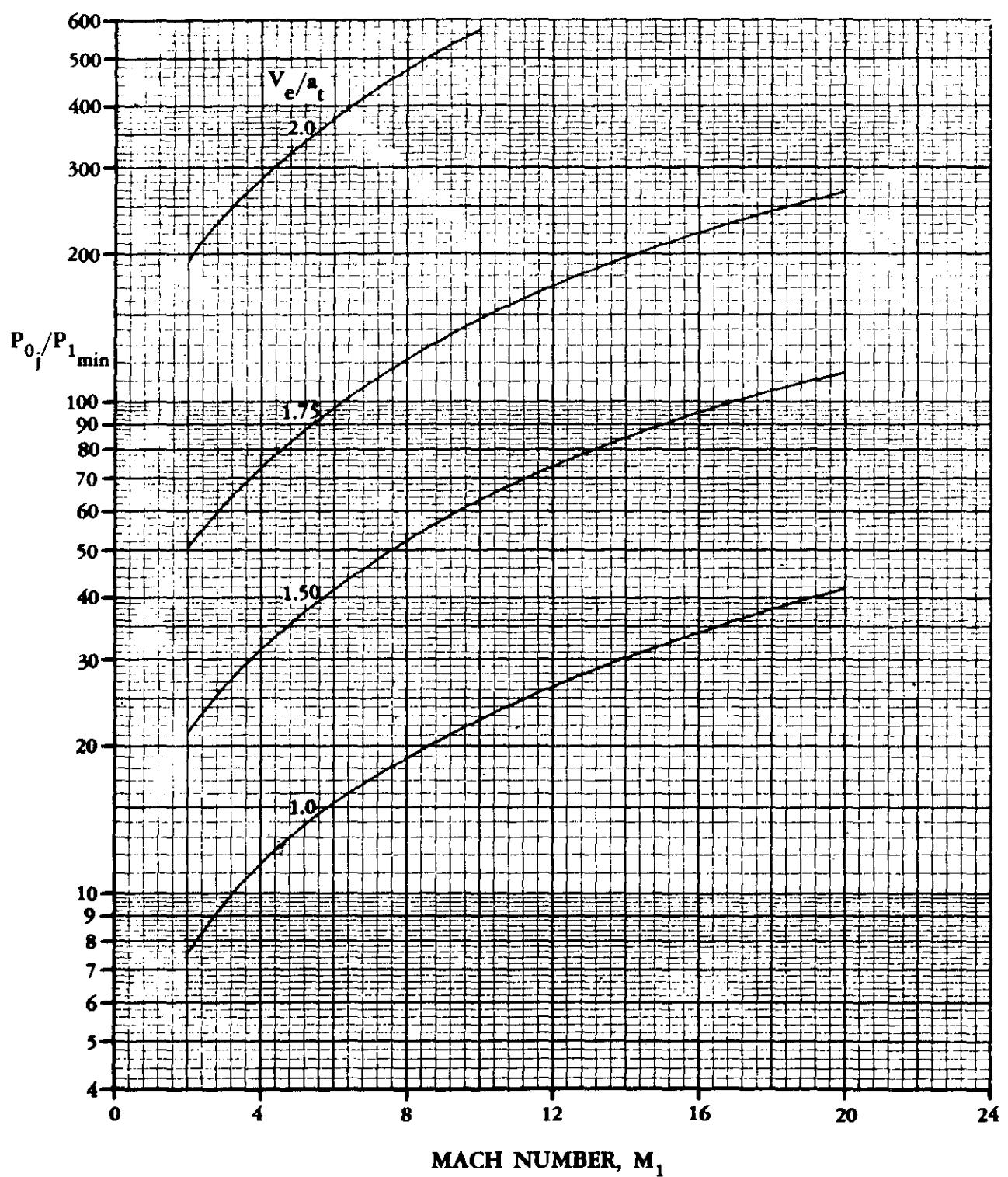


FIGURE 6.3.2-41 AMPLIFICATION FACTOR FOR INCLINED SUPERSONIC JETS



**FIGURE 6.3.2-42 AMPLIFICATION FACTOR FOR INCLINED SUPERSONIC JETS**



**FIGURE 6.3.2-43 MINIMUM JET PRESSURE RATIO FOR CHOKED NOZZLE FLOW**

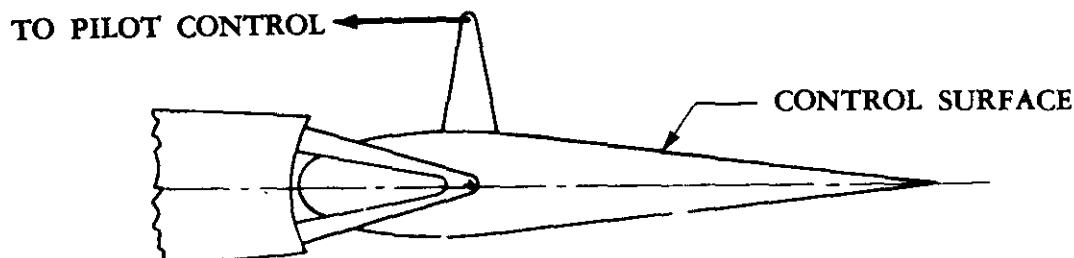
### 6.3.4 AERODYNAMICALLY BOOSTED CONTROL-SURFACE TABS

Aerodynamically boosted control-surface tabs have been successfully used to reduce the forces on reversible-control systems for many years. Linear methods from Reference 1 are presented herein for estimating the stick forces for a variety of the most commonly used control-surface-tab systems. Because of the compressibility effects on tabs at high speeds, the application of these methods should be restricted to subsonic flow; i.e., speeds below the surface critical Mach number or not above a Mach number of 0.90, whichever is least.

In order that the Datcom user may better understand the complex design considerations for a tab system, a general discussion (essentially taken from Reference 1) of pertinent design parameters for control-surface-tab systems is presented. For more details regarding tab systems the reader is referred to References 1 through 6. For a discussion and method of springy tabs or downsprings, the reader is specifically referred to Reference 6.

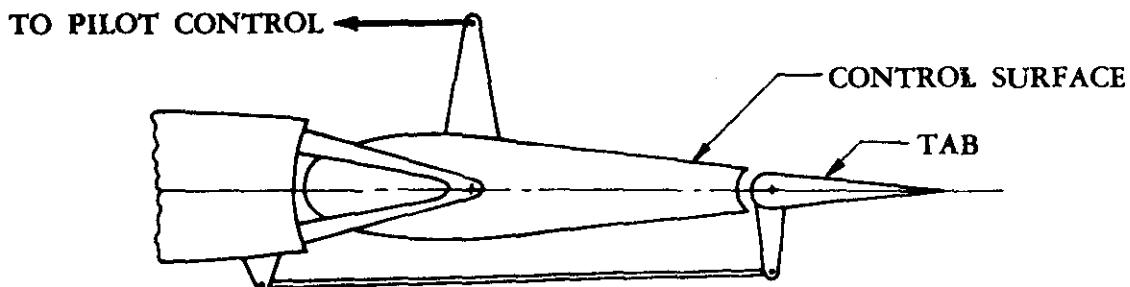
#### System Description

Aerodynamically boosted control systems can be divided into two distinct classifications: direct-control systems and indirect-control systems. Aerodynamic boost in direct-control systems includes nose aerodynamic balance, internal pressure balance on the main control surface, and may also include a tab "geared" to the main control surface. Sketch (a) illustrates the simple form of direct control without a tab, called "pure direct control."



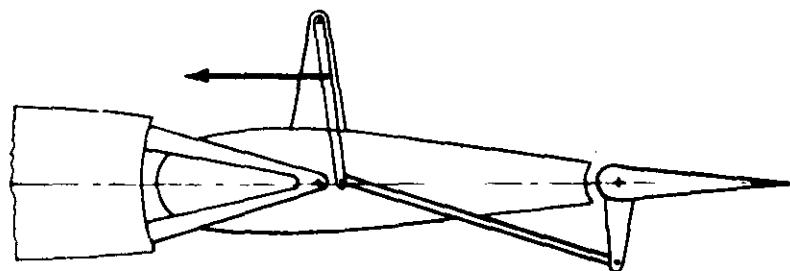
SKETCH (a) PURE DIRECT CONTROL

Sketch (b) illustrates the simple form of direct control with a tab, called a "geared tab."

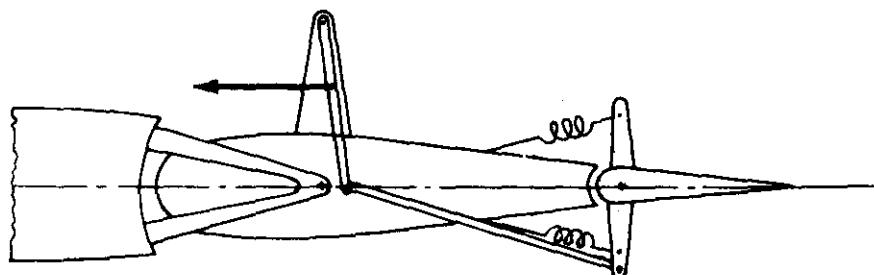


SKETCH (b) GEARED TAB

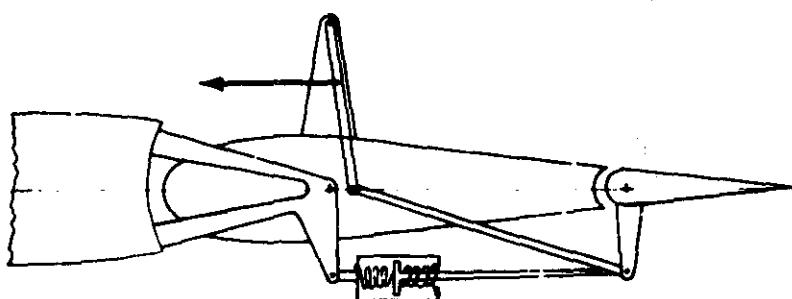
The most commonly used aerodynamically boosted control systems\* fall into the indirect-control classification. Indirect-control systems may be subdivided into two types, one in which the pilot has direct control over both the tab and the main control surface and one in which he controls only the tab. Those systems in which the pilot has direct control over both the tab and the main control surface are referred to as link-tab systems. The three types of link-tab systems are plain linked tab, spring tab, and geared spring tab, shown schematically in Sketch (c).



PLAIN LINKED TAB



SPRING TAB



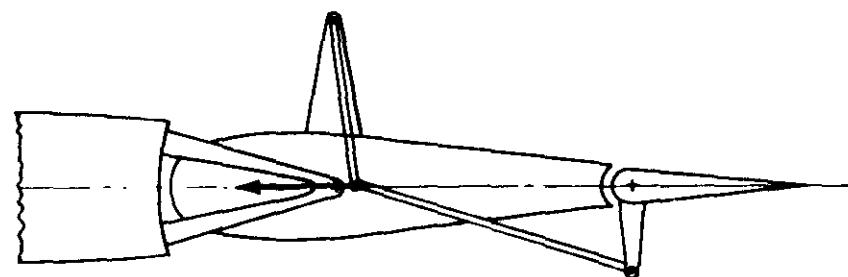
GEARED SPRING TAB

SKETCH (c)

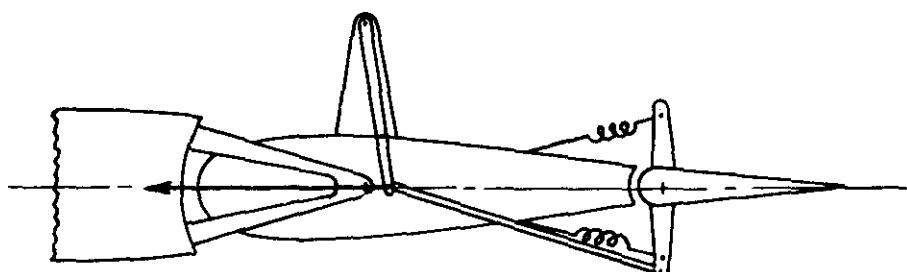
\*The control surface may be either an elevator, aileron, or rudder, throughout the discussion.

The fundamental relationship of the three tab systems is depicted in Sketch (c). It is evident that a spring-tab system is a plain linked tab with a spring added. The geared spring tab includes all the components of a spring tab, but with the spring arranged in series with a geared tab link.

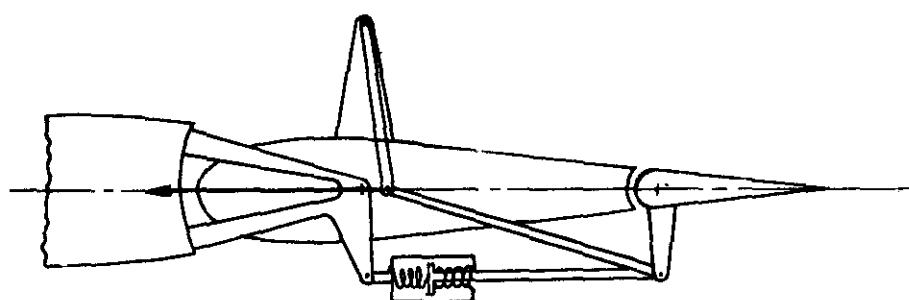
The second type of indirect-control system is distinguished from the link-tab systems in that the pilot controls only the tab and is therefore called the pure-flying-tab system. The three types of flying-tab systems are the pure flying tab, spring flying tab, and the geared flying tab as shown schematically in Sketch (d).



PURE FLYING TAB



SPRING FLYING TAB



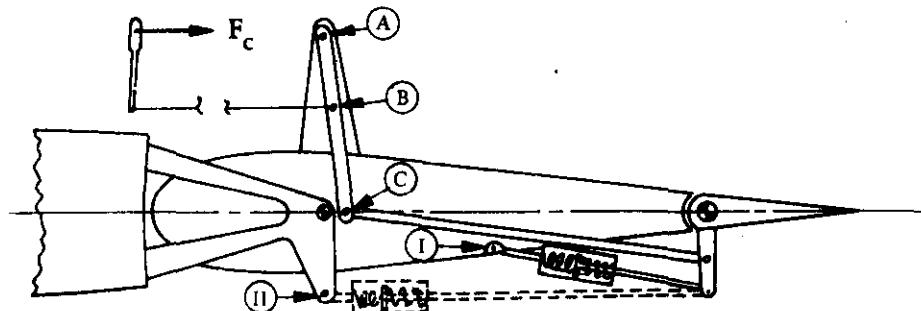
GEARED FLYING TAB

SKETCH (d)

Again, the fundamental relationship of the three tab systems is evident in Sketch (d).

It should be noted that both the plain linked tab and the pure flying tab have been called "servo-tabs" in much of the literature. However, since they are not identical systems, because of the different location of the cockpit control connecting point, it is important to maintain some distinction between the two.

In making any comprehensive analysis of aerodynamically boosted control-surface-tab systems, it is desirable first to reduce the special cases to be considered to the minimum number. Such a study reveals that all of the previously mentioned systems are but special cases of one general system. A schematic illustration of this general tab system is shown in Sketch (e). Table 6.3.4-A which accompanies the generalized control system, describes the specific tab system as a function of the cockpit control connecting point, along with the presence of a spring and its location.



GENERALIZED CONTROL SYSTEM SCHEMATIC DIAGRAM  
SKETCH (e)

TABLE 6.3.4-A

Cockpit Control Connecting Point	Tab Spring Configuration	Type of Control System
A	No Spring	Pure Direct Control
A	II	Geared Tab
B	No Spring	Plain Linked Tab
B	I	Spring Tab
B	II	Geared Spring Tab
C	II	Geared Flying Tab
C	I	Spring Flying Tab
C	No Spring	Pure Flying Tab

For a complete understanding of this general control-tab system, it is essential that the system kinematics are clearly understood. The key feature of the tab linkage is the fact that point C in Sketch (e) is not fixed to the control surface; i.e., it is free to translate; whereas, point A in Sketch (e) is fixed to the control surface and can translate only with movement of the control. It should also be noted that the spring configuration I in Sketch (e) corresponds to the case where the tab gearing link is connected to the hinge bracket at the main control-surface hinge line.

### Key Linkage Parameters

The tab-system designer determines the type of tab system and the system force characteristics by his selection of three key linkage parameters. These key linkage parameters are:

- o The aerodynamic boost link ratio  $R_L$ , which is an index to the relative location of the pilot connecting point (A, B, or C in Sketch (e))
- o The tab spring effectiveness  $k$
- o The tab gearing  $\beta$ , which is determined by the connecting linkage between the tab and the hinge bracket

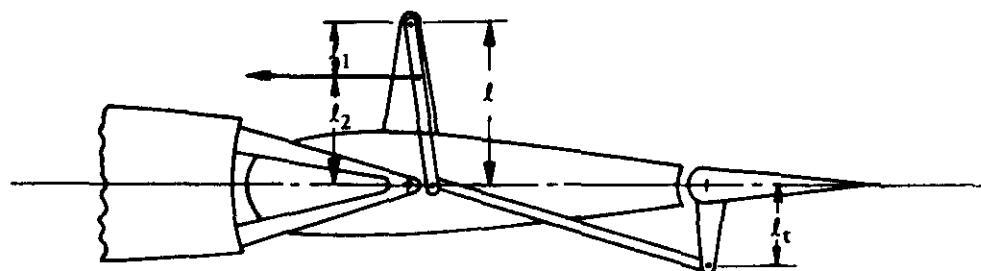
#### Boost Link Ratio $R_L$

The boost link ratio  $R_L$  is specifically defined as the rate of change of the tab deflection with respect to control-surface deflection with the control column fixed; i.e.,

$$R_L = \left( \frac{\partial \delta_{tc}}{\partial \delta_c} \right)_{\substack{\text{stick} \\ \text{fixed}}} \quad 6.3.4-a$$

For a general tab system as shown in Sketch (f), the value of  $R_L$  can be approximated by the system geometry by

$$R_L = \frac{l_2}{l_1} \frac{l}{l_t} \quad 6.3.4-b$$



SKETCH (f)

From this relationship, the value of  $R_L$  can be seen as a direct indication of the cockpit control connecting point. Thus, when the value of  $R_L$  is zero, the tab system corresponds to a pure flying tab as shown in Sketch (d). Likewise, when the value of  $R_L$  is infinite, the tab system becomes a direct-control system (with a free-floating tab).

### Tab Spring Effectiveness $k$

The tab spring effectiveness  $k$  is defined as the rate of change of moment on the tab due to the spring with respect to tab deflection, based on the product of tab area and chord; i.e.,

$$k = - \left( \frac{\partial M_{tc}}{\partial \delta_{tc}} \right)_{\text{spring}} \frac{l}{S_{tc} \bar{c}_{tc}} \quad 6.3.4-c$$

Thus, typical units of  $k$  could be lb/ft<sup>2</sup>-deg or lb/in.<sup>2</sup>-deg.

### Control Tab Gearing Ratio $\beta$

The control-tab-gearing ratio  $\beta$  is specifically defined as the rate of change of the tab deflection with respect to control-surface deflection with  $k = \infty$  and the stick free; i.e.,

$$\beta = \left( \frac{\partial \delta_{tc}}{\partial \delta_c} \right)_{\substack{\text{stick} \\ \text{free}}} \quad \text{with } k = \infty \quad 6.3.4-d$$

So, for a tab system without any connecting linkage between the tab and the hinge bracket, the value of  $\beta$  is zero, i.e., no gearing. For a geared system, the specific value of  $\beta$  is determined by the location of the connecting linkage relative to the control-surface hinge line.

### Linkage-Parameter Effects on Forces

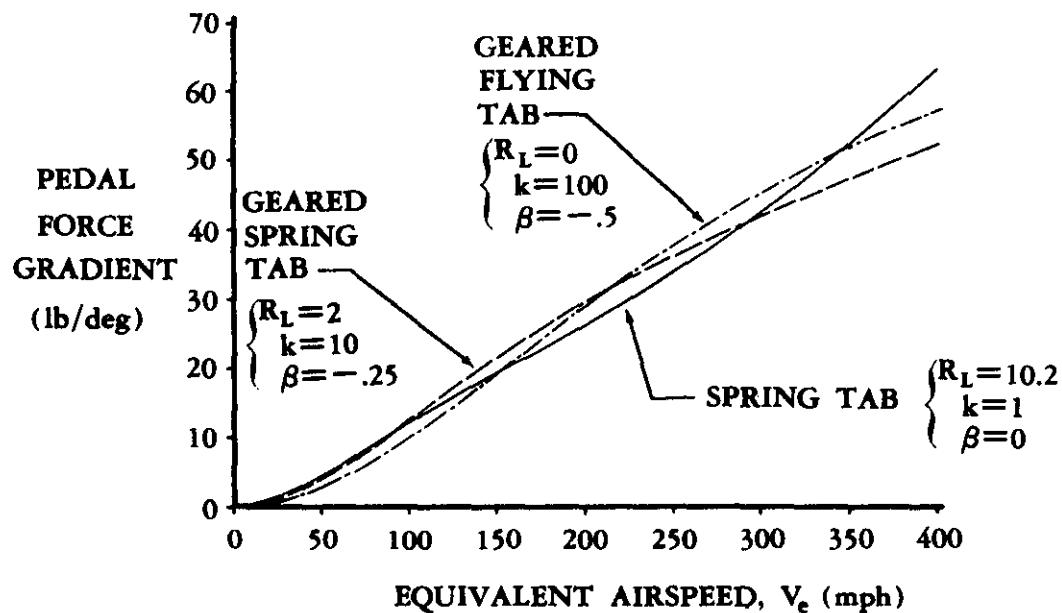
For discussion purposes, consider a plain-linked-tab system on a control surface that requires a pilot force of two hundred pounds to control the main surface, tab free, and a two-pound pilot force for a pure-flying-tab control. By applying one pound of pilot force to the tab, one-half the total work required to move the main surface is performed by the tab itself. Then by applying one hundred pounds of force to the main surface, the remaining one-half of the work is made up by the pilot directly, and the total pilot effort is 100 + 1 or 101 pounds. Thus, the link ratio  $R_L$  defines the proportions of the force division. At infinite link ratio, the pilot force will be two hundred pounds; at zero link ratio, two pounds. Therefore, a reduction in link ratio  $R_L$  results in a reduction of pilot force.

The use of a spring on the tab increases the tab hinge moments, and therefore increases the forces of a plain-linked-tab system. In the preceding example the force required to move the tab may be increased to, say, twenty pounds. For the same linkage, then, the total pilot force would be 100 + 10 or 110 pounds. Essentially, the spring effect adds an element of locked-tab hinge moment and reduces slightly the free-tab contribution. (This concept may be more clearly understood by referring to Equations 6.3.4-k and -o, which divide the control column force into contributions due to the free-tab, locked-tab, and gearing components.) Since the increase due to the locked-tab element is always greater than the corresponding decrease in the free-tab contribution, the pilot force will increase with increasing tab spring effectiveness.

Tab gearing  $\beta$  in the boost direction always reduces the pilot forces (by an increment rather than by a percentage), although the magnitude of the effect depends upon the values of the tab spring effectiveness  $k$  and the link ratio  $R_L$ . The effects of the spring and link ratio, however, are not so simply stated. Here both the magnitude and direction of the effect of one depend upon the value of the other and also on the tab gear ratio. In order to understand the interrelations between these parameters, it is necessary first to examine the "aerodynamic" characteristics of a spring. By this is meant the relationship of aircraft speed to the spring effect.

Normal aerodynamic coefficients are of course independent of speed if compressibility and aeroelastic effects are neglected. However, the spring characteristics are represented aerodynamically as  $(k/q)$  where  $q$  is the local dynamic pressure of the airstream. At zero airspeed the aerodynamic spring characteristic is infinite for all finite values of  $k$ . However, at infinite airspeed the aerodynamic spring characteristic is zero for all values of  $k$ . Hence, the characteristics of any system incorporating a tab spring correspond to those with the tab locked as in pure direct control (or geared as a geared tab) at zero airspeed, and to a system with no spring at infinite airspeed.

The individual effects of the linkage parameters are interrelated, but are nevertheless independent of the type of system used. It may be surmised that "special tab arrangements" are in themselves not that significant. What is more important is the matter of choosing proper values of the linkage parameters for a design application, rather than choosing a particular type of system. To illustrate this point, Sketch (g) shows three different tab systems for a particular control surface on an aircraft. Each tab system has been adjusted to yield nearly equivalent force characteristics over the speed range considered.



SKETCH (g)

## DATCOM METHOD

The Datcom Method presents the fundamental relationship between the pilot forces and the tab and control-surface moments from which the control-column forces are evaluated.

The control-column force equations are presented in such a manner that the individual contributions of the various factors, i.e., tab-free, tab-fixed, and gearing contributions can be readily identified. It should be noted that two control-column force equations are presented, both of which define a general tab control system for an elevator, rudder, aileron, or other control system having linear characteristics. The two equations presented are based on different independent variables for the convenience of the user (they provide identical values of control-column force).

Because of the lengthy control-column force equations, a summary table and shorthand notation has been used to simplify the presentation of equations. In order to facilitate this presentation, the following general notation list is provided.

### NOTATION\*

SYMBOL	DEFINITION
$A_c$	$= \frac{S_{tc} \bar{c}_{tc}}{S_c \bar{c}_c}$
$B_1$	$= \left( \frac{\partial C_{h_c}}{\partial \delta} \right)_{\delta_{tc}, \alpha_s, \delta_{tt}}$
$B_2$	$= \left( \frac{\partial C_{h_c}}{\partial \delta_{tc}} \right)_{\delta_c, \alpha_s, \delta_{tt}}$
$B_3$	$= \left( \frac{\partial C_{h_c}}{\partial \alpha_s} \right)_{\delta_c, \delta_{tc}, \delta_{tt}}$
$B_4$	$= \left( \frac{\partial C_{h_c}}{\partial \delta_{tt}} \right)_{\delta_c, \delta_{tc}, \alpha_s}$
$\bar{c}_{( )}$	surface mean aerodynamic chord (movable surfaces are defined by their area aft of the hinge line, and the MAC is of that area)
$C_{h_c}$	is the hinge-moment coefficient of the particular control surface, i.e., $H_c / q S_c \bar{c}_c$ (either an elevator, rudder, or aileron)
$C_{h_{tc}}$	is the hinge-moment coefficient of the control tab, i.e., $H_{tc} / q S_{tc} \bar{c}_{tc}$
$C_L$	lift coefficient, positive up or to the right

\*Units are not specified for derivatives, lengths, or areas. It is up to the user to choose his units and be consistent throughout.

SYMBOL	DEFINITION
$C_{L_s}$	lift coefficient of surface to which the main control surface is attached, i.e., $C_{L_H}$ , $C_{L_V}$ , or $C_{L_W}$ (total lift, including lift due to control deflection, tab deflection, and angle of attack)
$C_{L_H}$	is the horizontal-tail lift coefficient (total lift, including lift due to control deflection, tab deflection, and angle of attack)
$C_{L_V}$	is the vertical-tail lift coefficient (total lift, including lift due to control deflection, tab deflection, and angle of attack)
$C_{L_W}$	is the wing lift coefficient (total lift, including lift due to control deflection, tab deflection, and angle of attack)
$C_{L_\alpha}$	airplane lift-curve slope
$C_{L_{\alpha_H}}$	airplane lift-curve slope with respect to the tail angle of attack
$C_1$	$= \left( \frac{\partial C_{L_s}}{\partial \delta_c} \right)_{\delta_{tc}, \delta_{tt}, \alpha_s}$
$C_2$	$= \left( \frac{\partial C_{L_s}}{\partial \delta_{tc}} \right)_{\delta_c, \alpha_s, \delta_{tt}}$
$C_3$	$= \left( \frac{\partial C_{L_s}}{\partial \alpha_s} \right)_{\delta_c, \delta_{tc}, \delta_{tt}}$
$C_4$	$= \left( \frac{\partial C_{L_s}}{\partial \delta_{tt}} \right)_{\delta_c, \alpha_s, \delta_{tc}}$
$D_1$	$= \left( \frac{\partial C_{h_{tc}}}{\partial \delta_c} \right)_{\delta_{tc}, \alpha_s}$
$D_2$	$= \left( \frac{\partial C_{h_{tc}}}{\partial \delta_{tc}} \right)_{\delta_c, \alpha_s}$
$D_3$	$= \left( \frac{\partial C_{h_{tc}}}{\partial \alpha_s} \right)_{\delta_c, \delta_{tc}}$
$E_1$	$= B_1 / C_1$
$E_2$	$= B_2 - C_2 E_1$
$E_3$	$= B_3 - C_3 E_1$
$E_4$	$= B_4 - C_4 E_1$
$F_c$	control-column force in lb (pull force is positive)

SYMBOL	DEFINITION
F	elevator stick force in lb (pull force is positive)
$F_p$	rudder-pedal force in lb (push on left pedal is positive)
$F_1$	= $D_1/C_1$
$F_2$	= $D_2 - C_2 F_1$
$F_3$	= $D_3 - C_3 F_1$
$F_4$	= $-C_4 F_1$
$G_{( )}$	pilot gearing factor (see Equations 6.3.4-f and -f')
$G_{\max}$	maximum stick gearing (see Equation 6.3.4-i)
$H_{( )}$	control hinge moment
k	tab spring effectiveness, in lb/ft <sup>2</sup> -deg (see Equation 6.3.4-c)
n'	airplane normal acceleration or load factor in g's
q	local dynamic pressure (lb/ft <sup>2</sup> )
$q_\infty$	free-stream dynamic pressure (lb/ft <sup>2</sup> )
$R_1, R_2$	shorthand notation for tab and main surface hinge moments and key linkage parameters, obtained from Table 6.3.4-B
$R_L$	aerodynamic boost link ratio (see Equations 6.3.4-a and -b)
$S_{( )}$	surface area (movable surfaces are defined by their area aft of the hinge line)
$T_1, T_2$	shorthand notation for tab and main surface hinge moments and key linkage parameters, obtained from Table 6.3.4-C
V	airspeed
W	aircraft weight
$x_c$	fore and aft displacement of control column, positive forward
$x_{c \max}$	maximum displacement of control column, positive forward

SYMBOL	DEFINITION
$x_p$	fore and aft displacement of right rudder pedal, positive forward
$\alpha$	angle of attack, positive for lift increase
$\alpha_s$	angle of attack of the surface to which the main control surface is attached, i.e., $\alpha_H$ , $\alpha_V$ , or $\alpha_W$
$\alpha_H$	angle of attack of the horizontal tail
$\alpha_V$	angle of attack of the vertical tail
$\alpha_W$	angle of attack of the wing
$\beta$	control-tab gear ratio (see Equation 6.3.4-d)
$\epsilon$	downwash at the horizontal tail
$\Delta_r$	= $-\delta_{tc\max}/\delta_{c\max}$ for a maximum control deflection (the value of $\Delta_r$ is positive because $\delta_{tc\max}$ and $\delta_{c\max}$ will have opposite signs)
$\delta_{c\max}$	the maximum deflection of the main control surface, in degrees
$\delta_{( )}$	surface deflection, positive for trailing edge down or to the left, in degrees
$\sigma$	air density ratio, $\rho/\rho_0$
$\phi_\beta$	lift efficiency factor for a geared tab system, $1 + \beta C_2/C_1$

#### SUBSCRIPTS

c	main control surface (elevator, rudder, aileron, etc.)
e	elevator
H	horizontal tail
p	control pedal
r	rudder
s	surface to which the main control surface is attached, i.e., horizontal tail, vertical tail, or wing
tc	control tab
tt	trim tab

### Fundamental Relationships

The following relationship from Reference 1 is derived from basic considerations of system equilibrium and fundamental laws, giving a relationship between pilot forces and the tab and control surface moments, as

$$F_c = G_c H_c = G_{tc} H_{tc} = -G_c R_L H_{tc} \quad 6.3.4-e$$

where the control-surface stick gearing  $G_c$  and the tab stick gearing  $G_{tc}$  are defined as

$$G_c = \frac{1}{57.3 \left( \frac{\partial x_c}{\partial \delta_{c,tc}} \right)} \quad 6.3.4-f$$

$$G_{tc} = \frac{1}{57.3 \left( \frac{\partial x_c}{\partial \delta_{tc}} \right)_c} \quad 6.3.4-f'$$

Using Equation 6.3.4-e, the aerodynamic boost link ratio  $R_L$  can be expressed as a function of the stick and tab gearing, i.e.,

$$R_L = \frac{-G_{tc}}{G_c}$$

Since the aerodynamic boost link ratio must be positive, it becomes evident that the control surface stick gearing  $G_c$  and the tab stick gearing  $G_{tc}$  must have opposite signs.

The particular form of Equation 6.3.4-e that is used is dependent upon the value of the boost link ratio; i.e.,

$$F_c = G_c H_c \quad \text{for } R_L = \infty$$

$$F_c = G_{tc} H_{tc} \quad \text{for } R_L = 0$$

$$F_c = -G_c R_L H_{tc} \quad \text{for } 0 < R_L < \infty$$

The control surface moments  $M_c$  for a general tab system (see Sketch (e)) can be expressed as\*

$$H_c = S_c \bar{c}_c q [B_1 \delta_c + B_2 \delta_{tc} + B_3 \alpha_s + B_4 \delta_{tt} + \frac{k}{q} A_c \beta (\delta_{tc} - \beta \delta_c)] \quad 6.3.4-g$$

\*These moment equations are applicable for symmetrical, untwisted control surfaces that yield a value of zero for  $H_c$  and  $H_{tc}$  when  $\delta_c$ ,  $\delta_{tc}$ ,  $\delta_{tt}$ , and  $\alpha_s$  are all zero.

and the tab surface moments  $M_{tc}$  for a general tab system can be expressed as\*

$$H_{tc} = S_{tc} \bar{c}_{tc} q [D_1 \delta_c + D_2 \delta_{tc} + D_3 \alpha_s - \frac{k}{q} (\delta_{tc} - \beta \delta_c)] \quad 6.3.4-h$$

Equation 6.3.4-e is the primary aerodynamic relationship from which the stick forces are evaluated. It defines not only the force-moment relationships, but also the system equilibrium. Therefore, analysis of any control system can be made if the control-surface and control-tab hinge-moment characteristics and the system motion characteristics are known.

Another significant parameter is the maximum stick gearing  $G_{c_{max}}$  defined by

$$G_{c_{max}} = \frac{1}{57.3 \left( \frac{\partial x_c}{\partial \delta_c} \right)_{max}} \quad 6.3.4-i$$

The stick gearing  $G_c$  is related to the maximum stick gearing by the following:

$$\frac{G_c}{G_{c_{max}}} = \frac{R_L + \Delta_r}{R_L} \quad 6.3.4-j$$

From this equation it is evident that the value of the ratio  $G_c/G_{c_{max}}$  is greater than one. This simply means that the cockpit control travel must be greater than that required to bottom the control with the tab fixed. Sufficient control travel must exist to bottom the control surface and the control surface tab simultaneously, while allowing for cable stretch.

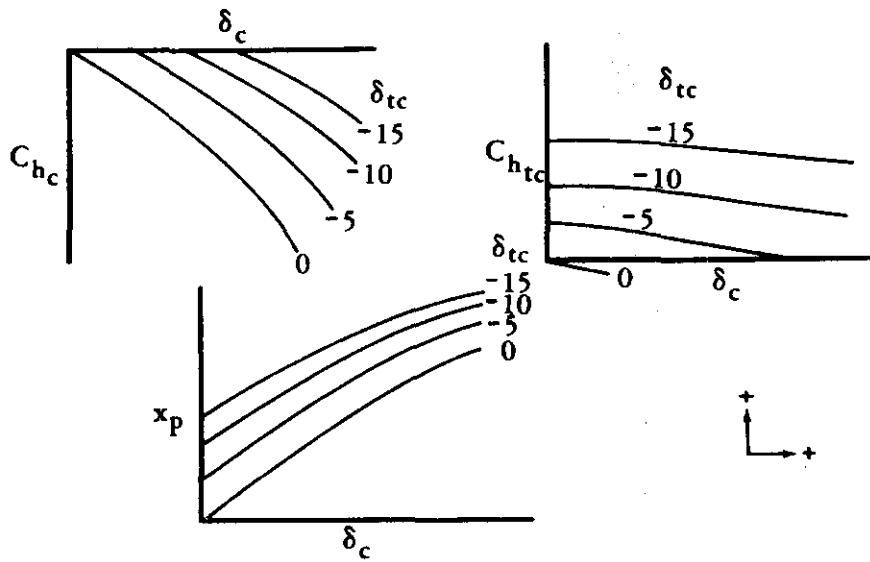
### Control Column Forces

The analysis of a typical tab system requires detailed knowledge of the tab and control hinge-moment characteristics as a function of the main-control-surface angle of attack. For a particular angle of attack, Sketch (h) illustrates the typical hinge-moment and gearing data required to analyze any tab control system.

These data should preferably be obtained from wind-tunnel-test data or may be estimated by using the hinge-moment methods of Section 6.1.6. Because of the lengthy control-column force equations, a summary table and shorthand notation will be used to simplify the presentation of the equations. The format in which the control-column force equations are presented, i.e., tab-free, tab-fixed, and gearing contributions, is used so that the contribution of the various factors can be more readily identified.

---

\*These moment equations are applicable for symmetrical, untwisted control surfaces that yield a value of zero for  $H_c$  and  $H_{tc}$  when  $\delta_c$ ,  $\delta_{tc}$ ,  $\delta_{tt}$ , and  $\alpha_s$  are all zero.



SKETCH (h)

The two control-column force equations presented herein are modifications of Equation 6.3.4-e, with the variable  $\delta_{tc}$  being eliminated. These equations are for a general tab control system on an elevator, rudder, aileron, or other control system having linear aerodynamic characteristics. (For example, when evaluating an elevator tab system, the terms  $\bar{C}_c$ ,  $\delta_c$ ,  $C_{hc}$ ,  $\alpha_s$ , etc., become  $\bar{C}_e$ ,  $\delta_e$ ,  $C_{he}$ ,  $\alpha_H$ , etc., respectively.) The first equation is based on the independent variables  $\delta_c$ ,  $\alpha_s$ , and  $\delta_{tt}$ ; while the second equation is based on the independent variables  $C_L$ ,  $\alpha_s$ , and  $\delta_{tt}$ . Either equation may be used depending upon the preference of the user.

The first equation for estimating the control-column force characteristics, based on the independent variables  $\delta_c$ ,  $\alpha_s$ , and  $\delta_{tt}$ , is

$$F_c = G_{c_{max}} S_c \bar{C}_c q \left[ \begin{array}{l} C_{hc_{tab}} \\ \text{free} \end{array} \right] R_1 + \left[ \begin{array}{l} C_{hc_{tab}} \\ \text{locked} \end{array} \right] R_2 + \Delta C_{hc_{tab}} \left[ \begin{array}{l} R_2 \\ \text{gearing} \end{array} \right] \quad 6.3.4-k$$

where

$G_{c_{max}}$  is the maximum stick gearing available as defined by Equation 6.3.4-i. The value of  $G_{c_{max}}$  is finite for all tab systems with a finite boost link ratio. However, for flying-tab systems where  $R_L = 0$ , the value of  $G_{c_{max}}$  is zero. To avoid a problem when using Equation 6.3.4-k, the user should realize that the  $R_1$  and  $R_2$  terms for flying-tab systems in Table 6.3.4-B contain the parameter  $\Delta_r$ . The product of  $G_{c_{max}}$  and  $\Delta_r$  yields  $G_{tc_{max}}$  or the maximum gearing of the tab, which has a finite value. Thus, for flying-tab systems a finite value of  $G_{c_{max}}$  is not possible; however, Equation 6.3.4-k is still applicable when  $G_{tc_{max}}$  is used to replace the product of  $G_{c_{max}}$  and  $\Delta_r$ .

$q$  is the dynamic-pressure ratio. This value must be consistent with whatever value is used to nondimensionalize the hinge-moment coefficients in Equations 6.3.4-l, -m, and -n. If the hinge-moment coefficients are based on wind-tunnel-test data, they are probably nondimensionalized with respect to the free-stream dynamic-pressure ratio. If the Datcom is used to estimate the hinge-moment coefficients, the local dynamic-pressure ratio should be used. (Local dynamic-pressure ratio may be obtained from Section 4.4.1 for an empennage panel.)

$$C_{h_c}^{tab\_free} = \left( B_1 - D_1 \frac{B_2}{D_2} \right) \delta_c + \left( B_3 - D_3 \frac{B_2}{D_2} \right) \alpha_s + B_4 \delta_{tt} \quad 6.3.4-l$$

$$C_{h_c}^{tab\_locked} = B_1 \delta_c + B_3 \alpha_s + B_4 \delta_{tt} \quad 6.3.4-m$$

$$\Delta C_{h_c}^{gearing} = (\beta B_2 + \beta A_c D_1 + \beta^2 A_c D_2) \delta_c + (\beta A_t D_3) \alpha_s \quad 6.3.4-n$$

The values for  $R_1$  and  $R_2$  are found from Table 6.3.4-B as a function of the specific type of tab system. This table also summarizes values for the three key linkage parameters  $R_L$ ,  $k$ , and  $\beta$  for each specific type of tab system, using an "F" to denote finite values for the parameters.

The second equation for estimating the control-column force characteristics, based on the independent variables  $C_{L_s}$ ,  $\alpha_s$ , and  $\delta_{tt}$ , is

$$F_c = G_{c_{max}} S_c \bar{c}_c q \left[ C_{h_c}^{tab\_free} T_1 + C_{h_c}^{tab\_locked} T_2 + \Delta C_{h_c}^{gearing} T_2 \right] \quad 6.3.4-o$$

where

$G_{c_{max}}$  is the maximum stick gearing available as defined by Equation 6.3.4-i. The same comments made about  $G_{c_{max}}$  for spring tab systems, when using Equation 6.3.4-k, also apply to the application of Equation 6.3.4-o (see discussion following Equation 6.3.4-k).

$q$  is the dynamic-pressure ratio as defined above for Equation 6.3.4-k. (Consistent with whatever value was used to nondimensionalize the hinge-moment coefficients in Equations 6.3.4-p, -q, and -r.)

TABLE 6.3.4-B

Specific Type of System	Linkage			$R_1$	$R_2$
	$R_L$	$k$	$\beta$		
Geared Tab	$\infty$	$\infty$	$F^*$	0	1
Pure Direct Control	$\infty$	$\infty$	0	0	1
Geared Spring Tab	F	F	F	$\frac{(R_L + \Delta_r)}{R_L + \frac{B_2}{A_c D_2} - \frac{k}{qD_2} (R_L - \beta)}$	$-\frac{(k/qD_2)(R_L + \Delta_r)}{R_L + \frac{B_2}{A_c D_2} - \frac{k}{qD_2} (R_L - \beta)}$
Spring Tab	F	F	0	$\frac{(R_L + \Delta_r)}{R_L + \frac{B_2}{A_c D_2} - \frac{k}{qD_2} (R_L)}$	$-\frac{(k/qD_2)(R_L + \Delta_r)}{R_L + \frac{B_2}{A_c D_2} - \frac{k}{qD_2} (R_L)}$
Plain Linked Tab	F	0	0	$\frac{(R_L + \Delta_r)}{R_L + \frac{B_2}{A_c D_2}}$	0
Geared Flying Tab	0	F	F	$\frac{\Delta_r}{\frac{B_2}{A_c D_2} + \frac{k}{qD_2} \beta}$	$-\frac{(k/qD_2) \Delta_r}{\frac{B_2}{A_c D_2} + \frac{k}{qD_2} \beta}$
Spring Flying Tab	0	F	0	$\frac{\Delta_r}{\frac{B_2}{A_c D_2}}$	$-\frac{(k/qD_2) \Delta_r}{\frac{B_2}{A_c D_2}}$
Pure Flying Tab	0	0	0	$\frac{\Delta_r}{\frac{B_2}{A_c D_2}}$	0

\*Denotes a finite value.

$$C_{h_{c_{tab\_free}}} = \left( E_1 - F_1 \frac{E_2}{F_2} \right) C_{L_s} + \left( E_3 - F_3 \frac{E_2}{F_2} \right) \alpha_s + \left( E_4 - F_4 \frac{E_2}{F_2} \right) \delta_{tt} \quad 6.3.4-p$$

$$C_{h_{c_{tab\_locked}}} = E_1 C_{L_s} + E_3 \alpha_s + E_4 \delta_{tt} \quad 6.3.4-q$$

$$\Delta C_{h_c \text{gearing}} = \beta \left( E_1 \frac{C_2}{C_1} + A_c \frac{F_2}{C_1} + \frac{E_2}{C_1} + A_c \phi_\beta F_1 \right) C_{L_s} + \beta \left( E_3 \frac{C_2}{C_1} - \beta A_c C_3 \frac{F_2}{C_1} - C_3 \frac{E_2}{C_1} + \phi_\beta A_c F_3 \right) \alpha_s + \beta \left( E_4 \frac{C_2}{C_1} - \beta A_c C_4 \frac{F_2}{C_1} - C_4 \frac{E_2}{C_1} + \phi_\beta A_c F_4 \right) \delta_{tt}$$

6.3.4-r

The values for  $T_1$  and  $T_2$ , along with values for the key linkage parameters, are found from Table 6.3.4-C as a function of the specific type of tab system.

TABLE 6.3.4-C

Specific Type of System	Linkage			$T_1$	$T_2$
	$R_L$	$k$	$\beta$		
Geared Tab	$\infty$	$\infty$	$F^*$	0	$1/\phi_\beta$
Pure Direct Control	$\infty$	$\infty$	0	0	1
Geared Spring Tab	F	F	F	$\frac{(R_L + \Delta_r)}{R_L + \frac{E_2}{A_c F_2} - \frac{k}{qF_2} \phi_\beta (R_L - \beta)}$	$\frac{-(k/qF_2)(R_L + \Delta_r)}{R_L + \frac{E_2}{A_c F_2} - \frac{k}{qF_2} \phi_\beta (R_L - \beta)}$
Spring Tab	F	F	0	$\frac{(R_L + \Delta_r)}{R_L + \frac{E_2}{A_c F_2} - \frac{k}{qF_2} (R_L)}$	$\frac{-(k/qF_2)(R_L + \Delta_r)}{R_L + \frac{E_2}{A_c F_2} - \frac{k}{qF_2} (R_L)}$
Plain Linked Tab	F	0	0	$\frac{(R_L + \Delta_r)}{R_L + \frac{E_2}{A_c F_2}}$	0
Geared Flying Tab	0	F	F	$\frac{\Delta_r}{\frac{E_2}{A_c F_2} + \frac{k}{qF_2} \phi_\beta (\beta)}$	$\frac{-(k/qF_2) \Delta_r}{\frac{E_2}{A_c F_2} + \frac{k}{qF_2} \phi_\beta (\beta)}$
Spring Flying Tab	0	F	0	$\frac{\Delta_r}{\frac{E_2}{A_c F_2}}$	$\frac{-(k/qF_2) \Delta_r}{\frac{E_2}{A_c F_2}}$
Pure Flying Tab	0	0	0	$\frac{\Delta_r}{\frac{E_2}{A_c F_2}}$	0

\*Denotes a finite value.

6.3.4-17

## Tab Lift Loss

In achieving large control-column force reductions, tabs generate loads opposite to those on the main control surface. Thus, the net lift or efficiency of the main control surface is reduced by some amount. A typical value for loss in lift efficiency for a transport-type aircraft is 15%. The majority of the lift losses range from 5 to 20%. The maximum loss will occur for the pure flying-tab system. The efficiency of a control surface employing a tab may be expressed as

$$\eta = 1 - \frac{\Delta C_{L_{tc}} \text{ (lift loss due to tab)}}{\Delta C_{L_c} \text{ (lift increment due to control surface)}} \quad 6.3.4-s$$

This can also be expressed as

$$\eta = 1 + \left( \frac{\partial C_{L_c}}{\partial \delta_{tc}} \right) \left( \frac{\partial \delta_c}{\partial C_{L_c}} \right) \frac{\delta_{tc}}{\delta_c} \quad 6.3.4-t$$

For most cases, the critical case occurs when the trim tab angle and the angle of attack are zero, allowing  $\delta_{tc}/\delta_c$  to be expressed as

$$\frac{\delta_{tc}}{\delta_c} = \frac{B_1 + R_L A_c D_1 + \frac{k}{q} \beta A_c R_L - \frac{k}{q} A_c \beta^2}{B_2 + R_L A_c D_2 - \frac{k}{q} A_c R_L + \frac{k}{q} A_c \beta} \quad 6.3.4-u$$

Thus, the efficiency of a tab system can be evaluated by using Equation 6.3.4-t where Equation 6.3.4-u is used for the relationship of  $\delta_{tc}/\delta_c$ .

## Design Criteria

The design of tab boost systems can be a complex iterative process involving many variables. The mechanical limitations vary for various aircraft designs. However, Table 6.3.4-D (from Reference 1) presents a summary of the practical design criteria that will apply to most systems.

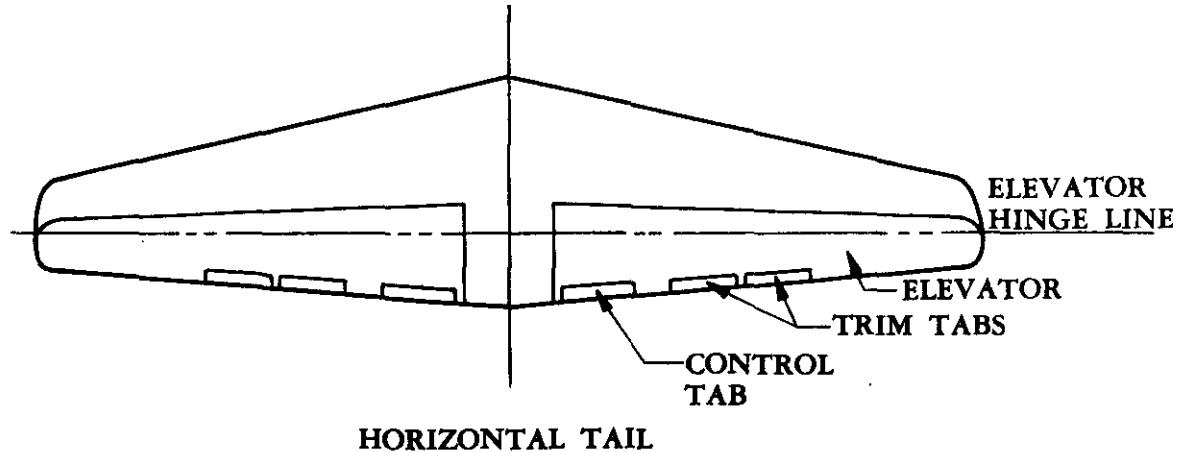
**TABLE 6.3.4-D**  
**SUGGESTED DESIGN CRITERIA**  
**FOR AERODYNAMIC BOOST SYSTEMS**

Parameter	Maximum Range of Values	Design Limitations
Link Ratio $R_L$	0, .1 to 10, $\infty$	Mechanical-Linkage Design
Spring Rate $k$	Any	Minimum Value Depends on Preload
Gear Ratio $\beta$	0 to $-\left( .002 + \frac{\partial C_{h_c}}{\partial \delta_c} \right) \left( \frac{\partial C_{h_c}}{\partial \delta_{tc}} \right)$	Nonlinearity and Overbalance
Spring Preload	Min. Value: As required to overcome tab system friction  Max. Value: No more than required to obtain desired force level	Good Tab Centering  Minimize Variation of Elevator Control Forces with Speed
Tab Size	Minimum: To control main surface to maximum deflection  Maximum: To give  $\frac{\partial C_{h_c}}{\partial \delta_c} / \frac{\partial C_{h_c}}{\partial \delta_{tc}} = 0.5$	Adequate Tab Power  Overbalance with Free Tab
$\frac{\partial C_{h_c}}{\partial \delta_c} = B_1$	$-B_1 > 0.002$	Overbalance and Nonlinearity

The following sample problem illustrates the use of the control-column force equations as applied to a given elevator spring-tab control system. No attempt is made herein to present a numerical example of the design of a tab boost system.

#### Sample Problem

Given: An elevator spring-tab control system on a transport-type aircraft.



Horizontal Tail Characteristics:

$$S_e \bar{c}_e G_{e_{\max}} = 162.0 \text{ ft}^2$$

$$\alpha_H = 2.5^\circ \quad \delta_{tt} = -3.0^\circ \quad \delta_e = 10^\circ$$

$$B_1 = \frac{\partial C_{h_e}}{\partial \delta_e} = -0.0040 \text{ per deg} \quad B_2 = \frac{\partial C_{h_e}}{\partial \delta_{tc}} = -0.0046 \text{ per deg}$$

$$B_3 = \frac{\partial C_{h_e}}{\partial \alpha_H} = -0.0017 \text{ per deg} \quad B_4 = \frac{\partial C_{h_e}}{\partial \delta_{tt}} = -0.0044 \text{ per deg}$$

$$\delta_{e_{\max}} = 15^\circ, -30^\circ \quad q = 150 \text{ lb/ft}^2 \text{ (sea level)}$$

Tab Characteristics:

$$R_L = 4.1 \quad k = 0.244 \text{ lb/ft}^2 \text{ deg} \quad \beta = 0 \quad \delta_{tc_{\max}} = \pm 20^\circ$$

$$A_e = \frac{S_{tc} \bar{c}_{tc}}{S_e \bar{c}_e} = 0.0169 \quad D_1 = \frac{\partial C_{h_{tc}}}{\partial \delta_e} = -0.0025 \text{ per deg}$$

$$D_2 = \frac{\partial C_{h_{tc}}}{\partial \delta_{tc}} = -0.0085 \text{ per deg} \quad D_3 = \frac{\partial C_{h_{tc}}}{\partial \alpha_H} = -0.0014 \text{ per deg}$$

Compute the control-column force required to deflect the elevator  $10^\circ$  TED at a free-stream dynamic pressure of  $150 \text{ lb/ft}^2$ .

Determine the values of  $R_1$  and  $R_2$  for a spring-tab system

$$R_1 = \frac{R_L + \Delta_r}{R_L + \frac{B_2}{A_e D_2} - \frac{k}{q D_2} R_L} \quad (\text{Table 6.3.4-B})$$

$$R_1 = \frac{4.1 + \frac{20.0}{15.0}}{4.1 + \frac{-0.0046}{(0.0169)(-0.0085)} - \frac{(0.244)(4.1)}{150.0(-0.0085)}} \\ = \frac{5.433}{36.907} = 0.1472$$

$$\begin{aligned}
R_2 &= \frac{-\frac{k}{qD_2} (R_L + \Delta_r)}{R_L + \frac{B_2}{A_e D_2} - \frac{k}{qD_2} R_L} = -\frac{k}{qD_2} R_1 \quad (\text{Table 6.3.4-B}) \\
&= \frac{-(0.244)}{(150.0)(-0.0085)} (0.1472) \\
&= 0.02817
\end{aligned}$$

Determine the tab-free hinge-moment coefficient

$$\begin{aligned}
C_{h_{e_{\text{tab free}}}} &= \left( B_1 - D_1 \frac{B_2}{D_2} \right) \delta_e + \left( B_3 - D_3 \frac{B_2}{D_2} \right) \alpha_H + B_4 \delta_{tt} \quad (\text{Equation 6.3.4-l}) \\
&= \left[ -0.0040 + 0.0025 \left( \frac{-0.0046}{-0.0085} \right) \right] 10 + \left[ -0.0017 + 0.0014 \left( \frac{-0.0046}{-0.0085} \right) \right] 2.5 \\
&\quad + (-0.0044)(-3.0) \\
&= -0.01563
\end{aligned}$$

Determine the locked-tab hinge-moment coefficient

$$\begin{aligned}
C_{h_{e_{\text{tab locked}}}} &= B_1 \delta_e + B_3 \alpha_H + B_4 \delta_{tt} \quad (\text{Equation 6.3.4-m}) \\
&= (-0.0040) 10 + (-0.0017) 2.5 + (-0.0044)(-3.0) \\
&= -0.03105
\end{aligned}$$

Solution:

$$\begin{aligned}
F_s &= G_{e_{\max}} S_e \bar{c}_e q \left[ C_{h_{e_{\text{tab free}}}} R_1 + C_{h_{e_{\text{tab locked}}}} R_2 + \Delta C_{h_{e_{\text{tab gearing}}}} R_2 \right] \quad (\text{Equation 6.3.4-k}) \\
F_s &= (162.0)(150) [(-0.01563)(0.1472) + (-0.03105)(0.02817) + 0] \\
&= (162.0)(150)(-0.003175) \\
&= -77.16 \text{ lb}
\end{aligned}$$

Therefore, for the given tab system, a push force of 77.16 lb is required to achieve an elevator deflection of 10° at a free-stream dynamic pressure of 150 lb/ft².

## REFERENCES

1. Dunn, O. R.: Aerodynamically Boosted Surface Controls and Their Application to the DC-6 Transport. IAS Paper presented May 24, 1949. (U)
2. Kolk, W. R.: Modern Flight Dynamics. Prentice-Hall, Inc., Englewood Cliffs, N.J., 1961. (U)
3. Perkins, C. D., and Hage, R. E.: Airplane Performance Stability and Control. John Wiley and Sons, Inc., N.Y., 1949. (U)
4. Toll, T. A.: Summary of Lateral-Control Research. NACA TR 868, 1947. (U)
5. Mendelsohn, R. A.: A Semigraphical Method of Computing Stick Forces for Spring-Tab Controls Having Nonlinear Hinge-Moment Characteristics. Jour. of Aero. Sci., February 1948. (U)
6. Woodcock, R. J., and Drake, D. E.: Estimation of Flying Qualities of Piloted Airplanes. AFFDL-TR-65-218, 1966. (U)